

THIRD EDITION

**Intermolecular
and Surface
Forces**

Jacob N. Israelachvili



Fundamental Constants

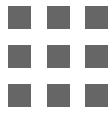
Constant	Symbol	SI	CGS
Avogadro's constant	N_A, N_0	$6.022 \times 10^{23} \text{ mol}^{-1}$	$6.022 \times 10^{23} \text{ mole}^{-1}$
Boltzmann's constant	$k, k_B = R/N_A$	$1.381 \times 10^{-23} \text{ J K}^{-1}$	$1.381 \times 10^{-16} \text{ erg/deg}$
Molar gas constant	$R = N_A k$	$8.314 \text{ J K}^{-1} \text{ mol}^{-1}$	$8.314 \times 10^7 \text{ erg/mole-deg}$
Electronic charge	$-e$	$1.602 \times 10^{-19} \text{ C}$	$4.803 \times 10^{-10} \text{ esu}$
Faraday constant	$F = N_A e$	$9.649 \times 10^4 \text{ C mol}^{-1}$	$9.649 \times 10^4 \text{ C/mole}$
Planck's constant	$h (\hbar = h/2\pi)$	$6.626 \times 10^{-34} \text{ J s}$	$6.626 \times 10^{-27} \text{ erg sec}$
Permittivity of free space	ϵ_0	$8.854 \times 10^{-12} \text{ C}^2 \text{ J}^{-1} \text{ m}^{-1}$	1
Mass of $\frac{1}{12}$ of ^{12}C atom*	u	$1.661 \times 10^{-27} \text{ kg}$	$1.661 \times 10^{-24} \text{ gm}$
Mass of hydrogen atom	m_H	$1.673 \times 10^{-27} \text{ kg}$	$1.673 \times 10^{-24} \text{ gm}$
Mass of electron	m_e	$9.109 \times 10^{-31} \text{ kg}$	$9.109 \times 10^{-28} \text{ gm}$
Gravitational constant	G	$6.674 \times 10^{-11} \text{ N m}^2 \text{ kg}^{-2}$	$6.674 \times 10^{-8} \text{ cm}^3/\text{gm-sec}^2$
Standard gravity	g	$9.80665 \text{ m s}^{-2} (\text{N kg}^{-1})$	980.665 cm/sec^2
Speed of light in vacuum	c	$2.998 \times 10^8 \text{ m s}^{-1}$	$2.998 \times 10^{10} \text{ cm/sec}$

*Atomic mass unit (also denoted by a.m.u. and a.u.), which is also the modern unit of molecular weight, the Dalton (Da).



Intermolecular and Surface Forces

This page intentionally left blank



Intermolecular and Surface Forces

Third Edition

Jacob N. Israelachvili

*UNIVERSITY OF CALIFORNIA
SANTA BARBARA, CALIFORNIA, USA*



ELSEVIER

AMSTERDAM • BOSTON • HEIDELBERG • LONDON • NEW YORK • OXFORD
PARIS • SAN DIEGO • SAN FRANCISCO • SINGAPORE • SYDNEY • TOKYO

Academic Press is an imprint of Elsevier



Academic Press is an imprint of Elsevier
225 Wyman Street, Waltham, MA 02451, USA
525 B Street, Suite 1900, San Diego, CA 92101-4495, USA
The Boulevard, Langford Lane, Kidlington, Oxford, OX51GB, UK
Radarweg 29, PO Box 211, 1000 AE Amsterdam, The Netherlands

Third edition 2011

Copyright © 2011, Elsevier Inc. All rights reserved.

No part of this publication may be reproduced, stored in a retrieval system or transmitted in any form or by any means electronic, mechanical, photocopying, recording or otherwise without the prior written permission of the publisher

Permissions may be sought directly from Elsevier's Science & Technology Rights Department in Oxford, UK: phone (+44) (0) 1865 843830; fax (+44) (0) 1865 853333; email: permissions@elsevier.com. Alternatively you can submit your request online by visiting the Elsevier web site at <http://www.elsevier.com/locate/permissions>, and selecting: Obtaining permission to use Elsevier material

Notice

No responsibility is assumed by the publisher for any injury and/or damage to persons or property as a matter of products liability, negligence or otherwise, or from any use or operation of any methods, products, instructions or ideas contained in the material herein. Because of rapid advances in the medical sciences, in particular, independent verification of diagnoses and drug dosages should be made

Library of Congress Cataloging-in-Publication Data

Israelachvili, Jacob N.

Intermolecular and surface forces / Jacob N. Israelachvili. – 3rd ed.

p. cm.

Includes bibliographical references and index.

ISBN 978-0-12-391927-4 (alk. paper)

1. Intermolecular forces. 2. Surface chemistry. I. Title.

QD461.I87 2011

541'.226–dc22

2010031067

ISBN: 978-0-12-391927-4

For information on all Academic Press publications
visit our website at elsevierdirect.com

Printed and bound in USA

10 11 12 10 9 8 7 6 5 4 3 2 1

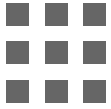
Working together to grow
libraries in developing countries

www.elsevier.com | www.bookaid.org | www.sabre.org

ELSEVIER

BOOK AID
International

Sabre Foundation



Contents

Preface to the Third Edition	xvii
Preface to the Second Edition	xix
Preface to the First Edition	xxi

PART ONE THE FORCES BETWEEN ATOMS AND MOLECULES	1
1. Historical Perspective	3
1.1. The Four Forces of Nature	3
1.2. Greek and Medieval Notions of Intermolecular Forces	3
1.3. The Seventeenth Century: First Scientific Period	5
1.4. The Eighteenth Century: Confusion, Contradictions, and Controversy	7
1.5. The Nineteenth Century: Continuum <i>versus</i> Molecular Theories	8
1.6. Intermolecular Force-Laws and Interaction Potentials: Long- and Short-Range Forces	9
1.7. First Successful Phenomenological Theories	12
1.8. First Estimates of Molecular Sizes	15
1.9. The Twentieth Century: Understanding Simple Systems	16
1.10. Recent Trends	17
<i>Problems and Discussion Topics</i>	18
2. Thermodynamic and Statistical Aspects of Intermolecular Forces	23
2.1. The Interaction of Molecules in Free Space and in a Medium	23
2.2. Self-Energy and Pair Potential	25
2.3. The Boltzmann Distribution and the Chemical Potential	26

2.4. The Distribution of Molecules and Particles in Systems at Equilibrium	27
2.5. The Van der Waals Equation of State (EOS)	30
2.6. The Criterion of the Thermal Energy kT for Gauging the Strength of an Interaction	31
2.7. Classification of Forces and Pair Potentials	34
2.8. Theoretical Analyses of Multimolecular Systems: Continuum and Molecular Approaches	35
2.9. Molecular Approaches via Computer Simulations: Monte Carlo (MC) and Molecular Dynamics (MD)	37
2.10. Newton's Laws Applied to Two-Body Collisions	39
2.11. Kinetic and Statistical Aspects of Multiple Collisions: the Boltzmann Distribution	43
<i>Problems and Discussion Topics</i>	49
3. Strong Intermolecular Forces: Covalent and Coulomb Interactions	53
3.1. Covalent or Chemical Bonding Forces	53
3.2. Physical and Chemical Bonds	54
3.3. Coulomb Forces or Charge-Charge Interactions, Gauss's Law	55
3.4. Ionic Crystals	58
3.5. Reference States	59
3.6. Range of Electrostatic Forces	60
3.7. The Born Energy of an Ion	61
3.8. Solubility of Ions in Different Solvents	62
3.9. Specific Ion-Solvent Effects: Continuum Approach	66
3.10. Molecular Approach: Computer Simulations and Integral Equations of Many-Body Systems	67
<i>Problems and Discussion Topics</i>	68
4. Interactions Involving Polar Molecules	71
4.1. What Are Polar Molecules?	71

4.2. Dipole Self-Energy	73
4.3. Ion-Dipole Interactions	73
4.4. Ions in Polar Solvents	78
4.5. Strong Ion-Dipole Interactions in Water: Hydrated Ions	78
4.6. Solvation Forces, Structural Forces, and Hydration Forces	80
4.7. Dipole-Dipole Interactions	81
4.8. Magnetic Dipoles	83
4.9. Hydrogen Bonds	83
4.10. Rotating Dipoles and Angle-Averaged Potentials	84
4.11. Entropic Effects	86
<i>Problems and Discussion Topics</i>	88
5. Interactions Involving the Polarization of Molecules	91
5.1. The Polarizability of Atoms and Molecules	91
5.2. The Polarizability of Polar Molecules	93
5.3. Other Polarization Mechanisms and the Effects of Polarization on Electrostatic Interactions	94
5.4. Interactions between Ions and Uncharged Molecules	96
5.5. Ion-Solvent Molecule Interactions and the Born Energy	98
5.6. Dipole-Induced Dipole Interactions	99
5.7. Unification of Polarization Interactions	99
5.8. Solvent Effects and “Excess Polarizabilities”	100
<i>Problems and Discussion Topics</i>	105
6. Van der Waals Forces	107
6.1. Origin of the Van der Waals-dispersion Force between Neutral Molecules: the London Equation	107
6.2. Strength of Dispersion Forces: Van der Waals Solids and Liquids	109
6.3. Van der Waals Equation of State	113
6.4. Gas-Liquid and Liquid-Solid Phase Transitions in 3D and 2D	115
6.5. Van der Waals Forces between Polar Molecules	117

6.6. General Theory of Van der Waals Forces between Molecules	119
6.7. Van der Waals Forces in a Medium	122
6.8. Dispersion Self-Energy of a Molecule in a Medium	126
6.9. Further Aspects of Van der Waals Forces: Anisotropy (Orientation), Nonadditivity (Many-Body), and Retardation Effects	127
<i>Problems and Discussion Topics</i>	130
7. Repulsive Steric Forces, Total Intermolecular Pair Potentials, and Liquid Structure	133
7.1. Sizes of Atoms, Molecules, and Ions	133
7.2. Repulsive Potentials	136
7.3. Total Intermolecular Pair Potentials: Their Form, Magnitude, and Range	136
7.4. Role of Repulsive Forces in Noncovalently Bonded Solids	140
7.5. Packing of Molecules and Particles in Solids	142
7.6. Role of Repulsive Forces in Liquids: Liquid Structure	145
7.7. The Effect of Liquid Structure on Molecular Forces	147
<i>Problems and Discussion Topics</i>	148
8. Special Interactions: Hydrogen-Bonding and Hydrophobic and Hydrophilic Interactions	151
8.1. The Unique Properties of Water	151
8.2. The Hydrogen Bond	152
8.3. Models of Water and Associated Liquids	156
8.4. Relative Strengths of Different Types of Interactions	157
8.5. The Hydrophobic Effect	158
8.6. The Hydrophobic Interaction	161
8.7. Hydrophilic Interactions	163
<i>Problems and Discussion Topics</i>	166
9. Nonequilibrium and Time-Dependent Interactions	169
9.1. Time- and Rate-Dependent Interactions and Processes	169

9.2. Rate- and Time-Dependent Detachment (Debonding) Forces	171
9.3. Energy Transfer (Dissipation) during Molecular Collisions: the Deborah Number	175
9.4. Energy Transfer during Cyclic Bonding-Unbonding Processes	178
9.5. Relationships between Time, Temperature, and Velocity (Rate) in Complex Processes	182
<i>Problems and Discussion Topics</i>	185
PART TWO THE FORCES BETWEEN PARTICLES AND SURFACES	189
10. Unifying Concepts in Intermolecular and Interparticle Forces	191
10.1. The Association of Like Molecules or Particles in a Medium	191
10.2. Two Like Surfaces Coming Together in a Medium: Surface and Interfacial Energy	196
10.3. The Association of Unlike Molecules, Particles, or Surfaces in a Third Medium	197
10.4. Particle-Surface and Particle-Interface Interactions	198
10.5. Engulfing and Ejection	200
10.6. Adsorbed Surface Films: Wetting and Nonwetting	201
<i>Problems and Discussion Topics</i>	203
11. Contrasts between Intermolecular, Interparticle, and Intersurface Forces	205
11.1. Short-Range and Long-Range Effects of a Force: Qualitative Differences in the Interactions of Particles and Small Molecules	205
11.2. Interaction Potentials between Macroscopic Bodies	208
11.3. Effective Interaction Area of Two Spheres: the Langbein Approximation	211
11.4. Interactions of Particles Compared to Those between Atoms or Small Molecules	212

11.5. Interaction Energies and Interaction Forces: the Derjaguin Approximation	215
11.6. “Body Forces” and “Surface Forces”	220
<i>Problems and Discussion Topics</i>	220
12. Force-Measuring Techniques	223
12.1. Direct and Indirect Measurements of Intermolecular, Interparticle, and Surface Forces	223
12.2. Different Direct Force-Measuring Techniques	227
12.3. Mechanics of Direct Force Measurements and Problems of Interpretation	231
12.4. Measuring Force-Distance Functions, $F(D)$	234
12.5. Instabilities	235
12.6. Measuring Adhesion Forces and Energies	237
12.7. Measuring Forces between Macroscopic Surfaces: the SFA, OP/OS and Related Techniques	239
12.8. Measuring Forces between Microscopic (Colloidal) and Nanoscopic Particles: AFM and TIRM Techniques	245
12.9. Measuring Single-Molecule and Single-Bond Interactions: OT and MC Techniques	248
<i>Problems and Discussion Topics</i>	250
13. Van der Waals Forces between Particles and Surfaces	253
13.1. Van der Waals Force-Laws for Bodies of Different Geometries: the Hamaker Constant	253
13.2. Strength of Van der Waals Forces between Bodies in a Vacuum or Air	254
13.3. The Lifshitz Theory of Van der Waals Forces	256
13.4. Particle-Surface Interactions	259
13.5. Nonretarded Hamaker Constants Calculated on the Basis of the Lifshitz Theory	260
13.6. Van der Waals Forces between Conducting Media	261
13.7. Theoretical and Experimental Hamaker Constants for Interactions in a Vacuum or Air	263

13.8. Applications of the Lifshitz Theory to Interactions in a Medium	264
13.9. Repulsive Van der Waals Forces: Disjoining Pressure and Wetting Films	267
13.10. Van der Waals Forces at Large Separations: Retardation Effects	270
13.11. Electrostatic Screening Effects in Electrolyte Solutions	274
13.12. Combining Relations	274
13.13. Surface and Adhesion Energies	275
13.14. Surface Energies of Metals	280
13.15. Forces between Surfaces with Adsorbed Layers	281
13.16. Experiments on Van der Waals Forces	282
<i>Problems and Discussion Topics</i>	284
14. Electrostatic Forces between Surfaces in Liquids	291
14.1. The Charging of Surfaces in Liquids: the Electric “Double-Layer”	291
14.2. Charged Surfaces in Water: No Added Electrolyte—“Counterions Only”	293
14.3. The Poisson-Boltzmann (PB) Equation	293
14.4. Surface Charge, Electric Field, and Counterion Concentration at a Surface: “Contact” Values	294
14.5. Counterion Concentration Profile Away from a Surface	296
14.6. Origin of the Ionic Distribution, Electric Field, Surface Potential, and Pressure	298
14.7. The Pressure between Two Charged Surfaces in Water: the Contact Value Theorem	300
14.8. Limit of Large Separations: Thick Wetting Films	303
14.9. Limit of Small Separations: Osmotic Limit and Charge Regulation	305
14.10. Charged Surfaces in Electrolyte Solutions	306
14.11. The Grahame Equation	308
14.12. Surface Charge and Potential of Isolated Surfaces	309

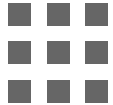
14.13. Effect of Divalent Ions	311
14.14. The Debye Length	312
14.15. Variation of Potential ψ_x and Ionic Concentrations ρ_x Away from a Surface	313
14.16. Electrostatic Double-Layer Interaction Forces and Energies between Various Particle Surfaces	314
14.17. Exact Solutions for Constant Charge and Constant Potential Interactions: Charge Regulation	318
14.18. Asymmetric Surfaces	321
14.19. Ion-Condensation and Ion-Correlation Forces	322
14.20. More Complex Systems: Finite Reservoir Systems and Finite Ion-Size Effects	325
14.21. Van der Waals and Double-Layer Forces Acting Together: the DLVO Theory	326
14.22. Experimental Measurements of Double-Layer and DLVO Forces	331
14.23. Electrokinetic Forces	334
14.24. Discrete Surface Charges and Dipoles	335
<i>Problems and Discussion Topics</i>	338
15. Solvation, Structural, and Hydration Forces	341
15.1. Non-DLVO Forces	341
15.2. Molecular Ordering at Surfaces, Interfaces, and in Thin Films	342
15.3. Ordering of Spherical Molecules between Two Smooth (Unstructured) Surfaces	345
15.4. Ordering of Nonspherical Molecules between Structured Surfaces	347
15.5. Origin of Main Type of Solvation Force: the Oscillatory Force	349
15.6. Jamming	354
15.7. Experimental Measurements and Properties of Oscillatory Forces	355
15.8. Solvation Forces in Aqueous Systems: Monotonically Repulsive “Hydration” Forces	361

15.9. Solvation Forces in Aqueous Systems: Attractive “Hydrophobic” Forces	370
<i>Problems and Discussion Topics</i>	378
16. Steric (Polymer-Mediated) and Thermal Fluctuation Forces	381
16.1. Diffuse Interfaces in Liquids	381
16.2. The States of Polymers in Solution and at Surfaces	381
16.3. Repulsive “Steric” or “Overlap” Forces between Polymer-Covered Surfaces	387
16.4. Interparticle Forces in Pure Polymer Liquids (Polymer Melts)	393
16.5. Attractive “Intersegment” and “Bridging” Forces	394
16.6. Attractive “Depletion” Forces	398
16.7. Polyelectrolytes	402
16.8. Nonequilibrium Aspects of Polymer Interactions	404
16.9. Thermal Fluctuations of and Forces between Fluid-Like Interfaces	405
16.10. Short-Range Protrusion Forces	406
16.11. Long-Range Undulation Forces	408
<i>Problems and Discussion Topics</i>	411
17. Adhesion and Wetting Phenomena	415
17.1. Surface and Interfacial Energies	415
17.2. Adhesion Energies versus Adhesion Forces	419
17.3. Highly Curved Surfaces and Interfaces: Clusters, Cavities, and Nanoparticles	422
17.4. Contact Angles and Wetting Films	429
17.5. Wetting of Rough, Textured, and Chemically Heterogeneous Surfaces	434
17.6. Contact Angle Hysteresis	439
17.7. Adhesion of Solid Particles: the JKR and Hertz Theories	442
17.8. Adhesion Hysteresis	448
17.9. Adhesion of Rough and Textured Surfaces	452

17.10. Plastic Deformations	453
17.11. Capillary Forces	456
<i>Problems and Discussion Topics</i>	461
18. Friction and Lubrication Forces	469
18.1. Origin of Friction and Lubrication Forces	469
18.2. Relationship between Adhesion and Friction Forces	476
18.3. Amontons' Laws of (Dry) Friction	481
18.4. Smooth and Stick-Slip Sliding	482
18.5. Lubricated Sliding	485
18.6. Transitions between Liquid- and Solid-Like Films	490
18.7. The "Real" Area of Contact of Rough Surfaces	493
18.8. Rolling Friction	494
18.9. Theoretical Modeling of Friction Mechanisms	495
<i>Problems and Discussion Topics</i>	497
PART THREE SELF-ASSEMBLING STRUCTURES AND BIOLOGICAL SYSTEMS	501
19. Thermodynamic Principles of Self-Assembly	503
19.1. Introduction: Soft Structures	503
19.2. Fundamental Thermodynamic Equations of Self-Assembly	504
19.3. Conditions Necessary for the Formation of Aggregates	509
19.4. Effect of Dimensionality and Geometry: Rods, Discs, and Spheres	510
19.5. The Critical Micelle Concentration (CMC)	512
19.6. Infinite Aggregates (Phase Separation) versus Finite Sized Aggregates (Micellization)	513
19.7. Hydrophobic Energy of Transfer	514
19.8. Nucleation and Growth of Aggregates	515
19.9. 2D Structures on Surfaces: Soluble and Insoluble Monolayers	520

19.10. Line Tension and 2D Micelles (Domains)	521
19.11. Soluble Monolayers and the Gibbs Adsorption Isotherm	524
19.12. Size Distributions of Self-Assembled Structures	524
19.13. Large and More Complex Amphiphilic Structures	527
19.14. Effects of Interactions between Aggregates: Mesophases and Multilayers	528
<i>Problems and Discussion Topics</i>	530
20. Soft and Biological Structures	535
20.1. Introduction: Equilibrium Considerations of Fluid Amphiphilic Structures	535
20.2. Optimal Headgroup Area	536
20.3. Geometric Packing Considerations	538
20.4. Spherical Micelles	540
20.5. Nonspherical and Cylindrical Micelles	543
20.6. Bilayers	544
20.7. Vesicles	548
20.8. Curvature/Bending Energies and Elasticities of Monolayers and Bilayers	550
20.9. Other Amphiphilic Structures and the Transitions between Them	558
20.10. Self-Assembly on Surfaces and Interfaces: 2D Micelles, Domains, and Rafts	562
20.11. Biological Membranes	564
20.12. Membrane Lipids	564
20.13. Membrane Proteins and Membrane Structure	567
<i>Problems and Discussion Topics</i>	569
21. Interactions of Biological Membranes and Structures	577
21.1. Van der Waals Forces	577
21.2. Electrostatic (Double-Layer) and DLVO Forces	579

21.3.	Repulsive Entropic (Thermal Fluctuation, Steric-Hydration) Forces: Protrusion, Headgroup Overlap, and Undulation Forces	585
21.4.	Attractive Depletion Forces	593
21.5.	Attractive Hydrophobic Forces	595
21.6.	Biospecificity: Complementary, Site-Specific and Ligand-Receptor (LR) Interactions	599
21.7.	Bridging (Tethering) Forces	603
21.8.	Interdependence of Intermembrane and Intramembrane Forces	605
21.9.	Biomembrane Adhesion, Bioadhesion	607
21.10.	Membrane Fusion	611
	<i>Problems and Discussion Topics</i>	613
22.	Dynamic Biointeractions	617
22.1.	Subtleties of Biological Forces and Interactions	617
22.2.	Interactions that Evolve in Space and Time: Some General Considerations	617
22.3.	Biological Rupture and Capture: the Bell and Jarzynski Equations	619
22.4.	Multiple Bonds in Series and in Parallel	622
22.5.	Detachment versus Capture Processes: Biological Importance of “Rare Events”	626
22.6.	Dynamic Interactions between Biological Membranes and Biosurfaces	626
22.7.	Self-Assembly versus Directed Assembly: Dynamic Phases and Tunable Materials	628
22.8.	Motor Proteins, Transport Proteins, and Protein Engines	630
	<i>Problems and Discussion Topics</i>	631
	References	635
	Index	661



Preface to the Third Edition

Updating the first and second editions of *Intermolecular and Surface Forces* was not easy. The field has exploded in many directions, both at the fundamental and applied levels, and into new areas. New terms have appeared such as complex fluids, soft matter, nanoscience, nanotechnology, nano-structured materials, biomimicry, and bio-inspired systems. Biological systems are being increasingly understood and copied at all length scales, accompanied by an increasing appreciation of dynamic (nonequilibrium, time- and rate-dependent) interactions. Ever more sophisticated experimental techniques and powerful computers now allow for highly complex systems to be studied and analyzed. Computers can now accurately mimic complex systems and even derive new equations without actually understanding what is going on (in the traditional sense).

The third edition contains updated material and also expands into new fields where molecular forces play a role, such as friction, lubrication, and dynamic (non-equilibrium) interactions. The aim has remained to provide basic physical insights and simple theoretical methods for calculating or estimating the magnitudes of various interactions—linking the fundamental science with practical and engineering applications. The focus is on fundamental aspects that may be applied to different phenomena rather than particular systems or the hot topics of the day.[†]

There are now many more worked examples scattered throughout each chapter and more end-of-chapter problems. The Worked Examples are intended to illustrate different ways of solving problems, both numerical and conceptual, that do not simply involve plugging numbers into an equation. The problems and discussion topics at the end of each chapter are similar, but they are often more subtle, and in some cases open-ended—in other words, ripe for discussion. Difficult problems are starred (*), and many problems have the answers provided but not how to solve them.

In preparing the third edition I have been helped by many. I am particularly grateful to Erika Eiser, Suzanne Giasson, Yu Tian, Eric Kaler, Joe Zasadzinski, Dan Schwartz, William Ducker, Marjorie Longo, Hongbo Zeng, Carlos Drummond, Stefan Karpitschka, Tonya Kuhl, Uzi Landman, Mark Robbins, Patricia McGuiggan, Kai Kristiansen, Roger Horn, Hugo Christenson, Yuval Golan, Xavier Banquy, Travers Anderson, Wren Greene, Malte Hammer, Jing Yu, Nataley Belman, Hernan Makse, Swapan Ghosh, Ayao Kitahara, Brian Vincent, Phil Pincus, and Dov Levine. Special thanks to Marina Ruths for her thorough reading and critical comments, Nancy Emerson for helping to organize the manuscript and references, Dottie McLaren for the illustrations, and Trudi Carey for her loving support.

Santa Barbara, California
December 29, 2009

[†]As another example of change, today's "hot" topic should really be described as "cool."

This page intentionally left blank



Preface to Second Edition

Since 1985, when the first edition of this book appeared, there has been much experimental and theoretical progress in this multidisciplinary subject. The nature of some “old” forces have been clarified while “new” forces have been discovered. The subject has matured into a rigorous discipline and a unifying area of chemistry, physics, and biology, and many university courses now routinely contain material on molecular and surface interactions. On the more practical side, many industrial and chemical engineering processes are now beginning to be understood and controlled at the fundamental level. It is with these developments in mind, together with the feedback I received from numerous colleagues, that the second edition was prepared.

The second edition is basically an updated version of the first, but it contains more than 100 problems. Most appear at the end of each chapter, but some appear as worked examples in the text. These problems should enhance the suitability of the book as an advanced undergraduate or graduate textbook. The problems have been devised to stimulate the mind; many are based on genuine research problems, others are tricky, some are extensions of the text into more advanced areas, and a few are open-ended to invite further reading, discussion, and even speculation.

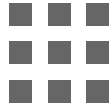
The text itself has been expanded to include recent developments in the areas of surface-force measurements, solvation and structural forces, hydration and hydrophobic forces, ion-correlation forces, thermal fluctuation forces, and particle and surface interactions in polymer melts and polymer solutions.

I am grateful to many colleagues who commented on the first edition, and I have used their suggestions in writing the second. In particular, my thanks go to Hans Lyklema, Håkan Wennerström and Jacob Klein, to Helen Vydra and Josefina Israelachvili for typing the manuscript, to Dottie McLaren for drawing many of the figures, to my wife Karina who supported me throughout, and finally to my students who have sat through my lectures and by their questions have unwittingly contributed the most.

Santa Barbara, California

October 24, 1989

This page intentionally left blank



Preface to the First Edition

Intermolecular forces embrace all forms of matter, and yet one finds very few university courses devoted to all aspects of this important subject. I wrote this book with the aim of presenting a comprehensive and unified introduction to intermolecular and surface forces, describing their role in determining the properties of simple systems such as gases, liquids, and solids, but especially of more complex, and more interesting, systems. These are neither simple liquids nor solids, but rather a myriad of dissolved solute molecules, small molecular aggregates, or macroscopic particles interacting in liquid or vapor. It is the forces in such systems that ultimately determine the behavior and properties of everyday things: soils, milk and cheese, paints and ink, adhesives and lubricants, many technological processes, detergents, micelles, biological molecules and membranes, and we ourselves—for each of us is one big biocolloidal system composed of about 75% water, as are most living organisms.

This subject therefore touches on a very broad area of phenomena in physics, chemistry, chemical engineering, and biology, in which there have been tremendous advances in the past 15 years. These advances can be viewed in isolation within each discipline or within a broader multidisciplinary framework. The latter approach is adopted in this book, where I have tried to present a general view of intermolecular and surface forces with examples of the various and often seemingly disparate phenomena in which they play a role.

Because of the wide range of topics covered and the different disciplines to which the book is addressed, I have presumed only a basic knowledge of the “molecular sciences”: physics (elementary concepts of energy and force, electrostatics), chemistry (basic thermodynamics and quantum mechanics), and mathematics (algebra and elementary calculus). The mathematical and theoretical developments, in particular, have been kept at a simple, unsophisticated level throughout. Vectors are omitted altogether. Most equations are derived from first principles followed by examples of how they apply to specific situations. More complicated equations are stated but are again carefully explained and demonstrated.

In a book such as this, of modest size yet covering such a wide spectrum, it has not been possible to treat each topic exhaustively or rigorously, and specialists may find their particular subject discussed somewhat superficially.

The text is divided into three parts, the first dealing with the interactions between atoms and molecules, the second with the interactions between “hard” particles and surfaces, and the third with “soft” molecular aggregates in solution such as micelles (aggregates of surfactant molecules) and biological membranes (aggregates of lipids and proteins). While the fundamental forces are, of course, the same in each of these categories, they manifest themselves in sufficiently different ways that, I believe, they are best treated in three parts.

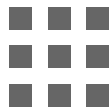
The primary aim of the book is to provide a thorough grounding in the theories and concepts of intermolecular forces so that the reader will be able to appreciate which forces are important in whatever system he or she is dealing with and to apply these theories correctly to specific problems (research or otherwise). The book is intended for final-year undergraduate students, graduate students, and nonspecialist research workers.

I am deeply grateful to the following people who have read the text and made valuable comments for improving its presentation: Derek Chan, David Gruen, Bertil Halle, Roger Horn,

Stjepan Marcelja, John Mitchell, Håkan Wennerström, and Lee White. My thanks also extend to Diana Wallace for typing the manuscript and to Tim Sawkins for his careful drawing of most of the figures. But above all, I am indebted to my wife, Karina, without whose constant support this book would not have been written.

Canberra, Australia

October 24, 1984



Units, Symbols, Useful Quantities and Relations

Much of the published literature and equations on intermolecular and surface forces are based on the CGS system of units. In this book the *Système International* (SI) is used. In this system the basic units are the **kilogram** (kg) for mass, the **meter** (m) for length, the **second** (s) for time, the **kelvin** (K) for temperature, the **ampère** (A) for electrical quantities, and the **mole** (mol) for quantity of mass. Some old units such as gramme (1 gm = 1 g = 10^{-3} kg), centimeter (1 cm = 10^{-2} m), ångstrom ($1 \text{ \AA} = 10^{-10}$ m) and degree centigrade ($^{\circ}\text{C}$) are still commonly used, although they are not part of the SI system. The SI system has many advantages over the CGS, not least when it comes to forces. For example, force is expressed in newtons (N) without reference to the acceleration due to the earth's gravitation, which is implicit in some formulae based on the CGS system. Note that units, prefixes, words, and abbreviations are usually unitalicized—that is, in text format (e.g., J, K, m, N, volts V), whereas variables are italicized (e.g., stiffness K , mass m , number N , maximum number N_{\max} , velocity or volume V).

Derived SI Units

Quantity	SI Unit	Symbol	Definition of Unit									
Energy	Joule	J	$\text{kg m}^2 \text{s}^{-2}$ (also Nm and CV)									
Force	Newton	N	$\text{J m}^{-1} = \text{kg m s}^{-2}$									
Power	Watt	W	$\text{J s}^{-1} = \text{kg m}^2 \text{s}^{-3}$									
Pressure	Pascal	Pa	N m^{-2}									
Electric charge	Coulomb	C	A s									
Electric potential	Volt	V	$\text{J A}^{-1} \text{s}^{-1} = \text{J C}^{-1}$									
Electric field	Volt/meter		V m^{-1}									
Frequency	Hertz	Hz	s^{-1}									
Fraction	10^{12}	10^9	10^6	10^3	10^{-1}	10^{-2}	10^{-3}	10^{-6}	10^{-9}	10^{-12}	10^{-15}	10^{-21}
Prefix symbol	T	G	M	k	d	c	m	μ	n	p	f	z

Definitions of Terms and Symbols Used in the Text

- a Atomic or molecular radius (m), surfactant headgroup area (m^2)
 a, b Constants in equations of state
 a_0 Bohr radius, atomic unit (a.u.) of length 0.053 nm, optimum headgroup area (m^2)
 A, A_{ijk} Hamaker constant for media i and k interacting across medium j (J), area (m^2), Helmholtz free energy

c, C	Interaction constant (J m^6), aqueous solute concentration in mole fraction units ($\text{mol dm}^{-3}/55.5$ or $\text{M}/55.5$), concentration number density (m^{-3}), volume fraction
d	Distance, diameter (m)
D	Distance between two surfaces (m)
Da	Dalton unit of molecular weight (same as MW)
E	Electric field strength (V m^{-1}), energy (J, eV, erg)
F	Force (N) or, when between two planar surfaces, force per unit area (N m^{-2})
G	Gibbs free energy
h, H	Height (m), enthalpy, hardness (Pa), hour (also hr)
I	Ionization potential (J)
i	$\sqrt{-1}$
k_a	Area compressibility modulus (J m^{-2} or N m^{-1})
k_b	Bending or curvature modulus (J)
k, K	Elastic modulus (N m^{-2}), spring constant or stiffness (N m^{-1})
K_a	Reaction constant, association constant (M^{-1})
K_d	Dissociation constant ($K_d = 1/K_a$)
l, ℓ	Length (m), unit segment length in polymer chain (m)
l_p	Persistence length of worm-like chain polymer (m)
l_c	Critical hydrocarbon chain length (m)
L	Latent heat (J mol^{-1}), thickness of polymer brush layer (m)
m, M	Mass (kg), molarity, molar mass, molecular weight (also MW), mean aggregation number
M	Concentration ($\text{mol dm}^{-3}, 10^3 \text{ mol m}^{-3}$, moles/liter)
M_W, M, MW	Molecular weight, molar mass (g mol^{-1}), atomic mass (g), mass of atom or molecule $\times N_0$, mass of atom or molecule/mass of $\frac{1}{12}$ of ^{12}C atom, Da (if not specified, e.g., PEO 1,000, assume Da)
n, N	Refractive index; number of atoms, molecules, moles, bonds, segments in a polymer chain, micelle aggregation number
p, P	Pressure (N m^{-2})
P_L, P_Y	Laplace pressure, yield stress (Pa)
pK	$-\log_{10}[\text{concentration or activity of } \text{H}^+ \text{ ions in M}]$
Q, q	Charge (C)
r, R	Radius (m), interatomic distance (m), atomic or molecular radius (m)
r_K	Kelvin radius (m)
R_g, R_F	Radius of gyration of polymer (m), Flory radius of polymer (m)
s	Mean distance between polymer anchoring sites (m)
S	Entropy, solubility
t	Time (s)
T	Temperature (K)
T_M, T_B	Melting or boiling points (K or $^\circ\text{C}$)
T_c, T_m	Lipid chain melting temperature
u	Dipole moment (C m)
U	Molar cohesive energy (J mol^{-1}), internal energy (J mol^{-1})
v, V	Volume (m^3), velocity or speed (m s^{-1}), molar volume (m^3)
w, W, W_0	Interaction free energy, pair potential (J). Between two planar surfaces: Work of adhesion, cohesion or interaction free energy per unit area (J m^{-2})
x, y, z	Position along the x-, y- or z- axis, arbitrary variables

\dot{x}	Time derivative of variable x , for example, velocity = dx/dt (m s^{-1})
\ddot{x}	Acceleration, $d(dx/dt)/dt = d^2x/dt^2$ (m s^{-2})
X	Dimensionless concentration (e.g., mole fraction)
Y	Young's modulus (N m^{-2})
z	Valency
α	Polarizability ($\text{C}^2 \text{ m}^2 \text{ J}^{-1}$), interaction energy parameter (J or J m^{-1})
γ	Surface tension (N m^{-1}), surface energy (J m^{-2}), $\tanh(e\psi_0/4kT) \rightarrow \tanh[\psi_0(\text{mV})/103]$ at 298 K
γ_i, γ_{AB}	Interfacial energy (J m^{-2})
Γ	Surface coverage, surface density, 2D density (number per m^2)
δ	Stern layer thickness (m), elastically or plastically deformed distance (m)
$\varepsilon(\nu)$	Dielectric permittivity at frequency ν
ε	Relative permittivity, static dielectric constant at zero frequency $\varepsilon(0)$, strain
ϵ	Energy (J or J m^{-1})
$\theta, \phi, \psi, \alpha$	Angle (deg or rad), contact angle (deg)
θ	Theta temperature of solvent ($^\circ\text{C}$, K)
κ	Inverse Debye length (m^{-1})
$\lambda, \lambda_0, \lambda_0$	Characteristic exponential decay length, wavelength (m), line tension (N)
ξ	Correlation length (m)
μ	Chemical potential, coefficient of friction (COF)
μ^i, μ^o	Standard part of chemical potential due to molecular interactions
ν, ν_1	Frequency (s^{-1} or Hz), ionization frequency (s^{-1})
ρ	Number density (m^{-3}) or mass density (kg m^{-3})
σ	Atomic or molecular diameter (m), surface charge density (C m^{-2}), standard deviation
τ, τ_o, τ_0	Characteristic relaxation time (s), lifetime (s), stress (N m^{-2} , Pa)
η	Viscosity (Pa s)
Ω	Solid angle
ψ, ψ_0	Electrostatic potential (V), surface potential (V)
Π	Two-dimensional surface pressure (N m^{-1})
\approx, \sim	Approximately equal to, roughly equal to
$>, <$	Greater than, less than
\lesssim, \gtrsim	Slightly greater than/less than
\leq	Less than or equal to
\geq	Greater than or equal to
\gg, \ll	Much greater than, much less than
\equiv	Equivalent to
\propto	Proportional to
\parallel, \perp	Parallel to, perpendicular or normal to
Δ	Change or difference in
$ X $	"Modulus" (positive or absolute value) of X
$\langle X \rangle, \bar{X}$	Average or mean of X
$[X]$	Concentration of X
$\rightarrow, \Rightarrow, \Rightarrow$	Approaches, implies, leads to
$1 2, \alpha \beta$	Interface between media 1 and 2 or phases α and β
■ ■ ■	Start or end of Worked Example

Abbreviations

e.g., eg	For example (from the Latin <i>exempli gratia</i>)
cf.	Compare with (from the Latin <i>confer</i>), contrast with
i.e., ie	That is, that is to say (from the Latin <i>id est</i>)
viz.	Namely (from the Latin, <i>videlicet</i>)
etc.	More of the same type (from the Latin <i>etcetera</i>)
et al.	And others (from the Latin <i>et alii</i>)
Ch.	Chapter
Log	In or \log_e (logarithm to base e)
<i>Ibid</i>	From same place as the previous reference/citation (from the Latin <i>ibidem</i>)
*	Difficult problem
Sect.	Section
FCC	Face Centered Cubic (see also HCP)
HCP	Hexagonal Close Packed (see also FCC)
1D, 2D, 3D	One-dimensional, two-dimensional, three-dimensional
RH	Relative humidity, p/p_{sat} for water vapor
STP	Standard temperature and pressure: $T = 25^\circ\text{C} = 298.15\text{ K}$, $P = 1\text{ atm} = 1.013 \times 10^5\text{ Pa}$. Some authorities have adopted $T = 20^\circ\text{C} = 293.15\text{ K}$ and $P = 100\text{ kPa}$.
CMC (CAC)	Critical micelle (aggregation) concentration

Conversion from CGS to SI

$1\text{ \AA\ (\"{a}ngstrom)} = 10^{-10}\text{ m} = 10^{-8}\text{ cm} = 10^{-4}\text{ }\mu\text{m} = 0.1\text{ nm}$
$1\text{ liter} = 10^{-3}\text{ m}^3 = 1\text{ dm}^3$
Density, $\rho(\text{kg m}^{-3}) = 10^3\rho(\text{g/cm}^3)$
Molecular weight, $M(\text{kg mol}^{-1}) = 10^{-3}M(\text{gm/mole})$
$1\text{ erg} = 10^{-7}\text{ J}$
$1\text{ cal} = 4.184\text{ J}$
$1\text{ kcal mole}^{-1} = 4.184\text{ kJ mol}^{-1}$
$1\text{ }kT = 4.114 \times 10^{-14}\text{ erg} = 4.114 \times 10^{-21}\text{ J at }298\text{ K (~25}^\circ\text{C)}$
$= 4.045 \times 10^{-14}\text{ erg} = 4.045 \times 10^{-21}\text{ J at }293\text{ K (~20}^\circ\text{C)}$
$= 4.281 \times 10^{-14}\text{ erg} = 4.281 \times 10^{-21}\text{ J at }310\text{ K (body temperature, ~37}^\circ\text{C)}$
$1\text{ }kT\text{ per molecule} = 0.592\text{ kcal mole}^{-1} = 2.478\text{ kJ mol}^{-1}\text{ at }298\text{ K}$
$1\text{ eV} = 1.602 \times 10^{-12}\text{ erg} = 1.602 \times 10^{-19}\text{ J}$
$1\text{ eV per molecule} = 23.06\text{ kcal mol}^{-1} = 96.48\text{ kJ mol}^{-1}$
$1\text{ cm}^{-1}\text{ (wave number unit of energy)} = 1.986 \times 10^{-23}\text{ J}$
$1\text{ dyne} = 1\text{ g cm s}^{-2} = 10^{-3}\text{ kg }10^{-2}\text{ m s}^{-2} = 10^{-5}\text{ N}$
$1\text{ dyne cm}^{-1} = 1\text{ erg cm}^{-2} = 1\text{ mN m}^{-1} = 1\text{ mJ m}^{-2}$ (unit of surface tension or energy)
$1\text{ dyne cm}^{-2} = 10^{-1}\text{ Pa or N m}^{-2}$ (unit of pressure).
$1\text{ atm} = 1.013 \times 10^6\text{ dyne cm}^{-2} = 1.013\text{ bar} = 1.013 \times 10^5\text{ Pa (N m}^{-2}\text{)}$
$1\text{ Torr} = 1\text{ mm Hg} = 1.316 \times 10^{-3}\text{ atm} = 133.3\text{ Pa (N m}^{-2}\text{)}$
$0^\circ\text{C} = 273.15\text{ K (triple point of water)}$
$1\text{ esu} = 3.336 \times 10^{-10}\text{ C}$
$1\text{ poise (P)} = 1\text{ dyne s cm}^{-2} = 0.1\text{ N s m}^{-2} = 0.1\text{ Pa s (unit of viscosity)}$
$1\text{ Stokes (St)} = \text{cm}^2\text{ s}^{-1} = 10^{-4}\text{ m}^2\text{ s}^{-1}$ (unit of kinematic viscosity: viscosity/density)
$\text{Debye (D)} = 10^{-18}\text{ esu} = 3.336 \times 10^{-30}\text{ C m}$ (unit of electric dipole moment)

Conversion from SI to CGS

$$1 \text{ nm} = 10^{-9} \text{ m} = 10 \text{ \AA} = 10^{-7} \text{ cm}$$

$$1 \text{ J} = 10^7 \text{ erg} = 0.239 \text{ cal} = 6.242 \times 10^{18} \text{ eV} = 5.034 \times 10^{22} \text{ cm}^{-1} = 7.243 \times 10^{22} \text{ K}$$

$$1 \text{ kJ mol}^{-1} = 0.239 \text{ kcal mole}^{-1} = 0.404 \text{ } kT \text{ per molecule at 298 K}$$

$$1 \text{ N} = 10^5 \text{ dyne} \equiv \text{mass or weight of 0.102 kg (102 gm) in a gravitational field of } g = 9.81 \text{ m s}^{-2}$$

$$1 \text{ Pa} = 1 \text{ N m}^{-2} = 10 \text{ dyne cm}^{-2} = 9.872 \times 10^{-6} \text{ atm} = 7.50 \times 10^{-3} \text{ torr} = 1.45 \times 10^{-4} \text{ psi (lb/in}^2)$$

$$1 \text{ bar} = 10^5 \text{ N m}^{-2} = 10^5 \text{ Pa} = 0.9868 \text{ atm} = 750.06 \text{ mm Hg}$$

Useful Quantities and Relations, Other Conversions

Mass of any atom or molecule = M/N_0 (also MW/N_0) g

Mean volume occupied per molecule = $M/(N_0 \times \text{mass density}) \text{ m}^3$

Converting mass density ρ_m (kg m^{-3}) to number density ρ_n (molecules m^{-3}): $\rho_n = \rho_m N_0/M$

Molar concentration: $1 \text{ M} = 1 \text{ mol dm}^{-3}$ (mole/litre) = 6.022×10^{26} molecules per m^3

Number density (solution concentration): $\rho = M \times 6.022 \times 10^{26}$ molecules per m^3

Standard volume of ideal gas = $22.414 \times 10^{-3} \text{ m}^3 \text{ mol}^{-1}$ (22.414 liters/mole)

$$4\pi\varepsilon_0 = 1.113 \times 10^{-10} \text{ C}^2 \text{ J}^{-1} \text{ m}^{-1}$$

$$kT/e = RT/F = -25.69 \text{ mV at 298 K (~25°C)} = -26.72 \text{ mV at 310 K (~37°C, body temperature)}$$

$$1 \text{ C m}^{-2} = 1 \text{ unit charge per } 0.16 \text{ nm}^2 (16 \text{ \AA}^2)$$

$$\kappa^{-1} (\text{Debye length}) = 0.304/\sqrt{M} \text{ nm for 1:1 electrolyte at 298 K (25°C)}$$

$$\text{Mass of the earth} = 5.976 \times 10^{24} \text{ kg}$$

$$\text{Density of earth (mean)} = 5.518 \times 10^3 \text{ kg m}^{-3}$$

Values of gravitational acceleration, g : Standard gravity (9.80665 m s^{-2}), Equator (9.780 m s^{-2}), North and south poles (9.832 m s^{-2}), New York (9.801 m s^{-2}), London (9.812 m s^{-2}).

Some Geometric Relations for Truncated Sphere and Cap of Height d (Shaded)

Height of cap: $d = R(1 - \cos \theta)$, $\sin \theta = r/R$

Chord theorem: $r^2 = (2R - d)d \approx 2Rd$ for $R \gg d$

Volume of sphere: $\frac{4}{3}\pi R^3$; surface area of sphere = $4\pi R^2$

Volume of cap: $\frac{1}{3}\pi d^2(3R - d) = \frac{1}{3}\pi R^3(2 + \cos \theta)(1 - \cos \theta)^2$

Volume of truncated sphere: $\frac{4}{3}\pi R^3 - \text{volume of cap}$

Area of curved surface of cap: $2\pi R d = 2\pi R^2(1 - \cos \theta)$

Area of curved surface of sphere: $2\pi R(2R - d) = 2\pi R^2(1 + \cos \theta)$

Area of flat circular base of cap: $\pi r^2 = \pi(2R - d)d = \pi R^2 \sin^2 \theta$

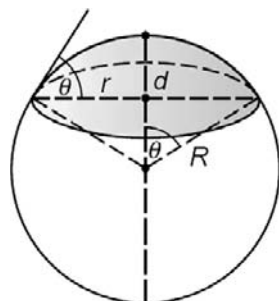


FIGURE I

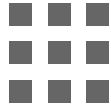
Table i. Some Properties of Water at 1 atm Pressure

Property	Values at Different Temperatures						
	Ice	0°C (273.15 K)	10°C (283 K)	20°C (293 K)	25°C (298 K)	37°C (body temp)	50°C (323 K)
Dielectric constant (permittivity) at zero frequency, ϵ	91.6	87.9	84.0	80.2	78.4	74.2	69.9
Refractive index at 589 nm, n	1.309	1.3343	1.3341	1.3334	1.3329	1.3313	1.3294
Surface tension/energy, γ (mJ m ⁻²)	~109	75.6	74.2	72.8	72.0	70.1	67.9
Density, ρ (gm/cm ³ = kg m ⁻³ /1000)	0.9167	0.9999 [†]	0.9997	0.9982	0.9970	0.9933	0.9880
Viscosity, η (mPa s)	10 ¹⁴ Glacier ice	1.79	1.31	1.00	0.89	0.69	0.55

Additional properties: Mass of water molecule: 2.99×10^{-26} kg. Dipole moment: 1.84 D. Rotational correlation time of water molecule in liquid water: $\tau_{\text{rot}} \approx 2$ ps.

[†]Density maximum 1.0000 at 4°C.

This page intentionally left blank



Definitions and Glossary

These days, online information is so good and readily accessible that it is no longer necessary to define or introduce basic terms or concepts in a text book. The reader should refer to such sources whenever new or unfamiliar terms are used, such as *simple harmonic motion*, *resonance frequency*, the *Grotthuss Mechanism*, the *Vroman effect*, and *von Schröder's Paradox*. It is for this reason that this glossary is so short.

Amphiphile Molecules such as surfactants and lipids where one part is hydrophilic (the “headgroup”) and the other is hydrophobic, usually a long hydrocarbon chain.

Classical An adjective that describes nonquantum mechanical systems whose molecules obey Boltzmann statistics.

Colloid A colloid is a dispersion of particles in solution. The size of colloidal particles is in the microscopic regime, ranging from 0.005 to 100 μm . Only one dimension of a particle needs to be in this range to qualify it as a colloidal particle—for example, a 5 nm thick lipid bilayer of macroscopic area. Particles in the size range from 1 to 100 nm are now referred to as **nanoparticles**, this being the range of sizes where atomic properties make the transition to microscopic or macroscopic properties.

Critical micelle concentration (CMC), critical aggregate concentration (CAC) The concentration at which further addition of solute molecules to a solvent makes them go into finite sized micelles (aggregates) while the monomer concentration remains unchanged at the CMC (CAC).

Directed assembly See **Self-assembly**.

Energy dissipated The energy that one system (molecule, particle or lattice) *transfers* to another system during an interaction. This can be in the form of translational kinetic energy or heat (e.g., internal vibrational and rotational energy).

Engineering conditions Range of time, length, mass, temperature, and so on, encountered in everyday phenomena (see Table 9.1).

Equilibrium Mechanical equilibrium is one where a small deviation from the “equilibrium” state brings the system back to that state; thermodynamic equilibrium is the lowest free-energy state—the state of “true” equilibrium. A system in mechanical equilibrium is not necessarily in the true equilibrium state, from which it may be separated by an energy barrier. A state can also be in thermal equilibrium (the temperature is uniform throughout), but not in mechanical or thermodynamic equilibrium. See Section 22.2 for more on nonequilibrium systems.

Extensive Thermodynamic term for property that depends on the number of molecules N or moles n or the total volume V of the system—for example, the mass or total energy of the system. Cf. **Intensive, Specific**.

Intensive Thermodynamic term for property that does not depend on the size or number of molecules in a thermodynamic system, for example, pressure, temperature, viscosity, surface tension. Cf. **Extensive, Specific**.

Self-assembly The natural (spontaneous, thermodynamically driven) organization of atoms and molecules into multimolecular structures. **Directed** or **engineered assembly** refers to

xxx Definitions and Glossary

external energy-requiring processes that lead to nonequilibrium, but often long-lived, structures, or to a stable steady-state organization but only so long as there is a constant rate of energy input.

Specific (i) Thermodynamic term for **intensive** property produced by dividing one **extensive** property by another—for example, specific molecular volume (volume occupied per molecule) $v = V/N$, specific molar volume $v = V/n$. Cf. **Intensive**, **Extensive**. (ii) Biological term for interaction or bond between two specialized groups that uniquely recognize each other. Specific bonds do not have to be strong. Also **complementary**, **lock-and-key**, **ligand-receptor (L-R or LR)** bonding.

The Forces between Atoms and Molecules

This page intentionally left blank

Historical Perspective

1.1 The Four Forces of Nature

It is now well-established that there are four distinct forces in nature. Two of these are the *strong* and *weak interactions* that act between neutrons, protons, electrons, and other elementary particles. These two forces have a very short range of action, less than 10^{-5} nm, and belong to the domain of nuclear and high-energy physics. The other two forces are the *electromagnetic* and *gravitational interactions* that act between atoms and molecules (as well as between elementary particles). These forces are effective over a much larger range of distances, from subatomic to practically infinite distances, and are consequently the forces that govern the behavior of everyday things (Figure 1.1). For example, electromagnetic forces—the source of all intermolecular interactions—determine the properties of solids, liquids, and gases, the behavior of particles in solution, chemical reactions, and the organization of biological structures. Gravitational forces account for tidal motion and many cosmological phenomena, and when acting together with intermolecular forces, they determine such phenomena as the height that a liquid will rise in small capillaries and the maximum size that animals and trees can attain (Thompson, 1968).

This book is mainly concerned with intermolecular forces. Let us enter the subject by briefly reviewing its historical developments from the ancient Greeks to the present day.

1.2 Greek and Medieval Notions of Intermolecular Forces

The Greeks were the first to consider forces in a nonreligious way. They found that they needed only two fundamental forces to account for all natural phenomena: Love and Hate. The first brought things together, while the second caused them to part. The idea was first proposed by Empedocles around 450 B.C., was much “improved” by Aristotle, and formed the basis of chemical theory for 2000 years.

The ancients appear to have been particularly inspired by certain mysterious forces, or influences, that sometimes appeared between various forms of matter (forces that we would now call magnetic or electrostatic). They were intrigued by the “action-at-a-distance” property displayed by these forces, as well as by gravitational forces, and they were moved to reflect upon their virtues. What they lacked in concrete experimental facts they more than made up for by the abundant resources of their imagination (Verschuur, 1993). Thus, magnetic forces could cure diseases, though they could also cause

4 INTERMOLECULAR AND SURFACE FORCES

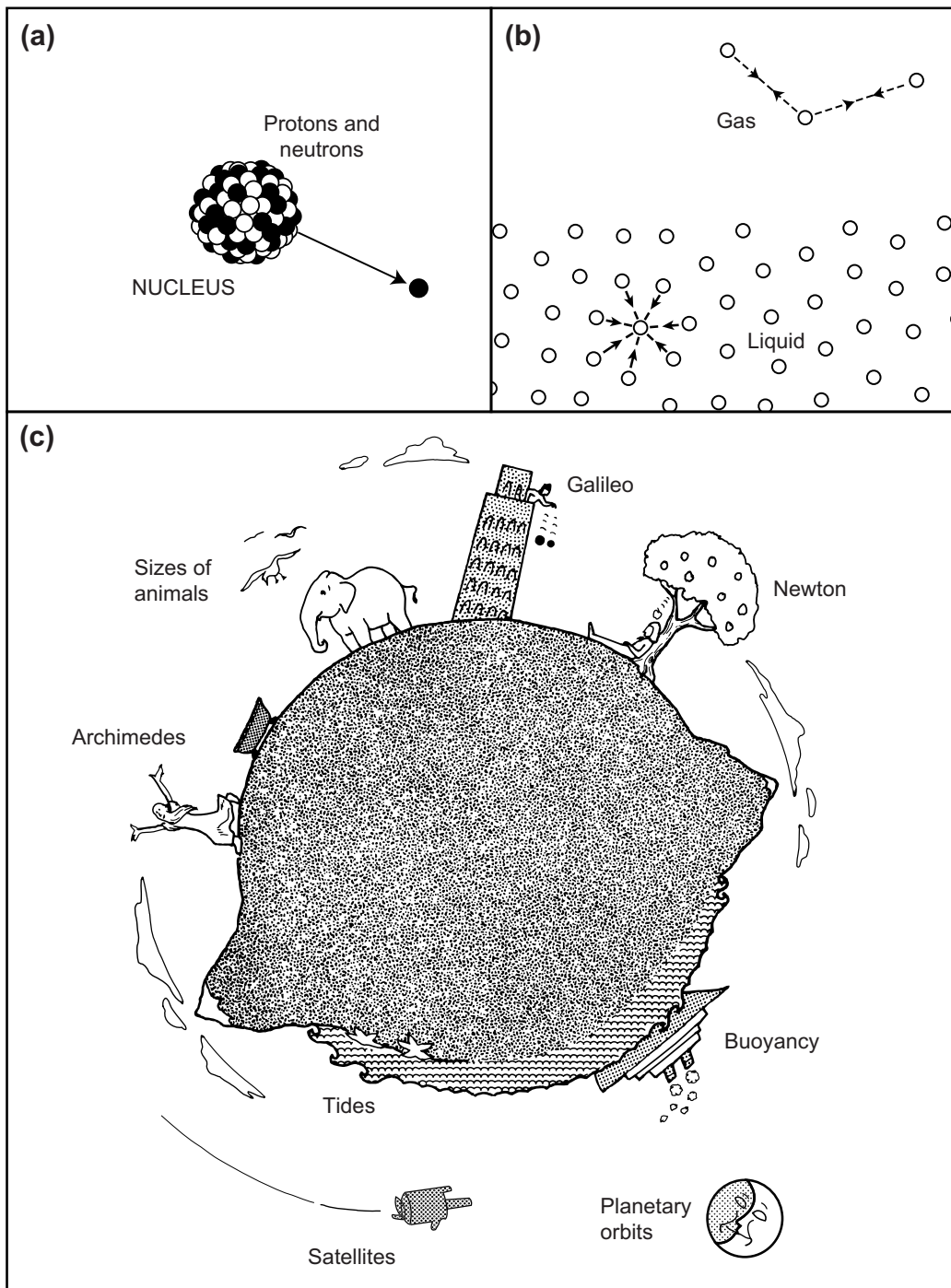


FIGURE 1.1 The forces of nature. **(a)** Strong nuclear interactions hold protons and neutrons together in atomic nuclei. Weak interactions are involved in electron emission (β decay). **(b)** Electrostatic (intermolecular) forces determine the cohesive forces that hold atoms and molecules together in solids and liquids. **(c)** Gravitational forces affect tides, falling bodies, and satellites. Gravitational and intermolecular forces acting together determine the maximum possible sizes of buildings, mountains, trees, and animals.

melancholy and thievery. Magnets could be used to find gold, and they were effective as love potions and for testing the chastity of women. Unfortunately, some magnetic substances lost their powers if rubbed with garlic (but they usually recovered when treated with goat's blood). Electric phenomena were endowed with attributes no less spectacular, manifesting themselves as visible sparks in addition to a miscellany of attractive or repulsive influences that appeared when different bodies were rubbed together. All these wondrous practices, and much else, were enjoyed by our forebears until well into the seventeenth century and may be said to constitute the birth of our subject at the same time as alchemy, astrology, and the search for perpetual motion machines, which paved the way for chemistry and physics.

Still, notwithstanding the unscientific or prescientific nature of these practices, some important conceptual breakthroughs were made that deserve to be recognized. Ask any schoolboy or schoolgirl what the three most memorable scientific discoveries of antiquity are, and they will very likely mention Archimedes, Galileo, and Newton (see Figure 1.1). In each case, what happened (or is alleged to have happened) is well known, but what is less well known are the *conceptual* breakthroughs whose implications are with us today. Put into modern jargon, when Archimedes (287–212 B.C.) discovered Archimedes' Principle, he had discovered that the force of gravity on a body can change—even its sign from attraction to repulsion—when it is placed in a medium that it displaces. Later we shall see that such displacement effects occur with many other types of interactions, such as van der Waals forces, with important consequences that in some cases have only recently been appreciated.

1.3 The Seventeenth Century: First Scientific Period

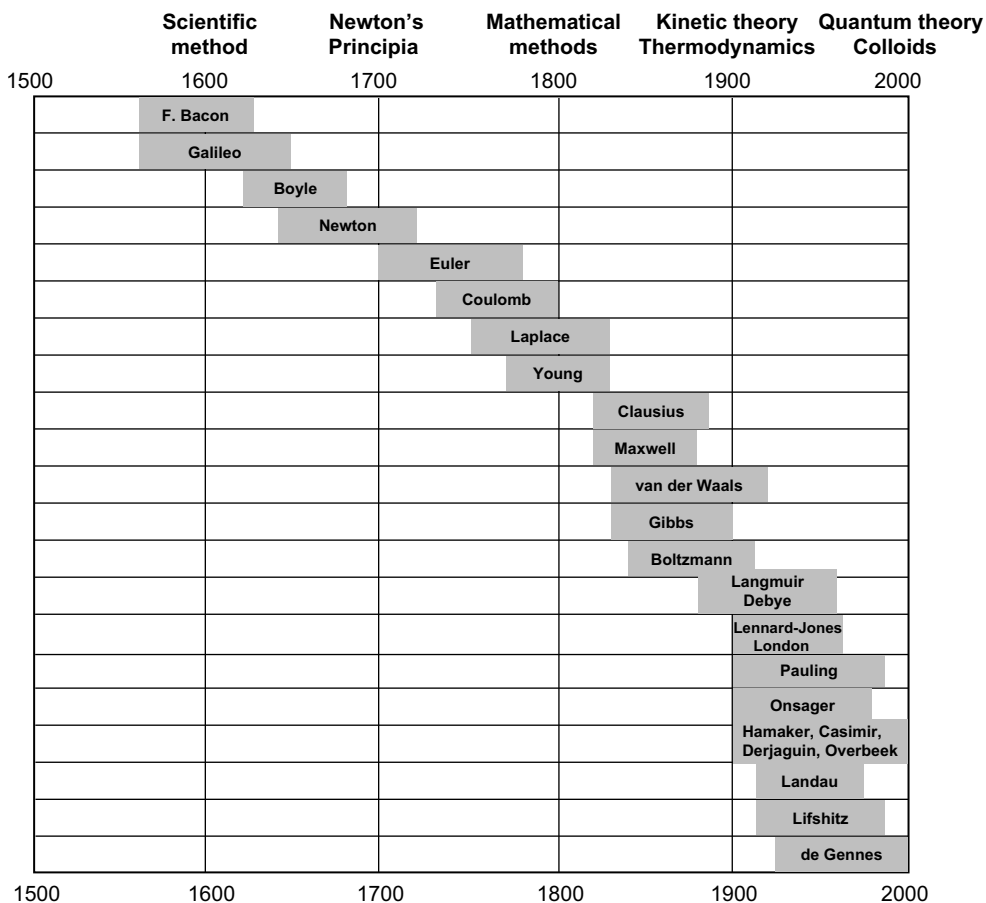
The notion of doing experiments to find out how nature works was an unknown concept until Galileo (1564–1642) demonstrated its power in his classic experiments on gravity, the motion of bodies, optics, astronomy, and proving the existence of a vacuum. In this he introduced the modern “scientific method” (Table 1.1).

But Galileo also introduced a new way of thinking that was not purely metaphysical. As an example, his experiment of throwing two different balls from the Tower of Pisa was conducted only after he had worked out the answer by applying a new form of reasoning—what we would today call “scaling arguments”—to Aristotelean Physics (see Problem 1.1), and his testing of his hypothesis by *direct experiment* was at the time also highly novel.¹ This is also true of Newton’s discovery of the Law of Gravitation when an apple fell on his head. We must pause to think about how many previous heads, when struck by a falling apple, were prompted to generalize the phenomenon to other systems

¹Galileo’s English contemporary Francis Bacon (1561–1626) may be credited with the introduction of inductive reasoning and the first to practice experimental research. Unfortunately, his first experiment was also his last: While testing the effects of cold on preserving meat by stuffing a disemboweled chicken with snow, he caught a chill and died.

6 INTERMOLECULAR AND SURFACE FORCES

Table 1.1 Scientists Who Made Major Contributions to Our Understanding of Intermolecular Forces (including some whose contribution was indirect)



such as the orbit of the moon around the earth when acted on by the same force—a thought process that requires a leap of the imagination by a factor of 10^6 in time, 10^8 in distance, and 10^{24} in mass.

But trouble was just round the corner. In 1662 Robert Boyle (1627–1691) published his famous gas law, $PV = \text{constant}$. Twenty-five years later, Isaac Newton (1642–1727) published his famous law of gravity. Boyle's Law suggested that molecules repel each other (the pressure P in $PV = \text{constant}$ is repulsive), while gravity suggested that they attract. Newton also concluded that the molecules of a gas must ultimately attract each other, since they condense into liquids or solids. These apparent contradictions sowed the first of many seeds that were to lead to heated controversies in the two centuries to come.

Worked Example 1.1

Question: If the experimental observation that $PV = \text{constant}$ is a result of the repulsion between the stationary molecules of a gas, what is the distance-dependence of this force? More generally, what would be the force function if $P \propto (1/V)^m \propto \rho^m$, where ρ is the density? Do not use any concepts that came after the eighteenth century.

Answer: In the eighteenth century, matter and space were believed to be made up of “corpuscles” that were *stationary*. There was no kinetic theory of gases, no collisions between molecules, and no thermodynamics. The concept of potential energy was still unknown, and everything was described in terms of mechanical forces that were mediated by some intervening medium or fluid known as the “aether” or “caloric.”

Let the repulsive force between two molecules be given by $+C/r^n$. Consider a cube of gas with sides of length L and volume $V = L^3$. Let there be N molecules within this volume, each occupying a volume $v = r^3$, where r is the distance between any two molecules. We therefore have $N = V/v = L^3/r^3$, so that for constant N , $r \propto L$. Now, each side of area L^2 will have L^2/r^2 molecules, which will exert a total normal force of $(C/r^n) \times (L^2/r^2)$ and, therefore, a pressure of $P = \text{Force/Area} = (C/r^n) \times (L^2/r^2)/L^2 = C/r^{n+2}$. Thus, if experimentally $P \propto 1/V$, we may write $P \propto 1/V \propto 1/L^3 \propto 1/r^3$ (since $r \propto L$), and we finally obtain $n = 3 - 2 = 1$, implying that the repulsive intermolecular force-law is $F = +C/r$. More generally, for $P \propto (1/V)^m \propto \rho^m$, we obtain $n = 3m - 2$.

1.4 The Eighteenth Century: Confusion, Contradictions, and Controversy

The above conclusion, and much else—including his gravitational force-law and the development of the calculus—was published by Newton in his famous *Principia* (1687, 1713, 1726).² But in spite of the tremendous advances made by Newton, the period between his *Principia* and the beginning of the nineteenth century was marked by confusion, contradictions, and controversy (Rowlinson, 2002). Here are some of the most notable ones:

- The derivation of an inverse distance law to account for the behavior of gases was known (even by Newton) to be unphysical when integrated over many molecules and/or large distances (see Section 1.6).
- Newton’s law of gravity required an instantaneous force to act across a vast vacuum. The idea of “action at a distance” with no intervening substance or mechanism for its transmission led to accusations that this was tantamount to invoking some

²The three dates refer to the three editions of this—probably the most influential scientific text of all time. It includes his *Opticks*, published in 1704. The calculus, discovered jointly with Leibniz in the 1680s, allowed for the mathematical analysis and development of scientific theories.

8 INTERMOLECULAR AND SURFACE FORCES

supernatural or occult force that the new field of “natural philosophy” was supposed to avoid.

- When considering the forces between particles over distances from the very large to the very small, an unsettling picture emerged where these forces start off being attractive (the gravitational force), then repulsive (in gases, as concluded in Worked Example 1.1), then attractive again (to account for solids and liquids), and finally repulsive (to account for the fact that matter does not disappear into itself). The notion of a generic oscillatory force between all particles was proposed by Boskovich (1711–1787), and heat was believed to be a substance (caloric) that increased the repulsive part of this interaction.
- The observations that the capillary rise of liquids did not depend on the capillary wall thickness, however thin,³ implied that interparticle forces must be of very *short range*. However, the equally undeniable fact that the liquid rises to a substantial height, even in tubes having macroscopic inner radii, suggested that these forces must be of *long range*, since they are able to reach the liquid molecules in the center of the tube.

But the eighteenth century also saw major advances in pure and applied mathematics by Euler, LaGrange, Laplace, and others (see Table 1.1) that proved to be invaluable for analyzing and interpreting experimental data.

1.5 The Nineteenth Century: Continuum *versus* Molecular Theories

The first half of the nineteenth century saw a continuation of the controversy about whether matter was a continuum or made up of molecules (atoms, particles, or corpuscles), with the balance slowly tilting toward the *continuum* picture. Newton had believed that matter, including light, was made of particles, but Young’s work on optical interference fringes showed that light behaved like waves. There were also theoretical successes in explaining many physical phenomena in terms of continuum field theories without the need to invoke molecules. And so the belief in molecules declined. According to Maxwell (1831–1879), the main reason that, by the mid-nineteenth century, no one believed in molecules any longer was not because anyone had shown that they did not exist but because “all those who believe in molecules are now dead.”

Much of the progress during the nineteenth century came from work on liquid surfaces, especially the capillary rise of liquids in glass tubes. In 1808 Clairaut suggested that capillarity could be explained if the attraction between the liquid and glass molecules was different from the attraction of the liquid molecules for themselves. It was also

³These experiments and many others were performed by Francis Hauksbee (1666–1713), who was Newton’s “demonstrator” at the Royal Society.

noticed that the height of rise of a liquid column does not depend on the capillary wall thickness, which led to the conclusion that these forces must be of very short range or, in the language of the time, extended over “insensible” distances.⁴

The latter half of the nineteenth century saw the return of molecules, thanks to the successes of the new kinetic theory and the van der Waals equation of state, both of which required attracting molecules to explain them. Clausius (1822–1888), Maxwell (1831–1879), van der Waals (1837–1923), and Boltzmann (1844–1906) were the main players⁵ in unifying continuum theories such as thermodynamics and mean-field theories with molecular theories through the new field of statistical mechanics (see Table 1.1). But the origin of the forces themselves remained a mystery until the advent of quantum theory in the 1920s.

1.6 Intermolecular Force-Laws and Interaction Potentials: Long- and Short-Range Forces

An important theoretical advance of the nineteenth century, thanks to the mathematical developments of the previous century, was the use of energy to analyze interactions and the properties of many-body systems; this allowed progress to be made in various areas, including thermodynamics. William Rankine (1820–1872) is generally considered to have pioneered the science of *energetics* whereby the vector forces and motions of Archimedes, Galileo, and Newton were replaced by scalar energy functions.⁶ As we shall see, in many cases the two approaches are equivalent, but where time- and rate-dependent interactions are involved, they are not. In other words, the force is not always simply the derivative of the energy-distance function (see Problems 1.4, 1.5, and 9.1, 9.4). New terms were coming into usage in addition to simple *energy* and *force*: internal energy, available energy, energy or force per unit length, per unit area, per unit volume (energy density), internal pressure, applied pressure, and more, and it remains an intellectual challenge to this day to be able to clearly distinguish among the many different types of energies and forces (Figure 1.2).

During the nineteenth century, it was believed that one simple universal force law or *potential energy function*, similar to Newton’s law for the gravitational force, would eventually be found to account for all intermolecular attractions. To this end, a number of *interaction potentials* were proposed that invariably contained the masses of the molecules, attesting to the belief at the time that these forces are related to gravitational forces.

⁴Although, as was noted in Section 1.4, the same phenomenon also seemed to suggest that these forces act over large distances.

⁵Or *natural philosophers*, as they were still called. Articles by Maxwell, Rayleigh, and others in the ninth edition of the encyclopedia Britannica of 1878 are still a good read. This edition was the last attempt to include the whole of science, as it was then known, in one encyclopedia.

⁶Many others contributed to the development of the concept of energy in different fields (see Chapter 2).

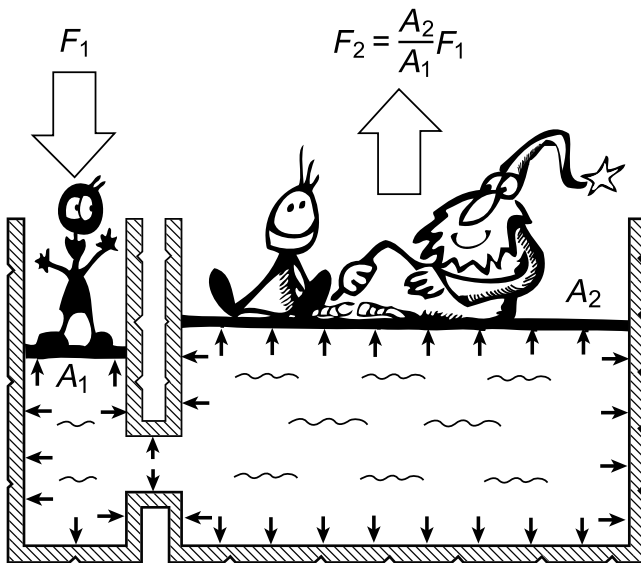


FIGURE 1.2 When discussing the “strength” of an interaction, it is important to clearly distinguish among the forces, energies, pressures, and so on. All of these have different units: force (N), energy (J), pressure (N m^{-2} or Pa), and so on. As will become apparent in future chapters, a bond may have a high bond energy but a low force needed to break it. Thus, simply talking about the “strength” of a bond may not mean anything. This figure illustrates the difference between force (F) and pressure (Force/Area = F/A), where a light load or force F_1 on the left lifts a heavier load F_2 on the right. At equilibrium, the pressure within a liquid at the same level must be the same everywhere (continuous), so motion occurs in the direction where the pressure, not the force, is lowest. In Chapter 9 we shall see how the difference between force and energy also requires consideration of the time (rate) and the temperature of an interaction. [Source: Figure reproduced from Watkins, 2000.]

Thus, typical attempts to model interaction potentials⁷ $w(r)$ for two molecules were of the form $w(r) = -Cm_1m_2/r^n$, which is related to the *force law* $F(r)$ between the molecules by

$$F(r) = -dw(r)/dr = -nCm_1m_2/r^{n+1}, \quad (1.1)$$

where m_1, m_2 are the molecular masses, r their separation, C a constant, and n some integer believed to be 4 or 5,⁸ which may be compared with $n = 1$ for the gravitational interaction:

$$w(r) = -Gm_1m_2/r, \quad G = 6.67 \times 10^{-11} \text{ N m}^2 \text{ kg}^{-2}. \quad (1.2)$$

It is instructive to see how the power-law index n was so chosen. It arose partly from a frantic attempt to fit experimental data to equations containing n as an adjustable

⁷Also *pair potential*, in units of energy (Joules, J).

⁸See footnote 3 in Chapter 6 to find out why Eq. (1.1) was almost successful. For an account of the lively theoretical activities of this time, see the introductory “History of Intermolecular Forces” in Margenau and Kestner (1971).

parameter but also from an appreciation of the fact, first noted by Newton, that if intermolecular forces are not to extend over large distances, the value of n must be greater than 3. Why this is so can be simply established as follows: Suppose the attractive potential between two molecules or particles to be of the general form $w(r) = -C/r^n$, where n is an integer. Now consider a region of space where the number density of these molecules is ρ . This region can be a solid, a liquid, a gas, or even a region in outer space extending over astronomical distances. Let us add all the interaction energies of one particular molecule with all the other molecules in the system. The number of molecules in a region of space between r and $(r+dr)$ away will be $\rho 4\pi r^2 dr$ (since $4\pi r^2 dr$ is the volume of a spherical shell of radius r and thickness dr —in other words, of area $4\pi r^2$ and thickness dr). The total interaction energy of one molecule with all the other molecules in the system will therefore be given by

$$\begin{aligned} \text{total energy} &= \int_{\sigma}^L w(r) \rho 4\pi r^2 dr = -4\pi C \rho \int_{\sigma}^L r^{2-n} dr \\ &= \frac{-4\pi C \rho}{(n-3)\sigma^{n-3}} \left[1 - \left(\frac{\sigma}{L}\right)^{n-3} \right] \\ &= -4\pi C \rho / (n-3) \sigma^{n-3} \quad \text{for } n > 3 \text{ and } L \gg \sigma, \end{aligned} \quad (1.3)$$

where σ is the diameter of the molecules and L is the size of the system—for example, the dimensions of a solid or the size of the box containing a gas. We can see that since σ must be smaller than L (i.e., $\sigma/L < 1$), large distance contributions to the interaction will disappear only for values of n greater than 3—that is, for $n = 4, 5, 6, \dots$. But for n equal to or smaller than 3,⁹ the second term in Eq. (1.3) will be greater than 1, and the contribution from more distant molecules will dominate over that of nearby molecules. In such cases the size of the system must be taken into account, as occurs for gravitational forces where $n = 1$ and where distant planets, stars, and even galaxies are still strongly interacting with one another (see Problem 1.3).

In later chapters we shall see that theoretical derivations of intermolecular force potentials do indeed predict that n usually exceeds 3, at least asymptotically (at large distances), and it is for this reason that the intrinsic bulk properties of solids, liquids, and gases do not depend on the volume of material or on the size of the container (unless these are extremely small) but only on the forces between molecules in close proximity to one another.¹⁰ The two most common interactions that give rise to long-range forces are the gravitational force ($n = 1$) and the forces between magnetic or electric dipoles ($n = 3$). The latter forces lie on the borderline between short- and

⁹For $n = 3$, the second term in Eq. (1.3) is $\log(\sigma/L)$, which is considered to be long-ranged.

¹⁰Standard thermodynamics, which assumes that certain thermodynamic functions such as energy are intensive properties, implicitly relies on intermolecular forces being short-ranged (Jund et al., 1995). However, as will become apparent, the effective range of some intermolecular forces between particles and surfaces can extend out to 100 nm or more, which can have important implications for submicroscopic and nano-sized systems.

long-range—their interaction energy decaying as $\log r$, which continues to increase, but only very weakly, as r approaches infinity. It is for this reason that magnetic dipoles can mutually align themselves along the same direction in a magnetic material and why we can feel magnetic forces (such as the earth's magnetic field) over very large distances. Such interactions also arise in electro-dipolar and liquid-crystalline media, giving rise to a long-ranged “ordering” of the molecules.¹¹

Returning to the latter part of the nineteenth century, hopes for an all-embracing force law dwindled as it became increasingly apparent that no suitable candidate would be forthcoming to explain the multitude of phenomena quantitatively. However, by this time the modern concept of surface tension forces was becoming established, as was the recognition that these forces are the same as those that hold molecules together in solids and liquids, and that in both cases they arise from interactions acting over very short distances. In addition, it was shown how these very short-range surface tension forces can account for such *macroscopic* phenomena as capillarity, the shapes of liquid drops on surfaces, the contact angle between coalescing soap bubbles, and the breakup of a jet of water into spherical droplets (Figure 1.3). Thus, it was established that very short-range forces can lead to very long-range (i.e., macroscopic) effects. It is therefore wrong to associate long-range *effects* with long-range *forces*. In fact, the opposite is usually the case—for what is more important is the *strength* of the interaction, and, as we shall see, short-range forces tend to be stronger than long-range forces. Further developments were forthcoming from quite different quarters: from work on gases rather than liquids or surfaces.

1.7 First Successful Phenomenological Theories

In an attempt to explain why real gases did not obey the ideal gas law ($PV = RT$ per mole of gas, where P is the pressure, V the molar volume, R the gas constant, and T the temperature),¹² the Dutch physicist J. D. van der Waals (1837–1923) considered the effects of attractive forces between molecules (at a time when the very existence of molecules as we know them today was still being hotly debated). In 1873 he arrived at his famous equation of state for gases and liquids,

$$(P + a/V^2)(V - b) = RT, \quad (1.5)$$

¹¹For molecules that are constrained to move on a surfaces, as occurs in monolayers, the critical index n for a long-ranged interaction changes from 3 to 2. Thus, the interaction of dipoles is short-ranged when these are confined to move on a surface (in two dimensions), even though it is long-ranged in three dimensions. The reason for this is that the total energy in 3D involves an averaging or integration over volume elements of $4\pi r^2 dr$ (cf. Eq. 1.3), while in 2D it involves averaging over area elements of $2\pi r dr$ (see Problem 2.2). In general, the exponent n has to exceed the “dimensionality” of the system for the interaction to be short-ranged.

¹²The Ideal Gas Law is a combination of Boyle's Law, $PV = \text{constant}$ and the later works by Charles, Guy-Lussac, and Dalton that showed that $P \propto T$ at constant V .

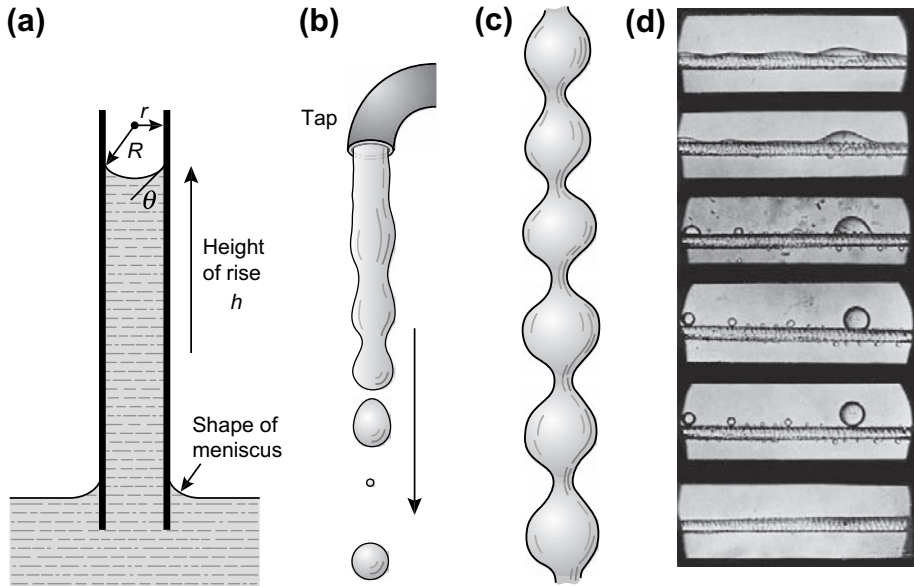


FIGURE 1.3 Long-range effects produced by short-range forces. (a) Capillary rise of liquids in narrow channels or pores. (b) Shape of water filament flowing out from a tap. (c) Unduloid shape of a spider's web, a “frozen” intermediate state of (b). (d) Action of detergent molecules in removing oily dirt from a fabric. Top to bottom: Progressive addition of detergent diminishes the contact area of oily droplets on fiber until they finally detach. [Source: (d) from Adam and Stevenson, 1953.]

in which he subtracted the term b from the volume to account for the finite size of molecules and added the term a/V^2 to the external (measured) pressure P to account for the attractive intermolecular forces now known as *van der Waals forces*.

By the early twentieth century, it was recognized that intermolecular forces are not of a simple nature, and the pursuit of one basic force law gave way to a less ambitious search for semiempirical expressions that could account for specific phenomena. In this vein Mie, in 1903, proposed an interaction pair potential of the form

$$w(r) = -A/r^n + B/r^m, \quad (1.6)$$

which for the first time included a repulsive term as well as an attractive term. This was the first of a number of similar laws that successfully accounted for a wide range of phenomena, and it is still used today, as is the van der Waals equation of state. Later we shall see how the parameters in potentials such as the Mie potential can be related to the constants a and b in the van der Waals equation of state. Lamentably, it was soon found that many different potentials with a wide range of (adjustable) parameters would satisfactorily account for the same experimental data, such as the elasticity of solids or the PVT behavior of gases. Thus, while such empirical equations were useful, the nature and origin of the forces themselves remained a mystery.

Worked Example 1.2

Question: The Lennard-Jones potential

$$w(r) = -A/r^6 + B/r^{12} \quad (1.7)$$

is a special case of the Mie potential, Eq. (1.6).¹³ In this potential the attractive (negative) contribution is the van der Waals interaction potential, which varies with the inverse-sixth power of the distance (Chapter 6). Make a sketch of how the energy $w(r)$ and force $F(r)$ vary with r . What does the Lennard-Jones potential predict for (i) the separation $r = r_e$ when the energy is at the minimum (equilibrium) value, w_{\min} ; (ii) the ratio of w_{\min} to the purely attractive van der Waals component of the interaction potential at r_e ; (iii) the ratio of r_e to r_0 defined by $w(r_0) = 0$; (iv) the ratio of r_s to r_0 , where r_s is the separation where the magnitude of the (attractive adhesion) force is maximum, F_{\max} ; and (v) the effective spring constant k of the bond for small displacements about the equilibrium position?

In the interaction between two atoms, the values of A and B are known to be $A = 10^{-77} \text{ J m}^6$ and $B = 10^{-134} \text{ J m}^{12}$. What is w_{\min} for this interaction in units of kT at 298 K, the spring constant in units of N m^{-1} , and the maximum adhesion force F_{\max} between the two atoms? Is this force measurable with a sensitive balance?

Answer:

- Figure 1.4 shows scaled plots of $w(r)$ and $F(r)$ for the given values of A and B , showing the various zero points, minima, points of inflection, and asymptotic values of the energy and force functions, and the relationship between them.
- $w(r)$ is minimum when $dw/dr = 0$. This occurs at $r = r_e = (2B/A)^{1/6} = 0.355 \text{ nm}$.
- Substituting r_e into Eq. (1.7) gives

$$w(r_e) = w_{\min} = -A^2/4B = -A/2r_e^6 = -2.5 \times 10^{-21} \text{ J} \rightarrow 2.5 \times 10^{-21}/4.1 \times 10^{-21} = 0.61 \text{ } kT$$
at 298 K.
- $w_{\min}(r_e)/w_{\text{VDW}}(r_e) = (-A/2r_e^6)/(-A/r_e^6) = \frac{1}{2}$.
- Since $w(r) = 0$ at $r = r_0 = (B/A)^{1/6}$, we obtain $r_e/r_0 = 2^{1/6} = 1.12$. Thus, $r_0 = 0.316 \text{ nm}$.
- The force is given by $F = -dw/dr$, and F_{\max} occurs at $d^2w/dr^2 = 0$ —that is, when
 $r = r_s = (26B/7A)^{1/6}$. Thus, $r_s/r_0 = (26/7)^{1/6} = 1.24$, and $r_s = (26B/7A)^{1/6} = 0.3935 \text{ nm}$.
- $F_{\max} = -dw/dr = -6A/r^7 + 12B/r^{13}$ at $r = r_s = 0.3935 \text{ nm}$.
Thus, $F_{\max} = -(126A^2/169B)/(26B/7A)^{1/6} = -1.89 \times 10^{-11} \text{ N} = -18.9 \text{ pN}$ (attractive).
- The effective spring constant or stiffness is defined by

$$k = |(dF/dr)_{r_e}| = d^2w/dr^2 = 42A/r^8 - 156B/r^{14}$$
 at $r = r_e = (2B/A)^{1/6}$, giving

$$k = |42A(2B/A)^{-4/3} - 156B(2B/A)^{-7/3}| = 18(A^7B^{-4}/2)^{1/3} = 14.3 \text{ N m}^{-1}$$
.
- The best conventional laboratory balance can measure down to $0.1 \mu\text{g}$ (about 10^{-9} N). To measure weaker forces, one needs specialized techniques. The *Atomic Force Microscope* (AFM) can measure forces down to 1 pN (see Section 12.8), while forces as small as 10^{-15} N (1 fN) can now be measured between molecules or small colloidal particles in solution using various optical techniques (see Chapter 12).

¹³ Proposed by Lennard-Jones in 1924 after quantum theory had shown that the attractive exponent in the Mie potential is 6. The inverse 12 exponent was chosen for mathematical convenience, it being shown that any number within 14 ± 5 gave equally good agreement with the experimental data available at the time.

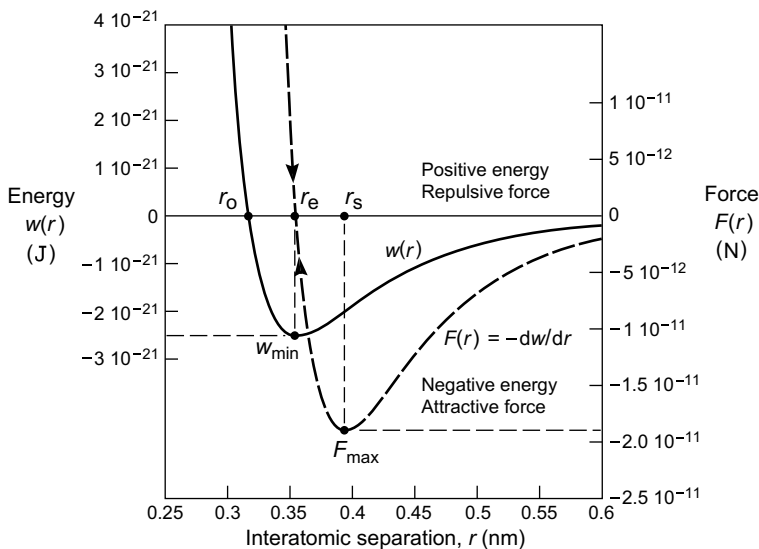


FIGURE 1.4 Typical van der Waals interaction energy (or potential) function $w(r)$ and force function $F(r)$ between two atoms, which are related by $F(r) = -dw/dr$. The separation r_e is the equilibrium separation, where the force is zero and the energy is a minimum, and r_s is the point at which the two atoms or particles separate spontaneously from r_s when pulled apart by a force F_{\max} (the “adhesion” or “pull-off” force). The plotted curves are for a Lennard-Jones potential, Eq. (1.7), with parameters $A = 10^{-77} \text{ J m}^6$ and $B = 10^{-134} \text{ J m}^{12}$ (see Worked Example 1.2).

1.8 First Estimates of Molecular Sizes

At a meeting of the Royal Society of London in 1774, Benjamin Franklin (1706–1790) reported on his interesting observation at Clapham pond on which he had dropped a teaspoonful of olive oil. As the oil spread on the water surface, it “stilled the waves”—a phenomenon that was already known to ancient seafarers. Franklin noticed that this smoothing effect extended a quarter of an acre and no more. It is remarkable that neither he nor anyone in his illustrious audience thought of dividing the volume ($\sim 1 \text{ cm}^3$) by the area ($\sim 1000 \text{ m}^2$) to get a dimension ($\sim 1 \text{ nm}$) for the size of the surface layer and hence of the molecules. This division was done by Lord Rayleigh, but not until 1890—more than one hundred years later!

The first successful attempt to estimate the size of molecules was made in 1815 by Thomas Young (1773–1829), who realized that the surface tension γ (in units of J m^{-2} or N m^{-1}) and the cohesive energy or latent heat of a material U (in units of J m^{-3} or N m^{-2}) were related via the range of the intermolecular forces and/or the molecular size. In terms of the notation used here, $U \approx 6\rho w(\sigma) \approx 6w(\sigma)/(4\pi r^3/3)$ (Section 2.2) and $\gamma \approx 3w(\sigma)/2(\pi r^2)$ (Section 13.13), so that we obtain

$$r \approx 3\gamma/U. \quad (1.8)$$

The latent heat of water is 40.7 kJ per mole (see Table 2.1), and one mole of water occupies 18 cm^3 or $18 \times 10^{-6} \text{ m}^3$, from which one can estimate U to be $(40.7 \times 10^3) \times (10^6/18.0) =$

$2.3 \times 10^9 \text{ J m}^{-3}$. Thus, for water Young obtained $r \approx 3 \times 0.070 / 2.3 \times 10^9 = 0.09 \text{ nm} \approx 1 \text{ \AA}$, which is remarkably close to the radius of a water molecule. Unfortunately, Young published his calculation in an obscure article and under a pseudonym (see F.O., 1815), and it was ignored.

The first calculations in the framework of the new kinetic theory were carried out during the second half of the nineteenth century, much along the lines of Young, by van der Waals, Waterson, Hodges, and, in his first paper, by Einstein (see Rowlinson (2002) for details).

1.9 The Twentieth Century: Understanding Simple Systems

By the beginning of the last century, our subject had reached the end of its first scientific phase, coinciding (not unexpectedly) with the end of the classical era of physics and chemistry. But a number of important conceptual changes had also occurred. The period that had started with Newton and ended with van der Waals, Boltzmann, Maxwell, and Gibbs saw the abandonment of the purely mechanistic view of intermolecular forces and the adoption of thermodynamic and probabilistic concepts such as free energy and entropy. It was now appreciated that heat is also a form of energy but different from mechanical energy and not due to some substance or intermolecular potential—for example, that the pressure of an ideal gas does not arise from any particular repulsive intermolecular potential between the molecules; indeed, it arises even when there is no interaction between the molecules and even for molecules of arbitrarily small size.

Accompanying these conceptual developments, it became apparent that there is a big gap between knowing the pair potential or force law between any two molecules and understanding how an ensemble of such molecules will behave. For example, the mere knowledge that air molecules attract one another does not mean that they will condense into a liquid or a solid at any given temperature or pressure. Even today, there is no ready recipe for deriving the properties of condensed phases from the intermolecular pair potentials, and vice versa.

Only with the elucidation of the electronic structure of atoms and molecules and the development of the quantum theory in the 1920s was it possible to understand the origin of intermolecular forces and to derive expressions for their interaction potentials (Margenau and Kestner, 1971; Stone, 1996). It was soon established that all intermolecular forces are essentially electrostatic in origin. This is encapsulated in the *Hellman-Feynman theorem*, which states that once the spatial distribution of the electron clouds has been determined by solving the Schrödinger equation, the intermolecular forces may be calculated on the basis of straightforward classical electrostatics. This theorem greatly simplified notions of the nature of intermolecular forces.¹⁴

¹⁴Later we shall encounter a very useful analogous theorem—the “contact value theorem”—which gives the force between two surfaces once the density distribution of molecules, ions, or particles in the space between them is known.

Thus, for two charges, we have the familiar inverse-square Coulomb force, while for moving charges we have electromagnetic forces, and for the complex fluctuating charge distributions occurring in and around atoms, we obtain the various interatomic and intermolecular bonding forces familiar to physics, chemistry, and biology.

This seems marvelously simple. Unfortunately, exact solutions of the Schrödinger equation are not easy to come by. In fact, it is even too difficult to solve (exactly) something as simple as two hydrogen atoms, let alone two water molecules, interacting in a vacuum. For this reason, it has been found useful to classify intermolecular interactions into a number of seemingly different categories, even though they all have the same fundamental origin.¹⁵ Thus, such commonly encountered terms as ionic bonds, metallic bonds, van der Waals forces, hydrophobic interactions, hydrogen bonding and solvation forces are a result of this classification, often accompanied by further divisions into strong and weak interactions and short-range and long-range forces. Such distinctions can be very useful, but they can also lead to confusion—for example, when the same interaction is “counted twice” or when two normally distinct interactions are strongly coupled.

1.10 Recent Trends

Today, as more and more information and interest is accumulating on microscopic, mesoscopic, and nanoscopic (molecular-scale) systems and processes, there is a natural desire to understand and control these phenomena by manipulating the operative forces. Until recently there were three main areas of activity. The first was largely devoted to the forces acting between simple atoms and molecules in gases, where various quantum mechanical and statistical mechanical calculations are able to account for many of their *physical* properties (Hirschfelder et al., 1954). The second area was concerned with the *chemical* bonding of ions, atoms, and molecules in solids (Pauling, 1960),¹⁶ while the third dealt with the longer-ranged interactions between surfaces and small “colloidal” particles suspended in liquids (Verwey and Overbeek, 1948; Hunter, 2001; Evans and Wennerström, 1999)—an area that is traditionally referred to as *colloid science*.

More recently the scope of endeavor has broadened to include liquid structure, surface and thin film phenomena; “complex fluids” (structured multicomponent systems); “soft matter”; “self-assembling” nano- and meso-systems; “quantum dots”; smart, responsive, and adaptable materials; and the interactions of biological and biomimetic molecules and structures, all of which are considered in this book. Not only are static (equilibrium, time-independent) systems and interactions being investigated but increasingly also dynamic (nonequilibrium, time-evolving) systems.

As was mentioned above, there are no ready theoretical recipes for deriving the *equilibrium* (static) properties of condensed phases from the intermolecular pair potentials (and vice versa). The situation is even more complex for *nonequilibrium*

¹⁵Most physicists believe that at least two of the four fundamental forces of nature are likewise related.

¹⁶Linus Pauling's book *The Nature of the Chemical Bond* is the most highly cited science book of all time.

(dynamic) processes that are rate- and/or time-dependent and that give rise to such phenomena as transport phenomena, adhesion hysteresis, friction, and irreversible wear. Recent theoretical trends have therefore focused on obtaining semirigorous equations that are nevertheless adequate for treating multimolecular and multicomponent systems, but even then one may need to resort to a computer to analyze such complex systems. Indeed, it is now not uncommon for a Monte Carlo or Molecular Dynamics computer simulation (Chapter 2) to result in a totally new equation that accurately describes, and can make predictions on, a particularly complex system or dynamic process. In the past, equations were obtained either from observation (experiment) or derived analytically or from other equations. To some, the insights gained by “computer experiments” do not carry the same intellectual satisfaction as a traditional scientific discovery or breakthrough, but they have become the main and often only reliable tool for analyzing highly complex processes.

The subject has become so broad that a tendency has developed for different disciplines to adopt their own concepts and terminology,¹⁷ to emphasize quite different aspects of interactions that are essentially the same, or even make “discoveries” that are well known in other fields. For example, in chemistry and biology, emphasis is placed almost entirely on the *short-range* force fields around atoms and molecules, rarely extending more than one or two atomic distances. The language of the present-day molecular biologist is full of terms such as *molecular packing*, *specific binding sites*, *lock and key mechanisms*, and *docking*, all of which are essentially short range. In the different though closely related area of colloid science, the emphasis is quite often on the *long-range* forces, which may determine whether two surfaces or particles are able to get close enough in the first place before they can interact via the types of short-range forces mentioned above. In this discipline one is more likely to hear about electric double-layer forces, van der Waals forces, steric polymer interactions, and so forth—all of which are essentially long ranged.

But this situation is also changing: pressured by the sheer complexity and all-embracing nature of our subject, the barriers between certain areas of physics, chemistry, biology, and engineering are rapidly disappearing, with a “return” to a state where science, engineering, and mathematics are no longer regarded as independent disciplines (see Problem 1.7).

PROBLEMS AND DISCUSSION TOPICS

1.1 Consider the following dialog.

Aristotle: Now, Plato, let us lay the foundations of the physics of motion. We agree that the motion of any natural body is caused by its need for fulfillment?

¹⁷Even the words *force* and *interaction* have become ambiguous. In this book I use *force* when specifically referring to a force (a vector, having magnitude in units of N and direction), while *interaction* covers all the effects that two bodies may have on each other, including the torques, induced shape-changes, molecular rearrangements, and the forces between them.

Plato: Yes, my dear Aristotle.

Aristotle: And that each body is naturally carried to its appropriate place, which may be up or down?

Galileo: But by what impetus is this movement accomplished?

Aristotle: Ah, let me complete the theory, Simplisticus. Every body experiences a natural impulse commensurate with its virtue of weight or lightness. So two bodies which differ from one another owing to excess of weight or of lightness, but are alike in other respects, move faster over an equal distance akin to the ratio which their magnitudes bear to one another.

Galileo: I see. Actually, my name is Galileo. So a heavier body falls faster than a lighter body?

Aristotle: Of course. That is the obvious conclusion.

Galileo: But then if a heavy body falls faster than a light body, I infer from your theory that an even heavier body falls more slowly!

Aristotle: How is that?

Galileo: For if I join the two bodies together by a string, the lighter will slow down the heavier, while the heavier will speed up the lighter. They will therefore fall at a rate intermediate between the two bodies falling alone. But since I tied them together, the two bodies have been turned into a single mass which is heavier than either. So surely it should fall faster than either body. We are therefore faced with a paradox.

It appears to me that the only way to resolve this paradox is to conclude that all bodies must fall at the same rate.

Aristotle: Your paradox is indeed intriguing.

Galileo: How about we do an experiment with two balls to test it?

Aristotle: Eh?

Question: Is either of them right? If you think Galileo is right, explain how he could arrive at the correct answer when none of the postulates are based on any experimental observation.¹⁸ [This problem furnishes a good example of Rothchild's Rule: "*For every phenomenon, however complex, someone will eventually come up with a simple and elegant theory. This theory will be wrong.*" For further reading on early ideas on gravitation, see Aristotle's *Physics*, Book IV; Galileo Galilei, *Discorsi e dimostrazioni matematiche, intorno à due nuove scienze*, Leyden, Elzevirs, The Netherlands (1638); Jammer (1957), and Hesse (1961).]

1.2 (i) Starting from Eq. (1.2), derive the expression for the gravitational pressure P_0 at the center of a liquid sphere of radius R and uniform mass density ρ , and

(ii) estimate the radius R of a water sphere for which $P_0 = 1$ atm. [Ans. (i)

$$P_0 = \frac{2\pi}{3}G\rho^2R^2. \text{ (ii) } R = 27 \text{ km.}]$$

¹⁸Galileo (1564–1642) and Francis Bacon (1561–1626) are usually credited with introducing the novel idea of doing experiments to test theories and discover the wonders of nature. However, it was not until 1675 that experiments were first introduced into university courses—at the University of Leiden, where Galileo's book was published. The first PhD degrees for original research rather than teaching were not awarded until early in the 19th century, in Germany.

- 1.3** Consider the universe as composed of particles, stars, and galaxies distributed randomly but uniformly within a spherical region of space of average mass density ρ and radius R . The particles interact via the inverse square gravitational force-law given by Eq. (1.2). One particle of mass m is at a finite distance r from the center. What is the force acting on this particle when (i) $r \gg R$, (ii) $r \ll R$, and (iii) $R = \infty$ (infinite universe)? What are the implications of your results for the effect of faraway particles on neighboring particles when all interact via an inverse square force? [For a related phenomenon involving light, find out about *Olbers' Paradox*.]
- 1.4** Two atoms interact via a Lennard-Jones potential, Eq. (1.7), with interaction constants $A = 10^{-77} \text{ J m}^6$ and $B = 10^{-134} \text{ J m}^{12}$ (as in the Worked Example 1.2). Consider two such atoms in contact—that is, sitting in their potential energy minimum at a mean separation r_e from each other, when they start being pulled apart by a constant externally applied force of $F_0 = 10 \text{ pN}$.

Plot the *net* force $F(r)$ and energy $w(r)$ experienced by each atom as a function of the interatomic separation, r . Explain how each plot predicts the same new equilibrium separation, r_e . Determine this new value, and calculate the ratio of r_e to the equilibrium spacing at $F = 0$ —that is, under no external force.

By trial and error, graphically determine what force will just cause the two atoms to fly apart to infinity. Again plot the net force and energy functions, $F(r)$ and $w(r)$, for this case, and briefly explain how each determines the adhesion or pull-off force F_0 and the “metastable” separation, $r_e = r_s$, just before the two atoms fly apart. From your graph, determine the pull-off force and the ratio of r_s to the equilibrium spacing r_e at $F = 0$ (give your results with your measuring error) and compare both values to the theoretical values.

Your results are strictly valid only at zero temperature ($T = 0 \text{ K} = -273^\circ\text{C}$). Discuss qualitatively whether and how your answers will be different *in practice*—in other words, in a genuine laboratory experiment carried out at room temperature and over a finite time.

[*Suggestion:* Choose your axes carefully so that you use the maximum space for displaying the essential features of your plots (suggested range for r : 0.25 to 0.60 nm). In practice, due to thermal effects such as Brownian motion, your answer will depend on the time the force is applied, as discussed in Chapters 9 and 22.]

- 1.5** This problem is similar to Problem 1.4 except that the externally applied force comes from a spring (force proportional to spring deflection or displacement) rather than remaining constant (independent of spring displacement or position). Consider the approach of two atoms where, as illustrated in Figure 1.5, the lower is part of a solid surface and the other is at the end of a fine tip that is slowly brought down vertically. We may model this system as if the top atom is suspended from the end of a spring of effective stiffness K . If $K = 0.1 \text{ N/m}$, calculate the value of r at which an instability occurs and the tip “jumps” into

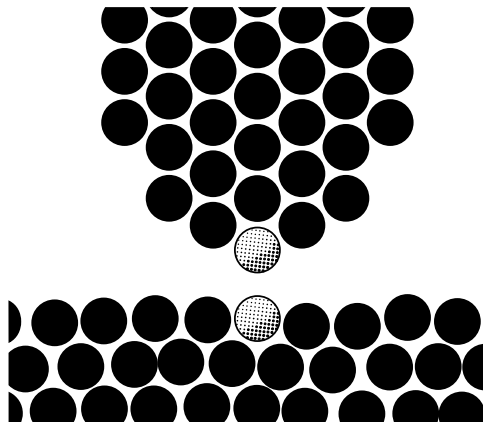


FIGURE 1.5 Idealized geometry of nano-tip near a substrate surface in an Atomic Force Microscope (AFM) experiment.

contact with the surface. Will another instability—and an outward “jump”—occur when the surfaces are separated? In reality, will the top atom or the whole tip tend to move sideways during the approach and separation process? Assume that the atoms interact with the same Lennard-Jones potential as in Problem 1.4 or Worked Example 1.2.

[*Hint:* As in the case of Problem 1.4, to understand this problem fully, it is instructive to be able to solve it graphically as well as numerically. First, plot the force $F(r)$ against r . Next, find at what point (or points) on the curve the slope is $+0.1 \text{ N/m}$. Draw a line through the point that has this slope, and find where it cuts the curve again at another point. If you think about it, these two points on the line give the start and end points of a “jump.” Alternatively, this problem can also be solved by considering the full energy-distance plots.]

[*Answer to numerical part:* There is an instability and an inward jump from $r = 0.48 \text{ nm}$ and another instability and an outward jump on separation from $r = 0.41 \text{ nm}$. From your graphical solution you should also find the end points of these two jumps. Such mechanical instabilities occur when measuring intermolecular forces using an atomic force microscope or the forces between macroscopic surfaces using a surface forces apparatus, both of which are described in Chapter 12. They are also important in determining the displacements of atoms from their equilibrium lattice positions when two *incommensurate* crystal lattices are in contact.]

- 1.6 Do the following “kitchen sink” experiment: On a dry day, turn on a tap and let water run out of it slowly in a thin but continuous filament as in Figure 1.3(b). Comb your hair with a plastic (nonconducting) comb and watch your hair “stand on end”, i.e., watch your hairs repel one another with a long-range force. Now hold the comb horizontally and bring it toward the running water filament near the exit

of the tap and watch the water stream bend toward the comb, i.e., observe the *attractive* long-ranged force. Does this force decay with time or only after the comb is allowed to touch the water? Does the material of the comb, what it is rubbed against, or the humidity of the air have any affect on the results of either experiment? What is going on? How can you further test your hypothesis? [By the end of Chapter 5, you should be able to fully answer this phenomenon.]

- 1.7** Many believe that technological advances stem from basic scientific research, which leads to new discoveries, followed by their development into new products and technologies. Others claim that the reverse process is true: that the “products” come first—a result of trial and error—followed by their slow but steady improvement over the centuries, and that only much later does science come in, first to explain what is going on and only later to improve the product further. Make an in-depth historical inquiry into the practical and scientific development of an object whose utility is based on its strength or adhesion, changing the forces between its constituent molecules or particles, or the forces that it is used to generate. Possible examples could include glue, cement, latex paint, the height of buildings, glass, boomerangs, processed food, and medicines.

Thermodynamic and Statistical Aspects of Intermolecular Forces

2.1 The Interaction of Molecules in Free Space and in a Medium

While this book is not primarily concerned with thermodynamics or statistical mechanics, it is nevertheless appropriate to begin by considering some fundamental thermodynamic and statistical principles without which a mere knowledge of interaction forces will not always be very meaningful. In this chapter we shall introduce a number of simple but important thermodynamic relations and then illustrate how these, when taken together with the strengths of intermolecular forces, determine the properties of a system of many molecules. Analyses of more complex “self-assembling” structures are considered in Part III.

At the most basic molecular level we have the interaction potential $w(r)$ between *two* molecules or particles. This is usually known as the *pair potential* or, especially when an interaction takes place in a solvent medium, the *potential of mean force*. The interaction potential $w(r)$ is related to the force between two molecules or particles by $F = -dw(r)/dr$. Since the derivative of $w(r)$ with respect to distance r gives the force, and thus the maximum work that can be done by the force, $w(r)$ is often referred to as the *free energy* or *available energy*.

In considering the forces between two molecules or particles in liquids, several effects are involved that do not arise when the interaction occurs in free space. This is because an interaction in a medium always involves many solvent molecules—that is, it is essentially a *many-body interaction*. Some of these effects are illustrated in Figure 2.1 and will now be described.

1. For two solute molecules in a solvent, their pair potential $w(r)$ includes not only the direct solute-solute interaction energy but also any changes in the solute-solvent and solvent-solvent interaction energies as the two solute molecules approach each other. A dissolved solute molecule can approach another only by displacing solvent molecules from its path (Figure 2.1a). The net force therefore also depends on the attraction between the solute molecules and the solvent molecules. Thus, while two molecules may attract each other in free space, they may repel each other in a medium if the work that must be done to displace the solvent exceeds that gained by the approaching solute molecules.

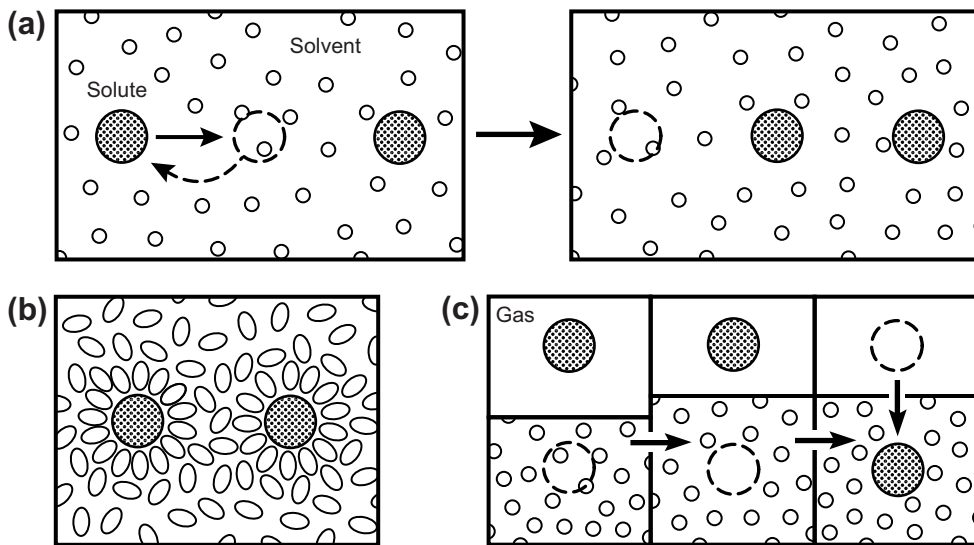


FIGURE 2.1 Some solvent effects involved in the interactions of dissolved solute molecules or particles. (a) Displacement of solvent by two approaching solute molecules. (b) Solvation (reordering) of solvent molecules by solute. (c) Cavity formation by solvent prior to solute insertion.

2. Solute molecules often perturb the local ordering or “structure” of solvent molecules (Figure 2.1b). If the free energy associated with this perturbation varies with the distance between the two dissolved molecules, it produces an additional “solvation” or “structural” force between them.
3. Solute-solvent interactions can change the properties of dissolved molecules, such as their dipole moment and charge (degree of ionization). The properties of dissolved molecules may therefore be different in different media.
4. Finally, when an individual molecule is introduced into a condensed medium, we must not forget the cavity energy expended by the medium when it forms the cavity to accommodate the guest molecule (Figure 2.1c). Since the formation of a cavity requires solvent molecules to be separated from one another, we see that the energetics of introducing a solute into a solvent also involves the solvent-solvent interactions.

These effects are obviously interrelated and are collectively referred to as *solvent effects* or *medium effects*. They manifest themselves to different degrees, depending on the nature and strength of solute-solute, solute-solvent, and solvent-solvent interactions. In later chapters we shall investigate the various functional forms of $w(r)$ for different types of forces and examine how solvent effects influence intermolecular and interparticle interaction potentials. In this chapter, we shall address ourselves to the thermodynamic implications arising from the existence of interaction potentials without, at this stage, inquiring as to their origins.

2.2 Self-Energy and Pair Potential

When an individual molecule is in a medium (gas or liquid), it has what may be called a “cohesive energy” or “self-energy,” μ^i , associated with it. This is given by the sum of its interactions with all the surrounding molecules, which includes any change in the energy of the solvent brought about by the presence of the solute molecule. In many cases one needs to know the value of μ^i , which refers to an *isolated* molecule in a medium rather than its pair potential $w(r)$ with another individual molecule. How are μ^i and $w(r)$ related? Let us first consider a molecule in the gas phase where $w(r)$ is usually a simple power law of the form

$$\begin{aligned} w(r) &= -C/r^n && \text{for } r \geq \sigma \quad (\text{where } n > 3), \\ &= \infty && \text{for } r < \sigma, \end{aligned} \quad (2.1)$$

where σ is the so-called *hard sphere diameter* of the molecules. We may now calculate μ^i by summing all the pair potentials $w(r)$ over all of space (as was done in Section 1.6) and obtain

$$\mu_{\text{gas}}^i = \int_{\sigma}^{\infty} w(r) \rho 4\pi r^2 dr = -4\pi C\rho / (n-3)\sigma^{n-3}. \quad (2.2)$$

This result will be used later for deriving the van der Waals equation of state.

When a molecule is introduced from vapor into a condensed phase such as a liquid or a solid, μ^i must also include the cavity energy (see Figure 2.1c). For example, in a liquid or solid composed of spherical molecules, each molecule can have up to 12 other molecules in contact with it (known as *close-packing*). If a molecule is introduced into its own liquid medium, then 12 liquid molecules must first separate from one another to form the hole. This costs $-6w(\sigma)$ in breaking the 6 “bonds” holding the 12 molecules together, where $w(\sigma)$ is the pair potential of two molecules in contact at $r = \sigma$ —that is, when their centers are separated by twice their radii, which equals their diameter, σ . $w(\sigma)$ is generally referred to as the “bond energy”.

On introducing the guest molecule, 12 new bonds are formed costing $+12w(\sigma)$. The net energy change is therefore

$$\mu_{\text{liq}}^i \approx 6w(\sigma) \quad (2.3)$$

which is *half* the total interaction energy of the molecule with its 12 nearest neighbors. Thus, the molar cohesive energy of a simple liquid (or solid) may be expected to be

$$U = -N_0 \mu_{\text{liq}}^i \approx -6N_0 w(\sigma) \quad (2.4)$$

It is interesting that a derivation similar to Eq. (2.2) also predicts a similar value for U : in a pure liquid (or solid) the number density of molecules ρ would be equal to

$$\rho = 1/(\text{molecular volume}) = 1/[(4\pi/3)(\sigma/2)^3] \quad (2.5)$$

where $\sigma/2$ is the molecular radius, and so we find that

$$\mu_{\text{gas}}^i = \frac{1}{2} \int_{\sigma}^{\infty} w(r) \rho 4\pi r^2 dr = \frac{-12C}{(n-3)\sigma^n} \approx \frac{12}{(n-3)} w(\sigma) \quad (2.6)$$

which for the van der Waals interaction where $n = 6$ (Chapter 6), gives

$$\mu_{\text{liq}}^{\text{i}} \approx 4w(\sigma) \quad \text{or} \quad U \approx -4N_0 w(\sigma). \quad (2.7)$$

As a rule of thumb, we may therefore expect that the cohesive energy of a molecule in a pure liquid or solid will be somewhere between four and six times the pair energy—the higher value being applicable to simple spherical molecules that condense into close-packed structures.

An *accurate* calculation of a molecule's free energy μ^{i} in a liquid from the pair potential $w(r)$ is extremely difficult. The mean number of molecules surrounding any particular molecule is not known in advance. It can be as high as 12 (for simple spherical molecules such as the noble gases) and as low as 4 (for water). Further, the density ρ of neighboring molecules is not uniform locally, but rather it depends on the distance r from the reference molecule (cf. Figure 2.1b). Thus, ρ in Eq. (2.2) should really be a function of r —that is, $\rho(r)$. This is known as the *density distribution function*, which can be measured (see Chapters 7 and 15) but can only be approximately determined *a priori*.

For a *solute* molecule dissolved in a (different) *solvent* or *medium*—that is, when it is surrounded by different molecules—the calculation of its free energy in the medium becomes even more difficult. Again, if we consider the simplest case of a solute molecule (s) surrounded by 12 solvent molecules (m) of similar size, then the change in cohesive energy on transferring the solute molecule from free space into the medium will be

$$\mu_{\text{liq}}^{\text{i}} \approx -[6w_{\text{mm}}(\sigma) - 12w_{\text{sm}}(\sigma)] \quad (2.8)$$

because 6 solvent pairs (mm) must first be separated before the solute molecule can enter the medium and interact with the 12 solvent molecules (sm). Note that if the solvent and solute molecules are the same, then $w_{\text{mm}}(\sigma) = w_{\text{sm}}(\sigma)$, and Eq. (2.8) reduces to the earlier result, $\mu^{\text{i}} \approx 6w_{\text{mm}}(\sigma)$, as expected. Modern theoretical techniques for studying such complex many-body interactions are described in Sections 2.8 and 2.9.

Finally, it is important to note that the effective pair potential between two dissolved solute molecules in a medium is just the change in the sum of their self-energies μ^{i} as they approach each other.

2.3 The Boltzmann Distribution and the Chemical Potential

If the molecular interaction energy of a particular type of molecule or particle has different values μ_1^{i} and μ_2^{i} in two regions of a system (e.g., a liquid in equilibrium with its vapor, or two coexisting phases), then at equilibrium the concentrations X_1 and X_2 of these molecules in the two regions are given by the well-known *Boltzmann distribution*

$$X_1 = X_2 \exp [-(\mu_1^{\text{i}} - \mu_2^{\text{i}})/kT] \quad (2.9)$$

which may also be written as

$$\mu_1^i + kT \log X_1 = \mu_2^i + kT \log X_2 \quad (2.10)$$

where log means \log_e or \ln . Strictly, Eqs. (2.9) and (2.10) are exact only when molecules mix ideally in both regions—that is, for a dilute system.

If there are many different regions (phases or states) in a system, each with different energies μ_n^i , but at the same temperature and pressure, then the condition of equilibrium is simply an extension of Eq. (2.10) to all the phases—that is,

$$\mu_n^i + kT \log X_n = \text{constant} = \mu, \quad \text{for all states } n = 1, 2, 3, \dots \quad (2.11)$$

Thus, there will be a flow of molecules between all the different states of the system until Eq. (2.11) is satisfied, that is, equilibrium is reached when the value of $\mu_n^i + kT \log X_n$ is uniform throughout. The quantity μ is known as the *chemical potential*, and it gives the total free energy per molecule; it includes the interaction energy as well as the contribution associated with its thermal energy. The $k \log X_n$ factor gives the (ideal) entropy of confining the molecules and is known by a variety of names: the ideal gas entropy, the configurational entropy, the entropy of confinement, the ideal solution entropy, the translational entropy, the entropy of dilution, and the entropy of mixing. The dimensionless concentrations X_n are usually expressed as mole fractions or volume fractions. For a pure solid or liquid, $X_1 = 1$, so that $\log X_1 = 0$.

2.4 The Distribution of Molecules and Particles in Systems at Equilibrium

The requirement of equality of the chemical potentials, as expressed by Eq. (2.11), provides a very general and useful starting point for formulating conditions of equilibrium within a molecular framework and may be applied to both simple and complex multicomponent systems—for example, electrolyte solutions, discussed in Part II, and “self-assembling” molecular structures such as surfactant micelles and lipid bilayers, discussed in Part III. In this chapter we shall consider some simpler cases.

Suppose we wish to calculate how the number density ρ of molecules in the earth’s atmosphere varies with altitude z . If we only consider gravitational forces, we may write

$$\mu_z^i + kT \log \rho_z = \mu_0^i + kT \log \rho_0$$

so that

$$\rho_z = \rho_0 \exp[-(\mu_z^i - \mu_0^i)/kT]. \quad (2.12)$$

Since $(\mu_z^i - \mu_0^i) = mgz$, where m is the molecular mass and g the gravitational acceleration, we immediately obtain the gravitational or barometric distribution law:

$$\rho_z = \rho_0 \exp(-mgz/kT) \quad (2.13)$$

which gives the density at height z in terms of the density at ground level ρ_0 .

Similarly, for charged molecules or ions, each carrying a charge e , if ψ_1 and ψ_2 are the electric potentials (in units of volts) in two regions of a system, then $(\mu_2^i - \mu_1^i) = e(\psi_2 - \psi_1) = e\Delta\psi$, and we obtain

$$\rho_2 = \rho_1 \exp[-e(\psi_2 - \psi_1)/kT] = \rho_1 \exp(-e\Delta\psi/kT) \quad (2.14)$$

which is known as the *Nernst equation*.

Worked Example 2.1

Question: At what height is the density of the earth's atmosphere half of the value at sea level? Assume $T = 25^\circ\text{C}$.

Answer: Using Eq. (2.13), we may write

$$\frac{\rho_z}{\rho_0} = \frac{1}{2} = \exp\left(-\frac{mgz}{kT}\right) = \exp\left(\frac{-1.67 \times 10^{-27} \times 28 \times 9.8 \times z}{1.38 \times 10^{-23} \times 298}\right) = \exp(-2.1 \times 10^{-4}z)$$

so that $z = -\log_e(0.5)/1.1 \times 10^{-4} = 6.2 \times 10^3 \text{ m} = 6 \text{ km}$.

Units check for mgz/kT (See Table of Fundamental Constants and pages xxvi–xxvii): $\text{kg}(\text{m s}^{-2})\text{m}/(\text{J K}^{-1})\text{K} \rightarrow (\text{J s}^2\text{m}^{-2})\text{m}^2\text{s}^{-2}/\text{J} \rightarrow 1$ (dimensionless, as required). ✓

Worked Example 2.2

Question: For what potential difference $\Delta\psi$ between two regions of space will their charge density (ionic concentration) differ by a factor of 2?

Answer: Using Eq. (2.14), we may write

$$\frac{\rho_2}{\rho_1} = 2 = \exp\left(-\frac{e\Delta\psi}{kT}\right) = \exp\left(\frac{+1.60 \times 10^{-19} \times \Delta\psi}{1.38 \times 10^{-23} \times 298}\right) = \exp(38.9 \Delta\psi)$$

so that $\Delta\psi = (\psi_2 - \psi_1) = \log_e(2)/38.9 = 1.78 \times 10^{-2} \text{ V} = 17.8 \text{ mV}$.

Units check for $e\Delta\psi/kT$ (See Table of Fundamental Constants and pages xxvi–xxvii): $\text{C V}/(\text{J K}^{-1})\text{K} \rightarrow \text{C}(\text{J C}^{-1})/\text{J} \rightarrow 1$. ✓

Note that for $\Delta\psi = -17.8 \text{ mV}$, $\rho_2/\rho_1 = 0.5$, which is still a factor of 2. The complete answer is therefore $\Delta\psi = \pm 17.8 \text{ mV}$.

In Worked Examples 2.1 and 2.2, the interactions energies did not arise from local intermolecular forces but from forces imposed by externally applied gravitational or electric fields. Let us now consider a two-phase system where $\mu_1^i - \mu_2^i$ is the difference in energy due to the different intermolecular interactions in the two phases. If one of the phases ($n = 1$) is a pure solid or liquid ($X_1 = 1$ so that $\log X_1 = 0$), we have

$$\mu_1^i = \mu_2^i + kT \log X_2,$$

thus,

$$X_2 = X_1 \exp[-(\mu_2^i - \mu_1^i)/kT] = 1 \times \exp(-\Delta\mu^i/kT). \quad (2.15)$$

Here, for example, μ_2^i could be the energy of molecules in solution relative to their energy in the solid, μ_1^i , when X_2 is their *solubility*.

Worked Example 2.3

Question: Consider two immiscible liquids such as water and oil. If a spherical oil molecule of radius r is taken out of the oil phase and placed in the water phase, the unfavorable energy of this transfer is proportional to the area of the solute (oil) molecule newly exposed to the solvent (water) multiplied by the *interfacial energy*, γ_i , of the oil-water interface (see Chapter 17). The interfacial energy of the bulk cyclohexane–water interface is $\gamma_i = 50 \text{ mJ m}^{-2}$, and the radius of a cyclohexane molecule is 0.28 nm. Estimate the solubility of cyclohexane in water at 25°C in units of mol dm⁻³ (mole/liter or M) and comment on your result.

Answer: $\Delta\mu^i/kT = 4\pi r^2 \gamma_i/kT = 4 \times 3.142 \times (0.28 \times 10^{-9})^2 \times (50 \times 10^{-3})/4.12 \times 10^{-21} = 12.0$. Thus, $X_2/X_1 = e^{-12} = 6 \times 10^{-6}$ in mole fraction units. Since this is very small, phase 2 is almost pure water (55.5 mole/liter), and we may assume phase 1 to be almost pure cyclohexane so that $X_1 \approx 1$. Thus, the solubility of cyclohexane in water is calculated to be $X_2 \approx 55.5 \times 6 \times 10^{-6} = 3.4 \times 10^{-4} \text{ M}$. The literature value is $7 \times 10^{-4} \text{ M}$ —about twice the calculated value. Note, however, that if the transfer energy $\Delta\mu^i$ were only 6% less—that is, $\Delta\mu^i/kT = 11.3$ instead of 12.0—the correct value would have been obtained. Thus, if this problem had been posed in reverse—that is, if we had been given the solubility and asked to estimate the molecular radius—our result would have differed from the correct value by only 3% (instead of differing by 50%). This example shows that macroscopic models often work surprisingly well at the molecular level, but it depends on what one is calculating. Thus, molecular sizes can usually be accurately estimated from experimental values (e.g., of solubility) using macroscopic or continuum models, as this example shows. In contrast, theoretical interaction *energies* have to be calculated very accurately if they are to predict measurable quantities, such as solubility, with reasonable accuracy.

In each of the above three examples, it was assumed that only one type of interaction contributes to the chemical potential. More generally, if the two regions or phases are composed of different chemical species, are at different heights, Δz , and have a potential difference of $\Delta\psi$ volts between them, then if the three interactions are independent of one another, their energies will be *additive*, and the distribution equation for the solute molecules or particles becomes

$$X_2 = X_1 \exp[-(\Delta\mu^i + mg\Delta z + e\Delta\psi)/kT]. \quad (2.16)$$

Many interactions, however, are not additive, especially in a (solvent) medium: the presence of a third body often affects that between two bodies, or different types of interactions are not independent of each other but coupled in some way—for example, van der Waals and structural forces (Chapters 6 and 7).

2.5 The Van der Waals Equation of State (EOS)

We proceed with a consideration of the role of intermolecular interactions in determining Equations of State, starting with an analysis of a vapor in equilibrium with liquid. If the gas molecules interact through an attractive pair potential $w(r) = -C/r^n$, Eq. (2.2) may be expressed as

$$\mu_2^i = \mu_{\text{gas}}^i = -4\pi C\rho/(n-3)\sigma^{n-3} = -A\rho, \quad (2.17)$$

where $A = 4\pi C/(n-3)\sigma^{n-3} = \text{constant}$. For molecules of finite size, we may also write

$$X_2 = 1/(v - B) = \rho/(1 - B\rho) \quad (2.18)$$

for the effective density of the nonideal gas molecules, where v is the (measured) gaseous volume occupied per molecule and $B = 4\pi\sigma^3/3$ is the excluded volume, since σ is the closest distance that one molecule can approach another. We therefore have for the chemical potential of a gas:¹

$$\mu = -A\rho + kT \log[\rho/(1 - B\rho)]. \quad (2.19)$$

Now the pressure P is related to μ via the well-known thermodynamic relation

$$(\partial\mu/\partial P)_T = v = 1/\rho \quad \text{or} \quad (\partial P/\partial\rho)_T = \rho(\partial\mu/\partial\rho)_T \quad (2.20)$$

Thus, we find

$$P = \int_0^\rho \rho \left(\frac{\partial\mu}{\partial\rho} \right)_T d\rho = \int_0^\rho \left[-A\rho + \frac{kT}{(1-B\rho)} \right] d\rho = -\frac{1}{2}A\rho^2 - \frac{kT}{B} \log(1 - B\rho),$$

and for $B\rho < 1$, we can expand the \log_e term as

$$\log(1 - B\rho) = -B\rho - \frac{1}{2}(B\rho)^2 + \dots \approx -B\rho \left(1 + \frac{1}{2}B\rho \right) \approx -B\rho / \left(1 - \frac{1}{2}B\rho \right) \approx -B / \left(v - \frac{1}{2}B \right),$$

so that

$$P = -\frac{\frac{1}{2}A}{v^2} + \frac{kT}{(v - \frac{1}{2}B)} \quad \text{or} \quad (P + a/v^2)(v - b) = kT, \quad (2.21)$$

which is the van der Waals equation of state in terms of the molecular parameters

$$a = \frac{1}{2}A = 2\pi C/(n-3)\sigma^{n-3} \quad \text{and} \quad b = \frac{1}{2}B = \frac{2}{3}\pi\sigma^3. \quad (2.22)$$

Note that b depends only on the molecular size, σ , and thus on the stabilizing repulsive contribution to the total pair-potential. Thus, conceptually, the constants a and b can be

¹The complete expression for the chemical potential also includes additional purely temperature-dependent terms. One of these is the translational kinetic energy $\frac{3}{2}kT$ per molecule. Since the kinetic energy depends only on T , this term does not contribute to the pressure, since it drops out of the derivation of the van der Waals equation when we calculate $(\partial\mu/\partial\rho)_T$ in Eq. (2.20). Another purely temperature-dependent term is $kT \log \lambda_T^3$, where $\lambda_T = (h^2/2\pi mkT)^{1/2}$ is known as the *de Broglie wavelength* or *thermal wavelength*, and where m is the molecular weight of the particles or molecules. λ_T^3 has units of volume, which ensures that the density $\lambda_T^3\rho$ is dimensionless. Boltzmann statistics apply whenever $\lambda_T^3\rho \ll 1$, which holds for all atoms and molecules at STP. This is also known as the classical limit (see footnote 3).

thought of as accounting for the attractive and repulsive forces between the molecules. In Chapters 6 and 7, we shall see how a and b can be related to other properties of molecules. The van der Waals equation is neither rigorous nor exact but merely one of many equations that have been found useful for describing the properties of gases (PVT data) and gas-liquid phase transitions.

The parameters of the van der Waals EOS contain only one length parameter σ , which disguises an important relationship between the size of the interacting molecules or particles and the range of the forces (or the volume encompassed by the interaction). To see this, let us consider a square-well potential of width Δ , depth w_0 , with the hard wall at the molecular diameter, $r = \sigma$. This potential can therefore be defined as

$$\left. \begin{aligned} w(r) &= \infty && \text{for } r < \sigma \\ w(r) &= -w_0 && \text{for } \sigma \leq r \leq (\sigma + \Delta) \\ \text{and} \quad w(r) &= 0 && \text{for } r > (\sigma + \Delta). \end{aligned} \right\} \quad (2.23)$$

Proceeding now in the same way as above, we find that $a = \frac{2}{3}\pi w_0[(\sigma + \Delta)^3 - \sigma^3] \propto w_0 \times \text{interaction volume}$, which may be compared with the value of a in the VDW EOS, $a = 2\pi C/(n-3)\sigma^{n-3} = -C/\sigma^n \times 2\pi\sigma^3/(3-n) \propto w_0 \times \text{molecular volume}/(n-3)$. Thus, while the excluded volume term, b , is unchanged, the interaction term of the square-well potential depends on the *interaction volume* rather than the *molecular volume*. To appreciate the implications of this, consider molecules of the same size σ and binding energy w_0 , but with one set having a much shorter-range interaction Δ . This will reduce their magnitude of a , and in the limit of $\Delta \ll \sigma$ the EOS approaches $P = kT/(V - b)$, and the critical point disappears. Such systems exhibit no gas-liquid transition—that is, no liquid phase. They include small particles and many-atom molecules such as C_{60} . The phase behavior of macromolecules and colloidal particles is discussed further in Chapters 6, 7, and 11.

2.6 The Criterion of the Thermal Energy kT for Gauging the Strength of an Interaction

As we have seen, the fundamental significance of the thermal energy kT has to do with the partitioning of molecules among the different energy levels of a system. The magnitude of kT is also often used as a rough indicator of the strength of an interaction, the idea being that if the interaction energy exceeds kT , it will “win out” over the opposing, randomizing, or disorganizing effect of thermal motion. However, molecular motion or disorder can appear in various ways—for example, as translational or positional disorder or as orientational disorder, and it is important to recognize how it manifests itself.

Let us first consider how strong the intermolecular attraction must be if it is to condense molecules into a liquid at a particular temperature and pressure. This amounts to finding the relation between the interaction (or cohesive) energy and the boiling point.

Now, at standard atmospheric temperature and pressure (STP, where $T = 273\text{ K}$, $P = 1\text{ atm}$) one mole of gas occupies a volume of $\sim 22,400\text{ cm}^3$, while in the condensed state a typical value would be about 20 cm^3 . Equating chemical potentials for gas and liquid molecules in equilibrium with each other gives

$$\mu_{\text{gas}}^{\text{i}} + kT \log X_{\text{gas}} = \mu_{\text{liq}}^{\text{i}} + kT \log X_{\text{liq}}, \quad (2.24)$$

and since the magnitude of $\mu_{\text{liq}}^{\text{i}}$ greatly exceeds $\mu_{\text{gas}}^{\text{i}}$, we may write

$$\mu_{\text{gas}}^{\text{i}} - \mu_{\text{liq}}^{\text{i}} \approx -\mu_{\text{liq}}^{\text{i}} \approx kT \log(X_{\text{liq}}/X_{\text{gas}}) \approx kT \log(22,400/20) \approx 7kT. \quad (2.25a)$$

If the gas obeys the gas law $PV \approx RT$, then at any other temperature the log term becomes $\log(22,400 \times T/20 \times 273)$. It is straightforward to verify that the log term is not very sensitive to temperature and that in the range $T = 100$ to 500 K , the log term changes by only 13%. Over this range of temperature we therefore find

$$-\mu_{\text{liq}}^{\text{i}} \approx 7kT_B \quad \text{or} \quad -N_0\mu_{\text{liq}}^{\text{i}}/T_B \approx 7N_0k = 7R, \quad (2.25b)$$

where T_B is the boiling temperature. This is an important result. First, it shows that the boiling point of a liquid is simply proportional to the energy needed to take a molecule from liquid into vapor. For one mole of molecules, the energy of vaporization U_{vap} is given by Eq. (2.25b) as $U_{\text{vap}} = -N_0\mu_{\text{liq}}^{\text{i}}$, while the enthalpy or latent heat of vaporization, L_{vap} , is related to U_{vap} by

$$L_{\text{vap}} = H_{\text{vap}} = U_{\text{vap}} + PV \approx U_{\text{vap}} + RT_B. \quad (2.26)$$

Thus, the above equations predict

$$L_{\text{vap}}/T_B \approx (U_{\text{vap}}/T_B) + R \approx 7R + R = 8R \approx 70\text{ J K}^{-1}\text{ mol}^{-1}. \quad (2.27)$$

We have derived, very crudely, the well-known empirical relationship, known as *Trouton's rule*, which states that the latent heat of vaporization is related to the normal boiling point of a liquid (at 1 atm) by

$$L_{\text{vap}}/T_B \approx \text{constant} \approx 80\text{ J K}^{-1}\text{ mol}^{-1}, \quad (2.28)$$

which corresponds to a cohesive energy $\mu_{\text{liq}}^{\text{i}}$ of about $9kT$ per molecule or $\frac{3}{2}kT$ per bond.

Conversely, and more intuitively, one may say that at a given temperature T a gas will condense into a liquid at a pressure P or gas density ρ_{gas} when the product of ρ_{gas} (which is small) with $e^{-\mu_{\text{liq}}^{\text{i}}/kT}$ (which is large) reaches that of the condensed liquid or solid phase—that is,

$$\rho_{\text{gas}} \exp(-\mu_{\text{liq}}^{\text{i}}/kT) \approx \rho_{\text{liq}}. \quad (2.29)$$

Trouton's rule, Eq. (2.28), applies to a great variety of substances, as illustrated in Table 2.1, and it shows that the boiling point of a substance provides a reasonably accurate indication of the strength of the cohesive forces or energies holding molecules together in condensed phases. For solids, L_{vap} and T_B are replaced by the heat of sublimation and the sublimation temperature, respectively.

Table 2.1 Boiling Points T_B and Latent Heats of Vaporization L_{vap} of Some Common Substances

Substance		T_B at 1 atm (K)	L_{vap} (kJ mol $^{-1}$)	L_{vap}/T_B ^a (J K $^{-1}$ mol $^{-1}$)
Neon	Ne	27	1.8	65
Nitrogen	N ₂	77	5.6	72
Argon	Ar	88	6.5	74
Oxygen	O ₂	90	6.8	76
Methane	CH ₄	112	8.2	73
Hydrogen chloride	HCl	118	16.2	86
Ammonia	NH ₃	140	23.4	97
Hydrogen fluoride	HF	293	32.6	111
Ethanol	C ₂ H ₅ OH	352	39.4	112
Benzene	C ₆ H ₆	353	20.8	87
Water	H ₂ O	373	40.7	109
Acetic acid	CH ₃ COOH	391	24.2	62
Iodine	I ₂	456	41.7	91
Sodium	Na (metal)	1156	91.2	79
Lithium	Li (metal)	1645	129	78

^aFor most “normal” substances, L_{vap}/T_B falls in the range of 75 to 90 J K $^{-1}$ mol $^{-1}$ (Trouton’s rule). Higher values can usually be traced to cooperative association of molecules in the liquid (e.g., HF, NH₃, C₂H₅OH, and H₂O), while lower values to association—for example, dimerization—in the vapor, as occurs for CH₃COOH (see Figure 8.2d).

Equation (2.28) also tells us that molecules will condense once their cohesive energy μ^i with all the other molecules in the condensed phase exceeds about $9kT$. Since we previously saw (Eq. 2.3) that $\mu^i \approx 6w(\sigma)$, we may further conclude that if the pair interaction energy of two molecules or particles in contact exceeds about $\frac{3}{2}kT$, then it is strong enough to condense them into a liquid or solid (see Table 6.1). It is for this reason that the thermal energy $\sim \frac{3}{2}kT$ can be used as a standard reference for gauging the cohesive strength of an interaction potential, though it is essential to note that this indicator, and Trouton’s rule, are valid only because of the particular value of the atmospheric pressure on the earth’s surface. This pressure determines that a gas molecule will occupy a volume of about 4×10^{-20} cm 3 at or near STP, which is needed for deriving Eqs. (2.25)–(2.27).

It is also worth mentioning that the notion that molecules go into the vapor phase because of the kinetic energy $\frac{3}{2}kT$ they acquire is not correct. Their kinetic energy does not disappear in a liquid or solid; the molecule’s motion is merely restricted to a narrower region of space around a potential-energy minimum. The average translational kinetic energy of a molecule $\frac{3}{2}mv^2$, where v is its mean velocity, is $\frac{3}{2}kT$ irrespective of whether it is in the gas, liquid, or solid state.

So far, the Boltzmann distribution has been used to find the spatial or density distribution of molecules in different regions of a system. The Boltzmann distribution can also be used to determine the *orientational distribution* of molecules. For example, if the pair potential also depends on the mutual orientation of two anisotropic molecules—that

is, if $w(r)$ is also angle-dependent so that it may be written as $w(r, \theta)$ —then the angular distribution of two molecules at a fixed distance r apart will be

$$X(\theta_2) = X(\theta_1)\exp\left\{-\frac{w(r, \theta_2) - w(r, \theta_1)}{kT}\right\}, \quad (2.30)$$

and here again, the factor kT appears as a convenient energy unit, but this time it appears for the strength of orientation-dependent interactions needed to mutually align molecules (e.g., solvent molecules around a dissolved solute molecule, discussed in Chapters 4 and 5). We shall not here consider the very complex energies also associated with the rotational and vibrational states of molecules in solids, liquids, and gases, but more the relationships among the various energies of molecules, and how these relate to their individual and collective properties are discussed further in Section 2.8–2.11.

2.7 Classification of Forces and Pair Potentials

Intermolecular forces can be loosely classified into various categories. One may divide them into categories of “opposites”—in other words, attractive or repulsive, short-ranged or long-ranged, strong or weak, and isotropic or directional. These are important distinctions, but they are also ambiguous and confusing. A force that has the same physical origin may be both short-ranged and long-ranged, or it may be attractive in one solvent and repulsive in another. This way of classification can also result in the same force being “counted twice” in any theoretical analysis. To avoid such pitfalls, it is best to classify forces according to their different physical or chemical origin, although even here we shall see that the forces among large particles or extended surfaces lend themselves to different modes of classification from those occurring between two atoms or molecules; this is because the collective interaction of many molecules, which always includes entropic effects (see below), cannot be easily related to the individual pair potentials.

First, some forces are *purely electrostatic* in origin, arising from the *Coulomb force* between charges. The interactions among charges, ions, permanent dipoles, quadrupoles, and so forth fall into this category. Electrostatic forces include *polarization interactions* that arise from the dipole moments induced in atoms and molecules by the electric fields of nearby charges and permanent dipoles. All electrostatic interactions in a solvent medium involve polarization effects. The electrostatic forces between electro-neutral² molecules or assemblies that are free to mutually orient are generally attractive, and they occur even at zero temperature ($T = 0$ K).

Second, some forces have a purely *entropic* origin. They arise from the collective behavior of molecules at finite temperatures ($T > 0$) and therefore cannot be described in terms of a pair potential or force-law between two molecules. The pressure of an ideal gas, given by

²An electroneutral molecule or particle has an equal number of positive and negative charges. The postulate of charge conservation implies that whenever a body is charged, there must be an equal and opposite charge somewhere else that balances or “neutralizes” this charge. There is a further implicit assumption in physics that the universe is overall electroneutral.

$P = nRT/V$, is an example of a “repulsive” entropic force (P is an *outward* pressure) that has a purely entropic origin for molecules obeying Boltzmann statistics. Other forces that fall into this category are *osmotic forces* and various *thermal fluctuation forces*.

Third, and last, some forces are *quantum mechanical* in nature. Such forces give rise to *covalent* or *chemical bonding* (including van der Waals–dispersion forces, acid-base, and charge-transfer interactions) and to the repulsive *steric forces* that balance the attractive forces at very short distances (due to the Pauli exclusion principle). Quantum systems are characterized by having discrete (quantized) energy levels.³

These three categories should not be considered as rigid: for certain types of forces—for example, van der Waals forces—an unambiguous classification is not possible, while some intermolecular interactions (e.g., magnetic forces—the “electrostatic” forces between moving charges) will rarely be mentioned because for the systems we shall consider they are always very weak.

Falling into the above categories are a number of fairly distinct interactions whose pair potentials in a vacuum are given in Table 2.2.⁴ In the following chapters these will be investigated in turn, and in the process we shall introduce important conceptual aspects of intermolecular forces, especially for interactions occurring in a medium. In a condensed medium, whether liquid or solid, the electrostatic force between two molecules is not always given by simply dividing the vacuum interaction by the medium’s dielectric constant, ϵ . Entropic forces can be very complex, involving many different degrees of motion, and the interactions among large molecules, particles, or surfaces can be very different from the summed pair potentials of Table 2.2.

Fortunately, of the many different interactions listed in Table 2.2, not more than three or four generally arise or dominate in any one situation, and the challenge is to identify these. Only in biological systems (covered in Part III) is it not uncommon for five or more interactions to be operating simultaneously.

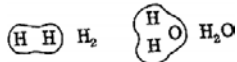
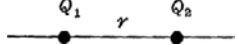
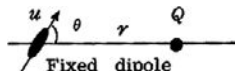
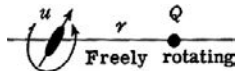
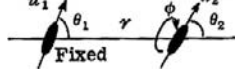
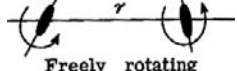
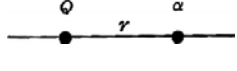
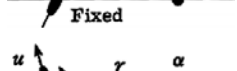
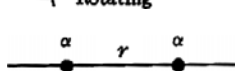
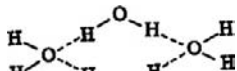
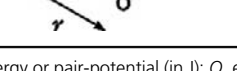
2.8 Theoretical Analyses of Multimolecular Systems: Continuum and Molecular Approaches

One of the greatest difficulties for establishing the pair-potentials in multicomponent multimolecular systems is how to deal with the suspending medium which cannot always be treated as a structureless continuum defined solely in terms of its bulk properties, such

³The energy distribution of any system can be described in terms of Boltzmann statistics such as the continuous Gaussian distribution of a Maxwell-Boltzmann gas, known as the *classical limit*, or in terms of the occupancy of discrete energy states—the approach of *statistical mechanics*. Elementary particles such as electrons and nucleons that have a small mass or are highly confined obey Fermi-Dirac or Bose-Einstein statistics; their energies and other properties are quantized.

⁴Some of the pair potentials contain the temperature, T , and one may ask, What is the temperature of a molecule in a vacuum? The temperature of a molecule is defined by the energy of its internal states—for example, of rotation, vibration, and so on—as determined by its collisions with other molecules (see Section 2.10) or with photons. The latter exist as background radiation at a certain temperature T , even in a vacuum, and equilibrate with the molecules in the system.

Table 2.2 Common Types of Interactions and their Pair-Potentials $w(r)$ between Two Atoms, Ions, or Small Molecules in a Vacuum ($\epsilon = 1$)^a

Type of interaction	Interaction energy $w(r)$
Covalent, metallic	
Charge-charge	 $+Q_1 Q_2 / 4\pi \epsilon_0 r$ (Coulomb energy)
Charge-dipole	 $-Qu \cos \theta / 4\pi \epsilon_0 r^2$
	 $-Q^2 u^2 / 6(4\pi \epsilon_0)^2 k T r^4$
Dipole-dipole	 $-u_1 u_2 [2 \cos \theta_1 \cos \theta_2 - \sin \theta_1 \sin \theta_2 \cos \phi] / 4\pi \epsilon_0 r^3$
	 $-u_1^2 u_2^2 / 3(4\pi \epsilon_0)^2 k T r^6$ (Keesom energy)
Charge-non-polar	 $-Q^2 \alpha / 2(4\pi \epsilon_0)^2 r^4$
Dipole-non-polar	 $-u^2 \alpha (1 + 3 \cos^2 \theta) / 2(4\pi \epsilon_0)^2 r^6$
	 $-u^2 \alpha / (4\pi \epsilon_0)^2 r^6$ (Debye energy)
Two non-polar molecules	 $-\frac{3}{4} \frac{h v \alpha^2}{(4\pi \epsilon_0)^2 r^6}$ (London dispersion energy)
Hydrogen bond	 Complicated, short range, energy roughly proportional to $-1/r^2$

^a $w(r)$ is the interaction free energy or pair-potential (in J); Q , electric charge (C); u , electric dipole moment (C m); α , electric polarizability ($C^2 m^2 J^{-1}$); r , distance between the centers of the interacting atoms or molecules (m); k , Boltzmann constant ($1.381 \times 10^{-23} J K^{-1}$); T , absolute temperature (K); h , Planck's constant ($6.626 \times 10^{-34} J s$); v , electronic absorption (ionization) frequency (s^{-1}); ϵ_0 , dielectric permittivity of free space ($8.854 \times 10^{-12} C^2 J^{-1} m^{-1}$). The force $F(r)$ is obtained by differentiating the energy $w(r)$ with respect to distance r : $F = -dw/dr$. The stabilizing repulsive "Pauli Exclusion" interactions (not shown) usually follow an exponential function $w(r) \propto \exp(-r/r_0)$, but for simplicity they are usually modeled as power laws: $w(r) \propto +1/r^n$ (where $n = 9-12$).

as its bulk density ρ or bulk dielectric constant ϵ . Such "medium effects" or "solvent effects" necessarily involve the simultaneous interactions of many molecules, both solvent and solute, and they become particularly severe when dealing with short-range interactions

that determine, for example, adhesion and bonding forces. There are two basic approaches to this problem. The first is to “work down” from the continuum to the molecular level. In this approach one usually assumes that at least some of the bulk properties of the system—for example, the dielectric constant or density of the solvent or solute—hold right down to molecular dimensions. In the second approach one starts from the interactions occurring at the atomic and molecular levels and then attempts to “build up” the properties of the whole system. This dichotomy of approaches will be a recurring theme in theoretical treatments and modeling of various intermolecular forces.

These two approaches are variously referred to as *continuum* and *molecular* or *atomistic* theories, or combinations of the two. These include *analytical methods* involving integral equations, *mean field theories*, *primitive models*, *finite element analyses*, and so on, and *numerical methods* involving various types of computer simulations. For details of these different theoretical techniques see Chaikin and Lubensky (1995). For more specialized texts on statistical mechanical methods see Hill (1960, 1963, 1964, 2002), Landau and Lifshitz (1980), McQuarrie (2000), Chandler (1987), and Davis (1996). Computer simulations are discussed below.

2.9 Molecular Approaches via Computer Simulations: Monte Carlo (MC) and Molecular Dynamics (MD)

In reality two solute molecules do not see themselves surrounded by a homogeneous liquid medium but rather by discrete molecules of a given size and shape, and, for water, possessing a large quadrupole moment (four concentrations of charge in the molecule). In recent years, much effort has been invested in developing molecular theories of liquids and of solute-solvent, solute-solute, and surface-surface interactions in liquids and, even more recently, in solids such as metals that often require solving quantum mechanical equations. In the molecular approach each molecule is individually modeled in terms of its known structure (including all the interatomic bond lengths, bond angles, atomic radii, charge distributions, etc.). A computer then works out how an “ensemble” of such molecules will behave when they are allowed to interact according to some interaction potential, such as the Lennard-Jones potential, Eq. (1.7), for simple molecules, or more complex potentials for more complex molecules (e.g., water). Such *computer simulations* or *computer experiments* are increasingly providing unique insights into the properties of different systems at the molecular level.

The two most popular types of computer simulations are the *Monte Carlo* (MC) and *Molecular Dynamics* (MD) techniques (Allen and Tildesley, 1987; Leach, 2001; Frenkel and Smit, 2002). In the MC technique a number of molecules (or ions or particles) are confined in a box or cell. One molecule, chosen at random, is then moved to a different position, also chosen at random (hence “Monte Carlo”). The computer then determines whether to accept or reject this move, depending on

whether the total energy of the system has decreased or increased. This process is repeated many times until there is no further change in the energy and other computed properties of the system, at which point the system is deemed to have reached thermodynamic equilibrium.

In the MD technique the computer first calculates the force on each molecule arising from all the other molecules and then, by solving Newton's equations of motion, determines how the molecule moves in response to this force. This computation is done simultaneously and continuously for all the molecules in the box, from which their trajectories can be followed in space and time. A Molecular Dynamics simulation always gives the same final result as an MC simulation for the equilibrium state of a system, but MD requires more calculations than MC. On the other hand, an MD simulation is usually more revealing because it provides information on how molecules actually move (hence molecular "dynamics"). Thus, with MD one can also study time-dependent phenomena, nonequilibrium effects, fluid flow, and other transport phenomena, which cannot be done easily with MC.

In a classical MD simulation the equations of motion of a set of N particles interacting through a prescribed pair- or many-atom potentials and subject to appropriate boundary conditions are solved on a computer. A typical simulation of this kind may involve up to 10 million atoms or molecules, and the potentials may be physical (Lennard-Jones or Coulombic) or chemical (quantum mechanical). In the latter case the computer solves Schrödinger's equation for the electronic degrees of freedom, concomitantly with Newton's equations for the nuclear degrees of freedom, to predict chemical interactions such as bond making and breaking. Such "first-principles" simulations are much more time consuming and are typically limited to several hundred atoms.

A typical MD simulation consisting of 10^4 to 10^6 atoms on a parallel computer takes about 10^{-2} to 1 second (or 10^{-6} s per atom in 2009) to compute all the interaction forces and to advance each atom by one move or time step. Each move or "timestep" corresponds to 0.01 \AA in distance and $\sim 10^{-15}\text{ s}$ (1 fs) of "real" time. In order for atoms to move 10 \AA (1 nm) in distance, a simulation needs to run several hundred to several thousand steps. To simulate 1000 time steps for a 10,000 atom system therefore takes $1000 \times 10,000 \times 10^{-6}\text{ s} \approx 10\text{ s}$ of computer time. Yet, this simulates only 1 ps of real time—the time of a single bond vibration. Thus, for a system of 10,000 atoms, to simulate molecular rotations ($\sim 1\text{ ns}$ of real time) takes $\sim 10^4\text{ s}$; to simulate slow molecular reorientations of polymers or the collision of two colloidal particles ($\sim 1\text{ \mu s}$ of real time) takes approximately 100 days, while 1 s of real time would currently require 300,000 years using a single processor. Large simulations often involve 10^9 atoms using hundreds of "parallel processors" to simulate several ns of real time.

Nevertheless, a properly executed computer simulation, whether MC or MD, is regarded as providing the *exact* solution to any well-defined problem, and all other (analytic) theories stand or fall depending on how well their predictions can be supported

by computer simulation. Of course, the *correctness* of the results depends on using the correct interaction potentials in the first place, a matter that can only be established by comparison with real (as opposed to computer) experiments.

Computer simulations provide the most powerful theoretical tools available today for studying an almost endless variety of interesting phenomena, ranging from the way NaCl ionizes in water to the interactions of polymers and proteins, to dynamic phenomena such as friction, material failure mechanisms, and (biological) cell-surface interactions. And they can even be used to derive new equations by simply sampling the whole parameter space of a system and then fitting the “results” to an algebraic equation, just as one would do in a laboratory experiment.

2.10 Newton's Laws Applied to Two-Body Collisions

As mentioned above, in a typical molecular (or particle) dynamics computer simulation, the equilibrium state of a system is computed by simply solving Newton's equations of motion based on the forces acting on each molecule due to its net interaction with all the other molecules. Does this mean that all the complexities and subtleties of a complex thermodynamic system, including its temperature, entropy, the Boltzmann distribution, the distinction between its “total” and “free” energies, and its continuous and discrete energies, are all contained in Newton's three simple laws? For nonquantum systems the answer is “Yes”—in fact, they are already contained in two of the three laws, as will now be demonstrated.

Figure 2.2 shows two colliding spherical molecules of different masses m and M moving with velocities v_0 and V_0 before the collision and v_1 and V_1 after the collision. For simplicity we shall assume that all motion takes place in the same direction,

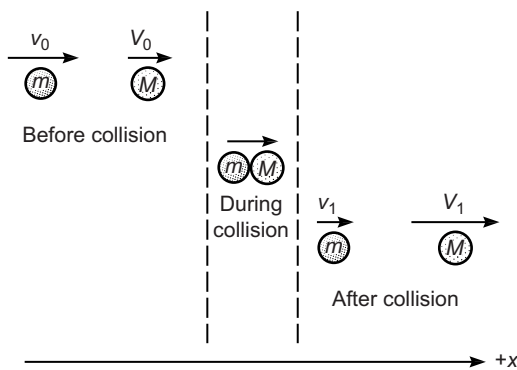


FIGURE 2.2 Two colliding molecules. In general, the velocities before and after the collision can be positive or negative. The situation during the collision can be very complex and depends on the intermolecular pair potential (cf. Worked Examples 2.4 and 2.5, and Figure 2.3).

parallel to the x -axis. The collision itself involves the molecules interacting with their specific pair potential, but here we shall restrict ourselves to a consideration of what properties of the system can be understood without requiring a detailed knowledge of the pair potential. We start by asking how the velocities v_1 and V_1 after the collision are related to those before the collision, v_0 and V_0 , which—thanks to Newton's laws—leads us to the principle of the conservation of (kinetic) energy. Thus, using the second law—force (F) = mass (m) \times acceleration (dv/dt , d^2x/dt^2 or \ddot{x})—we may write for the change in energy ΔE during a collision that takes the first mass m from position x_0 to x_1 , and its velocity from v_0 to v_1 :

$$\Delta E_m = E_1 - E_0 = \int_{E_0}^{E_1} dE = \int_{x_0}^{x_1} F dx = \int_{x_0}^{x_1} m \frac{dv}{dt} dx = m \int_{v_0}^{v_1} \frac{dx}{dt} dv = m \int_{v_0}^{v_1} v dv = \frac{1}{2} m(v_1^2 - v_0^2), \quad (2.31)$$

where $E = \frac{1}{2}mv^2$ is the *translational kinetic energy* of a moving mass m traveling at velocity v .

Now, applying Newton's third law—"For every action there is an equal and opposite reaction"—we may write a similar equation for the second mass M , where the value of F at any time is equal to $-F$. This force acts only during the collision—that is, when both molecules move through the same distance $x_2 - x_1$, so that we may write for the second mass:

$$\Delta E_M = - \int_{x_0}^{x_1} F dx = -\Delta E_m = -M \int_{x_0}^{x_1} \frac{dV}{dt} dx = -\frac{1}{2} M(V_1^2 - V_0^2). \quad (2.32)$$

the worked example below shows that $\Delta E_{\text{tot}} = \Delta E_m + \Delta E_M = 0$ —that is, the total kinetic energy is conserved during a collision *independently of the nature of the pair potential*. However, as the Worked Example 2.5 shows, additional, "internal" pair potentials do affect the above results; these can arise from the vibrational and rotational energies of the covalently bound atoms that make up the molecules.

Before we proceed, we can derive another important relation that describes the principle of conservation of *momentum* that, for a molecule of mass m moving at velocity v , is defined by mv . One can derive this conservation law by looking at the above collision from a moving frame of reference traveling at a constant velocity V relative to the original (rest) frame. Adding or subtracting V from each of the velocities in Eqs. (2.31) and (2.32), and assuming that the total energy is also conserved in a moving frame, we immediately obtain the desired result: $m(v_1 - v_0) + M(V_1 - V_0) = 0$.

The principles of the conservation of energy and momentum between two colliding molecules or particles (see Figure 2.2) are independent of their pair potentials and may be written in the below suitable forms:

$$\frac{1}{2}mv_0^2 + \frac{1}{2}MV_0^2 = \frac{1}{2}mv_1^2 + \frac{1}{2}MV_1^2 \quad \text{and} \quad \frac{mv_0 + MV_0}{\substack{\text{Momentum before} \\ \text{collision}}} = \frac{mv_1 + MV_1}{\substack{\text{Momentum after} \\ \text{collision}}} \quad (2.33)$$

Energy before collision Energy after collision

Worked Example 2.4

Question: The interaction potential for two identical particles each of mass m has a maximum value (energy barrier) of magnitude W at some finite separation. One particle approaches another, initially stationary, particle at velocity v . What is the minimum velocity v at which the particles will just touch, i.e., come into contact?

Answer: One's first inclination is to simply equate the kinetic energy of the moving particle $\frac{1}{2}mv^2$ with W —that is, $v = \sqrt{2W/m}$. This would be correct if the stationary particle remained stationary—for example, if it had infinite mass. But since its mass is finite and the same as that of the approaching particle, it will start to move as soon as the approaching particle enters its force field. At the point when the particles “just touch,” they must be moving at the same velocity V that, due to the principle of conservation of momentum, must be given by $2mV = mv$ —that is, $V = \frac{1}{2}v$, and at this point we may write: $\frac{1}{2}mv^2 = W + \frac{1}{2}(2m)V^2 = W + \frac{1}{4}mv^2$. Thus, $\frac{1}{4}mv^2 = W$, and so $v = \sqrt{4W/m}$ is the correct answer. A simpler way of solving this type of problem is to look at it from the symmetrical center of mass reference frame, which moves at velocity $\frac{1}{2}v$ relative to the stationary “laboratory” frame. In this frame each particle is approaching the other at the same velocity $\frac{1}{2}v$, one from the left and the other from the right, so that their *relative* velocity is still v . When the particles touch, $v = 0$ for each particle, so we have $\frac{1}{2}m(\frac{1}{2}v)^2 + \frac{1}{2}m(\frac{1}{2}v)^2 = W$, which gives the same result.

However, such apparently simple interactions can be very much more subtle when considered in fine detail, as Worked Example 2.5 shows.

Worked Example 2.5

Question: A molecule or small particle of mass m traveling at velocity v approaches a similar, stationary molecule of equal mass. What are the resulting motions of the two molecules? Assume that all the motions are along a straight line (in 1D).

Answer: Strictly, this question has no unique answer because of insufficient information. Referring to Figure 2.2 and inserting $m = M$ and $V_0 = 0$ in Eqs. (2.33), we immediately obtain $v_1 = 0$ for the first molecule and $V_1 = v_0$ for the second. In other words, the velocities have been exchanged, and, as in the case of a billiard ball hitting another ball head on, the first molecule comes to rest as the second moves with a velocity exactly equal to the original velocity of the first molecule.⁵

But what if the second molecule is composed of two atoms, as shown in Figure 2.3, each having mass $\frac{1}{2}m$ with the two connected by a string, which can be modeled as a square-well potential? If both atoms are initially stationary ($V'_0 = V''_0 = 0$), then the collision of the first molecule will be with an atom of mass $\frac{1}{2}m$ rather than m . Inserting these values into Eqs. (2.33) now leads to quite different velocities after the first collision: $v_1 = +\frac{1}{3}v_0$ for the first molecule, and $V'_1 = +\frac{4}{3}v_0$ for the first (left) atom of the second molecule. The first molecule therefore continues to move forward at some finite velocity, rather than coming to rest. Meanwhile, the first atom moves forward at four times that velocity until it hits the second atom. At this point,

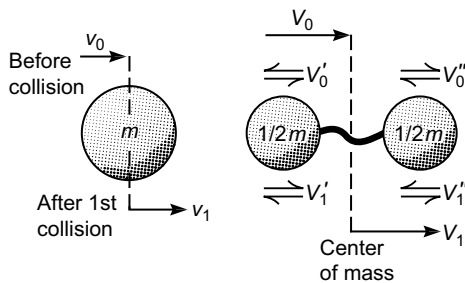


FIGURE 2.3 Molecule colliding with stationary diatomic molecule having the same net mass m . The two atoms of the second molecule interact with a square-well potential, which is analogous to a flexible string that only resists being extended beyond its taught length.

because the masses of the atoms are the same, there will be an exchange of velocities between them, exactly as in the above example: the first atom will come to rest as the second moves forward at velocity $V_1'' = +\frac{4}{3}v_0$. Then, once the string becomes taught, there will be an exchange of velocities once again, and so on.

The final situation is therefore one in which the first molecule moves forward at velocity $\frac{1}{3}v_0$, while the second molecule moves forward with its atoms continually exchanging their velocities between 0 and $\frac{4}{3}v_0$. In other words, the *center of mass* of the second molecule moves at constant velocity $V_1 = \frac{2}{3}v_0$, and when they are viewed from this position, the atoms will be seen to be moving back and forth symmetrically (vibrating) with velocities $\pm\frac{2}{3}v_0$. An overall momentum and energy balance now shows that the momentum of the first molecule has decreased by $m(v_0 - v_1) = m(v_0 - \frac{1}{3}v_0) = \frac{2}{3}mv_0$, while that of the second, as determined from the motion of its *center of mass*, has increased by the same amount, given by mV_1 . As regards the energy, the first molecule has lost $\frac{1}{2}m[v_0^2 - (\frac{1}{3}v_0)^2] = \frac{4}{9}mv_0^2$ (8/9ths its original energy), while the second has gained $\frac{1}{2}m(\frac{2}{3}v_0)^2 = \frac{2}{9}mv_0^2$ in translational energy of its center of mass and $2 \times \frac{1}{2}(\frac{1}{2}m)(\frac{2}{3}v_0)^2 = \frac{2}{9}mv_0^2$ in internal kinetic or vibrational energy of its two atoms (again, with respect to its center of mass). Thus, half of the energy “lost”⁶ or transferred by the first molecule has gone into internal, purely thermal energy and half to translational or purely kinetic energy of the second molecule.

This result is therefore quite different from the first, and it would be different still if the second molecule were composed of more atoms or if its initial state were different—for example, possessing some initial vibrational energy of its own (V_0' , $V_0'' \neq 0$ in Fig. 2.3) or if both molecules possessed internal energy. Such issues, involving the way energy and momentum are transferred or exchanged between interacting molecules and particles, also have important consequences for understanding nonequilibrium (dynamic, irreversible, and energy dissipating)⁶ processes such as friction.

⁵Actually, there is also another, trivial, purely mathematical solution where neither velocities change—the first molecule passes, ghostlike, *through* the second molecule. This solution is unphysical.

⁶Terms such as energy *lost* or *dissipated* can be misleading. By the First Law of Thermodynamics, energy is never lost but is simply transferred to another molecule or converted from mechanical—for example, kinetic—energy into internal energy or heat (see Chapters 9 and 18).

Worked Example 2.6

Question: Consider the back-and-forth 1D motion of a molecule in a chamber and its collisions with the opposite walls to derive an expression relating the mass m and mean velocity v of the molecule to k and T . Use the empirical Equation of State of an Ideal Gas: $PV = RT$, in which there are no intermolecular interactions.

Answer: During a collision of a gas molecule with the wall, its velocity changes from $+v$ to $-v$. The force f that the molecule applies to the wall while it is in “contact” with it can be obtained from Newton’s law $f = m dv/dt = 2mv/\tau$, where τ is the time of the collision. Now, if there are n molecules in the chamber whose sides are of length L , then the total time-averaged pressure on each wall of area L^2 will be given by $P = (\text{total time-averaged force}/L^2) = nf \times (\text{number of times each molecule strikes the wall per second}) \times (\text{the time that the molecule is in contact with the wall per collision})/L^2 = n(2mv/\tau)(v/2L)\tau/L^2 = nmv^2/L^3 = nmv^2/V$, where $V = L^3$ is the volume of the chamber. Thus, $PV = nmv^2$. Equating nmv^2 with $RT = nkT$ per mole of gas gives

$$mv^2 = kT \quad (2.34)$$

which is one of the fundamental equations of kinetic theory.

It is interesting to note in Worked Example 2.6 that in the derivation of the pressure of an ideal gas—that is, one where there are no forces between the molecules (or any collection of molecules or particles at a temperature T)—neither their size nor the “real area of contact” between the gas and the wall enters into the calculation. This is conceptually important, as will become apparent later when we consider other forces acting on surfaces, such as friction forces.

2.11 Kinetic and Statistical Aspects of Multiple Collisions: the Boltzmann Distribution

The principle of the conservation of energy and momentum during collisions can be extended to the multiple collisions of many molecules, as occurs in a gas or condensed phase, to obtain its equilibrium “classical”⁷ thermodynamic properties. As an illustrative example of this, consider a chamber (Figure 2.4) whose wall molecules of mass M are moving along the x-axis at the same velocity $\pm V_0$, which also defines its temperature T_0 according to Eq. (2.34). The chamber is stationary—that is, it has zero net momentum—so that at any time half the molecules are moving to the left at velocity V_0 and half are moving to the right at the same velocity. This type of situation can arise if there is a square-well potential between the wall molecules where the molecules simply bounce back and forth.

⁷That is, excluding quantum mechanical effects.

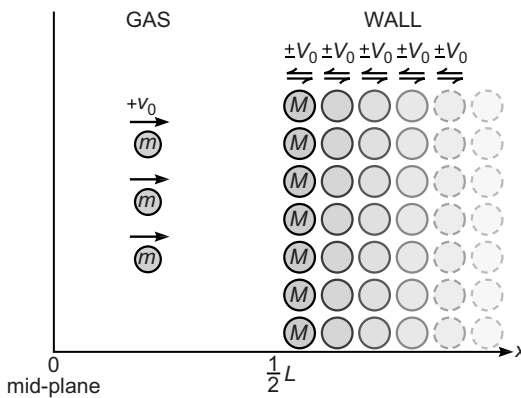


FIGURE 2.4 Gas molecules just prior to their first collision with wall molecules. Only the right half of the chamber is shown; the system is assumed to be symmetric about the mid-plane. After a few back and forth collisions the gas molecules will have the same mean (kinetic) energy as the wall (reservoir) molecules.

Now consider the interior of the chamber, which is empty except for gas molecules of mass m that are initially all located on a plane through the center. At time $t = 0$, let all the molecules have the same velocity v_0 , with half of them moving to the left and half to the right. This ensures that the center of mass of the whole system is not moving even though all of the molecules are—the wall molecules with velocity $\pm V_0$ and the gas molecules with velocity $\pm v_0$. This distinction between overall motion and internal motion is conceptually important for establishing the correct relationships between velocity (and other internal motions) and temperature. Unless stated otherwise, we shall ignore the internal vibrational and rotational motions of the molecules (cf. Worked Example 2.5) and concentrate only on their translational motions in the x direction.

When (half of) the gas molecules, whose velocities are identical and equal to v_0 , reach the wall, they collide with the wall molecules whose velocities are split equally between $+V_0$ and $-V_0$. The rebound velocities of the gas molecules will therefore also be split equally between two values given by solving the simultaneous equations Eqs. (2.33) for $V_0 = \pm V_0$. After a few lines of straightforward algebra, we find that the velocities and kinetic energies of the gas molecules after their first collision with the wall molecules may be written as

$$v_1 = \left(\frac{m - M}{M + m} \right) v_0 \pm \frac{2MV_0}{(M + m)} \quad (2.35)$$

and

$$\frac{1}{2} mv_1^2 = \frac{1}{2} mv_0^2 + \frac{2Mm}{(M + m)^2} \left[(MV_0^2 - mv_0^2) \pm (M - m)V_0 v_0 \right], \quad (2.36)$$

where 50% take the + sign and 50% take the - sign. The *mean* kinetic energy of the rebounding molecules is therefore

$$\begin{aligned}\frac{1}{2}m\bar{v_1^2} &= \frac{1}{2}mv_0^2 + \frac{4Mm}{(M+m)^2} \left(\frac{1}{2}MV_0^2 - \frac{1}{2}mv_0^2 \right) \\ &= \frac{1}{2}MV_0^2 + \left(\frac{m-M}{M+m} \right)^2 \left(\frac{1}{2}mv_0^2 - \frac{1}{2}MV_0^2 \right).\end{aligned}\tag{2.37}$$

Before proceeding further, it is worth noting some important thermodynamic implications of Eq. (2.37). The factor $4Mm/(M + m)^2$ varies between 0 (for $M \gg m$ or $M \ll m$) and 1 (for $M = m$). Thus, the mean energy of the gas molecules $\frac{1}{2}m\bar{v_1^2}$ always gets closer to that of the wall molecules $\frac{1}{2}mV_0^2$, or in other words, the difference in the mean energies of the gas and wall molecules always diminishes after collisions.⁸ The exception is in the limit of highly unequal masses when $4Mm/(M + m)^2 = 0$ and when $\frac{1}{2}m\bar{v_1^2}$ remains unchanged at $\frac{1}{2}mv_0^2$. This is analogous to an elastic ball bouncing off a hard floor. In the case of equal masses, when $M = m$, $\frac{1}{2}m\bar{v_1^2}$ becomes equal to the energy of the wall molecules $\frac{1}{2}mV_0^2$ already after the first collisions. This is analogous to a billiard ball hitting a stationary or slow-moving billiard ball.⁹ We can already see some important thermodynamic implications here whereby the gas molecules are beginning to “thermally” equilibrate with the wall or “reservoir,” and we can also see that this equilibration can be rapid—effectively complete after a few collisions.

We now proceed to see what happens after further collisions of the gas molecules with the two walls, where their velocities after the n^{th} collision is denoted by v_n . We shall assume that the wall behaves as an isothermal heat reservoir or “heat bath”—in other words, that its molecules always rapidly equilibrate to the mean reservoir energy or temperature (by collisions with other wall molecules) after each collision with a gas molecule, so in subsequent collisions with gas molecules the velocity of the wall molecules will always be taken to be $\pm V_0$ with equal probability.¹⁰

After the first collisions of the molecules, their velocities are equally split into two values given by Eq. (2.35), which may be written in the simplified form

$$v_1 = Av_0 \pm BV_0\tag{2.38}$$

⁸The assumption that the wall or reservoir is not moving is crucial here. Before the collisions, the two wall molecules must be moving in opposite directions and have zero net momentum. A low-energy molecule *can* transfer energy to a high-energy molecule during a *single* collision (see Problem 2.6).

⁹... where their velocities are exchanged. For example, after hitting a stationary ball, the first ball comes to rest as the second ball moves ahead at the same velocity. Note that all of these collisions are “elastic” and “energy conserving,” even though the resulting velocities can be very different. An elastic collision clearly does not mean that the colliding mass has to bounce back with its velocity unchanged. In addition, since momentum is conserved, the center of mass of the whole system does not change: the momentums and kinetic energies of the molecules simply redistribute.

¹⁰While the overall energy remains unchanged, there is a transfer or exchange of energy between the gas and wall molecules, given by Eq. (2.37). For example, energy will flow from the gas to the wall if $\frac{1}{2}m\bar{v_1^2} > \frac{1}{2}mV_0^2$.

$$\text{where } A = \left(\frac{m - M}{M + m} \right), \quad B = \frac{2M}{(M + m)} = +\sqrt{\frac{M}{m}(1 - A^2)}. \quad (2.39)$$

As the molecules bounce back and forth between the two walls of the chamber, each subsequent collision n doubles the number of different velocities (energy states), which are related to the previous ones by replacing v_0 and v_1 in Eq. (2.38) by v_{n-1} and v_n . The corresponding velocities after each collision can therefore be expressed in terms of v_0 , V_0 , m , and M as.

$$\begin{aligned} v_1 &= Av_0 \pm BV_0 \\ v_2 &= Av_1 \pm BV_0 = A(Av_0 \pm BV_0) \pm BV_0 = A^2v_0 \pm (1 \pm A)BV_0 \\ v_3 &= Av_2 \pm BV_0 = A(A^2v_0 \pm ABV_0 \pm BV_0) \pm BV_0 = A^3v_0 \pm (1 \pm A \pm A^2)BV_0 \\ &\vdots \\ v_n &= Av_{n-1} \pm BV_0 = A^n v_0 \pm (1 \pm A \pm A^2 \pm A^3 \pm \cdots \pm A^{n-1})BV_0, \end{aligned} \quad (2.40)$$

where after n collisions there are 2^n velocity or energy states having energies $\frac{1}{2}mv_n^2$. Actually, there are twice this number of states if we allow for the initial velocity to be $\pm v_0$ rather than just $+v_0$. The calculation of the *mean* energy $\frac{1}{2}\bar{m}v_n^2$ is simple because when we multiply v_n by itself, each \pm term cancels out with another \pm term. We therefore find¹¹

$$\begin{aligned} \frac{1}{2}\bar{m}v_n^2 &= \frac{1}{2}m \left[A^{2n}v_0^2 + (1 + A^2 + A^4 + A^6 + \cdots + A^{2(n-1)})B^2V_0^2 \right] \\ &= \frac{1}{2}MV_0^2 + A^{2n} \left(\frac{1}{2}mv_0^2 - \frac{1}{2}MV_0^2 \right) = \frac{1}{2}MV_0^2 + \left(\frac{m - M}{M + m} \right)^{2n} \left(\frac{1}{2}mv_0^2 - \frac{1}{2}MV_0^2 \right). \end{aligned} \quad (2.41)$$

Note that for $n = 1$, the above reduces to Eq. (2.37).

Equation (2.41) reveals many interesting and important general features of the kinetic behavior of confined molecules, whether gas, liquid, or solid. These will now be discussed in turn.

First, as $n \rightarrow \infty$, since $A = (m - M)/(M + m) \leq 1$, we have $\frac{1}{2}\bar{m}v_n^2 \rightarrow \frac{1}{2}MV_0^2$. Thus, the mean kinetic energy of the molecules always eventually equilibrates with that of the chamber wall—that is, the reservoir.

Second, the closer together the masses of the gas and wall molecules, the faster the equilibration of the mean energy, which is essentially complete after the first collision when $m = M$, i.e., when $m - M = 0$.

Third, Problem 2.7 asks you to establish that the final distribution or probability $X(E_i)$ of energies $\frac{1}{2}mv_i^2$ about the mean energy $\bar{E} = \frac{1}{2}mV_0^2$ is proportional to $e^{-\Delta E_i/MV_0^2}$. Comparing this with the experimentally measured distribution at temperature T ,

¹¹We use the algebraic relation: $(1 + A^2 + A^4 + A^6 + \cdots + A^{2(n-2)}) = (1 - A^{2n})/(1 - A^2)$, and the relationships between A , B , m , and M given by Eq. (2.39).

$X(\Delta E_i) = e^{-\Delta E_i/kT}$, allows us to relate the mean kinetic energies with the equilibrium temperature T by¹²

$$\frac{1}{2}mv_n^2 = \frac{1}{2}MV_0^2 = \frac{1}{2}kT \quad (2.42)$$

and

$$X(\Delta E_i) \propto e^{-\frac{1}{2}mv_i^2/kT} = e^{-\Delta E_i/kT}, \quad (2.43)$$

which is the Boltzmann distribution¹³ of the gas molecules in 1D after they have reached their equilibrium state. Recalling that at time $t = 0$ all of the gas molecules started off at an arbitrary velocity v_0 , we see that irrespective of the starting conditions, every molecule ends up with a time averaged mean kinetic energy of $\frac{1}{2}kT$ ($\frac{3}{2}kT$ in 3D) and a Boltzmann distribution whose spread is also determined by kT .

The above analysis provides a simple derivation of the Second Law of Thermodynamics:¹⁴ that heat flows from a higher to a lower temperature until, at thermodynamic equilibrium, the temperature is the same everywhere. It also shows that even for molecules that start off at a (discrete) velocity that is already equal to their final (mean) velocity—that is, molecules whose kinetic energy or “temperature” is already equilibrated with the reservoir—the *distribution* of velocities will increase about the initial value until it reaches the Maxwell-Boltzmann distribution. This has important implications for understanding the meaning of entropy at the molecular level. Thus, while the total energy of the gas has not changed, the fact that some molecules now have much higher and some much lower energies than the mean implies that processes or reactions that require a certain “activation energy” can now take place, which could not occur before.

Fourth, one may note that the equilibrium state is a very dynamic one where the molecules are continually changing both their velocities and positions but keeping within

¹²At room temperature the mean velocity of a molecule of molecular weight M is therefore $(1.381 \times 10^{-23} \times 298/M \times 1.673 \times 10^{-27})^{1/2} \approx 1,600/\sqrt{M} \text{ m s}^{-1}$, which is of the order of 1 km/s for molecules of low molecular weight.

¹³Also known as the Maxwell-Boltzmann distribution, the Boltzmann factor, and, mathematically, a Gaussian function.

¹⁴Actually, there are many quite different statements of the Second law involving work, heat, temperature, spontaneity, reversibility, randomness, and/or entropy. The first law, which states the conservation of energy, however, is simple and straightforward. It was stated in 1842 by an unlikely person, one Julius von Mayer, a surgeon, who observed that the blood of people in the tropics was a deeper red, which indicated a lower consumption of oxygen and, therefore, of energy, which he proceeded to generalize to all energy. In 1840, James Joule (1784–1858) measured the mechanical equivalent of heat, although much earlier, in 1798, Benjamin Thompson (also Count Rumford, 1753–1814) carried out friction experiments that disproved the Caloric Theory of heat, thereby sowing the seed for the birth of thermodynamics. Thompson failed to measure the mechanical equivalent of heat, but he succeeded in leading one of the most exciting lives that any scientist could hope for.

a well-defined distribution.¹⁵ This distribution is the same even for a *single* gas molecule as long as it is averaged over a long enough time. In particular, one should not think of the equilibrium *state* as having an equilibrium *structure*: there is no fixed structure or distance between molecules or particles in the equilibrium state; indeed, one can readily establish that in the above example of gas molecules in a chamber their kinetic energies are never repeated (see Problem 2.7). Put differently, the number of occupied states always increases with the number of collisions, or time. There are other interesting thermodynamic and statistical aspects that can be understood based on the above approach, including the implications of time reversal, which are left for discussion (Problem 2.7) and later considerations.

The above four-part analysis has taken us about as far as we can go for obtaining insights into the interactions of molecules and particles that do not interact with each other via some type of pair potential¹⁶ (cf. Worked Example below). It illustrates what a Molecular Dynamics simulation does and shows how complex behavior can arise even from the simplest conservation laws of energy and momentum. It also allows for an entry into many nonequilibrium, “energy dissipating” processes that will be considered in later chapters.



Worked Example 2.7

Question: A molecule interacts with a surface with a Lennard-Jones potential, Eq. (1.7), with interaction constants $A = 10^{-77} \text{ J m}^6$ and $B = 10^{-134} \text{ J m}^{12}$. Consider two such surfaces or walls separated by $D = 1.0 \text{ nm}$. Calculate and plot the potential energy profile and the density distributions of the molecules between the two walls at $T = 300 \text{ K}$ and 22 K . Use suitable scaling (normalization) factors so the three curves are on the same graph. Discuss the likely phase state or states of the molecules at 300 K and 22 K . What additional information do you need to completely solve this problem?

Answer: Assuming that interaction energies are additive scalar quantities, the potential energy $E(x)$ at any point x between the two walls is given by simply adding the two Lennard-Jones potentials of the walls: $E(x) = -\frac{A}{x^6} + \frac{B}{x^{12}} - \frac{A}{(D-x)^6} + \frac{B}{(D-x)^{12}}$. The distribution, $\rho(x)$,

defined by the number density of molecules at x , is given by the Boltzmann factor: $\rho(x) = \rho_0 e^{-E(x)/kT}$, where ρ_0 is a constant determined by the number of molecules N per unit area between the walls such that $\int_{x=0}^{x=D} \rho(x) dx = N$. Inserting the appropriate numbers into the above two equations yields the plots shown in Figure 2.5. Without knowing the number of molecules in the system, we cannot say whether there will be a phase separation between the vapor and surface layers—that is, whether the surface molecules condense into a liquid or solid phase at either temperature.¹⁷ The full analysis would also require

¹⁵Transient local deviations, “rare events”, or *fluctuations* away from the average play very important roles in many, especially biological, systems (Chapter 22).

¹⁶Actually, a “square-well” pair potential was implicitly assumed for the wall molecules, in which the molecules bounce back and forth at velocity V_0 corresponding to a temperature $T = mV_0^2/k$. One may also argue that hard-sphere molecules have been modeled with a repulsive hard-wall potential determined by their size.

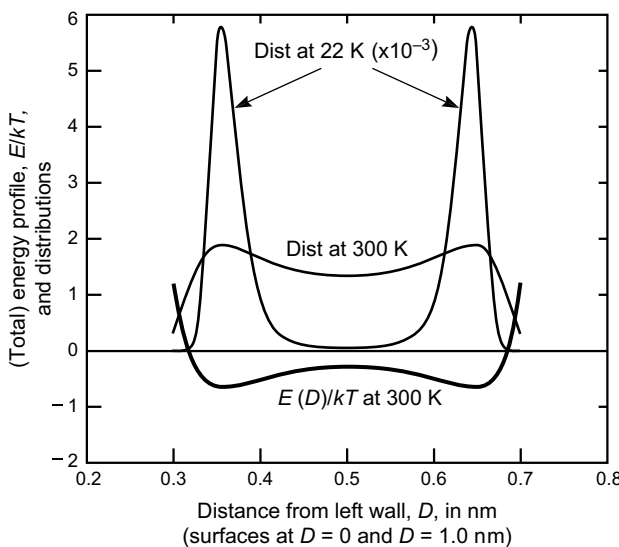


FIGURE 2.5 Energy profile $E(D)$ and density distributions $\rho(D)$, the latter in arbitrary units.

knowledge of the pair potential between the gas molecules, which are here considered to be noninteracting with each other.

¹⁷Because of the short-range nature of the surface forces, any condensed liquid or solid phase condensed at the surface will be molecularly thin. This is in contrast to the bulk liquid phase (e.g., the sea) occurring when long-range gravitational forces “condense” water vapor on the earth’s surface.



PROBLEMS AND DISCUSSION TOPICS

- 2.1** Show that for a mole of gas the van der Waals equation of state, Eq. (2.21), is

$$(P + N_0^2 a/V^2)(V - N_0 b) = RT, \quad (2.44)$$

and clearly explain the difference between the volume of the gas V , the free volume, and the excluded volume.

- 2.2*** For molecules constrained to interact on a surface (as occurs on adsorption and in surface monolayers) there is a “two-dimensional” van der Waals equation of state, analogous to the three-dimensional one (Eq. 2.21). This may be written as

$$(\Pi + a/A^2)(A - b) = kT, \quad (2.45)$$

where Π is the externally applied surface pressure (in units of $N\ m^{-1}$), A the mean area occupied *per molecule*, and a and b are constants. Derive this equation for molecules of diameter σ interacting with a van der Waals-type interaction pair potential given by $w(r) = -C/r^6$. Find the expressions for a and b in terms of C and σ ,

and for C in terms of a and b . [Hint: Two-dimensional systems are an abstraction. All real systems are three-dimensional. It is often best to consider a “two-dimensional system” as a three-dimensional system or film whose thickness is constant but finite and equal to the size of the molecules.]

Under what conditions could a be negative, and what are the implications of this? Can this approach, which predicts the existence of a gas-liquid transition, be extended to one dimension? [Hint: Carefully check the initial assumptions of this approach.]

- 2.3** (i) Why do the attractive forces between the molecules of a gas affect the pressure of the gas on a wall, while the attractive forces between the gas molecules and the wall molecules do not?
- (ii) The 3D pressure P of a gas is analogous to the 2D tension Π or γ of a liquid surface, and both can be treated within the framework of a van der Waals equation of state (cf. Eqs. 2.21 and 2.45). However, the pressure of a gas is trying to *increase* the volume of the gas, while the surface tension is trying to *decrease* the area of the liquid. Resolve this apparent paradox.
- (iii) Why is there no simple rule, such as Trouton’s Rule, relating the latent heat of melting to the melting temperature?
- 2.4** An atom of molecular weight $M = 50$ Da is confined to a solid lattice at 25 °C, where it “sits” in a square well potential (hard walls on both sides) of free width 0.02 nm. What is its vibration or collision frequency? Check with the literature to see whether your answer is reasonable. If it is not, explain why not. [Answer: $v \approx 10^{13} \text{ s}^{-1}$.]
- 2.5** (i) In the language of computer simulations what are *periodic boundary conditions* and what is the meaning of *ergodicity*? How does a Grand Canonical simulation differ from other, simpler simulations?
- (ii) How do the below factors limit the reliability of a simulation: (a) the use of a cell of finite size; (b) the artificial imposition of periodic boundary conditions or symmetry planes; (c) the use of a finite number of molecules or particles; (d) the finite time of a simulation; (e) the need to start the simulation with the particles in some arbitrary configuration; (f) the possibility that the system becomes trapped in a local, rather than global, energy minimum?
- (iii) Consider a colloidal dispersion of particles in a liquid where, due to surface-induced solvent structuring effects, the viscosity of the liquid is much higher near the surface of the particles than in the bulk. Thus, during a Brownian collision, two approaching particles would be slowed down and therefore experience an additional, effectively repulsive, hydrodynamic force. Would this effect modify the equilibrium velocity or spatial distribution of the particles? What other possible effects would an increased viscosity near the surfaces have on any measurable properties of the colloidal dispersion?
- 2.6** Two atoms or molecules having the same mass m collide. (i) One of the masses is initially stationary. Show that after the collision the two molecules move in

directions at 90° to each other. (ii) The two masses move at an angle θ relative to each other and have very different initial velocities V and v , where $V \gg v$. Under what conditions will V increase, in other words, will kinetic energy flow from the less energetic to the more energetic molecule? Does this contradict thermodynamic expectations? [Hint: Both of these problems can be solved geometrically.]

- 2.7*** By analyzing the binomial coefficients of the series given by Eqs. (2.40) and (2.41) for the discrete values of the energies $\frac{1}{2}mv_n^2$ after n collisions of gas molecules with the chamber walls, show (i) that the kinetic energy “states” rapidly approach a Gaussian distribution about a mean value of $\frac{1}{2}MV_0^2 = \frac{1}{2}kT$ and with a standard deviation of $MV_0^2 = kT$, Eqs (2.42) and (2.43); (ii) that the “energy states” remain “discrete” but continually increase in number with time (i.e., with the number of collisions); (iii) that the (mathematically) discrete energy values never repeat themselves; and (iv) that eventually, at any instant, each molecule “occupies” a different energy state—that is, each has a different energy from any of the other molecules. [Suggestion: It is instructive to choose a suitable value for A and plot the different energies after one, two, three, and so on, collisions to see how the Maxwell-Boltzmann distribution, Eq. (4.43), unfolds and then checking how it is more or less established after five or six collisions.]

For discussion: The problem, as posed, is “deterministic.” How realistic is this? What are the consequences of “time reversal”? That is, if the velocities of the gas and wall molecule were suddenly reversed, will a point be reached where all the molecules will have the same velocity and position? If so, does this imply a decrease in the “randomness” and “entropy” of the system, which is not allowed by thermodynamics? [Hint: Carefully consider the effect of time reversal on the velocities of both the gas and wall molecules, and do not confuse equilibrium distributions with transient fluctuations.]

- 2.8*** Consider the two-molecule collision in Figure 2.3 as analyzed in Worked Example 2.5. The solution obtained is independent of the length of the string. However, as the string is made progressively shorter, the two atoms of mass $\frac{1}{2}m$ should eventually behave as one of mass m , which gives a totally different result. Resolve the paradox, and explain what determines whether the diatomic molecule interacts like two independent masses or a single mass.
- 2.9** Does the expression for the pressure $P = \rho kT$ apply to photons (radiation pressure)? Use Wien’s Distribution Law for the density of photons within a frequency band $d\nu$ in free space (“black body”) at a temperature T : $8\pi\nu^2 d\nu/c^3[\exp(h\nu/kT) - 1]$. [Answer: Yes. $P = 8\pi^5 k^4 T^4 / 15c^3 h^3$.]

This page intentionally left blank

Strong Intermolecular Forces: Covalent and Coulomb Interactions

3.1 Covalent or Chemical Bonding Forces

Like two hydrogen atoms and one oxygen atom that combine to form a water molecule, when two or more atoms come together to form a molecule, the forces that tightly bind the atoms together within the molecule are called *covalent forces*, and the interatomic bonds formed are called *covalent* or *chemical bonds*. Closely allied to covalent bonds are metallic bonds. In both cases the bonds are characterized by the sharing of the electrons between the two or more atoms so that the discrete nature of the atoms is lost.

Depending on the position an atom (or element) occupies in the periodic table, it can participate in a certain number of covalent bonds with other atoms. This number, or stoichiometry, is known as the atomic *valency*; for example, it is zero for the inert gases (e.g., argon) that cannot normally form covalent bonds with other atoms—one for hydrogen, two for oxygen, three for nitrogen, and four for carbon and silicon—and thus water H₂O (H—O—H), hexane C₆H₁₂ (H₃C—CH₂—CH₂—CH₂—CH₂—CH₃), and so on. However, atoms can also form double or triple bonds where more than one electron is shared with a neighboring atom, as in carbon dioxide CO₂ (O=C=O) and acetylenic compounds (—CH₂—C≡C—CH₂—). A further characteristic of covalent bonds is their *directionality*; that is, they are directed or oriented at well-defined angles relative to each other. Thus, for multivalent atoms, their covalent bonds determine the way they will coordinate themselves in molecules or in crystalline solids to form an ordered three-dimensional lattice. For example, they determine the way carbon atoms arrange themselves to form the perfectly ordered diamond structure. Rotational freedom is another important property of covalent bonds. Thus, the carbon-carbon single bond allows for rotation about the bond, but double and triple bonds do not.¹ The ability to rotate or not has important consequences for the flexibility and stability of molecular and macromolecular structures such as crystals and proteins.

Covalent forces are of short range—that is, they operate over very short distances of the order of interatomic separations (0.1–0.2 nm). Table 3.1 shows the strength of some

¹This does not mean that all C—C bonds rotate under all conditions. The C—C bonds of saturated straight-chained hydrocarbons (—CH₂—CH₂—CH₂—CH₂—) rotate in the liquid state, as well as in some so-called gel and liquid-crystalline states, but not in the solid crystalline state. In contrast, the C—C bonds of fluorocarbons (—CF₂—CF₂—CF₂—CF₂—) cannot rotate freely due to the bulkiness (steric repulsion) of the fluorine atoms. Such molecules are always rigid and do not melt.

Table 3.1 Strengths of Covalent Bonds^a

Bond Type	Strength (kJ mol ⁻¹)	Bond Type	Strength (kJ mol ⁻¹)
C≡N (HCN)	870	Si—O	370
C=O (HCHO)	690	C—C (C ₂ H ₆)	360
C=C (C ₂ H ₄)	600	C—O (CH ₃ OH)	340
O—H (H ₂ O)	460	N—O (NH ₂ OH)	200
C—H (CH ₄)	430	F—F (F ₂)	150

^aThe strength of a covalent bond can depend on the type of other bonds nearby in the molecule. For example, the C—H bond strength can be as low as 360 kJ mol⁻¹ (in H—CHO) and as high as 500 kJ mol⁻¹ (in H—C≡N). Note that 100 and 1000 kJ mol⁻¹ correspond to 40 and 404 *kT* per bond, respectively, at 298 K.

common covalent bonds. As can be seen, they are mainly in the range 100–300 *kT* per bond (200–800 kJ mol⁻¹), and they tend to decrease in strength with increasing bond length—a characteristic property of most intermolecular interactions.

3.2 Physical and Chemical Bonds

The complex quantum mechanical interactions that give rise to covalent bonding will not be a major concern in this book, which is devoted more to the forces between unbonded *discrete* atoms and molecules. These are usually referred to as *physical forces*, and they give rise to *physical bonds*, in contrast to chemical forces, which give rise to *chemical* or *covalent bonds*.

Covalently bonded atoms make up molecules and crystals² with well-defined structures that cannot normally melt or liquify without totally breaking the bonds. They therefore tend to sublime (vaporize), decompose, or undergo a chemical reaction above some temperature rather than go through the conventional solid → liquid → gas states that are characteristic of physically bonded molecules.

Physical bonds usually lack the specificity, stoichiometry, and strong directionality of covalent bonds. They are therefore the ideal candidates for holding molecules together in liquids, since the molecules can move about and rotate while still remaining “bonded” to one another. Strictly, physical “bonds” should not be considered as bonds at all, for during covalent binding the electron charge distributions of the uniting atoms change completely and merge, whereas during physical binding they are merely perturbed, the atoms remaining as distinct entities. Nevertheless, physical binding forces can be as strong as covalent bonds, and even the weakest is strong enough to hold together all but the smallest atoms and molecules in solids and liquids at STP as well as in colloidal and biological assemblies. These properties, coupled with the long-range nature of physical forces, make them the regulating forces in all phenomena that do not involve chemical reactions.

²The difference between a molecule and a crystal can be a moot one. A diamond is strictly a large single molecule of covalently bonded carbon atoms.

3.3 Coulomb Forces or Charge-Charge Interactions, Gauss's Law

The inverse-square Coulomb force between two charged atoms, or ions, is by far the strongest of the physical forces that we are considering here; it is even stronger than most chemical binding forces.

The electric field E at a distance r away from a charge Q_1 is defined by³

$$E_1 = \frac{Q_1}{4\pi\epsilon_0\epsilon r^2} \text{ V m}^{-1}, \quad (3.1)$$

where ϵ is the *dielectric permittivity* or *constant* of the medium.⁴ This field, when acting on a second charge Q_2 at r , gives rise to a force known as the Coulomb force or Coulomb Law:

$$F(r) = Q_2 E_1 = \frac{Q_1 Q_2}{4\pi\epsilon_0\epsilon r^2} \text{ N.} \quad (3.2)$$

The free energy for the Coulomb interaction between two charges Q_1 and Q_2 is therefore given by

$$\begin{aligned} w(r) &= \int_{\infty}^r -F(r) dr = - \int_{\infty}^r \frac{Q_1 Q_2}{4\pi\epsilon_0\epsilon r^2} dr = + \left[\frac{Q_1 Q_2}{4\pi\epsilon_0\epsilon r} \right]_{\infty}^r \\ &= \frac{Q_1 Q_2}{4\pi\epsilon_0\epsilon r} = \frac{z_1 z_2 e^2}{4\pi\epsilon_0\epsilon r} \text{ J,} \end{aligned} \quad (3.3)$$

where the “reference state” of zero energy is taken to be at $r = \infty$. The expression on the right of Eq. (3.3) is commonly used for ionic interactions in aqueous solutions where the magnitude and sign of each ionic charge is given in terms of the elementary electron charge ($e = 1.602 \times 10^{-19}$ C) multiplied by the ionic valency z . For example, $z = +1$ for monovalent *cations* such as Na^+ ; $z = -1$ for monovalent *anions* such as Cl^- ; $z = +2$ for divalent cations such as Ca^{2+} ; and so on. For like charges, both w and F are positive and the force is repulsive, while for unlike charges they are negative and the force is attractive.

Let us put the strength of the Coulomb interaction into perspective. For two isolated ions (e.g., Na^+ and Cl^-) in contact, r is the sum of the two ionic radii (0.276 nm), and the binding energy is

$$w(r) = \frac{-(1.602 \times 10^{-19})^2}{4\pi(8.854 \times 10^{-12})(0.276 \times 10^{-9})} = -8.4 \times 10^{-19} \text{ J.}$$

In terms of the thermal energy $kT = (1.38 \times 10^{-23})(300) = 4.1 \times 10^{-21}$ J at 300 K, this energy turns out to be of order 200 kT per ion pair in a vacuum—similar to the energies of covalent bonds (see Table 3.1). Only at a separation r greater than about 56 nm will the Coulomb energy fall below kT . The *force* needed to break the ionic

³Since a positive charge gives rise to a positive field, this definition, which is based purely on convention, implies that electric field lines E go from *positive* to *negative* charges.

⁴The dielectric permittivity is a function of the frequency ν and so should strictly be written as $\epsilon(\nu)$. At zero frequency (i.e., under static conditions), it is referred to as the *dielectric constant* and denoted by either $\epsilon(0)$ or simply ϵ .

bond is $F = w(r)/r = 8.4 \times 10^{-19}/0.276 \times 10^{-9} \approx 3 \text{ nN}$, which is also similar to the force needed to break a covalent bond. We have thus established that the Coulomb interaction is very strong and of long range, although much weakened in water and in media of high ϵ . The strong ionic bond means that most ionic compounds are crystalline solids at room temperature. And unlike covalent crystals, the nondirectionality of the ionic bond allows these compounds to melt and become true liquids at some, usually high, temperature at which they form *molten salts* or *ionic liquids*.



Worked Example 3.1

Question: Show (1) that the Coulomb force on a charge q near a flat surface of uniform charge density σ (in unit of charge per unit area or C m^{-2}) is independent of the distance of the charge from the surface, and (2) that the force on a charge q near a sphere containing a net charge Q uniformly distributed on its surface is the same as if all of charge Q were concentrated at the center of the sphere.

Answer: (1) Consider a circular strip of radius r and width dr on the charged surface (Figure 3.1a). Its charge is $2\pi r dr \sigma$. Position the charge q on the x -axis passing through the center of the circle at a distance $x = z$ from the surface. The distance between the charge and the circular strip is therefore $[z^2 + r^2]^{1/2}$. If θ is the angle subtended by the circular strip $\cos \theta = z/[z^2 + r^2]^{1/2}$, and the normal field at any point x is given by integrating the resolved field due to the strip—that is,

$$E_x = \int_{r=0}^{r=\infty} \frac{2\pi r dr \sigma \cos \theta}{4\pi \epsilon_0 [z^2 + r^2]} = \frac{z\sigma}{2\epsilon_0} \int_0^\infty \frac{r dr}{[z^2 + r^2]^{3/2}} = \frac{\sigma}{2\epsilon_0}, \quad (3.4)$$

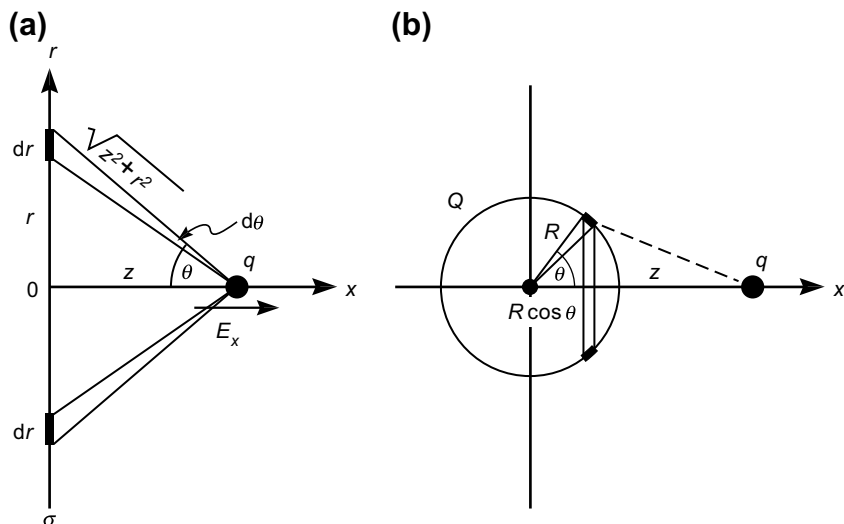


FIGURE 3.1 Calculation of the electric fields and forces acting on a charge q at a distance z from (a) a flat surface of charge density σ , and (b) the center of a uniformly charged sphere of total charge Q .

which is independent of z . Thus, the field, and hence the force on the charge, $q\sigma/2\varepsilon_0$ is independent of its distance from the surface. Put differently, the charge density “seen” or “felt” at any point due to a charged surface or layer is independent of how far the point is from that layer. This is an example of *Gauss’s Law*.

(2) This part of the example or question will be solved by calculating the electric potential at the charge q . Let the center of the sphere (of radius R) be at $x = 0$ (Figure 3.1b) and position the charge on the x -axis at $x = z$, where $z > R$. Let $\sigma = Q/4\pi R^2$ be the surface charge density of the sphere. Consider a circular strip on the sphere centered at $x = R \cos \theta$ of radius $R \sin \theta$ and width $R d\theta$. The distance between the charge and the circular strip is therefore

$$\sqrt{(R \sin \theta)^2 + (z - R \cos \theta)^2} = \sqrt{z^2 - 2zR \cos \theta + R^2}, \text{ so that the potential at } x = z \text{ is}$$

$$\psi_z = \int_0^\pi \frac{2\pi R^2 \sigma \sin \theta d\theta}{4\pi \varepsilon_0 [z^2 - 2zR \cos \theta + R^2]^{1/2}} = \frac{Q}{4\pi \varepsilon_0 z}. \quad (3.5)$$

which is independent of the radius of the sphere. Thus, the electric field $E = -d\psi/dz$, and force on the charge $F = qE$ is the same as for a point charge Q located at the center of the sphere. It can also be shown that the force will be unchanged if all the charge is distributed uniformly throughout the sphere.

[Comment: Either of the two results could have been obtained by summing the potential (a scalar quantity) and then differentiating with respect to z , as in (2), or by summing the resolved force (a vector), as in (1). If the medium has dielectric constant ϵ , then ε_0 becomes replaced by $\varepsilon_0 \epsilon$ in the above two equations. The above examples are illustrations of Gauss’s Law, which also applies to other $1/r^2$ forces such as the gravitational force. Gauss’s Law is very useful for determining electrostatic fields and forces (cf. Problem 3.5).]

In practice, to ensure overall charge neutrality, there must always be a countercharge somewhere else, and this may affect the net field experienced by the charges q in the two examples in Worked Example 3.1. For example, if there is a surface of opposite charge density $-\sigma$ parallel to a surface of charge density $+\sigma$, as in a capacitor (Figure 3.2), the fields inside and outside the capacitor plates can be determined by simply adding the fields $\pm\sigma/2\varepsilon_0\varepsilon$ from the two plates.⁵ As can be seen from Figure 3.2, the two fields augment each other between the plates and cancel out each other outside the plates. The fields will therefore be given by

$$E_{\text{in}} = -\sigma/\varepsilon_0\varepsilon \quad \text{between the plates,}$$

$$\text{and} \quad E_{\text{out}} = 0 \quad \text{outside the plates (independent of } \varepsilon_1 \text{ and } \varepsilon_2 \text{).} \quad (3.6)$$

The force per unit area, or pressure, between the two surfaces may be calculated from the field $E_1 = -\sigma/2\varepsilon_0\varepsilon$ of the first surface acting on the charge $\sigma_2 = +\sigma$ of the second

⁵Electrostatic potentials and the corresponding resolved fields and forces obey the “superposition principle,” meaning that they can be simply added—for example, $F_{\text{total}} = F_1 + F_2 + F_3 + \dots$ with no higher-order terms such as F_1^2 or $F_1 F_2$.

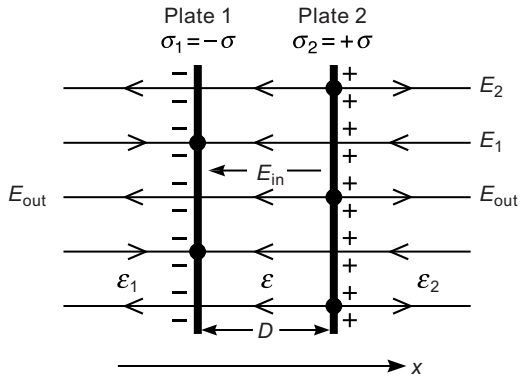


FIGURE 3.2 Two plane parallel surfaces (the two conducting plates of a capacitor or condenser) carrying equal and opposite charges $\pm\sigma$ per unit area. Note the signs and directions of the field lines, which are purely conventional (see footnote 3). In practice, the capacitor will slowly discharge if there is no external voltage to keep the attracting charges apart. Conversely, spontaneous charge separation can arise at interfaces separating dissimilar materials or phases of the same material.

surface, or vice versa, to give $F = \sigma_2 E_1 = \sigma_1 E_2 = -\sigma^2/2\epsilon_0\epsilon$. Thus, the two surfaces attract each other. Note that the field and pressure are independent of the intersurface separation.

Finally, since the force $F = -\sigma^2/2\epsilon_0\epsilon$ acting on each plate is a constant, the electric field energy of an infinite parallel plate capacitor is

$$\text{Electric field energy} = +\sigma^2 D / 2\epsilon_0\epsilon \text{ per unit area,} \quad (3.7)$$

where D is the separation between the plates (see Figure 3.2). This result can also be readily derived from the general equation for the energy of an electric field (Eq. 3.12): $\frac{1}{2}\epsilon_0\epsilon \int E^2 dV$.

3.4 Ionic Crystals

Coulomb forces (also known as *ionic forces*) hold the sodium and chloride ions together in the rigid salt lattice composed of alternate sodium and chloride ions, and the bond they give rise to is often referred to as the *ionic bond*. However, the above calculation of the binding energy of an *isolated* pair of Na^+Cl^- ions is too simplistic for estimating the mean energy of an ionic bond in a lattice. As we saw before, Coulomb forces are of very long range due to the $1/r$ distance dependence of $w(r)$. Therefore, for an accurate determination of the lattice energy, the Coulomb energy of an ion with all the other ions in the lattice has to be summed, not only to its nearest neighbors. Thus, in the NaCl crystal lattice, each Na^+ has 6 nearest-neighbor Cl^- ions at $r = 0.276$ nm, 12 next-nearest-neighbor Na^+ ions at $\sqrt{2}r$, 8 more Cl^- ions at $\sqrt{3}r$, and so on.

The total interaction energy for a pair of Na^+Cl^- ions in the lattice is therefore

$$\begin{aligned}\mu^{\text{i}} &= -\frac{e^2}{4\pi\epsilon_0 r} \left[6 - \frac{12}{\sqrt{2}} + \frac{8}{\sqrt{3}} - \frac{6}{2} + \dots \right] \\ &= -\frac{e^2}{4\pi\epsilon_0 r} \left[6 - 8.485 + 4.619 - 3.000 + \dots \right] \\ &= -1.748 \frac{e^2}{4\pi\epsilon_0 r} = -1.46 \times 10^{-18} \text{ J}.\end{aligned}\quad (3.8)$$

The constant 1.748 is known as the *Madelung constant* and has different values for other crystal structures, varying between 1.638 and 1.763 for crystals composed of monovalent ions such as NaCl and CsCl, rising to about 5 for monovalent-divalent ion pairs such as CaF₂, and higher for multivalent ions such as SiO₂ and TiO₂. However, it is clear that the net (binding) energy is negative and that it is of the same order as for isolated ion pairs. To obtain the theoretical *molar lattice energy* or *cohesive energy* U of an NaCl crystal, we must multiply the above by Avogadro's number N_0 —thus,

$$U = -N_0\mu^{\text{i}} = (6.02 \times 10^{23})(1.46 \times 10^{-18}) = 880 \text{ kJ mol}^{-1}. \quad (3.9)$$

This is about 15% higher than the measured value due to our neglect of the repulsive forces at contact that lower the final binding energy. These very short-range repulsive forces will be discussed in Chapter 7. The above value for the molar lattice energy of NaCl is fairly representative of other alkali halide energies, which range from about 600 to 1000 kJ mol⁻¹ going from RbI to LiF—that is, increasing with decreasing ionic size. Ionic bonds are therefore seen to be as strong as covalent bonds (Table 3.1).

An interesting and important conclusion of the above type of analysis is that in any system that is overall electrically neutral—that is, where the net charge of the system is zero—the charges attract each other.⁶

3.5 Reference States

It is important to always have the right reference state in mind when considering intermolecular interactions. Any value for the energy is not very meaningful unless referred to some state with which it is being compared. Thus, when ions come together to form a condensed phase from the gaseous state, the reference state is at $r = \infty$, and the interaction occurs in a vacuum ($\epsilon = 1$). It is for this reason that Eq. (3.8) for the lattice energy of ionic crystals does not contain the dielectric constant of the medium (e.g., $\epsilon \approx 6$ for NaCl). On the other hand, if two ions are interacting in a condensed liquid medium, the reference state is also at $r = \infty$, but the dielectric constant now appears in the denominator of any expression for the Coulomb interaction, since the interaction is now occurring entirely within the solvent medium.

⁶This is in the absence of entropic interactions, or at zero temperature ($T = 0 \text{ K}$). At finite temperatures, when the repulsive entropic pressure is included, $P = \rho kT$, the net interaction can be attractive or repulsive, as occurs for colloidal systems.

Different types of interactions can manifest great subtleties with regard to their reference states. In the case of the Coulomb interaction, the above statements are actually not strictly correct: the true lowest energy states of sodium and chlorine atoms at infinity—that is, of the isolated atoms—are the uncharged (neutral) states Na and Cl rather than Na^+ and Cl^- . When the two neutral atoms come together from a large separation, at a certain finite separation (of order ~1 nm) a quantum mechanical *charge exchange* or *charge transfer* interaction takes place whereby an electron jumps spontaneously from the sodium atom to the chlorine atom. The two neutral atoms suddenly turn into oppositely charged ions and now attract each other with a strong Coulomb force. This phenomenon is referred to picturesquely as the *Harpooning Effect*. Likewise, on separating the two ions from contact, at the same finite separation an electron will jump back, and the long-range Coulomb force will disappear and become replaced by the much weaker short-range van der Waals force. This effect also occurs between dissimilar surfaces, where it is known as *contact electrification* or *triboelectricity* (cf. Problem 1.6 and later chapters).

3.6 Range of Electrostatic Forces

The Coulomb interaction may be compared to the gravitational interaction that also follows an inverse-square force-law, is long-ranged, and is “additive.”⁷ In terms of magnitudes, the Coulomb interaction between two small ions is stronger than the gravitational one by a factor of $(e^2/4\pi\epsilon_0)/Gm^2 \sim 10^{33}$ (or a factor of 10^{43} for two electrons). However, while the gravitational force in a vacuum is always attractive, the Coulomb force on a charged particle generally involves many nearby and distant charges that are both positive and negative—in other words, both attractive and repulsive. Thus, in spite of the apparent simplicity of the form of the Coulomb force, the net electrostatic interaction on a body is usually very complex, difficult to calculate, and of much shorter range than expected for a simple inverse-square force-law.

For example, in a crystal lattice each positive charge has a negative charge next to it so that they form a dipole whose field decays asymptotically as $1/r^3$ rather than $1/r^2$ (Chapter 4). But each dipole has another next to it, and the field of the resulting quadrupole decays as $1/r^4$, and so on. Thus, the field outside an ionic lattice is seen to be short-ranged even though it is made up of many long-ranged contributions. In fact, it decays exponentially with a decay length that is smaller than the spacing between the ions (Section 14.24). Likewise, a positive ion moving freely in aqueous solution always has a higher density of negative ions surrounding it; its electric field becomes *screened*, again exponentially, and decays more rapidly away from the ion than from an isolated ion. As will be analyzed in Chapter 14, the effective or net Coulomb interaction between ionic

⁷An additive interaction is one in which the interaction energy or force between two molecules or bodies does not depend on the presence of other bodies. Additive forces obey the “superposition principle” (see footnote 5).

crystals, charged surfaces, and dissolved ions is of much shorter range than the inverse-square pair potential would suggest, although still longer-ranged than covalent forces. Interestingly, a single defect in an ionic lattice or crystal, such as a vacancy (a missing anion or cation) in the surface layer, produces a field that is equivalent to a single charge, which is stronger and of longer range than that of the millions of ions of the perfect (defect-free) lattice.

3.7 The Born Energy of an Ion

When a single ion is in a vacuum or in a medium, even though it may not be interacting with other ions, it still has an electrostatic free energy associated with it. This energy is equal to the electrostatic work done in forming the ion that in a vacuum is referred to simply as the *self-energy*, while in a medium it is referred to as the *Born or solvation energy* of the ion. The Born energy is an important quantity since it determines among other things the extent to which ions will dissolve and partition in different solvents. Let us see how the Born energy arises.

Imagine the process of charging an atom or sphere of radius a by gradually increasing its charge from zero to its full charge Q . At any stage of this process let the ionic charge be q , and let this be incremented by dq . The work done in bringing this additional charge from infinity to $r = a$ is therefore, from Eq. (3.3), putting $Q_1 = q$, $Q_2 = dq$, and $r = a$,

$$dw = \frac{q dq}{4\pi\epsilon_0\epsilon a} \quad (3.10)$$

so that the total free energy of charging the ion, the Born energy, is

$$\mu^i = \int dw = \int_0^Q \frac{q dq}{4\pi\epsilon_0\epsilon a} = \frac{Q^2}{8\pi\epsilon_0\epsilon a} = \frac{(ze)^2}{8\pi\epsilon_0\epsilon a}. \quad (3.11)$$

The Born energy gives the electrostatic free energy of an ion in a medium of dielectric constant ϵ . It is positive because the energy is unfavorable; that is, it is the energy of keeping a net charge Q distributed on the surface of a sphere against its own electrostatic repulsion.

The Born energy can also be obtained from the energy of the electric field of the ion. From basic electrostatic theory (Guggenheim, 1949; Landau and Lifshitz, 1984), the free energy density of an electric field E arising from a charge or any distribution of charges is $\frac{1}{2}\epsilon_0\epsilon E^2$ per unit volume. Thus, in general,

$$\mu^i = \frac{1}{2}\epsilon_0\epsilon \int E^2 dV, \quad (3.12)$$

and by integrating the energy density of an ion over all of space, we immediately obtain the following Born energy:

$$\mu^i = \frac{1}{2}\epsilon_0\epsilon \int_a^\infty \frac{Q^2}{(4\pi\epsilon_0\epsilon r^2)^2} 4\pi r^2 dr = + \frac{Q^2}{8\pi\epsilon_0\epsilon a}. \quad (3.13)$$

In Chapter 5 we shall see how the Born energy can also be obtained by summing the pair potentials of an ion with its surrounding solvent molecules.

From Eq. (3.11) we see that the change in free energy on transferring an ion from a medium of low dielectric constant ϵ_1 to one of high dielectric constant ϵ_2 is negative—that is, it is energetically favorable and equal to

$$\begin{aligned}\Delta\mu^i &= -\frac{z^2e^2}{8\pi\epsilon_0 a} \left[\frac{1}{\epsilon_1} - \frac{1}{\epsilon_2} \right] J \\ &= -\frac{28z^2}{a} \left[\frac{1}{\epsilon_1} - \frac{1}{\epsilon_2} \right] kT \text{ per ion at } 300 \text{ K}\end{aligned}\quad (3.14)$$

or

$$\Delta G = N_0 \Delta\mu^i = -\frac{69z^2}{a} \left[\frac{1}{\epsilon_1} - \frac{1}{\epsilon_2} \right] \text{ kJ mol}^{-1} \quad (3.15)$$

where a is given in nanometers. Thus, if one mole of monovalent cations and anions are transferred from the gas phase ($\epsilon = 1$) into water ($\epsilon = 78$), the gain in the molar free energy will be, assuming $a = 0.14$ nm for both the cations and anions,

$$\Delta G = -\frac{2 \times 69}{0.14} \left[1 - \frac{1}{78} \right] \approx -1000 \text{ kJ mol}^{-1}. \quad (3.16)$$

Equation (3.15) provides the basis for calculating the partitioning of ions between different solvents. Note that the Born energy does not include the energy expended by solvents in forming the cavities for accommodating the ions; these are generally small compared to the large Born energy.

3.8 Solubility of Ions in Different Solvents

Closely related to partitioning is the solubility of ions in different solvents. Both the Coulomb energy and the Born energy are useful for understanding why ionic crystals such as Na^+Cl^- , in spite of their very high lattice energies, dissociate in water and in other solvents with high dielectric constants. If we consider the Coulomb interaction, Eq. (3.3), we immediately see that the electrostatic attraction between ions in a medium is reduced by a factor ϵ . This is a somewhat superficial approach to the problem, since the Coulomb law is strictly not valid at very small interionic distances where the molecularity of the medium makes the continuum description (in terms of ϵ) break down. However, this approach does predict the right trends, so let us follow it up.

On the simplest level we may consider the difference in energy on going from the associated state to the dissociated state to be roughly given by Eq. (3.3). Thus, the free energy change on separating two monovalent ions such as Na^+ and Cl^- from contact in a solvent medium of dielectric constant ϵ is

$$\Delta\mu^i \approx \frac{+e^2}{4\pi\epsilon_0\epsilon(a_+ + a_-)}, \quad (3.17)$$

where a_+ and a_- are the ionic radii of Na^+ and Cl^- . This energy is positive, since the attractive Coulomb interaction will always favor association. However, some fraction

of the ions will always dissociate due to their entropy of dilution (Chapter 2). The concentration X_s of ions forming a saturated solution in equilibrium with the solid will therefore be given by Eq. (2.15):

$$X_s = e^{-\Delta\mu^i/kT} = \exp\left[-\frac{e^2}{4\pi\epsilon_0\epsilon(a_+ + a_-)kT}\right], \quad (3.18)$$

where the value of the dimensionless parameter X_s may be identified with the solubility of an electrolyte in water, or in any solvent, in mole-fraction units. Thus, for NaCl in water, where $(a_+ + a_-) = 0.276$ nm, $\epsilon = 78$ at $T = 298$ K, we expect very roughly $X_s \approx e^{-2.6} \approx 0.075$ in mole fraction unit, which may be compared with the experimental value of 0.11 mole/mole (360 g/liter).

While Eq. (3.18) is far too simplistic to quantitatively account for the solubilities of all electrolytes, it does predict the observed trends for monovalent salts reasonably well. For example, it predicts that the solubility X_s of a salt in different solvents is proportional to $e^{-\text{const}/\epsilon}$, where ϵ is the solvent dielectric constant. Thus, a plot of $\log X_s$ against $1/\epsilon$ should yield a straight line passing through the origin (defined at $X_s = 1$ and $\epsilon = \infty$). This is more or less borne out in practice, as shown in Figure 3.3, for NaCl in different solvents. The large solubilizing power of water to ions is therefore seen as arising quite simply from its high dielectric constant (Table 3.2) and not because of some special property of water. In the case of the amino acid glycine, the line is still straight but does not pass through the origin for reasons discussed in the following chapter.

From Eq. (3.18) we may also expect larger ions to be more soluble than smaller ions. This too is usually borne out in practice: alkali halide salts with large ionic radii, such as CsBr and KI, are generally much more soluble in various solvents than salts such as NaF and LiF; the latter has the smallest interionic distance and is the least soluble of the alkali halides in water.



Worked Example 3.2

Question: From the data of Figure 3.3, estimate the interionic spacing between a sodium and a chloride ion when they are in contact. Compare your result with the known value of 0.28 nm in the NaCl crystal.

Answer: The slope of the NaCl line in Figure 3.3 is $2.303 \times 5/0.069 = -167$. Using Eq. (3.18), this corresponds to an interionic spacing given by $(a_+ + a_-) = (1.602 \times 10^{-19})^2 / 4\pi(8.854 \times 10^{-12})(4.1 \times 10^{-21})(167) = 3.4 \times 10^{-10}$ m = 0.34 nm. This is about 0.06 nm larger than in the pure, dry crystal. Given the gross assumptions that were made in deriving Eq. (3.18), it is surprising that the calculated value differs from the correct value by only 20%.



The solubility of an electrolyte is strictly determined by the difference in the free energy of the ions in the solid lattice from that in solution. In the above approach, we did not consider the lattice energy specifically, but it is also possible to approach the



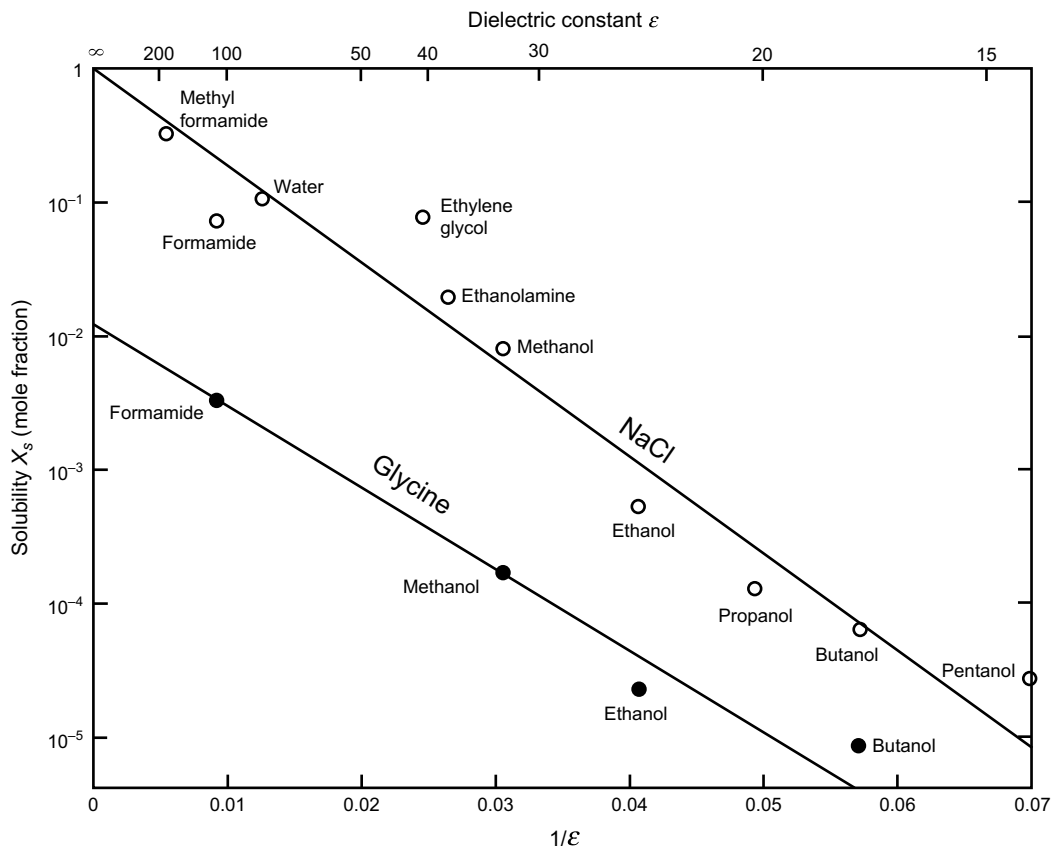


FIGURE 3.3 Solubilities of sodium chloride ($\text{NaCl} \rightleftharpoons \text{Na}^+ + \text{Cl}^-$) and glycine ($\text{NH}_2\text{CH}_2\text{COOH} \rightleftharpoons \text{NH}_3^+ + \text{CH}_2\text{COO}^-$) in solvents of different static dielectric constants ϵ at 25°C . Solubility (in mole fraction units) is plotted as $\log X_s$ as a function of $1/\epsilon$. For NaCl, the line passes through $X_s = 1$ at $-\epsilon = \infty$, which from Eq. (3.18) suggests that the interaction of $\text{Na}^+ + \text{Cl}^-$ with these solvents is purely Coulombic. For glycine, the line tends to a finite value ($X_s < 1$) as ϵ tends to infinity, indicative of some additional type of solute-solute attraction – the van der Waals interaction (Chapter 6). Note that all the solvents are hydrogen-bonding liquids (Chapter 8). Non-hydrogen-bonding liquids are less effective as solvents for ionic species; for example, the solubility of NaCl in acetone ($\epsilon = 20.7$) is $X_s = 4 \times 10^{-7}$ while that of glycine in acetone is $X_s = 2 \times 10^{-6}$. Solubility data were taken from GMELINS *Handbuch*, Series 21, Vol. 7 for NaCl, and from the CRC *Handbook of Chemistry and Physics* for glycine.

problem in a way that takes the lattice energy into account: by splitting up the dissociation process into two well-defined stages. The first is the dissociation of the solid into isolated gaseous ions, and the second is the transfer of these ions into the solvent. In this approach (see, e.g., Dassent, 1970; Pass, 1973) the energy associated with the first stage is simply the positive lattice energy, while the second stage reduces this by the negative Born energies of transferring the ions from the gas phase ($\epsilon = 1$) into the solvent medium of dielectric constant ϵ . However, for water, the theoretical Born energies turn out to be much too large, even larger than the lattice energies [compare Eq. (3.9) with Eq. (3.16)],

Table 3.2 Static Dielectric Constants ϵ of Some Common Liquids and Solids at 25°C^a

Compound	ϵ	Compound	ϵ
Hydrogen-bonding		Polymers	
Methyl-formamide	HCONHCH ₃	182.4	Nylon 3.7–4.2
Formamide	HCONH ₂	109.5	PTFE, Fluorocarbons 2.0, 2.1–3.6
Hydrogen fluoride	HF (at 0°C)	84	Polycarbonate 3.0
Water	H ₂ O	78.5	Polystyrene 2.4
Water	D ₂ O	77.9	Silicone oil 2.8
Formic acid	HCOOH (at 16°C)	58.5	Glasses
Ethylene glycol	C ₂ H ₄ (OH) ₂	40.7	Fused quartz SiO ₂ 3.8
Methanol	CH ₃ OH	32.6	Soda glass 7.0
Ethanol	C ₂ H ₅ OH	24.3	Borosilicate glass 4.5
n-Propanol	C ₃ H ₇ OH	20.2	Crystalline solids
Ammonia	NH ₃	16.9	Diamond (carbon) 5.7
Acetic acid	CH ₃ COOH	6.2	Crystalline quartz SiO ₂ 4.5
			Micas 5.4–7.0
Non-hydrogen-bonding, polar			Sodium chloride NaCl 6.0
Acetone	(CH ₃) ₂ CO	20.7	Alumina Al ₂ O ₃ 8.5
Chloroform	CHCl ₃	4.8	
Nonpolar			Misellaneous
Benzene	C ₆ H ₆	2.3	Piezoelectric materials »1, up to 10 ⁴
Carbon tetrachloride	CCl ₄	2.2	Water (liquid at 0°C) 87.9
Cyclohexane	C ₆ H ₁₂	2.0	Water (ice at 0°C) 91.6–106.4
Dodecane	C ₁₂ H ₂₆	2.0	Paraffin (liquid) 2.2
Hexane	C ₆ H ₁₄	1.9	Paraffin wax (solid) 2.2
			Liquid helium (2–3 K) 1.055
			Air (dry) 1.00054

^aThe dielectric constant is a measure of the extent of reduction of electric fields and, consequently, of the reduced strengths of electrostatic interactions in a medium.

and so to obtain agreement with measured solubility and other thermodynamic data, it has been found necessary to “correct” the crystal lattice radii of ions by increasing them by 0.02 to 0.10 nm when the ions are in water. The larger effective sizes of ions in water arise from their *solvation* or *hydration shells* (discussed in Chapter 4), although it has also been argued that the lower cutoff (Born) radius a in Eq. (3.13) should naturally be closer to the radius of the centers of the solvent molecules around the ion, not the bare ion radius (Stecki, 1961). Either way, this approach is unsatisfactory for predicting ionic solubilities because the solubility is given by the small difference between two large values so even a small “correction” to one of them results in a large difference in the result. However, it does show, once again, that the effective radii of (monovalent) ions in water are close to their bare ion radii.

While both the Coulomb and Born energy approaches usually predict the right trends, neither is quantitatively reliable because they both ignore the complex and

sometimes specific interactions that can occur between dissolved ions and the solvent molecules in their immediate vicinity. This problem has already been referred to as the *solvent effect* (cf. Sections 2.1 and 2.8), and it is particularly acute for small multivalent ions.

3.9 Specific Ion-Solvent Effects: Continuum Approach

To understand the role of the solvent in Coulomb interactions, we must investigate how a solvent affects the electric fields around dissolved ions. Ultimately, we shall have to consider the origin of the dielectric permittivity, ϵ , since this is what defines the “solvent” in all equations for electrostatic interactions. As already mentioned in Section 2.8, one can analyze such phenomena in terms of *continuum* and/or *molecular* theories. We start with the continuum approach and attempt to assess its limitations by examining in more detail the origin of the Born and Coulomb energies. We shall focus in particular on the small distance regime where the contribution to the net interaction energy is greatest and where the continuum picture is most likely to break down.

In Section 3.7 it was shown how the Born energy, Eq. (3.13), may be obtained by integrating the electric field energy over all of space. The derivation of Eq. (3.13) provides some important insights: First, the electrostatic self-energy is seen *not* to be concentrated on the ion itself, but rather it is spread out over the whole of space around the ion; thus, if in Eq (3.13) we integrate from $r = a$ to $r = R$ (rather than to $r = \infty$), we find that the energy contained within a finite sphere of radius R around the ion is

$$\frac{Q^2}{8\pi\epsilon_0\epsilon} \left[\frac{1}{a} - \frac{1}{R} \right]. \quad (3.19)$$

For example, for an ion of radius 0.1 nm, 50% of its energy will be contained within a sphere of radius 0.2 nm, and 90% within a radius of 1.0 nm. Thus, if the Born energy equation is to be applicable in a condensed medium, the value of the dielectric constant of the medium must already be equal to the bulk value at approximately 0.1 nm away from the ion, a distance that is smaller than even the smallest solvent molecule.

Second, it can be shown that the Coulomb interaction in a medium can also be derived from the change in the electric field energy, integrated over the whole of space, when two charges are brought together. The Coulomb interaction can therefore be considered as the change in the Born energies of two charges as they approach each other. This is conceptually important, since it shows that the Coulomb interaction in a medium is not determined by the dielectric constant in the region *between* two charges but by its value in the region *surrounding* (as well as between) the charges. It is for this reason that the strength of the Coulomb interaction of two oppositely charged ions will be reduced in a solvent medium even if the ions still remain in contact—that is, even before there are

any solvent molecules between them! This is yet another manifestation of the long-range nature of electrostatic interactions. And it clearly shows why the extremely strong ionic “bond” is so easily disrupted in a medium of high dielectric constant such as water, in marked contrast to the short-range covalent bonds, which—though often weaker—are not generally affected by a solvent.

We have now established how a solvent medium affects the electrostatic Born and Coulomb energies of ions. We have seen that it is the value of ϵ of the locally surrounding medium that is important and that if the standard expressions for the Born and Coulomb energies (and other interaction energies that depend on ϵ) are to apply, the bulk value of ϵ must be attained already within the first shell of surrounding solvent molecules (see Epstein et al., 1983). In Chapter 4 we shall see that for water near monovalent ions, this is more or less expected on theoretical grounds. Experimentally, too, this is often the case, and we may recall how the Coulomb and Born energies are able to predict, at least semiquantitatively, the solubilities of monovalent ionic salts in different solvents. But we shall also encounter numerous instances where such continuum theories totally break down at small intermolecular distances.

3.10 Molecular Approach: Computer Simulations and Integral Equations of Many-Body Systems

In the molecular approach, both the solute ions and the solvent molecules are treated as discrete particles having a certain size, shape, and charge distribution. These interact with one another via a combination of Lennard-Jones potentials (between the neutral atoms of the molecules) and Coulomb potentials between the charged groups. Since many molecules, each having multiple pair potentials, are involved, one needs to resort to sophisticated theoretical techniques that can handle many-body interactions or a computer simulation, as described in Chapter 2. Computer simulations and integral equation methods have revealed that the interaction potentials between two monovalent ions in a medium such as water exhibit short-range oscillations that merge at large separations (>0.8 nm) with the continuum inverse-square Coulomb force-law (dashed curve in Figure 3.4). The oscillations have a periodicity slightly less than the diameter of the water molecule $\sigma_{\text{H}_2\text{O}}$ and reflect the ordered structuring of water around each ion, with the electropositive water hydrogens facing anions and the electronegative oxygens facing cations. Note that for the larger and less hydrated ions such as K^+ and Na^+ the energy at contact—for example, at $r = \frac{1}{2}(\sigma_{\text{K}^+} + \sigma_{\text{Cl}^-})$ —is reasonably well described by the continuum equation. However, around the smaller, more hydrated ion of Li^+ , and even more so around multivalent ions, the first layer of water molecules is more strongly bound so as to eliminate the primary contact energy minimum altogether. Such *solvent structuring* effects have already been mentioned (cf. Figure 2.1) and are discussed in more detail in Chapters 4, 7, and 15, with particular attention to water being given in Chapter 8.

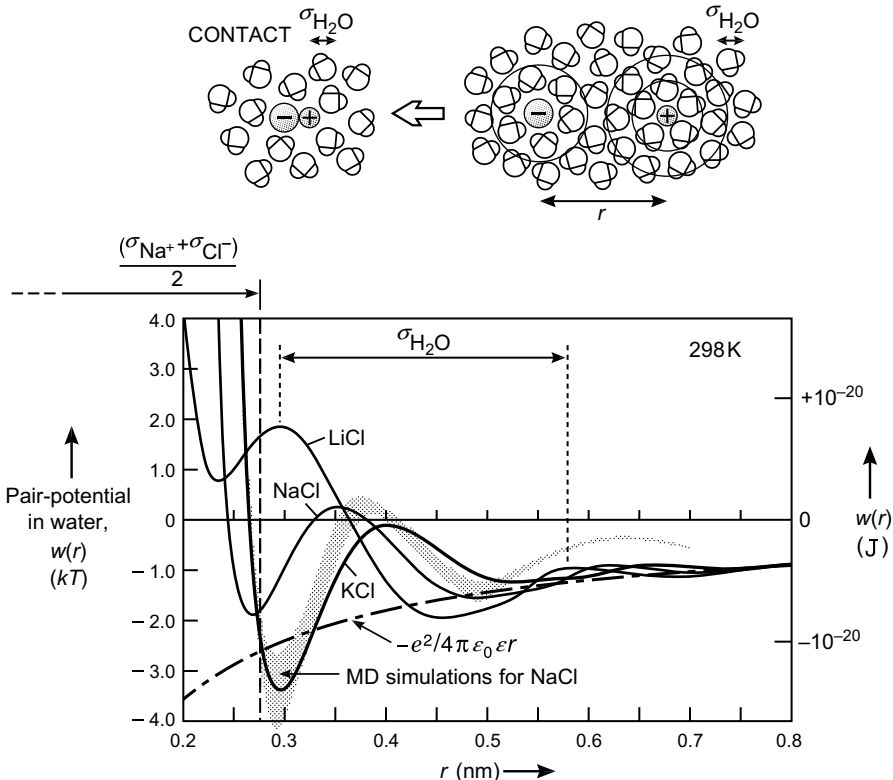


FIGURE 3.4 Theoretical calculations based on Molecular Dynamics (MD) and Integral Equations of the potentials of mean force for three alkali halide ion pairs in water in units of $kT = 4.1 \times 10^{-21}$ J (left-hand ordinate) and joules (right-hand ordinate) at 298 K (25°C). Shaded curve: MD simulations for $\text{Na}^+ \cdots \text{Cl}^-$ at 300 K based on two different models of water, the SPC and SPC/E models (Dang et al., 1990). Thin lines: Analytical Integral Equations calculations based on a modified TIPS model of water (Pettitt and Rossky, 1986). Different models of water are discussed in Section 8.3. The dashed line gives the monotonically decaying continuum energy based on the Coulomb law, Eq. (3.3), using $\epsilon = 78$. The inset shows the orientation of discrete water molecules around monovalent anions and cations that give rise to their primary and secondary hydration shells and the ‘oscillatory’ solvation or hydration forces, which are described in more detail in later chapters.

PROBLEMS AND DISCUSSION TOPICS

- 3.1** It is often argued that the Lennard-Jones potential, $w(r) = -A/r^6 + B/r^{12}$, is applicable to chemical bonds as well as physical bonds, where the attractive van der Waals term remains unchanged and where only a difference in the repulsive coefficient, B , distinguishes between the two types of interactions.

Consider two atoms for which $A = 10^{-77}$ J m⁶, and where their equilibrium separation is at $r_0 = 0.35$ nm and $r_0 = 0.15$ nm for the case of physical and chemical binding, respectively. Assuming the above hypothesis to be true, calculate the

values of w_{\min} in each case and then argue whether your result tends to support the above view.

- 3.2** (i) The ionic bond in a vacuum is very strong, but it is much reduced in water due to its high dielectric constant. Calculate the expected Coulomb energy and force needed to detach an Na^+ and a Cl^- ion from contact in water at 298 K, and discuss the implications of your results for the lifetime of the Na^+Cl^- dimer in water and for practical measurements of the detachment force. Assume that both ions are hard spheres. [Answer to numerical part: $w(\sigma) = -10.7 \times 10^{-21} \text{ J}$ (cf. Figure 3.4), $F(\sigma) = -3.9 \times 10^{-11} \text{ N} = 39 \text{ pN}$.]
- (ii) How many negatively charged ions can be put into contact around one positively charged ion of the same radius such that the net Coulombic energy of the cluster is still negative (i.e., energetically favorable)? Is your answer physically meaningful, and, if so, in what situations?
- 3.3** Two solid spheres, 1 and 2, of density 1.0 g/cm^3 and 10.0 g/cm^3 , respectively, are in an inert liquid medium 3 of density 2.0 g/cm^3 and dielectric constant 2.0 (Figure 3.5). Sphere 1 carries a charge $+e$, and sphere 2 carries a charge $-e$. If the spheres have the same radius R , calculate the value of R for there to be no long-range force between them at any separation D .
- 3.4** Use Eq. (3.12) for the energy of an electric field to derive the total energy and force per unit area between two surfaces of charge density $+\sigma$ and $-\sigma$ as a function of their separation. In Figure 3.2, what are the fields and forces if the surfaces maintain their equal and opposite charge densities $\pm\sigma$ but the dielectric constants ϵ of the three media are different?
- 3.5** A sphere has charge uniformly distributed on its surface. Show that the electric field is everywhere zero inside the sphere (refer to Worked Example 3.1).
- 3.6** Look up the values for the solubility of KCl in some of the same solvents as those in Figure 3.3. Use these to determine a value for the interionic spacing of K^+Cl^- , and compare this with the value obtained for Na^+Cl^- (see Worked Example 3.2). Is your result reasonable?
- 3.7*** Show that if a charged liquid drop evaporates into the air, there will come a point at which it will become unstable and break up into smaller charged droplets. This is

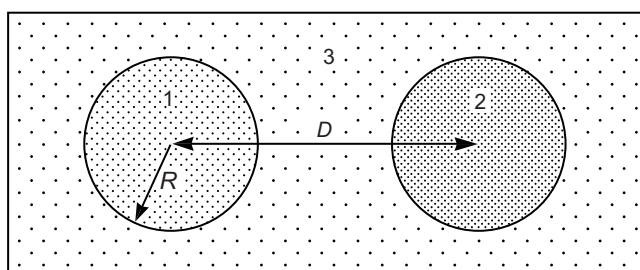


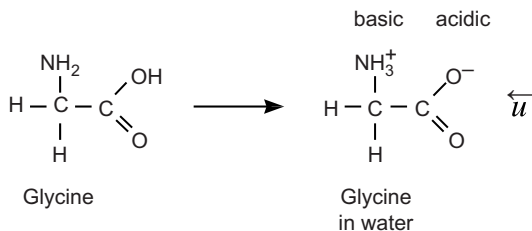
FIGURE 3.5

known as the *Rayleigh limit*. If the charge on the drop is $Q = 100e$ and if the liquid is water that has a surface tension of $\gamma = 73 \text{ mN m}^{-1}$ (numerically equal to the surface energy in units of mJ m^{-2}), at what drop radius R will this happen and what will be the nature of the fragmentation? [Suggestion: Start by distinguishing between the mechanical and thermodynamic instabilities in this problem. Answer: A spontaneous mechanical instability occurs at $R = 8.6 \text{ nm}$ when the charges will fly apart, taking the water with them. The resulting, smaller droplets will continue to evaporate and fragment until only singly charged nano-drops remain whose (thermodynamically) equilibrium radius will depend on the water vapor pressure (relative humidity).]

Interactions Involving Polar Molecules

4.1 What Are Polar Molecules?

Most molecules carry no net charge, but many possess an *electric dipole*. For example, in the HCl molecule the chlorine atom tends to draw the hydrogen's electron toward itself, and this molecule therefore has a permanent dipole. Such molecules are called *dipolar* or simply *polar* molecules. The dipoles of some molecules depend on their environment and can change substantially when they are transferred from one medium to another, especially when molecules become ionized in a solvent. For example, the amino acid molecule glycine contains an acidic group on one side and a basic group on the other. In water at neutral pH, the NH₂ group acquires a proton and the OH group loses a proton to the solution to produce a dipolar molecule:



Quite often the magnitude of the positive and negative charges are not the same, and these molecules therefore possess a net charge in addition to a dipole. Such molecules are then referred to as *dipolar ions*. Polarity can also arise from internal charge displacements within a molecule, producing *zwitterionic* molecules or groups. In larger molecules, or "macromolecules," such as proteins the net dipole moment is usually made up of a distribution of positive and negative charges at various locations of the molecules. It should already be apparent that the interactions and the solvent effects of polar molecules can be very complex.

The *dipole moment* of a polar molecule is defined as

$$u = ql, \quad (4.1)$$

where l is the distance between the two charges $+q$ and $-q$. The direction of the dipole moment is as shown in the above figure. For example, for two electronic charges $q = \pm e$ separated by $l = 0.1 \text{ nm}$, the dipole moment is $u = (1.602 \times 10^{-19}) (10^{-10}) = 1.6 \times 10^{-29} \text{ C m} = 4.8 \text{ D}$. The unit of dipole moment is the *Debye*, where $1 \text{ Debye} = 1 \text{ D} = 3.336 \times 10^{-30} \text{ C m}$,

Table 4.1 Dipole Moments of Molecules, Bonds, and Molecular Groups (in Debye Units: $1 \text{ D} = 3.336 \times 10^{-30} \text{ C m}$)^a

Molecules				
Alkanes	0^b	H_2O		1.85 ^c
C_6H_6 (benzene)	0^d	$\text{C}_n\text{H}_{2n+1}\text{OH}$ (alcohols)		1.7
CCl_4	0	$\text{C}_6\text{H}_{11}\text{OH}$ (cyclohexanol)		1.7
CO_2	0^e	OMCTS ^f		0.42
CO	0.11	CH_3COOH (acetic acid)		1.7
CHCl_3 (chloroform)	1.06	$\text{C}_2\text{H}_4\text{O}$ (ethylene oxide)		1.9
HCl	1.08	CH_3COCH_3 (acetone)		2.9
HF	1.91 ^c	HCONH_2 (formamide)		3.7 ^c
NH_3	1.47	$\text{C}_6\text{H}_5\text{OH}$ (phenol)		1.5
CH_3Cl	1.87	$\text{C}_6\text{H}_5\text{NH}_2$ (aniline)		1.5
NaCl	8.5	$\text{C}_6\text{H}_5\text{Cl}$ (chlorobenzene)		1.8
CsCl	10.4	$\text{C}_6\text{H}_5\text{NO}_2$ (nitrobenzene)		4.2
Bond Moments				
$\text{C}-\text{H}^+$	0.4	$\text{C}-\text{C}$	0	C^+-Cl 1.5–1.7
$\text{N}-\text{H}^+$	1.31	$\text{C}=\text{C}$	0	N^+-O 0.3
$\text{O}-\text{H}^+$	1.51	C^+-N	0.22	$\text{C}^+=\text{O}$ 2.3–2.7
$\text{F}-\text{H}^+$	1.94	C^+-O	0.74	$\text{N}^+=\text{O}$ 2.0
Group Moments				
C^-CH_3	0.4	C^-COOH	1.7	Adenine ~3
C^-OH	1.65	C^-OCH_3	1.3	Thymine ~4
C^-NH_2	1.2–1.5	C^-NO_2	3.1–3.8	Guanine ~7
				Cytosine ~8

^aData compiled from Wesson (1948), Smyth (1955), Davies (1965), Landolt-Börnstein (1982), and Jasien and Fitzgerald (1990).^bDepends on conformation (e.g., cyclopropane has a dipole moment).^cHydrogen-bonding molecules can have different dipole moments in the gas, liquid, and solid phases, as well as in different solvents.^dBenzene has six C^-H^+ dipoles pointing radially out, giving rise to a zero net dipole moment but that also attracts cations to the center of the molecule.^e CO_2 has two $\text{C}^=\text{O}^-$ dipoles pointing in opposite directions, giving rise to a zero net dipole moment.^fOctamethyl cyclotetrasiloxane, a quasi-spherical molecule of low polarity that is commonly used as a model solvent or solute in fundamental studies of intermolecular interactions.

which corresponds to two unit charges separated by about 0.2 \AA ($\sim 0.02 \text{ nm}$). Small polar molecules have moments of the order of 1 D, some of which are listed in Table 4.1. Permanent dipole moments occur only in asymmetric molecules and thus not in single atoms. For isolated molecules, they arise from the asymmetric displacements of electrons along the covalent bonds, and it is therefore not surprising that a characteristic dipole moment can be assigned to each type of covalent bond. Table 4.1 also lists some of these *bond moments*, which lie parallel to the axis of each bond. These values are approximate but very useful for estimating the dipole moments of molecules and especially of parts of

molecules by vectorial summation of their bond moments. For example, the dipole moment of gaseous H₂O, where the H–O–H angle is $\theta = 104.5^\circ$, may be calculated from

$$u_{\text{H}_2\text{O}} = 2u_{\text{OH}} \cos\left(\frac{1}{2}\theta\right) = 2 \times 1.51 \cos(52.25^\circ) = 1.85 \text{ D.}$$

4.2 Dipole Self-Energy

A dipole possesses an electrostatic self-energy μ^{i} that is analogous to the Born self-energy of an ion. The dipole self-energy is quite simply the sum of the (positive) Born energies of the two charges $\pm q$ at infinity plus the (negative) Coulomb energy of bringing the two charges $+q$ and $-q$ together to form the dipole. Let us estimate this for two ions of equal radius a brought into contact to form a hypothetical dipolar molecule of length equal to the sum of the two ionic radii, $l = 2a$. We therefore have

$$\mu^{\text{i}} = \frac{1}{4\pi\varepsilon_0\varepsilon} \left[\frac{q^2}{2a} + \frac{q^2}{2a} - \frac{q^2}{r} \right] = +\frac{q^2}{8\pi\varepsilon_0\varepsilon a} \quad \text{or} \quad +\frac{u^2}{4\pi\varepsilon_0\varepsilon l^3}, \quad (4.2)$$

where $r = l = 2a$. The dipole self-energy is therefore seen to be of roughly the same magnitude as the Born energy of an individual ion, Eq. (3.11), and its dependence on the dielectric constant of the medium is also the same. We may therefore expect that the solubility of polar molecules in different solvents should likewise increase with their value of ε . While this is generally the case, as shown in Figure 3.3 for glycine, Eq. (4.2) for polar molecules is somewhat model dependent and not as useful as the Born equation for ions. First, unlike the charge of an isolated ion, the dipole moment does not uniquely define the charge distribution of a dipolar molecule: a moment of $u = 1$ D could correspond to charges $\pm e$ separated by $l = 0.02$ nm, but it could also correspond to charges of $\pm \frac{1}{2}e$ separated by $l = 0.04$ nm. These two possibilities give significantly different values for the dipole self-energy. Second, the dipole moment u can vary from solvent to solvent (Davies, 1965). And third, since molecules are usually much bigger than ions, there are additional large energy terms arising from nonelectrostatic solute-solvent interactions, such as the van der Waals self-energy, which are not included in Eq. (4.2) (see Problem 4.3).

4.3 Ion-Dipole Interactions

The second type of electrostatic pair interaction we shall consider is that between a charged atom and a polar molecule—for example, between Na⁺ and H₂O. As an illustrative example, we shall derive the interaction potential for this case from basic principles. Figure 4.1(a) shows a charge Q at a distance r from the center of a polar molecule of dipole moment u subtending an angle θ to the line joining the two molecules. If the length of the dipole is l , with charges $\pm q$ at each end, then the total interaction energy will be the sum of the Coulomb energies of Q with $-q$ at B and Q with $+q$ at C :

$$w(r) = -\frac{Qq}{4\pi\varepsilon_0\varepsilon} \left[\frac{1}{AB} - \frac{1}{AC} \right], \quad (4.3)$$

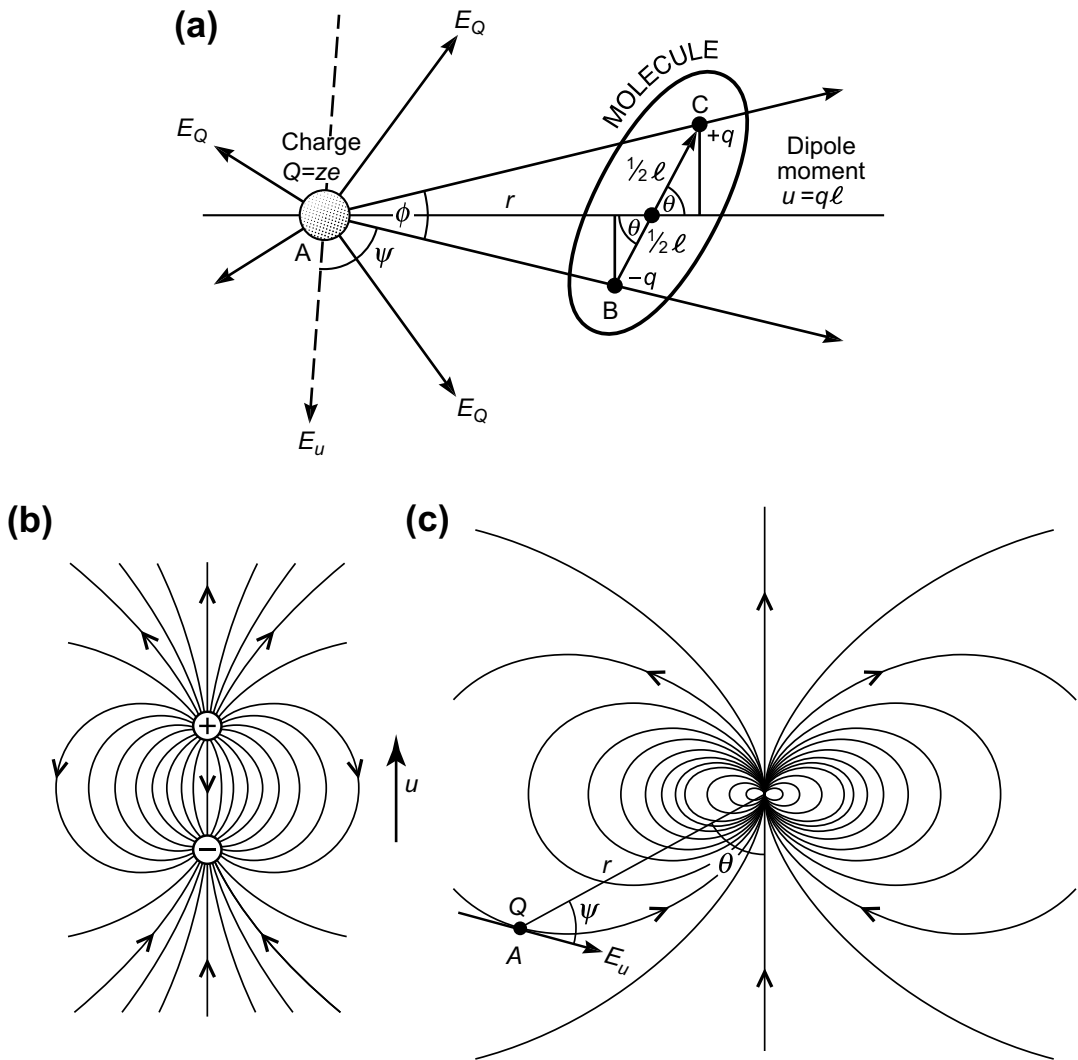


FIGURE 4.1 Ion-dipole interactions. The field of the ion (assumed positive) is E_Q , while that of the dipole (acting on the ion) is E_u . By definition, the direction of an electrostatic dipole is from B to C in panel (a)—that is, along the direction of the field emanating from the dipole, as shown in panels (b) and (c), not the internal field.

where

$$\begin{aligned}
 AB &= \left[\left(r - \frac{1}{2}l \cos \theta \right)^2 + \left(\frac{1}{2}l \sin \theta \right)^2 \right]^{1/2} \approx r - \frac{1}{2}l \cos \theta, \\
 AC &= \left[\left(r + \frac{1}{2}l \cos \theta \right)^2 + \left(\frac{1}{2}l \sin \theta \right)^2 \right]^{1/2} \approx r + \frac{1}{2}l \cos \theta,
 \end{aligned} \tag{4.4}$$

where the approximate values are in the limit of $r \gg l$ —that is, at large separations compared to the dipole length.¹ In the point dipole approximation limit, the interaction energy becomes

$$\begin{aligned} w(r) = w(r, \theta) &= -\frac{Qq}{4\pi\epsilon_0\epsilon} \left[\frac{1}{r - \frac{1}{2}l \cos \theta} - \frac{1}{r + \frac{1}{2}l \cos \theta} \right] \\ &= -\frac{Qq}{4\pi\epsilon_0\epsilon} \left[\frac{l \cos \theta}{r^2 - \frac{1}{4}l^2 \cos^2 \theta} \right] \\ &= -\frac{Qu \cos \theta}{4\pi\epsilon_0\epsilon r^2} = -\frac{(ze)u \cos \theta}{4\pi\epsilon_0\epsilon r^2}. \end{aligned} \quad (4.5)$$

Note that since the electric field of the charge acting on the dipole is $E(r) = Q/4\pi\epsilon_0\epsilon r^2$, we see that in general the energy of a permanent dipole u in a field E may be written as

$$w(r, \theta) = -uE(r)\cos \theta. \quad (4.6)$$

Equation (4.5) gives the free energy for the interaction of a charge Q and a “point dipole” u (for which $l = 0$) in a medium. Thus, when a cation is near a dipolar molecule, maximum attraction (i.e., maximum negative energy) will occur when the dipole points away from the ion ($\theta = 0^\circ$), while if the dipole points toward the ion ($\theta = 180^\circ$) the interaction energy is positive and the force is repulsive. Figures 4.1b and c show the field lines of a finite-sized dipole and a point dipole, respectively. Also shown in Figure 4.1c is the direction of the force on a charge, which is seen not to point along r —that is, along the line joining their centers (see Worked Example 4.1).

Figure 4.2 shows how the pair-potential $w(r)$ varies with distance for a monovalent cation ($z = +1$) interacting with a dipolar molecule of moment 1 D in a vacuum. The solid curves are based on the exact solution calculated from Eqs. (4.3) and (4.4), while the dashed curves are for the point-dipole approximation, Eq. (4.5), which shows itself to be surprisingly accurate down to fairly small separations. Only at ion-dipole separations r below about $2l$ does the approximate equation deviate noticeably (>10%) from that obtained using the exact formula. Thus, if the dipole moment arises from charges separated by less than about 0.1 nm, Eq. (4.5) will be valid at all physically realistic intermolecular separations. However, for greater dipole lengths—as occur in zwitterionic groups, highly polarizable molecules, and media—the deviations may be large, thereby requiring that the energy be calculated in terms of the separate Coulombic contributions. In such cases the interactions are always stronger than expected from Eq. (4.5), as can be inferred from Figure 4.2.

It is also evident from Figure 4.2 that the ion-dipole interaction is much stronger than kT at typical interatomic separations (0.2–0.4 nm). It is therefore strong enough to bind ions to polar molecules and mutually align them. Let us calculate the vacuum interaction

¹This is not the same as the molecular length or diameter σ . Dipoles are usually embedded inside molecules so that $l < \sigma$, which renders the approximate forms of Eq. (4.4) fairly accurate in many cases.

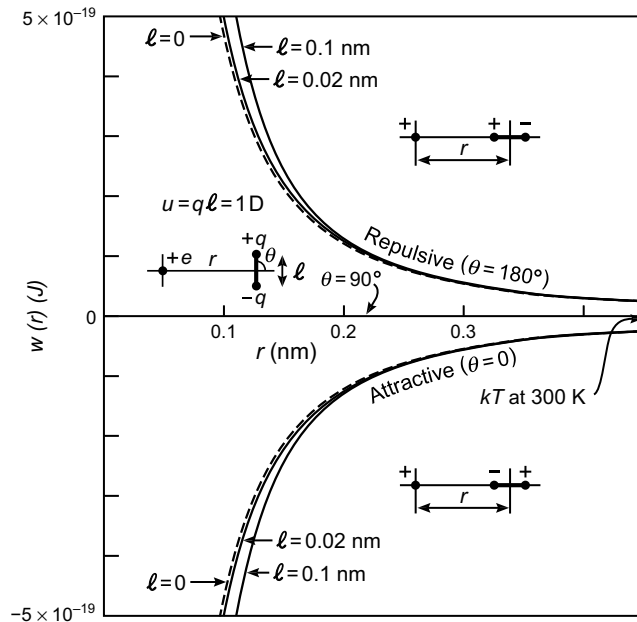


FIGURE 4.2 Charge-dipole interaction energy in vacuum ($\epsilon = 1$) between a unit charge e and a dipole of moment $u = q l = 1$ D (1 Debye) oriented at different angles θ to the charge. Solid lines are exact solutions, Eqs. (4.3) and (4.4), for finite sized dipoles with $l = 0.02$ nm and $l = 0.10$ nm; dashed lines are exact solutions for $l = 0$, which correspond to the approximate point-dipole formula, Eq. (4.5). Note that for typical interatomic spacings ($r \approx 0.3\text{--}0.4$ nm) the strength of the pair interaction greatly exceeds the thermal energy kT at 300 K.

between some common ions and water molecules. We shall assume that the water molecule may be treated as a simple spherical molecule of radius 0.14 nm with a point dipole of moment 1.85 D. This is a gross oversimplification: the distribution of charges in a water molecule is much more complex than for a simple dipole, as will be discussed later. But for our present purposes, we may ignore this complication. Thus, for the monovalent ion Na^+ ($z = 1$, $a = 0.095$ nm) near a water molecule ($a = 0.14$ nm, $u = 1.85$ D), the maximum interaction energy will be given by Eq. (4.5) as

$$\begin{aligned} w(r, \theta = 0^\circ) &= -\frac{(1.602 \times 10^{-19})(1.85 \times 3.336 \times 10^{-30})}{4\pi(8.854 \times 10^{-12})(0.235 \times 10^{-9})^2} = 1.6 \times 10^{-19} \text{ J} \\ &= 39 \text{ } kT \quad \text{or} \quad 96 \text{ kJ mol}^{-1} \quad \text{at 300 K} \end{aligned}$$

which compares surprisingly well with the experimental value of 100 kJ mol^{-1} (Saluja, 1976). For the smallest monovalent ion Li^+ ($a = 0.068$ nm), this rises to about 50 kT , or 125 kJ mol^{-1} (experimental value: 142 kJ mol^{-1}), while for the small divalent cations Mg^{2+} ($z = 2$, $a = 0.065$ nm) and Be^{2+} ($z = 2$, $a = 0.03$ nm), it rises to about 100 kT and 150 kT , respectively.

The strongly attractive interaction between ions and water is responsible for promoting the nucleation of raindrops around ions that are liberated after a lightning bolt

in thunderclouds. In other types of clouds, the nucleation of water occurs around uncharged particles, molecules, or molecular groups that nevertheless have a strong affinity for water. Such groups are referred to as *hydrophilic*, *hygroscopic*, or *deliquescent* and are discussed in Chapter 8.

Worked Example 4.1

Question: In Figure 4.1a, what is the net electrostatic force experienced by the ion, and in which direction does it act? What implications does your result have for (1) how a free ion moves when it is in the force field of a fixed dipolar molecule, and (2) how a free dipolar molecule moves when it is close to a fixed charge?

Answer: This problem can be solved in a similar way to that used to derive the interaction energy of the ion with the dipole, Eqs. (4.3)–(4.5). However, energy is a scalar quantity that only requires a knowledge of its magnitude at any point, whereas the field and resulting force is a vector quantity that requires a knowledge of both its magnitude and direction at any point. Referring to Figure 4.1a and using the approximate forms of Eq. (4.4) for $r \gg l$, the field at A due to the charge $-q$ at B is of magnitude $E_- = q/4\pi\epsilon_0 \cdot AB^2 \approx (q/4\pi\epsilon_0 r^2)(1 + \frac{l}{r} \cos\theta)$ and acts along the AB direction—that is, at an angle $-\phi/2$ to r . Similarly, the field at A due to the charge $+q$ at C is of magnitude $E_+ = q/4\pi\epsilon_0 \cdot AC^2 \approx (q/4\pi\epsilon_0 r^2)(1 - \frac{l}{r} \cos\theta)$ and acts along the CA direction—that is, at an angle $+\phi/2$ to r . For $r \gg l$, the angle ϕ is small and may be approximated by $\sin(\phi/2) \approx l \sin\theta/2r$ and $\cos(\phi/2) \approx 1$. Resolving the total field at A into its components E_{\parallel} and E_{\perp} parallel and perpendicular to r , we obtain $E_{\parallel} = (E_- - E_+) \cos(\phi/2) \approx (q/4\pi\epsilon_0 r^2) \frac{2l}{r} \cos\theta$ and $E_{\perp} = (E_- + E_+) \sin(\phi/2) \approx (q/4\pi\epsilon_0 r^2) \frac{l}{r} \sin\theta$. The magnitude and direction ψ of the resulting dipolar field at A is therefore given by $E_u = \sqrt{E_{\parallel}^2 + E_{\perp}^2} = (ql/4\pi\epsilon_0 r^3) \sqrt{4 \cos^2\theta + \sin^2\theta}$ and $\tan\psi = E_{\perp}/E_{\parallel} = \sin\theta/2 \cos\theta$. So the answer is (cf. Figure 4.1c)

$$F = QE_u = \frac{Qu (1 + 3 \cos^2\theta)^{1/2}}{4\pi\epsilon_0 r^3} \quad (4.7)$$

and

$$\tan\psi = \frac{\tan\theta}{2}. \quad (4.8)$$

A free charge will therefore move along the field lines E_u or lines of force QE_u of a fixed dipole, as drawn in Figure 4.1c. In contrast, a free dipole near a fixed charge will experience a torque, causing it to rotate until its negative charge $-q$ points toward the positive charge $+Q$, after which it will move in a straight line (along r) toward the charge. In both cases, however, the actual trajectories will be much more complex due to inertial and viscous effects, since the full equations of motion must include both inertial terms of the type $m\ddot{x}$ and viscous terms of the type $\eta\dot{x}$. Then, on coming into contact, additional steric effects—determined by the specific sizes and shapes of the ion and dipolar molecules—ultimately determine their lowest energy configuration.

4.4 Ions in Polar Solvents

When ion-water interactions take place in bulk water, the above energies are reduced by a factor of about 80, the dielectric constant of water. Even then, however, the strength of the interaction will exceed kT for small divalent and multivalent ions, and it is by no means negligible for small monovalent ions. But before we proceed, it is essential to understand what this interaction energy means. It cannot be the energy gained on bringing a water molecule up to an ion *in bulk water*, since this process must also involve removing one of the water molecules that was originally in contact with the ion and placing it where the guest water molecule was before it started on its journey. That is, the whole process is no more than an *exchange* of two water molecules and cannot result in any overall change of free energy.

However, clearly, a water molecule in bulk water is in a different state from a water molecule near an ion, and then we want to know the energy difference associated with these two states. Referring to Eq. (4.5) for the ion-water interaction in bulk water, we note that it contains an orientation term $\cos \theta$. At large separations the water molecules would be randomly oriented relative to the ion, and if they remained randomly oriented right up to the ion, the interaction energy *would* be zero, since the spatial average of $\cos \theta$ is zero. For an ion in a polar solvent, Eq. (4.5) therefore gives us an estimate of the free energy change brought about by *orienting* the polar solvent molecules around the ion—that is, the reference state of zero energy is for randomly oriented dipoles.

We have therefore established that the ion-dipole energies calculated for ions in water are comparable to or greater than kT and, from Eq. (2.30), reflect the strong aligning effect that small ions must have on their surrounding water molecules.

4.5 Strong Ion-Dipole Interactions in Water: Hydrated Ions

For small or multivalent ions in highly polar solvents such as water,² the strong orientation dependence of their ion-dipole interaction will tend to orient the solvent molecules around them, favoring $\theta = 0^\circ$ near cations and $\theta = 180^\circ$ near anions (cf. inset in Figure 4.2). Thus, in water Li^+ , Be^{2+} , Mg^{2+} , and Al^{3+} ions have a number of water molecules orientationally bound to them. Such ions are called *solvated ions* or *hydrated ions*, and the number of water molecules they bind—usually between 4 and 6 is known as their *hydration number* (Table 4.2). It should be noted, however, that these bound water molecules are not completely immobilized and that they do move and exchange with bulk water, albeit more slowly. The hydration number is more of a qualitative indicator of the degree to which ions bind water rather than an exact value.

²Water is not only polar but also a hydrogen-bonding liquid (Chapter 8). Not all polar molecules are hydrogen-bonding, but all hydrogen-bonding molecules are polar. Some interactions are due to the polarity (i.e., finite dipole moment) of molecules, others to their hydrogen-bonding, and some to both. This can be confusing, and as discussed in Chapter 8, there is still no unambiguous and clear-cut distinction between these two interactions.

Table 4.2 Hydrated radii and Hydration Numbers of Ions in Water (Approximate)

Ion	Bare ion radius (nm)	Hydrated radius (nm)	Hydration number (± 1)	Lifetime/exchange rate (s)
H_3O^+	—	0.28	3	—
Li^+	0.068	0.38	5	5×10^{-9}
Na^+	0.095	0.36	4	10^{-9}
K^+	0.133	0.33	3	10^{-9}
Cs^+	0.169	0.33	1	5×10^{-10}
Be^{2+}	0.031	0.46	4 ^a	10^{-3}
Mg^{2+}	0.065	0.43	6 ^a	10^{-6}
Ca^{2+}	0.099	0.41	6	10^{-8}
Al^{3+}	0.050	0.48	6 ^a	0.1–1
Cr^{3+}	0.052	—	6 ^a	>3 hrs
OH^-	0.176	0.30	3	
F^-	0.136	0.35	2	
Cl^-	0.181	0.33	1	$\sim 10^{-11}$
Br^-	0.195	0.33	1	$\sim 10^{-11}$
I^-	0.216	0.33	0	$\sim 10^{-11}$
NO_3^-	0.264	0.34	0	
$\text{N}(\text{CH}_3)_4^+$	0.347	0.37	0	

The hydration number gives the number of water molecules in the primary hydration shell (Fig. 3.4), though the total number of water molecules affected can be much larger and depends on the method of measurement. Similarly, the hydrated radius depends on how it is measured. Different methods can yield radii that can be as much as 0.1 nm smaller or larger than those shown. Table compiled from data given by Nightingale (1959), Amis (1975), Saluja (1976), Bockris and Reddy (1970), and Cotton and Wilkinson (1980).

^aNumber of water molecules forming a stoichiometric complex with the ion—for example, $[\text{Be}(\text{H}_2\text{O})_4]^{2+}$.

Closely related to the hydration number is the effective radius or *hydrated radius* of an ion in water, which is larger than its real radius (i.e., its crystal lattice radius), as shown in Table 4.2. Because *smaller* ions are more hydrated due to their more intense electric field they tend to have *larger* hydrated radii than larger ions. However, *very small* ions such as Be^{2+} have lower hydration numbers because they are too small for more than 4 water molecules to pack around them. Hydration numbers and radii can be deduced from measurements of the viscosity, diffusion, compressibility, conductivity, solubility, and various thermodynamic and spectroscopic properties of electrolyte solutions, and the results rarely agree with one another (Amis, 1975; Saluja, 1976).

More insight into the nature of ion hydration can be gained by considering the average time that water molecules remain bound to ions. In the pure liquid at room temperature the water molecules tumble about with a mean reorientation time or *rotational correlation time* of about 10^{-11} s. This also gives an estimate of the lifetime of the water-water bonds formed in liquid water (the hydrogen bonds).³ But when the water molecules are

³These times may be compared to the *intramolecular* vibrational or stretching time of the water molecule of approximately 10^{-14} s.

near ions, various techniques, such as oxygen nuclear magnetic resonance, x-ray and neutron diffraction, and IR or Raman spectroscopy, show that the mean lifetimes or exchange rates of water molecules in the first hydration shell⁴ can be much longer, varying from 10^{-11} s to many hours (Hertz, 1973; Cotton and Wilkinson, 1980). For very weakly solvated ions (usually large monovalent ions) such as $\text{N}(\text{CH}_3)_4^+$, Cl^- , Br^- , and I^- , these lifetimes are not much different from that for water in bulk water, and they can even be shorter (referred to as *negative hydration*).

Cations are generally more solvated than anions of the same valency, since they are smaller—having lost rather than gained an electron. Thus, for K^+ , Na^+ , and Li^+ , the residence times of water molecules in the primary hydration shells are about 10^{-9} s. Divalent cations are always more strongly solvated than monovalent cations, and for Ca^{2+} and Mg^{2+} , the bound water lifetimes are about 10^{-8} s and 10^{-6} s, respectively. Even longer lifetimes are observed for very small divalent cations such as Be^{2+} (10^{-3} s), while for trivalent cations such as Al^{3+} and Cr^{3+} these can be seconds or hours. In such cases the binding is so strong that an ion-water complex is actually formed of fixed stoichiometry (see Table 4.2). In fact, these quasi-stable complexes begin to take on the appearance of (charged) molecules and are often designated as such—for example, $[\text{Mg}(\text{H}_2\text{O})_6]^{2+}$, $[\text{Be}(\text{H}_2\text{O})_4]^{2+}$. Small divalent and especially trivalent cations have a weak but well-defined second hydration shell (Bergström et al., 1991).

Protons H^+ always associate with one water molecule, which goes by the name of the *hydronium ion* or *oxonium ion* H_3O^+ , while three water molecules are solvated around this ion to form $\text{H}_3\text{O}^+(\text{H}_2\text{O})_3$. Likewise, the hydroxyl ion OH^- is believed to be solvated by three water molecules forming $\text{OH}^-(\text{H}_2\text{O})_3$. The structure of the hydronium ion H_3O^+ is believed to be planar, with two positive charges and one negative charge at the three apices of an equilateral triangle.

4.6 Solvation Forces, Structural Forces, and Hydration Forces

The first shell of water molecules around a strongly solvated ion is usually referred to as the *first* or *primary hydration shell*. This is where the water molecules are “structured” most—in other words, restricted in their positional and orientational “order”⁵ and in their motion. But the effect does not end there; it propagates beyond the first shell, only much more weakly. This is because the water molecules in the first hydration shell interact directly with the charged ion (a solute-solvent interaction), while those in the second and subsequent shells interact only with other water molecules (solvent-solvent interaction) and only indirectly with the ion. The effect on the water structure is therefore very much

⁴Also known as the *primary* hydration shell and the *inner* hydration shell (Fig. 3.4).

⁵Various “order parameters” are commonly used to define the degree to which molecules sample different regions or angles of space. These vary between 0 for a totally random distribution of molecules (corresponding to complete “disorder”) to 1 for totally immobilized, identically orientated molecules.

weaker beyond the first layer and can often be ignored—although this really depends on what interaction or phenomenon one is looking at—except around small multivalent ions such as Cr^{3+} and Al^{3+} .

Later we shall find that other types of interactions can also lead to a modified molecular ordering around solute molecules and surfaces and that the effect decays roughly exponentially with distance, extending a few molecular diameters. We may refer to this region of modified *solvent structure* as the *solvation zone* wherein the properties of the solvent (e.g., density, positional and orientational order, and mobility) are significantly different from the corresponding bulk values, as was shown schematically in Figure 2.1b.

The existence of a solvation zone around dissolved ions, molecules, or particle surfaces in a solvent medium occurs whenever there are strong solute-solvent interactions (e.g., strong ion-dipole interactions in water) and has some important consequences. First, it affects the local dielectric constant of the solvent, since the solvent molecules no longer respond to an electric field as they would in the bulk. The restricted mobility of water molecules around small ions would suggest that the effective dielectric constant should be lower in the solvation zone than in the bulk liquid. However, since the dielectric constant of ice is actually higher than that of liquid water (see Figure 8.1), the reverse may occur (see Epstein et al., 1983). At present these effects are not well understood, but it is clear that solvation zones cannot be treated entirely in terms of continuum theories, since they arise from highly specific solute-solvent and modified solvent-solvent interactions occurring at the molecular level.

Second, when the solvation zones of two solvated molecules or surfaces overlap, a short-range force arises that again cannot be treated in terms of continuum models. For example, if the local dielectric constant of water around strongly solvated ions differs from 80, the short-range Coulomb interaction would be modified (Fig. 3.4). But this is only one aspect of the problem. There has been much recent theoretical and experimental activity aimed at unraveling all the subtle effects associated with these solvent-mediated interactions that they are now usually referred to as *solvation* or *structural forces* and, when water is the solvent, *hydration* forces. The nature of solvation forces are investigated further in Chapters 7 and 15.

4.7 Dipole-Dipole Interactions

When two polar molecules are near each other, there is a dipole-dipole interaction between them that is analogous to that between two magnets. For two point dipoles of moments u_1 and u_2 at a distance r apart and oriented relative to each other as shown in Table 2.2, the interaction energy may be derived by a procedure similar to that used in Section 4.3 to obtain the energy for the charge-dipole interaction, and we find

$$w(r, \theta_1, \theta_2, \phi) = -\frac{u_1 u_2}{4\pi\epsilon_0\epsilon r^3} [2 \cos \theta_1 \cos \theta_2 - \sin \theta_1 \sin \theta_2 \cos \phi]. \quad (4.9)$$

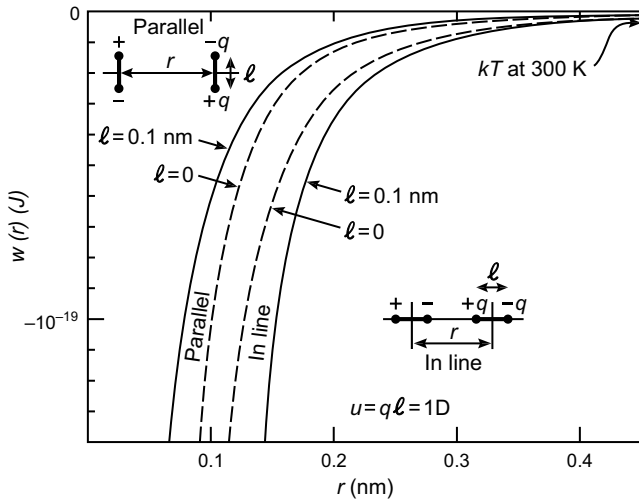


FIGURE 4.3 Dipole-dipole interaction energy in a vacuum between two dipoles each of moment 1 D. Note how much weaker this interaction is compared to the charge-dipole interaction (Figure 4.2) and the large effect of finite dipole size.

Equation (4.9) shows that maximum attraction occurs when two dipoles are lying in line, when the energy is given by

$$w(r, 0, 0, \phi) = -2u_1u_2/4\pi\epsilon_0\epsilon r^3, \quad (4.10)$$

while for two dipoles aligned parallel to each other, the energy $w(r, 90^\circ, 90^\circ, 180^\circ)$ is half of this value at the same interdipole separation, r . Equation (4.9) also shows that for two equal dipoles of moments 1 D, their interaction energy in a vacuum will equal kT at $r = 0.36$ nm when the dipoles are in line and at $r = 0.29$ nm when parallel (or antiparallel). Since these distances are of the order of molecular separations in solids and liquids, we see that at normal temperatures dipolar interactions (alone) are strong enough to bind only very polar molecules.

Figure 4.3 shows the variation of the pair interaction energy with distance for two dipoles of moments 1 D approaching each other at different orientations; the solid curves are the exact solutions for finite-sized dipoles, here assumed to be of length $l = 0.1$ nm, while the dashed curves are based on Eq. (4.9) for two point dipoles. In general we find that, even more than for the charge-dipole interaction, significant deviations from the ideal behavior now occur for $r < 3l$, when Eq. (4.9) can no longer be used. At these smaller separations it is again necessary to analyze the interaction in terms of its individual charge-charge (Coulombic) contributions, of which there will be four such terms for each pair of dipoles.

The above calculations, and Figure 4.3, appear to indicate that two dipoles always prefer to mutually orient themselves in line, but this is true only for the same value of r . Most dipolar molecules are also anisotropic in shape being longer along the direction of the dipole, so in practice the centers of two such cigar-shaped molecules can come

significantly closer together when they align in parallel, thereby making this interaction the more favorable one.

4.8 Magnetic Dipoles

Magnetic dipole-dipole forces have the same inverse cube pair-potential as electric dipoles— $w(r) \propto m_1 m_2 / r^3$ —where m_1, m_2 are the *magnetic* dipole moments. However, the magnetic forces between molecules are much weaker than the electrostatic forces, although they become more important for larger molecules or particles, as occurs for magnetic colloids and ferrofluids. This is because electric dipole moments usually increase in proportion to the length or diameter of a molecule—say, L —so for two contacting dipoles, their electric dipole-dipole interaction energy will go as $L^2/L^3 \propto 1/L$. In contrast, magnetic dipole moments usually increase with the volume of the molecule or particle, so the corresponding interaction energy goes as $L^6/L^3 \propto L^3$. Thus, magnetic interactions become more important for larger particles. As a further comparison, the gravitational interaction energy varies as $L^6/L \propto L^5$, so for very large particles (planets, etc.) their gravitational interaction eventually takes over as the dominant one.

Magnetic colloidal particles,⁶ as well as spherical beads with bar magnets inside them, tend to associate into linear strings where all the dipoles point in the same direction along the string. This occurs because, as shown by Eq. (4.9), two dipoles at a given separation have the greatest attraction for each other when they are “in-line.” Applying an external magnetic field will orient these strings along the field. In more concentrated systems the strings associate with one another to form bundles and, eventually, a close-packed lattice of magnetic particles.

4.9 Hydrogen Bonds

The electric dipole-dipole interaction is not as strong as the previous two electrostatic interactions we considered—the charge-charge and ion-dipole interactions—and for dipole moments of order approximately 1 D, it is already weaker than kT at distances of about 0.35 nm in a vacuum, while in a solvent medium this distance will be even smaller. This means that the dipole-dipole interaction, unlike the ion-dipole interaction, is usually not strong enough to lead to any strong mutual alignment of polar molecules in the liquid state. There are some exceptions, however, such as water, whose small size and large dipole moment does lead to short-range association in the liquid. A glance at Table 4.1 shows that the bond moments of O[−]–H⁺, N[−]–H⁺, and F[−]–H⁺ are unusually large. Since the electron-depleted H atom also has a particularly small size, this means that other *electronegative* atoms such as O[−], N[−], and F[−] can get quite close to these highly polar

⁶The interactions of colloidal particles are discussed in detail in Part II. Their size is in the microscopic regime (anything from 0.01 to 100 μm), and they are generally in a liquid medium where they remain “dispersed.” A “colloid” is a dispersion of colloidal particles in solution.

X^-H^+ groups and thus experience an unusually strong field. The resulting bond is known as the *hydrogen bond*, which is depicted by $-\text{X}^-\cdots\text{H}^+-$. Hydrogen bonds can be strongly attractive and moderately directional, so they can orient neighboring molecules such as H_2O , NH_3 , and HF , and groups such as $>\text{C}=\text{O}$, in both the solid, liquid, and gaseous states. Such liquids are called *associated liquids* (cf. Table 2.1).

The hydrogen bonding interaction is no more than a particularly strong type of directional dipole-dipole interaction. Because of the small size of the $-\text{H}^+$ group, it is far stronger than that predicted by the point dipole approximation (compare the energies of the dashed and solid lines at the same separation r in Figure 4.3). This interaction is discussed further in Chapter 8. For the moment, we will proceed to investigate the opposite situation: when the orientation dependencies of dipole-dipole and ion-dipole interaction energies are much *weaker* than the thermal energy kT and, therefore, unable to fully align molecules.

4.10 Rotating Dipoles and Angle-Averaged Potentials

At large separations or in a medium of high ϵ , when the angle dependence of the interaction energy falls below the thermal energy kT , dipoles can now rotate more or less freely. However, even though the values of $\cos \theta$, $\sin \theta$, and so on, when averaged over all of space are zero, the angle-averaged *potentials* are not zero, since there is always a Boltzmann weighting factor that gives more weight to those orientations that have a lower (more negative) energy.

In general, the angle-averaged free energy $w(r)$ of an instantaneous orientation-dependent free energy $w(r, \Omega)$ is given by the *potential distribution theorem* (Rushbrooke, 1940; Widom, 1963; Landau and Lifshitz, 1980)

$$e^{-w(r)/kT} = \int e^{-w(r,\Omega)/kT} d\Omega / \int d\Omega = \left\langle e^{-w(r,\Omega)/kT} \right\rangle, \quad (4.11)$$

where $d\Omega = \sin \theta d\theta d\phi$ corresponds to the *polar* and *azimuthal* angles θ and ϕ (see Table 2.2/cf. Figure 4.1) and the integration is over all of angular space. Accordingly, the denominator in Eq. (4.11) becomes

$$\int d\Omega = \int_0^{2\pi} d\phi \int_0^\pi \sin \theta d\theta = 4\pi \quad (4.12)$$

so that in general we may write

$$e^{-w(r)/kT} = \left\langle e^{-w(r,\theta,\phi)/kT} \right\rangle = \frac{1}{4\pi} \int_0^{2\pi} d\phi \int_0^\pi e^{-w(r,\theta,\phi)/kT} \sin \theta d\theta. \quad (4.13)$$

At this point we may note that the spatially averaged values of some angles:⁷

⁷This is in three dimensions. In two dimensions—for example, on a surface—the only difference is that $\langle \cos^2 \theta \rangle = \langle \sin^2 \theta \rangle = \frac{1}{2}$.

$$\begin{aligned}
 \langle \cos^2 \theta \rangle &= \frac{1}{4\pi} \int_0^\pi \cos^2 \theta \sin \theta d\theta \int_0^{2\pi} d\phi = \frac{1}{3}, \\
 \langle \sin^2 \theta \rangle &= \frac{2}{3}, \\
 \langle \sin^2 \phi \rangle &= \langle \cos^2 \phi \rangle = \frac{1}{2}, \\
 \langle \sin \theta \rangle &= \langle \cos \theta \rangle = \langle \sin \theta \cos \theta \rangle = 0, \\
 \langle \sin \phi \rangle &= \langle \cos \phi \rangle = \langle \sin \phi \cos \phi \rangle = 0.
 \end{aligned} \tag{4.14}$$

When $w(r, \Omega)$ is less than kT , we can expand Eq. (4.11):

$$e^{-w(r)/kT} = 1 - \frac{w(r)}{kT} + \dots = \left\langle 1 - \frac{w(r, \Omega)}{kT} + \frac{1}{2} \left(\frac{w(r, \Omega)}{kT} \right)^2 - \dots \right\rangle,$$

thus

$$w(r) = \left\langle w(r, \Omega) - \frac{w(r, \Omega)^2}{2kT} + \dots \right\rangle. \tag{4.15}$$

The angle-averaged free energy for the *charge-dipole interaction* is therefore, using Eq. (4.5) for $w(r, \Omega)$,

$$\begin{aligned}
 w(r) &= \left\langle -\frac{Qu \cos \theta}{4\pi\epsilon_0\epsilon r^2} - \left(\frac{Qu}{4\pi\epsilon_0\epsilon r^2} \right)^2 \frac{\cos^2 \theta}{2kT} + \dots \right\rangle \\
 &\approx -\frac{Q^2 u^2}{6(4\pi\epsilon_0\epsilon)^2 kTr^4} \quad \text{for} \quad kT > \frac{Qu}{4\pi\epsilon_0\epsilon r^2},
 \end{aligned} \tag{4.16}$$

which is attractive and temperature dependent. Thus, for a monovalent ion interacting with the polar solvent molecules of a medium of dielectric constant ϵ , Eq. (4.16) will supersede Eq. (4.5) at distances larger than $r = \sqrt{Qu/4\pi\epsilon_0\epsilon kT}$, which for a monovalent ion in water, setting $Q = e$, $u = 1.85$ D, $\epsilon = 80$, becomes roughly 0.2 nm (i.e., about 0.1 nm out from an ion of radius 0.1 nm). We can now see why only water molecules of the first shell around ions sometimes become strongly restricted in their motion, and we may anticipate that this should be the sort of range around an ion over which the properties of the solvent may be substantially different from the bulk values.

For the *dipole-dipole interaction*, a similar Boltzmann averaging of the interaction energy, Eq. (4.11), over all orientations (which now involves averaging over two polar angles θ_1 and θ_2 , and one azimuthal angle ϕ as shown in Table 2.2) leads to an angle-averaged interaction free energy of

$$w(r) = -\frac{u_1^2 u_2^2}{3(4\pi\epsilon_0\epsilon)^2 kTr^6} \quad \text{for} \quad kT > \frac{u_1 u_2}{4\pi\epsilon_0\epsilon r^3}. \tag{4.17}$$

The Boltzmann-averaged interaction between two permanent dipoles is usually referred to as the *orientation* or *Keesom* interaction. It is one of three important interactions, each varying with the inverse sixth power of the distance, that together contribute to the total *van der Waals* interaction between atoms and molecules. Van der Waals forces will be discussed collectively in Chapter 6.

Equations (4.16) and (4.17) show that beyond a certain distance the interaction energies fall faster than $1/r^3$. In view of the analysis of Section 1.6, this confirms that neither ion-dipole nor dipole-dipole forces can produce long-range alignment effects in liquids. Note that the expressions for these interactions become modified in two dimensions—for example, for molecules interacting on a surface (see footnote 7 and Problem 4.5)—but the distance-dependence does not change, so neither does the above conclusion.

All the energy expressions derived so far give the *free* energies of the interactions, strictly the Helmholtz free energies (Rushbrooke, 1940), since the interactions are implicitly assumed to occur at constant volume. From basic thermodynamics the Helmholtz free energy A of any system or interaction is related to the *total* internal energy U by the well-known Gibbs-Helmholtz equation

$$U = A + TS = A - T(\partial A / \partial T)_V = -T^2 \partial(A/T) / \partial T, \quad (4.18)$$

where S is the entropy of the system. Thus, for the angle-averaged dipole-dipole (Keesom) interaction in a vacuum ($\varepsilon = 1$), we find

$$U = -\frac{2u_1^2 u_2^2}{3(4\pi\varepsilon_0)^2 kTr^6}, \quad (4.19)$$

which is twice the *free* energy, Eq. (4.17), with which it is often confused in the literature. Note, too, that in condensed phases, the Helmholtz and Gibbs free energies, A and G , are essentially the same, since they are related by $G = A + PV$, where the PV term is usually small.

The distinction between A and U does not arise for temperature-independent pair interactions, since then $U = A - T(\partial A / \partial T)_V = A$.

4.11 Entropic Effects

The reason why the interaction free energy (the energy available for doing work or the energy that gives the force) is less than the total internal energy of two interacting dipoles is because some of the energy is taken up in aligning the dipoles as they approach each other. This unavailable part of the energy is associated with the entropic contribution to the interaction. Let us complete this chapter by considering these entropic effects a bit further.

From Eq. (4.18) the free energy may be written as⁸

$$A = U - TS = U + T(\partial A / \partial T) \quad (4.20)$$

⁸In this section, *intensive* thermodynamic variables are denoted in bold type, and *extensive* variables by normal font.

so there is an entropic contribution $T(\partial A/\partial T)$ that must be added to the total energy (or subtracted from it if it is negative) before we can know the available energy of an interaction. For example, for both the charge-dipole and dipole-dipole angle-averaged interactions in a vacuum, we find that since $A \propto -1/T$,

$$T(\partial A/\partial T) = -A, \quad (4.21)$$

so that

$$A = U - A = \frac{1}{2}U. \quad (4.22)$$

Thus, half the total energy is absorbed internally, that is, unavailable for work, during the interaction. This is analogous to the situation in Worked Example 2.5 in Section 2.10 where half of the energy transferred from one molecule to another during a collision went into internal (thermal vibrational) energy and half to kinetic energy of the molecule. In the present case the internal energy is taken up in decreasing the rotational freedom of the dipoles as they become progressively more aligned on approach. Since A is negative, the entropic contribution $T(\partial A/\partial T)$ to the free energy is *positive*—that is, unfavorable—and since $S = -(\partial A/\partial T)$ is negative, we would say that the interaction is associated with a *loss of entropy* (cf. Problem 4.8).

Entropic effects can arise even if the interaction energy does not have an explicit temperature dependence. All that is required is for the interaction to take place in a solvent of finite dielectric constant, or even in a vacuum if the dielectric constant of the molecule or particle appears in the expression for the pair potential or self-energy (as occurs in the case of van der Waals forces). This is because dielectric constants are usually temperature-dependent, especially in the case of polar solvents such as water. For example, for the Coulomb energy $A = +Q_1 Q_2 / 4\pi\epsilon_0\epsilon r$, we find that

$$TS = -T\left(\frac{\partial A}{\partial T}\right) = \frac{Q_1 Q_2}{4\pi\epsilon_0\epsilon r}\left(\frac{T}{\epsilon}\frac{\partial\epsilon}{\partial T}\right) = A\left(\frac{T}{\epsilon}\frac{\partial\epsilon}{\partial T}\right), \quad (4.23)$$

and likewise for the Born energy, $A = +Q^2 / 8\pi\epsilon_0\epsilon a$,

$$TS = -T\left(\frac{\partial A}{\partial T}\right) = \frac{Q^2}{8\pi\epsilon_0\epsilon a}\left(\frac{T}{\epsilon}\frac{\partial\epsilon}{\partial T}\right) = A\left(\frac{T}{\epsilon}\frac{\partial\epsilon}{\partial T}\right), \quad (4.24)$$

while for the angle-averaged charge-dipole and dipole-dipole interactions in a medium, we obtain

$$TS = -T\left(\frac{\partial A}{\partial T}\right) = A\left(1 + \frac{2T}{\epsilon}\frac{\partial\epsilon}{\partial T}\right), \quad (4.25)$$

where the first contribution to the entropy is associated with the orientational motion of the interacting *solute* dipoles as before [cf. Eq. (4.21)] and the second with the *solvent* molecules.

All the above entropic contributions that depend on $\partial\varepsilon/\partial T$ arise from changes in the configurations of the solvent molecules associated with these interactions. For water,

$$\frac{T}{\varepsilon} \frac{\partial\varepsilon}{\partial T} = -1.36 \quad \text{at } 25^\circ C, \quad (4.26)$$

which is negative. This allows us to make a number of interesting predictions concerning the effects of interactions on the surrounding water molecules. Thus, for the Born interaction, Eq. (4.24) shows that S is negative. We may therefore conclude that the solvation of ions by water is accompanied by a *decrease* in entropy, which indicates once again that water molecules become restricted in their translational and rotational freedom when they solvate ions. On the other hand, Eq. (4.23) shows that when two ions of *opposite* sign approach each other in a medium, the entropy of the solvent *increases*. This occurs because some of the motionally restricted water molecules around the ions are liberated into the solvent as the ions come together.

The above considerations bring out the remarkable feature of the dielectric constant in that it contains information on the entropic changes of the solvent and solute molecules involved in an interaction. We shall make use of this property again when we consider other types of interactions.

PROBLEMS AND DISCUSSION TOPICS

- 4.1** A free, positively charged ion A is placed close to a fixed dipolar molecule in a liquid medium. By considering the electric field lines emanating from the dipole (see Figure 4.1b and c), in what direction will A move if it is placed (i) somewhere along the long axis (along $\theta = 0$), and (ii) somewhere along the perpendicular bisector (at $\theta = 90^\circ$) of the dipolar molecule? In another situation, A is a free cigar-shaped dipolar molecule. (iii) How will A orient and then move with respect to the fixed dipole when it is placed in the same two positions as the above? Under natural or laboratory-controlled conditions, an ion or molecule is not “placed” somewhere but nevertheless “gets there” due to random or directed motion. Describe some of these motions.
- 4.2** Certain linear molecules such as $O=CH-CH=CH-CH=CH-NH_2$ containing conjugated bonds are easily polarizable by an electric field that causes intramolecular charge separation resulting in a highly dipolar molecule such as $\overset{-}{O}-CH=CH-CH=CH-CH=N^+H_2$. A nonpolar but easily polarizable molecule of length $l = 1$ nm acquires a dipole moment $u = el$ due to a potential of $\psi = 1$ V acting along its length. The resulting unit charges $\pm e$ at either end of the molecule are pulled by the field $E = \psi/l$ in opposite directions, which acts to *increase* the length of the molecule. However, these same charges attract each other with a Coulomb force that acts to *decrease* the length of the molecule. Does the molecule expand or contract? [Hint: In this example consider whether the charge separation and induced dipole has occurred due to an internal Harpooning effect.]

- 4.3** Look at Figure 3.3. Assume glycine to be a molecule with a dipole of unit charges $\pm e$ at a distance l apart. Estimate l from the data of Figure 3.3. Also, from the intercept of the line estimate the additional nonelectrostatic free energy contribution associated with the transfer of a molecule of glycine into a polar medium. If the glycine molecule is assumed to be spherical with diameter σ equal to l (as obtained previously), what would be the free energy per unit surface area γ of this non-electrostatic transfer process? Are the values you obtain for l , σ , and γ reasonable?
- 4.4***
- (i) What is the energy of a macroscopic sphere of material A and radius a in a liquid medium B , where γ_i is the interfacial energy of the A - B interface? For water and hydrocarbon liquids (e.g., alkanes, oils, etc.) the value of γ_i is about 50 mJ m^{-2} . Estimate the solubility of small hydrocarbon molecules such as methane in water at 20°C , in mole fraction units, assuming that these molecules behave as small macroscopic spheres of radius $a = 0.2 \text{ nm}$, and compare your result with the experimental value of approximately 0.0027 mole/mole .
 - (ii) An inert nonpolar oil is in contact with an aqueous 1:1 electrolyte solution (i.e., a salt of monovalent ions such as NaCl) whose cations and anions have the same bare-ion radii of $a = 0.10 \text{ nm}$. If the salt concentration in the water is 1 mM ($10^{-3} \text{ mol/litre}$), calculate the ionic concentration in the oil phase. Assume that the dielectric constants of oil and water are 2.0 and 78, respectively, and that the temperature is $T = 25^\circ\text{C}$. What would be the concentration if the ions had a radius of 0.08 nm ?
 - (iii) In practice, the concentration of ions in nonpolar hydrocarbon liquids is found to be much higher than any value calculated based on bare-ion radii—for example, Eq. (3.11) for the Born energy—because ions can enter these liquids surrounded by a certain number of water molecules—that is, as hydrated ions. Show that by going into the hydrocarbon phase ($\epsilon_{\text{hc}} \approx 2$) with a single layer of water ($\epsilon_w \approx 78$) around it, the total self-energy energy of the hydrated ion in oil is much reduced. Derive an expression for the radius and self-energy of the hydrated ion (assume a hydrocarbon-water interfacial energy of $\gamma_i = 50 \text{ mJ m}^{-2}$). Estimate the optimal radius of these hydrated ions in oil and their hydration number, and then calculate a new and more realistic value for the concentration of ions in the oil. Does your answer also explain why the partitioning and diffusion of monovalent ions in hydrocarbon liquids is roughly the same for ions of a different size? Would you expect the experimental values of the solubilities or partitioning of ions to be higher or lower than your calculated result? [Answer to (iii): Radius of hydrated ion $\approx 0.36 \text{ nm}$, largely independent of a , self-energy $\approx 56 \text{ kT}$, down from $\approx 136 \text{ kT}$ for an unhydrated ion of radius $a = 0.1 \text{ nm}$.]
- 4.5***
- (i) Derive Eq. (4.17) for the angle-averaged interaction potential for two dipolar molecules in free space.
 - (ii) Show that the angle-averaged potential for two dipolar molecules constrained to interact on a surface with their dipoles freely rotating but always lying in the plane of the surface—the two-dimensional Keesom

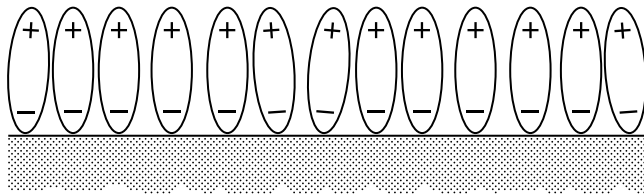


FIGURE 4.4

energy—is $w(r) = -5u_1^2 u_2^2 / 8(4\pi\epsilon_0)^2 kTr^6$. You will need to derive the corresponding two-dimensional values of $\langle \cos^2 \theta \rangle$, $\langle \sin^2 \theta \rangle$, and so on, that replace those of Eq. (4.14). (iii) Obtain an expression for the mean interaction energy per molecule for a surface monolayer consisting of mobile molecules whose dipoles are aligned *perpendicular* to the surface, as shown in Figure 4.4, where each molecule occupies a mean area A . Assume the dipoles have charges $\pm e$ a distance l apart (the dipole moment being $u = el$). What is the main difference between the last two interactions (ii) and (iii) concerning their contributions to two-dimensional phase transitions? [Hint: Consider the signs of their contributions to the two-dimensional van der Waals equation of state.]

- 4.6 Without resorting to mathematical calculation, deduce whether the electrostatic force between two similar but free surfaces each composed of a lattice of vertical dipoles as shown in Figure 4.4 is attractive or repulsive. Consider both the symmetric and asymmetric cases—in other words, where the dipoles of the two lattices point toward each other (symmetric case), and (ii) where they all point in the same direction (asymmetric case). [Answer: Attractive in both cases.]
- 4.7 The angle averaged Helmholtz free energy A of the dipole-dipole interaction $w(r)$ is related to the angle-dependent potential $w(r, \Omega)$ via Eq. (4.11): $e^{-w(r)/kT} = \langle e^{-w(r,\Omega)/kT} \rangle$. Show that for $w(r, \Omega) < kT$, the internal energy $U(r)$ is related to $w(r, \Omega)$ via

$$U(r) = \left\langle w(r, \Omega) e^{-w(r,\Omega)/kT} \right\rangle, \quad (4.27)$$

and use this to derive Eq. (4.19).

- 4.8 In Section 4.11 it is shown that the entropy change associated with certain electrostatic and attractive dipolar interactions is negative, and yet by the Second Law of Thermodynamics all spontaneous interactions must be accompanied by an increase in entropy. Resolve this apparent paradox.

Interactions Involving the Polarization of Molecules

5.1 The Polarizability of Atoms and Molecules

We now enter the last category of electrostatic interactions that we shall be considering: those that involve molecular *polarization*. This involves the dipole moments induced in molecules by the electric fields emanating from nearby molecules. Actually, we have already been much involved with polarization effects: whenever the macroscopic dielectric constant of a medium entered into our consideration, this was no more than a reflection of the way the molecules of the medium are polarized by the local electric field. Here we shall look at these effects in more detail, starting at the molecular level. We shall find that apart from the purely Coulombic interaction between two charges or permanent dipoles in a vacuum, all the other interactions are essentially polarization-type interactions.

All atoms and molecules are polarizable. Their (dipole) *polarizability* α is defined according to the strength of the *induced* dipole moment u_{ind} they acquire in a field E —that is,

$$u_{\text{ind}} = \alpha E. \quad (5.1)$$

For a nonpolar molecule, the polarizability arises from the displacement of its negatively charged electron cloud relative to the positively charged nucleus under the influence of an external electric field. For polar molecules, there are other contributions to the polarizability, discussed in the next section. For the moment, we shall concentrate on the polarizabilities of nonpolar molecules, which we shall denote by α_0 .

As a simple illustrative example of how polarizability arises, let us imagine a one-electron “Bohr” atom whose electron of charge $-e$ circles the nucleus of charge $+e$ at a distance R ; this would also define the radius of the atom (Figure 5.1a). If under the influence of an external field E the electron orbit is shifted by a distance l from the nucleus (Figure 5.1b), then we have for the induced dipole moment,

$$u_{\text{ind}} = \alpha_0 E = el. \quad (5.2)$$

Now the *external* force F_{ext} on the electron due to the field E is

$$F_{\text{ext}} = -eE,$$

which must be balanced at equilibrium by the attractive force between the displaced electron orbit and the nucleus. This is none other than the Coulomb force

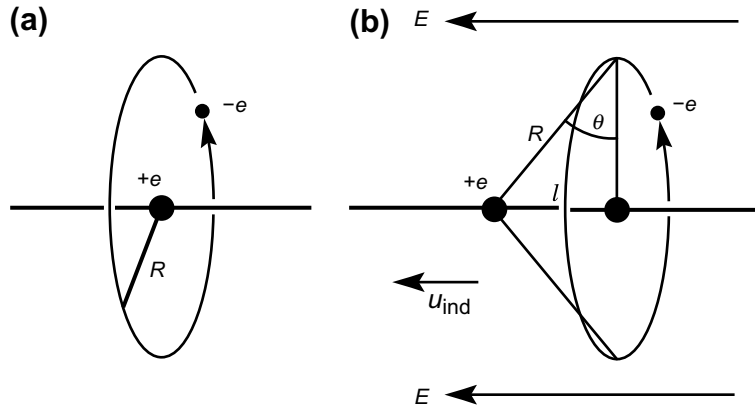


FIGURE 5.1 Induced dipole in a one-electron atom. (a) No external field, $u_{\text{ind}} = 0$. (b) In an external field E the electron's orbit is shifted by a distance l from the positive nucleus so that the induced dipole moment is $u_{\text{ind}} = el = \alpha_0 E$, where the polarizability in this case is $\alpha_0 = 4\pi\epsilon_0 R^3$.

$-e^2/4\pi\epsilon_0 R^2$ resolved along the direction of the field. The *internal* (restoring) force is therefore

$$F_{\text{int}} = \frac{-e^2}{4\pi\epsilon_0 R^2} \sin \theta \approx \frac{-e^2 l}{4\pi\epsilon_0 R^3} \approx \frac{-eu_{\text{ind}}}{4\pi\epsilon_0 R^3}. \quad (5.3)$$

At equilibrium, $F_{\text{ext}} = F_{\text{int}}$, which leads to

$$u_{\text{ind}} = 4\pi\epsilon_0 R^3 E = \alpha_0 E, \quad (5.4)$$

from which we obtain for the polarizability

$$\alpha_0 = 4\pi\epsilon_0 R^3. \quad (5.5)$$

The unit of polarizability is therefore $4\pi\epsilon_0 \times (\text{volume})$ or $\text{C}^2 \text{m}^2 \text{J}^{-1}$. For a one-electron atom of radius $R = 0.1 \text{ nm} = 10^{-10} \text{ m}$, its theoretical polarizability is therefore $\alpha_0 = 4\pi(8.854 \times 10^{-12}) \times 10^{-30} = 1.1 \times 10^{-40} \text{ C}^2 \text{m}^2 \text{J}^{-1}$. The polarizability of atoms and molecules that arises from such electronic displacements is known as the *electronic polarizability*. Its magnitude, apart from the $4\pi\epsilon_0$ term, is usually less than but of the order of the $(\text{radius})^3$ of the atom or molecule. For example, the experimental value for water is $\alpha_0/4\pi\epsilon_0 = 1.48 \times 10^{-30} \text{ m}^3 = (0.114 \text{ nm})^3$, where 0.114 nm is about 15% less than the radius of a water molecule (0.135 nm).

Table 5.1 lists the electronic polarizabilities of some common atoms and molecules. Since the electronic polarizability is associated with displacements of electron clouds, it has long been recognized that the polarizability of a molecule can be obtained by simply summing the characteristic polarizabilities of its covalent bonds, since these are where the polarizable electrons are mostly localized. Table 5.1 also lists some *bond polarizabilities*. As can be seen, the polarizability of methane, CH_4 ,

Table 5.1 Electronic Polarizabilities α_0 of Atoms, Molecules, Bonds, and Molecular Groups^a

Atoms and Molecules					
He	0.20	NH ₃	2.3	CH ₂ =CH ₂	4.3
H ₂	0.81	CH ₄	2.6	C ₂ H ₆	4.5
H ₂ O	1.45–1.48	HCl	2.6	Cl ₂	4.6
O ₂	1.60	CO ₂	2.9	CHCl ₃	8.2
Ar	1.63	CH ₃ OH	3.2	C ₆ H ₆	10.3
CO	1.95	Xe	4.0	CCl ₄	10.5
Bond Polarizabilities					
C—C aliphatic	0.48	C—H	0.65	C—Cl	2.60
C···C aromatic	1.07	O—H	0.73	C—F	0.73
C=C	1.65	C—O	0.60	Si—Si	2.24
C≡C	2.39	C=O	1.36	Si—H	1.27
Molecular Groups					
C—O—H	1.3	—CH ₂ —	1.84	CF ₃	2.4
C—O—C	1.1	CH ₃	2.0	Si—O—Si	1.4
C—NH ₂	2.0	—CF ₂ —	2.0	Si—OH	1.6

^aPolarizabilities α_0 are given in volume units of $(4\pi\epsilon_0)\text{\AA}^3 = (4\pi\epsilon_0)10^{-30} \text{ m}^3 = 1.11 \times 10^{-40} \text{ C}^2 \text{ m}^2 \text{ J}^{-1}$. Note that when molecules are dissolved in a solvent medium, their polarizability can change by up to 10%. Data compiled from *CRC Handbook of Chemistry and Physics*, 87th Edition (2006–2007), Denbigh (1940), Hirschfelder et al., (1954), and Smyth (1955).

is simply four times that of the C—H bond (i.e., $\alpha_{\text{CH}_4} = 4\alpha_{\text{C—H}}$). Likewise, the polarizability of ethylene, CH₂=CH₂, is given by $4\alpha_{\text{C—H}} + \alpha_{\text{C=C}}$. This additivity procedure is often accurate to within a few percent, but it can fail for molecules in which the bonds are not independent of each other (delocalized electrons, as in benzene) or when nonbonded lone-pair electrons that also contribute to the polarizability are present, as in H₂O and other hydrogen-bonding groups. Under such circumstances it has been found useful to assign polarizabilities to certain molecular groups. Some *group polarizabilities* are also included in Table 5.1. For example, the polarizability of CH₃OH is $3\alpha_{\text{C—H}} + \alpha_{\text{C—O—H}} = 4\pi\epsilon_0(3 \times 0.65 + 1.28) \times 10^{-30} = 4\pi\epsilon_0(3.23 \times 10^{-30}) \text{ m}^3$.

5.2 The Polarizability of Polar Molecules

In Section 5.1 we considered the polarizability arising solely from the electronic displacements in atoms and molecules. A freely rotating dipolar molecule (whose time-averaged dipole moment is zero) also has an *orientational* or a *dipolar polarizability*, arising from the effect of an external field on the Boltzmann-averaged orientations of the rotating dipole. Thus, in the presence of an electric field E , these orientations will no longer time-average to zero but will be weighted along the field. If at any instant the

permanent dipole u is at an angle θ to the field E , its resolved dipole moment along the field is $u \cos \theta$, and its energy in the field from Eq. (4.6) is $-uE \cos \theta$, so the angle-averaged induced dipole moment is given by

$$\begin{aligned} u_{\text{ind}} &= \left\langle u \cos \theta e^{uE \cos \theta / kT} \right\rangle \\ &= \frac{u^2 E}{kT} \left\langle \cos^2 \theta \right\rangle = \frac{u^2}{3kT} E, \quad uE \ll kT \end{aligned} \tag{5.6}$$

Since u_{ind} is proportional to the field E , we see that the factor $u^2/3kT$ provides an additional contribution to the molecular polarizability. This is the *dipolar* or *orientational* polarizability, defined by

$$\alpha_{\text{dip}} = u^2/3kT. \tag{5.7}$$

The total polarizability of a polar molecule is therefore given by the

$$\text{Debye-Langevin equation } \alpha = \alpha_0 + u^2/3kT, \tag{5.8}$$

where u is its permanent dipole moment. Thus, for example, a polar molecule of moment $u = 1 \text{ D} = 3.336 \times 10^{-30} \text{ C m}$ at 300 K will have a dipolar polarizability of

$$\alpha_{\text{dip}} = \frac{(3.336 \times 10^{-30})^2}{3(1.38 \times 10^{-23})300} = 9 \times 10^{-40} \text{ C}^2 \text{ m}^2 \text{ J}^{-1} = (4\pi\epsilon_0)8 \times 10^{-30} \text{ m}^3,$$

which is a value that is comparable to the electronic polarizabilities α_0 of molecules (cf. Table 5.1).

In very high fields or at sufficiently low temperatures such that $uE \gg kT$, a dipolar molecule will become completely aligned along the field. When this happens (e.g., water near a small ion), the molecule's dipolar polarizability is no longer given by Eq. (5.7), but the electronic polarizability contribution is still given by Eq. (5.5). In such cases, because the dipoles are already fully aligned, they no longer respond or "react" to the field, and their dipolar polarizability therefore *falls*, i.e., saturates.

5.3 Other Polarization Mechanisms and the Effects of Polarization on Electrostatic Interactions

An induced dipole gives rise to a "reaction" dipole field E_r , as shown in Figure 5.2, that enhances or opposes the inducing field E , depending on the location. In a condensed liquid or solid medium consisting of many polarizable molecules, when the reaction fields of all the induced dipoles are added up, the resulting field is known as the "polarization" field, E_p , which always opposes the inducing field E . This means that in any medium, two fields are always present: the original field E and an opposing polarization field E_p . The field E is the same inside and outside the medium, but E_p depends on the nature of the molecules making up the medium.

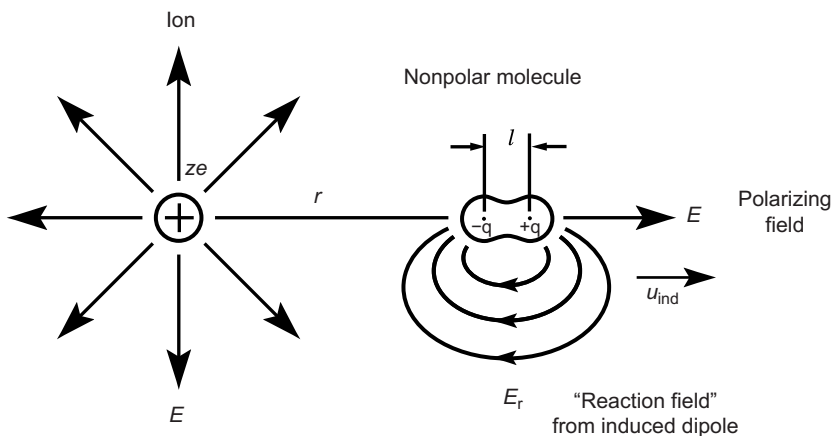


FIGURE 5.2 A neutral (nonpolar) molecule in a field E will acquire an induced dipole of moment $u_{\text{ind}} = ql = \alpha E$. The resulting force on the neutral molecule is therefore $F = q\Delta E$, where ΔE is the difference in E at either end of the dipole. Thus, $F = q(dE/dr)l = \alpha E(dE/dr)$ so that the interaction free energy is $w(r) = -\int F dr = -\frac{1}{2}\alpha E^2$ which is Eq. (5.14). This equation is quite general. If the polarizing field E is due to an ionic charge, we obtain Eq. (5.13); if due to a dipole, we obtain Eq. (5.22).

The net force on a charge Q in a medium is therefore made up of two parts that may be written as $F = (E + E_p)Q = E_{\text{eff}}Q$, where E_{eff} is the effective or total field acting on the charge. For example, the Coulomb force, $F = Q^2/4\pi\epsilon_0\epsilon r^2$, implies that the effective and polarization fields are related to the applied field E via

$$E_{\text{eff}} = E/\epsilon \quad \text{and} \quad E_p = -\left(\frac{\epsilon - 1}{\epsilon}\right)E. \quad (5.9)$$

Thus, for $\epsilon = 1$ (vacuum, gas), $E_{\text{eff}} = E$ and $E_p = 0$ —that is, there is no polarization field. For $\epsilon \gg 1$ (water, conducting medium), $E_{\text{eff}} \rightarrow 0$ and $E_p \rightarrow -E$ —that is, the polarization field almost balances the applied field. Electrostatic forces, which depend on E_{eff} , are therefore much reduced in media that have high dielectric constants.

As could be expected, the dielectric constant ϵ is related to α , with higher values for α resulting in higher values for ϵ . This relationship connects the molecular and continuum electric properties of matter and is discussed in Sections 5.5 and 5.8. However, in condensed phases there can be additional contributions to the dielectric constant of a medium that are not accounted for by the (discrete and noncooperative) electronic and dipolar polarizabilities of its individual molecules. In a condensed phase, charges can be displaced (polarized) over distances that are significantly larger than the sizes of the molecules—for example, via electron or proton hopping hydrogen-bonded networks, as is believed to occur in water, or through other conducting pathways as occurs in metals and piezoelectric materials. These large charge displacements give rise to large induced dipoles and, therefore, to the high effective polarizabilities and dielectric constants characteristic of such materials.

Worked Example 5.1

Question: An electric field is applied across a conducting medium such as a metal or salt solution whose dielectric constant is infinite ($\epsilon = \infty$). According to Eq. (5.9), there should be no net field and therefore no force on any charge inside the medium. And yet ions and electrons do conduct through such media. Resolve this paradox.

Answer: This example nicely illustrates the advantages of treating the field inside a medium as made up of *two* parts, E and E_p , having quite different origins, rather than a single effective field E_{eff} . The result also depends on whether charge is allowed to pass from one electrode to the other—in other words, whether or not the two ends are electrically connected.

Referring to Figure 5.2 as soon as the field E is applied across the medium, but before any charges have had time to become displaced by this field, the net field is E , and this field *will* act on and move any free charges inside the medium. This displacement, which is equivalent to a transient current, is what sets up the polarization field E_p . Once the charges have been displaced, they will accumulate at each end, and if they cannot move further, the system will equilibrate in this configuration. On the other hand, if the two ends are electrically connected (e.g., by a wire) and the field is maintained (e.g., by a battery), these charges will move through the wire and neutralize each other, thereby bringing the system back to its original state. The process will now be repeated or, more correctly, conduct charges through the medium continuously.

5.4 Interactions between Ions and Uncharged Molecules

When a molecule of polarizability α is at a distance r from an ion of charge ze , the electric field of the ion $E = ze/4\pi\epsilon_0\epsilon r^2$ will induce in the molecule a dipole moment of

$$u_{\text{ind}} = \alpha E = \alpha ze/4\pi\epsilon_0\epsilon r^2. \quad (5.10)$$

Worked Example 5.2

Question: Estimate the distance by which the electron cloud of a methane (CH_4) molecule is shifted relative to the center of the molecule due to the presence of a bare sodium ion whose center is 0.4 nm from the center of the molecule. Assume that the interaction occurs in air ($\epsilon = 1$)

Answer: For a monovalent ion such as Na^+ , the electric field at a distance of 0.4 nm from its center is $E = e/4\pi\epsilon_0 r^2 = (1.602 \times 10^{-19})/(4 \times 3.142 \times 8.854 \times 10^{-12})(0.4 \times 10^{-9})^2 = 9.0 \times 10^9 \text{ V m}^{-1}$. The induced dipole moment on a methane molecule is therefore, using Table 5.1,

$$\begin{aligned} u_{\text{ind}} &= \alpha_0 E = 4\pi\epsilon_0(2.6 \times 10^{-30})(9.0 \times 10^9) = 2.60 \times 10^{-30} \text{ C m} \\ &= 2.60 \times 10^{-30}/3.336 \times 10^{-30} = 0.78 \text{ D}. \end{aligned}$$

From Eq. (5.2) this corresponds to a unit charge separation in the molecule of $l = u_{\text{ind}}/e = 0.016 \text{ nm}$, which is about 8% of the molecular radius of methane (of 0.2 nm).

However, if we consider that four or more of the hydrogen electrons in CH₄ may be displaced simultaneously, this distance falls to $l = 0.004$ nm, or about 2% of the molecular radius. On the other hand, if we allow that the effective quantity of charge displaced may be some fraction of e , these distances will be greater.



From Worked Example 5.2, it appears that induced dipole moments can be of order 1 Debye, which is quite large. We may therefore anticipate that the forces associated with induced dipole moments may likewise be quite large.

We shall now consider the interaction between an ion and an uncharged molecule (see Figure 5.2). The induced dipole will point away from the ion if it is a cation and toward the ion if it is an anion. In either case this will lead to an attractive force between the ion and the polarized molecule. The “reflected” or “reaction” field of the induced dipole E_r acting back on the ion is, using Eq. (5.21)/Worked Example 4.1,

$$E_r = -2u_{\text{ind}}/4\pi\epsilon_0\epsilon r^3 = -2\alpha E/4\pi\epsilon_0\epsilon r^3 = -2\alpha(ze)/(4\pi\epsilon_0\epsilon)^2 r^5, \quad (5.11)$$

so that the attractive force and energy will be

$$F(r) = (ze)E_r = -2\alpha(ze)^2/(4\pi\epsilon_0\epsilon)^2 r^5, \quad (5.12)$$

$$w(r) = -\int_{\infty}^r F dr = -\alpha(ze)^2/2(4\pi\epsilon_0\epsilon)^2 r^4 \quad (5.13)$$

$$= -\frac{1}{2}\alpha E^2, \quad (5.14)$$

where $E = ze/4\pi\epsilon_0\epsilon r^2$ is the field acting on the molecule. Note that this energy is half that expected for the interaction of an ion with a similarly aligned *permanent* dipole, which from Eq. (4.6) is

$$w(r) = -uE = -\alpha E^2. \quad (5.15)$$

This happens because when a dipole moment is *induced* (rather than being *permanent* or *fixed*), some energy is taken up in polarizing the molecule. If we return to the example of Figure 5.2, we see that this is the energy absorbed internally in displacing the positive and negative charges in the molecule and may be calculated by integrating the internal force F_{int} of Eq. (5.3) with respect to the charge separation from 0 to ℓ —that is,

$$w_{\text{int}}(r) = \int_0^{\ell} F_{\text{int}} dl = \int_0^{\ell} \frac{e^2 l dl}{4\pi\epsilon_0 R^3} = \frac{(el)^2}{8\pi\epsilon_0 R^3} = \frac{(\alpha E)^2}{2\alpha} = \frac{1}{2}\alpha E^2. \quad (5.16)$$

Thus, a factor $+\frac{1}{2}\alpha E^2$ must be added to Eq. (5.15) to obtain the *free* energy for the ion-induced dipole interaction, Eq. (5.14). An alternative derivation of Eq. (5.14) is given in Figure 5.2.

We may now insert the value for the total polarizability of polar molecules, $\alpha = \alpha_0 + u^2/3kT$, into Eq. (5.13) and obtain for the net ion-induced dipole interaction free energy

$$w(r) = -\frac{(ze)^2 \alpha}{2(4\pi\epsilon_0\epsilon)^2 r^4} = -\frac{(ze)^2}{2(4\pi\epsilon_0\epsilon)^2 r^4} \left(\alpha_0 + \frac{u^2}{3kT} \right), \quad (5.17)$$

and we may note that the temperature-dependent term is identical to Eq. (4.16) derived earlier by a different method.

5.5 Ion-Solvent Molecule Interactions and the Born Energy

It is instructive to see how the ion-induced dipole interaction is related to the Born energy of an ion in a medium, which was previously discussed in Chapter 3. Let us first compute the total interaction energy of an ion in a medium with all the surrounding solvent molecules. For an ion of radius a , this can be calculated as before by integrating $w(r)$ of Eq. (5.13) or (5.17) over all of space:

$$\mu^i = \int_a^\infty w(r) \rho 4\pi r^2 dr = - \int_a^\infty \frac{\rho \alpha (ze)^2 4\pi r^2 dr}{2(4\pi\epsilon_0\epsilon)^2 r^4} = -\frac{\rho \alpha (ze)^2}{8\pi\epsilon_0^2\epsilon^2 a}, \quad (5.18)$$

where ρ is the number of solvent molecules per unit volume (the number density). To proceed further, we have to make some connection between the molecular and continuum properties of the solvent. This requires us to find a relation between the molecular polarizability α and the dielectric constant ϵ of a medium. This is a very complex problem and still not well understood. However, the value of $(\rho\alpha)/\epsilon_0$ in the Eq. (5.18) may in a first approximation be associated with the *electric susceptibility* χ of a medium. This is the polarizability per unit volume of a medium and is related to the dielectric constant ϵ by

$$\chi = (\epsilon - 1). \quad (5.19)$$

The change in free energy $\Delta\mu^i$ when an ion goes from a medium of dielectric constant ϵ_1 to one of ϵ_2 is therefore (since $d\chi = d\epsilon$)

$$\Delta\mu^i = - \int_{\chi_1}^{\chi_2} \frac{(ze)^2}{8\pi\epsilon_0\epsilon^2 a} d\chi = - \int_{\epsilon_1}^{\epsilon_2} \frac{(ze)^2}{8\pi\epsilon_0\epsilon^2 a} d\epsilon = -\frac{(ze)^2}{8\pi\epsilon_0 a} \left[\frac{1}{\epsilon_1} - \frac{1}{\epsilon_2} \right] \quad (5.20)$$

which is the change in Born energy, Eq. (3.14).

We have now seen how the Born energy—which was previously derived using a *continuum* analysis—can also be derived from a *molecular* approach. Furthermore, the molecular approach has the added advantage of providing insight into the limitations of the Born equation. Thus, for an ion in a polar solvent, we may expect the Born equation to be valid as long as the polarizabilities of the solvent molecules do not depend on their distance from the ion—that is, as long as the polarizing field E and solvent dipole moment

u are not so large that the Debye-Langevin equation, Eq. (5.8), breaks down. We have already seen in Chapter 4 that for ions in a polar solvent such as water, this condition is satisfied except for very small or multivalent ions.

5.6 Dipole-Induced Dipole Interactions

The interaction between a polar molecule and a nonpolar molecule is analogous to the ion-induced dipole interaction just discussed except that the polarizing field comes from a permanent dipole rather than a charge. For a fixed dipole u oriented at an angle θ to the line joining it to a polarizable molecule (Table 2.2), the electric field of the dipole acting on the molecule was previously shown to be (see Worked Example 4.1)

$$E = u(1 + 3 \cos^2 \theta)^{1/2} / 4\pi\epsilon_0\epsilon r^3, \quad (5.21)$$

which means the interaction energy is

$$w(r, \theta) = -\frac{1}{2}\alpha_0 E^2 = -u^2\alpha_0(1 + 3 \cos^2 \theta)/2(4\pi\epsilon_0\epsilon)^2 r^6. \quad (5.22)$$

For typical values of u and α_0 , the strength of this interaction is not sufficient to mutually orient the molecules, as occurs in ion-dipole or strong dipole-dipole interactions. The effective interaction is therefore the angle-averaged energy. Since the angle average of $\cos^2 \theta$ is $1/3$, Eq. (5.22) becomes

$$w(r) = -u^2\alpha_0/(4\pi\epsilon_0\epsilon)^2 r^6, \quad (5.23)$$

while more generally, for two molecules possessing permanent dipole moments u_1 and u_2 and polarizabilities α_{01} and α_{02} , their net dipole-induced dipole energy is

$$w(r) = -\frac{[u_1^2\alpha_{02} + u_2^2\alpha_{01}]}{(4\pi\epsilon_0\epsilon)^2 r^6}. \quad (5.24)$$

This is often referred to as the *Debye interaction* or the *induction interaction*. It constitutes the second of three inverse sixth power contributions to the total van der Waals interaction energy between molecules. The first we have already encountered in the angle-averaged dipole-dipole or Keesom interaction, Eq. (4.17), which incidentally may also be obtained from Eq. (5.23) by replacing α_0 by $\alpha_{\text{dip}} = u^2/3kT$ so that for two dipoles u_1 and u_2 , it gives the Keesom free energy:

$$w(r) = -\frac{u_1^2 u_2^2}{3(4\pi\epsilon_0\epsilon)^2 k T r^6}.$$

5.7 Unification of Polarization Interactions

Apart from the straight Coulomb interaction between two charges, all the other interactions we have considered have involved polarization effects, either explicitly for neutral molecules of polarizability α_0 or implicitly for rotating polar molecules that effectively

behave as polarizable molecules of polarizability $\alpha = \alpha_0 + \alpha_{\text{dip}}$. For completeness, we may note that all these angle-averaged interactions may be expressed in one general equation; thus, for a charged polar molecule 1 interacting with a second polar molecule 2, we may write

$$w(r) = -\left(\frac{Q_1^2}{2r^4} + \frac{3kT\alpha_1}{r^6}\right) \frac{\alpha_2}{(4\pi\epsilon_0\varepsilon)^2} \quad (5.25)$$

$$= -\left[\frac{Q_1^2}{2r^4} + \frac{3kT}{r^6}\left(\frac{u_1^2}{3kT} + \alpha_{01}\right)\right]\left(\frac{u_2^2}{3kT} + \alpha_{02}\right)\Big/\left(4\pi\epsilon_0\varepsilon\right)^2, \quad (5.26)$$

where Q_1 is the charge of the first molecule and u_1 , u_2 , α_{01} , α_{02} are the dipole moments and electronic polarizabilities of the two molecules. Each of the six terms arising from the Eq. (5.26) may be identified (cf. Table 2.2) with a previous derivation (except for the small van der Waals $\alpha_{01}\alpha_{02}$ term discussed later). The unification of these various interactions is conceptually important, for it shows them all to be essentially polarization-type forces. If none of the molecules carries a net charge ($Q_1 = 0$), Eq. (5.26) gives the Keesom-orientation and Debye-induction contributions to the total van der Waals force between two molecules. The third and last contributor to van der Waals forces—the *dispersion force*—will be introduced in the next chapter.

Equation (5.26) is also useful for rapidly estimating the relative strengths of charge, dipole, and electronic polarizability contributions in an interaction. Thus, for typical values of $Q_1 = e = 1.6 \times 10^{-19}$ C, $u_1 = 1$ D = 3.3×10^{-30} C m, $\alpha_{01} = (4\pi\epsilon_0)3 \times 10^{-30}$ m³, and $r = 0.5$ nm, at $T = 300$ K the ratio of the three terms in the square brackets

$$\frac{Q_1^2}{2r^4} : \frac{u_1^2}{r^6} : \frac{3kT\alpha_{01}}{r^6}$$

is about 800:3:1.¹ For water, however, because of its large dipole moment u and unusually small polarizability α_0 , the ratio $u^2 : 3kT\alpha_0$ is about 20:1; that is, the permanent-dipole-associated interactions of water always dominate over electronic polarization effects. Note, too, that the effectiveness of a dipolar interaction depends on $u^2/r^6 \sim (u/\sigma^3)^2$ rather than on the absolute value of the dipole moment. In other words, for a molecule to be considered as highly polar, it must have a high dipole moment *per molecular volume* and not simply a high u .

5.8 Solvent Effects and “Excess Polarizabilities”

The interaction between molecules or small particles in a solvent medium can be very different from that of isolated molecules in free space or in a gas. The presence of a suspending medium does more than simply reduce the interaction energy or force by

¹If we include the ion-ion Coulomb interaction energy $Q_1^2/4\pi\epsilon_0 r$ as the first term, these ratios become 25,000:800:3:1 in a vacuum.

a factor ϵ or ϵ^2 , as might appear from Eq. (5.26) and other equations derived earlier. First, the intrinsic dipole moment and polarizability of an isolated gas molecule may be different in the liquid state or when dissolved in a medium. This depends in a complicated way on its interactions with the surrounding solvent and can usually only be found by experiment. Second, as already discussed in Section 2.1, a dissolved molecule can move only by displacing an equal volume of solvent from its path; hence, the polarizability α in a medium must represent the *excess polarizability* of a molecule or particle over that of the solvent and must vanish when a dissolved particle has the same properties as the solvent. Qualitatively, we may say that if no electric field is reflected by a particle, it is “invisible” in the solvent medium and consequently does not experience a force.

The problem of knowing the excess or effective polarizability can be approached by treating a dissolved molecule or a small particle as a dielectric medium of a given size and shape. This *continuum* approach has an obvious advantage, since the dielectric constant of a medium is usually known. Accordingly, a molecule i may be modeled as a dielectric sphere of radius a_i and dielectric constant ϵ_i . Now in a medium of dielectric constant ϵ (Figure 5.3a), such a dielectric sphere will be polarized by a field E and acquire an excess dipole moment given by

$$u_{\text{ind}} = 4\pi\epsilon_0\epsilon \left(\frac{\epsilon_i - \epsilon}{\epsilon_i + 2\epsilon} \right) a_i^3 E \quad (5.27)$$

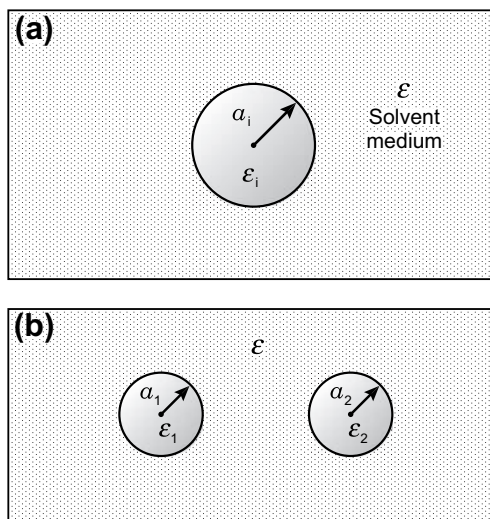


FIGURE 5.3 A dissolved molecule or small solute particle can be modeled as a sphere of radius a_i and dielectric constant ϵ_i . Its total polarizability in a medium of dielectric constant ϵ is $\alpha_i = 4\pi\epsilon_0\epsilon a_i^3(\epsilon_i - \epsilon)/(\epsilon_i + 2\epsilon)$, Eq. (5.28). As far as intermolecular forces are concerned, a vacuum can be considered as a “medium” with a dielectric constant of $\epsilon = 1$.

so that its effective or *excess polarizability* in the medium is

$$\alpha_i = 4\pi\epsilon_0\epsilon \left(\frac{\epsilon_i - \epsilon}{\epsilon_i + 2\epsilon} \right) a_i^3 = 3\epsilon_0\epsilon \left(\frac{\epsilon_i - \epsilon}{\epsilon_i + 2\epsilon} \right) v_i, \quad (5.28)$$

where $v_i = \frac{4}{3}\pi a_i^3$, is the volume of the molecule or sphere. This equation shows that for a dielectric sphere of high ϵ_i in free space (where $\epsilon = 1$), its polarizability is roughly $\alpha_i \approx 4\pi\epsilon_0 a_i^3$, as previously found for a simple one-electron atom, Eq. (5.5). Further, if $\epsilon_i < \epsilon$, the polarizability is negative, implying that the direction of the induced dipole is opposite to that in free space or when $\epsilon_i > \epsilon$.

If we substitute Eq. (5.28) into Eq. (5.25), we obtain the important result

$$w(r) = - \left[\frac{Q_1^2}{8\pi\epsilon_0\epsilon r^4} + \frac{3kT}{r^6} \left(\frac{\epsilon_1 - \epsilon}{\epsilon_1 + 2\epsilon} \right) a_1^3 \right] \left(\frac{\epsilon_2 - \epsilon}{\epsilon_2 + 2\epsilon} \right) a_2^3 \quad (5.29)$$

which allows us to conclude the following:

1. The net force between dissolved molecules or small particles in a medium (Figure 5.3b) can be zero, attractive, or repulsive, depending on the relative magnitudes of ϵ_1 , ϵ_2 , and ϵ .
2. Ions will be attracted to dissolved molecules of high dielectric constant (highly polar molecules or media where $\epsilon_2 > \epsilon$) but repelled from molecules of low dielectric constant (nonpolar molecules where $\epsilon_2 < \epsilon$).
3. The interaction between any two identical uncharged molecules ($\epsilon_1 = \epsilon_2$) is always attractive regardless of the nature of the suspending medium. Interestingly, two microscopic air bubbles, for which $\epsilon_1 = 1$, also attract each other in a liquid.

The above approach will generally predict the right qualitative trends, but it is quantitatively somewhat model-dependent in that it treats solute molecules as if they were a uniform medium having bulk dielectric properties. It is essentially a continuum treatment where the molecular properties appear only in determining the molecular radius or volume. This may be valid for larger molecules, macromolecules, and small particles in solution but may fail for small molecules, especially when they are close together. Let us therefore end this chapter by looking into the reasonableness of treating a molecule as if it were a dielectric sphere. From Eq. (5.28) we see that for isolated molecules in the gas phase ($\epsilon = 1$), their *total* polarizability should be given by

$$\frac{\alpha}{(4\pi\epsilon_0)} = \left(\frac{\epsilon - 1}{\epsilon + 2} \right) \frac{3v}{4\pi}, \quad (5.30)$$

where ϵ is now the static dielectric constant of the molecules, assumed to be the same as that of the condensed state (e.g., the liquid state). Equation (5.30) is known as the Clausius-Mossotti equation.

If we are interested in the *electronic* polarizability α_0 , then the value of ϵ in Eq. (5.30) is that measured in the visible range of frequencies and equals n^2 , where n is the refractive index of the medium. Thus, for the *electronic* polarizability, we may write

Table 5.2 Molecular Polarizabilities as Determined from Molecular and Bulk Properties^{a,b}

Molecule	Polarizabilities Deduced from Gas (Molecular) Properties				Polarizabilities Deduced from Condensed Phase (Continuum) Properties					
	u_{gas} meas. (D) ^c	$\frac{\alpha_0}{4\pi\epsilon_0}$ measured (10^{-30} m ³)	$\frac{\alpha}{4\pi\epsilon_0}$ from $\alpha = \alpha_0 + \frac{u^2}{3kT}$	Molecular Weight, M (10^{-3} kg mol ⁻¹)	Mass Density ρ (10^3 kg m ⁻³)	Refractive Index n	Dielectric Constant ϵ	$\frac{\alpha_0}{4\pi\epsilon_0}$ from $\left(\frac{n^2-1}{n^2+2}\right) \frac{3M}{4\pi N_0 \rho}$	$\frac{\alpha}{4\pi\epsilon_0}$ from $\left(\frac{\epsilon-1}{\epsilon+2}\right) \frac{3M}{4\pi N_0 \rho}$	
			(10^{-30} m ³)					(10^{-30} m ³)	(10^{-30} m ³)	
CCl ₄	carbon tetrachloride	0	10.5	10.5	153.8	1.59	1.460	2.2	10.5	11.2
C ₆ H ₆	benzene	0	10.3	10.3	78.1	0.88	1.601	2.3	10.4	10.5
CHCl ₃	chloroform	1.06	8.2	17.5 (20°C) 21.1 (-63°C)	119.4	1.48	1.446	4.8 (20°C) 6.8 (-63°C)	8.5	17.9 (20°C) 21.1 (-63°C)
H ₂ O	water	1.85	1.5	29.7	18.0	1.00	1.333	80	1.5	6.9
(CH ₃) ₂ CO	acetone	2.85	6.4	73.4	58.1	0.79	1.359	21	6.4	25.3
CH ₃ OH	methanol	1.69	3.2	26.8	32.0	0.79	1.329	33	3.3	14.7
C ₂ H ₅ OH	ethanol	1.69	5.2	28.8	46.1	0.79	1.361	26	5.1	20.7
<i>n</i> -C ₆ H ₁₃ OH	hexanol	1.69	12.5	36.1	102.2	0.81	1.418	13	12.6	40.0
C ₆ H ₅ OH	phenol	1.45	11.2	26.4	94.1	1.07	1.551	10 (60°C)	11.1	26.1

^aAll values at 20°C unless stated otherwise.^b α_0 , electronic polarizability; α , total polarizability.^c1 D = 3.336×10^{-30} C m.

$$\frac{\alpha_0}{(4\pi\epsilon_0)} = \left(\frac{n^2 - 1}{n^2 + 2}\right) \frac{3\nu}{4\pi}, \quad (5.31)$$

which is known as the Lorenz-Lorentz equation. At high frequencies, above about 10^{12} Hz, molecular dipoles can no longer respond to a field and the total polarizability is determined entirely by the electronic polarizability.

Table 5.2 shows the experimental values for the electronic polarizabilities α_0 and dipole moments u of isolated molecules in the gas phase, from which their total polarizabilities α may be obtained from Eq. (5.8):

$$\alpha = \alpha_0 + u^2/3kT.$$

Table 5.2 also shows the polarizabilities α_0 and α as calculated from Eqs. (5.30) and (5.31) in terms of the purely bulk properties of the liquids: the refractive index n , the dielectric constant ϵ , the molecular weight M , and mass density ρ , from which the volume occupied per molecule (the inverse number density) is given by

$$\nu = M/\rho N_0. \quad (5.32)$$

It is evident that for all the molecules listed in Table 5.2, their electronic polarizabilities α_0 are excellently described by Eq. (5.31). In contrast, the total polarizabilities α are well described by Eq. (5.30) only for weakly polar molecules such as CHCl_3 and $\text{C}_6\text{H}_5\text{OH}$. For small highly polar molecules such as H_2O and $(\text{CH}_3)_2\text{CO}$, the agreement is not good but improves for progressively larger molecules (cf. $\text{CH}_3\text{OH} \rightarrow \text{C}_2\text{H}_5\text{OH} \rightarrow \text{C}_6\text{H}_{13}\text{OH}$ and $\text{C}_6\text{H}_5\text{OH}$), as expected. It is not possible to ascertain whether the lack of agreement for highly polar molecules is due to the inapplicability of Eq. (5.30) or to a changed dipole moment of the molecules in the liquid state. However, we may safely conclude that Eqs. (5.30)–(5.31) serve as quantitatively reliable equations for determining the polarizabilities of all but very small highly polar molecules, and we may expect that Eq. (5.28) for the excess polarizability and Eq. (5.29) for the interaction energy should be likewise applicable.

But we are still not in a position to estimate the strength of the total interaction between neutral or polar molecules. There is one final contribution to the total force that must be considered before we can do that. This is the van der Waals-dispersion force.



Worked Example 5.3

Question: A light beam is directed onto a small uncharged colloidal particle that is suspended in water. What will be the nature of the electric polarization force on the particle if the beam is (1) collimated (uniform) and (2) focused on a point just ahead or just behind the particle? What additional forces are involved in such situations?

Answer: Light is an electromagnetic field so it will polarize the particle, causing charges $\pm q$ to become separated by a distance l (cf. Figure 5.2). In a uniform field there is no net polarization force on the particle, since the forces on the two charges cancel each other out. If, however, the electric field is not uniform, having a finite gradient dE/dr , the forces acting on the two charges will no longer cancel out but will be given by $F = q(dE/dr)\ell = u_{\text{ind}}(dE/dr) = \alpha E(dE/dr)$,

where α is the excess polarizability. Note that this force is the same as that obtained by differentiating the energy of Eq. (5.14): $F = -dw/dr$. Since the frequency of light waves is approximately 10^{15} Hz, only the electronic polarizabilities, determined by the refractive indices of the media, contribute to the excess polarizability of the particle. If the refractive index of the particle is greater than that of water (positive excess polarizability), the particle will be drawn in the direction of the increasing electric field or light intensity—that is, toward the focal point from either side, as in the case of Figure 5.2, where the ion is the effective focal point. For negative excess polarizability the particle will be driven away from the focal point—that is, driven in the direction of the weaker electric field. This analysis forms the basis of a powerful technique to move and measure the interactions of large macromolecules and small colloidal particles, known as Optical Tweezers and Optical Trapping (see Section 12.9). However, it ignores radiation, heating, and magnetic forces, which can be more important in some systems.

PROBLEMS AND DISCUSSION TOPICS

- 5.1 When an electric field is applied across a nonconducting liquid containing large colloidal particles, it is found that they align as shown in Figure 5.4. Explain this phenomenon and suggest one condition when the particles will not align (ignore gravitational effects). At low particle densities one often observes individual particles shuttling back and forth between the two electrode surfaces. Explain this effect in more detail than is given in Figure 5.4.
- 5.2 What does Table 5.2 tell us about the ability of nonpolar, polar, and hydrogen bonding molecules to rotate freely in the gas phase compared to their mobility in the condensed phase?
- 5.3 The following room temperature properties of liquid chloroform (CHCl_3) are given in Table 5.2: electronic polarizability α_0 ; dipole moment μ ; refractive index n ; and mass density ρ_m . Assuming that none of these changes with temperature, calculate the dielectric constant of liquid chloroform at 20°C and at its freezing point of -63.5°C ,

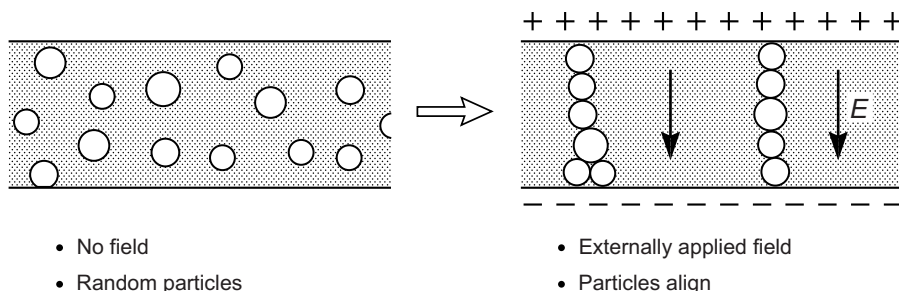


FIGURE 5.4 If the particles are conductors in a nonconducting medium, they can pick up electrons from the bottom surface and then be shuttled to the top, where they unload their “cargo”, and then pick up a proton and return to discharge it at the bottom surface. The processes are then repeated, giving rise to back-and-forth shuttling (and a current) so long as the electric field E is maintained across the gap.

and compare your answer with the measured values of $\epsilon = 4.8$ and 6.8 , respectively. What would you expect ϵ to be at a temperature just below the freezing point—that is, for solid chloroform?

- 5.4** According to the Debye–Langevin and Clausius–Mossotti equations, Eqs. (5.8) and (5.30), a high dielectric constant arises for molecules with large dipole moments. This appears to be the case for water. However, when water freezes, the dielectric constant of crystalline ice is actually higher than that of the liquid, even though one would expect a substantial decrease due to the restricted rotation of the now immobilized molecules. Does this mean that another polarization mechanism must be operating with water (other than the electronic and rotating dipole mechanisms described in this Chapter)? If so, propose a physically realistic theory for this phenomenon.

Van der Waals Forces

6.1 Origin of the Van der Waals-dispersion Force between Neutral Molecules: the London Equation

The various types of physical forces described so far are fairly easy to understand, since they arise from straightforward electrostatic interactions involving charged or dipolar molecules. But there is another type of force that—like the gravitational force—acts between *all* atoms and molecules, even totally neutral ones such as helium, carbon dioxide, and hydrocarbons. These forces have been variously known as dispersion forces, London forces, charge-fluctuation forces, electrodynamic forces, and induced-dipole-induced-dipole forces. We shall refer to them as *dispersion forces*, since it is by this name that they are most widely known. The origin of this name has to do with their relation to the dispersion of light in the visible and UV regions of the spectrum, as we shall see. The literature on this subject is quite voluminous, and the reader is referred to books and reviews by¹ London (1937), Hirschfelder et al. (1954), Moelwyn-Hughes (1961), Margenau and Kestner (1971), Israelachvili (1974), Mahanty and Ninham (1976), and Parsegian (2006).

Dispersion forces make up the third and perhaps most important contribution to the total van der Waals force between atoms and molecules, and because they are always present (in contrast to the other types of forces that may or may not be present, depending on the properties of the molecules), they play a role in a host of important phenomena such as adhesion; surface tension; physical adsorption; wetting; the properties of gases, liquids, and thin films; the strengths of solids; the flocculation of particles in liquids; and the structures of condensed macromolecules such as proteins and polymers. Their main features may be summarized as follows:

1. They are long-range forces and, depending on the situation, can be effective from large distances (greater than 10 nm) down to interatomic spacings (about 0.2 nm).
2. These forces may be repulsive or attractive, and in general the dispersion force between two molecules or large particles does not follow a simple power law.
3. Dispersion forces not only bring molecules together but also tend to mutually align or orient them, though this orienting effect is usually weaker than with dipolar interactions.
4. Dispersion forces are not *additive*; that is the force between two bodies is affected by the presence of other bodies nearby. This is called the *nonadditivity* of an interaction.

¹Many of the old, classic papers on this subject remain surprisingly up to date.

Dispersion forces are quantum mechanical in origin and amenable to a host of theoretical treatments of varying complexity, the most rigorous of which would take us into the world of quantum electrodynamics. Their origin may be understood intuitively as follows: For a nonpolar atom such as helium, the time average of its dipole moment is zero, but at any instant there exists a finite dipole moment given by the instantaneous positions of the electrons about the nuclear protons. This instantaneous dipole generates an electric field that polarizes any nearby neutral atom, inducing a dipole moment in it. The resulting interaction between the two dipoles gives rise to an instantaneous attractive force between the two atoms, and the time average of this force is finite. For a simple semiquantitative understanding of how these forces arise, we may consider the following model based on the interaction between two Bohr atoms.

In the Bohr atom an electron is pictured as orbiting around a proton. The smallest distance between the electron and proton is known as the *first Bohr radius* a_0 and is the radius at which the Coulomb energy $e^2/4\pi\varepsilon_0 a_0$ is equal to $2h\nu$ —that is,

$$a_0 = e^2/8\pi\varepsilon_0 h\nu = 0.053 \text{ nm}, \quad (6.1)$$

where h is the Planck constant and ν the orbiting frequency of the electron.² For a Bohr atom, $\nu = 3.3 \times 10^{15} \text{ s}^{-1}$, so that $h\nu = 2.2 \times 10^{-18} \text{ J}$. This is the energy of an electron in the first Bohr radius and is equal to the energy needed to ionize the atom—the *first ionization potential*, I .

The Bohr atom has no permanent dipole moment. However, at any instant there exists an instantaneous dipole of moment, $u = a_0e$, whose field will polarize a nearby neutral atom, giving rise to an attractive interaction that is entirely analogous to the dipole-induced dipole (Debye) interaction discussed in Chapter 5. The energy of this interaction in a vacuum will therefore be given by Eq. (5.23) as

$$w(r) = -u^2\alpha_0/(4\pi\varepsilon_0\varepsilon)^2r^6 = -(a_0e)^2\alpha_0/(4\pi\varepsilon_0)^2r^6,$$

where α_0 is the electronic polarizability of the second Bohr atom, which from Eq. (5.5) is approximately $4\pi\varepsilon_0 a_0^3$. Using this expression for α_0 and Eq. (6.1) for a_0 , we immediately find that the above interaction energy can be written approximately as

$$w(r) \approx -\alpha_0^2 h\nu/(4\pi\varepsilon_0)^2 r^6. \quad (6.2)$$

Except for a numerical factor, Eq. (6.2) is the same as that derived by London in 1930 using quantum mechanical perturbation theory. London's famous expression for the dispersion interaction energy between two identical atoms or molecules is (London, 1937)

$$w(r) = \frac{-C_{\text{disp}}}{r^6} = -\frac{3}{4}\alpha_0^2 h\nu/(4\pi\varepsilon_0)^2 r^6 = -\frac{3}{4}\alpha_0^2 I/(4\pi\varepsilon_0)^2 r^6 \quad (6.3)$$

²In the literature $h\nu$ is often expressed as $\hbar\omega$, where $\hbar = h/2\pi$ and $\omega = 2\pi\nu$.

and for two dissimilar atoms,³

$$w(r) = -\frac{3}{2} \frac{\alpha_{01}\alpha_{02}}{(4\pi\epsilon_0)^2 r^6} \frac{h\nu_1\nu_2}{(\nu_1 + \nu_2)} = -\frac{3}{2} \frac{\alpha_{01}\alpha_{02}}{(4\pi\epsilon_0)^2 r^6} \frac{I_1 I_2}{(I_1 + I_2)}. \quad (6.4)$$

London's equation has since been superseded by more exact, though more complicated, expressions (see Section 6.6), but it can be relied upon to give fairly accurate values for interactions in a vacuum although these are usually lower than more rigorously determined ones.

From the above simple model we see that while dispersion forces are quantum mechanical (in determining the instantaneous, but fluctuating, dipole moments of neutral atoms), the ensuing interaction is still essentially electrostatic—a sort of quantum mechanical polarization force. And we may further note that the $1/r^6$ distance dependence is the same as that of the two other polarization interactions, the Keesom and Debye forces discussed in Section 5.6, that together contribute to the net van der Waals force. But before we consider these three interactions collectively, let us first investigate the nature of dispersion forces.

6.2 Strength of Dispersion Forces: Van der Waals Solids and Liquids

To estimate the strength of the dispersion energy, we may consider two atoms or small molecules with $\alpha_0/4\pi\epsilon_0 \approx 1.5 \times 10^{-30} \text{ m}^3$ and $I = h\nu \approx 10^{-18} \text{ J}$ (a typical ionization potential in the UV). From Eq. (6.3) we find that for two atoms in contact at $r = \sigma \approx 0.3 \text{ nm}$, we obtain $w(\sigma) = -4.6 \times 10^{-21} \text{ J} \approx 1 \text{ kT}$. This is very respectable energy, considering that the interaction appears at first sight to spring up from nowhere. But when we recall that the inducing (instantaneous) dipole moment of even a small hydrogen (Bohr) atom is of order $a_0e \approx 2.5 \text{ D}$, we can appreciate why the dispersion interaction is by no means negligible. Thus, while very small nonpolar atoms and molecules such as argon and methane are gaseous at room temperature and pressure, larger molecules such as hexane and higher molecular weight hydrocarbons are liquids or solids, held together solely by dispersion forces. The solids are referred to as van der Waals solids, and they are characterized by having weak undirected “bonds” and therefore low melting points and low latent heats of melting.

For spherically symmetrical inert molecules such as neon, argon, methane, and C_{60} , the van der Waals solids they form at low temperatures are closely packed structures with 12 nearest neighbors per atom. Their lattice energy (12 shared “bonds” or six full “bonds” per molecule) is therefore approximately $6w(\sigma)$ per molecule, though if the attractions of

³Of purely historical interest, since ionization potentials do not differ much among different molecules, the dispersion interaction between two dissimilar molecules is given roughly by $w(r) \propto -\alpha_1\alpha_2/r^6$. Further, since α is roughly proportional to the molecular volume (Section 5.1), and the mass densities of different materials are also not very different, we find $w(r) \propto -m_1m_2/r^6$, which has the same form as the gravitational force-law except for the distance exponent.

Table 6.1 Strength of Dispersion Interaction between Quasi-Spherical Nonpolar Molecules of Increasing Size^d

Interacting Molecules	Molecular Diameter σ (nm) (From Figure 7.1)	London Constant			Molar Cohesive Energy, U (kJ mol ⁻¹)			Boiling Point, T_B (K)	
		Polarizability $\alpha_0/4\pi\epsilon_0$ (10 ⁻³⁰ m ³)	Ionization Potential $I = h\nu_1$ (eV) ^b	Theoretical Eq. (6.3)	Measured from Gas Law Eq. (6.14) ^a	Theoretical Eq. (6.5)	Measured $L_m + L_v$ (approx.)	Theoretical (Section 2.6) $\frac{3\alpha_0^2 h\nu_1}{4(4\pi\epsilon_0)^2 \sigma^6 (1.5k)}$	Measured
				$C_{\text{disp}} =$ $3\alpha_0^2 h\nu_1 / 4(4\pi\epsilon_0)^2$ (10 ⁻⁷⁹ J m ⁶)					
Ne–Ne	0.308	0.39	21.6	3.9	3.8	2.0	2.1	22	27
Ar–Ar	0.376	1.63	15.8	50	45	7.7	7.7	85	87
CH ₄ –CH ₄	0.400	2.60	12.6	102 ^c	101 ^c	10.9	9.8	121	112
Xe–Xe	0.432	4.01	12.1	233	225	15.6	14.9	173	165
CCl ₄ –CCl ₄	0.550	10.5	11.5	1520	2960	23.9	32.6	265	350

^aVan der Waals constants *a* and *b* taken from the *Handbook of Chemistry and Physics*, CRC Press, 56th ed.

^b1 eV = 1.602 × 10⁻¹⁹ J.

^cAs an example of the reliability of the approximate equations for C_{disp} , Eqs. (6.3) and (6.14), ab initio calculation for two CH₄ molecules (Fowler et al., 1989; Szczesniak et al., 1990) give $\sim 114 \times 10^{-79}$ J m⁶, which is about 10% higher than the theoretical value given here. The most reliable experimental value, based on a number of different types of measurements (Thomas and Meath, 1977), is $C_{\text{disp}} = 124 \times 10^{-79}$ J m⁶, which is about 20% higher than the value given here.

^dSee Pacheco and Ekardt (1992) for simple expressions and computed values for C_{disp} for metal atoms and small metal clusters.

more distant neighbors are also included, the factor of 6 rises to 7.22.⁴ The expected *molar lattice energy* or *molar cohesive energy* of a van der Waals solid is therefore

$$U \approx 7.22 N_0 \left[\frac{3\alpha_0^2 h\nu}{4(4\pi\epsilon_0)^2 \sigma^6} \right], \quad (6.5)$$

where σ is the equilibrium interatomic distance in the solid. Thus, for argon, since $\alpha_0/(4\pi\epsilon_0) = 1.63 \times 10^{-30} \text{ m}^3$, $I = h\nu = 2.52 \times 10^{-18} \text{ J}$, and $\sigma = 0.376 \text{ nm}$, we obtain $U \approx 7.7 \text{ kJ mol}^{-1}$. This may be compared with the latent heat of melting plus vaporization for argon of $L_m + L_v = 7.7 \text{ kJ mol}^{-1}$, which is approximately equal to the latent heat of sublimation or the molar cohesive energy U (ignoring the small PV term at this temperature). The value of $U \approx 10 \text{ kJ mol}^{-1}$ is typical for small nonpolar molecules, and it shows that the cohesive energies of van der Waals solids are one to two orders of magnitude weaker than those of covalent and ionic solids.

Table 6.1 shows the calculated and experimental values for the cohesive energies of a number of van der Waals solids composed of small spherical atoms or molecules. The good agreement obtained is to some extent fortuitous, since the computed values neglect the following:

- The very short-range stabilizing repulsive forces (Chapter 7) and many-body effects (Section 6.9) that can *lower* the final binding energy at contact by up to 50%.
- Other attractive forces, such as those that arise from other absorption frequencies and fluctuating quadrupole and higher-multipole interactions, which can *raise* the final binding by up to 50%. (see legend to Table 6.1).

These two opposing effects partially cancel each other out so the final results look more impressive than they really are.

At the end of Section 5.7 it was mentioned that the effective strength of a dipole-dipole interaction depends not on the dipole moment u but on the dipole moment per unit volume u/σ^3 . This factor usually *decreases* with increasing molecular size. Similarly, Eq. (6.3) shows that the effective strength of a van der Waals “bond” depends not on α but on $(\alpha/\sigma^3)^2$. However, as the Worked Example 6.1 shows, this factor stays roughly constant with molecular size. Thus, we may expect that dispersion forces become increasingly more important than dipolar forces for larger molecules.



Worked Example 6.1

Question: Many atoms or small molecules have ionization potentials I close to $2 \times 10^{-18} \text{ J}$. If their polarizability can be modeled in terms of the Bohr atom (Section 6.1), show that the strength of a typical van der Waals “bond” is always approximately a few kT at room temperature, irrespective of the size or polarizability of the molecules.

⁴This lattice summation is analogous to obtaining the Madelung Constant of ionic solids (Section 3.4), except that for the rapidly decaying dispersion force, only the nearest neighbors contribute.

Answer: The strength of a van der Waals “bond” is given by $w(r)$ at a separation $r = 2a$, where a is the molecular radius. From the Bohr atom model of polarizability, $\alpha_0 = 4\pi\varepsilon_0 a^3$, putting $r = 2a$ into the London equation, Eq. (6.3), we obtain $w(2a) \approx \frac{3}{4}Ia^6/(2a)^6 \approx \frac{3}{4}(I/64) \approx \frac{3}{4}(2 \times 10^{-18})/64 \approx 2 \times 10^{-20}$ J, which is a few kT and is independent of a or α_0 .

For larger spherical molecules with diameters greater than about 0.5 nm, the simple London equation can no longer be used. Clearly, as molecules grow in size, their center-to-center distance ceases to have any significance as regards the strength of the cohesion energy. This is because the dispersion force no longer acts between the centers of the molecules but between the centers of electronic polarization within each molecule, which, as we saw in Chapter 5, are located at the covalent bonds. Thus, for CCl_4 , the calculated value for the cohesion energy is too small (see Table 6.1) because the distance between the polarizable electrons of the two molecules is now significantly less than the equilibrium intermolecular separation of 0.55 nm. In Chapter 11 we shall investigate the interactions between spheres and particles whose radii are much larger than interatomic spacings.

Likewise, the simple London equation or Eq. (6.5) cannot be applied to asymmetric (nonspherical) molecules such as alkanes, polymers, and cyclic or planar molecules. To compute the binding energies within or between such complex molecules, the molecular packing in the solid or liquid must be known (which, of course, transforms any theoretical endeavor from the predictive to the confirmatory), and the different contributions arising from different parts of the molecules must be considered separately. Under such conditions the exact dispersion interaction is difficult to compute, but some simplifying assumptions can often be made to arrive at reasonable working models. Let us consider one such model for normal alkanes, of general formula $\text{CH}_3-(\text{CH}_2)_n-\text{CH}_3$, where each molecule may be considered as a cylinder of diameter $\sigma = 0.40$ nm composed of CH_2 groups spaced linearly at intervals of $l = 0.127$ nm, corresponding to the projected CH_2-CH_2 distance along an alkane chain. If we now consider one such molecule surrounded by six close-packed neighboring cylinders, we may sum the dispersion energy of any one CH_2 group in the central molecule with all the CH_2 groups in the six surrounding molecules (similar to the lattice sum carried out in Section 3.4 for the ionic lattice energy). Thus, there will be 6 CH_2 groups at $r = \sigma$, 12 at $r = [\sigma^2 + l^2]^{1/2}$, 12 at $r = [\sigma^2 + (2l)^2]^{1/2}$, and so on. The molar cohesive energy per CH_2 group will therefore be given by the following rapidly converging series:

$$U = \frac{3\alpha_0^2 h\nu}{4(4\pi\varepsilon_0)^2} \left[\frac{6}{\sigma^6} + \frac{12}{[\sigma^2 + l^2]^3} + \frac{12}{[\sigma^2 + (2l)^2]^3} + \dots \right] \frac{N_0}{2}. \quad (6.6)$$

Now for CH_2 groups, $\alpha_0/4\pi\varepsilon_0 = 1.84 \times 10^{-30}$ m³, and $h\nu = 1.67 \times 10^{-18}$ J, so we obtain

$$U \approx 6.9 \text{ kJ mol}^{-1} \text{ per CH}_2 \text{ group.} \quad (6.7)$$

Table 6.2 Strength of Dispersion Interaction between Linear-Chain Alkane Molecules

Molecule	Number of C–C Bonds <i>n</i>	Molar Cohesive Energy (kJ mol ⁻¹) Theoretical Eq. (6.7)	Measured <i>L_m</i> + <i>L_v</i>	Boiling Point <i>T_B</i> (K)
CH ₄	0	9.8 (measured)	9.8	112
C ₆ H ₁₄	5	44.3	45.0	342
C ₁₂ H ₂₆	11	85.7	86.1	489
C ₁₈ H ₃₈	17	127.1	125.9	590

Table 6.2 shows the experimental values for the latent heats of melting plus vaporization of alkanes together with the computed values based on Eq. (6.7). Experimentally it is found that for straight-chained alcohols, carboxylic acids, amides, esters, and so on, the cohesive energy increases by between 6 and 7.5 kJ mol⁻¹ per added CH₂ group. These good agreements between theory and experiment show two important aspects of dispersion forces: their nondirectionality and near-additivity.

The above analysis also shows that, in general, for straight-chain molecules one expects a direct proportionality between their latent heat, their molecular polarizability, their boiling point, their molecular length (number of “segments” or “monomer units”), and their molecular weight. This linearity is not followed by spherical molecules. Also, for long, *flexible* chains (e.g., high MW polymers), the molecules are no longer straight but coil up on themselves in the bulk solid or liquid;⁵ some segments now interact intramolecularly as well as intermolecularly.

6.3 Van der Waals Equation of State

Let us now see how the van der Waals interaction potential between two molecules can be related to the constants *a* and *b* in the van der Waals equation of state

$$(P + a/V^2)(V - b) = RT \text{ per mole.} \quad (6.8)$$

We shall again consider the molecules to be *hard spheres* of diameters σ , whose pair interaction energy is given by

$$w(r) = -\frac{3\alpha_0^2 h\nu}{4(4\pi\epsilon_0)^2 r^6} = -\frac{C}{r^6}, \quad r \geq \sigma \\ = \infty, \quad r < \sigma. \quad (6.9)$$

In Section 2.5 we found that the constant *a* is given by

$$a = 2\pi C/(n - 3)\sigma^{n-3} = 2\pi C/3\sigma^3 \quad \text{for } n = 6.$$

⁵Polymer chains in liquids (polymer melts) begin to coil significantly once their length exceeds their characteristic “persistence length” (see Chapter 16). Coiled molecules in solids form amorphous rather than crystalline solids.

This value, however, was derived for the case where the van der Waals equation was expressed in terms of molecular parameters, Eq. (2.21): $(P + a/v^2)(v - b) = kT$. Since $v = V/N_0$, we see that when V is the molar volume of the gas, then

$$a = 2\pi N_0^2 C / 3\sigma^3 \quad (6.10)$$

The London dispersion force coefficient C is therefore related to the van der Waals constant a by

$$C = 3\sigma^3 a / 2\pi N_0^2. \quad (6.11)$$

The constant b is obtained from the volume unavailable for the molecules to move in: the “excluded volume” per mole. Since one molecule cannot get closer than σ to another, the excluded volume for the pair is $\frac{4}{3}\pi\sigma^3$, or $\frac{2}{3}\pi\sigma^3$ per molecule as previously derived in Section 2.5. Thus,

$$b = \frac{2}{3}\pi N_0 \sigma^3 \quad (6.12)$$

per mole, which is four times the molar volume of the molecules. The molecular diameter is therefore given by

$$\sigma = (3b/2\pi N_0)^{1/3}. \quad (6.13)$$

Combining the above with Eq. (6.11), we finally obtain for the interaction constant

$$C = 9ab/4\pi^2 N_0^3 = 1.05 \times 10^{-76} ab \text{ J m}^6, \quad (6.14)$$

where a is in $\text{dm}^6 \text{ atm mol}^{-2}$ and b in $\text{dm}^3 \text{ mol}^{-1}$. For example, for methane, CH_4 , the experimental values are $a = 2.25 \text{ dm}^6 \text{ atm mol}^{-2}$ and $b = 0.0428 \text{ dm}^3 \text{ mol}^{-1}$, giving $C = 101 \times 10^{-79} \text{ J m}^6$, which is in remarkably good agreement with the theoretical value of $3\alpha_0^2 h v / 4(4\pi\epsilon_0)^2 = 102 \times 10^{-79} \text{ J m}^6$ calculated on the basis of the London equation. Table 6.1 also shows how good this agreement is for the other molecules listed, except for the largest molecule CCl_4 , which, as already discussed, must have a stronger interaction than can be accounted for by applying the London equation between molecular centers.

For molecules constrained to interact on a surface, as occurs on adsorption and in surface monolayers, there is an analogous equation to the van der Waals equation of state. This two-dimensional analog may be written as (cf. Problem 2.2)

$$(\Pi + a/A^2)(A - b) = N_0 kT = RT, \quad (6.15)$$

per mole of a “2D gas”, where Π is the external surface pressure (in N m^{-1}), A is the molar area, and a and b are constants as before. It is easy to verify that for an intermolecular pair potential of the form $w(r) = -C/r^6$, the constants a and b now become

$$a = \pi CN_0^2 / 4\sigma^4, \quad b = \frac{1}{2}\pi N_0 \sigma^2. \quad (6.16)$$

Figure 6.1 shows the P - V and Π - A phase diagrams predicted by the 3D and 2D van der Waals equations of state. The figure also shows other types of commonly encountered phase transitions.

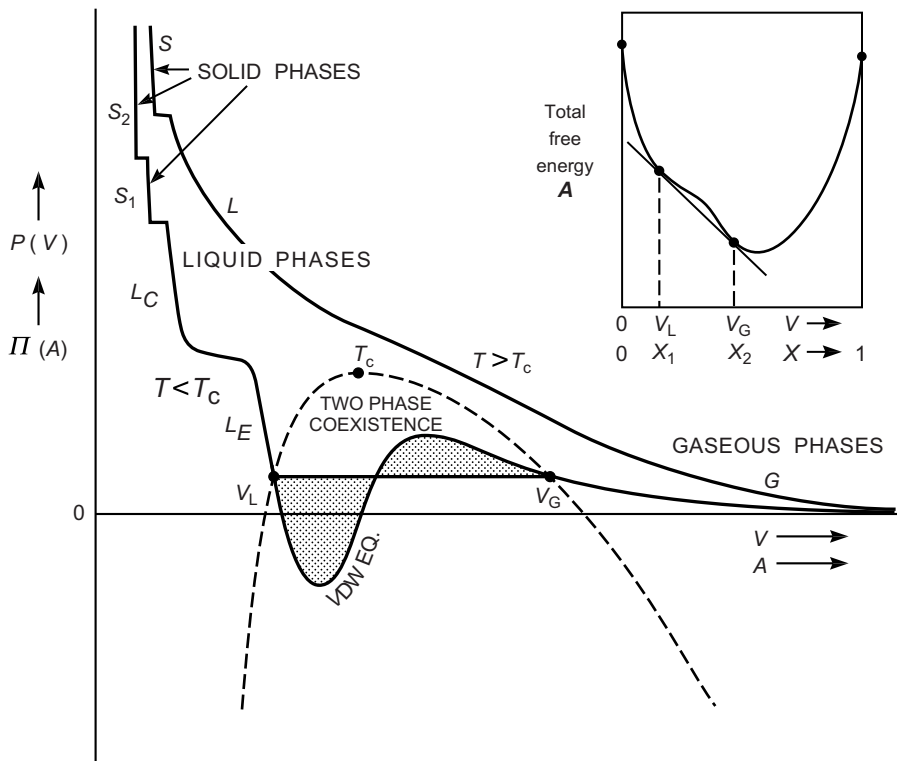


FIGURE 6.1 Typical pressure-volume (P - V) and pressure-area (Π - A) curves encountered in 3D and 2D systems, the latter occurring on surfaces and in monolayers (Pallas and Pethica, 1985, 1987). Such curves or phase diagrams are described by equations of state derived from measurements or from expressions for the free energy as a function of volume V or area A or, for two component mixtures, the mole fraction X . The lowest total free energy path is obtained by the so-called common tangent construction (inset) or, equivalently, the *Maxwell construction*, which separates the shaded region into equal areas above and below the constant pressure coexistence line. The end points define the two-phase coexistence region, here defined by V_G and V_L , of the gas-to-liquid phase transition. Other phase transitions are shown by other horizontal coexistence lines. Transitions involving nonhorizontal lines, such as the liquid expanded-to-liquid condensed (L_E - L_C) transition, which is often seen in lipid monolayers, are not first-order transitions between two thermodynamic phases and are discussed in Part III. For the 3D van der Waals equation of state, $(P + a/V^2)(V - b) = RT$, the critical point, defined by $(dP/dV)_T = (d^2P/dV^2)_T = 0$, occurs at $T_c = 8a/27Rb$, $V_c = 3b$, and $P_c = a/27b^2$.

6.4 Gas-Liquid and Liquid-Solid Phase Transitions in 3D and 2D

Both the three-dimensional and two-dimensional van der Waals equations of state can be applied to more complex systems—for example, to the interactions of small colloidal particles in a liquid and surfactant molecules on the surface of water or at an oil-water interface.⁶ Both equations predict the existence of a gas-liquid coexistence regime at

⁶By convention, a *surface* refers to a condensed (liquid or solid) phase exposed to a vacuum or vapor. An *interface* separates two condensed phases.

some particular pressure as long as the temperature T is below the critical temperature, T_c . This first-order gas-liquid *phase transition* is primarily due to the attractive forces between the molecules or particles. For molecules or particles that interact as hard-spheres, or between which there is a purely *repulsive* force as often occurs on surfaces (cf. Chapter 7), the constant a in Eqs. (6.8) and (6.15) becomes zero or negative. The resulting equations then predict a monotonic decrease of V with P , or A with Π , with no gas-to-liquid transition—for example, no gas-liquid two-phase region or a boiling temperature.

At sufficiently high pressures where the density approaches the close-packing density, there is always a liquid-to-solid transition from a disordered (liquid) state to an ordered crystalline (solid) state, as shown in Figure 6.1. This type of transition can arise even in the absence of any attractive forces, and it is known as an *Alder* or *Kirkwood-Alder transition* (Alder et al., 1968). Alder transitions are intimately related to the excluded volume and geometry of molecules or particles, and they arise because the only way they can get closer together is by going from a disordered or random liquid-like configuration to an ordered solid-like one (Figures 6.2a and b), which cannot be done continuously.

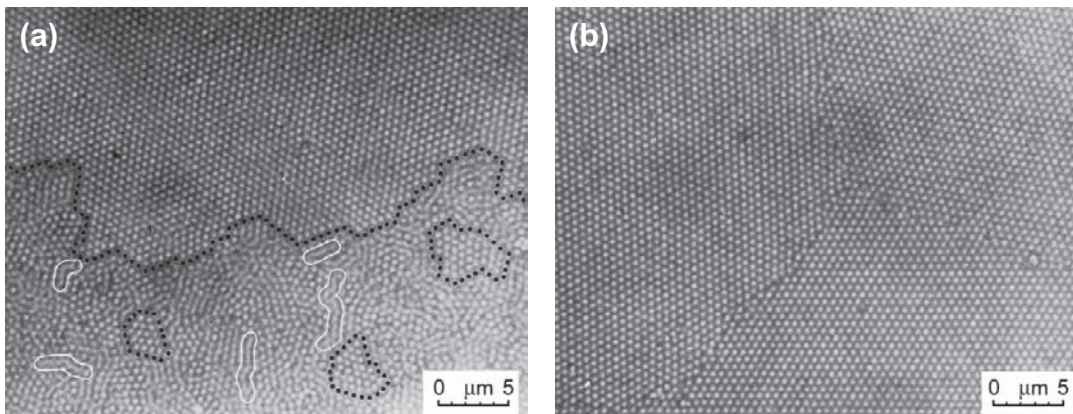


FIGURE 6.2 Optical microscope views of 400 nm diameter colloidal particles interacting via a purely repulsive short-range force in aqueous solutions. **(a)** Liquid-solid coexistence regime—that is, a two-phase region—occurs at intermediate particle densities. In the ordered solid phase the particles are in rapid thermal (Brownian) motion but are constrained to remain within their lattice sites—that is, the motion is highly localized. In the disordered liquid phase the particles can traverse over large distances and appear to do so in a snakelike fashion, known as *reptation* (see the smeared outlines within the liquid domain arising from the finite exposure time). Note the diffuse nature of the solid-liquid “interface” (dotted line), and bear in mind that it is continually fluctuating and will have a completely different shape a short time later. Molecular Dynamics simulations indicate that the same concepts and behavior apply at the molecular level (Glaser and Clark, 1990). **(b)** At higher molecular or particle densities, there is only a single solid phase or “colloidal crystal.” However, in real systems, there are grain boundaries between solid domains or grains, where defects and impurity molecules tend to collect and where the molecular motion is either more restricted (more solidlike) or, as is the case here, less restricted (more liquidlike). Such grain boundaries slowly grow in time, one at the expense of the other (see Figure 19.6). [Micrographs courtesy of Sei Hachisu; see also Okamoto and Hachisu, 1977.]

Molecules on surfaces or in monolayers at an interface often have more complex phase diagrams because, in spite of the reduced dimensionality, there is an increase in the number of different molecular species and interactions involving molecules at the surface or interface with those in the vapor, liquid, or solid phases on both sides of the interface.

6.5 Van der Waals Forces between Polar Molecules

Three distinct types of forces contribute to the total long-range interaction between polar molecules, collectively known as the van der Waals force: the *induction* force, the *orientation* force, and the *dispersion* force. Each has an interaction free energy that varies with the inverse sixth power of the distance. Thus, for two dissimilar polar molecules, we have

$$\begin{aligned} w_{\text{VDW}}(r) &= -C_{\text{VDW}}/r^6 = -[C_{\text{ind}} + C_{\text{orient}} + C_{\text{disp}}]/r^6 \\ &= - \left[(u_1^2 \alpha_{02} + u_2^2 \alpha_{01}) + \frac{u_1^2 u_2^2}{3kT} + \frac{3\alpha_{01}\alpha_{02}h\nu_1\nu_2}{2(\nu_1 + \nu_2)} \right] / (4\pi\varepsilon_0)^2 r^6. \end{aligned} \quad (6.17)$$

Table 6.3 shows how these three forces contribute to the net van der Waals energies of some molecules. The table reveals some interesting and important properties of van der Waals interactions:

- *Dominance of dispersion forces.* Dispersion forces generally exceed the dipole-dependent induction and orientation forces except for small highly polar molecules, such as water. The relative unimportance of dipolar forces is clearly seen in the hydrogen halides: as we go from HCl to HI, the strength of the total van der Waals interaction increases while the dipole moments diminish. Note, too, that in the interaction between two dissimilar molecules of which one is nonpolar, the van der Waals energy is almost completely dominated by the dispersion contribution.
- *Comparisons with experimental data.* The agreements between the computed (theoretical) values for C_{VDW} and those obtained from the gas law coefficients a and b are surprisingly good, even for NH_3 and H_2O . It is also possible to estimate the molar cohesive energies of polar molecules (London, 1937), though the agreement is not as good as for the nonpolar spherical molecules listed in Table 6.1, partly because the effective diameters σ of polar (and therefore asymmetrical) molecules are not well defined. For example, for CH_3Cl of molecular diameter $\sigma \approx 0.43$ nm, using Eq. (6.5) we obtain $U \approx 29$ kJ mol $^{-1}$ compared to the experimental value for $L_m + L_v$ of ~ 26 kJ mol $^{-1}$, while for water ($\sigma = 0.28$ nm) with only four nearest neighbors per molecule (see Chapter 8), we find $U \approx 70$ kJ mol $^{-1}$ compared to the measured value of ~ 50 kJ mol $^{-1}$.
- *Interactions of dissimilar molecules.* The van der Waals interaction energy between two dissimilar molecules A and B is usually intermediate between the values for $A-A$ and $B-B$. In fact, the coefficient C_{VDW} for $A-B$ is often close to the geometric mean of $A-A$ and $B-B$. Thus, for $\text{Ne}-\text{CH}_4$, the geometric mean (see Table 6.3) is $\sqrt{4 \times 102} = 20$, which may be compared with the computed value of 19, while for $\text{HCl}-\text{HI}$ we obtain $\sqrt{123 \times 372} = 214$ compared to the computed value of 205. This procedure affords

Table 6.3 Induction, Orientation, and Dispersion Free Energy Contributions to the Total Van der Waals Energy in a Vacuum for Various Pairs of Molecules at 293 K

Similar Molecules		Van der Waals Energy Coefficients C (10^{-79} J m^6)						$\text{Total VDW Energy } C_{VDW}$		Dispersion Energy Contribution to Total (Theoretical) (%)
		Electronic Polarizability $\frac{\alpha_0}{4\pi\epsilon_0} (10^{-30}\text{m}^3)$	Permanent Dipole Moment $u (\text{D})^a$	Ionization Potential $I = h\nu_I (\text{eV})^b$	$C_{ind} \frac{2u^2\alpha_0}{(4\pi\epsilon_0)^2}$	$C_{orient} \frac{u^4}{3kT(4\pi\epsilon_0)^2}$	$C_{disp} \frac{3\alpha_0^2 h\nu_I}{4(4\pi\epsilon_0)^2}$			
Ne–Ne	0.39	0	21.6	0	0	4	4	4	100	100
CH ₄ –CH ₄	2.60	0	12.6	0	0	102	102	101	100	100
HCl–HCl	2.63	1.08	12.7	6	11	106	123	157	86	
HBr–HBr	3.61	0.78	11.6	4	3	182	189	207	96	
HI–HI	5.44	0.38	10.4	2	0.2	370	372	350	99	
CH ₃ Cl–CH ₃ Cl	4.56	1.87	11.3	32	101	282	415	509	68	
NH ₃ –NH ₃	2.26	1.47	10.2	10	38	63	111	162	57	
H ₂ O–H ₂ O	1.48	1.85	12.6	10	96	33	139	175	24	
Dissimilar Molecules		$\frac{u_1^2\alpha_{02} + u_2^2\alpha_{01}}{(4\pi\epsilon_0)^2}$			$\frac{u_1^2u_2^2}{3kT(4\pi\epsilon_0)^2}$	$\frac{3\alpha_{01}\alpha_{02}h\nu_1\nu_2}{2(4\pi\epsilon_0)^2(\nu_1 + \nu_2)}$				
Ne–CH ₄				0	0	19	19 ^c	—	100	
HCl–HI				7	1	197	205	—	96	
H ₂ O–Ne				1	0	11	12	—	92	
H ₂ O–CH ₄				9	0	58	67	—	87	

^a1 D = 3.336×10^{-30} Cm.

^b1 eV = 1.602×10^{-19} J.

^cThis approximate value may be compared with the ab initio calculation by Fowler et al., (1989) that gives $23 \times 10^{-79} \text{ J m}^6$.

a convenient way to estimate the van der Waals interactions between unlike molecules when direct experimental data are not available. However, for interactions involving highly polar molecules, such as water, it breaks down. For example, for H₂O–CH₄ (see Table 6.3), the net interaction is actually much less than that of H₂O–H₂O or CH₄–CH₄. Thus, water and methane are attracted to themselves more strongly than they are attracted to each other. It is partly for this reason that nonpolar molecules are not miscible (do not mix) with water but separate out into different phases in water. Such compounds (hydrocarbons, fluorocompounds, oils, fats) are known as *hydrophobic* (from the Greek, meaning “water fearing”), and their low water solubility and their propensity to separate into clusters or phases in water are known as the *hydrophobic effect*. Table 6.3, however, reveals only part of the story: in liquid water the temperature-dependent dipole-dipole interaction is greatly modified, and there are important solvation-type interactions, as will be discussed later.

6.6 General Theory of Van der Waals Forces between Molecules

The London theory of dispersion forces has two serious shortcomings. It assumes that atoms and molecules have only a single ionization potential (one absorption frequency), and it cannot handle the interactions of molecules in a solvent. In 1963 McLachlan presented a generalized theory of van der Waals forces that included in one equation the induction, orientation, and dispersion force and that could also be applied to interactions in a solvent medium. McLachlan’s expression for the van der Waals free energy of two molecules or small particles 1 and 2 in a medium 3 is given by the series (McLachlan, 1963a, b, c; 1964, 1965)

$$w(r) = -\frac{C_{\text{VDW}}}{r^6} = -\frac{6kT}{(4\pi\epsilon_0)^2 r^6} \sum_{n=0,1,2,\dots}' \frac{\alpha_1(iv_n)\alpha_2(iv_n)}{\epsilon_3^2(iv_n)}, \quad (6.18)$$

where $\alpha_1(iv_n)$ and $\alpha_2(iv_n)$ are the polarizabilities of molecules 1 and 2, and $\epsilon_3(iv_n)$ is the dielectric permittivity of medium 3, at *imaginary* frequencies iv_n , where

$$v_n = (2\pi kT/h)n \approx 4 \times 10^{13} n \text{ s}^{-1} \quad \text{at 300 K} \quad (6.19)$$

and where the prime over the summation (\sum') indicates that the zero frequency $n = 0$ term is multiplied by $\frac{1}{2}$. McLachlan’s equation looks complicated, but it is actually quite straightforward to compute once we realize that $\alpha(iv_n)$ and $\epsilon(iv_n)$ are *real* quantities that are easily related to measurable properties, as we shall now see. For a molecule with one absorption frequency (the ionization frequency), ν_I , its electronic polarizability at *real* frequencies ν is given by the damped simple harmonic oscillator model

$$\alpha(\nu) = \alpha_0/[1 + i\kappa(\nu/\nu_I) - (\nu/\nu_I)^2], \quad (6.20)$$

where the damping coefficient κ is usually small ($\kappa \ll 1$) and can be ignored. Note that since most absorption frequencies are in the ultraviolet region (typically, $\nu_I \approx 3 \times 10^{15} \text{ s}^{-1}$),

the value of α in the visible range of frequencies, $\nu = \nu_{\text{vis}} \approx 5 \times 10^{14} \text{ s}^{-1}$, is essentially the same as α_0 because then $(\nu_{\text{vis}}/\nu_1)^2 \ll 1$.

If the molecule also possesses a permanent dipole moment u , there is an additional dipolar polarizability contribution that is given by Eq. (5.7) as $\alpha_{\text{dip}} = u^2/3kT$. This, however, is the time-averaged or “zero frequency” value. At finite frequencies the full frequency-dependent expression for the dipole polarizability is

$$\alpha_{\text{dip}}(\nu) = u^2/3kT(1 - i\nu/\nu_{\text{rot}}), \quad (6.21)$$

where ν_{rot} is some average rotational relaxation frequency for the molecule that is usually in the far infrared or microwave region of frequencies (typically, $\nu_{\text{rot}} \approx 10^{11} \text{ s}^{-1}$). Equations (6.20) and (6.21) for $\alpha(\nu)$ are complex, containing both real and imaginary parts. The imaginary parts are a measure of the energy absorbed by a molecule when it is stimulated by light.

The total polarizability of a molecule in free space as a function of $i\nu_n$ (replacing ν by $i\nu_n$) may now be written as

$$\alpha(i\nu_n) = \frac{u^2}{3kT(1 + \nu_n/\nu_{\text{rot}})} + \frac{\alpha_0}{1 - \kappa(\nu_n/\nu_1) + (\nu_n/\nu_1)^2} \quad (6.22)$$

which is a *real* function of ν_n . At zero frequency ($\nu_n = 0$) this reduces to the Debye-Langevin equation, Eq. (5.8), as expected:

$$\alpha(0) = u^2/3kT + \alpha_0. \quad (6.23)$$

The variation of $\alpha(i\nu_n)$ with frequency ν for a simple polar molecule is shown schematically in Figure 6.3.

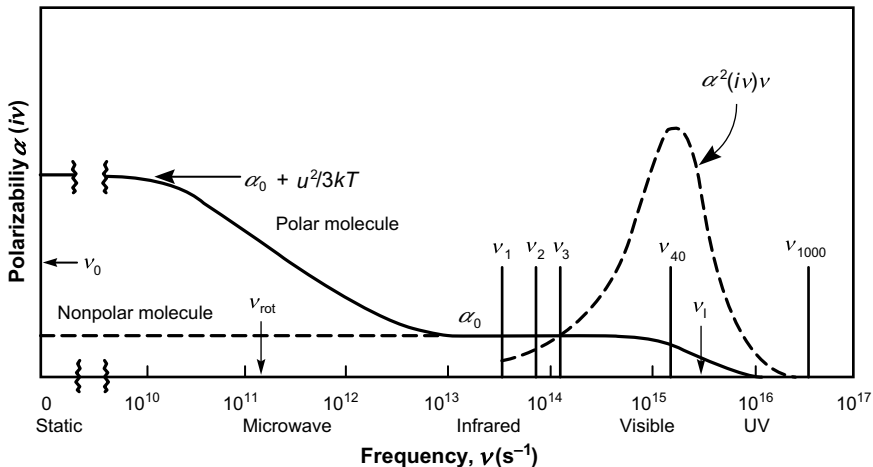


FIGURE 6.3 The molecular polarizability $\alpha(iv)$ as a function of frequency ν of a simple polar molecule as given by Eq. (6.22). The frequencies $\nu_n = 4 \times 10^{13} n \text{ s}^{-1}$, at which $\alpha(iv)$ contributes to the van der Waals energy (at 300 K), are shown as a series of vertical lines. The area under the dashed curve of $\alpha^2(iv)v$ shows how different regions of the spectrum contribute to the net dispersion energy.

We may now return to McLachlan's expression, Eq. (6.18). The first term in the series is that for $n = 0$ (i.e., $\nu_n = 0$), so from the above, we immediately obtain the "zero frequency contribution" to $w(r)$:

$$\begin{aligned} w(r)_{\nu=0} &= -\frac{3kT}{(4\pi\varepsilon_0)^2 r^6} \alpha_1(0)\alpha_2(0) \\ &= -\frac{3kT}{(4\pi\varepsilon_0)^2 r^6} \left[\frac{u_1^2}{3kT} + \alpha_{01} \right] \left[\frac{u_2^2}{3kT} + \alpha_{02} \right], \end{aligned} \quad (6.24)$$

which is identical to the second part of Eq. (5.26) and includes both the orientation (Keesom) and induction (Debye) interaction energies discussed earlier.

Let us now turn to the nonzero frequency terms ($n = 1, 2, 3, \dots$) of Eq. (6.18). The summation entails calculating the values of $\alpha(iv_n)$ at the discrete frequencies given by Eq. (6.19). Now, as shown in Figure 6.3, at normal temperatures the first frequency $\nu_{n=1} \approx 4 \times 10^{13} \text{ s}^{-1}$ is already much greater than ν_{rot} , so $\alpha(iv_n)$ is effectively determined solely by the electronic polarizability contribution in Eq. (6.22). Further, since $\nu_{n=1}$ is still much smaller than a typical absorption frequency $\nu_I \approx 3 \times 10^{15} \text{ s}^{-1}$, it is clear that the frequencies ν_n are very close together in the UV region. We may therefore replace the sum of discrete frequencies Σ by an integration over n —that is, $dn = (h/2\pi kT)d\nu$ —so that

$$kT \sum_{n=1,2,\dots}^{\infty} \rightarrow \frac{h}{2\pi} \int_{\nu=\nu_1}^{\nu=\infty} d\nu. \quad (6.25)$$

Applying this to Eq. (6.18), we obtain for the "finite frequency" free energy contribution to $w(r)$:

$$w(r)_{\nu>0} = -\frac{3h}{(4\pi\varepsilon_0)^2 \pi r^6} \int_0^{\infty} \alpha_1(iv) \alpha_2(iv) d\nu, \quad (6.26)$$

where, because $\nu_1 \ll \nu_I$, the lower integration limit ν_1 has been replaced by $\nu = 0$. Finally, by substituting the electronic polarizability as expressed by Eq. (6.22) into the above, putting $\kappa = 0$, and integrating using the definite integral

$$\int_0^{\infty} \frac{dx}{(a^2 + x^2)(b^2 + x^2)} = \frac{\pi}{2ab(a+b)}, \quad (6.27)$$

we obtain

$$w(r)_{\nu>0} \approx -\frac{3\alpha_{01}\alpha_{02}}{2(4\pi\varepsilon_0)^2 r^6} \frac{h\nu_{I1}\nu_{I2}}{(\nu_{I1} + \nu_{I2})} \quad (6.28)$$

which is the London equation. The complete McLachlan formula is particularly suitable for computing the dispersion forces between molecules that have a number of different absorption frequencies or ionization potentials, for which the simple London expression breaks down.

6.7 Van der Waals Forces in a Medium

The theory of McLachlan is also naturally applicable to the interactions of molecules or small particles in a medium (McLachlan, 1965). In this case the polarizabilities $\alpha(iv)$ in Eq. (6.18) are the *excess polarizabilities* of the molecules, as discussed in Section 5.8, and for a small spherical molecule 1 of radius a_1 in a medium 3 (Figure 6.4a), the excess polarizability is given by Eq. (5.28) as

$$\alpha_1(v) = 4\pi\varepsilon_0\varepsilon_3(v) \left(\frac{\varepsilon_1(v) - \varepsilon_3(v)}{\varepsilon_1(v) + 2\varepsilon_3(v)} \right) a_1^3 \quad (6.29)$$

The zero-frequency contribution to $w(r)$ in Eq. (6.18) is therefore

$$w(r)_{v=0} = -\frac{3kTa_1^3a_2^3}{r^6} \left(\frac{\varepsilon_1(0) - \varepsilon_3(0)}{\varepsilon_1(0) + 2\varepsilon_3(0)} \right) \left(\frac{\varepsilon_2(0) - \varepsilon_3(0)}{\varepsilon_2(0) + 2\varepsilon_3(0)} \right), \quad (6.30)$$

where $\varepsilon_1(0)$, $\varepsilon_2(0)$, and $\varepsilon_3(0)$ are the static dielectric constants of the three media. Equation (6.30) is the same as that previously derived and discussed in Section 5.8 in connection with the orientation and induction forces in a medium. We shall return to it again after first considering the finite frequency “dispersion” contribution. Substituting Eq. (6.29) into Eq. (6.18), and replacing the summation by the integral of Eq. (6.25), the dispersion energy may be written as

$$w(r)_{v>0} = -\frac{3ha_1^3a_2^3}{\pi r^6} \int_0^\infty \left(\frac{\varepsilon_1(iv) - \varepsilon_3(iv)}{\varepsilon_1(iv) + 2\varepsilon_3(iv)} \right) \left(\frac{\varepsilon_2(iv) - \varepsilon_3(iv)}{\varepsilon_2(iv) + 2\varepsilon_3(iv)} \right) dv. \quad (6.31)$$

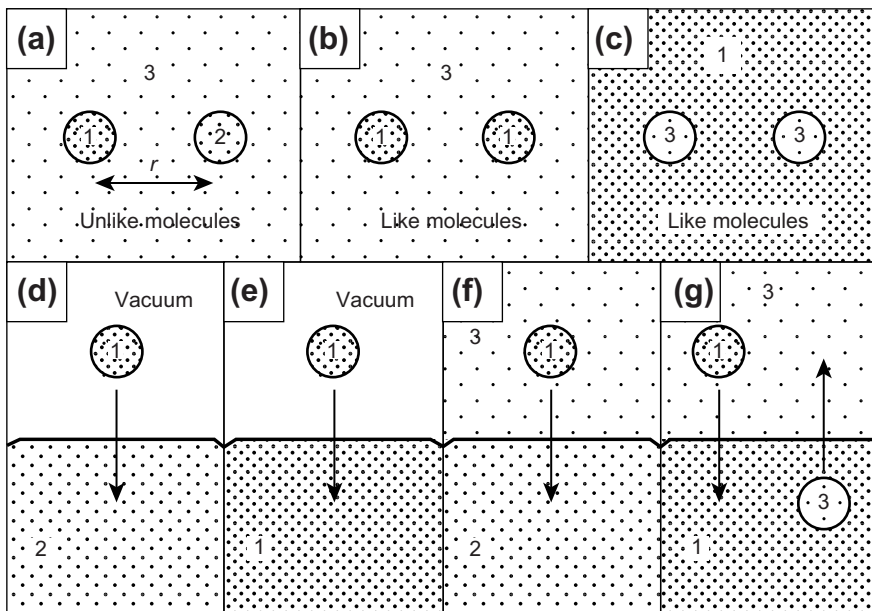


FIGURE 6.4 (a–c) Molecules of radii a (diameter $\sigma = 2a$) interacting in a solvent medium. (d–g) Transfer of molecules from one medium to another.

Unfortunately, complete data on the frequency-dependent absorption of materials are not always available, and it is necessary to adopt models that suitably represent the dielectric behavior of the media. In the previous section we saw how it was possible to derive London's result for the dispersion force by treating molecules as simple harmonic oscillators. Similarly, for a dielectric medium that has one strong electronic absorption peak at a frequency ν_e (which is usually slightly different from that of the isolated molecules in the gas ν_1), we may express its dielectric permittivity at frequencies $\nu > \nu_{n=1}$ as

$$\varepsilon(\nu) = 1 + (n^2 - 1)/[1 - (\nu/\nu_e)^2] \quad (6.32)$$

so that

$$\varepsilon(iv) = 1 + (n^2 - 1)/[1 + (\nu/\nu_e)^2], \quad (6.33)$$

where n is now the refractive index, roughly equal to $\sqrt{\varepsilon(\nu_{\text{vis}})}$. Substituting the preceding into Eq. (6.31) and integrating as before, we obtain

$$w(r)_{\nu>0} = -\frac{\sqrt{3}h\nu_e a_1^3 a_2^3}{2r^6} \frac{(n_1^2 - n_3^2)(n_2^2 - n_3^2)}{(n_1^2 + 2n_3^2)^{1/2}(n_2^2 + 2n_3^2)^{1/2}[(n_1^2 + 2n_3^2)^{1/2} + (n_2^2 + 2n_3^2)^{1/2}]}, \quad (6.34)$$

where, for simplicity, it is assumed that all three media have the same absorption frequency ν_e . The total van der Waals interaction free energy of two identical molecules 1 in medium 3 (Figure 6.4b) is therefore

$$w(r) = w(r)_{\nu=0} + w(r)_{\nu>0} \approx - \left[3kT \left(\frac{\varepsilon_1(0) - \varepsilon_3(0)}{\varepsilon_1(0) + 2\varepsilon_3(0)} \right)^2 + \frac{\sqrt{3}h\nu_e}{4} \frac{(n_1^2 - n_3^2)^2}{(n_1^2 + 2n_3^2)^{3/2}} \right] \frac{a_1^6}{r^6}. \quad (6.35)$$

The above equations highlight a number of important aspects of van der Waals forces in a solvent medium:

- (i) Since $h\nu_e \gg kT$, we find, as for interactions in free space, that the $\nu > 0$ dispersion force contribution is usually, but not always, greater than the $\nu = 0$ dipolar contribution. For example, in the case where $\varepsilon = n^2 \approx 2$ and $\nu_e = 3 \times 10^{15} \text{ s}^{-1}$, the ratio of the two contributions will be $h\nu_e/2\sqrt{3}kT \approx 140$.
- (ii) The van der Waals force is much reduced in a solvent medium. For example, for two nonpolar molecules of refractive index $n_1 = n_2 = 1.5$, the strength of the dispersion force in a solvent of $n_3 = 1.4$ will be reduced from its value in free space (where $n_3 = 1$) by a factor of

$$\frac{(1.5^2 - 1)^2 (1.5^2 + 2)^{-3/2}}{(1.5^2 - 1.4^2)^2 (1.5^2 + 2 \times 1.4^2)^{-3/2}} \approx 32.$$

- (iii) It is worth comparing the $\nu > 0$ dispersion contribution of Eq. (6.35) with London's equation for the free space interaction. If we put $n_3 = 1$, we obtain

$$w(r)_{\nu>0} = -\frac{\sqrt{3}\hbar\nu_e a_1^6}{4r^6} \frac{(n_1^2 - 1)^2}{(n_1^2 + 2)^{3/2}} \quad (6.36)$$

whereas London's result is

$$w(r) = -\frac{3\hbar\nu_1 \alpha_0^2}{4(4\pi\epsilon_0)^2 r^6} = -\frac{3\hbar\nu_1 a_1^6}{4r^6} \frac{(n_1^2 - 1)^2}{(n_1^2 + 2)^2}. \quad (6.37)$$

The reason for the apparent discrepancy is that the absorption frequency of an isolated molecule ν_1 is different from that of the condensed phase ν_e . It is a simple matter to ascertain that if $\alpha(\nu)$ and $\epsilon(\nu)$ are related by the Clausius-Mossotti-Lorenz-Lorentz equations: $\alpha(\nu) \propto [\epsilon(\nu) - 1]/[\epsilon(\nu) + 2]$, then the two absorption frequencies are formally related by

$$\nu_e = \nu_1 \sqrt{3/(n_1^2 + 2)} \quad (6.38)$$

so that when this is put into Eq. (6.36), we obtain the result based on London's formula, Eq. (6.37).

- (iv) The dispersion force between similar molecules is always attractive, while that between dissimilar molecules can be attractive or repulsive. The latter occurs when n_3 is intermediate between n_1 and n_2 in Eq. (6.34). Examples of repulsive van der Waals forces are presented in Chapter 13. In contrast, the interaction between identical molecules is always attractive due to the symmetry of Eq. (6.35), and we may further note that if the solute and solvent molecules, 1 and 3, are interchanged (Figures 6.4b → c), the expression for the van der Waals force between the two solute (ex-solvent) molecules remains practically the same.

The above equations provide a semiquantitative criterion for determining which liquids are likely to be miscible and which are not. As a rule of thumb, it is known that "like dissolves like." This becomes readily apparent from Eq. (6.35), where we see that the smaller the difference between n_1 and n_3 , the smaller the attraction between two solute molecules (Figures 6.4b, c) and the less will be their tendency to associate (i.e., separate out into different phases). Since Eq. (6.35) basically depends on the magnitude of $(n_1^2 - n_3^2)^2$ we may expect two liquids to become immiscible once $(n_1^2 - n_3^2)^2$ becomes too large. Now this can be written as

$\left[\sqrt{(n_1^2 - 1)^2} - \sqrt{(n_3^2 - 1)^2} \right]^2$, which from the Lorenz-Lorentz equation, Eq. (5.31), is roughly proportional to $\left[\sqrt{(\alpha_{01}^2/a_1^6)} - \sqrt{(\alpha_{03}^2/a_3^6)} \right]^2$ or

$$w(\sigma) \propto [\sqrt{U_1} - \sqrt{U_3}]^2, \quad (6.39)$$

where U_1 and U_3 are the cohesive energies or latent heats of vaporization of the two liquids [cf. Eq. (6.5)]. This semiquantitative derivation forms the basis of Hildebrand's "solvent solubility parameter", δ , which is equal to the square root of the cohesive energy density of a liquid (Small, 1953). It is found that if two nonpolar

liquids have similar values for δ —that is, if $(\delta_1 - \delta_2)^2$ is small—they are miscible and the binary mixture is nearly ideal—for example, it shows little deviation from Raoult's law. For a review of solubility relationships, see Kumar and Prausnitz (1975).

- (v) In some instances, the dispersion force between two molecules in a solvent is very small, and then the zero-frequency contribution dominates the interaction. The best-known cases concern fluorocarbons and the lower molecular weight alkanes in water whose refractive indices are very close to that of water (compare $n_{\text{CH}_4} \approx 1.30$, $n_{\text{C}_4\text{H}_{16}} \approx 1.33$ and $n_{\text{C}_5\text{H}_{12}} \approx 1.36$ with $n_{\text{H}_2\text{O}} \approx 1.33$). When these molecules interact in water (or vice versa), the major contribution is now not the dispersion force but rather the first term in Eq. (6.35), and since $\epsilon_{\text{H}_2\text{O}}(0) \approx 80$ while $\epsilon_{\text{alkane}}(0) \approx 2$, this term is large and reduces to approximately

$$w(r)_{\nu=0} \approx \frac{-kTa_1^6}{r^6} \quad (6.40)$$

which is purely entropic. Equation (6.40) shows that there is an increase in entropy as two alkane molecules approach each other in water, which is indicative of an increase in the degrees of freedom of the water molecules. It has long been known that the “hydrophobic interaction” between small hydrocarbon molecules in water is mainly entropic, but the measured values to date suggest a far stronger interaction than would be expected from Eq. (6.40). Thus, for two small molecules of radius a , we would expect a free energy of dimerization of order $kT(a/2a)^6 \approx kT/64$, or about 0.04 kJ mol^{-1} at 25°C (not enough to induce immiscibility), whereas the experimental values are at least 100 times larger: approximately 10 kJ mol^{-1} for CH_4 , C_6H_6 , and C_6H_{12} (Tucker et al., 1981). This lack of agreement is related to the breakdown in the simple model of the excess polarizability involving highly polar solvent or solute molecules, as discussed in Section 5.8. The unique and unusual properties of water, both as a solvent and as a medium for solute-solute interactions, are further investigated in Chapter 8 and in Part II.

Worked Example 6.2

Question: Two different nonpolar solute molecules repel each other via van der Waals dispersion forces in a different nonpolar solvent medium.

- In another three-component system, the optical properties of one of the solutes and the medium have been reversed. Will the two solute molecules now (a) repel each other, (b) attract each other, or (c) either of these?
- Repeat the above analysis for the case where the two solute molecules initially attract each other in the medium.
- Could the outcomes be different if one or more of the three media are highly polar?

Answer: Consider the three media A, B, and C as having refractive indices in the ratio 1:2:3, respectively. The interaction of A and C in medium B may be denoted by A|B|C or, in terms of the relative magnitudes of the refractive indices, by 1|2|3.

- The initial *repulsive* configurations must be 1|2|3 and, therefore, 2|1|3 or 1|3|2 after the exchange of properties. Since the refractive index of the medium is now either lower or higher than those of both solute molecules, the resulting interaction is attractive in both cases, so the answer is (b).
 - The initial *attractive* configurations must be 2|1|3 or 1|3|2 and, therefore, 1|2|3, 2|3|1, 3|1|2 or 1|2|3 after the exchange of properties. The first and fourth configurations are repulsive (and identical), while the second and third are attractive, so the answer is (c).
 - If one or more of the three media are polar—for example, if we have both a refractive index and dielectric contribution to the van der Waals interaction—the above conclusions will not change, as can be easily verified by using different values for n_i and ϵ_i . But the rigorous answer to all three of the questions is ultimately a thermodynamic one, independent of the type of interaction giving rise to the effect. Thus, considering bodies 1 and 2 in medium 3, cases 1 and 2 can be expressed in terms of interfacial energies as $\gamma_{12} - \gamma_{13} - \gamma_{32} = \pm \epsilon$, where $+\epsilon$ implies repulsion and $-\epsilon$ attraction. After switching the properties of 1 and 3, we have to determine the sign of $\gamma_{23} - \gamma_{13} - \gamma_{12}$ (remember that $\gamma_{ij} = \gamma_{ji}$), which can be expressed as $\gamma_{23} - \gamma_{13} - \gamma_{12} = -2\gamma_{13} - \epsilon$ for case 1 and $-2\gamma_{13} + \epsilon$ for case 2. Since γ_{ij} and ϵ are always positive, we find that in case 1 the resulting interaction is always attractive, while in scenario 2 it can go either way. The answer is therefore no.
-



6.8 Dispersion Self-Energy of a Molecule in a Medium

The concept of a dispersion self-energy of a molecule is analogous to the Born self-energy of an ion (Chapter 3), and, as for ions, it provides insight into the solubility and partitioning of molecules in different solvents. There are a number of different approaches to this problem (Mahanty and Ningham, 1976). We shall adopt the simplest, which nevertheless brings out the essential physics. Let us consider the transfer of a molecule 1 of diameter σ from free space into a medium 2 (Figure 6.4d), where it becomes surrounded by 12 solvent molecules of similar diameter. The free energy change is therefore given by the (positive) energy needed to first create a cavity, which involves breaking six solvent-solvent “bonds,” plus the (negative) energy of placing molecule 1 in the cavity, which involves the formation of 12 new solute-solvent “bonds.” Thus, for this process,

$$\Delta\mu_{\text{disp}}^{\text{i}} \approx \frac{3h\nu_1}{4(4\pi\epsilon_0)^2\sigma^6}[6\alpha_{02}^2 - 12\alpha_{01}\alpha_{02}], \quad (6.41)$$

where ν_1 is assumed to be the same for the solute and solvent molecules. We may already note that if medium 2 = medium 1 (Figure 6.4e), the above reduces to the result based on the London equation, Eq. (6.5), which gives the cohesive energy of the pure liquid or solid.

More generally, the free energy of transfer of a molecule 1 from medium 3 into medium 2 (Figure 6.4f) is therefore given by

$$\Delta\mu_{\text{disp}}^{\text{i}} \approx \frac{3h\nu_1}{4(4\pi\epsilon_0)^2\sigma^6}[(6\alpha_{02}^2 - 12\alpha_{01}\alpha_{02}) - (6\alpha_{03}^2 - 12\alpha_{01}\alpha_{03})], \quad (6.42)$$

which, using Eq. (5.31), is roughly proportional to

$$\Delta\mu_{\text{disp}}^{\text{i}} \propto -(\alpha_{02} - \alpha_{03})(2\alpha_{01} - \alpha_{02} - \alpha_{03}) \propto -(n_2^2 - n_3^2)(2n_1^2 - n_2^2 - n_3^2), \quad (6.43)$$

which can be positive or negative. In particular, the above shows that solute transfer is always energetically favored ($\Delta\mu_{\text{disp}}^{\text{i}}$ negative) into the solvent whose refractive index is closer to that of the solute molecule—a further manifestation of the “like dissolves like” rule (see Problem 6.2). If medium 2 = medium 1 (Figure 6.4g), the above reduces to

$$\Delta\mu_{\text{disp}}^{\text{i}} \approx -\frac{6(3hv_1)}{4(4\pi\varepsilon_0)^2\sigma^6}[\alpha_{01} - \alpha_{03}]^2 \quad (6.44)$$

$$\propto -(\sqrt{U_1} - \sqrt{U_3})^2 \propto -(n_1^2 - n_3^2)^2, \quad (6.45)$$

which is always negative and that applies equally to the two transfer processes shown in Figure 6.4g. Thus, it is always *energetically* favorable for a solute molecule to move into its own environment. It is interesting that the above is essentially the same result that was obtained in the previous section, Eq. (6.39), and leads to the same semi-empirical solubility relations as contained in the “solubility parameter” criterion. In particular, the very low solubility of alkanes and hydrocarbons in water, where $n_1 \approx n_3$, is once again seen not to be governed by their dispersion interaction but by other factors.

The above relationships and rule-of-thumb criteria, while useful, are limited to dispersion interactions and thus require that the solutes and solvents be nonpolar and have no strong electrostatic or hydrogen-bonding interactions. In Chapter 10 we shall develop similar relationships, based on cohesive energies, that can be applied to other phenomena as well (such as wetting).

6.9 Further Aspects of Van der Waals Forces: Anisotropy (Orientation), Nonadditivity (Many-Body), and Retardation Effects

In this final section we shall look at three important additional features of van der Waals forces: their dependence on the relative orientation of molecules (not only their separation, r); the contribution of other nearby “third body” molecules to the pair potential $w(r)$, and the modified expression for $w(r)$ at large separations. Similar features are encountered in other, such as H-bonding, interactions.

6.9.1 Anisotropy of Dispersion Forces

The polarizabilities of all but spherically symmetric molecules are anisotropic, having different values along different molecular directions. This arises because the electronic polarizabilities of bonds, which are a measure of the response of the electrons to an

external field, are anisotropic (Hirschfelder et al., 1954). For example, the longitudinal and transverse polarizabilities of the C–H bond are $\alpha_{\parallel}/4\pi\epsilon_0 = 0.79 \times 10^{-30} \text{ m}^3$ and $\alpha_{\perp}/4\pi\epsilon_0 = 0.58 \times 10^{-30} \text{ m}^3$; the mean value (quoted in Table 5.1) is $\frac{1}{3}(\alpha_{\parallel} + 2\alpha_{\perp})/4\pi\epsilon_0 = 0.65 \times 10^{-30} \text{ m}^3$. One consequence of the anisotropy in α is that the dispersion force between molecules becomes dependent on their mutual orientation (see Hirschfelder et al., 1954; Israelachvili, 1974). In nonpolar liquids the effect is not important, since the molecules are tumbling rapidly, and their *mean* polarizability is what matters. But in solids and liquid crystals the anisotropic attractive forces can sometimes be an important factor in driving molecules or molecular groups into favorable mutual orientations—for example, in determining the specific configurations of polymers and proteins, the ordering of molecules in liquid crystals, and the temperature-dependent phase transitions of lipid bilayers and monolayers.

The orienting effects of the anisotropic dispersion forces are usually not as strong as those of dipole-dipole and hydrogen-bonding forces. More importantly, for asymmetric molecules, the repulsive steric forces⁷ are also orientation-dependent, reflecting their asymmetric shape, and this is usually the dominating factor in determining how molecules mutually align themselves in liquids and especially in solids (see Chapter 7). For example, even for two methane molecules, their London dispersion coefficient C_{disp} is significantly higher in the $\text{H}_3\text{—CH}\cdots\text{HC—H}_3$ configuration, when the C–H bonds of two molecules are pointing toward each other, than in the $\text{H—CH}_3\cdots\text{H}_3\text{C—H}$ configuration. But the highest binding energy occurs in the latter configuration because the centers of the molecules can come closer together in this configuration (Szczesniak et al., 1990). The opposing effects of attractive dispersion and repulsive steric forces occur in most asymmetric systems—when the orientation of maximum interaction energy is also the one where the molecules can come closest together, which is the orientation that wins out.

6.9.2 Nonadditivity of Van der Waals Forces and Many-Body Effects

Unlike gravitational and Coulomb forces, van der Waals forces are not generally *pairwise additive*: the force between any two molecules is affected by the presence of other molecules nearby, so one cannot simply add all the pair potentials of a molecule to obtain its net interaction energy with all the other molecules. This is because the field emanating from any one molecule reaches a second molecule both directly and by “reflection” from other molecules, since they, too, are polarized by the field. This effect adds an additional contribution to the total van der Waals interaction energy. As shown in Figure 6.5 (see also Problem 6.4), the effect of the three-body interaction on the energy or force depends on the relative disposition of the molecules and can be positive or negative, so the net effect is usually small. For example, for a methane trimer in the triangular configuration, it is estimated that the three-body correction to the two-body (pair) interaction is less than 1% (Szczesniak et al., 1990). The overall effect of multiple- or multibody (including 4-body, 5-body, etc.) interactions usually results in an overall reduction in the strength of the

⁷Also known as “exchange repulsion.”

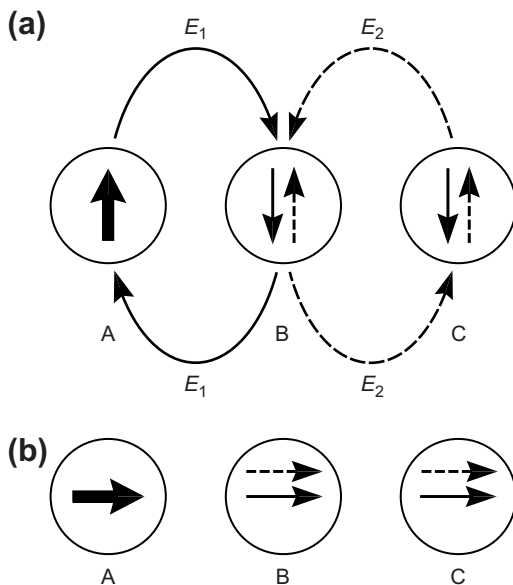


FIGURE 6.5 Reflected polarization fields of three atoms A, B, and C in line. **(a)** The instantaneous dipole moment of A is normal to the vertical line (thick arrow). The field of this dipole E_1 induces antiparallel dipoles in B and C (thin arrows), which are both attracted to A (the direct pair interaction). However, the induced dipole field E_2 of B induces a secondary dipole in C (dashed arrow) that is repelled from A. Likewise, the induced dipole field of C causes a secondary repulsion between B and A. The net three-body interaction energy for this configuration is therefore less favorable than the direct two-body (pair) interactions. **(b)** The instantaneous dipole moment of A is here parallel to the horizontal line (thick arrow). This induces parallel dipoles in B and C (thin arrows) that, again, are both attracted to A. However, the induced dipole field of B induces a secondary dipole in C (dashed arrow) that is now also attracted to A. Likewise, the induced dipole field of C causes a secondary attraction between B and A. The net three-body interaction energy for this configuration is therefore *more* favorable than the two-body interaction. When averaged over all possible configurations, the net effect is an overall slight enhancement of the attractive interaction (Margenau and Kestner, 1971). See Problem 6.4 for the case of three molecules located at the corners of a triangle.

summed pair interactions. But although small, many-body effects can be important because they do involve all the molecules in a lattice—for example, the total energy contributions, including many-body effects, to the lattice energies of the isotropic rare gas atoms, such as argon and xenon, determine that they pack as face-centered cubic (FCC) solids and not as hexagonal close-packed (HCP) solids. The nonadditive property of van der Waals forces is more important in the interactions between large particles and surfaces in a medium (Chapter 13).

6.9.3 Retardation Effects

When two atoms are an appreciable distance apart, the time taken for the electric field of the first atom to reach the second and return can become comparable with the period $1/\nu$ of the fluctuating dipole itself (cf. the distance traveled by light during one rotation

of a Bohr atom electron is $c/v = 3 \times 10^8 \text{ m s}^{-1}/3 \times 10^{15} \text{ s}^{-1} \approx 10^{-7} \text{ m}$ or 100 nm). When this happens, the field returns to find that the direction of the instantaneous dipole of the first atom is now totally different from the original and is less favorably disposed to an attractive interaction. With increasing separation above $r \sim 30 \text{ nm}$, the dispersion energy between two atoms begins to decay even faster than $-1/r^6$, approaching a $-1/r^7$ dependence by $r \sim 100 \text{ nm}$ (see Problem 6.5). This is called the *retardation effect*, and the dispersion forces between molecules and particles at large separations are called *retarded forces*.

For two molecules in free space, retardation effects begin at separations above 5 nm and are therefore of little interest. However, in a medium, where the speed of light is slower, retardation effects come in at smaller distances, and they become particularly important when macroscopic bodies or surfaces interact in a liquid medium, as we shall see in later chapters. Note that it is only the dispersion energy that suffers retardation; the zero-frequency orientation and induction energies remain nonretarded at all separations, so as the separation increases, these initially weak contributions ultimately dominate the interaction. Thus, as r increases to very large separations, the distance-dependence of the van der Waals energy between two molecules has the curious progression: $-1/r^6 \rightarrow -1/r^7 \rightarrow -1/r^6$.

PROBLEMS AND DISCUSSION TOPICS

- 6.1** Consider a molecule in a medium at a distance r from a straight-chained linear molecule composed of polarizable molecular groups⁸—for example, the CH₂ groups of an alkane molecule. By summing or integrating the pair potentials between the molecule and the molecular groups, show that the intermolecular van der Waals pair potential varies as $1/r^5$. Is this the same distance-dependence as for two straight-chained linear molecules that are parallel to each other?
- 6.2** A solution consists of solute molecules 1 dissolved in a liquid medium 2, where the refractive indices of 1 and 2 are $n_1 = 1.45$ and $n_2 = 1.50$. The solution is brought into contact with another liquid 3 that is completely immiscible with 2. It is found that most of the solute molecules 1 transfer from medium 2 into medium 3. What is the refractive index n_3 of medium 3? Assume that only dispersion forces are operating. Repeat the analysis for the case where $n_1 = 1.50$ and $n_2 = 1.45$. [Hint: It is not enough to calculate the change in the solute's dispersion self-energy on either side of the 2-3 interface; one must also establish that the solute is attracted from one side and repelled from the other. *Answer:* $1.45 < n_3 < 1.50$ in both cases.]
- 6.3*** Two nonpolar solute molecules 1 and 2 interact in a slightly polar medium 3 at 298 K. The interaction is dominated entirely by van der Waals forces, and the molecules may be considered to behave as small spheres with the same dielectric

⁸In the case of polymers, such groups are known as “segments” or “monomer units”; in the case of proteins, they are known as amino acid (AA) “residues.”

properties as the bulk materials whose properties are $n_1 = 1.40$, $n_2 = 1.50$, $n_3 = 1.45$, $\varepsilon_1 = n_1^2$, $\varepsilon_2 = n_2^2$, $\varepsilon_3 = 6.0$. If the absorption frequency ν_e of all three media is the same and equal to $3 \times 10^{15} \text{ s}^{-1}$, will the equilibrium interaction potential be (a) attractive at all separations, including contact, (b) repulsive at all separations, including contact, or (c) repulsive at small separations but attractive (adhesive) at some finite separation?

If your answer is (a) or (c), is the adhesion energy strong enough to lead to aggregation or phase separation of the solute in the solvent above some critical concentration (the solubility)?

- 6.4** The simple treatment used to derive the London equation for the dispersion interaction energy between two isolated molecules A and B (Section 6.1) can be extended to include the effect of a third molecule C. This arises because an additional component of the electric field from A reaches B by “reflection” from C (Figure 6.5). Consider three identical molecules of polarizabilities α and ionization potentials $I = h\nu$ sitting at the corners of a triangle with sides of length r_1 , r_2 , and r_3 . Ignoring numerical factors, derive a simple approximate expression in terms of α , I , r_1 , r_2 , and r_3 for the additional three-body interaction energy. On the basis of this equation, obtain a rough estimate for the magnitude of the three-body energy relative to the two-body (pair) interaction for the case when the three molecules are in contact—that is, when $r_1 = r_2 = r_3 = \sigma$. Explain, in qualitative terms, why the three-body contribution is negative (favorable) when three identical molecules are in line, as in Figure 6.5, but positive when in the symmetrical triangular configuration. [For further reading on three-, four-, and many-body effects, see Margenau and Kestner (1971).]
- 6.5*** Once two molecules (or particles) are sufficiently far apart, the simple model, based on two Bohr atoms, used to derive the London equation (Section 6.1) no longer holds. This is because the field reflected by the second atom returns to find that the direction of the original dipole has changed during the time it takes light to travel the distance $2r$. The extent of this change depends on the time it takes the Bohr electron to rotate about the nucleus—that is, it depends on the ionization frequency ν_I .⁹ Thus, in general, the inducing and induced dipoles become increasingly less correlated the farther two atoms or molecules are from each other, and this results in a weaker (retarded) dispersion attraction than that given by the London formula. By considering the McLachlan theory (Section 6.6), it is clear that at any given separation r not all frequencies will contribute to the interaction, so Eq. (6.26) should not really be integrated to $\nu = \infty$. By considering how some appropriate cutoff frequency must replace the upper integration limit in the derivation of the London equation, obtain an expression for the dispersion interaction potential between two identical molecules valid at all separations. Check that your equation predicts that the retarded dispersion energy is about half the (extrapolated)

⁹This “dynamic” explanation is strictly not correct (H. Wennerström - private communication).

nonretarded value at a separation of $r \approx c/\nu_I \approx 3 \times 10^8/3 \times 10^{15} \approx 100$ nm for typical values of ν_I , and comment on this result.

[*Answer:*

$$w(r) = \{-3h\nu_I\alpha_0^2/4(4\pi\varepsilon_0)^2r^6\}[2(\tan^{-1}x + x/(1+x^2))/\pi], \quad (6.46)$$

where $x = c/2\nu_Ir$, and where the term in curly brackets is the (nonretarded) London energy, Eq. (6.3). Thus, the term in square brackets is the correction term for retardation. For $r \gg c/2\nu_I$ ($x \ll 1$), $2(\tan^{-1}x + x/(1+x^2))/\pi \rightarrow 4x/\pi = 2c/\pi\nu_Ir$, giving $w(r) = -3\alpha_0^2hc/2\pi(4\pi\varepsilon_0)^2r^7$. In the limit of large separations the rigorously derived retarded dispersion interaction is given by the *Casimir-Polder* equation

$$w(r) = -23\alpha_0^2hc/8\pi^2(4\pi\varepsilon_0)^2r^7 \quad (6.47)$$

which is approximately 60% of the approximate equation, Eq. (6.46). Retardation effects come in at much smaller separations (see Section 13.10) because the dipoles cease to be correlated well before the electron has made a complete revolution.]

Repulsive Steric Forces, Total Intermolecular Pair Potentials, and Liquid Structure

7.1 Sizes of Atoms, Molecules, and Ions

At very small interatomic distances, the electron clouds of atoms overlap, and there arises a strong repulsive force that determines how close two atoms or molecules can ultimately approach each other. These repulsive forces are sometimes referred to as *exchange repulsion*, *hard core repulsion*, *steric repulsion*, or—for ions—the *Born repulsion*, and they are characterized by having very short ranges and increasing very sharply as two molecules come together. Strictly speaking, they belong to the category of quantum mechanical or chemical forces discussed earlier, and unfortunately there is no general equation for describing their distance dependence (see Table 2.2). Instead, a number of empirical potential functions have been introduced over the years, all of which appear to be satisfactory as long as they have the property of a steeply rising repulsion at small separations. The three most common such potentials are the *hard sphere potential*, the *inverse power-law potential*, and the *exponential potential*. Let us begin by considering the first one.

If atoms are considered as hard spheres—that is, incompressible—the repulsive force suddenly becomes infinite at a certain interatomic separation. This simple model reflects the observation that when different atoms pack together in liquids and solids, they often do behave as hard spheres, or “billiard balls,” of fixed radii characteristic for each atom. Defined in this way the radius of an atom (whether isolated or covalently bound) or a spherical molecule is then called its *hard sphere radius* or *van der Waals packing radius*. Results obtained from *x-ray* and neutron diffraction studies on solids, especially crystals, and from gas solubility, viscosity, and self-diffusion data on liquids often yield values that agree to within a few percentage points. The van der Waals packing radii of most atoms and small molecules lie between 0.1 and 0.2 nm, some of which are illustrated in Figure 7.1.

Similar concepts apply to ions in ionic crystals, where the characteristic packing radius is referred to as the *bare ion radius*. The bare ion radius is quite different from the hydrated ion radius of the ion in water, discussed in Section 4.5. Some bare ion radii are also shown in Figure 7.1. Note that anions are generally bigger than cations; this is because they have gained rather than lost electrons; this also causes an additional internal electrostatic repulsion between the electrons, which tends to further inflate the ion.

	Li^+	Na^+	K^+	NH_4^+	Cs^+	$\text{N}(\text{CH}_3)_4^+$
Monovalent cations						
	0.068	0.095	0.133	0.148	0.169	0.347
Divalent cations	Be^{2+} 	Mg^{2+} 	Fe^{2+} 	Ca^{2+} 	Ba^{2+} 	
	0.031	0.065	0.076	0.099	0.135	
Trivalent cations	Al^{3+} 	$\text{Fe}^{3+}, \text{Cr}^{3+}$ 	La^{3+} 			
	0.050	0.064	0.104			
Monovalent anions	F^- 	OH^- 	Cl^- 	Br^- 	I^- 	NO_3^-
	0.136	0.176	0.181	0.195	0.216	0.264
Spherical molecules	Ne 	Ar 	Kr 	Xe 	CH_4 	CCl_4
	0.154	0.188	0.201	0.216	0.20	0.275
Effective radii of nonspherical molecules and groups (approximate)	H_2O 0.14	O_2 0.18	NH_3 0.18	HCl 0.18	HBr 0.19	
	CH_3OH 0.21	CH_3Cl 0.215	CHCl_3 0.255	C_6H_6 0.265	C_6H_{12} 0.285	
	$-\text{CH}_3$ group 0.20	$-\text{CH}_2-$ group 0.20	$-\text{NH}_2$ group 0.17	$-\text{OH}$ group 0.145	Aromatic ring thickness 0.37	
Exposed radii of atoms covalently bonded in molecules		F 0.11	O 0.15	N 0.15	C 0.17	
	Cl 0.18	S 0.18	Br 0.19	P 0.19	I 0.20	
Covalent bond radii of atoms		$-\text{H}$ 0.03	$-\text{C}$ 0.077	$-\text{N}$ 0.070	$-\text{O}$ 0.066	$-\text{F}$ 0.064
			$=\text{C}$ 0.067	$=\text{N}$ 0.062	$=\text{O}$ 0.062	$-\text{Cl}$ 0.099
						$-\text{P}$ 0.110
			$\equiv\text{C}$ 0.060	$\equiv\text{N}$ 0.055		$-\text{Br}$ 0.114
						$-\text{Si}$ 0.117

FIGURE 7.1 Effective packing radii (in nm) of atoms, molecules, and ions, drawn to scale.

It is also recognized that the distance between the atomic centers of two atoms connected by a covalent bond can be expressed as the sum of their *covalent bond radii* (Figure 7.1). Single-bond covalent radii are usually about 0.08 nm shorter than the nonbonded (van der Waals) radii.

By considering both the covalent and van der Waals radii of individual atoms in a molecule and the bond angles between them, one can establish the effective van der Waals radius of a molecule. This concept is strictly valid only for small, nearly spherical molecules such as CH₄, but Bondi (1968) has described procedures for calculating the effective van der Waals radii of molecules and molecular groups, some of which are included in Figure 7.1. For very asymmetric molecules that cannot be considered even as quasi-spheres, one has to consider their van der Waals dimensions along different molecular axes. For example, in alkanes, the effective radius of the cylinder-like paraffin chain is about 0.20 nm, while its total length is 0.127 nm per CH₂–CH₂ link along the chain (0.154 nm along the bond) plus approximately 0.20 nm for each hemispherical CH₃ group at each end.

There are many different methods for measuring the radii of atoms and molecules. These include PVT and spectroscopic data on gases, viscosity, solubility, and diffusion data on both gases and liquids, and compressibility, electron, x-ray, and neutron diffraction data on liquids and solids. The values for molecular sizes deduced from these different methods can differ by as much as 30%, as illustrated in Table 7.1. This is because each method measures a slightly different property. Thus, molecular radii $\sigma/2$ determined from the van der Waals equation of state coefficient b , Eq. (6.12), $b = \frac{2}{3}\pi N_0 \sigma^3$

$$\sigma/2 = (3b/2\pi N_0)^{1/3}/2 = 0.463b^{1/3} \text{ nm } (b \text{ in dm}^3 \text{ mol}^{-1}) \quad (7.1)$$

gives the smallest value, since it reflects the sizes of molecules during collisions when they approach each other closer than their equilibrium separation. Values determined from the viscosity and self-diffusion of molecules in liquids (Ertl and Dullien, 1973; Dymond, 1981; Evans et al., 1981) usually yield results similar to those obtained from crystal packing (i.e., the van der Waals radii), while radii calculated from the mean molecular volume occupied in the liquid state (even assuming close-packing),

$$\frac{4}{3}\pi(\sigma/2)^3 = 0.7405(M/N_0\rho), \quad (7.2)$$

Table 7.1 Radii of Molecules ($\sigma/2$) Deduced from Different Methods

Molecule	Minimum Radius (nm) From van der Waals coefficient b , ^a Eq. (7.1)	Mean Radius (nm) From van der Waals packing radius (from Figure 7.1)	Maximum Radius (nm) From volume occupied in liquid at 20°C, Eq. (7.2)
CH ₃ OH	0.19	0.21	0.23
CHCl ₃	0.22	0.26	0.29
C ₆ H ₆	0.23	0.27	0.30
CCl ₄	0.24	0.28	0.305

^aConstants b taken from the *Handbook of Chemistry and Physics*, CRC Press, 56th ed.

yield the highest values, as shown in the last column of Table 7.1, because in the liquid state the mobile molecules are on average 5 to 10% farther apart than in the close-packed crystalline solid.

7.2 Repulsive Potentials

Returning now to our discussion of repulsive potentials, the *hard sphere* or *hard core potential* can be described by

$$w(r) = +(\sigma/r)^n \quad \text{where } n \rightarrow \infty. \quad (7.3)$$

Since for $r > \sigma$ the value of $w(r)$ is effectively zero, while for $r < \sigma$ it is infinite, this expression nicely describes the hard sphere repulsion where σ is the hard sphere diameter of an atom or molecule, which may be associated with twice the van der Waals radius.

Two other repulsive potentials are worthy of note: the *power-law potential*

$$w(r) = +(\sigma/r)^n, \quad (7.4)$$

where n is now an integer (usually taken between 9 and 16), and the *exponential potential*

$$w(r) = +ce^{-r/\sigma_0}, \quad (7.5)$$

where c and σ_0 are adjustable constants, with σ_0 of the order of 0.02 nm. Both of these potentials are more realistic in that they allow for the finite compressibility or “softness” of atoms. The power-law potential has little theoretical basis, while the exponential potential has some theoretical justification. It is generally recognized, however, that their common usage is due mainly to their mathematical convenience.

7.3 Total Intermolecular Pair Potentials: Their Form, Magnitude, and Range

The total intermolecular pair potential is obtained by summing the attractive and repulsive potentials. Figure 7.2a illustrates the two main types of repulsive potentials just discussed and the shapes of the potential functions they lead to when a long-range inverse power attractive term is added (Figure 7.2b). The best known of these is the *Lennard-Jones, L-J, or “6-12” potential*:

$$w(r) = -A/r^6 + B/r^{12} = 4\epsilon[(\sigma/r)^{12} - (\sigma/r)^6], \quad (7.6)$$

which is widely used because of its simplicity and inverse sixth-power attractive van der Waals term. The particular mathematical form given for the Lennard-Jones potential in Eq. 7.6 is commonly used, though it is well to note that the parameter σ is different from the molecular diameter. Thus, for the Lennard-Jones potential, $w(r) = 0$ at $r = \sigma$, and the minimum energy occurs at $r = 2^{1/6}\sigma = 1.12\sigma$ (Figure 7.2b). The minimum energy is $w(r) = -\epsilon$, where the attractive van der Waals contribution is -2ϵ while the repulsive energy contribution is $+\epsilon$. Thus the inverse 12th-power repulsive term decreases the

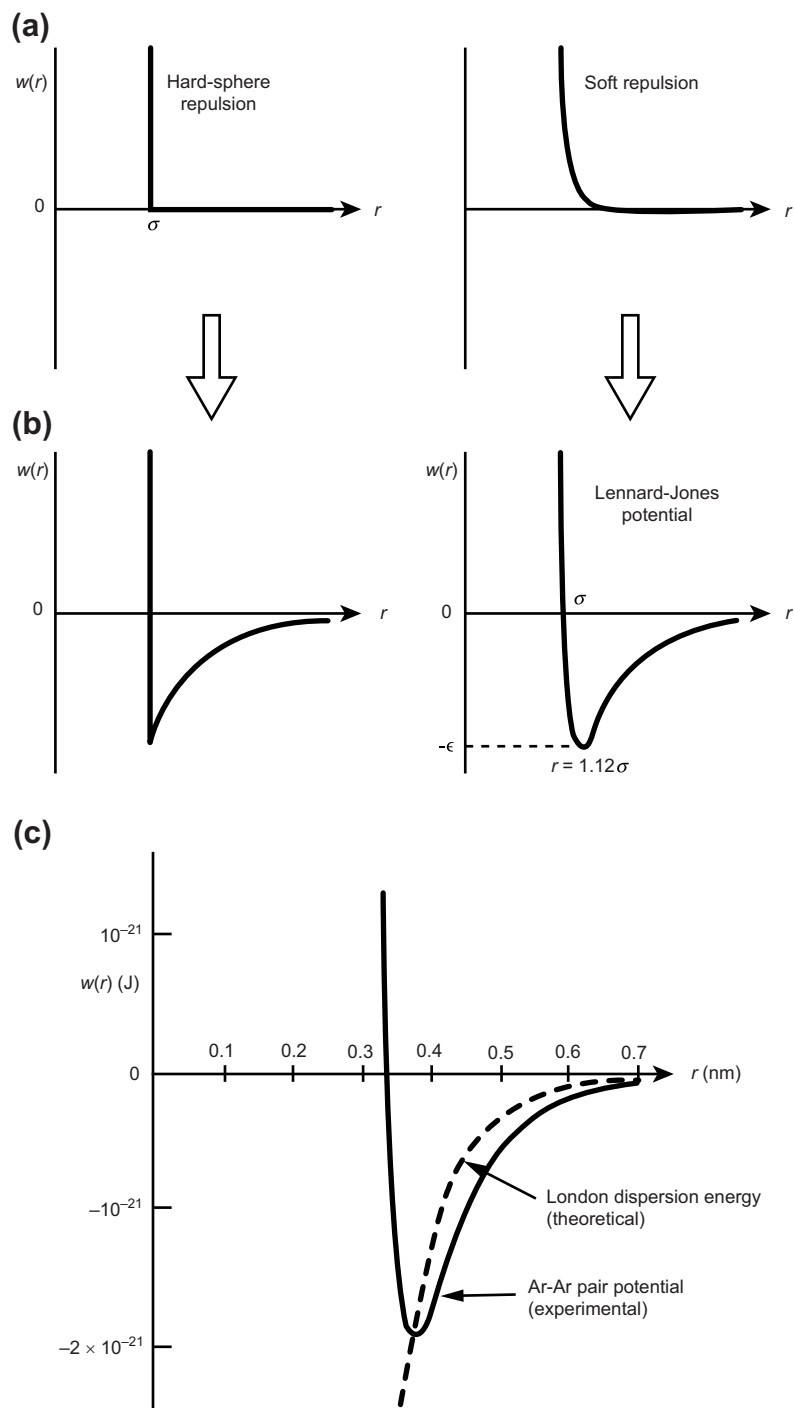


FIGURE 7.2 (a) Repulsive potentials. (b) Full pair potentials obtained by adding an attractive long-range potential to the preceding repulsive potentials. The packing diameter of a molecule is given by the value of r at the potential energy minimum. (c) Experimental Argon-Argon potential compared with the London dispersion energy. [(c) adapted from Parsons et al., 1972.]

Table 7.2 Different Potential Functions

Name/Type	Functional Form	Where It Arises
<i>Individual Attractive or Repulsive Potential Functions</i>		
Power law	$\pm A/r^n$	Attractive forces
Exponential	$+Ae^{-r/r_A}$ $-Ae^{-\kappa r}$	Repulsive steric forces; attractive electrostatic forces in solution
Hard wall	$w(r) = \infty$ at $r = \sigma$ $w(r) = 0$ at $r > \sigma$ Also expressible as $w(r) = +(\sigma/r)^n, n \rightarrow \infty$	Any infinitely sharp repulsion at $r = \sigma$
Yukawa, screened Coulomb	$\pm Ae^{-r/r_0}/r$, where $r_0 \approx 0.2\text{\AA}$ for Yukawa, Debye length κ^{-1} for electron gases and ionic solutions	Quantum mechanical forces; ionic interactions in solution
<i>Total Potential Functions (Combinations of the above)</i>		
Mie or $n-m$ potential Sutherland ^a ($m = \infty$)	$\frac{A}{r^n} + \frac{B}{r^m}, m > n$	Atoms, ions, and small molecules, physical and chemical bonds
Lennard-Jones ^a	$\frac{A}{r^6} + \frac{B}{r^{12}}$	Atoms and small molecules
Coulomb-hard wall ^a	$-(A/r) + (\sigma/r)^n, n \rightarrow \infty$	Ion-ion interaction in a vacuum
Buckingham (exp-6)	$\frac{A}{r^6} + Be^{-r/r_0}$	Physical and chemical bonds
Morse	$-Ae^{-r/r_A} + Be^{-r/r_B}$	General interatomic potential ^b
Triangular	$-A(r_0 - r)$ $w(r) = \infty$ at $r = 0$ $w(r) = 0$ at $r > r_0$	Polymer-surface and polymer bridging forces (Sections 9.2)
Square-well	$w(r) = \infty$ at $r < \sigma$ $w(r) = \text{constant} = -w_o$ $\sigma < r < r_0$ $w(r) = 0$ at $r > r_0$	Interactions of large molecules; polymer bridging forces (Problem 21.9)
Parabolic	$+A(r_0 - r)^2$ $F = -dw/dr = \pm 2A(r - r_0)$	Typical “elastic” energy around a potential energy minimum at r_0

^aSpecial forms of the Mie potential.

^bThe Morse potential is commonly used for covalent (chemical) bonds, but it is also arguably better suited for van der Waals interactions near the potential energy minima (Hart and Rappé, 1992).

strength of the binding energy at equilibrium by 50% (from -2ϵ to $-\epsilon$). This may be compared to the hard sphere repulsion potential where the binding energy at equilibrium would be just the van der Waals energy at contact (at $r = \sigma$). It is for this reason that the lattice energies of ionic crystals and van der Waals solids, calculated on the basis of a hard sphere repulsion, are sometimes too large (cf. Section 3.4). But quite often the hard sphere potential together with a London dispersion attraction gives excellent results when compared with the experimental molar lattice energies of nonpolar solids (cf. Table 6.1). This is because the attractive forces are usually stronger than predicted by

the simple London equation, which ignores contributions from other absorption frequencies, quadrupole interactions, and so forth. On the other hand, the repulsive potentials are believed to be steeper than $1/r^{12}$ and therefore weaker at the equilibrium separation than those given by the Lennard-Jones potential. All these effects conspire to make the hard sphere potential a reasonable one for predicting contact energies and phase behavior, but only for atoms and small molecules (see later and also Section 2.5). Figure 7.2c nicely illustrates this fortuitous cancellation of errors: here we see the experimentally determined pair potential for argon (Parsons et al., 1972) together with the London dispersion energy, $w(r) = -50 \times 10^{-79}/r^6$ J, taken from Table 6.1. Note how the theoretical dispersion attraction passes through the experimental curve almost exactly at its minimum value.

The pair potential function most commonly used so far has been the Mie and Lennard-Jones potentials. Other types of potentials also arise, especially for interactions involving more complex molecules such as polymers and for electrostatic interactions in aqueous solutions. Table 7.2 summarizes some of these potentials, many of which will be encountered in later chapters. Some potential functions have been adopted simply for their mathematical convenience, as in the case of the Mie, L-J, and Morse potentials, while others arise naturally in specific systems or situations, as in the case of the Yukawa, triangular, and square-well potentials. In many cases it is not crucial whether one uses the “correct” potential, whereas in others it is. For example, the Morse and exp-6 potentials do not increase indefinitely as $r \rightarrow 0$ and so cannot be used in this limit.

The repulsive term must be accurately known for determining certain interactions, especially dynamic and energy-dissipating processes (see the next section and Section 9.3), and even the values of the integers n or m in the Mie potential can be important, as illustrated in the following example.



Worked Example & Discussion Topic 7.1

Question: Interaction power-law potentials such as the Lennard-Jones potential, Eq. (7.6), and the Mie potential, Eq. (1.6), have a well-defined energy minimum at a well-defined distance but a “range” that is not well defined, since the attraction never disappears (except at $r = \infty$). Analyze the value of any discussion about “the range of an interaction.”

Answer: Traditionally, chemical bonds are considered as short-ranged, while physical bonds as being due to long-range forces, decaying as $-1/r^n$, which even for $n > 3$ is strictly (mathematically) of infinite range for any finite value of n . One may define the “effective range” as the distance at which the pair interaction equals kT , but this turns out not to be very useful for gases or condensed phases composed of many molecules whose separations vary from $r = \sigma$ to $r = \infty$. Neither the L-J potential nor the van der Waals equation of state ($P + a/V^2)(V - b) = kT$) contain a length scale that is indicative of “range”: these equations are in terms of σ , n , and the contact energy $w_0 = -C/\sigma^n$, where the only length scale is the diameter of the molecule, σ , which tells us nothing about the range of the interaction. A similar

conclusion applies to ionic crystals (Section 3.4), where the molar lattice energy is again essentially given by the ion-ion contact energy even though the Coulomb pair energy is still higher than kT at $r = 50$ nm.

Strictly, as we saw in Section 6.2, the L-J potential should not be applied to molecules consisting of more than a few atoms because the centers of the interacting atoms no longer coincide with the centers of the molecules. For such molecules, as well as for small colloidal particles, the square-well potential is a better model. The square-well potential (see Section 2.5) contains two length parameters σ and $(\sigma + \Delta)$, where the latter clearly defines the range of the interaction. Yet, as was seen in Section 2.5, the interaction *volume*, $\frac{4}{3}\pi[(\sigma + \Delta)^3 - \sigma^3]$, encompassed by the interaction (in units of m^3) is more meaningful than the interaction *range*, Δ (in m). For the square-well potential as $\Delta \rightarrow 0$, $a \rightarrow 0$, while for a Mie potential as $n \rightarrow \infty$, $a \rightarrow 0$, which leads to $P = kT/(V - b)$ in both cases, and the attractive *energy* has no effect, regardless of how deep it is! The critical point disappears, and there is no longer a gas-liquid transition or coexistence (but there is still a fluid-solid transition—the *Kirkwood-Alder* transition). Thus, the range of an interaction is a phrase to be avoided, at least for simple intermolecular potentials (unless $n \leq 3$). For $n > 3$ the only length scale that appears in equations is the molecular size, σ , which gives no indication of the range over which effects will be observed (cf. Figure 1.3). Later, when we consider complex colloidal-surface and polymer-associated interactions in liquids, where a number of different types of forces, both attractive and repulsive, may be occurring simultaneously, we will see that the different ranges of different forces contributing to the overall interaction *can* be very meaningful.

7.4 Role of Repulsive Forces in Noncovalently Bonded Solids

We now turn to the role of the repulsive parts of the intermolecular potential functions in solids. More often than not, it is these that determine many of their properties. The reason for this is that for many types of attractive interactions, their orientation or angle dependence is weak—that is, they are only weakly directional or anisotropic. This is particularly so for van der Waals forces. In contrast, the orientation dependence of the stabilizing repulsive force, which reflects the asymmetric shape of a molecule, often has a large effect. Thus, when molecules or ions come together in the condensed state, the way they can pack together—which is reflected in their relative sizes and shapes—now becomes a major consideration in determining their lattice structure, density, rigidity, internal energy, and so on.

They also determine their melting points but not their boiling points. To see why this is so, recall that latent heats of vaporization are closely associated with the cohesive energies in solids and liquids (Table 2.1). Thus, it is the *attractive* forces that mainly determine latent heats of vaporization and, by Trouton's rule, also their boiling points. Melting points, however, are determined by the geometry of molecules. If their shapes allow them to comfortably pack together into a lattice, they will tend to remain in this state and will therefore have a high melting point. If their shapes do not allow for good

packing, the melting point will be low. Note, too, that latent heats of melting are usually fairly small, an indication that on melting few “bonds” are broken; the main effect is a rearrangement of molecular ordering. Since the shape of a molecule is determined by its van der Waals dimensions, which is effectively a statement about its repulsive force, we can now see why repulsive forces are mainly responsible for melting, while attractive forces are mainly responsible for boiling.

This somewhat broad generalization can be illustrated by the melting points and boiling points of some hydrocarbons, shown in Table 7.3. Here we clearly see that the T_B values are not affected much by branching or by replacing a single C–C bond by a double C=C bond, since the intermolecular attractive forces are not much changed. But the T_M values are lowered dramatically because the regular crystalline packing of the all-*trans* chains is no longer possible when a “kink” is present somewhere along the otherwise linear molecules. Note how the effect of a single kink persists even for the 16-carbon hexadecane molecule. The last row of Table 7.3 shows that fluorocarbons exhibit similar trends. Note, however, that while their boiling temperatures are similar,

Table 7.3 Effect of Double Bonds and Chain Branching on Melting and Boiling Points of Hydrocarbons

Hydrocarbon		T_M (°C)	T_B ^a (°C)
C ₆ H ₁₄	<i>n</i> -Hexane	−95	69
C ₆ H ₁₂	1-Hexene	−140	63
C ₆ H ₁₂	2-Hexene (<i>cis</i>)	−141	69
C ₆ H ₁₄	2-Methyl pentane	−154	60
C ₈ H ₁₈	<i>n</i> -Octane	−57	126
C ₈ H ₁₆	1-Octene	−102	121
C ₈ H ₁₆	2-Octene (<i>cis</i>)	−100	126
C ₈ H ₁₈	2-Methyl heptane	−120	119
C ₁₂ H ₂₆	<i>n</i> -Dodecane	−10	216
C ₁₂ H ₂₄	1-Dodecene	−35	213
C ₁₆ H ₃₄	<i>n</i> -Hexadecane	18	287
C ₁₆ H ₃₂	1-Hexadecene	4	285
C ₁₈ H ₃₂	<i>n</i> -octadecane	28	317
C ₁₈ H ₃₀	1-octadecene	18	315
C ₁₈ H ₃₀	9-octadecene ^b	−30.5	—
Hydrocarbon versus Fluorocarbon		T_M (°C)	T_B ^a (°C)
C ₁₂ H ₂₆	<i>n</i> -Dodecane	−10	216
C ₁₂ F ₂₆	<i>n</i> -Perfluoro-octadecane	100	184 (est ^c)

^aAt 760 mm Hg.

^b*Cis* double bonds in biological lipid chains usually occur near the center of the chains where they are most effective in fluidizing bilayers.

^cLe and Weers (1995).

if generally lower than those of hydrocarbons of the same carbon number, their melting points are significantly higher. This is due to the rotational inflexibility of the bulky C–F groups about the C–C bonds resulting in rigid molecules that can pack tightly together.

For some molecules, however, the orientation dependence of their attractive forces plays the dominant role in determining their solid- and liquid-state properties. This is, of course, especially true of covalent bonds but also when strongly directional dipolar and hydrogen-bonding interactions are involved. A particularly notable example of this phenomenon is the water molecule whose interactions are so remarkable (and important) that they are given special attention in the next chapter.

Most molecules are far from spherical, and both their size and shape determine how they will pack in their different solid or liquid-crystalline phases, or “order” in the liquid state.¹ The sizes and shapes of large complex and asymmetric molecules such as surfactants, lipids, polymers, proteins, and other biological macromolecules, are particularly important in determining how they can pack together, “self-assemble,” or fold into structures such as micelles, membranes, and proteins in water, which in turn determines many of their properties, as will be discussed in Part III.

7.5 Packing of Molecules and Particles in Solids

Packing mismatches are particularly important in the interactions of nano-, micro- and macroscopic particles. For example, a concentrated dispersion of spherical colloidal particles of uniform diameter can order into a solidlike lattice, but when a few larger spheres are present, these will tend to associate into clusters or collect at certain interfacial regions or grain boundaries (see Figure 6.2b) rather than be randomly dispersed. This effect also occurs at the atomic level, where impurity atoms usually migrate to the grain boundaries of solids

To put the above discussion on a more quantitative basis, we may start by considering a close-packed lattice of identical spherical molecules or particles. The maximum volume fraction or density of close-packed spheres is $\pi/3\sqrt{2} = 0.74$, or 74% of the total volume, where each sphere has 12 nearest neighbors. This is known as close-packing (CP), and it occurs in the FCC and HCP lattices of many van der Waals solids, metals, C₆₀ (buckyballs), and spherical colloidal particles that form colloidal crystals in solution (cf. Figure 6.2). Clearly, such a close-packed structure must be both solid *and* crystalline (Figure 7.3a).

There is also a noncrystalline but solid structure in which spherical molecules or particles are randomly ordered yet as close-packed as they can be (Figure 7.3b). This is known as *random close-packing* (RCP), which occurs at a packing density of approximately 64% and where on average each sphere has about eight contact points

¹Most compounds exhibit a number of different solid and liquid-crystalline phases, both in the bulk and in surface monolayers. However, there is usually only one kind of (isotropic) liquid and gas phase.

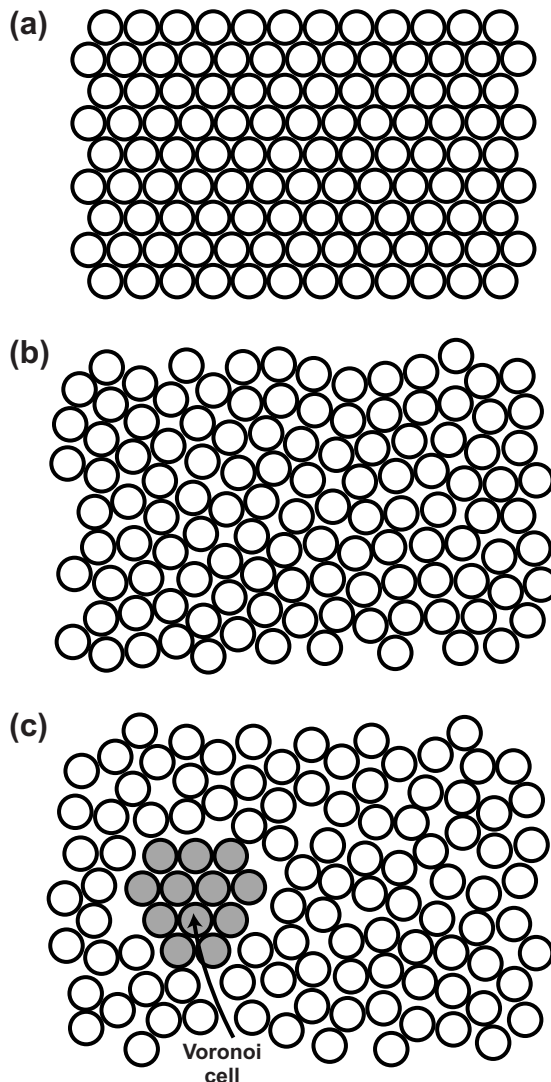


FIGURE 7.3 (a) Close-packed spheres at the maximum bulk density of $\pi/3\sqrt{2} = 74\%$. In 2D—for example, on a surface—the close packed density is significantly higher, $\pi/2\sqrt{3} = 91\%$, if the molecules are treated as discs, but if they are treated as spheres between two mathematically flat walls, the density is much lower, $\pi/3\sqrt{3} = 60\%$. (b) Randomly close-packed spheres at a density of 63.5%. (c) The critical density for free flow of randomly ordered spheres is 55.5%, which is referred to as the *random loose-packing* density. However, flow can also be achieved by the molecules ordering themselves into strings, ordered domains (Voronoi cells), or “shear bands” (*ordered loose-packing*) at densities that are higher than the random loose-packing or even the random close-packing density (see Problem 7.1).

Table 7.4 Maximum Packing Densities

Shape of Molecules or Particles	Close-Packing (CP) = Maximum Density	Random Close-Packing (RCP)	Random Loose-Packings (RLP)
Spheres (3D)	$\pi/3\sqrt{2} = 0.74^a$	0.635	0.555 ^b
Discs, cylinders (2D) ^c	$\pi/2\sqrt{3} = 0.91$	~0.82	~0.82
Ellipsoids	>0.74	>0.635	>0.555

^aApplies to Face Centered Cubic (FCC) and Hexagonal Close Packed (HCP) lattices.

^bFlow occurs at the RLP density after the material has expanded (dilated) to this density. Voronoi cells (see Figure 7.3c) increase the density at which flow can occur up to almost 60%, known as the jamming point.

^cInteractions on surfaces (2D) occur much more efficiently due to the higher densities attainable and the higher probability that diffusing molecules will meet each other than in the bulk (3D). This has important implications for catalytic and biological interactions. Data from Onoda and Liniger (1990); Jaeger and Nagel (1992); Williams (1998).

with its neighbors.² When small hard spheres are poured into jar that is then tightly closed, the density of the spheres is likely be at the random close-packing density. There will be no long-range crystalline order, but neither will the spheres be able to move collectively or flow, since the structure has become “frozen” into an *amorphous solid*. For bulk flow to occur, the spheres have to be able to move past each other. This requires some additional free volume that is not available in the random close-packing configuration. The density at which a collection of random hard spheres can flow is about 55% (Figure 7.3c) and is known as *random loose packing* (RLP).

Clearly, when compacted molecules or particles (e.g., sand) are forced to flow or shear, they can do this only by expanding first, a phenomenon known as “dilatancy.” We shall see later that this plays an important role in friction and lubrication. Similar effects occur with nonspherical molecules, such as alkanes, where the additional factors of bond rotation and molecular flexibility further complicate the packing configurations under both static and dynamic (e.g., flow) conditions. Table 7.4 lists the maximum packing densities for spheres and discs interacting in 3D and 2D, respectively.

Worked Example 7.2

Question: What is the maximum possible volume fraction that can be occupied by a collection of spherical particles that have very different radii? What does your result suggest for the strength of a composite or granular material made up of polydisperse rather than monodisperse molecules or particles?

Answer: Consider first a close-packed structure composed of spheres having the same radius. The density of this structure is 74%, leaving 26% of void space. Now fill up this void

²74.048% is the maximum density possible for *any* distribution of spheres. This statement—the *Kepler Conjecture* of 1611—appeared to be self-evident but did not satisfy mathematicians who wanted a rigorous proof that no non-close-packed configuration could have a higher density. The Kepler Conjecture was finally proved only in 1998 by Thomas Hales and Sam Ferguson in a 250+-page proof plus endless computer time. The journal to which it was submitted, *Annals of Mathematics*, asked a panel of 12 referees to review it. In 2003, after four years, they concluded that the proof was probably correct.

space with much smaller close-packed spheres. Continue this process indefinitely, finally pouring liquid into the remaining pores. The volume fraction occupied will therefore be $0.74 + 0.74(1 - 0.74) = 0.93$ after the first filling, $0.93 + 0.74(1 - 0.93) = 0.98$ after the second, and 1.0 at the end. The answer is the same if the particles are randomly close-packed.³ Of course, if we consider the molecules themselves to occupy only about 74% of the volume in the solid or liquid states, the answer would be about 74%, not 100%.

The greatly increased number of adhesive contacts makes a structure of polydisperse particles stronger than one of monodisperse spheres, even when the latter are close-packed. However, this conclusion, which implicitly assumes that all the particles are made of the same material and interact via the same intermolecular forces, does not apply as a general rule at the molecular level because different molecules are likely to have very different pair-potentials.

³The random close-packed density of polydisperse spheres is the same as for monodisperse spheres: about 64%. ■ ■ ■

7.6 Role of Repulsive Forces in Liquids: Liquid Structure

When a solid melts, the ordered molecular structure that existed in the solid is not completely lost in the liquid. This phenomenon has led to such concepts as *liquid structure* and *molecular ordering* in liquids, with important consequences both for our understanding of the liquid state and for the way molecules and particles interact in liquids (Pryde, 1966; Kohler, 1972; Croxton, 1975; Kruus, 1977; Maitland et al., 1981; Chandler, 1987; Allen and Tildesley, 1987; Ciccotti et al., 1987; de Gennes and Prost, 1995; Larson, 2000). The occurrence of “structure” in liquids arises first and foremost from the geometry of molecules, and as such it reflects the repulsive forces between them. Let us see what it is all about by first considering the molecular events that take place as a solid is heated through its melting point.

Imagine a close-packed FCC lattice at 0 K, where each molecule is surrounded by 12 nearest neighbors at a distance $r = \sigma$; six next-nearest neighbors at $r = \sqrt{2}\sigma$, 24 at $r = \sqrt{3}\sigma$, and so on. Figure 7.4a shows the number n of molecules to be found at a radial distance r away from any central or reference molecule. Ideally, the ordered crystalline structure extends indefinitely—that is, there is long-range order.

At a higher temperature, but still below the melting point, the mean distance between the molecules increases slightly, and the amplitude and frequency of molecular vibrations also increase, but the ordered lattice structure is maintained. The number density of molecules around the reference molecule now looks like Figure 7.4b, and since it is now spread out in space rather than being a set of discrete lines, one can no longer talk of the number n at r but more of the probability of finding a molecule at r . In other words, the discrete values have become replaced by a density distribution function.

At the melting point the ordered lattice structure abruptly breaks down. This occurs once the amplitude of the molecular vibrations reaches a point where the molecules can

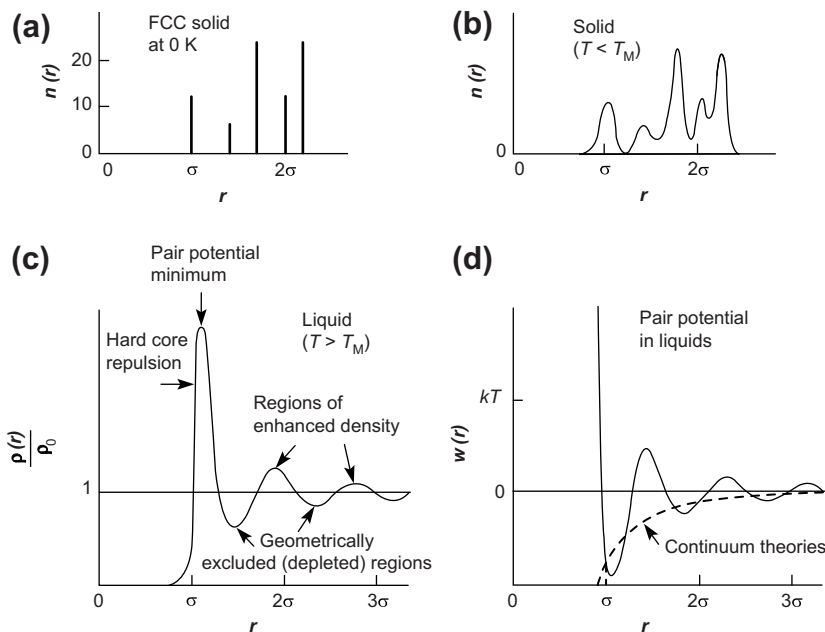


FIGURE 7.4 Radial density distribution functions: (a) for a close-packed FCC solid at 0 K; (b) for a solid at a finite temperature below its melting point T_M ; (c) for a liquid. Such data are obtained from x-ray and neutron scattering experiments on liquids. (d) Pair potential for two molecules in a liquid whose density distribution function is shown on the left, computed from $\rho(r) = \rho_0 \exp[-w(r)/kT]$.

move out of their confined lattice sites—in other words, they can now move past each other (cf. Figure 7.3c and Problem 7.1). Theoretically, for hard spheres, this ability should occur at a volume fraction close to the random-packing density of 0.64, which is 86% of the crystalline close-packed density and corresponds to a volume expansion of about 16% (Bondi, 1968). This is borne out by experiments where on melting, the increased volume is usually of this order, especially for spherical molecules (cf. 15 to 16% for Ne, Ar, Kr, Xe, and CH_4 , 17.5% for *n*-hexane, and 20% for benzene). But it can be much larger (e.g., 31% for polyethylene) or much smaller, and even negative, as for water.

But even in the liquid state, the molecules are still very much restricted in their motion and in the way they can position themselves with respect to one another. The 16% increase in the space available is not much; it corresponds to only a 5% increase in the mean intermolecular separation, and the tendency to pack into an ordered lattice persists in the liquid. Thus, our spherical reference molecule will now have only slightly fewer nearest neighbors, about 9 to 11 instead of 12, which will tend to group around it in a nonrandom way. The next-nearest neighbors will likewise order around the first group but with a smaller degree of correlation. Eventually, at larger distances, there will be no correlation at all with respect to the reference molecule. This short-range order extends over a few molecular diameters and characterizes the liquid state (recall that in the crystalline solid the order extends indefinitely).

Thus, at a distance r radially away from any reference molecule, the liquid density profile $\rho(r)$ looks like Figure 7.4c. The density profile or pair distribution function $\rho(r)$ is usually plotted as $\rho(r)/\rho_0$, where ρ_0 is the density of the bulk liquid. $\rho(r)/\rho_0$ is commonly referred to as the radial distribution function. At large distances, it always approaches unity as $\rho(r)$ approaches ρ_0 .

The magnitude and range of molecular ordering in liquids are enhanced by increasing the external pressure and lowering the temperature, as may be expected. Rigid hard sphere molecules exhibit more short-range order or structure than easily deformable molecules, such as hexane, where internal bond flexibility allows for greater configurational freedom to pack in different ways. The net effect, however, is that the density $\rho(r)$ usually oscillates with distance away from any molecule and only reaches the bulk liquid value ρ_0 at some distance away. Thus, in general, a liquid medium near a molecule or surface will not have the properties of a structureless continuum for which the density would be equal to the bulk value right up to contact.

It is important to stress that the existence of short-range liquid order or “structure” near another molecule, whether a dissolved solute molecule or another solvent molecule, or near a surface does not imply that the liquid is locally in the “solidlike” state. Short-range order is a characteristic property of the liquid state. Thus, attributing an “icelike structure” to water around a guest molecule or at a surface because of the short-range order observed around the guest molecule can be highly misleading. This structure is determined by the guest molecule or surface and not by the solidlike properties of the host (in this case water) molecules. Further aspects of this important conceptual matter are discussed in Chapters 15, 16, and 21.

7.7 The Effect of Liquid Structure on Molecular Forces

For two solute molecules or particles 1 dissolved in a liquid medium 2, the problem becomes exceedingly complicated. Three pair correlation functions may now be identified: $\rho_{11}(r)$ for the solute-solute density profile (i.e., the variation of $\rho_1(r)$ away from another solute molecule within the solvent medium); $\rho_{22}(r)$ for the solvent-solvent density profile; and $\rho_{12}(r)$ for the solute-solvent density profile. Each of these will exhibit oscillatory behaviors that are interdependent, depending on the sizes of the molecules and on the nature of the solute-solute, solute-solvent, and solvent-solvent forces. For example, solute-solvent interactions will affect the ordering of solvent molecules around a solute molecule, which in turn affects the solute-solute density profile.

How does all this affect the interaction between two dissolved molecules? In Chapter 2 we saw that the effective pair potential (or potential of mean force) between two solute molecules at a distance r apart is related to their density $\rho(r)$ at r by the Boltzmann relation:

$$\rho_{11}(r)/\rho_0 = \exp[-w_{11}(r)/kT]. \quad (7.7)$$

Thus, $w_{11}(r)$ tends to zero at large r , where $\rho(r)/\rho_0 \rightarrow 1$, but oscillates with distance at smaller separations; $w_{22}(r)$ behaves similarly. Such a pair potential is shown schematically

in Figure 7.4d. We see therefore how liquid structure can dramatically influence the interaction between dissolved molecules already at large distances. Unfortunately there is a lack of any direct experimental measurements of the pair potentials $w(r)$ or force functions $F(r)$ of solute molecules interacting in a solvent medium. However, measurements using an Atomic Force Microscope (AFM) found an oscillatory force profile between a nano-sized tip and a surface (Cleveland et al., 1995), although uncertainties about the exact separation and precise local geometry of the interaction zone in AFM experiments (cf. Figure 1.5) have so far precluded any detailed comparisons with theory. But this is not the case for interacting surfaces,⁴ and in Chapter 15 we shall see how solvent structure arises and affects the forces between macroscopic surfaces at distances below a few molecular diameters, for which both theoretical and experimental data are available.

PROBLEMS AND DISCUSSION TOPICS

- 7.1** Derive Eq. (7.2), which shows that the volume fraction or density of an assembly of close-packed spheres is $\pi/3\sqrt{2} = 0.74$, or 74%. Describe a realistic structure of identical spheres that allows for bulk shear flow to occur at a density *above* the random close-packing density of 64%.
- 7.2** Calculate the van der Waals coefficient a of a saw-tooth potential of depth $-\epsilon$ at $r = \sigma$ increasing linearly to zero at $r = \sigma + \Delta\sigma$. Is a proportional to the *volume* encompassed by the range of the attraction? How different is this potential from the Lennard-Jones potential?
- 7.3** (1) A colloidal dispersion consists of irregularly shaped particles in aqueous solution. Initially the forces between the particles are repulsive so that they remain dispersed. The pH of the solution is then changed so the forces become attractive (see Chapter 14), and the particles aggregate into “flocs” and fall out of the solution. It is commonly observed that when the precipitation occurs rapidly, the density of the particles in the flocs is low, while if the precipitation is slow, the particle density is higher and approaches that of random close-packing. Explain this inverse correlation between flocculation time and particle density.
(2) Describe, with sketches, the different types of molecular ordering that occur in isotropic liquids and in nematic and smectic liquid crystals. Discuss which geometric and other factors favor liquid-crystal formation, and smectic or nematic phases.
- 7.4** Plot the pressure-volume (PV) and temperature-volume (TV) phase diagrams for a gas-liquid system based on the van der Waals equation of state, $P = kT/(V - b) - a/V^2$, where the parameters a and b are defined by (see Sections 2.5 and 6.3) $a = 2\pi C/3\sigma^3$ and $b = 2\pi\sigma^3/3$, where $\sigma = 0.5$ nm and $C = 3 \times 10^{-76}$ J m⁶.
(1) Plot the PV curves at different temperatures, choosing your ranges and units of temperature (K), pressure (bar, Pa, or N m⁻²), and volume (m³ or nm³) to clearly

⁴Methods directly measuring the forces between molecules and surfaces are described in Chapter 12.

display the different phases of the system. By applying the Maxwell Construction to the van der Waals loops in the curves, draw the tie-lines and the boundary of the single-phase and two-phase regions, and identify the critical point. From your plots, deduce the boiling temperature of the liquid at $P \approx 1$ MPa (10 bar). [Answer: The critical point should occur at $T = T_c = 8a/27Rb = 412$ K, $P = P_c = a/27b^2 = 2.7 \times 10^6$ Pa, and $V = V_c = 3b = 7.9 \times 10^{-28}$ m³ (~ 0.8 nm³), which corresponds to a volume fraction of $\frac{4}{3}\pi(\sigma/2)^3/8 \times 10^{-28}$, or about 8%. On the PV plot, at $P \approx 1$ MPa, the two-phase coexistence tie-line occurs at $T \approx 330$ K (57°C), which defines the boiling temperature at this pressure.] (2) Repeat this procedure to obtain the TV phase diagram, and verify that you obtain the same critical point. (3) By estimating the latent heat of vaporization using the approximate equation $L_{\text{vap}} \approx 6N_0C/\sigma^6$ and applying Trouton's Rule, one obtains a significantly higher value for the boiling temperature than 330 K. Account for this effect.

- 7.5*** Plot the temperature-composition phase diagrams for the four cases where the forces between the solute molecules in a solvent are as drawn in Figure 7.5.

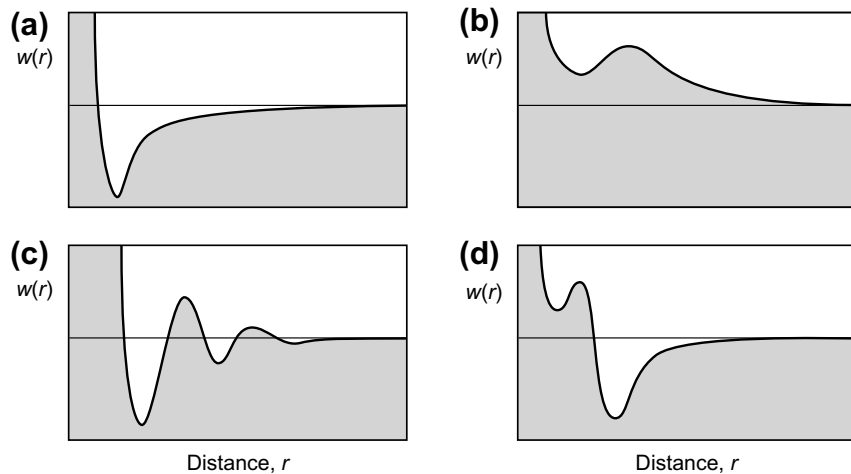


FIGURE 7.5

This page intentionally left blank

Special Interactions: Hydrogen-Bonding and Hydrophobic and Hydrophilic Interactions

8.1 The Unique Properties of Water

Water is such an unusual substance that it has been accorded a special place in the annals of phenomena dealing with intermolecular forces, and two types of “special interactions”—the *hydrogen bond* and the *hydrophobic effect*—are particularly relevant to the interactions of water. The literature on the subject is vast (Franks, 1972–1982; Ball, 1999), not only because water is the most important liquid on earth but also because it has so many interesting and anomalous properties.

For a liquid of such a low molecular weight, water has unexpectedly high melting and boiling points and latent heat of vaporization.¹ There are, of course, many other substances of low molecular weight and high melting and boiling points, but these are invariably ionic crystals or metals whose atoms are held together by strong Coulombic or metallic bonds. These properties of water point to the existence of an intermolecular interaction that is stronger than that expected for ordinary, even highly polar, liquids.

The density maximum at 4°C exhibited by liquid water, and the unusual phenomenon that the solid (ice) is less dense than the liquid, indicates that in the ice lattice the molecules prefer to be farther apart than in the liquid. We may further conclude that the strong intermolecular bonds formed in ice persist into the liquid state and that they must be strongly orientation-dependent, since water adopts a tetrahedral coordination (four nearest neighbors per molecule) rather than a higher packing density (cf. 12 nearest neighbors characteristic of close-packed van der Waals solids where the “bonds” are nondirectional). Water has other unusual properties, such as a very low compressibility and unusual solubility properties both as a solute and as a solvent (discussed later in this chapter).

If liquid water is strange, solid water (ice) is even stranger (Hobbs, 1974). The high molecular dipole moment and high dielectric constant of liquid water may at first appear to be related via the Debye-Langevin and Clausius-Mossotti equations (5.8) and (5.30). But unlike any typical polar liquid whose dielectric constant falls abruptly as it solidifies

¹If one follows the linear reduction in the boiling points of the homologous alcohols of general formula $C_nH_{2n+1}OH$, viz. C_4H_9OH , C_3H_7OH , C_2H_5OH , CH_3OH , one would conclude that the final member of this group, HOH, or water, H_2O , should be a gas at room temperature. In contrast, the boiling points of the *n*-alkanes, C_nH_{2n+2} , do continue to decrease monotonically right down to methane CH_4 ($n = 1$) and even H_2 ($n = 0$).

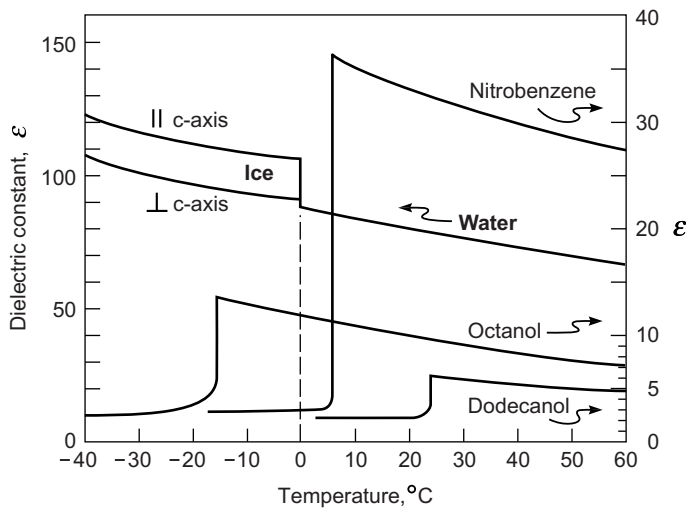


FIGURE 8.1 Static dielectric constants as a function of temperature of some “normal” polar liquids and water. For all the normal liquids ϵ falls abruptly on freezing to a value that is close to the square of the refractive index, indicating that the thermal rotations of the dipolar molecules have stopped. However, for water, ϵ rises on freezing and continues to rise to -70°C , after which it falls. The high polarizability may be due to proton hopping along the H-bond network (see Figure 8.2a) rather than molecular rotations. [Data compiled from Landolt-Börnstein (1982), Hasted (1973), and Hobbs (1974). Two classic papers that discuss the dielectric constants of water and ice are Pauling (1935) and Hollins (1964).]

due to the freezing of the molecular (i.e., dipolar) rotations, when water freezes into ice, the dielectric constant actually increases (Figure 8.1), and it is still increasing at -70°C (Hasted, 1973). It is highly unlikely that this phenomenon can be explained in terms of the conventional picture of rotating dipolar molecules. The proton conductivity and mobility in ice is also higher than in the liquid (Kunst and Warman, 1980; Hobbs, 1974). Both these phenomena suggest that the ice lattice affords some easy pathways for the movement of charges, particularly protons, via a “proton hopping” mechanism along the hydrogen-bonding network (Pauling, 1935; Hollins, 1966). Such a mechanism appears to persist into the liquid state, and is known as the *Grotthus Mechanism* (Agmon, 1995). Thus, to understand the secrets of liquid water, one may first have to unravel those of ice.

8.2 The Hydrogen Bond

The previous section indicates that some unusually strong and orientation-dependent bonds are involved in the interactions between water molecules. It is a straightforward matter to ascertain which bond is responsible for this interaction by simply looking at the distances between various atomic centers in the ice lattice (Figure 8.2a). The *intramolecular* O–H distance is about 0.10 nm, as expected for this covalent bond (see Figure 7.1), but the *intermolecular* O···H distance is only 0.176 nm, much less than the 0.26 nm expected from summing the two van der Waals radii but still larger than the

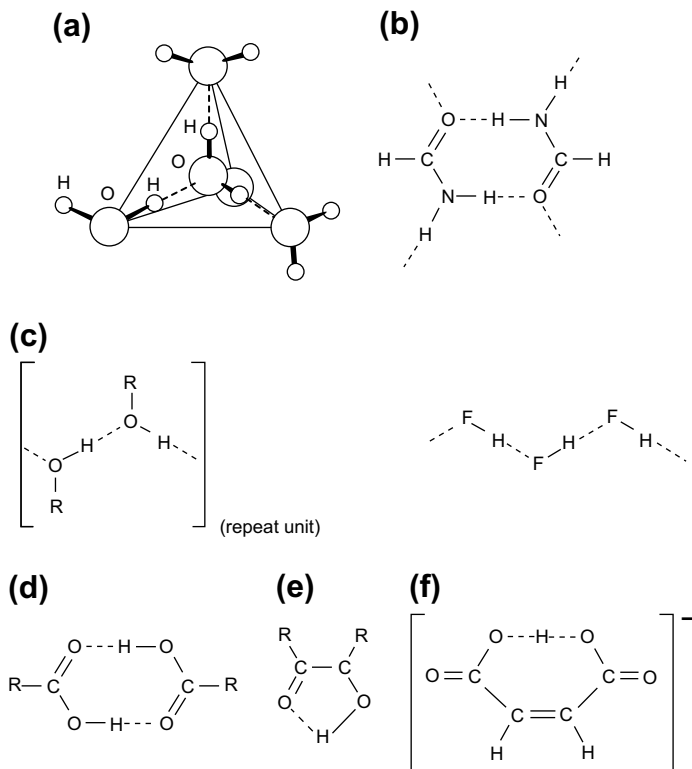


FIGURE 8.2 Different types of hydrogen bonds and hydrogen-bonded structures. Linear hydrogen bonds have the lowest energy, but some H bonds with a $\text{H}\cdots\text{H}$ angle of 20° or more also occur (cf. Figure 8.3). (a) Three-dimensional structures (e.g., ice). (b) Two-dimensional (layered) structures (e.g., formamide). (c) One-dimensional (chain and ring) structures (e.g., alcohols, HF). (d) Dimers (e.g., fatty acids). (e) Intramolecular H bond (not always linear). (f) Symmetric H bond (H atom shared). The structure of the hydronium ion H_3O^+ is believed to be planar, with two positive charges and one negative charge at the three apexes of an equilateral triangle.

covalent distance of 0.10 nm. Thus, the intermolecular $\text{O}\cdots\text{H}$ bond is implicated, which at first sight appears to possess some covalent character. Such bonds are known as *hydrogen bonds*, and the reader is referred to Pauling (1960), Coulson (1961), Joesten and Schaad (1974), Jeffrey (1997), and Schuster et al., (1976) for the voluminous literature on the subject.

Hydrogen bonds are not unique to water; they exist to varying degrees between electronegative atoms (e.g., O, N, F, and Cl) and H atoms covalently bound to similar electronegative atoms. These bonds are special in that they only involve hydrogen atoms, which, by virtue of their tendency to become positively polarized and their uniquely small size, can interact strongly with nearby electronegative atoms, resulting in an effective H-mediated “bond” between two electronegative atoms (see Section 4.9).

Originally, it was believed that the hydrogen bond was quasi-covalent and that it involved the sharing of an H atom or proton between two electronegative atoms. But it is

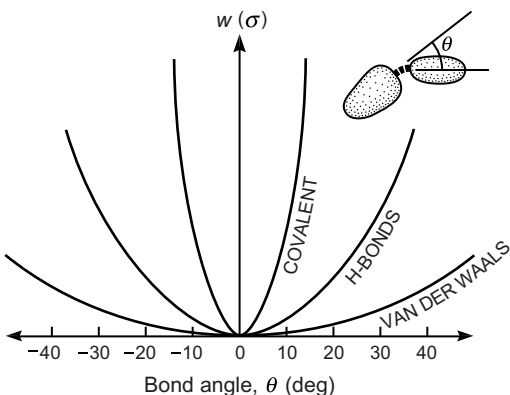


FIGURE 8.3 Orientation-dependence of different types of bonds (schematic). Covalent bonds are the most “directional” with binding energies $w(\sigma)$ of order $\sim 100 \text{ kJ mol}^{-1}$ at room temperature. Hydrogen bonds are less directional (varying up to $\sim 20^\circ$) and have lower energies ($\sim 10 \text{ kJ mol}^{-1}$), while van der Waals bonds are not directional or only weakly directional and have the lowest energy of all ($\sim 1 \text{ kJ mol}^{-1}$). Note, however, that there is no simple relationship between the strength and directionality of bonds; for example, ionic bonds are very strong and yet totally nondirectional.

now accepted (Coulson, 1961; Umeyama and Morokuma, 1977) that the hydrogen bond is predominantly an electrostatic (Coulombic) interaction.² With few exceptions, the H atom is not shared but remains closer to and covalently bound to its parent atom. Accordingly, the hydrogen bond between two groups XH and Y is usually denoted by X–H \cdots Y. Nevertheless, certain characteristics of hydrogen bonds do make them appear like weak covalent bonds. For example, they are not only fairly strong but also fairly directional (Figure 8.3). This endows them with the ability to form weak three-dimensional “structures” in solids, whereas in liquids the short-range order can be of significantly longer range whenever hydrogen bonds are involved, giving rise to the term *associated liquids*.

The strengths of most hydrogen bonds lie between 10 and 40 kJ mol^{-1} or approximately $5\text{--}10 \text{ kJ mol}^{-1}$ per bond at 298 K (Joesten and Schaad, 1974), which makes them stronger than a typical van der Waals bond ($\sim 1 \text{ kJ mol}^{-1}$ or $\sim 1 \text{ kT}$) but still much weaker than covalent or ionic bonds ($\sim 500 \text{ kJ mol}^{-1}$ or $\sim 100 \text{ kT}$).

Even though the hydrogen bond is now believed to be a purely electrostatic, Coulomb-like interaction (Coulson, 1961), there is no simple equation for the interaction potential, at least not one that is predictive or sufficiently accurate. One does find that the strengths of hydrogen bonds tend to follow a $1/r^2$ distance dependence, which is the same as that expected for the charge-dipole interaction, previously given by Eq. (4.5) as

$$w(r) = -Q_{\text{H}^+} u \cos \theta / 4\pi\epsilon_0 er^2. \quad (8.1)$$

This equation may be expected to apply because, as explained in Sections 4.9, the positive H atom is so small that its interaction with a dipole falls in between the

²However, proton hopping between water molecules adds an additional important, and not yet explored, feature that is not present in most other H-bonding molecules or interactions.

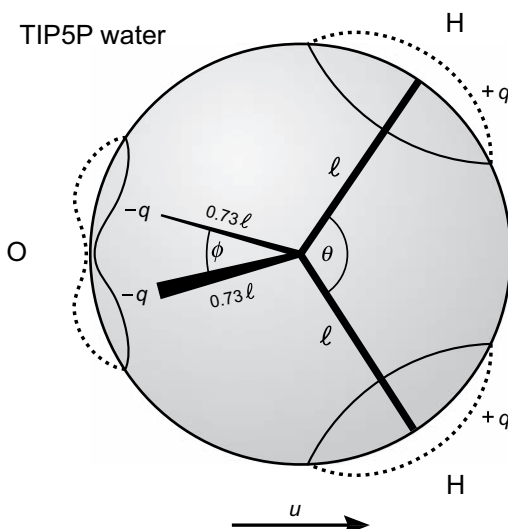


FIGURE 8.4 Some common models for the water molecule. There are more than 40 models (Guillot, 2002). Most models are based on a particular charge distribution of the two positive hydrogen atoms and around the negative oxygen atom. In SPC-type models the charges are distributed on a plane. In ST2 and TIP5 models the charges are on tetrahedral arms; for example, for TIP5P, $q = 0.24e$, $l = 0.096 \text{ nm}$, $\theta = 104.5^\circ$, and $\phi = 109.5^\circ$ (Mahoney and Jorgensen, 2000). No model can account for all the properties of water in all its phases. For example, the TIP5 model can “predict” the dielectric constant of liquid water and density maximum at 4°C but not the expansion coefficient or phase diagram of water. [ST2: After an earlier model by F. H. Stillinger and A. Rahman; SPC: Simple point charge; TIP: Transferable intermolecular potential.]

charge-charge and dipole-dipole interactions. But the magnitude of this charge Q_{H^+} is not the full electronic charge $+e$ and is not known in advance. And neither is r . For example, for the water-water H-bond, if we inserted into Eq. (8.1) the values $Q = 0.24e = 0.4 \times 10^{-19} \text{ C}$ (see the model of water in Figure 8.4), $u_{\text{H}_2\text{O}} = 1.5 \text{ D} = 5 \times 10^{-30} \text{ C m}$ (the dipole moment of water), $r = 0.176 + (0.100/2) = 0.226 \text{ nm}$ (the distance between H^+ and the center of the $\text{O}^- \text{H}^+$ dipole), $\theta = 0$, and $\epsilon = 1$, we obtain $w(r) \approx -3.4 \times 10^{-20} \text{ J} = 20.4 \text{ kJ mol}^{-1} = 4.9 \text{ kcal/mole}$. This agrees very well with the literature value of 4.5 kcal/mole for the water-water H-bond.

Hydrogen bonds can occur intermolecularly as well as intramolecularly and can happily exist in a nonpolar environment. They are consequently particularly important in macromolecular and biological assemblies, such as in proteins, linking different segments together inside the molecules, and in nucleic acids, where they are responsible for the structure of the DNA molecule.³ Their involvement in setting up one-, two-, and three-dimensional macromolecular structures is sometimes referred to as *hydrogen-bond polymerization* (illustrated in Figure 8.2a, b and c).

³But not the energy that holds the two strands together, which are believed to be due to non-orientation-specific hydrophobic forces (see Section 8.6).

8.3 Models of Water and Associated Liquids

Hydrogen bonds play a particularly prominent role in water, since each oxygen atom with its two hydrogens can participate in four such linkages with other water molecules: two involving its own H atoms and two involving its unshared (lone-pair) electrons with other H atoms. To see exactly how this arises, we require some picture of the charge distribution within the water molecule. Numerous models have been proposed (Allen and Tildesley, 1987; Ciccotti et al., 1987; Mahoney & Jorgensen, 2000; Guillot, 2002), but no single model has been able to satisfactorily account for the properties of water in all three phases (ice, liquid, and vapor) and especially its unusual interactions, discussed below, such as the hydrophobic interaction. Figure 8.4 shows one of the TIP5 models of water that is similar to some of the other models (Guillot, 2002) and so provides a good introduction to the various approaches being applied to understand water.

In most models the water molecule is modeled with positive charges centered on each hydrogen atom and two compensating negative charges on the opposite side of the oxygen atom, representing the two unshared electron pairs. The four charges are located along four tetrahedral arms radiating out from the center of the O atom. The interaction between any two water molecules is assumed to involve an isotropic Lennard-Jones potential and 16 Coulombic terms representing the interaction between each of the four-point charges on one molecule with the four on the other. The net Coulombic interaction obviously depends on the mutual orientation of the two molecules. When many molecules are involved, their equilibrium configurations and various physical properties can only be solved on a computer. Computer simulations show that in ice (solid water) the molecules order so that each oxygen atom is tetrahedrally coordinated to four other oxygens, with a hydrogen atom lying in the line joining two oxygen atoms. It is this preferred linearity of the O–H···O bond in water that endows it with its strongly directional nature.

In liquid water the tendency to retain the icelike tetrahedral network remains, but the structure is now disordered and labile. The average number of nearest neighbors per molecule rises to about five (hence the higher density of water on melting), but the mean number of H bonds per molecule falls to about 3.5 whose lifetimes are estimated to be about 10^{-11} s. Other strongly hydrogen-bonding molecules, such as formamide, ammonia, and HF, also retain some of their ordered crystalline structure in the liquid state over short distances. Such liquids are known as *associated liquids*. It is also believed that the H-bond structure in such liquids is cooperative in the sense that the presence of H bonds between some molecules enhances their formation in nearby molecules, thereby tending to propagate the H-bonded network. If so, the interaction is nonpairwise additive, which presents serious problems in theoretical computations of aqueous and other systems involving cooperative associations. The origin of this cooperativity may lie in the way that a well-structured network of H-bonds provides for the movement of protons, which increases the entropy of the system (Pauling 1935), and we may note that the diffusion coefficient of protons in ice is significantly higher than in liquid water.

It is instructive to note that the tetrahedral coordination of the water molecule is also at the heart of the unusual properties of water, probably more than the hydrogen bonds themselves. As a rule of thumb, molecules that can participate in only two H bonds can link up into a one-dimensional chain or ring (e.g., HF and alcohols, as shown in Figure 8.2). Likewise, atoms of valence two such as selenium and tellurium can form long chains of covalently bonded atoms. Atoms that can participate in three bonds (e.g., arsenic, antimony, and carbon in graphite) can form strong two-dimensional sheets or layered structures that are held together by weaker van der Waals forces. But only a tetrahedral or higher coordination allows for a three-dimensional network to form. For example, it is the tetrahedral coordination characteristic of carbon and silicon that allows for their almost infinite variety of associations whether in chain molecules (e.g., polymers, proteins, DNA), cyclic compounds, or two- and three-dimensional crystals (e.g., diamond, quartz, sheet silicates, and clays). The former are the basis of the endless variety of organic compounds and “life,” and the latter of geological rocks and natural minerals.

8.4 Relative Strengths of Different Types of Interactions

In earlier chapters we saw that molar cohesive energies and other properties can be computed fairly accurately for molecules with only one type of attractive force (e.g., pure Coulombic or pure dispersion). Usually, however, two or more interactions occur simultaneously, and it becomes difficult to apply simple potential functions, especially when orientation-dependent dipolar and H-bonding interactions are involved. In spite of this complexity, some general patterns do emerge when we compare the boiling points of different compounds, which is a measure of the cohesive forces holding molecules

Table 8.1 Relative Strengths of Different Types of Interactions as Reflected in the Boiling Points of Compounds^a

Molecule		Molecular Weight (Da)	Dipole Moment (D)	Boiling Point (°C)
Ethane	CH ₃ CH ₃	30	0	-89
Formaldehyde	HCHO	30	2.3	-21
Methanol	CH ₃ OH	32	1.7	64
<i>n</i> -Butane	CH ₃ CH ₂ CH ₂ CH ₃	58	0	-0.5
Acetone	CH ₃ COCH ₃	58	3.0	56.5
Acetic Acid	CH ₃ COOH	60	1.5	118
<i>n</i> -Hexane	CH ₃ (CH ₂) ₄ CH ₃	86	0	69
Ethyl propyl ether	C ₅ H ₁₂ O	88	1.2	64
1-Pentanol	C ₅ H ₁₁ OH	88	1.7	137

^aIn order to make comparisons meaningful, molecules have been put into three groups of similar molecular weights and size. Within each group the first molecule is nonpolar and interacts purely via dispersion forces, the second is polar, and the third also interacts via H-bonds.

together in condensed phases (Table 2.1). Such a comparison is made in Table 8.1, where we see that the weakest interactions are the dispersion and dipolar interactions, followed by H-bonding interactions. Then there is a large jump to the much stronger covalent and ionic interactions, not shown in Table 8.1. Note (1) the dominance of H-bonding forces even in very polar molecules such as acetone, and (2) the increasing importance of dispersion forces for larger molecules. However, though dispersion forces are the ones mainly responsible for bringing molecules together, they lack the specificity and directionality of dipolar and H-bonding interactions, and it is these that often determine the *structural* details of macromolecules and higher-order assemblies, such as polymer crystals, polypeptides (proteins), and polynucleotides (DNA and RNA).

8.5 The Hydrophobic Effect

So far in this chapter we have considered the interactions of water molecules with other water molecules. Now we shall investigate the equally interesting interactions of water with other compounds—that is, when water acts as a solvent or as a solute.

The strong inclination of water molecules to form H-bonds with each other influences their interactions with nonpolar molecules that are incapable of forming H-bonds (e.g., alkanes, hydrocarbons, fluorocarbons, inert atoms, vapor). When water molecules come into contact with such a molecule or small vapor cavity (bubble), they are faced with an apparent dilemma: no matter in which direction the water molecules face, it would appear that one or more of the four charges per molecule will have to point toward the inert solute molecule and thus be lost to H-bond formation. Clearly the best configuration would have the least number of tetrahedral charges pointing toward the unaccommodating species, so the other charges can point toward the water phase and be able to participate in H-bond attachments much as before. There are many options to salvaging lost H-bonds. If the nonpolar solute molecule is not too large, it is possible for water molecules to pack around it without giving up any of their hydrogen-bonding sites. Examples of such arrangements are shown in Figure 8.5. Since we have already established (Chapter 6) that the dispersion interaction between water and hydrocarbons is not very different from that between water and water or, for that matter, between hydrocarbon and hydrocarbon, we see that the main effect of bringing water molecules and nonpolar molecules together is the reorientation or restructuring of the water molecules so they can participate in H-bond formation more or less as in bulk water—in other words, without necessitating any breakage of H-bonds. To do this, the H-bonds may have to bend from their most favorable linear configuration, but as shown in Figure 8.3, the energetic cost is small.

Thus, thanks to the uncanny ability of tetrahedrally coordinated H-bonded molecules to link themselves together around almost any inert molecule, whatever its size or shape, the apparent dilemma mentioned earlier is often easily solved. Indeed, since water molecules in the liquid state participate on average in about 3.0–3.5 H-bonds, it would appear from Figure 8.5a that around certain inert solute molecules the water molecules

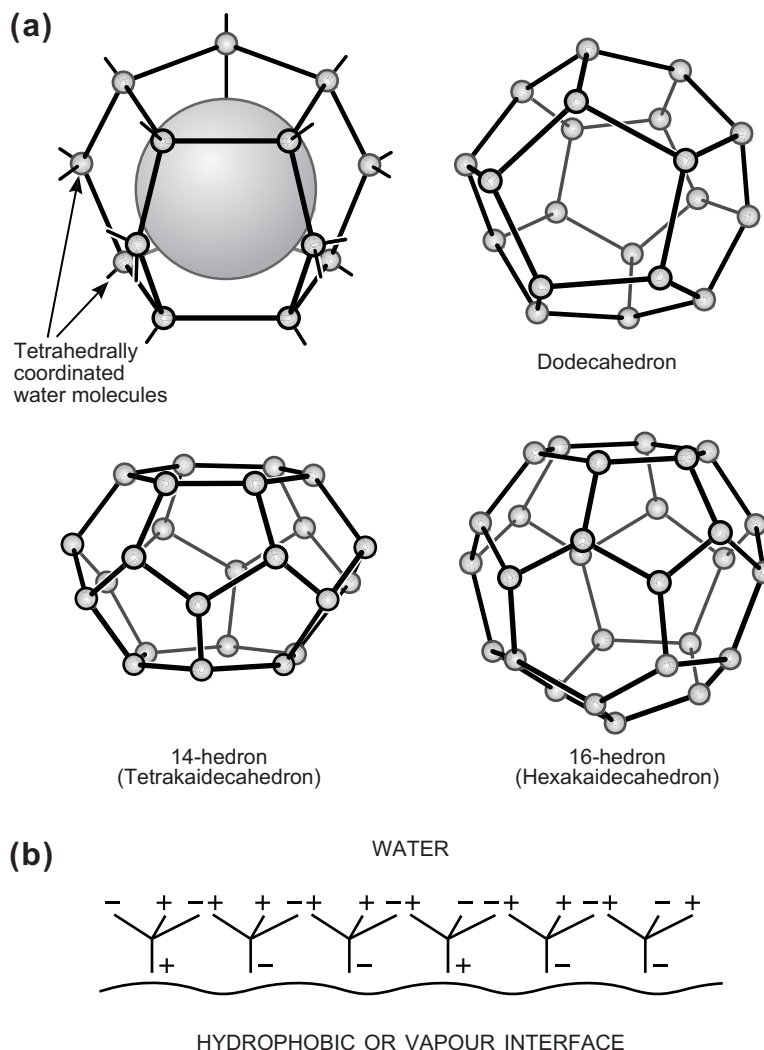


FIGURE 8.5 (a) “Clathrate cages” and “gas hydrates” (Holder et al., 2001) formed by water molecules around small dissolved nonpolar (hydrophobic) solute molecules, where each water molecule can participate in up to four H-bonds. The water molecules forming these cages are more ordered than in the bulk liquid, thus their loss of entropy and resulting unfavorable free energy, but they are surprisingly stable, especially at low temperatures and high pressures. The polyhedral cages can organize into solidlike super-lattices, trapping high concentrations of gases such as methane CH_4 and CO_2 . (b) Water structure at an extended hydrophobic-water interface, including the air-water interface, where each water molecule becomes more ordered in order to participate in three H-bonds (the maximum possible). Note that since hydrophobic surfaces are inert, the charge pointing toward the surface can be one of the two positive H^+ atoms or, more likely, one of the two negative lone-pair electrons on the larger O^- atom. This is the reason for the negative potential of -15 to -40 mV of air-water and hydrocarbon-water interfaces (Farrell and McTigue, 1982; Marinova et al., 1996). This is in contrast to the even more restricted structuring at hydrophilic surfaces, shown in Figure 8.6.

could actually have a higher coordination (of four) and thus have an even lower energy (strictly, enthalpy) than in the bulk liquid. It is also clear that the sizes and shapes of nonpolar solute molecules are fairly critical in determining the water structure adopted around them and that the structures adopted around small solute molecules may be very different from those adopted at surfaces (Figure 8.5b). This phenomenon is often referred to as *hydrophobic solvation* or *hydrophobic hydration*. At present there is no simple theory for such solute-solvent interactions. However, both theoretical and experimental studies do indicate that the reorientation, or restructuring, of water around hydrophobic solutes or surfaces is *entropically* very unfavorable, since it disrupts the existing water structure and imposes a new and more ordered structure on the surrounding water molecules.

It is for this reason that the hydrocarbons are so sparingly soluble in water, characterized by a highly unfavorable free energy of solubilization that is mainly entropic and, as we saw in Chapter 6, cannot be accounted for by continuum theories of van der Waals forces. For example, the free energy of transfer of methane (CH_4) and *n*-butane (C_4H_{10}) molecules from bulk liquid into water at 25°C are about 14.5 and 24.5 kJ mol^{-1} , respectively. For *n*-butane, this is split up as follows:

$$\Delta G_{\text{transfer}} = \Delta H - T\Delta S = -4.3 + 28.7 = +24.5 \text{ kJ mol}^{-1}.$$

Thus, the decrease in entropy contributes 85% to this interaction, and for many other hydrocarbons (e.g., benzene) the entropic contribution to $\Delta G_{\text{transfer}}$ is even higher.

It is also observed that for different hydrocarbons, the free energy of transfer is roughly proportional to the surface areas of the molecules, an indication that the number of reoriented water molecules is more or less determined by the non-H-bonding areas exposed to them. Thus, for methane, whose van der Waals radius is $a = \sigma/2 = 0.2 \text{ nm}$,⁴ the surface area per molecule is about $4\pi a^2 \approx 0.50 \text{ nm}^2$. The free energy of transfer, $\Delta G_{\text{transfer}} = 14.5 \text{ kJ mol}^{-1}$, when calculated per unit surface area—that is, $(14.5 \times 10^3)/(6.022 \times 10^{23}) \times (0.5 \times 10^{-18}) = 0.048$ —turns out to be 48 mJ m^{-2} . Similarly for the cylindrically shaped *n*-butane molecule ($\text{CH}_3\text{—CH}_2\text{—CH}_2\text{—CH}_3$), whose surface area is given by $4\pi a^2 + 2\pi a(3l) \approx 1.0 \text{ nm}^2$, where $l = 0.1275 \text{ nm}$ is the C–C distance along an alkane chain (see Section 7.1). Using the above value of $\Delta G_{\text{transfer}} = 24.5 \text{ kJ mol}^{-1}$, we deduce a corresponding surface free energy of 41 mJ m^{-2} . These values are very close to the interfacial free energies γ_i of bulk hydrocarbon-water interfaces that generally lie between 40 and 50 mJ m^{-2} . However, there are important differences in the interactions between hydrophobic molecules or groups and hydrophobic surfaces, discussed further in Chapters 15 and 21. The high surface tension of water, about 72 mJ m^{-2} , may also be taken as an example of this mainly entropic effect, since air behaves as an inert, non-H-bonding “medium” in this sense.

Conversely, water molecules are highly insoluble in nonpolar solvents, but here the effective surface energy of transfer is significantly larger than 50 mJ m^{-2} (see Problem 8.2).

⁴This is the effective radius in the liquid state at room temperature. The van der Waals packing radius in the solid crystal is about 0.185 nm, or about 7.5% smaller (see Section 7.1).

Clearly, when water molecules in the bulk liquid have to rearrange their coordination to accommodate a foreign solute molecule, the price is high. However, when a single water molecule is completely extracted out from its water environment, the price is even higher. We shall return to considerations of surface energies and their relation to hydrophobic and other surface phenomena in later chapters.

The immiscibility of inert substances with water, and the mainly entropic nature of this incompatibility, is known as the *hydrophobic effect* (Kauzmann, 1959; Tanford, 1980), and such substances (e.g., hydrocarbons and fluorocarbons) are known as hydrophobic substances.⁵ Similarly, hydrophobic surfaces do not get “wetted” by water; when water comes into contact with such surfaces, it rolls up into small lenses and subtends a large contact angle on them (see Chapter 17).

8.6 The Hydrophobic Interaction

Closely related to the hydrophobic effect is the hydrophobic interaction, which describes the unusually strong attraction between hydrophobic molecules and surfaces in water—often stronger than their attraction in free space. For example, the van der Waals interaction energy between two contacting methane molecules in free space is -2.5×10^{-21} J (Table 6.1), while in water it is -14×10^{-21} J. Similarly, the surface tensions of most saturated hydrocarbons lie in the range $15\text{--}30\text{ mJ m}^{-2}$, while their interfacial tensions with water are in the range $40\text{--}50\text{ mJ m}^{-2}$. In Section 6.7 we saw that this strong interaction in water cannot be accounted for by the conventional theory of van der Waals forces, which predicts a reduced interaction in water. Because of its strength, it was originally believed that some sort of “hydrophobic bond” was responsible for this interaction. But it should be clear from what has just been described that there is no bond associated with this mainly entropic phenomenon, which arises primarily from the rearrangement of H-bond configurations in the overlapping solvation zones as two hydrophobic species come together and is therefore of much longer range than any typical bond.

To date there have been very few measurements, whether direct or indirect, of the hydrophobic interaction between dissolved nonpolar molecules in water, mainly because they are so insoluble. Tucker and colleagues (1981) reported values, based on thermodynamic data, of $\Delta G_{\text{dimer}} = -8.4$ and -11.3 kJ mol^{-1} for the free energies of dimerization of benzene-benzene and cyclohexane-cyclohexanol, respectively, whereas calculated values for two methane molecules have ranged from -3 to -8.5 kJ mol^{-1} (Smith et al., 1992; Ben Naim et al., 1973). The theoretical problem is horrendously difficult because the hydrophobic interaction between two molecules is much more complex, involves many other molecules, and is of a longer range than that arising from any simple additive pair-potential.

⁵Hydrophobic means “water-fearing,” but it is important to note that the interaction between a hydrophobic molecule and water is actually attractive, due to the dispersion force. However, the interaction of water with itself is much more attractive. Water simply loves itself too much to let some substances get in its way.

The complex connectivities of the H-bonding network and the role of proton hopping in modifying the effective local polarizability of water must also be included in any theory or computer simulation. Thus, there is as yet no satisfactory theory of the hydrophobic interaction between solute molecules in water, though a number of promising theoretical approaches have been proposed (Dashevsky and Sarkisov, 1974; Pratt and Chandler, 1977; Marcelja et al., 1977; Pangali et al., 1979; Luzar et al., 1987; Nicholson and Parsonage, 1982; see also Faraday Discussions No. 146, 2010). The hydrophobic interactions between extended surfaces are discussed in Chapters 15 and 21.

Israelachvili and Pashley (1982b) measured the hydrophobic force law between two macroscopic curved hydrophobic surfaces in water and found that in the range 4–10 nm the force decayed exponentially with distance with a decay length of about 1 nm (an exponential distance-dependence for the interaction had previously been proposed by Marcelja et al., 1977). Based on these findings, it was proposed that for small solute molecules the hydrophobic pair-potential $w_H(r)$ is exponential, proportional to the diameter of the molecules or molecular groups σ , and may be expressed as

$$\begin{aligned} w_H(r) &\approx -20 \sigma e^{-(r-\sigma)/D_H} \quad \text{kJ mol}^{-1} \\ &\approx -8 \sigma e^{-(r-\sigma)/D_H} \quad kT \text{ at } 298 \text{ K}, \end{aligned} \quad (8.2)$$

where σ is in nm and where D_H is the characteristic hydrophobic decay length of order about 1.0 nm. The free energy of dimerization is therefore, putting $r = \sigma$ in the above equations,

$$\Delta G_{\text{dimer}} = w_H(\sigma) \approx -20 \sigma \text{ kJ mol}^{-1} \approx -8 \sigma kT \text{ at } 298 \text{ K}, \quad (8.3)$$

where again σ is in nm. For example, for cyclohexane ($\sigma = 0.57$ nm), this gives $\Delta G_{\text{dimer}} \approx -11.4 \text{ kJ mol}^{-1}$ ($\sim 5 kT$) in agreement with the measured value of $-11.3 \text{ kJ mol}^{-1}$. As regards the hydrophobic force needed to separate two molecules from contact, this would be given by

$$F_H(\sigma) = -(dw_H/dr)_{r=\sigma} \approx -3 \times 10^{-11} \sigma (\text{nm}) \quad \text{N at } 298 \text{ K}. \quad (8.4)$$

Thus, for $\sigma \approx 0.5$ nm, we would expect an adhesion force of about 15 pN.

Equation (8.2) indicates that for molecules of diameter approximately 0.5 nm, the strength of the hydrophobic interaction has fallen to below kT by $r = 2$ nm. Thus, if kT is taken as a criterion for the effective range of an interaction, the hydrophobic interaction has a range of 1.5–2.0 nm (15–20 Å) for molecules such as methane, cyclohexane, and benzene. This is about seven times greater than the range of the inverse sixth van der Waals interaction potential for hydrocarbons, which, from Eq. (6.40), is of the order of the radius of the molecules or molecular groups.⁶ This long range has important implications for understanding the dynamics of self-assembling amphiphilic molecules into micelles and bilayers, the folding of proteins, hydrophobic aggregation, and the fusion mechanisms of bilayers and biological membranes, discussed in Part III. However, the effect of

⁶Actually, when it comes to determining the *rate* of aggregation or association, it is the *volume* encompassed by an interaction that matters, not the distance. The effective enhancement factor is therefore $7^3 \approx 350$.

electrolyte ions in aqueous solutions is still not resolved or understood: different anions and cations can either increase or decrease the strength of the attraction between small hydrophobic solutes (Holz et al., 1993). Further aspects of the hydrophobic interactions between extended surfaces and colloidal particles are discussed in Part II (cf. Chapter 15), where an attempt is also made to establish its still mysterious origin, either as a structural force (due to water structure or a “depletion force”), as an enhanced van der Waals attraction (due to giant fluctuating dipoles arising from proton-hopping or a charge-correlation effects), or as a capillary force due to bridging of vapor bubbles.

Worked Example and Discussion Topic 8.1

Question: The hydrophobic attraction between molecules such as surfactants, proteins, and polymers in water results in their spontaneous self-assembly into large well-ordered structures such as micelles and biological organelles (see Chapter 20). This association appears to increase the order and thus lower the entropy of the universe, in contradiction with the second law of thermodynamics. Resolve this paradox.

Answer: This is more of a discussion topic and involves a number of issues. There is usually more than one contribution to the total entropy change during any process. While it is true that the coming together of the hydrophobic (solute) molecules is associated with a decrease in their entropy of mixing, this is more than offset by the increase in the configurational entropy of the water (solvent) molecules, as discussed at the end of Sections 4.11 and 6.7.

Moreover, the above statement, while true, nevertheless does not go to the heart of this problem which is actually much more fundamental, since it can be posed for any attractive pair potential that leads to association, whether physical or chemical, with or without a solvent. Association necessarily implies the formation of a two-phase system, with some molecules remaining behind in the dilute phase, and *their* entropy—which must also be taken into account—increases. When the entropy changes of all the molecules involved in this spontaneous aggregation process are added up, including the heat of reaction, the net result will always be an increase.

8.7 Hydrophilic Interactions

While there is no phenomenon actually known as the hydrophilic effect or the hydrophilic interaction, such effects can be recognized in the propensity of certain molecules and groups to be water-soluble and to strongly repel each other in water, in contrast to the strong attraction exhibited by hydrophobic groups. Hydrophilic (i.e., water-loving) groups prefer to be in contact with water rather than with each other, and they are often *hygroscopic* (taking up water from vapor). Some hydrophilic polymer networks can swell in water to 1000 times their original size, forming *hydrogels*. As might be expected, strongly hydrated ions and zwitterions are hydrophilic. But some uncharged and even nonpolar molecules can be hydrophilic if they have the right geometry and if they contain atoms capable of H-bonding with water—for example, the O atoms in C=O, —OH

Table 8.2 Hydrophilic Groups and Surfaces

Molecules and ions			
Alcohols (CH_3OH , $\text{C}_2\text{H}_5\text{OH}$, glycerol)		Polyelectrolytes (polysaccharides)	
Sugars (glucose, sucrose)		Soluble proteins	
Chaeotropes (urea)		Nucleic acids DNA, RNA	
Polyethylene oxide ($-\text{CH}_2\text{CH}_2\text{O}-$) _n		Na^+ , Li^+ , Mg^{2+}	
Molecular groups ^a			
	Anionic	Zwitterionic	
Carboxylate	$-\text{COO}^-$	Phosphatidylcholine (lecithin)	$-\text{OPO}_2^- \text{OCH}_2\text{CH}_2\text{N}^+(\text{CH}_3)_3$
Sulfonate	$-\text{SO}_3^-$		
Sulfate	$-\text{SO}_4^-$		
Phosphate ester	$-\text{OPO}_2^- \text{O}-$		
		Polar (nonionic)	
	Cationic	Amine	$-\text{NH}_2$
Trimethyl ammonium	$-\text{N}^+(\text{CH}_3)_3$	Amine oxide	$-\text{NO}(\text{CH}_3)_2$
Dimethyl ammonium	$>\text{N}^+(\text{CH}_3)_2$	Sulfoxide	$-\text{SOCH}_3$
		Phosphine oxide	$-\text{PO}(\text{CH}_3)_2$
Solid Surfaces			
Hydroxylated silica (below 600°C, surface characterized by silanol Si-OH groups ^b)			
Swelling clays (montmorillonite)			
Chromium			
Gold (when clean)			
Polar groups that are not hydrophilic when attached to a long hydrocarbon (hydrophobic) chain ^a			
Alcohol	$-\text{OH}$	Amide	$-\text{CONH}_2$
Ether	$-\text{OCH}_3$	Nitroalkanes	$-\text{NO}, -\text{NO}_2$
Mercaptan	$-\text{SH}$	Aldehyde	$-\text{CHO}$
Amines	$-\text{NH}(\text{CH}_3), -\text{N}(\text{CH}_3)_2$	Ketone	$-\text{COCH}_3$

^aCompiled from a longer list given by Laughlin (1978, 1981).

^bAbove 600°C, a dehydroxylation reaction takes place where two adjacent Si—OH groups liberate a water molecule (H_2O) and combine to form a hydrophobic siloxane Si—O—Si group. Dehydroxylated silica surfaces are hydrophobic.

(alcohol) and ethylene-oxide groups, and the N atoms in amines. Table 8.2 lists some common hydrophilic molecules and molecular groups, as well as some hydrophilic surfaces that are wetted by water or that repel each other in aqueous solutions. From this table we see that a polar group is not necessarily hydrophilic and that a nonpolar group is not always hydrophobic!

Figure 8.6 shows the structuring of water believed to occur at a hydrophilic surface, which may be compared with the structuring at a hydrophobic surface shown in Figure 8.5b. The differences are subtle but important for understanding why the interactions between hydrophilic and hydrophobic surfaces are so different—a “normal” van der Waals attraction with a short-range steric repulsion between two hydrophilic surfaces and an enhanced, hydrophobic attraction between two hydrophobic surfaces. Thus, the

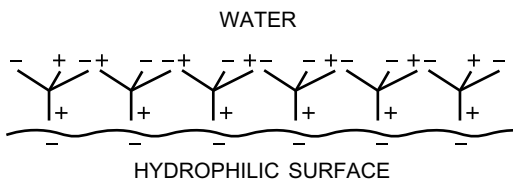


FIGURE 8.6 Water structure at a hydrophilic-water interface—for example, at a negatively charged or electronegative (H-bonding acceptor) surface, where the water molecules are forced to orient in a certain direction with one of the two positive H^+ atoms pointing toward the surface. This severely limits the way the first layer of water molecules can orient with respect to its neighbors, a restriction that does not arise on hydrophobic surfaces (Figure 8.5b). The structuring of water around an ion or small hydrophilic solute molecule is shown in Figure 3.4.

strong *and* directional binding of water to a hydrophilic surface or solute molecule adds an additional steric barrier, increasing the range of the repulsive force or the effective size of the molecule (cf. Problem 8.5). In addition, the orienting of all the water molecules in a certain direction partially restricts charge transport processes such as proton-hopping. No such directional binding occurs to a hydrophobic or vapor interface, where the water molecules, while positionally ordered, are freer to orient as they please. This allows for charge transport and proton-hopping to occur as in the bulk liquid, which in turn “switches on” the entropically driven hydrophobic interaction (see Chapter 15).

The above argument illustrates why the ordering or structuring of water at different surfaces, and its effect on interaction forces, causes so much confusion. At least three different types of ordering and order parameters can be identified: positional ordering into layers, which affects the oscillatory forces (Sections 7.6 and 7.7); orientational ordering, which affects electrostatic and entropic charge-transfer interactions; and mean density variations near the surfaces, which can give rise to the additional “steric” repulsion between hydrophilic surfaces and a “depletion” attraction between hydrophobic surfaces (cf. Chapter 15).

Certain molecules, when dissolved in water, have a drastic effect on other solute molecules, which is believed to be due to their effectiveness in altering or disrupting the local water structure. For example, when urea, $(\text{NH}_2)_2\text{C}=\text{O}$, is dissolved in water, it can cause proteins to unfold, and there have been attempts to categorize such nonionic but highly potent compounds into structure makers and structure breakers. Such molecules are commonly referred to as *chaotropic agents* or *chaotropes*, a term that was coined to convey the idea that their disruption of the local water structure leads to chaos (not the least of which being produced in the minds of those trying to understand this phenomenon).

It appears, therefore, that hydrophilic and hydrophobic interactions, unlike Coulombic and dispersion interactions, are interdependent and not additive. Indeed, one would not expect them to be, since both are determined by the structure of the water H-bonds adopted around dissolved groups. For example, as listed in Table 8.2, the hydrophilicity of some hydrophilic groups, for instance the $-\text{OH}$ group, can be completely neutralized when they are attached to a long alkyl chain such as $-(\text{CH}_2)_{11}\text{CH}_3$. Conversely, as described in

Section 19.7, the hydrophobic energy per CH₂ group of an alkane chain is much reduced when a hydrophilic head-group is attached to the end of the chain.

PROBLEMS AND DISCUSSION TOPICS

8.1 Are there any elements or compounds other than water that expand on freezing? In what ways are their bonding and physical properties unusual and/or similar to those of water?

8.2 The solubilities of cyclohexane (C₆H₁₂) and benzene (C₆H₆) in water are, respectively, 55 and 1800 parts per million by weight at 20°C. Calculate the solubilities in mole fraction units. Assuming that these organic molecules can be considered as macroscopic spheres with radii as given in Figure 7.1, calculate their interfacial energies per unit surface area exposed to water and compare your results with the known values for γ_{12} given in Table 17.1.

The measured solubility of water in cyclohexane and benzene is, respectively, 59 and 620 parts per million by weight at 20°C. By using the same argument as in Section 8.5 and a value of 0.14 nm for the radius of the water molecule, calculate the values for γ_{12} obtained from this reciprocal set of solubility data. Comment on possible reasons for the total lack of agreement in this case.

8.3 The strength of the attractive hydrophobic interaction increases with temperature. This often leads to molecular association (partial immiscibility or phase separation into two phases), *above* some critical temperature, known as a *lower consolute temperature*, which is in addition to the two-phase region that occurs *below* the “normal” critical point. Draw and describe the full temperature-composition phase diagrams for (a) a “normal” or typical two-component liquid-liquid system and (b) a hydrophobic solute in water. Identify the various lower- and upper-consolute temperatures. Applying the van der Waals equation of state to a hydrophobic solute dissolved in a solvent, explain why a temperature-dependent pair potential that is simply proportional to the temperature T —for example, $w(r) = -CT/r^n$, where C and n are constants, as in Eq. (6.40)—is not sufficient to produce a lower consolute point.

8.4 Polymethylene oxide, $[-\text{CH}_2-\text{O}-]_n$, is hydrophobic, but polyethylene oxide, PEO $[-\text{CH}_2-\text{CH}_2-\text{O}-]_n$, which has one more hydrophobic CH₂ group per segment, is hydrophilic and miscible with water. Give possible reasons for this.

8.5* Consider the below model for the effect of hydration (water binding) on the interaction of dissolved hydrophilic solute molecules in water: the solvent molecules (water, of diameter $\sigma_w = 0.25$ nm) bind to the solute molecules of diameter $\sigma_s = 0.4$ nm up to a maximum of one monolayer. The binding decreases with temperature, obeying an equation that is analogous to the *Langmuir adsorption isotherm* (Adamson, 1976, 1990), which gives for the effective diameter of the hydrated solute molecule:

$$\sigma = \sigma_s + 2\sigma_w(1 - e^{-E_0/kT}), \quad (8.5)$$

where $E_0 = 1.75 \times 10^{-21}$ J is the “activation energy.” Note that the hydrated solute diameter decreases from $\sigma = \sigma_s + 2\sigma_w = 0.9$ nm at low temperatures to $\sigma = \sigma_s = 0.4$ nm at high temperatures as the molecule becomes “dehydrated” with increasing temperature. For dilute solutions, the osmotic pressure P as a function of the mean volume occupied by each solute molecule V can be described by the van der Waals equation of state, $(P + a/V^2)(V - b) = kT$, where the parameters a and b were previously shown to be given by (see Sections 2.5 and 6.3): $a = 2\pi C/3\sigma^3$ and $b = 2\pi\sigma^3/3$, and where the van der Waals coefficient in this case is $C = 5 \times 10^{-76}$ J m⁶. Note that both a and b are now temperature-dependent. (1) Plot the PV curves for this system at different temperatures, carefully choosing your ranges of temperature, pressure, and volume to show all the different phases of the system. Draw in the single-phase and two-phase regions (cf. Problem 7.4). (2) How realistic is this model for hydrophilic or amphiphilic molecules in water, such as PEO (cf. Fig. 21.10), that often exhibit a transition from a one-phase to a two-phase system above some critical temperature, known as the *lower consolute temperature*. In practice, how can one tell whether a lower consolute temperature is due to hydrophobic attraction or dehydration? [Answer to numerical part: You should find a lower consolute point at $T = 290$ K, $P = 1.24 \times 10^6$ Pa and $V = 1.3$ nm³ per molecule, corresponding to an unhydrated volume fraction of $\frac{4}{3}\pi(\sigma_s/2)^3/1.3 \times 10^{-27} = 0.026$. There are two more critical points, one at a lower and one at a higher temperature.]

This page intentionally left blank

Nonequilibrium and Time-Dependent Interactions

9.1 Time- and Rate-Dependent Interactions and Processes

So far, time has played little role in our analysis of the forces and energies between molecules. This is because we have always been assuming equilibrium conditions, with the implicit assumption that neither the interaction potential nor the force changes with time, as opposed to distance or location. We have also assumed that the force is independent of the rate or velocity of relative motion of the interacting molecules.

It is not always easy to distinguish between equilibrium and nonequilibrium phenomena. Some equilibrium interactions or conditions can be more readily derived via a dynamic model, as in the case of the retarded van der Waals force (Section 6.9). Conversely, some properties that can be derived from equilibrium theories actually only reflect a long-lived kinetically trapped state, as in the case of the elastic properties of materials or the state of carbon in the form of diamond.

The general equation of motion of a molecule or particle of mass m at position x at time t is

$$m\ddot{x} + \eta\dot{x} + Kx + F(x, \dot{x}, t) = 0, \quad (9.1)$$

where η is the viscous coefficient, K the elastic coefficient (spring stiffness), and $F(x, \dot{x}, t)$ is the combined intermolecular, externally applied and reaction (friction) forces. This chapter deals with this term and the subtle and often unintuitive processes that give rise to hysteretic (irreversible), energy dissipating,¹ time-, rate- and history-dependent interactions. Chapters 17, 18 and 22 discuss further aspects of “dynamic” interactions. As we shall see, the temperature, which does not enter directly into Eq. (9.1), usually plays a key role in such interactions.

Consider a molecule bound to a surface by a potential much like the one shown in Figure 1.4. It was previously calculated (see Worked Example 1.2) that the depth of the well is $w_{\min} = -2.5 \times 10^{-21}$ J and that an adhesion force of $F_{\max} = 18.9$ pN is needed to pull the molecule out of the well. But this is true only at zero temperature ($T = 0$ K). At any finite temperature the surface molecule will be continuously struck by the molecules

¹The commonly used expressions “energy dissipation” and “energy loss” can be misleading given that the First Law of Thermodynamics states that energy is always conserved. Thus, energy can be exchanged or transferred, but it is never lost. The term “energy dissipation” will be used to define the amount of kinetic or heat energy that a molecule or particle transfers to another during an interaction.

of the lattice, which have a Boltzmann distribution of velocities about kT (Chapter 2). Many of the lattice molecules will have energies in excess of the mean energy w_{\min} , which is only 0.61 kT at 298K, and when one of these hits the surface molecule, it will acquire enough energy to leave the surface. The force needed to detach the surface molecule is therefore zero, since the molecule will come off naturally. Even if w_{\min} is well above kT , there will always be a molecule of that energy that *eventually* hits the surface molecule and knocks it out of the lattice. This phenomenon is nothing more than the everyday process of evaporation, but it reveals four important features that are crucial to understanding such processes:

- (1) To fully describe the detachment (knock out) of the molecule requires some specification of the time of the observation or experiment. Thus, if the average time of molecular vibrations or collisions in the lattice is τ_0 , then the mean lifetime of the molecule on the surface (or of any bond in a many-body system) will be given by (Bell, 1978)

$$\tau = \tau_0 e^{-w_0/kT} \quad (9.2a)$$

or, in terms of the rates,

$$\nu = \nu_0 e^{+w_0/kT}, \quad (9.2b)$$

where $\nu_0 = 1/\tau_0$ is the collision frequency and where w_0 is the depth of the potential well (the same as w_{\min} in the above example).² If w_0 is large ($>kT$) and negative, $\tau \gg \tau_0$, and Eq. (9.2) shows that whether a molecule remains bound or becomes free depends on the time of the experiment—the “measurement,” “observation,” or “waiting” time.

- (2) Even at zero pulling force, the molecule will eventually detach (escape) from the surface. Thus, the above calculated value of $F_{ad} = 18.9$ pN is meaningless unless one also specifies the time and temperature of the measurement. On the other hand, the potential energy function does not depend on these parameters. This is an important conceptual difference between force and energy.
- (3) The departing molecule will have received kinetic and potential energy that is in excess of the mean energy of the molecules in the lattice. Thus, the temperature of the lattice will fall as a consequence of this energy loss. Of course, under equilibrium conditions, another molecule from the vapor will have settled on the surface, so, on average, there is no change. This highly improbable and localized evaporation is referred to as a “fluctuation” rather than a spontaneous thermodynamic change of the system. Indeed, thermodynamic laws apply only to the mean properties of the molecules of a system that remain unchanged when averaged over space and time

²Equation (9.2) is sometimes erroneously explained in terms of the probability that the surface molecule can “tunnel through” the energy barrier w_0 even when its thermal energy kT is much lower than w_0 . However, a classical collision is purely deterministic: there is no tunneling: The probability enters into the Boltzmann distribution of the energies of the *bulk* molecules, that is, in the lattice, that impart their energy to the surface molecule. The bulk can be a solid, liquid, or gas.

(which is why neither the size of the system nor the time enter into thermodynamic equations).

- (4)** No pair-potential can fully describe this interaction, which is really a multitude of interactions or molecular collisions following each other in space and time. It is more appropriately to think of the interaction as a “process” (Hänggi et al., 1990).

As we shall see, such time- and temperature-dependent processes are particularly important in many-body and biological systems, and in systems in the steady-state but requiring a continuous input of energy—for example, during frictional sliding (Chapter 18) and in biological systems (Chapter 22). They involve either time-dependent or energy-dissipating effects, or both, and are difficult to understand at the molecular level, which is nevertheless where we shall start.

9.2 Rate- and Time-Dependent Detachment (Debonding) Forces

The following example illustrates why different results can be obtained when measurements of adhesion or unbinding forces are made at different rates or over different times even though the potential energy function is the same.



Worked Example 9.1

Question: When a linear chain molecule such as an alkane or short-chained polymer is pulled out from the bulk phase, the energy varies linearly with the distance pulled, r (Figure 9.1, inset). Such a system can be modeled with the “triangular” interaction potential listed in Table 7.2 as

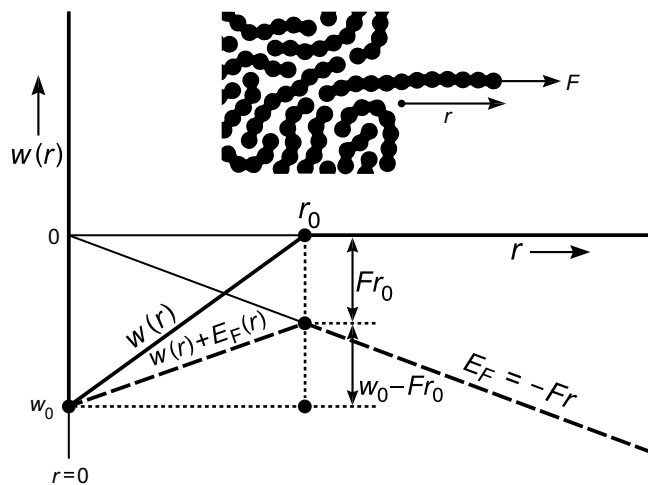


FIGURE 9.1 Bond characterized by a triangular potential function, as occurs when chain molecules are pulled out from the bulk liquid by applying a normal force F to one end of the molecule (inset).

$w(r) = -A(r_0 - r)$, which has a “hard wall” at $r = 0$, an attractive (negative) energy of constant slope that varies linearly from $w = -Ar_0 = w_0$ at $r = 0$, to $w = 0$ at $r = r_0$, and zero energy beyond r_0 , as shown by the thick solid lines in Figure 9.1. This potential function may be said to constitute the “bond” holding each molecule to the surface. In one particular system, $w_0 = -10^{-19}$ J and $r_0 = 1.5$ nm (if the chain is a hydrocarbon chain, this would correspond to about 10 carbon groups with a pull-out energy of 10^{-20} J or about 2.5 kT per group). The molecules have an average vibration time in their potential wells of $\tau_0 = 10^{-8}$ s. (i) What is the natural lifetime τ of the “bond”? (ii) At time $t = 0$ a fixed pulling force of $F = 10$ pN is applied to the molecule. Estimate the time at which the molecule will detach from the surface at $T = 25^\circ\text{C}$. (iii) Derive the expression for the effective (time- and temperature-dependent) adhesion force in terms of F , w_0 , r_0 , τ and the time t . (iv) What is the meaning of the force defined by the maximum value of dw/dr ?

Answer: Figure 9.1 shows the interaction potential function $w(r)$ for this system (thick solid lines), together with the energy E_F corresponding to a constant applied force F (thin solid line), and the total energy, $w(r) + E_F(r)$ (thick dashed lines).

- (i) The mean natural lifetime of the bond under no external force is given by Eq. (9.2a) as

$$\tau = \tau_0 e^{-w_0/kT} = 10^{-8} \exp(10^{-19}/4.1 \times 10^{-21}) = 10^{-8} e^{24.4} = 391 \text{ sec.}$$

- (ii) Under a constant pulling force of $F = 10$ pN = 10^{-11} N, the energy barrier is seen to have fallen from w_0 to $(w_0 - Fr_0)$ so that the mean lifetime is now given by

$$\begin{aligned} \text{Bond lifetime: } &= \tau_0 e^{-(w_0 - Fr_0)/kT} = \tau e^{-Fr_0/kT} = 10^{-8} \exp[(10^{-19} - 10^{-11} \\ &\quad \times 1.5 \times 10^{-9})/(4.1 \times 10^{-21})] = 10^{-8} e^{20.7} = 10 \text{ sec.} \end{aligned} \quad (9.3a)$$

- (iii) Equation (9.3a) can be rearranged to give

$$F(t) = kT \ln(\tau/t)/r_0, \quad (9.3b)$$

which gives the effective (time- and temperature-dependent) adhesion force, although it is more correct to consider Eq. (9.3b) as giving the most probable force needed to separate two bodies after a time t . Further aspects of this important equation are discussed in Chapter 22.

- (iv) The adhesion or pull-off force defined by $F_{\max} = -(dw/dr)_{\max} = 6.7 \times 10^{-11}$ N (67 pN) is the force that would pull out the molecule immediately, or spontaneously—that is, within one molecular vibration of 10 ns. A higher pulling force would detach the molecule even faster, but then additional inertial and viscous terms (cf. Eq. 9.1) must be included in the analysis.
-



Worked Example 9.1 and the potential energy functions shown in Figure 9.1 are but one of many different scenarios that arise in real situations. First, the interaction potential can be a Lennard Jones potential (cf. Problem 9.1), a square-well potential (cf. Problem 21.9), or some much more complicated three-dimensional “energy landscape”.

Second, the externally applied force need not be a constant force but an elastic force—that is, one whose energy varies parabolically with distance, as illustrated later in

Figure 9.4. This arises when the surface molecule is held by another compliant surface or material, and it produces very different effects, as also occurs in the case of friction forces, discussed in Chapter 18.

Third, the energy-distance function $w(r)$ may be different under different experimental conditions. Thus, referring to the inset in Figure 9.1, if the molecule is held at a different point along its length, or if it is not held at all, the way the molecule leaves the surface will be different from that shown, which also changes the functional form of $w(r)$ from the simple line shown in the figure. For example, under equilibrium (purely thermal) conditions—that is, in the absence of any external force—the molecule (a hydrocarbon chain, polymer, or protein) may fold up into a ball before coming off the surface. The calculated values for the lifetimes and time-dependent forces in Worked Example 9.1 must therefore be recognized as being highly model-dependent.

Fourth, in many cases a molecule is pulled away from a surface or from another molecule at some constant *velocity*, rather than a constant *force*. This occurs when two surfaces are separated from adhesive contact (Chapter 17) or sheared past each other at a given velocity or shear rate (Chapter 18). The former gives rise to *adhesion hysteresis*; the latter determines the energy dissipating mechanisms that determine the friction and lubrication forces between two shearing surfaces. In the simple case considered above, the bond lifetime was given by Eq. (9.3), which can be written as

$$\tau = \tau_0 e^{-(w_0 - Fr_0)/kT} = \tau_0^* e^{-Fr_0/kT}, \quad (9.4)$$

where

$$\tau_0^* = \tau_0 e^{-w_0/kT} \quad (9.5)$$

is the equilibrium lifetime of the bond—that is, under zero external force. These equations can be rearranged to give the *time-dependent* detachment force (cf. Eq. (9.3b)):

$$F(t) = kT \ln(\tau_0^*/t)/r_0. \quad (9.6)$$

If the molecule is being pulled at a constant velocity v , then one may express the effective measuring or waiting time t by the time it takes the anchoring point to move the length of the bond r_0 . Thus, we may put $t \approx r_0/v$ in the log term above, and write

$$F(v) = kT \ln(\tau_0^* v / r_0) / r_0 \quad (9.7)$$

which gives the rate-dependent detachment force. The above shows that the pull-off force is expected to increase logarithmically with the pulling rate.³ It is often easier to measure detachment forces at different rates rather than different waiting times, and this has been achieved using the AFM technique, as shown in Figure 9.2.

It is important to stress that all of the above equations, and the results shown in Figure 9.2, are probabilistic. They do not predict exactly when detachment will occur for

³Unfortunately, there is no commonly accepted jargon for describing these interaction so the following words or phrases are often used synonymously: *detachment force*, *rupture force*, *pulling force*, *adhesion force*, *binding or unbinding force (or rate)*, and *loading or unloading force (or rate)*. Likewise, the lifetimes of bonds are sometimes described in terms of the *molecular residence time*, *occupancy time*, or *escape rate*.

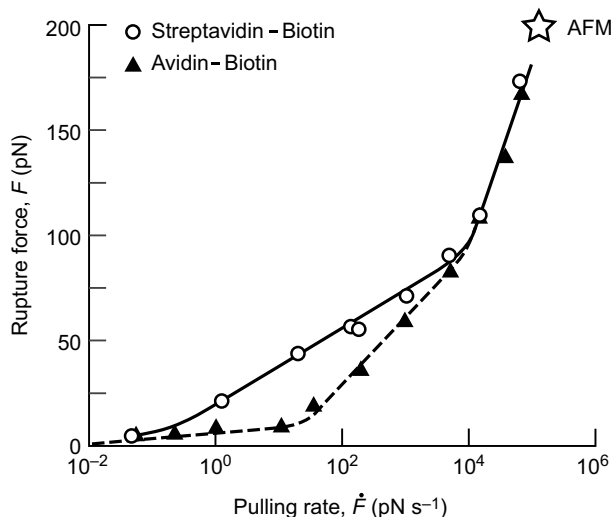


FIGURE 9.2 Force Probe and Atomic Force Microscopy (AFM) results of the detachment (unbinding) forces measured as a function of pulling rates for the streptavidin-biotin and avidin-biotin systems. These biological molecules interact via strong and highly specific bonds known as receptor-ligand or complementary interactions, described in Chapter 22. (Adapted from Evans and Ritchie, 1997.) The binding forces (the reverse of the unbinding forces) between such molecules can also be time- and rate-dependent, as discussed in Chapter 22.

a given force, or the force at which detachment will occur after a given time or pulling rate. They only give the most probable detachment times and forces, with a broad distribution about the mean. The uncertainties are due to the Boltzmann distribution of the energies and collision frequencies, $\nu_0 = 1/\tau_0$, of the material molecules that collide with the escaping molecule. For molecules in a condensed solid or liquid phase, their collision time may be estimated from their mean velocity v_0 and the width of the potential well r_0 . Thus, putting $\frac{1}{2}mv_0^2 = \frac{1}{2}kT$, we obtain

$$\tau_0 \approx 2r_0/v_0 \approx 2r_0\sqrt{m/kT}. \quad (9.8)$$

For example, for a molecule of MW = 200 Da in a potential well of width $r_0 = 0.5$ nm at room temperature, we expect a *collision* or *vibration* time of $\tau_0 \approx 10^{-11}$ s. However, viscous effects usually increase this time. In a gas, r_0 is the mean free path of the molecules, and the average time between such “nonbonded” collisions is much longer. Another way of estimating the collision times of strongly bonded atoms or molecules is in terms of their natural frequency of vibration in their potential energy minimum where the shape of the energy curve can be approximated by a parabola (cf. Table 7.2 and Problem 9.2). From the simple harmonic oscillator model the natural or resonance frequency is

$$\nu_0 = \frac{1}{\tau_0} = \frac{1}{2\pi}\sqrt{\frac{K}{m^*}}, \quad (9.9)$$

where K is the stiffness or effective spring constant of the potential well (in units of $N\ m^{-1}$), and m^* is the *reduced mass* of the molecules (in units of Kg). In the case of

a diatomic molecule composed of two atoms of mass m_1 and m_2 , $m^* = m_1m_2/(m_1 + m_2)$. We shall see how these characteristic frequencies and times play a key role in energy dissipating interactions.

There are many systems where detachment times can be months or centuries, so under a given force or pressure, the system may appear to reach equilibrium quickly, when in fact it is very far from equilibrium. And similar effects can arise when molecules or particles come together or associate rather than dissociate.⁴ These effects manifest themselves as creep in solids and glassy materials, or the slow aging seen in many colloidal and biological systems. Such systems may continue to change indefinitely (for example, under the influence of a constant force or pressure), or they may slowly transit from one state to another—for example, undergo a slow phase separation.

9.3 Energy Transfer (Dissipation) during Molecular Collisions: the Deborah Number

The above processes are all “thermally activated” processes, where the finite temperature of the system provides a mechanism for molecules to overcome a fixed energy barrier that is usually much higher than their mean or average energy. This gives rise to temperature-dependent effects, which translate into time- and rate-dependent processes or reactions such as those described by Eqs. (9.6) and (9.8). But there are also time- and rate-dependent interactions that do not depend on the temperature, at least not directly, as the following examples show.

In Section 2.10, a paradoxical situation arose during an analysis of colliding molecules. Specifically, it was found that when a monatomic molecule collides with a stationary diatomic molecule having the same total mass (cf. Figure 2.3), the first molecule may either come to rest ($v_1 = 0$) or it may continue with a velocity that is one-third of its original velocity ($v_1 = \frac{1}{3}v_0$). Given the way the problem was posed (see Worked Example 2.5 and Problem 2.8), there was no way of telling which of these conclusions is correct: both solution obey the principles of the conservation of energy and momentum. Indeed, if either of the colliding molecules were to consist of many atoms, even if their mass remained unchanged, there would be many other possible solutions to the problem. And yet the initial conditions were very simple: two molecules of equal mass colliding with each other head on, which is suggestive of a simple and unique solution. To resolve the paradox, one needs to first explain what determines whether a diatomic molecule interacts like two coupled masses or a single mass.

The missing but crucial bits of information were the unstated *times* of the various inter- and intramolecular collisions. The interaction actually consists of a “process”

⁴The dynamics of attachment or capture processes, as opposed to detachment, are considered in Chapters 17, 18, and Part III in the sections devoted to adhesion, aggregation, friction, and biological association.

involving at least two quite different collisions: the first molecule (assumed to be a single atom) colliding with the first atom of the diatomic molecule, followed by the collision of this atom with the second atom. If the two collisions occur at the same place and time, as is implicitly assumed for colliding hard spheres, the two molecules behave as two billiard balls, and all the energy of the first is transferred to the second (i.e., $v_1 = 0$). If the two collisions are independent, occurring at different places and times, the second solution to the problem, $v_1 = \frac{1}{3}v_0$, will be the correct one.

But these are only two of an almost infinite number of possibilities that can arise if the molecules are composed of many atoms that interact through specified potentials (so far the atoms have been assumed to be noninteracting hard spheres). For example, if the repulsive potentials are inverse power or exponential rather than hard-sphere, each inter-atomic interaction will take a finite time *and* occur over a finite distance. Under such conditions, the two atoms of the diatomic molecule will start to interact with each other before the first molecule has ceased to interact with the first, colliding, atom in Fig. 2.3. The solution to the problem requires a knowledge of the intra- and intermolecular pair potentials, which are almost certainly different, and involves solving three coupled equations of motion of the type of Eq. (9.1): one for the molecule and two for the two atoms. There is no simple or analytic solution to this *three-body* problem, but if the diatomic atoms are strongly bound together (e.g., via a covalent bond) so that the *intramolecular* interaction time (~molecular vibration time) is much shorter than the weaker van der Waals *intermolecular* interaction time (~collision time), the diatomic molecule will act as a single unit and the first solution ($v_1 = 0$) will be the correct one. In this case one may say that all the energy of the molecule has been transferred ("dissipated" or "lost") during the collision, whereas in the former case eight-ninths of the energy is transferred.

To put this complex but important effect into full perspective, Figure 9.3(a) shows a three-body system of balls and springs that provides many insights into dissipative interactions where between 0% and 100% of the initial energy may be transferred during a collision. In this model, mass **1** represents a "free" molecule or particle of mass m that moves at velocity v_0 toward a surface or lattice whose first two layers consist of molecules **2** and **3** of masses M that are bound together by an attractive parabolic (spring) potential of stiffness k_2 . The molecule-surface interaction is nonadhesive, and is modeled as a purely repulsive compression spring potential represented by half a parabola of stiffness k_1 . Deceptively simple in its appearance, this system is very rich in physical insights. Different relative values of the masses and spring constants lead to very different outcomes, where the initial translational kinetic energy of **1** is distributed among its final kinetic energy and the translational and vibrational (heat) energies of masses **2** and **3**. Solutions to the equations of motion show that after the collision the first mass can be totally reflected, totally stopped, continue forward at the same velocity v_0 , etc.—in other words, that it can have any velocity between 0 and $\pm v_0$ (Figure 9.3b). Analysis of this problem further shows that the essential determinant of the amount of energy transferred is the ratio of the collision time or *interaction time* (which depends on the masses

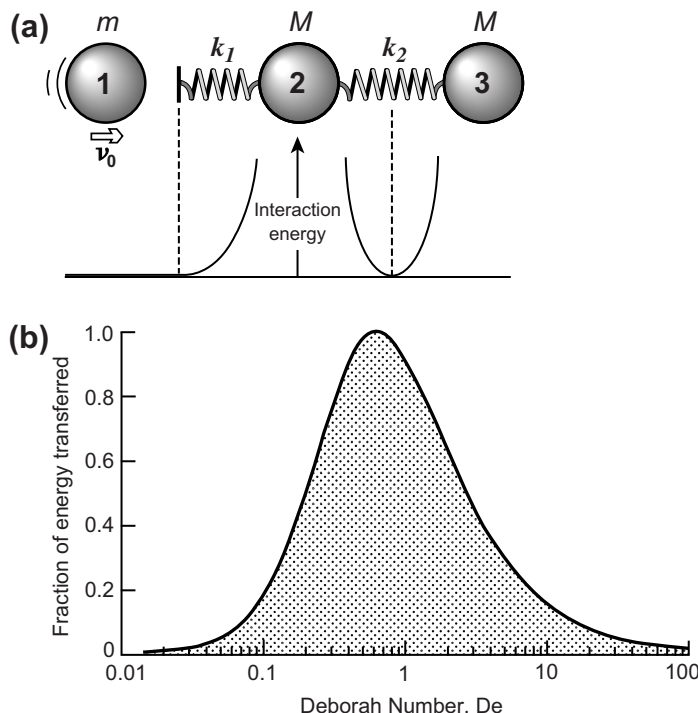


FIGURE 9.3 Energy transfer modeled by (a) the collision of an atom or molecule 1 with the first two surface atoms of a many-atom material. (b) Fraction of energy transferred calculated for $k_1 = 1$, $k_2 = 10$, $m = 1$, and varying M . The system relaxation time is defined as the simple harmonic period of masses M , given by Eq. (9.9), and the interaction time is the collision time, that is, the time atom 1 is in contact with atom 2 via spring k_1 . For low and high Deborah Numbers, atom 1 retains most of its original energy, that is, little energy is transferred to the diatomic molecule, atoms 2 and 3. However, for $De \ll 1$ the atom is reflected, while for $De \gg 1$ it continues along its original direction.

and spring constants) to the characteristic *relaxation time* of masses 2 and 3, defined by Eq. (9.9). This dimensionless ratio is known as the *Deborah Number*, De , which can be defined as

$$De = \frac{\text{System relaxation time}}{\text{Interaction time}}, \quad (9.10)$$

although other commonly used definitions replace the “interaction time” by the “observation time,” “measurement time,” or “transit time.” It is found that maximum energy is transferred when $De \approx 1$.⁵ When the collision time is much larger or smaller

⁵The simplest everyday example of maximum energy transfer occurring when $De = 1$ is in “forced simple harmonic motion” where a mass is suspended from a spring is oscillated at the same frequency as the natural frequency ν_0 of the spring-mass system, Eq. (9.9), at which frequency the amplitude of motion of the mass, and hence the energy transferred, is maximum.

than the system characteristic time—that is, when $De \gg 1$ or $De \ll 1$ —mass **1** is found to retain most of its kinetic energy.

The plot of Figure 9.3b is independent of v_0 or the temperature because we assumed parabolic potential functions whose characteristic frequencies, cf. Eq. (9.9), are independent of the velocities or temperature of the interacting atoms; just as the period of a simple pendulum is independent of the (maximum) velocity of the bob during the swing, or the amplitude of the swing, or the temperature. This means that the parabolic potential is unsuited for analyzing most dynamic and energy-dissipating interactions. In more complex systems, described by more realistic interaction potentials, both the velocity v_0 and temperature become important factors that affect both the Deborah Number and the energy dissipated (see the following section and Problem 9.4).

It is also important to note that in this one-dimensional analysis any additional energy modes and degrees of freedom of the second molecule were not considered. These rotational and vibrational modes, if present, will also be involved in the interaction, sharing in the energy transferred from mass **1** and giving rise to more than one Deborah Number. Further, if atoms **2** and **3** are only the first two atoms of a lattice the energy transfer or exchange becomes even more complex and can be rigorously analyzed only by a computer simulation (see Figure 9.7). Chapters 17 and 18 discuss further aspects of energy exchange as it pertains to adhesion, friction and lubrication forces.

9.4 Energy Transfer during Cyclic Bonding-Unbonding Processes

Molecular interactions often involve cyclic or repetitive processes, unlike the “one-way” detachment or collision processes that were analyzed in Sections 9.2 and 9.3. For example, in the Carnot Cycle or Engine, one considers a system that starts and ends at the same point in the PV phase diagram and calculates the work done, or energy dissipated, during the cycle. Different processes have different PVT cycles and different theoretical efficiencies that are important for determining how they will function as engines or machines during continuous running—that is, when energy is continuously fed to the system.

Analogous situations arise at the molecular level—for example, when molecules from one surface are brought into contact with another surface and then separated, or when one surface is slid across another surface (frictional sliding), or when a gas is compressed and then decompressed. In each case, one may consider the process as a cycle⁶ and analyze it at the molecular level.

Figures 9.4 and 9.5 shows how the total force and potential energy of a molecule or macroscopic body changes as it is first brought toward another body or surface and then

⁶The not-so-obvious “cycle” during frictional sliding may be understood by considering that in the steady-state it involves the forced displacement of a molecule from one lattice site to the next, where after each jump the molecule finds itself in the same state as before the jump. The only difference is in the initial and final positions of the molecule (see Figure 18.5).

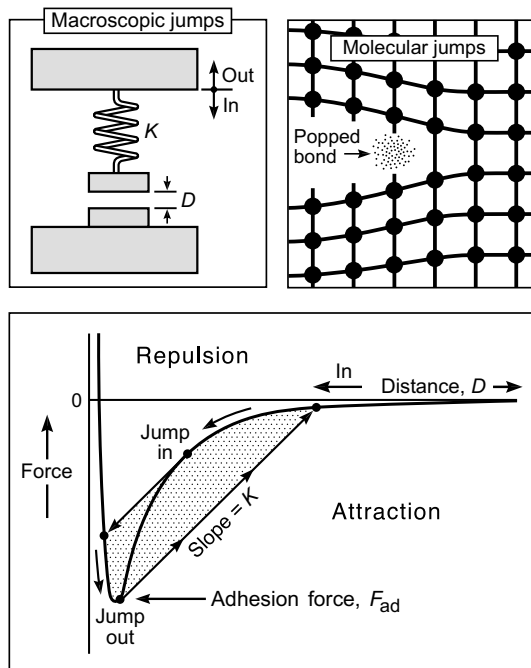


FIGURE 9.4 Force-distance functions for two atoms, molecules, or macroscopic bodies interacting via an attractive Lennard Jones-type force, where one or both are held by a spring-like force. Spontaneous inward and outward jumps occur from the positions shown as the two bodies are brought together or separated.

separated from it, to return to its original position. This is what happens during a typical loading-unloading or bonding-debonding cycle. In practice, the molecule or particle may be held by a spring-like force, or it may be pushed or pulled by a constant force. The former arises for molecules attached to a solid surface (Figure 9.5a) or, in force-measurements, to an AFM tip; the latter arises in experiments using Optical Tweezers, gravity, or fluid flow (cf. Figure 9.1), or when the spring stiffness is so low that it effectively acts as a constant force over small displacements.

In Figure 9.4 the molecule or particle is held by a spring-like force, which can be modeled as a magnet suspended from the end of a spring. The anchoring point of the molecule is defined by the point where $F = 0$ for the spring force, which is also where $E = 0$ in the energy minimum of the parabolic potential that represents the spring (Figure 9.5). This position is essentially the same as the center of mass of the body that holds the molecule. As the molecule is brought toward the surface, at some point—when the gradient of the force dF/dD exceeds K —the molecule will jump into contact with the surface. On separating, it will jump apart from a point where again $dF/dD > K$ (cf. Problem 1.5). These mechanical instabilities occur only for sufficiently weak supporting materials (small K). Since the jumps occur spontaneously, they cannot be reversible: the kinetic energy acquired by the molecule during each jump is converted into heat energy as the molecule comes to rest after the jump. Thus, it appears that regardless of how

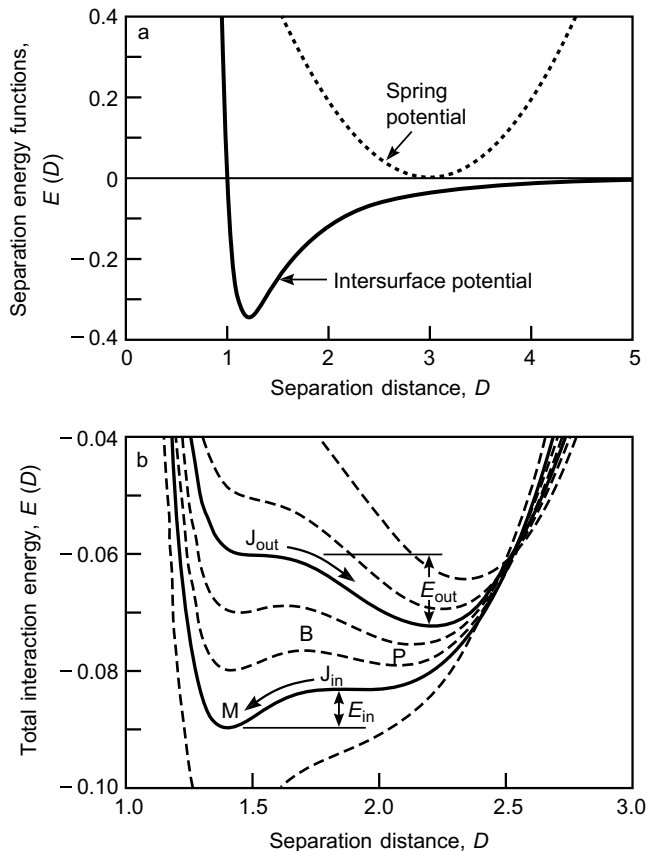


FIGURE 9.5 Top curves: separate intermolecular and spring potential functions. Bottom curves: total energy curves, comprising the sum of the intermolecular and spring potentials at different molecule-surface separations. The spontaneous inward and outward jumps occur from J_{in} and J_{out} .

slowly the molecule is brought toward the surface or separated from it, the spontaneous jumps into and out of contact ensure that the cycle will be dissipative; that is, not all the external work done on the molecule during the loading-unloading cycle will be recovered, and the system will be hotter at the end of each cycle. Such effects occur when bonds are forcibly broken during adhesive failure or crack propagation (Figure 9.4) and during frictional sliding (Chapter 18).

Figure 9.5 shows the same process on an Energy-Distance plot. Such energy plots afford a much better way of analyzing both thermodynamic stability and how energy is dissipated in a cyclic process. At first, it may appear that the energy lost as heat will always be given by $E_{in} + E_{out}$. However, more careful analysis shows that the amount of energy dissipated also depends on the *rate* or *velocity* at which the molecules or bodies are brought toward each other and separated—that is, on the *interaction time*. To see this, first imagine that the two bodies are moved very slowly, so slowly that at any position P in Figure 9.5 there is enough

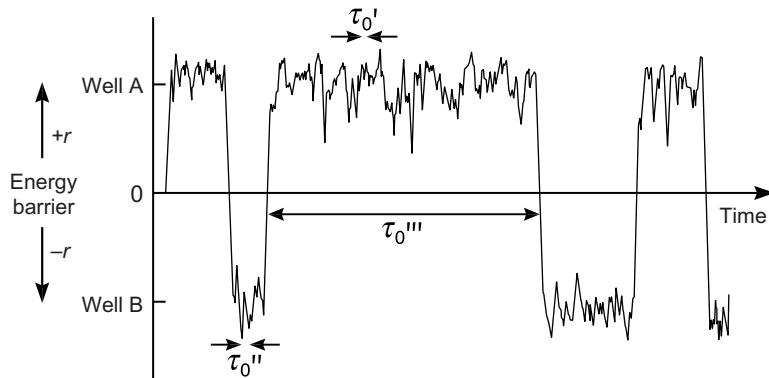


FIGURE 9.6 Theoretical computation of space-time trajectory of particle between two potential wells separated by an energy barrier, conceptually similar to those shown in Figures 9.5 and 9.7. Note the random thermal fluctuations within each well and less frequent larger jumps between the wells. This system has three mean relaxation times, two short, τ'_0 and τ''_0 , involving vibrations within each well, and one long, τ'''_0 , involving transitions between the two wells. (From Hänggi et al., 1985.)

time for them to sample the *whole* of the energy curve (“landscape” or “phase-space”). That is, they have sufficient time to undergo spontaneous thermally activated jumps over the energy barrier at B and back again many times during this Boltzmann averaging process (Figure 9.6), so the system is always at its true time-averaged thermodynamic equilibrium state (recall that thermodynamic equilibrium refers to an unchanging *distribution*, not a *constant* distance or structure). Depending on the energy landscape of the system, this averaging time could be as short as picoseconds or longer than the age of the universe—that is, from 10^{-12} to 10^{+17} s, a range of 29 decades. Thus, if the measurement or *interaction* time is much longer than this *relaxation* time ($t = \tau'''_0$ in Figure 9.6), the spontaneous mechanical jumps at J_{in} and J_{out} will cease to have any special significance; they will simply be lost in all the hops and jumps and other fluctuations that occur during the overall thermal averaging: no energy will be dissipated as heat, and the approach and separation will be reversible. We may conclude, therefore, that for sufficiently low Deborah Numbers ($De \ll 1$), the cycle will always be at equilibrium, thermodynamically reversible, and nondissipating.

The other extreme of very rapid approach and separation is equally intriguing, for now we find that following the spontaneous jump in from J_{in} the two bodies do not come to rest *immediately* at the minimum point M. Rather, they will oscillate about this minimum with a gradually diminishing amplitude as they release their extra kinetic energy of impact to the lattice as heat, eventually coming to “rest” at M (where they will continue to vibrate about the minimum with their mean thermal energy $\frac{1}{2}kT$). If the two bodies are pulled apart before they have had the time to dissipate their kinetic energy—that is, if their time in contact, the *interaction* time, is significantly shorter than the *relaxation time* of lattice vibrations about M ($t < \tau'_0$ in Figure 9.6)—then the two bodies will be whisked apart before they have had time to lose their extra kinetic energy. They will now lose it by going back up the energy curve and return to their original configuration with little or no change in their energy. Thus, under very rapid approach-separation rates, corresponding

now to $De \gg 1$, the energy dissipation will again be small. However, unlike the case for $De \ll 1$, where the system is always at thermodynamic equilibrium, here the reversibility is due to the fact that there is not sufficient time for energy transfer to occur—that is, the process is very far from equilibrium.

Maximum dissipation occurs at $De \approx 1$ when there is sufficient time for the kinetic energy gained during the interaction to be transferred to the bodies (as heat) but not sufficient time for the molecules to sample the whole of space at all stages of the interaction. These effects mirror the very similar dissipation seen with the colliding molecules modeled in Figure 9.3, which was also depended on De but where the dissipation was not velocity- or temperature-dependent. In most real cases, both the velocity and temperature play an important role. Thus, the faster the bodies are made to approach and separate, the shorter will be the interaction time, while the higher the temperature, the shorter (faster) will be the relaxation times.

Similar considerations apply to more complex collisions (Fig. 9.7), and to shearing surfaces during frictional sliding where the interaction time is the “transit” time it takes a molecule of one surface to traverse a lattice spacing of the other surface (Chapter 18).

9.5 Relationships between Time, Temperature, and Velocity (Rate) in Complex Processes

While there is no general proof that maximum dissipation occurs when the Deborah Number is close to 1, this appears to be the case in most systems, including some purely thermodynamic systems such as a perfect gas undergoing a compression-decompression cycle at different rates (Problem 9.4). A complex system usually has a number of different characteristic relaxation times that depend on the temperature and that can span many orders of magnitude, from nanoseconds to years. They are therefore important in very

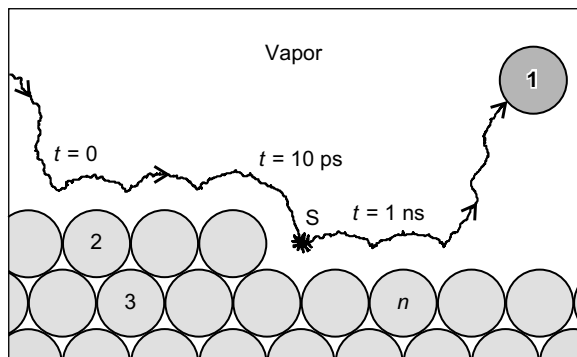


FIGURE 9.7 A ~ 1 ns snapshot of a monatomic molecule in a three energy state system showing the path of the molecule and how it has spent its time partly in the vapor (depending on the volume of the chamber), partly traveling along the surface (~ 10 ps), and partly in the solid state or phase at S (~ 1 ns). The scenario shown here is a more realistic example of the system in Figure 9.3 involving three atoms, 1, 2, and 3, where molecule n is the one that kicks molecule 1 off the surface.

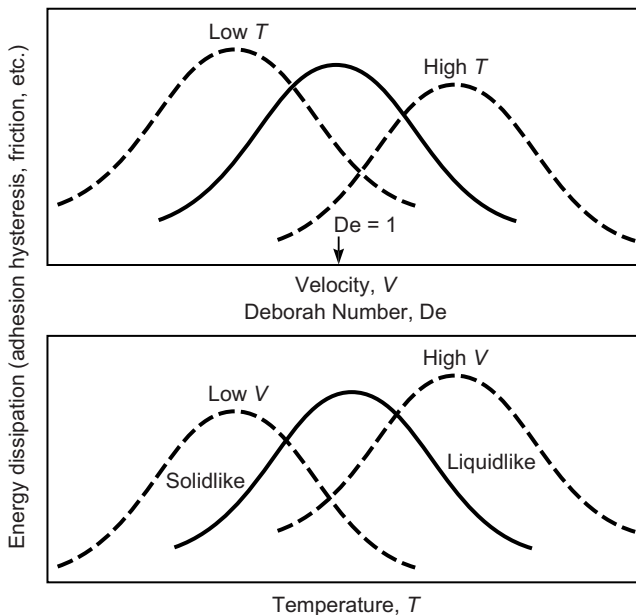


FIGURE 9.8 Typical energy dissipation/transfer vs velocity curve. Such “dynamic” phase diagrams⁷ are useful for representing energy losses in adhesion and frictional processes as a function of the loading-unloading rate or sliding velocity. Energy dissipation in general may also be plotted as a function of the dimensionless Deborah Number, De , defined by Eqs. (9.10) and (9.12). See Chapters 18 and 22 on the use of such phase diagrams for describing friction and lubrication phenomena, and complex dynamic biological processes.

different phenomena from chemical reactions to material creep and continental drift (plate tectonics). Typically, one presents the energy dissipated in such systems by plotting the work done against the time (velocity, rate, or frequency) or the temperature. The first is proportional to the dimensionless Deborah Number. Most interactions have a characteristic *interaction length* δ_0 that is associated with the relaxation time τ_0 , which allows one to also define a characteristic velocity $v_0 = \delta_0/\tau_0$. The interaction length is typically the distance between the atoms or molecules in the body, but it can be longer in the case of polymeric or structured materials and, in the case of adhesion, friction, and granular flow, many microns if it represents the distance between surface asperities, the grain size or the particle size. For a given experimental velocity v , the interaction time t is therefore

$$t = \delta_0/v, \quad (9.11)$$

which allows us to write the Deborah Number as

$$De = \frac{\text{System relaxation time}}{\text{Interaction time}} = \frac{\tau_0}{t} = \frac{\tau_0 v}{\delta_0} = \frac{v}{v_0}. \quad (9.12)$$

⁷Not to be confused with “real” phase diagrams, which represent states at thermodynamic equilibrium. Dynamic phase diagrams represent states at “steady-state” equilibrium.

The effect of temperature is more complex. In a first approximation it enters into Eq. (9.12) through its effect on the relaxation time via Eqs. (9.2) and (9.8), but it also affects the interaction length δ_0 , especially in complex multicomponent systems. The relationship between time (velocity, frequency) and temperature is known as *time-temperature superposition* (Ferry, 1980).

Figure 9.8 shows the type of bell-shaped energy dissipation *vs* velocity curve that is characteristic for most energy dissipation interactions or phenomena ranging from a simple damped harmonic oscillator to complex viscoelastic behavior (Ferry, 1980; Barnes et al., 1989), adhesion hysteresis (Chapter 17), friction and lubrication (Chapter 18), and energy losses during granular and colloidal flow (Mehta, 1994; Russel et al., 1999; Hiemenz and Rajagopalan, 1997). All of these phenomena may be considered to involve nonequilibrium interactions or processes in the sense that they require a continuous input of energy or that the outcome depends on the path taken. We end Part I of this book by considering one further example that nicely illustrate the principles covered in this and previous chapters.



Worked Example/Discussion Topic 9.2

Question: What is the difference between a liquid and a solid?

Answer: In the scientific literature one will find two distinguishing definitions: (1) a liquid flows but a solid doesn't; that is, a liquid has a viscosity, while a solid has an elastic modulus. (2) A liquid has only short-range molecular order but a solid, especially a crystalline solid, has long-range, essentially infinite, order. Concerning the first distinction/definition, consider a cup on a table. Given sufficient time, which may be on the order of 10^9 years or 10^{16} s, it will be seen to flow (cf. Problem 9.3). This is because at any finite temperature all materials, even crystalline solids, have defects. Atoms will be jumping in and out of these defects, and there will be a slight Boltzmann-averaged weighting in favor of the downward direction due to gravity. This will cause the cup to flow downward at a "velocity" that will be proportional to the gravitational force at any point. This is the same as defining the viscosity of a liquid, except that here the viscosity will be extremely large. But it is still a quantitative rather than a qualitative difference. On the other extreme, if a liquid is struck very rapidly (in less than 10^{-11} s). It will respond elastically—that is, like a solid. Thus, whether a material is a liquid or solid is seen to depend on our observation or measurement time—that is, on the Deborah Number. Given the enormous range of sizes, relaxation times, and other properties that different materials and phenomena can have (Table 9.1), it is clear why many of our ideas are formed by our rather narrow range of human perceptions.⁸ The second definition, in terms of the range of molecular ordering, is not dependent on time but can be ambiguous for solids that have ordered domains of finite size that can be arbitrarily large or small. This issue deserves further discussion.

⁸Also "engineering conditions." For example, shear rates lower than 10^{-6} s⁻¹ are difficult to achieve or measure even though many natural phenomena occur at much lower rates.



Table 9.1 Range of Dimensions of Everyday Things and Phenomena (Ranges of human perceptions are indicated by the darker shading.)

	10^{-30}	10^{-24}	10^{-18}	10^{-12}	10^{-6}	1	10^6	10^{12}	10^{18}	10^{24}	10^{30}
Temperature (K)							Star				
Energy* (J)		Bond*				†			††		
Force (N = 100 gm)			Bond*		Touch & Feel						
Pressure (bar, atm)					Touch	Star					
Speed (m/s)				Creep	Snail	Plane	Light				
Distance, size (m)				Atom	Cell	House	Solar				
Time (s)			Mol.	collision*	Bang	1 day	1M years	Universe			
Mass (kg)	Electron	Molecule	DNA	Cell	Pea	Animal	Ship	Asteroid	Earth	Sun	
Density (kg m^{-3})		Outer space			Air	Metals	Stars	Nuclei			
No. of molecules							Cell			Animals	

* Per molecule. † Sitting/running, J per second (Watts). †† Volcanos, hurricanes, J per day.

PROBLEMS AND DISCUSSION TOPICS

- 9.1 (i)** Plot the bond lifetime as a function of pulling force for Worked Example 9.1. Use a logarithmic scale for the time (the y -axis) and a linear scale for the force (the x -axis). The plot should then be a straight line. How do you expect the line to change at pulling forces in excess of 70 pN?
- (ii)** Two atoms interact via a Lennard-Jones potential, Eq. (1.7), with interaction constants $A = 10^{-77} \text{ J m}^6$ and $B = 10^{-134} \text{ J m}^{12}$ (cf. Problem 1.4 and Worked Example 1.2). Plot the detachment force as a function of the pulling time at 298 K assuming the atoms to have a MW of 100 Da. Your plot will be approximate and model-dependent. Justify all the assumptions you make.
- 9.2** Equations (9.8) and (9.9) give different expressions for the collision times of bonded atoms or molecules. Use both equations to estimate τ_0 for a diatomic molecule of total mass 200 Da at 300 K whose atoms interact via the Lennard Jones potential of Problem 9.1(ii). Comment on the similarity or difference in the calculated values.
- 9.3* (i)** Ignoring the effects of gravity and other external forces, the shape of lowest energy of any condensed isotropic material is a sphere, since this has the lowest

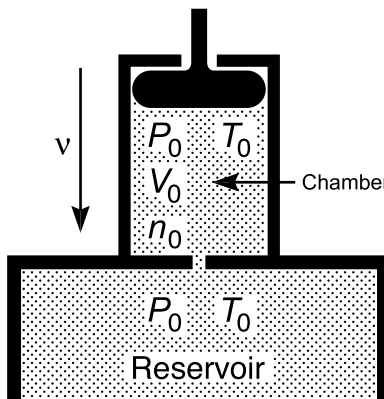


FIGURE 9.9

surface area for any given volume. Liquids quickly adopt this shape, and all solids should, regardless of their initial shape, if given sufficient time. Estimate this time for a solid metal cluster/particle consisting of a fixed number $N = 10^6$ of spherical atoms of molecular weight 100 Da and atomic radius $r = 0.1$ nm, where the energy per bond is $\epsilon = 10 kT$ (each internal, or bulk, atom may be assumed to participate in 12 bonds with its nearest neighbors). The cluster may be considered to be in a sealed chamber at $T = 300$ K and in equilibrium with its saturated vapor. (*Suggestion:* Consider first whether the solid is more likely to change its shape via bulk “viscous” flow,⁹ via surface diffusion of atoms, or via diffusion through the vapor. *Hint:* You have been given sufficient information to estimate many of the static and dynamic properties of the particle, such as its surface energy, fraction of vacancies, molecular surface diffusion rate, escape rate into the vapor, and so on.)

- (ii) Assuming that in the solid phase the atoms are arranged in a close-packed crystalline lattice with 12 nearest-neighbors per atom, and that different faces of the crystal have different surface energies, discuss whether, in general, the shape of lowest energy is indeed a sphere or a faceted polyhedron.

9.4* An ideal gas is contained in a small chamber that is connected to a large gas reservoir via a small orifice (Figure 9.9). Initially, the pressure, temperature, volume, and molar quantity of gas in the chamber are as shown in the figure above, and the gas is in equilibrium with the reservoir. At time $t = 0$ the piston is moved downward at a constant velocity v , defined by $v = dV/dt$, where V is the volume of the gas in the small chamber. When the piston has compressed a fraction ϕ of the gas ($0 < \phi < 1$), it immediately reverses direction and returns to its starting position at the same velocity, $-v$. The rate of flow of gas from the chamber to the reservoir is proportional

⁹See the famous “Pitch Drop Experiment”.

to the instantaneous difference in pressure between them and is given by $dn/dt = -\alpha(P - P_0)$, where P is the pressure and n is the molar quantity of gas inside the chamber, and α is a constant. The reservoir may be assumed to be at the same pressure and temperature at all times, and the outside pressure may also be assumed to be constant throughout the cycle (you may take it to be zero). You may also assume isothermal conditions at all times.

- (i) Explain, using simple language, why in the limits of very low and very high velocities, the compression-decompression cycles are reversible and no work is done by the piston—that is, $\Delta W = 0$. (You may assume that at the highest velocities the speed is still well below the velocity of the molecules or where inertial effects have to be considered.)
- (ii) Derive an expression for the mechanical work done on the gas during one cycle, defined by $\Delta W = \phi P dV$, as a function of $P_0 V_0$, αRT , v and ϕ ($0 < \phi < 1$).
Hint: The solution to the differential equation $\frac{dy}{dx} = Q(x) - P(x)y$ is $y e^{\int P dx} = \int Q e^{\int P dx} dx + c$.
- (iii) Show that the Deborah Number for this system, being the ratio of the characteristic relaxation time τ_r for the gas to diffuse through the hole between the two chambers to the total time τ_t of the cycle (the experimental, observation or transit time), is¹⁰ $De = \tau_r/\tau_t = v/\alpha RT$.
- (iv) For a system where $\phi = 0.9$, plot the dimensionless work done during a cycle $\Delta W/P_0 V_0$ as a function of De from $De = 0.01$ to $De = 100$, and verify that the maximum work done—that is, the maximum energy “dissipated”—occurs when the Deborah Number is close to 1.

[Answer: (i) This is a thermodynamic example of energy dissipation during a compression/decompression cycle of an ideal gas. In this example, work is done on the piston as it is moved down to some fraction of the volume of the upper chamber, and back again. Because gas flows out and back into this chamber during the compression/decompression cycle the total work done will depend on the velocity at which the piston is moved (assumed to be the same for both the down and up strokes). If carried out very slowly the gas has sufficient time to pass through the small hole between the two chambers so that it is at constant pressure throughout the cycle. The work done by the piston on compression will therefore equal that done (on the piston) on decompression, and the total work done will be zero. In the other extreme of rapid compression/decompression, there is no time for any gas to pass through the hole, the two chambers are therefore effectively decoupled during the cycle, and again the process is reversible. However, at intermediate rates, some gas will pass through the hole during the downstroke and not be able to get back by the time the piston has returned to its initial position. Even after the piston has stopped

¹⁰Note that the Deborah Number is here also the ratio of the experimental to characteristic rates of volume change of the gas.

moving, gas will continue to flow back into the upper chamber, but no more work will be done on the piston. For such cases a finite amount of work will be done by the piston per cycle. It will be shown that maximum work is done when the cycle time is approximately equal to the characteristic time for the gas to diffuse through the hole between the two chambers—that is, when the Deborah Number is close to 1. This system is analogous to some frictional processes where the hops between asperities or lattice sites (cf. Figure 18.5) can be modeled as compression/decompression cycles.]

The Forces between Particles and Surfaces

This page intentionally left blank

Unifying Concepts in Intermolecular and Interparticle Forces

10.1 The Association of Like Molecules or Particles in a Medium

In this second part of the book, we shall be looking at the physical forces between particles and surfaces. While the fundamental forces involved are the same as those already described (i.e., electrostatic, van der Waals, solvation forces), they can manifest themselves in quite different ways and lead to qualitatively new features when acting between large particles or extended surfaces. These differences will be discussed in the next chapter. In this chapter we look at the similarities and see how the ideas developed in Part I also apply to the interactions of macroscopic particles and surfaces. We shall find that, independently of the type of interaction force involved, certain semiquantitative relations describing molecular forces—known as *combining relations*—are applicable quite generally to all systems—that is, to the interactions of molecules, particles, surfaces, and even complex multicomponent systems.

Let us start by noting that for any type of interaction between two molecules A and B, the interaction energy at any given separation is always, to a good approximation, proportional to the product of some molecular property of A times some molecular property of B (rather than, say, their sum). Let us denote these properties by \mathbf{A} and \mathbf{B} . Referring to Table 2.2, we find, for example, that for the charge-nonpolar-molecule interaction we may write $\mathbf{A} \propto Q_A^2$ and $\mathbf{B} \propto \alpha_B$; for the dipole-dipole interaction, $\mathbf{A} \propto u_A$ or u_A^2 and $\mathbf{B} \propto u_B$ or u_B^2 , while for the dispersion interaction we have $\mathbf{A} \propto \alpha_A$ and $\mathbf{B} \propto \alpha_B$. Note that even for the gravitational interaction (Eq. 1.1), we may put $\mathbf{A} \propto$ mass of A, and $\mathbf{B} \propto$ mass of B.

Thus, for many different types of interactions, we may express the binding energies of molecules A and B in contact as

$$W_{AA} = -\mathbf{A}^2, \quad W_{BB} = -\mathbf{B}^2 \quad (\text{for like molecules}) \quad (10.1)$$

and

$$W_{AB} = -\mathbf{AB} \quad (\text{for unlike molecules}), \quad (10.2)$$

where only for the purely Coulombic charge-charge interaction are the signs reversed—for example, positive for two like charges (Table 2.2). Let us now consider a liquid consisting of a mixture of molecules A and B in equal amounts. If the molecules are randomly *dispersed* (Figure 10.1a), then on average an A molecule will have both A and B molecules

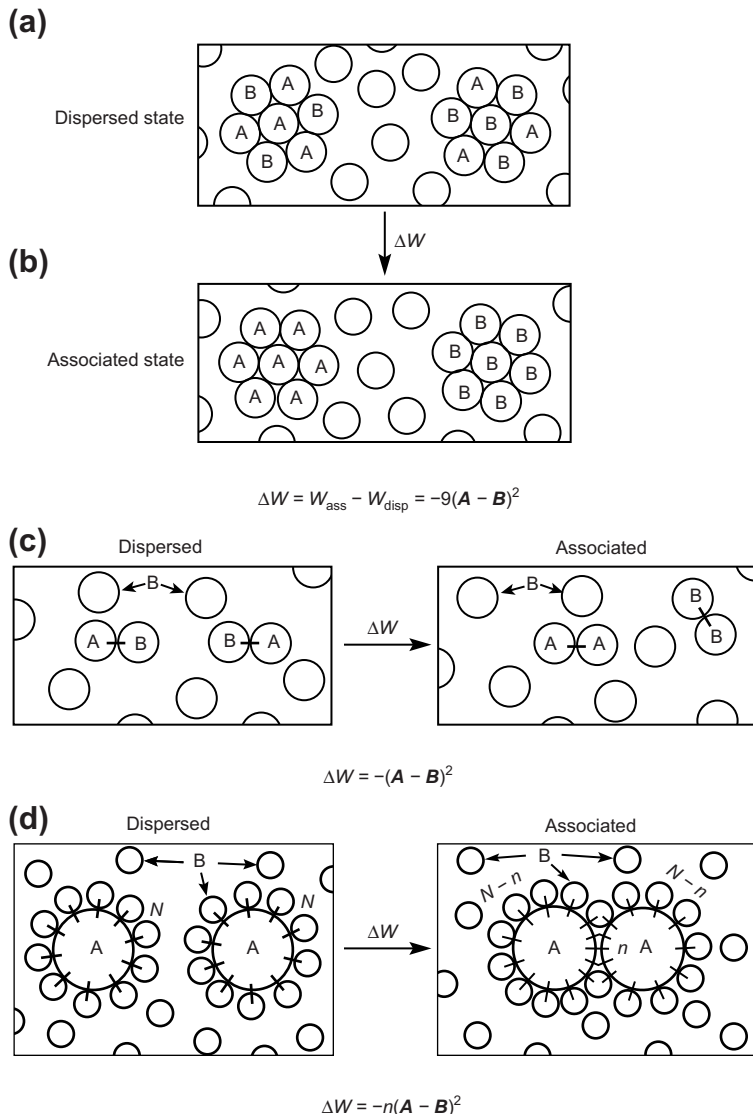


FIGURE 10.1 (a) Two central molecules A and B surrounded by an equal number of A and B molecules in a solvent. Since there are three A–A “bonds,” three B–B “bonds,” and 18 A–B “bonds,” we may write $W_{\text{disp}} = -(3A^2 + 3B^2 + 18AB)$. (b) Seven A molecules and seven B molecules have associated in two small clusters. There are now 12 A–A “bonds” and 12 B–B “bonds,” so that $W_{\text{ass}} = -12(A^2 + B^2)$. The net change in energy on going from the dispersed to the associated state is therefore $\Delta W = W_{\text{ass}} - W_{\text{disp}} = -9(A - B)^2$. Note that there is no change in the number of A and B molecules exposed to the solvent. Thus, ΔW does not involve any term due to the interaction with the surrounding medium if it is unchanged during the redistribution of the A and B molecules. (c) Two A molecules associating in a medium of B molecules. Here $W_{\text{disp}} = -2AB$, and $W_{\text{ass}} = -(A^2 + B^2)$, so that $\Delta W = -(A - B)^2$. (d) Two large particles A associating in a medium of small solvent molecules B. This involves the replacement of $2n$ A–B “bonds” by n A–A “bonds” and n B–B “bonds.” $W_{\text{disp}} = -2NAB$, $W_{\text{ass}} = -2(N - n)AB - nA^2 - nB^2$, so that $\Delta W = -n(A - B)^2$. Note that n is proportional to the adhesion area or effective “contact area” of the two particles, which is proportional to their radii (see Worked Example 10.1).

as nearest neighbors, and similarly for molecule B. However, if the molecules are *associated*, then the molecular organization of nearest neighbors around molecules A and B will be as in Figure 10.1b. The difference in energy between the associated and dispersed clusters will therefore be $\Delta W = -9(A - B)^2$, where we note that in this two-dimensional case nine A–A “bonds” and nine B–B “bonds” have replaced 18 A–B “bonds.” In three dimensions with 12 nearest neighbors around each central molecule, and starting with six A and six B molecules around each A and B molecule, we would find (Problem 10.1) that $\Delta W = -22(A - B)^2$ and that 22 A–A and 22 B–B “bonds” have been formed on association. For the simplest case of two associating A molecules (Figure 10.1c), we have $\Delta W = -(A - B)^2$.

Thus in general we may write

$$\Delta W = W_{\text{ass}} - W_{\text{disp}} = -n(A - B)^2, \quad (10.3)$$

where n is always equal to the number of like “bonds” that have been formed in the process of association, irrespective of how many molecules are involved or their relative sizes (Figure 10.1d). Further, since $(A - B)^2$ must always be positive, we see that in general $\Delta W < 0$ —that is, $W_{\text{ass}} < W_{\text{disp}}$. We may therefore conclude that the associated state of like molecules is energetically preferred to the dispersed state. In other words, *there is always an effective attraction between like molecules or particles in a binary mixture.*



Worked Example 10.1

Question: Two rigid macroscopic spheres of radius R are in adhesive contact as in Figure 10.1(d). What is their “effective” contact area—that is, the area that determines the number of intermolecular bonds n between them?

Answer: This can be a subtle problem. The answer depends on whether the intermolecular forces are long-range or short-range compared to the sizes of the particles. However, since we are here considering the adhesion of macroscopic spheres, we may assume the forces to be of short-range, effectively acting over a distance of the size of the molecules of the solvent or particles. Thus, referring to Figure 10.2 (left), we need to determine the area that excludes solvent molecules, of radius a , between the surfaces. That is, we need to determine πr^2 in terms of R and a .

From the geometric construction of Figure 10.2 (right) we apply Pythagoras’s theorem: $AC^2 = AB^2 + BC^2 = AD^2 + BD^2 + BD^2 + DC^2$. Thus: $4R^2 = a^2 + 2r^2 + (2R - a)^2$, which simplifies to

$$r^2 = (2R - a)a \approx 2Ra \quad \text{for } R \gg a. \quad (10.4)$$

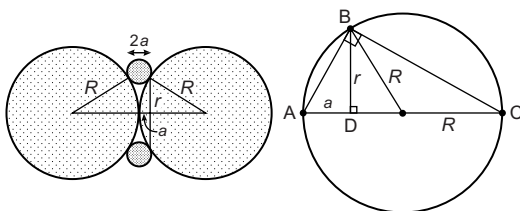


FIGURE 10.2

This relation, known as the *chord theorem*, is important for deriving many of the equations in later chapters. Thus, for two large spheres in contact their effective “area of contact” or effective “interaction area” is given by $\pi r^2 \approx 2\pi Ra$, where a is a measure of the range of the forces (usually of the order of molecular dimensions). Note that the effective area of interaction is proportional to R .

It is a simple matter to show that for two contacting spheres of different radii, R_1 and R_2 , their effective interaction area is $4\pi R_1 R_2 a / (R_1 + R_2)$, and that for two parallel cylinders it is $2[R_1 R_2 a / (R_1 + R_2)]^{1/2}$ per unit length.

Equation (10.3) can be developed further to provide more general insights into the interactions of like solute molecules and particles in a medium. First, Eq. (10.3) may be expressed in a number of different forms:

$$\Delta W = -n(\mathbf{A} - \mathbf{B})^2 = -n(\mathbf{A}^2 + \mathbf{B}^2 - 2\mathbf{AB}) \quad (10.5)$$

$$= -n(\sqrt{-W_{AA}} - \sqrt{-W_{BB}})^2 = +n(W_{AA} + W_{BB} - 2W_{AB}), \quad (10.6)$$

where ΔW may be readily seen to be the same as the interaction pair potential $w(\sigma)$ in the medium (at contact). Second, since $-nW_{AA}$ and $-nW_{BB}$ are roughly proportional to the respective molar cohesion energies U_A and U_B , we find that

$$\Delta W \propto -n(\sqrt{U_A} - \sqrt{U_B})^2 \quad (10.7)$$

which is essentially the same as Eq. (6.39), previously derived for the specific case of dispersion forces. If W_{AA} and W_{BB} are sufficiently different (i.e., if the molecules are very different; for example, A polar, B nonpolar), then ΔW will be large enough to overcome the entropic drive to disorder resulting in a low solubility (immiscibility) or phase separation. The immiscibility of water and hydrocarbons and the “like-dissolves-like” rule, previously discussed in Sections 6.7 and 6.8, are examples of this phenomenon. Furthermore, since $\Delta W \propto n$, larger particles or polymers of higher molecular weight are more likely to phase separate than smaller particles or molecules, and indeed the vast majority of polymers are immiscible with each other.

Third, Eq. (10.3) shows that the value of $\Delta W/n$ for molecules of type A coming into contact in medium B is the same as for the inverse case of molecules of type B associating in medium A. This reciprocity property was previously noted for the specific case of van der Waals forces (Section 6.7).

Finally, Eqs (10.3) and (10.5) clearly show that the interaction of two solute molecules A in a solvent medium B is intimately coupled to the strength of the solvent-solvent interaction. Thus, the attraction between two particles in water or between two protein molecules in a lipid bilayer is not independent of the surrounding water-water or lipid-lipid interactions.

While the preceding semiquantitative criteria have broad applicability, there are two very important exceptions: First, for the Coulomb interaction between charged atoms or ions, since the sign of ΔW is reversed, the dispersed state (Figure 10.1a) is the favored

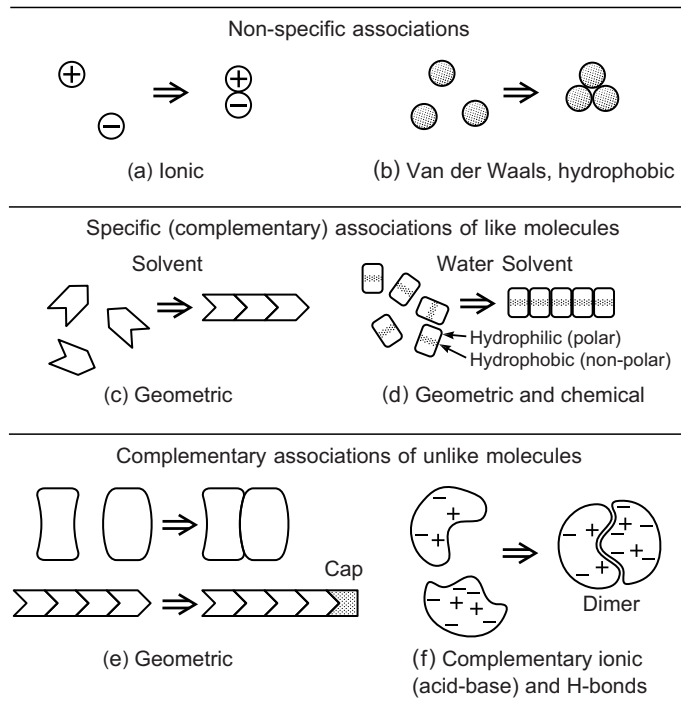


FIGURE 10.3 Nonspecific (a, b) and specific interactions (c to f) between molecules. Specific interactions can lead to orientationally specific associations of like molecules or to preferential association of unlike molecules. Such effects can be due to molecular geometry (molecular shape or “topology”) and/or chemical effects (specific bonds), and they are particularly common in the interactions of biological molecules as discussed in Chapters 21 and 22.

one. Thus, in ionic crystals (e.g., Na^+Cl^-), the cations and anions are nearest neighbors in the lattice. However, once oppositely charged ion pairs associate to form electroneutral dipoles, these can then be treated as units that do obey the preceding relations.

There are certain classes of molecules and interactions that do not readily fall into this simple pattern because the strength of the bond between two different molecules cannot be expressed simply in terms of $W_{AB} = -\mathbf{A}\mathbf{B}$. Such interactions are called *specific* interactions and, in the case of biological molecules, *complementary* or *lock-and-key* interactions (Chapter 21). Figure 10.3 shows examples of how such specific interactions arise. They can result from the complementary shapes of molecules, in which like molecules cannot fit together, whereas unlike molecules can; or they can be the result of an inherently specific interatomic bond, such as the hydrogen-bond (Figure 8.2). In the latter

case, a molecule such as acetone, $\text{CH}_3\text{C}(=\text{O})\text{CH}_3$, cannot form H-bonds with another

similar molecule, but it can do so with water via its C=O group, and for this reason, acetone is miscible with water. Such strongly hydrophilic groups (see Table 8.2) repel each other in water due to their strong binding to water, and their specific interactions cannot be described in terms of the simple equations presented above.

10.2 Two Like Surfaces Coming Together in a Medium: Surface and Interfacial Energy

The previous approach may be readily applied to the interaction of two macroscopic surfaces in a liquid. Let us start with two flat surfaces of A, each of unit area, in a liquid B. We may equate ΔW of Eq. (10.6) with the (negative) free energy change of bringing these two surfaces into adhesive contact in the medium. This energy, or work, is defined as twice the *interfacial energy* γ_{AB} of the A-B interface, which is positive by convention. Thus,

$$\Delta W = -2\gamma_{AB} \quad \text{or} \quad \gamma_{AB} = -\frac{1}{2}\Delta W = \frac{1}{2}n(\mathbf{A} - \mathbf{B})^2. \quad (10.8)$$

The factor 2 arises because by bringing these two surfaces into contact, the two initially separate media of A have merged into one, so we have effectively eliminated *two* unit areas of the A-B interface. Now, let there be n bonds per unit area. In Eq. (10.6) nW_{AB} is therefore the energy change of bringing unit area of A into contact with unit area of B *in a vacuum*. This is known as the *adhesion energy* or *work of adhesion* per unit area of the A-B interface. Likewise, nW_{AA} is the (negative) energy change of bringing unit areas of A into contact in a vacuum, known as the *cohesion energy* or *work of cohesion*. Note that two unit areas of A are eliminated in this process. By convention, the cohesion energy is related to the (positive) *surface energy* γ_A by $nW_{AA} = -2\gamma_A$ —that is,

$$\gamma_A = -\frac{1}{2}nW_{AA} = \frac{1}{2}nA^2, \quad (10.9a)$$

or simply,

$$\gamma = -\frac{1}{2}W \quad \text{per unit area,} \quad (10.9b)$$

and similarly for γ_B . Note that the *interfacial energy* $\gamma_{AB} = \frac{1}{2}n(\mathbf{A} - \mathbf{B})^2$ of the A-B interface is very different, both phenomenologically and quantitatively, from the adhesion energy $W_{AB} = -n\mathbf{AB}$ of surfaces A and B.¹ These different surface energies will be discussed in more detail in Chapter 17; for the moment, we simply note that for two surfaces Eq. (10.6) may be expressed in the form²

$$\gamma_{AB} = \gamma_A + \gamma_B - |W_{AB}| \quad \text{per unit area.} \quad (10.10)$$

¹For example, the *interfacial energy* of two similar surfaces in contact ($\mathbf{A} = \mathbf{B}$) is zero even as their *surface energy* is not.

²In some conventions the sign of W for the work of adhesion or cohesion is positive (i.e., $W > 0$) because the reference state of zero energy is taken as the contact state ($D = 0$). This is in contrast to the negative values for $W(D)$ and $w(r)$ where, again by convention, the reference states are the fully separated states at $D = \infty$ or $r = \infty$.

This important thermodynamic relation is valid for both solid and liquid interfaces. It gives the free energy (always negative³) of bringing unit areas of surfaces A into contact in liquid B, and vice versa, since $\gamma_{AB} = \gamma_{BA}$.

All the preceding equations belong to an important class of expressions known as *combining relations* or *combining laws*. They are extremely useful for deriving relationships between various energy terms in a complex system, and are often used for obtaining approximate values for parameters that cannot be easily measured. For example, if we return to Eq. (10.6), we may also write it as

$$\Delta W = n(W_{AA} + W_{BB} - 2\sqrt{W_{AA}W_{BB}}) \quad (10.11)$$

so that Eq. (10.10) becomes

$$\gamma_{AB} = \gamma_A + \gamma_B - 2\sqrt{\gamma_A\gamma_B} = (\sqrt{\gamma_A} - \sqrt{\gamma_B})^2, \quad (10.12)$$

a useful expression that is often used to estimate the interfacial energy γ_{AB} solely from the surface energies or surface tensions of the pure liquids, γ_A and γ_B , in the absence of any data on the energy of adhesion W_{AB} . We shall encounter these and other combining relations again later.

10.3 The Association of Unlike Molecules, Particles, or Surfaces in a Third Medium

Let us now proceed from two-component to three-component systems, starting with a consideration of the mixture shown in Figure 10.4. For two unlike molecules or particles A and B coming together in the solvent medium composed of molecules of type C (Figure 10.4 a → b), we find that the process can be split up into four elementary steps as follows:

$$\Delta W = W_{ass} - W_{disp} \propto -AB - C^2 + AC + BC = -(A - C)(B - C). \quad (10.13)$$

This is a very interesting result because it shows that the energy of association can now be positive or negative. If positive, the particles effectively repel each other and therefore remain dispersed in medium C.

It is instructive to consider how an effective repulsion has arisen from interaction potentials that are all purely attractive to begin with. The phenomenon may be thought of as *Archimedes' principle* being applied to intermolecular forces. In the case of gravitational forces we all know that iron sinks while wood rises in water. Thus, wood is effectively experiencing a repulsion from the earth when in water. This is because it is lighter than water, and if it were to descend, it would have to displace an equal volume of water and therefore drive it upward to replace the space previously occupied by the wood. Since water is denser and thus more attracted to the earth than wood, the whole process would be

³Actually, the interfacial energy can be positive, which implies that two surfaces or molecules of A repel each other in medium B, and vice versa. The separation of molecules A will continue until no aggregates remain—that is, until the AB interface disappears. Thus, if there is an interface, ΔW must be negative (and γ_{AB} must be positive).

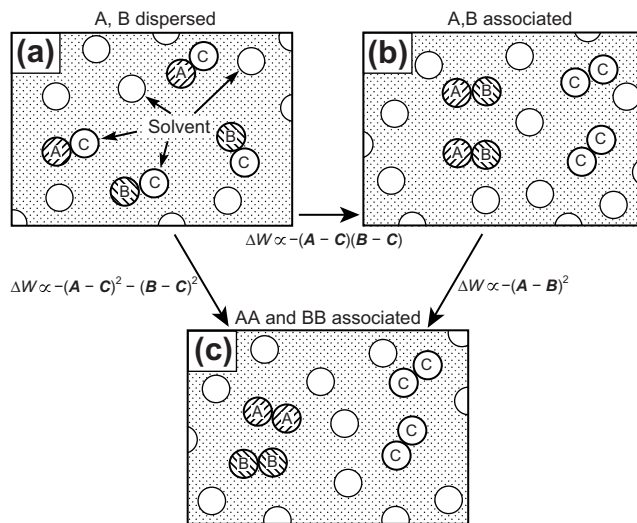


FIGURE 10.4 (a) and (b) Two unlike molecules or particles **A** and **B** may attract or repel each other in a third medium **C**. Repulsion will occur (ΔW positive) if the properties of **C** are intermediate between those of **A** and **B**—for example, for gravitational forces, if the density of **C** (e.g., water) is between that of **A** (e.g., iron) and **B** (e.g., wood). In such cases the dispersed state (a) is energetically favored. (c) The associated state of like molecules has a lower energy than either (a) or (b).

energetically unfavorable—in other words, the energy lost in water going up is not recovered by the energy gained in wood coming down. This displacement principle applies to all interactions in a medium, including intermolecular interactions (cf. Problem 10.4).

Equation (10.13) tells us that if **C** is intermediate between **A** and **B**, two particles (or surfaces) will repel each other, an effect that was previously noted for van der Waals forces (Section 6.7) where the operative properties of media **A**, **B**, and **C** are their dielectric constants and refractive indices. However, the association or dissociation of **A** and **B** in medium **C** is not the end of the story. As shown in Figure 10.4, whatever the relation between **A**, **B** and **C**, the most favored final state will be that of particles **A** associating with particles **A**, **B** with **B**, and **C** with **C** (Figure 10.4c).

This procedure may be extended to mixtures with more species. We may therefore generalize our earlier conclusion: *there is always an effective attraction between like molecules or particles in a multicomponent mixture* (again with the proviso that the interactions are not dominated by Coulombic or H-bonding forces). And in addition, *unlike particles may attract or repel each other in a solvent*.

10.4 Particle-Surface and Particle-Interface Interactions

The preceding analysis can be extended to the case of a particle **C** near an interface dividing two immiscible liquid media **A** and **B** (Figure 10.5). Four situations may arise:

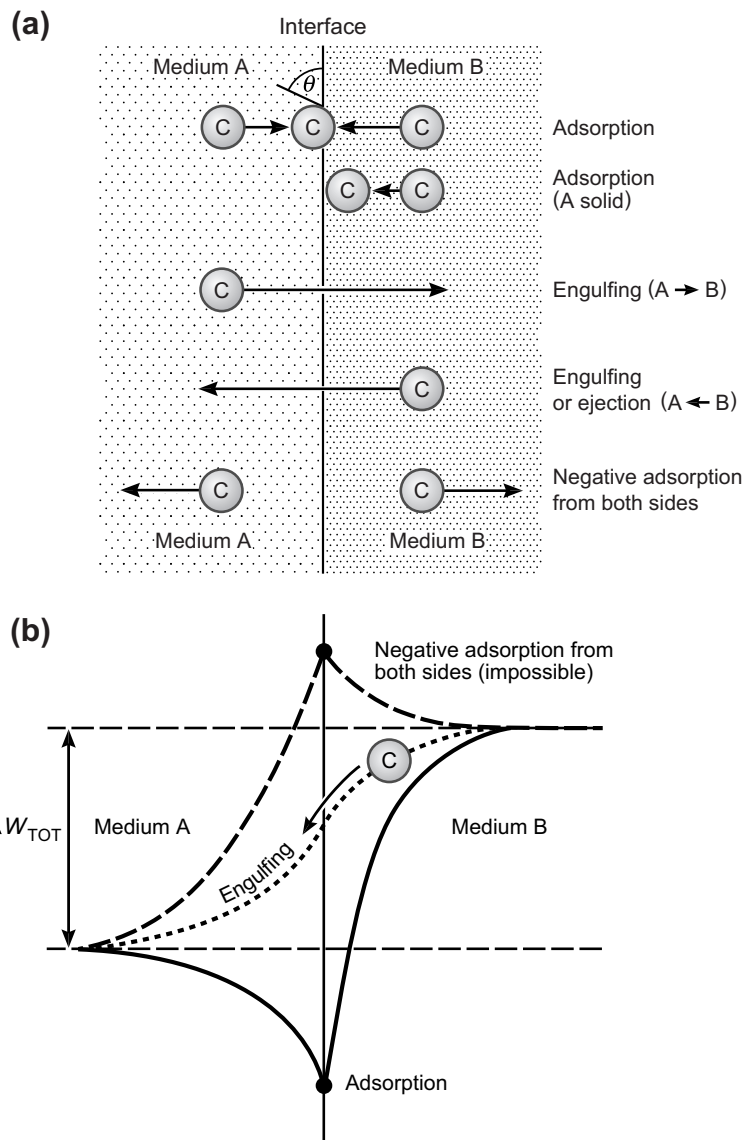


FIGURE 10.5 (a) Different possible modes of interaction of a particle C with a liquid-liquid interface. (b) Corresponding schematic energy versus distance profiles (assumed monotonic) for $\Delta W_{\text{tot}} < 0$. In the case of adsorbed particles, their configuration at the interface depends on their shape and whether the two media A and B are liquid or solid. If both media are liquid and the particle is spherical, it will pass through the interface or subtend a finite contact angle θ at the interface. If medium B is solid, particle C could adsorb on, but not penetrate into or pass through, the interface.

- *Adsorption*: The particle is attracted to the interface from either side.
- *Desorption*: The particle is repelled from the interface on either side of it (also known as “negative adsorption”).
- *Engulfing*: The particle is (1) attracted from one side (left or right) but (2) repelled from the other side (right or left).

Applying Eq. (10.13) we may write for the energy change of a particle coming up to the interface shown in Figure 10.5:

$$\text{from the left: } \vec{\Delta W} \propto -(\mathbf{C} - \mathbf{A})(\mathbf{B} - \mathbf{A}), \quad (10.14)$$

$$\text{from the right: } \vec{\Delta W} \propto -(\mathbf{C} - \mathbf{B})(\mathbf{A} - \mathbf{B}). \quad (10.15)$$

The preceding equations predict the following possibilities, illustrated in Figure 10.5a: First, if the particle’s properties \mathbf{C} are intermediate between those of media A and B (i.e., if $\mathbf{A} > \mathbf{C} > \mathbf{B}$ or $\mathbf{A} < \mathbf{C} < \mathbf{B}$), both $\vec{\Delta W}$ and $\vec{\Delta W}$ are negative. The particle will therefore be attracted to the interface from either side, leading to adsorption at the interface. The adsorption of amphiphilic molecules at hydrocarbon-water interfaces is an example of such a phenomenon. Amphiphilic molecules such as detergents and surfactants (derived from the words ‘surface-active’) are partly hydrophilic and partly hydrophobic and so have properties intermediate between the two liquids. Second, if $\mathbf{A} > \mathbf{B} > \mathbf{C}$ or $\mathbf{A} < \mathbf{B} < \mathbf{C}$ (\mathbf{B} intermediate), $\vec{\Delta W}$ will be negative, but $\vec{\Delta W}$ will be positive. The particle will therefore be attracted to the interface from the left but repelled from the right (engulfing by medium B). Finally, if $\mathbf{B} > \mathbf{A} > \mathbf{C}$ or $\mathbf{B} < \mathbf{A} < \mathbf{C}$ (\mathbf{A} intermediate), $\vec{\Delta W}$ will be positive, but $\vec{\Delta W}$ will be negative, and the particle will now be attracted from the right but repelled from the left (reverse engulfing or ejection from medium B). Since these six combinations exhaust all the possibilities, we see that repulsion from both sides of an interface (i.e., negative adsorption from both sides) cannot occur and that either adsorption or engulfing will be the rule. It is for this reason that surfaces are so prone to adsorbing molecules or particles from vapor or solution.

In the following two sections we discuss the cases of engulfing and adsorption in turn.

10.5 Engulfing and Ejection

The special case of engulfing or ejection involves the complete transfer of a particle from the interior of one bulk medium into another. The total energy of transfer $\vec{\Delta W}_{\text{tot}}$ from medium A into medium B can be determined by combining Eqs (10.14) and (10.15) to give

$$\begin{aligned} \vec{\Delta W}_{\text{tot}} = \Delta W_{\text{A} \rightarrow \text{B}} &= \vec{\Delta W} - \vec{\Delta W} \propto -(\mathbf{C} - \mathbf{A})(\mathbf{B} - \mathbf{A}) + (\mathbf{C} - \mathbf{B})(\mathbf{A} - \mathbf{B}) \\ &\propto (\mathbf{B} - \mathbf{C})^2 - (\mathbf{A} - \mathbf{C})^2 \end{aligned} \quad (10.16a)$$

$$\propto \gamma_{\text{BC}} - \gamma_{\text{AC}} \quad (10.16b)$$

where γ_{BC} and γ_{AC} are the interfacial energies of the respective particle-media interfaces. Thus, a particle will always move into a medium where its interfacial energy is lowest ($\Delta\vec{W}_{tot} < 0$), which in the case of engulfing by medium B implies that $\gamma_{BC} < \gamma_{AC}$. For example, for a spherical particle of surface area $4\pi r^2$, its change in energy on going from bulk medium B to bulk medium A is

$$\Delta W_{A \rightarrow B} = \text{Surface area} \times (\gamma_{BC} - \gamma_{AC}) = 4\pi r^2 (\gamma_{BC} - \gamma_{AC}). \quad (10.17)$$

This energy determines the partitioning of particles and molecules between different phases according to the Boltzmann factor $e^{-\Delta W/kT}$, where the free energy of transfer ΔW can be seen to be the same as the change in self-energy μ_0^i of the particle or molecule, discussed in Chapter 2. Since ΔW is proportional to the area of a molecule or particle, the partitioning becomes increasingly more pronounced for larger molecules—for example, polymers of higher MW—even when the *type* of interaction (e.g., van der Waals) remains the same.

The preceding two equations for the energy of engulfing or transfer should not be taken to imply that engulfing will occur whenever γ_{BC} and γ_{AC} are different, which they usually are. We also have to exclude the possibility of adsorption and desorption, and when this is done (see Worked Example below), one finds that the necessary condition for engulfing may be expressed in terms of the interfacial energies as

$$\gamma_{BC} + \gamma_{AC} > \gamma_{AB}. \quad (10.18)$$

Worked Example 10.2

Question: Obtain Eq. (10.18) from first principles—that is, from a consideration of the conditions necessary for engulfing based only on the elementary pair potentials **AB**, **AC**, and **BC**.

Answer: From the discussion following Eqs. (10.14) and (10.15), it is clear that for engulfing to occur from either side of the interface, $\Delta\vec{W}_A$ and $\Delta\vec{W}_B$ must have opposite signs. This means that $\Delta\vec{W}_A \times \Delta\vec{W}_B < 0$. In terms of the elementary potentials, this may be expressed as $(C - A)(B - A) \times (C - B)(A - B) < 0$, and since $(B - A)(A - B) = -(A - B)^2$ must be negative, this equation immediately simplifies to $(C - A)(C - B) > 0$. In terms of the elementary interactions as defined by Eq. (10.8), Eq. (10.18) is equivalent to $\frac{1}{2}n(B - C)^2 + \frac{1}{2}n(A - C)^2 > \frac{1}{2}n(A - B)^2$. When this equation is expanded, the $\frac{1}{2}nA^2$ and $\frac{1}{2}nB^2$ terms cancel and one is left with $(C - A)(C - B) > 0$, which is the necessary condition for engulfing.

10.6 Adsorbed Surface Films: Wetting and Nonwetting

The above examples and Figure 10.5 apply only to isolated particles or molecules of C; in other words, they apply only to dilute concentrations of C below its solubility limit in media A and B. At higher concentrations the molecules or particles of C may associate into a separate phase either in media A or B, or at the A–B interface. Which of these

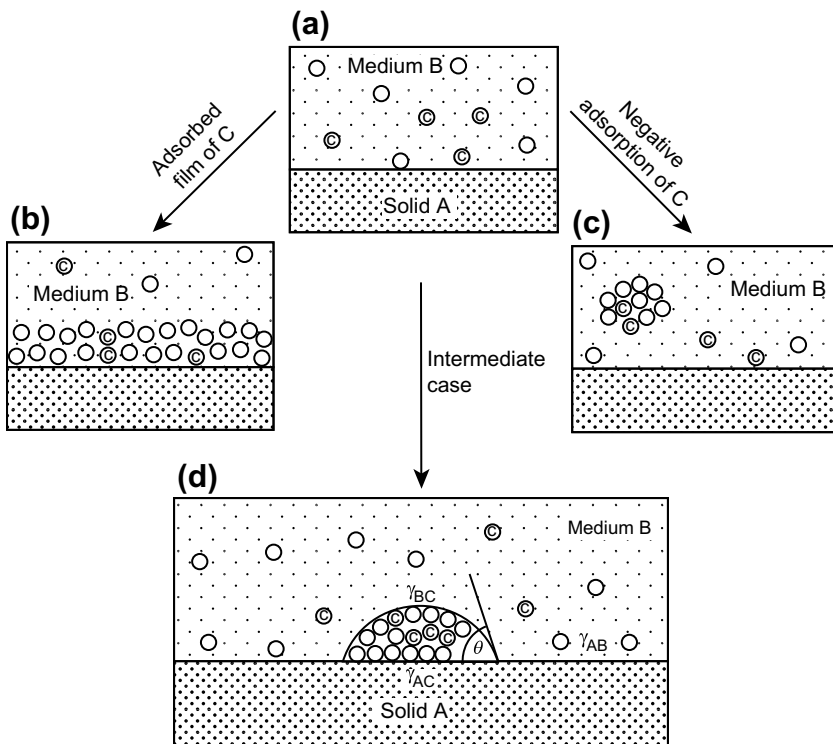


FIGURE 10.6 (a) Low concentration of solute molecules **C** in medium **B** (i.e., below saturation). (b) *Wetting film*: an adsorbed film of **C** develops and grows in thickness as the concentration of **C** in **B** approaches saturation. This corresponds to $\cos \theta > 1$ in Eq. (10.19). (c) *Unwetting*: resulting from repulsion between **C** and **A** in medium **B** above saturation. This corresponds to $\cos \theta < -1$ in Eq. (10.19). (d) *Partial wetting*: intermediate case between the two above, corresponds to $1 > \cos \theta > -1$.

happens depends on the relative magnitudes of **A**, **B**, and **C**. In this final section we shall consider the factors favoring the formation of thick adsorbed liquid films on a solid surface (the case of a liquid film or droplet adsorbed at a liquid-liquid or solid-liquid interface is further considered in Chapter 17).

In Figure 10.6a we have, initially, a solid surface of **A** in contact with a binary liquid mixture of solute molecules **C** in solvent **B**. Again there are three possibilities:

- For **C** intermediate between **A** and **B**, molecules **C** will be attracted to **A**, while molecules **B** will be repelled from it, and an adsorbed monolayer or film of **C** will be energetically favorable (Figure 10.6b). In this case, **C** is said to completely *wet* the surface.
- For **B** intermediate between **A** and **C** (Figure 10.6c), the roles of **B** and **C** are reversed, favoring adsorption of **B** and negative adsorption of **C**. In this case, **C** does not adsorb or wet the surface (whereas **B** will wet the surface if **C** were the solvent). This is known as *nonwetting*, *unwetting* or *dewetting*.

- Finally, when A is intermediate, both molecules B and C are attracted to the solid surface. Under such circumstances no uniformly adsorbed film of B or C will form, but different regions of the interface will collect macroscopic droplets of the B or C phase (Figure 10.6d). This is known as *partial-wetting* or *incomplete wetting*.

It is left as an exercise for the interested reader (see problem 10.5) to ascertain that when the total surface energies of the whole system is minimized, the *contact angle* θ formed by these droplets (Figure 10.6d) is given by

$$\cos \theta = (\mathbf{B} + \mathbf{C} - 2\mathbf{A}) / (\mathbf{B} - \mathbf{C}), \quad (10.19)$$

which leads to values of $\cos \theta$ between 1 and -1 (θ between 0° and 180°) only when A is intermediate between B and C . Equation (10.19) may also be written in the forms

$$\gamma_{AC} + \gamma_{BC} \cos \theta = \gamma_{AB} \quad (\text{Young equation}) \quad (10.20)$$

$$\gamma_{BC}(1 + \cos \theta) = \Delta W_{ABC} \quad (\text{Young – Dupré equation}), \quad (10.21)$$

where ΔW_{ABC} is the adhesion energy per unit areas of surfaces A and C adhering in medium B . These important fundamental equations will be derived using a different approach and discussed further in Chapter 17.

The purpose of the phenomenological discussion of this chapter is to illustrate how a few basic notions concerning two-particle interaction energies can be applied to progressively more complex situations, and vice versa—that is, how fairly complex situations can arise from, and be understood in terms of, the simplest possible pair potential, Eq. (10.2), as was illustrated in the Worked Example 10.2. However, this type of nonspecific approach, while conceptually useful, has its limits in that it does not take into account the way interaction energies vary with distance. Two particles or surfaces may have an adhesive energy minimum at contact, but if the force law is not monotonic—it may be repulsive before it becomes attractive closer in—the particles will remain separated—that is, they effectively repel each other. In addition, as we have seen, certain important interactions do not follow these simple rules. Only a quantitative analysis in terms of the magnitudes of the operative forces and their distance dependence can provide a full understanding of interparticle and interfacial phenomena.

PROBLEMS AND DISCUSSION TOPICS

- 10.1** Figures 10.1a and b show that in two dimensions the associated state (b) is energetically more favorable than the dispersed state (a) by a factor of $-9(\mathbf{A} - \mathbf{B})^2$. Calculate this energy in the case of three dimensions—that is, for a spherical cluster of 12 molecules surrounding the central molecule. [Answer: $\Delta W = -22(\mathbf{A} - \mathbf{B})^2$.]
- 10.2** In the examples of Figure 10.1 a–c, all the molecules or particles have the same radius, r or a . In Sections 5.1 and 6.1, it was shown that the polarizability of

a molecule is proportional to its volume—that is, to r^3 , which appears in the numerator of the London equation for the van der Waals pair potential. Show that for the more realistic case where $W = -\mathbf{AB}/(r_A + r_B)^6$ and where $\mathbf{A} \propto r_A^3$ and $\mathbf{B} \propto r_B^3$, the associated state is still the energetically favored one.

- 10.3** Show that for the geometries of Figures 10.1 and 10.2, $n \approx R/a$, which leads to the following important approximate relation:

$$\text{Adhesion or binding energy of particles} \approx \text{Binding energy of atoms} \times \frac{\text{Radius of particles}}{\text{Radius of atoms}}. \quad (10.23)$$

For which systems or conditions does the above relation not hold?

- 10.4*** An incompressible spherical particle has the same density and optical properties as water at 30°C, and all its properties may be assumed to be independent of temperature and pressure. It is suspended in a vertical column of water across which there is a uniform temperature gradient. In one case the top is maintained at 50°C, the bottom at 10°C. In another, the temperatures are reversed. In which directions do the following four forces act on the particle in the above two cases: gravitational (buoyancy) forces, van der Waals forces, forces due to viscous flow, and the forces due to Brownian motion—that is, osmotic pressure, thermal pressure or the molecular collisions of the water molecules. If your answer is “zero force,” state whether the “equilibrium” is stable or unstable—that is, whether the particle will return to the center if it is displaced from it by a small amount up or down, or whether it will continue to move away from the center.
- 10.5*** Derive Eq. (10.19) by finding the condition that minimizes the total surface energy of the system. [Hint: Consider all the surface energies of a truncated sphere of constant volume on a surface, including the curved and flat liquid areas, A_c and A_f , and the flat area A_s of the solid surface. You should find that the minimum energy condition is $dA_c/dA_f = \cos \theta$, which leads to Eq. (10.19).]
- 10.6** Two immiscible liquids B and C are in contact with a solid surface A, where there is a finite contact angle θ between the B–C interface and A, as shown in Figure 10.6d. Would you expect θ to change as one approaches the critical point of the B–C system, and if so how would this be seen visually?
- 10.7** What is the relative surface density of B and C molecules at the solid surface of A in Figure 10.6(a) if B and C are miscible and present in equal amounts (a 50/50 mixture)? Under what conditions will the densities at the surface be the same as in the bulk?

Contrasts between Intermolecular, Interparticle, and Intersurface Forces

11.1 Short-Range and Long-Range Effects of a Force: Qualitative Differences in the Interactions of Particles and Small Molecules

We are told that when an apple fell on Newton's head, it set in motion a thought process that eventually led Newton to formulate the law of gravity. The conceptual breakthrough in this discovery was the recognition that the force that causes apples to fall to the ground is the same force that holds the moon in a stable orbit around the Earth.

On Earth, gravity manifests itself in many different ways: in determining the height of the atmosphere, the capillary rise of liquids, and the behavior of waves and ripples. In biology it decrees that animals that live in the sea (where the effect of gravity is almost negligible) can be larger than the largest possible land animal; that heavy land animals such as elephants must have short, thick legs, while a man or a spider can have proportionately long, thin legs; that larger birds must have progressively larger wings (e.g., eagles and storks), while smaller birds, flies, and bees can have relatively small light wings; that only small animals can carry many times their own weight (e.g., ants); and much else (Thompson, 1968). But beyond the immediate vicinity of Earth's surface and out to the outer reaches of space, this same force now governs the orbits of planets, the shapes of nebulae, black holes and galaxies, the rate of expansion of the universe, and, ultimately, its age. The first group of phenomena—those occurring locally on Earth's surface—may be thought of as the *short-range* effects of the gravitational force, while the second and very different types of phenomena occurring on a cosmological scale may be thought of as the *long-range* effects of gravity.

Intermolecular forces are no less versatile in the way the same force can have very different effects at short and long range, though here "short range" usually means at or very close to molecular contact ($<1\text{ nm}$), while "long-range" forces are rarely important beyond 100 nm ($0.1\text{ }\mu\text{m}$). In Part I we saw that the properties of gases and the cohesive strengths of condensed phases are determined mainly by the interaction energies of molecules in contact $w(\sigma)$ —that is, molecules interacting with their immediate neighbors. For example, the van der Waals pair energy of two neighboring molecules is at least 64 times stronger than that between the next-nearest neighbors [$1/\sigma^6$ compared to $1/(2\sigma)^6$]. Only the Coulomb interaction is effectively long ranged in that the energy decays

slowly, as $1/r$, and remains strong at large distances. However, in a polar medium such as water the strength of the Coulomb interaction is much reduced due to the high dielectric constant and the requirement of electroneutrality, which leads to dipole formation and ionic screening effects (Chapter 14).

We may therefore conclude that the properties of solids and liquids are determined mainly by the molecular binding forces—that is, by the strength of the interactions at or very near molecular contact—with the long-range nature of the interactions, such as the exact distance dependence of the force laws, playing only a minor role.

A very different situation arises when we consider the interactions of macroscopic particles or surfaces, for now when all the pair potentials between the molecules in each body is summed, we shall find (1) that the net interaction energy is proportional to the size (e.g., radius) of the particles, so that the energy can be very much larger than kT even at separations of 100 nm or more, (2) that the energy and force decay much more slowly with the *absolute* separation distance, but much faster when compared to the *size* (e.g., the diameter) of the particles, and (3) the kinetics of macromolecular and interparticle interaction can be very different—usually much slower—than those between small atoms and molecules.¹ All these characteristics can make the interactions between macromolecules, nanoparticles, colloidal particles, and macroscopic bodies both quantitatively and qualitatively different from those between small molecules even though the same basic force may be operating in each case.

Furthermore, if the force law is not monotonic (not purely attractive or repulsive), then all manner of behavior may arise depending on the specific form of the long-range distance dependence of the interaction. This is illustrated in Figure 11.1. For example, consider the purely attractive interaction of Figure 11.1a. If both small molecules and particles experience the same type of interaction, both will be attracted to each other, and the thermodynamic properties of an assembly of molecules in the gas or condensed phase will be determined by the depth of the potential well at contact, as will the adhesion energy of two particles. However, for the energy law in Figure 11.1b, two small molecules will still attract each other, since the energy barrier is negligibly small compared to kT , but two macroscopic particles will effectively repel each other, since the energy barrier, which is proportional to their size, is now too high to surmount. Under such circumstances particles dissolved in a medium will remain dispersed even though the ultimate *thermodynamic equilibrium state* is the aggregated state.

We thus encounter another important difference between molecular and particle interactions—namely, that particles can be (and often are) trapped in some *kinetic* or *metastable* state if there is a sufficiently high repulsive energy barrier that prevents them from accessing all parts of their interaction potential over some reasonable time period. To put this in terms of the strengths of interactions, whether attractive or repulsive: *strong*

¹In general the stronger the interaction (adhesion or binding energy), the *longer* it takes a system of macromolecules or particles to equilibrate. This apparently counterintuitive effect arises because strong binding does not easily allow particles to rearrange into their lowest-energy configuration.

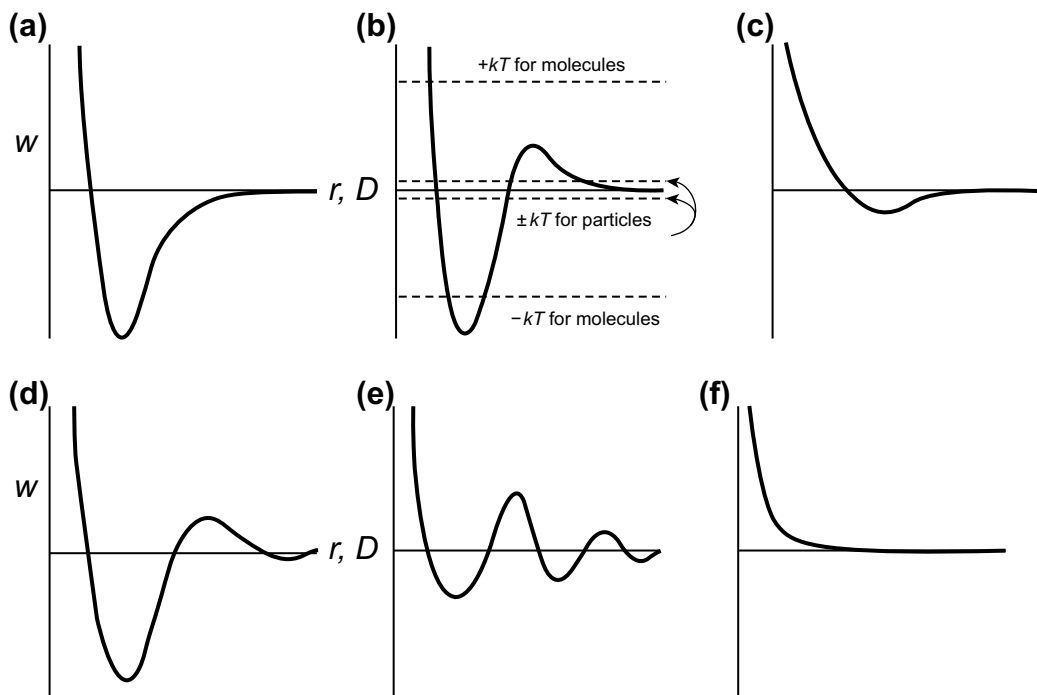


FIGURE 11.1 Typical interaction potentials encountered between molecules and macroscopic particles in a medium. (a) This potential is typical of vacuum interactions but is also common in liquids. Both molecules and particles attract each other. (b) Molecules attract each other; particles effectively repel each other. (c) Weak minimum. Molecules effectively repel, particles attract. (d) Molecules attract strongly, particles attract weakly in the outer minimum. (e) Molecules attract weakly, particles attract strongly. (f) Molecules repel, particles repel.

forces usually result in *slow* kinetics.^{Footnote 1} This sounds contradictory, given that one might expect a faster response from a larger driving force. However, we will encounter many situations where this is not the case, including colloidal aggregation (cf. Problem 7.3) and so-called “jamming” processes (Section 15.6).

Figure 11.1 illustrates some other types of commonly occurring intermolecular and intersurface potential functions and the different effects they can have on molecule-molecule and particle-particle interactions. In the following chapters we shall see how such interaction potentials actually arise and the effects they produce in different systems.



Worked Example 11.1

Question: Consider a 10% by weight dispersion of glass particles of radius $a = 100 \text{ nm}$ in water at room temperature interacting via a potential as shown in Figure 11.1b. Estimate what the energy barrier would have to be (in units of kT) for the particles to remain dispersed over a period of one day.

Answer: The mean Brownian velocity, v , per particle will be given by $\frac{1}{2}mv^2 \approx \frac{1}{2}kT$, where $m = 1.3 \times 10^{-17}$ kg is the particle mass (assuming a density of 3×10^3 kg m $^{-3}$). Thus, we obtain $v = 0.018$ m s $^{-1}$. The number of particles per unit volume is 8×10^{18} m $^{-3}$, so that their mean separation is about 5×10^{-7} m (500 nm). Thus the time between collisions will be about $5 \times 10^{-7} / 0.018 = 2.8 \times 10^{-5}$ s, so that the number of collisions per day will be $60 \times 60 \times 24 / 2.8 \times 10^{-5} \approx 3 \times 10^9$. We therefore require the condition that the probability of two colliding particles overcoming their energy barrier ΔW should be less than $1/(3 \times 10^9) = 3.2 \times 10^{-10}$. Putting $3.2 \times 10^{-10} = e^{-\Delta W/kT}$ we obtain $\Delta W = 22 kT$. Thus, the energy barrier should be in excess of about 25 kT to ensure kinetic stability—that is, that most of the particles remain dispersed over a 24-hour period. (Note: The preceding approach is known as the “ballistic” approach; a more rigorous calculation that includes the viscous drag on particle diffusion shows that the collision rate would be significantly lower and that an energy barrier of only 16 kT is needed to keep the system stable.)

There is yet another important difference in the interactions of particles as opposed to small molecules. This concerns the repulsive or steric forces that stabilize the attraction. Between atoms and molecules this is usually expressed in terms of a repulsive contribution to the pair potential—for example, a function of the form $w(r) = +(\sigma/r)^n$ (cf. Section 7.2). However, between large particles, the stabilizing repulsive force comes from the elastic (or plastic) deformations of the particles themselves, which depends on their bulk elastic properties and that cannot be readily described in terms of a potential function. These aspects are described in detail in Chapter 17.

Finally, the interactions of “soft particles”—for example, those composed of surfactant, polymer, and certain biological molecules—are particularly subtle due to the interdependence of the intraparticle and interparticle forces. The sizes and shapes of such “self-assembling” molecular aggregates in water, for example, are regulated by the short-range *intraparticle* interactions between the molecules, which are sensitive to electrolyte type and concentration, pH, temperature, and so on. On the other hand, the long-range *interparticle* interactions between these aggregates—those that determine whether they will attract or repel each other—are sensitive to the same variables. Thus, different parts of the intermolecular interaction potential govern very different properties in these systems. The interdependence of short-range and long-range forces and, consequently, of intra-particle and interparticle forces is particularly important for understanding the structure and interactions of micelles, vesicles, microemulsion droplets, copolymers, biological membranes, and other biological structures, discussed in Part III.

11.2 Interaction Potentials between Macroscopic Bodies

In this section we shall relate the pair potentials between small molecules to those between molecules and surfaces, and between large particles of different geometries. At some point we shall also investigate the meaning of “small” and “large.”

Molecule-Surface Interaction

Let us once again assume that the pair potential between two atoms or small molecules is purely attractive and of the form $w(r) = -C/r^n$. Then, with the further assumption of *additivity*, the net interaction energy of a molecule and the planar surface of a solid made up of like molecules (Figure 11.2a) will be the sum of its interactions with all the molecules in the body. For molecules in a circular ring of cross-sectional area $dxdz$ and radius x , the ring volume is $2\pi x dxdz$, and the number of molecules in the ring will be $2\pi\rho x dxdz$, where ρ is the number density of molecules

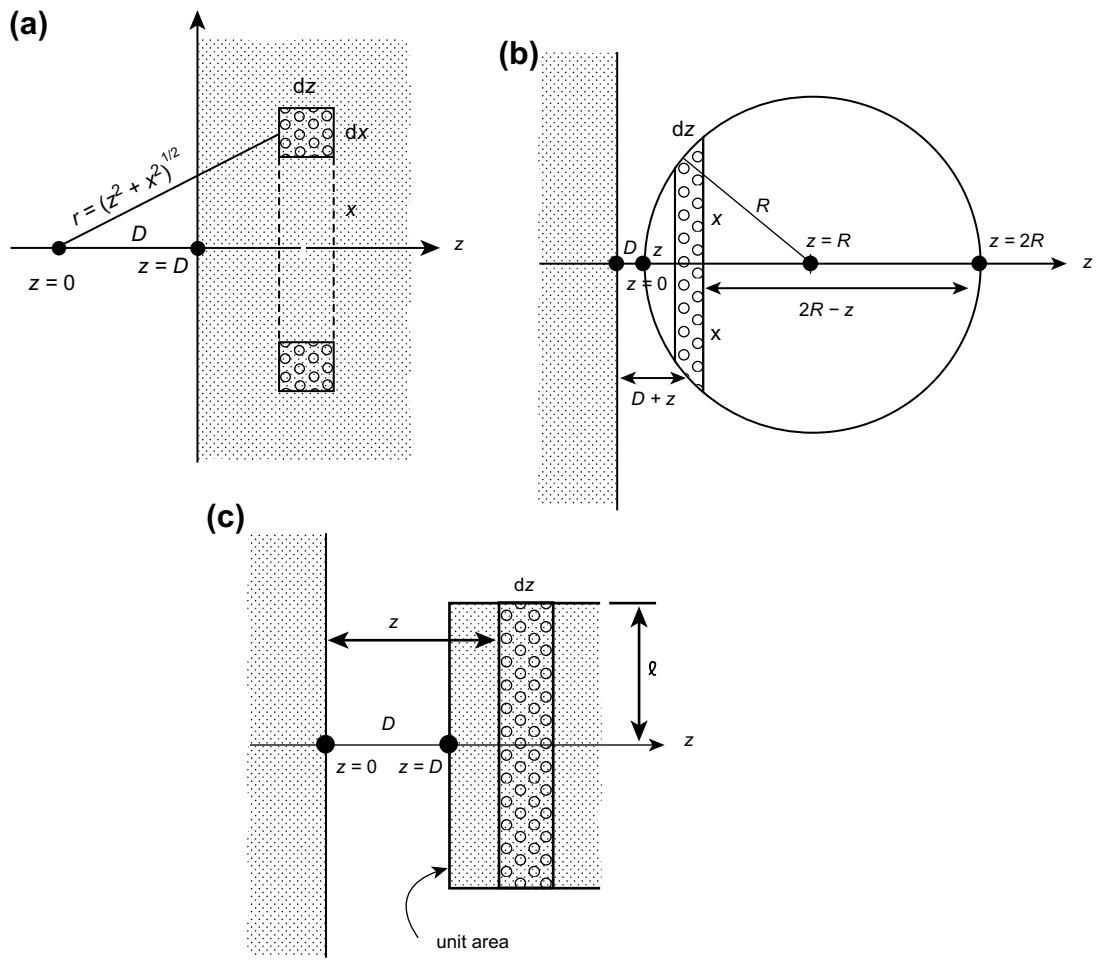


FIGURE 11.2 Methods of summing (integrating) the interaction energies between molecules in condensed phases to obtain the interaction energies between macroscopic bodies. **(a)** Molecule near a flat surface or "wall." **(b)** Spherical particle near a wall ($R \gg D$). **(c)** Two planar surfaces ($l \gg D$).

in the solid. The net interaction energy for a molecule at a distance D away from the surface will therefore be

$$\begin{aligned} w(D) &= -2\pi C\rho \int_{z=D}^{z=\infty} dz \int_{x=0}^{x=\infty} \frac{x dx}{(z^2 + x^2)^{n/2}} = -\frac{2\pi C\rho}{(n-2)} \int_D^\infty \frac{dz}{z^{n-2}} \\ &= -2\pi C\rho/(n-2)(n-3)D^{n-3} \quad \text{for } n > 3, \end{aligned} \quad (11.1)$$

which for $n = 6$ (van der Waals forces) becomes

$$w(D) = -\pi C\rho/6D^3. \quad (11.2)$$

The corresponding force, $F(D) = -dw(D)/dD = -\pi C\rho/2D^4$, could, of course, have been derived in a similar way by summing (integrating) all the pair forces resolved along the z -axis.

Sphere-Surface and Sphere-Sphere Interaction

We can now calculate the interaction energy of a large sphere of radius R and a flat surface (Figure 11.2b). First, from the chord theorem, Eq. (10.4), we know that for the circle: $x^2 = (2R - z)z$. The volume of a thin circular section of area πx^2 and thickness dz is therefore $\pi x^2 dz = \pi(2R - z)z dz$, so that the number of molecules contained within this section is $\pi\rho(2R - z)z dz$, where ρ is the number density of molecules in the sphere. Since all these molecules are at a distance $(D + z)$ from the planar surface, the net interaction energy is, using Eq. (11.1),

$$W(D) = -\frac{2\pi^2 C\rho^2}{(n-2)(n-3)} \int_{z=0}^{z=2R} \frac{(2R-z)z dz}{(D+z)^{n-3}}. \quad (11.3)$$

For $D \ll R$, only small values of z ($z \approx D$) contribute to the integral, and we obtain²

$$W(D) = -\frac{2\pi^2 C\rho^2}{(n-2)(n-3)} \int_0^\infty \frac{2Rz dz}{(D+z)^{n-3}} = -\frac{4\pi^2 C\rho^2 R}{(n-2)(n-3)(n-4)(n-5)D^{n-5}}, \quad (11.4)$$

which for $n = 6$ (van der Waals forces) becomes

$$W(D) = -\pi^2 C\rho^2 R/6D. \quad (11.5)$$

Note that the interaction energy is proportional to the radius of the sphere and that it decays as $1/D$, very much slower than the $1/r^6$ dependence of the intermolecular pair interaction.

For $D \gg R$, we may replace $(D + z)$ in the denominator of Eq. (11.3) by D , and we then obtain

$$W(D) = -\frac{2\pi^2 C\rho^2}{(n-2)(n-3)} \int_0^{2R} \frac{(2R-z)z dz}{D^{n-3}} = -\frac{2\pi C\rho(4\pi R^3 \rho/3)}{(n-2)(n-3)D^{n-3}}. \quad (11.6)$$

²To avoid confusion, we shall use W and D to denote the interaction free energies of macroscopic bodies whose surfaces are at a distance D apart, reserving w and r for the interactions of atoms and molecules.

Since $4\pi R^3 \rho / 3$ is simply the number of molecules in the sphere, the above is essentially the same as Eq. (11.1) for the interaction of a molecule (or small sphere) with a surface.

It is left as an exercise for the interested reader to show that for two spheres of equal radii R whose surfaces are at a small distance D apart ($R \gg D$), their interaction energy is one-half that given by Eq. (11.4) or (11.5), while for two spheres far apart ($D \gg R$) the energy varies as $-1/D^n$, as for two molecules. At intermediate separations ($R \approx D$) the expression for the interaction potential is more complicated but remains analytic (see Section 13.1 for the case of van der Waals forces, and Hamaker, 1937).

Surface-Surface Interactions

We can now calculate the interaction energy of two planar surfaces at a distance D apart. For two infinite surfaces, the result will be infinity, so we have to consider the energy per unit surface area. Let us start with a thin sheet of molecules of unit area and thickness dz at a distance z away from an extended surface of larger area (Figure 11.2c). From Eq. (11.1) the interaction energy of this sheet with the surface is $-2\pi C\rho(\rho dz)/(n-2)(n-3)z^{n-3}$. Thus, for the two surfaces, we have

$$W(D) = -\frac{2\pi C\rho^2}{(n-2)(n-3)} \int_0^\infty \frac{dz}{z^{n-3}} = -\frac{2\pi C\rho^2}{(n-2)(n-3)(n-4)D^{n-4}}, \quad (11.7)$$

which for $n = 6$ becomes

$$W(D) = -\pi C\rho^2 / 12D^2 \quad \text{per unit area.} \quad (11.8)$$

It is important to note that Eqs. (11.7) and (11.8) are for unit area of one surface interacting with an infinite area of another surface. In practice this usually amounts to two unit areas of both surfaces, but it is strictly applicable only when D is small compared to the lateral dimensions of the surfaces.

11.3 Effective Interaction Area of Two Spheres: the Langbein Approximation

When two large spheres or a sphere and a flat surface are close together, one sometimes wants to know what their “effective area” of interaction is. First, we may note that no matter how large a sphere becomes, it *never* approaches the behavior of a flat surface. Its interaction energy will increase linearly with radius R , Eq. (11.4), but the distance dependence of the interaction (energy $\propto -1/D^{n-5}$) will not change to that for two planar surfaces (energy $\propto -1/D^{n-4}$). However, the concepts of an “effective interaction zone” and “effective interaction area,” A_{eff} , are useful. If we compare Eq. (11.4) for a sphere near a surface with Eq. (11.7) for two surfaces, we find that the interaction of a sphere and a surface is the same as that of two planar surfaces *at the same surface separation D* if their area is

$$A_{\text{eff}} = 2\pi RD/(n-5) = 2\pi RD \quad \text{for } n = 6 \text{ (van der Waals forces).} \quad (11.9)$$

Now from Figure 11.2b and the chord theorem, Eq. (10.4), this area is simply equal to πx^2 when $z = D$ (as long as $R \gg D$). In other words, the effective area of interaction of a sphere with a surface is the circular zone centered at a distance $-D$ from the surface (inside the sphere). This is known as the *Langbein approximation*.

As can be seen from Eq. (11.9), the effective area of interaction is not a fixed value but increases linearly with both R and D . For example, for a sphere of radius $R = 1 \mu\text{m}$ at a distance $D = 1 \text{ nm}$ from a wall, the effective interaction area is about $2\pi RD \approx 6 \times 10^{-15} \text{ m}^2$ or $6,000 \text{ nm}^2$, which corresponds to a circle of radius $\sim 45 \text{ nm}$. At contact, when $D \approx 0.3 \text{ nm}$, this radius falls to 25 nm , though in practice elastic flattening generally significantly increases the contact area of “real” adhering particles due to their finite elasticity (see Section 17.7). For both of the above reasons, the effective area for curved surfaces is not as useful quantitatively as might be hoped. In addition, it also depends on the form of the interaction potential, being different for different power-laws ($n \neq 6$), as well as for an exponential potential (Problem 11.6).

11.4 Interactions of Particles Compared to Those between Atoms or Small Molecules

Size Effects on Interparticle Interaction Potentials

We have already seen (cf. Table 6.1) that for molecules that interact via van der Waals forces, once their diameters are greater than about 0.5 nm , they must already be considered as particles or else the strength of their interactions will be underestimated. A rough scaling relation for the effect of particle size was previously derived as Eq. (10.23):

$$\text{Adhesion or binding energy of particles} \approx \text{Binding energy of atoms} \times \frac{\text{Radius of particles}}{\text{Radius of atoms}}. \quad (11.10)$$

Another important scaling effect concerns the size of interacting particles relative to the range of their interaction potential or, more correctly, the volume of the particle relative to the volume encompassed by the interaction. In Sections 2.5 and 7.3 we saw once this ratio increases above a certain critical value, the system is always above the gas-liquid critical point—that is, there is no liquid state or gas-liquid phase transition. This phenomenon occurs for nanoparticles as small as 1 nm interacting through short-range van der Waals force—for example, C_{60} , which has no liquid phase (Hagen et al., 1993), as well as larger colloidal particles in water that aggregate straight into crystals from the gas phase (Figure 11.3) unless the forces between them are long-ranged (Figure 6.2) (Gast et al., 1983a, b; Meijer and Frenkel, 1991; Lekkerkerker et al., 1992; Pusey et al., 1994; in't Veld et al., 2007). However, such systems can still exhibit fluid-solid and solid-solid transitions (cf. Figure 6.1).

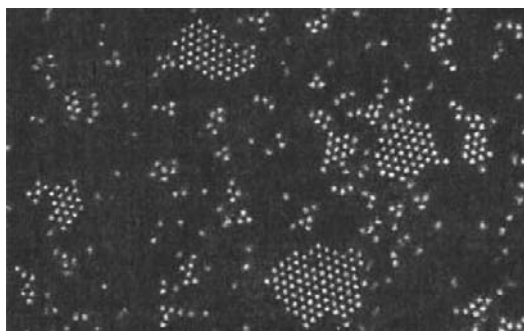


FIGURE 11.3 Small ($<1\text{ }\mu\text{m}$) colloidal particles interacting through an attractive force of shorter range than the size of the particles, showing no gas-liquid coexistence—that is, no liquid phase—only a gas-solid coexistence. Note that the solid (crystalline or amorphous) aggregates also exhibit very different rheological properties from those of ordinary liquids, behaving more like a weak gel—for example, cracking along “grain boundaries” rather than flowing. [Micrographs courtesy of Sei Hachisu; see also Okamoto and Hachisu, 1977.]

Skin Depth or Surface-Area-to-Volume Scaling Effects

Some intrinsic properties of particles are “additive,” given by summing the contributions from the individual atoms or molecules. Others are “nonadditive,” depending on cooperative effects. For example, the optical properties such as the dielectric constant and refractive index of clusters of noble gas atoms and hydrocarbons were previously seen to be additive (Section 5.8)—that is, calculable by summing the single-molecule contributions. In contrast, many properties, especially of associated liquids and metals, are not additive: their strength, melting temperatures, chemical activity, AC conductivity, and opto-electronic properties are often determined within a surface layer, attaining their maximum value only after a certain critical “skin-depth” or “proximity length” λ from the surface has been reached. Table 11.1 gives the values of λ for the more important physical and chemical properties of thin films, small particles, and highly curved surfaces.

Skin depth effects can result in certain *collective* properties peaking at some critical particle size even though *individual* particles show no such effect (Min et al., 2008). In addition, nanostructured materials can become harder or softer as the particle size decreases—harder if they are polycrystalline with dislocations that are no longer present below a certain size, or softer because of the reduced number of bonds, on average, holding the atoms together in the cluster.

Dynamic and Nonequilibrium Effects

Many important dynamic effects are strongly influenced by particle size. First, as particles increase in size, their van der Waals adhesion energies and forces, E_{ad} and F_{ad} , increase linearly with R —that is, $E_{\text{ad}} \propto R$. For atomically sized particles, E_{ad} is of order kT , but for particles larger than 1–2 nm, E_{ad} becomes much larger than kT . Since the adhesion (or binding) energy appears as $e^{-E_{\text{ad}}/kT}$ in equations to do with bonding lifetimes, dynamics,

Table 11.1 Skin-Depths and Proximity Lengths, λ , of Some Common Material Properties

Property	Equations for Particles or Thin Films of Radius or Film Thickness R	λ
Cohesive energy, latent heat ¹	$E_R = E_{\text{bulk}} \left(1 - \frac{\lambda}{R}\right)$	0.3–2 nm
Surface tension ¹	Tolman equation: $\gamma(R) = \frac{\gamma(\infty)}{(1 + \lambda/R)}, \quad \gamma(\infty) = \gamma_{\text{bulk}}$	0.3–5 nm
Melting point depression of metals ¹	$T_R = T_{\text{bulk}} \left(1 - \frac{\lambda}{R}\right)$	1–3 nm
Vapor pressure	Kelvin equation: λ depends on the relative humidity or vapor pressure.	0.3–10 nm
Chemical reactivity		
Covalent bonds		0.5 nm
Electron transfer	See “Harpooning effect.”	0.7–1.0 nm
Opto-electronic properties		
AC conductivity (metals)	$\lambda \propto 1/\sqrt{\text{frequency}}$	$\sim 1 \mu\text{m}$ at 1 GHz
DC (conducting polymers)		~ 2 molecules
Band gap energy		2–30 nm

¹The first three properties are intimately related. Table adapted from Min et al., (2008).

relaxations, and equilibration times, nanoparticle systems become increasingly nonequilibrium systems—that is, kinetically trapped in whatever state they were prepared. Such systems can show slow “aging effects” such as deformational creep.

Long equilibration or relaxation times have serious experimental and practical implications, especially for *self-assembly* interactions where spontaneous, naturally occurring ordering or organization is supposed to be driven by thermodynamics. When thermodynamics no longer dictates the self-assembly pathway (or does so only after a very long time), the particles become ordered not by *self-assembly* but by *directed-assembly* or *engineered-assembly*, which is driven by the externally applied forces on the system during their preparation such as normal or shear stresses, gravity (buoyancy effects in solution), and magnetic or electric fields. Directed assembly depends on the method of preparation and the previous history of the sample and is discussed further in Chapter 22.

Another dynamic effect has to do with surface diffusion. In comparison to large particles, the diffusion of molecules or atoms, such as in gold, over the surface of a nanoparticle is rapid, with important consequences. For example, since the mean-square distance diffused is proportional to the time t , as described by the diffusion equation, $\langle x \rangle^2 \propto Dt$, at constant D , if a surface molecule takes 1 year to diffuse to the other side of a 10 μm particle, it will take about 30 seconds to diffuse to the other side of a 10 nm nanoparticle. This has profound implications for particle coalescence, diffusion-limited aggregation, diffusion-controlled deformations, chemical reactions (sintering),

and other changes in particle assemblies when studied over laboratory or “engineering” time-scales. In general, larger particles take much longer to become ordered and, conversely, disordered. For these reasons, many nanoparticle assemblies and colloidal systems are nonequilibrium ones.

11.5 Interaction Energies and Interaction Forces: the Derjaguin Approximation

So far we have been dealing mainly with interaction *energies* rather than the *forces* experienced by molecules and small particles. This is because most experimental data on molecular interactions are of a thermodynamic nature and therefore more readily understood in terms of interaction energies, as we saw in Part I. However, between macroscopic particles and certain large molecules and nanoparticles it is the forces between them that are usually easier to measure, and of greater interest, than their interaction energies.³

It is therefore desirable to be able to relate the force law $F(D)$ between two curved surfaces to the interaction free energy $W(D)$ between two planar surfaces. Luckily, a simple relation exists for the two geometries most commonly encountered: two flat surfaces and two spheres (a sphere near a flat surface being a special case of two spheres, with one sphere very much larger than the other). A glance at Eq. (11.4) shows that for the additive intermolecular pair potential $w(r) = -C/r^n$, the value of $F(D)$ for a sphere near a flat surface is

$$F(D) = -\frac{\partial W(D)}{\partial D} = -\frac{4\pi^2 C \rho^2 R}{(n-2)(n-3)(n-4)D^{n-4}} \quad (11.11)$$

This force law can be seen to be simply related to $W(D)$ per unit area of two planar surfaces, Eq. (11.7), by

$$F(D)_{\text{sphere}} = 2\pi R W(D)_{\text{planes}}. \quad (11.12)$$

This is a very useful relationship, and while it was derived for the special case of an additive inverse power potential, it is in fact valid for any type of force law, as will now be shown.

Assume that we have two large spheres of radii R_1 and R_2 a small distance D apart (Figure 11.4). If $R_1 \gg D$ and $R_2 \gg D$, then the force between the two spheres can be obtained by integrating the force between small circular regions of area $2\pi x dx$ on one surface and the opposite surface, which is assumed to be locally flat and at a distance $Z = D + z_1 + z_2$ away. The net force between the two spheres (in the z direction) is therefore

³Other qualitative differences between the forces and energies of an interaction, such as the effect of time on measured forces but not the energies (Chapters 9 and 22), and that high binding energies do not necessarily imply high binding forces (Section 17.2), are considered elsewhere in the book.

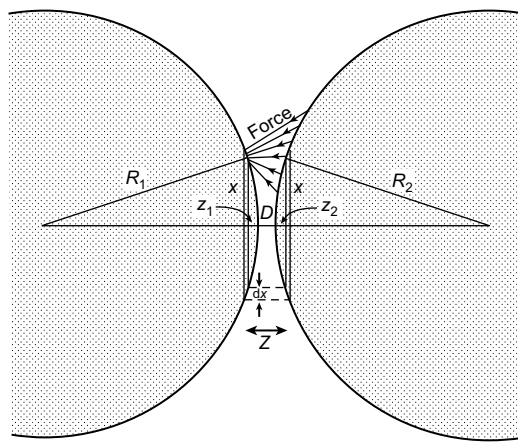


FIGURE 11.4 The Derjaguin approximation (Derjaguin, 1934), which relates the force law $F(D)$ between two spheres to the energy per unit area $W(D)$ of two flat surfaces by Eq. (11.16): $F(D) = 2\pi[R_1R_2/(R_1 + R_2)]W(D)$.

$$F(D) = \int_{Z=D}^{Z=\infty} 2\pi x \, dx f(Z), \quad (11.13)$$

where $f(Z)$ is the normal force per unit area between two flat surfaces. Since from the Chord Theorem $x^2 \approx 2R_1z_1 = 2R_2z_2$, we have

$$Z = D + z_1 + z_2 = D + \frac{x^2}{2} \left(\frac{1}{R_1} + \frac{1}{R_2} \right) \quad (11.14)$$

and

$$dZ = \left(\frac{1}{R_1} + \frac{1}{R_2} \right) x \, dx, \quad (11.15)$$

so that Eq. (11.13) becomes

$$F(D) = \int_D^\infty 2\pi \left(\frac{R_1R_2}{R_1 + R_2} \right) f(Z) dZ = 2\pi \left(\frac{R_1R_2}{R_1 + R_2} \right) W(D), \quad (11.16)$$

which gives the force between two spheres in terms of the energy per unit area of two flat surfaces at the same separation D . Eq. (11.16) is known as the *Derjaguin approximation* (Derjaguin, 1934). It is applicable to any type of force law, whether attractive, repulsive, or oscillatory, as long as the range of the interaction and the separation D are much less than the radii of the spheres. It is a useful equation for interpreting experimental data—for example, for comparing theory with experiment—since it is generally easier to theoretically derive the interaction *energy* for two planar surfaces, while it is usually easier to measure the *force* between curved surfaces, such as two spherical particles or a sphere and a surface. Equation (11.16) is also useful for comparing force data among different experiments, since all forces and energies are

predicted to scale by a simple geometric factor that depends only on the local radii of the interacting surfaces. It has been well verified experimentally, as discussed in Chapters 13–17.

From the Derjaguin approximation, Eq. (11.16), we may deduce the following:

- If one sphere is very large so that $R_2 \gg R_1$, we obtain $F(D) = 2\pi R_1 W(D)$, which is the same as Eq. (11.12) and corresponds to the limiting case of a sphere of radius R_1 near a flat surface. For two equal spheres of radii $R = R_1 = R_2$, we obtain $F(D) = \pi R W(D)$, which is half the value for a sphere near a flat surface.
- For two spheres in contact ($D = \sigma$), the value of $W(\sigma)$ can be associated with -2γ , where γ is the conventional surface energy per unit area of a surface. Eq. (11.16) then becomes

$$F(\sigma) = F_{\text{ad}} = \frac{-4\pi\gamma R_1 R_2}{(R_1 + R_2)} \quad (11.17)$$

which gives the *adhesion force* F_{ad} between two spheres in terms of their surface energy γ . Adhesion forces are discussed in Chapter 17.

- Perhaps the most intriguing aspect of the Derjaguin approximation is that it tells us that the distance dependence of the force between two curved surfaces can be quite different from that between two flat surfaces even though the same type of force is operating in both. This is illustrated in Figure 11.5, where we see that a purely repulsive force between two curved surfaces can be attractive between two planar surfaces

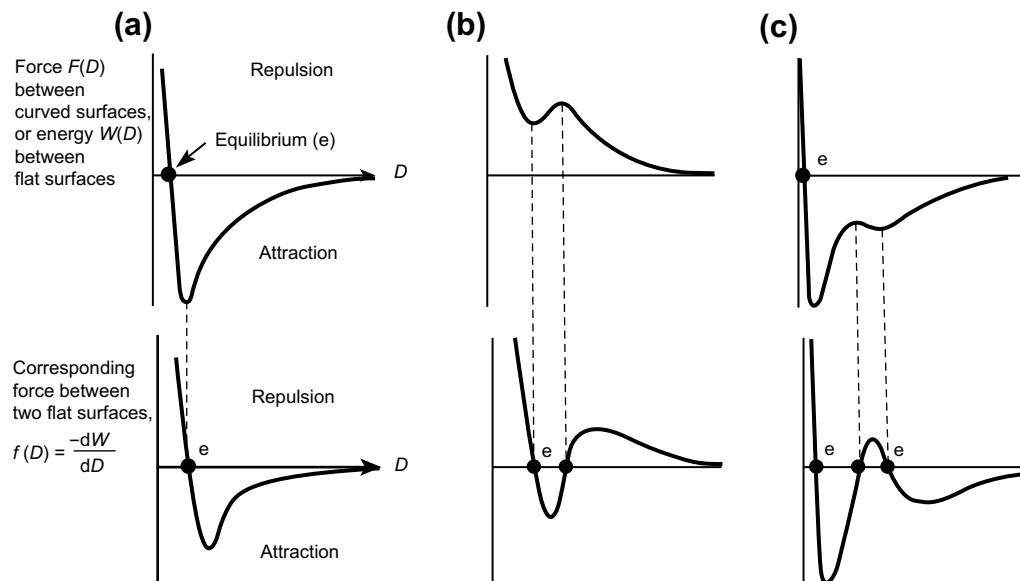


FIGURE 11.5 Top row: force laws between two curved surfaces (e.g., two spherical particles). Bottom row: corresponding force laws between two flat surfaces. Note that stable equilibrium occurs only at points marked e where the force is zero ($f = 0$) and the force curve has negative slope; the other points where $f = 0$ are unstable.

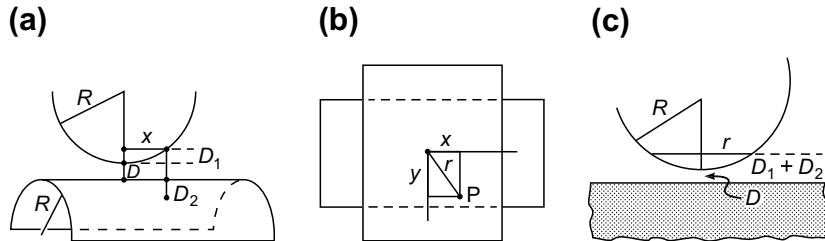


FIGURE 11.6 (a) and (b): Geometry of two crossed cylinders. (c) Equivalent geometry of a sphere near a flat surface.

(over a certain distance regime), with a stable equilibrium at some finite separation (Figure 11.5b). Conversely, a purely attractive force between curved surfaces can become repulsive between two planar surfaces (Figure 11.5c). This has important implications for the interactions of nonspherical particles—for example, faceted colloidal particles whose interaction between their flat faces can be both quantitatively and qualitatively different from the interaction between their curved regions.

The mathematical approach used to derive Eq. (11.16) for spherical particles can be applied to other curved geometries. For example, it may be readily shown that for two cylinders of radii R_1 and R_2 crossed at an angle θ to each other, the Derjaguin approximation becomes

$$F(D) = 2\pi\sqrt{R_1 R_2} W(D)/\sin \theta, \quad \text{for } D \ll R_1, R_2. \quad (11.18)$$

For two cylinders of equal radii $R = R_1 = R_2$, crossed at right angles to each other as shown in Figures 11.6a and b, we have $\theta = 90^\circ$, $\sin \theta = 1$, and the above reduces to the same result as for a sphere of radius R near a flat surface. In other words, the interaction of two orthogonal cylinders is the same as that of a sphere and a wall (Figure 11.6c) if all three radii are the same. This is therefore a convenient, and common, geometry used in surface force measurements (Chapter 12).



Worked Example 11.2

Question: Two orthogonal cylinders of equal radius R are separated by a small distance D ($D \ll R$). Using purely geometrical arguments, show that the surface geometry around the contact region is the same, to first order, as for a sphere of the same radius R at the same distance D from a flat surface.

Answer: Referring to Figures 11.6a and b, and using the Chord Theorem, Eq. (10.4), we have $x^2 = 2RD_1$ and $y^2 = 2RD_2$. Referring to Figure 11.6b, this implies $2R(D_1 + D_2) = x^2 + y^2 = r^2$. Thus, $D_1 + D_2$ is constant if r is constant—that is, if point P describes a circle. Since the above equation is indistinguishable from that for a sphere of the same radius near a flat surface, Figure 11.6c, we have proved that as far as forces (and many other properties) are concerned, the two geometries are locally equivalent.



Table 11.2 Different Types of Intertparticle Forces in Liquids^a

Type of Interaction	Other Names (Subclasses)	Attractive or Repulsive	Special Features (and Whether a Body or Surface Force)
Van der Waals (Ch. 13)	Dispersion, dipole-induced-dipole, charge-fluctuation, ion-correlation ^b , Debye, Keesom, Casimir.	Either: attractive between like particles	Weak but ubiquitous body force. Force can change sign at some finite distance.
Electrostatic (Ch. 14)	Coulomb, ionic, salt-bridge, dipolar, hydrogen-bonding, charge-transfer (harpooning), double-layer ^b .	Either: repulsive between like charges, attractive between electro-neutral systems	Strong, long-ranged force arising in polar solvents. Usually a surface force.
Solvation (Ch. 15)	Structural, epitaxial, hydration (in water), depletion ^b , hydrophobic ^c .	Either, including oscillatory	Surface force that modifies the local liquid structure.
Entropic (Ch. 16)	Steric, osmotic, thermal fluctuation/undulation/protrusion, polymer bridging, depletion ^b , double-layer ^b .	Usually repulsive	Surface force that arises from the confinement of solvent or solute molecules between the surfaces.
Short-range physical (Ch. 17, 19)	Adhesive, cohesive, surface tension, wetting, capillary.	Usually attractive	Can be either a body or surface force
Short range chemical (Ch. 3)	Covalent, quantum mechanical, metallic, exchange, steric, hard core, Born.	Either: ultimately repulsive at small distances	Strong short-ranged surface forces, largely independent of the suspending liquid medium.
Specific (Ch. 21)	Complementary (electrostatic or geometric), host-guest, lock-and-key, ligand-receptor, antibody-antigen.	Attractive (specific but not necessarily strong)	Single or multiple noncovalent bond arising from perfect fit of ion or molecule into host pocket or lattice site. Main “recognition” interaction of biological molecules.
Nonequilibrium (Ch. 9, 18, 22)	Viscous (drag), friction, shear, lubrication, hydrodynamic, energy dissipating, hysteretic.	Either (depends on externally applied forces)	Involves continuous or transient motion of molecules or particles. Heat generating.

^aUnless specifically mentioned, the interactions refer to the pair-potentials of like particles. Mixtures of different (unlike) particles can be very complex, even when the difference is only in their size.

^bForces that are difficult to classify unambiguously, or that are made up of two equally important contributions.

^cClassification still unknown or controversial.

11.6 “Body Forces” and “Surface Forces”

Some of the relations derived in this chapter were based on the assumption that all the molecules in one body interact with all the molecules in the other body. Other relations, such as the Derjaguin Approximation, simply assumed that two surfaces interact via a certain force per unit area without asking where this force comes from. The first type of interaction is known as a “body force,” where all the molecules within the bodies are involved. But there are situations where only the surfaces attract or repel each other, when the interaction is referred to as a “surface force.” For example, in Section 3.3 it was shown that the Coulomb interaction between two charged spheres is the same regardless of whether the charges are distributed evenly on their surfaces (a “surface force”) or throughout their bulk (a “body force”). In this case, the distinction between a surface and a body force may therefore not be important, but in others it can be very important.

One way to distinguish between the two is to think what would happen if the material behind the surfaces were to be removed. Thus, in the case of van der Waals forces, the total force would change, so this is a body force. But in the case of two spheres with charges on their surfaces, the force would be unchanged, so this is a surface force.

In future chapters we shall encounter situations where this distinction is important. For example, an attractive *surface* force between two bodies pulls the bulk interior of one body toward the other, whereas for an attractive *body* force all parts of the interior are pulled together. The coupling between the surface and interior therefore become important in determining the outcome of such interactions, particularly between “soft” particles. Thus, in the case of adhering soft elastic bodies or fluid-like colloidal particles (e.g., vesicles, emulsion droplets), these deform during an interaction, and one must know between which parts of the materials the forces originate before one can calculate or understand their equilibrium shapes.

Table 11.2 lists the most common forces encountered between macroscopic particles and extended surfaces interacting in liquids. This table is analogous to Table 2.2 in Part I that referred to interatomic, interionic, and intermolecular forces. Table 11.2 also summarizes the special features of the different interactions—for example, whether attractive or repulsive, or whether a surface or body force—and indicates the different chapters devoted to each of them.

PROBLEMS AND DISCUSSION TOPICS

- 11.1** In Section 2.6 it was shown that under the conditions on the earth’s surface (STP) any intermolecular adhesion energy greater than about kT ($\sim 4 \times 10^{-21}$ J at $T = 298$ K) will lead to (partial) condensation of the vapor into a solid or liquid phase. The total density of matter in the universe, of which 90% is dark matter, is estimated at 3×10^{-30} g/cm³—that is, about 10^{30} times less dense

than liquid water. In addition, the average temperature of space is 2.7 K, so that “ kT ” is also very different. Assuming that in space only van der Waals interactions occur between the molecules, would these be strong enough to condense them (into cold planets) at the very low temperature and extremely low density of space? [Answer: Yes, if the intermolecular binding energy is greater than about 5×10^{-22} J, which is the case for all but the smallest molecules.] Is it valid to apply such thermodynamic concepts to the universe? How would gravitational forces affect your analysis?

- 11.2*** Two spheres have very different radii ($R_1 \gg R_2$) whose molecules interact via a nonretarded van der Waals force at all separations. Show that their interaction energy will vary as $-1/D^n$ at small separations, as $-1/D^m$ at intermediate separations, and as $-1/D^p$ at large separations, where n, m and p are different integers. Identify n, m , and p , and the approximate range of D relative to R_1 and R_2 over which each force-law operates.
- 11.3** Show that the van der Waals interaction energy $W(D)$ per unit length for two parallel cylinders of radii R_1 and R_2 whose surfaces are separated by a distance D (where $R_1, R_2 \gg D$) is

$$W(D) = -\frac{\pi^2 C \rho_1 \rho_2}{12\sqrt{2} D^{3/2}} \left(\frac{R_1 R_2}{R_1 + R_2} \right)^{1/2} \quad \text{per unit length.} \quad (11.19)$$

- 11.4** Derive Eq. (11.18) for the interaction between two crossed cylinders.
- 11.5** The repulsive pressure between two flat surfaces interacting in a liquid medium is given by $P = Ce^{-\kappa D}$, where $C = 100$ Pa and $\kappa^{-1} = 20$ nm are constants, and where D is the separation between the surfaces (such long-range repulsive forces can arise from electrostatic or polymer-mediated interactions in liquids). Consider a large spherical colloidal particle of radius $R = 1 \mu\text{m}$ interacting with a flat surface in the liquid medium via the same interaction. When the surface of the particle is at a distance $D_0 = 10$ nm from the flat surface, (i) what is the net repulsive force between the particle and the surface, and (ii) what fraction of the total force comes from surface separations greater than $2D_0$? [Answers: (i) 7.6 pN; (ii) $e^{-\kappa D_0} = 0.61$.] If the spherical particle is made of iron and is suspended in water, what will be its average equilibrium distance from the surface?
- 11.6** The repulsive pressure between two flat surfaces interacting in a particular aqueous solution is described by $P = Ce^{-\kappa D}$, as in Problem 11.5. Consider a spherical colloidal particle of radius R interacting with a flat surface in this solution, where the two surfaces are at a distance D_0 apart ($D_0 \ll R$).
- (i) Calculate their “effective” area of interaction—that is, the area at which two flat surfaces, separated by the same distance D_0 , would have the same force as that between the sphere and the flat surface. Relate your result to the distance D_0 between the flat surface and the circular section through the sphere having this area.

- (ii) Repeat the above calculations for the case where the interaction is a purely attractive van der Waals force, where the pressure between two flat surfaces is now given by $P = -A/6\pi D^3$, where A is a constant. [cf. the Langbein approximation.]
- 11.7** The repulsive pressure between two flat surfaces is described by $P = Ce^{-\kappa D}$, as in Problem 11.5. Show that the force between a cylinder of radius R at a distance D ($D \ll R$) from a parallel surface is⁴
- $$F(D) = \sqrt{2\pi R/\kappa} Ce^{-\kappa D} \quad \text{per unit length.} \quad (11.20)$$
- 11.8** Obtain an expression for the repulsive part of the force-law between two flat surfaces by summing the repulsive $+B/r^{12}$ term of the Lennard-Jones potential. Is your expression physically meaningful? [Answer: No, but it's a nice exercise.]
- 11.9** For what types of interactions or under what conditions will the Derjaguin approximation not apply?
- 11.10** Do you expect the boiling point of a small droplet or cluster composed of van der Waals molecules to be higher or lower than that of the bulk liquid?
- 11.11*** A first-order phase transition occurs in a thin fluid film confined between two flat solid surfaces of unit area when they are brought together in a liquid medium. The fluid is in equilibrium with the bulk liquid reservoir outside the film. Sketch what the force F versus distance D curves look like between (i) the two flat surfaces, and (ii) two spheres. [Hint: Note that between two flat surfaces the force F per unit area as a function of the separation D is the same as the pressure P as a function of the volume V .]

⁴It is interesting to note that the exponential interaction potential remains purely exponential with the same decay length for all geometries. This is in contrast to the inverse power-law interaction, such as the van der Waals, where the index n is different for different geometries.

Force-Measuring Techniques

12.1 Direct and Indirect Measurements of Intermolecular, Interparticle, and Surface Forces

When we come to consider experimental measurements of intermolecular forces, we are confronted with a bewildering variety of data and techniques to draw upon. This is because almost any measurement of a physical or chemical property, whether in physics, chemistry, biology or engineering, is in some respect a measurement of intermolecular forces. For example, we have already seen how such a common property as the boiling point or phase state of a substance provides information on the strength of intermolecular binding energies. It is therefore difficult to make a list of experimental measurements of intermolecular forces; it is far better to draw upon whatever relevant data exists as the situation arises. This was done in Part I at the atomic and molecular levels, and we shall continue with this practice in Parts II and III at the nanoscopic, microscopic, and macroscopic levels. However, different types of measurements do provide different insights and information. Thus, some experiments provide purely thermodynamic data, whereas others may give the binding energies of molecules or particles in contact, either directly or indirectly, and still others may allow for a direct measurement of the complete force-law $F(D)$ but may be restricted to measuring only repulsive forces. It is therefore appropriate to start by categorizing experiments according to the type of information they provide, and we shall start by recapitulating some of those already mentioned (Figure 12.1).

- (i) Thermodynamic data on gases, liquids, and solids (e.g., PVT data, boiling points, latent heats of vaporization, lattice energies) provide information on the short-range attractive potentials between molecules. Adsorption isotherms provide information on the interactions of molecules with surfaces.
- (ii) Physical data on gases, liquids, and solids (e.g., molecular beam scattering experiments, viscosity, diffusion, compressibility, NMR, x-ray, light and neutron scattering, and optical microscopy of liquids and solids) provide information on the short-range interactions of molecules and colloidal particles, especially their repulsive forces, and their involvement in the structure of condensed phases (e.g., their ordering in liquid crystals and colloidal crystals).
- (iii) Thermodynamic data on liquid mixtures and multicomponent systems (e.g., phase diagrams, solubility, partitioning, miscibility, osmotic pressure) provide information on short-range solute-solvent and solute-solute interactions.

Experimental data like (i)–(iii) often provide thermodynamic information only, so that direct access to the intermolecular potential functions—that is, their

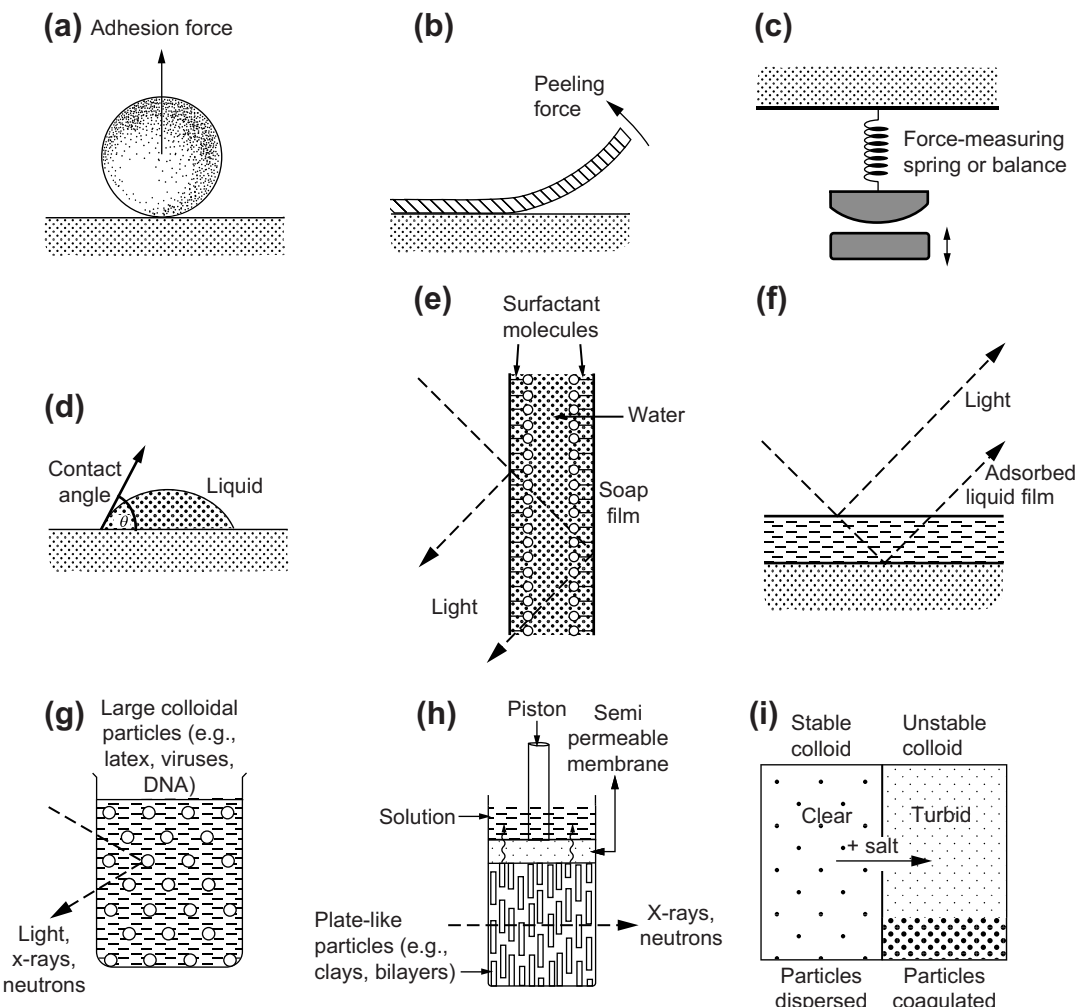


FIGURE 12.1 Different types of measurements that provide information on the forces between particles and surfaces. (a) Adhesion measurements (practical applications: xerography, particle adhesion, powder technology, ceramic processing). (b) Peeling measurements (practical applications: adhesive tapes, material fracture and crack propagation). (c) Direct measurements of force as a function of surface separation (practical applications: testing theories of inter-surface forces). (d) Contact angle measurements (practical applications: testing wettability and stability of surface films, detergency). (e) Equilibrium thickness of thin free films (practical applications: soap films, foams). (f) Equilibrium thickness of thin adsorbed films (practical applications: wetting of hydrophilic surfaces by water, adsorption of molecules from vapor, various magnetic and opto-electronic films, protective coatings and lubricant layers, biosensors). (g) Interparticle spacing in liquids using various spectroscopic and scattering techniques (practical applications: colloidal dispersions, paints, pharmaceutical dispersions, nano- and microstructured composite materials, measuring intermacromolecular and interparticle forces). (h) Sheet-like particle spacings in liquids (practical applications: clay and soil swelling behavior, microstructure of soaps and biological membranes, composite materials). (i) Coagulation studies (practical application: basic experimental technique for testing the stability and coagulation rates of colloidal dispersions).

distance dependence—is not possible. Thus, experimental PVT data may be compared with the van der Waals equation of state (Chapter 6), which contains terms to account for both the attractive and repulsive forces, but it does not give any information on the nature and range of the force laws themselves. To gain this information, some more direct measurement of forces is required. Of the various methods that have been devised for measuring molecular forces, the most direct employ macroscopic bodies or extended surfaces suspended from springs, where distances can be measured to 0.1 nm, where the forces are large and measurable, and where entropic (thermal) effects are negligible. It is from such experiments that much hard data on intermolecular and surface interactions have emerged.

- (iv) Particle detachment and peeling experiments (Figures 12.1a, b) provide information on particle adhesion forces and the adhesion energies of solid surfaces in contact (i.e., attractive short-range forces). Such experiments are important in powder technology, xerography, ceramic processing, the making of adhesive films, and in the understanding of granular flow and how cracks propagate in solids.
- (v) Measuring the force between two macroscopic surfaces as a function of surface separation can provide the full force law of an interaction (Figure 12.1c). Such *direct* force measurements are described in detail in the following sections.
- (vi) Various surface studies such as surface tension and contact angle measurements give information on liquid-liquid and solid-liquid adhesion energies (Figure 12.1d). When contact angles are measured under different atmospheric environments or as a function of rate or time these relatively simple experiments can provide surprisingly deep insights into the states of surfaces and adsorbed films, and of molecular reorientation times at interfaces.
- (vii) The thicknesses of free soap films and liquid films adsorbed on surfaces (Figures 12.1e, f) can be measured as a function of salt concentration or vapor pressure. Such experiments provide information on the long-range repulsive forces stabilizing thick wetting films. Various optical techniques (e.g., reflected intensity, total internal reflection spectroscopy, or ellipsometry) have been used to measure film thickness to within 0.1 nm.
- (viii) Equilibrium or mean interparticle separations and motions in liquids can be measured using NMR, light scattering, x-ray scattering and neutron scattering (Figures 12.1g, h). In such experiments the particles can be globular or spherical (e.g., micelles, vesicles, colloidal particles, latex particles, viruses), sheet-like (e.g., clays, lipid bilayers), or rod-like (e.g., DNA, rod-like nanoparticles). The interparticle forces can be varied by changing the solution conditions, and their mean separation can be varied by changing the quantity of solvent, for example, by changing the hydrostatic or osmotic pressure via a semipermeable membrane. Notable among these techniques are the *Compressibility Cell*, *Osmotic Pressure* and *Osmotic Stress* techniques developed by Homola and Robertson (1976), and

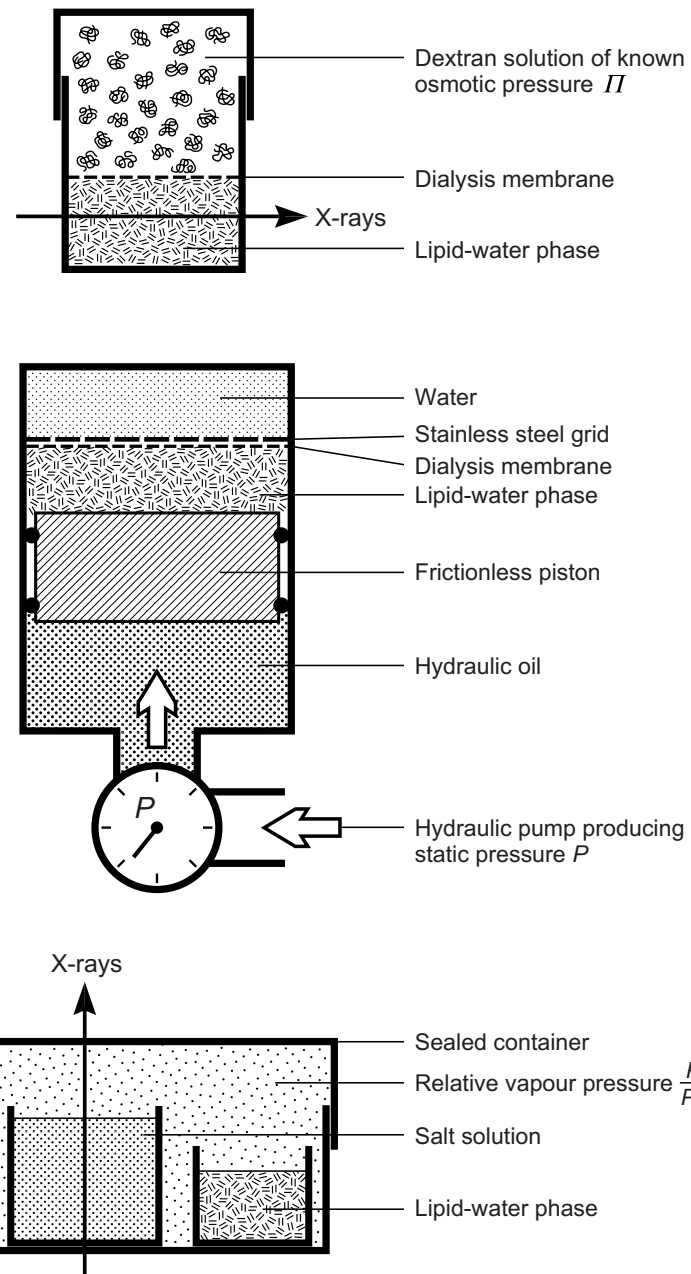


FIGURE 12.2 Osmotic Stress (OS) or Osmotic Pressure (OP) techniques: three setups commonly used for varying the osmotic pressure of a colloidal or biocolloidal dispersion while monitoring the structures in the solution and their mean separation using x-rays and/or neutron scattering (Wiener and White, 1992). [Adapted from Parsegian et al., 1979.]

LeNeveu et al., (1976), shown in Figure 12.2. By measuring the osmotic pressure as a function of interlamellar or interparticle separations,¹ the interaction force between surfaces can be obtained from the deviations from ideality in the PVT data. Such techniques are still *indirect* and are usually limited to measuring only the repulsive parts of a force-law.

- (ix) In coagulation studies on colloidal dispersions (Figure 12.1i) the salt type or concentration, pH or temperature of the suspending liquid medium (usually water) is changed until the dispersion becomes “unstable” and the particles coalesce (*precipitate, coagulate, or flocculate*). Coagulation rates can be very fast or very slow (see Worked Example 11.1). Such studies provide information on the interplay of repulsive and attractive forces in systems consisting of many particles that often involve many-body and/or nonpairwise additive interactions.

12.2 Different Direct Force-Measuring Techniques

Most of the methods shown in Figure 12.1 do not give the force-law (the force as a function of distance) but rather the adhesion force or minimum energy at some particular state—not necessarily the equilibrium state, of the system. Other methods, such as osmotic pressure measurements (see Figure 12.2), involve the collective interactions of many molecules or particles so that the data gained tend to be of a statistical or thermodynamic nature and not directly translatable into a force-law. The most unambiguous way to measure a force-law is to position two bodies close together and directly measure the force between them, such as from the deflection of a spring, very much as one would measure the force between two magnets. While the principle of direct force measurements is usually very straightforward, the challenge comes in measuring very weak forces at very small separations that must be controlled and measured to within 0.1 nm. Other challenges come in the interpretation of the data, which is often not as straightforward as it may initially appear. The different techniques and their unique capabilities and challenges will be described below after first considering the “philosophy” and “mechanics” of measuring forces.

Figure 12.3a shows the generic configuration of two interacting surfaces, whether under natural or laboratory (surface force measuring) conditions. The “system”² is always characterized by at least three important parameters: the surface geometry such as the surface radii R_i , the force function $F(D)$, and the compliance, stiffness, or effective elastic modulus K of the substrate material or force-measuring spring. The last is important because it is related to the means by which the forces are measured or

¹For most colloidal particles and flexible sheets or membranes their thermal motion means that one always measures a *distribution* about their mean spacing. This distribution can be quite large.

²By “system” is meant the two surfaces as well as their supporting materials and any moving parts and, in the case of a force-measuring instrument, the translators and detectors; in essence, the whole apparatus or device.

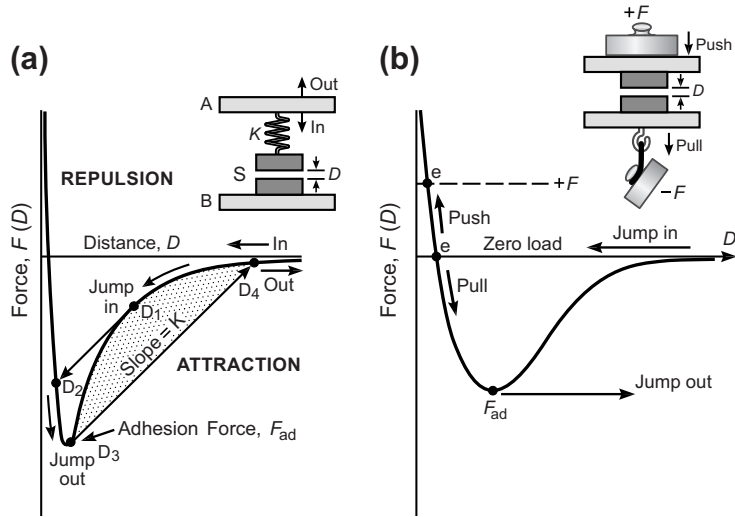


FIGURE 12.3 Measuring forces via (a) a spring (externally applied force \propto spring displacement: $F_{ext} = K\Delta D$), and (b) a constant force ($F_{ext} = \text{constant}$). For the typical force-law or force-distance curves $F(D)$ shown, instabilities occur at the positions shown, manifested by an inward jump on the way in (on approach) and an outward jump on the way out (on separation). (a) These jump instabilities will occur only if the effective spring constant K is lower than the maximum slope of the $F(D)$ curve. Thus, if the system is infinitely stiff ($K = \infty$) there will be no instabilities on approach or separation. In contrast, if a constant external force $+F$ is applied to one of the surfaces (b), K is effectively zero, and jumps will occur to the upper equilibrium points at e on approach, and out from F_{ad} on separation. No equilibrium is possible at surface separations between the **Jump in** and **Jump out** points.

“felt.” Thus, as shown in Figure 12.3a, the location **A** at which the force is detected or measured—for example, from the stress or strain of the substrate or spring—is different from the location **S** where the force acts. These two locations are connected by material of compliance K (and mass m , which is also an important factor when measuring dynamic interactions). Other important factors in any force measurement are the means by which the surfaces are moved and how and where the various displacements are measured (Leckband and Israelachvili, 2001). In the schematics of Figure 12.3a, it is assumed that the surfaces are moved by displacing the base of the supporting material **B** or spring at **A** and that the force is detected at **A**. When K is finite—that is, when the supporting materials are not infinitely rigid ($K = \infty$)—then as the surfaces are moved toward or away from each other, instabilities can occur depending on the force function $F(D)$. For a Lennard-Jones type of interaction, Figure 12.3a shows how these can lead to instabilities, manifested by an inward jump from D_1 to D_2 as the surfaces are brought toward each other, and to an outward jump from D_3 to D_4 when they are separated; there are no stable positions between D_1 and D_3 . These jumps occur when the slopes of the force dF/dD equal the stiffness K (see Problem 1.5). For infinitely stiff systems or for purely repulsive forces there are no jumps or instabilities.

Worked Discussion Topic 12.1

Question: Thermodynamic equilibrium requires that the same state is achieved regardless of the way one approaches it. What is the thermodynamically equilibrium separation D in Figure 12.3a in the region between D_2 and D_4 ?

Answer: This question is more of a play on words. Thermodynamics talks about the equilibrium “state” of a system, not about an equilibrium “separation” between any two or more objects. There is no thermodynamically equilibrium *distance* any more than there is one between the molecules of a gas, only a Boltzmann *distribution* of distances or an *average* distance. Thus, the two surfaces will move back and forth due to their thermal motion, sampling all distances while spending more time at those separations where the energy is least (cf. Figure 9.5). For macroscopic bodies these times are astronomical so that the system is never or rarely at *thermodynamic* equilibrium (which would require us to observe it over astronomical times). However, the system is at *mechanical* and *thermal* equilibrium.

Table 12.1 shows the typical range and strengths of the interaction energies and adhesion forces associated with differently sized particles, which in turn determines the most suitable experimental techniques for studying them. These particles have been separated into molecular, nanoscopic, microscopic, and macroscopic. The techniques used to study them are listed in the lower rows of Table 12.1 and are described in more detail in later sections in this chapter, or in Part III if they are used mainly for measuring biological interactions—for example, between model or living cells. For a review of both biological and nonbiological force-measuring techniques see Leckband and Israelachvili (2001).

Regarding the resolution, range or sensitivity with which different techniques can be used to measure forces, these can be defined in terms of the *energies*, the *forces*, the *pressures* or the *distances* at which reliable measurements can be made.³ For example, consider an AFM with a force measuring error of $\Delta F = \pm 10$ pN, which is being used to measure the force between a flat surface and a tip of radius $R = 20$ nm, where the van der Waals Hamaker constant (see Table 13.2) is $A = 10^{-20}$ J. This AFM will therefore be able to reliably measure the van der Waals force, given by $F = -AR/6D^2$, out to $D \approx 1.8$ nm. In comparison, a technique such as the SFA that is being used to measure the force between two cylindrical surfaces of radii $R = 20$ mm to within a much lower resolution of $\Delta F = \pm 10$ nN will nevertheless be able to measure the same van der Waals force out to $D \approx 58$ nm. This is approximately 30 times larger than the *distance* resolution of the AFM, even though the *force* resolution of the SFA is a factor of approximately 1,000 lower. The range of distances over which a technique can measure forces is therefore determined by $\Delta F/R$ rather than by ΔF .

³The effective measuring range depends on the measuring *error* which is typically 3 times greater than the *resolution*, *sensitivity*, or *detection limit* of the instrument.

Table 12.1 Typical Length Scales and Magnitudes for Noncovalent Interactions and the Ten Most Common Techniques for Measuring Them

Typical Parameters	Atomic (physical bonds, atoms and small molecules, submolecular groups)	Nanoscopic (macromolecules, nanoparticles, small aggregates)	Microscopic (small colloidal particles, vesicles, biological cells)	Macroscopic (large particles, flat surfaces)
Particle radius	0.1 nm	1 nm	1 μ m	1 mm
Binding or adhesion energy	$1 kT$	$10 kT$	$1000 kT$	$10^6 kT, 100 \text{ mJ/m}^2$
Adhesion force or pressure	$10^{-11} \text{ N} = 10 \text{ pN}$	$10^{-10} \text{ N} = 100 \text{ pN}$	$10^{-7} \text{ N} = 100 \text{ nN}$	$10^{-4} \text{ N} = 100 \mu\text{N}$ $10^8 \text{ N/m}^2 = 10^3 \text{ atm}$
Range of interaction ^a	0.2 nm	2 nm	20 nm	50 nm
Suitable Experimental Techniques ^b				
Atomic Force Microscopy (AFM)	with tip	with tip	with bead	
Micro Cantilever (MC)	☆	☆	☆	
Optical Tweezers or Optical Trapping (OT)	☆	☆	☆	
Micro Pipette Aspiration (MPA) ^c and Bio Force Probe (BFP) ^c	☆	☆	☆	
Total Internal Reflection Microscopy (TIRM)			☆	
Reflectance Interference Contrast Microscopy (RICM) ^c				☆
Surface Forces Apparatus (SFA)				☆.
Osmotic Pressure (OP) or Osmotic Stress (OS)				☆
Shear Flow Detachment (SFD) ^c		☆		☆

^aRange is here defined as the distance D at which the interaction energy $W(D)$ is of the same order as the thermal energy $kT \approx 4 \times 10^{-21} \text{ J}$ at 25°C .

^bSome techniques can only be used to measure attractive (e.g., adhesion) forces, some only repulsive forces, and some can measure both.

^cThe MPA, BFP, RICM and SFD techniques are devoted mainly to biological-type measurements—for example, between vesicles or living cells, described in Part III.

Table adapted from Leckband and Israelachvili (2001).

12.3 Mechanics of Direct Force Measurements and Problems of Interpretation

When measuring forces between surfaces having some fixed geometry, it is far simpler to measure the forces between curved surfaces than between two flat surfaces. This is because there are no alignment problems when measuring the force between, say, a sphere and a flat surface, whereas two flat surfaces have to be totally flat and perfectly aligned at the atomic level, as well as dust-free, over a large area for reliable measurements to be made. This is usually impossible to achieve, and for this reason most force-distance measurements are conducted between curved surfaces, the most common geometries being a sphere and a flat, two spheres, or two crossed cylinders (Problem 12.4). From the measured force function $F(D)_{\text{curved}}$ one can determine the corresponding energy of interaction between the two bodies by integrating the measured force:

$$W(D)_{\text{curved}} = - \int_{\infty}^D F(D)_{\text{curved}} dD. \quad (12.1)$$

And one can obtain the corresponding interaction energy $W(D)_{\text{flat}}$ per unit area between two flat parallel surfaces using the Derjaguin Approximation (cf. Figure 11.4). For example, for the case of a rigid sphere of radius R near a flat surface, or for two orthogonally crossed cylinders each of radius R , we have (cf. Eq. 11.12 and 11.18)

$$W(D)_{\text{flat}} = F(D)_{\text{curved}} / 2\pi R, \quad (12.2)$$

from which the corresponding pressure $P(D)_{\text{flat}}$ (force per unit area) between two flat surfaces⁴ can be obtained by a straightforward differentiation:

$$P(D)_{\text{flat}} = -dW_{\text{flat}}/dD = -(dF_{\text{curved}}/dD)/2\pi R. \quad (12.3)$$

Note that all the above equations are in terms of the *measured* force $F(D)_{\text{curved}}$.

All real surfaces are elastic—that is, they are not completely rigid—and they tend to deform by flattening when pressed together under a large external force or “load.” In the case of flattened surfaces, the mean or average pressure can be obtained directly from the measured force or load using

$$P = F/A, \quad (12.4)$$

where A is the measured contact area. However, as will become apparent, this pressure is unlikely to be uniform across the contact area. In the case of adhering surfaces, these will flatten even under no external force, and the interpretation of the results now becomes much more complex (see Section 12.6 below and Section 17.7).

Figure 12.4 illustrates the parameters that, ideally, should be measured in a force experiment, in addition to any other system-specific parameters and environmental variables. In practice, no technique measures all of these parameters; indeed, there is usually no need to do so because some of these parameters are related, for example, via

⁴Because pressure is defined per unit area, one cannot talk about the pressure between two curved surfaces, only the force between them.

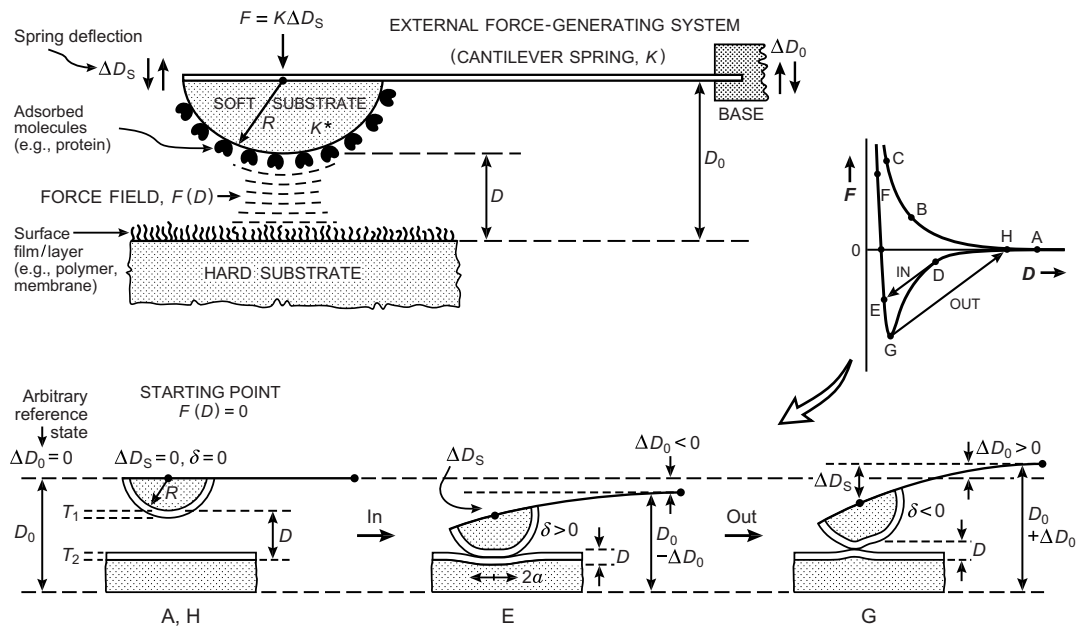


FIGURE 12.4 Generic geometry for force-measuring techniques that employ springs, showing the relevant parameters that must be controlled and/or measured, preferably as a function of time t , during a force measurement: the force F , the undeformed surface radius R , the surface separation D , the spring deflection ΔD_s , the force-measuring (cantilever) spring constant K such that $F(D) = K\Delta D_s$, the effective stiffness of the material K^* and its elastic deformation δ (see JKR theory in Chapter 17 and Figure 12.5), the flattened area $A = \pi a^2$ of the surfaces when in contact, and the film thicknesses T_1 and T_2 . One can define a laboratory reference distance D_0 such as that when the base is moved the change in the surface separation ΔD is given by Eq. (12.6): $\Delta D = \Delta D_0 \pm \Delta D_s \pm \delta$.

Eq. (12.6), and some may not be needed or may be of no interest. However, the more of these parameters that can be independently controlled and directly measured in any experiment, the more complete and unambiguous will the data be. The two most common types of limitations are:

- A lack of any direct measurement of the *local* geometry R , the *absolute* surface separation D , and the adsorbed layer thicknesses T_1 and T_2 (Figure 12.4). In many cases, the presence of particles or contaminant layers may not be easy to establish.
- Some interactions take a long time to equilibrate due to slow molecular rearrangements at the surfaces or in the adsorbed layers as they overlap during an interaction. If the forces are weak, it may be impossible to distinguish a slowly changing force from thermal drift. There is a pressing need to develop spectroscopic techniques that can be used in conjunction with force measurements for *in situ* measurements of molecular ordering during interactions.

Figure 12.4 shows a typical surface force-measuring system using a cantilever spring to generate and/or measure the force between two particle surfaces. The externally applied force is here shown to be generated by a spring, but other means are used such as light

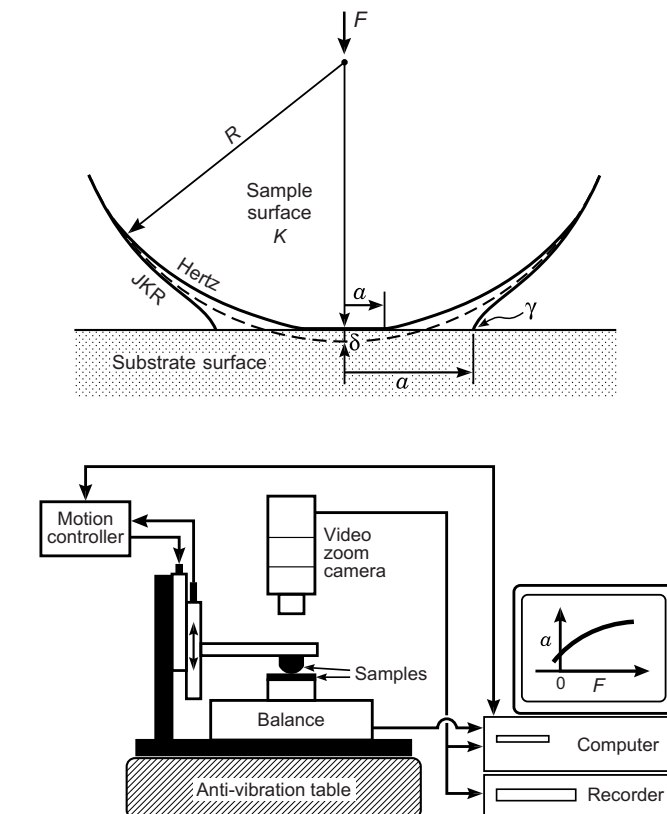


FIGURE 12.5 A JKR apparatus named after the Johnston-Kendall-Roberts theory of adhesion mechanics (Johnson et al., 1971), developed by Tirrell and coworkers (Mangipudi et al., 1995; Tirrell, 1996) to study the adhesion forces and deformations of macroscopic solids. The device allows for the measurement of the molecular contact radius a as a function of the applied load F , including negative loads. The results can then be used to test theories of adhesion and contact mechanics such as the JKR and Hertz theories (Chapter 17). This technique also enables the measurement of surface energies γ via Eq. (11.17) or Eq. (12.10).

pressure, osmotic pressure, electric or magnetic fields, buoyancy forces (weights), and fluid flow (viscous forces).

In the representative example shown in Figure 12.4, the upper particle or “tip” of local undeformed radius R is supported on a “force-measuring” spring of stiffness K defined such that a force F displaces the spring by a distance $\Delta D_S = F/K$. However, if the substrate materials have a finite stiffness K^* ,⁵ they will also deform by a finite amount δ given by $\delta = F/K^*$. Thus, we can write:

$$F = K\Delta D_S = K^*\delta. \quad (12.5)$$

⁵These materials include the surface layers of thickness T_1 and T_2 shown in Figure 12.4. For n elastic supporting materials in series, $1/K^* = 1/K_1^* + 1/K_2^* + \dots + 1/K_n^*$. In Figure 12.4 the lower substrate surface is assumed to be flat ($R = \infty$).

The preceding simple equations provide the basis for measuring the force, whether attractive or repulsive, at any surface separation so long as one can calibrate the cantilever spring stiffness K and independently measure the surface separation D (and therefore ΔD), and the spring deflection ΔD_S . The force can also be obtained from the elastic deformation of the substrate material $F = K^* \delta$, but this method is generally highly inaccurate and model-dependent: δ is usually difficult to measure, and the substrate stiffness K^* is usually not constant. However, this approach does form the basis of specialized techniques for measuring adhesion forces and the deformations associated with adhesion interactions, as shown in Figure 12.5.

With most force-measuring techniques D and ΔD_S cannot be measured directly so that other indirect but still accurate approaches have been adopted, each suited to that particular technique. In techniques where the forces are being measured with a spring the path A → H in Figure 12.4 (top right) shows the various stages of an interaction on approach and separation. When the forces are purely repulsive they take the *reversible* path A → B → C → B → H, and when they are attractive they follow the *irreversible* path A → D → E → F → G → H. The surfaces can be brought toward each other or separated by moving the lower substrate surface up or down or, equivalently,⁶ moving the base of the cantilever spring up or down by a known amount ΔD_0 . In each case, to determine the force, one tries to simultaneously measure the separation between the surfaces D and the deflection of the cantilever spring ΔD_S , and use Eq. (12.5). However, to obtain a full picture, one also needs to know the local (initial, undeformed) radius of the substrate R , its deformation during the interaction δ , the contact area πa^2 , and any other relevant factors such as changes in the adsorbed layer thicknesses, T_1 and T_2 . Note that the four displacements are related by

$$\Delta D_S = \Delta D_0 - \Delta D \pm \delta. \quad (12.6)$$

As we shall see, with some techniques the applied forces are generated, not by springs, but via some externally applied force field or pressure, which could be magnetic, electric, optical (using light pressure), flow (using liquids), or osmotic (using concentration gradients, as in the OP technique of Figure 12.2). In such cases it is sometimes only possible to measure repulsive forces, as in the OP technique, or attractive (adhesion) forces, as in the OT and SFD techniques, and various parameters such as the absolute surface separation D , local geometry, or substrate deformations may be totally inaccessible.

12.4 Measuring Force-Distance Functions, $F(D)$

The full force-law $F(D)$ between spring-supported surfaces can be measured in a number of ways. The simplest is to start with the surfaces well separated at some initial separation D where there is no detectable force between them—that is, where $F = 0$ (Fig. 12.4A). The

⁶Actually, the two processes are not equivalent. In a liquid medium, the viscous forces generated by the two motions are obviously quite different.

base of the force-measuring spring is now moved by a known (precalibrated) amount ΔD_0 to a new position where the surfaces come to equilibrium at a (new) separation D . During this process, the surface separation has changed by ΔD , the force-measuring spring has deflected by ΔD_S , and the surfaces have deformed by δ . If there is still no detectable force at D , then we shall find that $\Delta D = \Delta D_0$ and $\Delta D_S = \delta = 0$. However, if there is a finite force F at D , this force can be obtained using Eq. (12.5): $F = K\Delta D_S$, which could be attractive ($\Delta D_S < 0$) or repulsive ($\Delta D_S > 0$). The spring displacement ΔD_S may be measured directly, or by measuring the change in surface separation ΔD and substrate deformation δ (where $\delta > 0$ for compression or indentation, $\delta < 0$ for tension, extension) and then using Eq. (12.6) to get ΔD_S .

In many cases the force-measuring spring stiffness K is much weaker than the substrate stiffness δ , so that $\Delta D_S \gg \delta$. The force at D is then given by

$$F(D) = K\Delta D_S = K(\Delta D_0 - \Delta D). \quad (12.7)$$

If the initial position was at a finite force F_i and separation D_i , or if the surfaces are now moved to a new position by moving the base of the spring further by ΔD_0 , the final force F_f at D_f is given by

$$F_f(D_f) = F_i(D_i) + K(\Delta D_0 - \Delta D), \quad (12.8)$$

which reduces to Eq. (12.7) when $F_i = 0$. The above simple equations provide the basis for measuring the force, whether attractive or repulsive, at any surface separation.

With some techniques it is not possible to measure all of these parameters directly, especially the absolute separation D or ΔD , and some alternative or indirect method is then used. Often, only K and the relative displacements ΔD_0 and ΔD_S can be accurately measured. In such cases, the change in the force and surface separation after a displacement, assuming rigid surfaces ($\delta = 0$), are given by Eqs. (12.8) and (12.6):

$$D_f = D_i + \Delta D = D_i + (\Delta D_0 - \Delta D_S) \quad (12.9a)$$

and

$$F_f(D_f) = F_i(D_i) + K_S(\Delta D_0 - \Delta D) = F_i(D_i) + K_S\Delta D_S. \quad (12.9b)$$

Such techniques suffer from a lack of knowledge of the absolute separation D , and we need to assume that any adsorbed surface layers are infinitely rigid, which is rarely the case. The measurement of the absolute separation between two interacting molecules or surfaces remains the most difficult part of any force-measuring technique, and is the most problematic when comparing the results of force measurements with theory. Other serious uncertainties are the local radius R and contact area a , which are particularly important when measuring short-range and adhesion forces.

12.5 Instabilities

Measuring equilibrium forces may not always be feasible. One often encounters instabilities, where the force changes abruptly at a particular separation. This can occur when

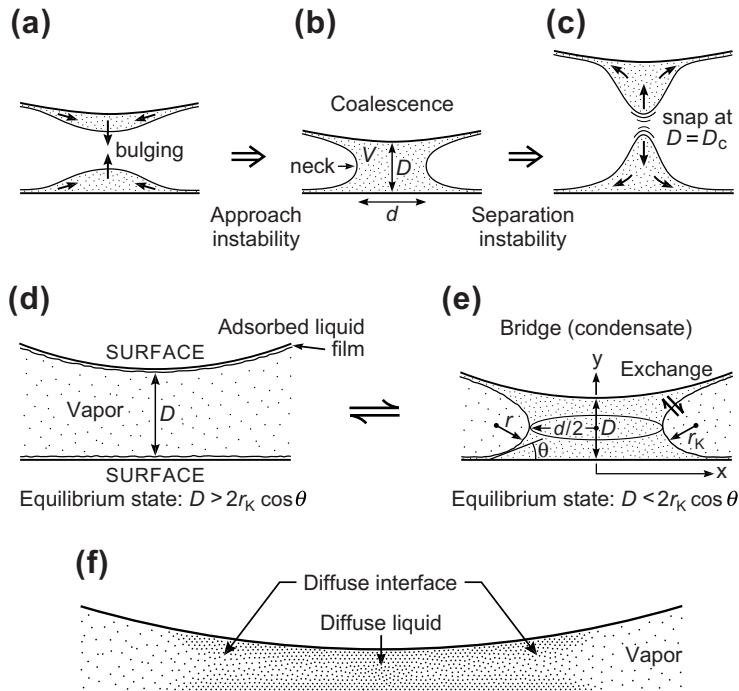


FIGURE 12.6 The different geometries of liquid bridges can give rise to instabilities in the “capillary forces” measured on approach or separation of two surfaces. Shown here are the rapid *mechanical* instabilities and slower *thermodynamic transitions* that can occur on approach (**a**→**b**) and separation (**b**→**c**) of two surfaces with a liquid film on each. At (**c**) a mechanical instability (rapid snapping) occurs at a critical distance $D_c \propto V^{1/3}$, where V is the (constant) volume of the liquid. At thermodynamic equilibrium (**d** and **e**), V is no longer constant; instead, the mean curvature of the liquid-vapor interface is now constant and equal the Kelvin radius r_K (Ch. 17). Some transitions in confined geometries and thin films can be slow and/or continuous rather than abrupt (Stroud et al., 2001).

a force-measuring spring of low stiffness K is used or when a phase transition occurs between the surfaces at a particular separation, as illustrated in Figure 12.6.

Mechanical Instabilities

The most common type of instability, illustrated in Figure 12.3a, involves an attractive force whose slope dF/dD exceeds the stiffness K of the springs holding the surfaces (or, more correctly, the overall stiffness of the whole instrument with the loading points defined by the two surfaces). For the simple force-distance curve shown in Figure 12.3a, there is an instability on approach and another on separation. Such instabilities, which depend on the net force between the two surfaces, may be referred to as *mechanical instabilities*.

Another type of mechanical instability, known as a *Rayleigh instability*, occurs when there is a liquid bridge between two surfaces (Figure 12.6b) that can snap, giving rise to an instability in the *capillary force*. It can be shown (see Section 17.11) that when the surfaces are separated to a critical distance given by $D_c \approx \pi d \approx (4\pi V)^{1/3}$, the bridge becomes

unstable and breaks up into one or two hemispherical droplets or lenses (Figure 12.6c), at which point the force between the two surfaces drops abruptly to zero.

Mechanical instabilities present problems when forces are being measured to determine the equilibrium (thermodynamic) interaction potentials which, ideally, should be measured under “ergodic” or “quasi-static” conditions—that is, infinitely slowly. Yet, no matter how slowly two bodies are brought together or separated from each other, a rapid jump will occur at an instability which cannot be avoided. The measured force at any given separation will therefore be different from the equilibrium force, and there will also be additional viscous and frictional forces (see Chapters 9, 18, and 22 for discussions on all aspects of nonequilibrium interactions).

Energetic Instabilities

As analyzed in Worked Example 17.9 and Problems 17.1 and 17.2, when two surfaces are separated, another type of instability could precede the Rayleigh instability. This instability would occur when the *energy* of one or more isolated droplets on the surfaces is less than that of the bridge, again for the same total volume of liquid. This energetic instability, however, does not occur spontaneously, as does the mechanical instability. There is usually a large activation energy between the different states, so that a “fluctuation” is needed to trigger the transition, as in the case of nucleation, and this can take a very long time.

Thermodynamic Instabilities

The preceding two cases apply to droplets of constant volume, which means that they are not in thermodynamic equilibrium with the surrounding vapor reservoir. Thermodynamic equilibrium requires that the chemical potential of the molecules in the bridge be equal to those in the vapor, which may be undersaturated, saturated, or supersaturated. This requirement, in turn, means that the surface curvature of the droplets (r_K in Figure 12.6e) must be the same everywhere at all values of D . This curvature depends on the relative vapor pressure and is given by the Kelvin Equation, Eq. (17.44). Thus, if molecules are allowed to exchange freely with the vapor, as D changes, the volume V of the bridge will also change, as will its shape. At some values of D the bridge may disappear altogether (evaporate, when D is increased) or appear (condense, when D is decreased), accompanied by a change in the capillary force between the surfaces. Again, these processes may take a long time, especially for involatile (strictly, partially volatile) liquids. Liquid bridges having different contact angles between curved surfaces are considered in Chapter 17.

12.6 Measuring Adhesion Forces and Energies

The adhesion or “pull-off” force F_{ad} needed to separate the two bodies from contact can be obtained from Eq. (12.5): $F_{ad} = K\Delta D_S$, where ΔD_S is the distance the two surfaces “jump” apart when they separate (Figure 12.4 G → H). This method is applicable even at

the microscopic or molecular levels, and it forms the basis of all direct force measuring methods that use springs for determining binding and adhesion forces. In techniques where a *constant* force is applied via, for example, a uniform external field, Eq. (12.5) does not apply, since there is no spring holding the particles. To separate the surfaces the force or field is gradually increased until, at some (known) value, the surfaces jump apart. However, there is no “jump distance”—under the influence of a constant force the particles will continue to move indefinitely.

All surfaces deform elastically when they interact regardless of whether the force between them is repulsive or attractive. The softer and larger they are, the larger is the absolute deformation. The most common type of deformation is a simple flattening, as shown in Figure 12.4E and Figure 12.5, but in general surface deformations due to interactions are much more complex, as shown in Figure 12.4G and discussed in Chapters 17 and Part III.

Only a few of these cases are currently amenable to direct observation or rigorous theoretical analysis, the primary one being the case of the forces and deformations of two elastic spherical surfaces during adhesive contact and separation. The adhesion of elastic bodies belongs to a field known as “adhesion mechanics” or “contact mechanics,” of which the central theories are the Hertz and Johnson-Kendall-Roberts (JKR) theories (Johnson, 1985), which are covered in detail in Section 17.7. The Hertz theory applies to nonadhering surfaces ($\gamma = 0$), the JKR theory to adhering surfaces (γ finite). Here we give some of the more important equations of these theories that are needed for interpreting the results of adhesion measurements using techniques such as the “JKR apparatus” shown in Figure 12.5.

The adhesion force F_{ad} between two elastic spheres of radius R_1 and R_2 is related to the *work of adhesion* W or *surface energy* ($\gamma = -\frac{1}{2}W$ for two similar materials in vacuum) by the simple relation⁷

$$F_{\text{ad}} = \frac{3}{2}\pi\bar{R}W = -3\pi\bar{R}\gamma. \quad (12.10)$$

where $\bar{R} = R_1R_2/(R_1 + R_2)$. F_{ad} is in units of N , and W and γ refer to the energies per unit area of the materials (in units of $N\text{ m}^{-1}$ or $J\text{ m}^{-2}$) as defined in Sections 10.2 and 17.1. It is interesting that the adhesion force depends on the geometry of the particles but not on their elastic modulus K . However, other relevant parameters do depend on K . Thus, for a spherical particle of radius R interacting with a flat surface, the following important relations apply (see Chapter 17):

- At zero load (normal force, $F = 0$) the contact radius a is finite and given by $a_0 = (12\pi R^2\gamma/K)^{1/3}$, and the elastic deformation of the particle’s surface is $\delta = +a_0^2/3R$ —that is, the surface is under compression. For example, for a sphere of stiffness $K = 10\text{ GPa}$ (corresponding to a hard polymer)⁸ and radius $R = 5\text{ }\mu\text{m}$ adhering to a flat surface with a surface energy of $\gamma = 30\text{ mJ m}^{-2}$, the flattened contact radius

⁷The adhesion force is also referred to as the “pull-off,” “binding,” “separation,” and “detachment” force.
⁸Table 17.2 lists the stiffnesses of some materials that are commonly encountered in force measurements.

and displacement at zero external load will be $a = 0.14 \mu\text{m}$ and $\delta = 1.3 \text{ nm}$, respectively (Fig. 12.5). Such measurements afford a way of measuring surface energies from equilibrium contact area and/or displacements measurements, in addition to the pull-off forces.

- At low loads F close to $\pm F_{\text{ad}}$, as F approaches the (negative) pull-off force the displacement δ changes from positive (compression) to negative (tension), as shown in Figures 12.4 and 17.12. Note that zero displacement ($\delta = 0$) occurs not when $F = 0$ or $a = 0$, but when $F = 0.89F_{\text{ad}}$ (a negative value) and $a = 0.76a_0$ (see Figure 17.14).
- Under a large compressive load ($F \gg |F_{\text{ad}}|$) or for low adhesion energies ($\gamma \approx 0$) the JKR and Hertz theories converge and the displacement is then given by

$$\delta = \frac{a^2}{R} = \frac{F^{2/3}}{K^{2/3}R^{1/3}} \propto F^{2/3}. \quad (12.11a)$$

and the contact area is also proportional to $F^{2/3}$:

$$\pi a^2 = \pi(RF/K)^{2/3}. \quad (12.11b)$$

Thus, the effective stiffness of a Hertzian or JKR junction, defined by $K^* = F/\delta$, is not a constant but depends on F . This also means that the deformation or “indentation” of a soft substrate surface or tip “appears” as a short-range repulsion of the form $F(D) \propto D^{3/2}$. It is often not easy to distinguish the elastic flattening of surfaces that are already in contact from a “real” repulsive force $F(D)$ acting between two separated surfaces in a liquid medium.

The issue of surface contamination by adsorbed polymers or other surface-active molecules from vapor or solution is another problem that is often difficult to detect; such “soft” contaminants can modify a surface force even at the submonolayer level. Large “hard” particles trapped between two surfaces will also modify an interaction, although these are usually easier to detect. For example, in the case of a hard particle of height H trapped between two bulk materials of elastic modulus K and adhesion energy W per unit area, the lateral extent of the elastic deformation r is given by (K. L. Johnson, private communication)

$$r = H^3(K/W)^2. \quad (12.12)$$

As an example, if a particle of height 10 nm is trapped between two surfaces having the stiffness as hard rubber ($K \approx 10^8 \text{ N m}^{-2}$) where the adhesion energy is $W = 60 \text{ mJ m}^{-2}$, we obtain: $r \approx 3 \times 10^{-6} \text{ m} = 3 \mu\text{m}$. Thus, a circle of diameter 6 μm is affected, which can be easily “seen” even with a low-powered optical microscope if one of the surfaces is transparent.

12.7 Measuring Forces between Macroscopic Surfaces: the SFA, OP/OS and Related Techniques

The first direct measurements of intermolecular forces were those of Derjaguin and coworkers (1954, 1956) who measured the attractive van der Waals forces between a convex

lens and a flat glass surface in vacuum. An electro-torsion balance was used to measure the forces and an optical technique was used to measure the distance between the two glass surfaces.⁹ Measurements were made in the distance regime 100–1,000 nm, and the results fell within 50% of the predictions of the Lifshitz theory of van der Waals forces (Chapter 13). Surface roughness prevented measurements to be made at smaller separations.

These experiments opened the way for the slow but steady progress that lead to the highly sophisticated and versatile techniques that are used today for measuring the interactions between molecularly smooth surfaces in vapors or liquids at the ångstrom resolution level. Both static (i.e., equilibrium) and dynamic (e.g., viscous) forces can now be studied with unprecedented precision providing information not only on the fundamental interactions in liquids but also into the structure of liquids adjacent to surfaces and other interfacial phenomena. In the following sections, various techniques that can directly measure the force-laws between bodies of *macroscopic*, *microscopic* (colloidal), *nanoscopic*, and *atomic* dimensions, respectively, will be described.

12.7.1 Surface Forces Apparatuses (SFA)

During the last 40 years various direct force-measuring techniques have been developed which allow for the full force-laws to be measured between two surfaces at the ångstrom resolution level. Tabor and Winterton (1969) and Israelachvili and Tabor (1972, 1973) developed apparatuses for measuring the van der Waals forces between molecularly smooth mica surfaces in air or vacuum. The results using these new techniques confirmed the predictions of the Lifshitz theory of van der Waals forces (Chapter 13) down to surface separations as small as 1.5 nm. These techniques were then further developed for making measurements in liquids, which opened up a whole world of new phenomena of relevance to a much wider spectrum of science. We shall now describe one such apparatus which has become a standard research tool in many laboratories.

Figure 12.7 shows a surface forces apparatus (SFA Mark II) with which the force between two surfaces in controlled vapors or immersed in liquids can be directly measured (Israelachvili and Adams, 1978; Israelachvili, 1987b). The normal and lateral distance resolutions are about 0.1 nm and 1 μm, respectively, and the force sensitivity is about 10^{-8} N (10^{-6} g). Modified versions have been developed by Klein (1980), Parker et al., (1989a), Israelachvili and McGuiggan (1990), Frantz et al., (1996), Restagno et al., (2002) and Israelachvili et al., (2010). Tonck et al., (1988) and Frantz et al., (1996) extended the SFA method to opaque materials, replacing the optical technique for measuring distances (see below) by a capacitance method (for reviews on the SFA technique and its applications, see Christenson, 1988; Israelachvili, 1989; Horn, 1990; Leckband, 1995; Patel and Tirrell, 1989; Claesson et al., 1996; Craig, 1997; Kumacheva, 1998; Schneider and Tirrell, 1999; Leckband and Israelachvili, 2001; Ruths and Israelachvili, 2010; Israelachvili et al., 2010).

⁹Historically, probably the first apparatus specifically designed to measure weak forces other than gravitational forces was the 1785 torsion balance of Coulomb (1736–1806) who used it to measure electrical forces.

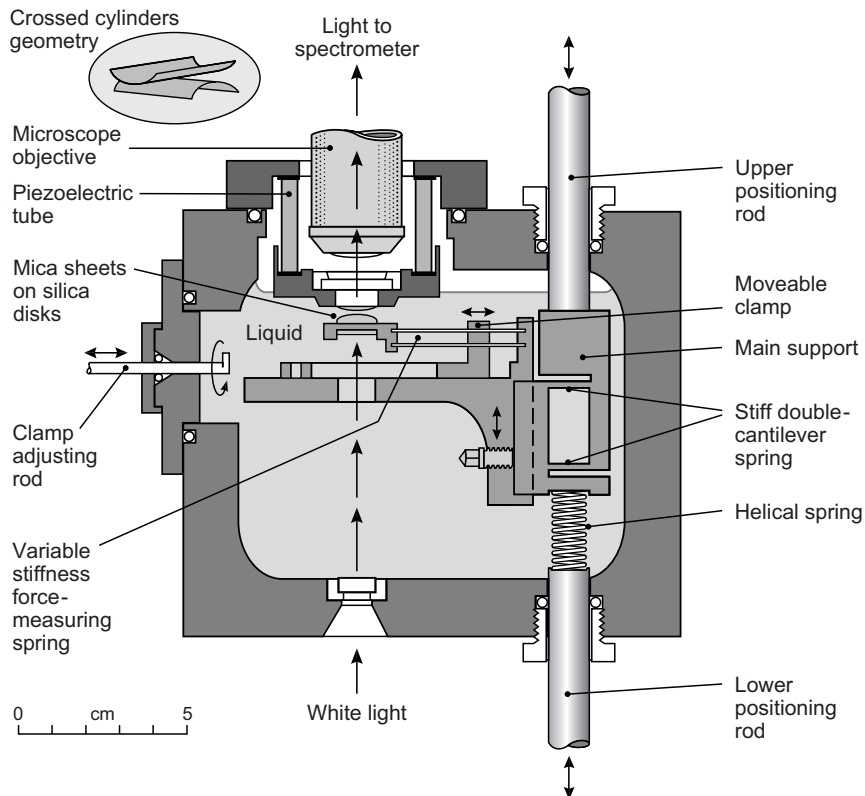


FIGURE 12.7 Surface Forces Apparatus (SFA) for directly measuring the force-laws between surfaces in liquids or vapors at the ångstrom resolution level. With the SFA technique two atomically smooth surfaces immersed in a liquid can be brought toward each other in a highly controlled way (the surface separation being controlled to 1 Å). As the surfaces approach each other, they trap a very thin film of liquid between them, and the forces between the two surfaces (across the liquid film) can be measured. In addition, the surfaces can be moved laterally past each other and the shear forces also measured during sliding. The results on many different liquids have revealed ultrathin film properties that are profoundly different from those of the bulk liquids—for example, that liquids can support both normal loads and shear stresses and that molecular relaxations can take 10^{10} times longer in a 10 Å film than in the bulk liquid. Only molecular theories, rather than continuum theories, can explain such phenomena. However, most long-range interactions are adequately explained by continuum theories.

The SFA contains two curved molecularly smooth surfaces of mica (of radius $R \approx 1$ cm) between which the interaction forces are measured using a variety of (interchangeable) force-measuring springs. The two surfaces are in a crossed cylinder configuration which is locally equivalent to a sphere near a flat surface or to two spheres close together (see Section 11.5).

In most SFA experiments, the surfaces are visualized optically with Multiple Beam Interferometry (MBI) using “fringes of equal chromatic order” (FECO) (Israelachvili, 1973a; Tolansky, 1948, 1955; Heuberger et al., 1997). From the positions of the colored FECO fringes seen in the spectrogram the thickness of adsorbed layers and the absolute distance

between the two surfaces can be measured, as can the refractive index of the medium between them. The latter allows for reasonably accurate determinations of the quantity of material—for example, lipid monolayer or polymer film, deposited or adsorbed on the surfaces. And from the *shapes* of the FECO fringes one obtains the shapes of the surfaces and of any thin film trapped between them. A great benefit of the FECO optical technique is that thermal drifts of the surfaces can be directly monitored and controlled.

While the lateral resolution is no better than that of an ordinary optical microscope, the normal resolution is 1 Å. This nevertheless allows for direct visualization of various interfacial phenomena involving extended surfaces, ranging from the contact radius a of adhering surfaces, to the surface deformations during sliding, to observing cavitation effects in thin films, to the fusion of lipid bilayers. These can be visualized as they occur through an eyepiece or recorded for later analysis.

The distance between the two surfaces is controlled by use of a three-stage mechanism of increasing sensitivity: The coarse control (upper rod) allows positioning to within about 1 μm, the medium control (lower rod, which depresses the helical spring and which in turn bends the much stiffer double-cantilever spring by 1/1000 of this amount) allows positioning to about 1 nm. Finally, a piezoelectric crystal tube—which expands or contracts vertically by about 1 nm per volt applied axially across its cylindrical wall—is used for positioning to 0.1 nm.

In a typical SFA experiment, two transparent mica sheets (each about 2 μm thick) are first coated with a semireflecting approximately 50 nm thick layer of silver before they are glued onto the curved silica disks (silvered sides down). Once in position in the apparatus, as shown in Figure 12.7, white light is passed vertically up through the two surfaces and the emerging beam is then focused onto the slit of a grating spectrometer. The beam emerging from the spectrometer can then be viewed directly through an eyepiece or recorded on a video camera as described above. The two surfaces can be brought into contact first in the absence of any surface-adsorbed species (to measure the fringe positions corresponding to $D = 0$) and then after adsorption of a layer from solution (to measure T_1 and T_2 in Figure 12.4). During subsequent force runs, the two surfaces are made to approach each other at various rates, and the interaction zone is simultaneously “observed” by monitoring the FECO fringes. This gives the separation D at any instant as well as ΔD and any deformations of the surfaces (Figure 12.4). The displacements ΔD_0 are obtained from the (known) displacements of the micrometer-piezo drives, from which ΔD_S is obtained using Eq. (12.6). This allows for the force-law $F(D)$ to be determined over any distance regime using Eq. (12.5) or (12.7).

Once the force F as a function of distance D is known for the two surfaces (of radius R), the force or energy between surfaces having a different geometry or radius can be easily deduced using Eqs (12.1)–(12.4) or some variant of the Derjaguin Approximation (Section 11.5). Furthermore, the adhesion or interfacial energy W per unit area between two flat surfaces is related to F by Eq. (12.10): $W = 2F_{\text{ad}}/3\pi R$. Thus, for $R \approx 1$ cm, and given the measuring sensitivity in F of about 10^{-8} N, the sensitivity in measuring adhesion and interfacial energies is therefore about 10^{-3} mJ m⁻² (erg/cm²). At the other extreme,

pressures as high as 0.5 GPa or 5,000 atm can be attained using stiff springs and small radius disks ($R \sim 1$ mm or less).

Over the past few years SFAs have identified and quantified most of the fundamental interactions occurring between surfaces in both aqueous solutions and nonaqueous liquids. These include the attractive van der Waals and repulsive electrostatic “double-layer” forces, oscillatory (solvation or structural) forces, repulsive hydration forces, attractive hydrophobic forces, steric interactions involving polymeric systems, viscous forces, capillary and adhesion forces, friction and lubrication forces, charge-transfer interactions, and the interactions between biological molecules such as specific ligand-receptor interactions. These forces are described in the following chapters.

Though mica, because of its molecularly smooth surface and ease of handling, is the primary surface used in SFA studies, there is currently much interest in developing alternative surfaces with different chemical and physical properties. Mica itself can be used as a substrate for adsorbing or depositing thin films of other materials such as metal or metal oxides, lipid monolayers or bilayers, polymers and proteins. Alternative materials to mica sheets can also be used, so long as they are transparent, such as sapphire (Horn et al., 1988), silica (Horn et al., 1989a; Vigil et al., 1994), and various polymer films (Mangipudi et al., 1994; Merrill et al., 1991).

A limitation of the SFA technique is its low lateral resolution. However, a tremendous advantage of the direct visualization of the contact region with FECO is that any damage of the surfaces, or undesirable particle or contamination, can be easily and immediately detected (cf. Eq. (12.12)), usually accompanied by a change in the measured force. On the other hand, the large area means that surfaces have to be extremely particle free or else these will become trapped in the contact zone; only one particle can spoil an otherwise good experiment.

Another limitation, and one currently shared with most other techniques, is that molecular composition and structure (e.g., molecular orientations) can only be inferred from the forces or FECO fringes rather than measured directly. For these reasons, it is now increasingly common to complement SFA measurements with two or more other techniques that can be used either before, during (*in situ*), or after the SFA experiments, in order to characterize the morphology and composition of the surfaces. These include various optical microscopy and spectroscopy techniques such AFM (Drummond, 2002), electron-microscopy (Bailey et al., 1990), light absorption spectroscopy (Grunewald and Helm, 1996), Second Harmonic Generation and/or Sum Frequency Generation (Frantz et al., 1996; Mamedov et al., 2002), x-ray and neutron-scattering and reflectivity for analyzing thin-film structure (Safinya et al., 1986; Golan et al., 2001), XPS or ESCA for chemical analysis (Chen et al., 1992), and Fluorescence Spectroscopy (Mukhopadhyay et al., 2002) to measure molecular-scale orientations and diffusion.

As with all other techniques, one can also compare SFA-measured forces with those obtained using other direct force-measuring techniques and/or with indirect methods for measuring interparticle interactions, such as light scattering. Indeed, in one study, excellent agreement was obtained between SFA force measurements on macroscopic

surfaces of radius $R \sim 1\text{ cm}$ with measured Second Virial Coefficients of suspended colloidal particles of radii approximately 5 nm (Gee et al., 1990a).

SFAs can take on various interchangeable attachments that allow for different types of interactions and phenomena to be studied (Israelachvili et al., 2010). These now include attachments for measuring the viscosity of liquids in very thin films (Chan and Horn, 1985; Israelachvili, 1986, 1989; Perkin et al., 2006; Cottin-Bisson et al., 2005), and friction and lubrication forces (Ruths and Israelachvili, 2010). Recent innovations have included applying electric fields or measuring the currents across films during experiments (Horn et al., 1992; Frechette and Vanderlick, 2001; Akbulut et al., 2007), and enhancing the force sensitivity and distance resolution to 0.1–0.25 Å (Frantz et al., 1996; Heuberger et al., 2001, and Zäch et al., 2003) which now allow for the fine details of a force curve to be measured at the sub-molecular level.

12.7.2 Osmotic Pressure (OP) or Osmotic Stress (OS) Techniques

In the Osmotic Stress technique (Figure 12.2) forces or, more strictly, pressures are measured between colloidal particles, clay sheets, lipid bilayers, and biological macromolecules such as viruses and DNA that form ordered colloidal structures or “arrays” in solution (Homola and Robertson, 1976; LeNeveu et al., 1976; Lyle and Tiddy, 1986; McIntosh et al., 1992a; 1992b; McIntosh, 1994; Parsegian et al., 1979; Rand and Parsegian, 1989; Leikin et al., 1993; Onsager, 1949; Podgornik et al., 1989; Rau et al., 1984). The structure of these ordered phases can be studied using x-ray and/or neutron scattering techniques (Caffrey and Bilderback, 1983; Parsegian et al., 1979; Wiener and White, 1992). This provides the mean separation between the particle surfaces as well as additional information on the thermal undulations of soft membranes or DNA bending modes.

The measurements of the mean interparticle separation D is accompanied by a measurement of the osmotic pressure P of the solution using one of three methods shown in Figure 12.2 whose suitability depend on the range of pressures under investigation. In some cases, especially when measuring the pressure between lipid bilayers, different values are obtained depending on which method is used. This has been attributed to the slow relaxation times that are needed for these systems to equilibrate or reequilibrate after a change in the solution conditions, which requires the slow diffusion of water and ions in or out a stack of semipermeable bilayers. Equilibrium values can be obtained only after long equilibration times (Katsaras, 1998), giving the osmotic pressure P as a function of the mean interbilayer separation D or the distance between linear macromolecules such as DNA. Only repulsive forces can be measured using the OP technique, and it is generally not a simple matter to extract the interaction potential $W(D)$ or force-law $F(D)$ between the particles from the measured osmotic pressure $P(D)$ of the solution since this also includes large entropic contributions. For example, for a solution containing *noninteracting* solute molecules, their osmotic pressure is given by $P = \rho RT$ where ρ is the solute number density. This repulsive pressure is large even for dilute solutions and yet arises from purely entropic effects—that is, when there is no actual force, attractive or repulsive, between the

suspended particles. In Chapter 21 we compare the results of force measurements between phospholipid bilayers using the OP and SFA techniques.

Worked Discussion Topic 12.2

Question: In a SFA (or AFM) experiment two rigid substrate surfaces, each supporting a soft, elastic membrane such as a lipid bilayer composed of molecules in the fluid state (see Figure 12.4 and 21.2) are brought together in water. There is a monotonically repulsive electrostatic or hydration pressure between the charged membrane surfaces across the water film. In a separate experiment, stacks of the same bilayers are studied using the OP technique where the spacing between the bilayer surfaces is changed by osmotic control (see Figure 12.2 and 21.5). As the surfaces come closer together in each type of experiment, will the membranes become thinner or thicker?

Answer: In the SFA experiment, as the water gap distance D falls, the bilayers are increasingly compressed due to the repulsive pressure between them. This causes them to become thinner, the excess lipid being forced out of the contact zone into the noninteracting region that acts as a “reservoir.” In the OP experiment the situation is different. The bilayer stack is fully confined within a sealed chamber (Figure 12.2) and there is no lipid reservoir. Thus, as the water is sucked out osmotically from the chamber and D falls, the system must adjust to the increasingly unfavorable (repulsive) interaction energy by a different rearrangement of its constituent molecules. Imagine that we remove the chamber from the semipermeable membrane and observe what happens as the system relaxes (while we keep it sealed at the same total volume and lipid-water volume fraction). The unfavorable energy can obviously be reduced by an increase in D . But at fixed lipid-water volume fraction this can only be achieved by having the bilayers thicken in the same proportion. Thus, the bilayers become thicker until a new equilibrium is reached where the unfavorable electrostatic and elastic energies are a minimum. If the total energy becomes too unfavorable, a phase transition to a different, nonlamellar structure may occur (see Problem 21.4).

12.8 Measuring Forces between Microscopic (Colloidal) and Nanoscopic Particles: AFM and TIRM Techniques

12.8.1 Atomic Force Microscopy (AFM)

The AFM (Figure 12.8) is in principle similar to the SFA except that forces are measured not between two macroscopic surfaces but between a fine tip and a surface (Binnig et al., 1986; Hansma et al., 1988; Rugar and Hansma, 1990). Tip radii can be as small as one atom and larger than 10 μm . Of most current interest are the smaller tips, where in principle one could directly measure the force between an individual atom or molecule and a surface, or even between two individual atoms (see Figure 1.5).

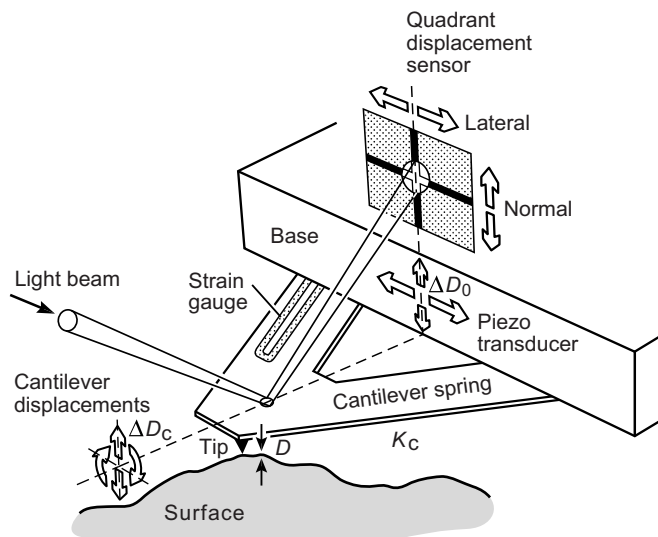


FIGURE 12.8 Atomic Force Microscope (AFM), originally designed for imaging the topology of surfaces via the forces experienced by a “tip” moving normally or laterally across the sample surface. The tip is attached to the end of the cantilever spring whose deflection ΔD_c gives the normal and/or lateral force acting on the tip. These deflections are monitored on a quadrant position sensitive detector (PSD) such as a photodiode array by following the movement of a light beam after it has bounced off the end of the cantilever surface. An XYZ piezoelectric transducer moves the tip relative to the sample surface (it can move either the cantilever spring support or the substrate surface). In some AFM instruments the “beam bouncing” detection method is replaced by resistance strain gauges attached to the cantilever arms, as shown.

As previously discussed, the adhesion force between an atomic- or molecular-sized tip and a surface should be in the range 10–3,000 pN depending on whether the bonding arises from a van der Waals bond or a covalent or ionic bond. These adhesion forces are often reduced by a factor of 10–100 in liquids. On the other hand, they would increase in linear proportion to the radius of the tip. Currently, most AFMs have a sensitivity of 1–10 pN that determines over what range different forces can be measured and the radius of the tip R necessary to measure a force at finite separations D . A whole new micro- and nano-fabrication technology has arisen devoted to fabricating nano-sharp tips and highly sensitive micron-sized scanners and force-sensing devices for AFM work¹⁰ (Binnig et al., 1986; Hansma et al., 1988; Rugar and Hansma, 1990; Cleveland, 1993). Spring stiffnesses K_c as small as 0.01 N/m can be used and displacements ΔD as small as 0.1 nm accurately measured using a variety of laser-optical sensing techniques. These determine the force sensitivity of the AFM, which is given by $(K_c)_{\min} \times (\Delta D_s)_{\min} \approx (0.01) \times (10^{-10}) = 10^{-12}$ N = 1 pN in this case.

¹⁰Atomic Force Microscopes (AFMs) come under the more general category of Scanning Probe Microscopes (SPMs) that evolved from the original Scanning Tunneling Microscope (STM) of Binnig and Rohrer (1982). Other instruments, such as the Friction Force Microscope (FFM) or Lateral Force Microscope (LFM) are more specialized instruments for measuring both normal and lateral forces.

Forces between individual molecules and small clusters of molecules have been measured using ultra-fine tips (Florin et al., 1994; Moy, 1994; Lee et al., 1994; Wong et al., 1998). These usually involve polymers and biological macromolecules, and will be described in later chapters.

Ducker et al., (1991, 1992) were the first to attach a micron-sized quartz sphere (bead) to the end of an AFM cantilever spring to measure the long-range repulsive electrostatic force (see Figure 14.16) between the sphere and a flat surface in aqueous salt solutions out to surface separations of 60 nm. This has become a standard way to fabricate tips with microscopic radii in the range 0.1–10 μm . In later chapters, comparisons will be made between forces measured using the AFM with micron-sized tips and other microscopic or macroscopic force-measuring techniques.

As its ambiguous name suggests, the Atomic Force Microscope is a tool for imaging by measuring forces, which is traditionally known as profilometry. Thus, a smooth surface that has a heterogeneous force landscape, for example, due to a distribution of charged and uncharged surface groups, cannot be easily distinguished from a bumpy surface whose molecules all interact via the same force. Interpreting the results of an AFM experiment is therefore not always straightforward. The absolute distance between the surfaces (D in Figure 12.8) which is required for obtaining a force-distance function, $F(D)$, is not directly measurable (Biggs et al., 2005). Difficulties in measuring the deformations of soft materials during an interaction, thermal drifts, and slow time-dependent interactions further complicate the interpretation of results. However, there are also advantages: due to the small radii of the tips, particulate contamination is much less of a problem, and forces can be measured quickly because hydrodynamic (viscous) forces are negligible.

12.8.2 Total Internal Reflection Microscopy (TIRM)

The forces between two colloidal particles in a liquid can be weaker than 10^{-13} g (10^{-15} N) and yet still be important in determining the properties of the system. Prieve and coworkers (Prieve, 1999; Prieve and Frej, 1990; Prieve et al., 1990) introduced a method for measuring such minute forces, specifically between a colloidal particle and a surface (Figure 12.9). Consider a particle of radius 1 μm having twice the density of water. When placed in a container of water its effective mass will be $4 \times 10^{-14} \text{ N}$ ($4 \times 10^{-12} \text{ g}$). The particle will slowly move downwards, but if there is a repulsive force between it and the bottom surface of the container it will come to equilibrium at some finite distance D_0 from the surface. In Chapters 13–16 we shall see that repulsive forces of this magnitude can easily arise from long-range van der Waals, electrostatic and polymer-mediated interactions in liquids. Thus, the equilibrium surface separation D_0 could be many tens of nanometers although the particle will generally execute large Brownian motion about D_0 , which is therefore more of a mean than an exact value (see Problem 12.5).

The technique developed by Prieve and coworkers uses total internal reflection microscopy (TIRM) for measuring the distance between an individual colloidal particle of

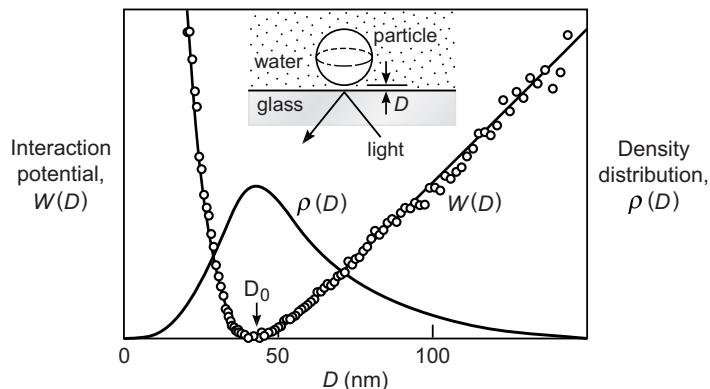


FIGURE 12.9 Measuring repulsive colloidal forces with the Total Internal Reflection Microscopy (TIRM) technique. Measured density distribution $\rho(D)$ and corresponding potential energy profile $W(D)$ for $10\text{ }\mu\text{m}$ polystyrene sphere near a glass surface in a 1 mM NaCl solution (Prieve and Frej, 1990; Prieve et al., 1990). The steep repulsion close in is due to the “double-layer” interaction (Chapter 14); the linear attraction farther out is due to the gravitational potential. Note that there is no real *equilibrium separation* between the sphere and the surface, only a distribution of distances about the mean distance, D_0 . This “distribution” defines the thermodynamic equilibrium state of the particle.

diameter approximately $10\text{ }\mu\text{m}$ hovering over a surface (Figure 12.9). The surface is usually made of transparent glass, and a laser beam is directed at the particle from below. From the intensity of the reflected beam one can record the motion of the particle about its mean separation D_0 in real time to an accuracy of about 5 nm . By analyzing how the reflected light intensity varies with space and time, the time-averaged spatial distribution function $\rho(D)$, which gives the distances sampled on either side of the equilibrium distance, is obtained. From the distribution function, one can determine the interaction potential $W(D)$ or force-law $F(D)$ on either side of the equilibrium distance. The TIRM technique provides data on a variety of interparticle interactions under conditions that closely reproduce those occurring in colloidal dispersions.

More recently, radiation pressure has also been used to modulate the force acting on the colloidal particle (Prieve, 1999). Closely related to the TIRM technique is the Reflectance Interference Contrast Microscopy (RICM) technique for studying membrane-substrate interactions involving large flexible (thermally mobile) surfaces such as those of giant lipid bilayer vesicles and biological cells. The RICM technique is described in Chapter 21.

12.9 Measuring Single-Molecule and Single-Bond Interactions: OT and MC Techniques

12.9.1 Optical Tweezers or Optical Trapping (OT)

Optical trapping employs radiation pressure via gradients in light intensity to generate a force on a “functionalized” or “derivatized” particle, viz., a particle to which specific

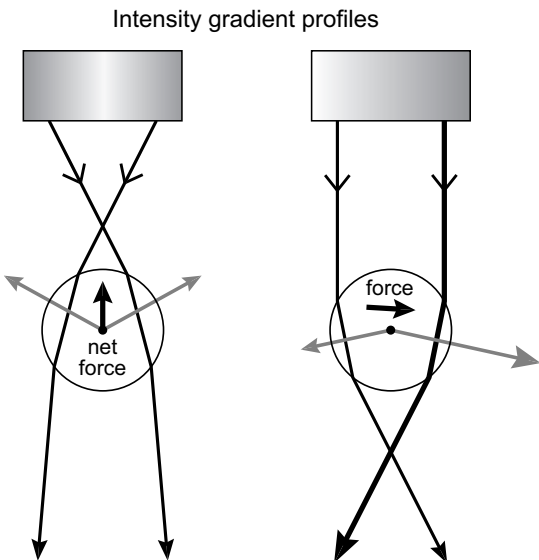


FIGURE 12.10 Optical Tweezers or Optical Trapping. The two ray optics diagrams illustrate the different ways used to generate optical forces on a dielectric sphere using focused beams. (a) When a laser beam is focused slightly above or below the center of the particle, it pulls the particle upward or downward ($\pm z$ direction) into the focal point or “trap.” (b) A light beam that also has a lateral intensity gradient shifts the particle in the x-y plane as well. If the refractive index of the particle is less than that of the medium, the forces are in the opposite direction. Radiation pressure also contributes to the net force on the particle, even for collimated beams. [Adapted from Svoboda and Block (1994).]

molecules or molecular groups have been attached. The force drives the particle toward the region of highest intensity, for example, toward a charge (cf. Figure 5.2) or the focal point of a laser beam (Figure 12.10). The use of optical traps or “tweezers” to manipulate small particles was first demonstrated in 1986 (Chu et al., 1986; Ashkin et al., 1986, 1987; Ashkin, 1992) and rapidly developed as a powerful technique for studying mainly biological interactions (Block, 1992; Sterba and Sheetz, 1998; Svoboda and Block, 1994). As shown in Figure 12.10, three-dimensional light intensity gradients are used to manipulate the position of a particle or to pull or push it against another derivatized particle. The practical range of applied forces is from one to hundreds of piconewtons, the high end being determined by the amount of heating that can be tolerated.

In more recent designs (Visscher et al., 1996; Dai and Sheetz, 1999; Gijs et al., 2000), the position of the particle is also monitored by recording the deflection of the laser beam, similar to the approach used in AFM measurements. In this way, ~ 1 nm displacements can be measured, and force-distance profiles $F(D)$ obtained, although the absolute value of D is usually not known. A distinct advantage of optical trapping techniques is the high degree of control one has over the applied force, which can be rapidly increased or abruptly terminated, and where loading and unloading rates can be easily changed. This facility gives the tweezers perhaps the best time-dependent control of the forces between small particles.

Optical trapping experiments have been mainly devoted to studying the interactions of polymers and biological molecules, for example, biopolymer stretching forces and the traction forces of “motor” proteins, which are described in Chapters 21 and 22.

12.9.2 Micro Cantilever (MC)

The Microfiber Cantilever (Essavaz-Roulet et al., 1997; Schmitz et al., 2000) operates on a similar principle to the AFM (Figure 12.8) where a thin glass fiber replaces the cantilever spring *and* probe tip of the AFM. The fiber is usually derivatized with a molecule of interest, and is brought into contact with a bead or particle that has also been specifically functionalized. The bead is then retracted, and the fiber deflects in proportion to the force exerted by the bead. As in SFA and AFM measurements, the adhesion force is determined from the deflection (jump distance) of the fiber ΔD_S when the bond breaks according to Eq. (12.5). The location of the fiber relative to the bead is visualized by optical microscopy to an accuracy of about 1 μm . Fiber stiffnesses are typically very low, of order $K_S \approx 10^{-5}$ N/m, which determines the force sensitivity of $K_S \Delta D_S \approx 10^{-5} \times 10^{-6} \approx 10^{-11}$ N or about 10 pN, which is similar to that of the AFM, but neither the absolute intersurface distance D nor the local geometry of the contact site R is usually known.

As with the OT technique, the MC technique has been mainly used to measure biomolecular bond strengths and the traction forces exerted by motor proteins and migrating cells. It has also been used for making “dynamic” force measurements, for example, investigating the dynamics of bio-specific receptor-ligand bonds by varying the pulling rate or time, as previously discussed in Chapter 9. These, too, are further described in Chapter 21.

PROBLEMS AND DISCUSSION TOPICS

- 12.1** In SFA and AFM experiments where two attracting surfaces are slowly brought toward each other, the force-measuring cantilever spring deflects before the jump-in instability (Figure 12.3a). Consider an attractive force-law of the type $F(D) = -C/D^n$. If the spring deflects by ΔD_S to the point where the surfaces jump into contact, and if the jump in distance is D_J , show that $D_J/\Delta D_S = -n$.
- 12.2** The pair potential of two atoms consists of an attractive van der Waals term with a coefficient of $C = 10^{-77}$ J m⁶, and a hard-wall repulsion at $r = 0.2$ nm. What is the adhesion force between (i) an atom and a flat solid surface, and (ii) a solid sphere of radius $R = 100$ nm and a flat solid surface? Compare the adhesion forces (calculated at $D = r = 0.2$ nm) with the forces when the surfaces are at $D = 2.0$ nm from each other. Each solid may be assumed to be composed of the same atoms of diameter σ at their maximum (close packed) density.

If in each of the above cases the atom or sphere is suspended from a spring of stiffness $K = 0.1$ N/m that is slowly brought down toward the surface, calculate (i) the gap distance, D_J , at which the atom (or sphere) will spontaneously “jump” into

contact with the flat surface, (ii) the attractive force and deflection of the spring ΔD_s just before the jump at $D = D_j$, and (iii) the adhesion force and distance the surfaces jump apart on separation.

In a particular type of AFM experiment the atom or sphere are attached to the end of a long elastic “tip” (Figure 12.8), and the jump distance D_j is assumed to be the same as the deflection of the cantilever spring between the start and end of a jump. Will this assumption overestimate or underestimate the real jump-in distance between the two surfaces? Consider the following effects: soft sphere, stiff tip; stiff sphere, soft tip; surfaces covered with a thin adsorbed layer of water; rough surfaces.

- 12.3** Each surface atom of a solid is held to the bulk material by a Lennard-Jones (L-J) potential, Eq. (1.7), with parameters $A = 10^{-77} \text{ J m}^6$ and $B = 10^{-134} \text{ J m}^{12}$. The bulk material is totally rigid—that is, of infinite stiffness. Two such surfaces are brought together. If each surface atom is commensurate and interacts with the opposing surface via the same L-J potential, (i) will the two surfaces come into contact equilibrium (i.e., merge into one continuous material) smoothly or via instability jumps of the surface atoms? (ii) If there are two layers of L-J atoms at each surface instead of one, over what range of surface separations D (where $D = 0$ corresponds to the separation when the two surfaces are in contact equilibrium) will there be no stable equilibrium (see Figure 12.3a)? (iii) What are the implications of your results for the gap width and geometry of cracks in solid materials? [Answer to (i): Via instability jumps. First calculate the maximum slope of the force-distance curve and then show that it is greater than the effective “spring constant” of $k = 7.1 \text{ N m}^{-1}$ arising from the two van der Waals bonds (see Worked Example 1.2 and Problem 1.5).]
- 12.4** The four most common geometries for measuring the forces between microscopic or macroscopic surfaces are: a sphere and a flat surface, two spheres, two crossed cylinders, and two flat parallel surfaces. Discuss the experimental advantages and disadvantages of each of these geometries, and give one realistic example where each is the most convenient or appropriate geometry to use for a particular system or type of information required.
- 12.5** Glass surfaces usually become negatively charged in water, acquiring a surface charge density of one electron charge per 10 nm^2 (one charge per $1,000 \text{ \AA}^2$). Small glass spheres of radius $R = 10 \mu\text{m}$ are placed in a 1 mM NaCl aqueous solution in a glass beaker at 25°C . In Problem 14.9, it is found that this gives rise to a repulsive interaction energy of $W(D) = +5.8 \times 10^{-16} e^{-D/9.61} \text{ J}$, where D is in nm. Estimate the mean separation at which the spheres will settle (execute Brownian motion) above the flat surface of the beaker. Assume a density of 3 gm/cm^3 for the spheres. Plot the density distribution function $\rho(D)$ of the spheres about their mean positions, as illustrated in Figure 12.9. Measuring this distribution is the basis of the TIRM force-measuring technique described in Section 12.8.2. [Answer: the mean separation is 63.4 nm , and the distribution has a half-width of about 2 nm .]

- 12.6** In a particular experiment forces were measured between two surfaces at separations from $D = 1$ to 100 nm. The data points show a monotonically decreasing (but not linear) repulsion with increasing D from $F = 100$ to 1 nN. The scatter (random error) is about $\pm 10\%$ in both F and D for each data point. How would you establish whether the force-law is a power law of the type $F(D) = C/D^n$ or $F(D) = C/(D - D_0)^n$ or an exponential $F(D) = Ce^{-D/D_0}$, and how would you determine the constants C , n , and D_0 ? You may illustrate your answer with graphical plots of imaginary data.
[Suggestion: Plot your “data” on linear, semilog, and log-log plots.]
- 12.7** Many force-measuring techniques involve particles or substrate surfaces suspended from a spring immersed in a liquid medium. Imagine such a particle initially suspended in a pure liquid. Some polymer is added to the liquid which adsorbs to the particle’s surface. The adsorption is “weak” in the sense that (i) the “coverage” is low—the adsorbed polymer coils remain well-separated from each other, and (ii) only 10% of the segments are actually bound to the surface at any time—the remaining 90% are “floating” in the solvent like seaweed. Will the changed weight of the substrate after the adsorption be determined by the 10% of surface-bound segments or by the full 100% of adsorbed polymer molecules? What other effects does the fraction of bound-to-unbound segments have on the effective (measured) weight or inertia of a suspended body?

Van der Waals Forces between Particles and Surfaces

13.1 Van der Waals Force-Laws for Bodies of Different Geometries: the Hamaker Constant

As we saw in Part I, van der Waals forces play a central role in all phenomena involving intermolecular forces, for while they are not as strong as Coulombic or H-bonding interactions, they are always present and can be important both at small and large separations. Let us begin by deriving the van der Waals interaction energies in a vacuum for pairs of bodies of different geometries. Starting at the simplest level, we shall assume that the interaction is *nonretarded* and *additive*. In Chapter 11 we saw that for an interatomic van der Waals pair potential of the form $w(r) = -C/r^6$, one may sum (integrate) the energies of all the atoms in one body with all the atoms in the other and thus obtain the “two-body” potential for an atom near a surface (Eq. 11.2), for a sphere near a surface (Eq. 11.5), or for two flat surfaces (Eq. 11.8). This procedure can be carried out for other geometries as well (cf. Problems 11.3 and 11.4). The resulting interaction laws for some common geometries are shown in Figure 13.1, given in terms of the conventional *Hamaker constant*

$$A = \pi^2 C \rho_1 \rho_2 \quad (13.1)$$

after Hamaker¹ (1937), who together with Bradley (1932), Derjaguin (1934), and de Boer (1936), did much of the earlier work that advanced understanding of the forces between macroscopic bodies.

Typical values for the Hamaker constants of condensed phases, whether solid or liquid, are about 10^{-19} J for interactions in *a vacuum*. For example, if each body is composed of atoms for which $C = 10^{-77}$ J m⁶ (cf. Table 6.1) and of number density $\rho = 3 \times 10^{28}$ m⁻³ (corresponding to atoms of radius ~0.2 nm), the Hamaker constant is

$$A = \pi^2 10^{-77} (3 \times 10^{28})^2 \approx 10^{-19} \text{ J (100 zJ or } 10^{-12} \text{ erg)}.$$

Let us consider three cases more specifically. First, for hydrocarbons, treating them as an assembly of CH₂ groups, we have $C \approx 5 \times 10^{-78}$ J m⁶ and $\rho = 3.3 \times 10^{28}$ m⁻³ per CH₂ group, from which we obtain $A \approx 5 \times 10^{-20}$ J. This is shown below, together with similarly calculated values for carbon tetrachloride and water.

¹Many years after the Second World War, Hamaker, who had left science long before, accidentally discovered that he was famous.

Table 13.1 Hamaker Constants Determined from Pairwise Additivity, Eq. (13.1)

Medium	VDW Constant, $C (10^{-79} \text{ J m}^6)$	Density of Atoms, $\rho (10^{28} \text{ m}^{-3})$	Hamaker Constant, $A = \pi^2 C \rho^2 (10^{-19} \text{ J})$
Hydrocarbon	50	3.3	0.5
CCl ₄	1500	0.6	0.5
H ₂ O	140	3.3	1.5

Note that all three Hamaker constants are similar even though the media are composed of molecules differing greatly in polarizability and size. This is not a coincidence. It arises because the coefficient C in the interatomic pair potential is roughly proportional to the square of the polarizability α , which in turn is roughly proportional to the volume v of an atom (Section 5.1). And since $\rho \propto 1/v$, we see that $A \propto Cp^2 \propto \alpha^2 \rho^2 \propto v^2/v^2 \propto \text{constant}$. Of course, this is a gross oversimplification; nevertheless, the Hamaker constants of most condensed phases *are* found to lie in the range $(0.4 - 4) \times 10^{-19} \text{ J}$.

13.2 Strength of Van der Waals Forces between Bodies in a Vacuum or Air

Taking $A = 10^{-19} \text{ J}$ as a typical value, we can now estimate the strength of the van der Waals interaction between macroscopic bodies in a vacuum (or air). Thus, for two spheres of radius $R = 1 \text{ cm} = 10^{-2} \text{ m}$ in contact at $D \approx 0.2 \text{ nm}$, their adhesion force will be

$$\begin{aligned} F &= -AR/12D^2 = -(10^{-19} \times 10^{-2})/12(2 \times 10^{-10})^2 \\ &= -2 \times 10^{-3} \text{ N (or } 0.2 \text{ g)} \end{aligned}$$

while at $D = 10 \text{ nm}$ the force will have fallen by a factor of 2500 to about 10^{-6} N , or 0.1 mg. Note that these forces are easily measurable using conventional methods.²

Turning now to the interaction *energy*, at $D = 10 \text{ nm}$, the energy is $-AR/12D \approx -10^{-14} \text{ J}$, or about $2 \times 10^6 \text{ kJ}$, and even for particles with radii as small as $R = 20 \text{ nm}$ their energy exceeds kT at $D = 10 \text{ nm}$.

For two planar surfaces in contact ($D \approx 0.2 \text{ nm}$), the adhesive pressure will be

$$P = -A/6\pi D^3 \approx -7 \times 10^8 \text{ N m}^{-2} \approx 7000 \text{ atm},$$

while at $D = 10 \text{ nm}$ the pressure is reduced by a factor of about 10^5 to a still-significant 0.05 atm. At contact the *adhesion energy* will be $-A/12\pi D^2 \approx -66 \text{ mJ m}^{-2}$, which corresponds to a surface energy of $\gamma = -\frac{1}{2}W = 33 \text{ mJ m}^{-2}$. This is exactly of the order expected for the surface energies and tensions of van der Waals solids and liquids, discussed later. We see, therefore, that the van der Waals interaction between macroscopic particles and surfaces is large, and not only when the bodies are in contact. Later we shall

²Indeed, they were already being measured in the 1930s, and the results appeared to “agree” with the theoretical predictions. However, we now know that the glass surfaces used were rough, and that what was being measured were *capillary forces* that are of similar magnitude (see Section 17.11).

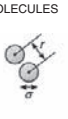
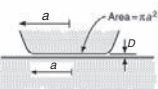
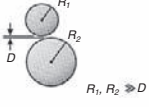
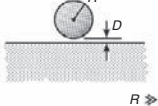
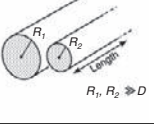
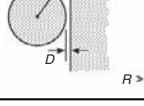
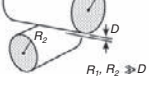
Geometry of bodies with surfaces D apart ($D \ll R$)		Van der Waals Interaction*	
		Force, $F = -dW/dD$	
Two atoms or small molecules	TWO ATOMS or SMALL MOLECULES  $r \gg \alpha$	$-C/r^6$	$-6C/r^7$
Two flat surfaces (per unit area)	TWO FLAT SURFACES  $r \gg D$	$W_{\text{flat}} = -A/12\pi D^2$	$-A/6\pi D^3$
Two spheres or macromolecules of radii R_1 and R_2	TWO SPHERES  $R_1, R_2 \gg D$	$\frac{-A}{6D} \left(\frac{R_1 R_2}{R_1 + R_2} \right)$	$\frac{-A}{6D^2} \left(\frac{R_1 R_2}{R_1 + R_2} \right)$ Also $F = 2\pi \left(\frac{R_1 R_2}{R_1 + R_2} \right) W_{\text{flat}}$
Sphere or macromolecule of radius R near a flat surface	SPHERE ON FLAT  $R \gg D$	$-AR/6D$	$-AR/6D^2$ Also $F = 2\pi R W_{\text{flat}}$
Two parallel cylinders or rods of radii R_1 and R_2 (per unit length)	TWO PARALLEL CYLINDERS  $R_1, R_2 \gg D$	$\frac{-A}{12\sqrt{2}D^{3/2}} \left(\frac{R_1 R_2}{R_1 + R_2} \right)^{1/2}$	$\frac{-A}{8\sqrt{2}D^{5/2}} \left(\frac{R_1 R_2}{R_1 + R_2} \right)^{1/2}$
Cylinder of radius R near a flat surface (per unit length)	CYLINDER ON FLAT  $R \gg D$	$\frac{-A\sqrt{R}}{12\sqrt{2}D^{3/2}}$	$\frac{-A\sqrt{R}}{8\sqrt{2}D^{5/2}}$
Two cylinders or filaments of radii R_1 and R_2 crossed at 90°	CROSSED CYLINDERS  $R_1, R_2 \gg D$	$\frac{-A\sqrt{R_1 R_2}}{6D}$	$\frac{-A\sqrt{R_1 R_2}}{6D^2}$ Also $F = 2\pi\sqrt{R_1 R_2} W_{\text{flat}}$

FIGURE 13.1 Van der Waals interaction energy W and force F between macroscopic bodies of different geometries in terms of their Hamaker Constant, A . Negative F implies attraction (A positive); positive F means repulsion (A negative). The Hamaker constant A is defined as $A = \pi^2 C \rho_1 \rho_2$ where ρ_1 and ρ_2 are the number of atoms per unit volume in the two bodies and C is the coefficient in the atom-atom pair potential (top row). More rigorous methods for calculating Hamaker constants are described in Sections 13.4 and 13.5. For other geometries, see Parsegian (2006).

see that in a medium the interaction strength is reduced by about an order of magnitude and that under certain conditions it can become repulsive.

The geometries shown in Figure 13.1 are the most common ones encountered in practice, but there are also cases where the sizes of the particles are comparable to their separation—that is, when the assumption that $D \ll R$ is not valid. The most common situation involves two spheres of radii R_1 and R_2 whose surfaces are separated by a distance D . This geometry was first considered by Hamaker (1937) who derived the following general equation for the nonretarded van der Waals interaction valid at *all* separations:

$$W(D) = -\frac{A}{6} \left\{ \frac{2R_1 R_2}{(2R_1 + 2R_2 + D)D} + \frac{2R_1 R_2}{(2R_1 + D)(2R_2 + D)} + \ln \frac{(2R_1 + 2R_2 + D)D}{(2R_1 + D)(2R_2 + D)} \right\}. \quad (13.2)$$

One may readily verify (cf. Problem 13.3) that in the various limits of large or small R_1 and R_2 relative to each other and to D , Eq. (13.2) simplifies to the expressions for two spheres close together ($W \propto -1/D$), a sphere near a flat surface ($W \propto -2/D$), a sphere far from a flat surface ($W \propto -1/D^3$), or two spheres far apart ($W \propto -1/D^6$). In the latter case one obtains

$$W(D) = -\frac{16AR_1^3 R_2^3}{9D^6} = -\left(\frac{4}{3}\pi R_1^3 \rho_1\right)\left(\frac{4}{3}\pi R_2^3 \rho_2\right)\frac{C}{D^6} = -\frac{n_1 n_2 C}{D^6}, \quad (13.3)$$

which is the London equation for two molecules (or small particles or “nanoparticles”)³ consisting of $n_1 = \frac{4}{3}\pi R_1^3 \rho_1$ and $n_2 = \frac{4}{3}\pi R_2^3 \rho_2$ atoms (or molecules), respectively. For two identical spheres close together, the Hamaker equation shows that at a separation D equal to only 1% of R the van der Waals interaction energy is already ~10% less than the short-distance limit given by $W(D) = -AR/12D$. In other words, the various limiting equations of Figure 13.1 for macroscopic bodies are strictly correct only for values of D very much smaller than R ($D < R/100$).

13.3 The Lifshitz Theory of Van der Waals Forces

The assumptions of simple pairwise additivity inherent in the formulae of Figure 13.1 and the definition of A of Eq. (13.1) ignore the influence of neighboring atoms on the interaction between any pair of atoms. First, as we saw in Section 5.8 the effective polarizability of an atom changes when it is surrounded by other atoms. Second, recalling our earlier simple model of the dispersion interaction between two Bohr atoms 1 and 2, if a third atom 3 is present, it too will be polarized by the instantaneous field of atom 1, and its induced dipole field will also act on atom 2. Thus, the field from atom 1 reaches atom 2 both directly and by reflection from atom 3 (see Figure 6.5). The existence of multiple reflections and the extra force terms to which they give rise is a further instance where straightforward additivity breaks down, and the matter becomes very complicated when many atoms are present (see Problem 6.4). In rarefied media (gases) these effects are small, and the assumptions of

³See footnote 2 in Chapter 11. See Pacheco and Ekardt (1992) for simple expressions and computed values for the coefficient C in Eq. (13.3) for metal atoms and small metal clusters.

additivity hold, but this is not the case for condensed media. Further, the additivity approach cannot be readily extended to bodies interacting in a medium.

The problem of additivity is completely avoided in the *Lifshitz theory*, where the atomic structure is ignored and the forces between large bodies, now treated as continuous media, are derived in terms of such bulk properties as their dielectric constants and refractive indices. However, before we proceed, it is well to point out that all the expressions in Figure 13.1 for the interaction energies remain unchanged even within the framework of continuum theories. The only thing that changes is the way the Hamaker constant A is calculated.

The original Lifshitz theory (Lifshitz, 1956; Dzyaloshinskii et al., 1961) requires a thorough working knowledge of quantum field theory for its understanding, and it is probably due to this that it was initially ignored by most scientists who persisted with the additivity approach of Hamaker. Later, Langbein, Ninham, Parsegian, Van Kampen, and others, showed how the essential equations could be simplified and also derived using simpler theoretical techniques (for reviews and texts see Israelachvili and Tabor, 1973; Israelachvili, 1974; Mahanty and Ninham, 1976; Hough and White, 1980; Bergström, 1997; Parsegian, 2006). Here we shall adopt the simplest of these using a modified additivity approach.

We have already seen that the van der Waals interaction is essentially electrostatic, arising from the dipole field of an atom “reflected back” by a second atom that has been polarized by this field. Let us first analyze this reflected field when the first atom is replaced by a charge Q and the second atom is replaced by a macroscopic body such as a planar surface. From Table 2.2 we know that the interaction energy of a charge with a molecule (Figure 13.2a) is given by

$$w(r) = -C/r^n = -Q^2\alpha_2/2(4\pi\epsilon_0\epsilon_3)^2r^4, \quad (13.4)$$

where α_2 is the excess polarizability of molecule 2 in medium 3. When molecule 2 is replaced by a medium (Figure 13.2b) the interaction between the charge in medium 3 and the surface

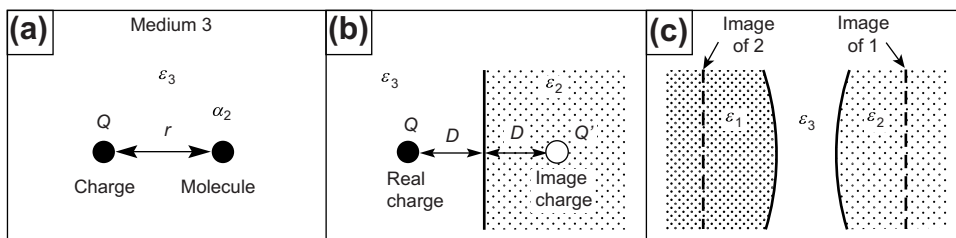


FIGURE 13.2 Image charges and image fields. (a) A charge interacts with a neutral molecule because of the field reflected by the molecule on becoming polarized. (b) Likewise, a charge interacts with a surface because of the field reflected by the surface. This reflected field is the same as if there were an ‘image’ charge Q' at a distance $2D$ from Q . Similarly, a dipole near a surface will see an image of itself reflected by the surface. If $\epsilon_2 > \epsilon_3$, the force is attractive; if $\epsilon_2 < \epsilon_3$, it is repulsive. (c) Two surfaces will see an image of each other reflected by the other surface that gives rise to the van der Waals force between them. In principle, the reflected or image fields are the same as occur when one looks at a glass surface or a mirror. Metal surfaces reflect most of the light falling on them, and the van der Waals force between metals is much stronger than that between dielectric media.

of medium 2 may be obtained by the method of additivity, Eq. (11.1), which gives $W(D) = -2\pi C\rho_2/(n-2)(n-3)D^{n-3}$. Inserting values for C and $n = 4$ from Eq. (13.4) gives

$$W(D) = -\pi Q^2 \rho_2 \alpha_2 / 2(4\pi\epsilon_0\epsilon_3)^2 D. \quad (13.5)$$

However, it is well known that a charge Q in a medium of dielectric constant ϵ_3 at a distance D from the plane surface of a second medium of dielectric constant ϵ_2 experiences a force as if there were an “image” charge of strength $-Q(\epsilon_2 - \epsilon_3)/(\epsilon_2 + \epsilon_3)$ at a distance D on the other side of the boundary—that is, at a distance $2D$ away from the real charge. This force is therefore given by

$$F(D) = \frac{-Q^2}{(4\pi\epsilon_0\epsilon_3)(2D)^2} \left(\frac{\epsilon_2 - \epsilon_3}{\epsilon_2 + \epsilon_3} \right), \quad (13.6)$$

which corresponds to an interaction energy of

$$W(D) = \frac{-Q^2}{4(4\pi\epsilon_0\epsilon_3)D} \left(\frac{\epsilon_2 - \epsilon_3}{\epsilon_2 + \epsilon_3} \right). \quad (13.7)$$

Equating Eq. (13.7) with Eq. (13.5), we immediately find that

$$\rho_2 \alpha_2 = 2\epsilon_0 \epsilon_3 (\epsilon_2 - \epsilon_3) / (\epsilon_2 + \epsilon_3). \quad (13.8)$$

This is an important result, giving the excess bulk or volume polarizability of a planar dielectric medium 2 in medium 3 in terms of the purely macroscopic properties of the media. The nonretarded Hamaker constant for the interaction of two media 1 and 2 across a third medium 3 (Figure 13.2c) may now be expressed in terms of McLachlan’s equation, Eq. (6.18), for C , and Eq. (13.8) for $\rho_1 \alpha_1$ and $\rho_2 \alpha_2$ as follows:

$$\begin{aligned} A &= \pi^2 C \rho_1 \rho_2 = \frac{6\pi^2 k T \rho_1 \rho_2}{(4\pi\epsilon_0)^2} \sum_{n=0,1,2,\dots}^{\infty} \left(\frac{\alpha_1(iv_n) \alpha_2(iv_n)}{\epsilon_3^2(iv_n)} \right) \\ &= \frac{3}{2} k T \sum_{n=0,1,2,\dots}^{\infty} \left[\frac{\epsilon_1(iv_n) - \epsilon_3(iv_n)}{\epsilon_1(iv_n) + \epsilon_3(iv_n)} \right] \left[\frac{\epsilon_2(iv_n) - \epsilon_3(iv_n)}{\epsilon_2(iv_n) + \epsilon_3(iv_n)} \right] \end{aligned} \quad (13.9)$$

Replacing the sum Σ' by the integral of Eq. (6.25), we end up with the expression for the nonretarded Hamaker constant based on the Lifshitz theory⁴

$$A \approx \frac{3}{4} k T \left(\frac{\epsilon_1 - \epsilon_3}{\epsilon_1 + \epsilon_3} \right) \left(\frac{\epsilon_2 - \epsilon_3}{\epsilon_2 + \epsilon_3} \right) + \frac{3h}{4\pi} \int_{\nu_1}^{\infty} \left(\frac{\epsilon_1(iv) - \epsilon_3(iv)}{\epsilon_1(iv) + \epsilon_3(iv)} \right) \left(\frac{\epsilon_2(iv) - \epsilon_3(iv)}{\epsilon_2(iv) + \epsilon_3(iv)} \right) d\nu, \quad (13.10)$$

where ϵ_1 , ϵ_2 , and ϵ_3 are the static dielectric constants of the three media, $\epsilon(iv)$ are the values of ϵ at imaginary frequencies, and $\nu_n = (2\pi kT/h)n = 4 \times 10^{13} n \text{ s}^{-1}$ at 300 K. The first term in Eq. (13.10) gives the zero-frequency energy of the van der Waals interaction and includes the Keesom and Debye dipolar contributions. The second term gives the dispersion energy and includes the London energy contribution. Equations (13.9) and (13.10) are not exact but are only the first terms in an infinite series for the nonretarded Hamaker constant. The other terms, however, are small and rarely contribute more than 5%.

⁴Also known as the DLP theory after Dzyaloshinskii et al., (1961).

13.4 Particle-Surface Interactions

For a spherical particle 1 of radius $R_1 = R$ near a flat surface (Figure 13.3), inserting $R_2 = \infty$ and $R_1 = R$ into the full Hamaker equation, Eq. (13.2), gives a particularly simple general expression for the force that is useful for interpreting the results of AFM and TIRM experiments where the radius R of the particle or “probe tip” may be comparable to the separation D (Argento and French, 1996):

$$F = -\frac{dW}{dD} = -\frac{2AR^3}{3(2R+D)^2D^2} \quad (13.11a)$$

which further simplifies in the limits of small and large D to:

$$F = -AR/6D^2 \text{ for } D \ll R \text{ (cf. Figure 13.1)} \quad (13.11b)$$

and

$$F = -2AR^3/3(D+R)^4 \text{ for } D \gg R, \quad (13.11c)$$

where in the latter case the effective separation distance of $(D + R)$ is from the surface to the center of the molecule or particle.

For the case shown in Figure 13.3a, A is given by Eq. (13.9) or (13.10). But if the particle or molecule 1 is in medium 2 (Figure 13.3b), we must exchange $\varepsilon_2(iv)$ and $\varepsilon_3(iv)$ in the equations for A . Equation (13.11) therefore has interesting consequences when the dielectric media 2 and 3 are liquids, or at least permeable to particle 1, for it predicts that the particle will behave in one of two ways depending on the relative values of the dielectric permittivities:

- The particle will be attracted to the interface from either side of it (e.g., if ε_1 is intermediate between ε_2 and ε_3).
- The particle will be attracted toward the interface from one side and then repelled from the other side (e.g., if $\varepsilon_1 > \varepsilon_3 > \varepsilon_2$, the particle will be driven from right to left in Figure 13.3).

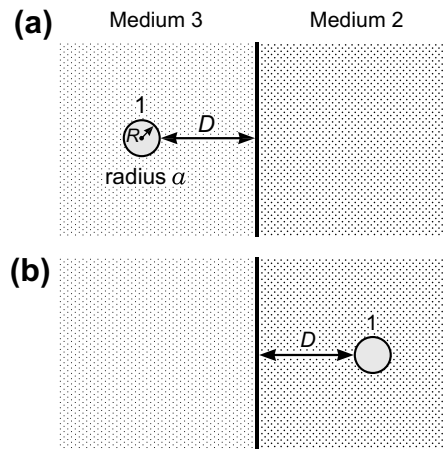


FIGURE 13.3

Thus, in the absence of constraints or other forces the van der Waals interaction alone may promote the migration of small uncharged particles across liquid interfaces. Note that repulsion from both sides of the interface never occurs. These effects are entirely analogous to those previously discussed in Section 10.4 in nonspecific terms. The application of the Lifshitz theory to explain the engulfing or rejection of particles by moving solid-liquid interfaces has been extensively studied by Van Oss et al., (1980).

13.5 Nonretarded Hamaker Constants Calculated on the Basis of the Lifshitz Theory

To obtain the Hamaker constant for any system we first need to know how the dielectric permittivity of the media vary with frequency, after which we can integrate Eq. (13.10) to obtain A . The dielectric permittivity $\varepsilon(iv)$ of a medium varies with frequency v in much the same way as does the atomic polarizability of an atom, discussed in Section 6.6. Thus, $\varepsilon(v)$ and $\varepsilon(iv)$ can usually be represented by a complex function of the form (Mahanty and Ninham, 1976; Parsegian, 2005)

$$\varepsilon(v) = 1 + \frac{\text{constant}}{(1 - iv/v_{\text{rot}})} + \frac{\text{constant}}{(1 - v^2/v_e^2)}, \quad (13.12)$$

so that $\varepsilon(iv)$ is a *real* function of v given by

$$\varepsilon(iv) = 1 + \frac{(\varepsilon - n^2)}{(1 + v/v_{\text{rot}})} + \frac{(n^2 - 1)}{(1 + v^2/v_e^2)}, \quad (13.13a)$$

$$\varepsilon(0) = 1 + (\varepsilon - n^2) + (n^2 - 1) = \varepsilon, \quad \varepsilon(\infty) = 1, \quad (13.13b)$$

where v_{rot} is the molecular rotational relaxation frequency, which is typically at microwave and lower frequencies ($v_{\text{rot}} < 10^{12} \text{ s}^{-1}$), v_e is the main electronic absorption frequency in the UV typically around $3 \times 10^{15} \text{ s}^{-1}$, and n is the refractive index of the medium in the visible—that is, $n^2 = \varepsilon_{\text{vis}}(v)$.

Since $v_1 \approx 4 \times 10^{13} \text{ s}^{-1} \gg v_{\text{rot}}$, the summation of Eq. (13.9) that gives the dispersion energy is determined solely by the electronic absorption [last term in Eq. (13.13a)]. We may therefore substitute an expression of the form

$$\varepsilon(iv) = 1 + (n^2 - 1)/(1 + v^2/v_e^2) \quad (13.14)$$

for each medium into Eq. (13.10) and integrate using the definite integral of Eq. (6.27). If the absorption frequencies of all three media are assumed to be the same, we obtain the following approximate expression for the nonretarded Hamaker constant for two macroscopic phases 1 and 2 interacting across a medium 3:

$$\begin{aligned} A_{\text{total}} &= A_{v=0} + A_{v>0} \approx \frac{3}{4} kT \left(\frac{\varepsilon_1 - \varepsilon_3}{\varepsilon_1 + \varepsilon_3} \right) \left(\frac{\varepsilon_2 - \varepsilon_3}{\varepsilon_2 + \varepsilon_3} \right) \\ &+ \frac{3h\nu_e}{8\sqrt{2}} \frac{(n_1^2 - n_3^2)(n_2^2 - n_3^2)}{(n_1^2 + n_3^2)^{1/2}(n_2^2 + n_3^2)^{1/2}\{(n_1^2 + n_3^2)^{1/2} + (n_2^2 + n_3^2)^{1/2}\}}. \end{aligned} \quad (13.15)$$

For the “symmetric case” of two identical phases 1 interacting across medium 3, Eq. (13.15) reduces to the simple expression

$$A = \frac{3}{4}kT \left(\frac{\varepsilon_1 - \varepsilon_3}{\varepsilon_1 + \varepsilon_3} \right)^2 + \frac{3h\nu_e}{16\sqrt{2}} \frac{(n_1^2 - n_3^2)^2}{(n_1^2 + n_3^2)^{3/2}}. \quad (13.16)$$

The above expressions for A apply to any of the geometries listed in Figure 13.1. Four interesting aspects of these equations may be noted:

1. The van der Waals force between two *identical* bodies in a medium is always attractive (A positive), while between *different* bodies in a medium it can be attractive or repulsive (A negative).
2. The van der Waals force between any two condensed bodies in a vacuum or air ($\varepsilon_3 = 1$ and $n_3 = 1$) is always attractive.
3. The Hamaker constant for two similar media interacting across another medium remains unchanged if the media are interchanged. Thus, if no other forces are operating, a liquid film in air will always tend to thin under the influence of the attractive van der Waals force between the two surfaces, or in other words, two air phases (or bubbles) attract each other in a liquid.
4. The dispersion energy contribution can be very high when one of the media has a high refractive index—for example, when $n_1 \gg n_3$ in Eq. (13.16), as occurs for conducting media (discussed below). However, the purely entropic zero-frequency contribution $A_{\nu=0}$ can never exceed $\frac{3}{4}kT$, or about 3×10^{-21} J at 300 K. For interactions between nonconducting (dielectric) media across a vacuum, where the dispersion energy contribution $A_{\nu>0}$ is typically $\sim 10^{-19}$ J, the zero-frequency contribution is usually small, less than 5%. But, as will be seen, for some interactions in a medium the zero-frequency contribution can dominate over the dispersion contribution.

A number of authors have given more complex analytic formulae for A when the interacting media have different absorption frequencies (Horn and Israelachvili, 1981; Parsegian, 2006), while others have described simple numerical procedures for computing Hamaker constants for media with many absorption frequencies when the more exact equation (13.9) must be used (Gregory, 1970; Pashley, 1977; Hough and White, 1980; Prieve and Russel, 1988; Bergström, 1997).

13.6 Van der Waals Forces between Conducting Media

The above analysis applies to what are normally referred to as dielectric or nonconducting media or materials. For interactions involving conducting media (including aqueous solutions), metals, semiconductors, and piezoelectric materials that have high dielectric constants or refractive indices, Eq. (13.16) would suggest that their Hamaker constant should be very high, or even infinite, as $n_1 \rightarrow \infty$. However, in such media the polarizable charges (be they electrons, protons, or free ions in solution) are not bound to a particular atom or molecule as was implicitly assumed in Chapter 5 when deriving

expressions for the electronic and dipolar polarizabilities of molecules. The freer flow of charges does give rise to higher values for α , ϵ , and n , but the expressions for these as a function of the frequency ν are also different. Thus, for metals the dielectric permittivity is given approximately by

$$\epsilon(\nu) = 1 - \nu_e^2/\nu^2, \quad (13.17)$$

so that

$$\epsilon(iv) = 1 + \nu_e^2/\nu^2, \quad \epsilon(0) = \infty \quad \text{and} \quad \epsilon(\infty) = 1, \quad (13.18)$$

where ν_e is the so-called plasma frequency of the free electron gas, typically in the range $(3\text{--}5) \times 10^{15} \text{ s}^{-1}$. Substituting the above equation in Eq. (13.10) and integrating as before, we obtain for two metals interacting across a vacuum (assuming $\nu_e \approx 4 \times 10^{15} \text{ s}^{-1}$, $h\nu_e \approx 3 \times 10^{-18} \text{ J}$)

$$A = \frac{3}{4} kT + (3/16\sqrt{2})h\nu_e \approx 4 \times 10^{-19} \text{ J}. \quad (13.19)$$

Thus, due to their high polarizability as reflected by their high dielectric constants and refractive indices, the Hamaker constants of metals can be up to an order of magnitude higher than those of nonconducting media. Note, too, that the zero-frequency temperature-dependent term contributes less than 1% to the interaction between metals.

For two metal nanoparticles (see footnote 2 in Chapter 11) separated by distances D larger than their radii a , their van der Waals interaction is expected to be given by inserting Eq. (13.19) into Eq. (13.3), which gives

$$W(D) = -\frac{C}{D^6} = -\frac{16AR^6}{9D^6} = -\frac{h\nu_e R^6}{3\sqrt{2}D^6} \approx -\frac{h\nu_e a^6 N^2}{3\sqrt{2}D^6}, \quad (13.20)$$

where N is the number of atoms per cluster. For example, for metals of atomic radii $a \approx 0.2 \text{ nm}$, the van der Waals coefficient C is predicted to be $\sim 4.5 \times 10^{-77} N^2 \text{ J m}^6$, giving $\sim 3 \times 10^{-75} \text{ J m}^6$ for $N = 8$, $\sim 2 \times 10^{-74} \text{ J m}^6$ for $N = 20$, and $\sim 7 \times 10^{-74} \text{ J m}^6$ for $N = 40$. More rigorous calculations predict values that are very similar to these—for example, $C = 3.9 \times 10^{-75} \text{ J m}^6$ for $N = 8$, and $C = 8.4 \times 10^{-74} \text{ J m}^6$ for $N = 40$ sodium atoms (Pacheco and Ekardt, 1992). Accurate experimental values are more difficult to come by, but see the list compiled by Standard and Certain (1985).

As might be expected, the strength of the van der Waals interaction between a dielectric (nonconducting) medium and a metal (conducting) medium falls somewhere in between the two symmetrical systems. The corresponding Hamaker constant can again be derived using Eq. (13.10), where $\epsilon_1(iv)$ and $\epsilon_3(iv)$ are given by Eq. (13.13) but where $\epsilon_2(iv)$ is now given by Eq. (13.17). This results in the following approximate equation (Lipkin et al., 1997):

$$A \approx \frac{3}{8\sqrt{2}} \left(\frac{n_1^2 - n_3^2}{n_1^2 + n_3^2} \right) \frac{h\sqrt{\nu_1\nu_3} \cdot \nu_2}{(\sqrt{\nu_1\nu_3} + \nu_2) / \sqrt{n_1^2 - n_3^2}}, \quad (13.21)$$

where n_1 , n_3 , ν_1 , ν_3 refer to the dielectric/ceramic material and intervening liquid, respectively, and ν_2 to the metal.

The van der Waals forces between either dielectric or conducting media at large separations, where retardation effects come in, are discussed in Section 13.10.

13.7 Theoretical and Experimental Hamaker Constants for Interactions in a Vacuum or Air

Table 13.2 gives some Hamaker constants for two identical phases interacting across a *vacuum* or air as calculated using the approximate equations derived above, putting $n_3 = \varepsilon_3 = 1$, together with more rigorously computed values. Experimentally determined values are

Table 13.2 Nonretarded Hamaker Constants for Two Identical Media Interacting in a Vacuum (Inert Air) at Room Temperature

Medium	Dielectric Constant ε	Refractive Index n	Absorption Frequency ν_e (10^{15} s^{-1})	Hamaker Constant A (10^{-20} J)		
				Eq. (13.16) $\varepsilon_3 = 1$	Exact solutions ^a	Experiment ^b
Liquid He	1.057	1.028	5.9	0.057		
Water	80	1.333	3.0	3.7	3.7–5.5	
<i>n</i> -Pentane (C_5H_{12})	1.84	1.349	3.0	3.8	3.75	
<i>n</i> -Octane	1.95	1.387	3.0	4.5	4.5	
<i>n</i> -Dodecane	2.01	1.411	3.0	5.0	5.0	
<i>n</i> -Hexadecane	2.05	1.423	2.9	5.1	5.2	
Hydrocarbon (crystal)	2.25	1.50	3.0	7.1		10
Diamond	5.66	2.375	2.6	28.9	29.6	
Cyclohexane (C_6H_{12})	2.03	1.426	2.9	5.2		
Benzene (C_6H_6)	2.28	1.501	2.1	5.0		
Carbon tetrachloride (CCl_4)	2.24	1.460	2.7	5.5		
Acetone ($(CH_3)_2CO$)	21	1.359	2.9	4.1		
Ethanol (C_2H_5OH)	26	1.361	3.0	4.2		
Polystyrene	2.55	1.557	2.3	6.5	6.6–7.9	
Polyvinyl chloride	3.2	1.527	2.9	7.5	7.8	
PTFE (Teflon)	2.1	1.359	2.9	3.8	3.8	
Silica (SiO_2)	3.8	1.448	3.2	6.3	6.5	5–6
Mica	5.4–7.0	1.60	3.0	10	7–10	13.5
CaF_2	7.4	1.427	3.8	7.0	7.0	
Silicon (Si)	11.6	3.44	0.80	18	19–21	
Silicon nitride (Si_3N_4)	8	1.98	2.45	17	17	
Silicon carbide (SiC)	10.2	2.65	1.8	25	25	
α -Alumina, sapphire (Al_2O_3)	10.1–11.6	1.75	3.2	15	15	
Zirconia ($n-ZrO_2$)	18	2.15	2.1	18	20	
Zinc sulfide (ZnS)	8.5	2.26	1.6	16	15–17	
Metals (Au, Ag, Cu)	∞	—	3–5	25–40	20–50	
				Eq. (13.19)		

^aExact solutions computed by Hough and White (1980), Parsegian and Weiss (1981), H. Christenson (1983, thesis), Velamakanni (1990, thesis), Senden et al., (1995), French et al., (1995), Bergström et al., (1996), Bergström (1997), Parsegian (2006).

^bExperimental values from Israelachvili and Tabor (1972), Derjaguin et al., (1978), and other literature sources.

also included where available. Note the good agreement between values calculated on the basis of the approximate equations and those computed more rigorously by solving the full Lifshitz equation. Note, too, the reasonably good agreement between theory and experiment. We may also compare the values of A of Table 13.2 with those obtained from a summation of additive pair potentials given in Table 13.1. Thus, for hydrocarbons and CCl_4 , the agreement is surprisingly good, but for media of high ϵ such as water the additivity approach overestimates the value of A mainly because it overestimates the zero-frequency contribution.⁵

It is important to stress that the Lifshitz theory is a continuum theory and so can only be used when the interacting surfaces are farther apart than molecular dimensions. In Sections 13.13 and 13.14 we shall investigate the applicability of the Lifshitz theory for determining short-range forces, including the adhesion energies of bodies in contact.

Worked Example 13.1

Question: A region of a charged cloud consists of spherical water droplets (aerosol particles) of radius $R = 0.5 \mu\text{m}$ each carrying $n = 100$ electronic charges of the same sign distributed evenly on their surfaces. The droplets repel each other via a Coulombic force, but they also attract via a van der Waals force with a Hamaker constant of $4 \times 10^{-20} \text{ J}$ (cf. second row of Table 13.2). (1) What is the maximum energy or “energy barrier” W_{\max} for coalescence and at what surface separation D_{\max} does it occur? (2) At what velocity v would each droplet have to be traveling to have sufficient kinetic energy to overcome this barrier?

Answer: (1) Let us initially assume that $D_{\max} \ll R$, so that the total interaction energy may be written as $W(D) = +n^2 e^2 / 4\pi\epsilon_0(2R + D) - AR/12D$, which for $R \gg D$ has a maximum at $D_{\max} = \sqrt{4\pi\epsilon_0 AR^3 / 3n^2 e^2} = 27 \text{ nm}$. This is 5% of R , at which distance the Hamaker equation, Eq. (13.2), shows that the van der Waals energy is about 30% less than given by $-AR/12D$. The more rigorously calculated distance at W_{\max} is $D_{\max} = 23 \text{ nm}$, at which distance we obtain $W_{\max} = +2.2 \times 10^{-18} \text{ J}$, which is about $530 kT$ at 298 K . Most of this energy comes from the first term in the above expression for $W(D)$. (2) If two identical droplets approach each other at velocity v , they will overcome the energy barrier if their combined kinetic energies $2(\frac{1}{2}mv^2)$ just equals W_{\max} . This gives $v = \sqrt{W_{\max}/m} = \sqrt{W_{\max}/\frac{4}{3}\pi R^3 \rho} = [(2.2 \times 10^{-18})/\frac{4}{3}\pi(0.5 \times 10^{-6})^3 \times 1000]^{1/2} = 6.5 \text{ cm/s}$. Note, however, that if one of the droplets is stationary, the velocity of the other is given by equating $\frac{1}{2}(\frac{1}{2}mv^2)$ with W_{\max} , not $\frac{1}{2}mv^2$ with W_{\max} (see Worked Example 2.4).

13.8 Applications of the Lifshitz Theory to Interactions in a Medium

The Lifshitz theory is particularly suitable for analyzing interactions in a medium. As a graphic example of this, Figure 13.4 shows how $\epsilon(iv)$ varies with frequency for water and

⁵Or, conversely, the Lifshitz theory underestimates A . This arises because of the breakdown of the Clausius-Mossotti equation, Eq. (5.30), and similar equations such as Eq. (13.8) that relate the dielectric permittivity ϵ to the molecular polarizability α . These equations suggest that even as $\epsilon \rightarrow \infty$, α can never exceed some finite value, which is unphysical.

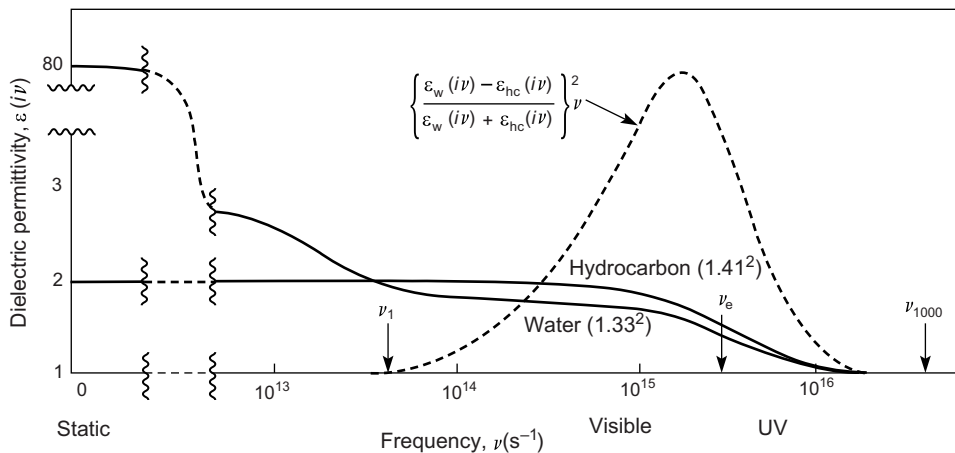


FIGURE 13.4 Dielectric permittivity $\epsilon(i\nu)$ as a function of frequency ν for water and hydrocarbon (water interacting across hydrocarbon, and vice versa). In the visible and UV range these are given by

$$\begin{aligned}\epsilon_w(i\nu) &= 1 + \left(n_w^2 - 1\right) / \left(1 + \nu^2/\nu_e^2\right), \quad n_w = 1.33, \\ \epsilon_{hc}(i\nu) &= 1 + \left(n_{hc}^2 - 1\right) / \left(1 + \nu^2/\nu_e^2\right), \quad n_{hc} = 1.41,\end{aligned}$$

where $\nu_e = 3.0 \times 10^{15} \text{ s}^{-1}$ for both. The total Hamaker constant for this system at 300 K is about $0.45 \times 10^{-20} \text{ J}$.

a typical hydrocarbon such as dodecane. Both of these liquids have roughly the same absorption frequency of about $\nu_e \approx 3.0 \times 10^{15} \text{ s}^{-1}$. The area under the dashed curve at frequencies above ν_1 is roughly proportional to the nonretarded dispersion energy of two hydrocarbon phases across a water film, for which we obtain, using Eq. (13.16),

$$A_{\nu>0} = \frac{3(6.63 \times 10^{-34})(3 \times 10^{15})}{16\sqrt{2}} \frac{(1.41^2 - 1.33^2)^2}{(1.41^2 + 1.33^2)^{3/2}} \approx 0.17 \times 10^{-20} \text{ J}.$$

Concerning the zero-frequency contribution, water exhibits strong absorptions at lower frequencies and consequently has a high static dielectric constant of $\epsilon = 80$. In contrast, the dielectric constant of hydrocarbons remains the same right down to zero-frequency, where $\epsilon = n^2 \approx 2.0$. The large difference between ϵ_w and ϵ_{hc} leads to a large zero-frequency contribution to the Hamaker constant of

$$A_{\nu=0} = \frac{3}{4}kT \left(\frac{80-2}{80+2}\right)^2 \approx 0.28 \times 10^{-20} \text{ J at 300 K},$$

giving a total value for A of $(0.28 + 0.17) \times 10^{-20} \approx 0.45 \times 10^{-20} \text{ J}$.

Thus, the interaction between hydrocarbons across water is dominated by the mainly entropic, zero-frequency contribution $A_{\nu=0}$, which is about 50% higher than the dispersion contribution $A_{\nu>0}$. Furthermore, while the total strength of the interaction is about 10% of that in a vacuum (cf. Table 13.1), the zero-frequency contribution is actually *higher* than in a vacuum.

Ninham and Parsegian (1970), Gingell and Parsegian (1972), and Hough and White (1980) considered the hydrocarbon-water system in great detail and found that the theoretical A for this system lies in the range $(4\text{--}7) \times 10^{-21}$ J depending on the refractive index of the hydrocarbon. Note that as far as van der Waals forces are concerned the interaction of hydrocarbon across water is the same as for water across hydrocarbon.

Table 13.3 Hamaker Constants for Media 1 and 2 Interacting across Medium 3 at Room Temperature

Interacting Media (Note: For Symmetrical Systems $A_{131} = A_{313}$)			Hamaker Constant A (10^{-20} J)		
1	3	2	Eq. (13.15) ^a	Exact Solutions ^b	Experiment ^c
Air (water)	Water (air)	Air (water)	3.7	3.7	
Pentane	Water	Pentane	0.28	0.34	
Octane	Water	Octane	0.36	0.4	
Dodecane	Water	Dodecane	0.44	0.4–0.5	0.5 ^d
Hexadecane	Water	Hexadecane	0.49	0.4–0.5	0.3–0.6 ^d
PTFE	Water	PTFE	0.29	0.33	
Polystyrene	Water	Polystyrene	1.4	0.95–1.3	
Water	Hydrocarbon	Water	0.3–0.5	0.34–0.54	0.3–0.9
Silica (SiO_2)	Dodecane	Silica (SiO_2)	0.07	0.10–0.15	
Fused quartz (SiO_2)	Octane	Fused quartz (SiO_2)	0.13	—	
Fused quartz	Water	Fused quartz	0.63	0.5–1.0	
Mica	Hydrocarbon	Mica	0.35–0.81	0.85	0.5–0.8
Mica	Water	Mica	2.0	1.3–2.9	2.2
α -Alumina (Al_2O_3)	Water	α -Alumina (Al_2O_3)	4.2	2.7–5.2	6.7
Silicon nitride (Si_3N_4)	Water	Silicon nitride (Si_3N_4)	8.2	5–7	
Zirconia ($n\text{-ZrO}_2$)	Water	Zirconia ($n\text{-ZrO}_2$)	13	7–9	
Silicon carbide (SiC)	Water	Silicon carbide (SiC)	21	11–13	
Ag, Au, Cu	Water	Ag, Au, Cu	—	10–40	40 (gold)
Water	Pentane	Air	0.08	0.11	
Water	Octane	Air	0.51	0.53	
Octane	Water	Air	−0.24	−0.20	
Fused quartz	Water	Air	−0.87	−1.0	
Fused quartz	Octane	Air	−0.7	—	
Fused quartz	Tetradecane	Air	−0.4	—	−0.5
Silicon nitride	Diiodomethane ^a	Fused quartz	−1.3	−0.8	"Repulsion"
CaF_2 , SrF_2	Liquid He	Vapor	−0.59	−0.59	−0.58

^aBased on dielectric data of Table 13.2, assuming mean values for ν_e . Values for diiodomethane: $\epsilon = 5.32$, $n = 1.76$, $\nu_e = 2.3 \times 10^{15} \text{ s}^{-1}$ (Meurk et al., 1997).

^bExact solutions computed by Sabisky and Anderson (1973), Hough and White (1980), Parsegian and Weiss (1981), Christenson (1983, thesis), Horn et al., (1988a), Velamakanni et al., (1990), Senden et al., (1995), Bergström et al., (1996), Bergström (1997), Parsegian (2006).

^cExperimental values from Israelachvili and Tabor (1972), Sabisky and Anderson (1973), Requena et al., (1975), Derjaguin et al., (1978), Israelachvili and Adams (1978), Lis et al., (1982), Ohshima et al., (1982), Horn et al., (1988a), Israelachvili et al., (1989), Velamakanni et al., (1990), Meurk et al., (1997), Vigil et al., (1994).

^dPure hydrocarbon-water and other hydrophobic-water interfaces experience an additional hydrophobic attraction which is fully or partially shielded when the interfaces contain hydrophilic groups, as occurs in the interactions between surfactant and lipid bilayers (see Chapters 14 and 21).

Experimental A values for hydrocarbon-water systems have been determined from studies on lipid bilayers (Table 13.3).

Table 13.3 gives some computed values of A for interactions across various media based on the Lifshitz theory, together with measured values where these are available. As can be seen, the agreement between theory and experiment is good. Note the much smaller Hamaker constants compared to those for interactions across a vacuum, especially for media of low refractive index (cf. Table 13.2). In contrast, for metals, because of their high values for ϵ and n , the high Hamaker constant in vacuum is not much affected by an intervening dielectric medium.

13.9 Repulsive Van der Waals Forces: Disjoining Pressure and Wetting Films

We have already seen in Chapter 6 how repulsive van der Waals forces can arise in a medium and again in Chapter 10 how repulsive forces in general can be understood intuitively. Equation (13.15) shows that the Hamaker constant will be negative, resulting in repulsion, whenever the dielectric properties of the intervening medium are intermediate between those of the two interacting media. Indeed, one of the early successes of the Lifshitz theory was in the quantitative explanation of the wetting properties of liquid helium due to a negative Hamaker constant (Dzyaloshinskii et al., 1961).

It is well known that liquid helium avidly spreads on almost any surface. Thus, if liquid helium is placed in a beaker, it rapidly climbs up the walls and down the other side, and eventually leaves the beaker altogether. The reason for this peculiar behavior is that the dielectric permittivity of liquid helium, $\epsilon = n^2 = 1.057$, is lower than that of any other condensed medium. Thus, there will be a negative Hamaker constant and a repulsive van der Waals force across an adsorbed liquid helium film exposed to helium vapor, which will act to thicken the film so as to lower its energy. But when liquid helium climbs up a smooth wall the gain in van der Waals energy is at the expense of gravitational energy, and so the equilibrium film thickness will decrease with height (Figure 13.5). Sabisky and Anderson (1973) measured the thickness as a function of the height of liquid helium films at 1.38 K on atomically smooth surfaces of CaF_2 , SrF_2 and BaF_2 . As the height increased the thickness decreased. Let us look at this interesting phenomenon of *wetting films* in more detail.

Consider unit area of a film of mass m , density ρ and thickness D at a height H above the flat liquid-vapor surface of Figure 13.5. The total free energy of this mass will be

$$G(D) = -\frac{A}{12\pi D^2} + mgH = -\frac{A}{12\pi D^2} + \rho g HD \quad (\text{since } m = \rho D). \quad (13.22)$$

The equilibrium film thickness at H will be given when $\partial G / \partial D = 0$ —that is,

$$A/6\pi D^3 + \rho g H = 0, \quad (13.23)$$

which gives for the thickness profile as a function of height H

$$D = (-A/6\pi\rho g H)^{1/3}. \quad (13.24)$$

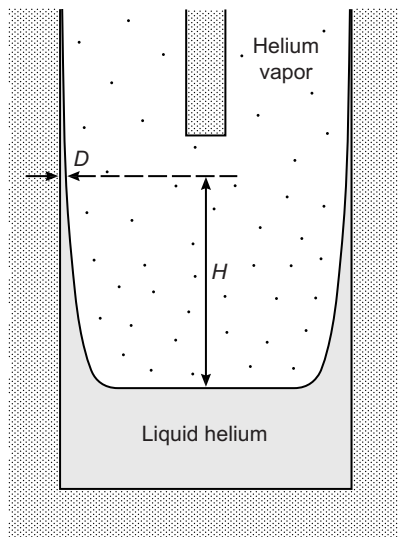


FIGURE 13.5 Liquid helium climbs up the walls of containers because of the repulsive van der Waals force across the adsorbed (or condensed) film. At equilibrium the work done against gravity mgH is balanced by the work done by the repulsive van der Waals force acting to expand or “disjoin” the film. Thermodynamic considerations, discussed in the text, show that the film will have the same thickness on a surface at the same height H even when it is not in contact with the bulk liquid, as in the case of a rod of the same material inserted into the beaker.

Equation (13.24) has solutions for positive D only when A is negative. In the case of liquid helium on a CaF_2 surface, from Table 13.3 we have $A = -5.9 \times 10^{-21} \text{ J}$, and for helium $\rho = 1.4 \times 10^2 \text{ kg m}^{-3}$. Thus, we expect for the film profile $28/\sqrt[3]{H(\text{cm})} \text{ nm}$. Sabisky and Anderson (1973) measured $D = 2.8 \text{ nm}$ at $H = 1,000 \text{ cm}$, exactly as expected. But at $H = 1 \text{ cm}$ they obtained $D = 21.5 \text{ nm}$ instead of $D = 28 \text{ nm}$. This is due to retardation, which was observed for films thicker than 6 nm.

Repulsive van der Waals forces also occur across thin liquid hydrocarbon films on alumina (Blake, 1975) and quartz (Gee et al., 1989). The thicknesses of such films were varied either by pressing a gas bubble in the liquid against the solid surface or by changing the vapor pressure above the film (see below). The measured variation of the repulsive pressure with thickness in the range 0.5–80 nm was found to be in excellent agreement with theory. Once again retardation effects are evident for films thicker than 5 nm.

Returning to Eq. (13.23), the first term is simply the repulsive van der Waals pressure across the film. In fact, we may write that equation in the more general form

$$P(D) = +\rho gH \quad (13.25)$$

which is valid for any repulsive (positive) pressure regardless of the origin of the interaction. Such a repulsive pressure $P(D)$ is often referred to as the *disjoining pressure* of a film.

It is important to appreciate that the equilibrium thickness of the helium film at any point on the surface of the beaker in Figure 13.5 does not rely on the film being in contact with the bulk liquid reservoir at the bottom of the beaker. If the surface is not in contact

with the bulk liquid, equilibrium will simply be established by condensation via the vapor (though it may take longer). This fact invites another way of looking at the equilibrium of films. Just above the flat liquid surface, the vapor pressure must be at the saturation value, p_0 , but at a height H the vapor pressure, p , will be below saturation. Now from Eq. (2.13) we have $p = p_0 e^{-\rho v g H / kT}$, so that the equilibrium condition, Eq. (13.25), may also be written as

$$P(D) = -(kT/v)\log(p/p_0) = -(RT/V)\log(p/p_0), \quad (13.26)$$

where v and V are the molecular and molar volumes, respectively, and where $P(D)$ is the repulsive pressure that can be due to any type of interaction. Since the relative vapor pressure, p/p_0 (also p/p_{sat}), can be controlled in a variety of ways (in addition to controlling the height of the film above the surface of the liquid) we see that Eq. (13.26) provides an alternative way of determining the equilibrium thicknesses of a wetting film in contact with its undersaturated vapor. Indeed, the method of “vapor pressure control” rather than “gravity control” of film thicknesses is usually far more practical, as the example below shows.



Worked Example 13.2

Question: (1) At what relative vapor pressure of *n*-octane will a 1.5 nm film adsorb on a horizontal quartz glass surface at 25°C? (2) If the same film is to be attained by having the surface placed above the bulk liquid level, what height should this be at? (3) Assuming that a curved meniscus experiences an additional *Laplace Pressure* given by the *Laplace equation*, Eq. (17.15), estimate the maximum curvature of the surface asperities that can be tolerated if the film thickness has to be uniform to within 10% of the calculated value. What other experimental parameters are crucial for this?

Answer: (1) For the quartz-octane-vapor system $A = -0.7 \times 10^{-20} \text{ J}$ (see Table 13.3). The molecular weight of octane, C₈H₁₈, is $114 \times 10^{-3} \text{ kg mol}^{-1}$, and the density of the liquid is $0.70 \times 10^3 \text{ kg m}^{-3}$. The molecular volume is obtained from Eq. (5.32) as: $v = M/\rho N_0 = (114 \times 10^{-3})/(0.70 \times 10^3)(6.02 \times 10^{23}) = 2.7 \times 10^{-28} \text{ m}^3$. Thus, to have an equilibrium film thickness of $D = 1.5 \times 10^{-9} \text{ m}$ (15 Å) at $T = 298 \text{ K}$ we require

$$\begin{aligned} p/p_0 &= \exp[-P(D)v/kT] = \exp[Av/6\pi D^3 kT] \\ &= \exp[-(0.7 \times 10^{-20})(2.7 \times 10^{-28})/6\pi(1.5 \times 10^{-9})^3(4.12 \times 10^{-21})] \\ &= 0.993 \text{ (i.e., 99.3\% of the saturated vapor pressure).} \end{aligned}$$

(2) Using equation (13.24), the height is

$$H = \frac{-A}{6\pi\rho g D^3} = \frac{(0.7 \times 10^{-20})}{6\pi(0.70 \times 10^3)(9.81)(1.5 \times 10^{-9})^3} = 16.0 \text{ m.}$$

Such a height is experimentally feasible but difficult (remember that the temperature must be kept exactly the same at both ends). To obtain even thinner films H becomes impractically large, whereas controlling the thickness via the vapor pressure actually becomes easier (why?).

(3) The van der Waals pressure across a 1.5 nm film of octane is $P(D) = -A/6\pi D^3 = +(0.7 \times 10^{-20})/6\pi(1.5 \times 10^{-9})^3 = 1.10 \times 10^5$ Pa (about 1 atm), while that across a film 10% thicker—that is, with $D = 1.65$ nm, is 0.83×10^5 Pa. The difference in pressure is $\Delta P = 0.27 \times 10^5$ Pa. From the Kelvin-Laplace equation, Eq. (17.15), such a pressure difference is established if the radius of the surface film is $r = 2\gamma/\Delta P$, where $\gamma = 22$ mJ/m² is the surface tension of octane at 25°C. Thus, if the surface has locally curved regions (asperities) of radii less than $r = 2(0.022)/(0.27 \times 10^5) = 1.6 \times 10^{-6}$ m, or 1.6 μm, the film thickness will vary from place to place by more than 10% of the mean value.

Other experimental parameters that must be carefully controlled: temperature, purity of liquid and vapor, cleanliness of surface.



Using a quartz crystal microbalance Panella and colleagues (1996) measured the equilibrium thicknesses (via the measured masses) of various adsorbed liquid films, including water, on metal surfaces as a function of the vapor pressure. They also reviewed the contradictory literature on this subject and concluded that for simple nonpolar liquids there is good quantitative agreement with the Lifshitz (DLP) theory “down to monolayer thicknesses.”

Negative Hamaker constants are also expected for water films on hydrocarbons and on quartz (see Table 13.3). Now, water does indeed wet quartz, but this is also due to the existence of other repulsive forces across the film such as electric double-layer forces (Chapter 14) and hydration forces (Chapter 15). However, water certainly does not wet hydrocarbons. This is due to the attractive *hydrophobic* force across the film, which is stronger than the repulsive van der Waals force (Chapter 15).

Repulsive van der Waals forces often occur between different types of polymers dissolved in organic solvents. Van Oss and colleagues (1980) estimated the Hamaker constants of 31 polymer pairs in different solvents. These varied from $A = +0.75 \times 10^{-20}$ J to $A = -0.38 \times 10^{-20}$ J. It was found that whenever the Hamaker constant exceeds about 0.03×10^{-20} J the polymers are immiscible with each other in the solvent, and phase separation occurs, while for $A < 0.03 \times 10^{-20}$ J, they are miscible. Another example of repulsive van der Waals forces is given below after a few words about retardation effects.

13.10 Van der Waals Forces at Large Separations: Retardation Effects

In Chapter 6 we saw that at distances beyond about 5 nm the dispersion contribution to the total van der Waals force begins to decay more rapidly due to retardation effects. For interactions between molecules, this is of little consequence. However, for interactions between macroscopic bodies, where the forces can still be significant at such large separations, the effects of retardation must often be taken into account. In the transition from nonretarded to retarded forces the dispersion force-law exponent increases from n to $n + 1$.

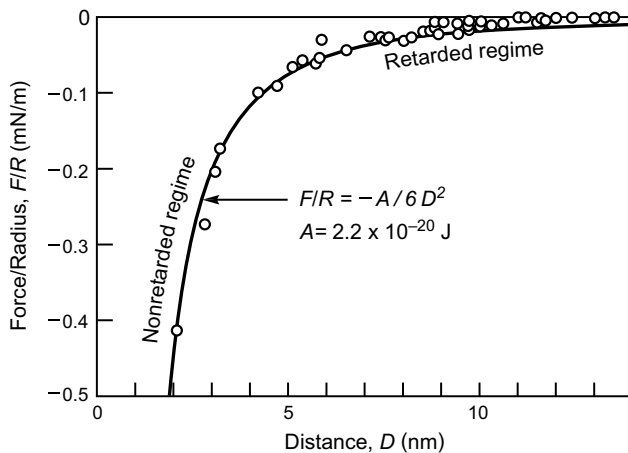


FIGURE 13.6 Attractive van der Waals force F between two curved mica surfaces of radius $R \approx 1$ cm measured in water and aqueous electrolyte solutions. The measured nonretarded Hamaker constant is $A = 2.2 \times 10^{-20}$ J. Retardation effects are apparent at distances above 5 nm where the measured forces are weaker than the extrapolated nonretarded force (solid line). [Data from SFA experiments with surfaces in the crossed-cylinder geometry, equivalent to a sphere of radius R near a flat surface or two spheres of radius $2R$, adapted from Israelachvili and Adams (1978) and Israelachvili and Pashley (unpublished).]

As an illustration of retardation effects, Figure 13.6 shows experimental results obtained for the van der Waals force law between two curved mica surfaces in aqueous electrolyte solutions (in a liquid medium such as water the full force-law also involves the electric double-layer force, so that some extrapolation and subtraction of this force must be done in order to obtain the purely van der Waals force contribution to the total interaction). For this system, the nonretarded Hamaker constant at distances below 5 nm was found to be $A = 2.2 \times 10^{-20}$ J, which is about 10% higher than the theoretical value (see Table 13.3). The experimental results clearly show the onset of retardation at separations above about 5 nm—the same distance as in the wetting film experiments described in the previous section. Strictly, however, the Hamaker constant is never truly constant at any separation but decreases progressively as D increases.⁶

While the full Lifshitz equation (Lifshitz, 1956; Dzaloshinskii et al., 1961) includes the effects of retardation, there is no *simple* equation for calculating the van der Waals force at all separations. Mahanty and Ninham (1976) and Parsegian (2006) have described numerical methods for computing the van der Waals force law at all distances by solving the full Lifshitz equation; and Gregory (1981), Russel et al., (1999) have proposed various approximate equations for dielectric media. The following equation, due to Gregory (1981), is particularly suitable for computing the dispersion Hamaker

⁶Some authors prefer to use the term “Hamaker coefficient” or “Hamaker function.”

“constant” in the transition region from nonretarded to retarded forces out to distances D of about 100 nm (the zero-frequency contribution remaining unchanged):

$$A = A_{\text{Non-ret}}/(1 + pD\nu_e/c) \approx A_{\text{Non-ret}}/(1 + pD/100 \text{ nm}), \quad (13.27)$$

where $p = 5.3$ for interactions between two planar surfaces, $p = 11$ for interactions between spheres, and $p = 14$ for the interactions between a sphere and a planar surface. For example, for two spheres, $W_{\text{disp}} \propto -1/D$ for the nonretarded force, which goes over to $W_{\text{disp}} \propto -1/D^2$ for the retarded force, the transition being half way complete at $D \approx 10$ nm in a vacuum, or less in a medium, in reasonably good agreement with the experimentally measured force (Figure 13.6).

As the separation approaches the fully retarded regime, two things happen: the inverse power-law dependence of the dispersion force increases by 1, but the zero-frequency temperature-dependent contribution remains unchanged since, as already pointed out in Section 6.9.3, it is not subject to retardation effects. Thus, retardation can have quite different effects depending on the media. For metals, where the nonretarded dispersion force is already high and well in excess of the zero-frequency contribution (cf. Eq. 13.19), the retarded dispersion force also remains high up to very large separations where, up to $D = 8 \mu\text{m}$, it dominates over the nonretarded zero-frequency contribution (see below). In contrast, for hydrocarbons interacting across water, where the short-distance nonretarded dispersion contribution is already smaller than the zero-frequency contribution (see Section 13.8), the long-range van der Waals force quickly becomes dominated by the only slightly weaker but nonretarded temperature-dependent contribution.

The fully retarded van der Waals energy between two surfaces interacting in a vacuum is given by (Lifshitz, 1956):

$$W(D) = -\frac{kT}{16\pi D^2} \left(\frac{\varepsilon - 1}{\varepsilon + 1} \right)^2 - \frac{\pi hc}{1440 D^3} \left(\frac{\varepsilon - 1}{\varepsilon + 1} \right)^2 f(\varepsilon) \quad \text{per unit area}, \quad (13.28)$$

where the first term is the normal nonretarded contribution, decaying as $1/D^2$, and where the second term decays as $1/D^3$. The function $f(\varepsilon)$ is roughly constant at $f(\varepsilon) \approx 0.35$ for $\varepsilon < 4$, and increases at higher ε , approaching 1 as $\varepsilon \rightarrow \infty$. Thus, for metals and other fully conducting media for which $\varepsilon = \infty$ the van der Waals force per unit area is

$$F(D) = -\frac{dW}{dD} = -\left(\frac{kT}{8\pi D^3} + \frac{\pi hc}{480 D^4} \right) \quad (13.29a)$$

$$= -\frac{1.64 \times 10^{-22}}{D^3} \left(1 + \frac{7.95 \times 10^{-6}}{D} \right) \text{ N m}^{-2} \text{ at } 298 \text{ K}. \quad (13.29b)$$

The second term in the above equation is the well-known Casimir equation (Casimir, 1948).⁷ For metals, therefore, the retarded dispersion force dominates the interaction out

⁷The Casimir theory preceded the Lifshitz theory, but the full Lifshitz theory includes the so-called *Casimir force*, which emerges naturally from it in certain limits.

to distances of approximately 10 μm , beyond which the interaction becomes once again “nonretarded.”

Retarded van der Waals forces have been measured between mica, glass, and metal surfaces in air or a vacuum out to distances of 1.2 μm (1200 nm), all in good agreement with the full Lifshitz theory. Indeed, the first direct measurements of van der Waals forces by Derjaguin and Abrikossova (1954) were of retarded forces between two quartz glass surfaces in the distance range 100–400 nm. More recently, the Casimir force between a 200 μm diameter metal sphere and a flat metal surface (see Problem 13.16) was measured by Mohideen and Roy (1998), the results agreeing excellently with theory over the distance regime from ~ 0.1 to $\sim 10 \mu\text{m}$; and repulsive Casimir forces have been measured by Munday et al., (2008).

Since only the dispersion force suffers retardation, and not the zero-frequency term, some very interesting effects can sometimes arise leading to a change in sign of the Hamaker constant at some finite separation. A particularly notable example of this phenomenon concerns the behavior of liquid hydrocarbons on water. Referring to Table 13.3, we note that the nonretarded Hamaker constant for a pentane film on water is very small, about $A \approx 10^{-21} \text{ J}$. This is made up of a negative zero-frequency contribution of $A_{\nu=0} = -0.8 \times 10^{-21} \text{ J}$ together with a positive dispersion contribution of $A_{\nu>0} = 1.6 \times 10^{-21} \text{ J}$ which dominates at small separations. At larger distances, however, $A_{\nu>0}$ becomes retarded and progressively decreases. Thus, at some small but finite distance the value of A changes sign from net positive to net negative. It is for this reason that pentane spreads on water: the van der Waals force across the film is repulsive, so tending to increase its thickness and thus favoring the spreading of the liquid on water. For the higher alkanes, the attractive dispersion force contribution is very much larger (cf. $A_{\nu>0} \approx 6 \times 10^{-21} \text{ J}$ for octane), and these hydrocarbons do not spread on water but collect as isolated lenses on the water surface (Figure 13.7).

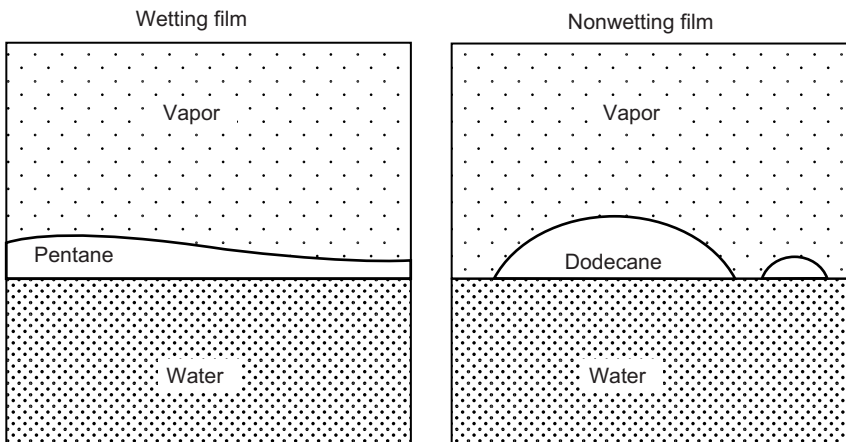


FIGURE 13.7

13.11 Electrostatic Screening Effects in Electrolyte Solutions

In Chapter 6 we saw that the zero-frequency contribution to the van der Waals force is essentially an electrostatic interaction. Now, in any medium containing free charges—for example, water containing free ions in solution or a metal containing free electrons—all electrostatic fields become “screened” due to the polarization (displacement) of these charges. A screened electric field decays roughly exponentially with distance according to $e^{-\kappa D}$, where the characteristic decay length, κ^{-1} , is known as the *Debye Screening length* or *Thomas-Fermi screening length* (see Section 14.14). Typical values for κ^{-1} in aqueous electrolyte solutions are approximately 10 nm in a 10⁻³ M solution and approximately 1 nm in a 0.1 M solution (see Eq. 14.37). Electrostatic screening affects only the zero-frequency contribution, $A_{\nu=0}$. The dispersion contribution, $A_{\nu>\nu_1}$, remains unscreened because the electrolyte ions cannot respond to, and are therefore not polarized by, such high frequencies.

Across an electrolyte solution the screened nonretarded Hamaker constant is given by (D. Y. C. Chan, private communication)

$$A \approx A_{\nu=0} e^{-\kappa D} + A_{\nu>\nu_1}. \quad (13.30)$$

The screening of $A_{\nu=0}$ is analogous to the retardation of $A_{\nu>\nu_1}$, but it usually comes in at much smaller separations. For example, in a 0.1 M aqueous NaCl solution the Debye screening length is about 1 nm, so that by $D = 2$ nm the zero-frequency contribution has already fallen to about 13% of its value at $D = 0$. Thus, for interparticle interactions across such a solution, at separations greater than 2 nm the attraction is effectively determined solely by the dispersion force.

Marra (1986a) measured the van der Waals force-law between two uncharged lipid bilayers in various salt solutions. Over the distance regime from 1 to 4 nm the nonretarded Hamaker constant was found to be $A = 7 \times 10^{-21}$ J in pure water, and $A = 3 \times 10^{-21}$ J in 0.1 M NaCl solution. The first value is slightly larger than expected for pure hydrocarbon across water (see Table 13.3) due to the additional contribution from the polarizable headgroups, while the second value is lower than the first by 4×10^{-21} J, consistent with the zero-frequency term being screened by the electrolyte ions.

13.12 Combining Relations

Combining relations or combining laws are frequently used for obtaining approximate values for unknown Hamaker constants in terms of known ones. Let us define A_{132} as the nonretarded Hamaker constant for media 1 and 2 interacting across medium 3 (Figure 13.2c). A glance at Eq. (13.9) shows that we may expect A_{132} to be approximately related to A_{131} and A_{232} via

$$A_{132} \approx \pm \sqrt{A_{131} A_{232}}. \quad (13.31)$$

From this we obtain

$$A_{12} \approx \sqrt{A_{11}A_{22}}, \quad (13.32)$$

where A_{12} is for media 1 and 2 interacting across a vacuum (i.e., with no medium 3 between them). This is a useful combining relation giving A_{12} in terms of the Hamaker constants of the individual media. Two other useful relations are (Israelachvili, 1972)

$$A_{131} = A_{313} \approx A_{11} + A_{33} - 2A_{13} \quad (13.33)$$

$$\approx (\sqrt{A_{11}} - \sqrt{A_{33}})^2, \quad (13.34)$$

which when combined with Eq. (13.31) gives

$$A_{132} \approx (\sqrt{A_{11}} - \sqrt{A_{33}})(\sqrt{A_{22}} - \sqrt{A_{33}}). \quad (13.35)$$

Note the similarity of these combining relations to those derived in Chapter 10.

As an illustration of the above relations, let us consider a few systems whose Hamaker constants are given in Tables 13.2 and 13.3. Thus, for the quartz-octane-air system, Eq. (13.35) would predict for A_{132} :

$$A_{132} \approx (\sqrt{6.3} - \sqrt{4.5})(0 - \sqrt{4.5}) \times 10^{-20} = -0.82 \times 10^{-20} \text{ J},$$

to be compared with the more rigorously computed value of -0.71×10^{-20} J. Likewise for the CaF₂-helium-vapor system, we expect

$$A_{132} \approx (\sqrt{7.2} - \sqrt{0.057})(0 - \sqrt{0.057}) \times 10^{-20} = -0.58 \times 10^{-20} \text{ J},$$

to be compared with -0.59×10^{-20} J.

For the system quartz-octane-quartz, Eq. (11.35) gives

$$A_{132} \approx (\sqrt{6.3} - \sqrt{4.5})^2 \times 10^{-20} = +0.15 \times 10^{-20} \text{ J},$$

compared to $+0.13 \times 10^{-20}$ J.

Combining relations are applicable only when dispersion forces dominate the interactions as in the above examples, but they break down when applied to media with high dielectric constants such as water or whenever the zero-frequency contribution $A_{y=0}$ is large. Thus, for hexadecane across water, Eq. (13.35) would predict a Hamaker constant of $(\sqrt{5.2} - \sqrt{3.7})^2 \times 10^{-20} \approx 0.13 \times 10^{-20}$ J, which is much smaller than the real value of 0.5×10^{-20} J.

In view of the ease with which Hamaker constants may be reliably computed using equations such as Eq. (13.15) or more rigorous numerical methods, the use of combining relations is not recommended. Parsegian (2006) has described methods for computing the Hamaker constants for both simple and complex dielectric media of different geometries, including layered surfaces (particles), and retardation effects (Casimir forces).

13.13 Surface and Adhesion Energies

Chapter 17 describes various phenomena that arise from the *surface energies* γ of solids and liquids (for a liquid, γ is usually referred to as its *surface tension*). Here we shall see

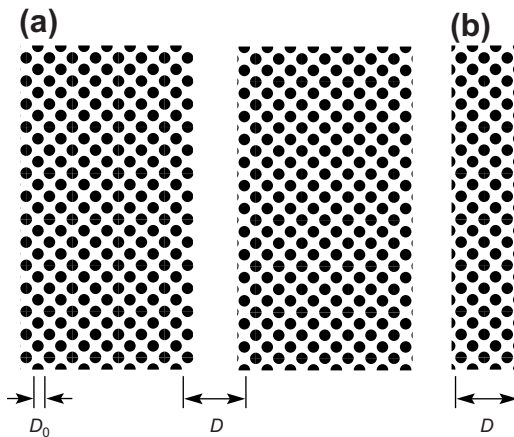


FIGURE 13.8 (a) Two planar “semi-infinite” media or “half-spaces.” The pairwise summation of London dispersion energies between *all* atoms leads to Eq. (13.37). For two surfaces close together, their total surface energy may therefore be written as $W = -2\gamma(1 - D_0^2/D^2)$. The long-range van der Waals interaction energy can be seen to be no more than a perturbation of the surface energy γ . A similar result is obtained for (b), a thin film.

how surface energies are determined from the intermolecular forces between two surfaces. But first, what do we mean by the surface energy of a material? Let us go back to Figure 11.2c and recall the pairwise summation of energies between all the atoms of one medium with all the atoms of the other medium which, for van der Waals forces, gave the interaction energy between two planar surfaces as $W = -A/12\pi D^2$. Had the summation been carried out between *all* the atoms of the system, including the atoms in the same medium, we should have obtained two additional energy terms:

$$W = -\text{constant} + A/12\pi D_0^2 \text{ per unit area,} \quad (13.36)$$

where the **constant** is simply the bulk cohesive energy, Eq. (6.5), of the atoms with their immediate neighbors at $D = D_0$ (Figure 13.8). The second (positive) term arises from the “unsaturated bonds” at the two surfaces. This term is always positive and shows that a free isotropic liquid or solid of a given volume will always try to minimize its surface energy by minimizing its surface area, which leads to its “balling up” into a sphere.⁸

Thus, apart from the bulk energy, the total energy of two planar surfaces at a distance D apart (see Figure 13.8) is given by

$$W = -\frac{A}{12\pi} \left(\frac{1}{D_0^2} - \frac{1}{D^2} \right) = -\frac{A}{12\pi D_0^2} \left(1 - \frac{D_0^2}{D^2} \right) \text{ per unit area.} \quad (13.37)$$

At $D = D_0$ (two surfaces in contact), $W = 0$, while for $D = \infty$ (two isolated surfaces),

⁸Anisotropic media such as crystals and liquid crystals have different surface energies (different values for A and D_0) for different faces, and their shape of minimum energy is more complex and, in general, nonspherical (Chapter 17).

or

$$W = -A/12\pi D_0^2 = -2\gamma \quad (13.38)$$

$$\gamma = A/24\pi D_0^2. \quad (13.39)$$

In other words, the surface energy γ equals half the energy needed to separate two flat surfaces from contact to infinity—that is, it is half the adhesion energy.

We may now test Eq. (13.39) to see how well it predicts the surface energies of materials. Unfortunately, it is not at all obvious what value to use for the interfacial contact separation D_0 . At first sight one might expect D_0 to be the same as the distance between atomic centers and thus be put equal to σ , as was done in Chapter 6. However, there are two problems. First, in the process of computing Hamaker constants by the Hamaker summation method the discrete and bumpy surface atoms were artificially “smeared out” into a continuum by transferring the energy *sum* to an *integral*. Our two “structured” surfaces were thereby transformed into two smooth surfaces, and this invalidates the use of Eq. (13.39) at interatomic distances (Tabor, 1982). Second, the continuum Lifshitz theory, which does predict similar values for A as the Hamaker summation method at large separations, is not expected to apply at atomic-scale distances.

Clearly a molecular approach is called for. Let us therefore first consider the matter in terms of the pairwise additivity of individual atoms or molecules which proved so successful in accurately calculating the cohesive energies of condensed phases (cf. Chapter 6). For an idealized planar close-packed solid, each surface atom (of diameter σ) will have only 9 nearest neighbors instead of 12. Thus, when it comes into contact with a second surface each surface atom will gain $3w = -3C/\sigma^6$ in binding energy. For a close-packed solid, each surface atom occupies an area of $\sigma^2 \sin 60^\circ$, and the bulk density of atoms is $\rho = \sqrt{2}/\sigma^3$. Thus, the surface energy should be approximately

$$\gamma \approx -\frac{1}{2} \left(\frac{3w}{\sigma^2 \sin 60^\circ} \right) \approx -\frac{\sqrt{3}w}{\sigma^2} \approx \frac{\sqrt{3}C\rho^2}{2\sigma^2} \approx \frac{\sqrt{3}A}{2\pi^2\sigma^2} \approx \frac{A}{24\pi(\sigma/2.5)^2}, \quad (13.40)$$

where $A = \pi^2 C \rho^2$ is the Hamaker constant as before.

Thus, to use Eq. (13.39): $\gamma = A/24\pi D_0^2$, for calculating surface energies γ we must use a “cut off” distance D_0 that is substantially less than the interatomic or intermolecular center-to-center distance σ (Israelachvili, 1973b; Aveyard and Saleem, 1976; Hough and White, 1980; Tabor, 1982). For example, for a typical value of $\sigma \approx 0.4$ nm, we should use $D_0 \approx \sigma/2.5 \approx 0.16$ nm. Table 13.4 gives the predicted surface and adhesion energies of a variety of compounds all based on the same cut-off separation of $D_0 = 0.165$ nm:

$$\gamma \approx A/24\pi(0.165 \text{ nm})^2. \quad (13.41)$$

It is remarkable that this “universal constant” for D_0 yields values for surface energies in such good agreement with those measured, even for very different liquids and solids. Only for highly polar H-bonding liquids, shown in the lower part of Table 13.4, does Eq. (13.41) seriously underestimate their surface energies, which is to be expected (Section 8.4). But for “ordinary” solids and liquids, even including acetone and ethanol,

Table 13.4 Comparison of Experimental Surface Energies with Those Calculated on the Basis of the Lifshitz Theory

Material (ϵ) in Order of Increasing ϵ	Theoretical	Surface Energy, γ (mJ m ⁻²)	
	A (10 ⁻²⁰ J)	Simple Theory $\gamma = A/24\pi D_0^2$ ($D_0 = 0.165$ nm)	Experiment ^a (20°C)
Liquid helium (1.057)	0.057	0.28	0.12–0.35 (4–1.6 K)
<i>n</i> -Perfluoro-pentane (1.72)	2.59	12.6	10.3
<i>n</i> -Pentane (1.8)	3.75	18.3	16.1
<i>n</i> -Octane (1.9)	4.5	21.9	21.8
Cyclohexane (2.0)	5.2	25.3	25.5
<i>n</i> -Dodecane (2.0)	5.0	24.4	25.4
<i>n</i> -Hexadecane (2.1)	5.2	25.3	27.5
PTFE (2.1)	3.8	18.5	18.3
CCl ₄ (2.2)	5.5	26.8	29.7
Benzene (2.3)	5.0	24.4	28.8
Rubber (2.35)	5.7	27.8	35
Polystyrene (2.6)	6.6	32.1	33
Polydimethyl-siloxane, PDMS (2.75)	4.4	21.4	21.8
Polyvinyl chloride (3.2)	7.8	38.0	39
Acetone (21)	4.1	20.0	23.7
Ethanol (26)	4.2	20.5	22.8
Methanol (33)	3.6	18	23
Glycol (37)	5.6	28	48
Glycerol (43)	6.7	33	63
Water (80)	3.7	18	73
Hydrogen peroxide H ₂ O ₂ (84)	5.4	26	76
Formamide (109)	6.1	30	58
Adhesion energy in a medium ^b $W = -2\gamma_i = -A/12\pi D_0^2$ (mJ m ⁻²)			
Mica in water and dilute NaCl and KCl solutions	2.0	19	~10

^aNote the good agreement between theory and experiment for γ (within 20%) except for the six strongly H-bonding liquids (in bold).

^bExperimental values compiled from pull-off force measurements between curved surfaces using Eq. (12.10): $W = 2F/3\pi R$ (McGuiggan and Israelachvili, 1990; Shubin and Kekicheff, 1993). The adhesion and interfacial energies of many systems have contributions from other short-range forces, both attractive and repulsive (see Table 21.1). Values taken from various sources including Drummond et al., (1996) and Drummond and Chan (1997).

Eq. (13.41) appears to be reliable to within 10 to 20%, which is within the accuracy that A can be computed. The apparent success of Eq. (13.41) provides us with the following simple formula for estimating the Hamaker constants of non-H-bonding solids and liquids from their surface energies:

$$A \approx 2.1 \times 10^{-21} \gamma, \quad (13.42)$$

where γ is in mJ m^{-2} (dyn/cm or erg/cm^2) and A is in joules (J).



Worked Example 13.3

Question: A “smectic” liquid crystal is composed of large nonpolar cigar-shaped molecules that order in the bulk in a close-packed configuration as shown in Figure 13.9. The molecules may be modeled as long rigid cylinders of total length L with hemispherical ends of radius R , where $L \gg R$. The forces between the molecules are due to an attractive dispersion force and a hard-core repulsion. When a liquid crystal is in contact with a surface it can orient either in the parallel or “planar” orientation, or in the perpendicular or “homeotropic” orientation, as shown in Figure 13.9. By treating the liquid crystal molecules as macroscopic bodies having a Hamaker constant A , which may be assumed to be the same as that of the surface, derive an expression for the adhesion energies W per unit area in the two cases in terms of A , the “cutoff” separation at contact D_0 , L , and R . Under what conditions will W be given by Eq. (13.38), and comment on the implications of your result.

Answer: In the homeotropic orientation, the surface density of molecules is $1/2\sqrt{3}R^2$, and each interacts with energy $-AR/6D_0$. The net adhesion energy is therefore

$$W_{\perp} = \frac{-A}{12\sqrt{3}RD_0} = \frac{-A}{12\pi D_0^2} \left(\frac{\pi D_0}{\sqrt{3}R} \right).$$

The planar orientation is more subtle, there now being both cylinders and hemispheres in contact with the surface, each at a different density that depends on L and R . But for $L \gg R$ the surface density of molecules is $1/(2RL)$ and each interacts with energy $-AR^{1/2}L/12\sqrt{2}D_0^{3/2}$. The net surface energy is therefore

$$W_{\parallel} = \frac{-A}{24\sqrt{2}RD_0^{3/2}} = \frac{-A}{12\pi D_0^2} \left(\frac{\pi^2 D_0}{8R} \right)^{1/2} = W_{\perp} \left(\frac{R}{2.7D_0} \right)^{1/2}.$$

As R approaches D_0 both energies approach the value for two “unstructured” planar surfaces, Eq. (13.38). But for $R \gg D_0$, (1) the adhesion energies fall below the values for two unstructured surfaces, and (2) the adhesion is higher for the planar orientation than for the homeotropic orientation, although the difference diminishes as R approaches D_0 . Thus, larger rigid molecules composed of the same atoms should have lower surface and adhesion energies and,

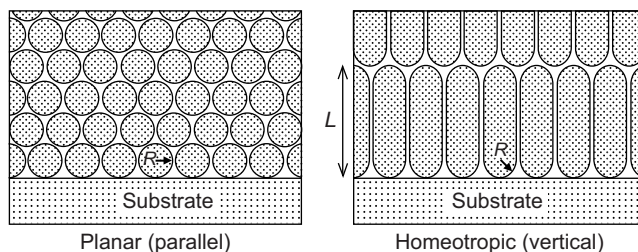


FIGURE 13.9

indeed, C₆₀ and fluorocarbons do tend to have unusually low values for γ even though the polarizabilities of their constituent atoms are high. This effect is analogous to the lower adhesion forces between rough surfaces and to the “Lotus Effect,” discussed in Chapter 17.



For the interaction between a dielectric and a metal surface, the Hamaker constant is given by Eq. (13.21), and we might expect that this equation should also predict good values for the adhesion energies of, for example, ceramic-metal interfaces. Thus, for alumina (Al₂O₃) adhering to eight different metal surfaces Eq. (13.21) predicts that the Hamaker constants should fall within the narrow range $(2.0\text{--}3.0) \times 10^{-19}\text{ J}$ (Lipkin et al., 1997), which, using a cut-off distance of $D_0 = 0.165\text{ nm}$, predicts adhesion energies in the range $W = -A/12\pi D_0^2 = -(190\text{--}280)\text{ mJ m}^{-2}$ ($0.19\text{--}0.28\text{ J m}^{-2}$) at room temperature. However, measured energies are significantly higher and vary over a wider range than these “predicted” values. The reason for this has been attributed to the smaller effective widths of metallic interfaces and the need to treat each system specifically, including the effects of lattice incommensurability for these asymmetric systems, rather than use a universal cut-off separation. When this is done, much better agreement between theory and experiment is obtained (Lipkin et al., 1997). However, the situation is quite different for two metal surfaces where the Lifshitz theory is totally inadequate to predict their adhesion energies—that is, predict the strength of “metallic bonds,” as discussed below.

13.14 Surface Energies of Metals

From the analysis of the previous section we might expect the surface energies of metals to be given by Eq. (13.41) using a Hamaker constant appropriate for metals—that is, $A \approx 4 \times 10^{-19}\text{ J}$ (see Table 13.2). This would predict $\gamma = -\frac{1}{2}W \approx 0.2\text{ J m}^{-2}$. While this value is higher than for nonmetallic compounds, it is still about an order of magnitude lower than typically measured values for metals, which vary from 0.4 to 4 J m⁻² (Table 13.5).

Table 13.5 Surface Energies of Metals

Material	Transition Temperatures		Surface Energy (Tension) γ (mJ m ⁻²) ^a		
	Boiling Point T_B (K) ^b	Melting Point T_M (K) ^b	Just Above T_M	Just Below T_M	At 300 K
Metals					
Aluminum	2,543	931	700	800	1,100
Silver	2,223	1,233	1,000	1,200	1,500
Copper	2,603	1,356	1,300	1,600	2,000
Iron	2,773	1,803	1,500	1,800	2,400
Tungsten	5,273	3,653	2,500	3,600	4,400
Nonmetals					
Silicon	2,623	1,683	750	~1,100	1,400
Ice	373	273	75	110	71

^aValues from Wawra (1975) and other standard references. Values for solids ($T < T_M$) are only approximate, the exact value of γ depends on the crystallographic plane.

^bAt 760 mm Hg.

Table 13.6 Calculated Surface Energies of Metallic Contacts: Effects of Lattice Mismatch

Type of Metal-Metal Interface	Surface Energy, γ (mJ m ⁻²) ^a	
	Lattices in Register (Commensurate)	Lattices Out of Register (Incommensurate)
Similar materials		
Al(111)-Al(111)	715	490
Zn(0001)-Zn(0001)	545	505
Mg(0001)-Mg(0001)	550	460
Dissimilar materials		
Al(111)-Zn(0001)		520
Zn(0001)-Mg(0001)		490
Al(111)-Mg(0001)		505

^aAs computed by Ferrante and Smith (1985), and Banerjee et al., (1991).

Clearly, the attractive forces between two metal surfaces cannot be accounted for by conventional van der Waals forces even though at larger separations they can (see Tables 13.2 and 13.3). The strong adhesion is believed to be due to short-range nonadditive electron exchange interactions which arise between two conducting surfaces at separations below 0.5 nm and give rise to so-called metallic bonds. A phenomenological expression for the interaction potential of two similar metallic surfaces is (Banerjee et al., 1991)

$$W(D) = -2\gamma \left[1 - \frac{(D - D_0)}{\lambda_M} \right] e^{-(D-D_0)/\lambda_M} \text{ per unit area,} \quad (13.43)$$

where λ_M is some characteristic decay length for metals, similar to the Fermi screening length. Minimum energy occurs at $D = D_0$, where $W(D_0) = -2\gamma$.

Ferrante and Smith (1985) have also computed the adhesion energies of metals when their lattices are not in perfect registry (referred to as “incommensurate” or “mismatched” lattices). This can arise between two similar metals if the contacting lattices are at some finite “twist angle” relative to each other, and it occurs between any two dissimilar metals whose lattice dimensions are different (Table 13.6). As might be expected, the atoms of two incommensurate lattices cannot pack together as closely as two commensurate lattices, and their adhesion energy is often significantly smaller than for commensurate interfaces.

An incommensurate interface between two similar lattices can arise from a finite twist angle but also when one lattice plane is simply shifted laterally (without rotation) over another by some fraction of the lattice spacing. The accompanying strained bonds and increase (dilatancy) of the *normal* spacing also lowers the adhesion energy. The energetics of both of these processes are crucial to an understanding of material failure (e.g., fracture) and friction, as will be discussed in Chapter 18.

13.15 Forces between Surfaces with Adsorbed Layers

The nonretarded van der Waals force between two surfaces 1 and 1' with adsorbed layers 2 and 2' across medium 3 (Figure 13.10) is given by the approximate expression (Israelachvili, 1972)

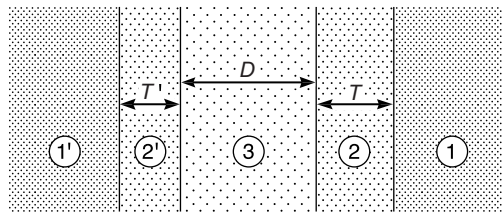


FIGURE 13.10

$$F(D) = -\frac{1}{6\pi} \left[\frac{A_{232'}}{D^3} - \frac{\sqrt{A_{121}A_{323}}}{(D+T)^3} - \frac{\sqrt{A_{1'2'1'}A_{323}}}{(D+T')^3} + \frac{\sqrt{A_{1'2'1'}A_{121}}}{(D+T+T')^3} \right]. \quad (13.44)$$

For the “symmetrical” case when medium 1 = medium 1', medium 2 = medium 2', and $T = T'$, this equation can be simplified using combining relations when it reduces to

$$F(D) = \frac{-1}{6\pi} \left[\frac{A_{232}}{D^3} - \frac{2A_{123}}{(D+T)^3} + \frac{A_{121}}{(D+2T)^3} \right]. \quad (13.45)$$

At small separations, when $D \ll (T + T')$, Eq. (13.44) becomes

$$F(D) = -A_{2'32}/6\pi D^3 \quad (13.46)$$

while at large separations, when $D \gg (T + T')$, we obtain

$$F(D) = -A_{1'31}/6\pi D^3. \quad (13.47)$$

Thus, as a rule of thumb we may say that the van der Waals interaction is dominated by the properties of the bulk or substrate materials at large separations and by the properties of the adsorbed layers at separations less than the thicknesses of the layers. In particular, this means that the adhesion energies are largely determined by the properties of any adsorbed films even when these are only a monolayer thick. Note that with adsorbed layers the long-range van der Waals forces can change sign over certain distance regimes depending on the properties of the five media. However, for a symmetrical system it can be shown that the interaction is always attractive regardless of the number and properties of the layers.

13.16 Experiments on Van der Waals Forces

The expression “experiments on van der Waals forces” is a rather vague one, since many important phenomena involve van der Waals interactions in one way or another. Thus, the measurement of the surface tensions of nonpolar liquids or the thickness of wetting films may be thought of as experiments on van der Waals forces, and we have seen how the results are in good agreement with theory. Other phenomena involving van der Waals interactions (e.g., physical adsorption, adhesion, the strength of solids) have also been extensively studied, but experiments of this type afford a poor way of

rigorously studying van der Waals forces, since they usually have to contend with many parameters that themselves are uncertain, so that it becomes difficult to compare the results with theory.

The most direct way to study van der Waals forces is simply to position two bodies close together and measure the force of attraction as a function of the distance between them, as described in Chapter 12. The pioneering measurements carried out by Derjaguin and colleagues in the USSR and Overbeek and colleagues in The Netherlands in the 1950s and 1960s were of this type. The bodies were made of glass, the force was determined by measuring the deflection of a sensitive spring or balance arm, and the distance between the highly polished surfaces was obtained by optical interference (using Newton's rings, for example). In this way the forces between various types of glass in air or a vacuum were successfully measured in the range 25–1200 nm, which is in the retarded force regime. In general, experiments with glass and metal-coated glass have yielded results in good agreement with the Lifshitz theory: the expected power law for the force was obtained, and the measured magnitudes of the forces agreed with theory within a factor of about two.

Unfortunately, experiments with glass were unable to provide accurate results for separations less than about 10 nm. For this, a much smoother surface was needed. This problem was resolved by making use of naturally occurring muscovite mica, which may be cleaved to provide molecularly smooth surfaces over large areas, and by employing a multiple beam interferometry technique for measuring surface separations to within ± 0.1 nm. In this way, Tabor and Winterton (1969) and later Israelachvili and Tabor (1972) and Coakley and Tabor (1978) measured the van der Waals forces between curved mica surfaces or metal-coated surfaces in air in the range 2–130 nm, where the agreement with theory was generally within 30%. These experiments also allowed for the first measurements of the transition from retarded to nonretarded forces. Experiments were also carried out down to separations of 1.4 nm with a surfactant monolayer of thickness 2.5 nm deposited on each mica surface. The results showed that for separations greater than about 5 nm the effective Hamaker constant is as for bulk mica, but that for separations less than 3 nm it is about 25% less and dominated by the properties of the monolayers, a result which is in accord with theoretical expectations (Section 13.15). For reviews of the earlier work on van der Waals forces, see Israelachvili and Tabor (1973), Israelachvili and Ninham (1977), Derjaguin et al., (1978), and van Blokland and Overbeek (1978, 1979).

After 1975, new experimental techniques such as the Surface Forces Apparatus, described in Section 12.7, were developed to directly measure the van der Waals forces between macroscopic surfaces in liquids (Israelachvili and Adams, 1978; Derjaguin et al., 1978; Israelachvili and McGuiggan, 1991; Israelachvili et al., 2010). Figure 13.6 showed results obtained for the van der Waals force between two mica surfaces in various electrolyte solutions in the distance range 2–15 nm, where again the agreement with theory is within 30%. It was also been verified that in liquids retardation effects come in at smaller separations than in air (above about 5 nm rather than 10 nm) and that the zero frequency contribution is screened in salt solution (Marra, 1986a).

More recently, with the advent of new microscopic and nanoscopic probe techniques such as the AFM and TIRM for measuring forces (Section 12.8), results have been obtained on microscopic and even nanoscopic particles. Most of these have been applied to measuring repulsive or short-range adhesion or solvation forces (described in later chapters), rather than the attractive van der Waals force-laws at finite separations, which are more difficult to measure using these techniques. Biggs and Mulvaney (1994), Ducker and Clarke (1994), Milling et al., (1996), and Meurk et al., (1997) measured the van der Waals forces between various AFM tips (usually of gold or silicon nitride) and various surfaces in various liquids, and generally confirmed that the forces are attractive or repulsive depending on the relative optical properties of the media, as expected from the Lifshitz theory. However, due to difficulties in determining the absolute separation D and tip geometry or radius R , detailed comparisons with theory are not always possible (Argento and French, 1996).

It is well to end this chapter on a reminder that in liquids, unlike in air or in a vacuum, other forces than van der Waals are also usually present, such as long-range electric double-layer forces (Chapter 14) and—at separations below a few molecular diameters—solvation forces (Chapter 15) and various steric, entropic and osmotic forces (Chapter 16). The major limitation of the Lifshitz theory is that it treats both the surfaces and the intervening solvent medium as structureless continuums, and consequently does not encompass molecular effects such as solvation forces and surface structural effects. We have seen in Chapter 7 that at very small separations the solvation force is expected to oscillate with distance with a periodicity equal to the molecular diameter—quite unlike the monotonic force law of the continuum Lifshitz theory. These, and other important short- and long-range forces are described in the following chapters.

PROBLEMS AND DISCUSSION TOPICS

- 13.1** Show that Eq. (10.23), which was derived for any nonspecific short-range interaction, applies to the van der Waals interaction between two macroscopic spheres.
- 13.2** The van der Waals pair potential for two atoms or small groups of diameter σ is given by $w(r) = -C/r^6$ for $r \gg \sigma$. Show that (i) the interaction between a molecule and a surface is given by $w(r) = -\pi C\rho/6r^3$, and (ii) the interaction between two parallel chain molecules (polymers) composed of monomer units of these groups is $w(r) = -3\pi C/8\sigma^2 r^5$ per unit length. Assume that $r \gg \sigma$ in all cases.
- 13.3** (i) Using Eq. 13.2 show that as two dissimilar spheres ($R_1 \gg R_2$) are separated from contact their nonretarded van der Waals interaction energy varies first as $-1/D$, then as $-1/D^3$, then as $-1/D^6$, and derive Eq. (13.3) in this large-distance limit.
(ii) For two similar spheres ($R_1 = R_2 = R$) at what surface separation D relative to R will the interaction energy W have fallen to 50% and 10% of the values given by the short-range limiting equation $W = -AR/12D$?

- 13.4** In Worked Example 13.1, for what value of n would the droplets coalesce spontaneously due to their thermal kinetic energy given by $\frac{1}{2}mv^2 = \frac{1}{2}kT$? Is this the reason why the discharge of electricity during a lightning strike is often followed by a downpour?
- 13.5** (i) Two identical hard spheres of density 10^4 kg/m^3 (10 g/cm^3) and radius R are in contact. Assuming a Hamaker constant of $A = 10^{-19} \text{ J}$, estimate the value of R at which their van der Waals and gravitational attraction are equal, and calculate the total force between them. (ii) If the first and second sphere also have charges $+Q$ and $-Q$ uniformly distributed on their surfaces such that the Coulombic force is also the same as each of the other two forces, what is Q in units of e , and what is the average distance between the charges on the surface?
- 13.6** A particle of radius R is sitting snuggly in (a) a hemispherical hole and (b) a cylindrical hole. Both the particle and substrate materials are the same and have an adhesion energy as defined by Eq. (13.38) for two flat surfaces: $W = -A/12\pi D_0^2$, and both are initially in molecular contact at the van der Waals cut-off distance, D_0 . Derive expressions for the forces, $F(z)$, and total energy differences, ΔE , of the particles between their initial and final positions at $z=0$ and $z=\infty$, respectively, in terms of R , A , and D_0 . Use a macroscopic approach, and verify or discuss the “reasonableness” of your results in the various limits. For nanoscopic particles would your answers overestimate or underestimate the real forces and energies? [Answer: The force and energy for configuration (a) are $F(z) = -AR^2/6D_0(D_0+z)^2$ and $\Delta E = -AR^2/6D_0^2 = -(2\pi R^2)(A/12\pi D_0^2) = 2\pi R^2 W = \text{surface area} \times \text{adhesion energy}.$]
- 13.7*** Two immiscible nonpolar liquids A and B are placed in a round container of radius 2 cm exposed to the atmosphere at STP. The volumes of the liquids are the same and equal to 50 ml each. The densities of A and B are 1.0 and 1.1 g/ml, and their refractive indices are 1.45 and 1.40, respectively. Explain what happens at the liquid-air interface and estimate the thickness of the film of liquid B at that interface. Assume that only nonretarded van der Waals forces are involved, and that the UV electronic absorption frequencies of the two liquids are the same and equal to $3 \times 10^{-15} \text{ s}^{-1}$. [Answer: 19.6 nm.]
- Describe, and illustrate with schematic drawings, what can occur at the container-liquid interfaces (with both A and B) depending on the optical properties of the container material relative to those of A and B.
- 13.8** Two metal surfaces are very close together (as may occur in a crack). The surfaces are not smooth but have asperities of mean radius $R = 10 \text{ nm}$. The elastic properties of the system are such that each asperity may be modeled as being held to its surface by a spring of stiffness $K = 3 \text{ N/m}$. Find the smallest distance that two asperities may remain at equilibrium before the system becomes unstable, and describe the nature of this instability. Assume that the Hamaker constant for the metal-metal van der Waals interaction is $A = 5 \times 10^{-19} \text{ J}$.

How would you estimate the effective stiffness K of the asperity in terms of the Young's Modulus of the metal and the asperity dimensions? How would you expect the critical distance for the instability to depend on the radius of the asperities?

- 13.9** A liquid film on a flat surface exposed to saturated vapor will grow indefinitely if the Hamaker constant across the film A_{SLV} is negative. However, this is not the case for a film on a curved surface. Derive a relation between the equilibrium thickness D of a film on the surface of a cylindrical fiber of radius R in terms of A_{SLV} , R and γ (the surface tension of the liquid). For a quartz fiber of radius $R = 10 \mu\text{m}$ in contact with a saturated vapor of octane at 20°C , calculate the equilibrium thickness of the film on the fiber surface ignoring gravitational effects. Is your calculated thickness likely to be an overestimate or an underestimate of the real value? Use Tables 13.3 and 13.4 and Eq. (17.15) for the Laplace pressure. [Answer: $D = 5.6 \text{ nm}$. For further reading on this phenomenon see Quéré et al., 1989.]
- 13.10** A liquid is in a beaker of radius R . Show that if $A_{SLV} < 0$, there is a thin wetting film on the inside of the beaker whose thickness D at a height H above the liquid surface is given by

$$D^3 = \frac{-A_{SLV}}{6\pi\rho g H [1 - \gamma/\rho g H(R - D)]}. \quad (13.48)$$

What happens at $H \approx \gamma/\rho g R$?

- 13.11*** A film of thickness D on a flat solid surface for which $A_{SLV} > 0$ is unstable and will eventually dewet the surface—that is, break up into one or more lenses (see Fig. 13.7). If there is a local fluctuation (ripple) in the thickness of the film, under what conditions will the ripple grow as an instability until the film dewets?
- 13.12** Describe graphically how the Hamaker “constant” A_{123} might vary with distance D for the liquid-liquid-solid system shown in Figure 13.11. Assume the film to be thin but the lens to be macroscopic, and ignore gravity.
- 13.13** Two van der Waals liquids A and B are completely miscible. A small quantity of A is dissolved in B. It is found that a very thin surface region of B is (i) depleted, and (ii) enhanced of molecules A (compared to their concentration in the bulk liquid). Argue whether you expect the surface tension of the mixture to be higher

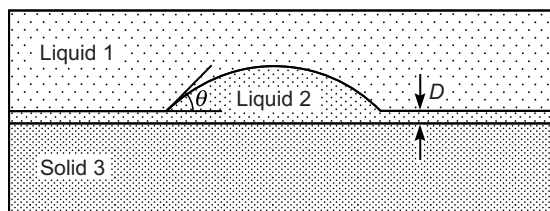


FIGURE 13.11 Liquid that does not wet a thin film of itself adsorbed on a surface (known as *autophobic*). The contact angles θ in such cases are usually small.

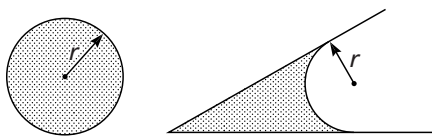


FIGURE 13.12 Liquid droplet (convex surface) and meniscus (concave surface) exposed to vapor or immersed in another (immiscible) liquid.

or lower than that of pure liquid B in cases (i) and (ii). Also discuss whether you expect the surface tension of pure liquid A to be higher or lower than that of pure liquid B.

- 13.14*** The molecules of two nonpolar liquids, A and B, are of equal size but have very different polarizabilities, with $\alpha_A \gg \alpha_B$. Would you expect the liquids to be miscible or immiscible? If the specific solubility of A in bulk liquid B is X_s , would you expect the specific solubility to be larger or smaller in (i) small droplets of B (convex meniscus), and (ii) a small volume of capillary condensed liquid in a wedge (concave meniscus)—see Fig. 13.12?

- 13.15** Colloidal nanoparticles of metals and inorganic materials often coagulate in nonpolar liquids (hydrocarbons, oils) because of the strongly attractive van der Waals forces between them. This is often a nuisance but can be prevented by coating the particles with a surfactant or polymer layer whose refractive index matches that of the liquid. Explain this phenomenon.

At an ACS conference, Dr Chan from Colloids Corp. describes a colloidal dispersion consisting of $0.5\text{ }\mu\text{m}$ diameter smooth silica spheres in oil where, by coating the spheres with a “matching layer” of surfactant, the depth of the potential energy well was reduced by a factor of 10 as ascertained by light scattering measurements. When asked about the thickness of the layer, Dr Chan replies that this is proprietary information. What was the thickness of the layer?

- 13.16** Use the Derjaguin Approximation to show that the Casimir force between a metal sphere and a flat metal surface is given by $F = -\pi^2 hc/720D^3$.

- 13.17** Derive the expression for the nonretarded force between two thin membranes 2 of thickness T whose surfaces are at a distance D apart in medium 1. Show that at a separation of $D = 2.2T$ the force between them is half that of the bulk materials at the same separation D . Also show that at larger separations, when $D \gg T$, the nonretarded interaction energy between two sheets approaches

$$W(D) = -A_{121}T^2/2\pi D^4. \quad (13.49)$$

- 13.18*** In Worked Example 13.3 and Figure 13.9: (i) Recalculate the adhesion energies for the case when L is not much larger than R , and establish that the two values converge when $L = 2R$. (ii) Which of the two configurations is energetically more favorable? [Note: this question is related to but is not the same as determining which adhesion energy is the greater.] (iii) If the length of the

molecules L is progressively decreased from an initially large value ($L \gg R$), is there a transition from one orientation to the other at some particular value of L/R ? (iv) Discuss whether any of your answers could change under the following two conditions: (a) the surface is not mathematically flat or smooth but “structured”—that is, it has atomic or molecular-scale corrugations, which is the situation in practice, and (b) the central regions of the liquid crystal molecules are highly polar. [Suggestion: You could look into the literature on this subject to find out how real liquid crystal and other linear-chain molecules orient at surfaces.]

- 13.19** Are there realistic situations where the strength (whether attractive or repulsive) of the van der Waals interaction (i) increases with distance, and (ii) is higher in a medium than in free space? [Hint: consider the effects of retardation, screening, surface geometry and surface layers or films on the overall interaction.]
- 13.20*** (i) Cylindrical nanorods with hemispherical ends (cigar-shaped) have two equal halves (along their length) of different composition A and B but the same cross-sectional diameter. How will two such particles associate in a liquid C where the only forces are the van der Waals and hard-core repulsive forces? (ii) Does your answer change if the ends are flat? (iii) If the two particles with hemispherical ends have different half-sections A and B, and A and D, respectively, analyze the different ways these could associate in a medium C. Derive the relevant equations (in terms of A , B , C , and D as in Chapter 10) that give the conditions for each type of association relative to the dissociated state, and illustrate each case with hypothetical numerical values. Assume that the cylindrical length of the particles is a few times their width, and that their width is significantly larger than the sizes of their atoms. [Answers: There is one lowest energy configuration in (i); there are two possible configurations in (ii), and five in (iii).]
- 13.21** Will the liquid helium film covering the bottom flat part of the rod in Figure 13.5 have a flat or curved liquid-vapor interface?
- 13.22*** Table 13.7 gives the refractive indices of some materials that constitute different nano-colloidal systems of spherical core-shell nanoparticles of core radii R in oil, where each core surface has a strongly bound layer of surfactant of thickness 1.5 nm (the nanoparticle diameters are therefore $2R + 3$ nm). Each medium can be assumed to have the same absorption frequency $\nu_e \approx 4 \times 10^{15} \text{ s}^{-1}$.

Table 13.7 Properties of Core-Shell Nanoparticles

Medium	Material	Refractive Index, n
Nanoparticle core of radius R	A – silica	1.45
	B – alumina (nonconducting)	1.75
	C – metal (conducting)	∞
Surfactant layer of thickness 1.5 nm	D – hydrocarbon	1.41
Suspending liquid	E – hydrocarbon (oil)	1.41

Estimate the Hamaker constants A and contact adhesion energies W_{ad} in kT units for the following symmetric and asymmetric systems (where “contact” refers to when the surfactant layers **D** touch in the oil medium **E**—that is, when the core surfaces are 3.0 nm apart):

- (i) Surfactant-coated cores of **A**, **B** and **C** each of core radii $R = 2$ nm.
- (ii) Same as (i) but for $R = 20$ nm.
- (iii) Same as (ii) but for the asymmetric *geometries* of spheres ($R = 20$ nm) on flat surfaces.
- (iv) Same as (iii) but for the asymmetric *geometries and compositions* where the flat surface is a conducting metal (e.g., of gold coated with a chemisorbed layer of thiol surfactant). Note that the third case (system) of (iv) is the same as the third case of (iii).
- (v) Estimate the magnetic moment of the particles in (ii) that will give rise to magnetic interaction energies at contact equal to the van der Waals adhesion energies.
- (vi) At what refractive index of the surfactant layers on silica will the van der Waals adhesion energy for silica-core particles in oil equal that between the alumina-core particles calculated in (ii)? [Answer to (i): For the symmetrical **AD-E-DA** system: $A = 0.6$ zJ, $W_{\text{ad}} = 0.008$ kT ; for the symmetrical **BD-E-DB** system: $A = 30$ zJ, $W_{\text{ad}} = 0.40$ kT ; for the symmetrical **CD-E-DC** system: $A \approx 350$ zJ, $W_{\text{ad}} \approx 4.6$ kT .]

This page intentionally left blank

Electrostatic Forces between Surfaces in Liquids

14.1 The Charging of Surfaces in Liquids: the Electric "Double-Layer"

Situations in which van der Waals forces alone determine the total interaction are restricted to a few simple systems—for example, to interactions in vacuum or to nonpolar wetting films on surfaces, both of which were discussed in Chapter 13. In more complex, and more interesting, systems long-range electrostatic forces are also involved, and the interplay between these two interactions has many important consequences.

As mentioned earlier the van der Waals force between similar particles in a medium is always attractive, so that if only van der Waals forces were operating, we might expect all dissolved particles to stick together (coagulate) immediately and precipitate out of solution as a mass of solid material. Our own bodies would be subject to the same fate if we remember that we are composed of 55–75% water. Fortunately this does not happen, because particles suspended in water or any liquid of high dielectric constant are usually charged and can be prevented from coalescing by repulsive electrostatic forces. Other repulsive forces that can prevent coalescence are solvation and steric forces, described in Chapters 15 and 16. In this chapter we shall concentrate on the electrostatic forces.

The charging of a surface in a liquid can come about in three ways:

1. By the ionization or dissociation of surface groups (e.g., the dissociation of protons from surface carboxylic groups ($\text{--COOH} \rightarrow \text{--COO}^- + \text{H}^+$), which leaves behind a negatively charged surface)
2. By the adsorption or binding of ions from solution onto a previously uncharged surface—for example, the adsorption of --OH^- groups to the water-air or water-hydrocarbon interfaces that charges them negatively, or the binding of Ca^{2+} onto the zwitterionic headgroups of lipid bilayer surfaces that charges them positively. The adsorption of ions from solution can, of course, also occur onto oppositely charged surface sites—for example, the adsorption of cationic Ca^{2+} to anionic --COO^- sites vacated by H^+ or Na^+ . Such surfaces are known as *ion exchangeable* surfaces. Ion exchange can take a surprisingly long time.
3. The above examples apply to isolated surfaces exposed to a liquid medium (usually water). A different type of *charge exchange* mechanism occurs between two dissimilar

surfaces very close together where, as previously mentioned in Section 3.5, charges—usually protons or electrons—hop across from one surface to the other. This gives rise to an electrostatic attraction between the now oppositely charged surfaces. Such “acid-base” type interactions are important for understanding short-range adhesion forces and are discussed in Chapter 17.

Whatever the *charging mechanism* (also referred to as *charge regulation*), the final surface charge of *co-ions* is balanced by an equal but oppositely charged region of *counterions*. Some of the counterions are bound, usually transiently, to the surface within the so-called *Stern* or *Helmholtz* layer, while others form an atmosphere of ions in rapid thermal motion close to the surface, known as the diffuse *electric double-layer*¹ (Figure 14.1). The difference between a “bound” ion and a “free” ion in the diffuse double-layer is analogous to the difference between a water molecule in the sea and in the atmosphere. However, because the distances involved in the latter case are of atomic dimensions, the distinction can sometimes become blurred.

Two similarly charged surfaces usually repel each other electrostatically in solution, though under certain conditions they may attract at small separations. Zwitterionic surfaces—that is, those characterized by surface dipoles but no net charge also interact electrostatically with each other, though here we shall find that the force is usually attractive.

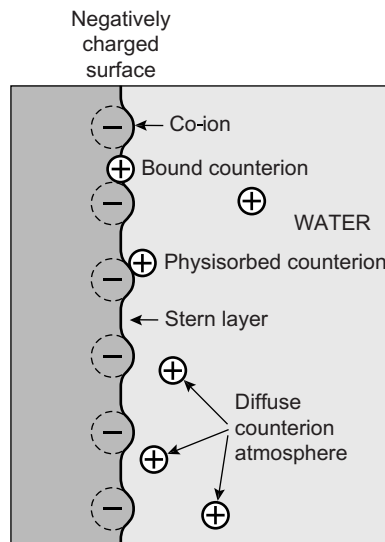


FIGURE 14.1 Ions bound to a surface are not rigidly bound but can exchange with other ions in solution; their lifetime on a surface can be as short as 10^{-9} s (1 ns) or as long as many hours.

¹Originally, the layers of co-ions and counterions were thought to behave like a capacitor whose two rigid plates carry equal but opposite charges (see Section 3.3). Hence the term “double-layer” [of charge]. Indeed, capacitors are excellent models for double-layers as far as their electrical properties are concerned.

14.2 Charged Surfaces in Water: No Added Electrolyte—“Counterions Only”

In the following sections we shall consider the counterion distribution and force between two similarly charged planar surfaces in a pure liquid such as water, where (apart from the H_3O^+ and OH^- ions from dissociated water) the only ions in the solution are those that have come off the surfaces. Such systems are sometimes referred to as “*counterions only*” systems, and they occur when, for example, colloidal particles, clay sheets, surfactant micelles or bilayers whose surfaces contain ionizable groups interact in pure water, and also when thick films of water build up (condense) on an ionizable surface such as glass. But first we must consider some fundamental equations that describe the counterion distribution between two charged surfaces in solution.

14.3 The Poisson-Boltzmann (PB) Equation

For the case when only counterions are present in solution, the chemical potential of any ion may be written as (cf. Sections 2.3 and 2.4):

$$\mu = ze\psi + kT \log \rho, \quad (14.1)$$

where ψ is the electrostatic potential ($E = -d\psi/dx$ is the electric field), and ρ the number density of ions of valency z at any point x between two surfaces (Figure 14.2). Since only differences in potential are ever physically meaningful, we may set $\psi_0 = 0$ at the midplane ($x = 0$), where also $\rho = \rho_0$ and $(d\psi/dx)_0 = 0$ by symmetry.

From the equilibrium requirement that the chemical potential be the same throughout (i.e., for all values of x), Eq. (14.1) gives us the expected Boltzmann distribution of counterions at any point x (the Nernst equation):

$$\rho = \rho_0 e^{-ze\psi/kT}. \quad (14.2)$$

One further important fundamental equation is required. This is the well-known Poisson equation for the net excess charge density at x :

$$ze\rho = -\epsilon_0 \epsilon (d^2\psi/dx^2) \quad (14.3)$$

which when combined with the Boltzmann distribution, Eq. (14.2), gives the Poisson-Boltzmann (PB) equation:

$$d^2\psi/dx^2 = -ze\rho/\epsilon_0 \epsilon = -(ze\rho_0/\epsilon_0 \epsilon) e^{-ze\psi/kT}. \quad (14.4)$$

When solved, the PB equation gives the potential ψ , electric field $E = -\partial\psi/\partial x$, and counterion density ρ , at any point x in the gap between the two surfaces. Let us first determine these values at the surfaces themselves. These quantities are often referred to as the *contact values*: ψ_s , E_s , ρ_s , and so on.

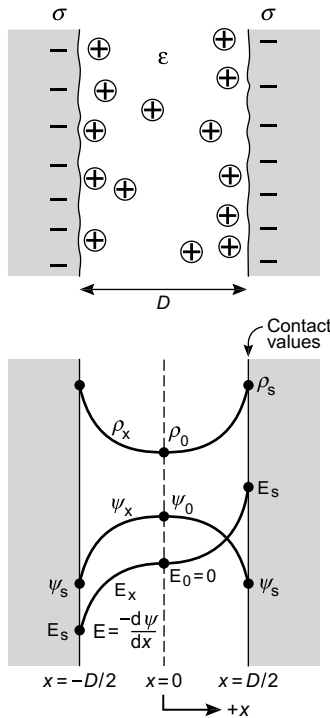


FIGURE 14.2 Two negatively charged surfaces of surface charge density σ separated a distance D in water. The only ions in the space between them are the counterions that have dissociated from the surfaces. The counterion density profile ρ_x and electrostatic potential ψ_x are shown schematically in the lower part of the figure. The “contact” values are ρ_s , ψ_s and $E_s = -(d\psi/dx)_s$.

14.4 Surface Charge, Electric Field, and Counterion Concentration at a Surface: “Contact” Values

The PB equation is a nonlinear second-order differential equation, and to solve for ψ we need two *boundary conditions*, which determine the two integration constants. The first boundary condition follows from the symmetry requirement that the field must vanish at the midplane—that is, that $E_0 = -(d\psi/dx)_0 = 0$. The second boundary condition follows from the requirement of overall *electroneutrality*—that is, that the total charge of the counterions in the gap must be equal (and opposite) to the charge on the surfaces. If σ is the surface charge density on each surface (in $C\ m^{-2}$) and D is the distance between the surfaces (see Figure 14.2), then the condition of electroneutrality implies that

$$\sigma = - \int_0^{D/2} z \epsilon \rho dx = +\epsilon_0 \epsilon \int_0^{D/2} (d^2 \psi / dx^2)^2 dx = -\epsilon_0 \epsilon (d\psi / dx)_{D/2} = -\epsilon_0 \epsilon (d\psi / dx)_S = -\epsilon_0 \epsilon E_S,$$

that is,

$$E_S = -\sigma / \epsilon_0 \epsilon, \quad (14.5)$$

which is essentially Gauss' Law (cf. Section 3.4). Equation (14.5) gives an important general boundary condition relating the surface charge density σ to the electric field E_s at each surface (at $x = \pm D/2$), which we may note is independent of the gap width D .



Worked Example 14.1

Question: Is the electric field near a charged surface in water sufficiently intense to immobilize the water molecules adjacent to it?

Answer: Assuming a high-charge density of $\sigma = -0.3 \text{ C m}^{-2}$ (which is one charge per 0.5 nm^2 —typical of a fully ionized surface), the electric field at the surface, Eq. (14.5), is $E_s = -\sigma/\epsilon_0\epsilon = -0.3/80(8.85 \times 10^{-12}) = -4.2 \times 10^8 \text{ V m}^{-1}$. We may compare this to the field just outside a monovalent ion in water. Using Eq. (3.1), the field at $r = 0.25 \text{ nm}$ from the center of an ion is $E_r = e/4\pi\epsilon_0\epsilon r^2 = 2.9 \times 10^8 \text{ V m}^{-1}$. Since this is comparable to the field at the charged surface, and since the fields of monovalent ions are usually not strong enough to immobilize water molecules around them (cf. Chapters 3–5), it is unlikely that water molecules will become significantly oriented, immobilized or “bound” to any but the most highly charged surfaces. However, other interactions with the surface, such as H-bonding, may lead to significant effects on the local water structure.



Turning now to the *ionic concentrations*, there exists an important general relation between the concentrations of counterions at either surface and at the midplane. Differentiating Eq. (14.2) and then using Eq. (14.4) we obtain

$$\frac{d\rho}{dx} = -\frac{ze\rho_0}{kT}e^{-ze\psi/kT}\left(\frac{d\psi}{dx}\right) = \frac{\epsilon_0\epsilon}{kT}\left(\frac{d\psi}{dx}\right)\left(\frac{d^2\psi}{dx^2}\right) = \frac{\epsilon_0\epsilon}{2kT}\frac{d}{dx}\left(\frac{d\psi}{dx}\right)^2, \quad (14.6)$$

hence

$$\rho_x - \rho_0 = \int_0^x d\rho = \frac{\epsilon_0\epsilon}{2kT} \int_0^x d\left(\frac{d\psi}{dx}\right)^2 = +\frac{\epsilon_0\epsilon}{2kT} \left(\frac{d\psi}{dx}\right)_x^2$$

so that

$$\rho_x = \rho_0 + \frac{\epsilon_0\epsilon}{2kT} \left(\frac{d\psi}{dx}\right)_x^2, \quad (14.7)$$

which gives ρ at any point x in terms of ρ_0 at the midplane and $(d\psi/dx)^2$ at x . In particular at the surface, $x = D/2$, we obtain using Eq. (14.5) the contact value of ρ

$$\rho_s = \rho_0 + \sigma^2/2\epsilon_0\epsilon kT. \quad (14.8)$$

This important result shows that the concentration of counterions at the surface depends only on the surface charge density σ and the counterion concentration at the midplane. It shows that ρ_s never falls below $\sigma^2/2\epsilon_0\epsilon kT$ even for isolated surfaces—that is, for two

surfaces far apart when $\rho_0 \rightarrow 0$. For example, for an isolated surface in water of charge density $\sigma = -0.2 \text{ C m}^{-2}$ (one charge per 0.8 nm^2) at 293 K

$$\rho_s = \sigma^2 / 2\epsilon_0 \epsilon kT = (0.2)^2 / (2 \times 80 \times 8.85 \times 10^{-12} \times 4.04 \times 10^{-21}) = 7.0 \times 10^{27} \text{ m}^{-3},$$

which is about 12 M. If these surface counterions are considered to occupy a layer of thickness $\sim 0.2 \text{ nm}$, the above value for ρ_s corresponds to a surface counterion density of $(7 \times 10^{27})(0.2 \times 10^{-9}) = 1.4 \times 10^{18} \text{ ions/m}^2$ or one charge per 0.7 nm^2 , which is about the same as the surface charge density σ . This is an interesting result, for it shows that regardless of the counterion distribution profile ρ_x away from a surface (Section 14.5), most of the counterions that effectively balance the surface charge are located in the first few ångstroms from the surface (Jönsson et al., 1980)—that is, right up against the surface, hence the term *double-layer*. However, for lower surface charge densities, since $\rho_s \propto \sigma^2$, the layer of counterions extends well beyond the surface and becomes much more diffuse, hence the term *diffuse double-layer*.

14.5 Counterion Concentration Profile Away from a Surface

The above equations are quite general and are the starting point of all theoretical computations of the ionic distributions near planar charged surfaces, even when the solution contains added electrolyte (Section 14.10 onwards). To proceed further for the specific case of counterions only (see Figure 14.2) we must now solve the Poisson-Boltzmann equation, Eq. (14.4), which can be satisfied by²

$$\psi = (kT/ze) \log(\cos^2 Kx) \quad (14.9)$$

or

$$e^{-ze\psi/kT} = 1/\cos^2 Kx, \quad (14.10)$$

where K is a constant given by

$$K^2 = (ze)^2 \rho_0 / 2\epsilon_0 \epsilon kT. \quad (14.11)$$

With this form for the potential we see that $\psi = 0$ and $d\psi/dx = 0$ at $x = 0$ for all K , as required. To solve for K we differentiate Eq. (14.9) and then use Eq. (14.5) to obtain for the electric fields

$$\text{at any point } x : E_x = -d\psi/dx = +(2kTK/ze)\tan Kx, \quad (14.12a)$$

$$\text{at the surfaces} : E_s = -(d\psi/dx)_s = +(2kTK/ze)\tan(KD/2) = -\sigma/\epsilon_0 \epsilon. \quad (14.12b)$$

²There are other mathematical solutions to this equation, but Eq. (14.9) is the only one that is physically realistic—that is, satisfying all the boundary conditions, as demonstrated further in the following.

The counterion distribution profile

$$\rho_x = \rho_0 e^{-ze\psi/kT} = \rho_0 / \cos^2 Kx \quad (14.13)$$

is therefore known once K is determined from Eq. (14.12) in terms of σ and D .



Worked Example 14.2

Question: Two charged surfaces with $\sigma = 0.2 \text{ C m}^{-2}$ are 2 nm apart ($D = 2 \text{ nm}$). Calculate the field, potential and counterion density at each surface, at 0.2 nm from each surface and at the midplane, assuming monovalent counterions.

Answer: From Eq. (14.12) we find that for $z = -1$, $K = 1.3361 \times 10^9 \text{ m}^{-1}$ at 293 K. From Eq. (14.11) this means that $\rho_0 = 0.40 \times 10^{27} \text{ m}^{-3}$, so that at the surface $\rho_s = \rho_0 / \cos^2(KD/2) = 7.4 \times 10^{27} \text{ m}^{-3}$. The same result is also immediately obtainable from Eq. (14.8), since, as we have previously established, $\sigma^2/2\varepsilon_0\epsilon kT = 7.0 \times 10^{27} \text{ m}^{-3}$. Thus, the counterion concentration at each surface ρ_s is about 18.5 times greater than at the midplane ρ_0 , which is only 1 nm away. Putting $K = 1.3661 \times 10^9 \text{ m}^{-1}$, $kT = 4.045 \times 10^{-21} \text{ J}$, $\sigma = 0.2 \text{ C m}^{-2}$, $\epsilon = 80$, $ze = 1.602 \times 10^{-19} \text{ C}$, and $D = 2 \times 10^{-9} \text{ m}$ into Eqs. (14.9), (14.12), and (14.13), we obtain:

	$\psi (\text{mV})$	$E (\text{V m}^{-1})$	$\rho (\text{m}^{-3})$
At $x = 1 \text{ nm}$ ("contact value" at surface)	74	2.8×10^8	7.4×10^{27} (12 M)
At $x = 0.8 \text{ nm}$ (0.2 nm from surface)	37	1.2×10^8	1.7×10^{27} (3 M)
At $x = 0$ ("midplane" value 1 nm from surface)	0	0	0.4×10^{27} (0.7 M)

Note the unphysically steep decrease in the ion density ρ near the surface over a distance of only 0.2 nm (2 Å).



Figure 14.3 shows how the counterion concentration varies with distance for the case of $\sigma = 0.224 \text{ C m}^{-2}$, $D = 2.1 \text{ nm}$, as calculated on the basis of (1) the Poisson-Boltzmann

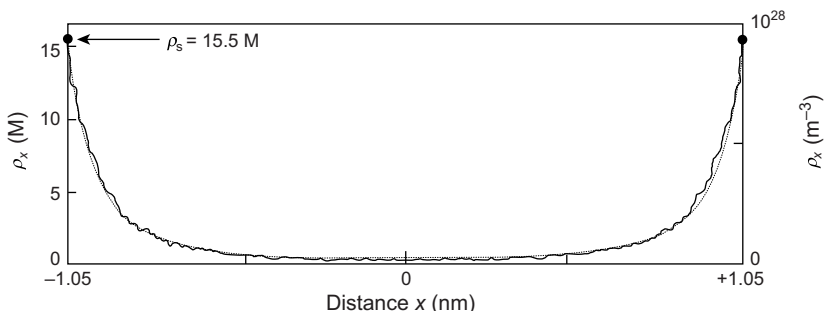


FIGURE 14.3 Monovalent counterion concentration profile between two charged surfaces ($\sigma = 0.224 \text{ C m}^{-2}$, corresponding to one electronic charge per 0.714 nm^2) a distance 2.1 nm apart in water. The smooth curve is obtained from the Poisson-Boltzmann equation; the other is from a Monte Carlo simulation by Jönsson et al., (1980).

equation as in the above example, and (2) a Monte Carlo simulation of the same system. The agreement is quite good though the Monte Carlo result gives a slightly higher counterion concentration very near the surfaces compensated by a lower concentration in the central region between the two surfaces.

14.6 Origin of the Ionic Distribution, Electric Field, Surface Potential, and Pressure

Before we proceed to calculate the force or pressure between two surfaces, it is instructive to discuss, in qualitative terms, how the counterion distribution, potential, field, and pressure between two surfaces arise. The first thing to notice is that if there were no ions between two similarly charged surfaces, there would be no electric field in the gap between them. This is because the field emanating from a planar charged surface, $E = -\sigma/2\epsilon_0\epsilon$, is uniform away from the surface (Section 3.3). The two opposing fields emanating from the two plane parallel surfaces therefore cancel out to zero between the two surfaces or plates (although they add up outside the two plates). Thus, when the counterions are introduced into the intervening region they do *not* experience an attractive electrostatic force toward each surface. The reason why the counterions build up at each surface is simply because of their mutual repulsion and is similar to the accumulation of mobile charges on the surface of any charged conducting material such as a metal. The repulsive electrostatic interaction between the counterions and their entropy of mixing alone determine their concentration profile ρ_x , the potential profile ψ_x and the field E_x between the surfaces (Jönsson et al., 1980), and we may further note that in all the theoretical derivations so far the only way the surface charge density σ enters into the picture is through Eq. (14.5), which is simply a statement about the total number of counterions in the gap.

Further, if the centers of the surface coions were not at the physical solid-liquid interface (at $x = \pm\frac{1}{2}D$) but at some small distance δ within the surface (Figure 14.4), the ionic distribution ρ_x , potential ψ_x , field E_x , and the pressure in the medium between $+\frac{1}{2}D$ and $-\frac{1}{2}D$ would not change. But the potential would be different if it were measured at $x = \pm(\frac{1}{2}D - \delta)$. This is the origin of the so-called *Stern* and *Helmholtz layers* (Stern, 1924; Verwey and Overbeek, 1948; Hiemenz, 1997) that separate the charged plane from the *Outer Helmholtz Plane* (OHP) from which the ionic atmosphere begins to obey the Poisson-Boltzmann equation. The combined thickness of the Stern and Helmholtz layers δ is of the order of a few ångstroms and reflects the finite size of the charged surface groups (coions) and transiently bound counterions, as illustrated in Figures 14.1 and 14.4. Clearly, within this region, whose thickness is determined by the finite (hard core) sizes of the ions, the PB equation cannot hold. If the dielectric constant of the Stern-Helmholtz layer is assumed to be uniform and equal to ϵ_δ it can be modeled as a capacitor (see Section 3.3) whence the additional drop in potential across this layer is given by

$$\psi_\delta = \sigma\delta/\epsilon_0\epsilon_\delta. \quad (14.14)$$

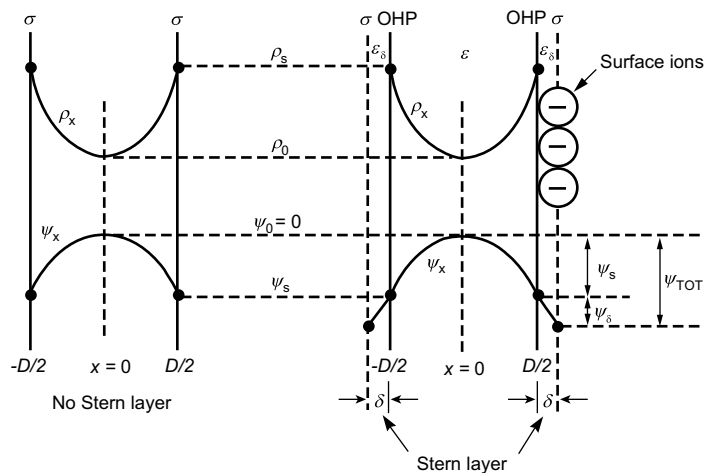


FIGURE 14.4 Stern layers of thickness δ at each surface dividing the planes of fixed charge density σ from the boundary of the aqueous solution—the OHP. There is an additional linear drop in potential across the Stern layer given by Eq. (14.14) so that the total potential drop is $\psi_{TOT} = \psi_\delta + \psi_s$. However, the counterion density and electrostatic potential within the aqueous region between the two OHPs at $x = D/2$ and $x = -D/2$, and the pressure between the two surfaces, are independent of δ .

For example, if $\delta = 0.2$ nm, $\sigma = 0.2$ C m⁻², and $\epsilon_\delta = 40$, we obtain $\psi_\delta = 130$ mV, which is actually higher than the potential drop across the diffuse double-layer, calculated in the previous worked example.

We now turn to the origin of the force or pressure between the two surfaces. Contrary to intuition, the origin of the repulsive force between two similarly charged surfaces in a solvent containing counterions and/or added electrolyte ions is entropic (osmotic), not electrostatic. Indeed, the electrostatic contribution to the net force is actually attractive. Consider an isolated surface, initially uncharged, placed in water. When the surface groups dissociate the counterions leave the surface against the attractive Coulombic force pulling them back. What maintains the diffuse double-layer is the repulsive osmotic pressure between the counterions which forces them away from the surface and from each other so as to increase their configurational entropy. On bringing two such surfaces together one is therefore forcing the counterions back onto the surfaces against their preferred equilibrium state—that is, against their osmotic repulsion but favored by the electrostatic interaction. The former dominates and the net force is repulsive.

On the other hand, to understand why the purely electrostatic part of the interaction is attractive recall that it involves an equal number of positive (counterion) and negative (surface) charges—that is, the system is overall electrically neutral. The net Coulombic interaction between a system of charges that are overall neutral always favors their association, as we saw in the case of ionic crystals in Chapter 3 and dipoles in Chapter 4.

There *are* situations where the electrostatic attraction does dominate over the entropic repulsion, giving rise to an overall attraction even between two equally charged surfaces or particles in solution. These cases are discussed in later Sections.

14.7 The Pressure between Two Charged Surfaces in Water: the Contact Value Theorem

We may derive an expression for the pressure of counterions in a confined space in the same way as the pressure of a van der Waals gas in a confined volume was derived in Section 2.5. Using Eq. (2.20), the repulsive pressure P of the counterions at any position x from the center (see Figure 14.4) is given by $(\partial P / \partial x')_{x,T} = \rho(\partial \mu / \partial x')_{x,T}$, where the chemical potential μ is given by Eq. (14.1). The change in pressure at x on bringing two plates together from infinity ($x' = \infty$, where $P = 0$) to a separation $x' = D$ at constant temperature is therefore

$$\begin{aligned} P_x(D) - P_x(\infty) &= P_x(D) = + \int_{\infty}^D [ze\rho(d\psi/dx')dx' + kT(d\rho/dx')dx'] \\ &= - \int_{x'=D}^{x'=\infty} [ze\rho(d\psi/dx')_x dx' + kT d\rho_x]. \end{aligned} \quad (14.15)$$

Note that in Eq. (14.15), the values are computed at a *fixed* point x within the ionic solution, which is not the same as the *variable* separation x' between the two surfaces. Replacing $ze\rho$ by the Poisson equation, Eq. (14.3), and using the relation

$$\frac{d}{dx} \left(\frac{d\psi}{dx} \right)^2 = 2 \left(\frac{d\psi}{dx} \right) \left(\frac{d^2\psi}{dx^2} \right)$$

Eq. (14.15) becomes

$$P_x(D) - P_x(\infty) = \left[-\frac{1}{2}\epsilon_0\epsilon \left(\frac{d\psi}{dx} \right)^2_{x(D)} + kT\rho_{x(D)} \right] - \left[-\frac{1}{2}\epsilon_0\epsilon \left(\frac{d\psi}{dx} \right)^2_{x(\infty)} + kT\rho_{x(\infty)} \right], \quad (14.16)$$

where the subscripts x mean that the values are calculated at x when the surfaces are at a distance D or ∞ apart. In the present case, since there are no electrolyte ions in the bulk solution, $\rho_0(\infty) = 0$, so that by Eq. 14.7, we have $P_x(\infty) = 0$, as expected.

The above important equation gives the pressure P at any point x between the two surfaces, and we may notice that it is split into two contributions. The first, being a square, is always negative—that is, *attractive* (except at the midplane, $x = 0$, where it is zero). This is the electrostatic field energy contribution, discussed qualitatively in the previous section. The second term is positive and hence repulsive. This is the entropic (osmotic) contribution to the force.

At equilibrium, $P_x(D)$ should be uniform throughout the gap—that is, independent of x —and it is also the pressure acting on the two surfaces. To verify this we note that using Eq. (14.7) the above may be written as

$$P_x(D) = kT[\rho_0(D) - \rho_0(\infty)] \quad (14.17a)$$

or

$$P_x(D) = kT\rho_0(D) \quad \text{since here } \rho_0(\infty) = 0. \quad (14.17b)$$

which is indeed independent of x and depends only on the increased ionic concentration, or osmotic pressure, at the midplane, $\rho_0(D)$, and thus on σ and D . We may therefore drop the subscript x from $P_x(D)$. It is instructive to insert Eq. (14.8) into the above equation, from which we obtain

$$P(D) = kT\rho_0(D) = kT[\rho_s(D) - \sigma^2/2\epsilon_0\epsilon kT],$$

that is,

$$P(D) = kT[\rho_s(D) - \rho_s(\infty)]. \quad (14.18)$$

Thus, the pressure is also given by the increase in the counterion concentration at the surfaces as they approach each other. This important equation, known as the *contact value theorem*, is always valid as long as there is no interaction between the counterions and the surfaces—that is, as long as there is no counterion adsorption so that the surface coion charge density remains constant and independent of D . It shows that the force or pressure is repulsive if the density of counterions at the surface increases as the two surfaces are brought together and attractive if it decreases.

The contact value theorem is very general and applies to many other types of interactions—for example, to double-layer interactions when electrolyte ions are present in the solution, to solvation interactions where $\rho_s(D)$ is now the surface concentration of solvent molecules (Chapter 15), to polymer-associated steric and depletion interactions where $\rho_s(D)$ is the surface concentration of polymeric groups (Chapter 16), and to various entropic or thermal fluctuation forces between fluid surfaces and biological membranes (Chapters 16 and 21). In the case of overlapping double-layers, the resulting force is often referred to as the *electric* or *electrostatic* double-layer force, even though, as we have seen, the repulsion is really due to entropic confinement.

Returning to Eq. (14.17b), the pressure may also be expressed in terms of K , as given by Eq. (14.11), by

$$P = kT\rho_0 = 2\epsilon_0\epsilon(kT/ze)^2K^2. \quad (14.19)$$

As an example let us apply this result to Worked Example 14.2, where for two surfaces with $\sigma = 0.2 \text{ C m}^{-2}$ at $D = 2 \text{ nm}$ apart, we found $K = 1.336 \times 10^9 \text{ m}^{-1}$. The repulsive pressure between them is therefore $1.7 \times 10^6 \text{ N m}^{-2}$, or about 17 atm. Note that this repulsion exceeds by far any possible van der Waals attraction at this separation. For a typical Hamaker constant of $A \approx 10^{-20} \text{ J}$ the van der Waals attractive pressure would be only $A/12\pi D^3 \approx 3 \times 10^4 \text{ N m}^{-2}$ or about 0.3 atm.

The above equations have been used successfully to account for the equilibrium spacings of ionic surfactant and lipid bilayers in water (Cowley et al., 1978). Figure 14.5 shows experimental results obtained for the repulsive pressure between bilayers composed of a mixture of charged and uncharged lipids in water using the Osmotic Pressure Technique (cf. Figures 12.1h and 12.2), together with the theoretical curve based on Eq. (14.19). The agreement is very good down to $D \approx 2 \text{ nm}$ and shows that the effective charge density of the anionic lipid headgroups is about $1e$ per 14 nm^2 . At smaller distances the measured forces are more repulsive than expected due to the steric-hydration interactions between the thermally mobile hydrophilic headgroups that characterize these fluid-like interfaces (cf. Problem 14.3 and Chapters 15, 16, and 21). Similar methods have been used to measure the repulsive electrostatic forces between

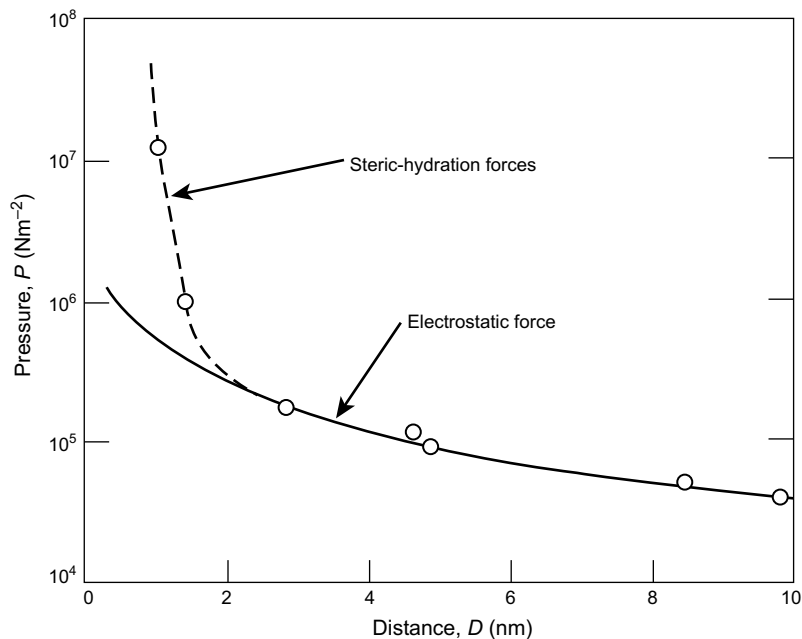


FIGURE 14.5 Measured repulsive pressure between charged bilayer surfaces in water. The bilayers were composed of 90% lecithin (phosphatidylcholine, PC), a neutral zwitterionic lipid, and 10% phosphatidylglycerol (PG), a negatively charged lipid. For full ionization, the surface charge density should be one electronic charge per 7 nm^2 , whereas the theoretical line through the experimental points suggests one charge per 14 nm^2 (i.e., about 50% ionization). Below 2 nm there is an additional repulsion due to “steric-hydration” forces. [Adapted from Cowley et al., (1978), ©1978 American Chemical Society.]

surfactant bilayers and biological membranes, both in pure water and in salt solutions (Diederichs et al., 1985; Dubois et al., 1992).

Repulsive electrostatic forces also control the long-range swelling of clays in water. Most naturally occurring clays are composed of lamellar aluminosilicate sheets about 1 to 2 nm thick whose surfaces dissociate in water giving off Na^+ , K^+ , and Ca^{2+} ions, and when placed in water they can swell to more than 10 times their original volume (Norrish, 1954). The swelling of clays is, however, a complex matter and also involves other forces at surface separations below about 3 nm (van Olphen, 1977; Pashley and Quirk, 1984; Kjellander et al., 1988a, b; Quirk, 1994).

In the case of charged spherical particles (e.g., latex particles³) in water, the long-range electrostatic repulsion between them can result in an ordered lattice of particles even when the distance between them is well in excess of their diameter (Takano and Hachisu, 1978). In such systems (cf. Figure 6.2) colloidal particles attempt to get as far apart from each other as possible but, being constrained within a finite volume of solution, are

³Latex particles are made from biological or synthetic polymers. Hydrophobic latex particles can be rendered water-soluble by grafting hydrophilic groups to their surfaces—for example, sulfonic acid groups to polystyrene particles.

forced to arrange themselves into an ordered lattice. For a review on colloidal crystals see Murray and Grier (1996).

Parsegian (1966) and Jönsson and Wennerström (1981) extended the above analysis to the interactions between cylindrical and spherical structures, and the results were used to analyze the relative stability of charged surfactant aggregates which form spontaneously in water. Such micellar structures are soft and fluid-like, and they change from being spherical to cylindrical to sheet-like (bilayers) as the amount of water is reduced (see Chapter 20).

Worked Example 14.3

Question: Two flat but dissimilar surfaces are pressed together with a pressure of 10 atm in pure water (monovalent counterions only, no added electrolyte) at 25°C. If the surfaces carry surface charges of densities $\sigma_1 = -0.04 \text{ C m}^{-2}$ and $\sigma_2 = -0.08 \text{ C m}^{-2}$, respectively, due to the surface dissociation of monovalent surface ions, what will be their equilibrium separation?

Answer: Referring to Figure 14.4 and the equations describing K , the ionic distribution, potential, and pressure for the *symmetrical* case, it is clear that the two halves of the system on either side of the midplane at $x = 0$ are completely independent of each other as long as ρ_0 and T are fixed (which determine K , ρ_x , ψ_x and P). For the *asymmetric* case, these same equations apply on either side of the plane at which $E = -d\psi/dx = 0$, which redefines $x = 0$. All that needs to be done is to find the distance D_1 and D_2 on either side of $x = 0$, where the surface charge densities are equal to σ_1 and σ_2 , respectively, as given by Eq. (14.12). Thus, from Eq. (14.19) a pressure of $P = 10 \text{ atm} = 1.013 \times 10^6 \text{ N m}^{-2}$ at 25°C corresponds to $K = (ze/kT)\sqrt{P/2\varepsilon_0\varepsilon} = (1.602 \times 10^{-19}/1.381 \times 10^{-23} \times 298.15) \times [(1.013 \times 10^6)/(2 \times 8.854 \times 10^{-12} \times 78.5)]^{1/2} = 1.05031 \times 10^9 \text{ m}^{-1}$. Inserting this value into Eq. (14.12) to get $\frac{1}{2}D$ for $\sigma_1 = -0.04$ and $\sigma_2 = -0.08 \text{ C m}^{-2}$ gives $\frac{1}{2}D_1 = 0.78 \text{ nm}$ and $\frac{1}{2}D_2 = 1.08 \text{ nm}$, respectively. The separation is therefore $D = \frac{1}{2}D_1 + \frac{1}{2}D_2 = 1.86 \text{ nm}$.

14.8 Limit of Large Separations: Thick Wetting Films

At large distances $D \rightarrow \infty$, in order to keep $\tan(KD/2)$ finite in Eq. (14.12b), K must approach π/D . In this limit the pressure, Eq. (14.19), therefore becomes

$$P(D) = 2\varepsilon_0\varepsilon(\pi kT/ze)^2/D^2, \quad (14.20)$$

that is,

$$P(D) \propto +1/D^2,$$

which is known as the *Langmuir equation*. The Langmuir equation has been used to account for the equilibrium thickness of thick wetting films of water on glass surfaces (Figures 12.1f and 14.6). Here the water-air surface replaces the midplane of Figure 14.2 so that for a film of thickness $d = D/2$, we have

$$P(d) = \varepsilon_0\varepsilon(\pi kT/ze)^2/2d^2, \quad (14.21)$$

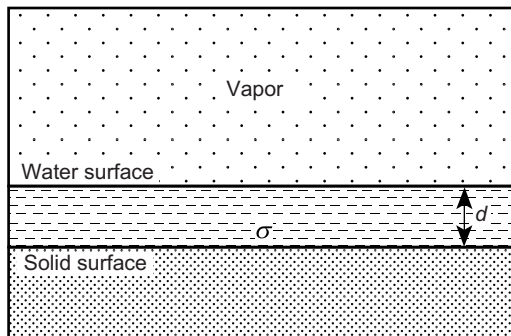


FIGURE 14.6 A water film on a charged (ionizable) glass surface will tend to thicken because of the repulsive “disjoining pressure” of the counterions in the film. If the vapor over the film is saturated, the film will grow indefinitely, but if it is unsaturated, the equilibrium thickness d will be finite as given by Eqs. (14.21) and (14.22).

which is sometimes referred to as the *disjoining pressure* of a film. This repulsive pressure is entirely analogous to the repulsive van der Waals force across adsorbed liquid films, such as helium (Section 13.9), that causes them to climb up or spread on surfaces. Note, however, that both the magnitude and range of the double-layer repulsion is usually greater than the van der Waals’ ($P \propto 1/d^2$ instead of $P \propto 1/d^3$).

In Section 13.9 we saw that the equilibrium thickness d of a wetting film is given by one or other of the following equivalent equations

$$P(d) = +mgH/v = -(kT/v)\log(p/p_{\text{sat}}), \quad (14.22)$$

where H is the height of the film above the surface of the bulk liquid, v and m the molecular volume and mass of the solvent ($\rho = m/v$), and p/p_{sat} the relative vapor pressure. Thus, if water condenses on a charged surface from undersaturated vapor, the film thickness d will increase to infinity as H approaches zero or, equivalently, as p approaches p_{sat} (100% relative humidity).

Langmuir (1938) first applied Eq. (14.21) to explain the then paradoxical “Jones-Ray Effect,” where the rise of water up a capillary tube is observed to be higher than expected from the Laplace Equation (Chapter 17). Langmuir’s explanation was that since the water also wets the inner surface of the capillary, the effective radius of the tube is smaller than the dry radius, and this leads to the higher capillary rise.

Derjaguin and Kusakov (1939) measured how the thickness of a water film on a quartz glass surface decreased when an air bubble was progressively pressed down on the film. The results were in rough agreement with the Langmuir equation. Read and Kitchener (1969) repeated these measurements and again found only rough agreement between theory and experiment: in the range 30–130 nm the measured film thicknesses were 10–20 nm thicker than expected theoretically. Later, Derjaguin and Churaev (1974), Pashley and Kitchener (1979), and Gee et al., (1990b) used the vapor pressure control method to measure the equilibrium film thickness and found that for $d < 30$ nm the films are *much* thicker than expected from Eq. (14.22). These effects are believed to be due to one or both

of the following: (1) The air-water and hydrocarbon-water interfaces are known to be negatively charged due to the preferential accumulation of OH^- ions or depletion of H_3O^+ ions at these interfaces (Taylor and Wood, 1957; Usui et al., 1981; Marinova et al., 1996; Beattie, 2007), so that for a given disjoining pressure P or vapor pressure p the film thickness would indeed be higher than given by Eq. (14.21), which assumes $\sigma = 0$ and $d\psi/dx = 0$ at that interface; and/or (2) the presence of even small amounts of soluble contaminants in the films will lower p_{sat} in Eq. (14.22), which will result in a large increase in the thickness of the film at any given value of p (Pashley, 1980).



Worked Example 14.4

Question: What are the thermodynamic equilibrium radii of the charged water droplets of Problem 3.7 after fragmentation in an atmosphere of relative humidity $p_{\text{vap}}/p_{\text{sat}} = 50\%$ at 20°C ?

Answer: The surface tension or energy of a surface γ is defined by the isothermal work done on changing the area of the surface: $dG = \gamma dA$. For a water droplet with a net charge Q uniformly distributed on its surface, $G = 4\pi R^2 \gamma_0 + Q^2/8\pi\epsilon_0 R$, where γ_0 is the surface tension of pure water ($\gamma_0 = 73 \times 10^{-3} \text{ N m}^{-1}$ at $T = 293 \text{ K}$), and $A = 4\pi R^2$ is the surface area. This gives $\gamma = \gamma_0(1 - Q^2/64\pi^2\epsilon_0\gamma_0R^3)$. At thermodynamic equilibrium, the Laplace pressure of the droplet, given by Eq. (17.15): $P = 2\gamma/R$, equals the pressure of the undersaturated vapor, given by Eq. (14.22): $P = -(RT/V)\log(p_{\text{vap}}/p_{\text{sat}})$, where $V = 18 \text{ ml}$ is the molar volume of water.⁴ When there is only one charge left per droplet, $Q = e$, the average equilibrium radius of each droplet will therefore be $(8.3 \times 293/18 \times 10^{-6})\log_e 0.5 = -9.4 \times 10^7 = 2 \times 0.073[1 - (1.602 \times 10^{-19})^2/(64\pi^2 \times 8.854 \times 10^{-12} \times 0.073R^3)]/R$, which is satisfied by $R = 0.37 \text{ nm}$, corresponding to a droplet containing about 6 water molecules around the ion.

⁴For water, based on molar parameters, $R/V = 8.3/18 \times 10^{-6} = 4.6 \times 10^5 \text{ N m}^{-2} \text{ K}^{-1}$. This can also be expressed in terms of molecular parameters: $k/v = 1.38 \times 10^{-23}/30 \times 10^{-30} \text{ N m}^{-2} \text{ K}^{-1}$.



14.9 Limit of Small Separations: Osmotic Limit and Charge Regulation

At small separations, as $D \rightarrow 0$, it is easy to verify from Eq. (14.12) that $K^2 \rightarrow -\sigma ze/\epsilon_0\epsilon kTD$ (note that K^2 is positive since σ and z must have opposite signs). Thus, the repulsive pressure P of Eq. (14.19) approaches infinity according to

$$P(D \rightarrow 0) = -2\sigma kT/zeD. \quad (14.23)$$

From Eqs. (14.13) and (14.11) we further find that as $D \rightarrow 0$ the counterion density profile between the surfaces becomes uniform and equal to

$$\rho_x \approx \rho_s \approx \rho_0 \approx -2\sigma/zeD \quad \text{at all } x. \quad (14.24)$$

Since $-2\sigma/zeD$ is the number density of counterions in the gap, this means that the limiting pressure of Eq. (14.23) is simply the osmotic pressure $P = \rho kT$ of an ideal gas at

the same density as the trapped counterions. This is known as the *osmotic limit*, which applies to any system where ions, atoms, or molecules remain confined or trapped between two surfaces as they approach each other. In the present case the trapping is due to the requirement of maintaining electroneutrality in the gap that prevents the counterions from going into the surrounding bulk liquid reservoir; in other cases it may be due to the covalent attachment of, for example, polymer molecules to the surfaces. Yet in other cases the trapped molecules may indeed leave the gap, in which case the density ρ is not proportional to $1/D$ and the resulting pressure can be repulsive, attractive, or oscillatory, as discussed in later chapters.

The infinite pressure as $D \rightarrow 0$ implied by Eq. (14.23) is, of course, unrealistic and arises from the assumption that the total number of ions in the gap does not change—that is, that $\sigma = \text{constant}$, which further implies that the surfaces remain fully ionized even when there is a very large pressure pushing the counterions back against the surfaces. In practice when two surfaces are finally forced into molecular contact the counterions are forced to readsorb onto their original surface sites. Thus, as D approaches zero the surface charge density σ also falls—that is, σ becomes a function of D . This is known as *charge regulation*, and its effect is to reduce the repulsion below that calculated on the assumption of constant surface charge. Charge regulation can also arise at isolated surfaces from changes in the solution conditions (rather than from a change in D). These two mechanisms are interdependent and are discussed further in Section 14.17. In addition, other effects and forces can also come in at small separations, and these can be equally important in determining the short-range and especially the adhesion forces at contact.

14.10 Charged Surfaces in Electrolyte Solutions

It is far more common for charged surfaces or particles to interact across or in a solution that already contains electrolyte ions (dissociated inorganic salts). In animal fluids, ions are present in concentrations of about 0.2 M, mainly NaCl or KCl with smaller amounts of MgCl₂ and CaCl₂. The oceans have a similar relative composition of these salts but at a higher total concentration, about 0.6 M. Note that even “pure water” at pH 7 is strictly an electrolyte solution containing 10^{-7} M of H₃O⁺ and OH⁻ ions, which cannot always be ignored. For example, for a charged isolated surface exposed to a solvent containing no added electrolyte ions (only the counterions), Eqs. (14.9) and (14.12) readily show that for the isolated surface, for which $D \rightarrow \infty$, we obtain $KD \rightarrow \pi$ and $\psi_s \rightarrow \infty$. As we shall see, this unrealistic situation is removed as soon as the bulk solvent contains even the minutest concentration of electrolyte ions.

The existence of a “bulk reservoir” of electrolyte ions has a profound effect not only on the electrostatic potential but also on the forces between charged surfaces, and in the rest of this chapter we shall consider this interaction as well as the total interaction when the ever-present van der Waals force is added. But to understand the double-layer interaction between two surfaces it is necessary to first understand the ionic distribution adjacent to an isolated surface in contact with an electrolyte solution. Consider an isolated surface, or

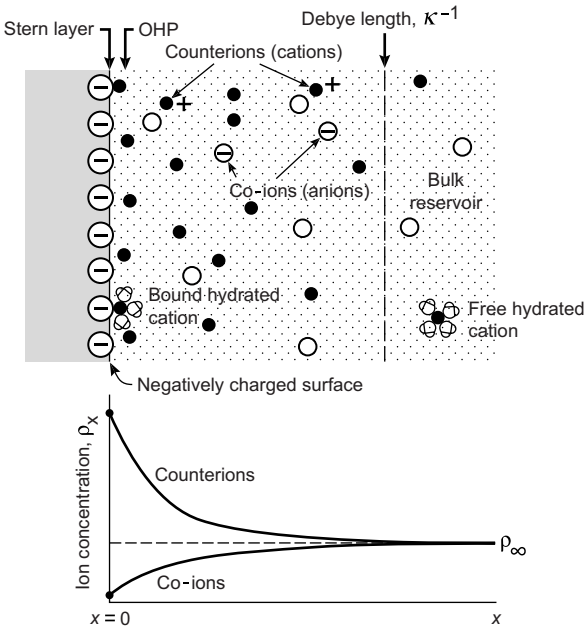


FIGURE 14.7 Near a negatively charged surface there is an accumulation of counterions (ions of opposite charge to the surface coions) and a depletion of coions, shown graphically below for a 1:1 electrolyte, where ρ_∞ is the electrolyte concentration in the bulk or “reservoir” at $x = \infty$. Counterions can adsorb to the surface in the dehydrated, partially hydrated, or fully hydrated state. The OHP is the plane beyond which the ions obey the Poisson-Boltzmann equation. This plane is usually farther out than the van der Waals plane.

two surfaces far apart, in an aqueous electrolyte (Figure 14.7). For convenience, we shall put $x = 0$ at the surface rather than at the midplane. Now, all the fundamental equations derived in the previous sections are applicable to solutions containing different types of ions i (of valency z_i) so long as this is taken into account by expressing the net charge density at any point x as $\sum_i z_i e \rho_{xi}$ and the total ionic concentration (number density) as $\sum_i \rho_{xi}$. Thus, Eq. (14.2) for the Boltzmann distribution of ions i at x now becomes.

$$\rho_{xi} = \rho_\infty i e^{-z_i e \psi_x / kT} \quad (14.25)$$

while at the surface, at $x = 0$, the contact values of ρ and ψ are related by

$$\rho_{0i} = \rho_\infty i e^{-z_i e \psi_0 / kT}, \quad (14.26)$$

where $\rho_{\infty i}$ is the ionic concentration of ions i in the bulk (at $x = \infty$) where $\psi_\infty = 0$. For example, if we have a solution containing $\text{H}^+ \text{OH}^- + \text{Na}^+ \text{Cl}^- + \text{Ca}^{2+} \text{Cl}_2^-$, etc., we may write

Solution values	Contact values
$[\text{H}^+]_x = [\text{H}^+]_\infty e^{-e \psi_x / kT},$	$[\text{H}^+]_0 = [\text{H}^+]_\infty e^{-e \psi_0 / kT},$
$[\text{Na}^+]_x = [\text{Na}^+]_\infty e^{-e \psi_x / kT},$	$[\text{Na}^+]_0 = [\text{Na}^+]_\infty e^{-e \psi_0 / kT},$
$[\text{Ca}^{2+}]_x = [\text{Ca}^{2+}]_\infty e^{-2e \psi_x / kT},$	$[\text{Ca}^{2+}]_0 = [\text{Ca}^{2+}]_\infty e^{-2e \psi_0 / kT},$
$[\text{Cl}^-]_x = [\text{Cl}^-]_\infty e^{+e \psi_x / kT},$	$[\text{Cl}^-]_0 = [\text{Cl}^-]_\infty e^{+e \psi_0 / kT},$

where $[\text{Na}^+]$, and so on are expressed in some convenient concentration unit such as M (1 M = 1 mol dm⁻³ and corresponds to a number density of $\rho = 6.022 \times 10^{26}$ m⁻³).

14.11 The Grahame Equation

Let us now find the total concentration of ions at an isolated surface of charge density σ . From Eq. (14.8) this is immediately given by

$$\sum_i \rho_{0i} = \sum_i \rho_\infty i + \sigma^2 / 2\epsilon_0 \epsilon kT \quad (\text{in number per m}^3). \quad (14.28)$$

Thus, for $\sigma = -0.2$ C m⁻² (corresponding to one electronic charge per 0.8 nm² or 80 Å²) at 25°C, we find $\sigma^2 / 2\epsilon_0 \epsilon kT = 7.0 \times 10^{27}$ m⁻³ = 11.64 M. For a 1:1 electrolyte such as NaCl, the surface concentration of ions in this case is

$$[\text{Na}^+]_0 + [\text{Cl}^-]_0 = 11.64 + [\text{Na}^+]_\infty + [\text{Cl}^-]_\infty = 11.64 + 2[\text{Na}^+]_\infty = 11.64 + 2[\text{NaCl}] \text{ M}, \quad (14.29a)$$

while for a 2:1 electrolyte such as CaCl₂,

$$[\text{Ca}^{2+}]_0 + [\text{Cl}^-]_0 = 11.64 + [\text{Ca}^{2+}]_\infty + [\text{Cl}^-]_\infty = 11.64 + 3[\text{Ca}^{2+}]_\infty = 11.64 + 3[\text{CaCl}_2] \text{ M}, \quad (14.29b)$$

where [NaCl] and [CaCl₂] are the bulk molar concentrations of the salts. The ions at the surface are, of course, mainly the counterions (e.g., Na⁺ or Ca²⁺ at a negatively charged surface) and their *excess* concentration at the surface over that in the bulk is seen to be (1) dependent solely on the surface charge density σ —that is, *independent* of the bulk electrolyte concentration—and (2) of magnitude sufficient to balance much of the surface charge (cf. Sections 14.4 and 14.15).

We may now find the relation between the surface charge density σ and the surface potential ψ_0 . Incorporating Eq. (14.26) into Eq. (14.28), we obtain for the case of a mixed NaCl + CaCl₂ electrolyte:

$$\begin{aligned} \sigma^2 &= 2\epsilon_0 \epsilon kT \left(\sum_i \rho_{0i} - \sum_i \rho_\infty i \right) \\ &= 2\epsilon_0 \epsilon kT \{ [\text{Na}^+]_\infty e^{-e\psi_0/kT} + [\text{Ca}^{2+}]_\infty e^{-2e\psi_0/kT} + [\text{Cl}^-]_\infty e^{+e\psi_0/kT} - [\text{Na}^+]_\infty - [\text{Ca}^{2+}]_\infty - [\text{Cl}^-]_\infty \}. \end{aligned}$$

On further noting that $[\text{Cl}^-]_\infty = [\text{Na}^+]_\infty + 2[\text{Ca}^{2+}]_\infty$ the above becomes

$$\sigma^2 = 2\epsilon_0 \epsilon kT \{ [\text{Na}^+]_\infty (e^{-e\psi_0/kT} + e^{+e\psi_0/kT} - 2) + [\text{Ca}^{2+}]_\infty (e^{-2e\psi_0/kT} + 2e^{+e\psi_0/kT} - 3) \},$$

so that finally we obtain the Grahame equation (Grahame, 1953)

$$\begin{aligned} \sigma &= \sqrt{8\epsilon_0 \epsilon kT} \sinh(e\psi_0/2kT) \{ [\text{Na}^+]_\infty + [\text{Ca}^{2+}]_\infty (2 + e^{-e\psi_0/kT}) \}^{1/2} \\ &= 0.117 \sinh(\psi_0/51.4) \{ [\text{NaCl}] + [\text{CaCl}_2]_\infty (2 + e^{-\psi_0/25.7}) \}^{1/2} \text{ C m}^{-2} \quad (14.30) \end{aligned}$$

at 25°C, where the bulk concentrations $[\text{NaCl}] = [\text{Na}^+]_\infty$ and $[\text{CaCl}_2] = [\text{Ca}^{2+}]_\infty$ are in M, ψ_0 in mV, and σ in C m⁻² (1 C m⁻² corresponds to one electronic charge per 0.16 nm² or

16\AA^2). For example, a surface having a typical potential of -75 mV in, say, physiological saline solution (150 mM NaCl) has a surface charge density of $\sigma = 0.117 \sqrt{0.150} \sinh(-75.0/51.4) = -0.0922 \text{ C m}^{-2}$. Thus, each charge occupies $0.16/0.092 \approx 1.7 \text{ nm}^2$ or $\sim 170\text{\AA}^2$, the mean separation between charges on the surface being about 13\AA . Equation (14.30) allows us to calculate σ once ψ_0 is known, or vice versa, from which the individual counterion concentrations at each surface ρ_{0i} can be obtained using Eqs. (14.26) or (14.27). We shall now consider some implications of the *Grahame equation*, bearing in mind that it does not predict σ or ψ_0 , but just relates them.

14.12 Surface Charge and Potential of Isolated Surfaces

For an aqueous 1:1 electrolyte solution such as NaCl against a negatively charged surface of $\sigma = -0.2 \text{ C m}^{-2}$, we obtain the potentials shown in the middle column of Table 14.1. Note that for no electrolyte we obtain an infinite potential, which is unrealistic; a pure liquid such as water will always contain *some* dissociated ions. It is for this reason that we did not consider an isolated surface in the absence of bulk electrolyte ions in Section 14.5. From Table 14.1 we find that at constant surface charge density the surface potential falls progressively as the electrolyte concentration rises. From the tabulated values of ψ_0 we can determine the ionic concentrations at the surface using Eq. (14.27). For example, in 10^{-7} M 1:1 electrolyte, where $\psi_0 \approx -477.1$ mV, we obtain $10^{-7} \times e^{+477.1/25.69} = 11.64 \text{ M}$ for the counterions, and $10^{-7} \times e^{-477.1/25.69} \approx 10^{-15} \text{ M}$ for the coions. In 1 M, where $\psi_0 = -67.0$ mV, we obtain 13.57 M and 0.07 M for the counterions and coions, respectively, which total 13.64 M. As expected, the *total* concentration of all the ions at the surface agrees exactly with that predicted by Eq. (14.29).

In most cases neither σ nor ψ_0 remains constant as the solution conditions change. This is because ionizable surface sites are rarely fully dissociated but are partially neutralized by the binding of specific ions from the solution. Such ions or surfaces are

Table 14.1 Variation of Surface Potential with Aqueous Electrolyte Concentration for a Planar Surface of Charge Density -0.2 C m^{-2} as Deduced from the Grahame Equation, Eq. (14.30).

1:1 Electrolyte Concentration (M)	Pure 1:1 Electrolyte Solution	ψ_0 (mV) Bulk Solution Also Contains 3 mM 2:1 Electrolyte
0 (hypothetical)	$-\infty$	-106
10^{-7} (pure water)	-477	-106
10^{-4}	-300	-106
10^{-3}	-241	-106
10^{-2}	-181	-105
10^{-1}	-123	-100
1	-67	-66

often referred to as *exchangeable* ions or surfaces, in contrast to those *inert* ions that do not bind to the surface. For example, if only protons can bind to a negatively charged surface, the equilibrium condition at the surface is given by the familiar *mass action equation* (Payens, 1955). Thus, for the reaction



where K_d is the surface dissociation constant. We may express the proton concentration at the surface as $[\text{H}^+]_0$, the concentration or surface density of negative (dissociated) surface sites as $[\text{S}^-]_0$, and the density of neutral (undissociated) sites as $[\text{SH}]_0$. The surface charge density σ is related to $[\text{S}^-]_0$ via $\sigma = -e[\text{S}^-]_0$. Proton concentrations $[\text{H}^+]$ are usually given in pH units, defined by $\text{pH} = -\log_{10}[\text{H}^+]$.⁵ The surface dissociation constant K_d is defined by

$$K_d = \frac{[\text{S}^-]_0 [\text{H}^+]_0}{[\text{SH}]_0} \quad (14.31)$$

$$= \frac{\sigma_0 \alpha}{\sigma_0 (1 - \alpha)} [\text{H}^+]_0 = \frac{\alpha}{(1 - \alpha)} [\text{H}^+]_\infty e^{-e\psi_0/kT}, \quad (14.32)$$

where σ_0 is the maximum possible charge density (i.e., if all the sites were dissociated) and α is the fraction of sites actually dissociated.

Another important property of an ionizable surface is its pK value, which is the *bulk* pH⁵ at which half of its charged sites are dissociated ($\alpha = 0.5$). At this point Eq. (14.32) shows that $K_d = [\text{H}^+]_\infty e^{-e\psi_0/kT}$. Thus, the pK can be directly equated with the dissociation constant. For example, if half the sites are dissociated at $[\text{H}^+]_\infty = [\text{H}^+]_\infty^{pK} = 10^{-4} \text{ M}$ (pH 4.0), we would say that the pK of the surface is 4.0. If both K_d and ψ_0 remain constant as the pH changes, then at any different $[\text{H}^+]_\infty$ or pH the fraction of dissociated sites can be written as

$$\alpha = \frac{K_d}{K_d + [\text{H}^+]_\infty e^{-e\psi_0/kT}} = \frac{[\text{H}^+]_\infty^{pK}}{[\text{H}^+]_\infty^{pK} + [\text{H}^+]_\infty} = \frac{10^{-4}}{10^{-4} + [\text{H}^+]_\infty}. \quad (14.33)$$

Thus, at pH 3 (corresponding to ten times the proton concentration at the pK) we find $\alpha = 0.09$, while at pH 5 (ten times lower proton concentration) we find $\alpha = 0.91$.

For a mixed 1:1 electrolyte consisting of inert (non-surface-binding) and surface-binding H^+ ions—for example, a mixture of NaCl and HCl—Eq. (14.32) can be combined with the Grahame equation to give the simultaneous equations

$$\sigma = \alpha \sigma_0 = K_d \sigma_0 / (K_d + [\text{HCl}]_\infty e^{-\psi_0/25.7}) = 0.117 \sinh(\psi_0/51.4) \sqrt{[\text{NaCl}]_\infty + [\text{HCl}]_\infty} \quad (14.34)$$

in which both σ and ψ_0 can now be totally determined in terms of the maximum charge density σ_0 and dissociation constant K_d . It is clear from the above that if K_d is very

⁵Note that if the pH is defined in terms of the concentration (number density) of protons, then the surface pH of $-\log_{10}[\text{H}^+]_0$ is different from the bulk pH of $-\log_{10}[\text{H}^+]_\infty$. However, if the pH is defined in terms of the *activity* of the protons, the two values are identical, since they are now being equated with the chemical potential of the protons.

large (high surface charge, weak binding of protons), then $\sigma \approx \sigma_0 \approx \text{constant}$, and we obtain the earlier result for the case of fixed surface charge density. However, if K_d takes on a more typical value, the effect can be quite dramatic. For example, if $K_d = 10^{-4} \text{ M}$, then for a surface of $\sigma_0 = -0.2 \text{ C m}^{-2}$ in a 0.1 M NaCl bulk solution at pH 7, we find $\psi_0 = -118 \text{ mV}$ and $\alpha = 0.91$ —that is, the protons have neutralized 9% of the surface sites, and ψ_0 is not very different from the value in the absence of protons (see Table 14.1). But at pH 5 we obtain $\psi_0 = -73 \text{ mV}$ and $\alpha = 0.36$ —that is, only 36% of the sites now remain dissociated even though the bulk concentration of HCl is a mere 0.01% of the NaCl concentration. Under such conditions the proton is referred to as a *potential determining ion*. Thus, both ψ_0 and σ will vary as the salt concentration or pH is changed, but the surface will always remain negatively charged.

More generally, a surface may contain both anionic (e.g., acidic) and cationic (e.g., basic) groups to which various cations and anions can bind. Such surfaces are known as *amphoteric*, and the *competitive adsorption* of ions to them can be analyzed by assigning a binding constant to each ion type, and then incorporating these into the Grahame equation (Healy and White, 1978; Chan et al., 1980a). The charge density of amphoteric surfaces (e.g., protein surfaces) can be negative or positive depending on the electrolyte conditions. At the *isoelectric point* (iep) or *point of zero charge* (pzc) there are as many negative charges as positive charges so that the mean surface charge density is zero ($\sigma = 0$), although it is important to remember that there may still be local regions of high negative or positive charge. Such discrete local charges become crucially important for determining the short-range and adhesion forces between amphoteric surfaces and biological macromolecules, and we return to consider such acid-base and protein-substrate interactions in later sections and in Part III.

14.13 Effect of Divalent Ions

The presence of divalent cations has a dramatic effect on the surface potential and counterion distribution at a negatively charged surface. For example, if all the NaCl solutions of Table 14.1 also contain $3 \times 10^{-3} \text{ M CaCl}_2$, the Grahame equation gives the potentials shown in the third column. We see that even at constant surface charge density, relatively small amounts of divalent ions substantially lower the magnitude of ψ_0 , in fact, about 100 times more effectively than increasing the concentration of monovalent salt. Indeed, ψ_0 is determined solely by the divalent cations once their concentration is greater than about 3% of the monovalent ion concentration, and for 2:1 electrolyte concentrations above a few mM, typical surface potentials are well below -100 mV irrespective of the 1:1 electrolyte concentration.

Further, even when the bulk concentration of Ca^{2+} is much smaller than that of Na^+ , the surface may have a much higher local concentration of Ca^{2+} . For example, in $100 \text{ mM NaCl} + 3 \text{ mM CaCl}_2$, where $\psi_0 = -100 \text{ mV}$ (see Table 14.1) the concentration of Ca^{2+} at the surface is $[\text{Ca}^{2+}]_0 \approx 3 \times 10^{-3} e^{+200/25.7} \approx 7 \text{ M}$ compared to $[\text{Na}^+]_0 \approx 0.1 e^{+100/25.7} \approx 5 \text{ M}$.

At such high surface concentrations (of *doubly charged* ions) divalent ions often bind chemically to negative surface sites, thereby lowering σ and reducing ψ_0 even further, and it is not unusual for surfaces to be completely neutralized ($\sigma \rightarrow 0, \psi_0 \rightarrow 0$) in the presence of mM amounts of Ca^{2+} . In the case of trivalent ions such as La^{3+} , bulk concentrations in excess of 10^{-5} M can neutralize a negatively charged surface and even lead to *charge reversal* wherein the cations continue to adsorb onto a surface that is already net positively charged (see Problem 3. 2(ii)).

As in the case of monovalent ion binding, the effect of divalent ion binding can be dealt with quantitatively by incorporating the appropriate binding constants into the Grahame equation (Healy and White, 1978; McLaughlin et al., 1981), and when many different ionic species (e.g., $\text{Ca}^{2+}, \text{H}^+$) compete for binding sites the variation of ψ_0 and σ with electrolyte concentration and pH can be quite complex. In most cases ion binding tends to lower both σ and ψ_0 as the concentrations of these ions increase, and we may anticipate that such effects lead to a substantial reduction in the repulsive double-layer forces between surfaces.

14.14 The Debye Length

For low potentials, below about 25 mV, the Grahame equation simplifies to

$$\sigma = \varepsilon_0 \varepsilon k \psi_0, \quad (14.35)$$

where

$$\kappa = \left(\sum_i \rho_\infty i e^2 z_i^2 / \varepsilon_0 \varepsilon k T \right)^{1/2} \text{m}^{-1}. \quad (14.36)$$

Thus, the potential becomes proportional to the surface charge density. Equation (14.35) is the same as Eq. (14.14) for a capacitor whose two plates are separated by a distance $1/\kappa$, have charge densities $\pm\sigma$, and potential difference ψ_0 . This analogy with a charged capacitor gave rise to the name *diffuse electric double-layer* for describing the ionic atmosphere near a charged surface, whose characteristic length or “thickness” is known as the Debye length, $1/\kappa$.

The magnitude of the Debye length depends solely on the properties of the solution and not on any property of the surface such as its charge or potential. For a monovalent electrolyte ($z = 1$) at 25°C (298K) the Debye length of aqueous solutions is

$$\kappa^{-1} = (\varepsilon_0 \varepsilon k T / 2 \rho_\infty e^2)^{1/2} = \left(\frac{8.854 \times 10^{-12} \times 78.4 \times 1.381 \times 10^{-23} \times 298}{2 \times 6.022 \times 10^{26} \times (1.602 \times 10^{-19})^2 M} \right)^{1/2} = 0.304 \times 10^{-9} / \sqrt{M} \text{ m.}$$

Thus,

$$\begin{aligned} & 0.304 / \sqrt{[\text{NaCl}]} \text{ nm} && \text{for 1:1 electrolytes (e.g., NaCl)} \\ 1/\kappa = & 0.176 / \sqrt{[\text{CaCl}_2]} \text{ nm} && \text{for 2:1 and 1:2 electrolytes (e.g., CaCl}_2, \text{ Na}_2\text{SO}_4) \\ & 0.152 / \sqrt{[\text{MgSO}_4]} \text{ nm} && \text{for 2:2 electrolytes (e.g., MgSO}_4) \end{aligned} \quad (14.37)$$

For example, for NaCl solution, $1/\kappa = 30.4 \text{ nm}$ at 10^{-4} M , 9.6 nm at 1 mM , 0.96 nm at 0.1 M , and 0.3 nm at 1 M . In totally pure water at pH 7, the Debye length is 960 nm , or about $1 \mu\text{m}$.

14.15 Variation of Potential ψ_x and Ionic Concentrations ρ_x Away from a Surface

The potential gradient at any distance x from an isolated surface is given by Eq. (14.7):

$$\sum_i \rho_{xi} = \sum_i \rho_{\infty i} + \frac{\epsilon_0 \epsilon}{2kT} \left(\frac{d\psi}{dx} \right)_x^2. \quad (14.38)$$

For a 1:1 electrolyte this gives

$$d\psi/dx = \sqrt{8kT\rho_{\infty i}/\epsilon_0 \epsilon} \sinh(e\psi_x/2kT),$$

which may be readily integrated using the integral $\int \operatorname{csch} X dX = \log \tanh(X/2)$ to yield

$$\psi_x = \frac{2kT}{e} \log \left[\frac{1 + \gamma e^{-\kappa x}}{1 - \gamma e^{-\kappa x}} \right] \approx \frac{4kT}{e} \gamma e^{-\kappa x}, \quad (14.39)$$

where⁶

$$\gamma = \tanh(e\psi_0/4kT) = \tanh[\psi_0(\text{mV})/103] \text{ at } 25^\circ\text{C}. \quad (14.40)$$

This is known as the *Gouy-Chapman* theory. For high potentials $\gamma \rightarrow 1$, while for potentials less than 25 mV, Eq. (14.39) reduces to the so-called *Debye-Hückel* equation

$$\psi_x \approx \psi_0 e^{-\kappa x}, \quad (14.41)$$

where again the Debye length $1/\kappa$ appears as the characteristic decay length of the potential [see Verwey and Overbeek (1948) and Hiemenz (1997) for a fuller discussion of the Gouy-Chapman and Debye-Hückel theories].

The above equations apply to *symmetrical* 1:1 electrolyte solutions, such as NaCl. Equations that apply to *asymmetrical* electrolytes—for example, 2:1 and 1:2 electrolytes such as CaCl₂ and Na₂SO₄—have been derived by Grahame (1953). These are more complicated than Eq. (14.39), but for low ψ_0 they all reduce to $\psi_x = \psi_0 e^{-\kappa x}$.

We now have all the equations needed for computing the ionic distributions away from a charged surface. For a 1:1 electrolyte, this is given by inserting Eq. (14.39) into Eq. (14.25) or (14.27). Figure 14.8 shows the variation of ψ_x and ρ_x for a 0.1 M 1:1 electrolyte, together with a Monte Carlo simulation for comparison. Note how the counterion density approaches the bulk value much faster than would be indicated by the Debye length. Indeed, for such a high surface charge density and potential the counterion distribution very near the surface is largely independent of the bulk electrolyte concentration, and it is left as an exercise for the reader to verify that even in 10^{-4} M the counterion profile over the first few ångstroms is not much different from that in 0.1 M (so long as σ remains the same).

⁶ $\tanh x = (e^x - e^{-x})/(e^x + e^{-x})$.

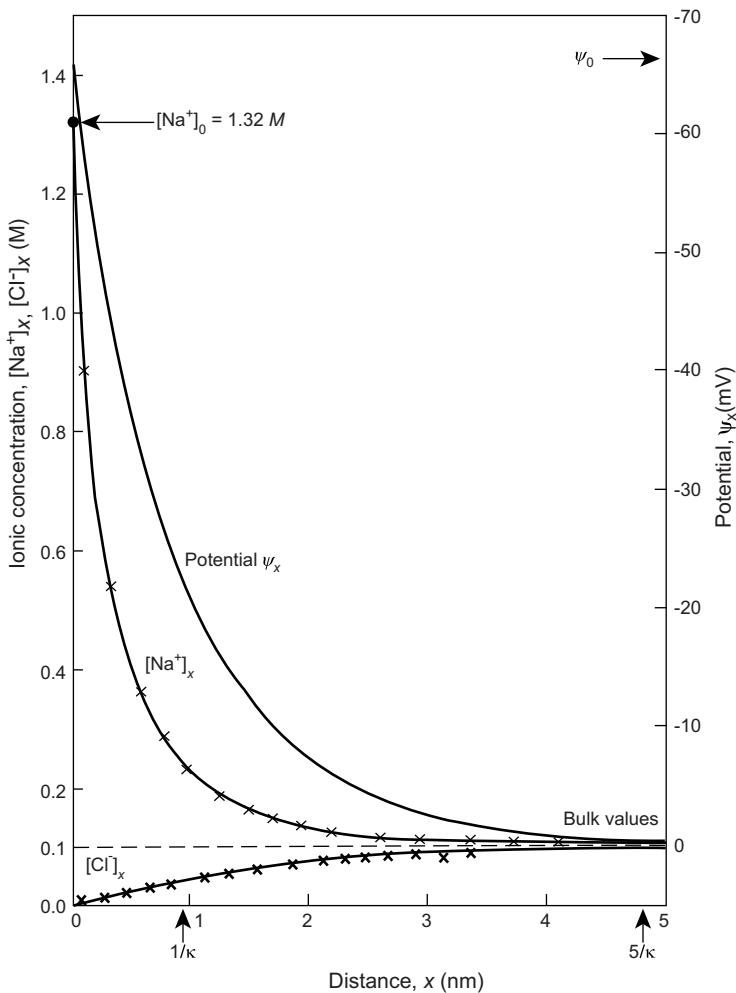


FIGURE 14.8 Potential and ionic density profiles for a 0.1 M monovalent electrolyte such as NaCl near a surface of charge density $\sigma = -0.0621 \text{ C m}^{-2}$ (about one electronic charge per 2.6 nm^2), calculated from Eqs. (14.39) and (14.25) with $\psi_0 = -66.2 \text{ mV}$ obtained from the Grahame equation. The crosses are the Monte Carlo results of Torrie and Valleau (1979, 1980). Note that the potential (and force between two surfaces) both decay asymptotically as $e^{-\kappa x}$, while the ionic concentrations decay much more sharply.

14.16 Electrostatic Double-Layer Interaction Forces and Energies between Various Particle Surfaces

The interaction pressure between two identically charged surfaces in an electrolyte solution (Figure 14.9) can be derived quite simply as follows. First, from Section 14.7 we note that at any point x the pressure $P_x(D)$ is given by

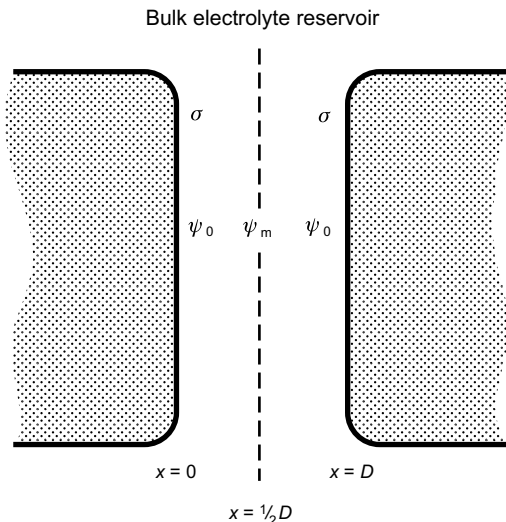


FIGURE 14.9

$$P_x(D) - P_x(\infty) = -\frac{1}{2}\epsilon_0\varepsilon \left[\left(\frac{d\psi}{dx} \right)_{x(D)}^2 - \left(\frac{d\psi}{dx} \right)_{x(\infty)}^2 \right] + kT \left[\sum_i \rho_{xi}(D) - \sum_i \rho_{xi}(\infty) \right]. \quad (14.42)$$

Second, from Eq. (14.7) we have

$$\sum_i \rho_{xi} = \sum_i \rho_{mi} + \frac{\epsilon_0\varepsilon}{2kT} \left(\frac{d\psi}{dx} \right)_x^2 \quad (14.43)$$

for any x or D , where $\sum \rho_{mi}$ is the total ionic concentration at the midplane at $x = \frac{1}{2}D$. Incorporating Eq. (14.43) into Eq. (14.42), and again putting $P_x(D = \infty) = 0$, yields two useful and equivalent expressions for the pressure:

$$P_x(D) = kT \left[\sum_i \rho_{0i}(D) - \sum_i \rho_{0i}(\infty) \right] = kT \left[\sum_i \rho_{mi}(D) - \sum_i \rho_{mi}(\infty) \right] \quad (14.44)$$

which, as before, is the uniform pressure across the gap (independent of position x) acting on the electrolyte ions and on the surfaces. The above result is essentially the same as Eqs. (14.17) and (14.18) and shows that P is simply the excess osmotic pressure of the ions at the surfaces or in the midplane. Since $\sum \rho_{mi}(\infty)$ is known from the bulk electrolyte concentration the problem reduces to finding the midplane concentration of ions $\rho_{mi}(D)$ when D is finite, and it is here that certain assumptions have to be made to obtain an analytic result (Verwey and Overbeek, 1948). For a 1:1 electrolyte such as NaCl, Eq. (14.44) may be written as

$$P = kT\rho_\infty [(e^{-e\psi_m/kT} - 1) + (e^{+e\psi_m/kT} - 1)] = 2kT\rho_\infty [\cosh(e\psi_m/kT) - 1] \quad (14.45)$$

$$\approx e^2\psi_m^2\rho_\infty/kT \quad \text{for } \psi_m < 25 \text{ mV}, \quad (14.46)$$

which assumes that the midplane potential ψ_m (not the surface potential ψ_0) is small. If we further assume that ψ_m is simply the sum of the potentials from each surface at $x = \frac{1}{2}D$ as previously derived for an isolated surface, then Eq. (14.39) gives $\psi_m \approx 2(4kT\gamma/e)e^{-\kappa D/2}$. Inserting this into Eq. (14.46) gives the final result for the repulsive pressure between two planar surfaces across a 1:1 electrolyte:

$$P = 64kT\rho_\infty\gamma^2e^{-\kappa D} = (1.59 \times 10^8)[\text{NaCl}]\gamma^2e^{-\kappa D} \text{ N m}^{-2} \quad \text{at } 25^\circ\text{C (298 K),} \quad (14.47)$$

where we note that $\gamma = \tanh(z\epsilon\psi_0/4kT)$ can never exceed unity. Equation (14.47) is known as the *weak overlap approximation* or *linear superposition approximation* (SLA) for the interaction between two similar surfaces at constant potential.

The interaction free energy per unit area corresponding to the above pressure is obtained by a simple integration with respect to D , and gives

$$W_{\text{flats}} = (64kT\rho_\infty\gamma^2/\kappa)e^{-\kappa D} \quad (14.48)$$

$$= 0.0482[\text{NaCl}]^{1/2} \tanh^2[\psi_0(\text{mV})/103]e^{-\kappa D} \text{ J m}^{-2} \quad (\text{for 1:1 electrolytes}) \quad (14.49)$$

$$= 0.0211[\text{MgSO}_4]^{1/2} \tanh^2[2\psi_0(\text{mV})/103]e^{-\kappa D} \text{ J m}^{-2} \quad (\text{for 2:2 electrolytes}), \quad (14.50)$$

where in the above equations the bulk concentrations $[\text{NaCl}]$ and $[\text{MgSO}_4]$ are in M. There is no simple expression for 2:1 or 1:2 electrolytes, or for mixed 1:1 and 2:1 electrolytes (Chan, 2002), but it is interesting to note that for surface potentials between 50 and 80 mV the values of $0.0482 \tanh^2 [\psi_0/103]$ and $0.0211 \tanh^2 [2\psi_0/103]$ differ by less than 20%, suggesting that either of the above equations provides a good approximation so long as the correct Debye length is used (which can always be accurately calculated using Eq. (14.36)).

Applying the Derjaguin approximation, Eq. (11.16), we may immediately write the expression for the force F between two spheres of radius R as $F = \pi RW$, from which the interaction free energy is obtained by a further integration (see Sader et al., 1995, for more accurate formulae for spheres):

$$W_{\text{spheres}} = (64\pi kTR\rho_\infty\gamma^2/\kappa^2)e^{-\kappa D} = 4.61 \times 10^{-11}R\gamma^2e^{-\kappa D} \text{ J} \quad (\text{for 1:1 electrolytes}). \quad (14.51)$$

We see therefore that the double-layer interaction between surfaces or particles of different geometries always decays exponentially with distance with a characteristic decay length equal to the Debye length. This is quite different from the van der Waals interaction where the decay is a power law having very different exponents for different geometries. Figure 13.1 gave the different expressions for the van der Waals forces and energies between bodies of different geometries in terms of their dimensions and the Hamaker Constant. Figure 14.10 is a similar figure for the double-layer forces and energies, given in terms of the dimensions of the particles, the Debye length κ^{-1} , and an “interaction constant” Z defined by

$$Z = 64\pi\epsilon_0\epsilon(kT/e)^2 \tanh^2(z\epsilon\psi_0/4kT) \text{ J m}^{-1} \text{ or N} \quad (14.52)$$

$$= (9.22 \times 10^{-11}) \tanh^2(\psi_0/103) \text{ J m}^{-1} \text{ at } 25^\circ\text{C or 298 K (room temperature)} \quad (14.53)$$

$$= (9.38 \times 10^{-11}) \tanh^2(\psi_0/107) \text{ J m}^{-1} \text{ at } 37^\circ\text{C or 310 K (physiological temperature)} \quad (14.54)$$

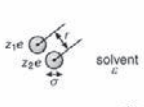
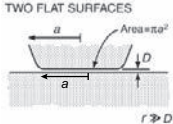
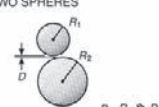
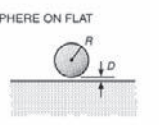
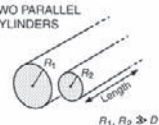
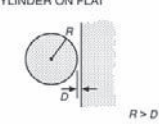
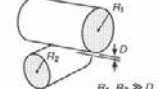
Geometry of bodies with surfaces D apart ($D \ll R$)		Electric 'Double-layer' Interaction	
		Energy, W	Force, $F = -dW/dD$
Two ions or small charged molecules	TWO IONS IN WATER 	$\frac{+z_1z_2e^2}{4\pi\epsilon_0\epsilon r} \frac{e^{-\kappa(r-\sigma)}}{(1+\kappa\sigma)}$	$\frac{+z_1z_2e^2}{4\pi\epsilon_0\epsilon r^2} \frac{(1+\kappa r)}{(1+\kappa\sigma)} e^{-\kappa(r-\sigma)}$
Two flat surfaces (per unit area)	TWO FLAT SURFACES 	$W_{\text{Flat}} = (\kappa / 2\pi) Ze^{-\kappa D}$	$(\kappa^2 / 2\pi) Ze^{-\kappa D}$
Two spheres or macromolecules of radii R_1 and R_2	TWO SPHERES 	$\left(\frac{R_1R_2}{R_1 + R_2} \right) Ze^{-\kappa D}$	$\kappa \left(\frac{R_1R_2}{R_1 + R_2} \right) Ze^{-\kappa D}$ Also $F = 2\pi \left(\frac{R_1R_2}{R_1 + R_2} \right) W_{\text{Flat}}$
Sphere or macromolecule of radius R near a flat surface	SPHERE ON FLAT 	$RZe^{-\kappa D}$	$\kappa RZe^{-\kappa D}$ Also $F = 2\pi RW_{\text{Flat}}$
Two parallel cylinders or rods of radii R_1 and R_2 (per unit length)	TWO PARALLEL CYLINDERS 	$\frac{\kappa^{1/2}}{\sqrt{2\pi}} \left(\frac{R_1R_2}{R_1 + R_2} \right)^{1/2} Ze^{-\kappa D}$	$\frac{\kappa^{3/2}}{\sqrt{2\pi}} \left(\frac{R_1R_2}{R_1 + R_2} \right)^{1/2} Ze^{-\kappa D}$
Cylinder of radius R near a flat surface (per unit length)	CYLINDER ON FLAT 	$\kappa^{1/2} \sqrt{\frac{R}{2\pi}} Ze^{-\kappa D}$	$\kappa^{3/2} \sqrt{\frac{R}{2\pi}} Ze^{-\kappa D}$
Two cylinders or filaments of radii R_1 and R_2 crossed at 90°	CROSSED CYLINDERS 	$\sqrt{R_1R_2} Ze^{-\kappa D}$	$\kappa \sqrt{R_1R_2} Ze^{-\kappa D}$ Also $F = 2\pi \sqrt{R_1R_2} W_{\text{Flat}}$

FIGURE 14.10 Electrostatic double-layer interaction energies $W(D)$ and forces ($F = -dW/dD$) between similar constant potential surfaces of different geometries in terms of the interaction constant Z defined by Eq. (14.52). For a monovalent 1:1 electrolyte such as NaCl ($z = 1$), $Z = 64\pi\epsilon_0\epsilon(kT/e)^2 \tanh^2(\psi_0/4kT) = (9.22 \times 10^{-11} \tanh^2(\psi_0/103)) \text{ J m}^{-1}$ at 25°C and $(9.38 \times 10^{-11}) \tanh^2(\psi_0/107) \text{ J m}^{-1}$ at 37°C (body temperature). The Debye length, κ^{-1} , is defined by Eq. (14.36).

where ψ_0 is in mV. The interaction constant Z is analogous to the Hamaker Constant A , and—apart from the electrolyte valency z —depends only on the properties of the surfaces. The other terms that appear in the expressions for the interaction energies and forces, such as κ , depend only on the solution and on the geometry and separation of the

surfaces. Note that the interaction constant Z is defined in terms of the surface potential ψ_0 of the isolated surfaces (at $D = \infty$), but it can also be expressed in terms of the surface charge density σ by applying the Grahame Equation.

As an example of the use of Figure 4.10, the double-layer energy for two identical spheres of radius R is given in the 4th row as $W(D) = Z R_1 R_2 e^{-\kappa D} / (R_1 + R_2) = \frac{1}{2} Z R e^{-\kappa D} = (4.61 \times 10^{-11}) R \tanh^2(\psi_0/103) e^{-\kappa D}$ J, which is the same as Eq. (14.51).

It is important to note that with increasing ionic strength, even though the Debye length falls due to the increased screening of the electric field, the asymptotic short-range force or energy can *increase*, depending on the geometry of the particles. This unintuitive result arises for those geometries in Figure 14.10, where κ appears in the numerator, for example, as occurs for both the energy and force between two planar surfaces. For such systems, as $D \rightarrow 0$ and $e^{-\kappa D} \rightarrow 1$, the repulsion at constant potential ($Z = \text{constant}$) is seen to increase with increasing ionic strength (increasing κ). This has important implications for the short-range and adhesion forces in aqueous solutions, as discussed later (cf. Figure 14.15).

At low surface potentials, below about 25 mV, all the above equations simplify to the following: For two planar surfaces,

$$P \approx 2\varepsilon_0 \varepsilon \kappa^2 \psi_0^2 e^{-\kappa D} = 2\sigma^2 e^{-\kappa D} / \varepsilon_0 \varepsilon \quad (14.55)$$

and

$$W \approx 2\varepsilon_0 \varepsilon \kappa \psi_0^2 e^{-\kappa D} = 2\sigma^2 e^{-\kappa D} / \kappa \varepsilon_0 \varepsilon \quad (14.56)$$

while for two spheres of radius R ,

$$F \approx 2\pi R \varepsilon_0 \varepsilon \kappa \psi_0^2 e^{-\kappa D} = 2\pi R \sigma^2 e^{-\kappa D} / \kappa \varepsilon_0 \varepsilon \quad (14.57)$$

and

$$W \approx 2\pi R \varepsilon_0 \varepsilon \psi_0^2 e^{-\kappa D} = 2\pi R \sigma^2 e^{-\kappa D} / \kappa^2 \varepsilon_0 \varepsilon \quad (14.58)$$

In the above, ψ_0 and σ are related by $\sigma = \varepsilon_0 \varepsilon \kappa \psi_0$, which, as we have seen, is valid for low potentials. These four equations are quite useful because they are valid for all electrolytes, whether 1:1, 2:1, 2:2, 3:1, or even mixtures as long as the appropriate Debye lengths are used as given by Eqs. (14.36)–(14.37). Thus, they are particularly suitable when divalent ions are present, since the surface charge and potential is often low due to ion binding.

14.17 Exact Solutions for Constant Charge and Constant Potential Interactions: Charge Regulation

All the expressions derived so far are accurate only for surface separations beyond about one Debye length. At smaller separations one must resort to numerical solutions of the Poisson-Boltzmann equation to obtain the exact interaction potential (Verwey and Overbeek, 1948; Devereux and De Bruyn, 1963; Honig and Mul, 1971) for which there are no simple expressions that cover all possible situations. Figures 14.11 and 14.12 show

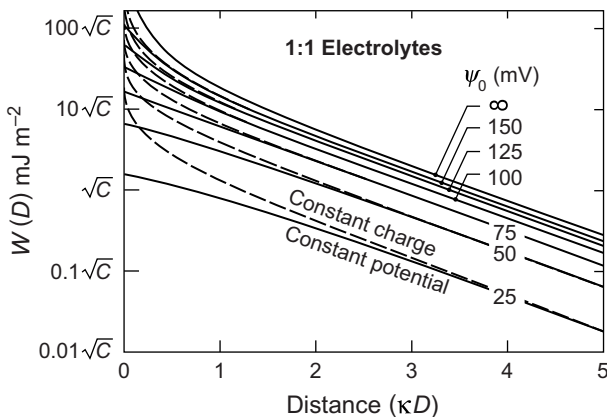


FIGURE 14.11 Repulsive double-layer interaction energy for two planar surfaces in a 1:1 electrolyte [exact solution kindly computed by M. Sculley, R. Pashley, and L. White based on Ninham and Parsegian (1971)]. ψ_0 is the potential of the isolated surfaces and C the electrolyte concentration in M, which is related to the Debye length by $1/\kappa = 0.304/\sqrt{C}$ nm. Theoretically, the double-layer interaction must lie between the constant-charge and constant-potential limits. (--) constant charge, (—) constant potential. However, these limits are based on the validity of the Poisson-Boltzmann (PB) equation; if other forces, such as ion-correlation, hydrophobic, or steric-hydration, are present, the interaction can be more attractive or more repulsive. At separations greater than $1/\kappa$ the forces and energies are well described by Eqs. (14.47)–(14.51) for $z = 1$.

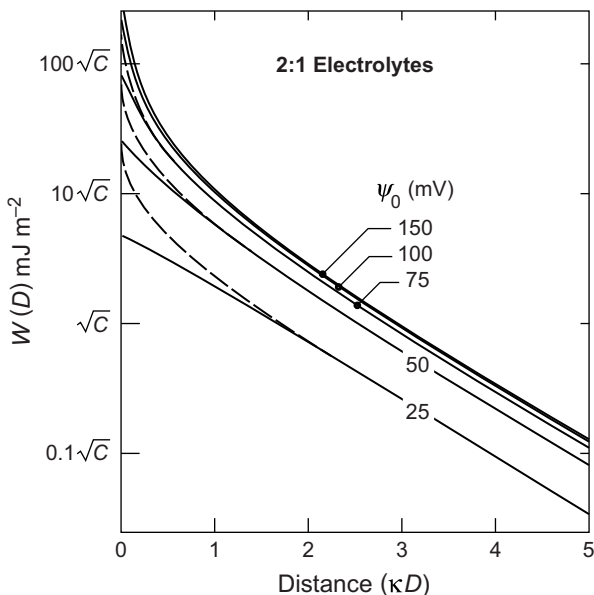


FIGURE 14.12 Repulsive double-layer interaction energy for two planar surfaces in a 2:1 electrolyte where the counterions—that is, the ions of opposite charge to those on the surface—are divalent [computed as in Figure 14.11]. For 1:2 electrolytes (where the counterions are monovalent) the interaction is approximately as for a 1:1 electrolyte but with the Debye length as for a 2:1 or 1:2 electrolyte—that is, Debye length $1/\kappa = 0.176/\sqrt{C}$ nm, where C is the electrolyte concentration in M. (--) constant charge, (—) constant potential. At separations greater than $1/\kappa$ the forces are well described by Eqs. (14.47)–(14.51) for $z = 2$.

plots of the exact numerical solutions for the double-layer interaction potentials of two planar surfaces in pure 1:1 and 1:2 electrolytes in the two limiting cases of constant charge and constant potential. The figures may be used for reading off the interaction energy of any 1:1 or 2:1 electrolyte at any desired concentration C , and surface separation D . This is because the energy scales with \sqrt{C} and the distance scales with the Debye length, κ^{-1} . The constant potential curves of Figure 14.11 compare reasonably well with the approximate expression of Eq. (14.48) even at small separations, and especially when ψ_0 is between 50 and 100 mV. In contrast, as shown by the dashed curves in Figures 14.11 and 14.12, interactions at constant charge are always greater than those at constant potential, especially at separations below 1–2 Debye lengths where they veer sharply upwards, becoming infinite as $D \rightarrow 0$, while the constant potential interaction tends toward a finite value.

In addition there is the question of charge regulation at small separations. In general, neither the surface charge density nor the potential remain constant as two surfaces come close together. Instead, as was discussed in Section 14.9, some of the counterions are forced back onto the surfaces thereby reducing σ . This affects the form of the interaction which now falls between the constant charge and constant potential limits. At large distances, beyond a few κ^{-1} , all the interaction pressures and energies merge and are well described by the equations based on the Linear Superposition Approximation as listed in Figure 14.10.

If there is no binding, the surface charge density remains constant, and in the limit of small D the number density of monovalent counterions between the two surfaces will approach a uniform value of $2\sigma/eD$. From Eq. (14.44) the limiting pressure in this case is

$$P(D \rightarrow 0) = kT \sum_i \rho_{mi} = -2\sigma kT/zeD = +|2\sigma kT/zeD|, \quad (14.59)$$

and

$$W(D \rightarrow 0) = (-2\sigma kT/ze)\log D + \text{constant}, \quad (14.60)$$

that is, as $D \rightarrow 0$ the pressure and the energy become infinite. Note that this is the same *osmotic limit* as in the case of no bulk electrolyte (counterions only), Eq. (14.23), and results from the limiting osmotic pressure of the “trapped” counterions.

If there is counterion binding as D decreases—that is, charge regulation— P falls below this limit, and the Poisson-Boltzmann equation must now be solved self-consistently by including the dissociation constants of the adsorbing ions (cf. Section 14.12). The computations have been described by Ninham and Parsegian (1971) and Healy et al., (1980), and simple numerical algorithms have been given by Chan et al., (1976, 1980b). So long as the Poisson-Boltzmann equation remains valid, the double-layer forces between two symmetrical charge-regulating surfaces always lie between the constant surface charge and constant surface potential limits shown in Figures 14.11 and 14.12.⁷ When the PB equation breaks down—for example, when the electrolyte contains multivalent

⁷Although Borkovec and Behrens (2008) have suggested that under certain conditions the double-layer interaction can be weaker than at constant potential.

counterions—or when other forces, such as ion-correlation forces, are present, then the resulting interaction can be very different and even change sign—that is, become attractive. And the situation becomes much more complex for asymmetric surfaces, even in the absence of charge regulation.

An often overlooked feature of a charge-regulating interaction is that as two surfaces approach each other there is a continual exchange of ions with the bulk reservoir. This takes time. If two surfaces are brought together quickly, the interaction may be at constant charge even though the equilibrium interaction is at constant potential (Raviv et al., 2002; Anderson et al., 2010).⁸ And the issue is not only determined by the diffusion of ions into and out of the interaction zone; quite often the ion exchange processes at the interfaces is slow (minutes) and is the rate-limiting part of the overall interaction.

14.18 Asymmetric Surfaces

For two surfaces of different charge densities or potentials the interaction energy can have a maximum or minimum at some finite distance, usually below $1/\kappa$. Approximate equations for the interactions of two surfaces of unequal but constant potentials were given by Hogg et al., (1966), Parsegian and Gingell (1972), Ohshima et al., (1982), and Chan et al., (1995), and for unequal charges by Gregory (1975), and Ohshima (1995). The “Hogg-Healy-Fuerstenau” equation (Hogg et al., 1966) for two planar surfaces of low constant potentials in 1:1 electrolyte is

$$W(D) = \frac{\varepsilon_0 \varepsilon k [2\psi_1 \psi_2 - (\psi_1^2 + \psi_2^2) e^{-\kappa D}]}{(e^{+\kappa D} - e^{-\kappa D})} \text{ J m}^{-2} \quad (14.61)$$

which leads to a pressure of

$$P(D) = -\frac{dW}{dD} = \frac{2\varepsilon_0 \varepsilon k^2 [(e^{+\kappa D} + e^{-\kappa D}) \psi_1 \psi_2 - (\psi_1^2 + \psi_2^2)]}{(e^{+\kappa D} - e^{-\kappa D})^2} \text{ N m}^{-2}. \quad (14.62)$$

Approximate expressions for constant charge interactions are more complicated. The following, proposed by Gregory (1975), is probably the simplest that is also reasonably accurate for 1:1 electrolytes

$$P(D) = \rho_\infty kT \left[2 \left\{ 1 + \left(\frac{ze(\psi_1 + \psi_2)/kT}{e^{+\kappa D/2} - e^{-\kappa D/2}} \right)^2 \right\}^{1/2} - \frac{\left\{ ze(\psi_1 - \psi_2)/kT \right\}^2 e^{-\kappa D}}{1 + \left(\frac{ze(\psi_1 + \psi_2)/kT}{e^{+\kappa D/2} - e^{-\kappa D/2}} \right)^2} - 2 \right] \text{ N m}^{-2}. \quad (14.63)$$

It is noteworthy that the double-layer forces between dissimilar surfaces can change sign, depending on the conditions. For example, for constant potential interactions at large separations, Eq. (14.62) tends to $P(\kappa D \gg 1) = 2\varepsilon_0 \varepsilon k^2 \psi_1 \psi_2 e^{-\kappa D}$. This is attractive when ψ_1 and ψ_2 have opposite signs and repulsive when they have the same sign, and it reduces

⁸For a colloidal system at equilibrium, all the interactions are given by the equilibrium interaction potentials even though the particles may be moving very rapidly in the solution. This is an example of *Detailed Balance*.

to Eq. (14.55) when $\psi_1 = \psi_2$. However, in the limit of $D \rightarrow 0$, Eq. (14.62) tends to $P(D \rightarrow 0) = -\varepsilon_0 \varepsilon k (\psi_1 - \psi_2)^2 / 2D^2$ which is always negative—that is, attractive.

The constant charge interaction at large separations, Eq. (14.63), reduces to $P(\kappa D \gg 1) = 4(\rho_\infty z^2 e^2 / kT) \psi_1 \psi_2 e^{-\kappa D} = 2\varepsilon_0 \varepsilon k^2 \psi_1 \psi_2 e^{-\kappa D} = 2\kappa^2 \sigma_1 \sigma_2 e^{-\kappa D} / \varepsilon_0 \varepsilon$, which is the same as the constant potential limit. However, in the limit of $D \rightarrow 0$, Eq. (14.63) tends to $P(D \rightarrow 0) = +|(\sigma_1 + \sigma_2) kT / zeD|$, which reduces to Eq. (14.59) when $\sigma_1 = \sigma_2$ and that is always positive—that is, repulsive (see Problem 14.4).

All of the above equations assume no charge regulation and that the surface charges are smeared out on each surface. Both of these assumptions are particularly dangerous when the two surfaces are different. Such surfaces usually contain ion-exchangeable sites, and their charges can often move about and redistribute as the surfaces come into contact. Some of these issues, especially those involving “competitive adsorption,” have been addressed by Ninham and Parsegian (1971), Prieve and Ruckenstein (1976), Chan et al., (1980), Pashley (1981), Van Riemsdijk et al., (1986), Carnie and Chan (1993), and Ettelaine and Buscall (1995), and are discussed again in later sections devoted to acid-base interactions and the adhesion of amphoteric and biological surfaces.

At very large separations, above 1 μm or the dimensions of colloidal particles, there is experimental evidence that the double-layer force can become weakly attractive even between identical particles, which can result in phase separation (Ise and Yoshida, 1996). Sogami and Ise (1984) have proposed a potential—the “Sogami potential”—to account for this effect, but it remains controversial both at the experimental and theoretical levels.

14.19 Ion-Condensation and Ion-Correlation Forces

We may recall that for a system of charges that is overall electrically neutral the net electrostatic (purely Coulombic) interaction is always attractive. This is the attraction that leads to the formation of ionic crystals discussed in Section 3.4. However, as discussed further in Section 3.8, in a medium of high dielectric constant such as water, the Coulomb interaction is much reduced and thermal effects can now win out, causing the dissolution of the ionic crystal. An important parameter that always arises when considering such effects is the *Bjerrum length* λ_B , which is the distance r between the centers of two unit charges when their Coulomb energy, $w(r) = e^2 / 4\pi\varepsilon_0\varepsilon r$, equals the thermal energy kT —that is,

$$\begin{aligned}\lambda_B &= e^2 / 4\pi\varepsilon_0\varepsilon kT \\ &= 0.72 \text{ nm in water at } 25^\circ\text{C} (\varepsilon = 78.3).\end{aligned}\quad (14.64)$$

The Bjerrum length appears often in equations associated with electrostatic interactions in electrolyte solutions, such as double-layer, ion-condensation, and ion-correlation interactions. For example, the Debye length, Eq. (14.36), can be expressed as $\sum_i (4\pi\lambda_B \rho_\infty z_i^2)^{1/2}$, and the solubility of a 1:1 electrolyte, Eq. (3.18), can be expressed

as $X_s \approx e^{-\lambda_B/(a_+ + a_-)}$, where $(a_+ + a_-)$ is the distance between the centers of the ions. In Section 3.8 we saw how this equation accounts for the higher solubility or dissociation of larger ions (larger $a_+ + a_-$). For example, when $(a_+ + a_-) = \lambda_B$ we expect full dissociation up to electrolyte concentrations of ~40% (mole/mole). For smaller and especially multivalent ions such as Ca^{2+} , their tendency to dissociate is much reduced, and such electrolytes or salts are much less soluble, and their ions in solution are often only partially dissociated (or partially associated).

A similar effect arises at charged surfaces. Consider a small sphere of radius R where the surface charges are separated by a mean distance d such that the total charge on the sphere is $Q = (4\pi R^2/d^2)e$. The Coulomb energy of bringing a small ion of radius a and charge ze up to the sphere is $zeQ/4\pi\epsilon_0\epsilon(R + a)$. For small similarly sized monovalent ions ($Q = e$, $z = 1$) this reduces to the expected equation: $w(r) = e^2/4\pi\epsilon_0\epsilon(2a)$, but for a large spheres ($R \gg a$) we obtain for the ion-surface binding energy:

$$w \approx zeQ/4\pi\epsilon_0\epsilon R \approx 4\pi z k T R \lambda_B / d^2. \quad (14.65)$$

This equation shows that at constant surface charge density (fixed d), the binding energy of a (counter)ion to an oppositely charged surface is higher (1) for larger spheres or particles (larger R), (2) the closer the surface co-ions are to each other (smaller d , higher σ), and (3) the higher the valency, z , of the binding counterion. The first two conclusions show that the size of a macromolecule or small colloidal particle is important in determining its surface charge density σ and potential ψ_0 —the smaller the particle, the more likely it is to be fully ionized.

The strength of ion binding also depends on the shapes or geometry of particles, being stronger for planar surfaces, then cylindrical surfaces then spherical surfaces—an effect that is referred to as *charge, ion or “Manning” condensation* (Manning, 1969; Ray and Manning, 1996). For example, planar surfaces are generally less than 10% ionized or dissociated, cylindrical (DNA or micelle) surfaces are typically ~20% ionized, small spherical micelles are ~25% ionized (Pashley & Ninham, 1987), while individual ionizable molecules, which can be considered as very small spheres, are often fully (close to 100%) ionized. Equation (14.65) also shows why this effect is more pronounced for multivalent counterions.

The effect of ion condensation is a reduced double-layer repulsion, especially between planar and cylindrical structures such as clay sheets, charged lipid bilayers, DNA, nanorods and microtubules in aqueous solutions, which is further enhanced when these contain calcium or polyvalent ions (Bloomfield, 1991; Podgornik et al., 1994; Tang et al., 1996). In reality, the binding energy of ions to surfaces in electrolyte solutions is much more complex than given by Eq. (14.65) and depends, among other things, on the absolute or relative values of R , a , λ_B , d , and κ^{-1} .

Whereas ion-condensation simply lowers the double-layer repulsion, there is another counterion effect between similarly charged surfaces that gives rise to an attraction. This is contrary to the Poisson-Boltzmann equation that predicts a repulsion at all separations between equally charged surfaces. This additional electrostatic force was first proposed

by Oosawa (1971) who considered the implications of having mobile (rather than fixed) counterions in each double layer. These mobile ions, he argued, constitute a highly polarizable (essentially conducting) layer at each interface whose fluctuations in density must give rise to an attractive van der Waals–like force with another double-layer. This force is not included in the Poisson-Boltzmann equation nor in the Lifshitz theory. Now known as the *ion-correlation or charge fluctuation force* (Jonsson, 1980; Guldbrand et al., 1984; Kjellander, 1988a) this attraction becomes significant at small distances (<4 nm), and it increases with the surface charge density and valency of the counterions—just as does the ion-condensation effect with which it is often associated (Rouzina and Bloomfield, 1996; Gronbech-Jensen, 1997).

In the first Monte Carlo study of the ionic density distributions, interaction energies and pressures between planar surfaces, spheres and cylinders, Wennerström and colleagues (1982) concluded that between surfaces of high charge density the attractive ion-correlation force can reduce the effective double-layer repulsion by 10–15% if the counterions are monovalent. However, with divalent counterions such as Ca^{2+} the ion-correlation attraction was found to exceed the double-layer repulsion—the net force becoming overall attractive—below about 2 nm, even in dilute electrolyte solutions. Such short-range attractive ion-correlation forces have been measured between anionic surfactant and lipid bilayers in CaCl_2 solutions, and they are believed to be responsible for the strong adhesion or limited swelling of negatively charged clay surfaces in the presence of divalent ions (Marra, 1986b, c; Khan et al., 1985; Kjellander et al., 1988a, b; Kjellander, 1990). Their importance in the interactions of colloidal, amphiphilic and biological surfaces have yet to be fully established.

Similar ion-correlation interactions can arise between the surface co-ions of two opposing surfaces if these are mobile, as occurs at surfactant and lipid bilayer and biological membrane surfaces. Indeed, it has been suggested that when both the counterions and coions are mobile, the final adhesion of the two surfaces can cause them to order into a thin crystalline lattice (Rouzina and Bloomfield, 1996). Such effects are usually specific and can be understood only by considering the surface charges as discrete and of a certain size rather than as smeared out over the surfaces (cf. Chapter 21).

Both ion-correlation and ion-condensation forces enhance adhesion; they are related (Rouzina, 1996; Shklovskii, 1999) but are difficult to separate, quantify or simulate and, so far, do not appear to be describable by a single simple force-law or potential function although some have been proposed (Lau et al., 2000). Experimental examples of both of these interactions are given in Part III.

Another effect that derives from the discreteness of surface charges is the “image force” produced by a surface coion and its image on the opposite surface. As shown in Figure 13.2, this produces a repulsive force when the two surfaces are in a medium (e.g., water) with a dielectric constant that is higher than those of the surfaces. However, Ohshima (1995) has argued that for certain charge-regulating mechanisms the image force can *reduce* the double-layer repulsion.

14.20 More Complex Systems: Finite Reservoir Systems and Finite Ion-Size Effects

We have seen how different are the interactions between charged surfaces in the absence and presence of a bulk “infinite” reservoir of electrolyte ions at some given concentration. In many cases the situation is not so simple. For example, the case of “counterions only,” discussed in Sections 14.2-14.9 changes when some electrolyte is present, and when the number of counterions coming off from the surfaces are comparable to the number of background electrolyte ions already present in the system, the equations for the ionic distributions and interaction forces become more complicated and can only be solved numerically (Dubois et al., 1992). Such systems arise when concentrated dispersions of clay sheets, micelles, bilayers or polyelectrolytes interact in pure water or dilute salt solutions (Dubois et al., 1992; Diederichs et al., 1985; Delville et al., 1993).

In some cases, simplifying assumptions can be made. Thus, it has been found that the Debye length of a micellar or polyelectrolyte solution is given by Eq. (14.36) but where only the background electrolyte ions and micellar or polyelectrolyte counterions contribute to the ionic concentrations in that equation but not the micelles or polyelectrolyte molecules themselves. For example, for a micellar system above the *critical micelle concentration* (cmc) consisting of completely dissociated surfactant monomers at a concentration X_{cmc} coexisting with micelles of concentration X_{mic} and aggregation number N of which a fraction f are ionized (typically $f \approx 0.25$), the Debye length is given by (Pashley and Ninham, 1987)

$$\kappa^2 = \frac{e^2}{\varepsilon_0 \varepsilon kT} [2X_{\text{cmc}} + (NX_{\text{mic}} - X_{\text{cmc}})f]. \quad (14.66)$$

Tadmor and colleagues (2002) derived a similar equation for polyelectrolyte solutions.

Finite ion size effects can play an important role in modifying the double-layer interactions between surfaces at small separations. First, as discussed in Section 14.6, the existence of a Stern Layer due to finite cation and/or counterion sizes does not necessarily affect the functional form of the ionic distribution away from a surface; but it does shift the plane of origin of the distribution (the Outer Helmholtz Plane or OHP) which effectively changes the way $D = 0$ is defined in equations for the forces. As will be discussed further below, this can have important consequences in the presence of another force, such as the van der Waals force, which may have a different plane of origin. Similar finite size effects arise in the case of van der Waals forces, but now with respect to the *solvent* molecules, as described in Chapter 15.

The previous sections have revealed the great complexity of double-layer forces, almost to the point where it may appear than any interaction is possible. However, as we shall see, there are many situations where the measured forces appear to be well described by the simplest continuum equations, such as those in Figure 14.10, right down to molecular contact.

14.21 Van der Waals and Double-Layer Forces Acting Together: the DLVO Theory

The total interaction between any two surfaces must also include the van der Waals attraction. Now, unlike the double-layer interaction, the van der Waals interaction potential is largely insensitive to variations in electrolyte concentration and pH, and so may be considered as fixed in a first approximation. Further, the van der Waals attraction must always exceed the double-layer repulsion at small enough distances since it is a power law interaction (i.e., $W \propto -1/D^n$), whereas the double-layer interaction energy remains finite or rises much more slowly as $D \rightarrow 0$. Figure 14.13 shows schematically the various types of interaction potentials that can occur between two similarly charged surfaces or colloidal particles in a 1:1 electrolyte solution under the combined action of these two forces. Depending on the electrolyte concentration and surface charge density or potential one of the following may occur:

- For highly charged surfaces in dilute electrolyte (i.e., long Debye length), there is a strong long-range repulsion that peaks at some distance, usually between 1 and 5 nm, at the *force* or *energy barrier*, which is often high (many kT).
- In more concentrated electrolyte solutions there is a significant *secondary minimum*, usually beyond 3 nm, before the energy barrier closer in. The potential energy minimum at contact is known as the *primary minimum*. For a colloidal system, even though the thermodynamically equilibrium state may be with the particles in contact in the deep primary minimum, the energy barrier may be too high for the particles to

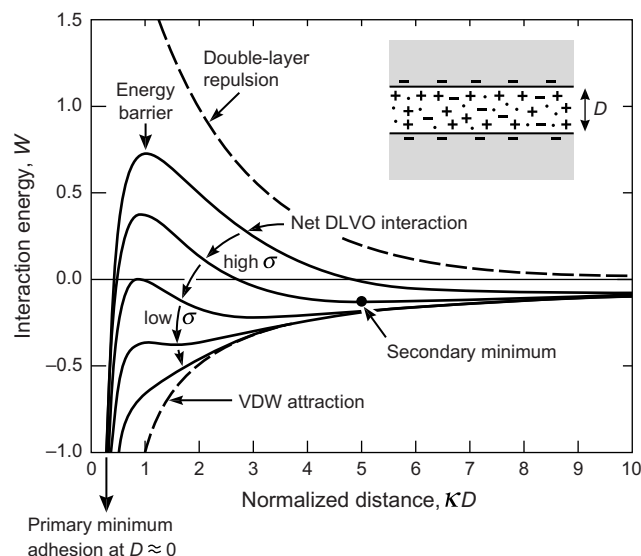


FIGURE 14.13 Schematic energy versus distance profiles of the DLVO interaction. The actual magnitude of the energy W is proportional to the particle size (radius) or interaction area (between two planar surfaces).

overcome during any reasonable time period. When this is the case, the particles will either sit in the weaker secondary minimum or remain totally dispersed in the solution. In the latter case the colloid is referred to as being *kinetically stable* (as opposed to *thermodynamically stable*).

- For surfaces of low charge density or potential, the energy barrier will be lower. This leads to slow aggregation, known as *coagulation* or *flocculation*. Below a certain charge or potential, or above some concentration of electrolyte, known as the *critical coagulation concentration*, the energy barrier falls below the $W = 0$ axis (middle curve in Figure 14.13) and the particles then coagulate rapidly. The colloid is now referred to as being *unstable*.
- As the surface charge or potential approaches zero the interaction curve approaches the pure van der Waals curve (lower dashed curve in Figure 14.13), and two surfaces now attract each other strongly at all separations.

The sequence of phenomena described above can be described quantitatively (see Worked Examples 14.5 and 14.6), and it forms the basis of the celebrated DLVO theory of colloidal stability, after Derjaguin and Landau (1941), and Verwey and Overbeek (1948). See also Hiemenz (1997), Hunter (2001), and Evans and Wennerström (1999).

The main factor inducing two (negatively charged) surfaces to come into adhesive contact in a primary minimum is the lowering of their surface charge or potential, brought about by decreasing the pH, increased cation binding, or increasing the screening of the double-layer repulsion by increasing the salt concentration. If the double-layer repulsion remains high on raising the salt concentration, two surfaces can still “adhere” to each other, but in the secondary minimum, where the adhesion is much weaker and easily reversible. On the other hand, as discussed below, in Section 14.16 and in Chapter 15, there are situations where particles first aggregate then redisperse as the salt concentration or pH is increased.

It is clear that one must have a fairly good idea of the charging process occurring at a surface before attempting to understand its double-layer interactions and the stability of colloidal dispersions, as Worked Examples 14.5 and 14.6 show.



Worked Example 14.5

Question: For a biocolloidal dispersion of $0.1\text{ }\mu\text{m}$ radius vesicles in a 100 mM NaCl solution at 37°C it has been established that the surface potential ψ_0 changes linearly with increasing pH from $\psi_0 = +50\text{ mV}$ at pH 5 to $\psi_0 = -50\text{ mV}$ at pH 7. Assuming that the vesicle dispersion remains effectively stable for energy barriers greater than about $25\text{ }kT$, calculate the range of pH over which the system is unstable—that is, the vesicles aggregate. Assume a Hamaker constant for the vesicles in the solution of $A = 10^{-20}\text{ J}$.

Answer: The vesicle-vesicle interaction energy at 37°C is

$$W(D) = \frac{1}{2}RZe^{-\kappa D} - AR/12D = (0.5 \times 10^{-7}) \times (9.38 \times 10^{-11}) \tanh^2(\psi_0/107)e^{-\kappa D} - (10^{-20} \times 10^{-7})/12D = (4.69 \times 10^{-18}) \tanh^2(\psi_0/107) e^{-D(\text{nm})/0.95} - (8.33 \times 10^{-20})/12D(\text{nm}).$$

Figure 14.14 shows the DLVO plots at $\psi_0 = \pm 24.5\text{ mV}$ (the “critical coagulation potential” where the energy

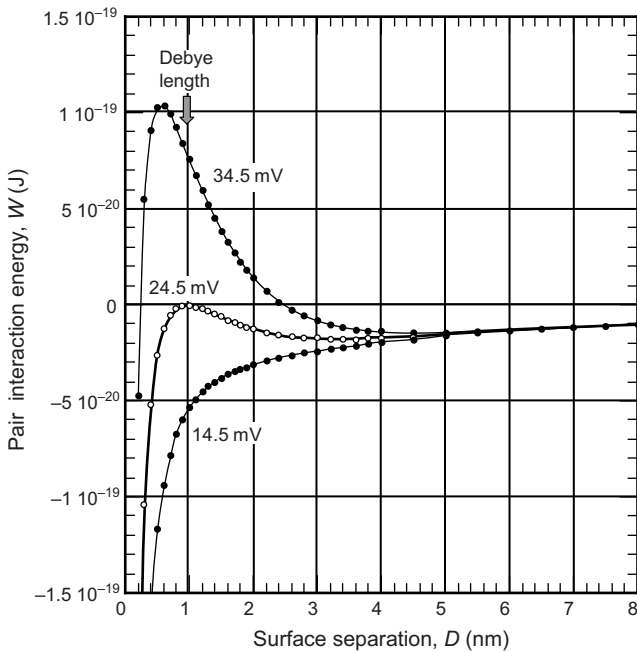


FIGURE 14.14 Computed DLVO energy profiles between amphoteric vesicles of radii 1,000 Å (0.1 μm) in 100 mM NaCl solution at 37°C. Note that at the “critical coagulation potential” (middle curve) the energy maximum at $W = 0$ occurs at the Debye length ($D = \kappa^{-1} = 0.95$ nm in 100 mM NaCl).

is everywhere negative resulting in rapid coagulation) as well as at ± 14.5 and ± 34.5 mV—that is, 10 mV on either side of the critical potential. The energy barrier exceeds $25 kT = 1.1 \times 10^{-19}$ J for potentials higher than about 35 mV (positive or negative), which correspond to pH values of $35/50 = 0.7$ above or below pH 6.0 (the “isoelectric point” or pI where $\psi_0 = 0$). Thus, the vesicles will aggregate at pH values between 5.3 and 6.7, although rapid coagulation will occur at pH values between 5.5 and 6.5. Strictly, the answer also depends on the vesicle concentration and on the depth of the primary minimum. The secondary minimum at ~4.5 nm is of depth 1.5×10^{-20} J or $3.5 kT$, which is not deep enough to cause aggregation except for larger vesicles at higher vesicle concentrations.

Worked Example 14.6

Question: For a number of colloidal systems it is found that the “critical coagulation concentration” (ccc) of the electrolyte varies with the inverse sixth power of the counterion valency z —that is, $\rho_\infty(\text{ccc}) \propto 1/z^6$. Is this empirical observation, known as the Schultze-Hardy rule, (Schultze, 1882, 1883; Hardy, 1900), consistent with the DLVO theory?

Answer: The total DLVO interaction potential between two spherical particles interacting at constant potential is

$$W(D) = (64\pi k T \rho_\infty \gamma^2 / \kappa^2) e^{-\kappa D} - AR/12D \quad (14.67)$$

By definition (see Figures 14.13 and 14.14), the critical coagulation concentration or condition occurs when both $W = 0$, and $dW/dD = 0$. The first condition leads to

$$\kappa^2/\rho_\infty = 768\pi kTD\gamma^2 e^{-\kappa D}/A,$$

while the second condition leads to $\kappa D = 1$, which shows that the potential maximum occurs at $D = \kappa^{-1}$ (the Debye length) as illustrated in Figure 14.14. Inserting this into the above equation leads to

$$\kappa^3/\rho_\infty = 768\pi kT\gamma^2 e^{-1}/A,$$

that is,

$$\kappa^6/\rho_\infty^2 \propto (T\gamma^2/A)^2.$$

Now, since $\kappa^2 \propto \rho_\infty z^2/\epsilon T$, the above equation implies that

$$z^6 \rho_\infty \propto \epsilon^3 T^5 \gamma^4 / A^2, \quad (14.68)$$

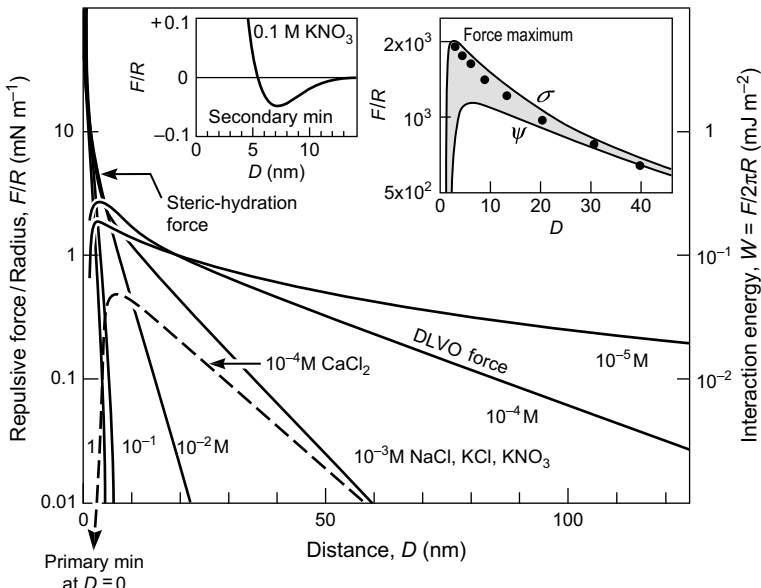


FIGURE 14.15 DLVO forces measured between two negatively charged mica surfaces in monovalent (10^{-5} to $1 \text{ M NaCl, KCl, KNO}_3$) and divalent (10^{-4} M CaCl_2) solutions. The shaded band in the right inset is the theoretical DLVO force in $10^{-4} \text{ M 1:1 electrolyte}$ using a Hamaker constant of $A = 2.2 \times 10^{-20} \text{ J}$ showing the constant charge σ and constant potential ψ limits. Theoretically, within the Poisson-Boltzmann formalism, we expect the interaction to fall between these two limits. At low ionic strengths, the forces are in good agreement with the DLVO theory right down to adhesive molecular contact in the primary minimum at $D = 0$. The left inset is the measured force in concentrated $0.1\text{--}1.0 \text{ M KNO}_3$ showing the emergence of a secondary minimum, and at even smaller separations there is an additional repulsive short-range steric-hydration force believed to be due to the finite hydrated size of the adsorbed monovalent cations (see Figure 14.7). Figure 14.18 shows a similar effect. [Data from SFA experiments with surfaces in the crossed-cylinder geometry, equivalent to a sphere of radius R near a flat surface or two spheres of radius $2R$, from Israelachvili and Adams, 1978; Pashley, 1981a; and Israelachvili, 1982.]

which is a constant if γ is constant, a condition that holds at high surface potentials ($\psi_0 > 100$ mV) where $\gamma = \tanh(z\psi_0/4kT) = 1$. In this limit, therefore, the critical coagulation concentrations do indeed scale as $\rho_\infty \propto 1/z^6$. For example, if coagulation occurs at 1 M with a 1:1 electrolyte, it will occur at $\frac{1}{64}$ M with a 2:2 electrolyte (or divalent counterions), and at $\frac{1}{729}$ M with a 3:3 electrolyte (or trivalent counterions). Thus, the Schultze-Hardy rule is consistent with the DLVO theory.

But wait. Is it not unreasonable to assume high surface potentials in divalent and trivalent electrolyte solutions? Let us investigate the case of low potentials. Here we have $\gamma \propto z\psi_0/T$, so that Eq. (14.68) now becomes

$$z^2 \rho_\infty \propto \epsilon^3 T \psi_0^4 / A^2, \quad (14.69)$$

which is constant if ψ_0 remains constant. Thus for low but constant potentials we obtain a modified form of the Schultze-Hardy rule: $\rho_\infty \propto 1/z^2$.

In real systems the surface potential is neither high nor constant, but usually falls to quite low values as the valency of the electrolyte counterions increases. For example, if $\psi_0 \propto 1/z$, then for *low* potentials we now obtain: $\rho_\infty \propto \psi_0^4/z^2 \propto 1/z^6$, which brings us back to the Schultze-Hardy rule. Clearly, the DLVO theory can be applied in more ways than one to explain the Schultze-Hardy rule.



Probably the most important practical issue in any quantitative interpretation of experimental results in terms of the DLVO theory is the question of the locations of the “planes of origin” of the double-layer and van der Waals forces. For the double-layer interaction $D = 0$ is defined at the plane where the PB equation commences to be valid—that is, at the OHP, which is generally at or a few ångstroms *further out* from the physical substrate-liquid interface due to the finite size of the surface cations or adsorbed counterions (14.4, 14.7 and 14.18) or the protruding or mobile surface-attached co-ions (Figures 15.14, 16.14, and Chapter 21). On the other hand, for the van der Waals force $D = 0$ is defined as the distance between the atomic or ionic centers, which is $\sim 2\text{\AA}$ *further in* from the physical solid-liquid interface (cf. Section 13.13). A difference of δ in the locations of $D = 0$ per surface (2δ for both surfaces) pushes the plane of origin of the double-layer interaction (the OHP) out to $D = 2\delta$ relative to the van der Waals interaction, which can totally change the DLVO interaction potential. It is remarkable that for values of δ as small as 0.2–0.3 nm the energy barrier and deep primary minimum can be totally eliminated, the force-law becomes repulsive at all separations down to “steric contact” at $D = 2\delta$, and its profile can be significantly modified out to distances as far as 5 nm (see Figs 15.14 and 15.15). This model was first proposed by Frens and Overbeek (1972) to explain the common phenomenon of colloidal stability in high salt, the spontaneous swelling of certain colloids in water, and *repeptization*—the reversible coagulation of colloidal particles (according to the DLVO theory coagulation in a primary minimum should never be reversible). This effect was later demonstrated experimentally by Marra and Israelachvili (1985) for charged lipid bilayers, by Vigil et al., (1994) for silica surfaces, and by Claesson et al., (1984) for adsorbing *counterions* (see Figure 14.18).

Worked Example 14.7

Question: The osmotic limit of Eq. (14.59) assumes that the trapped counterions have zero size. Applying the same finite-size correction as in the van der Waals equation of state, show that this introduces an effective Stern Layer of thickness $\delta = 16\pi a^3 \sigma / 3e$ per surface, where a is the ionic radius and σ the surface charge density. What is δ for (i) unhydrated and (ii) hydrated sodium counterions when each surface charge occupies an area of 1 nm^2 ?

Answer: The van der Waals excluded volume correction to the pressure is $P = kT/(V - b)$, where we may write $V = AD$ for surfaces of area A interacting across a gap width D . Thus, $P = kT/(AD - b) = kT/A(D - b/A)$, which effectively shifts the force curve for point counterions $F = PA = kT/D$ outwards by $D = b/A$. Since $b = 4 \times \text{total ionic volume in the gap} = 4(2\sigma A/e)^{4/3}\pi a^3$, the magnitude of this shift is

$$\delta = b/2A = 16\pi a^3 \sigma / 3e \text{ per surface,}$$

where σ/e is the number of charged sites per unit area. Thus, the *free* counterions in the diffuse double-layer increase the range of the short-range double-layer repulsion in the same way as does a finite Outer Helmholtz Plane or Stern Layer of thickness δ , which are normally associated with the surface *co-ions* or surface-*bound* counterions. Further aspects of this effect are discussed by Marcelja (1997, 2000). For a charge density of 1 nm^2 per unit charge ($\sigma/e = 10^{18} \text{ m}^{-2}$), inserting $a = 0.095 \text{ nm}$ for the radius of unhydrated sodium ions (Table 4.2) gives $\delta = 0.014 \text{ nm}$. In contrast, for hydrated ions, where $a \approx 0.36 \text{ nm}$, we obtain $\delta \approx 0.8 \text{ nm}$, which is a 50-fold increase that can have a very dramatic effect on the net DLVO interaction (see Worked Example 15.3).

14.22 Experimental Measurements of Double-Layer and DLVO Forces

Figure 14.15 shows the experimental results of direct force measurements between two mica surfaces in dilute 1:1 and 2:1 electrolyte solutions where the Debye length is large, thereby allowing accurate comparison with theory to be made at distances much smaller than the Debye length. The theoretical DLVO force laws (using exact solutions to the non-linear PB equation, which differ from the approximate equations of Section 14.16 only below κ^{-1}) are shown by the continuous curves. The agreement is remarkably good at all separations, even down to 2% of κ^{-1} , and indicates that the DLVO theory is basically sound. One may also conclude that the dielectric constant of water must be the same as the bulk value even at surface separations as small as 2 nm, since otherwise significant deviations from theory would have occurred (Hamnerius et al., 1978, showed that the dielectric constant of water remains unchanged even in 1 nm films). The surface potentials ψ_0 inferred from the magnitude of the double-layer forces agree within 10 mV with those measured independently on isolated mica surfaces by the method of electrophoresis (Lyons et al., 1981). Further, the surface charge density corresponding to

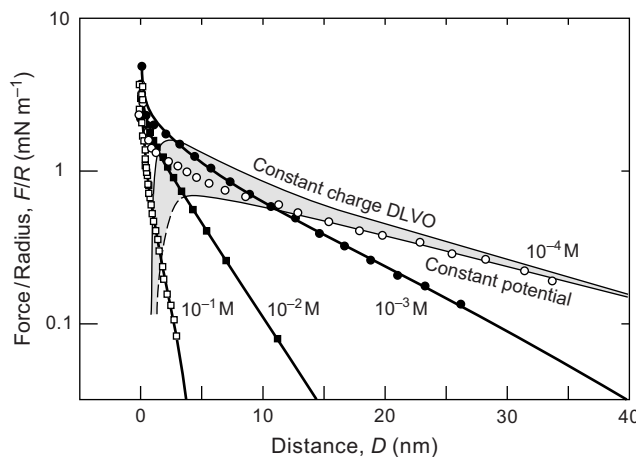


FIGURE 14.16 The first accurate measurement of double-layer forces using AFM, between a silica bead of radius $R \sim 1.5 \mu\text{m}$ and a flat silica surface in aqueous NaCl solutions. Note how the repulsive short-range double-layer and “hydration” forces increase with increasing ionic strength even though the range of the long-range double-layer repulsion decreases—an effect also seen in the forces between other surfaces such as mica (Figure 14.15). [Reproduced from Ducker and Seden, 1992, with permission.]

these potentials is typically $1e$ per 60 nm^2 . Thus, at separations below about 8 nm the surfaces are actually closer to each other than the mean distance between the surface charges, and yet the double-layer forces still behave as if the surface charges are smeared out. The reason for this will become clear in section 14.24.

Figure 14.16 shows the first AFM measurement of double-layer forces between two silica surfaces, by Ducker et al., (1991). Again the results are in good agreement with theory except at small separations where no adhesion was measured. As mentioned in the previous section, in the case of silica the lack of adhesion in aqueous electrolyte solutions is believed to be due to the protruding silicic acid groups on the silica surface, which carry the negative charges and define the OHP (see also Section 15.8 and Vigil et al., 1994).

Other SFA, AFM and Osmotic Pressure measurements of double-layer or DLVO forces have been carried out in various monovalent, divalent and multivalent electrolyte solutions (Pashley, 1981a,b, 1984; Pashley and Israelachvili, 1984; Horn et al., 1988a), between surfactant and lipid bilayers (Pashley and Israelachvili, 1981; Marra, 1986b,c; Marra and Israelachvili, 1985; Claesson and Kurihara, 1989; Pashley et al., 1986; Diederichs et al., 1985; Dubois et al., 1992; Delville et al., 1992, 1993; Anderson et al., 2010), across soap films (Derjaguin and Titijevskaia, 1954; Lyklema and Mysels, 1965; Donners et al., 1977), between silica, sapphire, and metal or metal oxide surfaces (Horn et al., 1988a, 1989; Smith et al., 1988; Meagher, 1992; Vigil et al., 1994; Larson et al., 1993), as well as in nonaqueous polar liquids (Christenson and Horn, 1983, 1985). The results on surfactant and lipid bilayers, and on biological molecules and surfaces, are discussed in more detail in later sections devoted to amphiphilic and biological systems. Here we shall concentrate more on solid, inorganic surfaces.

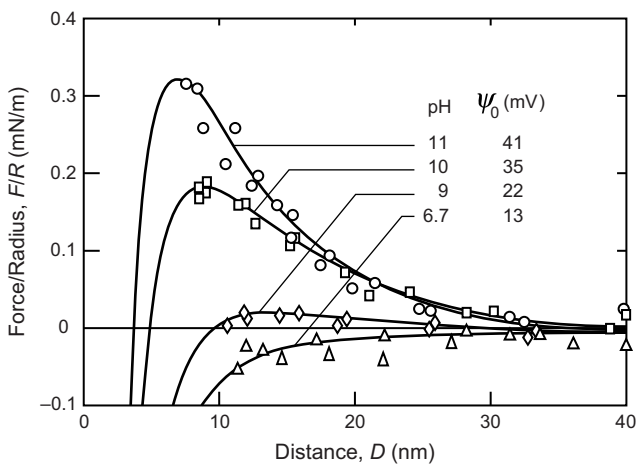


FIGURE 14.17 Classic DLVO forces measured between two sapphire surfaces in 10^{-3} M NaCl solutions at different pH. The continuous lines are the theoretical DLVO forces for the potentials shown and a Hamaker constant of $A = 6.7 \times 10^{-20}$ J. [Data from SFA experiments with surfaces in the crossed-cylinder geometry, equivalent to a sphere of radius R near a flat surface or two spheres of radius $2R$, adapted from Horn et al., 1988a.]

In general, the results have been in good agreement with the DLVO theory (Figure 14.17), often down to separations well below the Debye length (see Figure 14.15). When deviations do occur these can usually be attributed to the presence of other, non-DLVO, forces or to the existence of a Stern-layer or protruding counterions. A direct experimental measurement of Stern-layer stabilization is shown in Figure 14.18 where the counterions used in that study were unusually large. This shows that a short-range stabilizing repulsion, even in high salt, does not necessarily imply the existence of an additional non-DLVO force (such as a solvation or hydration force, discussed in Chapter 15). But it does require an explanation for what determines the finite value for δ .

As already noted, for certain geometries the double-layer repulsion at constant potential decreases at long-range but *increases* at short range with increasing ionic strength. This effect may explain the coagulation of colloidal particles and the collapse of certain charged polymers with increasing salt, followed by their redispersal and reexpansion on further increasing the concentration (Kallay et al., 1986; Drifford et al., 1996).

It is perhaps surprising that measured double-layer forces are so well described by a theory that, unlike van der Waals force theory, contains a number of fairly drastic assumptions, viz. the assumed smearing out of discrete surface charges, that ions can be considered as point charges, the ignoring of image forces, and that the PB equation remains valid even at small distances and high concentrations. One reason for this is that many of these effects act in opposite directions and tend to cancel each other out. As mentioned above, most experimental deviations in the forces from those expected from the DLVO theory are not due to any breakdown in the DLVO theory, but rather to the existence of a Stern-layer or to the presence of other forces such as ion-correlation,

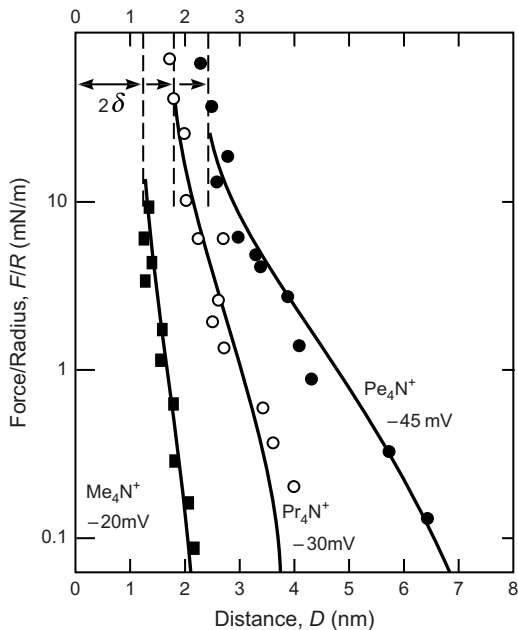


FIGURE 14.18 Example of Stern-layer effects due to the finite size of the counterions. Measured forces between two mica surfaces in various tetra-alkyl ammonium bromide solutions (Claesson et al., 1984). The continuous curves are the expected DLVO interactions assuming potentials as shown and Stern-layer thicknesses of δ per surface equal to the diameters (Born repulsion) of the adsorbed cations: $\delta = 0.6$ nm for methyl ammonium (Me_4N^+), $\delta = 0.9$ nm for propyl ammonium (Pr_4N^+), and $\delta = 1.2$ nm for pentyl ammonium (Pe_4N^+). Note how the outward shift in the OHP has eliminated the force maximum and primary minimum. [Data from SFA experiments with surfaces in the crossed-cylinder geometry, equivalent to a sphere of radius R near a flat surface or two spheres of radius $2R$.]

solvation, hydrophobic, or steric forces. These additional forces, are, of course, very important, especially in more complex colloidal and biological systems where they often dominate the interactions at short-range where most of the interesting things happen. Their consideration forms a large part of the rest of this book.

14.23 Electrokinetic Forces

When an electric field is applied across an electrolyte solution, any charged particles suspended in the solution will move toward the oppositely charged electrode—for example, a negatively charged colloidal particle will move toward the anode. This is known as electrophoretic flow and the force acting on the particle is known as the electrophoretic force. With regard to the electrolyte ions themselves, these will also move, the anions toward the anode and the cations toward the cathode. If the surfaces of the flow chamber are charged—for example, if the field is applied along a silica capillary tube whose surface is negatively charged—then the excess positively charged counterions in the solution will move toward the cathode. Since these counterions will be located within

the double-layer very close to the surface, the whole liquid column enveloped by these ions (including any particles within the column) will be dragged along with them. This is known as electro-osmotic flow.

The forces, flows and flow patterns generated by electrophoretic and electro-osmotic forces can be extremely complex, and depend on the geometry and size of the flow chamber and the suspended particles. For example, the negatively charged particle moving toward the anode by electrophoresis will also experience an opposing electro-osmotic force arising from the viscous drag of the suspending liquid moving in the opposite direction. If the diameter of the capillary tube is large compared to the diameter of the particle, the electrophoretic force wins out, but if it is small, the electro-osmotic force wins out and the particle will move with the liquid (Sen Gupta and Papadopoulos, 1997; Papadopoulos, 1999).

14.24 Discrete Surface Charges and Dipoles

The charge on a solid surface is obviously not uniformly spread out over the surface, as has been implicit in all the equations derived so far. For a surface with a typical potential of 75 mV in a 1 mM NaCl solution, the surface charge density as given by the Grahame equation is $\sigma = 0.0075 \text{ C m}^{-2}$, which corresponds to only one charge per 21 nm^2 or 2100 \AA^2 . In 0.1 M NaCl the same potential implies $1e$ per 2 nm^2 . Thus, the charges on real surfaces are typically 1–5 nm apart from each other on average. What effect does this have on the electrostatic interaction between two surfaces, especially at surface separations closer than the separation between the charges?

Let us consider a planar square lattice of like charges q as shown in Figure 14.19a. If d is the distance between any two neighboring charges, then the mean surface charge density is $\sigma = q/d^2$, and if this charge were smeared out, the electric field emanating from the surface would be uniform and given by $E_z = \sigma/2\epsilon\epsilon_0$. What, then, is the field of a surface lattice of discrete charges having the same mean charge density? To compute this field one must sum the contributions from all the charges. The resulting slowly converging series can be turned into a rapidly converging series by using a mathematical technique known as the Poisson summation formula (Lighthill, 1970). If x and y are the coordinates in the plane relative to any charge as the origin (Figure 14.19a), the field E_z along the z direction is given by the series (Lennard-Jones and Dent, 1928)

$$E_z = \frac{\sigma}{2\epsilon_0\epsilon} \left[1 + 2 \left(\cos \frac{2\pi x}{d} + \cos \frac{2\pi y}{d} \right) e^{-2\pi z/d} + \dots \right], \quad (14.70)$$

where the higher-order terms decay much more rapidly with distance z . The first term is the same as that of a smeared-out surface charge. The second term is interesting, for it shows that the excess field decays away extremely rapidly, with a decay length of $d/2\pi$, for example, about 0.3 nm for charges 2 nm apart. Thus, at $z = \frac{1}{2}d$ the electric field is at most 17% different from that of the smeared-out field, while at $z = d$ it has reached 99.3% of the smeared-out value! A similar conclusion is reached for other types

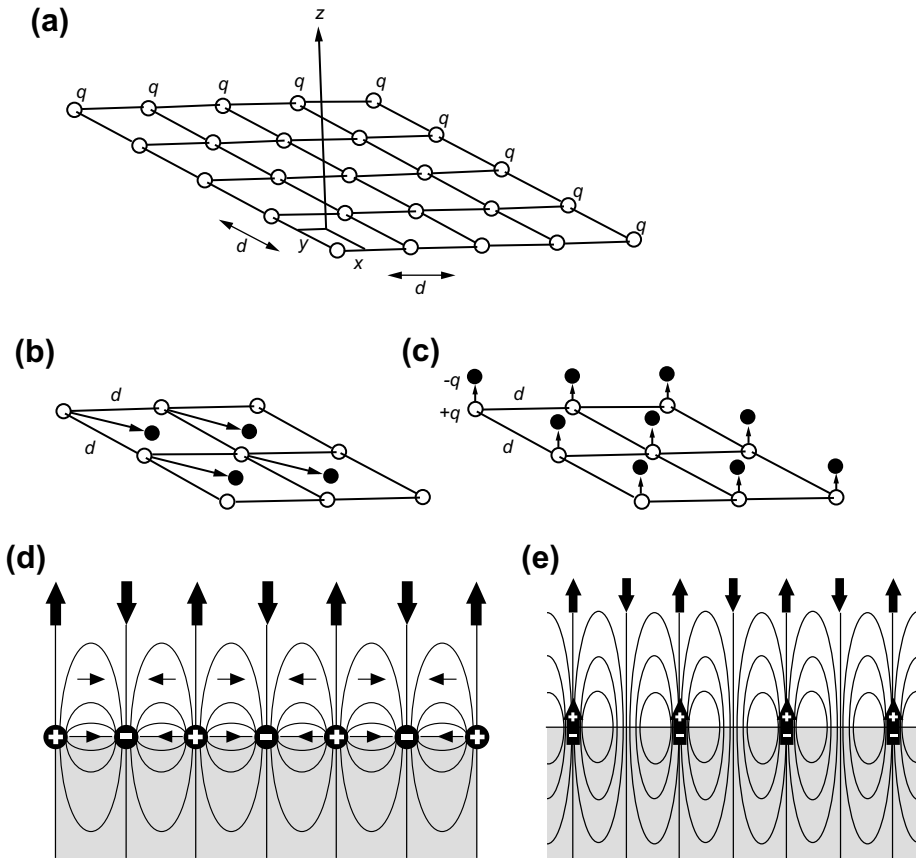


FIGURE 14.19 (a)–(c): Sections of infinite lattices of charges and dipoles. **(d) and (e):** Electric field lines and directions above electro-neutral surfaces consisting of discrete charges **(d)** and aligned dipoles **(e)**. Equations (14.71) and (14.72) show that within a very short distance away from each surface ($z \gtrsim d$) the average or mean field of a dipolar lattice is already effectively zero.

of lattices; for example, for a hexagonal lattice where neighboring ions are separated by a distance d , the mean surface charge density is $\sigma = 2q/\sqrt{3}d^2$ and the exponential decay length of the field is $\sqrt{3}d/4\pi$, which is even smaller than for a square lattice—that is, the field decays even faster. It is for these reasons that the smeared-out approximation works so well in considering the electrostatic interactions at and between charged surfaces (McLaughlin, 1989).

The above analysis can be readily extended to surfaces that have no net charge but that carry discrete surface dipoles. A common example of this is the dipolar or zwitterionic headgroups of lipid molecules that reside at the lipid-water interfaces of micelles, surface monolayers, and bilayers. The dipoles may align normally or parallel to the surfaces, and they can be either immobilized in a 2-D lattice or have (usually restricted) lateral and/or rotational mobility. The charged lattice of Figure 14.19a can be transformed into a lattice

of in-plane dipoles by adding charges of opposite sign at the center of each square (Figure 14.19b). By superimposing the fields of the positive and negative lattices using Eq. (14.70) it is easy to show that the electric field opposite a positive charge (at $x = 0$, $y = 0$) is

$$E_z = +(4q/\epsilon_0\epsilon d^2)e^{-2\pi z/d} + \dots, \quad (14.71)$$

while opposite a negative charge (at $x = \frac{1}{2}d$, $y = \frac{1}{2}d$), it is

$$E_z = -(4q/\epsilon_0\epsilon d^2)e^{-2\pi z/d} + \dots. \quad (14.72)$$

This geometry is equivalent to a dipolar or zwitterionic lattice whose dipoles, of length $d/\sqrt{2}$ and surface density $1/d^2$, are lying parallel to the surface.

For dipoles of length l comparable to d arrayed perpendicular to the surface, as in Figure 14.19c, the above two equations become replaced by $E_z \approx \pm(2q/\epsilon_0\epsilon d^2)e^{-2\pi z/d} + \dots$. This procedure can be readily extended to other lattices including three-dimensional ionic crystals. The end result is always that the field is positive or negative depending on the x , y coordinates and that it decays very rapidly to zero with increasing z .

If a second lattice of vertical dipoles is brought up to the first, the Coulombic interaction pressure between the two dipolar surfaces at a separation D will be given by

$$P(D) = \pm(2q^2/\epsilon_0\epsilon d^4)e^{-2\pi D/d} \quad (14.73)$$

depending on whether the approaching dipoles are exactly opposite each other or in register (+ sign, repulsion) or out of register (– sign, attraction). The pressure is anyway very small and in reality, since surface dipoles will not be on a perfect lattice but distributed randomly or moving about (e.g., zwitterionic head-groups on a lipid bilayer surface), the net pressure will average to zero in a first approximation, though a Boltzmann-averaged interaction will yield a weak but overall exponentially *attractive* force. A similar result is obtained if the dipoles are lying in the plane of the surfaces, as in Figure 14.19b.

The above results furnish yet another example of where the purely electrostatic interaction between a system of charges or dipoles that are overall electrically neutral produces an attractive force even though intuitively one might have expected two surfaces with vertical dipoles pointing towards each other to always repel each other. In the limit where the surface-bound dipoles are free to rotate *in all directions* the resulting interaction energy must be the same as the attractive van der Waals-Keesom interaction, which decays as $-1/D^4$ [Eq. (13.49)] but is screened if the interaction occurs across electrolyte solution (Section 13.11). Jönsson and Wennerström (1983) also considered the image force between individual dipoles and their image reflected by the other surface, and found that for surfaces of low dielectric constant interacting across water this contribution can be large and repulsive.

The interactions of finite-sized dipolar domains on surfaces, as occur in monolayers, lipid bilayers and biological membranes, are discussed in Chapters 20 and 21 (see also Problem 14.1).

PROBLEMS AND DISCUSSION TOPICS

- 14.1** Sketch the electric field lines of (i) a single dipole, (ii) an infinite lattice of vertical dipoles, and (iii) an infinite lattice of in-plane dipoles. Indicate the directions of the dipoles and fields with arrows. (iv) Without resorting to complex mathematical calculations show whether the normal Coulomb (dipole-dipole) force $F(z)$ between two similar parallel surfaces of type (ii) and (iii) is attractive or repulsive. Assume that the *surfaces* (not the *fixed dipoles* on each surface) can move freely in the x - y plane. (v) Sketch the electric field lines of a *finite* lattice of dipoles of type (ii) and (iii).
- 14.2** A glass surface is exposed to water vapor at 96% relative humidity (i.e., $p/p_{\text{sat}} = 0.96$). Estimate the equilibrium thickness D of the thin film of water adsorbed on the surface assuming (i) that only electrostatic double-layer forces are operating and that the surface is fully dissociated with a surface charge density of $\sigma = -0.1 \text{ C/m}^2$, (ii) that the monovalent counterions ($z = 1$) are uniformly distributed throughout the thin water film. [Answer: 0.46 nm.] With these same assumptions also estimate the repulsive electrostatic pressure between two such planar surfaces immersed in water at a distance $2D$ apart. [Answer: $5.6 \times 10^6 \text{ Pa}$ or 55 atm.] Is your estimate likely to be too high or too low, and how does it compare with the attractive van der Waals pressure between the surfaces at this separation? Will the van der Waals attraction eventually win out at some smaller, but physically realistic, plate separation? [Answer: ~0.4 nm.]
- 14.3** Calculate the repulsive pressure between two charged surfaces in pure water where the only ions in the gap are the counterions that have come off from the dissociating surface groups (i.e., no electrolyte present, no bulk reservoir). Assume a surface charge density of one electronic charge per 0.70 nm^2 and $T = 22^\circ\text{C}$. Plot your results as pressure against surface separation in the range 0.5–18 nm and compare these with the experimental results of Cowley et al., [*Biochemistry*, Vol. 17, 3163 (1978)] where in Figure 4b on page 3166 the authors plot their measured values for such a system (Δ points). What conclusions do you arrive at concerning the “hydration” forces between two pure phosphatidyl-glycerol (PG) bilayers at small separations?
- 14.4** Explain, in qualitative terms, why the double-layer interaction between two surfaces having unequal but constant charge densities is always repulsive at small separations, irrespective of the signs of σ_1 and σ_2 , and without resorting to complicated equations or mathematics show that it is given by $P(D \rightarrow 0) = +|(\sigma_1 + \sigma_2) kT/zeD|$, as given by Eq. (14.63) in this limit.
- 14.5** Split the double-layer interaction free energy into its enthalpic and entropic components and discuss the implications of your result.
- 14.6** The reason(s) why positively charged divalent counterions such as Ca^{2+} are better coagulants or flocculants of negatively charged surfaces or particles than monovalent ions such as Na^+ is because of one or more of the following:
- (i) They screen the electrostatic repulsion better.
 - (ii) They are more hydrated.

- (iii) They bind more readily and hence lower the surface charge.
 - (iv) They have additional ion-correlation attractive forces.
 - (v) They can bridge two surfaces by virtue of having two charges.
 - (vi) They disrupt the water structure more effectively.
 - (vii) They have a lower kinetic energy.
 - (viii) They dehydrate surfaces on binding to them.
 - (ix) They enhance the hydrophobic attraction.
 - (x) They are smaller than monovalent cations (cf. Figure 7.1).
- 14.7** Two different types of force-laws between colloidal particles in an aqueous solution are as shown in Figure 14.20. Describe how such potentials can arise. If the potentials are assumed to be independent of temperature, sketch how the temperature-composition phase diagrams could look like for these colloidal systems.
- 14.8** (i) Estimate the adhesion force between two smooth spheres of silica glass each of radius $R = 1 \mu\text{m}$ in air where the Hamaker constant is given in Table 13.2. Assume that contact occurs at a cut-off distance of $D_0 = 0.30 \text{ nm}$. (ii) What would be the adhesion *force* if the glass spheres are immersed in an aqueous 23 mM NaCl solution but remain uncharged, and what would be the adhesion *energy* in units of kT at 25°C (use Table 13.3)? (iii) If the glass surfaces acquire a surface potential of -40 mV , find the new adhesion force between the spheres in the aqueous solution. Is your answer unique—that is, are there multiple solutions to this problem? [Hints: To answer (iii), plot the force vs. distance and energy vs. distance curves.] (iv) It is found that if the aqueous solution is added to an initially dry compact powder of spheres the adhesion between the spheres is significantly higher than after the solution is vigorously stirred or sonicated, or if spheres are added individually (e.g., poured in) to the aqueous solution. Explain this phenomenon. Which is the thermodynamically more stable state of this system?
- 14.9** Glass spheres of radius $R = 10 \mu\text{m}$ are placed in a 1 mM NaCl solution in a glass beaker at 25°C. If the glass surfaces acquire a surface charge density of $1e$ per 10 nm^2 , show that the short-range ($D \ll R$) repulsive double-layer interaction potential is $W(D) = +5.8 \times 10^{-16} e^{-D/9.61} \text{ J}$, where D is in nm. See Problem 12.5 for an experimental follow-up to this problem.
- 14.10** A colloidal system containing unknown particles is dispersed in a dilute aqueous electrolyte solution at pH 6 where the dispersion is stable. The pH is steadily raised

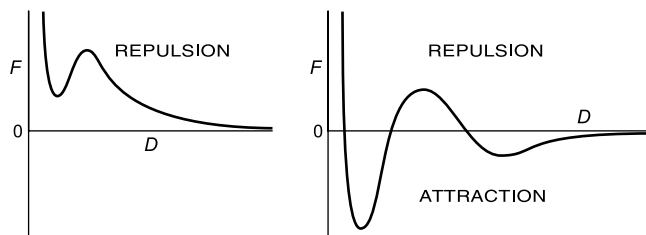


FIGURE 14.20

by adding NaOH. At pH 8 the particles coalesce, then at pH 10 they redisperse again, then at pH > 12 they aggregate again. Describe what is likely to be happening and how you could further test this. Note: the colloid may be homogeneous or a mixture of different particles.

- 14.11***How does the existence of an electric double-layer contribute to the lateral (2D) surface pressure Π or tension γ (in units of $N\ m^{-1}$ or $J\ m^{-2}$) of a fully charged surfactant monolayer at a water surface? Consider two limiting case: (i) The monolayer is totally insoluble so that all the surfactant molecules remain in the monolayer when it is compressed. In this case the lateral pressure is usually denoted by Π , and it varies with area A . (ii) The monolayer is soluble and can exchange its surfactant molecules with those in the bulk solution or reservoir that are at some fixed concentration. In this case the double-layer contribution to the pressure is denoted by γ_{el} , and is independent of area—that is, it is a constant. [Hint: First obtain an expression for the energy of a single double-layer, giving careful thought to the reference state. Refer to Payens, 1955; Chan and Mitchell, 1983; and Hunter, 1981, Chapter 7.]
- 14.12** When an electric field is applied across an electrolyte solution containing charged particles they are seen to move parallel or antiparallel to the field depending on the sign of their charge. Now, since almost all of the potential drop must occur across the double-layer at each electrode surface, there can be no electric field within the conducting electrolyte solution and thus no force on the charged colloidal particles. Why, then, do the particles move?
- 14.13** The particles of a colloid are disordered (gas-like) at high NaCl concentrations but become ordered at low concentrations. Explain this phenomenon. If the particle concentration is increased will the ionic concentration of this “order-disorder transition” increase or decrease?
- 14.14** Certain colloidal particles that interact via a DLVO type of interaction in a certain solution are sometimes seen to coagulate below and above a certain size (particle radius) but not at some intermediate range of sizes. Explain this effect, giving two possible reasons for the coagulation at large radii. [Hints: Do a scaling analysis, and do not forget the effect of buoyancy.]
- 14.15** A flat glass plate of refractive index 1.50 is placed in a sealed chamber together with a beaker containing liquid whose surface is kept at the same height as the top glass surface. In one case (a) the beaker contains a highly volatile nonpolar hydrocarbon liquid such as pentane and a small amount (~5%) of a “nonvolatile” but miscible hydrocarbon liquid such as hexadecane. What will be the *equilibrium* thickness of the liquid film that adsorbs on the top glass surface at STP? In another case (b) the beaker contains a saturated aqueous solution of potassium sulfate (check the relative humidity over such a solution at STP). If water wets the glass surface ($\theta = 0$), what will the equilibrium film thickness be now? [Answer: The film will grow indefinitely in each case, but there will be an initial rapid plateau, followed by a much slower growth.]

Solvation, Structural, and Hydration Forces

15.1 Non-DLVO Forces

When two surfaces or particles approach closer than a few nanometers, continuum theories of attractive van der Waals and repulsive double-layer forces often fail to describe their interaction. This is either because one or both of these continuum theories breaks down at small separations or because other non-DLVO forces come into play. These additional forces can be monotonically repulsive, monotonically attractive, or oscillatory, and they can be much stronger than either of the two DLVO forces at small separations.

As we saw in Chapter 7 short-range oscillatory solvation forces can arise when spherical liquid molecules are induced to order or “structure” into quasi-discrete layers between two surfaces or within any highly restricted space. Such oscillatory forces have a mainly geometric origin, the oscillatory force-function depending critically on the shapes of the liquid (solvent) molecules. Additional non-DLVO solvation forces can arise that decay monotonically with distance. These can be repulsive or attractive, and are less well understood. On the other hand, there are also non-DLVO forces that are due to surface-adsorbed polymers or to surface-specific (rather than solvent-specific) interactions; these should not be thought of as a “solvation” force and are considered in later chapters.

Solvation forces depend not only on the properties of the intervening liquid medium but also on the chemical and physical properties of the surfaces—for example, whether they are hydrophilic or hydrophobic, smooth or rough, amorphous or crystalline (atomically structured), homogeneous or heterogeneous, natural or patterned, rigid or fluid-like. These factors affect the structure that confined liquids adopt between two surfaces, which in turn affects the solvation force. It is therefore often difficult to distinguish between a solvation force—that is, one that arises from the intrinsic properties of the solvent molecules—and a surface force that depends on the properties of the surfaces or solute molecules. For example, consider two smooth surfaces that tightly bind a layer of solvent molecules. These surfaces will resist coming closer together than two solvent molecules, but this “steric” repulsion is due to the strong solvent-surface interaction rather than any solvent-solvent interaction. In contrast, if the surfaces are “inert”—that is, if there is no solvent-surface binding, there will still be a “solvation” force at small separation. As we shall see, this force now also depends on the properties of the solvent and is generally considered as part of the solvation force.

Solvation forces can be very strong at short-range, and they are therefore particularly important for determining the magnitude of the adhesion between two surfaces or particles in “contact” or at their potential energy minimum. We shall start by considering the most general type of solvation force: the oscillatory force arising from the discrete molecular nature of all condensed phases.

15.2 Molecular Ordering at Surfaces, Interfaces, and in Thin Films

The theories of van der Waals and double-layer forces discussed in the previous two chapters are both continuum theories, described in terms of the bulk properties of the intervening medium such as its density ρ , refractive index n , and dielectric permittivity ϵ . We have already seen in Chapters 7 and 8 that at small separations, below a few molecular diameters, these values are no longer the same as in the bulk, which implies that the short-distance intermolecular pair potential can be quite different from that expected from continuum theories. In particular, we saw that in general the liquid density profiles (density distribution functions) and interaction pair-potentials (potentials of mean force) between two solute molecules in a solvent medium oscillate with distance, with a periodicity close to the molecular diameter of the solvent molecules and with a range of a few solvent molecules. Similar short-distance interactions also arise between particles and extended surface, when they are referred to as *solvation* or *structural* forces, or—when the medium is water—*hydration* forces.

To understand how solvation forces arise between two planar surfaces, we must first consider the way liquid molecules order themselves at a single, isolated surface. We can then consider how this ordering becomes modified in the presence of a second surface, and how this determines the short-range interaction between the two surfaces in the liquid. The solvation (or structuring) of solvent molecules at a surface is in principle no different from that occurring around a small solute molecule, or even around another identical solvent molecule, which—as previously described—is determined primarily by the geometry of molecules and how they can pack around a constraining boundary [for some mainly theoretical reviews see Nicholson and Parsonage (1982), Ciccotti et al., (1987), and Evans and Parry (1990)].

Theoretical work and particularly computer simulations indicate that while liquid density oscillations are not expected to occur at a liquid-vapor or liquid-liquid interface (Figure 15.1a), a very different situation arises at a solid-liquid interface (Figure 15.1b). Here, attractive interactions between the wall and liquid molecules and the geometric constraining effect of the “hard wall” on these molecules force them to order (or structure) into quasi-discrete layers. This layering is reflected in an oscillatory density profile extending several molecular diameters into the liquid (Abraham, 1978; Rao et al., 1979). If the surface is idealized to be “mathematically” smooth, as shown in Figure 15.1b, the ordering of the molecules within each layer will be random or disordered—that is,

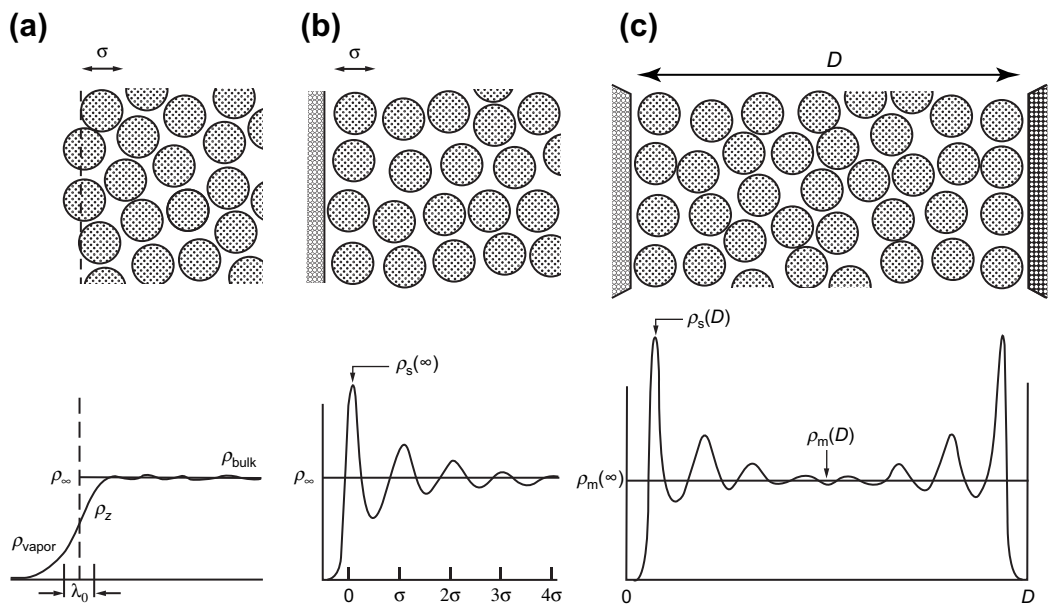


FIGURE 15.1 (a) Liquid density profile at a vapor-liquid interface. ρ_∞ is the bulk liquid density and λ_0 is the width or molecular-scale “roughness” of the interface. (b) Liquid density profile at an isolated solid-liquid interface. $\rho_s(\infty)$ is the “contact” density at the surface. (c) Liquid density profile between two hard walls a distance D apart. The contact and midplane densities $\rho_s(D)$ and $\rho_m(D)$ are a function of D as illustrated in Figures 15.2–15.4. Note that $\rho_m(\infty) = \rho_\infty$.

exhibiting only short-range liquid-like order. However, if the surface is itself structured, even at the atomic level (for example, a crystalline lattice), then there will be some epitaxially induced ordering also within the layers. In such cases we would say that there is both *out-of-plane* ordering and *in-plane* ordering, the first referring to the existence of ordered layers, the second referring to the existence of ordering *within* the layers themselves.

Experimentally, liquid layering adjacent to single, isolated surfaces have been measured directly only relatively recently, mainly using x-ray reflectivity techniques. Cheng et al., (2001) found about four water layers adjacent to mica surfaces, with a periodicity of $2.6 \pm 0.1\text{\AA}$. Other measurements have found similar density oscillations for both liquid metals (Huisman et al., 1997) and van der Waals liquids (Yu et al., 1999, 2000).

The constraining effect of two solid surfaces is much more dramatic (Figure 15.1c). Even in the absence of any attractive or structured wall-liquid interaction, geometric considerations alone dictate that the liquid molecules must reorder themselves so as to be accommodated between *two* walls, and the variation of this ordering with separation D gives rise to the solvation force between the confining surfaces. For simple spherical molecules between two hard, smooth surfaces the solvation force is usually a decaying oscillatory (but not sinusoidal) function of distance. For molecules with asymmetric shapes or whose interaction potentials are anisotropic or not pair-wise additive, the

resulting solvation force can be very complex and may also have a monotonically repulsive or attractive component. Likewise, if the confining surfaces are themselves not well-ordered, but rough or fluidlike, the oscillations will be smoothed out and the resulting solvation force will be monotonic. The effects of both the liquid and surfaces on the resulting solvation force are considered in more detail in the following sections.

Worked Example 15.1

Question: Derive an approximate expression for the molecular-scale thermal roughness of a liquid-vapor interface in terms of the intermolecular bond energy $w(\sigma)$ or surface energy γ , the molecular diameter σ and the temperature T . Estimate the magnitude of this roughness for a van der Waals and a metal liquid-vapor surface, and comment on the different effects these could have on the ordering of the liquid molecules and solvation forces at these surfaces.

Answer: Consider the thermal fluctuations of liquid molecules that cause a certain fraction of them to protrude beyond the surface into the vapor phase (Figure 15.1a). The additional energy of a molecule that protrudes a small distance z ($z < \sigma$) may be estimated by multiplying the additional area exposed $\pi\sigma z$ by the surface energy γ (note that the molecular-scale value of γ may not be the same as the macroscopic value; this is discussed later). The *protrusion energy* is therefore proportional to the distance the molecule or group protrudes from the surface. In keeping with our previous notation this may be expressed as

$$\text{Protrusion energy} = (\mu_z^i - \mu_0^i)_{\text{prot}} = \pi\sigma\gamma z = \alpha_p z, \quad (15.1)$$

where α_p is the energy per unit length of a protrusion (in units of J m^{-1}). Proceeding as we did when calculating the density profile of the earth's atmosphere (Section 2.4), we obtain for the density profile of molecular protrusions

$$\rho_z = \rho_\infty e^{-\alpha_p z/kT} = \rho_\infty e^{-\pi\sigma\gamma z/kT} \approx \rho_\infty e^{-\sqrt{3}\pi w(\sigma)z/\sigma kT}, \quad (15.2)$$

where $\rho_\infty = \rho_{\text{bulk}}$ is the bulk liquid density and where we have used $\gamma \approx \sqrt{3}w(\sigma)/\sigma^2$ from Eq. (13.40). The above shows that the liquid density decays exponentially from the surface according to

$$\rho_z = \rho_\infty e^{-z/\lambda_0},$$

where

$$\lambda_0 = kT/\alpha_p = kT/\pi\sigma\gamma \approx \sigma kT/5w(\sigma) \quad (15.3)$$

is the molecular *protrusion decay length* or *interfacial width* (Figure 15.1a). Equation (15.3) cannot apply once $z > \sigma$, since beyond this distance the molecule becomes detached from the surface and is then no longer part of the liquid but becomes part of the vapor. For chain molecules such as alkanes, surfactants and polymers the above equations remain valid out to much larger distances; we shall consider the consequences of this in Chapter 16.

For small spherical molecules we should expect the density to level off at $z \approx \sigma$ to a value corresponding to the saturated vapor pressure. That this is indeed so can be readily checked by putting $z = \sigma$ into Eq. (15.2) which reduces it to the result obtained in Sections 2.2–2.4—that is, $\rho_{\text{vap}} = \rho_{\text{bulk}} e^{-\mu_{\text{liq}}^i/kT} \approx \rho_{\text{bulk}} e^{-5w(\sigma)/kT}$.

The protrusion length of Eq. (15.3) is a measure of the molecular-scale roughness of a surface and is one of a number of contributions to the total “width” of a surface or interface, often denoted by ξ . Other contributions come from more macroscopic-scale thermal fluctuations such as those arising from capillary waves. For a van der Waals liquid, where typically $\sigma \approx 0.3$ nm and $\gamma \approx 25$ mJ m⁻², we obtain $\lambda_0 \approx 0.2$ nm (a computer simulation by Xia et al., 1992, gave a value of 0.3 nm for hydrocarbon liquids). It is a pure coincidence that the molecular-scale roughness has turned out to be of the same order as the molecular size. For many surfaces it can be much smaller. Thus, for a metal surface, where $\gamma > 300$ mJ m⁻², we find $\lambda_0 < 0.02$ nm. Liquid metal surfaces, by virtue of their high binding energies, are therefore very much smoother than van der Waals liquids. As a consequence of this, liquid metal molecules (or atoms) behave as if they are packing against a hard wall, as drawn in Figure 15.1b. It is for this reason that the surfaces of liquid metals are believed to have a layered or “stratified” structure (Rice, 1987). In contrast, little or no structuring is expected at a van der Waals liquid-vapor interface, which in turn implies only a weak and short-ranged solvation force. It is probably for this reason that measurements of the van der Waals forces across thin liquid films of helium and alkanes on solid surfaces are so well described by the Lifshitz theory down to film thickness of 1 nm (Section 13.9).



15.3 Ordering of Spherical Molecules between Two Smooth (Unstructured) Surfaces

In Section 14.7 we saw that the pressure between two surfaces is directly correlated with the density of the (liquid) molecules between the two surfaces. The system of spherical molecules between two smooth or “unstructured” surfaces that are also assumed to be hard (undeformable or incompressible) is the simplest system that one can imagine. Indeed, it is too simple to be truly realistic because no surface is smooth, i.e., mathematics flat, at the atomic level, and the effects of atomic corrugations are very important when the surfaces confine atoms or molecules having a comparable size. However, as we shall see, even this apparently simple system is amazingly complex and subtle, and its analysis serves to introduce the even more complex issues that arise between “real” surfaces interacting across “real” liquids.

Figure 15.2 shows how the structure of a confined liquid film changes as the number of molecular layers changes from three to two to one. For simplicity we shall assume a two-dimensional film, essentially treating the molecules as cylinders. We shall also assume that there are no interactions between the “hard-sphere” molecules, and that the surfaces are likewise inert. We further assume that the film molecules can exchange freely with molecules in a bulk liquid reservoir outside the film (not shown), and that the reservoir is at some finite “hydrostatic” pressure that keeps the molecules in the film (otherwise they will evaporate away).

The question now is: what are the configurations of maximum density as the film thickness falls from three layers to two layers? Knowing this will help determine the

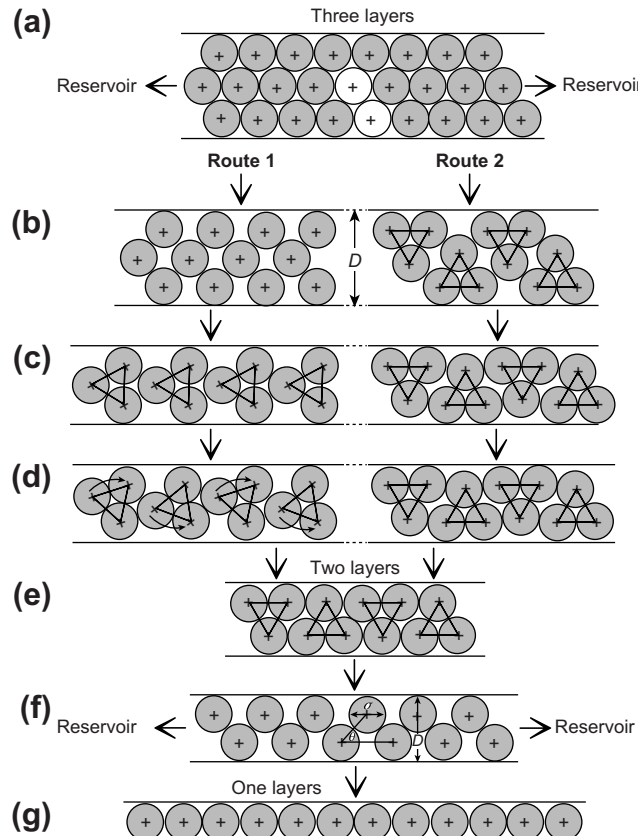


FIGURE 15.2 Possible structural rearrangements of 12 cylindrical molecules or small particles between two flat (unstructured) surfaces as the film thickness D decreases from three to two to one close-packed layers. **Route 1:** symmetric collapse of molecular layers into each other, followed by the final rotation of triangular units. **Route 2:** fixed triangular units slide along each other. Routes 1 and 2 display very different molecular orderings (film structure) and densities at each separation D that give rise to different solvation force functions between the surfaces (cf. Problems 15.1 and 15.2). The white molecules do not participate in Routes 1 or 2. Note that the film thicknesses D for $n = 3, 2$ and 1 layers are $(1 + \sqrt{3})\sigma = 2.73\sigma$, $(1 + \sqrt{3}/2)\sigma = 1.87\sigma$, and 1.00σ , respectively—that is, they are not simple multiples of the molecular diameter σ except for $n = 1$. Other possibilities are discussed in the text and illustrated in Figure 15.3.

free-volume available for the molecules to move about in as the gap distance falls.¹ In Figure 15.2 the three extreme configurations are shown as the close-packed configurations for three layers in (a), for the two layers in (e) and for one layer in (g). These are the obvious configurations of maximum packing density in these limits,² but the transition

¹Similar considerations arise for a bulk (3D) system of hard spheres.

²Although, depending on the temperature and externally applied pressure, the film may adopt a different configuration. Note, too, that so far nothing has been assumed about the phase state of the reservoir which could be a solid or a liquid.

between three and two layers is far from obvious. The figure shows two possible routes, which are by no means exhaustive (see below). The first, route 1, appears the more intuitive because the three layers simply open up and merge into two layers symmetrically. However, route 2 turns out to be the preferred path, both theoretically (cf. Problem 15.1) and experimentally, as has been found for concentrated colloidal particles confined in narrow slits (Cohen et al., 2004). The second transition, from two to one close-packed layers, is obvious, and shown in Figure 15.2 (e) → (g).

The situation for spheres, rather than cylinders, is much more complex, and the reader may readily ascertain that even the transition from two to one close-packed layers is not trivial. Thus, if two close-packed lattice planes of spheres simply collapse into each other as in the two-dimensional case depicted in Figure 15.2 (e) → (g), it is easy to establish that the final monolayer will have holes, showing that a more complicated transition must occur (Problem 15.1).

In the illustrations of Figure 15.2, the molecules remain fully ordered and touching at all stages of the transitions. This will occur only at very high pressures. In practice, depending on the reservoir pressure and temperature, the molecules will not be touching but will “expand” to increase their free volume for movement (cf. Sections 7.5–7.6). As D changes, the molecules may still remain ordered, or they may undergo a series of order-disorder transitions, becoming disordered or “liquid-like” at non-integral/fractional separations of σ , or some layers may remain ordered, while others do not, or there may be laterally separated domains of ordered and disordered molecules (Heuberger, 2001). Even more diverse structures can occur between structured surfaces, as discussed below.

15.4 Ordering of Nonspherical Molecules between Structured Surfaces

No surface is “unstructured,” and very few molecules are truly spherical or cylindrical. Figure 15.3 shows two new features that arise between more realistic “structured” surfaces as they transit from confining three layers to contact. First, there is a lateral shift in the lattice every time a layer is removed or added. Second, depending on the “commensurability” of the surface and solvent molecules, it may not be possible for the molecules to retain any long-range order—that is, remain structured, as D changes. In such cases the film becomes disordered—that is, it “melts” on going from, say, three layers to two layers or from two to one layer, as shown in Fig. 15.3A.

Incommensurability can arise from the different sizes and shapes of the surface and liquid molecules or from the surfaces alone. For example, the two surfaces may have different lattice dimensions or the same lattice but rotated at some “twist angle” relative to each other. And even if the two lattices are identical (commensurate) and “in registry” in the x - y plane, this may not be sufficient to ensure good—that is, low-energy—packing of the liquid molecules between them. In general, to maintain good packing as two surfaces approach each other in the z -direction, they must also be free to shift *laterally* in

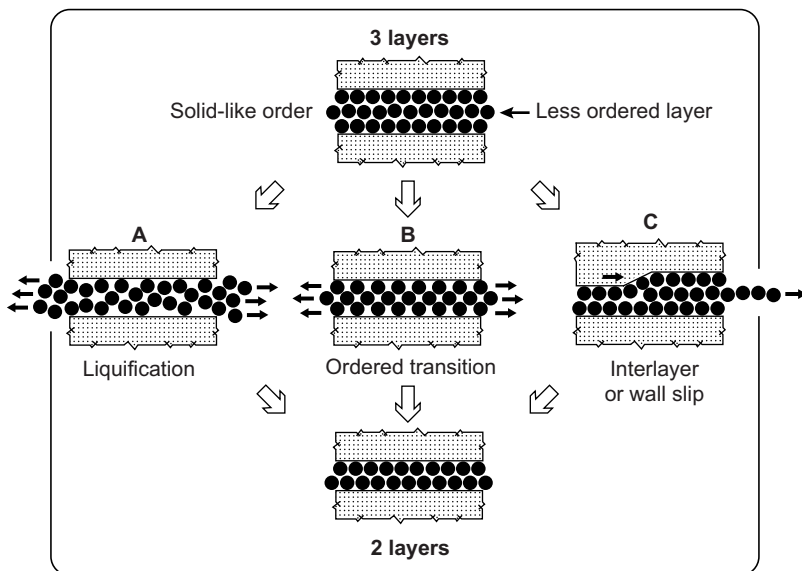


FIGURE 15.3 Possible alternative structural changes occurring in thin liquid or even solid films between two solid but deformable surfaces during transitions from 3 to 2 layers. In some cases, the reverse may occur: instead of a monolayer being expelled from the film (route C), a monolayer may force itself into the film (either from the right or into the page), thereby opening up and weakening the material. Examples of this are water penetrating into hydrophilic cracks in rocks and “swelling clays” such as montmorillonite causing rapid (and sometimes easily visible) swelling, and mercury and gallium penetrating into grain boundaries in aluminum causing the metal to break under the least force within 30 minutes. The type of change occurring depends on the lattice structure of the confining surfaces (here shown to be flat or “structureless”) and their commensurability with those of the film atoms or molecules.

the x-y plane, as can be readily seen by comparing panels (a), (e), and (g) in Figure 15.2. This means that epitaxial solidification of a confined film may be frustrated if the two lattices are not able to move laterally to accommodate the structured film between them. This effect has important implications both for the structure and phase state of confined films and for the solvation forces between the confining surfaces. Thus, for surfaces or particles that are free to also move laterally as they approach each other, the trapped liquid molecules will have a greater tendency to solidify and such films often display higher melting points than the bulk liquids. In contrast, surfaces that are not free to adjust, as occurs in cracks, grain boundaries, and narrow pores, tend to fluidize the molecules between them, and liquids in such films or “confined geometries” usually display *lower* melting points than the bulk liquids (Awshalom and Warnock, 1987).

The removal of the last layer is special, and it usually involves a different mechanism from the removal of the layers from thicker, multilayered films. For the last layer to be removed (or added), the surfaces themselves must deform from their planar state, as shown in Figure 15.3c. The ability to do this now depends on such factors as the surface structure and the elastic or plastic stiffness of the material (Luedtke and Landman, 1992). In some cases, no amount of pressure will remove the last layer, which will simply be

driven farther into the lattice of the material until it results in a grain boundary or an intercalation compound.

The ordering of nonspherical, such as linear chain, molecules between surfaces is even more complex, since now both the relative positions and mutual orientations of the molecules determine how they will pack together between two surfaces. Layering of such molecules may still occur, but a flexible hydrocarbon or polymer chain molecule may find different parts of the molecule in different layers (Gao et al., 1997a, b; Porcheron et al., 2001).

Overall, both for spherical and asymmetric molecules, the structure of a confined film is remarkably sensitive to the slightest changes in the atomic or molecular geometry, as well as to any roughness of the surfaces—a change of only 0.1 Å being able to produce dramatic changes in the structure and resulting solvation force.³

15.5 Origin of Main Type of Solvation Force: the Oscillatory Force

In Section 14.7 we saw that the repulsive electrostatic double-layer pressure between two charged surfaces separated by a solvent containing the counterions is given by the following equivalent equations:

$$P(D) = kT[\rho_s(D) - \rho_s(\infty)] = kT[\rho_m(D) - \rho_m(\infty)], \quad (15.4)$$

where ρ_s and ρ_m are the ionic densities at each surface and the midplane. Equation (15.4) also applies to solvation forces (Henderson, 1986, 1988; Evans and Parry, 1990) as long as there is no interaction between the walls and liquid molecules, where ρ_s and ρ_m are now the density of liquid molecules at each surface and the midplane (Figure 15.1b, c). Thus, a solvation force arises once there is a *change* in the liquid density at the surfaces and/or the midplane as they approach each other. For two inert surfaces this is brought about by changes in the molecular packing as was illustrated in Figures 15.2 and 15.3.

Figure 15.4a shows that $\rho_s(D)$ will be high only at surface separations that are close multiples of σ but must fall at intermediate separations. At large separations, as $\rho_s(D)$ approaches the value for isolated surfaces $\rho_s(\infty)$, the solvation pressure approaches zero. The resulting variation of the solvation pressure with distance is shown schematically in Figure 15.4b. Like the density profile, it is an oscillatory function of distance of periodicity roughly equal to σ and with a range of a few molecular diameters.

In the limit of very small separations, as the last layer of solvent molecules is finally squeezed out, we have $\rho(D \rightarrow 0) \rightarrow 0$ for both the surface and midplane layers. In this limit the solvation pressure approaches a finite value given by

$$P(D \rightarrow 0) = -\rho(\infty)kT \quad (15.5)$$

³This refers to the thermodynamically equilibrium force. But time can play an important role in practice. For example, confined molecules that bind strongly to each other or to the surface molecules may get “stuck” or “jammed” (see Section 15.6) and therefore not readily move to their new equilibrium position as the film thickness changes. Similar effects can occur if the external force is applied rapidly.

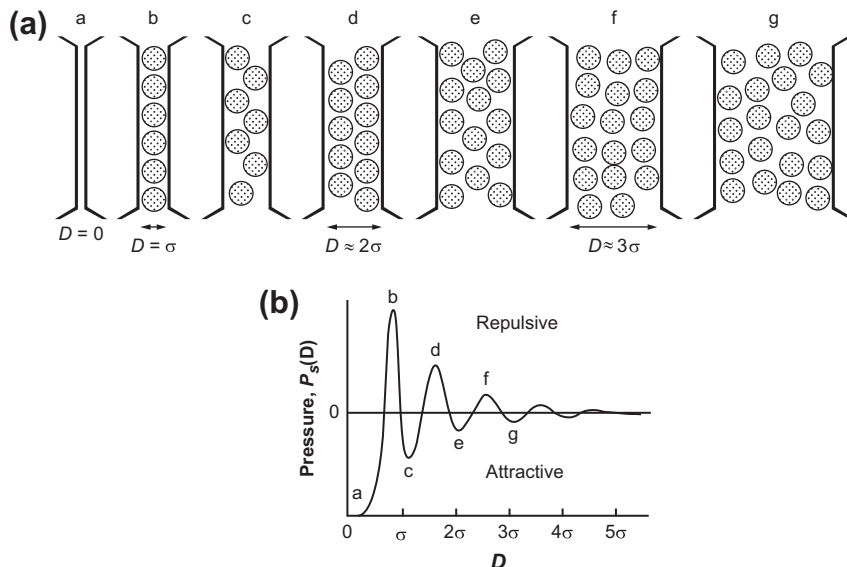


FIGURE 15.4 (a) Same geometry as Figure 15.1c, showing how the molecular out-of-plane ordering changes as the separation D changes. Note that the density of liquid molecules in contact with the surface $\rho_s(D)$ varies between maxima and minima. The molecules in the film are assumed to be free to exchange with those in the bulk reservoir. (b) Corresponding solvation pressure (schematic) as given by Eq. (15.4). The resulting oscillatory solvation force need not be symmetrical about the $P = 0$ axis, and it is often superimposed on a monotonic force as shown in Figure 15.5d. Note the multiple (“quantized”) and progressively deeper adhesive minima at g, e, c, and a (contact).

which means that the force at contact is negative—that is, attractive or adhesive. Equations (15.4) and (15.5) are important fundamental equations that crop up in many different systems, and we shall encounter them again when considering other entropic interactions.

Oscillatory forces do not require that there be any attractive liquid-liquid or liquid-wall interaction. All one needs is two hard smooth or crystalline walls confining molecules whose shapes are not too irregular (see below) and that are free to exchange with molecules in the bulk liquid reservoir. In the absence of any attractive forces between the molecules the bulk liquid density may be maintained by an external hydrostatic pressure which determines $\rho_m(\infty)$ or ρ_∞ . In real liquids, attractive intermolecular forces such as the van der Waals force play the role of the external pressure, but the (entropic) oscillatory force remains much the same. However, the two are not independent of each other, as Worked Example 15.2 shows.



Worked Example 15.2

Question: Making reasonable assumptions and approximations, calculate and plot or sketch the pressure as a function of distance $P(D)$ for (1) the entropic solvation and (2) the van der Waals interaction between the two smooth surfaces of Figure 15.2 as the confined liquid film

goes from two layers (e) to one layer (g) at $T = 298\text{K}$. Assume the confined molecules to be spheres of diameter $\sigma = 0.5 \text{ nm}$ but that they retain the two-dimensional symmetry of Figure 15.2. Also assume that all the molecules are nonpolar and nonconducting and that the refractive index and Hamaker constants of the surface and film molecules are the same and equal to $n = 1.50$ and to $A = 10^{-20} \text{ J}$.

Answer: (1) Referring to Figure 15.2f at any film thickness $D = (1 + \sin \theta)\sigma$ the lateral distance between molecular centers is $2\sigma \cos \theta$, so that in a first approximation the *mean* density of molecules in the film will be given by $\rho(D) = 1/\cos \theta(1 + \sin \theta)\sigma^3$ [since there are 2 molecules per rectangular “unit cell” of dimensions $2\sigma \cos \theta (1 + \sin \theta)\sigma \times \sigma$]. Assuming a bulk liquid density of $\rho(\infty) = \rho_\infty = 1/\sigma^3$, we therefore have $P(D) = -kT[1 - 1/\cos \theta(1 + \sin \theta)]/\sigma^3 = -3.3 \times 10^7[1 - 1/\cos \theta(1 + \sin \theta)] \text{ Nm}^{-2}$ for $\sigma = 0.5 \text{ nm}$ and $T = 298\text{K}$. The mean density reaches a minimum value at $\theta = 30^\circ$, where it is 0.77 of the bulk density. This occurs at $D = 0.75 \text{ nm}$ (exactly 1.5 molecular diameters) and corresponds to an attractive pressure of $-0.8 \times 10^7 \text{ N m}^{-2}$ (80 atm), compared to the reference (reservoir) pressure at $D = \infty$. An alternative approach is to consider that the density of the molecules in direct physical contact with the walls $\rho_s(D)$ varies as $1/\cos \theta$, falling progressively as D and θ decrease. The contact density reaches its lowest value of $0.5\rho_\infty$ as D approaches σ ($\theta \rightarrow 0$), corresponding to an attractive pressure of $-1.6 \times 10^7 \text{ N m}^{-2}$ (160 atm), just before it rises sharply at $D = \sigma = 0.5 \text{ nm}$ when all the molecules finally make contact with both surfaces (Figure 15.2g). Note that in both cases the shapes of the oscillations are far from simple sinusoidal functions (cf. Figure 2 in Porcheron et al., 2001).

(2) The van der Waals force across the film depends on the Hamaker constant which in turn depends on the mean refractive index of the film (Section 13.3). The Lorenz-Lorentz equation, Eq. (5.31), relates the refractive index to the density, which we have seen reaches a minimum value of $0.77\rho_\infty$ at $D = 0.75 \text{ nm}$. At this separation we therefore have $(n_{\text{film}}^2 - 1)/(n_{\text{film}}^2 + 2) = 0.77(1.50^2 - 1)/(1.50^2 + 2)$, which gives $n_{\text{film}} = 1.37$ (9% less than the bulk value). The Hamaker constant for interactions across this film A_{film} is related to that of the bulk material $A_{\text{bulk}} = 10^{-20} \text{ J}$ via Eq. (13.16) by $A_{\text{film}}/A_{\text{bulk}} = [(n_{\text{bulk}}^2 - n_{\text{film}}^2)^2/(n_{\text{bulk}}^2 + n_{\text{film}}^2)^{3/2}]/[(n_{\text{bulk}}^2 - 1)^2/(n_{\text{bulk}}^2 + 1)^{3/2}]$, which gives $A_{\text{film}} = 6.2 \times 10^{-22} \text{ J}$. The van der Waals pressure at $D = 0.75 \text{ nm}$ is therefore $-A/6\pi D^3 = 8 \times 10^4 \text{ N m}^{-2}$, which is also attractive, but not nearly as strong as the entropic solvation pressure at this separation, calculated above. However, if the dielectric properties of the surface and film molecules were different, the van der Waals contribution could be much larger although still not as large as the entropic contribution. Note that in this example the van der Waals pressure also oscillates, being zero (i.e., maximum) at separations where the film has the same mean density and refractive index as the bulk. These maxima coincide with the maxima of the entropic oscillatory forces.

It is instructive, and left as an exercise for the interested reader, to plot the various pressure-distance curves discussed above.

A number of theoretical studies and computer simulations of various confined liquids, including water, which interact via some form of the Mie potential have invariably lead to an oscillatory solvation force at surface separations below a few molecular diameters (van Megen and Snook, 1979, 1981; Snook and van Megen, 1980, 1981; Rickayzen and Richmond, 1985; Kjellander and Marcelja, 1985a, b; Tarazona and Vicente, 1985; Henderson and Lozada-Cassou, 1986, 1994; Evans and Parry, 1990;

Delville, 1992, 1993; Mitlin and Sharma, 1995; Kralchevsky and Denkov, 1995; Das et al., 1996; Trokhymchuk et al., 1999, 2001; Porcheron et al., 2001). In a first approximation the entropic solvation contribution to the total interaction energy may be described by an exponentially decaying cos-function of the form

$$W(D) \approx W(0)\cos(2\pi D/\sigma)e^{-D/\sigma} \quad \text{J m}^{-2} \quad (15.6a)$$

where, by definition,

$$W(0) = -2\gamma_i, \quad (15.6b)$$

where both the oscillatory period and the characteristic decay length of the envelope are close to σ . By differentiating Eq. (15.6) it is a simple matter to show that the solvation contribution to the interfacial *pressure* of two flat surfaces in contact at $D = 0$ is (cf. Eq. 15.5)

$$P(0) = -2\gamma_i/\sigma = -\rho_\infty kT \approx -kT/\sigma^3 \quad \text{N m}^{-2} \quad (15.7)$$

that is,

$$\gamma_i \approx kT/2\sigma^2, \quad (15.8)$$

which is the contribution of the entropic solvation interaction to the interfacial energy. Other semiempirical equations for the solvation interaction have been proposed by Tarazona and Vicente (1985), Kralchevsky and Denkov (1995), and Porcheron et al., (2001), for example, in terms of the pressure:

$$P(D) = -\rho_\infty kT\cos(2\pi D/\sigma)e^{-D/\sigma} \quad \text{N m}^{-2} \quad (15.9)$$

which reduces to Eq. (15.5) and (15.7) at $D = 0$ but that, when integrated, leads to a different functional form for $W(D)$ from that of Eq. (15.6).

Equation (15.8) may be compared with Eq. (13.40), which gives the van der Waals contribution to the interfacial energy as $\gamma_i = \frac{A}{24\pi D_0^2} \approx \frac{A}{24\pi(\sigma/2.5)^2} \approx 0.1A/\sigma^2$. Thus, for Hamaker constants smaller than about $5kT$ —that is, for $A < 2 \times 10^{-20}$ J—the oscillatory solvation interaction is expected to dominate the adhesion energy in a liquid. Table 13.3 shows that higher values for A in liquids arise only between metal and metal oxide and ceramic materials. Worked Example 15.2 shows the same trend: at contact ($D = 0$) the entropic solvation pressure would have been simply $-kT/\sigma^3 \approx 3 \times 10^7$ N m⁻² (300 atm), whereas the van der Waals contact pressure for $A = 6 \times 10^{-22}$ J would have been $0.1 A/\sigma^2 \approx 3 \times 10^6$ N m⁻², which is a factor of 10 smaller.

Thus, unless the Hamaker constant is high, we expect the oscillatory solvation force to dominate the adhesion of smooth inert surfaces and particles in simple liquids, *especially for small molecules* (see Sections 15.8 and 15.9 for the special case of water—one of the smallest of molecules).

It is important to appreciate that solvation forces do not arise simply because liquid molecules tend to structure into semiordered layers at surfaces. They arise because of the disruption or *change* of this ordering during the approach of a second surface. If there were no change, there would be no solvation force. This is already implicit in

Eq. (15.4). The two effects are of course related (Fig. 15.5): the greater the tendency toward structuring at an isolated surface, the greater the solvation force between two such surfaces, but there is a real distinction between the two phenomena that should always be kept in mind.

Real systems are often much more complex than the examples and illustrations discussed so far. The liquid molecules are usually nonspherical and interact via anisotropic orientation-dependent potentials both with each other and with the surfaces. Even when spherical, molecules are generally not hard spheres but soft—the softer the molecules or particles (e.g., micelles), the fewer and smoother the oscillations—that is, less sawtooth-shaped and more sinusoidal. Very soft particles, such as polymer “blobs,” may exhibit no oscillations at all, just a single energy minimum (see depletion forces). Similarly, the confining surfaces themselves are generally not smooth but corrugated or structured either at the atomic or nanoscopic level, or rough, easily deformable (soft) or fluid-like. These are the systems we shall be discussing in the rest of this chapter.

Any strongly attractive interaction between a surface and the liquid molecules adjacent to it leads to a denser packing of molecules at the walls (Abraham, 1978; Snook and van Megen, 1979) and thus to higher ρ_s values and a more short-range repulsive but still oscillatory force (Figure 15.5b). On the other hand, if the surface-liquid interaction is

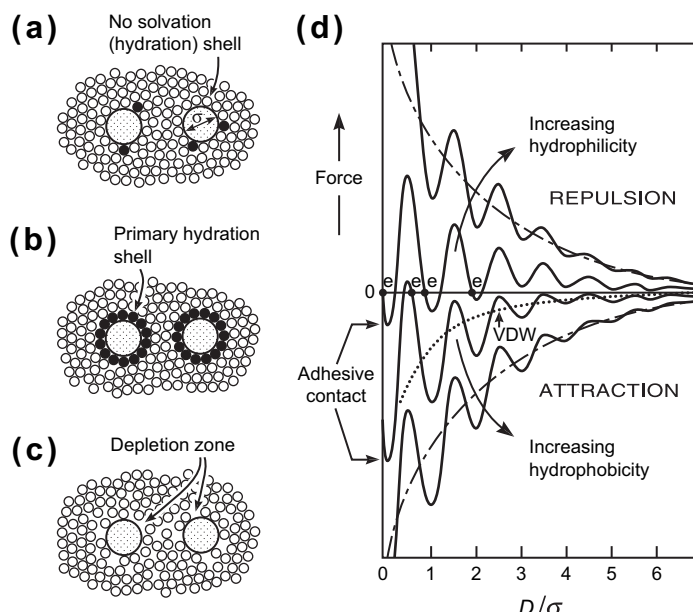


FIGURE 15.5 (a)–(c): Schematic diagrams of solvent structure, which can be both positional and orientational, at different surfaces. The resulting solvation force (d) is usually oscillatory, and appears to be additive with the monotonic long-range double-layer force (see Figure 15.8), but probably not the continuum van der Waals force (dotted line), which assumes a constant density between the surfaces. There are four equilibrium adhesion points in (d) indicated by the letter e.

much weaker than the liquid-liquid interaction the oscillatory force tends to be overall more attractive (Figure 15.5c). Such complex force-laws often show both a short-range oscillatory part and long-ranged monotonic part (in addition to any long-ranged DLVO force). Monotonic long-range solvation forces remain controversial and are discussed in Sections 15.8, 15.9 and Chapter 21.

To summarize, modern theories and simulations of liquids have shown how very complex structures and force-laws can arise across an assembly of molecules that interact even via the simplest possible pair potential. The confined liquids can take on properties that may be unrecognizable from their bulk properties, both quantitatively and qualitatively: they may structure into layers displaying “quantized” properties that change continuously or abruptly as the film thickness changes, analogous to a series of continuous or first-order phase transitions. These “phases” may be solid-crystalline, liquid-crystalline, glassy-amorphous, homogeneous, or separated into lateral or stratified domains. In particular, they can withstand a finite compressive force at a finite separation even when the final contact is adhesive.

15.6 Jamming

When molecules or particles become locked in a nonequilibrium configuration, they are said to become jammed. For example, if the two surfaces of Figure 15.3 or 15.4 are pressed together quickly, the molecules may not have time to leave the gap and go into the reservoir. Instead, they may remain in the same configuration, only more compressed. The jammed state (cf. Fig. 7.3) may be ordered or disordered. Everyday examples of jamming are (1) the supercooling of a liquid, which occurs in the bulk state (Uhlmann, 1972), and (2) the inability to remove a rod from a container full of sand, which is an example of jamming due to confinement. Polymers and anisotropically shaped molecules in liquids are particularly prone to becoming entangled in the bulk and sterically jammed when confined—an effect that can occur both at the molecular level (see sections on lubrication in Chapter 18)—and the macroscopic level—for example, when filters get clogged up with particles.

As was previously discussed in Section 7.5, the randomly close-packed particles (sand grains) need to expand or “dilate” before they can flow, which is prevented by the inflexible hard surfaces of the rod and container walls. Jamming is ultimately a result of insufficient “excluded volume” available for molecules or particles to rearrange. This volume has to exceed that of “random loose packing” for the molecules to be able to adopt a new structure (Table 15.1).

The force across a jammed film is generally more repulsive than the equilibrium force because transitions to lower energy configurations do not occur. The whole phenomenon depends critically on the rates at which the forces are applied. For example, if a van der Waals liquid is slowly compressed at a temperature just above its freezing point, it will rapidly crystallize because the freezing is driven by thermodynamic gradients, but if the compressive pressure is increased rapidly, freezing will take longer or not at all. In the

Table 15.1 Maximum Packing Densities, Expressed as Volume Fractions, of Spheres, Disks, Cylinders, and Rods in Different Critical Configurations (see also Table 7.4).

Packing Density (Fraction) f^a	Close-Packing f_{cp}	Random Close-Packng f_{rcp}	Random Loose-Packng f_{rlp}
Spheres (3-D)	0.74	0.64	0.55
Disks, cylinders (2-D)	0.91	~0.82	
Rods (1-D)	1.00	~0.75 ^b	

^aThe fraction f gives the actual volume occupied by the molecules, so that $(1 - f)$ gives the volume available for movement which is also referred to as the “excluded volume.” Restricted (localized) motion can occur for $f_{cp} > f_{rlp}$, while free flow over large distances can occur when $f < f_{rlp}$ or, in terms of the excluded volume, $(1 - f) > (1 - f_{rlp})$. The requirement for a compressed material to expand before it can flow is known as *dilatancy*.

^bMaximum density attained when cars of the same length l are allowed to park *at random* on a street until there is no gap between any two cars greater than l .

latter case, the jammed molecules will remain in the liquid state but exhibit a much higher viscosity (Liu and Nagel, 1998). The issue of jamming in thin interfacial films, especially its nonequilibrium and rate-dependent nature, is intimately related to such phenomena as adhesion hysteresis, friction, and lubrication and is taken up again in Chapter 18.

15.7 Experimental Measurements and Properties of Oscillatory Forces

In addition to the insights provided by recent computer simulations, there is also a rapidly growing literature on experimental measurements and other phenomena associated with solvation forces. The first systems that were studied were simple spherical molecules between smooth surfaces, but now more complex—for example, linear and branched—molecules and mixtures are being studied between different types of surfaces, including rough and patterned (textured, structured) surfaces.

Figure 15.6 shows the results obtained by Horn and Israelachvili (1981a, b) for two mica surfaces across an inert liquid of molecular diameter $\sigma \approx 0.9$ nm, together with a plot of a theoretically computed force law. Subsequent measurements of oscillatory forces between different surfaces across both aqueous and non-aqueous liquids have revealed their subtle nature and richness of properties (Christenson and Horn, 1985; Israelachvili, 1987b; Christenson, 1988a; Christenson and Yaminski, 1993). For example, their great sensitivity to the shape and rigidity of the solvent molecules and the confining surfaces. In particular, the oscillations can be smeared out if the molecules are irregularly shaped, such as branched, and therefore unable to pack into ordered layers, or when surfaces are rough even at the subångstrom level (Frink and van Swol, 1998). The main features of these forces will now be summarized, together with the different techniques used to measure them.

1. **Inert, spherical, rigid molecules.** In liquids such as CCl_4 , benzene, toluene, cyclohexane, and OMCTS whose molecules are roughly spherical and fairly rigid, the periodicity of the oscillatory force at room temperature is equal to the mean

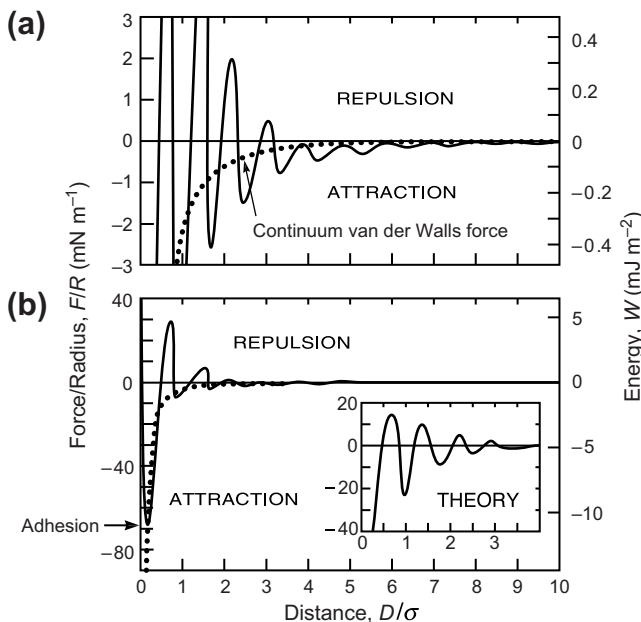


FIGURE 15.6 (a) Measured force F between two cylindrically curved mica surfaces of radius $R \approx 1$ cm in octamethylcyclotetrasiloxane (OMCTS), an inert silicone liquid whose nonpolar molecules are quasi-spherical with a mean molecular diameter of $\sigma \approx 0.9$ nm, at 22°C , plotted on a reduced distance scale. Dotted line: theoretical continuum van der Waals force computed for this system, given by $F/R = -A/6D^2$ and using a Hamaker constant of $A = 1.35 \times 10^{-20}$ J. The right hand ordinate gives the corresponding interaction energy per unit area of two flat surfaces according to the Derjaguin approximation: $W = F/2\pi R$. (b) The full experimental force law. The inset shows a theoretical force law computed for this system based on a molecular theory by Henderson and Lozada-Cassou (1985). [Experimental data from Horn and Israelachvili, 1981a, b.]

molecular diameter σ , usually within a few percentage points of the diameters obtained from x-ray, gas solubility, and diffusion data. Note that the periodicity is larger than for close-packed spheres (cf. Figure 15.2) due to the “thermal expansion” of the film. The exact value depends on many factors and is only coincidentally equal to the hard-core σ .

2. **Range of oscillatory forces.** The peak-to-peak amplitudes of the oscillations show a roughly exponential decay with distance with a characteristic decay length of 1.2 to 1.7σ . However, some systems manifest only a single, hard barrier at $D = \sigma$ arising from a strongly bound monolayer of solvent molecule (as in Figure 15.5b) with no further effects or only weak oscillations beyond $D = \sigma$ (Stuckless et al., 1997a, b).
3. **Magnitude of forces.** The oscillatory force generally exceeds the van der Waals force at separations below 5 to 10 molecular diameters (see Christenson and Yaminski, 1993, and Section 15.5), and for simple liquids, merges with the continuum van der Waals or DLVO force at larger separations.
4. **Effect on adhesion energy in a medium.** The depth of the potential well at contact ($D = 0$) corresponds to an interaction energy that is often close to the value expected

from the continuum Lifshitz theory of van der Waals forces, especially in cases where the Hamaker constant is high and the liquid molecules are large or surface-induced structuring effects are weak (Section 15.5 and Fig. 15.5a). For example, for the mica-OMCTS-mica system (where $\sigma_{\text{OMCTS}} \approx 0.9 \text{ nm}$) the Hamaker constant is about $1.35 \times 10^{-20} \text{ J}$. Using Eqs. (13.39)–(13.42) we obtain $W \approx -A/12\pi D_0^2 \approx -12 \text{ mJ m}^{-2}$ for the adhesion energy at contact. This may be compared with the value of $W \approx -11 \text{ mJ m}^{-2}$ obtained from the measured adhesion force (see Figure 15.6). For smaller molecules such as cyclohexane ($\sigma \approx 0.5 \text{ nm}$) and *n*-alkanes ($\sigma \approx 0.4 \text{ nm}$) the adhesion energy contribution from the solvation interaction, which varies as $1/\sigma^2$ (Eq. 15.8), increases sharply until it dominates over the van der Waals contribution. However, in series of detailed adhesion measurements Christenson and Yaminski (1993) concluded that the oscillatory solvation contribution dominates over the van der Waals contribution even for molecules as large as OMCTS. Sections 15.8 and 15.9 deal with the special case of the unusually small water molecule for which $\sigma \approx 0.27 \text{ nm}$.

5. **Temperature dependence.** Oscillatory solvation forces are not strongly temperature dependent and show no change when a liquid is supercooled below its freezing point. They should therefore not be viewed as a surface-induced “prefreezing” of liquids.
6. **Small flexible (soft) molecules.** Short-chained molecules such as *n*-hexane, and small branched chained molecules such as 2,2,4-trimethylpentane, have highly flexible bonds that can rotate freely. Such molecules may be considered as being internally “liquid-like” and, unlike the more rigid molecules described in 1–3, they have no need to order into discrete layers when confined between two surfaces. Consequently, their short-range structure and oscillatory solvation force does not extend beyond two to four molecules or some other packing dimension of the molecules.
7. **Linear chain molecules.** Homologous liquids of *n*-hexane, *n*-octane, *n*-decane, *n*-dodecane, *n*-tetradecane, and *n*-hexadecane (Christenson et al., 1987) exhibit similar oscillatory solvation force-laws (Figure 15.7). For such liquids, the period of the oscillations is about 0.4 nm, which corresponds to the molecular width and indicates that the molecular axes are preferentially oriented parallel to the surfaces (see Figure 15.7, inset). Similar results have been obtained with short-chained polymer melts such as polydimethylsiloxanes (Horn and Israelachvili, 1988; Horn et al., 1989b).
8. **Nonlinear (asymmetric) and branched chain molecules.** Irregularly shaped chain molecules with side groups or branching lack a symmetry axis and so cannot easily order into discrete layers or other ordered structure within a confined space. In such cases the liquid film remains disordered or amorphous and the force law is not oscillatory but monotonic. An example of this is shown in Figure 15.7 for iso-octadecane, where we see how a single methyl side-group on an otherwise linear 18-carbon chain has totally eliminated the oscillations. Similar effects occur with other branched hydrocarbons such as squalane ($\text{C}_{30}\text{H}_{62}$ with six $-\text{CH}_3$ side groups),

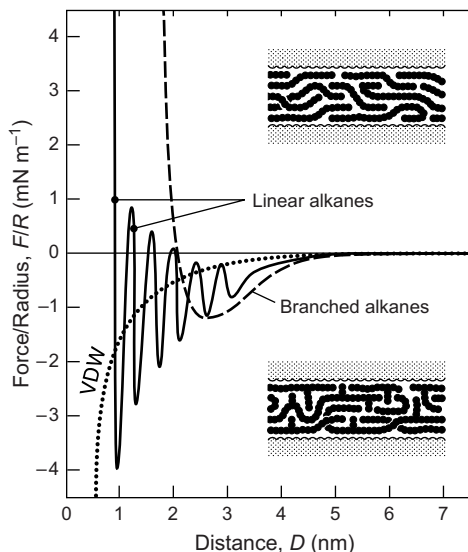


FIGURE 15.7 Measured force laws between mica surfaces across straight-chained liquid alkanes such as *n*-tetradecane and *n*-hexadecane (molecular width $\sigma \approx 0.4$ nm), and across the branched alkane (iso-paraffin) 2-methyloctadecane. The dotted line is the theoretical continuum van der Waals interaction. [Data from SFA experiments with surfaces in the crossed-cylinder geometry, equivalent to a sphere of radius R near a flat surface or two spheres of radius $2R$, adapted from Christenson et al., 1987, and Gee and Israelachvili, 1990.]

and branched polymer melts such as polybutadienes (Granick, 1995; Israelachvili and Kott, 1988). Theoretical analyses of such molecules by Gao et al., (1997a, b) suggest that the molecules do order into layers, but that the branching results in side-group mixing between layers; this mixing prevents the sharp transitions between the layers, which eliminates the discrete oscillations in the force (see lower inset in Fig. 15.7).

9. **Effect of polydispersity.** A small degree of polydispersity appears to have only a small effect on the force law so long as the mixture remains homologous. For example, a polydisperse mixture of *n*-alkanes or a polydisperse polymer melt exhibits similar equilibrium force-laws to those of the pure one-component liquids (though the times to reach equilibrium may differ significantly).
10. **Effects of miscible components (liquid mixtures).** Christenson (1985a) found that the forces between two mica surfaces across a mixture of OMCTS ($\sigma \approx 0.9$ nm) and cyclohexane ($\sigma \approx 0.55$ nm) are essentially the same as that of the dominant component if its volume fraction in the mixture exceeds 90%. However, for a 50/50 mixture the oscillations are not well defined, and their range is now less than for either of the pure liquids. It appears that a mixture of differently shaped molecules cannot order into coherent layers so that the range of the short-range structure becomes even shorter (note that this is not the case for mixtures of *homologous* molecules where the critical packing dimension, the molecular width, remains the same, as discussed in 9).

- 11. Effects of water and other immiscible polar components in nonpolar liquids.** The presence of even trace amounts of water can have a dramatic effect on the solvation force between two hydrophilic surfaces across a nonpolar liquid. This is because the preferential adsorption of water onto such surfaces disrupts the molecular ordering in the first few layers. This effect usually leads to a shift of the oscillatory force curve to lower, more adhesive, energies. At higher water concentrations a thick water film may form that changes the whole nature of the interaction, as discussed in Chapter 17.
- 12. Effect of molecular polarity (dipole moment) and H-bonds.** The measured oscillatory solvation force laws for highly polar and H-bonding liquids such as acetone, methanol, propylene carbonate, ethylene glycol, and water are surprisingly similar to those of non-polar liquids, displaying a similar periodicity, magnitude and range. However, H-bonding liquids may introduce an additional monotonic solvation force, as discussed in the following section. This would be in addition to any monotonic DLVO interaction that appears to be additive with the solvation interaction as shown in Figure 15.8 for propylene carbonate.

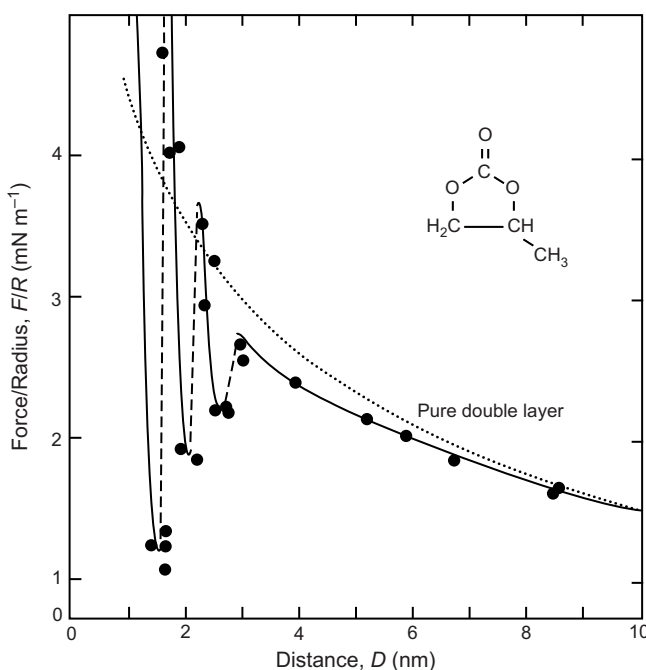


FIGURE 15.8 Measured force between two curved mica surfaces in propylene carbonate ($\sigma \approx 0.5 \text{ nm}$, $u = 4.9 \text{ D}$, $\varepsilon = 65$) containing 10^{-4} M electrolyte (tetraethyl-ammonium bromide). Beyond 8 nm and out to 50 nm (not shown) the force law is accurately described by double-layer theory (dotted line). Below 8 nm the van der Waals attraction reduces the net force below the purely double-layer curve, as expected from the DLVO theory, and below 3 nm the force is oscillatory. [Data from SFA experiments with surfaces in the crossed-cylinder geometry, equivalent to a sphere of radius R near a flat surface or two spheres of radius $2R$, reproduced from Christenson and Horn (1983) with permission.]

- 13. Effect of surface lattice structure and roughness.** It is now appreciated that the structure of the confining surfaces is just as important as the nature of the liquid for determining solvation forces. As previously discussed in Sections 15.4 and 15.5, between two surfaces that are completely smooth (or “unstructured”) the liquid molecules will be induced to order into layers, but there will be little inducement for ordering within the layers. In other words, there will be out-of-plane but no in-plane ordering. However, if the surfaces have a crystalline (periodic) lattice, this will induce in-plane “epitaxial” ordering, especially in the first layer, which will affect the oscillatory force. For example, McGuiggan and Israelachvili (1990) found that the adhesive minima in the oscillatory force between two mica surfaces across an aqueous solution are affected out to at least 4 water layers, becoming less deep as the “twist angle” between the two lattices deviates from 0° (the angle of perfect registry).

On the other hand, for surfaces that are *randomly* structured or rough, the oscillatory force becomes smoothed out and may disappear altogether, to be replaced by a purely monotonic solvation force (Christenson, 1986; Crassous et al., 1994). Apparently, a roughness greater than about $1/3^{\text{rd}}$ of the molecular diameter is enough to convert an oscillatory force to a monotonically decaying, usually repulsive, force (Gee and Israelachvili, 1990; Ruths et al., 2001; Frink and van Swol, 1998). This occurs even if the liquid molecules themselves are perfectly capable of ordering into layers. The situation of *symmetric* liquid molecules confined between *rough* surfaces, is therefore not unlike that of *asymmetric* molecules between *smooth* surfaces.

To summarize, for there to be an oscillatory solvation force, the liquid molecules must be able to be correlated over a reasonably long range. This requires that both the liquid molecules and the surfaces have a high degree of order or symmetry. If either is missing, so will the oscillations. A surface roughness of only a few ångstroms is often sufficient to eliminate any oscillatory component of a force law.

- 14. Effect of surface hardness or “fluidity.”** The above statement requires some qualification, because if the surfaces are soft or fluid-like, they may be induced to flatten and thereby allow for layering, resulting in an oscillatory force even across a free liquid film (Wassan and Nikolov, 2008); this effect would not occur between hard surfaces having the same (rough) topography. As might be expected, the short-range forces between hard, rough surfaces, whether in air or in a liquid medium, are determined by the mechanical compressibility of their surface asperities as soon as these meet each other. The range of this force is therefore determined by the heights of the highest asperities. Interestingly, both measurements and computations of the forces between various randomly rough and nanoparticle-coated surfaces show them to be either exponentially or linearly repulsive (Golan et al., 2001; Benz et al., 2006; Zappone et al., 2007; Yang et al., 2008; Akbulut et al., 2007; Min et al., 2008), an effect that appears to be related to the commonly observed density $\propto \log(\text{pressure})$ dependence in the compaction of rough colloidal particles—for example, during ceramic processing (Biesheuvel and Lange, 2001).

The situation of fluid-like surfaces that are “dynamically” rough is quite different from those of hard surfaces that are “statically” rough; the former also give rise to near-exponentially repulsive forces, which are discussed in Chapters 16 and 21.

15. **Effect of surface curvature and geometry.** It is easy to understand how layering and oscillatory forces arise between two flat, plane parallel surfaces, as illustrated in Figures 15.2–15.4. Between two curved surfaces—for example, two spheres as in Fig. 15.5—one might imagine the molecular ordering and oscillatory forces to be smeared out in the same way that they are smeared out between two randomly rough surfaces. However, this is not the case. Ordering can occur as long as the curvature or roughness is itself regular or uniform—that is, not random. For curved surfaces this is a natural consequence of the Derjaguin Approximation that related the interactions between smooth and curved surfaces (see Problem 15.5). Thus, oscillatory forces arise between the smallest solute molecules (Chapter 7), and they have been measured between highly curved AFM tips and surfaces in OMCTS, water, and other liquids (Hoh et al., 1992; O’Shea et al., 1992, 1994; Cleveland et al., 1995; Han and Lindsay, 1998).
16. **Oscillatory forces involving nano- and colloidal particles.** There is nothing in the theory of solvation forces that restricts it to atoms or small molecules or to pure liquids. They are expected to arise whenever packing constraints limit the ordering of particles in a confined geometry. Thus, concentrated solutions of hard silica particles, soft spherical micelles, and lipid bilayers have been found to exhibit oscillatory forces determined by the size of the particles, micelles, or the periodicity of the bilayers in the lamellar phase (Wassan and Nikolov 2008; Richetti et al., 1990; Richetti and Kékicheff, 1992; Moreau et al., 1994; Bergeron and Radke, 1992, 1995). The number and height of the oscillations depend on the concentration of particles, there being only one adhesive minimum in dilute systems, increasing to about 5 oscillations at high concentrations (Richetti and Kékicheff, 1992; Parker et al., 1992). However, in the case where there is long-range liquid-crystalline order already in the bulk phase, the oscillations extend much farther, although their strength increases at smaller separations (Horn et al., 1981; Moreau et al., 1994).

15.8 Solvation Forces in Aqueous Systems: Monotonically Repulsive “Hydration” Forces

The short-range forces between surfaces in water and aqueous salt solutions display some highly unusual properties that, in spite of the most intense experimental and theoretical studies, are still not understood. These forces can be strongly monotonically repulsive, attractive, oscillatory, or a combination of these. For example, certain clays and uncharged surfactant and lipid bilayers swell spontaneously or repel each other in aqueous solutions, and silica dispersions and other colloidal particles sometimes remain stable in very high salt. And yet for all these systems one would expect the surfaces or particles to remain in adhesive contact or coagulate in a primary minimum if the only

forces operating were the DLVO and/or oscillatory solvation forces. These monotonically repulsive forces have become known as “hydration” forces.

Historically, hydration forces were first proposed by Langmuir (1938), Derjaguin and Zorin (1955), and others to explain the unexpected stability of uncharged colloidal particles such as “coacervates” (giant vesicles) in solution, and subsequent experiments showed them to be monotonically repulsive, roughly exponential, and with a range of 10–30 Å between amphiphilic surfaces (Figure 15.9) and of longer range between hydrophilic mineral surfaces. The idea that these forces are due to “water structuring” at surfaces gained steady popularity, and the often observed exponential decay length of approximately 2.5 Å (see Figure 15.9) was believed to be due to some characteristic property of water such

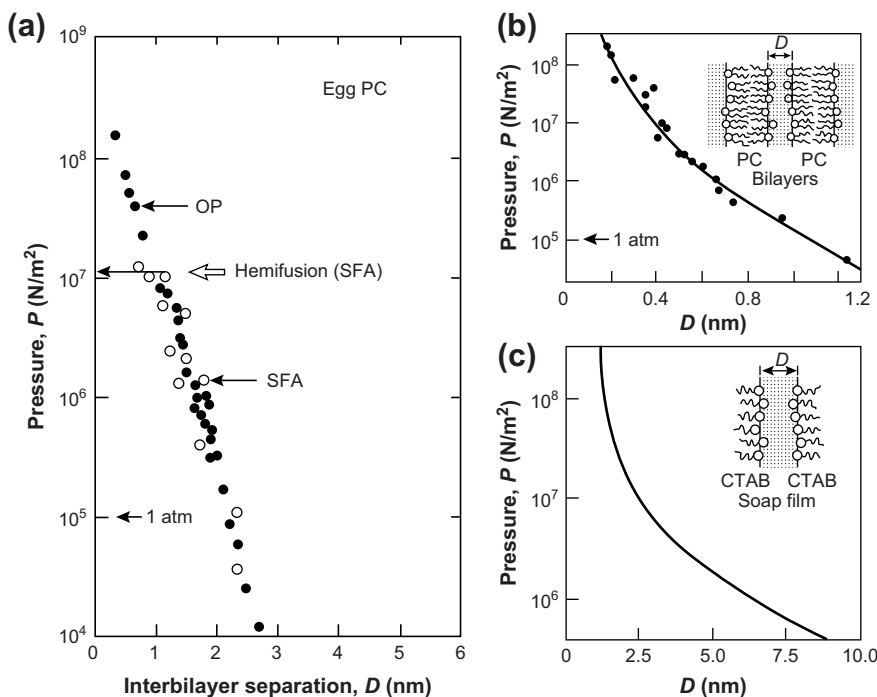


FIGURE 15.9 Monotonically repulsive short-range forces (pressures) measured between surfactant and lipid monolayers and bilayers in water. **(a)** Forces between uncharged egg-lecithin bilayers (see Table 19.1), measured independently by the Surface Forces Apparatus (SFA) and Osmotic Pressure (OP) techniques, described in Section 12.7. The force is essentially made up of the van der Waals attraction at long-range, beyond 3 nm (see Figure 15.17), and an exponential repulsion of decay length ~0.25 nm at short-range, as shown here. These short-range forces arise from a combination of steric and hydration effects between fluid-like interfaces, and have more to do with the dynamic structure of the surfaces than ordering of the solvent; they are considered in greater detail in Chapters 16 and 21. Figure adapted from Horn et al., (1988) and Helm et al., (1992). **(b)** Force (pressure) measured between fluid bilayers of the uncharged zwitterionic lipid dipalmitoyl-phosphatidylcholine (lecithin or DPPC) in water. The range of the repulsion is about 1.2 nm, below which it is roughly exponential with a decay length of ~0.14 nm. [From McIntosh and Simon, 1986.] **(c)** Force (pressure) measured across a soap film of the cationic surfactant CTAB or HTAB: $C_{16}H_{33}N(CH_3)_3^+Br^-$, showing a non-double layer repulsion below ~2 nm. [From Clunie et al., Reprinted with permission from Nature, Vol. 216, pp. 1203–1204. © 1967 MacMillan Journals Ltd.]

as its size. However, as theoretical work and computer modeling failed to confirm the existence of any type of exponentially repulsive hydration force associated with water structuring, other interpretations for their origin—based on the properties of the interacting *surfaces* rather than the *medium*—were offered and subsequently supported by further experimental and theoretical work. There are two types of such forces, those between fluid-like amphiphilic surfaces such as surfactant and lipid bilayers and those between solid hydrophilic mineral surfaces such as clay and silica surfaces.

Steric-hydration forces between fluid-like amphiphilic surfaces. Very strong short-range monotonically repulsive forces have been measured across soap films composed of various surfactant monolayers, between uncharged bilayers composed of lipids with uncharged sugar or zwitterionic head-groups, as shown in Figure 15.9, and between biological membranes. While the hydrophilicity of such surfaces is due to the presence of strongly hydrophilic groups, the repulsive force between them is essentially entropic—arising from the confinement of the thermally excited chains and head-groups protruding from these surfaces as they approach each other. Such forces are therefore more akin to the “steric” forces or “thermal fluctuation” forces between two polymer-covered or fluid-like interfaces, and they are considered in detail in Chapters 16 and Part III.

Monotonically repulsive hydration forces between solid hydrophilic surfaces. Monotonically repulsive hydration forces between solid mineral surfaces were first studied extensively between clay surfaces such as montmorillonite which swell spontaneously in water, known as *swelling clays* (van Olphen, 1977). More recently, they have been measured in detail between mica, silica, and other hydrophilic surfaces. Mica and silica surfaces present two very different types of monotonically repulsive hydration forces, which will now be considered in turn.

The monotonic hydration forces between mica surfaces (Figure 15.10) have been found to decay exponentially with decay lengths of about 1 nm with a range of about 3–5 nm. Empirically, therefore, the hydration repulsion between two hydrophilic surfaces appears to follow the simple equation

$$W(D) = +W_0 e^{-D/\lambda_0}, \quad (15.10)$$

where $\lambda_0 = 0.6\text{--}1.1$ nm for 1:1 electrolytes (Pashley, 1982), and where W_0 depends on the hydration of the surfaces but is usually below 3–30 mJ m⁻², higher W_0 values generally being associated with lower λ_0 values.

In a series of experiments to identify the factors that determine and regulate these hydration forces, Pashley (1981a, b; 1982, 1985) and Pashley and Israelachvili (1984) found that the interaction between molecularly smooth mica surfaces in *dilute* electrolyte solutions obeys the DLVO theory. However, at higher salt concentrations, specific to each electrolyte, hydrated cations bind to the negatively charged surfaces and—above this “critical hydration concentration”—give rise to a repulsive hydration force (see Figure 15.10). This is believed to be due to the hydration of the surfaces brought about by the binding of the cations to the negatively charged mica surfaces, the cations presumably retaining some of their water of hydration on binding. This conclusion was arrived at after

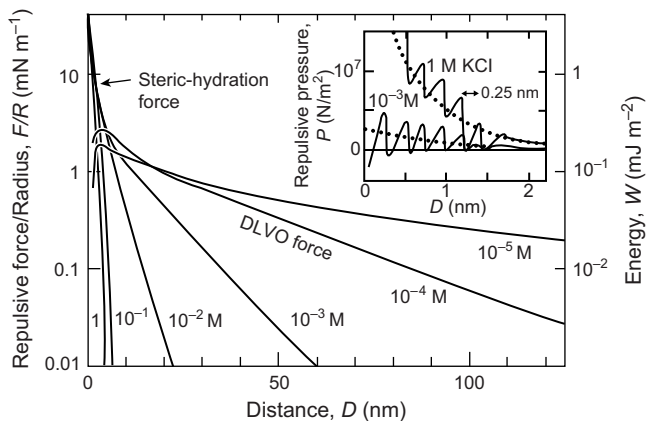


FIGURE 15.10 Measured forces between curved mica surfaces in KNO_3 or KCl solutions (qualitatively similar results are obtained in other electrolyte solutions). In 10^{-5} and 10^{-4} M the force follows the theoretical DLVO force law at all separations. At 10^{-3} M and higher concentrations more cations adsorb (bind) onto the surfaces and bring with them their water of hydration. This gives rise to an additional short-range hydration force below 3–4 nm (see inset and Fig. 15.11 for details). The hydration force is characterized by short-range oscillations of periodicity 0.24 ± 0.02 nm—about the diameter of the water molecule—superimposed on a longer-ranged exponentially repulsive tail of decay length close to the Debye length (cf. the qualitatively similar effect in the interactions between glass and silica surfaces, shown in Figure 15.13). The right-hand ordinate gives the interaction energy between two flat surfaces according to the Derjaguin approximation. [Data from SFA experiments with surfaces in the crossed-cylinder geometry, equivalent to a sphere of radius R near a flat surface or two spheres of radius $2R$, adapted from Israelachvili and Pashley, 1982a; Pashley, 1981a,b; Pashley, 1984.]

noting that the strength and range of the hydration forces increase with the hydration number of the cations (cf. Table 4.2) in the order $\text{Mg}^{2+} > \text{Ca}^{2+} > \text{Li}^+ \sim \text{Na}^+ > \text{K}^+ > \text{Cs}^+$. In acid solutions, where only protons bind to the surfaces, no hydration forces were observed (presumably because protons penetrate into the mica lattice) and the measured force laws were very close to those expected from DLVO theory at all proton concentrations (pH values). These observations are consistent with the well-known swelling behavior of clays (Cebula et al., 1980; Schramm and Kwak, 1982) where their tendency to swell increases as the interlayer counterion goes from cesium to lithium. However, the more hydrated the ions, the higher is their critical hydration concentration, that is, the higher is the concentration at which the hydration forces “kick in”. This is because these ions require a higher energy to (partially) dehydrate them on binding.

Israelachvili and Pashley (1983) also found that while the hydration force between two mica surfaces is overall repulsive below about 4 nm, it is not always monotonic below about 1.5 nm but exhibits oscillations of mean periodicity 0.25 ± 0.03 nm, roughly equal to the diameter of the water molecule. This is shown in Figures 15.10 and 15.11. In particular, they observed that the first three minima at $D \approx 0, 0.28$, and 0.56 nm occur at negative energies, a result that rationalizes observations on clay systems: clay platelets such as montmorillonite repel each other increasingly strongly down to separations of approximately 2 nm (Viani et al., 1984). However, the platelets can also stack into stable aggregates with water

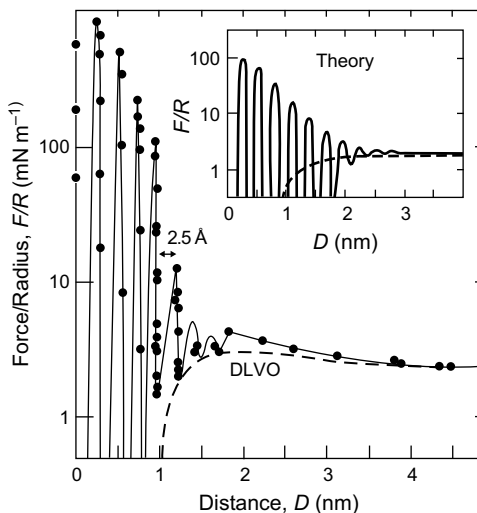


FIGURE 15.11 Measured short-range force between two curved mica surfaces of radii $R \approx 1$ cm in 10^{-3} M KCl. The force at distances above 4 nm is given in Figure 15.10. The dashed line shows the expected DLVO interaction. The values of F/R shown here have been plotted on the assumption of constant surface radius R ; however, due to elastic flattening of the glue supporting the mica surfaces at the high repulsive force barriers at separations below ~ 1 nm, the values of F/R at the force barriers (force maxima) are overestimates. *Inset:* Theoretical computation for the same system by Trokhymchuk et al., (1999) where both the periodicity of the oscillations and the exponential decay length of the envelope of the force maxima is about 0.27 nm. Similar force profiles have also been computed by Cherepanov (2004). The forces between aligned clay sheets show similar behavior, as measured using other techniques such as the Osmotic Stress Technique (Del Pennino, 1981; Viani, 1983). [Experimental data from SFA experiments with surfaces in the crossed-cylinder geometry, equivalent to a sphere of radius R near a flat surface or two spheres of radius $2R$, adapted from Israelachvili and Pashley, 1983.]

interlayers of typical thickness 0.25 and 0.55 nm between them (Del Pennino et al., 1981). In chemistry we would refer to such structures as stable hydrates of fixed stoichiometry, while in physics we may think of them as experiencing an oscillatory force.

These experiments showed that hydration forces can be modified or “regulated” by exchanging ions of different hydrations on surfaces. Such regulated hydration effects also occur with other surfaces and systems (Israelachvili, 1985), including amphiphilic surfaces, discussed in Section 21.3. For example, the force between two mercury surfaces obeys DLVO theory in various electrolyte solutions, but the surfaces fail to coalesce once ionic species (e.g., I^-) specifically bind to the surfaces at higher concentrations (Usui et al., 1967; Usui and Yamasaki, 1969).

Regarding “hydration regulation” in colloidal dispersions, the effects of different electrolytes on the hydration forces between colloidal particles can determine whether they will coagulate or not. Figure 15.12 shows the experimentally determined regions of stability and instability of amphoteric polystyrene latex particles whose surfaces expose $-COO^-$ and $-NH_3^+$ groups. In concentrated $CsNO_3$ solutions Cs^+ ions bind to the surfaces at high pH where there is no competition from protons. But the hydration forces are weak because Cs^+ is weakly hydrated, and the stability/instability regions are indeed explicable

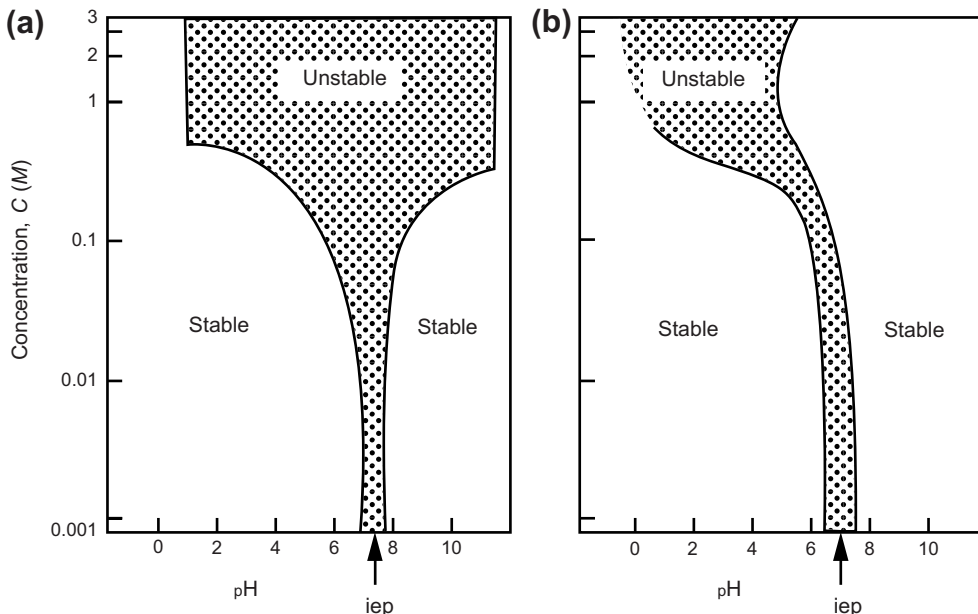


FIGURE 15.12 Domains of stability and instability (coagulation) of a dispersion of amphoteric “latex” particles whose surfaces contain COO^- and NH_3^+ groups. (a) In CsNO_3 solutions the behavior is “ideal”—that expected from DLVO theory. (b) In KNO_3 , and to an even greater extent in LiNO_3 , it is not—the expected coagulation does not occur in high salt above the isoelectric point ($\text{iep} = 7.2$). [From Healy et al., 1978.]

by DLVO theory. However, in concentrated KNO_3 and more so in LiNO_3 solutions the particles remain stable, even at the isoelectric point, because of the stronger hydration forces arising from the binding of the more hydrated K^+ and Li^+ ions. Similar effects occur in other colloidal systems. Thus, the effectiveness of monovalent cations as coagulants usually decreases according to the so-called “lyotropic series”: ⁴ $\text{Cs}^+ > \text{K}^+ > \text{Na}^+ > \text{Li}^+$ for monovalent ions, and $\text{Ca}^{2+} > \text{Mg}^{2+}$ for divalent ions (Hiemenz, 1977), consistent with the model experiments on mica and as expected from the increasing hydration of these ions.

Computer simulations on the interactions between alkali metal and chloride ions in water by Pettitt and Rossky (1986) also showed that the depth of the primary potential minimum becomes less deep than expected from the continuum Coulomb equation on going from K^+Cl^- to Na^+Cl^- to Li^+Cl^- , as shown in Figure 3.4. Likewise, between similar ions, the range of the repulsion in water appears to increase on going from K^+-K^+ to Na^+-Na^+ to Li^+-Li^+ . Later, Grand Canonical Monte Carlo simulations by Delville (1992, 1993) on the double-layer forces between clay surfaces found that sodium ions should cause clays such as montmorillonite to swell, but that potassium ions (which are found in micas) should not. The swelling was found to depend

⁴Or “Hofmeister lyotropic series,” after Franz Hofmeister (1888), who studied the effects of cations and anions on the solubility of proteins, later extended by others to other properties of proteins, hydrophobic interactions, and so on.

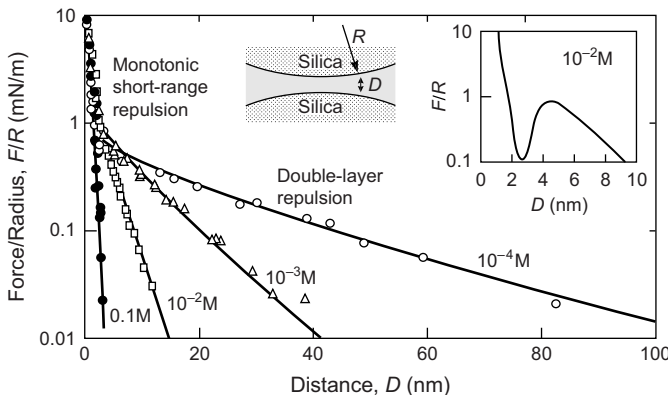


FIGURE 15.13 Experimental measurements of short-range exponentially repulsive non-DLVO forces between two silica surfaces in various aqueous NaCl solutions. Here the forces are pure double layer down to 3–5 nm below which there is a steep *monotonic* repulsion that decays roughly exponentially with a decay length 0.5–1.0 nm instead of the attractive van der Waals force expected from the DLVO theory or the oscillatory force expected from liquid structure theories. [Figure adapted from Horn et al., 1989a]. Similar forces have been measured between silica surfaces by Vigil et al., (1994), and by Ducker and Senden (1992) and Meagher (1992) using the AFM technique. When the short-range repulsion is monotonic, it is probably due to surface roughness (silica hairs in this case), dynamic roughness as in Figure 15.9, or a displaced OHP as in Figure 15.14.

critically on the binding location of the ions to the surfaces, which is investigated further in Worked Example 15.3.

Figure 15.13 shows the measured forces between silica surfaces in various aqueous electrolyte solutions measured by Horn et al., (1989a). Here, the steep short-range repulsion is somewhat different from that observed between mica surfaces: it is largely insensitive to the ionic conditions, and there is no oscillatory component. These hydration forces appear to be truly monotonic and “intrinsic” to the surfaces rather than being “regulatable” by changing the solution conditions. Similar forces have been measured between silica surfaces by Peschel et al., (1982), Meagher (1992), Ducker and Senden (1992), Vigil et al., (1994), and between glass fibers by Rabinovich et al., (1982), using different techniques. Likewise for the forces measured between alumina and silicon nitride surfaces in aqueous solutions although here, as for mica, there is also an oscillatory force at small separations (Ducker and Clarke, 1994). In most cases, the agreement between forces measured using the SFA and AFM techniques has been good (Ducker and Senden, 1992; Hartley et al., 1997).

In Section 14.21 we saw that when the plane of charge (the Outer Helmholtz Plane or OHP) is farther out than the physical solid-liquid interface (the van der Waals plane), the DLVO interaction becomes effectively more repulsive than if both are located in the same place—a few angstroms difference being enough to change an overall attractive DLVO force with a deep adhesive minimum at contact into a purely repulsive interaction at all separations. A similar effect was found to arise for free, but finite sized, counterions adsorbed on mica surfaces (Figure 14.18). Unlike mica and alumina, the silica surface is amorphous, and its negative surface charges (the silicic acid co-ion groups) are located at the ends of short silica hairs protruding a few ångströms from the surfaces (Iler, 1979).

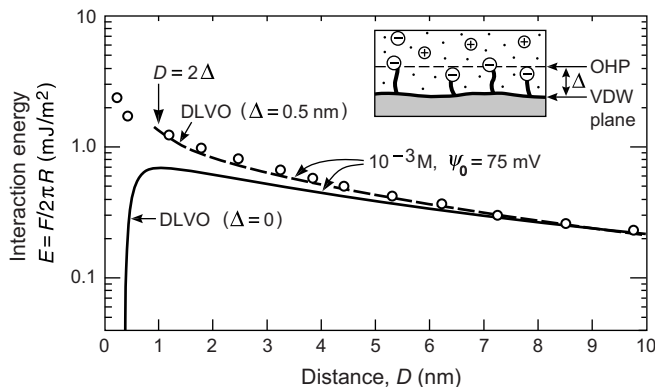


FIGURE 15.14 Measured forces F and corresponding energies E between smooth amorphous silica surfaces in 1 mM NaCl solution (Vigil et al., 1994). Solid line: Calculated DLVO force giving poor agreement with experiment except at large separations. Dashed line: Calculated DLVO force but now with an offset distance of $\Delta = 0.5$ nm per surface for the electrostatic Outer Helmholtz Plane (OHP), corresponding to 1 nm for both surfaces, while keeping the van der Waals plane at $D = 0$, giving good agreement with the measured force law. Silica surfaces are known to have charged silica hairs protruding from them, as shown in the inset (Iler, 1979). This analysis shows how *surface* (as opposed to *liquid*) structural effects occurring within a few ångströms of a surface can have a significant effect on the forces at much larger separations, in addition to eliminating any adhesive energy minimum.

Figure 15.14 illustrates how this effects in the interactions between silica surfaces, effectively eliminating any adhesion.

Worked Example 15.3

Question: The surface potential of a mineral surface in 100 mM NaCl solution at 298 K is measured to be -17.3 mV and the Hamaker constant is calculated to be $A = 8 \times 10^{-21}$ J. Under these conditions, it was further calculated that the DLVO force between two spheres or a sphere and a flat surface of this material should be attractive at all separations with the expectation of strong adhesion at contact. The force between a sphere and a flat surface was measured and found to be monotonically repulsive at all separations below about 4.5 nm, and roughly exponential from 4 down to 1 nm as shown by the \times points in Figure 15.15. It is suspected that this repulsion is a hydration force; but it may also be a DLVO force where the surface charges are located at a finite distance from each solid-liquid interface. Was the initial expectation of a purely attractive force correct? If so, how could you establish that the measured repulsion is due to a monotonically repulsive hydration force, a Stern Layer, or some other effect?

Answer: Figure 15.15 shows plots of the DLVO force-distance curves based on the following equation, taken from Figures 13.1 and 14.10 for this geometry, and including the effect of a shift in the Outer Helmholtz Plane (OHP) of δ per surface:

$$F(D)/R = \kappa Z e^{-\kappa(D-2\delta)} - A/6D^2 \quad \text{for } D > 2\delta, \quad (15.11)$$

where a strong steric repulsion is assumed at separations below 2δ . For the present system we have $\kappa^{-1} = 0.96 \times 10^{-9}$ m and $Z = (9.22 \times 10^{-11}) \tanh^2(\psi_0/103) = 2.55 \times 10^{-12}$ N. For $\delta = 0$ the force is indeed attractive ($F/R < 0$) at all separations, as shown in Figure 15.14 for $\Delta = 0$.

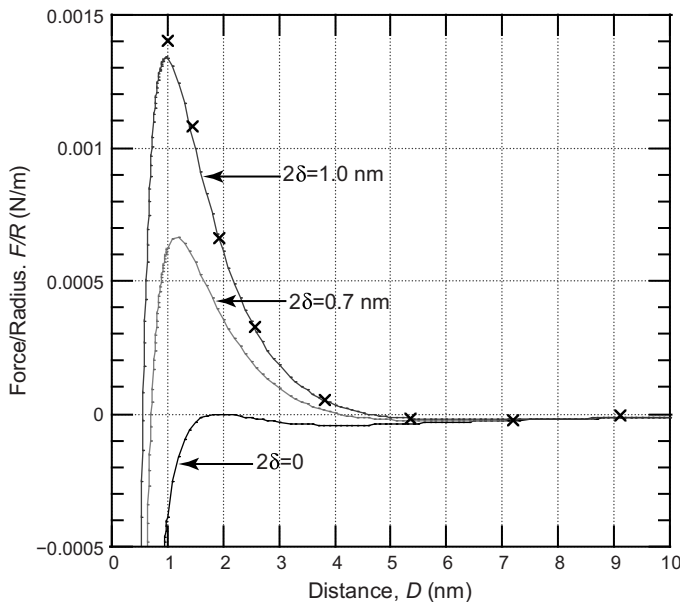


FIGURE 15.15 Experimentally measured (x) and theoretically computed DLVO forces (Eq. 15.11) including finite outward shifts in the OHP of Δ per surface for the double-layer forces.

For $\delta = 0.50$ nm the calculated curve passes nicely through the experimental points, and in the regime between $D \approx 4$ and $D \approx 1$ nm is indeed close to being exponential. (Even for $\delta = 0.35$ nm the net force is already repulsive ($F/R > 0$) at all separations below 4 nm.) The finite δ could be due to a finite layer of surface co-ions or surface-bound counterions, or to the finite size of the *free* counterions in the diffuse double-layers (see Worked Example 14.7). Each of these would be differently sensitive to changes in the electrolyte ions, their valency, ionic strength, and pH. Thus, to establish whether the short-range repulsion is a solvation force rather than simply a modified DLVO interaction, a series of experiments under different solution conditions would have to be carried out. These should be coupled to independent measurements of the surface potential (via zeta potential, streaming potential or electrophoresis measurements) to establish the whether the constant potential assumption is valid or whether a charge regulation or some other model of the double-layer force can account for the results (see last paragraph of this section). Surface structural studies (via AFM imaging, for example) and time- and rate-dependent force measurements may also be required.

The different locations of the van der Waals and double-layer planes, together with finite counterion size effects, are the most likely explanation for most of the monotonic hydration repulsion observed in many systems, including those where the repulsion can be regulated by ion exchange, and also when an oscillatory solvation force is superimposed on the monotonic force (Delville, 1993; Marcelja, 1997, 2000). This interpretation would place this type of force in the category of a steric repulsion—more associated with the overlapping of confined ionic groups than a true solvation force that is mediated

by the structure of the solvent molecules. For this reason such forces are now often referred to as “steric-hydration” forces.

Repulsive hydration forces are important in many phenomena. For example, they may be responsible for the unexpectedly thick wetting films of water on silica and other charged surfaces, discussed in Section 14.8. The fact that these forces can often be regulated by ion exchange makes them useful for controlling various technological processes such as clay swelling (Quirk, 1968, 1994), colloidal and bubble coalescence (Healy et al., 1978; Elimelech, 1990; Lessard and Zieminski, 1971; Craig et al., 1993), and ceramic processing and rheology (Velamakanni et al., 1990; Chang et al., 1994; Biesheuvel and Lange, 2001). In the latter case, the weakening of the strong adhesion by a short-range repulsive hydration force allows ceramic particles to roll over and adjust to each other more easily, resulting in higher packing densities.

Neither experiment nor theory has yet revealed the full nature of short-range monotonically repulsive solvation forces, which we return to again in later chapters devoted to adhesion forces and the short-range interactions of fluid-like and biological surfaces in water. Theoretical work and computer simulations by Jönsson (1981), Christou et al., (1981), Kjellander and Marcelja (1985a, b), Henderson and Lozada-Cassou (1986, 1994), Trokhymchuk et al., (1999), suggest that the solvation forces in water should be purely oscillatory and additive with the two DLVO forces. But other theoretical studies (Marcelja and Radic, 1976; Marcelja et al., 1977; Gruen and Marcelja, 1983; Jönsson and Wennerström, 1983; Schiby and Ruckenstein, 1983; Luzar et al., 1987; Attard and Batchelor, 1988) suggest a monotonic exponential repulsion or attraction, possibly superimposed on an oscillatory profile. Still others have argued that the monotonic and oscillatory hydration forces are intimately related to the double-layer interaction and cannot be separated from each other (Delville, 1992, 1993; Marcelja, 1997), even though they may be additive with the van der Waals and other types of interactions (Marcelja, 2000). For example, Delville (1992, 1993) concluded that the short-range forces in electrolyte solutions depend critically on the precise locations at which the counterions bind to the surfaces, and that a higher surface charge does not necessarily enhance the structuring or layering of the water molecules.

15.9 Solvation Forces in Aqueous Systems: Attractive “Hydrophobic” Forces

In contrast to some hydrophilic surfaces that exhibit an apparently enhanced repulsion in water, other “hydrophobic” surfaces experience an added attraction. The concept of “hydrophobicity” first arose to describe the low solubility and unexpectedly strong attraction between hydrocarbon molecules in water (Chapter 8). This concept was initially applied only to small solute molecules, and it was believed to be associated with the way water molecules could structure around them (cf. Figure 8.5). Hydrophobic solutes are invariably nonpolar—for example, hydrocarbons, fluorocarbons, vapor bubbles, or cavities—and are therefore “inert” to water—not being able to form polar, ionic or hydrogen bonds with them. Later, it was realized that extended surfaces of chemically similar

materials are also hydrophobic in the sense that (1) their mutual attraction in water and aqueous solutions is much greater than can be expected from the London or Lifshitz theories of van der Waals forces, and (2) water droplets have a large contact angle θ on them, typically $>90^\circ$. Some manifestations of hydrophobicity are illustrated in Figure 15.16.

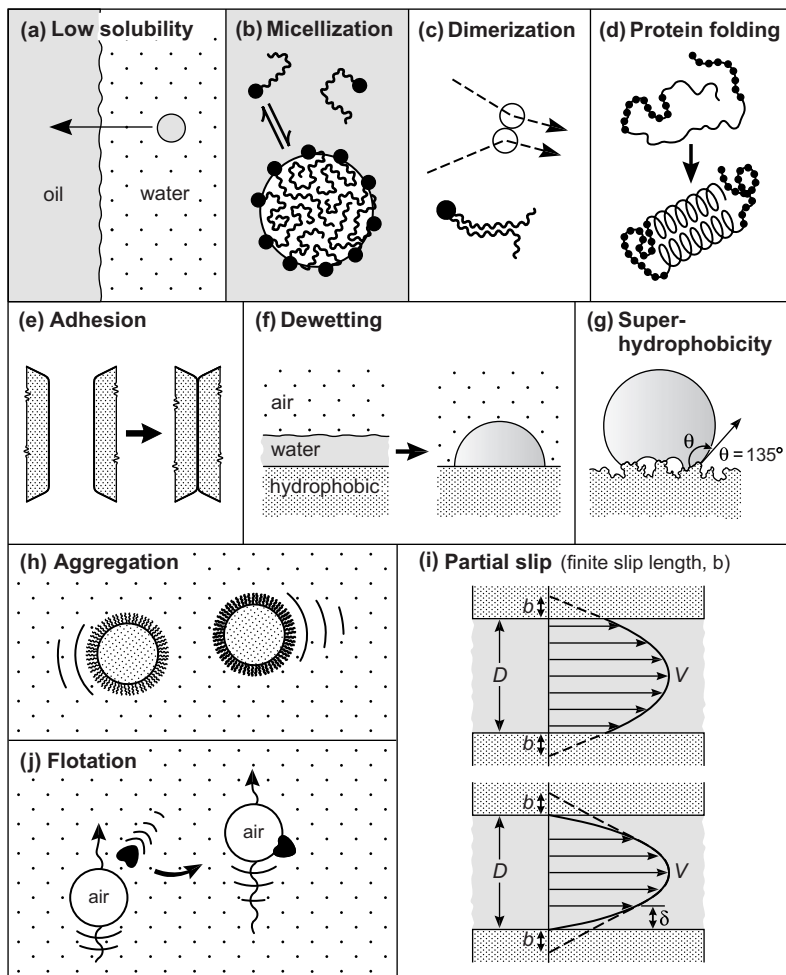


FIGURE 15.16 Manifestations of hydrophobicity and hydrophobic interactions. (a) Low solubility/immiscibility (see Chapter 8); (b) micellization (see Chapters 19 and 20); (c) dimerization and association of hydrocarbon chains; (d) protein folding; (e) strong adhesion (see Chapter 17); (f) nonspreadng of water on hydrophobic surfaces; (g) Superhydrophobic surfaces are found in plants and animals and, more recently, as man-made coatings. They serve as “self-cleaning” surfaces and, in the case of some aquatic animals, such as penguins, to trap air between their feathery skins that insulates them from heat loss in cold water; (h) rapid coagulation of hydrophobic particles or surfactant-coated surfaces; (i) partial slip boundary condition at a solid-liquid interface. Partial slip can arise from true partial slip (top figure) as occurs at a liquid-vapor interface, or zero wall slip (apparent partial slip, bottom figure) due to a reduced liquid density and viscosity within a depletion zone of thickness δ ($\neq b$) at the interface (see also Figure 15.5c) as may be occurring for water flowing past a hydrophobic surface; (j) hydrophobic particle attachment to rising air bubbles (basic mechanism of “froth flotation” used to separate hydrophobic and hydrophilic particles).

The strong attraction of hydrocarbon surfaces in water is reflected in the large interfacial energy, γ_i , of the hydrocarbon-water or “oil-water” interface. By definition, γ_i is half the adhesion energy $W_{hc/w/hc}$ needed to fully separate two hydrocarbon surfaces from contact in water, which is larger, rather than smaller, than the energy needed to separate the surfaces in air. According to the Lifshitz theory, the Hamaker constant for a typical hydrocarbon liquid of refractive index $n = 1.41$ was calculated in Chapter 13 to be about $5 \times 10^{-20} \text{ J}$ in air or vapor ($n = 1.00$), and about 10 times less for interactions in water ($n = 1.33$). This implies a surface energy of $\gamma \approx 25 \text{ mJ m}^{-2}$ for the hydrocarbon-air interface, as observed (Table 13.4), and an interfacial energy for the hydrocarbon-water interface of $\gamma_i \approx 2.5 \text{ mJ m}^{-2}$, which is only 5% of the measured value of $\gamma_i \approx 50 \text{ mJ m}^{-2}$.⁵

Where does the other, non-van der Waals, contribution of 95% come from? To answer this we may split up γ_i into three contributions as $\gamma_i = \gamma_{hc} + \gamma_w - W_{hc/w}$.⁶ Now, typical values for the first and last terms are $\gamma_{hc} \approx 25 \text{ mJ m}^{-2}$ and $W_{hc/w} \approx 50 \text{ mJ m}^{-2}$, *which are as expected from the Lifshitz theory*. Thus, it appears that the high interfacial energy is due entirely to the anomalously high value of the surface tension of (pure) water—the hydrocarbon surface behaving as normal van der Waals solid or liquid, both in its interaction with itself (which determines γ_{hc}) and with water (which determines $W_{hc/w}$).

Concerning the likely origin of other (non-van der Waals) contributions to the interaction of inert surfaces in water, we must first consider the oscillatory solvation force in water. Equation 15.8 showed that this contributes approximately $-kT/2\sigma^2$ to the interfacial energy γ_i . Since the water molecule has a relatively small diameter of $\sigma \approx 0.25 \text{ nm}$, this contribution is large and close to 33 mJ m^{-2} at room temperature. When added to the (much smaller) van der Waals–Lifshitz contribution, calculated above, we obtain $\gamma_{hc/w} \approx 35 \text{ mJ m}^{-2}$. This is less than but not too far from the measured value of $\sim 50 \text{ mJ m}^{-2}$, and it is mainly entropic. The oscillatory forces as $D \rightarrow 0$ is often referred to as the *depletion force*, since it determines the final adhesion as the last layer of molecules is finally “depleted” from between the two surfaces. We return to discuss the origin of hydrophobic forces at the end of this Section after considering the evidence.

Another phenomenon associated with hydrophobicity is the high contact angles of water on hydrophobic surfaces. Again, according to the Lifshitz theory, these should be small or zero. Thus, if only van der Waals forces were operating and if the refractive index of the (hydrocarbon) surface is greater than that of the liquid ($n_{hc} > n_w$), the adhesion energy of the solid-liquid interface should be greater than the adhesion energy of the liquid-liquid interface: $W_{hc/w} \geq 2\gamma_{hc}$. By the Young-Dupré equation, $W_{hc/w} = \gamma_w(1 + \cos \theta)$, the above condition implies that $\cos \theta \geq 1$ —that is, that the liquid should wet (spread on) the surface and, therefore, that $\theta \approx 0$. The contrast with measured values could not be more striking: typical contact angles of water on fully hydrocarbon surfaces

⁵The high value for γ_i appears to be related, qualitatively if not quantitatively, to the unexpectedly high free energy of transferring a hydrocarbon molecule into water (cf. Sections 8.5 and 8.6). However, the free energy of transfer is mainly entropic and increases with T (Tanford, 2000), while γ_i decreases with T .

⁶The adhesion energy for interactions in a medium, expressed as γ_i , γ_{12} , W_{121} or $W_{hc/w/hc}$, should not be confused with the adhesion energy in air or across a vacuum, expressed as W_{12} or $W_{hc/w}$ (Section 17.1).

are $\theta \approx 110^\circ$ (i.e., $\cos \theta \leq 0$), implying that the ratio $W_{\text{hc/w}}/\gamma_w$ is very much lower than expected if only van der Waals forces were operating. Again, the reason for this is not because $W_{\text{hc/w}}$ is too low, but because γ_w is too high. Thus, inserting $W_{\text{hc/w}} \approx 50 \text{ mJ m}^{-2}$ and $\gamma_w = 72 \text{ mJ m}^{-2}$ into the Young-Dupré equation gives $\theta = \cos^{-1}\{(50/72) - 1\} = 108^\circ$, as observed. We therefore arrive at the same conclusion as above, namely, that the unexpectedly high contact angle is due to some unusual surface property of water and not of the hydrocarbon surface that is actually surprisingly “normal.”

Thus, the answer to the question “What is a hydrophobic surface?” appears to be “Any ordinary, nonpolar surface.” Now, there *are* surfaces on which the water contact angle is small and where their adhesion in water *is* well-described by the Lifshitz theory. These surfaces are invariably polar and are discussed in Chapter 17. Here we shall concentrate on those surfaces that, together with water, give rise to a hydrophobic interaction. They are usually nonpolar but can also be polar—for example, the siloxane $\text{Si}-\text{O}-\text{Si}$ groups that appear on silica and clay surfaces and certain polymer groups are hydrophobic or partially hydrophobic, even when they are charged or highly polar.

Degrees of hydrophobicity. As we shall see, there are “degrees of hydrophobicity,” whether defined in terms of the interfacial energy γ_i , the magnitude and range of the hydrophobic force, or the contact angle of water on a hydrophobic or partially hydrophobic surface. The last is the easiest to measure and has become the unofficial measure of hydrophobicity. However, a generally accepted quantitative scale of surface hydrophobicity in terms of the contact angle or any other criterion does not yet exist,⁷ and it would be problematic because the contact angle depends on the surface chemistry, on whether the water is advancing or receding, and on the surface roughness (see Sections 17.5 and 17.6). For smooth surfaces, the contact angle can be quantified on the basis of the semiempirical Cassie equation (Cassie, 1948) which gives the contact angle of a surface composed of a fraction f_1 and $f_2 = (1 - f_1)$ of different, for example, hydrophobic and hydrophilic groups as

$$\cos \theta = f_1 \cos \theta_1 + f_2 \cos \theta_2, \quad (15.12)$$

where θ_1 and θ_2 are the contact angles of the pure hydrophobic and hydrophilic surfaces. A modified Cassie equation, more suited to van der Waals dispersion forces, has been proposed of the form (Gee et al., 1989)

$$\cos \theta = \sqrt{f_1^2 \cos^2 \theta_1 + f_2^2 \cos^2 \theta_2}. \quad (15.13)$$

Both of the above equations predict similar results, and have been found to be surprisingly accurate in predicting contact angles in experiments on mixed surfactant-coated surfaces of known composition (Drelich et al., 1996).

As an example of the Cassie equation, we may consider a fully hydrophobic surface for which $\theta = 115^\circ$ so that $\cos \theta_1 = -0.42$, and a hydrophilic surface for which $\theta = 0$ so that $\cos \theta_2 = 1.00$. For a surface composed of a 50–50 mixture of hydrophobic and hydrophilic groups, the Cassie equation predicts that $\cos \theta = \frac{1}{2} \times 1 - \frac{1}{2} \times 0.42 = 0.29$, so that $\theta = 73^\circ$.

⁷For amphiphilic molecules the HLB number provides such a scale (see Fig. 20.3).

For a surface with only 10% hydrophobic groups the contact angle is 31°. Thus, according to the Cassie equation, a surface may be said to be fully hydrophobic when $\theta > 90^\circ$; partially hydrophobic for θ between 45 and 90°, and weakly hydrophobic when θ is below 45° but still non-zero. Below we shall see that there is a correlation between the contact angle and other manifestations of hydrophobicity, such as the magnitude and range of the hydrophobic force between two surfaces in water.

Direct measurements of hydrophobic forces. There has been a steady accumulation of SFA and AFM measurements of the forces between various hydrophobic surfaces in aqueous solutions (Christenson and Claesson, 2001). These surfaces include (1) surfaces coated with physisorbed surfactant monolayers exposing hydrocarbon or fluorocarbon groups, (2) surfaces that have been rendered hydrophobic by chemical methylation or plasma etching (chemisorption), (3) water-air or water-vapor surfaces (for example, two air bubbles), and (4) various other surfaces, such as the (partially) hydrophobic siloxane surfaces of dehydroxilated silica. While the data is often equivocal, the majority of experiments have found that the hydrophobic force-law between macroscopic or colloidal surfaces is much stronger, longer-ranged, and has a different distance-dependence than the Lifshitz van der Waals force.⁸ Experimental difficulties arise because hydrophobic surfaces in water are prone to picking up impurities from solution, such as polymers or excess surfactants (Israelachvili et al., 1981), or air bubbles (Tyrrell and Attard, 2001), or cause physisorbed surfactants or amphiphilic polymer groups to overturn and expose their previously buried hydrophilic moieties. These effects can give rise to long-range steric, capillary, or electrostatic forces that can be repulsive or attractive.

Hydrophobic forces have been studied by both SFA and AFM techniques (Meyer et al., 2006), and are discussed in more detail in Section 21.5. The full force-law in pure water appears to follow a double exponential function of the type

$$F = -C_1 e^{-D/D_1} - C_2 e^{-D/D_2} \quad (15.14)$$

but there is uncertainty about the values of the four “constants,” and even whether there actually is such a “universal” force-law for the hydrophobic interaction (Hammer et al., 2010).

Helm et al. (1992) measured the forces between “depleted” lecithin bilayers in water as a function of increasing hydrophobicity of the two outer monolayers. This was achieved by progressively increasing (stressing) the amphiphilic molecules by depleting the lipids from the aqueous reservoir, thereby increasing their headgroup area and exposing more of the hydrocarbon chains to the aqueous phase. The results (see Figure 21.8 in Chapter 21) showed that with increasing hydrophobic area per molecule: (1) the attractive forces, which were initially van der Waals, became stronger and longer ranged, (2) the repulsive short-range steric-hydration force decreased in magnitude or range, and (3) the adhesion

⁸The hydrophobic force is not in principle particularly strong, only stronger than the van der Waals between hydrocarbon surfaces in water which happens to be particularly weak (cf. the Hamaker constants of $\sim 0.5 \times 10^{-20}$ J for hydrocarbons compared to $\sim 40 \times 10^{-20}$ J for metals and conducting surfaces in water, listed in Table 13.3)

energy $W(0)$ increased, eventually reaching over 1,000 times the original value (see inset). These results illustrate how the hydrophobic force-law $F(D)$ and adhesion energy $W(0)$ can change continuously as the surfaces change from being fully hydrophilic to fully hydrophobic.

Other ways of inducing hydrophobicity in lipid membranes is to stress them mechanically, electrically (electroporation) or osmotically so that they are forced to thin and/or stretch. In all cases, the enhanced adhesion force or surface energy $-W(0) = 2\gamma_i$ has been found to be proportional to the applied stress τ (see inset in Figure 21.8) which—because in a first approximation bilayers stretch elastically—is proportional to the additional hydrophobic area exposed at the bilayer-water interface. Significantly, for a fully depleted bilayer—for example, an inverted monolayer, the interfacial energy $W(0)$ approaches $2\gamma_i = 100 \text{ mN m}^{-1}$ (mJ m^{-2})—the value for a pure hydrocarbon-water interface (Helm et al., 1992; Chen et al., 1992; Kurihara and Kunitake, 1992; Leckband and Israelachvili, 2001). The biological implications of the interactions between biological surfaces (membranes and proteins) that expose hydrophobic patches are discussed in Chapter 21.

The results of AFM force measurements at the other extreme of very hydrophobic surfaces and large separations are shown in Figure 15.17. These experiments employed silanated silica surfaces of different hydrophobicities to measure both the force-laws $F(D)$ and corresponding contact angles. The results showed that the strength and range of the attraction changes linearly with $\cos \theta$, where θ is the contact angle of water on the hydrophobic

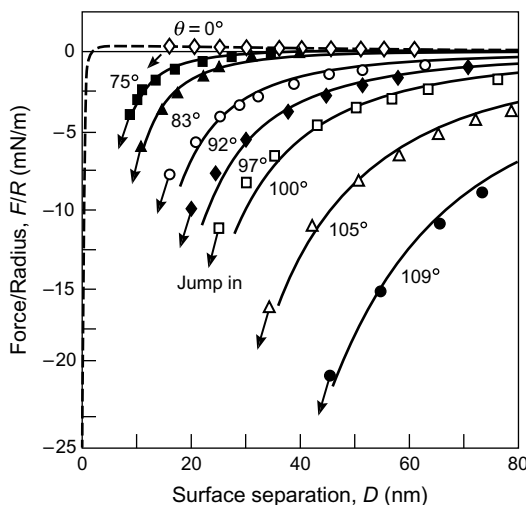


FIGURE 15.17 Force measurements between a partially hydrophobic silanated silica surface (contact angles θ from zero to 109° as shown) and a fully hydrophobic surface (θ fixed at 109°) measured by AFM (Yoon et al., 1997). Jump-in instabilities are indicated by arrows. The dashed curve is the theoretical DLVO force. The lines through the experimental points fit an inverse-square force-law, $F/R = -C_H/D^2$, the same as for the van der Waals force but with an effective Hamaker constant $A_{\text{eff}} = 6C_H$ that is orders of magnitude larger than even for metals or conductors, Eq. (13.19), which is believed to be the maximum possible. Recent SFA results also show a long-range attraction but not stronger than the van der Waals interaction between conductors and not as long-ranged (Meyer et al., 2006).

surface. However, the measured adhesion energies $W(0)$, as determined from the pull-off forces, were less than expected from the Young-Dupré equation.

Most of the early measurements of hydrophobic forces used mica or silica surfaces coated with a physisorbed monolayer of cationic surfactants, where the positively charged headgroups attached to the negatively charged surfaces thereby exposing the hydrocarbon ends of the molecules. However, when immersed in water, half of the surfactants flip to form bilayer domains,⁹ so that in water each surface consists of positively charged bilayer islands (domains, patches) floating on a negatively charged sea of bare mica or silica. When two such surfaces are brought close together the positive islands of each surface move laterally to face the negative sea of the other, giving rise to a strong long-range electrostatic attraction. Wood and Sharma (1995) were the first to employ robust, *chemisorbed* surfactant monolayers, which do not flip or rearrange when immersed in water, and measured an attraction extending out to ~10 nm, instead of >100 nm. This was probably the first direct measurement of the “true” hydrophobic force. Meyer and colleagues (2008) extended these studies using chemisorbed surfactants, and concluded that the hydrophobic attraction is stronger than the van der Waals attraction at separations less than 10–15 nm (where the second term in Eq. 15.14 dominates) and that it becomes even stronger in the last 1 nm before contact (where the first term dominates).

The long-range nature of the hydrophobic interaction has a number of important consequences, some of which were shown in Figure 15.16. It accounts for the rapid coagulation of air bubbles and hydrophobic particles in water (Xu and Yoon, 1990; Pugh and Yoon, 1994), and it may also account for the rapid folding of proteins (see Chapters 20 and 21). It also explains the ease with which water films rupture on hydrophobic surfaces (Tchaliowska et al., 1990). In this the van der Waals force across the water film is repulsive (Section 13.9) and therefore favors wetting, but this is more than offset by the attractive hydrophobic interaction acting between the two hydrophobic phases across water (remember that air is hydrophobic!).

The consequences of such strong long-range forces, especially if they are also long-ranged at the molecular level, could be very significant for understanding many biological processes because the hydrophobic interaction is the main interaction responsible for stabilizing surfactant micelles and biological membranes (Tanford, 1980) and macromolecules such as proteins and DNA (Cantor, 1980). Long-ranged hydrophobic forces may contribute to the rapid and directed folding of proteins, and hydrophobic forces are increasingly being implicated in the adhesion and fusion of biological membranes and cells, as discussed in Chapter 21. However, still unanswered is the crucial question of whether the hydrophobic interaction is long-ranged even between small molecules and sub-molecular groups, such as hydrocarbon chains or hydrophobic amino acid groups or “residues.” This is important for knowing whether long-range attractions are involved in, for example, biospecific recognition interactions and protein folding.

⁹The overturning of surfactants was first described by Langmuir (1937).

Origin and theories of hydrophobic forces. Like the monotonically repulsive hydration force, the origin of the hydrophobic force is still unknown, and it is still not clear whether it should be considered as a solvation force or as some kind of long-range electrostatic or van der Waals-like interaction (see Faraday Discussions No. 146, 2010). It appears, however, to be a *surface force* rather than a *body force* (Section 11.6).

Earlier in this Section we saw that due to small size of the water molecule the oscillatory solvation interaction does predict the right order of magnitude for the adhesion energy of two inert (nonpolar) surfaces in water, a value that is mainly entropic and much greater than the van der Waals contribution. However, the apparently monotonic profile and long range of measured hydrophobic forces are certainly not predicted by this model. There are currently three main theoretical approaches to modeling the hydrophobic force, based on one of the following mechanisms: *vapor bridges*, due to the attractive capillary (Laplace pressure) force between bridging nanoscopic bubbles; *water structure*, as an attractive solvation (hydration) force associated with changes in the density or ordering of water between two approaching hydrophobic surfaces; and *electrostatic*, as an attractive electrostatic van der Waals-like force between correlated charges or dipoles at the surfaces. We briefly consider these three mechanisms in turn.

Vapor bridges model. Hydrophobic surfaces or patches are prone to picking up air bubbles that bridge two approaching surfaces to give rise to a strongly attractive capillary force (see Section 17.11). It has been suggested that the long-range hydrophobic attraction is due to such bridges (Yaminsky and Ninham, 1993; Craig et al., 1993; Vinogradova et al., 1995), and AFM imaging of hydrophobic surfaces have sometimes shown high concentrations of such bubbles on the surfaces (Tyrrell and Attard, 2001). However, other AFM studies have not (Tsao et al., 1991) and optical measurements show that water between two hydrophobic surfaces has the same refractive index as in the bulk (Kekicheff and Spalla, 1994). A number of studies have found that the long-range hydrophobic interaction disappears when the water is deaerated (Craig et al., 1993), but it is not known whether this also applies to the short-range interaction (below 10 nm), and the high interfacial tension of the hydrocarbon-water interface of $\gamma_i = 50 \text{ mJ m}^{-2}$, which determines the strength of the attraction at contact, is unaffected by deaeration. How dissolved gases in water change the hydrophobic interaction is not yet understood, nor have the full implications of this effect for biological interactions and the colloidal stability of emulsions been explored. Thermodynamically, a vapor bubble should not be stable on *any* surface, whether hydrophilic or hydrophobic—that is, whatever the contact angle θ . But if $\theta > 90^\circ$, a vapor cavity bridging two hydrophobic surfaces will be stable (since the water surface can now be convex) and give rise to an attractive capillary force. However, hydrophobic forces arise even in the absence of a vapor bridge.

Water structure models. Early Molecular Dynamics simulations (Lee et al., 1984) already showed that water is differently structured¹⁰ at hydrophobic and hydrophilic surfaces (cf. Figs 8.5 and 8.6). More recent theories of the forces between two

¹⁰Structure can mean molecular orientation (a vector), density (a scalar), or a cooperative network.

hydrophobic surfaces, including analytic theories (Lum et al., 1999) and Grand Canonical Monte Carlo simulations (Luzar, 1987; Leung, 2000; Luzar, 2000; Bratko et al., 2001; Forsman et al., 1996), do indicate that a depletion-like mechanism is responsible for the hydrophobic interaction, where the region immediately adjacent to a hydrophobic surface is more vapor-like than liquid-like (cf. Figure 15.5c). The predicted interaction potential is a decaying oscillatory force superimposed on a monotonic attraction, but its range is much less than that measured. Unfortunately, current simulations with water are limited to gap widths below 1.5 nm so that a true comparison with experimental data is not yet possible. Support for a depletion model comes from the temperature-dependence of the hydrophobic interaction, and its pressure-dependence: the attraction gets weaker at high pressures which, presumably, collapses the depletion layer (Bratko et al., 2001).

Electrostatic models. These are essentially charge or dipole correlation models of the ion-correlation or van der Waals type (Attard, 1989; Tsao et al., 1993; Miklavic et al., 1994; Podgornik and Parsegian, 1995). Most involve mobile charges or dipoles, which can be due to mobile ionic or dipolar molecules or domains adsorbed to the surfaces (Tsao et al., 1993) or to the arrangements of the water molecules themselves. The latter mechanism would require that water molecules organize themselves differently at hydrophobic surfaces, and that this ordering is modified in the presence of another, approaching surface. Such an effect may be related to the peculiar dielectric and long-range proton-hopping properties of water (cf. Section 8.1) that allow for high local polarizations to occur. For any given positional arrangement of water molecules, whether in the liquid or solid state, there is an almost infinite variety of ways the H-bonds can be interconnected over three-dimensional space while satisfying the “Bernal-Fowler” rule that requires two donors and two acceptors per water molecule (Hobbs, 1974; Stanley and Teixeira, 1980; Stanley et al., 1981). In other words, the H-bonding “structure” may be quite distinct from the “molecular” structure. The energy and entropy associated with the H-bonding network can extend over a much larger region of space than the molecular correlations (Pauling, 1935; Hollins, 1964), and the perturbation of this network when water is under confinement could be at the root of the hydrophobic interaction.

Whatever the answer, it is clear that the situation in water is governed by much more than the simple molecular packing effects that seem to dominate the solvation or structural forces in simpler liquids.

PROBLEMS AND DISCUSSION TOPICS

- 15.1** (i) In Figure 15.2 show analytically or by geometrical construction that at any given separation D the density of close-packed (cylindrical) molecules taking Route 1 is lower than those taking Route 2. Discuss the implications of this for the preferred path and for the functional form of the solvation force between the two surfaces.
(ii) For spherical molecules, the transition between two and one close-packed layers shown in Figure 15.2 e → g is not the one of highest density at any separation D . Sketch top views of the transition of highest density, clearly showing the

location of the upper and lower spheres at each stage. Explain why there is no plane through which this transition can be represented by Figure 15.2 e → g. If you find two or more possible routes, argue which one is likely to follow the path of lowest energy. [Suggestion: Draw 18 close-packed circles forming 3 rows (lines) of 6 molecules each to represent the lower layer. Add 10 close-packed circles centered above the “holes” of the lower layer to represent the upper layer. Mark the centers of the lower and upper circles at each stage of the collapse.]

- 15.2** Consider the changing density of the molecules or particles in the gap and reservoir in the system shown in Figure 15.4b as the surfaces are separated from contact. How will the attractive solvation force or pressure initially change with the separation in the range from $D = 0$ to $D = \sigma$ if (i) the system is at constant volume, and (ii) the reservoir is at constant pressure? [Answer: (i) The attractive force *increases*; (ii) the attractive force remains constant.]
- 15.3** From a consideration of molecular size contribution to the solvation interaction between two surfaces, estimate the adhesive *force* per unit area (i.e., the pressure) between two flat surfaces in an inert liquid whose molecules occupy a volume of 40 \AA^3 . Compare this value with what would be expected from the van der Waals force, assuming a Hamaker constant of $8 \times 10^{-21} \text{ J}$. [Answer: The two pressures are about the same.]
- 15.4*** Figure 15.1c and Eq. (15.4) apply to dissolved solute molecules and ions, as well as to colloidal particles or nanoparticles dispersed in a solvent medium between the two surfaces. In the case of colloidal particles, since their radius is much larger than that of the solvent molecules, any ejection of a confined particle into the reservoir must be accompanied by its replacement by many solvent molecules. This means that ρ_s and ρ_m *increase* rather than *decrease* in Eq. (15.4), resulting in a repulsion rather than an attraction (as occurs for a single-component fluid). However, this is not the case: the depletion of particles or large macromolecules from a gap does result in a “depletion” attraction (see Section 16.6). Resolve this paradox.
- 15.5** Starting from the approximate expression for the decaying oscillatory potential (or pressure) between two flat but structured surfaces, Eq. (15.6), obtain an expression for the force between a large sphere of radius R and a flat surface. What does your answer indicate concerning the “smearing out” of oscillations between two curved surfaces? Will the same apply to surfaces that are randomly rough?
- 15.6** How do you envisage that the last layer of molecules are removed (squeezed out) between two *real*—that is, structured and elastically deformable, surfaces as they come into final molecular contact with no solvent molecules between them? Make atomic-scale drawings of all the crucial intermediate stages to illustrate your model(s).
- 15.7** A liquid droplet of a thermotropic liquid crystal in the nematic phase is placed on a solid surface. The molecules of the nematic can be considered as short rigid rods

(cigar-shaped) aligned in the same direction but having no long-range positional order. Discuss the factors that determine whether the molecules align parallel or perpendicular to the surface and how this affects the solvation force between two surfaces across the nematic liquid.

- 15.8** A colloidal dispersion is stable (i.e., the particles remain dispersed) when the solvent is pure water. On addition of a small amount of a certain electrolyte it becomes unstable (i.e., the particles coagulate). On progressive addition of the same electrolyte it becomes stable again, then unstable, then finally stable again at very high electrolyte concentration. Explain this phenomenon in qualitative terms, and suggest the likely nature of the surface of the colloidal particles and the type of electrolyte used.

Steric (Polymer-Mediated) and Thermal Fluctuation Forces

16.1 Diffuse Interfaces in Liquids

So far, the particle-solution interface has been assumed to be smooth and rigid, possessing a sharp, well-defined boundary. There are many instances where this is not the case, where interfaces are spatially diffuse, and where the forces between them depend on how their diffuse boundaries overlap. By a diffuse surface or interface we do not mean that it is simply “rough,” but rather that it has thermally mobile surface groups—that is, that it is dynamically rough, not statically rough. There are two common types of such diffuse interfaces.

First, there is the interface that is inherently mobile or fluid-like, as occurs at liquid-liquid, liquid-vapor, and some amphiphile-water interfaces. We have already seen in Section 15.2 (Figure 15.1a) that a simple liquid-vapor surface has molecular-scale thermal fluctuations or protrusions. Even though the scale of these fluctuations may be no more than a few ångstroms, this is sufficient to significantly affect the molecular structure of the surfaces and the forces between them. As we shall see, different types of fluctuations can arise depending on the shapes of the molecules and their specific interactions at an interface. In some cases the resulting protrusions can have quite large amplitudes. When two such surfaces or interfaces approach each other, their protrusions become increasingly confined into a smaller region of space and, in the absence of any other interaction, a repulsive force arises associated with the unfavorable entropy of this confinement. Such forces are essentially entropic or osmotic in origin and are referred to as “thermal fluctuation,” “entropically driven,” or “protrusion” forces.

The second type of a thermally diffuse interface occurs when chain molecules, attached at some point to a surface, dangle out into the solution where they are thermally mobile (like seaweed on the sea floor). On approach of another surface, the entropy of confining these dangling chains again results in a repulsive entropic force that, for overlapping polymer molecules, is known as the “steric” or “overlap” repulsion.

For both of the above examples, complex molecular rearrangements and other interactions can lead to quite complex interaction potentials. For example, the force may be attractive before it becomes repulsive. We shall start by considering the second of the above cases: the interactions of polymer-covered surfaces.

16.2 The States of Polymers in Solution and at Surfaces

A polymer is a macromolecule composed of many monomer units or segments. If all the monomer units are the same, it is called a homopolymer, and if different, a copolymer or

heteropolymer. Proteins are heteropolymers of amino acids where the segments are referred to as “groups” or “residues.” Some common polymers are listed in Table 16.1.

The molecular weight M_0 of a monomer unit is typically between 50 and 100 Da(=g/mol), while the total molecular weight $M = nM_0$ can range from 1,000 to above 10^6 . When in solution, a polymer chain can adopt a number of configurations depending on the net segment-segment forces in the liquid. A rigid polymer, such as DNA and actin, will be straight, and its fully extended length or *contour length* is therefore $L_c = nl$, where n is the number of segments and l the segment or monomer length. However, even rigid rods have some elastic flexibility, and, if sufficiently long, at a finite temperature they will undergo thermally induced bending fluctuations—the effective Brownian motion of a wire. Such polymers are called *wormlike chains*, and their natural mean (fluctuating) wavelength is called the *persistence length*. Since most wormlike chain polymers are biological, they are discussed in Part III.

The other type of polymer molecule is known as the *freely jointed chain*, where the segments behave like the links of a necklace, able to rotate freely about each other in any direction. If these rotations are truly free—that is, not perturbed by any segment-segment interactions—the polymer assumes the shape of a *random coil*, shown schematically in Figure 16.1b. An important length scale for an unperturbed coil is the *radius of gyration*, R_g , defined by

$$R_g = \frac{l\sqrt{n}}{\sqrt{6}} = \frac{l\sqrt{M/M_0}}{\sqrt{6}} \quad (16.1)$$

which may be taken as the effective size or lateral extent of the coil (sometimes referred to as a “blob”) in the solution. As an example, if $l = 1.0$ nm and the segment molecular weight is $M_0 = 200$, then for a polymer of $M = 10^6$ Da we obtain $R_g \approx 29$ nm. However, the real volume of the chain is only a small fraction of the volume encompassed by R_g . Thus, if the segment width σ is about the same as the segment length l , then the molecular volume is $\pi(l/2)^2 nl \approx nl^3$, while the volume encompassed by R_g is $R_g^3 \approx \frac{4}{3}\pi R_g^2 \approx 0.3l^3 n^{3/2}$. The ratio of these volumes is $\sim 3.5/\sqrt{n}$. Thus, for a polymer with $n = 1000$ segments, only about 10% of the molecular volume is actually occupied.

Equation (16.1) is valid as long as the solvent is “ideal” for the polymer—that is, as long as there are no interactions—attractive, repulsive, or excluded volume—between the segments in the solvent. In real (nonideal) solvents the effective size of a coil can be larger or smaller than the unperturbed radius R_g , and it is sometimes referred to as the *Flory radius*, R_F , where $R_F = \alpha R_g$. The *intramolecular expansion factor* α is unity in an ideal solvent (Flory, 1969). In a “good” solvent there is repulsion between the segments, α exceeds unity, the coil swells and becomes more “expanded” (Fig. 16.1c), and its Flory radius is given by

$$R_F \approx ln^{3/5}. \quad (16.2)$$

Polymers are completely soluble (miscible) in good solvents. In contrast, in a “poor” or “bad” solvent the segments attract each other, α is less than unity, and the coil shrinks. If the

Table 16.1 Some Common Polymers and Polymer Groups

Polymer	Characteristic linkage, Monomer unit	Uses
Polymer families		
Poly vinyls	—CH ₂ —CH(X)—	Plastics
Poly esters	—CO—O—	Clothing, containers
Poly siloxanes, silicones	—Si—O—	Lubricants, rubbers, paints
Poly amides	—NH—CO—	“Nylon,” fabrics, auto parts
Poly urethanes	—NH—CO—O—	Adhesives, flexible furniture
Cellulose	—C—O—	Paper, photographic film
Poly carbonates	—O—CO—O—	Optical equipment, CDs
Fluoropolymers	H replaced by F	Nonstick surfaces, thin film and boundary lubricants
Common hydrophobic polymers^a		
Poly ethylene (PE)	—CH ₂ —CH ₂ —	Coatings, containers, films
Poly styrene (PS)	—CH ₂ —CH(C ₆ H ₅)—	Packaging, housewares
Poly butadiene (PBD)	—CH ₂ = CH—CH = CH ₂ —	Latex paints, rubbers, tires
Poly dimethylsiloxane (PDMS)	—Si(CH ₃) ₂ —O—	Silicone oil, lubricants
Poly propylene (PP)	—CH ₂ —CH(CH ₃)—	Carpets, bottles, wrap films
Poly methyl methacrylate (PMMA)	—CH ₂ —CCH ₃ (CO ₂ CH ₃)—	Transparent windows, “plexiglass,” “perspex”
Poly tetrafluoroethylene (PTFE)	—CF ₂ —CF ₂ —	“Teflon,” inert, nonwetting, low adhesion-low friction surfaces, lubricants
Poly vinyl chloride (PVC)	—CH ₂ —CH(Cl)—	Plastic sheet, insulation, pipes
Common charged hydrophilic polymers		
Poly ethylene imine (PEI)	NH ₂ —(CH ₂ —CH ₂ —N ⁺ H] _n —	Neutralizes anionic colloids, ion-exchange resins
Polyelectrolytes, polyacrylates, sialic acid, sulphate, side groups	Poly acrylic acid —CH ₂ —CH(COO ⁻ H ⁺)—	Food additives, confections, ointments, lubricants
Common uncharged (H-bonding) hydrophilic polymers^a		
Poly ethylene oxide (PEO, PEG)	—CH ₂ —O—CH ₂ —	Detergents, cosmetics
Poly acrylamide (PAA)	—CH ₂ —CH(CONH ₂)—	Plastics, textiles, diapers
Poly vinyl alcohol (PVA)	—CH ₂ —CH(OH)—	Fibers, adhesives, textiles
Common biological polymers (polyelectrolytes)^b		
Poly isoprene	—CH ₂ —C(CH ₃) = CH—CH ₂ —	Natural rubber
Poly peptides (proteins)	H ₂ —[—NH—CHR—CO—] _n —OH R = amino acid (AA) group or “residue”	Biological “engines,” wool, silk, food additives (gelatin), steric stabilizers
Poly nucleotides (DNA, RNA)	>phosphate-sugar-base···	Gene therapy
Poly saccharides (sugars), HA ^c	Can be charged or H-bonding	Food additives, biolubricants

^aHydrophilic polymers are soluble in aqueous solutions, whereas hydrophobic polymers are soluble in organic solvents such as liquid hydrocarbons. In spite of their high molecular weight some polymers such as PBD and PDMS are liquid at room temperature. These are known as polymer melts.

^bInterestingly, biological polymers are generally linear—that is, not branched.

^cHyaluronic acid.

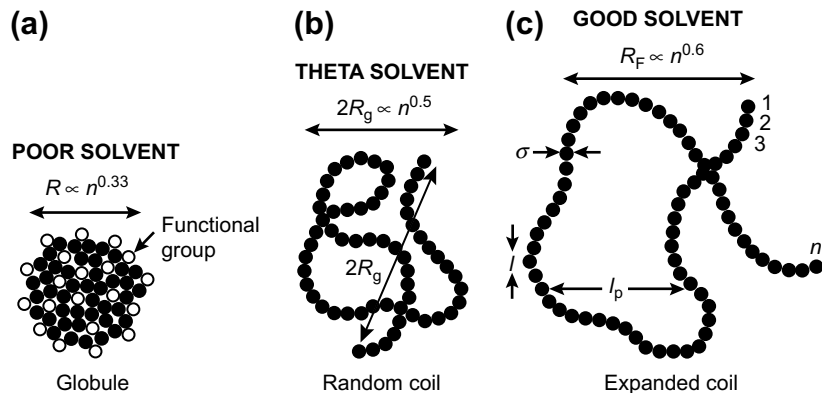


FIGURE 16.1 Different states of isolated polymer chains in solution, each chain is composed of n segments or monomer units of length l and width σ . The fully extended contour length is $L_c = nl$. (a) Collapsed (globular) state, (b) random coil (described by R_g), (c) expanded coil (described by R_F or l_p). While R_g should represent a radius – the root mean square radius of an unperturbed coil (Flory, 1953), and therefore half the diameter occupied by the coil in solution, in practice the range of repulsive steric and attractive depletion forces measured is found to be closer to R_g than to $2R_g$, and likewise for R_F (see Figs. 16.7b and 16.11). In contrast to *freely-jointed chains*, stiffer *wormlike chains* such as DNA are characterized by an elastic bending modulus; their characteristic length is known as the *persistence length*, l_p , being the mean distance between segments of the chain that are no longer correlated. The persistence length of DNA is about 50 nm.

segment-segment attractions are very strong, due to intraionic, van der Waals, hydrophobic, or H-bond interactions, the coil loses all semblance of randomness and collapses or “folds” into a compact structure (e.g., globular proteins and DNA) as illustrated in Fig. 16.1a.

A poor solvent can often be made into a good one by adding certain solutes or by raising (or lowering) the temperature above (or below) some critical value known as the *theta temperature* (T_θ or just θ), at which point $\alpha = 1$. A solvent at $T = T_\theta$, is known as an *ideal solvent* or a *theta solvent* (θ -solvent).

Another polymer-associated length is the *Kuhn length* for polymers with *restricted* or *semiflexible* chains that are not totally free to rotate about each segment-segment bond, but whose coils are not rigid or elastic either. The Kuhn length l_K is a theoretical construct giving the effective segment length where the polymer *can* be treated as a freely jointed chain; it is therefore longer than the segment length l but shorter than the *persistence length* l_p .

Polymers can adsorb avidly on surfaces, often reaching saturation adsorption at very low concentrations of a few parts per million in solution. If the state of an adsorbed unperturbed coil is the same as its state in solution (Figure 16.2a), the surface area covered per coil or “mushroom” will therefore be $\pi R_g^2 \approx \frac{1}{2}nl^2$. If again the segment width σ is assumed to be close to l , the contour area of a chain will be $nl\sigma \approx nl^2$. Thus, as a rough guide, the amount of polymer adsorbed at full surface coverage but without lateral overlap of the coils is quantitatively similar to that which would occur if all the coils were to lie flat and close-packed on the surface.

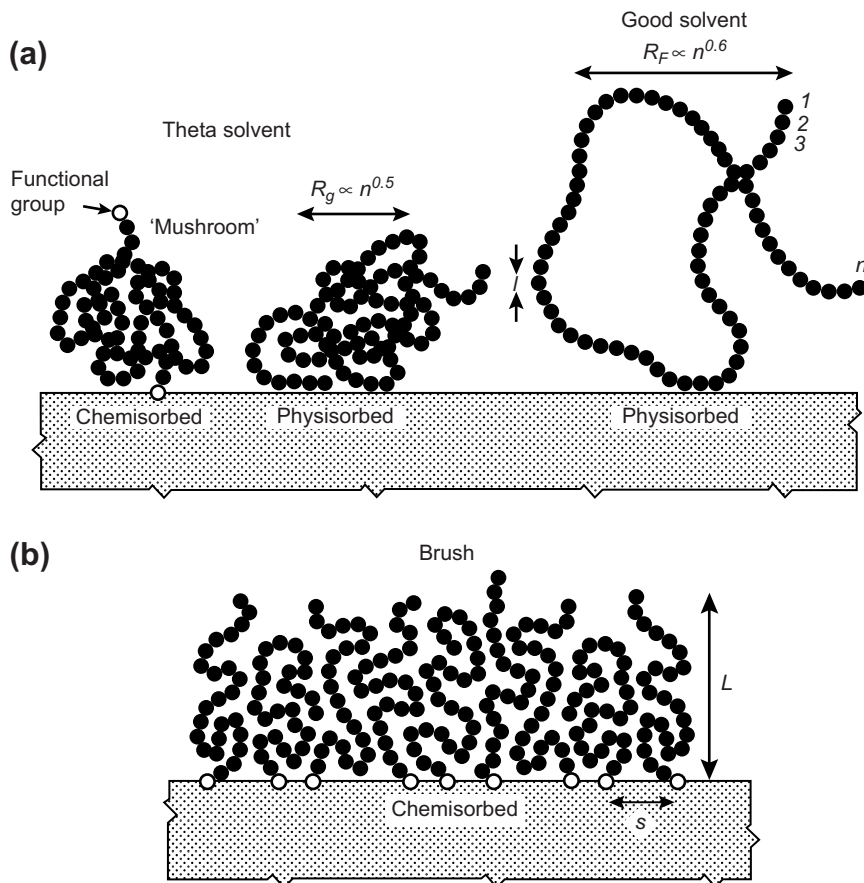


FIGURE 16.2 Different states of adsorbed polymers (see also Figures 16.3 and 16.13). The configuration of physisorbed and chemisorbed chains can be very different from their configuration in solution. The surface coverage Γ is defined as $\Gamma = 1/(\text{area occupied per adsorbed molecule}) \approx 1/s^2$ in units of m^{-2} , which is shown here for a brush. Chemisorbed chains are also referred to as end-grafted and, in the case of biological polymers, as specifically bound (see site-specific binding in Part III).

In practice the situation is far more complex, and various types of adsorptions are possible depending on the bulk polymer concentration, on whether the polymer is a homopolymer or a copolymer, and on whether the adsorption is via physical forces (physisorption) or by the grafting, anchoring or binding of specific “functional” groups via chemical bonds (chemisorption). If the coverage is high, the layer thickness will be greater than R_g or R_F , resulting in a “brush” (Figure 16.2b). Figure 16.3 shows a computer simulation of the density profiles and segment configurations as we go from low coverage (mushroom regime) to high coverage (brush regime) of a 30 segment end-grafted polymer in a θ -solvent.

There are many ways of experimentally studying the structure and dynamics of adsorbed polymer layers. These include Small Angle Neutron Scattering (SANS), Neutron

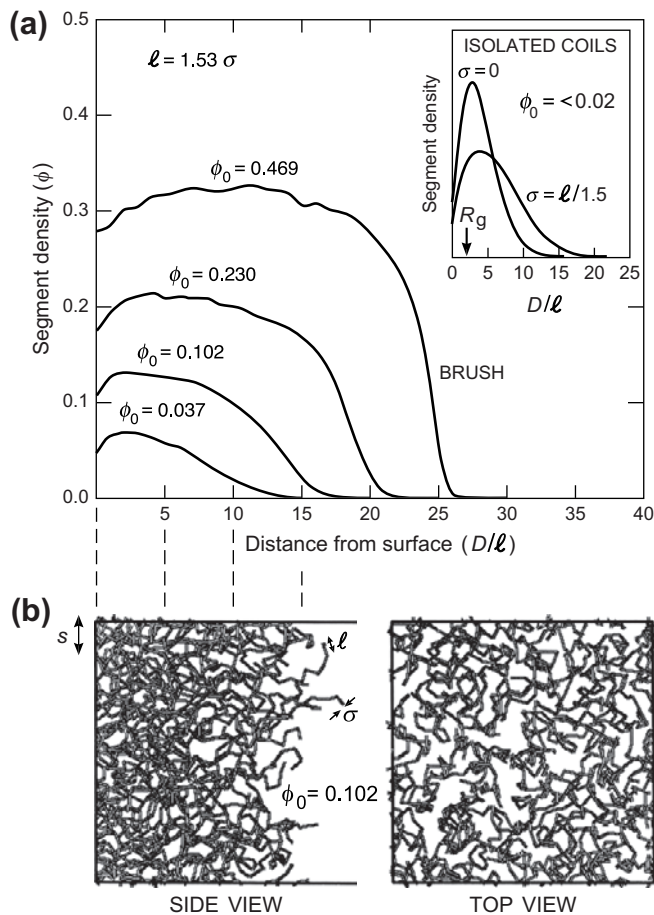


FIGURE 16.3 Computer simulations of the structure of end-grafted polymer layers exposed to a theta solvent showing the transition from a low coverage layer to a brush layer with increasing grafting density, ϕ_0 . Each polymer has $n = 30$ segments of diameter σ and length $\ell = 1.53\sigma$. From Eq. (16.1) we therefore obtain $R_g = 2.2\ell$. (a) Segment density profiles $\phi(D)$ for four different grafting densities, ϕ_0 , defined by the area fraction occupied by the grafted end-segments: $\phi_0 = \pi(\sigma/2)^2\Gamma$, where Γ is the number of grafting sites per unit area (the plotted segment densities do not include the density of the grafted end-segments themselves). Note that the grafted coils begin to overlap with each other on each surface once $\pi R_g^2\Gamma > 1$ —that is, for $\phi_0 > 0.02$. Inset: Density profile of an isolated coil (effectively for $\phi_0 < 0.02$) showing how excluded volume effects (finite σ) expands the coils and layer thickness. (b) Side and top views of coils for $\phi_0 = 0.102$, drawn on the same scale as above. [Computed by Young-Hwa Kim at Corporate Research Laboratories, 3M Corporation, St Paul, Minnesota (1989) using a grand canonical MC simulation. Similar results have been obtained by Murat and Grest, 1989.]

and x-ray Reflectivity, NMR, ellipsometry, Internal Reflection Spectroscopy, and various other scattering, reflectivity and spectroscopic techniques (for reviews see Takahashi and Kawaguchi, 1982; Cosgrove, 1990; Campbell et al., 2000).

The forces between surfaces with adsorbed polymer layers or across polymer solutions are usually measured using one of the standard force-measuring techniques described in

Chapter 12, such as the SFA technique. For recent reviews of all aspects of intersurface and interparticle forces involving polymers see Patel and Tirrell (1989), Ploehn and Russel (1990), Merrill et al., (1991), and Farinato and Dubin (1999).

Theoretically, polymer adsorption and the interactions between polymer-covered surfaces are examined using scaling and mean-field theories (de Gennes, 1979, 1981, 1982, 1985, 1987a; Scheutjens and Fleer, 1980, 1985; Cohen-Stuart et al., 1986; Fleer, 1988; Ingersent et al., 1986, 1990), and computer simulations as shown in Figure 16.3. For books on polymer dynamics and more complex polymer systems, see Doi and Edwards (1986) and Fredrickson (2006).

16.3 Repulsive “Steric” or “Overlap” Forces between Polymer-Covered Surfaces

When two polymer-covered surfaces approach each other, they experience a force once the outer segments begin to overlap—that is, once the separation is below a few R_g . This interaction usually leads to a repulsive osmotic force due to the unfavorable entropy associated with compressing (confining) the chains between the surfaces. In the case of polymers this repulsion is usually referred to as the *steric* or *overlap* repulsion, and it plays an important role in many natural and practical systems. This is because colloidal particles that would normally coagulate in a solvent can often be stabilized by adding a small amount of polymer to the dispersion. Such *polymer additives* are known as *protectives against coagulation*, and they lead to the *steric stabilization* of a colloid. Both synthetic polymers (Table 16.1) and biopolymers (proteins, gelatin) are commonly used in both nonpolar and polar solvents (e.g., in paints, toners, emulsions, cosmetics, pharmaceuticals, processed food, soils, and lubricants).

In this section we shall consider the purely repulsive steric force between two polymer-covered surfaces interacting in a liquid. Other polymer-associated interactions that can be attractive or that modify steric interactions will be considered in the following sections.

Theories of steric interactions are complex (Hesselink, 1971; Hesselink et al., 1971; Vrij, 1976; Scheutjens and Fleer, 1982; de Gennes, 1987a, Ingersent et al., 1986, 1990; Ruths et al., 1997). The forces depend on the coverage of polymer on each surface, on whether the polymer is simply *adsorbed* from solution (a reversible process where the coverage depends on the bulk polymer concentration) or irreversibly *grafted* onto the surfaces, and finally on the *quality* of the solvent for the polymer. Two limiting situations, corresponding to low and high surface coverage, will now be described.

We first consider the simplest case of the repulsive steric interaction between flat surfaces containing an adsorbed polymer layer of “mushrooms”—that is, end-grafted chains, in a θ -solvent (inset in Figure 16.4). In the limit of low surface coverage there is no overlap or entanglement of neighboring chains, and each chain interacts with the opposite surface independently of the other chains. For two such surfaces the repulsive

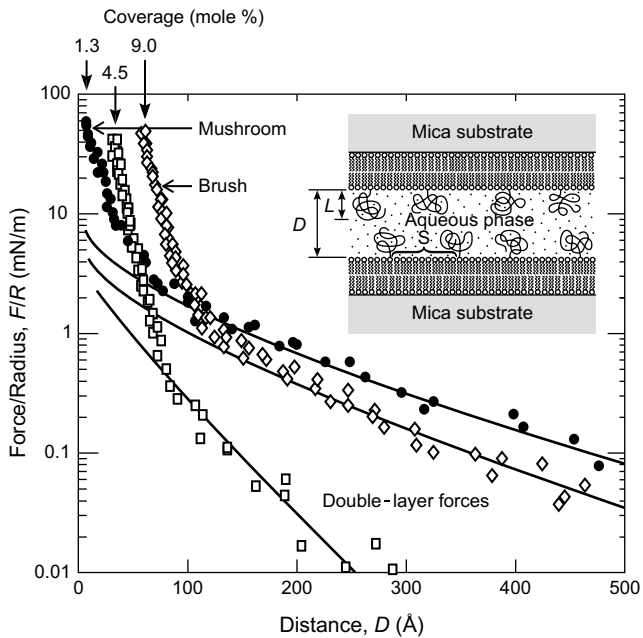


FIGURE 16.4 Forces between end-grafted uncharged polyethylene oxide surfaces at three different surface concentrations of DSPE-EO₄₅ in 0.5–4.2 mM KNO₃ solutions at 21°C, where the EO₄₅ coil has a Flory radius of $R_F = 3.5$ nm. The areas occupied by each DSPE-EO₄₅ and DSPE molecule is 0.43 nm², so that the transition from low coverage mushrooms to high coverage brushes occurs when the DSPE-EO₄₅ mole fraction is $f = 0.43/(3.5)^2 = 0.035$, or 3.5 mole %, which falls in the middle of the tested range from 1.3 to 9.0 mole %. At larger separations the repulsions are dominated by the double-layer forces between the negatively charged surfaces (the DSPE-EO₄₅ headgroups) because, in these dilute electrolyte solutions, the Debye lengths are longer than the characteristic decay lengths of the steric forces. See Figure 16.11 for the very different forces when the polymer is not attached or adsorbed to the surfaces. [Data from SFA experiments with surfaces in the crossed-cylinder geometry, equivalent to a sphere of radius R near a flat surface or two spheres of radius $2R$, adapted from Kuhl et al., 1994.]

energy per unit area is a complex series, but over the distance regime from $D = 8R_g$ down to $D = 2R_g$, it is roughly exponential (see Figure 1 of Dolan and Edwards, 1974) and is adequately given by

$$W(D) = 2\Gamma kTe^{-D^2/4R_g^2} + \dots \approx 36\Gamma kTe^{-D/R_g} \text{ J m}^{-2} \quad (16.3a)$$

or¹

$$W(D) \approx 36kTe^{-D/R_g} \text{ J per molecule} \quad (16.3b)$$

which corresponds to a pressure of

$$P(D) = -dW/dD \approx +36(\Gamma kT/R_g)e^{-D/R_g} \text{ N m}^{-2}, \quad (16.3c)$$

¹Li and Pincet (2007) proposed and satisfactorily tested a more accurate form for Eq. (16.3b) of $W(D) \approx 36kTe^{-\sqrt{3}D/R_g}$, while for dense mushrooms, where the chains overlap at the mid-plane, $D_{\text{eff}} \rightarrow \frac{1}{2}D$, and $W(D) \rightarrow 36kTe^{-\sqrt{3}D/2R_g}$.

where $\Gamma = 1/s^2$ is the number of grafted chains per unit area (the coverage) and s is the mean distance between attachment points. Equation (16.3) is valid for low coverages ($s > R_g$) when the layer thickness is roughly equal to R_g and therefore varies as $M^{0.5}$ in a θ -solvent. In good solvents the coils swell, the layer thickness varies as $M^{3/5}$ rather than $M^{1/2}$ (cf. Eq. 16.2), and the range of the repulsion is therefore greater than that given by Eq. (16.3).



Worked Example 16.1

Question: It is required to end-graft an uncharged water soluble polymer to the surface of a prosthetic device to function in the body where it will be exposed to surfaces of surface potential $\psi_0 = -75$ mV in 0.15 M NaCl saline solution at $T = 37^\circ\text{C}$. The biocompatible (biochemically inert) surface must also provide a soft repulsion to these and other surfaces such that under a pressure of 15 atm there is still an aqueous film of thickness 2.5 nm between the surfaces, thereby allowing for free fluid and solute flow—that is, a minimal increase in the local viscosity. To avoid inducing electrochemical effects the surface potential of the device is designed to also have a surface potential of $\psi_0 = -75$ mV. What should be the radius of gyration of the polymer?

Answer: From Eqs. (14.36) and (14.37) the Debye length is $\kappa^{-1} = 0.313/\sqrt{0.15} = 0.809$ nm, and Fig. 14.10 gives for the double-layer pressure at $D = 2.5$ nm and 37°C : $P_{\text{es}} = \frac{1}{2\pi}\kappa^2 Ze^{-\kappa D} = [9.38 \times 10^{-11}/2\pi \times (0.809 \times 10^{-9})^2]\tanh^2(75/107)e^{-2.5/0.809} \approx 3.8 \times 10^5$ Pa, which is 3.8 atm. The steric pressure P_{st} at 2.5 nm must therefore exceed 11.2 atm. For efficient cushioning, we desire the polymer coils to fully cover the surface but not to overlap (which would result in entanglements and a significant increase in the viscosity of the gap). Thus, $\Gamma \approx 1/R_g^2$. The steric pressure at $D = 2.5$ nm and 37°C should therefore be, using Eq. (16.3c), $P_{\text{st}} = 36(\Gamma kT/R_g) e^{-D/R_g} = 36(kT/R_g^3)e^{-D/R_g} > 11.2 \times 10^5$ Pa, giving $0.29 < R_g < 4.2$ nm. (The pressure at $D = 2.5$ nm is maximum for $R_g = 0.8$ nm.)



As we go from low coverage ($s > R_g$) to high coverage ($s < R_g$), the adsorbed or grafted chains are forced to extend away from the surface much farther than R_g or R_F . In the case of end grafted chains, as might be expected intuitively, the thickness of the “brush” layer L now increases linearly with the length of the polymer molecules—that is, L is proportional to M or n rather than to $M^{0.5}$ or $M^{0.6}$ as occurs at low coverages. More generally, for a brush in a θ -solvent its thickness, L , scales according to $L \propto M^\nu \propto n^\nu$, where ν varies from 0.5 to 1 as we go from very low to very high coverage. For a brush in a *good* solvent, where the segments repel each other and so do not become easily entangled, its thickness can be expressed in a number of equivalent forms (Alexander, 1977):

$$L = nl^{5/3}/s^{2/3} = \Gamma^{1/3}nl^{5/3} = R_F(R_F/s)^{2/3}, \quad (16.4)$$

where $\Gamma = 1/s^2$ as before. We may note that $L = R_F$ when $s = R_F$, as expected, and that for $s \ll R_F$, $L \propto n$ at fixed s , also as expected.

Once two flat brush-bearing surfaces are closer than $2L$ from each other, there is a repulsive pressure between them given by the Alexander-de Gennes equation (de Gennes, 1985, 1987a)

$$P(D) = \frac{kT}{s^3}[(2L/D)^{9/4} - (D/2L)^{3/4}] \text{ for } D < 2L. \quad (16.5)$$

For $D/2L$ in the range 0.2 to 0.9 the above pressure is roughly exponential and is adequately given by

$$P(D) \approx \frac{100}{s^3}kTe^{-\pi D/L} = 100I^{3/2}kTe^{-\pi D/L} \text{ N m}^{-2}, \quad (16.6a)$$

so that

$$W(D) \approx \frac{100L}{\pi s^3}kTe^{-\pi D/L} = 32I^{3/2}LkTe^{-\pi D/L} \text{ J m}^{-2}. \quad (16.6b)$$

The first term in Eq. (16.5) comes from the osmotic repulsion between the coils, which favors their expansion and so acts to increase D , while the second term comes from the elastic stretch energy of the chains, which favors contraction and so acts to decrease D . More accurate but more complex expressions for the force-laws have been derived by Milner et al., (1988) and Zhulina et al., (1990, 1991) that nevertheless predict a very similar force-law to the Alexander-de Gennes equation. In particular, the development by Zhulina et al., (1990, 1991) eliminates the abrupt disappearance of the force at $D = 2L$, making the exponential approximations of Eqs. (16.6a) and (16.6b) actually more accurate. Also, as discussed later in Section 21.3, while the Alexander-de Gennes equation was originally developed for high molecular weight coils, it has been found to quantitatively account for the forces between surfactant and lipid bilayers in water where the flexible hydrophilic headgroups consist of only a few segments (of ethylene oxide or sugar groups).

Figure 16.4 shows the results of SFA force measurements between two bilayer surfaces whose outer monolayers consist of a binary mixture of DSPE and the “PEGolated lipid” DSPE-EO₄₅. The ethylene-oxide (EO) coils are neutral (uncharged), and each is covalently attached at one end to a negatively charged DSPE headgroup, as shown in the inset to Figure 16.4. The remaining DSPE (not PEGolated) molecules are uncharged. Both the steric forces and double-layer forces were found to be well fitted by the equations for interacting mushrooms, brushes, and double-layers; these results also show that steric and double-layer forces can be “additive.”

More accurate tests of theories for interacting brushes have been carried out in nonaqueous solutions between uncharged surfaces with higher MW polymers attached to them. Figure 16.5 shows results obtained by Taunton et al., (1990) for the forces between two end-grafted polystyrene brushes in toluene, together with theoretical fits based on the full Alexander-de Gennes equation. The agreement is remarkably good. Interestingly, the interactions between pure PEGolated lipid bilayers with as few as four EO groups are also quantitatively accounted for by the Alexander-de Gennes equation (Problem 16.6).

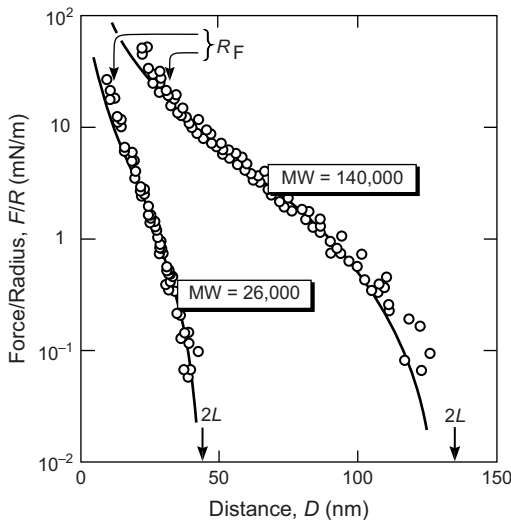


FIGURE 16.5 Measured forces between two polystyrene (PS) brush layers end-grafted onto mica surfaces in toluene (a good solvent for PS). Left curve: MW = 26,000, R_F = 12 nm; right curve: MW = 140,000, R_F = 32 nm. Both force curves were reversible on approach and separation. Solid lines: theoretical fits based on Eq. (16.5) with the following (measured) parameters: spacing between attachment sites: s = 8.5 nm, brush thicknesses: L = 22.5 nm and 65 nm, respectively. [Data from SFA experiments with surfaces in the crossed-cylinder geometry, equivalent to a sphere of radius R near a flat surface or two spheres of radius $2R$, adapted from Taunton et al., 1990.]

Further results on the interactions between biological surfaces that exhibit brush-like interactions are discussed in Chapter 21.

The steric forces between surfaces with end grafted chains are now fairly well understood both theoretically and experimentally. This is because they are reasonably well defined: each molecule is permanently attached to the surface at one end, the coverage is fixed, and the molecules do not interact either with each other or with the two surfaces. Di-block copolymers are often employed for producing mushroom or brushes: one of the blocks binds strongly to the surface, acting as the anchoring group, while the other protrudes into the solvent to form the diffuse polymer layer.

Things are much more complicated with physisorbed or weakly bound polymers. Many homopolymers do not have specific anchoring groups that chemisorb irreversibly to a surface. Instead, each coil binds *reversibly* at a number of points via weak physical “bonds” (see Figure 16.2a). Such adsorbed layers are highly dynamic, with individual segments continually attaching and detaching from the surfaces, and where whole molecules slowly exchange with those in the bulk solution or “reservoir”. The steric forces between such surfaces are more difficult to formulate because neither the amount of adsorbed polymer nor the number of binding sites per molecule remain constant as two surfaces approach each other. Further, bridging can now occur whereby different segments from the same coil bind to both surfaces. Indeed, the force between two such surfaces at any particular separation can take a long time to reach its true equilibrium

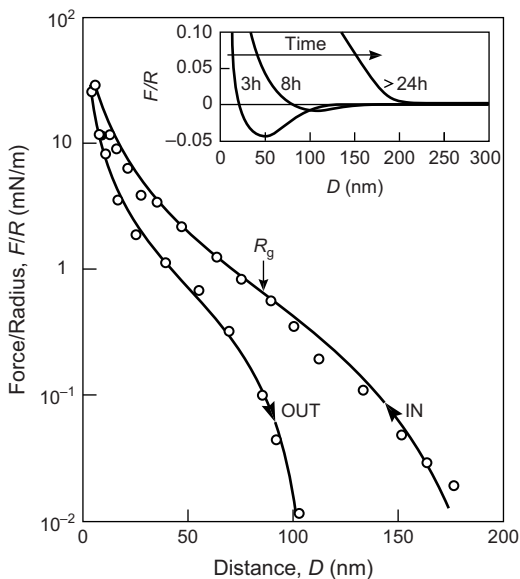


FIGURE 16.6 Effects of molecular weight and time: measured forces between two layers of PEO, MW = 1,100,000, R_g = 86 nm, physisorbed on mica from 150 $\mu\text{g}/\text{ml}$ PEO solution in aqueous 0.1 M KNO₃ (a good solvent for PEO). *Main figure:* Force after ~16 hrs adsorption time. Note the hysteresis (irreversibility) on approach and separation for this physisorbed polymer, in contrast to the absence of hysteresis with grafted chains (Figure 16.5). *Solid line:* Theoretical curve based on a modified form of the Alexander-de Gennes equation, Eq. (16.5). *Inset:* Evolution of the forces with the adsorption time. Note the gradual reduction—though not necessarily the disappearance—of the attractive bridging component. [Data from SFA experiments with surfaces in the crossed-cylinder geometry, equivalent to a sphere of radius R near a flat surface or two spheres of radius $2R$, adapted from Klein and Luckham, 1982, 1984a, 1984b; Luckham and Klein, 1990.]

value (many hours or even days at high MW), and measured force profiles are usually time- and history-dependent, approach and separation rate-dependent, and hysteretic. Figure 16.6 illustrates these effects in the case of the interaction between high MW PEO adsorbed on mica in aqueous solutions where the binding per segment is weak.

Note that the range of steric forces can be many times R_g , both for chemisorbed and physisorbed polymers. This can be due to a high surface coverage (cf. brush layers) or because $R_F \gg R_g$ due to the additional repulsive forces arising from the finite size of the confined segments (excluded volume effect) and, in aqueous solutions, from hydration layers and/or repulsive electrostatic interactions between charged segments. All these effects can lead to steric forces having a magnitude and range even greater than $10R_g$, especially in aqueous solutions (Klein, 1988; Patel and Tirrell, 1989).

At the other extreme of very small separations, $D \ll R_g$, polymer chains become increasingly compacted, and if the chains are not forced out from the contact region, the steric repulsion becomes even steeper than given by any of the above equations (cf. Figure 16.9). The repulsion eventually hits a “hard wall”—an effectively infinite repulsion at a finite separation that is determined by the excluded volume of the molecules (steric jamming).

16.4 Interparticle Forces in Pure Polymer Liquids (Polymer Melts)

Since a polymer molecule in a melt is surrounded by molecules of its own kind, one might expect its interactions to be very much the same as that of a polymer in a theta solvent. This is the essence of de Gennes's (1987b) scaling prediction that a monotonically repulsive potential similar to Eq. (16.3) applies between two surfaces in a polymer melt, but only if the molecules are terminally anchored to one of the surfaces. In the case of a melt where the molecules are not bound to the surfaces various theoretical studies have predicted that the force should be zero (de Gennes, 1987b; Kumar et al., 1988; Ten Brinke et al., 1988), attractive (Yethiraj and Hall, 1990), repulsive (Christenson et al., 1987), oscillatory (Madden, 1987; Yethiraj and Hall, 1989), or some combination of these. The matter is far from being clear or resolved. However, it appears that if only van der Waals forces are operating, the final contact should always be adhesive—that is, attractive—regardless of whether we have a physisorbed polymer from solution or a melt between the surfaces. The long relaxation times for attaining this lowest energy state may, however, preclude it being reached in experiments or practical situations.

On the experimental side, the forces between mica surfaces across pure polymer melts such as polydimethylsiloxane (PDMS), polybutadiene (PBD), and fluoropolymers have been measured by Horn et al., (1989b), Israelachvili and Kott (1988), and Montfort and Hadzioannou (1988). The measured forces generally exhibit oscillations at small distances, with a periodicity equal to the segment width, and a monotonically decaying weak repulsion farther out extending over distances of up to $10R_g$. The oscillations, with a final adhesive energy minimum at contact, are consistent with computer simulations (Yethiraj and Hall, 1989), while the smoothly decaying repulsive tail of these interactions may reflect the effective immobilization or surface anchoring of these polymers during the time course of the measurements. In contrast, the forces between inert hydrocarbon surfaces across short-chained hydrocarbon liquids exhibit a stronger than van der Waals attraction at all separations (Jansen et al., 1986; Gee and Israelachvili, 1990), which been attributed to the predominance of chain ends in these short-chained liquids that contribute an additional attractive component to the net interaction (Israelachvili et al., 1989).

Concerning the short-range oscillatory forces in melts, it has been found that irregularly shaped polymers—for example, those with large bumpy segments or randomly branched side groups—become entangled when confined and show fewer or no short-range oscillations, indicative of their inability to order into discrete, well-defined layers [Israelachvili and Kott (1988); Montfort and Hadzioannou (1988); Gee and Israelachvili (1990)]. Instead, the oscillations are replaced by a smooth monotonic repulsion, although, again, it is likely that when all the polymer is removed from between the surfaces, the contact interaction is attractive.

It is worth stressing that when polymer molecules are concentrated within an adsorbed surface layer or confined within a thin film between two surfaces, they become

jammed, and their molecular relaxation times can be many orders of magnitude higher than in the bulk. In some cases the molecules, which may be liquid in the bulk, freeze into a highly viscous or an amorphous glassy state between the surfaces (Van Alsten and Granick, 1990). In cases where the short-range forces are oscillatory (Chapter 15) the energy barriers and minima at finite separations may trap the surfaces more or less indefinitely in these potential wells. Consequently, it is unlikely that the measured force-laws, even though they often appear to be reversible and reproducible over the time-scales of the measurements, are ever at true *thermodynamic* equilibrium.

16.5 Attractive “Intersegment” and “Bridging” Forces

We now turn our attention to attractive polymer-mediated interactions, bearing in mind that the attraction may be operating only over a narrow distance regime and that the full force-law may have both attractive and repulsive regimes.

We have already noted that segments attract each other in a poor solvent. The attraction may be due to van der Waals or some solvation force, and if it is not too strong (or the polymer concentration is below the saturation concentration—see previous section), the main effect on an isolated coil in solution is that the coil radius shrinks below R_g . The coil does not totally collapse because the osmotic repulsion still wins out at some smaller radius. Stronger attractions can arise due to strong van der Waals, hydrophobic, H-bonding, and charge-specific interactions—for example, when a (usually biological) polymer contains a certain sequence of H-bonds or charged groups that can mate with a complementary sequence either on the same molecule (cf. β -sheets) or on a different polymer (cf. DNA, cadherin protein tethers). Such complementary interactions can lead to the total collapse of a polymer, as illustrated in Figure 16.1a, or ordered assemblies of macromolecules, and are discussed in Part III. Here we will consider the weaker, nonspecific interactions of homopolymers that do not phase separate out of solution but that do adsorb to surfaces.

As two polymer-coated surfaces come together in a poor solvent, the attraction between the outermost segments is felt as an initial “intersegment” attraction between the surfaces. Closer in, the steric overlap repulsion wins out, and the force becomes overall repulsive. Figure 16.7 shows that this is what is observed in the interactions between both chemisorbed and physisorbed polystyrene layers at temperatures below the theta temperature. Such force-laws are expected in all poor solvent conditions regardless of whether the polymer is a homopolymer or a copolymer, physisorbed or chemisorbed, or at low or high coverage.

As we go from poor to good solvent conditions—for example, by raising the temperature—the intersegment attraction vanishes, and if no other attractive force is operating, the force-law becomes purely repulsive at all separations. This is what is observed in the case of chemisorbed polystyrene on mica (Figure 16.7a). However, in the case of the physisorbed polymer (Figure 16.7b), even though the attraction has diminished, it has not completely disappeared above T_θ because of the residual attractive surface bridging force

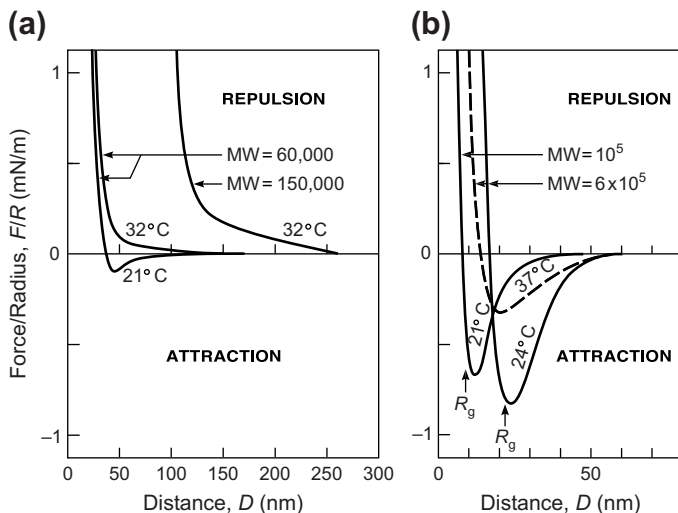


FIGURE 16.7 Effects of temperature: measured forces between mica surfaces covered with polystyrene below and above the theta temperature, θ , corresponding to poor and good solvent conditions. (a) End-grafted polystyrene brushes in toluene ($\theta \approx 35^\circ\text{C}$). Left curves: $MW = 60,000$, $R_g = 7$ nm; right curve: $MW = 150,000$, $R_g = 11$ nm. At $T = 21^\circ\text{C}$ (poor solvent conditions) the attraction is due to intersegment forces. At $T = 32^\circ\text{C}$ (good solvent conditions) there is no intersegment nor a bridging force and the attraction vanishes. Note that the forces scale roughly as M or R_g^2 —a characteristic feature of brush layers. (Adapted from Hadzioannou et al., 1986, and Patel, 1986.) (b) Physisorbed polystyrene in cyclohexane ($\theta = 34.5^\circ\text{C}$). Left curve: $MW = 100,000$, $R_g = 8.5$ nm. Right curves: $MW = 600,000$, $R_g = 21$ nm. At $T = 24^\circ\text{C}$ (poor solvent conditions) the attraction is due to both intersegment and bridging forces; at $T = 37^\circ\text{C}$ (good solvent conditions) only to bridging forces. The reduced range of the interaction at 37°C is due to the reduced adsorption of physisorbed polymer at the higher temperature. Note that the forces scale roughly as \sqrt{M} or R_g , which is indicative of low coverage rather than brush layers. [Data from SFA experiments with surfaces in the crossed-cylinder geometry, equivalent to a sphere of radius R near a flat surface or two spheres of radius $2R$, adapted from Klein, 1980, 1982, 1983, and Israelachvili et al., 1984.]

that is still operative in the latter but not the former case. Bridging forces can manifest themselves in many different ways and will now be described.

The net interaction of a polymer-covered surface with another depends not only on the segment-segment forces but also on the forces between the polymer and the opposite surface. These forces can be repulsive—for example, if the van der Waals force between the polymer and the opposite surface is repulsive in the solvent—or attractive, in which case they are referred to as “bridging” forces. There are two types of bridging forces: specific and nonspecific (Figure 16.8) or chemisorbed and physisorbed. Specific bridging forces (Figure 16.8, right) involve specific or chemisorbed end-functionalized binding groups or ligands attached to the ends of “tethers”; these occur mostly in biological systems and are discussed in Section 21.7. Physisorbed bridges involve all segments of a chain (Figure 16.8, left) and are more common in nonbiological colloidal systems (Almog and Klein, 1985; Hu et al., 1989; Ingersent et al., 1986, 1990; Ji et al., 1990; Ruths et al., 1997). Clearly, any polymer that naturally adsorbs to a surface from solution has the potential to form bridges between two such surfaces.

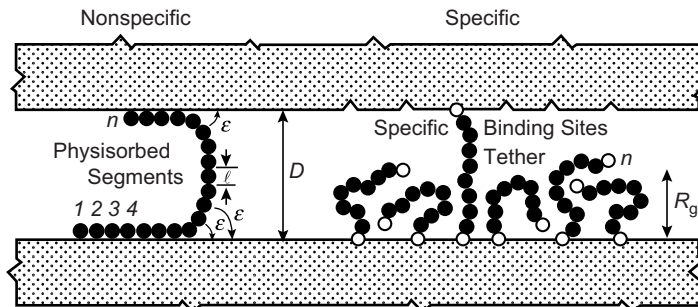


FIGURE 16.8 Examples of the two main types of bridging forces. These forces have a range of the contour length of the polymer tether $L_c = nl$, which for large n is much larger than R_g or R_f .

There are no simple expressions for the bridging forces between physisorbed polymers, where each chain can bind to both surfaces in more than one location (known as “trains”), with “loops” in between the trains and free ends or “tails” at each end. The conformation of the chains also depend on the previous history, exhibit very long relaxation times, and are rarely at equilibrium over reasonable time scales. Figure 16.8 (left) shows a simple type of bridging mechanism involving a homopolymer, where as each additional segment binds to one of the surfaces, it pulls it closer to the other surface by a segment length $\Delta D = -l$ accompanied by an energy change of $\Delta w = -\epsilon$, this being the binding energy per segment. The attractive energy and force per bridging molecule, tether, or tail are therefore given by

$$\begin{aligned} w(D) &= -\epsilon(L_c - D)/l \\ \text{and } F(D) &= -dw/dD = -\epsilon/l \end{aligned} \quad \left. \right\} \text{for } D < L_c, \quad (16.7a,b)$$

where $L_c = nl$ is the contour length, as before. If the tail density is $\Gamma = 1/s^2$ per surface, the interaction energy per unit area $W(D)$, and pressure $P(D)$, between two identical surfaces will be related to the above by $W(D) = 2\Gamma w(D)$ and $P(D) = 2\Gamma F(D)$, with the factor 2 appearing because each surface contributes equally. Note that the density of tails or bridges can be different from the surface coverage of the adsorbed molecules, both of which are defined by Γ . For example, a physisorbed molecule may have one, two, or more tails (cf. Figure 16.13). As regards the contribution of the bridging interaction to the adhesion energy at contact $W(D \rightarrow 0)$, which, by definition, is twice the interfacial energy γ_i , we obtain

$$\gamma_i = -\frac{1}{2}W(D \rightarrow 0) = \epsilon\Gamma L_c/l = \epsilon n\Gamma = \epsilon n/s^2. \quad (16.8)$$

As examples of bridging forces for four different types and strengths of binding: for $\epsilon = 0.1, 1, 10$, and $35 kT \Rightarrow \epsilon \approx 0.04, 0.4, 4$, and $15 \times 10^{-20} \text{ J}$, corresponding to a weak van der Waals bond, a strong van der Waals bond (in liquid), a H-bond, and a strong ionic or bio-specific ligand-receptor bond, and $l = 0.4 \text{ nm}$, the pulling forces per tether, Eq. (16.7b), will be 1, 10, 100, and 350 pN, respectively (see Table 21.1). If there are $n = 100$ segments per chain and the distance between tethers is $s = 10 \text{ nm}$, then the contribution of the bridging

interaction to the interfacial energy for $\varepsilon = 0.1\text{--}10 kT$ will be $\gamma_i = (0.04\text{--}4.0) \times 10^{-20} \times 100 / (10 \times 10^{-9})^2 = 0.4\text{--}40 \text{ mJ m}^{-2}$ —that is, of the same order but typically larger than the van der Waals contribution in a liquid; and the range of the bridging force, here $L_c = nl = 40 \text{ nm}$, is also usually much larger.

Note that the bridging force per molecule or tail, or between two planar surfaces, Eq. 16.7b, is constant—that is, it is independent of D . However, for a spherical particle of radius R near a planar surface, the bridging force will be determined by the Derjaguin approximation, giving:

$$F(D) = -4\pi R\varepsilon\Gamma(L_c - D)/l. \quad (16.9)$$

This force now varies linearly with D , from zero at $D = L_c$ to $F(D \rightarrow 0) = -4\pi R\varepsilon\Gamma L_c/l = -4\pi R\varepsilon n\Gamma = -4\pi R\gamma_i$ at contact. Note that this expression gives the same value for γ_i as Eq. (16.8).

Such “linear” bridging forces have been measured between certain surfaces (cf. Figure 16.7b), where the agreement with theory is sometimes very good (Figure 16.9). But linear or power-law bridging forces are by no means general: some bridging forces appear to be exponential, with a decay length close to R_g (Israelachvili et al., 1984; Ji et al., 1990) or, in the case of nonequilibrium situations, to follow some as yet unknown function (see Figure 16.6, inset). The bridging attraction between loops is expected to be weaker and of shorter range than between tails (see dashed curve in Figure 16.9a).

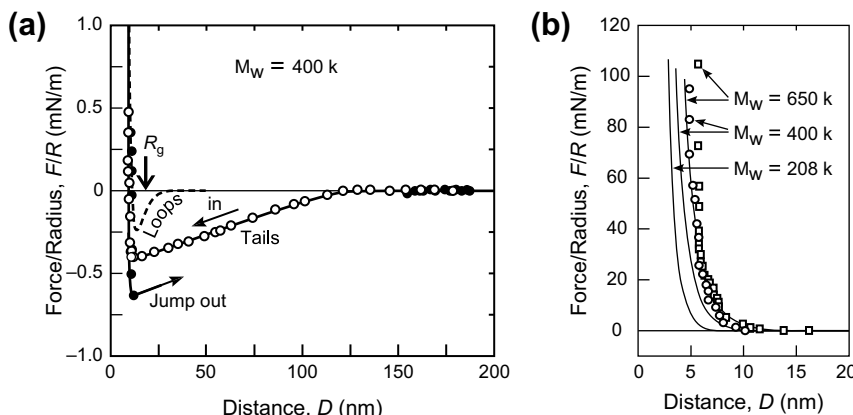


FIGURE 16.9 (a) Reversible bridging force measured on approach and separation between two physisorbed polystyrene (PS 400k) layers physisorbed on mica in cyclopentane at $T = 23^\circ\text{C}$, corresponding to near θ -conditions ($T_\theta = 19.5^\circ\text{C}$, $R_g = 18.3 \text{ nm}$), measured after an adsorption-equilibration time of 42 hr. The bridging attraction has a range of $L_c = 125 \text{ nm}$ (about 6% of the fully extended molecular length), and extrapolates to a value of $F/R = -4.5 \times 10^{-4} \text{ N m}^{-1}$ as $D \rightarrow 0$, which from Eq. (16.9) should be $-4\pi\varepsilon\Gamma L_c/l$. Assuming $\varepsilon \approx 0.1\text{--}1 kT$ and $l \approx 0.5 \text{ nm}$, we obtain a tail density of $\Gamma \approx (0.35\text{--}3.5) \times 10^{14} \text{ m}^{-3}$ per surface. The molecular coverage was measured to be roughly $4 \times 10^{14} \text{ m}^{-3}$ per surface, suggesting that between 10 and 100% of the adsorbed molecules contributed tails to the bridging force. The calculated curves for two other molecular weights are also shown. (b) Short-range stabilizing repulsive force between the two layers under very high compression. The near-exponential repulsion starts at $D \leq R_g$ and rapidly dominates over the attraction for $D < \frac{1}{2}R_g$ with an exponential decay length of $\sim 1 \text{ nm}$. This is much smaller than R_g and indicative of highly compressed (compacted) layers. For details of the theoretical analysis see Ruths et al., 1997.

Another type of bridging interaction occurs between surfaces connected by polymers with strongly or specifically bound end-groups, with the rest of the chains being noninteracting (see Figure 16.8, right). In this case the equilibrium (minimum energy), separation is at $D \approx R_g$, with repulsion closer in and an attraction farther out. Such interactions are common in biological systems where unfolded proteins and other types of biological polyelectrolytes bind specifically to two surfaces, trapping them within a broad potential well, and are described in Section 21.7 on “specific” bridging interactions.

16.6 Attractive “Depletion” Forces

Yet another type of attractive polymer-mediated interaction is that associated with polymers that are not attracted to or repelled from surfaces so that there is no adsorption at all. One might expect that under these circumstances there would be no interaction either, but this is not so (see Problem 16.3). The interaction is weak, attractive, and in certain cases can be the dominant one in a colloidal or biocolloidal system (see also Section 21.4).

Depletion forces have a similar *entropic* origin to the first potential energy minimum of the oscillatory solvation force (Figure 15.4b). They were first proposed by Asakura and Oosawa (Asakura, 1954; Asakura, 1958; see also Vrij, 1976; Joanny et al., 1979) to account for the unexpected attractive forces generated between large colloidal particles by dissolving nonadsorbing polymer and small colloidal particles in the solution. This force arises from the osmotic pressure between the bulk solution that contains polymer at a concentration ρ , and the polymer-depleted zone of radius r between the two surfaces that is free of polymer (Figure 16.10). The situation is as if there exists a circular semipermeable membrane of radius r surrounding the depletion zone; this “membrane” forces the water *out* from the inner solute-depleted region *into* the outer solute-concentrated reservoir, which acts to drive the two surfaces together.

Between two flat surfaces of finite area—that is, in a reservoir—the depletion pressure is therefore the same as the osmotic pressure, $P = -\rho kT$, but only for $D < R_g$. For example, for a 5% by weight solution of PEO of MW 8,000 in water (for which $R_g \approx 5 \text{ nm}$), the attractive pressure at 25°C will be $P = -\rho kT = -0.05(6.022 \times 10^{29})(4.11 \times 10^{-21})/8,000 = -1.55 \times 10^4 \text{ N m}^{-2}$ or about 0.15 atm. Note that just as in the case of the linear bridging force described above, this force is constant and independent of the separation D .

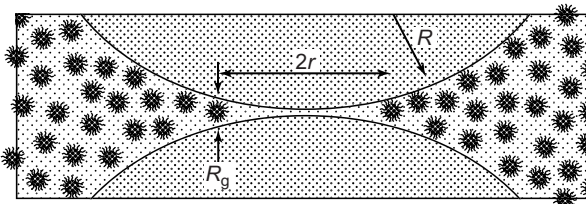


FIGURE 16.10 Depletion attraction: nonadsorbing solute molecules, macromolecules, small particles, or polymer coils produce a weak attraction between two macroscopic surfaces with a range of the size of the molecules (cf. Figures 7.4 and 15.5) or polymer coils (R_g or R_f).

between two planar surfaces. However, the force acts over a distance of only about R_g , rather than the fully extended length as in the case of bridging tethers—that is, a range that is a factor of $n^{1/2}$ smaller.

The depletion pressure $P = -\rho kT$, acting over a distance R_g , corresponds to an interaction energy between two planar (flat) surfaces that varies linearly with distance according to

$$W_f(D) = - \int_{R_g}^D P(D) dD = \int_{R_g}^D \rho k T dD = -\rho R_g k T (1 - D/R_g) \text{ per unit area (for } D < R_g\text{)}, \quad (16.10)$$

that is, the energy is zero at $D \geq R_g$ and decreases linearly to $W(0) = -\rho R_g k T$ at contact ($D = 0$), which corresponds to an interfacial energy contribution of

$$\gamma_i = -\frac{1}{2} W_f(D \rightarrow 0) = \frac{1}{2} \rho R_g k T = -\frac{1}{2} R_g P. \quad (16.11)$$

One may also calculate the depletion force F_c and energy W_c between two curved surfaces by first applying the Derjaguin approximation and then integrating. Thus, for two spheres of radius R the force and energy are therefore

$$F_c(D) = \pi R W_f(D) = -\pi R R_g \rho k T (1 - D/R_g) \quad (16.12a)$$

$$= -\pi R R_g \rho k T = -2\pi R \gamma_i \quad \text{at } D \rightarrow 0 \quad (16.12b)$$

and $W_c(D) = - \int_{R_g}^D F_c(D) dD = -\frac{1}{2} \pi R R_g^2 \rho k T (1 - D/R_g)^2 \quad (16.13a)$

which, in terms of the volume fraction of polymer “particles” in the solution, $\phi \approx \rho R_g^3$, can also be expressed as

$$W_c(D) \approx -\frac{1}{2} \pi (R/R_g) \phi k T (1 - D/R_g)^2. \quad (16.13b)$$

Note the similar functional forms for the distance-dependence of the depletion and bridging interactions (cf. Eq. 16.9). However, both the magnitudes and ranges of depletion forces are usually smaller.

As quantitative examples of the above equations, using the above values for a 5% by weight PEO 8,000 solution, the depletion contribution to the interfacial energy will be $\gamma_i = -\frac{1}{2} R_g P = -\frac{1}{2} (5 \times 10^{-9}) \times (1.55 \times 10^4) = 0.04 \text{ mJ m}^{-2}$. And two lipid bilayer vesicles of radius $R = 100 \text{ nm}$ in the same solution will experience an enhanced adhesion force due to depletion of $\pi R R_g \rho k T = 24 \text{ pN}$. This may be compared with the contribution from the van der Waals force for this system which is of order $AR/6D_0^2 \approx 1,000 \text{ pN}$ (assuming $D_0 = 0.3 \text{ nm}$).

The above equations show that for depletion forces to be significant we need a high bulk concentration of polymer molecules (high ρ or ϕ) as well as a large R_g (high MW). But since in practice it is not possible to have both— ρ cannot much exceed the concentration of close-packed coils, $1/R_g^3$, without causing entanglements and a breakdown of the implicit discrete coil assumption—the best practical way to attain a strong depletion attraction is to have as high a polymer concentration as possible, which in turn requires that R_g and thus the molecular weight be low, which will therefore be at the expense of the range of the attraction.

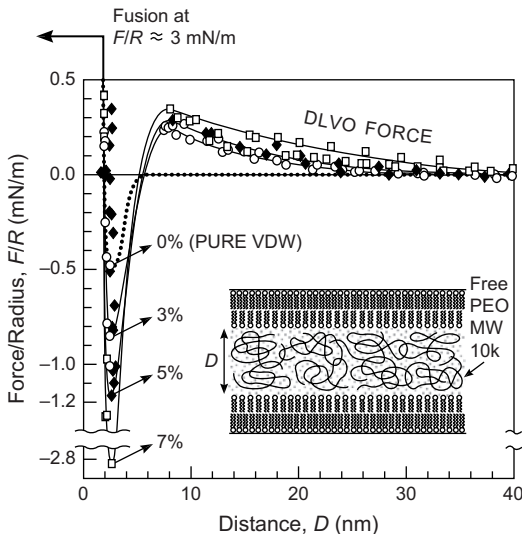


FIGURE 16.11 Attractive depletion forces in different weight % concentrations of non-adsorbing 10k PEO in water ($R_g \sim 5$ nm, $R_F \sim 9$ nm) measured between inert lecithin bilayers resulting in enhanced adhesion and fusion. The attractive force F/R in the absence of PEO is the van der Waals force, which is enhanced with increasing PEO concentration. The enhanced adhesion at contact ($D = 0$) is well-described by theory, Eq. (16.12b), when the PEO concentration ρ is replaced by the activity of PEO in aqueous solution at this concentration. The long-range repulsion is due to a weak double-layer force and/or to the long-range repulsive tail of the depletion force. [Data from SFA experiments with surfaces in the crossed-cylinder geometry, equivalent to a sphere of radius R near a flat surface or two spheres of radius $2R$, adapted from Kuhl et al., 1996, 1998.] Depletion forces are often used to aggregate colloidal and biological particles and, at higher polymer concentrations, they can induce lipid bilayers and cell membranes to fuse (Chapter 21).

Evans and Needham (1988) were the first to unambiguously measure the depletion energy of two interacting bilayer surfaces in a concentrated dextran solution using the MicroPipette Aspiration (MPA) technique (Chapter 12), and successfully verified Eq. (16.11). Subsequent force-distance measurements using the SFA technique (Kuhl et al., 1996) further showed that it is the activity rather than the concentration of the polymer that must be used for ρ in the equations (Figure 16.11). This is the reason why some polymers, such as PEO or PEG, are very effective depletants, having an activity coefficient well above unity.

Depletion forces are commonly used to aggregate fragile structures, such as biological cells and vesicles, where changing the electrolyte or pH is not an option, as in the following example.



Worked Example 16.2

Question: Uncharged but hydrophilic biocolloidal particles in a buffer solution were expected to interact only via the van der Waals force between them. The Hamaker constant was estimated to be $A = 5 \times 10^{-21}$ J, predicting an adhesion energy in excess of

$-A/12\pi D_0^2 = -3 \text{ mJ m}^{-2}$ assuming $D_0 \approx 0.2 \text{ nm}$. For the size and concentration of the particles in the suspension, it was calculated that any adhesion energy in excess of -2 mJ m^{-2} would result in coagulation or separation of the particles at 25°C , which was the desired aim of the assay. However, no separation occurred, and independent adhesion tests (cf. Chapters 12 and 17) showed that this was because the adhesion energy was only 0.5 mJ m^{-2} , six times less than expected. To induce coagulation but without changing the electrolyte conditions (for biological reasons) it was decided to add a benign, noninteracting, non-adsorbing polymer such as PEO that would cause the particles to aggregate. Assuming θ -conditions, a monomer molecular weight of $M_0 = 50$, and segment length $l = 0.5 \text{ nm}$, what would be the optimum segment number n and molecular weight of the polymer M to ensure coagulation?

Answer: The low adhesion energy of $W_{\text{ad}} = 0.5 \text{ mJ m}^{-2}$ suggests that a short-range repulsive hydration force or hard-wall “primary hydration layer” is preventing the hydrophilic particles from coagulating. The thickness of this layer D_h can be estimated from $A/12\pi D_h^2 = 0.5 \times 10^{-3}$ to be $D_h = 0.52 \text{ nm}$, or $\frac{1}{2}D_h = 0.26 \text{ nm}$ (about one water molecule per surface). Since a net adhesion energy of 2 mJ m^{-2} is required, an additional 1.5 mJ m^{-2} must therefore come from the depletion force at $D = D_h = 0.52 \text{ nm}$. Now, the highest polymer concentration that can be used without introducing entanglements is $\rho = 1/R_g^3$. Equation (16.10) then gives for the maximum depletion energy: $W = -(1 - D/R_g) kT/R_g^2$, which approaches $-kT/R_g^2$ as $D \rightarrow 0$. Thus, the maximum *strength* of the depletion interaction *decreases* with increasing R_g (or molecular weight), but its *range* (R_g) *increases* with molecular weight. It is instructive to plot W vs R_g for fixed $D = D_h = 0.52 \text{ nm}$ and $kT = 4.1 \times 10^{-21} \text{ J}$; the plot shows that $W > 1.5 \text{ mJ m}^{-2}$ only for R_g between 0.54 and 2.8 nm , with the maximum adhesion of 8 mJ m^{-2} occurring for $R_g = 0.8 \text{ nm}$. These limits arise because at high R_g the interaction is weak due to the limit on ρ , while for low R_g the range of the depletion interaction becomes smaller than the range of the dominating hydration repulsion. Inserting $R_g = 0.8 \text{ nm}$, $l = 0.5 \text{ nm}$, and $M_0 = 50$ into Eq. (16.1), we obtain for the optimum segment number $n = 6(R_g/l)^2 = 6(0.8/0.5)^2 = 15$ and $M = nM_0 = 770$, but higher MW values, up to 10^4 , would also coagulate the particles. (See Problem 16.5 for a follow-up question to this example.)



In the limit of small R_g and high ρ , the adhesive minimum becomes deeper and sharper, and eventually develops ripples transforming it into the first minimum of a decaying oscillatory force characteristic of a pure liquid or polymer melt (cf. Sections 15.5, 15.7 and 16.4).

It is often difficult to experimentally distinguish between attractive intersegment, depletion, bridging, and hydrophobic forces without carrying out a detailed study of the quantitative effects of all the contributing variables. And there can be additional subtleties when some of these interactions occur simultaneously with other, such as repulsive, polymer-mediated interactions. For example, polymers that adsorb to surfaces but repel each other in solution (good or θ -solvent conditions) can give rise to a weak depletion force between the two adsorbed layers at $D > R_g$ with a shorter-ranged steric repulsion closer in once the repelling chains overlap at $D < R_g$. A qualitatively similar interaction potential will arise if the chains attract each other in solution (poor solvent conditions). However, the quantitative features of these two interactions will be very different; for example, the

depletion attraction will be proportional to the polymer concentration, while the attraction in the good or θ -solvent will depend on the amount of polymer adsorbed.

16.7 Polyelectrolytes

Most water-soluble polymers are charged, PEO and some polysaccharides being notable exceptions (Table 16.1). Charged polymers, or polyelectrolytes, can be divided into *univalent polyelectrolytes*, where all the charges have the same sign, either negative or positive (acidic or basic groups), and *multivalent polyelectrolytes* or *polyampholytes*, where the molecules contain both negative (anionic) and positive (cationic) groups. The latter interact very differently from the former, both with surfaces, with other polymers, and internally (intrasegment interactions), and will be considered in Part III because they are typically found in biological systems—for example, as proteins.

Univalent polyelectrolytes can be synthetic or biological. Hyaluronic acid is an example of uniformly charged biological *polydisaccharide*, consisting of two sugar groups per repeat unit, where one contains a negatively charged carboxylic acid COO^- group. Such polymers adsorb to positively charged surfaces but are repelled from negatively charged surfaces (giving rise to a depletion attraction between them). Cationic polyelectrolytes often owe their charge to an ammonium group such as $-\text{N}^+(\text{CH}_3)_3$.

The segments of univalent polyelectrolytes generally repel each other, but they can be attracted (physisorbed) to or repelled (depleted) from surfaces depending on the relative strengths of the van der Waals and electrostatic forces. As in the case of uncharged polymers, attachment to a surface can also occur via covalent bonds (chemisorption) or, as in the case of many biological filaments or cytoplasmic domains, because they are a natural component of the surface molecules (the lipid head-groups or exposed protein domains).

The forces between surfaces with exposed physisorbed or chemisorbed polyelectrolytes are complex because of the many additional interactions, solution conditions, and variables that now come into play. Thus, in addition to van der Waals and excluded volume effects that are the main determinants of the interactions of uncharged polymers, the segment Kuhn length l_K and degree of dissociation α , the pH and type and concentration of electrolyte ions c in the bulk solution now become important factors. In addition, the charged state of the substrate surfaces is also involved in determining the conformation of the adsorbed coils and possible bridging forces. For asymmetric surfaces—commonly encountered in biological systems—the situations can become very complex and “specific”—that is, no longer describable by mean-field equations.

However, one simple and fairly general qualitative statement can be made: the initial overlap interaction between two univalent polyelectrolyte layers is repulsive due to both the steric and double-layer repulsions between the loops and tails. But quantitative equations depend on which of the above-mentioned “regimes” the system falls into (Pincus, 1991), and even for this relatively simple system there are various interaction regimes determined by which characteristic length scales dominate: the polyelectrolyte Kuhn and contour lengths, l_K and $nl_K = L_c$, the mean distance between surface binding

sites s , the mean separation between the ions in the bulk solution $c^{-1/3}$, where c is the concentration or density in units of m^{-3} , and the mean separation between the counterions within each layer, which is given by $s_c = (\text{number of counterions per molecule/volume occupied per molecule})^{-1/3} = (\alpha n/Ls^2)^{-1/3}$. For brushes of contour length greater than the other characteristic lengths or the Debye length, the forces have no double-layer asymptotic tail and are determined by a brush-like repulsion between the two overlapping polyelectrolyte layers. There are two distinct regimes (Pincus, 1991): the dilute “osmotic brush” regime ($s_c < c^{-1/3}$), where the brush thickness is

$$L = \alpha^{1/2} nl_K = \alpha^{1/2} L_c, \quad s_c c^{1/3} < 1, \quad (16.14)$$

where L is independent of c in this regime, and the concentrated “salt” regime where

$$L = n(\alpha l_K/s)^{2/3}/c^{1/3} = \alpha^{1/2} L_c/s_c c^{1/3}, \quad s_c c^{1/3} > 1, \quad (16.15)$$

where now the layer thickness decreases with increasing bulk electrolyte concentration according to $L \propto c^{-1/3}$. Figure 16.12 shows some force-distance curves for the type of interaction described above, between two mica surfaces, each covered by a brush layer of polystyrene sulphonate ($-\text{SO}_3^- \text{Na}^+$) in various NaNO_3 solutions. The agreement of the force measurements with the mean field theory developed for this type of system by Pincus (1991) was found to be excellent in both the osmotic and salt regimes (Balastre et al., 2002).

With multivalent counterions in the bulk solution, the preceding trends occur at lower bulk concentrations, and above some concentration the forces can become attractive. At

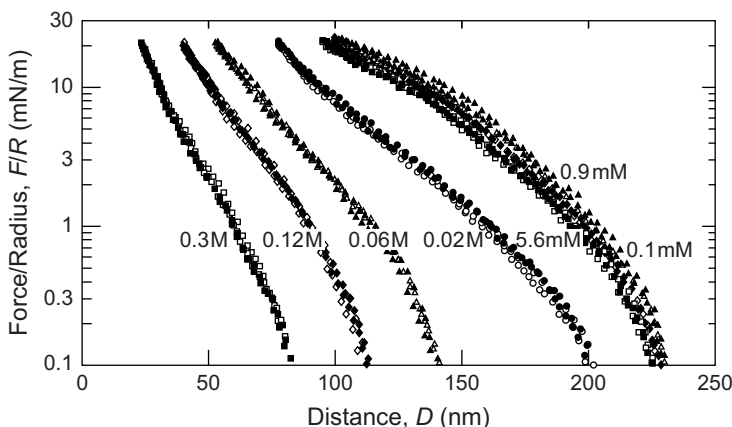


FIGURE 16.12 Forces between polyelectrolyte layers: measured forces between surfaces with end-grafted univalent polyelectrolyte molecules (high MW polystyrene sulphonate) interacting in various concentrations c (in M) of aqueous NaNO_3 solutions at 30°C . In low salt the layer thickness and repulsion is brush-like and independent of c , but does depend on the degree of dissociation α (fraction of Kuhn segments that are charged). At higher salt concentrations the range of the repulsion decreases as $1/c^{1/3}$. Both the magnitude and range of the measured forces in both the dilute “osmotic” and concentrated “salt” regimes are well-fitted by mean field theory for $\alpha \approx 0.2$. Note that here the polymer is charged but the surfaces are uncharged, whereas in Figure 16.4 the surfaces were charged and the polymer uncharged. [Data from SFA experiments with surfaces in the crossed-cylinder geometry, equivalent to a sphere of radius R near a flat surface or two spheres of radius $2R$, adapted from Balastre et al., 2002.]

even higher concentrations the binding of highly hydrated cations to the polyelectrolyte molecules can cause the layers to swell—reversing the trend at lower concentrations (Schneider et al., 2008), and similar to the effects seen with charged colloidal particles in concentrated solutions of highly hydrated electrolyte ions (cf. Figure 15.12).

16.8 Nonequilibrium Aspects of Polymer Interactions

So far, all the theories and equations given for polymer-mediated interactions have assumed equilibrium conditions, similar to those for the DLVO forces discussed earlier. This is usually fine for the DLVO forces, since when two surfaces or colloidal particles approach each other, both the electronic and ionic distributions can usually respond sufficiently rapidly to ensure that the van der Waals and double-layer forces they experience *will* be the equilibrium forces. Even the short-range oscillatory solvation forces in liquids are likely to quickly attain equilibrium if the solvent molecules are small and spherical. But one cannot always be sure that the equilibrium force law is operating between two surfaces interacting across a complex polymer system or even a pure polymer melt. Indeed, a distinctive feature of polymer interactions—one that has often been noted by experimentalists—is the extreme sluggishness with which equilibrium is attained once polymer molecules are confined within a narrow space (Van Alsten and Granick, 1990; Ruths et al., 1997). This leads to time-dependent and hysteresis effects in force measurements and to “aging” effects in colloidal systems.

At least four different molecular and ionic relaxation mechanisms can be taking place when polymers are confined between two surfaces or particles, each having its own relaxation time. First, solvent has to flow out through the network of increasingly entangled polymer coils; second, the coils themselves must reorder as they become confined (compressed), which may involve the formation of new segment-segment bonds; third, new binding sites and bridges (segment-surface bonds) may be formed between the polymer and the surfaces (including ion binding or exchange reactions, which can be surprisingly slow), and fourth, a certain fraction of polymer molecules may be forced to slowly leave (or enter) the gap region, requiring them to diffuse through the network of entangled coils on their way to or from the bulk solution. Most of these processes involve the concerted motions of many entangled molecules, which may require many hours or days even though the rate of similar molecular motions of the isolated coils in the bulk may take less than 10^{-6} s (a difference of a factor of 10^{10}).

Because of this, the interactions between compressed polymer layers are often far from equilibrium, exhibiting hysteresis, time-dependent, and history-dependent effects (cf. Figure 16.6). This is probably the most important factor that distinguishes polymer-mediated interactions from other interactions and one that must always be borne in mind when comparing theory with experiment.

Similar aging effects occur when polymers collapse onto themselves (as occurs during coil-to-globule transitions and protein folding) or adsorb on a surface. In each case the initial collapsed or adsorbed configuration is more of a reflection of the state of the

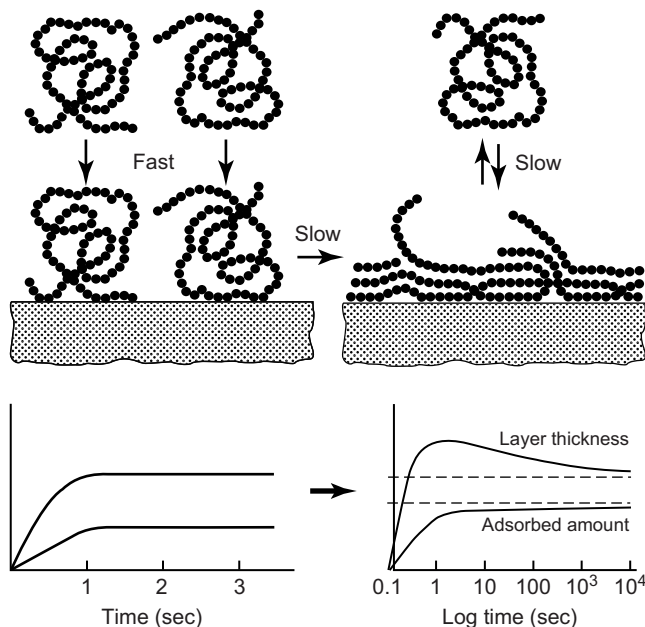


FIGURE 16.13 *Left:* Fast initial adsorption of polymer onto a surface (or on itself in the case of a coil-to-globule collapse). The initial adsorbed state is determined by the configuration of the polymer in solution before the conditions were changed to initiate the adsorption. The initial adsorption or collapse can take micro-seconds or many seconds. *Right:* A very long time may be needed to attain the final equilibrium state, which is usually very different from the initial state, in the adsorbed amount (coverage), the configuration of the molecules (conformation or order parameter), and the thickness of the layer.

molecules in the solution. The initial collapsed state is usually reached quickly, within μs or seconds, but it is not the final equilibrium state. For this to occur, it takes a much longer time as the now entangled polymers slowly rearrange (Figure 16.13). The mechanism of a rapid initial adsorption followed by a much slower relaxation toward equilibrium also occurs in many other systems.

16.9 Thermal Fluctuations of and Forces between Fluid-Like Interfaces

Not all surfaces or interfaces are rigid. Some structures such as micelles, bilayers, microemulsion droplets, and biological membranes are aggregates of weakly held amphiphilic or polymer molecules, discussed in Part III. These structures are thermally mobile or “fluid-like,” and their shape is constantly changing as their molecules twist, turn and bob in and out of the surfaces (Figure 16.14a).

As two such surfaces come together, they experience a number of repulsive “thermal fluctuation” forces associated with the entropic confinement (overlap) of their various fluctuation modes. These can be either collective molecular motions such as the

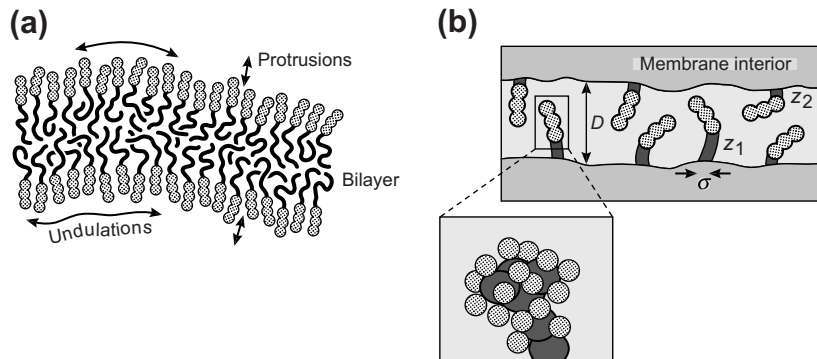


FIGURE 16.14 (a) Schematic illustrations of different types of mobile surfaces that give rise to repulsive thermal fluctuation forces (Pfeiffer et al., 1989). (b) Molecular-level protrusions and overlapping of amphiphilic molecules and their hydrophilic (hydrated) headgroups in water. Examples of thermal fluctuation and protrusion forces are given in Chapter 21.

undulating ripples of a thin membrane, or they can be molecular-scale protrusions similar to those discussed in Section 15.2. In either case, there is a repulsive force or pressure between two such surfaces that contains the inevitable ΓkT term characteristic of the osmotic repulsion between surfaces that confine solvent, ions or polymer molecules, except that Γ now represents the surface density of thermally active modes. The repulsive forces they give rise to have often been erroneously attributed to “water structure”—that is, to a repulsive “hydration force” or “solvation force” arising from the ordering of water or solvent in the thin film (typically of thickness 1–3 nm) between the surfaces. Ironically, rather than keeping the surfaces apart in the solvent, these interactions are an expression of the intermittent collisions—that is, *contact*—between the mobile molecules or their terminal groups at the surfaces, which has important biological implications discussed further in Chapter 21. We shall proceed by first considering the protrusion interaction.

16.10 Short-Range Protrusion Forces

A repulsive protrusion force arises when two amphiphilic surfaces come close enough together that their molecular-scale protrusions overlap (Figure 16.14b). This force is analogous to the steric repulsion between surfaces with adsorbed polymer layers. Here, however, as two surfaces approach each other their protruding segments are forced back *into* the surfaces, whereas with polymers the molecules are compressed but remain *between* the surfaces (for grafted chains) or they may forced out *laterally* into the bulk liquid (for adsorbed chains).

Protrusion forces are particularly important between amphiphilic surfaces interacting in aqueous and highly polar liquids (Israelachvili and Wennerström, 1992, 1996). To calculate the protrusion force between two amphiphilic surfaces in water, we first note that each protrusion is associated with a positive hydrophobic energy due to the

increased molecular hydrocarbon-water contact area. In a first approximation, this energy increases linearly with the distance z the molecules protrudes into the water (Figure 16.14b). We may thus define a “protrusion” potential as in Eq. (15.1):

$$\varepsilon(z_i) = \pi\sigma\gamma_i z_i = \alpha_p z_i, \quad (16.16)$$

where the *interaction parameter*, α_p , is in units of $J m^{-1}$. The density of protrusions extending a distance z from the surface is therefore expected to decay exponentially according to

$$\rho(z) = \rho(0)e^{-\alpha_p z_i/kT} = \rho(0)e^{-z_i/\lambda}, \quad (16.17)$$

where

$$\lambda = kT/\alpha_p = kT/\pi\sigma\gamma_i \quad (16.18)$$

is the protrusion decay length. Equations (16.17) and (16.18) were first used by Aniansson (1978) and Aniansson et al., (1976) to analyze the protrusion dynamics of surfactant molecules in and out of micelles and their exchange rates with the monomers in the bulk solution. For amphiphilic hydrocarbon molecules we have $\sigma \approx 0.3$ nm and $\gamma_i = (20-50) mJ m^{-2}$ giving $\alpha_p \approx (2-5) \times 10^{-11} J m^{-1}$ at $25^\circ C$, which corresponds to decay lengths in the range $\lambda \approx 1-2$ nm.

For immiscible polymer-polymer interfaces λ is known as the *interfacial width*, and since the interfacial tension is generally much lower, typically $\gamma_i \approx 1 mJ m^{-2}$, we expect λ to be much larger, typically >3 nm. The interfacial width of an immiscible polymer interface is usually expressed as $a_I = 2b/\sqrt{6\chi}$, where b is the segment size and χ is the Flory-Huggins interaction parameter, which is related to γ_i by (Helfand and Tagami, 1971; de Gennes, 1992; Binder, 1983)

$$\chi = 6(\gamma_i/b\rho kT)^2, \quad (16.19)$$

where ρ is the number density of the monomers. Putting $\rho \approx 1/b^3$ and $b = \sigma$ gives $a_I \approx kT / 3\sigma\gamma_i$ which shows that a_I and λ of Eq. (16.18) are essentially the same.

Measurements of the “roughness” of both amphiphilic (e.g., bilayer) and polymer interfaces usually give higher values for λ due to thermal undulations in the former (Section 16.11) and surface capillary waves in the latter system (Safinya et al., 1986; Wiener and White 1992; Shull et al., 1993).

Turning now to the protrusion force between two amphiphilic surfaces, let each surface have molecular protrusions of lateral dimensions σ , extending a distance z_i into the solution, and let there be Γ protrusion sites per unit area ($\Gamma \approx 1/s^2$). For two surfaces facing each other, whose protrusions are not allowed to overlap, the potential distribution theorem [cf. Eq. (4.11)] gives for the interaction free energy

$$\begin{aligned} W(D) &= -\Gamma kT \ln \left\{ \int_0^D dz_2 \int_0^{D-z_2} \exp[-\alpha_p(z_1 + z_2)/kT] dz_1 \right\} \\ &= -\Gamma kT \ln \left\{ (kT/\alpha_p)^2 [1 - (1 + D\alpha_p/kT)e^{-\alpha_p D/kT}] \right\} \end{aligned} \quad (16.20)$$

which gives the force per unit area (the protrusion pressure) as

$$P(D) = -\frac{\partial W}{\partial D} = \frac{(\Gamma\alpha_p^2 D/kT)e^{-\alpha_p D/kT}}{[1 - (1 + \alpha_p D/kT)e^{-\alpha_p D/kT}]} = \frac{\Gamma\alpha_p(D/\lambda)e^{-D/\lambda}}{[1 - (1 + D/\lambda)e^{-D/\lambda}]}.$$
 (16.21)

In the distance regime between 1 and 10 decay lengths, this force varies roughly exponentially and is adequately given by²

$$P(D) = 2.7\Gamma\alpha_p e^{-D/\lambda} \quad \text{for } \lambda < D < 10\lambda,$$
 (16.22)

where $\lambda \approx kT/\alpha_p$ is the protrusion decay length, as before. Equation (16.21) also predicts a steep upturn in the force once D falls below λ , when it diverges according to

$$P(D \rightarrow 0) = 2\Gamma kT/D.$$
 (16.23)

Note that this is the expected “osmotic limit,” $P = \rho kT$, for an ideal gas of protrusions (or any noninteracting particles) of density 2Γ per unit area (Γ per surface) confined uniformly within a gap of thickness D —that is, of density $\rho = 2\Gamma/D$. We have previously noted a similar small-distance limit for the double-layer repulsion between two surfaces of constant surface charge density (Eq. 14.23).

The protrusion pressure of Eq. (16.22) corresponds to an interaction energy per unit area of

$$W(D) = 2.7\Gamma\alpha_p\lambda e^{-D/\lambda} \approx 3\Gamma kTe^{-D/\lambda}.$$
 (16.24)

This may be compared with $W(D) \approx 36\Gamma kTe^{-D/R_g}$ for the interaction energy between surfaces with end-grafted chains, Eq. (16.3a).

In Chapter 21 we shall use the above equations as a basis for analyzing the short-range repulsive forces measured between surfactant and lipid bilayers in water and nonaqueous solvents.

16.11 Long-Range Undulation Forces

In addition to molecular-scale protrusions, all fluid-like structures also undergo collective thermal fluctuations at the macroscopic level that can be analyzed within a continuum framework. Fluid membranes or bilayers can be considered as weakly elastic sheets that have a number of characteristic modes of motion, the *undulatory* waves being the most important (Figure 16.15). These waves are determined by the membrane’s bending modulus, k_b , which can vary from $<10^{-21}$ to $>10^{-18}$ J depending on the state of the hydrocarbon chains—that is, whether they are in the fluid (liquid-like), amorphous (solid-like), or frozen (crystalline) state, which in turn depends on the temperature in relation to their various transition temperatures (see Section 20.8).

²These equations assume point molecules and headgroups. In practice, if the interacting hydrophilic groups are large or carry a primary hydration shell of strongly bound water molecules, their finite excluded volume b must be included as a correction term. In a first approximation, this may be done by replacing all free volumes V by $(V-b)$, or densities $\rho = 1/V$ by $1/(V-b) = \rho/(1-\rho b)$.

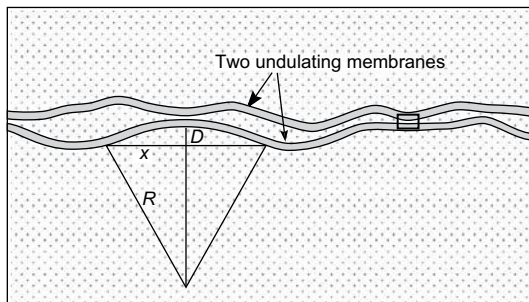


FIGURE 16.15 The thermal undulations of elastic sheets or membranes may be thought of as the analogue of the 3D Brownian motion of suspended particles in solution. Fibrous elastic polymers such as DNA also exhibit fluctuations. All of these structures experience a repulsion when their thermal ripples physically overlap—that is, bump into each other—which is essentially the osmotic pressure between them. Finite size corrections enhance the repulsion. Examples of undulation forces are given in Chapter 21. The small rectangle is panel (b) in Figure 16.14.

The undulation force arises from the entropic confinement of the undulating waves as two membranes approach each other. This force can be easily derived from the contact value theorem, which gives the entropic force per unit area between two surfaces as $P(D) = kT[\rho_s(D) - \rho_s(\infty)]$, where $\rho_s(D)$ is the volume density of molecules or molecular groups in contact with the surfaces when the distance between them is D . In the case of undulation forces these contacts can be associated with the thermally excited waves (undulation modes) of amplitude D as shown in Figure 16.15. Assuming each mode to have the geometry of a spherical cap, and ignoring numerical factors, the density of contacts (or modes) at $D = D$ and $D = \infty$ are

$$\rho_s(D) = 1/(\text{volume per mode}) = 1/\pi x^2 D,$$

and

$$\rho_s(\infty) = 0. \quad (16.25)$$

For the spherical cap geometry of an undulation mode the chord theorem gives $x^2 \approx 2RD$. The undulation pressure is therefore

$$P(D) = \frac{kT}{\pi x^2 D} \approx \frac{kT}{2\pi RD^2}. \quad (16.26)$$

Now, by definition, the elastic bending (or curvature) energy of a curved membrane with local radii R_1 and R_2 is

$$E_b = \frac{1}{2} k_b \left(\frac{1}{R_1} + \frac{1}{R_2} \right)^2 \quad \text{J per unit area} \quad (16.27a)$$

$$= 2k_b/R^2 \quad \text{for } R_1 = R_2 = R \quad (16.27b)$$

$$= 2\pi x^2 k_b/R^2 \quad \text{J per mode} \quad (16.27c)$$

since each mode occupies an area πx^2 . At temperature T we expect each mode to have energy $\sim kT$. Thus, $kT \approx 2\pi x^2 k_b / R^2 = 2\pi(2RD)k_b / R^2 = 4\pi D k_b / R$. Substituting this into Eq. (16.26) and ignoring numerical factors, we obtain $P(D) \approx (kT)^2 / k_b D^3$, which is the desired (approximate) expression for the repulsive undulation force. The exact expression, first derived by Helfrich (Helfrich, 1978; Servuss and Helfrich, 1989) is

$$P(D) = \frac{3\pi^2(kT)^2}{64k_b D^3} \approx \frac{(kT)^2}{2k_b D^3}. \quad (16.28)$$

The undulation force has been measured and the inverse third distance dependence verified experimentally (Safinya et al., 1986; Abillon and Perez, 1990). Note that the force has the same form as the nonretarded van der Waals force ($\propto 1/D^3$) but is of opposite sign. In many cases, especially involving bilayers, the magnitude is also similar. However, the modulus k_b is very sensitive to various factors, and so is the undulation force. Thus, charged membranes tend to have a higher k_b , and lowering the temperature below the liquid-solid transition temperature or chain melting temperature of a bilayer, T_m , can increase k_b significantly. Putting a membrane under tension, either mechanically or osmotically, also suppresses undulations and the undulation repulsion. All of these effects affect the adhesion between membranes or bilayers (see inset in Fig. 15.17). In contrast, the van der Waals force is little affected by these changes in the solution or system conditions.

Worked Example 16.3

Question: Unilamellar vesicles (Figure 19.1) consisting of uncharged lipid bilayers in the fluid state where their bending modulus is $k_b = 10^{-20}$ J are dispersed in an aqueous solution at 37°C (body temperature). Assuming that the Hamaker constant of bilayers is the same as for hydrocarbon sheets, are the vesicles expected to aggregate? If the melting temperature of the lipid chains is $T_m = 24^\circ\text{C}$, below which the bending modulus increases to above 10^{-19} J, what transformations, if any, do you expect to see in the vesicles as the temperature is lowered below T_m ?

Answer: From Section 13.7 the nonretarded, unscreened Hamaker constant in water is $A \approx 5 \times 10^{-21}$ J at 310 K (37°C). Since the van der Waals and undulation forces have the same distance dependence ($\propto 1/D^3$), one or the other interaction will win out at all separations depending on whether $P_{\text{VDW}} = -A/12\pi D^3$ is larger or smaller than $P_{\text{Und}} = (kT)^2/2k_b D^3$. The turning point occurs at $k_b = 6\pi(kT)^2/A = 7 \times 10^{-20}$ J, which is much higher than the value given at 310 K, implying that the undulation repulsion dominates over the van der Waals attraction at this temperature, thereby preventing the vesicles from aggregating. But at $T < T_m$, as k_b increases above 10^{-19} J, two changes will occur: first, the higher bending energy causes the bilayers to become less curved—that is, to grow and/or deform into faceted vesicles—and second, the attractive van der Waals forces now dominate over the undulation repulsion resulting in adhesion between the now flattened bilayers. The dispersed vesicles will therefore transform into stacks of flattened bilayers or large spherical multilamellar “liposomes” or “onions.”

PROBLEMS AND DISCUSSION TOPICS

- 16.1** Estimate the contour length and R_g of a polymer of MW 100,000 Da given that $l = 0.3$ nm. Two planar surfaces in a liquid have a Hamaker constant of $A = 10^{-20}$ J. They are covered with end-grafted mushrooms of the polymer at a coverage Γ of 1 molecule per 100 nm^2 . Estimate the equilibrium separation between the two surfaces at $T = 300$ K assuming that the intervening liquid is a theta-solvent for the polymer. What is the equilibrium separation if the interacting surfaces are not flat but spherical colloidal particles? Explain qualitatively why the equilibrium separation is smaller in this geometry.
- 16.2** A polymer is added to a suspension of aggregated colloidal particles in a liquid causing the particles to disperse. Does this mean that the polymer has adsorbed to the particle surfaces, replacing the adhesion by a monotonic repulsion? Assume room temperature conditions and that only van der Waals forces are operating between all the molecules and media.
- 16.3** Four scientists are arguing about the force between colloidal particles dispersed in a particular polymer solution at the theta temperature. The polymers are known not to adsorb on the particle surfaces in this solvent. **Dr. A:** When the particle surfaces are closer than R_g , there will be a depletion zone of reduced polymer density in the narrow gap between them. This leads to a repulsive force between the particles, because the polymer molecules in the more concentrated bulk solution want to get back into the gap, thereby pushing the surfaces apart. **Dr. B:** I disagree. The depletion must lead to an attractive force, because if you imagine the solutions in the gap and the bulk as two distinct phases (as in an osmotic pressure cell), solvent will want to diffuse out from the gap into the more concentrated bulk region, and this will act to pull the surfaces together. Thus, the force should be attractive, not repulsive. **Dr. C:** I agree that the force should be attractive, but for a different and much simpler reason. Since the concentration of polymer is less in the gap, the Contact Value theorem immediately tells us that the force must be attractive. **Dr. D:** But you have overlooked that when the polymer molecules move out of the gap, solvent molecules (which are presumably smaller) must come in to replace them. Thus there is actually a net *increase* in the overall number density of molecules in the gap, and according to the Contact Value theorem this will lead to a repulsion. **Dr. E:** This is really part of a more general phenomenon that applies to all systems composed of noninteracting particles (but of different sizes) where segregation effects can arise due entirely to entropic effects. If we look at the whole system it becomes apparent that as the larger particles come closer together (on the average) their entropy will decrease, but this is more than compensated by the increased entropy of the smaller particles that now fill the space vacated by the larger particles. In the present case the polymers act as the smaller particles and so there will be an effective attraction between the surfaces (of the larger particles).

Critically analyze these five arguments.

- 16.4 *** (i) For a square-well pair-potential between spherical particles of radius R having parameters defined by Eqs. (2.23) show that at temperatures above $\sim w_0 \Delta / Rk$ the phase diagram has only two phases, fluid and solid, as in Figure 11.3, rather than the conventional three phases, gas-liquid-solid, as in Figure 6.1. Note that this is tantamount to showing that the critical temperature is below T —that is, that $T_c < T$, which is characteristic of “hard-sphere” and granular systems. (ii) In systems where the attraction is determined solely by the depletion force (Section 16.6), assuming that the effective range of the attraction Δ is R_g , and that $R_g/R \ll 1$, show that there is no liquid phase at all temperatures T and interparticle adhesion energies w_0 at polymer volume fractions ϕ less than $\sim 2/\pi = 0.64$. [In practice no gas-liquid-solid phase regimes are found for $R_g/R < 0.25$ except at high volume fractions, typically for ϕ above ~ 0.5 (Ilett et al., 1995)].
- 16.5** In Worked Example 16.2, if the repulsive interaction is due to an effective hard wall of immobilized water molecules of thickness D_h , should the plane that defines $D = 0$ for the depletion interaction be at $D = 0$ (as assumed) or at $D = D_h$?
- 16.6** Compute the force-law in water between two bilayers of the poly[ethylene-oxide] surfactant $C_{12}EO_4$ (see Table 16.1). Assume that the interaction is determined mainly by headgroup overlap forces as modelled by the Alexander-de-Gennes theory, Eq. (16.5), for interacting brush layers. Use $L = 1.6$ nm (0.4 nm per EO group), $s = 0.93$ nm (mean spacing between groups), and $T = 25^\circ\text{C}$. Are these values reasonable? Compare your computed force profile with the measured force in the range $D = 1.5\text{--}3.2$ nm, i.e., from $\sim L$ to $2L$. (Lyle and Tiddy, 1986). Comment on whether the Alexander-de-Gennes theory really applies to this interaction or whether any agreement between theory and experiment is fortuitous.
- 16.7** Many force-measuring techniques involve particles or sheets suspended from a spring immersed in a liquid medium. Imagine such a particle initially suspended in a pure liquid. Some polymer is added to the liquid that adsorbs to the particle’s surface. The adsorption is “weak” in the sense that (i) the “coverage” is low—the adsorbed polymer coils remain well separated from each other, and (ii) only 10% of the segments are actually bound to the surface at any time—the remaining 90% are “floating” or “dangling” in the solvent like seaweed. Will the changed weight of the substrate after the adsorption be determined by only the 10% of surface-bound segments or all the adsorbed polymer molecules? [Answer: The weight will be determined by the full displaced mass of the adsorbed molecules.]
- 16.8 *** A thin membrane in solution has a small hole. A polymer molecule, held at one end, is pulled through the hole. Once 25% of the polymer is through the hole, it is released. What will the polymer do if it is driven only by entropic interactions? Assume θ -solvent conditions and an equal concentration of polymer in solution on either side.
- 16.9** A colloidal system is stable in the absence of polymer. A small amount of polymer is added and the colloidal particles coagulate, but if a large amount of polymer is

added, they redisperse. In another system no coagulation occurs when a small amount of polymer is added, but does occur at high polymer concentrations. Discuss the likely nature of the polymer, particle surfaces and solvent in each case.

- 16.10** Show that the depletion contribution to the adhesion energy of two spherical colloidal particles of radius R immersed in water containing non-adsorbing polymer “blobs” of radius R_g and volume fraction ϕ is approximately $-\phi kT(R/R_g)$. Under what conditions will the effective ϕ and R_g be different from the ideal, conventionally defined values?

This page intentionally left blank

Adhesion and Wetting Phenomena

17.1 Surface and Interfacial Energies

In Part I we saw how various interaction potentials between molecules arise, and we considered the implications of the energy minimum, or the “adhesion” energy, of molecules in contact. Here we shall look at phenomena involving particles and extended surfaces in adhesive contact, and it is best to begin by defining some commonly used terms and deriving some useful thermodynamic relations.

Work of adhesion and cohesion in a vacuum. These are the free energy changes, or reversible work done, to separate unit areas of two surfaces or media from contact to infinity in a vacuum (Figure 17.1a, b). For two different media ($1 \neq 2$), this energy is referred to as the work of adhesion W_{12} , while for two identical media ($1 = 2$), it becomes the work of cohesion W_{11} . If 1 is a solid and 2 a liquid, W_{12} is often denoted by W_{SL} . Note that since all media attract each other in a vacuum W_{11} and W_{12} are always positive—that is, of opposite sign to the reverse processes of bringing surfaces *into* contact from infinity (See footnote 2 in Chapter 10).

Surface energy, surface tension. This is the free energy change γ when the surface area of a medium is increased by unit area. Now the process of creating unit area of surface is equivalent to separating two half-unit areas from contact (Figure 17.1b, c), so that we may write

$$\gamma_1 = \frac{1}{2}W_{11}. \quad (17.1)$$

For solids γ_1 is commonly denoted by γ_s and is given in units of energy per unit area: mJ m^{-2} (the same as erg/cm^2). For liquids, γ_1 is commonly denoted by γ_L and is usually given in units of tension per unit length: mN m^{-1} (the same as dyn/cm), which is numerically and dimensionally the same as the surface free energy.

It is evident that the intermolecular forces that determine the surface energy of a substance are the same as those that determine its latent heat and boiling point (Section 2.6). As might be expected, substances such as metals with high boiling points ($T_B > 2000^\circ\text{C}$) usually have high surface energies ($\gamma > 1000 \text{ mJ m}^{-2}$), while lower boiling point substances have progressively lower surface energies. For example, for mercury: $\gamma = 485 \text{ mJ m}^{-2}$, $T_B = 357^\circ\text{C}$; for water: $\gamma = 73 \text{ mJ m}^{-2}$, $T_B = 100^\circ\text{C}$; for argon: $\gamma = 13.2 \text{ mJ m}^{-2}$, $T_B = -186^\circ\text{C}$; and for hydrogen: $\gamma = 2.3 \text{ mJ m}^{-2}$, $T_B = -253^\circ\text{C}$. In Section 13.13 we saw how the surface energies of all but strongly polar or H-bonding liquids and solids can be calculated reasonably accurately on the basis of current theories of van der Waals forces. Additional short-range forces that contribute to surface energies and adhesion are metallic bonds (Section 13.14) and charge exchange (including acid-base) interactions

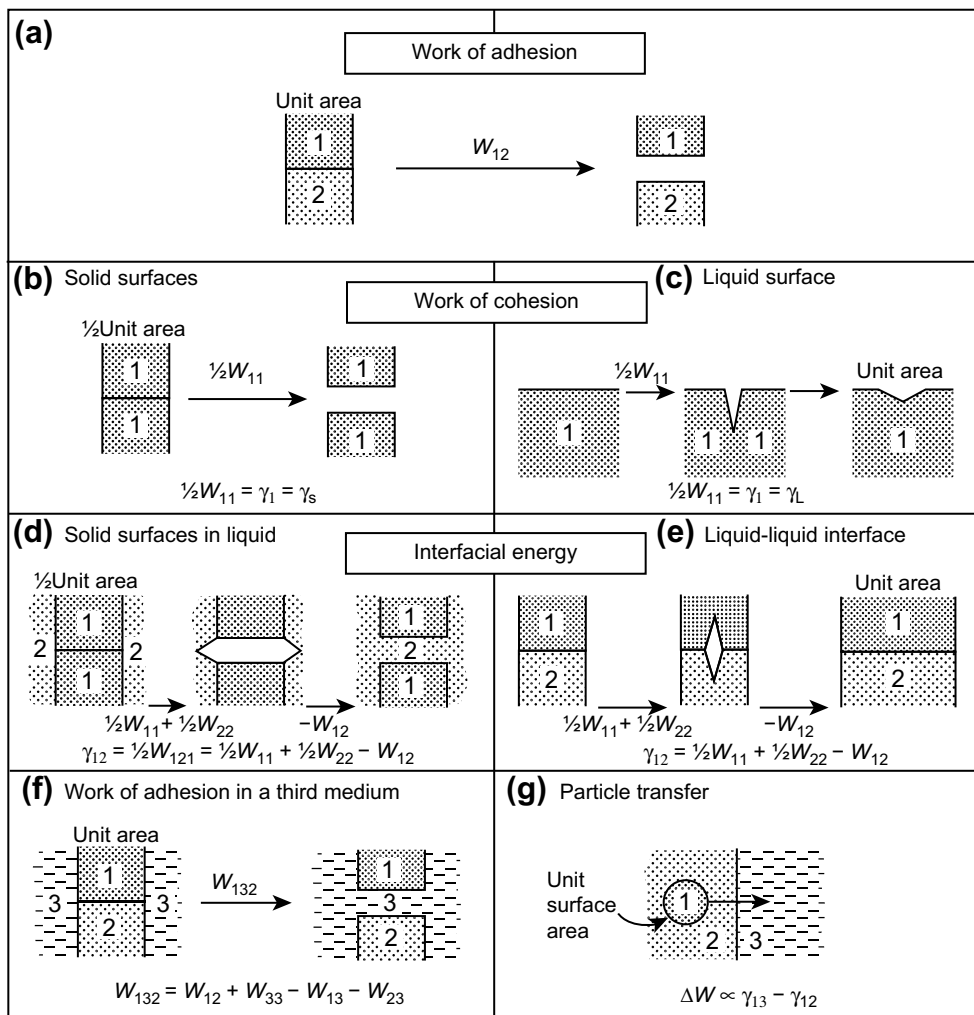


FIGURE 17.1 Definition of various energy terms associated with the adhesion of solid surfaces and the surface area changes of liquids. Note that W and γ are idealized thermodynamic quantities, assuming reversibility and smooth surfaces. In practice, only with liquids can the area be changed gradually and reversibly, as in (c). For solids, their adhesion, cohesion, and debonding processes, as in (a) or (b), usually involve plastic deformations with the dissipation of irreversible energy as heat. Note the positive sign of W (i.e., $W > 0$) for the work of adhesion/cohesion where, by convention, the reference state (of zero energy) is the contact state ($D = 0$), compared to the negative values for $W(D)$ and $w(r)$ where, again by convention, the reference states are at $D = \infty$, $r = \infty$.

where the spontaneous transfer of charge from one surface to another, dissimilar, surface generates an electrostatic attraction between the now oppositely charged surfaces (Dwight, 1997), a phenomenon that is also known as the “harpooning effect.”

It is important to appreciate that when the process of increasing the surface area of a medium takes place in a foreign vapor, such as laboratory air, some adsorption of vapor

molecules (e.g., water, hydrocarbons) may take place on the newly created surface. This has the effect of lowering γ_S and γ_L from their values in a vacuum, and the surface energies in vapor are denoted by γ_{SV} and γ_{LV} . For example, when mica is cleaved in high a vacuum the surface energy is $\gamma_S \approx 4500 \text{ mJ m}^{-2}$, but when cleaved in humid laboratory air it falls to $\gamma_{SV} \approx 300 \text{ mJ m}^{-2}$ (Bailey et al., 1970). The effects of adsorbed films and monolayers on surface energies are discussed in Chapter 19.

Interfacial energy. When two immiscible liquids 1 and 2 are in contact, the free energy change in expanding their “interfacial” area by unit area is known as their interfacial energy or interfacial tension γ_{12} or, in general, as γ_i . The energetics associated with this expansion process may be understood by splitting it into two hypothetical steps (Figure 17.1e): First, unit areas of media 1 and 2 are created, and are then brought into contact. The total free energy change γ_{12} is therefore

$$\gamma_{12} = \frac{1}{2}W_{11} + \frac{1}{2}W_{22} - W_{12} = \gamma_1 + \gamma_2 - W_{12}, \quad (17.2)$$

which is often referred to as the Dupré equation. As shown in Figure 17.1d, this energy is formally the same as that expended on separating two media 1 in medium 2 (W_{121}) or, conversely, of separating two media 2 in medium 1 (W_{212}). We may therefore also write

$$\gamma_{12} = \frac{1}{2}W_{121} = \frac{1}{2}W_{212}. \quad (17.3)$$

For a solid-liquid interface, γ_{12} is commonly denoted by γ_{SL} , so that the Dupré equation may be written as

$$\gamma_{SL} = \gamma_S + \gamma_L - W_{SL}. \quad (17.4)$$

Table 17.1 gives the surface and interfacial energies of some common substances. These values are always positive. When γ or γ_{12} is negative, the area wants to expand indefinitely, which means that 1 and 2 are miscible—that is, the interface eventually disappears (evaporates or dissolves).

If only dispersion forces are responsible for the interaction between media 1 and 2, we have previously seen that to a good approximation

$$W_{12} \approx \sqrt{W_{11}^d W_{12}^d} \approx 2\sqrt{\gamma_1^d \gamma_2^d} \quad (17.5)$$

so that Eq. (17.2) now becomes

$$\gamma_{12} \approx \gamma_1 + \gamma_2 - 2\sqrt{\gamma_1^d \gamma_2^d}, \quad (17.6)$$

where γ_1^d and γ_2^d are the dispersion force contributions to the surface tensions. Fowkes (1964) and Good and Elbing (1970) estimated that for water, the dispersion contribution to the total surface tension is $20 \pm 2 \text{ mN m}^{-1}$ or about 27% of the total. Note the near agreement between this value and the probably fortuitous theoretical estimates of 24 and 25% obtained in Tables 6.3 and 13.4. The remaining 53 mN m^{-1} arises from nondispersion (i.e., polar and H-bonding) interactions. Since water and hydrocarbon

Table 17.1 Surface and Interfacial Energies Selected from Different Classes of Materials at 20–25°C ($\text{mJ m}^{-2}\text{a}$)

Liquid 1	Surface Energy γ_1	Interfacial Energy γ_{12}
With water, H_2O ($\gamma_2 = 72\text{--}73$)		
<i>n</i> -hexane to <i>n</i> -hexadecane (sat) $\text{C}_n\text{H}_{2n+2}$	18–27	50–53
1-hexene to 1-dodecene (unsat) $\text{C}_n\text{H}_{2n}^b$	18–25	44–48
<i>iso</i> -alkanes/paraffins (branched) $\text{C}_n\text{H}_{2n+2}^b$	18–22	~48
Cyclohexane $\text{C}_6\text{H}_{12}^{20^\circ\text{C}}$	25	51
Paraffin wax (solid) $\text{C}_{20}\text{H}_{42}$ to $\text{C}_{40}\text{H}_{82}^c$	25	~50
PTFE (solid) $\text{CF}_3(\text{CF}_2)_n\text{CF}_3^{20^\circ\text{C}} c$	19	50
Carbon tetrachloride $\text{CCl}_4^{20^\circ\text{C}}$	27	45
Benzene C_6H_6 , toluene $\text{C}_6\text{H}_5\text{CH}_3$	28	34–36
Chloroform $\text{CHCl}_3^{20^\circ\text{C}}$	27	28
Diethyl ether $\text{C}_2\text{H}_5\text{OC}_2\text{H}_5^{20^\circ\text{C}}$	17	11
Cyclohexanol $\text{C}_6\text{H}_{11}\text{OH}^{20^\circ\text{C}}$	32	4
Mercury $\text{Hg}^{20^\circ\text{C}}$	486	415
With tetradecane, $\text{C}_{14}\text{H}_{32}$ ($\gamma_2 = 26$)		
Water, H_2O	72–73	53
Glycerol (1,2,3 propane-triol) $\text{C}_3\text{H}_5(\text{OH})_3^d$	64	31–36
1,3 propane-diol $\text{HO}(\text{CH}_2)_3\text{OH}$	49	21
Ethylene glycol (1,2 ethane-diol) $\text{C}_2\text{H}_4(\text{OH})_2$	48	18–20
1,2 propane-diol $\text{CH}_3\text{CH}(\text{OH})\text{CH}_2\text{OH}$	38	13
Formamide $\text{H}(\text{CO})\text{NH}_2$	58	29–32
Methyl-formamide $\text{H}(\text{CO})\text{NH}(\text{CH}_3)$	40	12
Dimethyl-formamide $\text{H}(\text{CO})\text{N}(\text{CH}_3)_2$	37	5

^aValues compiled from standard references, especially TRC Thermodynamic Tables for Hydrocarbons (1990), Jańczuk et al., (1993), Landolt-Börnstein (1982), Zografi and Yalkowsky (1974).

^bNote that C = C double bonds (unsaturation) and branching have only a small effect on the surface and interfacial energies of hydrocarbons with water.

^cNote that surface and interfacial tensions need not change when one or both of the phases change from liquid to solid.

^dAlso glycol, glycerine.

attract each other mainly via dispersion forces, the interfacial tension of a hydrocarbon-water interface should therefore be given by Eq. (17.6). Thus, for octane-water, putting $\gamma_1^d = 21.8 \text{ mN m}^{-1}$ and $\gamma_2^d = 20 \text{ mN m}^{-1}$, we calculate

$$\gamma_{12} \approx 21.8 + 72.75 - 2\sqrt{21.8 \times 20} \approx 52.8 \text{ mN m}^{-1}$$

which is very close to the measured value of 50.8 mN m^{-1} . This good agreement is obtained for many hydrocarbon-water interfaces, but the agreement is not so good for unsaturated hydrocarbons and aromatic molecules such as benzene and toluene (Fowkes, 1964; Good and Elbing, 1970).

Work of adhesion in a third medium, the “spreading pressure.” It is left as an exercise for the reader to establish that the energy change on separating two dissimilar media 1 and 2 in medium 3 (Figure 17.1f) is given by

$$W_{132} = W_{12} + W_{33} - W_{13} - W_{23} = \gamma_{13} + \gamma_{23} - \gamma_{12}. \quad (17.7)$$

Note that W_{132} can be positive (attraction between 1 and 2 in 3) or negative (repulsion between 1 and 2 in 3).

A negative W_{132} is often referred to as a “spreading pressure” or “spreading coefficient,” commonly denoted by S , C , or π , because when W_{132} is negative ($S > 0$), liquid 3 will displace liquid 2 and “spread on” or “totally wet” the surface of 1. This also implies that $\gamma_{13} + \gamma_{23} < \gamma_{12}$, which means that the two interfaces of 1|3 and 2|3 have a lower energy than the single interface of 1|2 or, alternatively, that the 1|2 interface will spontaneously split into two interfaces by the penetration of medium 3.

However, when W_{132} is positive ($S < 0$), we have $\gamma_{13} + \gamma_{23} > \gamma_{12}$, which is a necessary but not a sufficient or strong enough condition to allow us to conclude that medium 2 will spread on medium 1: partial spreading, with a contact angle between 0 and 180° (see Figure 17.6) is also a possibility, where both media 2 and 3 are in contact with 1. For full spreading of medium 2 on medium 1 we require that $\gamma_{13} > \gamma_{12} + \gamma_{23}$ —that is, $W_{132} < 0$.

Note that if medium 3 is a vacuum, $W_{132} \rightarrow W_{12}$, $\gamma_{13} \rightarrow \gamma_1$, $\gamma_{23} \rightarrow \gamma_2$, Eq. (17.7) reduces to Eq. (17.2) as expected, where W_{12} is always positive.

Surface energy of transfer. When a macroscopic particle 1 moves from medium 2 into medium 3 (Figure 17.1g) the change in energy per unit area of the particle’s surface is

$$\Delta W = \left(W_{12} - \frac{1}{2}W_{22} \right) - \left(W_{13} - \frac{1}{2}W_{33} \right) = \gamma_{13} - \gamma_{12}, \quad (17.8)$$

where $(W_{12} - \frac{1}{2}W_{22})$ is the energy required to first separate unit areas of media 1 and 2 and then bring into contact the newly created free surfaces of medium 2, and where $-(W_{13} - \frac{1}{2}W_{33})$ is the reverse operation for medium 1 with medium 3.

17.2 Adhesion Energies versus Adhesion Forces

We have already noted the conceptual differences between energies and forces. These differences are particularly manifest in adhesion and wetting phenomena, as illustrated in Worked Example 17.1.



Worked Example 17.1

Question: Consider the two adhering polymer surfaces of Figure 17.2 where the initial and final (fully separated) states are the same but where the paths between them are different. What are the adhesion forces in each case? Assume a Hamaker constant of $A = 6.5 \times 10^{-20}$ J and a square area of $1\text{ cm} \times 1\text{ cm}$.

Answer: Path (a) involves planar separation where the van der Waals adhesion force is given by $F_{\text{ad}} = A \times \text{area}/6\pi D_0^3 = (6.5 \times 10^{-20}) \times (0.01)^2/6\pi(1.65 \times 10^{-10})^3 = 7.7 \times 10^4$ N. Concerning the net change in energy, this is the same in both cases and is given by $W_{\text{ad}} = A \times \text{area}/12\pi D_0^2 = 6.3 \times 10^{-6}$ J. However, path (b) involves peeling of the surfaces over a distance of

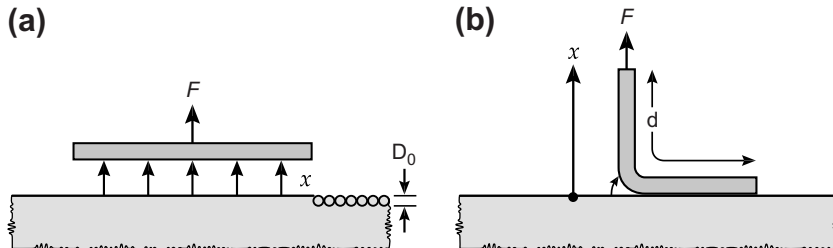


FIGURE 17.2 Two different paths for surfaces to separate, involving the same net change in energy ΔW or W_{ad} but requiring very different “adhesion” forces, F . In general, since $\Delta W = \int F dx$, we can see that depending on the path taken, which is prescribed by x , the force can be large or small as well as continually changing during the separation. Furthermore, even for a given path, the force can depend on the time or rate of separation, and can be higher or lower than the values calculated in Worked Example 17.1. This example illustrates how a soft adhesive polymer film¹ on a hard ceramic plate can provide a very strong adhesion force even when the surface energy of the polymer is low (i.e., involving only weak van der Waals forces).

$d = 1 \text{ cm} = 0.01 \text{ m}$ at a constant force of $F = W_{ad}/d = 6.3 \times 10^{-4} \text{ N}$ (cf. nonspecific bridging forces in Figures 16.8 and 16.9), which is 8 orders of magnitude less than for the planar separation.

Worked Example 17.1 shows how the same starting and ending states, and energy change, can nevertheless involve very different forces depending on the paths taken. This particular example also has practical implications: adhesive tape can be peeled away with little force as in Figure 17.2b, while an adhesive ceramic tile requires a substantially greater force even though the adhesive polymer layer may be the same. In the latter case, the stiff tile causes the surfaces to separate all at once, effectively mimicking the path of Figure 17.2a. Clearly, when referring to the “strength” of an interface or bond, one must specify whether one is talking about the energy or the force needed to break the contact.

An oft-asked question is: Since surfaces in a liquid separate in a vacuum before any liquid molecules can get between them (cf. Figure 15.4), shouldn’t the adhesion force and energy be given by the interaction in a vacuum? Strictly, yes: if the two surfaces were truly flat and rigid and separated while remaining parallel to each other, as in Figure 17.2a, the initial force *would* be that in a vacuum, falling as soon as the first layer of molecules enters the gap, then oscillating to zero as $D \rightarrow \infty$. But in practice two surfaces almost always separate by peeling, where the solvent molecules immediately enter between the surfaces at the bifurcation line. Similar effects occur in vapor due to adsorption; for example, the measured adhesion force of peeling or cleaving a mica sheet in air is less than 10% of the value in a vacuum.

The path taken is not only geometry-dependent but also rate-dependent: for very fast separations the adhesion force can reach very high values if there is not enough time for

¹A Pressure Sensitive Adhesive (PSA) is supposed to stick without any external pressure.

the surfaces to deform so that they can peel away, or for the solvent or vapor molecules to enter the gap or bifurcation line during the peeling process. Such large and rapidly changing adhesion forces can give rise to the phenomenon of cavitation in liquids (which can result in irreversible surface damage). Nonequilibrium and rate-dependent interactions lead to hysteresis effects, where again very different paths and forces can be experienced depending on the rates at which surfaces are moved, either normally (toward or away) or laterally relative to each other (friction forces). These issues are discussed in various other sections and chapters as they arise in different systems (see the Index). The important point to note is that in each of the detachment processes discussed above the net energy change is the same but the forces very different.

The thermodynamic “surface energy” and/or “surface tension” of a liquid is defined by a single parameter γ that can be expressed in units of energy (J m^{-2}) or, dimensionally equivalently, in units of force (N m^{-1}). This is somewhat unfortunate because it can lead to confusion, especially when considering rate-dependent nonequilibrium processes (Sections 17.6 and 17.8), nonplanar surfaces (Section 17.9), and surfaces with monolayers on them (Chapters 19 and 20). Here we shall consider some of the different ways of looking at the molecular origins of surface energy and tension, which will provide the basis for the discussions of the above three phenomena. Figure 17.3 shows three different ways of looking at how the concept of surface energy and tension γ arise at a bulk liquid-vapor interface. The three scenarios are equivalent but only when the following three conditions are satisfied: planar surfaces, pure single-component liquids, and equilibrium conditions.

In the first scenario, Figure 17.3a, two unit areas are brought together involving a change in energy of ΔW while eliminating *two* unit areas. In this case we can define $\gamma = \frac{1}{2}\Delta W$ per unit area, which is in units of J m^{-2} .

In the second scenario, Figure 17.3b, we consider a single surface with two imaginary parallel lines of length z going into the paper that attract each other with a force F per unit

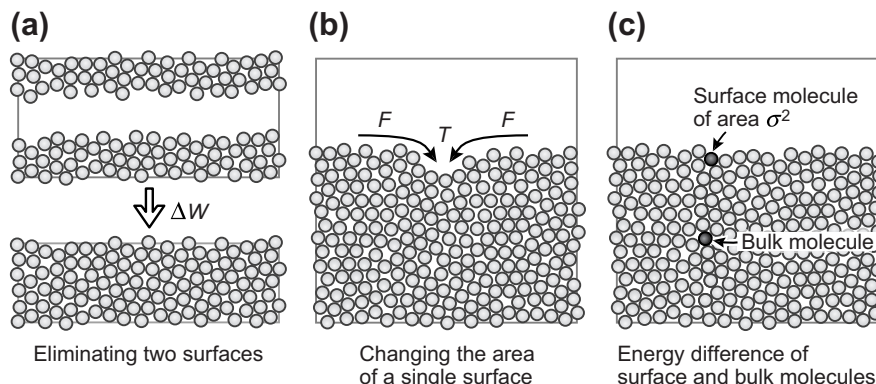


FIGURE 17.3 Different ways of looking at the origin of surface energies and surface tension forces of pure (single-component) systems. The situation can be very different when a liquid surface contains a monolayer or sub-monolayer of adsorbed molecules that are “insoluble” in the bulk liquid (see insoluble monolayers in Chapter 19).

length or tension, T . On closing the gap between the two lines by a lateral distance x , the area of the surface has decreased by $A = zx$ and the energy by $F \times \text{length of line} \times \text{distance moved} = Fzx = FA$. Assuming that we can equate this energy with the energy γA of the first scenario, we find that F is the same as the γ but now in units of force per unit length (N m^{-1}). This is the way surface tension was first conceived.

The third scenario also involves a single surface, Figure 17.3c, but with no motion or change in area, just a consideration of the equilibrium difference in the energy between a molecule at the surface and one in the bulk. In the bulk, let each molecule share 12 bonds of energy w with its nearest neighbors. On the surface the number of shared bonds will be 9. The difference is 3 shared bonds per molecule, or $1\frac{1}{2}$ full bonds per molecule. Thus, the energy per unit area relative to the bulk reference state is $\gamma = 3w/2 \times \text{area per molecule}$ which is the same as Eq. (13.40). We therefore see that the three scenarios of Figure 17.3 lead to the same numerical values for γ , but only under the conditions mentioned above.

The surface energies, tension, and stresses of surfaces with adsorbed species on them (e.g., surfactant and lipid monolayers on water) are described in Chapters 19 and 20. The surfaces of such two-component systems often exhibit very different properties from the single-component systems discussed here; for example, the monolayers may be elastic, with a tension that changes with the surface area rather than being independent of it.

17.3 Highly Curved Surfaces and Interfaces: Clusters, Cavities, and Nanoparticles

Here we shall investigate the validity of applying the concept of surface energy and tension to highly curved surfaces such as clusters, droplets, nanoparticles, cavities (holes, voids, bubbles) and even isolated molecules. Clearly the idea of a surface tension as exemplified in Figure 17.3c cannot be applied to a single atom or molecule since there is no “bulk energy” to compare the surface energy with. An atom or molecule surrounded by 12 nearest neighbors is the smallest cluster where such a comparison can be made.

But the concept of a surface or interfacial energy can be applied already to single molecules, since there is always an energy change associated with transferring a molecule from one medium to another or one location to another (as in Figure 17.1g), and this process can always be expressed in terms of $4\pi a^2 \gamma$ or $4\pi a^2 (\gamma_{13} - \gamma_{12})$, where a is the molecular radius. For small droplets or clusters two immediate questions arise: (1) How close will the surface energy of a cluster be to that of the planar bulk interface, and (2) how should one define a cluster—in terms of the number of molecules or the radius? If, as is commonly done, by the radius, problems of where to define the surface at the atomic or molecular level arise when, for example, we also want to define the radius of a hole vacated by a cluster or of one liquid in another since the atoms intercalate at the interface (see below).

Let us start by considering the reference planar surface: if $-w$ is the pair energy at molecular contact, then for a planar close-packed surface lattice, with three unsaturated bonds per surface molecule, the surface energy was previously found to be given by Eq. (13.40) as

$$\gamma \approx \sqrt{3}w/\sigma^2 = \sqrt{3}w/4a^2 \approx 0.43w/a^2 \text{ J m}^{-2} \quad \text{for a planar surface,} \quad (17.9)$$

where $\sigma = 2a$ is the molecular diameter. In contrast, for a single, isolated molecule, with 12 unsaturated bonds, its effective surface energy is

$$\gamma \approx 12w/2(4\pi a^2) \approx 0.48w/a^2 \text{ J m}^{-2} \quad \text{for a single atom,} \quad (17.10)$$

while for a cluster of 13 molecules, with seven unsaturated bonds per each of the 12 surface molecules (Figure 17.4), we obtain

$$\gamma \approx 7 \times 12w/2[4\pi(3a)^2] \approx 0.37w/a^2 \text{ J m}^{-2} \quad \text{for a 13-atom cluster,} \quad (17.11)$$

which is only slightly smaller than the value for the planar surface. Thus, we arrive at the remarkable conclusion that the magnitude of the effective surface energy γ of a very small cluster, or even an isolated molecule, is within 15% of that of the planar macroscopic surface. We encounter various experimental manifestations of this phenomenon in Section 8.5 and elsewhere in this book.

Equation 17.11 is qualitatively consistent with the Tolman Equation which gives the surface energy of a spherical droplet of radius R as (Tolman, 1949; Rowlinson and Widom, 1989).

$$\gamma(R) \approx \gamma(\infty)/(1 + \delta/R) \approx \gamma(\infty)(1 - \delta/R), \quad (17.12)$$

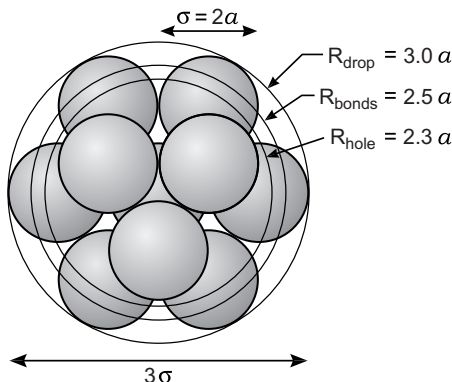


FIGURE 17.4 Cluster of 13 atoms or molecules: one central atom surrounded by 12 close-packed neighbors, six in the plane of the page with three above and three below. Note that each of the 12 surface atoms has 5 contact points with its neighbors in the cluster and therefore 7 with the next layer (of 42 molecules, not shown). These 84 contact points with the third layer may be thought of as the centers of the interatomic bonds. The number of spheres in complete-shell icosahedra are: 1, 13, 55, 147, 309, 561, . . . , and 74% of the volume is occupied. In 2D the sequence is: 1, 7, 19, . . . , and 91% of the area is occupied. In practice, real clusters are rarely close-packed structures.

where $\gamma(\infty)$ is the surface energy of the planar surface ($R = \infty$), and δ is an atomic-scale dimension. For the 13-atom cluster of radius $R = 3a$ our analysis would give $\gamma(R)/\gamma(\infty) = 0.37/0.43 = (1 - \delta/3a) \Rightarrow \delta = 0.4a$. The Tolman equation remains controversial: it is difficult to test experimentally, and its extension to cavities or to droplets in another medium, where γ_i replaces γ , is not obvious.

The cluster of Figure 17.4 shows a central atom surrounded by six atoms in the same plane, with three above and three below. This type of packing is referred to as hexagonal close packed (HCP), where, if continued, the “bilayers” alternate indefinitely. However, one can see that the three atoms in the lower plane, which are not seen because they are shielded by the three in the upper plane, could be rotated by 60° yet still give a close-packed structure. This type of packing is referred to as face centered cubic (FCC) where, if continued, “trilayers” alternate indefinitely. When next-nearest neighbor energies are considered one immediately sees that the HCP cluster is energetically favored over the FCC because the atoms of the two outermost layers are closer together. One would therefore expect spherical atoms, molecules, and nanoparticles to pack into HCP lattices rather than FCC, but both occur naturally, sometimes with a transition between them at some particular temperature. The reasons for these effects are subtle—the energy differences are typically $\sim 10^{-3} kT$ per particle—and have been attributed to 3- and higher-body interactions, multipole interactions, and entropy effects (Nieland and Venables, 1974; Woodcock, 1997).

The above discussion becomes even more complex when extended to curved surfaces that are not isolated droplets, such as the asperities on a rough surface, and to concave surfaces such as cavities or holes. Figure 17.5 shows a spherical cluster or droplet and its complementary hole. While the total surface energies of a droplet and its complementary cavity may be the same, convex and concave surfaces nevertheless exhibit both

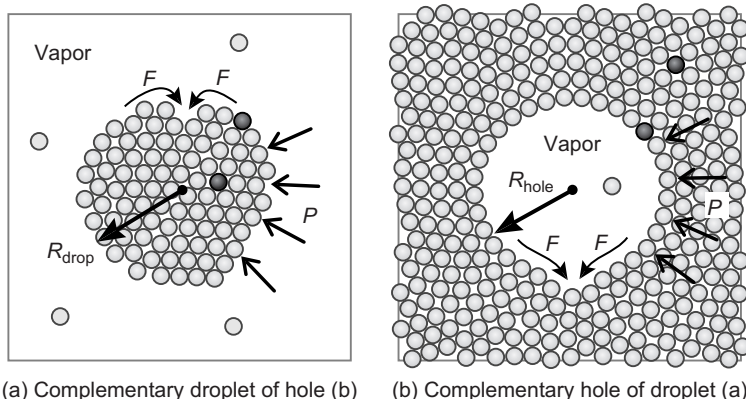


FIGURE 17.5 Small spherical cluster or nano-droplet (left) and complementary cavity or hole (right). For additive nearest-neighbor pair potentials, the total surface energy of the cluster and its complementary cavity (the one it was extracted from) must be the same, but other surface properties can be very different. For example, the surface energy *per surface atom* is greater in droplets or convex surfaces than in holes or concave surfaces because the former has fewer bonds than the latter. In contrast, the surface energy *per unit area* is somewhat arbitrary, since it depends on where the convex and concave radii are defined.

quantitative and qualitative differences. These include the definitions of the radii of curvature and areas per molecule, the resulting deformations when molecules are drawn into the bulk, and the different effects of cooperative (nonadditive) interactions. For example, in the case of the 13-atom cluster (Figure 17.4), each surface atom has 7 open bonds and there are therefore $12 \times 7 = 84$ of them, which must be the same as for the complementary hole. But while having the same total surface energy, the radii of the clusters and holes, R_{drop} and R_{hole} , are different when defined in terms of their outer and inner boundaries. Thus, in Figure 17.4, $R_{\text{drop}} = 3a$ but R_{hole} is smaller and given by $R_{\text{hole}} = (4\sqrt{2/3} - 1)a = 2.27a$, so that the surface energy of the hole is

$$\gamma \approx 7 \times 12w/2[4\pi(2.27a)^2] \approx 0.65w/a^2 \text{ J m}^{-2} \quad \text{for a 13-atom hole,} \quad (17.13)$$

which is greater than the surface energies of both the planar surface, Eq. (17.9), and the 13-atom cluster or drop, Eq. (17.11).

These differences in the surface energies of droplets and holes are partly due to the somewhat arbitrary definition of their radii (not to mention that small clusters are not even spherical). A more consistent definition of radius would be that of the sphere whose surface passes through the contact points—the effective bond centers defined by R_{bonds} in Figure 17.4—between the outermost spheres and the next layer of spheres. This would give the same radius for complementary spheres and holes. When this is done for the 13-atom cluster one obtains $R_{\text{drop}} = R_{\text{hole}} = \sqrt{19/3}a = 2.52a$, which is intermediate between $3.0a$ and $2.27a$, as expected. With this common radius, the surface energies of the 13-atom cluster and hole are now the same:

$$\gamma \approx 7 \times 12w/2[4\pi(2.52a)^2] \approx 0.53w/a^2 \quad \text{for a 13-atom cluster or hole,} \quad (17.14)$$

which is 23% higher than the value for a planar surface, Eq. (17.9). A higher value was also obtained for a single atom, Eq. (17.10). The problem of exactly where to define the boundaries of small particles comes up when considering other properties that involve their radius, length, area, or volume—for example, the strain, stress, defining the Young's modulus, and so on.



Worked Example 17.2

Question: A single 13-molecule cluster of medium 1 resides in a liquid medium 2. What is the effective interfacial energy of the cluster in terms of the bulk surface energy γ_1 ? What is it in the case of a single molecule of 1 in medium 2? Assume that both types of molecules have the same radius a , and that the pair contact energies are $-w_{11}$, $-w_{22}$, and $-w_{12}$. Discuss the implications of your results.

Answer: Following the method of calculating of the surface energy of a single surface in Section 13.13, the interfacial energy of the planar interface is $\gamma_1(\infty) \approx \frac{3}{2} \left(\frac{w_{11} + w_{22} - 2w_{12}}{\sigma^2 \sin 60^\circ} \right) = 0.43(w_{11} + w_{22} - 2w_{12})/a^2$. For a cluster of one material coexisting in another, the concept of a different outer and inner radius, as arises for isolated clusters and cavities, becomes

untenable. The common radius will be defined as the locus of the contact points or bonds, which occurs at $R = 2.52a$ for the 13-molecule cluster and at $R = a$ for the single molecule. The total change in energy per cluster can be determined by calculating the energy change of transferring the cluster from medium 2 into its own bulk medium 1, since this eliminates the interface which defines the reference state of zero energy. The transfer process is similar to the four-step process of Figure 17.1g involving a change in energy of $\Delta w = (w_{12} - \frac{1}{2}w_{22} + \frac{1}{2}w_{11} - w_{11}) = -\frac{1}{2}(w_{11} + w_{22} - 2w_{12})$ per bond at the interface. Since there are $5 \times 7 = 35$ such bonds at the 13-cluster interface, the interfacial energy is therefore $\gamma_i(R = 2.52a) \approx 35(w_{11} + w_{22} - 2w_{12})/2[4\pi(2.52a)^2] \approx 0.53(w_{11} + w_{22} - 2w_{12})/a^2 = 1.23\gamma_i(\infty)$. Applying the same argument to the single molecule “cluster” we obtain for its interfacial energy: $\gamma_i(R = a) \approx 12(w_{11} + w_{22} - 2w_{12})/2(4\pi a^2) = 1.1\gamma_i(\infty)$. The effect is therefore the same as for the surface tension—that is, resulting in an increased interfacial energy. The result is also unchanged on exchanging media 1 and 2. This trend arises because at a curved interface, whether concave or convex, there are always more higher energy 1-2 or 2-1 bonds than at the planar interface. Since the interfacial energy is positive—that is, unfavorable—the surfaces of smaller droplets tend to evaporate or dissolve faster than larger droplets.



Still, it is clear that for pair-wise additive interactions the surface energies per unit area of even the smallest nano-droplets and cavities are already very close to those of the planar surfaces and that any difference really depends on how their radii are defined. Thus, describing particles, whether ordered or amorphous, in terms of their radii can be confusing. It is also unnecessary. It is far better to analyze the energetics of clusters in terms of the energy *per molecule*—that is, to define clusters in terms of the number of molecules in the cluster rather than the radius of the cluster. Molecular and molar energies also enter naturally into basic equations of thermodynamics and statistical mechanics, whereas radii do not (see later sections on self-assembly and nucleation in Part III).

When expressed in terms of the energies per molecule, the picture changes completely: the 35 surface bonds of the 13-molecule cluster are shared with 42 molecules in the next layer. Thus, while per unit area the cluster and hole energies are similar, when reckoned *per surface molecule* the cluster energies are $35/42w = 3.5w$ per molecule and the hole energies are $42/42w = 1.0w$ per molecule, a difference of 350%. The differences are also large, especially for the cavity, when compared to the energies of the planar surfaces of $3.0w$ per molecule. This may be readily understood by considering that the molecules on a convex surface have fewer bonds, while those on concave surfaces have more bonds than those on planar surfaces. In the case of a single molecule, the cluster and hole energies are $6.0w$ (cf. Eq. 2.3) and $6w/12 = 0.5w$, respectively. The hole energy is now very small because each surface molecule is surrounded by 11 other molecules, making it effectively in the bulk state—the reference state of zero energy. Due to the much lower number of cohesive bonds holding molecules and small clusters, these are often in a different phase state from the bulk material. Thus small gold particles are liquid at temperatures where the bulk metal is solid (see below), and small volumes of liquid may have a density intermediate between the vapor and (bulk) liquid phase (Stroud et al., 2001).

The nanoparticle regime. The analysis so far has assumed that atoms and small molecules interact via additive pair potentials where long-range forces and many-body effects are not important. While this condition holds for van der Waals solids and liquids, it does not apply to metallic, semiconducting, ionic, and hydrogen-bonding compounds, where a certain number of atoms are needed for some property to reach the saturation or bulk value.

In Chapter 11, particularly Section 11.4, we considered how size affects the nonadditive properties of particles as they grow from single atoms to macroscopic bodies exhibiting bulk properties. For example, the high latent heats, melting points, surface energies, electronic and optical properties of metals, and semiconductors depend on the correlated (cooperative) interactions of many atoms. In very small droplets or ultrathin films these medium- to long-range correlations cannot occur, and some metal clusters with less than 15–30 atoms lose many of their bulk metallic properties and become indistinguishable from van der Waals substances. For example, the melting points of small droplets of gold are significantly lower than the bulk value of 1336 K, falling to 1000 K for a cluster of diameter 4 nm and to about 500 K for a diameter of 2.5 nm (Buffat and Borel, 1976). Similarly, Buffey and colleagues (1990) have found that small water clusters with about 20 molecules or less are probably in the liquid state already at 200 K due to the inability of a H-bonding network to develop in these clusters. A related effect occurs with thin water films: thus, between 0 and -20°C the surface of ice has a thin liquid layer on it—a phenomenon known as “surface melting”—which is responsible for the low friction of ice (Dash, 1989).

Thus, the different properties of clusters and nanoparticles are not so much to do with their size or curvature effects per se but on the reduced number of bonds at surfaces (even flat surfaces as in the case of the low friction of ice) and/or on the nonadditive (cooperative) intermolecular interactions. Further aspects of these “skin effects” and “proximity effects” were discussed in Section 11.4, and the role of nonequilibrium interactions in their assembly is discussed in Chapter 22 in Section 22.7 on self-assembly versus directed assembly.

The Laplace pressure. For surfaces with large, macroscopic radii, curvature effects are still important, since they give rise to a significant *Laplace pressure* P_L within the liquid or solid. Returning to Figure 17.5, the surface tension force of γ per unit length, when resolved normal to a circumferential circle of radius R gives a net force of $F = 2\pi R\gamma$ that acts to compress the droplet and that at equilibrium must be balanced by an internal pressure given by $P = \text{net force}/\text{area} = 2\pi R\gamma/\pi R^2 = 2\gamma/R$. More generally, for a surface with two orthogonal or “principal” radii, R_1 and R_2 :

$$P_L = \gamma(1/R_1 + 1/R_2). \quad (17.15)$$

Thus, for a spherical droplet or hole of radius R we obtain the above result, $P_L = 2\gamma/R$, while for a cylinder of radius R , $P_L = \gamma/R$.

The convention of defining the meniscus curvature relative to the condensed phase—for example, positive for liquid droplet but negative for a hole—can cause confusion

regarding the sign or direction of the pressure. It is best to remember that the Laplace pressure always drives the interface *in the concave direction*. Thus, the liquid in a drop (convex surface) experiences a positive (compressive) pressure, whereas a liquid containing a bubble or hole (concave surface) experiences a negative (tensile) pressure. The positive Laplace pressure on a droplet means that its molecules are compressed – much like the stretched elastic membrane of a balloon compresses the gas inside it, while around a concave surface the molecules are expanded, such as when liquid rises up a capillary tube or when a liquid droplet spreads between two sheets pulling them together (see Section 17.11 on capillary forces). This issue becomes most clearly apparent when we try to establish whether the pressure inside a liquid droplet immersed in another liquid is positive or negative: it is always positive since γ_i is always positive² (Section 17.1).

Worked Example 17.3

Question: Can the Laplace pressure be applied to curved surfaces having molecular dimensions?

Answer: Consider the limit of just two molecules in adhesive contact for which the “internal” Laplace pressure would be given by $P = 2\gamma/a$, where $\sigma = 2a$. In terms of molecular parameters, where the molecular contact area is $\sim \pi a^2$. Using Eq. (17.9) this pressure corresponds to a “Laplace force” of $f_{\text{Lap}} \approx 2[\sqrt{3}w(\sigma)/4a^2]\pi a^2/a = 2.7w(\sigma)/a$. Assuming a van der Waals pair potential of $w(r) = -C/r^6$ with a hard-wall cut-off at $r = \sigma$, the van der Waals adhesion force is $f(\sigma) = -6C/\sigma^7 = 6w(\sigma)/\sigma = 3.0w(\sigma)/a$. The Laplace and intermolecular forces are therefore calculated to be within 10% of each other. The concept and quantitative application of the Laplace pressure therefore appears to apply to molecular clusters including dimers, where it is seen to reduce to none other than the pair-interaction between two molecules.

Worked Example 17.3 shows that the Laplace pressure can be enormous, enough to make liquids rise many tens of meters in fine capillary tubes and to the tops of tall trees.³ For van der Waals liquids where, typically, $\gamma \approx 30 \text{ mJ m}^{-2}$, for $R = a = 0.3 \text{ nm}$, pressures as high as $2(30 \times 10^{-3})/(3 \times 10^{-10}) = 2 \times 10^8 \text{ Pa} \approx 2,000 \text{ atm}$ can therefore be attained. Situations where such highly curved (concave) menisci and high local pressures arise occur at cracks and contact boundaries—for example, between surfaces or their asperities. A liquid does not have to be present at such boundaries: the equation for the Laplace pressure applies equally to solids and liquids, and for solids where γ is usually much higher than for liquids the pressure will be correspondingly higher.

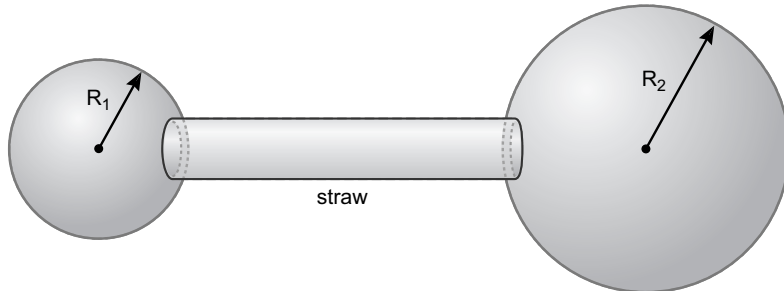
²The two liquids must be immiscible or partially miscible. A negative γ_i means that the droplet will eventually dissolve in the host liquid—in other words, that the interface will disappear, since it wants to *increase* its area.

³An analogous situation arises with gravitational pressure: in a star of mass M and radius R the compressive pressure at the center can be readily shown (by considering the pressure between two hemispheres) to be approximately $GM^2/4\pi R^4 \propto R^2$. However, due to the long-range nature of gravitational forces this pressure is not uniform but is highest at the center. It also increases rather than decreases with R , and can lead to the gravitational collapse of large stars into neutron stars with radii as small as 10 km.

There is one important fundamental difference between convex and concave surfaces, which concerns the thermodynamic equilibrium state of these surfaces. As shown in Section 17.11, a planar or concave surface can be stable in saturated or undersaturated vapor, respectively, but a convex surface is only metastable in oversaturated vapor. Oversaturated vapor spontaneously condenses until the vapor pressure reaches or falls below the saturated pressure and the liquid-vapor interface is planar, becomes concave or disappears (as when a hole closes up).

Worked Example 17.4

Question: A hollow cylindrical straw has two macroscopic soap bubbles of different radii, R_1 and R_2 , where $R_1 < R_2$, at each end. Air can flow freely between the bubbles through the straw, and their Laplace pressure is given by $P_L = 2\gamma/R_i$, where $\gamma = \text{const}$. No air flows through the soap films. What is the final stable configuration of the system?



Answer: The Laplace pressure difference will drive air from the smaller bubble to the larger one until the pressure has equilibrated throughout the system. This will occur when both bubbles have the same radius, R . The initially larger bubble will have grown and the initially smaller bubble will have shrunk, first to where its radius equals that of the straw diameter, then further—but now with *increasing* radius—to the point where it exists as a slightly convex bulge at the circular opening of the straw. Since both truncated “bubbles” have the same radius R and truncated contact area with the straw, they are geometrically complementary parts of a complete sphere of radius R . Assuming that the total internal volume (of the air and, therefore, bubbles) has not changed, the radius of the two end “bubbles” will therefore be given by $R^3 = R_1^3 + R_2^3$. In practice, if the gas is ideal, will R be larger or smaller?

17.4 Contact Angles and Wetting Films

Surface and interfacial energies determine how macroscopic liquid droplets deform when they adhere to a surface. In Figure 17.6a (top) a large initially spherical droplet 2 in medium 3 approaches and then settles on the rigid flat surface of medium 1. The final total surface energy of the system is therefore given by

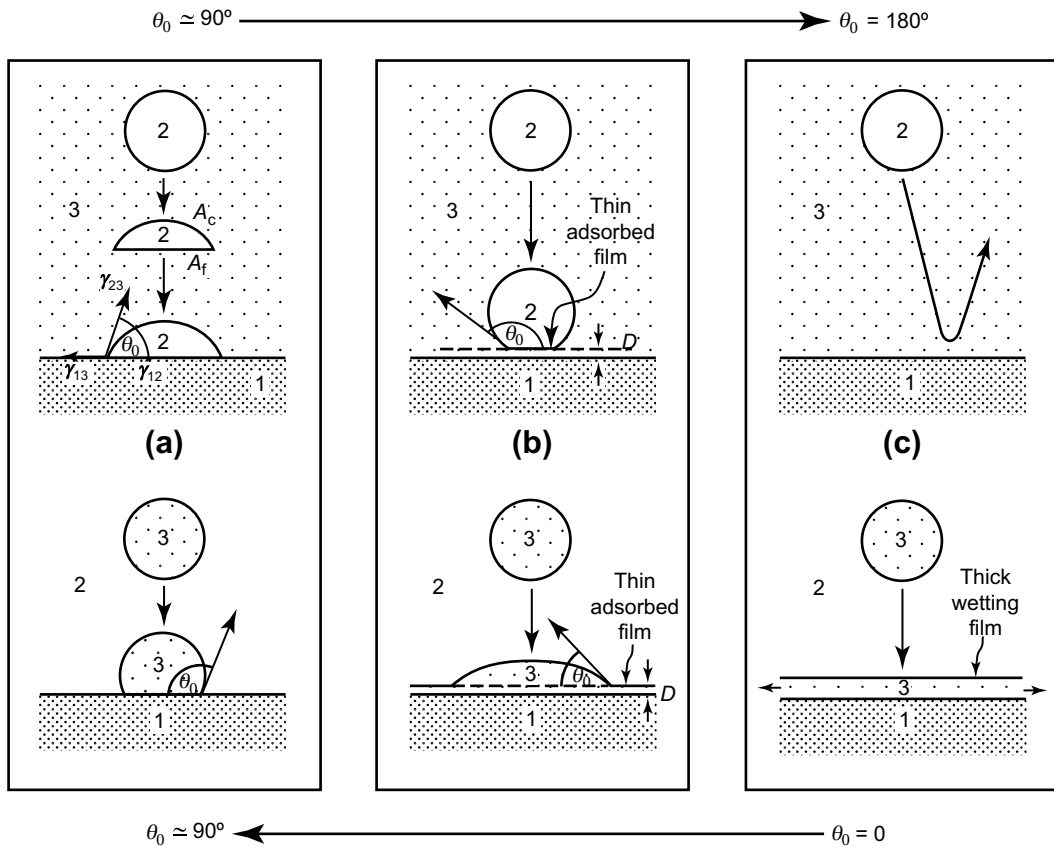


FIGURE 17.6 Contact angles and their manifestation from $\theta = 0$ to $\theta = 180^\circ$. Note that the upper and lower drawings in each box are formally equivalent on interchanging media 2 and 3 and replacing θ_0 by $(180^\circ - \theta_0)$. The thin adsorbed films in the middle panel are an example of “autophobicity”—the nonwetting of a liquid on a layer of itself. Such films can be molecularly thin with “quantized” thicknesses. For a spreading droplet on a surface they are referred to as precursor films.

$$W_{\text{tot}} = \gamma_{23}(A_c + A_f) - W_{132}A_f, \quad (17.16)$$

where A_c and A_f are the curved and flat areas of the droplet. At equilibrium: $\gamma_{23}(dA_c + dA_f) - W_{132}dA_f = 0$. For a droplet of constant volume, it is easy to show using straightforward geometry that $dA_c/dA_f = \cos \theta$. Thus, the equilibrium condition ($\theta = \theta_0$) is

$$\gamma_{23}(1 + \cos \theta_0) = W_{132} = \gamma_{13} + \gamma_{23} - \gamma_{12}, \quad (17.17)$$

or

$$\gamma_{12} + \gamma_{23} \cos \theta = \gamma_{13}, \quad (17.18)$$

which can also be derived by balancing the resolved interfacial tensions in the plane of the surface (Figure 17.6a).

It is also interesting to resolve the forces normal to the surface: if r is the radius of the contact circle, the net vertically resolved interfacial tension force acting at the rim of the droplet is $2\pi r\gamma_{23} \sin \theta_0$. This should be balanced by the Laplace pressure acting downward on the surface, which is given by $2\gamma_{23}/R$, where R and r are geometrically related by $r = R \sin \theta_0$. The net force due to the Laplace pressure is therefore $2\gamma_{23} \times \text{contact area}/R = 2\pi r^2 \gamma_{23}/R = 2\pi r\gamma_{23} \sin \theta_0$, which exactly balances the upwardly resolved surface tension force.

If media 2 and 3 are interchanged, as in Figure 17.6a (bottom), then Eq. (17.17) becomes

$$\gamma_{23}(1 + \cos \theta_0) = W_{123} = \gamma_{12} + \gamma_{23} - \gamma_{13}, \quad (17.19)$$

that is,

$$\gamma_{12} - \gamma_{23} \cos \theta_0 = \gamma_{13}, \quad (17.20)$$

or

$$\gamma_{23}(1 - \cos \theta_0) = W_{132}, \quad (17.21)$$

which is the same as Eq. (17.17) with θ_0 replaced by $180^\circ - \theta_0$. Thus, as might have been expected intuitively, the contact angle in Figure 17.6a (bottom) is simply $180^\circ - \theta_0$ of that in Figure 17.6a (top).⁴

The total “wetting” or “spreading” energy of the droplet on the surface is given by inserting the equilibrium condition, Eq. (17.17), into Eq. (17.16), giving $W_{\text{total}} = W_{\text{min}} = \gamma_{23}(A_c + A_f) - W_{132}A_f = [(A_c + A_f)/(1 + \cos \theta_0) - A_f]W_{132} = (A_c - A_f \cos \theta_0)W_{132}/(1 + \cos \theta_0)$. The minimum total energy can be expressed more conveniently in terms of the equilibrium contact angle θ_0 and initial radius of the spherical droplet, R_0 (Figure 17.6a):

$$W_{\text{total}} = W_{\text{min}} = 4^{2/3}\pi R_0^2 W_{132}(2 - 3 \cos \theta_0 + \cos^3 \theta_0)^{1/3}/(1 + \cos \theta_0) \quad (17.22a)$$

$$= 4^{2/3}\pi R_0^2 \gamma_{23}(2 - 3 \cos \theta_0 + \cos^3 \theta_0)^{1/3} \quad (17.22b)$$

$$= 4\pi R_0^3 \gamma_{23}/R. \quad (17.22c)$$

Thus, W_{min} is a maximum for $\theta_0 = 180^\circ$, when $\cos \theta_0 = -1$, $W_{132} = 0$, $R = R_0$, and the energy remains unchanged from the original value of $4\pi R_0^2 \gamma_{23}$ because there is no adhesion and therefore no adhesive flattening. The total energy of Eq. (17.22) decreases monotonically from $4\pi R_0^2 \gamma_{23}$ to zero as the contact angle decreases from 180° to zero (i.e., as the droplet spreads on the surface), and as R increases from R_0 to ∞ (i.e., as the Laplace pressure falls to zero). Thus, given a choice, a liquid prefers to wet the surface on which it has the lowest contact angle. As a corollary to this, if a (smooth) surface has

⁴By convention, the contact angle is always the angle measured within the liquid (not vapor) medium. For a liquid-liquid interface—that is, a liquid droplet in another liquid—there is no convention and one needs to specify the liquid within which the angle is defined.

a gradient in its chemical properties such that the contact angle of a particular liquid also varies on it, a droplet of this liquid placed on the surface will move to the region where it subtends the lowest contact angle. This qualitative conclusion could also have been arrived at, more or less immediately, by considering where the Laplace pressure within the droplet is least.

While the above results were derived for the specific case of a spherically shaped droplet on a flat surface, the contact angle is independent of the surface geometry (Adamson, 1976, Chapter 7). Thus, θ_0 is the same on a curved surface, inside a capillary, or at any point on an irregularly shaped surface. Further, the contact angle θ_0 as given by the above equations is a thermodynamic and thus a purely macroscopic, quantity—Independent of the nature of the forces between the molecules as long as these are of shorter range than the dimensions of the droplet. Thus, the contact angle tells us nothing about the microscopic contact angle or the shape of the liquid profile at the point where it meets the surface (Figure 17.7).

The above equations are more generalized forms of the famous equations of Young and Dupré derived for liquid droplets on surfaces exposed to vapor. Thus, if medium 3 in Figure 17.6a (top) is an inert atmosphere, Eqs. (17.17) and (17.18) become the Young-Dupré equation:

$$\gamma_2(1 + \cos \theta_0) = W_{12} \quad (17.23)$$

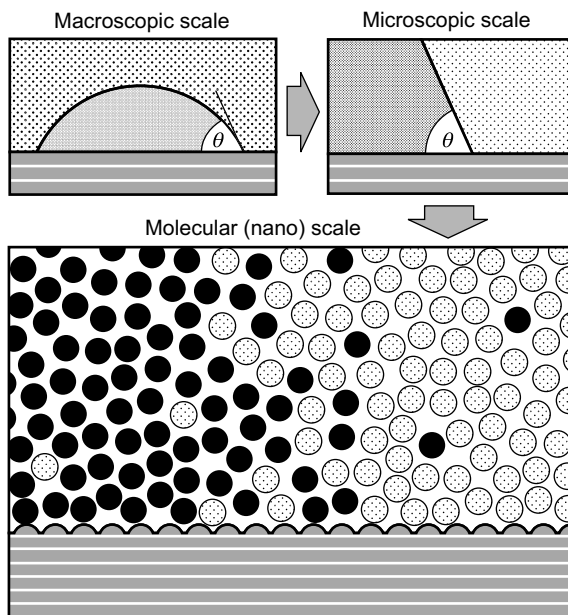


FIGURE 17.7 Schematic shape of a liquid-liquid interface as it meets a solid surface seen at the macroscopic, microscopic and molecular (nanoscopic) levels. The macroscopic contact angle, θ , does not tell us much about the shape of the interface at the molecular level.

and the Young equation:

$$\gamma_{12} + \gamma_2 \cos \theta_0 = \gamma_1. \quad (17.24)$$

For example, for water on paraffin wax, the measured values are $\theta_0 \approx 111^\circ$, $\gamma_1(\text{paraffin}) = 25 \text{ mJ m}^{-2}$, and $\gamma_2(\text{water}) = 73 \text{ mJ m}^{-2}$, from which we infer that $\gamma_{12} \approx 51 \text{ mJ m}^{-2}$ (cf. Table 17.1) and that $W_{12} \approx 47 \text{ mJ m}^{-2}$. Note that this is close to the value expected from $W_{12} \approx 2\sqrt{\gamma_1^d \gamma_2^d} \approx 2\sqrt{25 \times 20} \approx 45 \text{ mJ m}^{-2}$. In some studies all four parameters of the Young equation were independently measured (Pashley and Israelachvili, 1981; Israelachvili, 1982): This involved a droplet of $8 \times 10^{-4} \text{ M}$ HTAB surfactant solution on a monolayer-covered surface of mica for which $\gamma_1(\text{solid}) = 27 \pm 2 \text{ mJ m}^{-2}$, $\gamma_2(\text{liquid}) = 40 \text{ mJ m}^{-2}$, $\gamma_{12}(\text{solid-liquid}) = 11 \pm 2 \text{ mJ m}^{-2}$, and $\theta_0 = 64^\circ$, which agree with the Young equation.

In the case where medium 3 is a liquid, equilibrium can be attained at some finite distance D [Figure 17.6b (top)] where the interaction energy W_{132} is a minimum—for example, a weak secondary minimum (Section 14.21). In such cases the contact angle is usually very low. Such phenomena occur, for example, when dissolved air bubbles or oil droplets containing lipid or surfactant monolayers (emulsion droplets) adhere weakly to each other or to a surface (Figure 1.3d).

An analogous situation occurs when a liquid droplet attaches to a surface containing a thin physisorbed film of the same liquid [Figure 17.6b (bottom)]. Qualitatively, one may say that here a small contact angle forms because the liquid rests on a surface that is of its own kind. Note that this is formally the same as that of Figure 17.6b (top) with media 2 and 3 interchanged. Such cases occur quite often; for example, many different vapors, including water and hydrocarbons, adsorb as a monolayer on mica, and these liquids have a small but finite contact angle on mica of $\theta_0 < 6^\circ$.

If the interaction between 1 and 2 across 3 is monotonically repulsive, the liquid droplet is now repelled from the surface [Figure 17.6c (top)], and we must put $W_{132} = 0$. Such situations lead to the complete spreading of a liquid on a surface and the development of thick wetting films [Figure 17.6c (bottom)], previously discussed in Sections 13.9 and 14.8 as they arise due to van der Waals and electrostatic forces, respectively.

Contact angles can often be changed by chemically modifying surfaces or by addition of certain solute molecules into the medium that adsorb on the surfaces (Chapter 19). For example, addition of “surface-active” molecules such as detergents to water can cause the contact angle to increase from 0 to 180° (see Figure 1.3d). When quartz is preheated above 300°C its hydrophilic surface silanol groups $-\text{Si(OH)}-\text{Si(OH)}-$ give off water, leaving behind hydrophobic siloxane groups, $-\text{Si-O-Si}-$, and the contact angle rises from 0 to about 60° .

Electro-wetting. We have previously seen that spontaneous charge exchange, also known as contact electrification, can occur between two dissimilar surfaces, producing a capacitor (Figure 3.2) and an attractive force between the two surfaces (cf. Fig. 18.21). Similar effects occur when an external voltage or potential ψ is applied between two

surfaces or even across a single solid-liquid interface. The enhanced attraction is equivalent to an enhanced adhesion energy, which can be calculated from the general equation for the energy of an electric field, Eq. (3.12):

$$\text{Total electrostatic field energy} = \frac{1}{2}\epsilon_0\epsilon \int E^2 dV, \quad (17.25)$$

where V is the volume of space where the field intensity is E . For a parallel-plate capacitor of area A and thickness δ , $V = A\delta$, and the field $E = \psi/\delta$ is uniform. We can therefore write for the electrostatic adhesion energy contribution per unit area:

$$W_{\text{el}} = \frac{1}{2}\epsilon_0\epsilon\psi^2/\delta \quad \text{C V m}^{-2} (\text{or J m}^{-2}). \quad (17.26)$$

For example, using the numerical values following Eq. (14.14) to model the Stern layer of Figure 14.4: $\delta = 0.2 \text{ nm}$, $\epsilon = 40$, $\sigma = 0.2 \text{ C m}^{-2}$, we obtain $\psi = \sigma\delta/\epsilon_0\epsilon = 130 \text{ mV}$ and $W_{\text{el}} = 15.0 \text{ mJ m}^{-2}$. Much higher values can be obtained when ψ is applied externally: 0.5 Volt would increase the above adhesion energy to $\sim 220 \text{ mJ m}^{-2}$. When W_{el} is added to W_{12} in the Young-Dupré equation, Eq. (17.23), we can see that this will lead to a large decrease in the contact angle and/or total wetting of the surfaces by the liquid. Such *electro-wetting* and *electro-capillarity* effects are commonly used to control the contact angles and thus the wetting/spreading of liquids on surfaces (Mugele and Baret, 2005). However, the liquids and substrates need to be conducting (for example, electrolyte solutions on a metal substrate) in order for most of the field to fall across the gap between them.

17.5 Wetting of Rough, Textured, and Chemically Heterogeneous Surfaces

All the surfaces considered so far have been implicitly assumed to be both physically and chemically homogeneous. Most real surfaces are neither and, as we shall see, can also alter their shape and chemical composition during interactions—for example, when they come into or out of contact with another surface or liquid. To understand the subtle effects of chemical heterogeneity and surface roughness or “texture,” we may initially consider the two simple situations depicted in Figure 17.8, the first a molecularly smooth but chemically heterogeneous surface, the second a textured but chemically homogeneous surface.

Effect of chemical heterogeneity on contact angles. Figure 17.8a shows a smooth surface that is chemically different on either side of the line at P. This difference manifests itself in different contact angles, θ_1 and θ_2 , for a particular liquid L on these surfaces. The question is, What is the contact angle θ at P? The answer is that it is not uniquely defined, and can be anything between θ_1 and θ_2 —that is, $\theta_1 \leq \theta \leq \theta_2$. To see how this arises, consider the line at P to have a small but finite width, as shown in the expanded part of Figure 17.8a, where the chemical composition of the surface varies continuously from pure 1 to pure 2. Let f_1 and f_2 (where $f_1 + f_2 = 1$) be the local fractions (surface densities) of components 1 and 2 inside the transition regime or strip. Writing

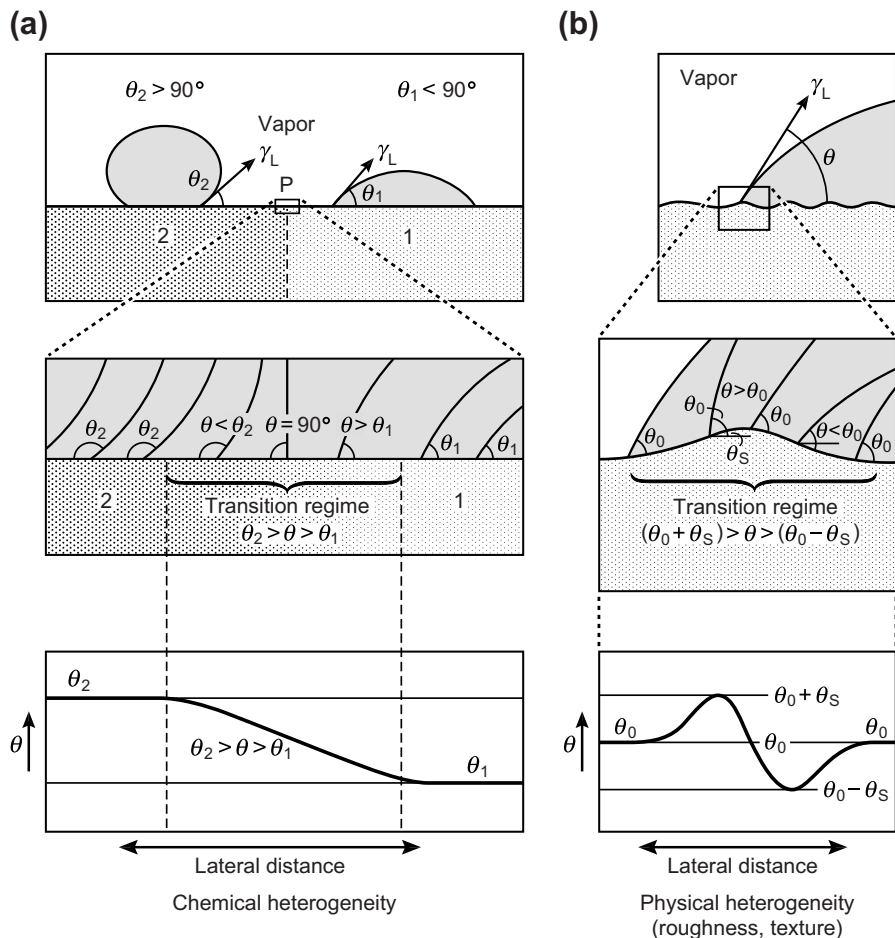


FIGURE 17.8 (a) Effects on the contact angle at a line separating two chemically different regions of a smooth surface. (b) Effect on the contact angle at a ridge separating two chemically homogeneous regions of an otherwise smooth surface. Note that the contact angle will be different depending on whether the liquid droplet is approaching from the left or right and also whether it is advancing or receding. The chemical and topographical heterogeneities shown here have been oversimplified to occur at a 1D line; real surfaces are usually much more complex, exhibiting heterogeneities in both 2D and 3D.

$\gamma_L(1 + \cos \theta_1) = W_{1L} \approx \sqrt{W_1 W_L}$ and $\gamma_L(1 + \cos \theta_2) = W_{2L} \approx \sqrt{W_2 W_L}$ for the Young-Dupré equations for the pure surfaces, then within the strip:

$$\gamma_L(1 + \cos \theta) \approx \sqrt{(f_1 W_1 + f_2 W_2) W_L} = \sqrt{f_1 W_1 W_L + f_2 W_2 W_L}, \quad (17.27)$$

which gives the following general relation for the contact angle at a chemically heterogeneous surface:

$$(1 + \cos \theta)^2 = f_1(1 + \cos \theta_1)^2 + f_2(1 + \cos \theta_2)^2. \quad (17.28)$$

This equation is similar to the Cassie Equation:

$$\cos \theta = f_1 \cos \theta_1 + f_2 \cos \theta_2 \quad (17.29)$$

which is more appropriate for surfaces with chemically distinct—that is, microscopic rather than nanoscopic, patches of compounds 1 and 2 (Cassie, 1948; Israelachvili and Gee, 1989). Both equations give the same limiting values as $f_1 \rightarrow 1$ and $f_2 \rightarrow 1$.

Returning to Figure 17.8a, we can see that within the strip at P the contact angle can take on any value between θ_1 and θ_2 , an effect that is one of the main causes of contact line “pinning” and contact angle hysteresis and hysteresis effects in adhesion and capillary forces (see Sections 17.6 and 17.8 and Problem 17.2).

Effects of surface topography on contact angles. Figure 17.8b illustrates the similar effects of a simple line ridge or depression on the local contact angle. Real textured surfaces are usually more ornate: they can be randomly rough, have a particular texture, or have a periodic profile or “pattern” such as the one shown in Figure 17.9. Each of these topographies, even the simplest periodic one, can result in complex and varied effects, including different apparent contact angles θ and wetting properties, hysteresis, sudden instabilities, time-dependent effects, and different local deformations of the surfaces (see later).

For textured surfaces the molecular or “real” area of liquid-solid contact is usually no longer the same as the macroscopic or “projected” area, defined by the circle where the macroscopic contact angle θ is defined—a distinction that does not arise with smooth surfaces. For such surfaces, we may replace W_{132} by ϕW_{132} in Eq. (17.17), where ϕ is the fraction by which the real area is greater or less than the projected area. For a liquid droplet on a surface in vapor the Young-Dupré equation then becomes

$$\gamma_L(1 + \cos \theta) = \phi W_{SL} \quad (17.30a)$$

which leads to

$$(1 + \cos \theta) = \phi(1 + \cos \theta_0), \quad (17.30b)$$

where W_{SL} and θ_0 are the values for molecularly smooth surfaces. Equation (17.30b) may be compared with the Wenzel Equation (Wenzel, 1936): $\cos \theta = \phi \cos \theta_0$ which, however, appears to be unphysical in that it predicts no effect of roughness when $\theta_0 = 90^\circ$.

The problem of roughness usually reduces to one of determining the value of the dimensionless parameter ϕ for a textured surface, where ϕ can be less or greater than 1. According to Eq. (17.30) for $\phi > 1$ the macroscopic contact angle θ is lower than θ_0 , while for $\phi < 1$ it is higher (for the simple reason that the liquid-surface adhesion per unit projected area must be higher or lower, respectively).

In spite of the generality and simplicity of Eq. (17.30) for macroscopic droplets the general situation is complex because ϕ is usually difficult to predict. Figure 17.9 shows a surface with a microscopically wavy but chemically homogeneous surface—that is, where the local (real) contact angle θ_0 is less than 90° in region (a) and greater than 90° in region (b). For each case we can envisage three scenarios: (1) a macroscopic droplet of liquid is placed on the surface, (2) a nanoscopic droplet is placed on the surface, and (3) the

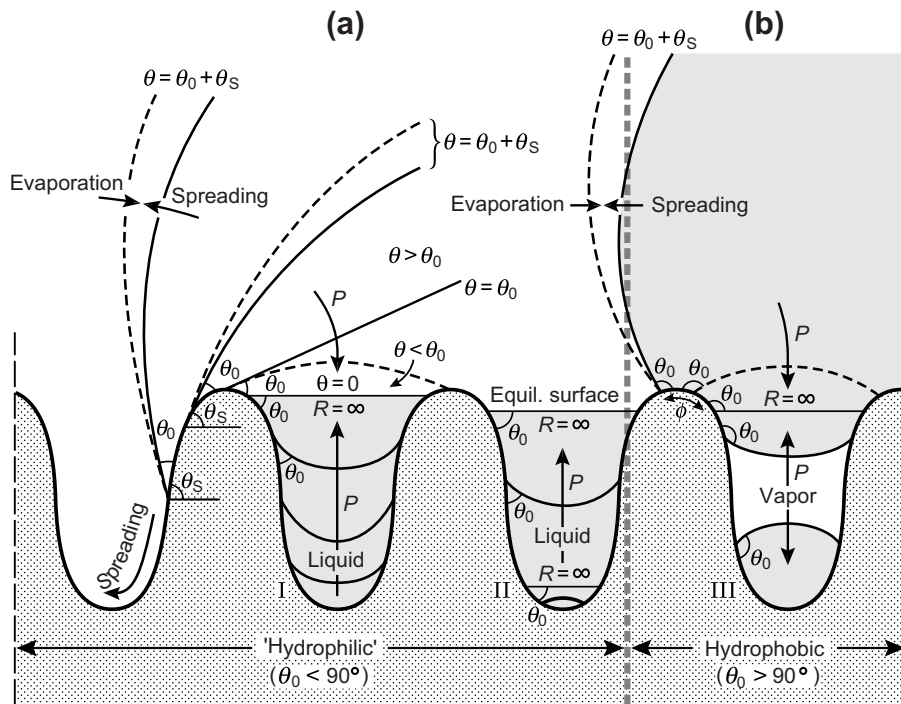


FIGURE 17.9 Wetting and spreading of a liquid on a periodically patterned surface when (i) a large droplet is placed on the surface, and (ii) the liquid condenses from saturated vapor where the ultimate, thermodynamically equilibrium, meniscus is flat—that is, $R = \infty$ (see Kelvin radius). (a) When the liquid has a low intrinsic contact angle, θ_0 , it will immediately spread and fill all the holes or wells. After the initial spreading, the concave liquid surfaces will grow (by condensation), while any convex surfaces will slowly evaporate, each driven by the Laplace pressures P in the directions shown. The final state will be a liquid surface with zero apparent contact angle ($\theta = 0$) and zero Laplace pressure ($R = \infty$). (b) When the liquid has a high intrinsic contact angle, θ_0 , all liquid surfaces are convex, as shown. The Laplace pressure drives all these surfaces to evaporate while reducing the real contact area to zero ($\phi \rightarrow 0$). Note that very high local Laplace pressures can cause elastic or plastic deformations of solid surfaces. The situations depicted here are more complex when the vapor is not saturated.

liquid condenses on the surface from vapor. For each of these scenarios we may further consider the initial (mechanical equilibrium) and final (thermodynamic equilibrium) configurations. Even ignoring the effects of gravity, the many different variables of this system (not to mention the crucial details of the surface topography) makes it difficult to arrive at any general conclusions regarding ϕ , and only a few of the more commonly encountered situations will be considered (see also Problems 17.8, 17.9, 17.12 and 17.28).

For liquids of low intrinsic contact angles, say $\theta_0 = 10^\circ$, Eq. 17.30 gives $\cos \theta = 1.9848\phi - 1$. Thus, θ can be zero, small or large depending very delicately on the precise value of ϕ . For example, for $\phi = 1.000$, we obtain $\theta = 10^\circ$, as expected. For $\phi < 1.000$ the contact angle θ will be greater than 10° , while for $\phi > 1.008$ the contact angle will be zero—that is, the liquid will completely wet the surface ($\theta = 0$). This is the situation that occurs in practice for low θ_0 systems on rough or textured surfaces (for example, water

on hydrophilic surfaces) once thermodynamic equilibrium has been attained, as illustrated in Figure 17.9a. Figure 17.9a also illustrates some nonequilibrium situations where the contact angle can be significantly higher than the intrinsic angle θ_0 .

Figure 17.9b shows the quite different situation where θ_0 is greater than 90° , when the equilibrium value of ϕ is now smaller than 1. As an example, consider a rough hydrophobic surface where the intrinsic water contact angle is $\theta_0 = 90^\circ$ and where only the tops of the asperities, constituting 20% of the projected area, are actually contacted by a water droplet sitting on the surface (see point ϕ in Figure 17.9b). The macroscopic contact angle will therefore be given by $(1 + \cos \theta) = \phi = 0.2 \Rightarrow \theta = 143^\circ$. Such surfaces are referred to as superhydrophobic, and the phenomenon is also known as the Lotus Effect (see also Fig. 15.16g). However, unless the vapor is supersaturated, convex water droplets should not be thermodynamically stable on hydrophobic (or any) surfaces and should eventually disappear through evaporation.

Worked Example 17.5

Question: The contact angle of water on the planar surface of Figure 17.9 is 30° . The central cavity I is exposed to saturated water vapor. Sketch the path taken by the water meniscus or droplet in this cavity. Ignore gravitational effects and the possible involvement of other cavities.

Answer: The path taken by the meniscus as liquid water condenses from vapor is shown by the lines $a \rightarrow e$ in Figure 17.10, where $\theta = 30^\circ$ in each case. State a is unstable and will tend to shrink (evaporate), b is metastable, c and d continue to grow, e is the stable state, and f is unstable and will shrink back to e . The path involves the nucleation of droplet b before further growth can proceed. The nucleation is energetically unfavorable and will be the rate-limiting part of the whole process—the greater the volume of water that needs to be nucleated, the longer will be this time.

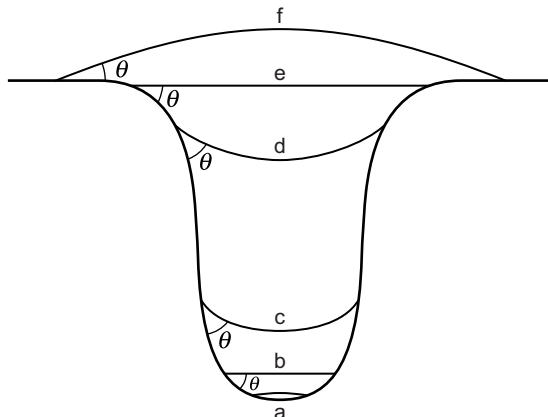


FIGURE 17.10

17.6 Contact Angle Hysteresis

The contact angle, being a thermodynamic quantity, should be expected to be a unique value for any particular system. But it is often found that when an interface advances along a surface, even a molecularly smooth surface, the “advancing” contact angle, θ_A , is larger than the “receding” angle, θ_R . This is known as *contact angle hysteresis*, and we have already seen in Figures 17.8 and 17.9 how it can come about due to chemical and physical heterogeneities of surfaces.

Figure 17.11 shows these and two additional effects that give rise to contact angle hysteresis: the additional effects being due to *changes* in the chemical and physical nature of the surfaces after they have come into contact with a liquid or another material (rather than having these properties fixed as in Figures 17.8 and 17.9). Other physico-chemical reactions, not shown in Figure 17.11, can also produce contact angle hysteresis—for example, when surfactant adsorbs to a surface from an advancing liquid. The role of time, advancing and receding rates, and previous history enter naturally into any contact angle hysteresis that is due to such effects since the changes are invariably associated with some characteristic relaxation, adaptation, or adsorption time.

Contact angle hysteresis can be very large, with advancing and receding angles sometimes differing by more than 90° , and it is often very difficult to tell which effect is responsible. When a receding interface is not retracing its original advancing or spreading path, the process is not thermodynamically reversible, and it is generally not immediately obvious which, if any, of the two contact angles represent the truly equilibrium value. The matter is not easy to resolve experimentally—for example, by allowing very long equilibration times—since advancing and receding angles can be stable for very long times. As the previous discussion and figures have shown, only on perfectly smooth and chemically homogeneous surfaces can we hope to obtain the “true” angle (and then only if the surfaces are infinitely rigid and chemically inert). There is also the nagging matter that a droplet with a convex surface cannot be at thermodynamic equilibrium with its vapor: it can only be in mechanical equilibrium.

The phenomenon of contact angle hysteresis is a manifestation of a much more general effect: the hysteresis in the adhesion energy W of two phases, where one or both of the phases are solid (Figure 17.11d). For a liquid droplet on a surface, it is the different values of W for the advancing and receding liquid with the surface that results in the different values for θ via the Young-Dupré equation, Eq. (17.23). For two solids, the difference manifests itself in different (irreversible) loading and unloading energies, time-dependent adhesion forces, and energy-dissipating friction forces (Chapter 18).

The existence of hysteresis and irreversibility usually means that a system is trapped in a transient or metastable nonequilibrium state. In the case of a liquid droplet on a solid surface this can be due to mechanical or chemical effects, as illustrated in Figure 17.12. Let us first consider the three liquid phases of Figure 17.12a. At the three-phase boundary, the three contact angles will be uniquely determined by the three interfacial tensions

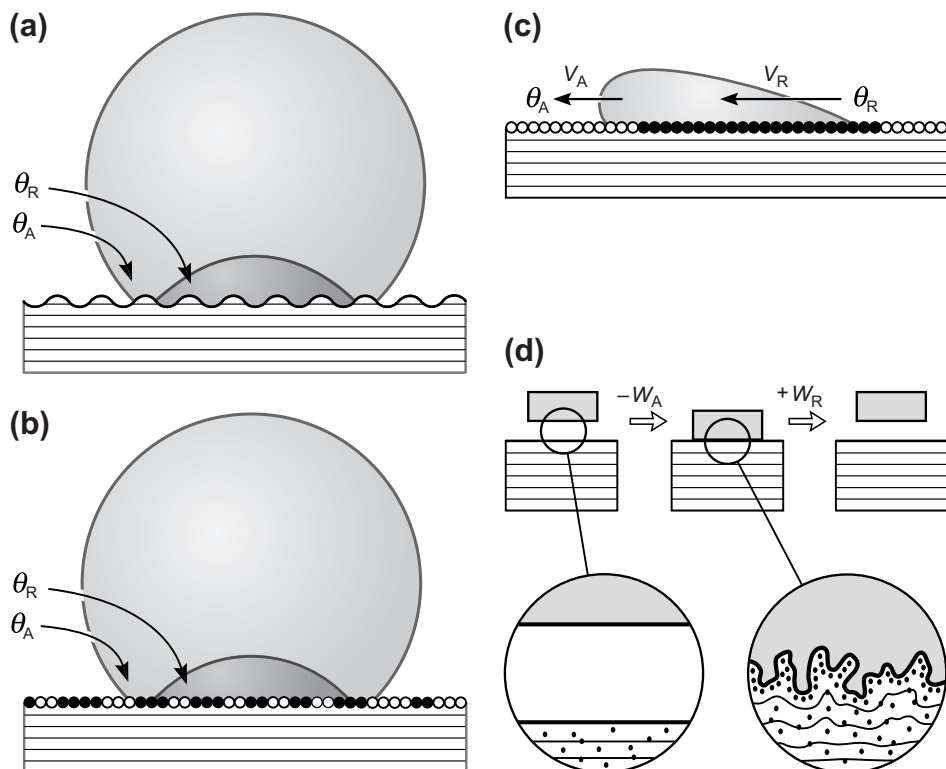


FIGURE 17.11 Contact angle and adhesion hysteresis. **(a)** Effect of surface roughness: liquid droplets on a rough surface where the microscopic contact angle is 90° in each case but the macroscopic (measured) advancing and receding contact angles, θ_A and θ_R , are very different. **(b)** Effect of chemical heterogeneity: droplets on a smooth but chemically heterogeneous surface where the adhesion energy W is different at different places. **(c)** The orientation of surface chemical groups often depends on the phase they are exposed to, resulting in molecular rearrangements and different adhesion energies and contact angles at the advancing and receding ends of the moving droplet. These angles are rate- and previous history-dependent—that is, depending both on the velocity of the moving “three-phase boundaries,” V , and the time the liquid has been in contact with the surface. **(d)** Interdiffusion and interdigitation, especially of viscoelastic and polymer-like materials, resulting in different adhesion energies on approach W_A and separation (retraction) W_R , which is analogous to the advancing and receding energies in panel (c). Note how both surfaces may look “perfect” before and after they are in contact but totally different when *in* contact.

according the triangle of forces rule or, equivalently, the requirement of the uniformity of the Laplace pressure in Liquid 1. When this condition is satisfied, true thermodynamic equilibrium will have been attained. Now consider the situation where the lower surface is a solid and where the three interfacial energies are unchanged. Clearly, the *equilibrium* geometry should also be unchanged, but in practice, if the solid is rigid and undeformable, the geometry will depend on the shape of the solid surface. Actually, a real solid *will* deform elastically or plastically with time; for example, starting from Figure 17.12b the system will slowly deform and approach the true equilibrium geometry of Figure 17.12c, but this may take billions of years.

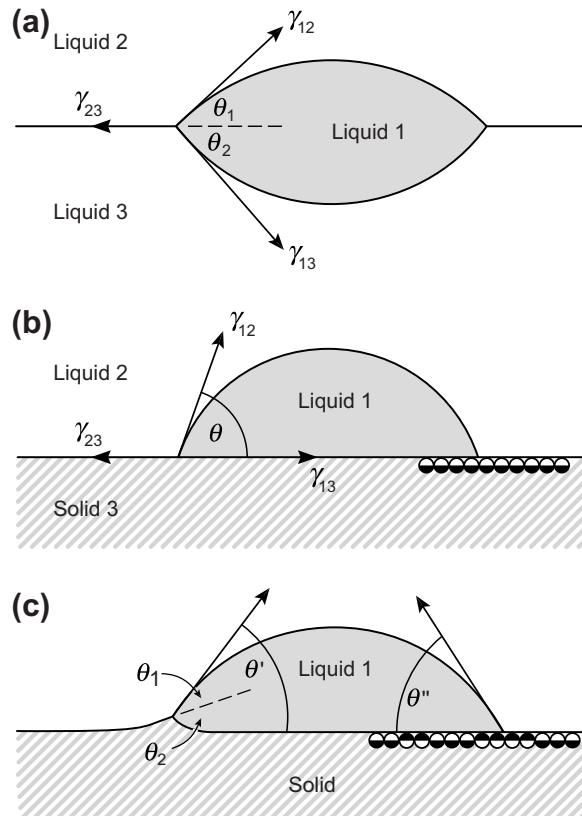


FIGURE 17.12 (a) Equilibrium configuration of liquid droplet (or lens) on another liquid. (b) Nonequilibrium (but mechanically stable) configuration of liquid droplet on a solid surface. Equation 17.31 shows that θ will be greater than θ_1 but less than $(\theta_1 + \theta_2)$. (c) Microscopic and molecular-scale deformations that can occur, usually at the three-phase boundary, to relax the vertical component of the interfacial tension.



Worked Example 17.6

Question:

1. Show that $\gamma_{12} \sin \theta_1 = \gamma_{13} \sin \theta_2$ in Figure 17.12a.
2. If $\theta_1 = \theta_2 = 45^\circ$ in Figure 17.12a, what is θ in Figure 17.12b?
3. What balances the vertical component of the tension $\gamma_{12} \sin \theta$ in Figure 17.12b? Ignore gravitational effects.

Answer:

1. At equilibrium the pressure throughout the system must be uniform. This implies that the Laplace pressures of the two interfaces are the same and that the curvature of each interface is uniform. The radii R_1 and R_2 of the upper and lower curved interfaces must therefore be related by $\gamma_{12}/R_1 = \gamma_{13}/R_2$. Since the radius of the three phase contact circle is

$r = R_1 \sin \theta_1 = R_2 \sin \theta_2$, we immediately obtain the desired result which shows that the resolved vertical components of the interfacial tensions are balanced, as expected.

2. Equating vertical components we have: $\gamma_{12} \sin \theta_1 = \gamma_{13} \sin \theta_2$. Equating horizontal components we obtain: $\gamma_{12} \cos \theta_1 + \gamma_{13} \cos \theta_2 = \gamma_{23}$ and $\gamma_{12} \cos \theta + \gamma_{13} = \gamma_{23}$. Eliminating γ_{12} , γ_{13} and γ_{23} from these three equations yields:

$$\cos \theta = \cos \theta_1 - (1 - \cos \theta_1) \sin \theta_1 / \sin \theta_2. \quad (17.31)$$

Inserting $\theta_1 = \theta_2 = 45^\circ$ into the above, we obtain $\theta = \cos^{-1}[\sqrt{2} - 1] = 65.5^\circ$.

3. The apparently unbalanced vertical component of the tension $\gamma_{12} \sin \theta$ is balanced by high local stresses on the solid surface. This can result in elastic or even plastic deformations which cause the surface to bulge upwards (Shanahan and de Gennes, 1986), as illustrated in Figure 17.12c, left. More importantly, it may lead to molecular rearrangements that alter the local surface energies so as to reduce these local stresses (Figure 17.12c, right). These stress relaxation effects usually act to reduce the final contact angle below θ .
-



All the above effects can lead to hysteresis and aging effects of contact angles and adhesion energies. Thus, values of θ and W will usually differ for advancing and receding boundaries, with W_R being generally larger than W_A , so that $\theta_A > \theta_R$. As already mentioned, these differences also depend on dynamic factors such as the rate at which the boundaries move (see Section 17.8 and Chapter 18).

17.7 Adhesion of Solid Particles: the JKR and Hertz Theories

The adhesion force of two rigid (incompressible) macroscopic spheres is simply related to their work of adhesion by

$$F_{\text{ad}} = 2\pi \left(\frac{R_1 R_2}{R_1 + R_2} \right) W, \quad (17.32)$$

where $W = W_{132}$ in the general case of two different bodies 1 and 2 interacting in a third medium 3. This general result is a direct consequence of the Derjaguin approximation, Eq. (11.16), and leads to the following special cases:

$$\text{for two identical spheres in liquid: } F = 2\pi R \gamma_{SL} \quad (17.33a)$$

$$\text{for two identical spheres in a vacuum: } F = 2\pi R \gamma_S \quad (17.33b)$$

$$\text{for a sphere on a flat surface in a vacuum: } F = 4\pi R \gamma_S \quad (17.33c)$$

$$\text{for a sphere on a flat surface in vapor: } F = 4\pi R \gamma_{SV} \quad (17.33d)$$

Real particles, however, are never completely rigid as in Figure 17.13a, and on coming into contact, they deform elastically under the influence of any externally applied load as well as the attractive intersurface forces that pull the two surfaces together, which gives rise to a finite contact area even under zero external load (Figure 17.13b). One of the first

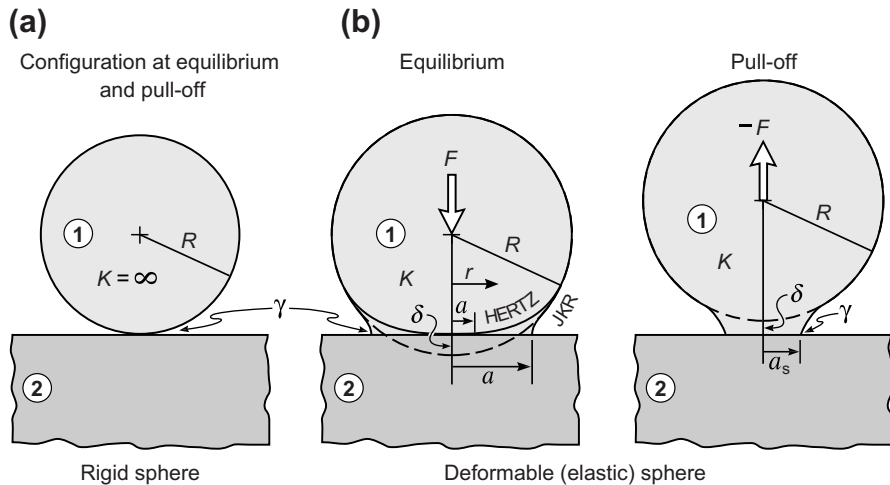


FIGURE 17.13 Hertz and JKR geometries of rigid and elastically deformable surfaces under external compressive (↓) or tensile (↑) loads F . (a) Rigid sphere on rigid surface. (b) Left: deformable (elastic) sphere on rigid surface in the absence (Hertz) and presence (JKR) of adhesion. (b) Right: elastic adhering sphere about to spontaneously separate from adhesive contact.

attempts at a rigorous theoretical treatment of the adhesion of elastic spheres is due to Johnson, Kendall and Roberts (1971), whose theory, the “JKR theory,” forms the basis of modern theories of “adhesion mechanics” or “contact mechanics” (Johnson et al., 1971; Johnson, 1996; Pollock, 1978; Barquins and Maugis, 1982; see also Fig. 12.5). In the JKR theory two spheres of radii R_1 and R_2 , elastic moduli K^5 and surface energy W_{12} per unit area, will flatten when pressed together under an external load or force, F , such that at mechanical equilibrium their contact area will have a radius a given by

$$a^3 = \frac{R}{K} \left[F + 3\pi RW \pm \sqrt{6\pi RWF + (3\pi RW)^2} \right] \quad (17.34a)$$

$$= \frac{R}{K} \left(\sqrt{\frac{3}{2}\pi RW} \pm \sqrt{F + \frac{3}{2}\pi RW} \right)^2, \quad (17.34b)$$

where $R = R_1 R_2 / (R_1 + R_2)$. For a sphere of radius R on a flat surface of the same material (Figure 17.13b) we may put $R_2 = \infty$, $R = R_1$ and $W = 2\gamma_{sv}$ in the above equation, so that under zero load ($F = 0$) the contact radius is finite and given by

$$a_0 = (6\pi R^2 W / K)^{1/3} = (12\pi R^2 \gamma_{sv} / K)^{1/3}. \quad (17.35)$$

The central displacement δ (see Figures 17.13b and c) is given by

$$\delta = \frac{a^2}{R} \left[1 - \frac{2}{3} \left(\frac{a_0}{a} \right)^{\frac{3}{2}} \right]. \quad (17.36)$$

⁵The elastic modulus K used here is related to E^* in Ken Johnson’s classic book *Contact Mechanics* (Johnson, 1996 edition) by $K = 4E^*/3$.

Figure 17.14 shows how the contact area (a) and displacement (b) vary with the load. The load-displacement curve in Figure 17.14b may be thought of as the force-distance profile of the JKR interaction potential. Thus, if the sphere is pulled by a constant force F , it will detach from the surface when F reaches the “adhesion force” (also separation, detachment or pull-off force) given by:

$$F_{\text{ad}} = -\frac{3}{2}\pi RW = -3\pi R\gamma_{sv} \quad (17.37)$$

and separation will occur abruptly at a contact radius of $a_s = a_0/4^{1/3} = 0.63a_0$. Thus, from a measurement of the adhesion force F_{ad} one may determine the surface or interfacial energy or, more generally, the work of adhesion W_{132} . These values may also be obtained by measuring (Fig. 12.5) then plotting the contact radius a or area πa^2 against the applied load F , and using Eq. (17.34) to determine W if R and K are known.

The load-displacement or force-distance relationship of a JKR interaction is a subtle one. If the externally applied force is constant (e.g., a gravitational “dead weight” or buoyancy force), then detachment will occur at $F = F_{\text{ad}}$ and $a = a_s$ as given above. But if it is applied by a spring or compliant element, as is common in SFAs, AFMs, indenters, machines, and devices, detachment will occur when the slope of the force-distance curve in Figure 17.14 equals that of the force-measuring spring (see Figure 12.3). In particular, since the finite stiffness of the materials is an inherent part of the JKR interaction, the force-distance curves show instabilities even when measured with an infinitely rigid spring: a “jump-in” instability on the way in (from I to II) and a “jump-out” instability on the way out (from V to VI), which in other systems are determined by the stiffness of the external supporting structure or force-measuring spring.

Another useful equation of the JKR theory gives the pressure or stress distribution within the contact circle as

$$P(x) = \frac{3Ka}{2\pi R}(1-x^2)^{\frac{1}{2}} - \left(\frac{3KW_{12}}{2\pi a}\right)^{\frac{1}{2}}(1-x^2)^{-\frac{1}{2}}, \quad (17.38)$$

where $x = r/a$ (see Figure 17.13b). Equation (17.38) shows that inside a JKR contact the pressure is positive (compressive) near the center but tensile toward the edge, where theoretically it diverges, becoming infinite as $r \rightarrow a$ ($x \rightarrow 1$). The theory also predicts an infinite strain at the contact boundary, with each surface bending infinitely sharply through 90°. Indeed, material failure in the form of plastic deformations and micro-cracks is often observed at the boundary of an adhesive junction, brought about – not because the two materials are being pulled apart—but because of the enormous *equilibrium* negative stresses at the rim. Figure 17.15 shows a computer simulation of a metallic nano-junction showing some plastic deformation at the boundary but also surprisingly good agreement with the overall (elastic) deformation predicted by the JKR theory.

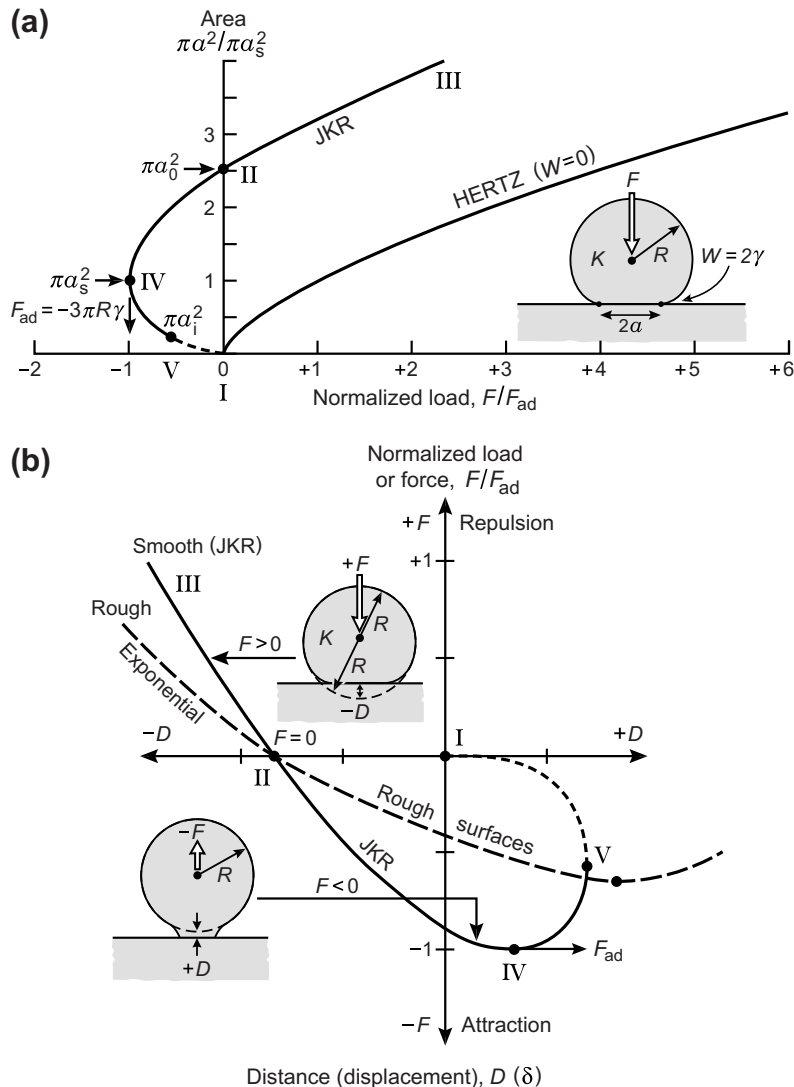


FIGURE 17.14 Need to add points I to V in both a and b. (a) Schematic “JKR plots” of the contact area versus load for adhering (JKR) and nonadhering (Hertzian) elastic spheres on a flat rigid surface, based on Eq. (17.34). (b) Effective JKR force-distance curve $F(D)$ for an elastic sphere on approach and separation from a rigid surface, where D is the same as the displacement δ in Figure 17.13b, given by Eq. (17.36), defined such that $D = \delta = 0$ at the point (I) when the sphere first touches the flat surface on approach (under no external force, $F = 0$) just before it spontaneously flattens and moves to point (II). Points (I) to (V) in (a) correspond to those in (b). The dashed curve in (b) illustrates the effect of roughness (Figure 17.17a).

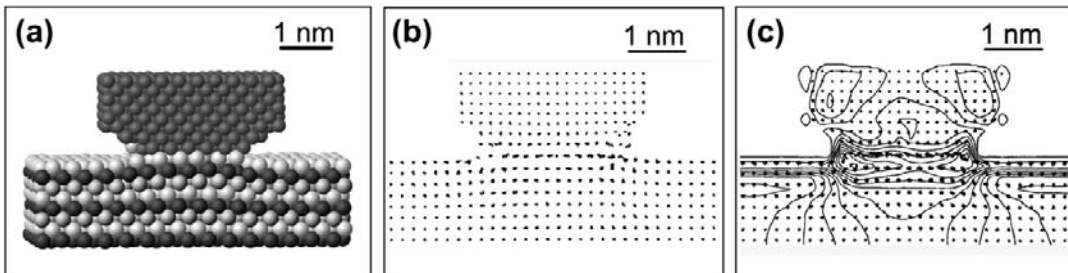


FIGURE 17.15 Simulation of an adhesive nano-junction between a nickel AFM tip and a (softer) gold surface just after the surfaces have jumped into contact, showing surprisingly good agreement with the JKR theory both for the mean positions of the atoms and the stress distribution, shown in (c). The image is a snapshot averaged over ~ 1 ps. The fuzziness of some of the atoms in (b) reflect their higher mobility in regions where they are less confined. [Adapted from Landman et al., (1990) *Science* 248, 454–461.]

It is interesting to note that, according to the JKR theory, a finite elastic modulus, K , while having an effect on the contact radius a or area πa^2 , has no effect on the adhesion force, Eq. (17.37)—an interesting and unexpected result that has nevertheless been verified experimentally (Merrill et al., 1991; Mangipudi et al., 1994). On the other hand, the total adhesion energy of two elastically deformable surfaces in equilibrium contact (at $F = 0$) is given by (Johnson, 1985)

$$E_0 = -0.6\pi a_0^2 W = -1.2\pi a_0^2 \gamma \quad (17.39)$$

which *does* depend on the modulus K via Eq. (17.35)—the lower the modulus K the higher the adhesion energy. This energy is 40% smaller than the purely surface energy needed to separate the two particles of equilibrium contact area πa_0^2 because of the additional positive (unfavorable) elastic energy stored in the system. Table 17.2 gives the K values of some common materials. Note the 11 orders of magnitude variation as we go from the hardest materials (e.g., diamond) to the softest (biological cells).

As elaborated in Section 17.2, the adhesion force provides information on the force that must be applied to spontaneously detach a particle from another—an essentially nonequilibrium process. In contrast, the energy tells us more about the equilibrium thermodynamic state of a system of particles, such as the probability of finding the particles dispersed or in contact (aggregated), and the mean lifetimes or spontaneous on- and off-rates of the particles in the absence of any external pulling force. Such issues become more important for smaller particles, such as nanoparticles, biological macromolecules and vesicles, where the interaction energies are often comparable to kT and where lifetimes fall in the range of “engineering interest” or “everyday experience” (Table 9.1): nanoseconds ($\sim 10^{-9}$ s) to many years ($\sim 10^{+9}$ s).⁶

⁶Since lifetimes are proportional to $e^{-E_0/kT}$ an order of magnitude change in E_0 —say, from $4kT$ to $40kT$ —will lead to a change in the lifetime of a bond or adhesive junction of more than 15 orders of magnitude.

Table 17.2 Young's Modulus ($Y = \text{Stress}/\text{Strain}$) of Some Common Materials

Nonbiological Materials (MPa) ^{a,b}	Biological Materials and Tissues (MPa) ^a
Weak gels	<1 ^c
Soft rubber	1–10
Hard rubber	100
Soft polymers (nylon, Teflon, PE)	500
Hard polymers (PMMA, PS, PVC)	3,000
Soft metals (Mg, Al), glass	40,000–80,000
Hard metals (bronze, steel, Ti)	100,000–200,000
SiC, WC, diamond	450,000–1,100,000
Brain matter	0.0005 (500 Pa)
Cells	0.001–0.1
Fluid lipid bilayers	50
Gel state bilayers	200
Soft, spongy bone	100
Protein crystals	100–1,000
Microtubules, virus capsids ^d	1,000
Hard bone, enamel	20,000–50,000

^a1 MPa = 10^6 N m⁻² = 145.0 psi (lb/in²).

^bSee Table 16.1 for full polymer names.

^cGels, aerogels, and foams can be as dense and stiff as a microstructured ceramic or so open and frail that they cannot hold their own weight ($K < 1$ kPa).

^dLayered materials composed of molecularly thin (2D) sheets have different Young's moduli in different directions. For example, graphene—the single molecule-thick sheet of single-walled microtubules and graphite—has a Young's modulus of 10^{12} Pa in the plane of the monolayer (Lee et al., 2008), which is the same as for diamond: the covalent C–C bonds are essentially the same in these three structures. In contrast, the Young's modulus of graphite in the direction normal to the layers, which are held together by van der Waals forces, is $\sim 10^{10}$ Pa. If one can talk about the Young's modulus in 1D, then an alkane chain also has a Young's modulus of $\sim 10^{12}$ Pa (Akhmatov, 1966).



Worked Example 17.7

Question: Two spherical metal particles of radius 0.1 mm, elastic modulus $K = 10^{11}$ N m⁻² and surface energy $\gamma = 1.0$ J m⁻² are in adhesive contact under zero external force. What is the compressive pressure between them at the center of the contact circle? The tensile strength of the material is 250 MPa. How far in from the boundary will the material fail? What will change with time if the particles are allowed to remain in contact indefinitely?

Answer: For two spheres of equal radii $R_1 = R_2 = 0.1$ mm, we may insert $R = 0.05$ mm and $W = 2\gamma = 2.0$ J m⁻² in the JKR equations. Since $F = 0$, the radius of the contact circle is $a = a_0 = (6\pi R^2 W/K)^{1/3} = 9.8 \times 10^{-7}$ m (0.98 μm). Using Eq. (17.38), the pressure at the center ($x = r/a = 0$) is therefore:

$$P(0) = (3Ka_0/2\pi R) - (3KW/2\pi a_0)^{1/2} = +(6K^2 W/\pi^2 R)^{1/3}. \quad (17.40)$$

Inserting the above values for K , W , and R we obtain a positive (compressive) pressure of $P(0) = 6.24 \times 10^8$ N m⁻² (~600 MPa or ~6,000 atm). With increasing radial distance r from the center the pressure changes from compressive to tensile at $x = 0.82$, and reaches a value equal to the tensile strength at $x = 0.88$, which corresponds to $r = 0.88a_0 = 0.88 \times 0.98 = 0.87$ μm, which is 110 nm from the boundary. Thus, tensile failure is expected to occur within this region, manifested by submicron cracks or plastic deformation (material flow) to relax the elastic stresses at the boundary.

At finite temperatures all materials are viscoelastic and will flow or creep, however slowly.⁷ Thus, with time, the adhering particles will deform to minimize the total surface and interfacial

energy. If the two metals are of the same material they will slowly coalesce (cold-weld): the interface will disappear and the two truncated spheres will slowly deform by bulk creep and/or surface diffusion⁸ until they form a single sphere or, if the materials are crystalline, a single faceted crystal. If the materials are different the interface will not disappear but the spheres will still deform until one material engulfs the other or they form a doublet, similar to two adhering soap bubbles. The final shapes of the particles will depend on the crystal structure and surface and interfacial energies of the different crystallographic faces of the two metals.

⁷See the fascinating *Pitch Drop Experiment* website, perhaps the longest ongoing experiment in history.

⁸Particle shape changes via surface diffusion occur much faster for smaller particles. Since the time to diffuse a distance x is proportional to x^2 , a (nano)particle with an initial radius of 10 nm will deform by surface diffusion 10^{10} times faster than one with a radius of 1 mm (see Section 11.4).



The Hertzian limit. For nonadhering surfaces ($W = 0, \gamma = 0$), as well as for very high loads ($L \gg L_{\text{ad}}$), all the equations of the JKR theory reduce to those of the earlier Hertz theory for nonadhering elastic spheres (Hertz, 1881; Johnson, 1985):

$$\text{Adhesion force and energy: } F_{\text{ad}} = 0, E_0 = 0 \quad (17.41\text{a})$$

$$\text{Contact radius: } a^3 = RF/K \quad (17.41\text{b})$$

$$\text{Displacement: } \delta = a^2/R = F/Ka \quad (17.41\text{c})$$

$$\text{Pressure: } P(x) = 3Ka(1 - x^2)^{\frac{1}{2}}/2\pi R = 3F(1 - x^2)^{\frac{1}{2}}/2\pi a^2. \quad (17.41\text{d})$$

The last equation shows that the pressure is zero at the edge ($x = 1, r = a$) and maximally compressive at the center ($x = r = 0$), where $P(0) = \frac{3}{2}F/\pi a^2$, which is 1.5 times the mean pressure across the contact circle. Unlike the situation in a JKR contact where the stress is (theoretically) infinite at the boundary, it is zero at the boundary of a Hertzian contact.

Apart from its breakdown within the last few nanometers of the bifurcation boundary, most of the equations of the JKR theory and all the equations of the Hertz theory have been experimentally tested for molecularly smooth surfaces and found to apply extremely well even at the submicron scale (see Figure 17.15 and Horn et al., 1987; Bhushan, 1995; Landman et al., 1990; Luedke and Landman, 1992; Carpick et al., 1996a, b; McGuigan et al., 2007).

In the following sections we shall investigate other common situations where the JKR theory breaks down or no longer applies. These involve systems where the surface energy changes with time, where the materials are viscoelastic (rather than elastic), and when surfaces are not smooth, all of which can give rise to hysteresis and time-dependent effects.

17.8 Adhesion Hysteresis

Just as in the case of a liquid droplet advancing or receding on a surface, a growing (advancing) and contracting (receding) contact area between two solid surfaces can also

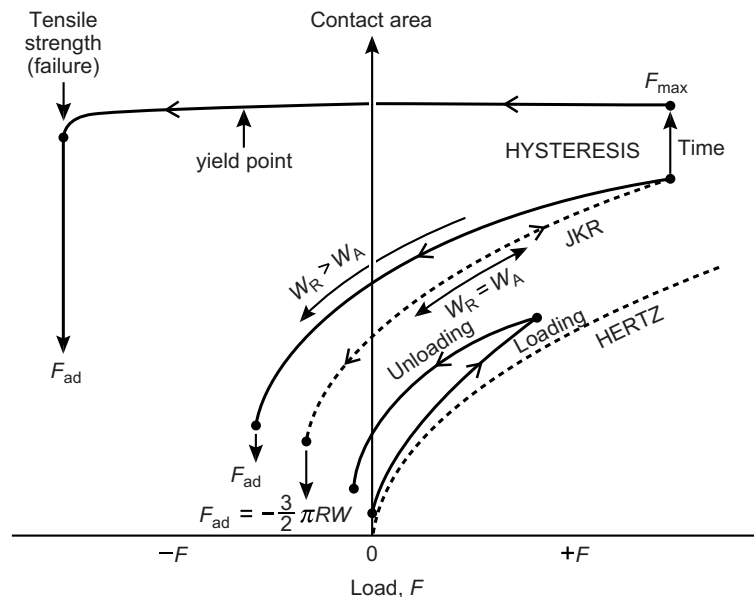


FIGURE 17.16 “JKR-plots” showing reversible and irreversible or “hysteretic” loading-unloading “JKR cycles” and “Hertz cycles.” Dashed curves show reversible paths; solid curves show hysteretic paths. In practice, W , R , and/or K can change with the contact time and loading-unloading rates. When these changes are large (compared to the initial values on loading) the unloading curve is no longer described by Eq. (17.34). For example, if two viscoelastic materials are allowed to remain in contact for a long time after loading, their contact area will increase even at constant load. They may also partially coalesce (increasing W), and if they are then separated quickly, the unloading path will correspond to that of a solid undergoing brittle or ductile failure, as shown in the top curve.

have different values for W or γ , referred to as W_A and W_R , giving rise to adhesion energy hysteresis (Figure 17.16) which is entirely analogous to contact angle hysteresis (Figure 17.11). With polymeric materials this effect arises because of chain interdigitations occurring across the contact interface that increase the effective contact area (or number of interfacial bonds) as a function of time (Figure 17.17b). With metals and inorganic solids such as silica, the effect can be due to slow coalescence or chemical sintering reactions (Figure 17.18). Both of these effects give rise to an adhesion energy on loading (coming on or advancing), W_A , that is less than the energy on unloading (coming off or receding), W_R , and thus to hysteresis effects and energy dissipation during a JKR loading-unloading cycle (see Figure 17.16).

Even the simplest adhesion processes are unlikely to be reversible, but involve energy dissipation,⁹ having profound effects for understanding why things actually stick together after they come into contact, and providing a link between adhesion and friction (Chapter 18). For example, if a body is attracted to a surface via a Lennard-Jones type

⁹As previously mentioned, “energy dissipation” is a misnomer, since energy is never dissipated in the sense of being “lost”; rather, it is converted into a different form. In this case, mechanical or kinetic energy is converted into heat.

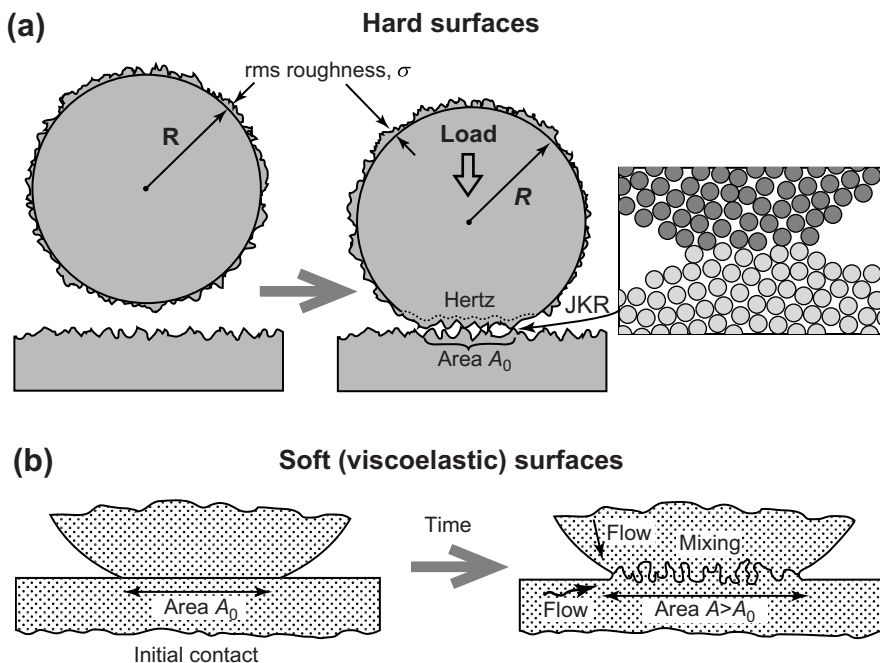


FIGURE 17.17 Examples of rough contacts and aging effects at hard and soft adhesion junctions. **(a)** Hard elastic materials exhibit lower adhesion forces than predicted by the JKR theory since the real (total molecular) area of contact is less than that predicted by the JKR theory, A_0 . Local junctions can be JKR-like, as in Figure 17.15, at the same time as the mean overall shape is closer to Hertzian. **(b)** The surfaces of soft and viscoelastic materials deform on coming into adhesive contact so that the real contact area A can exceed the JKR area, A_0 . The molecules of viscoelastic materials interpenetrate (mix) across the interface and flow with time resulting in time-dependent (aging) effects, manifested by a progressive increase in both the real (molecular) contact area and the apparent (projected) area and enhanced adhesion forces that can be as much as 10^4 higher than predicted by the JKR theory (which may be compared with the reduction in F_{ad} in the case of hard rough surfaces). If the two surfaces are different (immiscible), the interdigitation will saturate; if they are the same, it will continue to completion—that is, until there is no more interface between the now continuous material.

potential, one would think that if it is allowed to approach that surface it would stick to it. However, under ideal reversible conditions, it would simply bounce back at the same velocity ($-V$) as its original approach velocity ($+V$). If its kinetic or thermal energy is to change, some “energy transfer” or “internal friction” mechanism has to be operating (cf. Sections 2.10, 9.3 and Chapter 18), whereby the body ends up in the bottom of the potential well and the temperature of the surface, body, and surroundings has increased. Even the “jumps-into-contact,” as commonly seen and used to measure attractive forces, would not occur in the absence of an energy transfer mechanism. Since this issue forms the basis of understanding friction, further discussion on adhesion and surface energy hysteresis, and its intimate relationship to friction, is deferred to Chapter 18.

Another effect that gives rise to adhesion hysteresis in JKR plots is viscoelasticity of the material—that is, in K , which always has both a real (static elastic) and imaginary

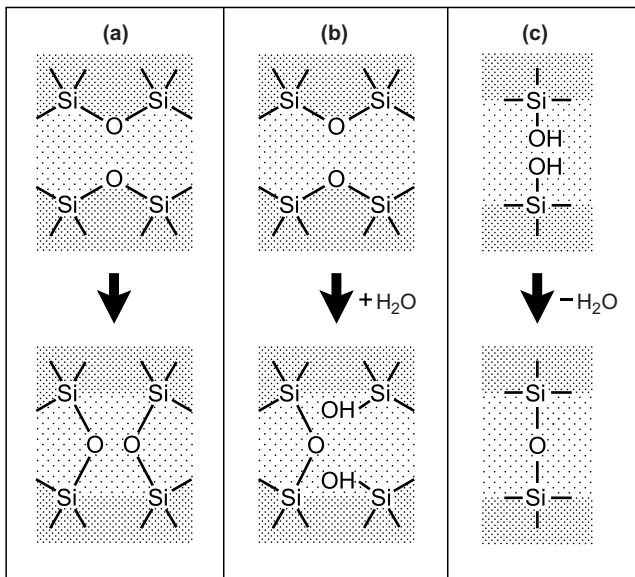


FIGURE 17.18 Slow chemical reactions can increase the adhesion of particles with time through the formation of covalent bonds. The examples show the sintering of silica or quartz (SiO_2) surfaces, in each case resulting in strong siloxane (Si-O-Si) across the interface, which eventually disappears. Such reactions may occur naturally (a), but they often involve the uptake of water from the atmosphere (b) or loss of water (c).

(dynamic energy dissipating) part, denoted by G' and G'' (Ferry, 1980).¹⁰ Viscoelastic junctions deform with the time they are left in contact (Figure 17.17b) and with the loading and unloading rates, both of which affect the JKR loading and unloading paths, as illustrated in Figure 17.16. It is often difficult to distinguish between an enhanced adhesion that is due to molecular interdigitation or sintering at the interface without an increase in the “apparent” (projected or macroscopic) contact area, and one due to bulk viscous flow that does increase the contact area.



Worked Example 17.8

Question: According to the JKR theory, the adhesion force needed to separate an elastic sphere from a flat surface is $\frac{3}{2}\pi RW$. Derive an approximate expression for the pull-off force when the materials are viscoelastic (as are many types of polymers) and where the separation is done very rapidly. What are the two adhesion forces for each of the above conditions when $R = 1 \text{ cm}$, $W = 100 \text{ mJ m}^{-2}$, and the “quasi-static” value of K is 100 MPa ?

Answer: In the limit of very rapid separation the surfaces do not have time to deform from their equilibrium shape (at $F = 0$) and therefore come apart while maintaining this geometry. Thus, the surfaces will separate not by peeling away from each other, which is implicit in a

¹⁰Strictly, K and G are different, being related by $G = Kf(\nu)$, where ν is the Poisson ratio whose typical value is 0.3.

JKR-type separation, but with the contact circle remaining in the planar geometry with a constant area of $\pi a_0^2 = \pi(6\pi R^2 W/K)^{2/3}$. The pull-off force for this type of separation is $F_{ad} = \pi a_0^2 W/D_0 = \pi(6\pi R^2 W^{5/2}/K)^{2/3}/D_0$, where $D_0 \approx 0.2$ nm is the effective range of the molecular forces. This adhesion force increases as K decreases even as the JKR force, $\frac{3}{2}\pi RW$, remains unchanged. Inserting the given values, we obtain $\frac{3}{2}\pi RW = 4.7$ mN, and $\pi a_0^2 W/D_0 = 24.0$ N, which is approximately 5,000 times larger.¹¹

¹¹It is for this reason that it is wise to peel away adhesive tape from paper slowly rather than quickly if you don't want to remove some of the paper as well.



Stick-slip adhesion. When two surfaces are separated from adhesive contact, either by peeling as in Figure 17.2b or through a JKR-type unloading path (Figure 17.16), even if the pulling force is increased at a steady rate the contact area may decrease in a “stick-slip” fashion. A similar effect can occur when a liquid boundary advances: sticking then slipping to the next sticking or “pinning” point, then slipping again. The sticking and slipping states are often described as the “static” and “kinetic” regimes of motion, but they actually represent regimes having finite but very different rates of motion—one very slow, the other very fast. The reasons for stick-slip adhesion and other types of forces showing “intermittent” behavior are explored in detail in the following chapter on friction and lubrication forces.

17.9 Adhesion of Rough and Textured Surfaces

The JKR and Hertz theories assume perfectly smooth surfaces. Most surfaces are rough or “textured,” and asperities as small as 1–2 nm can significantly lower their adhesion (Persson, 2000), but roughness can also increase the adhesion. Roughness and texture can come in many guises: surface asperities can be randomly rough or fractal, have uniform height but variable widths or uniform widths but variable heights, have a periodic pattern, and so on. For this reason there is as yet no general mathematical way of defining roughness (or surface topography) that covers all possible situations. In Section 17.5 we saw how texture can affect the wetting properties of surfaces, giving rise to very complex phenomena. Here we shall look at how different types of surface texture can affect their adhesion.

Figure 17.17a shows the deformations of a rough adhesive junction of RMS roughness σ . Locally, each asperity-asperity contact may be treated as a small JKR junction with a much smaller radius than the macroscopic particle radius R . The total adhesion force is therefore much smaller than the JKR adhesion force for the smooth surfaces ($\sigma = 0$). A schematic JKR force-distance curve for rough elastic particle surface is illustrated by the dashed line in Figure 17.14b. Recent experiments (Benz et al., 2006; Zappone et al., 2007) and modeling (Yang et al., 2008) suggest that the adhesion force decays exponentially with the roughness σ according to

$$F_{ad}(\sigma) = F_{ad}(0)e^{-\sigma/\sigma_0}, \quad (17.42)$$

where σ_0 is a constant and $F_{\text{ad}}(0)$ is the JKR adhesion force for smooth surfaces ($\sigma = 0$), and that the repulsive part becomes exponential rather than being described by Eqs (17.34) and (17.36). Since the net adhesion force of a rough junction is low, the mean overall (macroscopic) deformation of the junction closely follows a Hertzian shape even though the local micro- and nano-contacts are JKR-like (cf. Figure 17.17a). It has also been found that the repulsive parts of the loading-unloading curves of rough surfaces can be hysteretic, as illustrated in Figure 17.16. This effect can arise even when the surfaces and the asperities themselves are not deformed plastically (Section 17.10), and appears to be a consequence of having more contacts “on the way out” than “on the way in”—a situation that does not arise with a single asperity junction.

In contrast to the generally low adhesion of rough *elastic* surfaces, *viscoelastic* materials will flow once they come into adhesive contact so that the real contact area, or number of adhesive bonds at the interface, will increase with time until it *exceeds* the value for smooth surfaces, as illustrated in Figure 17.17b. In this case the initial roughness profile is completely lost soon after the surfaces come into contact, making the adhesion force larger rather than smaller than the ideal JKR value. In general, both molecular-level mixing and chemical bonding across the interface (interdigitation, interdiffusion, reptation, sintering, coalescence, cold welding), and bulk flow at the boundaries (viscous creep) can occur.

17.10 Plastic Deformations

The mechanical properties of viscoelastic and other types of nonelastic materials is outside the scope of this book, but the salient differences in the *contact mechanics* and *adhesion mechanics* of plastic and elastic solids will now be briefly described. At high loads, materials no longer deform elastically: deformations are no longer proportional to the applied load or reversible on releasing the load. The atoms or molecules “flow,” but the flow is unlike the flow in a liquid: it stops as soon as the load or stress is removed, as illustrated in Figures 17.19a and b for a compressive load. The *yield stress* (also *flow stress*) P_Y defines the transition or *yield point* from elastic to *plastic* (also *ductile*) behavior, where the strain no longer varies linearly with the applied pressure P —that is, where the elastic modulus is no longer constant (Figure 17.19c).

Complete *failure* or *fracture* of the material—for example, a material breaking into two parts on being stretched or sheared—occurs at the *failure* or *fracture strength* of the material. The yield stresses, and especially failure stresses, of nonelastic materials can be very different on compression and tension. For example, no material can be compressed beyond a strain of -1 ; however, some fibers may be stretched to many times their original length (strain $\gg 1$) before they finally snap. For these reasons the deformations (displacements), forces, and various yield points on loading (compression) and unloading (tension) are usually quite different, requiring these phenomena to be considered separately. Loading phenomena include indentation; unloading

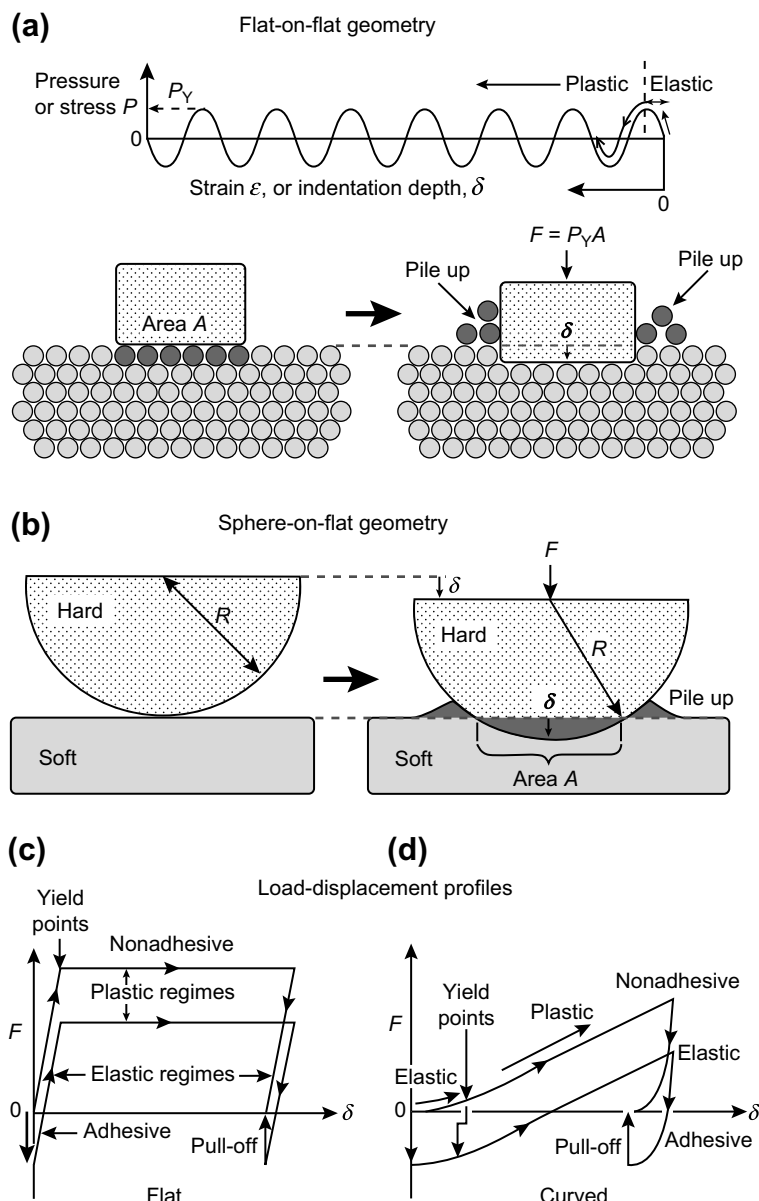


FIGURE 17.19 Deformations and associated forces of plastically deforming solids of different geometries. **(a)** Idealized pressure-distance curve when a crystal is compressed: after the initial elastic regime, atomic layers get pushed out, ideally one at a time, so long as the applied pressure is kept at the yield stress P_Y . The schematics show six extruded atoms that have piled up at the edges; these no longer contribute to the pressure. Panel **(c)** shows the load-displacement paths on loading and unloading for the flat-punch geometry for nonadhesive and adhesive contacts. Note that on unloading, the materials relax elastically before finally detaching (pull-off). Panels **(b)** and **(d)** show the same features for the sphere-on-flat geometry or between any two curved surfaces.

phenomena include extensive stretching or abrupt cracking failure (for brittle materials), and most of these processes involve nonequilibrium time-dependent “aging effects” such as creep.

Bodies under compression. Figure 17.19 illustrates the origin of plasticity, the transition from elastic to plastic flow, and why the “flow” stops or relaxes when the compressive stress is removed. The load-displacement curves are hysteretic (irreversible), which is quite different from those of elastically deforming bodies, described by the JKR theory (compare Figures 17.19c and d with Figure 17.14b). Two common geometries used in compression or indentation measurements are the “flat punch” and “round punch” geometries, where the punch is hard and is assumed not to deform as the softer material plastically deforms.

As shown in Figure 17.19c, for the *flat punch* geometry the elastic regime, where $P(\delta) \propto \delta$, is followed by the plastic regime, where $P = F/A = P_Y = \text{constant}$. The corresponding forces for the *round punch* geometry can be readily determined from the flat punch equations using the Derjaguin approximation, Eq. (11.16). Thus, for the elastic regime we obtain $F(\delta) = 2\pi R E(\delta) = 2\pi R \int P(\delta) d\delta \propto 2\pi R \delta^2$, and for the plastic regime we obtain $F(\delta) = 2\pi R \int P_Y d\delta = 2\pi R P_Y \delta + C$, where C is a constant determined by the extent of the elastic regime (see Problem 17.22). Thus, in the initial “elastic” regime we expect $F \propto \delta^2$ while in the plastic regime $F \propto \delta$, as illustrated in Figure 17.19d, and seen in most indentation measurements (Johnson, 1985; Oliver and Pharr, 1992). More recent nano-indentation measurements have revealed some of the discreteness (stick-slip) effects expected at the atomic scale (Cross et al., 2006).

For small deformations ($\delta \ll R$) and constant R , the chord theorem, Eq. (10.4), allows us to further simplify the above equation to give, in the plastic regime:

$$F(\delta) = 2\pi R P_Y \delta + \text{const.} = P_Y A + \text{const.} \quad (17.43a)$$

or, for small C ,

$$P_Y = F(\delta)/A. \quad (17.43b)$$

Thus, the permanently deformed area A is proportional to the load only—that is, independent of the indentation depth δ or radius R of the punch or ball. This relationship forms the basis of various methods to measure the *hardness* H of materials, which is defined by an equation similar to Eq. (17.43b)—for example, $H \propto \text{load}/\text{area}$ —where the area may be the actual or projected surface area of the indentation and where H is proportional to, but not the same as, the elastic limit or yield stress (Maugis & Pollock, 1984).

The loading-unloading paths of plastically deforming bodies are hysteretic, but in a different way from the hysteresis observed with rough elastic surfaces. In the latter case, the hysteresis is reversible on repeated loading-unloading cycles, while in the former it is not.

Bodies under tension. The situation of bodies under tension is much more complex. The unloading curves of Figures 17.19c and d, showing abrupt JKR-like detachment (pull-off) assume that the contact interface remains intact—that is, that the two surfaces have

not merged or coalesced. When there is full or partial coalescence, the junction ruptures or fractures, but the rupture mechanism depends on the geometry, the viscoelastic properties of the material, and the separation rate or force, and can involve stringing, fibrillation, Saffman-Taylor fingering and internal cavitation. The effective adhesion forces and energies can be 3 to 4 orders of magnitude higher than the ideal values for elastic solids—for example, $F_{\text{ad}} = 3\pi R\gamma_S$ for a sphere on flat geometry.

17.11 Capillary Forces

The mechanical and adhesive properties of many substances are very sensitive to the presence of even trace amounts of “condensable” vapors in the atmosphere—that is, vapors whose liquids form a small contact angle with the surface. For example, the stability of colloids in organic liquids, the adhesion of powders and sand (granular materials), the seismic properties of rocks, and the swelling of certain polymers into gels are markedly dependent on the relative humidity. All these effects are due in part to the *capillary condensation* of water at surface contact sites (e.g., in cracks, pores and hydrophilic molecular groups), which, as we shall see, can have a profound effect on the adhesion strength¹² of junctions, both large and small.

Liquids that wet or have a small contact angle on surfaces will spontaneously condense from vapor into cracks and pores (Figure 17.20a, b). At thermodynamic equilibrium the curvature of a concave meniscus (or convex droplet) surface ($1/r_1 + 1/r_2$) is related to the relative vapor pressure (relative humidity for water) by the Kelvin equation. The Kelvin equation can be derived from the general equation, Eq. (13.26), relating pressure to the relative vapor pressure: $P = (kT/\nu)\log(p/p_{\text{sat}}) = (RT/V)\log(p/p_{\text{sat}})$, where ν and V are the molecular and molar volumes, respectively, p the vapor pressure and p_{sat} the saturated vapor pressure. Equating P with the Laplace pressure, Eq. (17.15), we immediately obtain the *Kelvin equation*

$$r_K = \left(\frac{1}{r_1} + \frac{1}{r_2} \right)^{-1} = \frac{\gamma V}{RT \log(p/p_{\text{sat}})}, \quad (17.44)$$

where r_K is the *Kelvin radius*. For water at 20°C, $\gamma V/RT = 0.54$ nm. Thus, for a spherical concave water meniscus (putting $r_1 = r_2 = r$), we find $r_K = \infty$ at $p/p_{\text{sat}} = 1.0$ (saturated vapor), $r_K \approx -5.1$ nm at $p/p_{\text{sat}} = 0.9$, $r_K \approx -0.8$ nm at $p/p_{\text{sat}} = 0.5$, and $r_K \approx -0.23$ nm at $p/p_{\text{sat}} = 0.1$ (10% relative humidity).

What is the effect of a liquid condensate on the adhesion force between a macroscopic sphere and a surface (Figure 17.20c)? A simple derivation is to consider the *Laplace pressure* in the liquid: $P_L = \gamma_L (1/r_1 + 1/r_2) \approx \gamma_L/r_1$, since $r_2 \gg r_1$. The Laplace pressure acts on an area $\pi x^2 \approx 2\pi R d$ between the two surfaces, thus pulling them together with

¹²The commonly used term *adhesion strength*, like *bond strength*, is not recommended, since it is not clear whether it refers to the force or energy of the contact, which, as discussed in Sect. 17.2, are qualitatively different both in their units and the effects they give rise to.

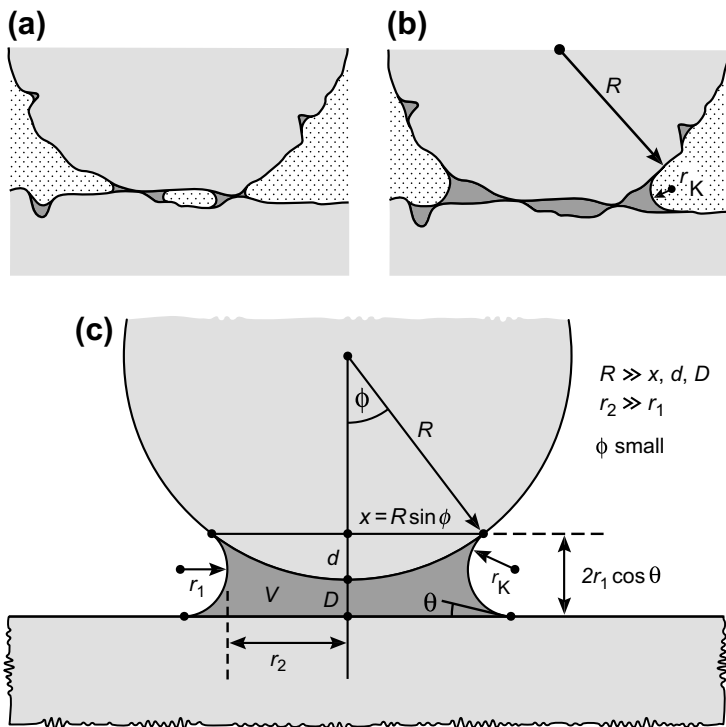


FIGURE 17.20 (a) and (b). Capillary condensation of liquids at contact junctions and in pores and cracks. The concave menisci formed give rise to a tensile Laplace pressure within the liquid which gets transmitted to the surrounding solid(s) causing particles to attract each other and pores and cracks to close. However, if the direct inter-surface force is repulsive in the liquid, the short range force will be repulsive which can cause microcracks to open rather than close. (c) Geometry of capillary bridge between a sphere and a flat. If the condensate is in thermodynamic equilibrium with the surrounding vapor, its mean radius of curvature is the Kelvin radius. In saturated vapor, condensation will continue until the liquid surface has zero mean curvature ($r_2 = -r_1$ everywhere); such a surface can be flat (planar) or a minimal surface (see Problem 17.19).

a force $F \approx -2\pi R d \gamma_L / r_1$. For small ϕ , $(d + D) \approx 2r_1 \cos \theta$, and we can express the Laplace pressure contribution to the adhesion force as

$$F(D) = -4\pi R \gamma_L \cos \theta \left(1 - \frac{D}{2r_1 \cos \theta} \right), \quad (17.45a)$$

or, equivalently,

$$F(D) = -\frac{4\pi R \gamma_L \cos \theta}{(1 + D/d)}. \quad (17.45b)$$

The additional force arising from the resolved normal surface tension around the circumference, $\sim 2\pi x \gamma_L \sin \theta$, is always small compared to the Laplace pressure contribution except for $\theta \approx 90^\circ$ when $\cos \theta \approx 0$ and $\sin \theta \approx 1$.

Worked Example 17.9

Question: A cylindrical liquid bridge of constant volume V and radius R is held by capillary forces between two hydrophobic surfaces (where $\theta = 90^\circ$) as shown in Figure 17.21. Calculate the normal force F between the two walls using two different methods: (1) by resolving forces, and (2) by considering the surface energies γ_L , γ_S , and γ_{SL} of the various surfaces and interfaces. You should, of course, arrive at the same result in each case. Ignore gravitational effects.

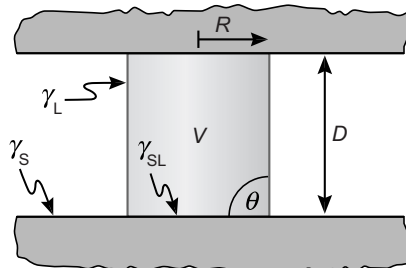


FIGURE 17.21 Liquid capillary bridge of constant volume $V = \pi R^2 D$ and contact angle $\theta = 90^\circ$. On increasing D liquid bridges become unstable and snap at the critical separation $D = D_c = 2\pi R = (4\pi V)^{1/3} \propto V^{1/3}$.

Answer: (1) Resolving the forces in the normal direction, we first have the compressive Laplace pressure acting on the surfaces by the liquid, giving rise to a (repulsive) force between them of $P_L \times \text{area} = (\gamma_L/R) \times (\pi R^2) = +\pi R \gamma_L$. The normally resolved surface tension force of $\gamma_L \cos \theta = \gamma_L$ per unit length acting along the circumference of length $2\pi R$ gives rise to an additional force at the boundary of $-2\pi R \gamma_L$. The total force is therefore

$$F(D) = -\pi R \gamma_L = -\gamma_L \sqrt{\pi V/D} \quad (\text{since } V = \pi R^2 D = \text{constant}). \quad (17.46)$$

Thus, the net force is attractive—pulling the surfaces together and varying as $1/D^{1/2}$.

(2) Since the contact angle is $\theta = 90^\circ$, the Young Equation, Eq. 17.24, tells us that $\gamma_{SL} = \gamma_S$. If A is the (constant) *total* area of each flat surface, the total surface energy of the system is $E = 2\pi RD\gamma_L + 2\pi R^2\gamma_{SL} + (2A - 2\pi R^2)\gamma_S = 2\pi RD\gamma_L + 2A\gamma_S$. Expressing E in terms of D and the constant volume V gives, $E = 2\gamma_L \sqrt{\pi VD} + 2A\gamma_S$, which on differentiating with respect to D gives Eq. (17.46).

Equation 17.45 shows that for a sphere and a flat surface the maximum capillary force occurs at contact, when $D = 0$, and is given by

$$F(D = 0) = F_{ad} = 4\pi R \gamma_L \cos \theta. \quad (17.47)$$

For surfaces with different contact angles, θ_1 and θ_2 , it is easy to show that the adhesion force is

$$F_{ad} = 2\pi R \gamma_L (\cos \theta_1 + \cos \theta_2). \quad (17.48)$$

The two forms of Eq. 17.45, although equivalent, apply to two quite different situations where the capillary forces vary differently with D even though the values at $D = 0$ are the same. The two situations correspond to those of thermodynamic equilibrium and constant liquid volume. In the first, the liquid bridge is at equilibrium with the vapor so that the mean curvature of the meniscus remains constant as D changes (via evaporation or condensation) and equal to the Kelvin radius, r_K —that is, $r_1 \approx r_K$ in Figure 17.20c. Since θ is also constant, Eq. (17.45a) applies, showing that the force-distance function is a straight line that cuts the $F = 0$ axis at $D = 2r_K \cos \theta$, at which separation the bridge finally disappears (see Problem 17.10). In the second scenario, the liquid is “involatile” or effectively of constant volume during the separation of the surfaces. Equation 17.45b now becomes more convenient, where $(d + D)$ is no longer constant but a function of V, R, D and θ . The attractive force is now longer-ranged, and at some separation D (proportional to $V^{1/3}$) a spontaneous Raleigh-like snap-off occurs (see Problem 17.2 and Willett et al., 2000).

A rigorous analysis of the meniscus shape and capillary force of even the simplest geometry is actually quite complicated. First, the liquid surface must have the same Laplace pressure and therefore the same mean curvature ($1/r_1 + 1/r_2$) throughout, and so in the case of the liquid neck just discussed cannot be circular, as indicated by the concave radius r_1 in Figure 17.20c, since the orthogonal radius r_2 cannot also be constant. Surfaces of constant mean curvature everywhere are known as *minimal surfaces*. The shape of the meniscus must also satisfy the boundary condition(s) of constant contact angle(s) at all points on the two surface(s) irrespective of their geometry.¹³ In the case of the capillary bridges between spheres and/or planar surfaces, more rigorous expressions, valid for large ϕ and different contact angles on each surface, have been derived by Orr et al., (1975).

One other important parameter must be included in the above expressions. This is the direct solid-solid contact adhesion force inside the liquid annulus, Eq (17.33). For a sphere and a flat surface the final result is therefore

$$F_{\text{ad}} = 4\pi R(\gamma_L \cos \theta + \gamma_{SL}) = 4\pi R\gamma_{SV}. \quad (17.49)$$

Fogden and White (1990) and Maugis and Gauthier-Manual (1994) considered the effects of JKR-type deformations on capillary forces and concluded that for strong solid-solid adhesion Eq. (17.49) becomes: $F_{\text{ad}} = 4\pi R(\gamma_L \cos \theta + 0.75\gamma_{SL})$, while if the meniscus radius is very small it becomes $F_{\text{ad}} = 3\pi R(\gamma_L \cos \theta + \gamma_{SL})$. Note, however, that if the solid-solid interaction in the liquid is short-range repulsive, this additional contribution will be negative and D will be finite at “contact equilibrium” (see Problem 17.13).

For two spheres, R is replaced by $(1/R_1 + 1/R_2)^{-1}$ in all the above equations.

Equations (17.47)–(17.49) for the adhesion forces are independent of the meniscus radius r_1 so that it is of interest to establish below what radius, relative vapor pressure or

¹³Although this has never been rigorously proved to the author.

RH, these equations break down—that is, when does γ_{SV} become γ_S ? McFarlane and Tabor (1950) verified that the adhesion force between glass spheres and a flat glass surface in close to saturated vapors of water, glycerol, decane, octane, alcohol, benzene, and aniline are all given by $F = 4\pi R\gamma_L \cos \theta$ to within a few percentage points. Fisher and Israelachvili (1981) measured the adhesion forces between curved mica surfaces in various vapors such as cyclohexane and benzene and found that $F = 4\pi R\gamma_L \cos \theta$ is already valid once the relative vapor pressures exceed 0.1–0.2, corresponding to meniscus radii of only ~0.5 nm—that is, about the size of the molecules. However, for water, a larger radius of ~2 nm appears to be needed before Eq. (17.47) is satisfied (Christenson, 1988b; Hirz et al., 1992). These results support the analysis in Sect. 17.3 that for molecules that interact via a simple Lennard-Jones (attractive van der Waals) pair-potential, their bulk surface energy is already manifest at very small curvatures.

Since real particle surfaces are often rough their adhesion in vapor is not always given by Eq. (17.47) or (17.49). For example, the adhesion of dry sand particles is very small, and even when slightly moist the adhesion is not much different since the condensed water is only bridging small asperities (Figure 17.20a). However, once r_K exceeds the asperity size but is still less than the particle radius R (Figure 17.20b), the adhesion force attains its full strength of $F = 4\pi R\gamma_L \cos \theta$ as found by McFarlane and Tabor (1950). However, when r_K exceeds R —that is, when the particles are effectively immersed in excess liquid—the adhesion is often again very low because the capillary term disappears. It is for this reason that one can only build sandcastles with moist sand, but not with dry or completely wet sand (R. Pashley, unpublished results).

Capillary condensation also occurs when water condenses from a solvent in which it is only sparingly soluble—for example, from hydrocarbon solvents where the solubility is usually below 100 ppm. In such circumstances the presence of even 20 ppm (i.e., 20–40% of saturation) can lead to a dramatic increase in the adhesion of hydrophilic colloidal particles. Indeed, it has long been known that trace amounts of water can have a dramatic effect on colloidal stability (Bloomquist and Shutt, 1940; Parfitt and Peacock, 1978), and surfactant association (Eicke, 1980) in nonpolar organic solvents. The enhanced agglomeration of metal ores and coal particles in oils by addition of water forms the basis of several industrial separation and extraction processes (Henry et al., 1980). Christenson (1983, 1985b) found that in the presence of small amounts (<100 ppm) of water the adhesion force between mica surfaces in benzene, octane, cyclohexane, and the liquid OMCTS is given by Eq. (17.47) to within 20% with γ_L replaced by the liquid-liquid interfacial energy γ_{12} . The enhanced adhesion in such systems arises because γ_{12} is typically 35–50 mJ m⁻² (see Table 17.1)—much higher than the solid-liquid interfacial energies in the anhydrous liquids.

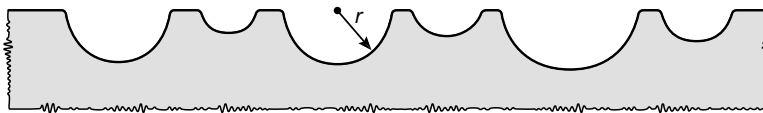
Finally, an interesting phenomenon occurs when two hydrophobic particles interact in water. If the contact angle exceeds 90° the above equations predict that a *vapor* cavity should “capillary condense” between the two surfaces, again resulting in a strongly adhesive force determined by the high value of the hydrophobic-water interfacial tension. This effect has been observed by Christenson et al., (1989) and Meyer et al., (2006).

PROBLEMS AND DISCUSSION TOPICS

- 17.1** In Worked Example 17.9 and Figure 17.21, the force between the two surfaces is given by the sum of the Laplace Pressure and resolved surface tension force. However, when calculating the height of rise h of a liquid in a capillary tube of radius r (Figure 1.3a), one considers either the Laplace Pressure ($2\gamma_L/R = 2\gamma_L/r \cos^{-1}\theta$ acting on area πr^2) or the resolved surface tension contribution ($\gamma_L \cos \theta$ acting along the circumference $2\pi r$), but not both. Each of these give the same result, viz. $\rho gh = 2\pi\gamma_L \cos \theta/r$, but only one actually contributes. Resolve this apparent paradox.
- 17.2*** (i) With increasing length D the liquid bridge in Figure 17.21 becomes *mechanically* unstable, becoming unduloid and eventually breaking up into two hemispheres (cf. Figure 1.3c). At what value of D will this occur? (ii) Show that the value of D at which the cylinder becomes *thermodynamically* unstable is smaller than this value, and discuss how these two instabilities manifest themselves in practice. Will this second type of instability lead to one, two, or more hemispheres? Would you expect similar instabilities to occur for a thin liquid film adsorbed on (iii) a cylinder and (iv) a flat surface? [Answer: (i) $D = 2\pi R = (4\pi V)^{1/3}$, where V is the (constant) volume of the liquid bridge.¹⁴ (ii) One hemisphere. (iii) Yes.]
- 17.3** Estimate the local tensile pressure acting normal to a solid surface at the point where a macroscopic liquid droplet of water meets the surface (see Fig. 17.12c). What effects could this have on the surface both at the microscopic and molecular levels? [Answer: $\gamma_L/\sigma \approx 50 \text{ mJ m}^{-2}/0.5 \text{ nm} \approx 100 \text{ MPa} \approx 1,000 \text{ atm.}$]
- 17.4** Why does the 3D pressure of a gas act to *increase* its volume but the 2D pressure of a liquid surface (the surface tension) acts to *decrease* the area?
- 17.5** Compounds 1 and 2 are both nonpolar liquids and interact only via van der Waals dispersion forces. The Hamaker constant of 1 is larger than that of 2 ($A_1 > A_2$). A small amount of 1 (the solute) is completely dissolved in 2 (the solvent).
- (i) Will the concentration of 1 below the surface of the solution be the same, greater than, or less than the bulk concentration? If there is a difference, estimate the distance range over which the concentration will be affected.
 - (ii) Will the surface tension of the solution be the same, greater than, or less than the value for the pure solvent 2?
 - (iii) What if $A_1 < A_2$?
 - (iv) How do your conclusions relate to the “Gibbs Adsorption isotherm”? [Answer: (i) Less than. (ii) Greater than. (iii) Greater than, less than.]
- 17.6** When gas dissolves in a liquid, does the surface tension increase or decrease? [Answer: Decrease.]

¹⁴This is known as the Raleigh Instability. If you think it is a difficult problem, it probably won't be any consolation to you to know that Joseph Plateau solved it more than 150 years ago, and he was blind.

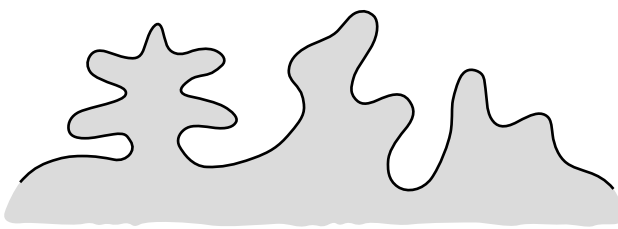
- 17.7** The 13-atom cluster of Figure 17.4 has 12 identically coordinated atoms in the 1st layer around the central atom. The second and subsequent layers build up to form quasi-spherical HCP clusters. (i) How many van der Waals “bonds” does each atom in the 1st layer make with its nearest neighbors? (ii) How many unsaturated bonds are there per atom in the 1st layer? (iii) How many bonds does each atom in the 1st layer make with those in the 2nd layer? (iv) What is the total number of bonds between the 1st and 2nd layers? (v) How many atoms form the 2nd layer? (vi) What is the average number of bonds that an atom in the 2nd layer makes with those in the first layer? (vii) Does each atom of the 2nd layer make the same number of bonds with those in the 1st layer? [Answer: (i) 5. (ii) 7. (iii) 7. (iv) 42. (v) 84. (vi) $84/42 = 2$. (vii) No. Six bond to 4 atoms, 24 bond to two atoms, and 12 bond to one atom, giving an average of exactly two per atom.¹⁵]
- 17.8** A hydrophobic surface on which water makes a 90° contact angle has a small circular area of radius r that is hydrophilic with a contact angle of 0° . A syringe slowly ejects water to the center of the hydrophilic circle. Describe, with sketches, how the contact angle changes as the water volume increases from zero to $\frac{4}{3}\pi r^3$, and then decreases again to zero. Repeat your analysis for a surface where the hydrophobic and hydrophilic areas are interchanged. Ignore gravitational effects.
- 17.9*** A wavy surface has shallow depressions that can be approximated by hemispherical cavities of various radii from $r = 5 \text{ mm}$ to $r = \infty$ (planar) as shown in the figure below. (i) A small liquid droplet of volume 2 mm^3 and intrinsic contact angle $\theta_0 = 15^\circ$ (on a planar surface) is placed on the surface. Assuming that the droplet can move about to find its location of lowest energy, without changing its volume, what radius cavity will it settle in? (ii) If the droplet can break up into smaller droplets, each settling in a different cavity, could this lower the total surface energy of the system? (iii) When the surface is exposed to saturated vapor, allowing for condensation to occur, sketch the final equilibrium state of the system. Identify both metastable and stable states. Ignore gravitational effects. [Answer: (i) In a cavity of radius $r = 8.2 \text{ mm}$.]



- 17.10** Derive Eq. (17.45) from the variation of the total surface energy of the system W with distance D , $F = -dW/dD$, assuming constant liquid volume V and small ϕ in Figure 17.20c.

¹⁵It is interesting to note that the 13-atom cluster exposes six 4-bond and eight 3-bond adsorption sites (see Figure 17.4), yet none of the 3-bond sites end up being occupied in the complete 55-atom cluster.

- 17.11*** Derive Eq. (17.45a) by differentiating the total energy of the system with respect to D for the case of constant chemical potential of the liquid and vapor molecules—that is, assuming thermodynamic equilibrium with the vapor reservoir, so that $r_1 = r_K$ at all separations D . [Hint: Since evaporation or condensation must occur as D changes, the free energy associated with this must be included in your energy balance (as a PdV term).]
- 17.12** The rough surface shown below is exposed to saturated vapor of a liquid that subtends a small contact angle ($\theta \approx 10^\circ$) on the surface. Draw the different stages of capillary condensation from the initial condensate to the final thermodynamic equilibrium configuration of the liquid-vapor interface, noting the mechanically stable, unstable and metastable states on the way. Repeat for when a liquid droplet is placed on the surface (note that the final equilibrium state should be the same). Repeat both of the above for a liquid of contact angle $\theta = 90^\circ$. Ignore gravitational forces. [Hint: Consider the Laplace pressure driving the meniscus to always move (by condensation or evaporation) in the concave direction.]



- 17.13** Water condenses at the junction of two spheres (glass marbles) of radius 1 cm. The contact angle is zero at both surfaces, the RH is 0.9 (90%), and the temperature is 20°C. What is the adhesion force in the case where (i) $\gamma_{SL} = 20 \text{ mJ m}^{-2}$ and (ii) $\gamma_{SL} = 0$, and there is a hard-wall repulsive hydration force at $D = 2.0 \text{ nm}$? [Answer to (ii): $3.7 \times 10^{-3} \text{ N}$ (~0.37 gm).]
- 17.14** For a microscopic solid sphere, would you expect its (i) density and (ii) boiling point to be larger or smaller than the bulk material?
- 17.15** A sphere having a density greater than water is carefully placed on a water surface where it is seen to float. Its contact angle with water is 90°. Sketch the geometry of the water surface around the sphere and explain how it is supported given that at the three-phase border all the forces are balanced by the Young equation.
- 17.16*** Two bodies floating on the surface of a denser liquid have contact angles as shown in Figure 17.22. (i) In each case, determine whether the force between the bodies due to surface tension effects is attractive or repulsive. (ii) Sketch the configuration of the bodies in the absence of gravity, where the liquid volume is large and its surface effectively flat. [Answer to (i): (a) Attractive, (b) attractive, (c) repulsive.]

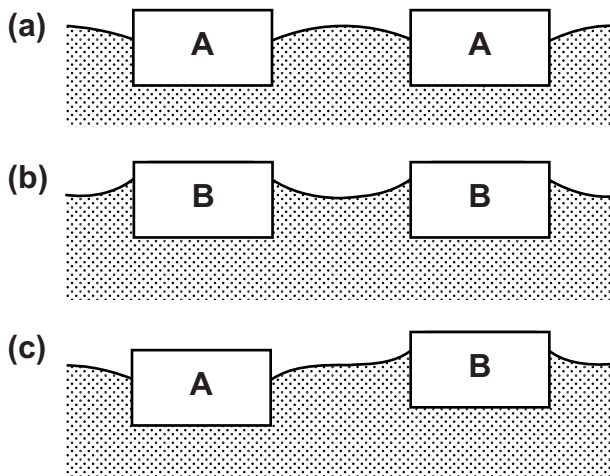


FIGURE 17.22

- 17.17** Two smooth cylindrical fibers of radii R_1 and R_2 are brought into contact with their axes at an angle α in an atmosphere of water vapor. Show that the adhesive capillary force between them is constant over a large range of relative humidity and is given by

$$F_{\text{ad}} = -4\pi\sqrt{R_1 R_2}(\gamma_{\text{SL}} + \gamma_{\text{LV}} \cos \theta)/\sin \alpha. \quad (17.50)$$

Would you expect Eq. (17.50) to overestimate or underestimate the adhesion at (i) low humidities ($\text{RH} < 50\%$), (ii) high humidities ($\text{RH} > 99\%$), and (iii) small fiber radii ($R < 1 \mu\text{m}$). What happens when $\alpha = 0^\circ$?

- 17.18** Prove that for two dissimilar particles—say, two spheres—if one has a contact angle θ the other must have a contact angle less than $(180 - \theta)$ for the capillary force between them to be attractive. What occurs in practice if the capillary force is predicted to be repulsive?
- 17.19*** Two plane parallel surfaces or spheres as in Figure 17.23 are connected by a liquid bridge that is axially symmetric around the vertical z axis. The bridge is in thermodynamic equilibrium with the surrounding saturated vapor ($\text{RH} = 100\%$). Show that the profile of the liquid-vapor interface is a catenary described by $r(z) = r_0 \cosh(z/r_0) = r_0(e^{+z/r_0} + e^{-z/r_0})/2$, where r_0 is the radius of the neck at its

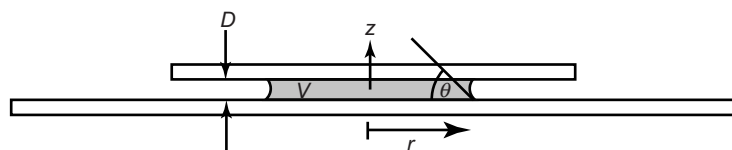


FIGURE 17.23

narrowest point (r_2 in Figure 17.20c). For two plane parallel surfaces (or $r_2 \ll R$) show that the equilibrium force-law $F(D)$ is

$$F(D) = -\pi D \gamma_L / \arctan h(\cos \theta), \quad (17.51)$$

where θ is the contact angle. What does it mean that the force is infinite when $\theta = 90^\circ$?

- 17.20** Why does the capillary force contribution to the total adhesion force between two rough surfaces often increase and then decrease as the RH increases from 0 to saturation (RH = 100%)?
- 17.21** A flat surface is brought down onto the flat end of a vertical elastic cylindrical pillar of length L and unit cross-sectional area, to which it adheres with surface energy W . The pillar is attached to a rigid substrate at its lower end. The flat surface is now retracted until the pillar detaches from it when it has stretched by ΔL . If the size of the molecules and effective range of the adhesion forces is σ , (i) what is the force on the surface (and pillar) at the moment of detachment, and (ii) how much energy has been expended by the surface to bring about the separation? If your answer to (ii) is greater than W , where has the excess energy gone to?
- 17.22** An assembly of nonadhering spheres in a square lattice, with 6-nearest neighbors per sphere, as shown in Figure 17.24, is subjected to a mean compressive pressure P . If K is the bulk elastic modulus of the material of the spheres (i) what is the effective modulus of the “granular material,” defined by $K_{\text{eff}} = \text{stress}/\text{strain} = P/(\Delta L/L)$, and (ii) what is the maximum pressure p_{max} experienced by the spheres—that is, at their points of contact with each other? If the particles are made of glass ($K = 50$ GPa), what is the maximum pressure actually felt by the particles when the mean applied pressure is $P = 1$ GPa? What do your results

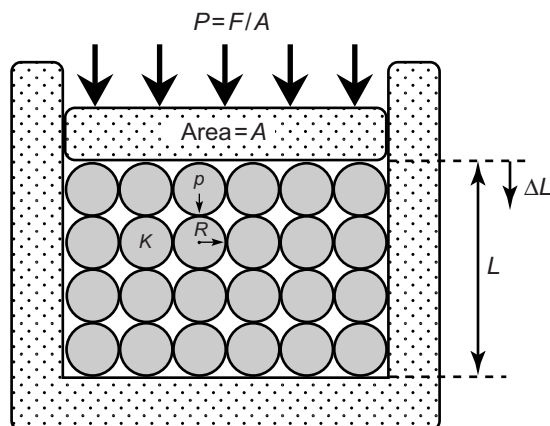


FIGURE 17.24

imply for how one thinks about the “elasticity” and yield stress of granular materials on compression? [Answer: (i) For this (Herzian) geometry, ΔL is not a linear function of the load F . Thus, K_{eff} is not a constant even when the spheres themselves deform elastically. (ii) $p_{\text{max}} = 6K^{2/3}P^{1/3}/\pi^{5/3} = 0.9K^{2/3}P^{1/3} = 12 \text{ GPa}$ (12 times the applied pressure).]

- 17.23*** A 6-sided right-angled cuboid crystal has sides of length a , b , and c in the x , y , and z directions, and the three pairs of faces have surface energies γ_a , γ_b , and γ_c , respectively. Show that the lowest total surface energy of a crystal, assumed to be of fixed volume $V = abc$, is when all six faces have the same surface energy—that is, $\gamma_a bc = \gamma_b ac = \gamma_c ab$.¹⁶
- 17.24** Give possible reasons for each of the following observations and how you could establish experimentally which ones are responsible.
- (i) The adhesion force increases with the *time* the surfaces are in contact.
 - (ii) The adhesion force increases with the *rate* at which the surfaces are pulled apart.
 - (iii) The adhesion force increases with the *relative humidity*.
 - (iv) The adhesion force is *lower* in water and salt solutions.
 - (v) The adhesion force is *higher* in water and salt solutions.
- 17.25** How would you expect the adhesion energy between two molecularly smooth surfaces to depend on the relative orientation of their surface crystallographic axes (“twist” angles)?
- 17.26*** A glass beaker contains equal volumes of 3 immiscible liquids that have stratified into 3 layers (phases) according to their density, with the heaviest liquid (No. 1) at the bottom and the lightest (No. 3) at the top. Only van der Waals forces are operating, and the Hamaker constants of the liquids and glass are in the order $A_2 > A_3 > A_1 > A_{\text{glass}} > A_{\text{air}}$. (i) Is there a thin film at any of the interfaces? (ii) What will be the disposition of the liquids in zero gravity?
- 17.27** Referring to Problem 1.2, at what radius will the gravitational pressure and the pressure due to surface tension be the same at the center of a sphere of liquid water? [Answer: $R = 10.0 \text{ m}$.]
- 17.28** Figure 17.10 shows six possible configurations of a liquid on a solid surface where the contact angle θ is the same for each. Which is the thermodynamically equilibrium configuration when the vapor above the surface is (i) slightly below and (ii) slightly above the saturated vapor pressure?
- 17.29** A surface contains two small (~5 mm) droplets or lenses of dissimilar liquids A and B that subtend contact angles $\theta_A = 30^\circ$ and $\theta_B = 10^\circ$. When droplet A is moved toward droplet B using a think glass rod, it is seen that droplet B moves away and that it is very difficult to make the droplets coalesce even though the liquids are mutually miscible. Explain this effect. [Hint: Consider that all liquids are at least partially volatile, and the possible effects of precursor films (see Fig. 17.6)].

¹⁶In practice, crystal shapes are determined more by the different rates at which the different faces grow.

- 17.30** Show that for a solid-liquid interface of the same material, for example, ice and liquid water, we expect $\gamma_{SV} \approx \gamma_{SL} + \gamma_{LV}$, and check whether this is indeed the case for water, and for one other material. [Hint: See Antonow's equation.]
- 17.31** Where is the missing point VI in Figure 17.14, mentioned in the text on the previous page?

This page intentionally left blank

Friction and Lubrication Forces

18.1 Origin of Friction and Lubrication Forces

We tend to think of forces in terms of a force-distance law where the force acting on a body can generate motion or acceleration according to Newton's second law, $F(x) = m\ddot{x}$. Friction and lubrication forces, however, act in a totally different way: they have no force-law and arise only as a *reaction* to motion or another force. Viscous and hydrodynamic forces also fall into this category. This chapter considers these types of forces, which are often referred to as nonconservation forces because they involve energy loss or dissipation or, more correctly, the transfer of energy from one body or form to another, usually mechanical, potential, or kinetic energy to heat. Chapter 9 was devoted to nonequilibrium interactions in general; this chapter is devoted to energy dissipating forces associated with friction, lubrication and wear—a field known as tribology (derived from the Greek word for rubbing).

The simplest example of an energy dissipating process is that of two colliding balls or “hard spheres,” where one of mass m and velocity v_0 collides with another of mass M and velocity V_0 (cf. Figure 2.2). After the collision the velocity of the first ball v_1 is given by Eq. (2.35) as

$$v_1 = \left[\frac{m - M}{m + M} \right] v_0 + \frac{2MV_0}{(m + M)}. \quad (18.1)$$

Thus, if the first ball is to lose all its (kinetic) energy to the second, v_1 must be zero, and Eq. (18.1) then gives $V_0 = (M - m)v_0/2M$. For example, if $M = m$, $V_0 = 0$, so that the second ball must initially be stationary, and the collision is like a fast billiard ball hitting a stationary one: the first one stops dead, while the second moves with the original velocity of the first ball. If $M \gg m$, we obtain $V_0 = +\frac{1}{2}v_0$, while if $M \ll m$, $V_0 = -mv_0/2M$,—in other words, the second much lighter ball—must approach the first at high speed (note the negative sign, and that $m/M \gg 1$).

Even the simplest case of $V_0 = 0$ is not without its subtleties. In this case the kinetic energy of the first ball after the collision is readily seen to be (see Section 2.11)

$$\frac{1}{2}mv_1^2 = \frac{1}{2}mv_0^2 - \frac{2m^2Mv_0^2}{(m + M)^2} = \frac{1}{2}mv_0^2 \left[\frac{1 - M/m}{1 + M/m} \right]^2. \quad (18.2)$$

The fraction of kinetic energy transferred from the first to the second mass is therefore

$$1 - \frac{\frac{1}{2}mv_1^2}{\frac{1}{2}mv_0^2} = \frac{4M/m}{(1 + M/m)^2}. \quad (18.3)$$

Figure 18.1 shows the fraction of the energy transferred as a function of the mass ratio M/m . Note the broad, Gaussian-like shape of the transfer function which peaks at

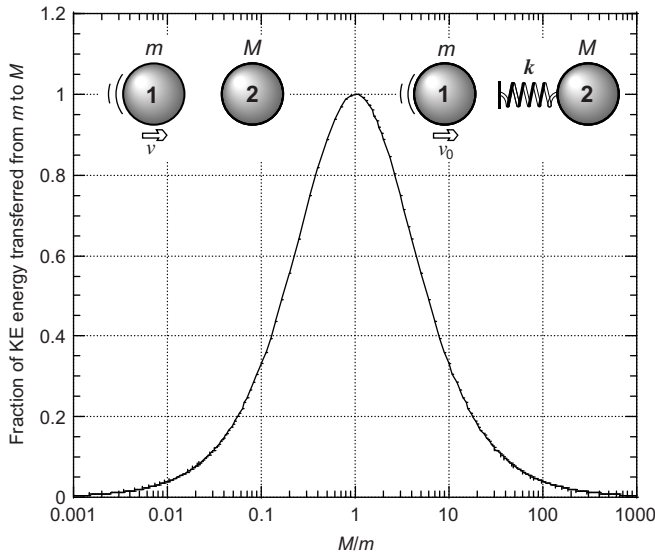


FIGURE 18.1 Illustration of a simple energy transfer process between hard spheres (left schematic) when a ball or molecule of mass m and initial velocity v_0 collides with a stationary ball (velocity $V_0 = 0$) of mass M . The fraction of kinetic energy transferred from the first to the second mass is $[1 - (\frac{1}{2}mv_1^2/\frac{1}{2}mv_0^2)]$, given by Eq. (18.3). Note that all of these collisions are “elastic”: the total kinetic energy is conserved even when the first molecule has “dissipated” or “lost” all its energy to the second. As shown in Worked Example 18.1, a finite stiffness k (soft elastic repulsion between the balls as shown in the right schematic) has no effect on the final kinetic energies of the two balls.

$M = m$ ($M/m = 1$), at which condition all the energy is transferred or—in common parlance—the molecule has “lost” or “dissipated” all its energy.

This simple example illustrates how a body that collides with another invariably loses some of its kinetic energy to the other body. The original motion is usually induced by an externally applied force, while the transferred kinetic energy starts off as a directional or vectorial motion of the receiving molecule and ends up being distributed as *random* motion among many molecules, that is, as “internal” kinetic energy, or heat. This is perhaps the simplest nontrivial way of thinking about the origin of friction. The full story is, however, much more complex.

As discussed in Sections 2.10 and 2.11, the meaning of “mass”, as it appears in the above equations, is not a simple matter. A large mass M can be made up n smaller masses m , and its behavior during collisions will depend on how the n masses are connected. For example, when a billiard ball is dropped onto a hard, concrete floor it will bounce back to almost its original height. In this case we may say that it hit a much larger mass, $M \gg m$, because no kinetic energy was transferred (cf. Eq. 18.3 when $M/m \gg 1$). In contrast, when it hits another ball of the same mass m , all the energy is transferred. But the ball also loses all its energy when it hits n identical billiard balls of mass m stacked up in a line.¹ What then is the

¹A popular coffee table gadget known as Newton’s Cradle nicely illustrates this effect, where a few balls hang in line from V-shaped strings. When the first ball strikes the second ball, only the last ball moves.

reason for the difference between n contacting balls each of mass m and a single ball having the same total mass nm ? The main reason is the assumption that each collision is instantaneous—that is, taking no time and occurring at a point. This is inherent in any hard sphere model, where the spheres do not interact with each other through any force-law, and are infinitely rigid. Many things change when these and other factors are taken into consideration.

To understand the role of the collision or interaction time, it is best to start by considering the simplest case of free (as opposed to forced) simple harmonic motion of bodies. The equation of motion of a mass m attached to a spring of spring constant k is $m\ddot{x} + kx = 0$. One of the solutions—that for simple harmonic motion—is $x(t) = A \sin(\omega t) = A \sin(2\pi\nu t)$, where A is the amplitude of the oscillations and where the period τ is related to the *natural frequency* ν by $\tau = 1/\nu = 2\pi/\omega$. Single and double differentiations of $x(t)$ give $\dot{x} = A\omega \cos \omega t$, and $\ddot{x} = -A\omega^2 \sin \omega t \rightarrow m\ddot{x} = -m\omega^2 x$. Thus, $\omega^2 = k/m$, giving for the period of the oscillations

$$\tau = 1/\nu = 2\pi/\omega = 2\pi\sqrt{m/k}, \quad (18.4)$$

which, interestingly and significantly, is independent of the amplitude A or maximum velocity $A\omega$ of the motion.



Worked Example 18.1

Question: In the top right schematic in Figure 18.1 the second, initially stationary, sphere is not hard but elastic, which in 1D can be modeled as if a spring of spring constant k (N/m) protrudes from the sphere. What is (1) the fraction of energy transferred, (2) the collision time τ , and (3) the distance D the first sphere travels during the collision, defined as the time the two spheres are “in contact” which in turn can be defined as the time the spring is under compression? Express your answers in terms of v_0 , k , M , and m , and compare them with the case of two hard spheres. What are typical values for τ and D in the collision of two inert, nonadhering atoms of MW 60 Da at room temperature?

Answer: Let the free length of the spring be L . Contact is made as soon as the first sphere touches the end of the spring and continues until the spring is once again of length L and the two spheres recede from each other. It is convenient to analyze this type of system from the center of mass frame of reference which moves at constant velocity $v = v_0m/(M + m)$ throughout the collision as determined by the conservation of momentum of the system: $v_0m = v(M + m)$. Within this reference frame the spring may be split into two independent lengths and effective spring constants on either side of the (stationary) origin: $LM/(M + m)$ and $k(M + m)/M$ on the left, and $Lm/(M + m)$ and $k(M + m)/m$ on the right. Also, within this frame spheres 1 and 2 approach the center with velocities $+v_0M/(M + m)$ and $-v_0m/(M + m)$, respectively.

- (1) At the end of the collision, within the center of mass frame of reference, sphere 1 has velocity $-v_0M/(M + m)$ because it executes simple harmonic motion during its interaction with the spring which brings it back to its original velocity but in the opposite direction. Its velocity in the “laboratory” frame is therefore

$-v_0M/(M+m) + v_0m/(M+m) = +v_0(m-M)/(M+m)$, and so its kinetic energy is $\frac{1}{2}mv_0^2[(1-M/m)/(1+M/m)]^2$, which is the same as Eq. (18.3). The fraction of energy transferred is therefore the same as for hard spheres, as plotted in Figure 18.1. Thus, a finite stiffness k has no effect on the final kinetic energy of the two balls.

- (2) The collision time τ is also best determined in the center of mass frame, where it is given by, applying Eq. (18.4),

$$\tau = 2\pi\sqrt{\text{mass/effective spring constant}} = 2\pi\sqrt{mM/k(M+m)}, \quad (18.5)$$

which is the same for both masses, as expected. For hard spheres, $k = \infty$, and $\tau = 0$.

For spheres of finite stiffness the collision time is finite. Thus, if other molecules are present nearby, the second molecule may already be interacting with them before its collision with the first molecule is over.

- (3) Since the collision is over when the spring reaches its original length, the first ball has traveled the same distance as the center of mass frame: $\tau v = 2\pi v_0 m^{3/2} M^{1/2} / k^{1/2} (M+m)^{3/2}$. For hard spheres, $k = \infty$, and $D = 0$.

For an atom or molecule of MW 60 Da, $m = 10^{-25}$ kg. The value of k can be estimated from the bulk elastic modulus which for van der Waals solids is typically $\sim 10^9$ N m $^{-2}$ —that is, ~ 1 GPa for a cube with sides of length 1 m. If the molecular diameter is taken as 0.4 nm, then k will be $10^9 \times (\text{number of molecules per unit length}) / (\text{number of molecules per unit area}) = 10^9 \times 4 \times 10^{-10} = 0.4$ N m $^{-1}$. Putting $m = M$ in Eq. (18.5) we obtain $\tau = 2.2 \times 10^{-12}$ s, which is a typical vibration time of weakly bound atoms. At room temperature the velocity of the moving molecule will be $v_0 \approx (k_B T/m)^{1/2} = 200$ m s $^{-1}$, so that the distance traveled during the collision (by both molecules) is $200 \times (2.2 \times 10^{-12}) = 4.4 \times 10^{-10}$ m = 0.44 nm, which is about the same as the atomic size.



Worked Example 18.1 does not consider what happens to either molecule or atom after the collision—that is, when the atoms proceed to collide with other atoms. Nor does it consider the situation when there are attractive forces between the atoms so that the collision inevitably involves other atoms that are in adhesive contact with the second atom. Furthermore, the spring model is qualitatively unrealistic because the period (and therefore collision time τ) of simple harmonic motion is independent of the velocity or amplitude, just as in the case of the period (swing time) of a pendulum. Real force-laws are not linear (parabolic for the energy), but power-laws or exponential functions, and this makes both the collision time τ and energy transferred nonharmonic and dependent on the velocity of the incoming atom or molecule.

Figure 18.2 shows a more realistic geometry and collision scenario, known as Coulomb friction, that begins to resemble the energy transferred during a real tribological system because it contains the following features: (1) There are now many molecules in the system that interact with each other through a more typical potential function such as the Lennard-Jones potential. (2) The top molecule or particle is subjected to continuing normal and lateral forces, allowing for off-axis collisions and an analysis of the time evolution or “dynamics” of the interaction that shows how an initially directional force (and kinetic

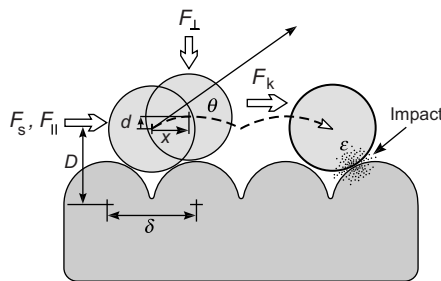


FIGURE 18.2 Schematic of the normal and lateral (friction, shear) forces, F_{\perp} and F_{\parallel} , and normal and lateral displacements, d and x , associated with moving a molecule or “top surface” laterally across a “bottom surface.” On impact a fraction ε of the kinetic energy acquired by the top molecule is transferred to the bottom surface. Note that the sub-ångstrom structure of the surface is crucially important in determining the friction force F_{\parallel} , but not the adhesion force F_{\perp} (see text). Also note the inherent asymmetry in this geometry: during sliding, the same top molecules are always in contact—that is, interacting—with the lower surface, while the bottom molecules are only transiently in contact with the top molecules during the finite time it takes the top area to move across them.

energy) becomes converted into heat (random kinetic energy). Nevertheless, this system is still somewhat idealized in that the surface is molecularly smooth, that plastic deformations (damage, wear) are not allowed, and that there is no “third body” such as a lubricant film between the surfaces, all of which will be considered later in this chapter.

When subjected to a purely lateral (horizontal) force F_{\parallel} , for the top atom or molecule to move laterally by a distance x across the bottom planar surface, it needs to rise by a distance d . The phenomenon of dilation is inherent in most processes where flow or motion is induced in a system initially at rest.² This requires that work or a force be applied to the system to overcome the forces that oppose the dilation. In the case of Figure 18.2, there are two such forces: the externally applied load normal force or load F_{\perp} the (internal) adhesion forces. The first requires that a lateral force of

$$F_{\parallel} = F_{\perp} \tan \theta = \mu F_{\perp} \quad (18.6)$$

be applied to initiate lateral motion, where μ is known as the static friction coefficient (Table 18.1). The second requires an additional force to overcome the intermolecular adhesion force holding the top molecule to the bottom left molecule. This contribution depends on the intermolecular pair potential. For two extended surfaces, the total friction force is therefore given by a term proportional to the load and a term proportional to the number of bonds³ that must be broken when the top layer of molecules rise (dilate) to move across the bottom layer. For molecularly smooth surfaces, the number of bonds is proportional to the contact area A , so that we may write

$$F_{\parallel} = \mu F_{\perp} + \sigma A, \quad (18.7)$$

²For example, when one steps on wet sand on a beach, the region just around the footprint becomes momentarily dry because the flow induced in the sand causes it to dilate.

³The term “bond” is used here in a loose, general sense, and includes van der Waals and other types of physical, noncovalent “bonds.”

Table 18.1 Friction Coefficients for Material 1 Sliding on Material 2 (dissimilar materials are shaded in gray).[†]

Material 1	Material 2	Friction coefficients in air ($\pm 50\%$)		Comments
		Static, μ_s	Sliding, μ_k	
Aluminum	Aluminum	1.5	1.4	
Mild steel	Mild steel	0.7	0.6	
Aluminum	Mild Steel	0.6	0.5	The crystal lattice incommensurability of different materials (steel and aluminum in this example) leads to a lower friction coefficient compared to the commensurate surfaces that can lock together.
Sapphire	Sapphire	0.2	0.2	
Diamond	Diamond	0.1		
Diamond	Metal	0.1		Both diamond and sapphire have hard, atomically smooth surfaces, and weak van der Waals bonding to other materials, resulting in low adhesion- and load-controlled friction forces.
Rubber	Solids	1.0–4.0		Despite its low adhesion energy, rubber can conform to surfaces to achieve a high contact area.
Teflon	Teflon			
Rough	Rough	0.04	0.04	
Smooth, flat	Smooth, flat	0.08	0.07	
Teflon	Smooth metals	0.1–0.3	0.1–0.3	Teflon and graphite readily transfer to the surfaces they are sliding against, so that the friction ends up between surfaces of the same two materials: Teflon on Teflon or graphite on graphite. Teflon has low μ because it flows and the CF_2 groups are rigid and do not interdigitate; graphite has low μ because it delaminates and rolls up into submicron roller bearings.
Graphite	Graphite	0.1		
Graphite	Steel	0.1		
Teflon	Steel			
Moving	Fixed	0.18	0.16	Friction forces are generally not symmetrical on exchanging the stationary and moving surfaces.
Fixed	Moving	0.27	0.27	Lower μ is usually due to continuous material transfer from the softer (fixed) surface to the contact area of the harder (moving) slider surface.
Teflon	Chromium plate			
Moving	Fixed	0.21	0.19	This is the case for Teflon and chromium, but not for Teflon and steel.
Fixed	Moving	0.09	0.08	
Ice	Ice	0.1	0.03	
Metal	Ice	0.02	0.02	At temperatures above -20°C a monolayer or two of water remains unfrozen on ice, which acts as a very effective liquid lubricant.
Cartilage in joints	Cartilage in joints	0.01	0.003	Biological systems have found ways to achieve very efficient “water-based” lubricant systems.

[†]Data taken from various sources including *ASM Handbook*, Vol. 18 (1992) pages 73–74.

where the first term is referred to as the load-controlled contribution, and the second the adhesion-controlled contribution, where σ is known as the shear stress. The first term is related to the structure or topography of the surfaces, and the second is related both to their structure and the intermolecular forces. Figure 18.3 further illustrates why load- and adhesion-controlled friction forces depend on the geometric properties of the system.

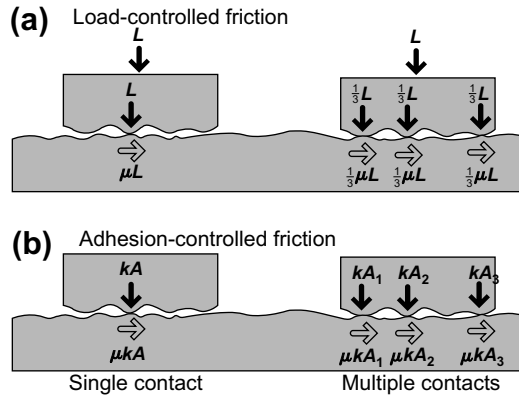


FIGURE 18.3 Illustration of the difference between load-controlled and adhesion-controlled friction. **(a)** Load-controlled friction forces are determined by the microscopic topography of the surfaces, defined by the friction coefficient μ (Eq. 18.6), which is assumed to be everywhere the same. For a given total load L or F_{\perp} the total friction force is therefore always given by $F_{\parallel} = \sum_n \mu(F_{\perp}/n) = \mu F_{\perp}$ —that is, it is independent of how the load is distributed, or the number of contacts n , or the “real” contact area. **(b)** Adhesion-controlled friction depends on the number of contacts n of area A_n that sum to give the total “real” area of contact A_{TOT} according to $F_{\parallel} = \sum_n \sigma A_n = \sigma A_{\text{TOT}}$ (Eq. 18.7).

It is important to distinguish between the lateral force needed to initiate motion and the force needed to continue the motion. Equation (18.7) gives us the force to move a molecule only to the next lattice site, where it hits the next molecule with the kinetic energy it has acquired on moving a distance δ from x to $x + \delta$ (see Figure 18.2). Whether the motion continues or not depends on what fraction ε of this kinetic energy is transferred to the bottom surface during the impact. The “static” friction coefficient to initiate motion μ_s is generally higher than that during sliding, when it is known as the “kinetic” friction coefficient, μ_k (see Table 18.1). Understanding the dynamic energy transfer processes of shearing surfaces is the key to understanding friction, and is the central topic of this chapter.

There are two more friction mechanisms in addition to the load-controlled and adhesion-controlled mechanisms described above; these are commonly referred to as *elastohydrodynamic (EHD) friction* and *rolling friction*. The first arises when a liquid film is present between the two shearing surfaces, giving rise to viscous and lubrication forces, although it can also arise when a thin surface layer of a solid undergoes “shear-induced melting”; the second arises when ball or roller bearings or wheels mediate the motion so that there is never any slip or shear at any interface, but where energy is still dissipated during the rolling.

Figure 18.4 shows the mechanical circuit of a typical tribological setup that is encountered in practice, showing the various parameters that determine the tribological behavior of the system. As can be seen, there are many parameters, not all of which can be directly measured even under ideal experimental conditions.

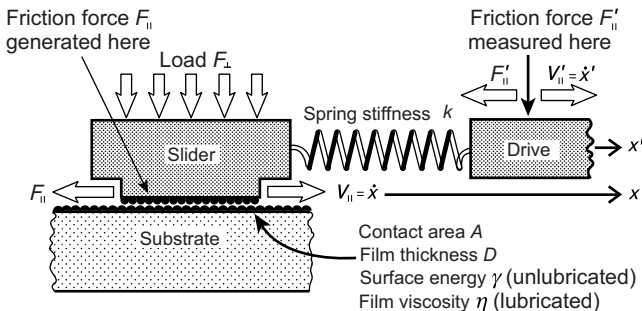


FIGURE 18.4 Schematic of a typical tribological setup and its equivalent mechanical circuit. It is important to note that friction forces are never measured or detected at the point where they are actually generated (the friction interface) but at some distance away that is coupled to the friction interface by a mechanical element or backing material that has its own inertia (a finite mass m , complex stiffness k , etc.). The applied or measured lateral force F'_{\parallel} is therefore different from the real friction force F_{\parallel} except in the case of smooth, steady-state sliding. Likewise, at any instant or time t , the measured lateral displacement x' and velocity $V'_{\parallel} = dx'/dt$ are different from the real interfacial displacement x and sliding velocity $V_{\parallel} = dx/dt = \dot{x}$. (See Problem 18.4.) In the setup shown the lateral force is applied via a spring; in other situations it can be applied as a constant force or (dead) load or via a pulley and weight. In the latter case the frictional response can be quite different, for example, exhibiting smooth sliding (slip) but no stick-slip motion. Neither Leonardo da Vinci nor Amontons mention stick-slip friction, probably because most of their experiments were conducted with constant loads.

18.2 Relationship between Adhesion and Friction Forces

While adhesion and friction forces have the same origin—that is, explicable in terms of the same interaction potential, such as the Lennard Jones potential—between the molecules of two surfaces, they are both quantitatively and qualitatively different. First, regarding magnitude, Figure 18.2 shows that the sub-ångstrom structure (topography or texture) of the surface is crucially important in determining the friction force F_{\parallel} , but this is not the case for the adhesion force F_{\perp} . Thus, if $w(\delta)$ is the van der Waals adhesion energy required to separate two spherical molecules of diameter δ from each other, the energy required to separate a molecule from the bottom surface would be $2w(\delta)$ for the 2-point contact shown in Figure 18.2, or $3w(\delta)$ for a 3-point contact (Section 13.13). If the bottom surface were mathematically flat, the adhesion energy would be $2w(\delta)$ —that is, not very different, showing that the adhesion is not very sensitive to the detailed atomic-scale structure of the surface.

In contrast, if the bottom surface were mathematically flat, the friction force would be zero, since no energy or force would be required to slide the top molecule across the laterally featureless surface (even if the adhesion energy and force were high), since there is now no normal dilation during the lateral motion. The very small (sub-ångstrom) but finite dilation d shown in Figure 18.2 is what ultimately determines the shear strength of an interface or of any solid, and what prevents steel from flowing like a liquid.

But there is a relationship between friction and adhesion *hysteresis*: the irreversible or nonrecoverable part of the energy during a loading-unloading cycle (Section 17.8). This is illustrated in Figure 18.5, which shows a hypothetical loading-unloading cycle on the left and a “friction cycle” (moving the top surface to the next lattice position) on the right. As can be seen, the friction cycle can be split into the two stages of an adhesion cycle simply by raising then bringing the surfaces down one lattice position to the left or right of the starting position. The only difference is that during frictional sliding the molecules of the two surfaces do not fully separate during a cycle as they do in an adhesion cycle where the surfaces are separated to infinity. Thus, any adhesion energy hysteresis in an adhesion cycle, defined by $(W_R - W_A) = 2(\gamma_R - \gamma_A)$ per unit area (see Figure 17.16), will be less in a friction cycle. We may define the fraction of energy transferred by ε , which is also illustrated in Figure 18.2. If $\varepsilon = 1$, the top surface will stop at the next lattice position. If $\varepsilon = 0$, the top surface will continue to move indefinitely across the bottom surface even if the externally applied force is switched off. In practice, ε lies between 0 and 1, its value depending on many factors.

Relating the energy lost during each loading-unloading cycle due to adhesion energy hysteresis, $2\varepsilon A(\gamma_R - \gamma_A) = 2\varepsilon A\Delta\gamma$ per unit area, to the frictional work done $F_{||}\delta$ to move the surfaces a lateral distance δ during each friction cycle we obtain for the adhesion-controlled friction force:

$$F_{||}\delta = 2\varepsilon A\Delta\gamma, \quad (18.8)$$

where $\Delta\gamma = (\gamma_R - \gamma_A) = \frac{1}{2}(W_R - W_A)$. Comparing with Eq. (18.7) gives us an expression for the shear stress: $\sigma = F_{||}/A = 2\varepsilon\Delta\gamma/\delta$. Equation (18.7) for the load- and adhesion-controlled friction forces can now be written as

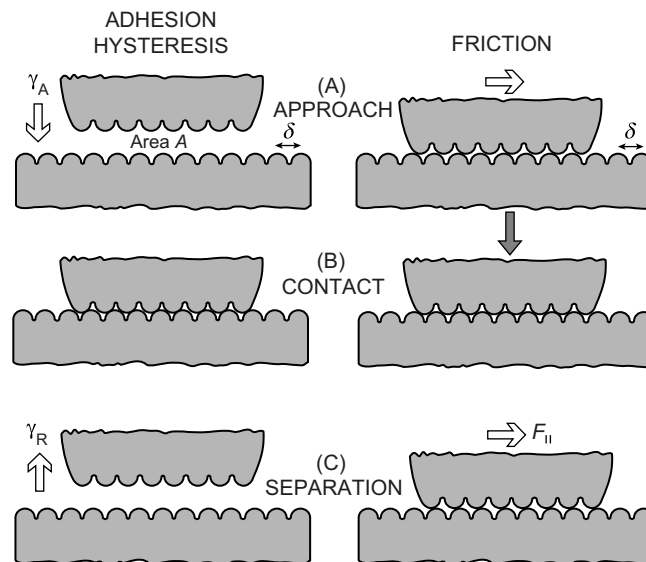


FIGURE 18.5 Relationship between adhesion hysteresis $(\gamma_R - \gamma_A) = \Delta\gamma$ and the “adhesion-controlled” friction force $F_{||}$.

$$F_{\parallel} = \mu F_{\perp} + \sigma A = \mu F_{\perp} + 2\varepsilon A \Delta\gamma/\delta. \quad (18.9a)$$

It is sometimes more convenient to express friction forces in terms of the stresses or pressures (force/area), in which case, dividing the above by the area A , we obtain for the total shear stress

$$P_{\parallel} = \mu P_{\perp} + \sigma = \mu P_{\perp} + 2\varepsilon \Delta\gamma/\delta, \quad (18.9b)$$

where P_{\perp} is the externally applied normal pressure. When the adhesion hysteresis is high, γ_R is usually much larger than γ_A , so that one can replace $\Delta\gamma$ by γ_R in the above equations.

The area A is problematic. It is generally referred to as the “real” contact area, in contrast to the projected or “apparent” contact area of, say, a rough interface where $A_{\text{real}} < A_{\text{app}}$, or an interdigitated interface where $A_{\text{real}} > A_{\text{app}}$ (Figures 17.11d and 17.17b). Even for an atomically or molecularly smooth surface, the area is not well defined because there is no definition for the contact area between two atoms or molecules. Strictly, the appropriate energy parameter should be the energy of the *bonds* made and (partially) broken during sliding, as depicted in Figure 18.2, which is also how these interactions are simulated in computer simulations—for example, in terms of Lennard-Jones potentials with no reference to any area. Still, for molecularly smooth surfaces interacting through noncovalent bonds the above equations provide surprisingly good semiquantitative descriptions of the friction forces, where the area implicitly represents the number of participating bonds, as illustrated below.

Worked Example 18.2

Question: The molecules of two planar close-packed (HCP or FCC) solid surfaces interact through an attractive van der Waals pair potential given by $w(r) = -C/r^6$, where $C = 10^{-77} \text{ J m}^6$. The molecules may be considered to behave as hard spheres of diameter $\delta = 0.4 \text{ nm}$. One such surface of area A is now slid laterally across the other (which may be considered to be of infinite extent) while subjected to a normal compressive load F_{\perp} . Show that the total friction force F_{\parallel} is approximately given by a relation of the form given by Eq. 18.7, where μ and σ are constants. From the values given for C and δ , estimate the values of the constants μ and σ , and the total friction force for a surface of area of $A = 1 \text{ cm}^2$ sliding under a load of 1 kg. What fraction of the friction force comes from intermolecular forces at this load? State and critically discuss any assumptions made.

Answer: Assuming perfect commensurability (perfect registry, zero “twist angle”) of the two surfaces in the HCP or FCC configuration and only nearest-neighbor interactions, the area per molecule is $\sqrt{3}\delta^2/2$ giving an adhesion energy of (see Section 13.13): $W = 2\gamma = (3C/\delta^6)/(\sqrt{3}\delta^2/2) = 2\sqrt{3}C/\delta^8 = 53 \text{ mJ m}^{-2}$ ($\gamma = 26 \text{ mJ m}^{-2}$). A top sphere initially sitting between three bottom spheres in the HCP or FCC lattice (cf. Figure 18.2) can slide or roll over the bottom lattice in a number of ways: over the top of one of the three bottom spheres (energetically expensive), between two adjacent spheres (the route of lowest energy), or any path in between. It is clear that the friction force will depend on the initial twist angle between the two lattices and the direction of sliding. Assuming perfect initial registry and a sliding path of lowest energy (least resistance), one may calculate that each sphere will remain in contact

with two adjacent spheres as it moves up between them at an angle θ to the horizontal given by $\tan \theta = 1/2\sqrt{2} = 0.35$ ($\theta = 19.5^\circ$). Thus, the load-controlled friction coefficient is $\mu = 0.35$.⁴

The adhesion-controlled contribution can be estimated by noting that a certain fraction of the total adhesion energy is consumed when the spheres of the top surface detach from those of the bottom surface in order to go over them. To estimate this energy we may consider the energy of a sphere when it is at the mid-point between two energy minimums—that is, when it is at the highest point between the two adjacent spheres. At this position the sphere is in contact with and therefore at a distance δ from the centers of the two adjacent spheres on either side of it in the crystal plane below, and $\sqrt{3}/2 \delta$ from the centers of the two spheres behind and in front of it. Its energy is therefore $-2C/\delta^6[1 + (2/3)^3] = -2.59C/\delta^6$, which is $0.41C/\delta^6$ or 14% higher than the value of $-3C/\delta^6$ for the sphere in its initial position in the potential energy minimum. The lateral distance moved to reach this high energy point is $\sqrt{3}\delta/2$.

Using the same analysis as above to derive Eq. (18.9a), and putting $\varepsilon = 1$, $\Delta\gamma = 0.14 \times 26 \text{ mJ m}^{-2}$, and $\delta = 0.4 \text{ nm}$, we obtain $F_{\parallel} = \mu F_{\perp} + 2\varepsilon A \Delta\gamma / (\sqrt{3}\delta/2) = \mu F_{\perp} + \sigma A = 0.35F_{\perp} + 2.1 \times 10^7 \text{ A}$. Finally, for $F_{\perp} = 1 \text{ kg} \approx 10 \text{ N}$, and $A = 1 \text{ cm}^2 = 10^{-4} \text{ m}^2$, $F_{\parallel} = 3.5 + 2.1 \times 10^3 \approx 2,100 \text{ N} (\approx 210 \text{ kg})$. Thus, 99.8% of the friction force comes from the adhesion contribution. Only at loads above 600 kg (pressures >60 MPa) will the load-dependent contribution exceed the adhesion contribution, which is assumed to be independent of the load.

The calculated shear stress of $\sigma \approx 2 \times 10^7 \text{ N m}^{-2}$ is close to measured shear strengths of molecularly/atomically smooth, noncovalent, van der Waals contacts (Figure 18.6), whose surface energy γ is also close to the calculated value of 26 mJ m^{-2} . It is also an upper bound for such contacts: at finite temperatures and for $\varepsilon < 1$ the friction forces will be lower.

A close analysis of the geometry of the shearing close-packed lattices shows that after the first hop from one lattice site to the next between two adjacent contacting molecules, the next hop must involve a different path—either above a molecule or between two molecules, but now moving at an angle to the original direction, either of which will involve a higher friction force.

⁴At the time of Leonardo da Vinci it was believed that all friction coefficients were exactly $\frac{1}{4}$, with values different from 0.25 reflecting some “nonideal” behavior of the system.



In Worked Example 18.2, the surface area A was given as constant, as in Figure 18.4. This situation applies to two flat surfaces. For curved surfaces—for example, a sphere sliding on a flat surface—the first term in Eq. (18.7) does not change, but the area A in the second term now depends on the load, as given by the JKR equations, or other equations of contact mechanics. At low loads the friction force is dominated by the adhesion contribution, but at high loads, where $A \propto F_{\perp}^{2/3}$, it is dominated by the load-dependent contribution μF_{\perp} . Figures 18.6–18.8 show some typically measured friction forces using the SFA and AFM techniques that illustrate many of the above points at the macroscopic, microscopic, and nanoscopic (molecular) scales.

It is clear that the parameters A , ε and δ in the above equations are the difficult ones to measure or calculate. However, we may note that δ/ε may be replaced by the

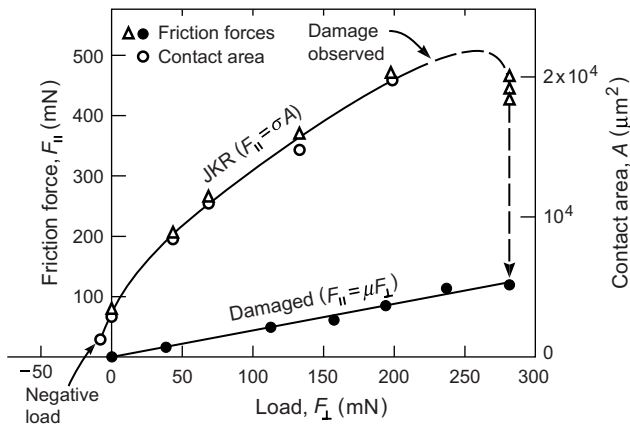


FIGURE 18.6 SFA-measured macroscopic friction forces F_{\parallel} (Δ , ●) and “real” contact areas A (○) versus normal load F_{\perp} for two molecularly smooth mica surfaces sliding in air in the crossed-cylinder configuration, which is equivalent to a sphere (of radius $R \approx 2$ cm) sliding on a flat surface. At these relatively low loads the friction force is adhesion-controlled—that is, directly proportional to the contact area—which is in turn well described by the JKR theory, even during sliding. The measured shear strength is $\sigma = 2.5 \times 10^7 \text{ N m}^{-2}$, close to the maximum theoretically expected value (see Worked Example 18.2), but falls to $\sigma = 4 \times 10^6 \text{ N m}^{-2}$ for two surfactant-coated (“boundary lubricated”) mica surfaces in air (not shown). Note the finite contact area and friction force even at negative loads. The adhesion force is also unchanged under these sliding conditions ($V < 10 \mu\text{m/s}$). The vertical arrow shows a transition to load-controlled friction after damage has occurred at high loads and/or sliding speeds, resulting in almost zero adhesion and a friction force that is now proportional to the load, $F_{\parallel} = \mu F_{\perp}$, with a coefficient of $\mu \approx 0.3$ for both the unlubricated and lubricated surfaces (●). [Adapted from Homola et al., 1989, 1990.]

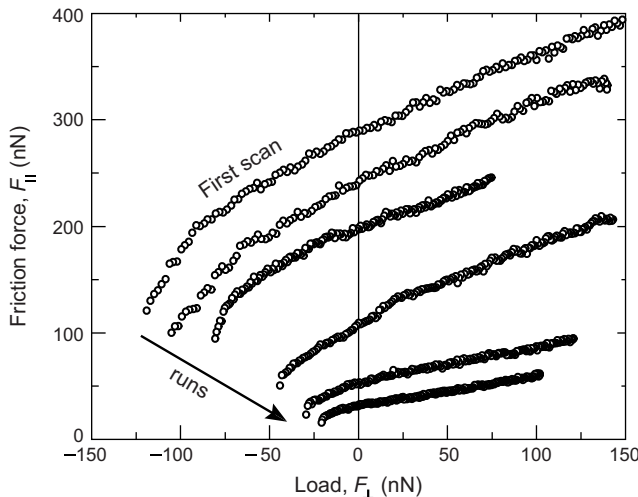


FIGURE 18.7 AFM-measured nanoscopic friction forces versus load, F_{\parallel} versus F_{\perp} , for a Pt-coated tip in contact with a mica surface in an ultra-high vacuum showing JKR-like force-load profiles as in Figure 18.6. With increasing back-and-forth sliding (number of runs) the surfaces have probably become damaged and the profiles tend to a straight line passing through the origin corresponding to load-controlled friction, $F_{\parallel} = \mu F_{\perp}$, with a friction coefficient of $\mu \approx 0.3$. (cf. similar effect observed in Fig. 18.6). [Adapted from Carpick et al., 1996 a,b.]

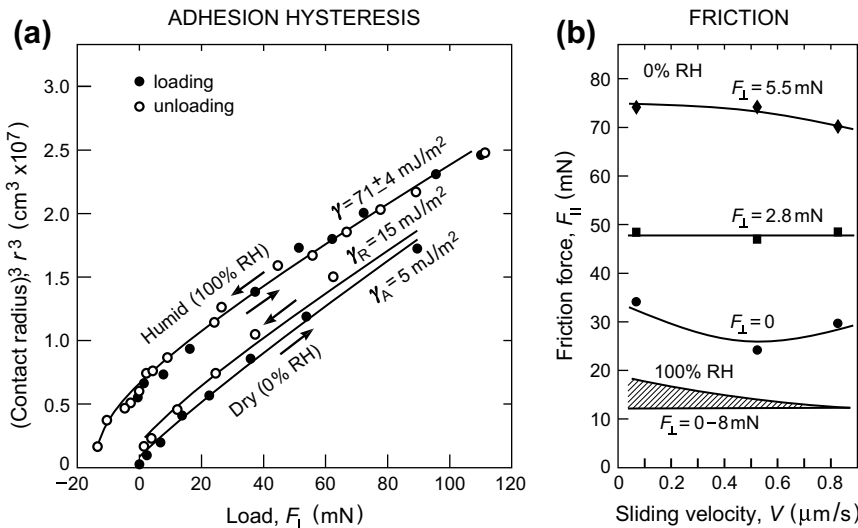


FIGURE 18.8 Example of the relationship between adhesion hysteresis (a) and the friction forces (b) for two silica surfaces sliding against each other in dry and humid air. The solid lines in (a) are JKR fits to the data points using the values for γ , γ_A , and γ_R , as shown. In dry air the measured values at zero load were $\Delta\gamma = 10 \text{ mJ m}^{-2}$, $A \approx 10^4 \mu\text{m}^2$, so that from Eq. (18.9a) we expect, putting $\delta \approx 1 \text{ nm}$ and $\varepsilon = 1$: $F_{\parallel} = 2\varepsilon A \Delta\gamma / \delta = 20 \text{ mN}$, which may be compared to the measured value of $\sim 30 \text{ mN}$ at $F_{\perp} = 0$ in (b). Note how the friction force is related to $\Delta\gamma$ but not to the actual magnitude of the adhesion energy γ , which in this case is actually higher when the friction force is lower. [Adapted from Vigil et al., 1994.]

distance traveled when all the potential energy introduced into the system to get the top surface moving has been dissipated. This distance can be a lattice or molecular dimension, or macroscopic, and it introduces the notion of static versus kinetic friction, stick-slip versus smooth sliding, lubricated versus unlubricated (or “dry”) friction, and time- and rate-dependent effects, which are considered in the following sections. But first, some comments on traditional views of friction.

18.3 Amontons’ Laws of (Dry) Friction

There are three Laws of Friction that are all wrong and are also attributed to the wrong person. These are Amontons’ Laws (Amontons, 1699) that were first studied and described by Leonardo da Vinci (1452–1519). Amontons’ laws are:

1. The friction force F_{\parallel} is directly proportional to the applied load, L or F_{\perp} .
2. The friction force is independent of the apparent area of contact, A .
3. The kinetic friction force is independent of the sliding velocity, V .

These laws were arrived at by observing the sliding of blocks of wood down inclined planes or when pulled by strings rolling over pulleys with weights hanging from their ends. There was little or no adhesion, so the friction was load-controlled, as described by

the first term of Eq. (18.6), which, since it does not contain the contact area or sliding velocity, therefore implicitly satisfies Amontons' three laws. Recent experimental and theoretical work has shown that the second law also applies to molecularly smooth surfaces—that is, to the “real” contact area—but, again, as long as there is no adhesion (Ruths et al., 2003; Landman et al., 2007; Ruths and Israelachvili, 2010). Strictly, Amontons' laws should apply only to dry (unlubricated) surfaces, since these were the systems that were originally studied. However, even for such surfaces the first two laws do not apply, since there is always some, and in many cases strong, adhesion.⁵ Thus, in general, the coefficient of friction as defined by Amontons, $\mu = F_{\parallel}/F_{\perp}$, is not constant or independent of the contact area, especially at low loads.

The issue of the velocity dependence of the friction force is more subtle, but here too the friction force is generally velocity-dependent, although often only weakly so. However, when plotted on a log scale (F_{\parallel} vs $\log V_{\parallel}$), the curves usually exhibit maxima and minima that give important information about the energy dissipating mechanisms underlying the friction process.

Classic tribology has a long and interesting history (Dowson, *History of Tribology*, 1998); it played a central role in determining how many people were needed to move the statues (colossi) of the pharaohs, refuting the caloric theory of heat, and giving birth to the field of thermodynamics,⁶ and it attracted the attention of Coulomb and Euler. Classic books on the subject are Bowden and Tabor's *The Friction and Lubrication of Solids* (1950), and Rabinowicz's *Friction and Wear of Materials* (1995). During the 1980s, computer simulations started to take over from the traditional, analytical, methods of modeling friction processes, ushering in the modern era of this discipline.

18.4 Smooth and Stick-Slip Sliding

When one surface is pushed across another, as illustrated in Figure 18.4, even when the driving velocity V'_{\parallel} is constant, the relative motion of the two surfaces may be nonuniform; that is, at any instant t , $V_{\parallel}(t) \neq V'_{\parallel}(t)$, $F_{\parallel}(t) \neq F'_{\parallel}(t)$, and $x(t) \neq x'(t)$. The most common type of nonuniform friction is “stick-slip” friction, where surfaces move in a sawtooth motion when the measured friction force is plotted versus time, known as a “friction trace” (Figure 18.9b). Stick-slip motion occurs in many systems and situations, including the squeaking of doors, the sound of a violin, the mating calls of grasshoppers, sensory perception (e.g., food texture or “mouthfeel”), earthquakes, and the motion of white blood cells (leukocytes) along the walls of blood cells (endothelial cells) as they look for foreign bodies such as antigens—one of the seek-and-search mechanisms of the immune system.

⁵In such situations, if μ is defined as F_{\parallel}/F_{\perp} in accordance with Amontons' first law, it diverges as $F_{\perp} \rightarrow 0$, which is often reported in the literature.

⁶Gibbs' PhD thesis (1863) was on the optimum geometry of the teeth of wheels and gears in steam engines and railroad brakes.

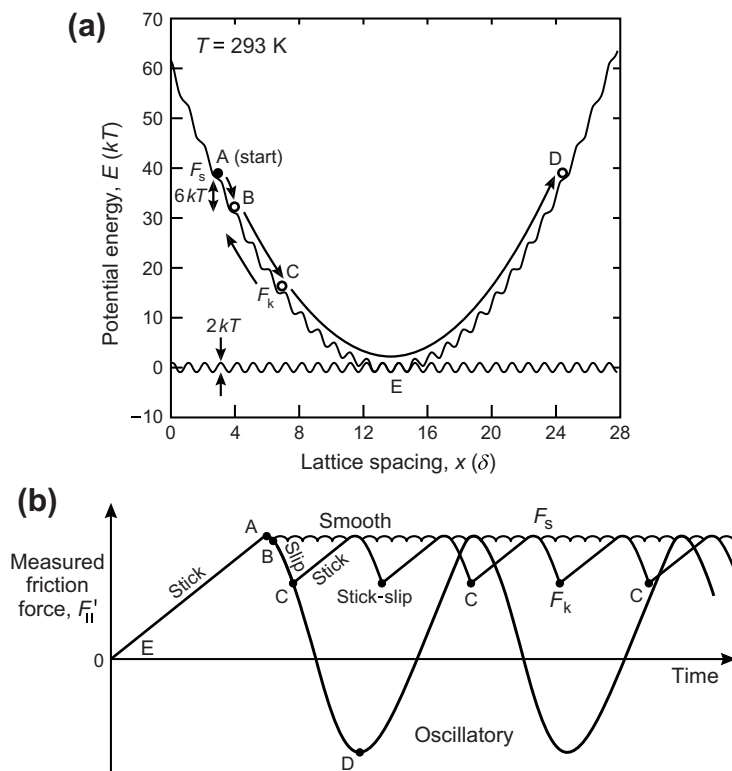


FIGURE 18.9 Interplay between the real friction force at the interface between two shearing surfaces and the measured or externally applied lateral force. Referring to Figure 18.4, at time $t = 0$ the DRIVE is moved to the right at constant velocity $V_{||}'$, i.e., $x'(t) = V_{||}'t$. The measured lateral force $F'_{||} = k(x' - x)$ is generally quite different from the real friction force $F_{||} = -dE/dx$ (see text). Overdamped systems exhibit smooth friction (A \rightarrow B \rightarrow A \rightarrow B \rightarrow ...); underdamped systems exhibit large stick-slip (A \rightarrow C \rightarrow A \rightarrow C \rightarrow ...) or oscillatory sliding (A \rightarrow D \rightarrow A \rightarrow D \rightarrow ...). All curves are schematic; some real friction traces are shown in Figure 18.11.

Stick-slip can be beneficial or detrimental: it is welcome as a way of generating beautiful sounds, but unwelcome when it appears as vibrations (noise) of machines. Damage and wear of materials is often caused by stick-slip motion.

There are two main mechanisms for stick-slip friction: the first applies to dry sliding, and the second to lubricated sliding, which is considered in the next section. In the simplest example of dry sliding of two molecularly smooth surfaces we may consider the intermolecular potential energy in the lateral x -direction to be represented by a sinusoidal function, $E(x) = E_0 \sin(2\pi x/\delta)$ per molecule, as shown in Figure 18.9a. The top surface is attached to a lateral spring, as in Figure 18.4, whose potential energy function is a parabola. The total potential energy is given by the sum of these two energies: $E(x) = nE_0 \sin(2\pi x/\delta) + \frac{1}{2}kx^2$, where n is the total number of molecules in the contact area. The lateral force is given by the derivative of the total energy, $F_{||} = -dE(x)/dx$. The total potential energy per molecule $E(x)/n$ is shown by the wavy curve in Figure 18.9a.

Initially, at time $t = 0$, the two surfaces are at rest in a potential energy minimum at **E**, and are not subjected to any normal or lateral force—that is, the parabola has its minimum also at **E**. At $t = 0$ the DRIVE is moved to the right at constant velocity V' , that subjects the stage to an increasing lateral force. At first, the STAGE or SLIDER will remain “stuck” at **E** as the molecules move up the wavy potential energy curve in Figure 18.9a, where they continue to sit in their local energy minimum. However, at some critical point, the local minimum becomes a stationary point of inflection or saddle point where both $dE/dx = 0$ and $d^2E/dx^2 = 0$ and the molecules will “slip” down from point **A**. This instability occurs at the point on the wavy curve where the spring force kx equals the maximum friction force $F_{\parallel} = 2\pi n E_0 / \delta$. For example, if $E_0 = 1 \text{ } kT$, $k = 1 \text{ N m}^{-1}$, $\delta = 0.5 \text{ nm}$, and the real contact area is $A = 100 \times 100 \text{ nm}^2$, then $n \approx A/\delta^2 = 4 \times 10^4$, and $x = 2\pi n E_0 / k\delta = 2.0 \times 10^{-6} \text{ m}$ at 295 K. Thus the spring will need to be stretched by $2.0 \mu\text{m}$ to initiate sliding (slip). At this point the friction force is $F_{\parallel} = 2\pi n E_0 / \delta = kx = 2.0 \times 10^{-6} \text{ N}$, or $\sim 50 \text{ pN}$ per molecule, and the shear stress is $F_{\parallel}/A = 2.0 \times 10^8 \text{ N m}^{-2}$.

Whether the slip ends at the next lattice point **B**, or the one after, or continues to **C**, or to the maximum point **D** now depends on k , V'_{\parallel} , and the energy transfer mechanisms operating in the system, previously discussed in Section 18.1. At low V'_{\parallel} , the jump from **A** to **B** will be fast compared to any movement of the SLIDER, and on reaching **B** the molecule will have acquired kinetic energy given by the spring energy difference from **A** to **B**, which is roughly $kx\delta/n = 2\pi E_0 = 6.3 \text{ } kT$ per molecule using the above values (shown in Fig. 18.9a). If all this energy is dissipated at **B**, as in Figure 18.1 when $m = M$, the friction will appear smooth, as shown by curve **A** in Figure 18.9b, where the molecular-scale ratcheting is not traditionally considered as stick-slip. According to Eq. (18.3) and Figure 18.1, the fraction of energy transferred between elastic bodies is independent of the collision velocity—that is, the kinetic energy of the colliding molecule; but, in general, for any realistic interaction potential, it does depend on the velocity.

If not all the energy is transferred at **B**, then the molecule will move on to the next minimum where the energy barrier to continue is now slightly higher. It may therefore stop at this minimum. Or it may traverse many lattice dimensions before the surfaces restick at **C** giving rise to the stick-slip friction trace shown by curve **C** in Figure 18.9b. If the system is highly “underdamped,” there will be sinusoidal oscillations as shown by curve **D**.



Worked Example 18.3

Question: Using the values of the above discussion, estimate the transient increase in the local temperature during smooth sliding.

Answer: As drawn in Figure 18.9a, smooth sliding implies that all the kinetic energy acquired by the top molecule as it falls from **A** to **B** is transmitted to the bottom molecule. This energy was calculated to be $2\pi E_0 \approx 6.3 \text{ } kT$, implying an increase in temperature of $\sim 6.3 \text{ } T$ or $\sim 1,900 \text{ K}$ at room temperature, which rapidly (within a few ps) becomes distributed among the molecules of both surfaces. We may note that this local temperature increase is determined by the intermolecular potential and not the sliding velocity. The latter, however, determines how

many such collisions will occur per unit time and, therefore, the rate at which the generated heat flows away from the shearing interfaces. Molecular dynamics simulations by Landman et al. (1989) and Xie et al. (2002) computed that even at slow sliding speeds there can be a 500–1000 K rise in the *local* temp, that is, in the first layer of surface atoms or molecules, which is rapidly dissipated by collisions.



By convention, the maxima and minima of a stick-slip friction trace are referred to as the “static” and “kinetic” friction, denoted by F_s and F_k in Figure 18.9, although these terms can be misleading: there is usually some motion (creep) before the slip; also F_k depends on V_{\parallel}' and k , and is not necessarily the same as the smooth, steady-state friction force that may occur at higher or lower sliding speeds. Thus, as the driving velocity is increased, the kinetic energy acquired by the molecule on reaching successive potential energy minima will be higher than under the “free fall” situation considered above. This will increase the slip distance. At even higher velocities the acquired kinetic energy during the slip exceeds the energy barriers encountered by the molecule and the system will oscillate, undergo chaotic motion, or slide smoothly at some low steady-state kinetic friction force.

A more rigorous analysis requires us to consider more realistic, nonharmonic, force functions where the collision lifetime depends not only on the masses of the molecules but also on the collision velocity, which in turn also depends on the sliding velocity. Still, in many cases the effect of sliding velocity on the friction force is weak, detectable only when varied over a few decades, hence the origin of Amontons’ third law.

If the shear force is a constant force, such as arises when a body slides down an inclined plane or when it is pulled along a horizontal plane by a string placed over a pulley with a weight at its end, the parabolic spring energy curve of Figure 18.9 becomes replaced by a straight line of slope equal to the mass of the weight. Once slip occurs, motion will continue indefinitely because the driving force does not decrease as the sliding distance x increases. In such situations, there is no stick-slip.

Before continuing with our investigation of the highly interesting phenomenon of stick-slip, we must first consider some of the other mechanisms that give rise to it.

18.5 Lubricated Sliding

When two surfaces are separated by a liquid film, the repulsive short-range solvation, double-layer, or steric-hydration force between them usually prevents the surfaces from coming into molecular contact. Instead, the liquid forms a stable film—the higher the applied pressure, the thinner the film. This film protects many surfaces from becoming damaged when they are sheared, and it also reduces the friction force or friction coefficient—the thicker and less viscous the film, the more effective it is as a “lubricant.” For two plane parallel surfaces of area A , separated by a distance D , and sliding at relative velocity V_{\parallel} , the viscous shear force is given by

$$F_{\parallel} = \eta A V_{\parallel} / D, \quad (18.10)$$

where η is the film viscosity (in Pa.s). Equation (18.10) is essentially the definition of the shear viscosity of a liquid: $\eta = \text{shear stress}/\text{shear rate} = (F_{\parallel}/A)/(V_{\parallel}/D)$ under conditions known as *Couette flow*.

Equation (18.10) clearly does not obey Amontons' laws except under certain highly specific conditions (see Problem 18.3): the friction force F_{\parallel} is now a direct function of the area A and sliding velocity V_{\parallel} , and the load does not even enter into the picture directly.

As an example of Eq. (18.10), if the two van der Waals surfaces of Worked Example 18.2 (which under dry sliding conditions have a shear stress of $\sigma \approx 2 \times 10^7 \text{ N m}^{-2}$) slide with a 1 nm thick liquid film between them at a velocity of $V_{\parallel} = 1 \text{ cm s}^{-1}$, the “lubricated” shear stress will be $\sigma = F_{\parallel}/A = 10^7 \eta$. For liquids such as water and low MW hydrocarbons the viscosity is typically $\eta \approx 10^{-3} \text{ Pa.s}$, so we expect $\sigma = 10^4 \text{ N m}^{-2}$, which implies a reduction in the friction force by more than 3 orders of magnitude simply by having a 1 nm thick layer of liquid between the surfaces.

But this is to ignore the dramatically altered physical properties of liquids confined in molecularly thin films that affect both the adhesion- and load-controlled friction forces. In Chapter 15 we saw that as the applied pressure increases and a liquid film thins, the molecules become increasingly ordered into solid-like layers. On shearing, the interface can slip in a number of ways, three of which are shown in Figure 18.10 for a highly idealized system of spherical molecules having the same radius but different interaction potentials for the solid and liquid molecules.

In the case of viscous slip (Figure 18.10c), Eq. (18.10) applies but the effective viscosity of the film, whose thickness D is determined by the normal load F_{\perp} , can now be orders of magnitude higher than that of the bulk liquid due to the jamming of the molecules between the surfaces. In the case of interlayer slip (Figure 18.10c'') the friction force is determined by similar considerations as in dry friction (Coulomb friction): there is an adhesion-controlled contribution that is now determined by the oscillatory force between the surfaces as they dilate, and a load-dependent term that is geometry-dependent.

As in the case of dry sliding, lubricated sliding can be smooth or exhibit stick-slip over certain ranges of the load and driving velocity. Some typical stick-slip profiles are shown in Figures 18.11 and 18.12, but in more complex mechanical systems—especially in machines composed of many inertial components—many other patterns can arise including steady sine waves and periodic profiles with beats.

Stick-slip cycles brought about by freezing-melting transitions belong to a class characterized by having a negative slope in the friction force versus velocity profile of the surfaces—that is, where $dF_{\parallel}/dV_{\parallel} < 0$ over some range of velocities V_{\parallel} . If the slope is everywhere positive, as when the friction is described by Eq. (18.10) and/or Figure 18.11a, there is no stick-slip, just smooth sliding. However, if $F_{\parallel}(V_{\parallel})$ has a maximum value F_{\parallel}^{\max} at some velocity, then as soon as the driving force reaches F_{\parallel}^{\max} , the surfaces (or the SLIDER in Figure 18.4) start to slip and V_{\parallel} increases. The friction force therefore falls below F_{\parallel}^{\max} due to the negative slope, causing the SLIDER to accelerate because the driving force is still at F_{\parallel}^{\max} . This process continues: the friction force continues to fall as V_{\parallel} continues to increase, producing a rapid “slip.” After a certain distance has been moved, the spring

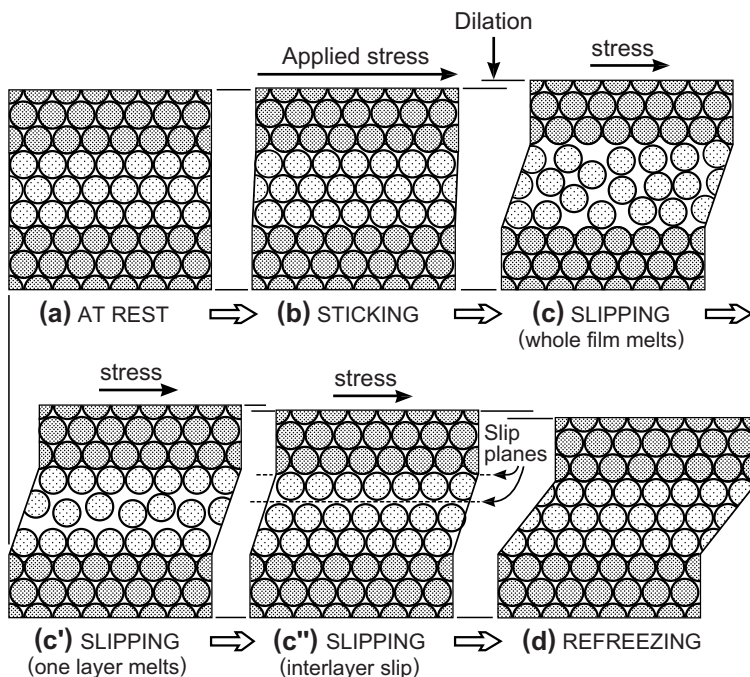


FIGURE 18.10 Different scenarios of lubricated sliding of simple spherical and short-chain molecules when the DRIVE in Figure 18.4 is moved. (a) Static loading: the liquid film becomes ordered into quasi-solid-like layers. (b) Under a shear force the film dilates by d (Fig. 18.2) then partially melts and slips by viscous flow (c, c') or along a lattice plane (c'') very much as during dry sliding. Slipping can also occur at one of the surfaces (wall slip, c''). Sliding can be smooth (as long as the motion of the DRIVE is maintained) or by stick-slip motion. In the latter case, the state at the end of each slip cycle (d) is the same as at the start (a).

itself begins to relax causing a slowdown in the slip, and it may even overshoot as shown in Figure 18.9b, causing rapid deceleration of the surfaces. At some point the surfaces stick again and the cycle is repeated.

In the case where shear-induced melting occurs, the friction force falls abruptly at some critical sliding velocity when the film “melts” and the surfaces slip, and then increases abruptly when the film resolidifies at some higher critical velocity and the surfaces stick again. Of course, the film does not have to resolidify: depending on the driving velocity, a film, once molten, may remain in this state as long as the surfaces continue to be sheared. In this case there is a high initial friction force, known as the stiction force or stiction spike, followed by smooth sliding at the lower kinetic friction force.

Not all liquids solidify or become ordered under confinement, and those that do not make the best lubricants for producing low friction forces.⁷ The inability to solidify can be

⁷Some lubricants such as those used in brakes and as clutch fluids need to exhibit *high* friction forces, while still protecting the shearing surfaces from wear.

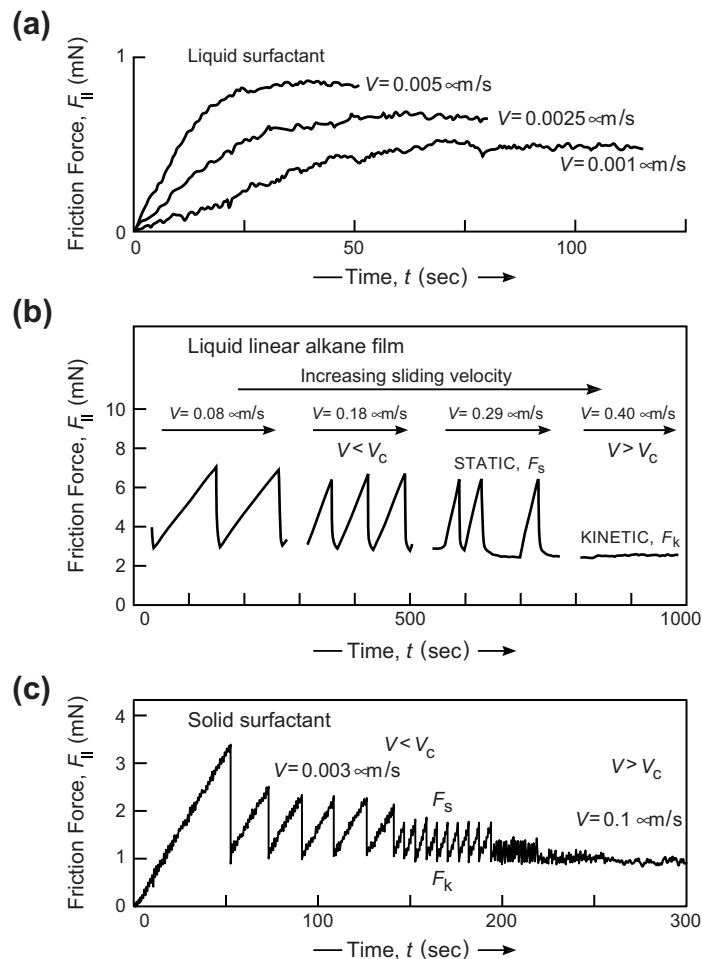


FIGURE 18.11 A tribological system can exhibit a number of smooth and stick-slip regimes at different sliding velocities, depending on the load, the inertia (stiffness and mass) of the moving surface, SLIDER or STAGE, the temperature, and of course the surfaces and lubricating material. Shown here are some recorded friction traces showing different types of smooth and stick-slip sliding patterns. **(a)** Smooth lubricated sliding of two mica surfaces coated with physisorbed calcium alkylbenzene sulfonate “boundary lubricant” monolayers, whose branched hydrocarbon chains are in a highly fluid state. Such surfactants are used as additives in lube oils. **(b)** Friction of a three-layer, $\sim 1.2 \text{ nm}$ thick, n -hexadecane film, showing stick-slip due to freezing-melting transitions of the type illustrated in Figure 18.10. The stick-slip disappears abruptly above some critical driving velocity V_c where the melted or disordered film is no longer able to resolidify (reorder) during the motion. Figure 18.12 shows the stick-slip profiles for films with different number of layers. **(c)** Stick-slip sliding of two mica surfaces coated with physisorbed phosphatidyl-ethanolamine monolayers, whose saturated, close-packed hydrocarbon chains are in the solid state. The transition from regular stick-slip to smooth sliding with increasing driving velocity occurs gradually, rather than abruptly, passing through a chaotic regime (see Section 18.9). [Adapted from Ruths and Israelachvili, 2010.]

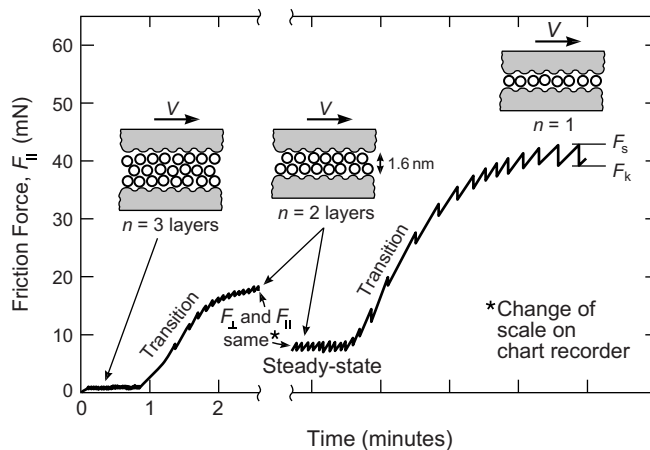


FIGURE 18.12 Friction traces showing “quantized” stick-slip for a liquid film of the nonpolar, quasi-spherical molecule octa-methyl-cyclo-tetra-siloxane (OMCTS, diameter ~ 0.8 nm) between two mica surfaces at increasing load and decreasing number of layers n (Gee et al., 1990). Similar results are obtained with other quasi-spherical molecules such as cyclohexane.

due to the surfaces, to the liquid, or to both. Thus, if the liquid and surface molecules are very different (“incommensurate”), the type of epitaxial ordering induced by confinement, shown in Figure 18.10, may not be possible (see also Table 18.1). In other cases the liquid itself may not be able to solidify because the molecules are too irregularly shaped to order, as occurs with branched hydrocarbon liquids and polymer melts (McGuigan et al., 2007; Gao et al., 1997a,b) or their entanglements may cause wall-slip rather than film-slip to occur (Fig. 18.10c’), which also helps reduce the friction force. Such fluids make good lubricants, such as greases, even though their bulk viscosity is high.

Third, if the surface itself is rough or dynamically “labile”—that is, fluid-like—as in the case of surfaces coated with surfactant monolayers or bilayers, the confined liquid cannot order and again the friction force will be low. This type of lubrication is very effective both with hydrocarbon liquids between surfactant monolayers exposing fluid chains (Yoshizawa et al., 1993), and water between surfactant bilayers exposing mobile hydrophilic head-groups (Drummond et al., 2003; Raviv et al., 2002a,b).

Finally, the forces between the surfaces may be sufficiently repulsive that they keep the surfaces well apart even under high loads such that the viscosity of the confined liquid does not increase too much above the bulk value. This commonly occurs in aqueous (water-based lubricant) systems including most biological systems, where the repulsive double-layer, short-range steric-hydration and entropic polymer-associated forces can be very strong (Raviv et al., 2002a,b; Perkin et al., 2009). In addition, the effective (thin film) viscosity of water is apparently not as enhanced as in oil-based systems, hence the low friction coefficients of some water-based lubricant systems and ice ($\mu \approx 0.02$; see Table 18.1) which are due to only 1–3 monolayers of liquid water between the shearing surfaces.

18.6 Transitions between Liquid- and Solid-Like Films

When confined to a thin film, both the static and dynamic properties of a liquid can be very different from those in the bulk. Regarding the dynamic properties, the shear viscosity usually increases, thereby enhancing the viscous force given by Eq. (18.10). But the thin-film viscosity also becomes non-Newtonian—that is, it also depends on the sliding velocity, V_{\parallel} , or shear rate, V_{\parallel}/D , exhibiting both “shear thickening” and “shear thinning” behavior whereby F_{\parallel} increases or decreases with increasing V_{\parallel} . The way the viscosity and friction of a film change with the load (pressure), sliding velocity and temperature follow certain trends that are encapsulated in the Williams-Landell-Ferry (WLF) theory, the “time-temperature superposition” principle, and the Deborah Number. The WLF theory (Ferry, 1980) was first developed to explain the complex nonlinear rheology of polymers, but it has since been recognized as applying to other energy-dissipating phenomena, including friction.

In the previous section we saw how smooth or stick-slip sliding can arise due to shear-induced melting of a film that produces a steep negative slope in the $F_{\parallel}(V_{\parallel})$ curve at some critical sliding velocity. In other systems the function $F_{\parallel}(V_{\parallel})$ can exhibit a number of maxima and minima at different velocities, giving rise to a series of smooth sliding interspersed by stick-slip (and slip-stick) sliding regimes. Such systems usually involve more complex lubricant films than the simple liquids described in Figures 18.10 and 18.12, and include boundary lubricant surfactant layers, mixed, branched and polydisperse hydrocarbons and higher MW polymer melts. Figure 18.13 illustrates a common scenario encountered in such systems, where the shearing surfaces are coated with a layer of chain-like molecules that can be in the solid or liquid state depending on the load, driving force, sliding velocity, previous history, and observation or experimental

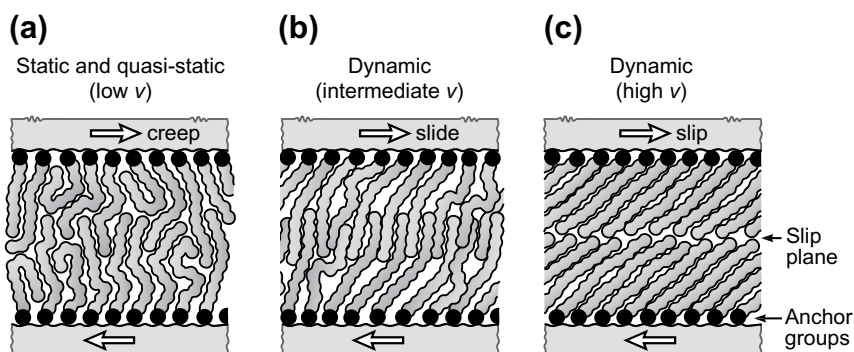


FIGURE 18.13 Two shearing surfaces, each coated with a surfactant “boundary lubricant” layer, where the state of the hydrocarbon chains determines the friction force. For chains in the fluid state (a) the film behaves like a liquid and the friction force is low. At intermediate velocities (b) the chains have time to interdigitate but not to completely disengage during the motion, giving rise to a higher friction force. At high sliding velocities (c) there is not enough time to interdigitate and the chains become shear-aligned, thereby offering low resistance (low friction) to sliding, as in (a). Polymer surfaces behave similarly.

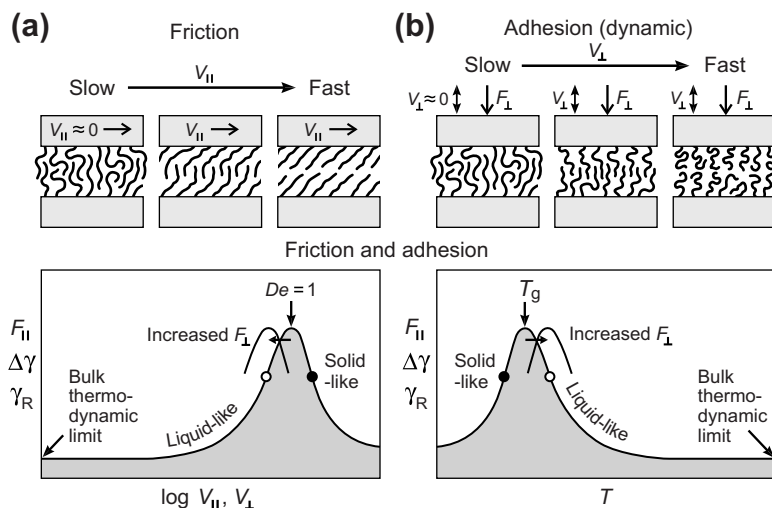


FIGURE 18.14 Dynamic friction phase diagrams showing the variation of the friction and adhesion forces with (a) sliding velocity, and (b) temperature, which are related by the time-temperature superposition principle (Ferry, 1980). Note that high friction forces F_{\parallel} are related to large adhesion hysteresis $\Delta\gamma$ or high effective adhesion forces γ_R via Eq. (18.8).

time (remember that it takes a finite time to melt or solidify). Freezing or nucleation times (on stopping) and melting times (on starting) can be surprisingly long, many seconds, and depend on the number of layers. Freezing and melting times are often similar, although freezing usually takes longer than melting (Yamada, 2003, 2009).

Let us consider the friction force as the driving force and sliding velocity increase gradually from zero at some fixed temperature where the film may be in the solid, amorphous or liquid state. Figure 18.13 shows the “static” film to be in the amorphous or solid state. Nevertheless, whatever the state of the film under static conditions, it will always flow to some extent as long as the temperature is finite. This is because of the defects such as vacancies that always exist in a film—even a solid crystalline film—at finite temperatures, and the continual hopping of molecules into and out of these defects biases the motion in the direction of the applied force, however small. Thus, under a force the film will flow, however slowly, and be describable by a shear viscosity, however large.⁸

Thus, as $V_{\parallel} \rightarrow 0$, $F_{\parallel} \rightarrow 0$, according to Eq. (18.10) for *any* system, although—due to the load-dependent confinement—the effective viscosity in Eq. (18.10) is usually very much higher than the bulk viscosity at that temperature. This is essentially the thermodynamic limit (Figure 18.14a), where the system can fully equilibrate at each position of the travel. In this sense, the film behaves like a liquid. Figure 18.14b shows the equivalent friction force–temperature phase diagram for this system, showing the thermodynamic,

⁸See The Pitch Drop Experiment, and the ongoing discussions regarding the existence or otherwise of “finite yield stress.” The viscosity of glucose decreases continuously from 10^{16} to 1 Pa.s as the temperature increases from 10°C to the glass transition temperature at ~150°C.

“liquid-like” limit at high T . The thermodynamic, high T or low V_{\parallel} regime is often inaccessible experimentally, since the time to equilibrate may be very long, requiring velocities, V_{\parallel} , below 1 nm/day or shear rates, V_{\parallel}/D , below 10^{-6} s^{-1} .

Before considering what happens on gradually increasing the sliding velocity V_{\parallel} , let us first look at the other extreme of very high V_{\parallel} . At high sliding velocities the chains have no time to interdigitate and so no new bonds are created (or broken) as the surfaces pass each other. Often, the surface molecules become shear-ordered or aligned, as illustrated in Figure 18.13c. In this regime, the system is far from equilibrium, and the film is effectively frozen or “solid-like” during the motion but with interfacial slip occurring easily between the two ordered layers. The friction force F_{\parallel} is low (Figure 18.14a). Similar shear-aligning effects also occur in the bulk at high shear rates, when it is known as “shear thinning.”

The intermediate regime between low and high V_{\parallel} is particularly interesting: in this regime F_{\parallel} can rise to very high values, as much as 3–4 orders of magnitude higher than the values at very low and very high V_{\parallel} . In this regime V_{\parallel} is still slow enough for the chains of Figure 18.13b to interdigitate naturally due to their thermal motion, but now too fast for the newly formed bonds to break without a large input of energy (the factor $F_{\parallel}\delta$ in Eq. (18.8)). This is the same regime that gives rise to high adhesion energy hysteresis. Regimes of high dissipation in their adhesion forces F_{ad} or friction forces F_{\parallel} occur when the sliding velocity, shear rate and/or temperature are close to the “characteristic” values of the system. In the case of sliding or shearing, the dimensionless Deborah Number, defined by (see also Section 9.3)

$$De = \frac{\text{characteristic relaxation time}}{\text{measurement or interaction time}} = \frac{\tau_0}{\tau_m} \quad (18.11)$$

distinguishes whether the system is in the high velocity, high shear rate, “solid-like” regime ($De > 1$) or in the low velocity, low shear rate, “liquid-like” regime ($De < 1$).

For many different types of systems, maximum energy transfer or dissipation occurs at $De \approx 1$. The simplest example is that of *forced simple harmonic motion*, where a spring supporting a mass m is driven by a stage with an oscillatory force $F_0 \cos \omega t$. The equation of motion of the mass is

$$m\ddot{x} + kx = F_0 \cos \omega t \quad (18.12a)$$

and the steady state solution is

$$x = \frac{F_0 \cos(\omega t + \phi)}{m(\omega_0^2 - \omega^2)}, \quad (18.12b)$$

where $\omega_0 = \sqrt{k/m}$ is the natural frequency of free oscillations, Eq. (18.4), F_0 is the amplitude, and ϕ is the phase difference in the oscillations of the mass and stage. The kinetic energy of the oscillating mass is $\frac{1}{2}m\dot{x}^2$ that, when averaged over a cycle, is $F_0^2\omega^2/4m(\omega_0^2 - \omega^2)^2$. Thus, for the same driving force F_0 maximum energy transfer from the stage to the oscillating mass occurs when the driving frequency ω (or interaction time) equals the natural frequency ω_0 (or characteristic time) of the system—that is, when $De = 1$.

The concept of the Deborah Number applies to many other energy dissipating (transferring) systems, including more complex cyclic processes and molecular collisions (Section 9.3), the viscoelasticity of polymers (Ferry, 1980), tribological processes (Ruths and Israelachvili, 2010), biological processes (Chapter 22), and various *resonance energy transfer* processes in optical and electrical systems.

When applied to tribological systems, the measurement or interaction time τ_m in Eq. (18.11) can refer to a frequency or the sliding velocity V_{\parallel} , where maximum energy transfer occurs at some critical velocity (Figure 18.14a). Inherent in such systems is the existence of a characteristic length, δ , that relates the sliding velocity to the measurement time via $\tau_m = \delta/V_{\parallel}$. Since the friction force peaks when $De \approx 1$ and falls at higher V_{\parallel} , this is also the regime where we expect stick-slip.

In the case of temperature, the *glass transition temperature* T_g characterizes the temperature at which energy dissipation is maximum (Figure 18.14b). Stick-slip usually occurs at $T < T_g$. However, as indicated in Figure 18.14, the load also has an effect on T_g , as well as on the relaxation time τ_0 . A higher load (pressure) usually drives a film toward the solid state, but it also increases its (relaxation) time to solidify *and* melt. The previous shearing history of a film therefore also plays a role in determining the instantaneous friction force, and is now routinely included in computer simulations and “rate-and-state” models of friction (Müser, 2008).

18.7 The “Real” Area of Contact of Rough Surfaces

In some disciplines, especially tribology, the question often arises: What is the “real” area of contact between two surfaces at the atomic or molecular level? As shown in Figure 17.17, for hard materials it can be very much smaller than the geometric or projected area, while for polymeric materials it can be much larger. In a classic experiment, Bowden and Tabor (1939) pressed together the rough surfaces of two hard conducting materials and measured the electric current and resistance between them. The resistance is the same as the inverse conductivity, which was found to be directly proportional to the load pressing the two materials together. From this result they concluded that the real area of contact, which was assumed to be proportional to the conductivity, is also directly proportional to the load.

Theoretical modeling of such systems is made difficult because at the molecular level there is no clear definition of “contact” as opposed to “not in contact.” A good operational definition (see Szlufarska et al., 2008; Mo et al., 2009; Cheng et al., 2010) is to consider those atoms that are closer than the separation at the potential energy minimum (r_e in Figure 1.4 or D_3 in Fig. 12.3) to be in contact; all others to be out of contact. The contact area is then given by multiplying the number of contacting atoms or “bonds” by the surface area of each atom. For nonadhering interactions, a certain “cut-off distance” is chosen to define the boundary between contacting and noncontacting atoms. Note that in all such procedures the contact area is ultimately defined in terms of the number of bonds across the interface, which is then converted into an area.

Using such approaches in computer simulations one usually finds, even for rough surfaces, that the real contact area A is roughly proportional to the applied load L when there is no adhesion between them (cheng et al., 2010), and we earlier saw (cf. Figure 18.6) that the friction force is also proportional to the load for nonadhering surfaces irrespective of how the real area varies with the load (Berman et al., 1998). Actually, more often one finds that the slope dA/dF_{\perp} , not the chord A/F_{\perp} , is a constant—that is, the line does not extrapolate back to the origin, which is also the case with simulations of the friction forces between nonadhering surfaces (Figure 18.16).

18.8 Rolling Friction

Another type of friction we shall consider is rolling friction (Bowden and Tabor, 2001), which occurs when a wheel or ball-bearing rolls and there is no slip (no shearing interface). Ball and roller bearings provide the best lubrication at high loads and speeds (see Worked Example below). But there is still some energy dissipation due to the hysteresis in the elasticity of any material.

When a sphere of radius R and elastic modulus K is under a load F_{\perp} the stored elastic energy, assuming Hertzian mechanics, is given by (see Section 17.7)

$$E_{\text{el}} = \int F d\delta = \int (Ka^3/R) d\delta = \int_0^{\delta} KR^{1/2} \delta^{3/2} d\delta = \frac{2}{5} KR^{1/2} \delta^{5/2} = \frac{2}{3} (F_{\perp}^5/K^2 R)^{1/3}, \quad (18.13)$$

where the flattened region is of diameter $2a$ given by Eq. (17.34a) Thus, during rolling the ball will be continually flattened and unflattened as its surface rolls a distance $2a$. If a fraction ε of this energy is unrecovered—that is, transformed into heat—then the friction force will be given by (cf. Eq. (18.8))⁹

$$F_{\parallel} = \varepsilon E_{\text{el}}/2a = \frac{1}{3} \varepsilon (F_{\perp}^5 / K^2 R)^{1/3} / (RF_{\perp}/K)^{1/3} = \frac{1}{5} \varepsilon F_{\perp} (F_{\perp}/KR^2)^{1/3} \propto F_{\perp}^{4/3}. \quad (18.14)$$

Thus, to have low rolling friction, it is desirable to have large wheels made of materials that have high K or hardness H and low ε . This is the reason why railway engines have *large* wheels made of *hardened* steel ($K = 10^{11} - 10^{12} \text{ N m}^{-2}$).

Worked Example 18.4

Question: At what load will the rolling friction force exceed the shear force for a wheel of radius $R = 10 \text{ cm}$, elastic modulus $K = 10^{11} \text{ N m}^{-2}$, where $\varepsilon = 0.1$ and $\mu = 0.2$? You may use the equations for spheres.

Answer: The ratio of the rolling to the sliding friction force is $\frac{1}{5} \varepsilon F_{\perp} (F_{\perp}/KR^2)^{1/3} / \mu F_{\perp} = \frac{1}{5} \varepsilon (F_{\perp}/KR^2)^{1/3} / \mu$, which in most practical situations is «1. Since rolling friction is proportional to $F_{\perp}^{4/3}$ rather than F_{\perp} we expect the former to exceed the latter at some high value of F_{\perp} . For the

⁹The distance over which the friction force acts depends on where the ball or wheel is pushed. It is $2a$ if at the center (the axle) as for a cart, but $4a$ if at the top (as for a ball bearing). It is for this reason that one needs only half the force to push a cart uphill when pushing the top of the wheel instead of the cart itself.

given values, this occurs at the impractically high load of $F_{\perp} = (5\mu/\varepsilon)^3 KR^2 = 10^3 \times 10^{11} \times 10^{-2} = 10^{12}$ kg. For all practical loads, the rolling friction is orders of magnitude lower than the load- or adhesion-controlled friction forces.



18.9 Theoretical Modeling of Friction Mechanisms

Modeling friction processes is difficult. There are the traditional empirical equations and scaling laws such as Amontons' Laws and the Stribeck Curve (Rabinowicz, 1995; Bowden and Tabor, 2001), analytic macroscopic models (Persson, 2000), computer simulations of molecular-scale tribological processes (Landman, 2005; Thompson and Robbins, 1990; Müser et al., 2003), and so-called "rate and state" models that also apply to seismic phenomena such as earthquakes (Ruina, 1983; Carlson and Batista, 1996; Müser, 2008). Some models apply to dry friction, others to lubricated friction. Some deal with the theoretically and experimentally challenging problems associated with rough surfaces, others try to predict surface damage (wear), which has not been covered in this chapter.

Computer simulations. Large-scale molecular and particle dynamics computer simulations are time-consuming but provide the best or most rigorous way to analyze both the equilibrium and dynamic properties of tribological systems at the molecular level in terms of the intermolecular forces. Figures 18.15 and 18.16 show the results of simulations of the friction forces between two slightly rough surfaces under adhesive and nonadhesive conditions. We may note the finite zero load friction force in the former, as expected from Eq. (18.7), and the similar *slopes* of the F_{\parallel} vs F_{\perp} curves, giving the same friction coefficient μ , for the adhesive and nonadhesive surfaces because their surface roughness (texture or structure) is the same.

Semiempirical (heuristic) "rate and state" models. Various models have been proposed that can handle macroscopic systems and/or long-term effects that cannot be analyzed by, for example, molecular dynamics computer simulations. "Rate and state"

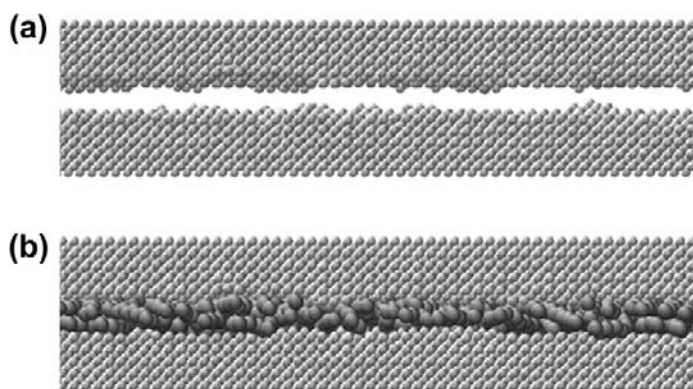


FIGURE 18.15 Rough surfaces of gold separated by vacuum (adhesive) and a liquid hexadecane film (nonadhesive). [Reproduced from Gao et al., (2004) with permission.]

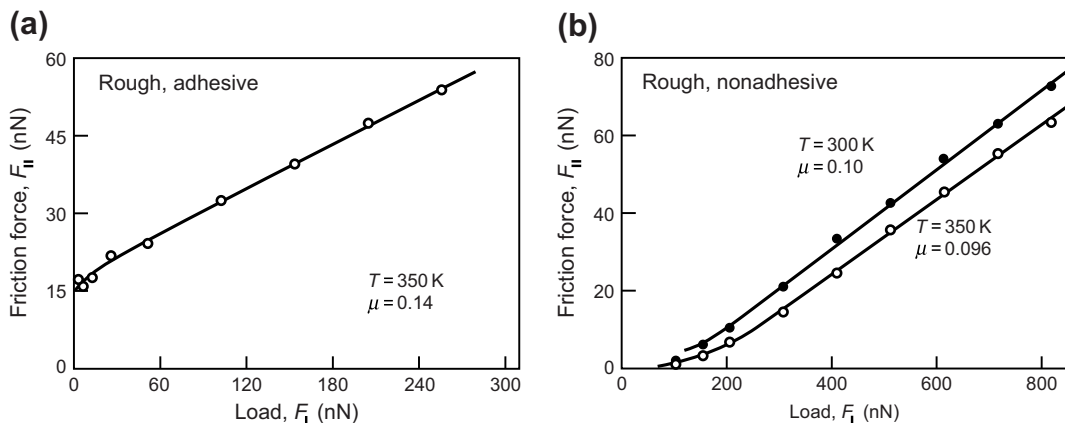


FIGURE 18.16 Molecular dynamics (MD) computer simulation of the friction forces between the two rough adhesive surfaces (a) and nonadhesive surfaces (b) of Figure 18.15. The sliding velocity was 1 m s^{-1} . [Reproduced from Gao et al., 2004, with permission.]

and “Shear Transformation Zone” (STZ) models are two examples where constitutive equations describe the time evolution of the system in terms of parameters such as the shear rate or sliding velocity and the state (liquid or solid) of the deforming material or shearing film. Such models have successfully described chaotic stick-slip motion (see

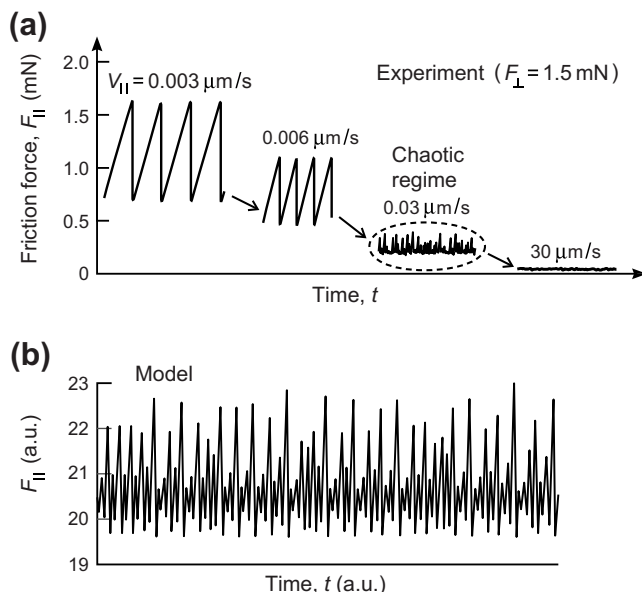


FIGURE 18.17 (a) Chaotic stick-slip regime measured in the transition from highly regular (periodic) stick-slip at low V_{\parallel} to smooth sliding at high V_{\parallel} for two shearing mica surfaces separated by a 1–2 nm thick film of a branched hydrocarbon liquid. (b) Analysis of the chaotic regime using the Shear Transformation Zone (STZ) model. [Courtesy of Carlos Drummond, Anaël Lemaître and Jean Carlson.]

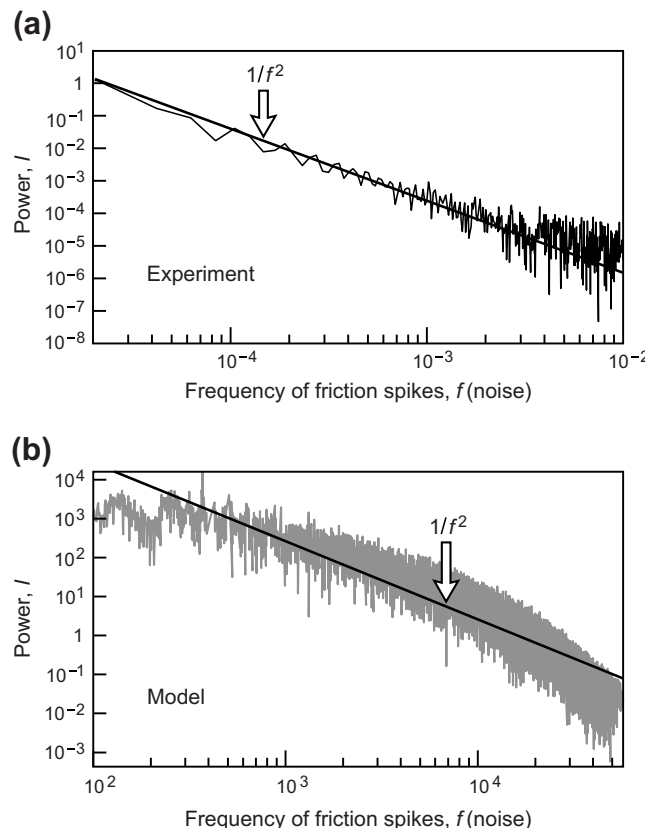


FIGURE 18.18 (a) Power spectrum corresponding to the chaotic stick-slip regime of Figure 18.17a. (b) Theoretical prediction based on the STZ model which has also been used successfully to analyze earthquakes (Ruina, 1983; Carlson and Batista, 1996). [Courtesy of Anaël Lemaître and Jean Carlson.]

Figures 18.11c and 18.17) and the power spectra of various slip and stress-weakening processes in both tribological and seismic (e.g., earthquake) phenomena (Figure 18.18).

During chaotic sliding the stick-slip spikes appear to be random, but neither the amplitude nor the frequency is random. The friction trace is “deterministic” but in a complex way that requires detailed analysis of the friction force *vs* time. The resulting power spectrum (Figure 18.18) gives the friction spike intensity I versus frequency f , which often follows a $1/f^n$ function where $n = 1$ or 2 . For example, if $I \propto 1/f^2$, a 10 times stronger earthquake is 3 times less likely. Unfortunately, deterministic models are not yet able to reliably predict earthquakes.

PROBLEMS AND DISCUSSION TOPICS

- 18.1** Analyze the *energy-distance* potential functions of Figure 18.9 in terms of the *force-distance* functions, clearly showing the initial instability (onset of slip) and

subsequent stick states. If the surface area of the stage is $100 \times 100 \text{ nm}^2$ and the mean intermolecular spacing is 0.5 nm, and a lateral force of 10 pN is required to move a molecule over its neighbors, calculate (i) the shear stress, and (ii) the maximum possible number of quantized stick states during a stick-slip cycle when using a spring of stiffness $k = 1 \text{ N m}^{-1}$. [Answers: (i) $4 \times 10^7 \text{ N m}^{-2}$; (ii) about 800.]

- 18.2** Figure 18.19 shows plots of the displacement of a DRIVE x' as a function of time t (see Figure 18.4) for a system where (i) the friction force $F_{\parallel} = \mu F_{\perp} = 0.4 K a$ is independent of the sliding velocity V_{\parallel} and distance x . On the same plot, draw in the following parameters as a function of time: the velocity of the DRIVE V'_x , the measured friction force F'_{\parallel} , the velocity of the SLIDER V'_{\parallel} , and the sliding distance x . (ii) Repeat (i) for the case where a Newtonian liquid film lubricates the surfaces and the friction force is given by Eq. (18.10).
- 18.3** Physiological fluids contain electrolytes and various biomolecules, and they are usually non-Newtonian both in the bulk and when confined between two surfaces. Two biological surfaces in physiological solution are repelled from each other by a short-range electrostatic, hydration or polymer-mediated force F_{\perp} or pressure $P_{\perp} = F_{\perp}/A$, given by $P_{\perp} = C/D^2 \text{ N/m}^2$, where $C = 10^{-10} \text{ N}$ and D is the film thickness. When the upper surface of area $A = 1 \text{ cm}^2$ slides at velocity $V_{\parallel} = 1 \text{ cm/s}$, the friction force is found to vary with the load as shown in Figure 18.20—that is, the system appears to obey Amontons' first law, exhibiting a constant friction coefficient of $\mu = 0.1$ (at constant V_{\parallel} and A) over the range of loads studied. Surprisingly, the friction force is found to also obey Amontons' other two laws—that is, $F_{\parallel} = \mu F_{\perp}$ where μ remains constant and equal to 0.1 independently of both V_{\parallel} and A .
- (i) Assuming that Eq. (18.10) for Couette flow applies, but with an effective thin film viscosity η_{eff} that is not a constant, what is the expression for η_{eff} as a function of μ , C , V_{\parallel} and D over the range of loads shown in Figure 18.20? (ii) What is the effective viscosity at $F_{\perp} = 100 \text{ N}$? Does the film "shear thicken" or "shear thin"? [Answer to (ii): 0.1 Pa.s]
- 18.4** (i) In which order would you expect the adhesion-controlled friction forces to decrease for the following surfaces: (a) two molecularly smooth surfaces,

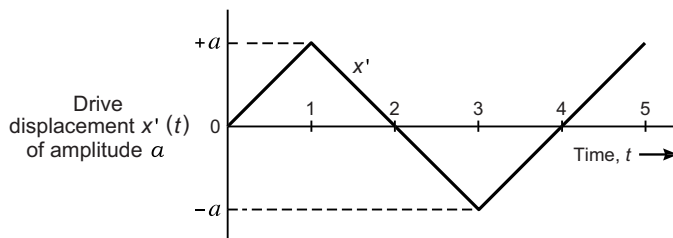


FIGURE 18.19

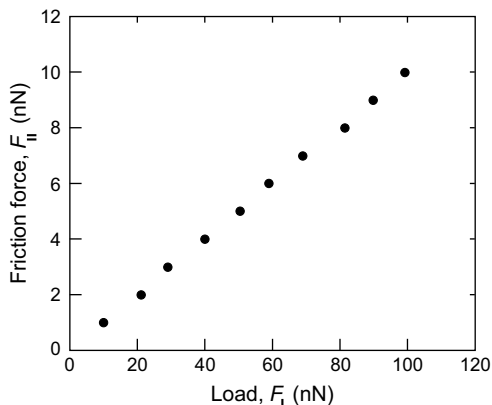


FIGURE 18.20

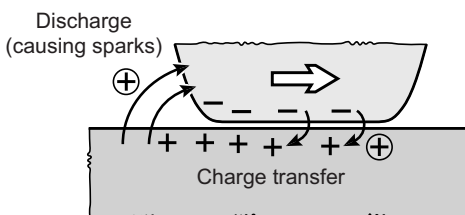
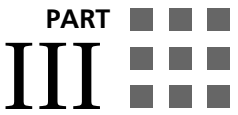


FIGURE 18.21 Spontaneous charge exchange between dissimilar surfaces is usually enhanced by rubbing. Such triboelectric charging can cause audible and visible sparks, for example, when walking on a carpet or rolling mercury in a horizontal glass tube.

(b) a rough surface sliding across a smooth surface, or (c) two rough surfaces? The materials and asperities of the two surfaces may be considered to be elastic in each case, with no plastic deformations occurring during sliding. (ii) When a liquid droplet moves along a solid surface, or a liquid filament moves forward in a capillary tube, if there is no slip at the solid-liquid interface, how can this motion happen at the molecular level?

- 18.5*** *Triboelectric effects* occur when there is spontaneous charge transfer or *contact electrification* between two dissimilar surfaces, which increases their adhesion force (see Section 17.4). The increased adhesion also increases the friction force, but the mechanism of *adhesion hysteresis* and *adhesion-controlled friction* due to charge exchange is different and much more complex than that due to van der Waals forces described in Section 18.2. Figure 18.21 shows how charges move between two sliding surfaces or asperities, illustrating the different effects occurring at the front and back ends of a contact junction. Discuss how the friction force is expected to be enhanced when the adhesion energy is increased by W_{el} as given by Eq. (17.26).



Self-Assembling Structures and Biological Systems

This page intentionally left blank

Thermodynamic Principles of Self-Assembly

19.1 Introduction: Soft Structures

In Part III we shall be looking at the interactions of molecular aggregates, such as micelles, microemulsions, bilayers, vesicles, biological membranes, and macromolecules such as proteins. Most of these structures form readily in aqueous solution by the spontaneous *self-association* or *self-assembly* of *amphiphilic* molecules (see Figures 19.1 and 19.2 and Table 19.1). These structures and the systems they form—sometimes collectively referred to as *associated* or *association colloids, complex fluids, and soft (structured) materials*—stand apart from the conventional colloidal particles discussed in Part II in one important respect: unlike solid particles or rigid macromolecules such as viruses, globular proteins, and DNA, they are soft and flexible—that is, *fluid-like*. This is because the forces that hold amphiphilic molecules together in micelles and bilayers are not due to strong covalent or ionic bonds but arise from weaker van der Waals, hydrophobic, hydrogen-bonding, and screened electrostatic interactions. Thus, if the solution conditions, such as the electrolyte concentration or the pH, of an aqueous suspension of micelles or vesicles is changed, not only will this affect the interactions between the aggregates, but it will also affect the intermolecular forces within each aggregate, thereby modifying the size and shape of the structures themselves. It is therefore necessary to begin by considering the factors that determine how and why certain molecules associate into various well-defined structures.

In Chapters 19 and 20 we shall be concerned with the thermodynamic and physical principles of self-assembly in general and of amphiphilic molecules such as surfactants and lipids in particular, while in Chapters 21 and 22 we shall investigate the various equilibrium and nonequilibrium forces and interactions between these structures. Chapter 22 also discusses the differences between structures that form spontaneously by *self-assembly* and those that are formed by *directed-assembly*.

Our first concern will be to formulate the basic equations of self-assembly in general statistical thermodynamic terms and then go on to investigate the relevant intermolecular interactions that determine into which structures different amphiphiles will assemble. We shall find that a very beautiful picture emerges that brings out the role of molecular geometry in determining the structures formed and from which many of the physical properties of these structures can be quantitatively understood without requiring a detailed knowledge of the very complex short-range forces operating between the polar headgroups and hydrocarbon chains. (By analogy, the van der Waals equation of state contains no information on the nature and range of intermolecular forces—that

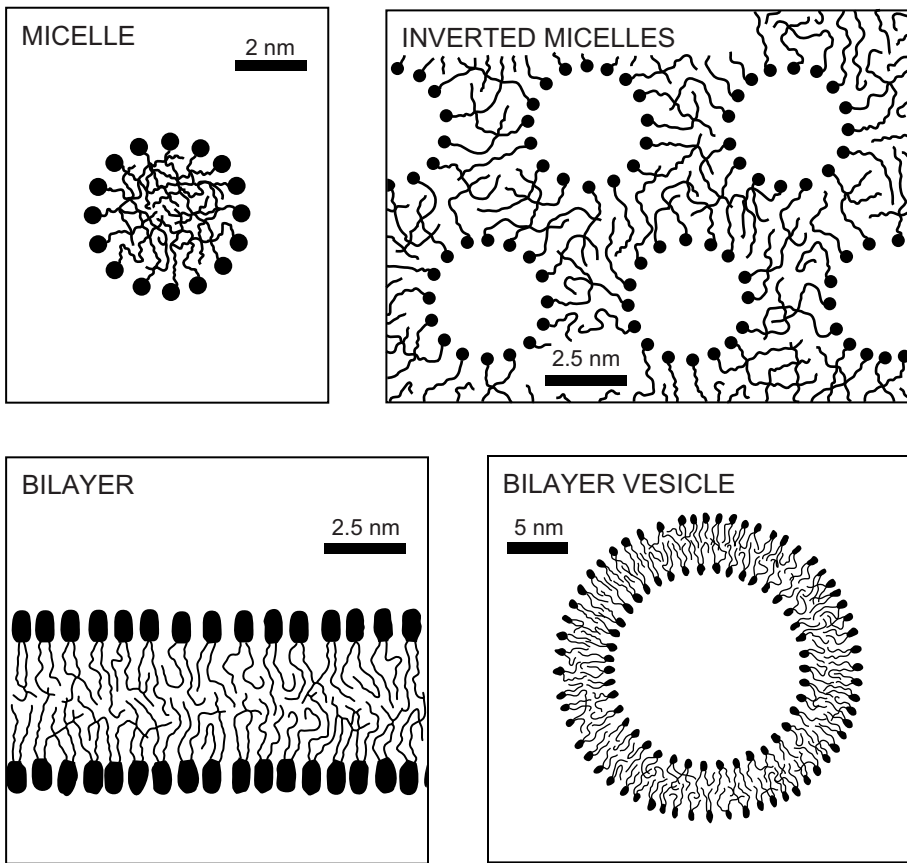


FIGURE 19.1 Surfactant and lipid amphiphiles: Amphiphiles such as surfactants and lipids (see Table 19.1) can associate into a variety of structures in aqueous solutions. These can transform from one to another by changing the solution conditions such as the electrolyte or lipid concentration, pH, or temperature. In most cases the hydrocarbon chains are in the fluid state allowing for the passage of water and ions through the narrow hydrophobic regions—for example, across bilayers. The lifetime of water molecules in lecithin vesicles is about 0.02 sec, while ions can be trapped for much longer times, about 8 hr for Cl^- and one month for Na^+ ions. Most single-chained surfactants form micelles, while most double-chained surfactants form bilayers, for reasons that are discussed in Chapter 20.

is, the force laws—and yet it provides a very satisfactory description of gas-liquid phase behavior. Indeed, when van der Waals in 1873 proposed his famous equation, he knew nothing about the origin and nature of van der Waals forces.)

19.2 Fundamental Thermodynamic Equations of Self-Assembly

The literature on this subject is voluminous and often confusing, the most rigorous treatment being that of Hall and Pethica (1967) based on Hill's classic books on small

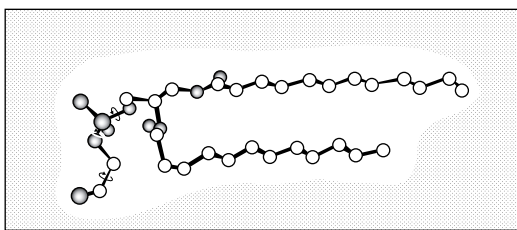


FIGURE 19.2 The zwitterionic phospholipid dilauryl-phosphatidyl-ethanolamine (DLPE) containing two saturated hydrocarbon chains, each with 12 carbons, and a hydrophilic (sometimes referred to as polar) headgroup (see also Table 19.1). DLPE is an amphiphile, characterized by having a solvophilic (hydrophilic) and a solvophobic (hydrophobic) region. Many self-assembling molecules can have more than two such regions, for example, polymer tri-blocks, allowing them to form more complex structures both in solution and in the pure state. When PE lipids self-assemble into a bilayer, the positive ammonium group of each molecule can come close to the negative phosphate group of its neighbor, thereby providing a fairly strong lateral dipole-dipole attraction holding the headgroups together. The bulkier headgroups of PC lipids do not allow for such tightly packed associations: their headgroup areas in bilayers are much larger and the bilayers more fluid-like.

systems thermodynamics (Hill, 1963, 1964, 2002). We shall follow the more simplified approach and notation of Tanford (1980) for micelles, which was later extended to larger lipid aggregates such as bilayers, vesicles, other micellar phases, and microemulsion droplets by Nagarajan and Ruckenstein (1977, 1979), Israelachvili et al., (1976, 1977, 1980a), Wennerström and Lindman (1979), Mitchell and Ninham (1981), and Evans and Wennerström (1999).

Equilibrium thermodynamics requires that in a system of molecules that form aggregated structures in solution (Figure 19.3) the chemical potential of all identical molecules in different aggregates must be the same. This may be expressed as

$$\mu = \mu_1^0 + kT \log X_1 = \mu_2^0 + \frac{1}{2} kT \log \frac{1}{2} X_2 = \mu_3^0 + \frac{1}{3} kT \log \frac{1}{3} X_3 = \dots$$

monomers dimers trimers

$$\text{or} \quad \mu = \mu_N = \mu_N^0 + \frac{kT}{N} \log\left(\frac{X_N}{N}\right) = \text{constant}, \quad N = 1, 2, 3, \dots, \quad (19.1)$$

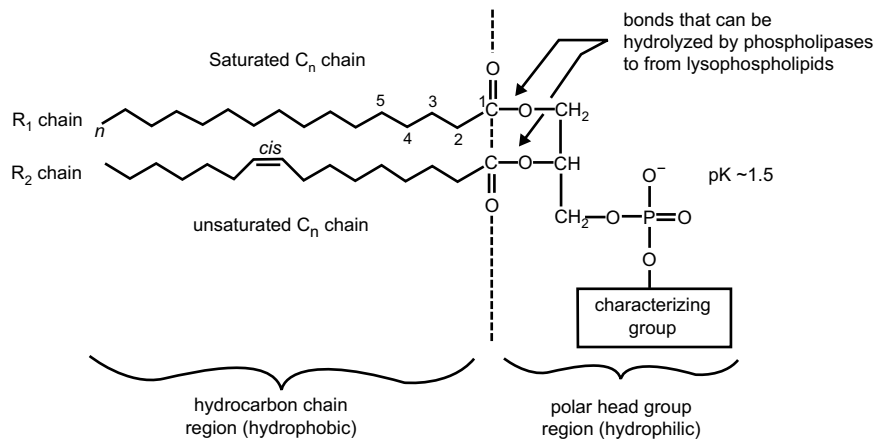
where μ_N is the mean chemical potential of a molecule in an aggregate of aggregation number N , μ_N^0 is the standard part of the chemical potential (the mean interaction free energy *per molecule*) in aggregates of aggregation number N , and X_N is the concentration (more strictly the activity) of molecules in aggregates of number N . $N = 1$, μ_1^0 , and X_1 correspond to isolated molecules or *monomers* in solution. Note that the energy *per aggregate* is $N\mu_N^0$. Equation (19.1) may also be derived using the familiar *law of mass action* as follows: referring to Figure 19.3 we may write

rate of association = $k_1 X_i^N$,

rate of dissociation $\equiv k_N(X_N/N)$

Table 19.1 Some Common Amphiphiles

Single-chained surfactants and lipids		
Anionic	$C_{12}H_{25}-O-SO_3^-Na^+$	Sodium dodecyl sulphate (SDS or NaDS)
Anionic	$C_{18}H_{37}-COO^-H^+$	Stearic acid
Cationic	$C_{16}H_{33}-N+(CH_3)_3Br^-$	Hexadecyl trimethyl ammonium bromide (HTAB or CTAB)
Nonionic	$C_{12}H_{25}-(O-CH_2-CH_2)_5-OH$	Pentaoyxethylene dodecyl ether ($C_{12}E_5$)
Zwitterionic	Lysolecithin (see below)	Single chained lipids (double-chained lipids after lysis)
Catanionic	CTAB-SDS dimer	Strong binding of anionic and cationic headgroups effectively form a double-chained surfactant
Bola	$(CH_2-CH_2-O)_5-C_{12}H_{25}-(O-CH_2-CH_2)_5$ or $E_5C_{12}E_5$	Alkyl chain with a headgroup at each end
Gemini	$[C_{12}H_{25}-N^+(CH_3)_2(CH_2)_n(CH_3)_2N^+-C_{12}H_{25}]_2Br^-$	Surfactants covalently linked by a 'spacer'

Double-chained phospholipids

Hydrocarbon chains^a
Normally contain 16–18
carbons per chain, the R_2
chain containing 1–3 *cis*

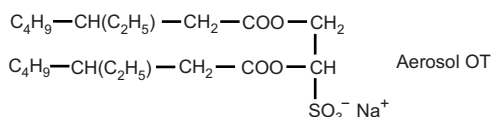
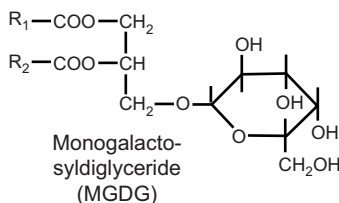
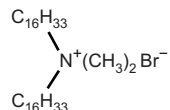
Name of phospholipid^b
...phosphatidic acid (anionic)

Characterizing group^c
—H $pK \sim 11$

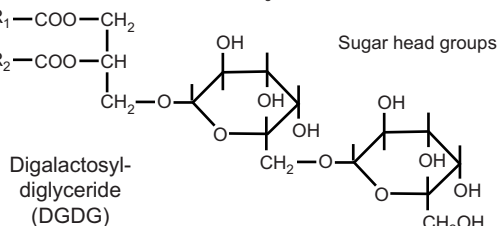
diC ₁₂ : dilauroyl...	... phosphatidyl choline or lecithin (zwitterionic)	$\text{--CH}_2\text{--CH}_2\text{--N}^+(\text{CH}_3)_3$
diC ₁₄ : dimyristoyl...	... phosphatidyl ethanolamine (zwitterionic)	$\text{--CH}_2\text{--CH}_2\text{--NH}_3^+ \text{ pK } \sim 11$
diC ₁₆ : dipalmitoyl...	... phosphatidyl glycerol (anionic)	$\begin{array}{c} \text{CH}_2\text{OH} \\ \\ \text{--CH}_2\text{--CH} \\ \\ \text{OH} \\ \\ \text{COO}^- \\ \\ \text{NH}_3^+ \end{array}$
diC ₁₈ : distearoyl...	... phosphatidyl serine (anionic)	$\begin{array}{c} \text{CH}_2\text{OH} \\ \\ \text{--CH}_2\text{--CH} \\ \\ \text{OH} \\ \\ \text{COO}^- \\ \\ \text{NH}_3^+ \end{array}$

Other double-chained surfactants and lipids^b

Dihexadecyl dimethylammonium bromide (diC₁₆ DAB)



Aerosol OT



^aAbout 50% of biological lipids have an unsaturated chain; these increase the fluidity and hydrophilicity of bilayers.

^bPhosphatidylcholines (lecithins) and phosphatidylethanolamines (cephalin) are the two major lipids found in animal membranes, while the galactolipids DGDG and MGDG are the major constituents of plant thylakoid membranes. Note that none of these carry a net charge at normal pH.

^cThe ionic states of the headgroups are given for aqueous dispersions at pH 7. At high pH (>11.5) phosphatidylethanolamine becomes negatively charged while at low pH (<1) it becomes positively charged.

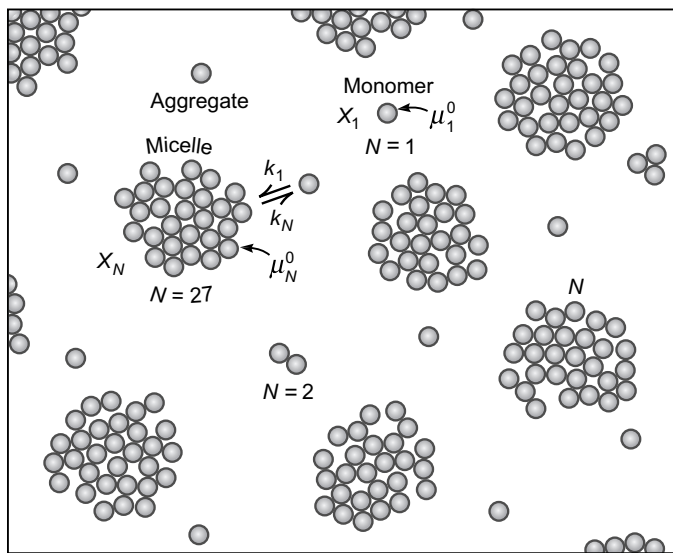


FIGURE 19.3 Definition of parameters used in the thermodynamic equations for the association of N monomers into an aggregate (e.g., a micelle). The mean lifetime of an amphiphilic molecule in a small micelle is very short, typically 10^{-5} – 10^{-3} s.

where

$$K = k_1/k_N = \exp[-N(\mu_N^0 - \mu_1^0)/kT] \quad (19.2)$$

is the ratio of the two “reaction” rates, giving the equilibrium constant, K . The above combine to give Eq. (19.1), which can also be written in the more useful (and equivalent) forms

$$X_N = N \{ (X_M/M) \exp[M(\mu_M^0 - \mu_N^0)/kT] \}^{N/M} \quad (19.3a)$$

$$\text{and, putting } M = 1, \quad X_N = N \{ X_1 \exp[(\mu_1^0 - \mu_N^0)/kT] \}^N, \quad (19.3b)$$

where M is any arbitrary reference state of aggregates (or monomers) with aggregation number M (or 1). Equations (19.3) together with the conservation relation for the total solute concentration C

$$C = X_1 + X_2 + X_3 + \dots = \sum_{N=1}^{\infty} X_N \quad (19.4)$$

completely defines the system. Depending on how the free energies μ_1^0, μ_N^0 are defined the dimensionless concentrations C and X_N can be expressed in volume fraction or mole fraction units [(mol dm⁻³)/55.5 or M/55.5 for aqueous solutions]. In particular, note that C and X_N can never exceed unity. Equation (19.3) assumes ideal mixing and is restricted to dilute systems where interaggregate interactions can be ignored. The effects of such interactions will be considered later.

Worked Example 19.1

Question: Certain types of solute molecules are found to self-assemble in solution into discrete macromolecular clusters with a fixed aggregation number N per cluster. The equilibrium between monomers (A) and aggregates (B) in the solution may be expressed in the form of a chemical reaction: $A + A + A + \dots = B$. Let X_A and X_B be the concentrations of A and B in mole fraction units, K the equilibrium constant for the reaction ($K \gg 1$), N the number of molecules per aggregate ($N \gg 1$), and let C be the *total* concentration of solute molecules in the solution.

- (1) Obtain a relation between K , N , C , and X_A , and show that for $K \gg 1$ and $N \gg 1$ the concentration of monomers, X_A , can never exceed $(NK)^{-1/N}$.
- (2) If $K = 10^{80}$ and $N = 20$ calculate the concentration of molecules in monomers, X_A , and monomers in aggregates, NX_B , at 2.0×10^{-5} , $C = 1.052 \times 10^{-4}$, and $C = 0.1$ (10% mole fraction). Comment on your findings. (Note that X_N in the notation of Eqs. (19.1)–(19.4) corresponds to NX_B in the present notation).

Answer: (1) Combining the two basic equations: $K = X_B/X_A^N$ and $C = X_A + NX_B$, we obtain $K = (C - X_A)/NX_A^N = \text{constant}$, or $X_A = [(C - X_A)/NK]^{1/N}$. Since the maximum possible value of $(C - X_A)$ is 1, we immediately find that X_A can never exceed $(NK)^{-1/N}$. For $K = 10^{80}$ and $N = 20$ this critical concentration is 0.86×10^{-4} .

(2) Putting $K = 10^{80}$ and $N = 20$ into the above equation gives $X_A = 10^{-4}[(C - X_A)/20]^{1/20}$. Solving this for the given values of C we find:

$$\text{at } C = 2.0 \times 10^{-5}, \quad X_A = 1.99999998 \times 10^{-5} \text{ and } NX_B = 2 \times 10^{-13},$$

$$\text{at } C = 1.052 \times 10^{-4}, \quad X_A = NX_B = 0.526 \times 10^{-4},$$

$$\text{at } C = 0.1, \quad X_A = 0.8 \times 10^{-4} \text{ and } NX_B = 0.09992.$$

Thus, for $C \ll 10^{-4}$ we have $X_A \approx C$ (i.e., most of the surfactant molecules remain dispersed as monomers). At $C \approx 10^{-4}$, we have $X_A \approx NX_B$ (i.e., the molecules partition equally between monomers and aggregates), while for $C \gg 10^{-4}$ we have $X_A \approx 10^{-4} \approx \text{constant}$, and $NX_B \approx C$ —that is, the monomer concentration remains unchanged at $\sim 10^{-4}$ as all the molecules go into aggregates. The critical concentration of $\sim 10^{-4}$, or $(NK)^{-1/N}$, is known as the *critical micelle concentration* (CMC) or *critical aggregate concentration* (CAC), and is discussed further in Section 19.5.

Little more can be said about aggregated dispersions without specifying the form and magnitude of μ_N^o as a function of N . This important matter will now be considered, and it is instructive to first proceed with a formal thermodynamic analysis of the equations derived so far.

19.3 Conditions Necessary for the Formation of Aggregates

Aggregates form only when there is a difference in the cohesive energies between the molecules in the aggregated and the dispersed (monomer) states. If the molecules in different-sized aggregates (including monomers) all experience the same interaction with

their surroundings, the value of μ_N^0 will remain constant in different aggregates (with different N , including $N = 1$), and Eq. (19.3) becomes

$$X_N = NX_1^N \quad \text{for } \mu_1^0 = \mu_2^0 = \mu_3^0 = \dots = \mu_N^0. \quad (19.5)$$

Since $X_1 < 1$, we must have $X_N \ll X_1$ so that most of the molecules will be in the monomer state ($N = 1$). If μ_N^0 increases as N increases, Eq. (19.3) shows that the occurrence of large aggregates becomes even less probable.

The necessary condition for the formation of large stable aggregates is that $\mu_N^0 < \mu_1^0$ for some value(s) of N —for example, when μ_N^0 progressively decreases as N increases or when μ_N^0 has a minimum value at some finite value of N . As we shall see, the exact functional variation of μ_N^0 with N also determines many of the physical properties of aggregates, such as their mean size and polydispersity. Further, since this variation may be a complex one, it is clear that a number of structurally different populations may coexist within a *single phase*¹ in thermodynamic equilibrium with each other (note that X_N in Eq. (19.3) is a *distribution function* and may peak at more than one value of N).

We shall now consider the functional forms of μ_N^0 for some simple structures, and by use of Eqs. (19.3)–(19.4) investigate their physical properties.

19.4 Effect of Dimensionality and Geometry: Rods, Discs, and Spheres

One-dimensional aggregates (rods, cylinders). As mentioned above, aggregates will form if μ_N^0 decreases with N . We shall now see that in a first approximation the dependence of μ_N^0 on N is usually determined by the geometrical shape of the aggregate. Let us begin by considering a suspension of rod-like aggregates made up of linear chains of identical molecules or monomer units (strings of beads) in equilibrium with monomers in solution. Let $-\alpha kT$ be the monomer-monomer “bond” energy in the aggregate relative to isolated monomers in solution (Figure 19.4). The total interaction free energy $N\mu_N^0$ of an aggregate of N monomers is therefore (remembering that the terminal monomers are unbonded)

$$N\mu_N^0 = -(N - 1)\alpha kT$$

that is,

$$\mu_N^0 = -(1 - 1/N)\alpha kT = \mu_\infty^0 + \alpha kT/N. \quad (19.6)$$

Thus, as N increases, the mean free energy μ_N^0 decreases asymptotically toward μ_∞^0 , which defines the “bulk” energy of a molecule in an infinite aggregate. A similar expression for μ_N^0 is obtained for any type of rod-like structure (e.g., a cylindrical micelle).

¹No matter how large the aggregates or structures, the system remains a single phase as long as the distribution of aggregates does not change as we go through the system. A two-phase system requires there to be a single interface separating the two phases (see Problem 19.8).

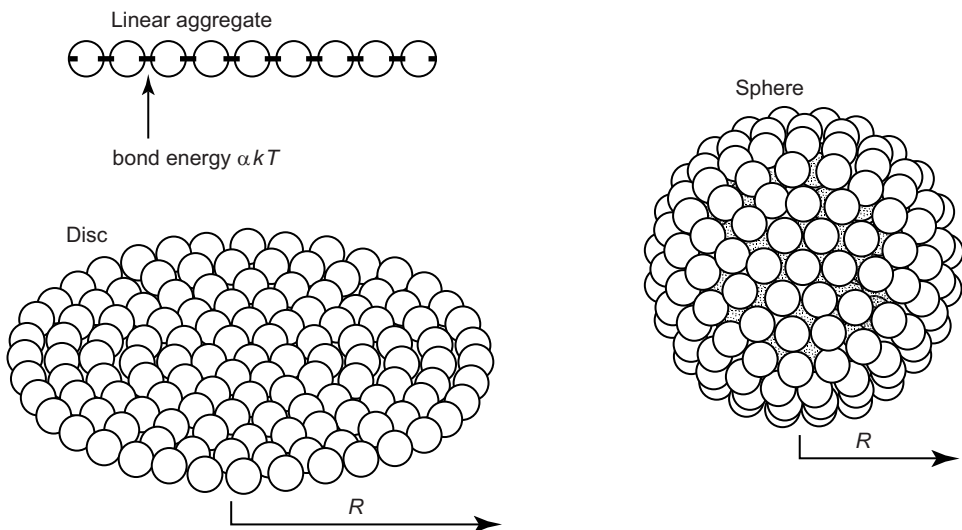


FIGURE 19.4 One-, two-, and three-dimensional structures formed by the association of identical monomer units in solution.

Two-dimensional aggregates (discs, sheets). Let us now look at disc-like or sheet-like aggregates (Figure 19.4). Here the number N of molecules per disc is proportional to the area πR^2 , while the number of unbonded molecules in the rim is proportional to the circumference $2\pi R$, and thus to $N^{1/2}$. The mean free energy per molecule in such an aggregate is therefore

$$\mu_N^0 = \mu_\infty^0 + \alpha kT/N^{1/2}, \quad (19.7)$$

where again α is some constant characteristic of the monomer-monomer and monomer-solvent interaction. As an example, consider the association of molecules that can only bind to each other in 2D to form sheets. If v is the volume per molecule and ℓ its mean size ($v \approx \ell^3$), then for a circular disk of radius R , $N = \pi R^2/v = \pi R^2/\ell^3$. The free energy of the disc is given by $N\mu_\infty^0 + 2\pi R\ell\gamma_i$, where μ_∞^0 is the bulk energy per molecule and γ_i the interfacial free energy per unit exposed area of the rim (Chapter 15). The additional edge or rim energy $2\pi R\ell\gamma_i$ can also be expressed as $2\pi R\lambda$, where $\lambda = \ell\gamma_i$ is the *line tension* (in units of N), representing the energy per unit length of the edge or rim.

In 2D we therefore have

$$\mu_N^0 = \mu_\infty^0 + \frac{2\pi(v/\pi)^{1/2}\ell\gamma_i}{N^{1/2}} = \mu_\infty^0 + \frac{\alpha kT}{N^{1/2}}, \quad (19.8a)$$

where

$$\alpha = 2\pi(v/\pi)^{1/2}\ell\gamma_i/kT \approx 2(\pi v)^{1/2}\lambda/kT. \quad (19.8b)$$

Three-dimensional aggregates (spheres, droplets). Finally, let us consider spherical aggregates or small solute droplets of radius R in a solvent (see Figure 19.4). Here N is

proportional to the volume $\frac{4}{3}\pi R^3$, while the number of unbonded surface molecules is proportional to the area $4\pi R^2$ and thus to $N^{2/3}$. We therefore have

$$\mu_N^0 = \mu_\infty^0 + \alpha kT/N^{1/3}. \quad (19.9)$$

As an example, consider the association of small hydrocarbon molecules such as alkanes in water. If v is the volume per molecule, then $N = 4\pi R^3/3v$. The free energy of the sphere is given by $N\mu_\infty^0 + 4\pi R^2\gamma_i$, where μ_∞^0 is the bulk energy per molecule and γ_i the interfacial free energy per unit area (Chapter 15). Hence,

$$\mu_N^0 = \mu_\infty^0 + \frac{4\pi R^2\gamma}{N} = \mu_\infty^0 + \frac{4\pi\gamma(3v/4\pi)^{2/3}}{N^{1/3}} = \mu_\infty^0 + \frac{\alpha kT}{N^{1/3}}, \quad (19.10a)$$

where $\alpha = \frac{4\pi\gamma_i(3v/4\pi)^{2/3}}{kT} \approx \frac{4\pi r^2\gamma_i}{kT}, \quad (19.10b)$

r being the effective radius of a molecule.

We see, therefore, that for the simplest shaped structures—rods, sheets, and spheres—the interaction free energy of the molecules can be expressed as

$$\mu_N^0 = \mu_\infty^0 + \alpha kT/N^p, \quad (19.11)$$

where α is a positive constant dependent on the strength of the intermolecular interactions and p is a number that depends on the shape or dimensionality of the aggregates. As we shall see, Eq. (19.11) also applies to other structures such as spherical vesicles in which the bilayers bend elastically. In particular, we note that for all these structures, μ_N^0 decreases progressively with N , which is a necessary (but not sufficient) condition for aggregate formation.

19.5 The Critical Micelle Concentration (CMC)

Given the general functional form of μ_N^0 of Eq. (19.11) we may now ask, at what concentration will aggregates form? Incorporating Eq. (19.11) into the two fundamental equations of self-assembly, Eqs. (19.3) and (19.4), leads to some very interesting conclusions. First, we note that

$$\begin{aligned} X_N &= N\{X_1 \exp[(\mu_1^0 - \mu_N^0)/kT]\}^N \\ &= N\{X_1 \exp[\alpha(1 - 1/N^p)]\}^N \approx N[X_1 e^\alpha]^N. \end{aligned} \quad (19.12)$$

Now, for sufficiently low monomer concentrations X_1 such that $X_1 \exp[(\mu_1^0 - \mu_N^0)/kT]$ or $X_1 e^\alpha$ is much less than unity, we have $X_1 > X_2 > X_3 > \dots$ for all α . Thus, at low concentrations most of the molecules in the solution will be isolated monomers—that is, $X_1 \approx C$, as shown in Figure 19.5. However, since X_N can never exceed unity, it is clear from Eq. (19.12) that once X_1 approaches $\exp[-(\mu_1^0 - \mu_N^0)/kT]$ or $e^{-\alpha}$, it can increase no further. The monomer concentration (X_1)_{crit} at which this occurs may be called the *critical aggregation*

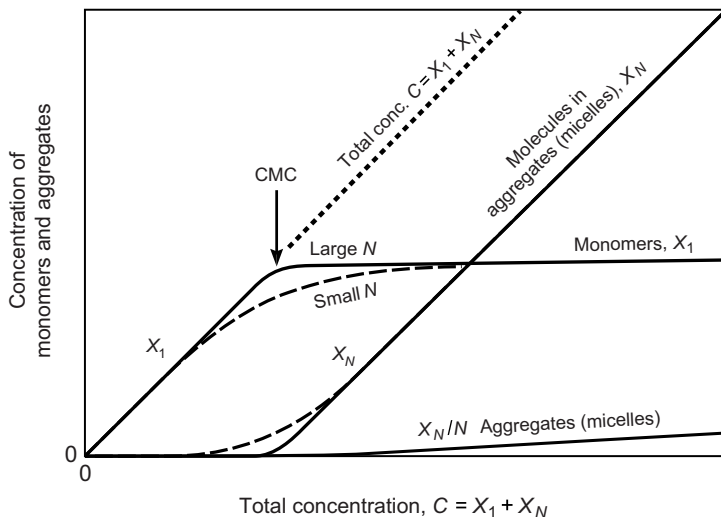


FIGURE 19.5 Monomer and aggregate concentrations as a function of total concentration (schematic). Most single-chained surfactants containing 12–16 carbons per chain have their CMC in the range 10^{-2} – 10^{-5} M, while the corresponding double-chained surfactants have much lower CMC values due to their greater hydrophobicity. Some important CMC values are listed in Table 19.2. The larger the aggregation number N (which usually means a larger aggregate) the sharper is the transition at the CMC. Similar sharp adsorption transitions or steps can occur when cluster-forming molecules adsorb on surfaces (Ruckenstein and Bhakta, 1994).

concentration (CAC), though it is common to use the traditional term *critical micelle concentration* (CMC) to denote the critical concentration of all self-assembled structures.² Thus, in general

$$(X_1)_{\text{crit}} = \text{CMC} \approx \exp[-(\mu_1^0 - \mu_N^0)/kT]. \quad (19.13)$$

If μ_N^0 is given by Eq. (19.11), we have the simple but important result:

$$(X_1)_{\text{crit}} = \text{CMC} \approx e^{-\alpha} \quad \text{for all } p. \quad (19.14)$$

These two equations define the concentration at which further addition of solute molecules results in the formation of more aggregates while leaving the monomer concentration more or less unchanged at the CMC (see Figure 19.5).

19.6 Infinite Aggregates (Phase Separation) versus Finite Sized Aggregates (Micellization)

What can we say about the nature of these aggregates? This now depends very much on their shape. For simple disc-like and spherical aggregates, Eq. (19.12) becomes

²Historically, when McBain discovered and claimed the stability of micelles in 1913 (McBain, 1913), most people had difficulties reconciling these small aggregates with the Gibbs phase rule, and they certainly did not consider the possibility of much larger equilibrium structures within a one-phase system.

$$X_N = N[X_1 e^\alpha]^N e^{-\alpha N^{1/2}} \quad \text{for spheres } \left(p = \frac{1}{2} \right) \quad (19.15)$$

$$X_N = N[X_1 e^\alpha]^N e^{-\alpha N^{2/3}} \quad \text{for spheres } \left(p = \frac{1}{3} \right). \quad (19.16)$$

Above the CMC where $X_1 e^\alpha \approx 1$, the above two equations may be approximated by $X_N \approx N e^{-\alpha N^{1/2}}$ and $X_N \approx N e^{-\alpha N^{2/3}}$, respectively. Now for any reasonable positive value of α , which is usually greater than 1, these equations show that apart from a few dimers, trimers, and so on, there will be very few aggregates of any appreciable size (e.g., with $N > 5$). Where do the molecules go above the CMC? The answer is quite simple: For discs and spheres, there is a phase transition to a separate phase, strictly to an aggregate of infinite size ($N \rightarrow \infty$) at the CMC: the micelles may be thought of as having left the one-phase system. Israelachvili and colleagues (1976) showed that such a transition to large macroscopic aggregates occurs whenever $p < 1$ in Eq. (19.11). This applies, quite generally, to all planar or disc-like aggregates composed of identical molecules, and it is for this reason that finite crystalline sheets, one-component lipid bilayers, and even biological membranes with exposed edges are rarely found floating about in solution. Above the CMC, infinite bilayers form spontaneously from lipid monomers, although they may close up on themselves to form vesicles (discussed later).

Likewise for simple spherical structures. Here, for example, we may consider the association of oil or alkane molecules in water. On adding oil to water the molecules disperse as monomers up to the critical concentration given by Eqs. (19.14) and (19.10),

$$(X_1)_{\text{crit}} \approx e^{-\alpha} \approx e^{-4\pi r^2 \gamma_i / kT}, \quad (19.17)$$

above which they will separate out into a bulk oil phase, which may be considered simply as a very large spherical aggregate (see Problem 19.2). For such a system (of two immiscible liquids) it is clear that what we are now talking about is the solubility of a solute in a solvent, where α is the free energy of transferring a solute molecule from the solute into the solvent phase. For example, if we consider the solubility of hydrocarbons in water, we may put $\gamma_i \approx 50 \text{ mJ m}^{-2}$ and $r \approx 0.2 \text{ nm}$ for a methane molecule. The free energy of transferring a methane molecule from bulk hydrocarbon liquid into water should therefore be approximately $4\pi r^2 \gamma_i \approx 2.5 \times 10^{-20} \text{ J}$, corresponding to $\alpha \approx 6$ or about 15 kJ mol^{-1} . Surprisingly, this crude theoretical estimate agrees well with the experimental value for the solubility or hydrophobic energy of transfer of methane into water (see Worked Example 2.3 and Problem 8.2).

Linear aggregates such as rods and cylinders, for which $p = 1$, exhibit some special and quite different properties from spheres and discs, and are considered separately in Sections 19.12 and 19.13.

19.7 Hydrophobic Energy of Transfer

The hydrophobic energy of transferring alkyl chains from water into bulk hydrocarbon (which determines their solubility) or into micelles (which determines their CMC) can be

analyzed in a similar fashion. Thus, for an alkane chain of radius $r \approx 0.2$ nm and an interfacial energy with water of $\gamma_i \approx 50$ mJ m⁻² as above, the hydrophobic energy per unit length will be $2\pi r \gamma_i \approx 6 \times 10^{-11}$ J m⁻¹. Now, since the CH₂–CH₂ distance along a chain is $\ell = 0.126$ nm, this energy corresponds to 8×10^{-21} J per CH₂ group added to the chain. We could therefore expect a decrease in the solubility by a factor of about $\exp[8 \times 10^{-21} / 4.1 \times 10^{-21}] \approx e^2 \approx 7$ per CH₂ group added to an alkane chain. Experimentally, one finds an increment of about 900 cal/mole or 3.8 kJ mol⁻¹ per CH₂ group at 25°C (Tanford, 1980), equivalent to 6.3×10^{-21} J. This corresponds to an increment in α of $6.3 \times 10^{-21}/kT \approx 1.5$ and thus to a lowering of the solubility of alkanes in water by $e^{-1.5} \approx 0.22$ —that is, by a factor of about 4—per added CH₂ group (see first row of Table 19.2). The lower energy is partially due to chains being partially coiled in water so that they expose a smaller hydrophobic area to water than do fully extended chains.

The above applies only to pure alkane chains being transferred from water into a pure bulk hydrocarbon phase. In the case of surfactant molecules being transferred into micelles or bilayers, the hydrophobic energy increment is even lower, ranging from 1.7 to 2.8 kJ mol⁻¹ per CH₂ group (Table 19.2). As discussed in Section 8.7, the reduced hydrophobicity of an amphiphilic chain compared to that of a pure alkane chain is believed to be due to the proximity of the hydrophilic headgroup, and to the higher chain ordering of chains within micelles that acts to reduce the energy even more (Aniansson, 1978). The above range of values means that typical micellar CMCs fall by a factor between 2 and 3 per CH₂ group added to the surfactant chain.

The important difference between alkanes and amphiphilic molecules is not so much in their solubility or CMC values but in the ability of amphiphiles to assemble into structures in which μ_N^0 reaches a minimum or constant value at some *finite* value of N . It is for this reason that the aggregates formed are not infinite (\rightarrow phase separation) but of finite size (\rightarrow micellization). The reasons for *why* and *how* amphiphilic molecules do this will be investigated fully in the following two chapters.

19.8 Nucleation and Growth of Aggregates

But even simple phase separation is not without its subtleties. Figure 19.6 (top) shows the stages of nucleation and the growth of simple solute droplets in a solvent or vapor medium once the solubility limit S or saturated vapor pressure P_{sat} have been exceeded. At this point thermodynamics tells us that a solute-rich phase will separate out from the solvent. Thermodynamics, however, does not tell us how long this process will take or its path. In many cases, once S has been exceeded, nothing happens: the system becomes supersaturated, and (spontaneous) separation occurs only at some higher concentration or only after a very long time. In most cases, however, small droplets nucleate (not necessarily at the bulk density) and grow by one or both of the following mechanisms: (1) coalescence, especially if the forces between the droplets are monotonically attractive, and/or (2) *Ostwald Ripening*, in which individual solute molecules are exchanged between the droplets by diffusion through the solvent.

Table 19.2 CMCs of Some Common Surfactants And Lipids Showing the Effects of Chain Length, Number of Chains, Chain Unsaturation, Type of Headgroup, Counterion, Cation, Salt, and Temperature (see Problem 20.1).

Surfactant ($R_n = C_nH_{2n+1}$)	Total number Carbon Atoms in Chains	CMC or Solubility, S^a (mM)	Increment of CMC per CH_2 Group (f)	Average Energy per CH_2 Group ^b ($\Delta G = RT \ln f$)
Pure n-Alkanes (no headgroup)	4-8	(Solubility) CMC \sim 30 nM $S \sim 5 \mu M$	4.4	3.7 kJ mol ⁻¹ (880 cal/mole)
Cholesterol				
Cationic				
Alkyl trimethylammonium bromides				
$R_{10}N(CH_3)_3^+Br^-$	10	66	2.1	
$R_{12}N(CH_3)_3^+Br^-$	12	15	2.1	1.8 kJ mol ⁻¹ (430 cal/mole)
$R_{14}N(CH_3)_3^+Br^-$	14	3.5	2.0	
$R_{16}N(CH_3)_3^+Br^-$ (CTAB or HTAB)	16	0.9		
Alkyl trimethylammonium chlorides				
$R_{10}N(CH_3)_3^+Cl^-$	10	63	1.8	
$R_{12}N(CH_3)_3^+Cl^-$	12	19	2.1	1.7 kJ mol ⁻¹ (400 cal/mole)
$R_{14}N(CH_3)_3^+Cl^-$	14	4.5	1.9	
$R_{16}N(CH_3)_3^+Cl^-$	16	1.3	2.0	
$R_{18}N(CH_3)_3^+Cl^-$	18	0.34		
Anionic				
Sodium alkyl sulfates				
$R_8SO_4^-Na^+$	8	130	2.0	
$R_{10}SO_4^-Na^+$	10	33.2	2.0	1.7 kJ mol ⁻¹ (410 cal/mole)
$R_{12}SO_4^-Na^+$ (SDS)	12	8.1	2.0	
$R_{14}SO_4^-Na^+$	14	2.0		
Nonionic				
Alkyl polyoxyethylene monoethers				
$R_8-(OCH_2CH_2)_6OH$ (C_8E_6)	8	9.8		
$R_{10}-(OCH_2CH_2)_6OH$ ($C_{10}E_6$)	10	0.90	3.3	2.9 kJ mol ⁻¹ (700 cal/mole)
$R_{12}-(OCH_2CH_2)_6OH$ ($C_{12}E_6$)	12	0.087	3.2	
Zwitterionic				
Lyso-phosphatidylcholines at 25°C				
$R_{10}-PC$	10	7.0	3.2	
$R_{12}-PC$	12	0.70	3.2	2.8 kJ mol ⁻¹ (680 cal/mole)
$R_{14}-PC$	14	0.070	3.2	
$R_{16}-PC$	16	0.007		

Effect of headgroup size (at 25°C)				
R ₁₂ -PC	12	0.70	3.2	680 cal/mole
R ₁₂ -PE	12	0.34	4.7	920 cal/mole
Effect of salt				
Sodium alkyl sulfates in 0.3M NaCl at 21°C (note the lower CMCs and higher increment factors than in salt-free water)	8	67	3.1	2.8 kJ mol ⁻¹ (670 cal/mole)
	10	6.9	3.1	
	12	0.7		
Counterion effects				
Dodecyl sulfate (40°C) in 0.02M of				
Cs ₂ SO ₄	12	3.0		
K ₂ SO ₄	12	3.5		
Na ₂ SO ₄	12	3.8		
Li ₂ SO ₄	12	4.0		
Co-ion effects				
Dodecyl sulfate (21°C) in 0.1M of				
NaF	12	1.45		
NaCl	12	1.45		
NaBr	12	1.43		
Nal	12	1.38		
Temperature effects				
	10°C	8.7		
	15°C	8.4		
R ₁₂ -SO ₄ ⁻ Na ⁺ (SDS)	20°C	8.3		
Sodium dodecyl sulfate	25°C	8.1 ← min		
	30°C	8.3		
	35°C	8.4		
	40°C	8.7		
Effect of mid-chain unsaturation ^c				
saturated R ₁₈ -SO ₄ ⁻ Na ⁺	18 sat	0.11		
trans R ₁₈ -SO ₄ ⁻ Na ⁺	18 trans	0.18		
cis R ₁₈ -SO ₄ ⁻ Na ⁺	18 cis	0.29		

(Continued)

Table 19.2 CMCs of Some Common Surfactants And Lipids Showing the Effects of Chain Length, Number of Chains, Chain Unsaturation, Type of Headgroup, Counterion, Coion, Salt, and Temperature (see Problem 20.1).—cont'd

Surfactant ($R_n = C_nH_{2n+1}$)	Total number Carbon Atoms in Chains	CMC or Solubility, S^a (mM)	Increment of CMC per CH ₂ Group (f)	Average Energy per CH ₂ Group ^b ($\Delta G = RT \ln f$)
Double-chained surfactants				
Di-alkyl dimethylammonium chlorides				
$R_8R_8-N(CH_3)_2^+Cl^-$	16	27	1.9	1.6 kJ mol ⁻¹ (380 cal/mole)
$R_{10}R_{10}-N(CH_3)_2^+Cl^-$	20	2.0	1.9	
$R_{12}R_{12}-N(CH_3)_2^+Cl^-$	24	0.15		
Di-alkyl sulfates (40°C)				
$R_7R_6-CH-SO_4^-Na^+$	14	9.70	1.5	
$R_7R_7-CH-SO_4^-Na^+$	15	6.65	1.6	1.2 kJ mol ⁻¹ (300 cal/mole)
$R_8R_7-CH-SO_4^-Na^+$	16	4.25	1.8	
$R_8R_8-CH-SO_4^-Na^+$	17	2.35	1.6	
$R_9R_9-CH-SO_4^-Na^+$	19	0.94		
$R_{14}R_{14}-CH-SO_4^-Na^+$	29	0.08		
Di-acyl phosphatidylcholines				
R_6R_6-PC	12	1.5×10^{-2} M	2.7	
R_8R_8-PC	16	3×10^{-4} M	2.7	2.1 kJ mol ⁻¹ (500 cal/mole)
$R_{10}R_{10}-PC$	20	5×10^{-6} M	2.2	
$R_{16}R_{16}-PC$ (DPPC)	32	5×10^{-10} M		

CMC and solubility values taken from Shinoda et al., (1963), Mukerjee and Mysels (1970), Haberland and Reynolds (1973), Tanford (1980), Cevc and Marsh (1987), Stafford et al., (1989), Marsh (1990), Gunstone et al., (1994), Huibers et al., (1996).

^aUnsaturated chains have similar interfacial energies with water as their saturated counterparts (Table 17.1) and are therefore expected to have similar CMCs. However, a double bond can change the chain melting temperature thereby having a large effect on the structure, CMC, elastic and dynamic properties of the resulting aggregates. Note that most biological lipids are unsaturated.

^bThis energy increment can also be expressed in terms of the protrusion energy per unit length of chain(s) protruding into the aqueous phase α where 1 kJ mol⁻¹ corresponds to $\alpha = 1.3 \times 10^{-11}$ J/m.

^cValues in water (no added salt) at 25°C unless stated otherwise. The so-called Krafft point of a surfactant is essentially its solubility—that is, the point at which the aggregates precipitate out of solution or form a separate phase (note that a micellar solution is a one-phase system – see Section 19.6).

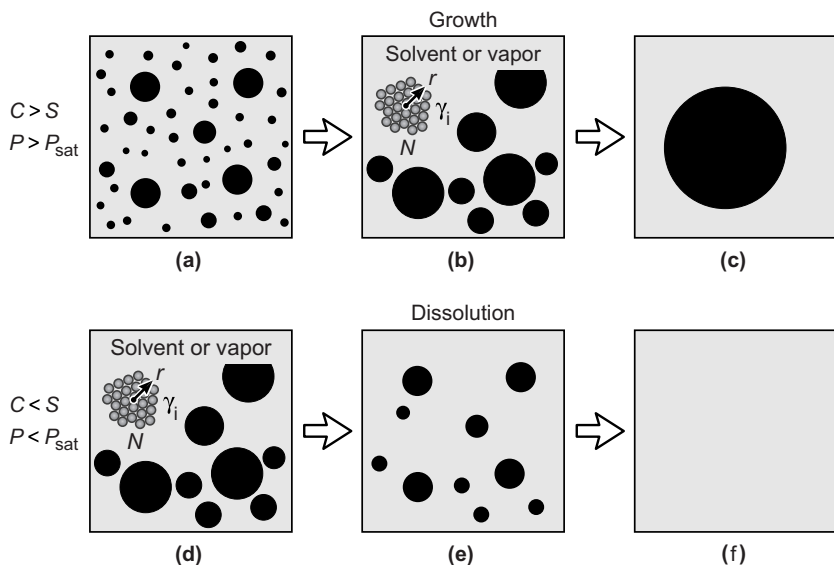


FIGURE 19.6 (a)→(c) Growth of droplets by Ostwald ripening whereby molecules diffuse through the solvent or vapor from the smaller to the larger particles. The same concepts apply to grain boundary growth (Figure 6.2) and to 2D and 1D clusters; for example, they apply to growing monolayer or bilayer domains on surfaces. 3D droplets grow with time as $R \propto t^{1/3}$, 2D domains grow as $R \propto t^{1/2}$, 1D filaments as Length $\propto t$. (d)→(f) During dissolution all the droplets shrink, unlike during growth when some grow and some shrink. [C is the concentration; S is the solubility limit.]

If the long-range colloidal forces between the droplets in the solvent are repulsive—for example, if they interact through DLVO forces—growth will occur through Ostwald Ripening, as illustrated in Figure 19.6a→c. Since the Laplace pressure $2\gamma_i/R$ is higher around the smaller droplets, solute molecules will diffuse from the smaller to the larger droplets³ (cf. Worked Example 17.4). Thus, the larger droplets will grow and the smaller ones will shrink. After a while, some of the “larger” droplets now find themselves to be the smaller ones because all the previously smaller ones have disappeared (Figure 19.6b). At this point these stop growing and begin to shrink. Eventually, only one droplet remains—this being the separate phase in what is now a two-phase system (Figure 19.6c).

Interestingly, during the reverse process of “dissolution” or evaporation, the system does not retrace the path it took during growth. For example, if the solution conditions are reversed at the stage corresponding to Figure 19.6b so that the droplets now dissolve back into the solvent, each one will shrink or bleb (Figure 19.6d→e) until all have disappeared (Figure 19.6f).

Another important issue is the activation energy and time to nucleate the first droplets. In Chapter 17 the Kelvin equation, Eq. (17.44), was derived giving the radius of the meniscus in equilibrium with vapor of pressure $p < p_{\text{sat}}$. The relationship

³One can also think of this preferential transfer as a consequence of the greater attraction of solute molecules to larger droplets.

$r_K \propto 1/\log(p/p_{\text{sat}})$ shows that for $p = p_{\text{sat}}$, $r_K = \infty$ —that is, a saturated vapor is in equilibrium with a flat surface. For $p > p_{\text{sat}}$ (supersaturation) as we have in Figure 19.6 (top row) a droplet (convex radius) will evaporate if $r < r_K$, but grow if $r > r_K$; and a liquid meniscus in a crack (concave radius as in Figures 17.9, 17.10, and 17.20) will always grow. For $p < p_{\text{sat}}$ (undersaturation) as we have in Figure 19.6 (bottom row), the equilibrium radius r_K is negative—that is, concave. All convex droplets now evaporate, while a concave meniscus in a crack will grow or shrink (evaporate) until its radius equals r_K . The Kelvin equation thus gives the critical nucleation size (Wennerström and Evans, 1999), which corresponds to an activation energy of $4\pi r_K^2 \gamma$. This can be expressed in terms of the number of molecules N_c in the critical droplet or cluster, giving⁴

$$\frac{N_c}{\text{in vapor}} = \frac{\frac{4\pi r_K^2 \gamma}{kT \log(p/p_{\text{sat}})}}{\frac{4\pi r_K^2 \gamma_i}{kT \log(C/C_{\text{sat}})}}, \quad (19.18)$$

where p_{sat} is the saturated vapor pressure of the condensing liquid and C_{sat} is the solubility (also S) of the nucleating liquid in the solution (see Problem 19.6, and Section 20.10 for nucleation of 2D domains in monolayers and bilayers).

19.9 2D Structures on Surfaces: Soluble and Insoluble Monolayers

Soluble monolayers are those whose molecules are in exchange equilibrium with some bulk reservoir containing excess molecules that determines the chemical potential of the molecules both in the bulk and in the monolayer. Insoluble monolayers are those whose molecules remain on the surface when the monolayer is expanded or compressed, either because the reservoir is too small or because not enough time is allowed for equilibrium to be attained.⁵ Soluble monolayers have an area-independent surface tension (discussed further below); insoluble monolayer do not and are akin to a gas in a chamber where the pressure depends on the volume. Indeed, in Section 6.3 (see also Problem 2.2) we saw that insoluble monolayers can be described by a 2D van der Waals equation of state given by Eq. (6.15): $(\Pi + a/A^2)(A - b) = kT$, where Π is the surface pressure or tension (in units of N m^{-1}), A is the area, and where a and b are constants (Pallas and Pethica, 1985). Thus, the tension Π (also often denoted by τ) has the same units as the surface tension or energy γ of a simple liquid (N m^{-1} or J m^{-2}), but unlike for a simple liquid, Π is not a constant (independent of the area A).

⁴The more traditional approach to obtain the critical nucleation radius by finding the maximum value of the (positive) surface and (negative) bulk energies, $4\pi r^2 \gamma - \frac{4}{3}\pi r^3 g$, can be shown to be the same as the Kelvin radius of Eq. (19.44) when g is defined in a certain way; see Problem 19.6.

⁵The latter is a kinetic rather than a thermodynamic argument, although in practice many “thermodynamic” reasons are really kinetic: the small reservoir may be sitting on a table next to a large water-filled trough into which the surfactants will eventually distil.

Further, unlike gases or simple solute molecules in a solvent, the interaction between amphiphiles on a surface can be repulsive, when a is negative. The interaction can also change sign, as occurs in DLVO interactions, which is discussed further in Chapter 20. We may note, too, that at any point on the Π - A curve if the area is changed by a small amount the monolayer behaves like an elastic sheet or membrane with an area modulus of

$$k_a = \text{change in surface pressure/fractional change in area} = A(d\Pi/dA) \text{ N m}^{-1}. \quad (19.19)$$

An insoluble monolayer can be continuous (single-phase) or two-phase, as described by Eq. (6.15). But it can also be broken into domains that are essentially 2D micelles that obey the equations derived in Sections 19.2–19.4 for 2D aggregates (see also Problem 19.2). However, the energetics of surfactant domains are complicated because the factor α in Eq. (19.11) is not always constant and can depend on the size, shape, or aggregation number of the domain. This is because more than one type of interaction contributes to α (one may note that three different molecular components are involved in determining α —the water “subphase,” the monolayer, and the vapor or liquid phase above). These different contributions are best understood in terms of the *line tension* at the edge of a domain.

19.10 Line Tension and 2D Micelles (Domains)

The concept of the line tension was introduced in Eq. (19.8) as a parameter that quantifies the (usually unfavorable) energy of the edge of a 2D aggregate or a 3-phase boundary line. Line tensions arise when the edge of a monolayer or droplet lens contributes an additional positive or negative energy to the total surface energy. The line tension λ is in units of energy per unit length (J m^{-1} or N) rather than energy per unit area and can be due to a number of different effects including van der Waals, hydrophobic, and electrostatic forces (Figure 19.7).



Worked Example 19.2

Question: Estimate the line tension of a surfactant or lipid monolayer on the water-air interface (Figure 19.7b) assuming that it exposes a hydrocarbon edge of thickness $\ell = 2 \text{ nm}$?

Answer: The line tension is $\lambda = \text{edge energy per unit length} = (\text{surface energy of edge, J m}^{-2}) \times (\text{area of unit length of edge, m}^2)/(\text{unit length, m}) = \ell\gamma = (27 \times 10^{-3}) \times (2.0 \times 10^{-9} \times 1.0)/(1.0) = 5.4 \times 10^{-11} \text{ J m}^{-1} = 5.4 \times 10^{-11} \text{ N}$. Typically measured values are 10^{-11} – 10^{-10} N for monolayer domains in the gel, crystalline, or solid state, as schematized in Figure 19.7b, and 10^{-14} – 10^{-12} N for fluid state monolayers and bilayers (Veatch and Keller, 2003).



Another contribution to λ comes from the charges present in the headgroups of surfactant or lipid molecules that can be modeled as a capacitor (Figure 19.7b and c)

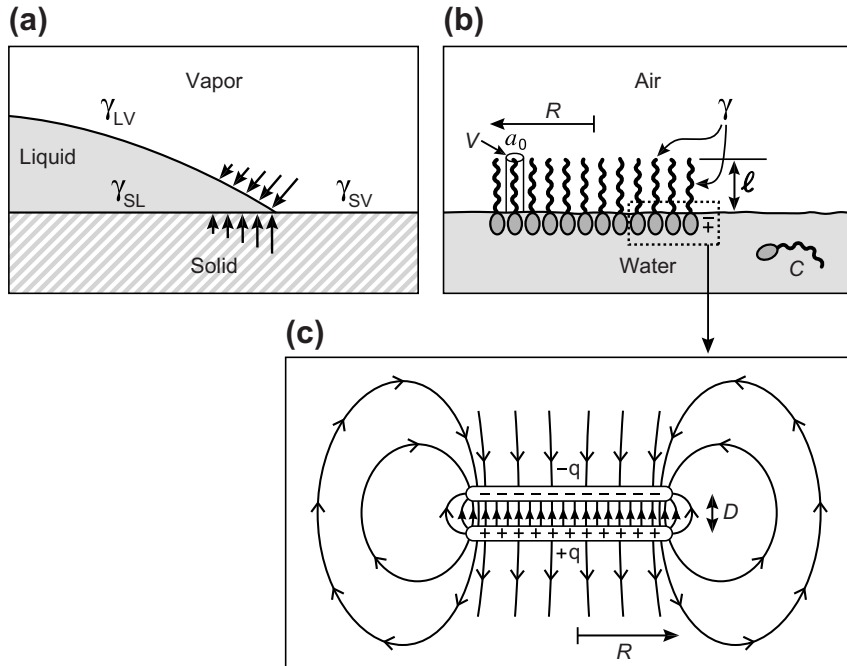


FIGURE 19.7 Three sources of line tension, λ (in units of N): (a) The edge of a liquid drop on a surface where the surface energies γ_{LV} and γ_{SL} near the three-phase line are changed due to the interaction across the thin liquid film in that region. For $\theta < 90^\circ$ the line tension is positive ($\lambda > 0$); for $\theta > 90^\circ$ it is negative ($\lambda < 0$). (b) The edge of a monolayer in the solid or crystalline state (see Worked Example 19.2). Monolayers and bilayers in the fluid state can deform to relax the high edge energy – effectively reducing the length ℓ in Eq. 19.22 for the same volume v , and these usually have much lower line tensions. (c) The edge of the charged or zwitterionic (dipolar) headgroup region of a surfactant or lipid monolayer where the electric field energy is different from the uniform field within the monolayer, giving rise to a negative line tension whose value depends on the domain radius R (Eq. 19.21).

consisting of charges $\pm q$, separated by a “dipole” distance D , occupying an area a_0 corresponding to a surface density of $\Gamma = 1/a_0$. The dipole moment u can therefore be expressed as $u = qD$ and the dipole moment density is $u\Gamma$. The energy per unit area of a capacitor with plates of charge density $\pm\sigma$, separated by a distance D in a medium of dielectric constant ϵ was previously given as $\sigma^2 D / 2\epsilon_0 \epsilon$ per unit area (see Figure 3.2 and Eq. 3.7). For a circular monolayer of radius R , the total energy is therefore expected to be $\pi R^2 \sigma^2 D / 2\epsilon_0 \epsilon = \pi R^2 (u\Gamma)^2 / 2\epsilon_0 \epsilon D$. However, this is to ignore the additional term from the edges where the electric field is distorted, as shown in Figure 19.7c. For $D \ll R$ the total electrostatic energy is⁶

$$\frac{\pi R^2 (u\Gamma)^2}{2\epsilon_0 \epsilon D} - \frac{R(u\Gamma)^2}{2\epsilon_0 \epsilon} \log\left(\frac{16\pi R}{eD}\right) = \frac{\pi R^2 (u\Gamma)^2}{2\epsilon_0 \epsilon D} \left\{ 1 - \frac{D}{\pi R} \log\left(\frac{16\pi R}{eD}\right) \right\}. \quad (19.20)$$

⁶In these equations $e = 2.718$. The correction term to the capacitance C of a condenser is known as Kirchhoff's formula, where the total energy is $Q^2/2C$ where Q is the total charge on each plate.

The first term in Eq. (19.20) is proportional to the area and therefore to the number of molecules in the monolayer, $N = \pi R^2 \Gamma$, while the second term is proportional to the perimeter, $2\pi R$, and therefore corresponds to a line tension contribution of

$$\lambda_{\text{el}} = -\frac{(u\Gamma)^2}{4\pi\varepsilon_0\varepsilon} \log\left(\frac{16\pi R}{eD}\right). \quad (19.21)$$

To this we must add the line tension contribution from the van der Waals or hydrophobic surface energy contribution obtained in Worked Example 19.2:

$$\lambda_{\text{hyd}} = \ell\gamma_i. \quad (19.22)$$

The total energy *per molecule* is therefore $\mu^0 = \text{Constant} + 2\pi R(\lambda_{\text{hyd}} + \lambda_{\text{el}})/N$, where $N = \pi R^2 \Gamma$, giving

$$\mu_N^0 = \mu_\infty^0 + \left[2\pi\gamma\ell - \frac{(u\Gamma)^2}{2\varepsilon_0\varepsilon} \log\left(\frac{16\pi R}{eD}\right) \right] / (\pi\Gamma)^{1/2} N^{1/2}. \quad (19.23)$$

This equation is of the form for disks, Eq. (19.7), except that now the line tension contribution—equivalent to the αkT term in Eq. (19.7)—is not a constant but increases then decreases as R and N increase. The minimum energy occurs at a domain radius of

$$R \approx (e^2 D / 16\pi) e^{4\pi\varepsilon_0\varepsilon\lambda_{\text{hyd}} / (u\Gamma)^2}, \quad (19.24a)$$

and aggregation number

$$M = \pi R^2 / a_0 \quad (19.24b)$$

although when entropic effects are included, the optimum radius is less and depends on the concentration of surfactants and the temperature (Hu et al., 2006). A similar equation was derived by McConnell and coworkers (McConnell, 1991) where the preexponential term is $(e^3 D / 4)$. As can be seen, since D is of order 0.5 nm, to obtain large domains requires a large value for $4\pi\varepsilon_0\varepsilon\lambda_{\text{hyd}} / (u\Gamma)^2$ —that is, a large hydrophobic line tension and/or small dipole moment density. For example, for $\lambda_{\text{hyd}} = 5 \times 10^{-11}$ N, $D = 0.5$ nm, q = electronic charge, $\varepsilon = 50$,⁷ and $\Gamma = 1/a_0 = 1/40\text{\AA}^2 = 2.5 \times 10^{18} \text{ m}^{-2}$, then $u\Gamma = 2.003 \times 10^{-10} \text{ C m}^{-1}$, and we obtain a domain radius of about 75 nm using Eq. (19.24a) and 2,600 nm = 2.6 μm using McConnell’s equation. Typically observed sizes of surfactant domains at the water-air interface range from the very small (nano sized) to the very large (many microns), but whether they are true equilibrium structures has yet to be established. These domains tend not to coalesce because of the long-range dipole-dipole repulsion between them (see electric field lines in Figure 19.7c). Their growth occurs via slow Ostwald ripening of surfactant diffusing on the water surface (see Figure 19.6).

2D micelles occur in both monolayers and bilayers, where they are also referred to as domains, patches and rafts. They are discussed further in Section 20.10 and Chapter 21.

⁷The dielectric constant of the hydrophilic headgroup region is unknown but is expected to be less than the value for bulk water.

19.11 Soluble Monolayers and the Gibbs Adsorption Isotherm

When the area of a soluble monolayer is compressed, the surfactants go into the solution, thereby keeping the surface coverage and pressure (tension) unchanged. The equilibrium between the molecules on the surface and those in solution is given by the Gibbs equation, which relates the change in the surface pressure Π (N m^{-1}) and change in the bulk surfactant monomer concentration X_1 to the coverage Γ (m^{-2}). Using the above notation, the Gibbs equation may be derived by considering the monolayer to be a very large aggregate of essentially infinite aggregation number so that for the monolayer $(kT/N)\ln(X_N/N)$ may be put equal to zero. Also, μ^0 in the monolayer can be written as $\mu^0 = \mu^0 - \Pi a$, where $-\Pi a$ accounts for the additional (negative) transfer free energy per surfactant molecule occupying an area a in the monolayer (Gruen and Wolfe, 1982). Thus at equilibrium

$$\mu_1^0 + kT \ln X_1 = \mu_N^0 + (kT/N) \ln (X_N/N) = \mu_\infty^0 + 0 - \Pi a, \quad (19.25)$$

where N refers to the micelles, if any, in solution. Differentiating the above gives the Gibbs equation⁸

$$\frac{1}{a} = \Gamma = -\frac{1}{kT} \left(\frac{\partial \Pi}{\partial \log X_1} \right)_T. \quad (19.26)$$

The Gibbs equation shows that on addition of solute molecules (any molecules) to a solvent (increasing X_1), if they adsorb at an interface (increasing Γ), then the surface tension, γ or Π , must fall. Amphiphiles such as surfactants, lipids, and proteins “go to the interface” and decrease γ , whereas ions are repelled from the water-air interface due to the image force (Figure 13.2c), so the surface tension of electrolyte solutions increases above the value for pure water.

19.12 Size Distributions of Self-Assembled Structures

Micelles, vesicles, and other structures in equilibrium with each other in solution usually have a finite distribution of sizes about some mean value. The distribution may be narrow (monodisperse) or broad (polydisperse), and it may be symmetrical or asymmetrical about the mean (Figure 19.8). Polydispersity should not be thought of as a defect but as a natural thermodynamic state, determined by a combination of thermodynamic equations and the intermolecular forces between the molecules within the aggregates. Here we shall investigate how polydispersity comes about thermodynamically, starting with a consideration of aggregates for which $p = 1$ in Eq. (19.11).

⁸Also the Gibbs Isotherm and Gibbs Adsorption Isotherm.

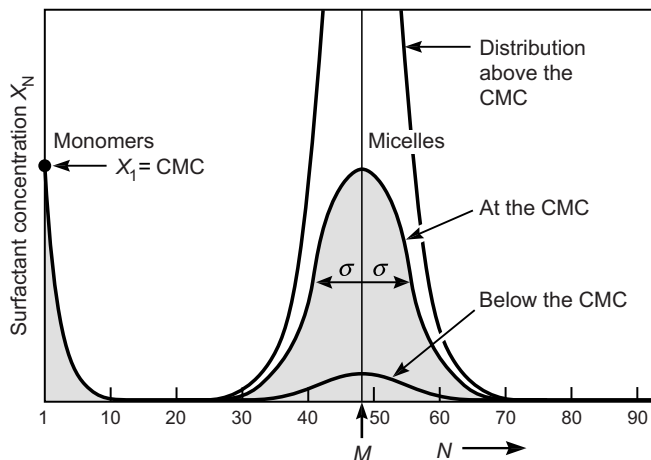


FIGURE 19.8 Distribution of molecules X_N as a function of aggregation number N . At the CMC (shaded region) we have $X_1 \approx X_M$, where the mean micellar aggregation number is M . For spherical micelles, the distribution about M is near Gaussian with standard deviation $\sigma \approx \sqrt{M}$ (Section 20.4).

Putting $p = 1$ in Eq. (19.12), we obtain

$$X_N = N[X_1 e^\alpha]^N e^{-\alpha}. \quad (19.27)$$

Thus, in contrast to Eqs. (19.15) and (19.16), the second exponential term is now a constant rather than a rapidly decreasing function of N . Since above the CMC we have $X_1 e^\alpha \leq 1$, this equation shows that $X_N \propto N$ for small N —that is, the concentration of molecules in these aggregates now *grows* in proportion to their size, and there is no phase separation. Only for very large N does the $[X_1 e^\alpha]^N$ term begin to dominate, eventually bringing X_N down to zero as N approaches infinity. The distribution is therefore highly polydisperse.

The case of $p = 1$ is in marked contrast to the case when $p < 1$ (as occurs for simple discs or spheres) where an abrupt phase transition to one infinitely sized aggregate occurs at the CMC and where the concept of a size distribution does not arise. Alternatively, for structures where $p > 1$ it can be shown that no finite or infinite sized aggregates form at any concentration so that again the concept of a size-distribution does not apply (except for the few very small aggregates or clusters of molecules that are always present). Thus, structures for which $p = 1$ appear to have special properties, and it is instructive to analyze this type of system in more detail.

The total concentration of molecules is given by inserting Eq. (19.27) into Eq. (19.4) as

$$\begin{aligned} C = \sum_{N=1}^{\infty} X_N &= \sum_{N=1}^{\infty} N[X_1 e^\alpha]^N e^{-\alpha} = [X_1 e^\alpha + 2(X_1 e^\alpha)^2 + 3(X_1 e^\alpha)^3 + \dots] e^{-\alpha} \\ &= X_1 / (1 - X_1 e^\alpha)^2, \end{aligned} \quad (19.28)$$

where we have made use of the identity $\sum_{N=1}^{\infty} Nx^N = x/(1-x)^2$.

Thus,

$$X_1 = \frac{(1 + 2Ce^\alpha) - \sqrt{1 + 4Ce^\alpha}}{2Ce^{2\alpha}}. \quad (19.29)$$

Note that at low concentrations C where $Ce^\alpha \ll 1$, this gives $X_1 \approx C$, whereas at high concentrations, well above the CMC such that $Ce^\alpha \gg 1$, the above simplifies to

$$X_1 \approx (1 - 1/\sqrt{Ce^\alpha})e^{-\alpha} \leq e^{-\alpha}; \quad (19.30)$$

that is, $X_1 \approx \text{CMC}$, as expected. Also, above the CMC, the density distribution of *molecules* in aggregates of N molecules is given by inserting Eq. (19.30) back into Eq. (19.27), yielding

$$X_N = N(1 - 1/\sqrt{Ce^\alpha})^N e^{-\alpha} \approx Ne^{-N/\sqrt{Ce^\alpha}} \quad \text{for large } N. \quad (19.31)$$

This function peaks when $\partial X_N / \partial N = 0$, which occurs at

$$N_{\max} = M = \sqrt{Ce^\alpha}, \quad (19.32)$$

while the *expectation value* of N , defined by $\langle N \rangle = \sum NX_N / \sum X_N = \sum NX_N / C$, is given by

$$\begin{aligned} \langle N \rangle &= \sqrt{1 + 4Ce^\alpha} \\ &\approx 1 && \text{below the CMC,} \\ &\approx 2\sqrt{Ce^\alpha} = 2M && \text{above the CMC.} \end{aligned} \quad (19.33)$$

Finally, from Eq. (19.12) the density distribution of *aggregates* above the CMC is

$$X_N/N = \text{Const.}e^{-N/M} \quad \text{for } N > M; \quad (19.34)$$

that is, the concentration of large aggregates decays exponentially with increasing N with a characteristic decay number of M . Thus, the distribution is very broad, with the concentration of aggregates first increasing with N for small aggregates and decaying gradually to zero at large N .

The above results should apply to all dilute *one-component* aggregates for which $p = 1$ in Eq. (19.11). This includes any chain-like (polymer-like) aggregates, cylindrical micelles, and fibrous structures such as microfilaments and microtubules.⁹ Later, we shall see that it also applies to spherical vesicles and microemulsion droplets whose membranes bend elastically. For all these structures, the mean aggregation number M is concentration-dependent, varying with the square root of the concentration C above the CMC; and from Eq. (19.32) we further note that it is also very sensitive to small changes in the interaction parameter α . Consequently, we may anticipate that the aggregation number and polydispersity of such structures in water should also be very sensitive to temperature, electrolyte concentration and pH.

⁹Biological cells control the size and polydispersity of fibrous structures by using a variety of “capping” agents.

Actually, there is a formal relationship between the mean aggregation number, M , the total surfactant concentration, C , and the polydispersity, σ (Figure 19.8). This relation

$$\sigma^2 \approx \partial \log \langle N \rangle / \partial \log C \quad (19.35)$$

is valid above the CMC (Israelachvili et al., 1976) and shows that whenever the distribution is highly polydisperse, the mean aggregation number is also very sensitive to the total surfactant concentration. Conversely, monodisperse structures have aggregation numbers that do not vary much with concentration.

Further quantifying micellar polydispersity requires input from the forces operating between the amphiphilic molecules in the aggregates. This is done below and in Chapter 20.

19.13 Large and More Complex Amphiphilic Structures

The values of the interaction parameter α and dimensionality factor p in Eq. (19.11) are constant only for aggregates composed of fairly simple molecules that self-assemble into simple geometric shapes such as spheres, discs, or rods. More complex amphiphilic molecules can have a size-dependent α (cf. the monolayer domains of Section 19.10) and/or assemble into more complex shapes such as vesicles, interconnected rods, or three-dimensional periodic structures (cf. Figure 20.8).

Before proceeding with an analysis of the size distributions of these structures, let us first consider what causes different amphiphilic molecules to aggregate into one or another of these structures in the first place. This is determined by the types of anisotropic binding forces acting between different parts of the amphiphilic molecules. For simple (nonamphiphilic) molecules such as alkanes in water whose hydrophobic interaction with each other is largely isotropic or *nondirectional*, we would expect them to coalesce and grow as small spherical droplets (for which the total surface energy is a minimum for any given N). And we have seen that for such aggregates, $p = \frac{1}{3}$ in Eq. (19.11), which results in a phase separation at the solubility limit (the effective CMC). Clearly, molecules that aggregate into linear (1D) or sheet-like (2D) structures must have asymmetric *directional* bonding. For example, cigar-shaped molecules may have their binding sites located at the ends of the molecules or radially around each molecule; the former will result in linear rod-like aggregates, the latter in sheet-like aggregates.

Further, if the molecules are also flexible, the structures they adopt will be more varied than any of the simple shapes so far considered. Thus, the energetically unfavorable regions at each end of a rod-like aggregate may be eliminated if the two ends bend and join together, resulting in a torus or toroidal micelle. Similarly, the unfavorable rim energy of a disc may be eliminated by its closing up into a vesicle, which is what happens with certain classes of surfactants and lipids. In all such cases, μ_N^0 no longer decays gradually with increasing N , as given by the simple equation, Eq. (19.11).

Instead, it often reaches a minimum value at some *finite* value of N (say $N = M$), or it reaches a low value at $N = M$ and then remains almost constant for $N > M$ (see Figure 20.7). Depending on the sharpness of the minimum, such a form for μ_N^0 generally results in monodisperse aggregates of mean aggregation number $N < M$, rather than infinite or polydisperse aggregates. As we shall see in the following chapter, this is what happens for certain types of vesicles and spherical micelles. Here we shall consider the consequences for the size distribution of micelles when μ_N^0 reaches a low value at some finite aggregation number M (at which internal, for example, bending stresses are relieved) and does not continue to decrease for $N > M$.

If μ_N^0 has a minimum value at $N = M$, the variation of μ_N^0 about μ_M^0 can usually be expressed in the parabolic form:

$$\mu_N^0 - \mu_M^0 = \Lambda(\Delta N)^2 \quad (19.36)$$

where $\Delta N = (N - M)$. In this case the distribution about $N = M$ is given by Eq. (19.3a) as

$$X_N = N \left\{ \frac{X_M}{M} \exp \left(-M\Lambda(\Delta N)^2 kT \right) \right\}^{N/M} \quad (19.37)$$

and so the distribution of X_N about M will be near Gaussian (Figure 19.8) with a standard deviation in the *aggregation number* of

$$\sigma = \sqrt{kT/2M\Lambda}. \quad (19.38)$$

Systems that fall into this category are spherical micelles and certain single bilayer vesicles, and we shall find (Section 20.4) that for typical values of M and Λ these can be fairly monodisperse with $\sigma/M \approx 0.1\text{--}0.3$.

19.14 Effects of Interactions between Aggregates: Mesophases and Multilayers

So far we have ignored interaggregate interactions. These cannot be ignored at high concentrations (low water content) where, especially for surfactant and lipid dispersions, transitions to larger and more ordered *mesophase* or liquid crystalline structures are commonly observed. These can be ordered arrays of cylinders (hexagonal or nematic phases), stacks of bilayers (lamellar, liposome, or smectic phases) or a complex three-dimensional network of interconnected surfaces (periodic structures forming bio-continuous and tricontinuous phases). Some of these structures are shown in Figure 20.8. Both attractive and repulsive forces between aggregates can lead to phase transitions that lead to ordered nano-structures, and it is worth considering these two very different scenarios in turn.

First, consider the case where there are strong repulsive electrostatic, steric, or hydration forces between the aggregates, which we shall assume are initially small spherical micelles. With increasing surfactant concentration the micelles are forced to

come closer together, which is energetically unfavorable. However, if the surfactants rearrange to form an ordered array of cylinders, it is a simple matter to ascertain (see Problem 20.13) that their surfaces can now be farther apart from each other. And if they order into a stack of bilayers, their surfaces can be even farther apart, all at the same surfactant concentration (same volume fraction). It is for this reason that many surfactant structures go from being small micelles to long cylinders to large liposomes as the surfactant content is progressively increased above about 10% by weight (Ekwall, 1975; Tiddy, 1980). Note that since these types of phase transitions arise from repulsive *interaggregate forces*, where the aggregates are trying to get as far apart as possible within a confined volume of solution, the different phases formed fill up the whole volume of the solution. In Chapter 20 we shall find that similar structural transitions also occur due to changes in the *intraaggregate forces* between the amphiphilic molecules within the aggregates, arising from changes in their molecular packing properties (preferred geometric shapes) when the solution conditions are changed.

In contrast, when the structural transitions are caused by *attractive* interaggregate forces, the larger structures may now either separate out from, or coexist with, the smaller aggregates or monomers in solution. Such attractive forces can be due to van der Waals or ion correlation forces—for example, between amphiphiles with nonionic or zwitterionic headgroups, and between charged headgroups in high salt or solutions containing divalent counterions. Let us again consider the transformation of small micelles or vesicles into large liposomes (multilamellar bilayers). Now, however, because the forces are attractive, the equilibrium separation between the bilayers in the liposomes will be at the potential-energy minimum, where the depth of the minimum is W_0 per unit area (illustrated for example in Figure 21.3). While the smaller micelles are clearly favored entropically, the liposomes could be thermodynamically more favorable if the value of W_0 is sufficiently large. An additional contribution is the difference in the bending energies of the two structures. The problem is to establish how these three effects compete in determining which structure is formed at the CMC and at higher concentrations.

If M is the micelle or vesicle aggregation number and \mathbf{M} the liposome aggregation number ($\mathbf{M} \gg M$), then equating the chemical potentials of molecules in all the possible dispersed and aggregated states gives at equilibrium

$$\begin{array}{lll} \mu_1^0 + kT \log X_1 & = \mu_M^0 + (kT/M) \log(X_M/M) & = \mu_{\mathbf{M}}^0 + (kT/\mathbf{M}) \log(X_{\mathbf{M}}/\mathbf{M}) \\ \text{monomers} & \text{micelles/vesicles} & \text{liposomes/superaggregates} \end{array} \quad (19.39)$$

or
$$(X_{\mathbf{M}}/\mathbf{M}) = \{(X_M/M) \exp[M(\mu_M^0 - \mu_{\mathbf{M}}^0)/kT]\}^{\mathbf{M}/M}. \quad (19.40)$$

The concentration at which $X_{\mathbf{M}} = X_M$ is therefore

$$(X_M)_{\text{crit}} \approx M \exp[-M(\mu_M^0 - \mu_{\mathbf{M}}^0)/kT]. \quad (19.41)$$

Thus, depending on M and the difference in the energies ($\mu_M^0 - \mu_{\mathbf{M}}^0$) per surfactant molecule in the micellar and liposome states (which includes contributions from both *intrabilayer* and *interbilayer* interactions) the latter may form spontaneously at the CMC,

or—if $(X_M)_{\text{crit}}$ is greater than the CMC—at some higher concentration, while the background concentration of monomers and the smaller aggregates remains unchanged. We may conveniently term such transitions first and second CMCs. If $M \gg M$, the concentration at which large aggregates begin to form will be sharp and in all respects analogous to the first CMC. Note, too, that if we put $M = 1$ in Eq. (19.41), it reduces to Eq. (19.13) for the first CMC. Indeed, if we consider the smaller aggregates as if they were “monomers,” Eqs. (19.40) and (19.41) are completely analogous to Eqs. (19.3) and (19.13).

Worked Example 19.3

Question: In a certain system the depth of the potential energy minimum between two lipid bilayers is $W_0 = 8 \times 10^{-2} \text{ mJ m}^{-2}$. If this is the only energy difference per molecule in a vesicle and in a liposome, estimate the “critical liposome concentration.” Assume that the surface area occupied by each lipid molecule is $a_0 = 0.70 \text{ nm}^2$, that each vesicle contains 3000 molecules, and that the liposomes are much larger than the vesicles.

Answer: The free energy difference per molecule in vesicles and liposomes is $\frac{1}{2} W_0 a_0 = (\mu_M^0 - \mu_M^0) \approx \frac{1}{2} \times 8 \times 10^{-5} \times 0.70 \times 10^{-18} = 2.8 \times 10^{-23} \text{ J}$, or 0.0068 kT at 298 K (Note: this corresponds to g_0 in Figure 21.3). If $M = 3000$ is the vesicle aggregation number, then from Eq. (19.41) a vesicle-to-liposome transition will occur at a lipid concentration of $(X_M)_{\text{crit}} = 3000 \exp[-3000 \times 0.0068] \approx 4 \times 10^{-6}$,—that is, at about $2 \times 10^{-4} \text{ M}$ (which may be compared with the first CMC of $\sim 10^{-10} \text{ M}$ typical of vesicle-forming lipids). This analysis, however, neglects any possible bending energy difference arising from the different bilayer curvatures in vesicles and planar bilayers which will also contribute to $(\mu_M^0 - \mu_M^0)$ in Eq. (19.41). Bilayer curvature effects are discussed in Section 20.8.

We have gone as far as is possible with a formal analysis of the statistical thermodynamics of self-assembly, and to proceed further we must now consider the different types of interactions occurring between amphiphilic molecules in aggregates more specifically. In Chapter 20 we shall quantify these interactions and in particular investigate how the geometric shape constraints of surfactant and lipid molecules restrict their assembly into aggregates of different shapes. The important conclusion to be drawn from this chapter is that once the aggregates’ shape is known many of their physical properties are necessarily given by the thermodynamic equations developed in this chapter, for example, a dilute dispersion of (one-component) cylindrical micelles must be polydisperse and their size must increase with concentration. Therein lies the beauty and power of thermodynamics.

PROBLEMS AND DISCUSSION TOPICS

- 19.1** In the so-called *pseudo-phase approximation* of the theory of micelles or clusters (Section 19.2), it is assumed that only two solute species exist in the solution: monomers and *monodisperse* micelles, all having the same aggregation number N .

Let X_1 and X_N be the concentrations of solute monomers and solute molecules in micelles, and $C = X_1 + X_N$ the total concentration in mole fraction units (mole/mole). Let the difference in the standard parts of the chemical potentials for the molecules in solution and those in micelles be $(\mu_1^0 - \mu_N^0) = 25 \text{ kJ mol}^{-1}$ at 25°C . Plot the concentration of monomers X_1 , monomers in clusters X_N , and clusters X_N/N , as a function of the total concentration C from $C = 10^{-5}$ to $C = 1$ at 25°C for $N = 10, 50$, and 500 as in Figure 19.5. What is the CMC for this system, defined as the maximum monomer concentration at large N and C ? If the CMC is instead defined as the total concentration C_0 at which the number of molecules in monomers and in micelles is equal, how does this definition differ from the previous one? [Answer: CMC = 4.5×10^{-5} mole/mole = 2.3 mM. $C_0 = 2 \times \text{CMC}$.]

- 19.2*** The formalism of Problem 19.1 applies to other systems and aggregation processes, including the gas-liquid PVT equation of state. Using the notation of Section 19.2 and the pseudo-phase approximation, the ideal osmotic pressure of a solution of clusters or aggregates is $P = kT(X_{\text{monomers}} + X_{\text{micelles}}) = kT(X_1 + X_N/N)$. Further, to include finite size (excluded volume) effects, all concentrations can be expressed as volumes, as in the van der Waals equation of state, by putting $X_i = 1/(V_i - b)$ —for example, $C = (X_1 + X_N) = 1/(V - b)$, where b is a constant. Show that the equation of state for this system is

$$P = \left[\frac{(N-1)}{N(V_1 - b)} + \frac{1}{N(V - b)} \right] kT, \quad (19.42)$$

where V_1 is not constant but a function of V , the critical aggregate concentration or volume V_c , and the aggregation number N . Assuming a gas or solution where the gas or solute molecules aggregate into clusters at $V_c = 1 \text{ liter/mole}$ where $b = 0.1 \text{ liter/mole}$, plot P vs V for a mole of the solute for $N = 1$ and 500 at 25°C . Show that as N goes from 1 to >500 the P – V curve goes from $P = kT/(V - b)$ to a van der Waals-type equation of state showing a first order gas-liquid phase transition with a coexistence regime between $V \approx V_c$ and $V \approx b$, as in Figure 6.1. What is the (approximately) constant pressure of this transition? For large N , show that at the onset of the transition from a one-phase gas to a two-phase gas-liquid coexistence the slope of the P vs V curve changes by a factor of $\sim N$. What does this tell you about whether the system is in the one-phase or two-phase regime when N is large but finite? [Answer: Transition pressure $\approx 2.75 \text{ MPa} = 27.5 \text{ atm}$.]

- 19.3*** Estimate the interfacial tension γ_i of an oil-water interface at 25°C where the aqueous phase contains surfactant micelles and where the interface contains a compact (liquid-condensed) surfactant monolayer. Assume that the total surfactant concentration in the aqueous phase is $C = 10^{-2} \text{ M}$ (well above the CMC), that the micelles have a mean aggregation number of $N = 100$, and that the headgroup area is $a_0 = 0.40 \text{ nm}^2$. Ignore curvature energy effects. [Answer: $\gamma_i \approx (kT/Na_0)\ln(N/C) \approx 1 \text{ mJ m}^{-2}$.]

Table 19.3 Experimental results on effectiveness of different liquids (L) on debonding a polymer film (B) from a surface (A)

Liquid or solution	γ_L Liquid-vapour	γ_{AL} Substrate-liquid	γ_{BL} Coating-liquid	Experimental observation ¹
Pure water	72.8	27.4	13.3	NS
Sodium dodecyl sulfate	37.2	0.9	1.6	S
Sodium diisoamyl sulfosuccinate	25.6	1.2	7.9	NS
TritonX-405	42.4	2.6	0.7	S

¹S = Spontaneous separation; NS = Did not Separate.

- 19.4** D. K. Owens [*J. Appl. Polymer Sci.*, **14**, 1725–1730 (1970)] reported the effects of immersing a surface of propylene (material A) coated with a thin film of the copolymer vinylidene chloride (material B) into water and various aqueous surfactant solutions, L. The interfacial energy of the substrate-film interface is $\gamma_{AB} = 3.5 \text{ mJ m}^{-2}$, while the other surface and interfacial energies are given in Table 19.3. In which liquids would you expect the coating to spontaneously separate (debond) from the surface?

Is it surprising that the lowering of the surface tension of water by addition of surfactant is not related to the effectiveness of the surfactant solution in separating the two surfaces—that is, to its effectiveness as a detergent?

- 19.5** The headgroups of a lipid bilayer totally immersed in water have a certain optimum headgroup area a_0 . The same lipids are spread to form a surface monolayer at the air-water interface. At what applied surface pressure π will the head-groups in the monolayer occupy the same area, a_0 ? [Answer: Theoretically, about $72 - 27 = 45 \text{ mJ m}^{-2}$. Experimental values range from 30 to 40 mJ m^{-2} .]
- 19.6** At what concentrations will a surfactant monolayer adsorb from solution on (i) the air-water interface, and (ii) a hydrophobic surface, given that the molecules self-assemble into free bilayers in bulk solution at a cmc of 10^{-6} M ? Assume an area per molecule of 50 \AA^2 . Will the adsorption transition be sharp, like a cmc?
- 19.7** The total free energy of a spherical droplet of radius r can be written in terms of its (positive, unfavorable) surface and (negative, favorable) bulk energies:

$$G = 4\pi r^2 \gamma - \frac{4}{3}\pi r^3 g, \quad (19.42)$$

where g is the bulk energy per unit volume. The critical radius for nucleation r_{crit} is then given when G is maximum—that is, when $dG/dr = 4\pi r(2\gamma - rg) = 0$ and $d^2G/dr^2 < 0$. Show that the critical radius r_{crit} and the Kelvin radius r_K of Eq. (17.44) are the same when G and g are expressed in terms of μ_N^0 , the number of molecules per droplet N , the molecular or molar volumes v or V , kT , and the dimensionless concentration X/X_{sat} .

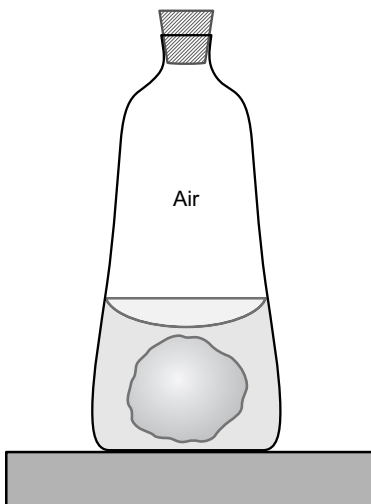


FIGURE 19.9

- 19.8** Can a dispersion of droplets of a pure, isotropic (nonamphiphilic) liquid ever be in true equilibrium in vapor or in a different liquid? An astronaut in a zero-gravity chamber has a bottle sitting on a shelf, as shown in Figure 19.9. The bottle contains a binary mixture of two liquids that form a single phase at the temperature and pressure of the chamber (and bottle). What is wrong with the figure? [Hint: at least two things are wrong, but one of them may not be what you might have immediately thought.]
- 19.9*** What is the standard deviation of the domains of mean radius 75 nm calculated in Section 19.10 based on Eqs (19.23)–(19.24) and (19.36)–(19.38)?
- 19.10** Explain the effects of the following solutes on the surface tension of water using the Gibbs isotherm, Eq. (19.26), and considerations of how the solute molecules interact with the water-air interface and/or with each other on the water surface: (i) Many sugars have no effect. (ii) Inorganic salts increase γ . (iii) Alcohols decrease γ . (iv) Surfactants decrease γ up to a point, above which γ remains unchanged. (v)* Surfactants and lipids produce a van der Waals type Π - A curve but the “coexistence line” is not horizontal—that is, not at constant pressure Π .
- 19.11*** (i) What is the 2D pressure Π_L that plays the same role as the 3D Laplace pressure P_L (cf. Eq. (17.15)) for a circular 2D immiscible monolayer domain of radius R and line tension λ ? (ii) What is the 2D Kelvin radius in terms of the line tension λ , the area per molecule a_0 , the surface concentration C relative to the saturation concentration C_{sat} , and the temperature T ? (iii) For a supersaturated monolayer in the vapor state at 25°C where $C/C_{\text{sat}} = 1.10$, $a_0 = 20 \text{ \AA}^2$, and $\lambda = 10^{-11} \text{ N}$, what is the critical domain radius above which the domains will spontaneously grow

(by Ostwald ripening) until there are only two-phases on the surface? [Answers: (i) Consider a circular monolayer on a surface as a 3D disk of variable radius R and fixed finite thickness ℓ to obtain

$$\Pi_L = \lambda/R \quad (19.43)$$

where Π is related to the 3D pressure by $\Pi = P\ell$, and where λ is the 2D line tension, defined by Eq. (19.22) as $\lambda = \ell\gamma$. (iii) 5.1 nm.]

Soft and Biological Structures

20.1 Introduction: Equilibrium Considerations of Fluid Amphiphilic Structures

Amphiphilic molecules such as surfactants, lipids, copolymers, and proteins can associate into a variety of structures in aqueous solutions that can transform from one to another when the solution conditions are changed—for example, the ionic strength, type of ions in the solution, the pH, or temperature. To understand these structural aspects one requires an understanding not only the thermodynamics of self-assembly (discussed in Chapter 19) but also the forces between the amphiphilic molecules within the aggregates and how these are affected by the solution conditions. These two factors (thermodynamics and intraaggregate forces), together with the strength of the interaggregate forces between aggregates in more concentrated systems, determine the equilibrium structures formed.

In this chapter we shall investigate the interaction forces between amphiphilic molecules within aggregates in more detail, and we shall see how these naturally lead to molecular packing considerations in determining which structures are formed naturally. In Chapter 21 we consider the forces and interactions between these structures and their consequences for the equilibrium state of the whole system. Nonequilibrium structures, formed by “directed-assembly” or “engineered-assembly” or during biological activity, are discussed in Chapter 22.

Before proceeding it is worth clarifying what one means by “equilibrium structures,” especially with reference to the Gibbs phase rule. Amphiphilic structures can be hard and solid-like, but they are more often soft or fluid-like, with the molecules in constant thermal motion within each aggregate: twisting, turning, diffusing, and bobbing in and out of the surface. Thus, unlike colloidal particles, soft amphiphilic structures have no definite size or shape, but only a distribution about some mean value. In Chapter 19 we saw that this distribution can sometimes be very broad.

We also saw that it is possible for the equilibrium distribution to peak at more than one value of N . Thus, in principle, small aggregates such as micelles can be in thermodynamic equilibrium with large aggregates such as vesicles, all within the same one-phase system. While it may appear that a large vesicle or liposome, being a macroscopic structure, should be considered as a separate phase, this is strictly not so. The sizes of the structures play no role in the thermodynamic definition of what constitutes a single phase, which merely requires that the properties be uniform throughout the phase (see Problem 19.8). Thus, in principle, structures may be very large and macroscopic and yet not constitute a separate phase if their number density in solution (or space) remains uniform

throughout the whole system which, of course, must be even larger. And “time” also plays a role here: the properties at any location must be averaged over a sufficiently long time to avoid any bias from fluctuations.

Genuine two-phase and three-phase systems can also occur, where monomers, micelles, vesicles, or liposomes separate out into distinct phases in equilibrium with each other while separated by a single meniscus or phase boundary. However, such phase separations can take a long time to reach equilibrium, so that it is often difficult to experimentally identify the true thermodynamic state of an amphiphilic system.

20.2 Optimal Headgroup Area

The major forces that govern the self-assembly of amphiphiles into well-defined structures such as micelles and bilayers, as well as three-dimensional networks, derive from the hydrophobic attraction at the hydrocarbon-water interface, which induces the molecules to associate, and the hydrophilic, ionic, or steric repulsion of the headgroups, which imposes the opposite requirement that they remain in contact with water. These two interactions compete to give rise to the idea of two “opposing forces” (Tanford, 1980) acting mainly in the interfacial region: the one tending to decrease and the other tending to increase the interfacial area a per molecule exposed to the aqueous phase (Figure 20.1).

The attractive interaction arises mainly from the hydrophobic or interfacial tension forces which act at the fluid hydrocarbon-water interface. This interaction may be

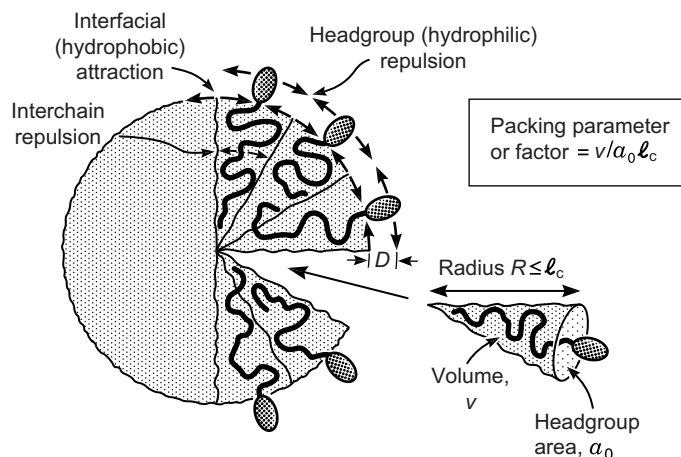


FIGURE 20.1 The hydrocarbon interiors in both micelles and bilayers are normally in the fluid state at room temperature (see Table 20.1). Repulsive headgroup forces and attractive hydrophobic interfacial forces determine the optimum headgroup area a_0 at which μ_N^* is a minimum (see Figure 20.2). The chain volume v and chain length l_c set limits on how the fluid chains can pack together, on average, inside an aggregate. Thus, the preferred molecular conformation depends on a_0 , v , and l_c . In stressed micelles or bilayers, the headgroup area a is larger or smaller than a_0 . Such stresses can come from compressing a monolayer or bilayer either normally or laterally, stretching it, or bending it.

represented by a positive interfacial free energy per unit area characteristic of the hydrocarbon-water interface of¹ $\gamma \approx 50 \text{ mJ m}^{-2}$, though as discussed in Sections 19.6 and 19.7 in the presence of a hydrophilic headgroup this value may be much reduced and closer to $\gamma \approx 20 \text{ mJ m}^{-2}$. Thus, the attractive interfacial free energy contribution to μ_N^0 may be simply written as γa where, in a first approximation, γ may be taken to lie between 20 and 50 mJ m^{-2} .

The repulsive contributions are too complex and difficult to formulate explicitly (Israelachvili et al., 1980a; Puvvada and Blanckstein, 1990). Between mobile hydrophilic headgroups these include a steric contribution, a hydration force contribution, and an electrostatic double-layer contribution if the headgroups are charged (Payens, 1955; Forsyth et al., 1977). Luckily, these separate contributions do not have to be known explicitly. This is because—as in the two-dimensional van der Waals equation of state—we expect the first term in any energy expansion to be inversely proportional to the surface area occupied per headgroup a (cf. pressure $\propto 1/\text{area}^2$ in Eq. (6.15)).

The total interfacial free energy per molecule in an aggregate may therefore be written, to first order, as

$$\mu_N^0 = \gamma a + K/a, \quad (20.1)$$

where K is a constant. We shall initially assume that both these forces act in the same plane at the hydrophobic-hydrophilic interface (see Figure 20.1). The minimum energy is therefore given when $d\mu_N^0/da = 0$, leading to

$$\mu_N^0(\min) = 2\gamma a_0, \quad a_0 = \sqrt{K/\gamma}. \quad (20.2)$$

a_0 will be referred to as the optimal surface area per molecule, defined at the hydrocarbon-water interface. The interfacial energy per molecule, Eq. (20.1) may now be expressed in the more convenient form

$$\mu_N^0 = 2\gamma a_0 + \frac{\gamma}{a}(a - a_0)^2 \quad (20.3)$$

in which the unknown constant K has been eliminated, so that μ_N^0 as a function of a is now in terms of the two known or measurable parameters, γ and a_0 .

We see therefore how the concept of opposing forces leads to the notion of an optimal area per headgroup at which the total interaction energy per lipid molecule is a minimum (Figure 20.2). Moreover, for truly fluid (liquid-like) hydrocarbon chains, the optimal area should not depend strongly on the chain length or on the number of chains, as is indeed found experimentally² (Gallop and Skoulios, 1966; Reiss-Husson, 1967; Lewis and Engelman, 1983b).

The above equations, while crude, contain the essential features of interamphiphile interactions in micelles, bilayers, and more complex structures. They imply that, to a first approximation, the interaction energy between lipids has a minimum at a certain

¹Elsewhere referred to as γ_i .

²This is true only when the area a exceeds $\sim 20 \text{ \AA}^2$ per chain, this being the value for fully compressed and aligned chains in the crystalline state (see Akhmatov (1966) for the lattice dimensions of hydrocarbon chains).

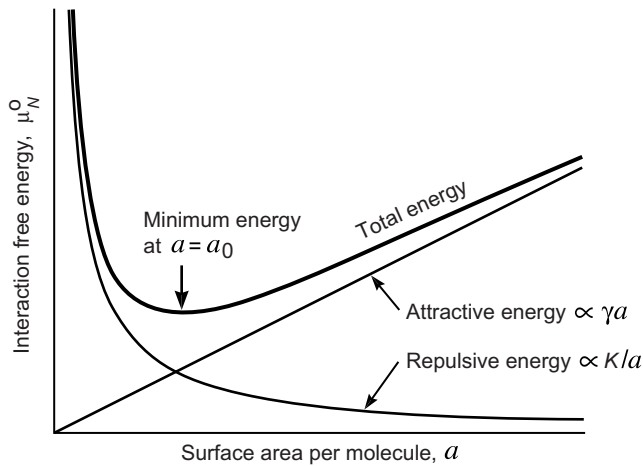


FIGURE 20.2 Optimal headgroup area a_0 at which the opposing forces of headgroup repulsion and interfacial (hydrophobic) attraction are balanced. For small deviations about the optimum area, the energy varies parabolically about a_0 , as described by Eq. (20.3), implying elastic-like behavior of the film when stretched.

headgroup area a_0 , about which the energy varies parabolically (i.e., elastically). The equations ignore three second-order but nevertheless important effects, some of which are discussed later: (1) specific headgroup interactions such as ionic bridging, (2) complex chain-chain interactions (since the hydrocarbon chains are never perfectly liquid-like), and (3) the effect of surface curvature on μ_N^0 .

The concept of opposing forces and optimum interfacial area arises for other types of amphiphilic molecules as well as for nonaqueous solvents—for example, polymer diblocks (AB) or triblocks (ABA or BAB) in liquids that are good solvents for A but not B. Such systems can give rise to a large variety of structures, discussed later in this chapter.

20.3 Geometric Packing Considerations

Having established the equations that adequately describe the interactions between simple amphiphilic molecules within an aggregate, we have yet to establish the most favored structures. The geometry or “packing properties” of the molecules now enter the picture. These depend on their optimal area a_0 , the volume v of their hydrocarbon chain or chains, which will be assumed to be fluid (deformable) but incompressible, and the maximum effective length that the chains can assume. We shall call this the critical chain length, ℓ_c . This length sets a limit on how far the chains can extend; smaller extensions are allowed but further extensions are not, these being energetically or entropically expensive, as in the case of polymers being extended well beyond R_g (see Section 21.7). The critical length ℓ_c is a semiempirical parameter, since it represents a somewhat vague cut-off distance beyond which hydrocarbon chains can no longer be considered as fluid. However, as may be expected, it is of the same order as, though somewhat less than, the fully extended molecular length of the chains ℓ_{\max} (Israelachvili et al., 1976, 1977; Gruen,

1985; Tanford, 1980). According to Tanford, for a saturated hydrocarbon chain with n carbon atoms:

$$\ell_c \leq \ell_{\max} \approx (0.154 + 0.1265n) \text{ nm}, \quad (20.4)$$

and

$$v \approx (27.4 + 26.9n) \times 10^{-3} \text{ nm}^3. \quad (20.5)$$

Note that for large n , $v/\ell_c \approx 0.21 \text{ nm}^2 \approx \text{constant}$, which is close to the minimum cross-sectional area that a hydrocarbon chain can have.³

Once the optimal surface area a_0 , hydrocarbon chain volume v , and critical length ℓ_c are specified for a given molecule—all these being measurable or estimable—one may ascertain which structures the molecules can pack into within these geometric constraints. A convenient parameter for analyzing these structures is the dimensionless number, $v/a_0\ell_c$, known as the critical “packing parameter” or “packing factor.” Figure 20.3 illustrates how the different interactions occurring at the headgroup and chain regions determine $v/a_0\ell_c$ and, in turn, the critical or limiting packing shapes that the molecules can adopt in the structures they assemble into. It is important to note that these are the *limiting* shapes; for example, when $v/a_0\ell_c = \frac{1}{2}$ in Figure 20.3, the molecules may pack into structures where they are *less* cone-shaped (structures to the right) than the one shown because their area and volume can remain equal to a_0 and v as their extension ℓ remains less than ℓ_c . But they cannot do this if they adopt a *more* conical shape (the more highly curved structures to the left).

It turns out that a great variety of different structures can be formed that satisfy the same critical packing parameter. However, since μ_N^0 will be roughly the same for all these structures (since a_0 is the same) entropy will favor the structure with the smallest aggregation number—say, at $N = M$ —and this structure is unique! Larger structures will be entropically unfavored, while smaller structures, where packing constraints force the surface area a to increase above a_0 , will be energetically unfavored.

Figure 20.4 shows the gradation in preferred structures with increasing $v/a_0\ell_c$ from spherical micelles ($v/a_0\ell_c \leq \frac{1}{3}$) to nonspherical (ellipsoidal) micelles ($\frac{1}{3} < v/a_0\ell_c < \frac{1}{2}$) to cylindrical or rod-like micelles ($v/a_0\ell_c \approx \frac{1}{2}$) to various interconnected structures ($\frac{1}{2} < v/a_0\ell_c < 1$) to vesicles and extended bilayers ($v/a_0\ell_c \approx 1$) and finally to a family of “inverted” structures ($v/a_0\ell_c > 1$). Each of these structures corresponds to the minimum-sized aggregate in which all the amphiphiles have minimum free energy.

In concentrated systems the preferred structures are also determined by the interactions *between* the aggregates, which cause transitions to ordered “mesophase” structures.⁴ Due to the short-range repulsive forces between the aggregates, with increasing

³About 0.18 nm^2 (18 \AA^2) in the monoclinic crystal (Akhmatov, 1966).

⁴A mesophase is a normal phase in the thermodynamic sense, but one that is structurally more complex than a simple liquid or solid phase. It can contain many small molecular aggregates that can be monodisperse or polydisperse, or it can have convoluted lamellar, rod-like, or tubular structures that link up with each other to form a three-dimensional network that extends indefinitely throughout the phase. These are known as periodic, bicontinuous or tricontinuous structures, some of which are shown in Figures 20.4, 20.8, and 20.10.

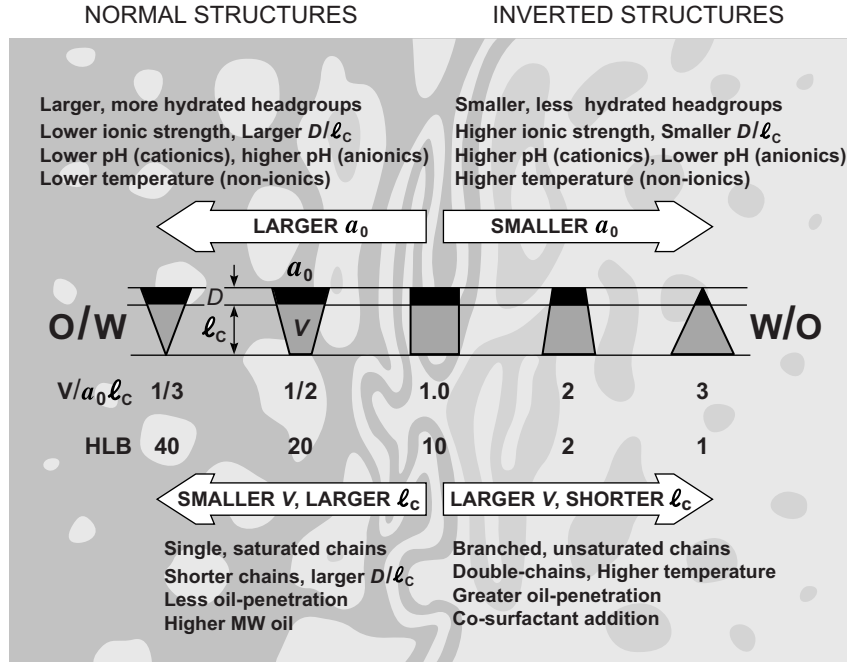


FIGURE 20.3 The various forces acting laterally between the hydrophilic headgroups (black regions), the hydrocarbon chains (grey regions), and at the hydrocarbon-water interface between them, that together determine the preferred packing geometry of surfactant and lipid molecules, defined in terms of the dimensionless packing parameter, $v/a_0\ell_c$. The lateral repulsive forces between the headgroups are located at a finite distance D from the hydrocarbon-water interface, which determines the bending or curvature energy contribution to μ_N^0 (Section 20.8). The dimensionless packing parameter $v/a_0\ell_c$ is linearly proportional to the *Hydrophile-Lipophile Balance* or HLB number (Becher, 1984), which is traditionally used to designate amphiphiles that form oil-in-water (O/W) micelles or inverted water-in-oil (W/O) micelles in surfactant-water-oil mixtures (discussed again later and also illustrated in Figures 20.4 and 20.9). [From Israelachvili, 1994a.]

amphiphile concentration (decreasing water content) the optimum area falls (see Problems 21.4 (iii) and 21.5) and the structures are driven to higher $v/a_0\ell_c$ values. They also become more ordered. Thus, referring to Fig. 20.4, at higher surfactant concentrations spherical micelles transform to ordered hexagonal (H phase) cylinders, cylindrical micelles to interconnected cubic (C phase) structures, and extended bilayers or lamellae to inverted (C_{II} or H_{II}) structures (Lee et al., 1993). These are first order phase transitions where each one-phase region is separated by a two-phase region as required by thermodynamics (see inset in Figure 6.1). Very similar transitions occur in polymer amphiphile systems (Bates and Fredrickson, 1990). We shall now consider the more important structures in turn.

20.4 Spherical Micelles

For molecules to assemble into spherical micelles, their optimal surface area a_0 must be sufficiently large and their hydrocarbon volume v sufficiently small that the radius of the

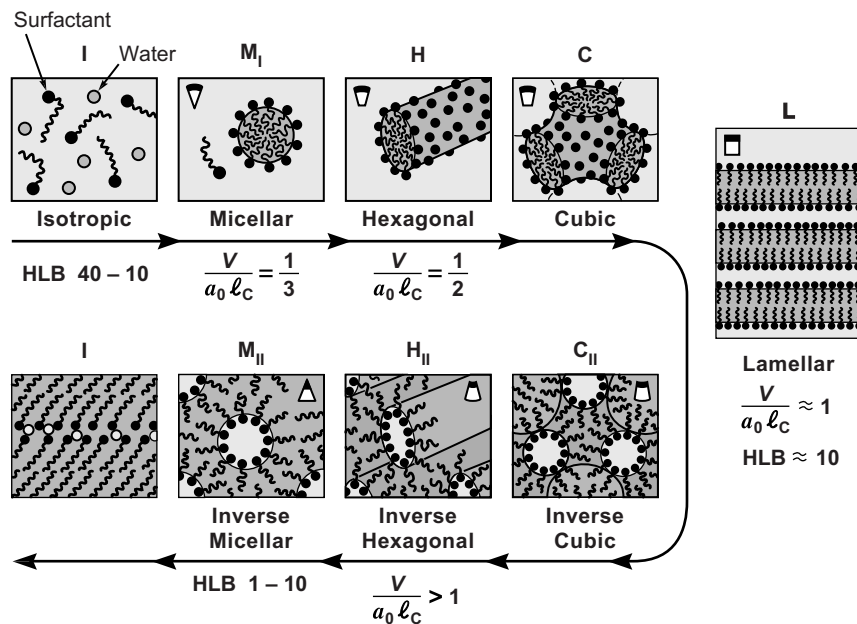


FIGURE 20.4 The different types of structures and “mesophases” formed by amphiphiles in aqueous solutions depending on their packing parameter, $v/a_0 \ell_c$. Figure 20.9 shows the somewhat different structures formed in the presence of oil (hydrocarbon), although both systems have similar designations: I for isotropic solutions of monomers, M for micellar, H for hexagonal (cylindrical), C for cubic (usually isotropically interconnected), L for lamellar, and subscripts I and II for normal and inverted (aqueous core) structures. There are many types of cubic and lamellar structures and phases that depend on the concentration of and interactions between the aggregates and also on the sign and magnitude of the curvature energy. [From Israelachvili, 1994a.]

micelle R will not exceed the critical chain length ℓ_c . From simple geometry we have, for a spherical micelle of radius R and mean aggregation number M (see Figure 20.1),

$$M = 4\pi R^2/a_0 = 4\pi R^3/3v, \quad (20.6)$$

namely,

$$R = 3v/a_0, \quad (20.7)$$

so that only for $\ell_c > R$ —that is,

$$v/a_0 \ell_c < \frac{1}{3} \quad (20.8)$$

will the amphiphiles be able to pack into a spherical micelle with their headgroup areas equal to a_0 and with the micelle radius R not exceeding ℓ_c .

An example of such micelle-forming amphiphiles is the 12-carbon chain sodium dodecyl sulfate surfactant (SDS) in water, shown in Figure 20.5, where experimentally $M \approx 74$ (Cabane, 1985). Putting $n = 12$ into Eq. (20.5) gives $v = 0.3502 \text{ nm}^3$. Equation (20.6) then gives $a_0 \approx 0.57 \text{ nm}^2$, and Eq. (20.7) gives for the optimal micelle radius: $R \approx 1.84 \text{ nm}$. Now for a 12-carbon chain, Eq. (20.4) gives $\ell_c \approx 1.67 \text{ nm}$, which is 0.17 nm (or 9%) short of

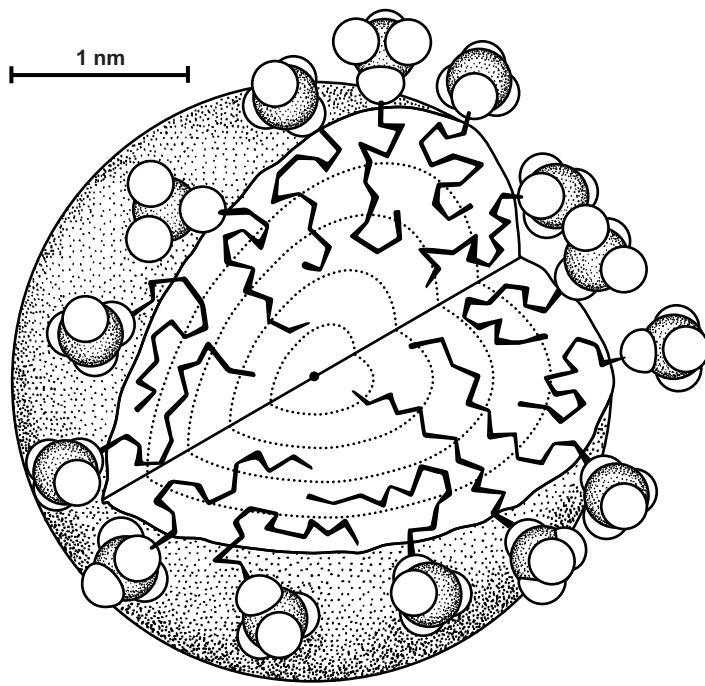


FIGURE 20.5 A sodium dodecylsulfate (SDS) micelle drawn to scale. The micelle contains 60 sodium dodecylsulfate molecules. The hydrocarbon chains pack at liquid hydrocarbon density in the core where they are almost as disordered as in the bulk liquid state. Each of the five spherical shells contains approximately the correct number of chain segments to ensure even chain packing density throughout. Note that all segments of the chain spend an appreciable proportion of time near the micelle surface. Thus, even though the core is almost completely devoid of water each segment samples the hydrophilic environment. Drawing based on calculations by Gruen and de Lacey (1984).

the required (optimal) radius for a sphere. Thus, for SDS micelles in water, $v/a_0\ell_c \approx 0.37$, which means that they just cannot pack into spheres and so must be slightly nonspherical.



Worked Example 20.1

Question: Below what aggregation number will SDS micelles in water be spherical and how could this be achieved in practice?

Answer: After some thought or algebra, using Eqs. (20.6)–(20.8), it becomes clear that the answer is simply

$$M = \frac{4\pi\ell_c^3}{3v} = \frac{4\pi[(0.154 + 0.1265 \times 12)10^{-9}]^3}{3[(27.4 + 26.9 \times 12)10^{-30}]} = 56.$$

We have seen that experimentally, $M = 74$ and $v/a_0\ell_c \approx 0.37$ for SDS in water. Since v and ℓ_c are fixed, the only way to reduce $v/a_0\ell_c$ to the required value of 0.33 is to raise a_0 by about 10%.

In practice, this could be achieved by raising the pH of the solution, which would increase the degree of ionization of the negatively charged headgroups, thereby increasing the repulsion between them (see Problem 14.11) and resulting in an increase in a_0 . The required value of a_0 is given by Eq. (20.8) as $3v/\ell_c = 0.63 \text{ nm}^2$. If the surfactant were cationic, we would decrease the pH.



The mean size of spherical micelles is relatively insensitive to the surfactant concentration above the CMC, and the micelles are fairly monodisperse. The standard deviation σ in the aggregation number about the mean (at $N \approx M$ where $a = a_0$) may be obtained by first noting that μ_N^0 of Eq. (20.3) can be written as

$$\mu_N^0 = \mu_M^0 + \frac{\gamma}{a}(a - a_0)^2. \quad (20.9)$$

Now for a spherical micelle, we have $N = 4\pi R^2/a = 4\pi R^3/3v = 36\pi v^2/a^3$. Equation (20.9) may therefore be expressed in the form of Eq. (19.36) as

$$\mu_N^0 - \mu_M^0 = A(N - M)^2, \quad \text{where } A = \gamma a_0 / 9M^2. \quad (20.10)$$

The distribution profile is therefore roughly Gaussian: $\exp(-(N - M)^2/2\sigma^2)$, with a standard deviation of (Israelachvili et al., 1976):

$$\sigma = \sqrt{(9kT/2\gamma a_0)M}. \quad (20.11)$$

Typically, for γ lying in the range 20–50 mJ m⁻² and $a_0 \approx 0.60 \text{ nm}^2$, we therefore expect

$$\sigma \approx \sqrt{M}. \quad (20.12)$$

For example, for $M \approx 60$, $\sigma \approx 8$. Aniansson and colleagues (1976) found that for a variety of sodium alkyl sulfate micelles, the value of σ lies between \sqrt{M} and $2\sqrt{M}$. The distribution or spread about M is thus fairly narrow but by no means sharp, as was illustrated in Figure 19.8.

20.5 Nonspherical and Cylindrical Micelles

Most lipids that form spherical micelles have charged headgroups, since this leads to a large headgroup area a_0 . Addition of salt partially screens the electrostatic inter-headgroup repulsion and thereby reduces a_0 . Surfactants and lipids that possess smaller headgroup areas such that $\frac{1}{3} < v/a_0\ell_c < \frac{1}{2}$ cannot pack into spherical micelles but can form cylindrical (rod-like) micelles. Falling into this category are single-chained lipids possessing charged headgroups in high salt (e.g., SDS, CTAB) or those possessing uncharged, nonionic, or zwitterionic headgroups (e.g., C₁₂E₅, lysolecithin), which are also fairly insensitive to ionic strength. However, the headgroups of nonionic surfactants are sensitive to temperature (see Figure 20.3).

As discussed in Section 19.12 rod-like aggregates must have very unusual properties: they are large and polydisperse, and their mean aggregation number is very sensitive to the total surfactant or lipid concentration C . According to Eq. (19.32), above the CMC

their mean aggregation number should increase proportionally to \sqrt{C} , which is indeed found to be the case experimentally (Mazer et al., 1976; Missel et al., 1980).⁵

It is important to note that the unusual properties of cylindrical micelles are due entirely to end effects: at each end the molecules are forced to pack into hemispherical caps with a headgroup area a determined by $v/a\ell_c = \frac{1}{3}$ so that $a > a_0$, since $v/a_0\ell_c > \frac{1}{3}$. The unfavorable energy of these end lipids determines the magnitude of the interaction parameter α in Eqs. (19.32) and (19.33), which increases as a_0 decreases. Since $\langle N \rangle = 2\sqrt{Ce^\alpha}$, it is not surprising that the growth or shrinkage of cylindrical micelles is very sensitive to changes in temperature, chain length, and—for ionic lipids—to ionic strength (Missel et al., 1980, 1983, 1989; Malliaris et al., 1985; Lin et al., 1990; Heindl and Kohler, 1996; Evans and Wennerström, 1999). For example, their sensitivity to increasing ionic strength arises from its effect on decreasing a_0 , which increases α and thus $\langle N \rangle$. Thus, the aggregation number of SDS micelles in 0.6 M NaCl is ~ 1000 compared to ~ 60 in water. Likewise, “rod” micelles of cationic surfactants increase in size with the bulk anion concentration in the order $\text{Cl}^- < \text{Br}^- < \text{NO}_3^- < \text{I}^-$, as the hydrated size of the anionic counterions fall (see Section 4.5). The unfavorable end energy of cylindrical micelles may be eliminated if the two ends join, thereby forming a toroidal micelle (the two-dimensional analog of a vesicle), but at the expense of configurational entropy and bending energy.

20.6 Bilayers

Amphiphiles that form bilayers are those that cannot pack into micellar structures due to their small headgroup area a_0 or because their hydrocarbon chains are too bulky to fit into such small aggregates while maintaining the surface area at its optimal value. For bilayer-forming lipids, the value of $v/a_0\ell_c$ must lie close to 1, and this requires that for the same headgroup area a_0 and chain length ℓ_c , their hydrocarbon volume v must be about twice that of micelle-forming lipids (for which $v/a_0\ell_c$ is in the range $\frac{1}{3}$ to $\frac{1}{2}$). Therefore, lipids with two chains are likely to form bilayers, and indeed most of them do. For example, single-chained lysolecithins (lyso-PCs) form small but nonspherical micelles, while lecithins (phosphatidyl cholines, PCs) with two alkyl chains, such as di-C₁₄ PC and di-C₁₆ PC, form bilayers (Figure 20.6). Similarly, the cationic CTAB forms micelles, while the double-chained homologs form bilayers. On the other hand, some single-chained surfactants may have a sufficiently large headgroup area that the chains can interdigitate, forming a thin but fairly rigid bilayer.

The doubling of the chains also affects other aggregate properties, both static and dynamic. First, it increases the hydrophobicity of the lipids, which in turn drastically lowers their CMC: compare the CMCs of common micelle-forming lipids (10^{-2} – 10^{-5} M) with those of bilayer-forming lipids (10^{-6} – 10^{-10} M). We shall return to comment on the biological significance of such low CMCs later. Second, it increases the lifetimes or

⁵Nature controls the unrestrained growth of rod-like structures such as actin and microtubules by employing capping agents.

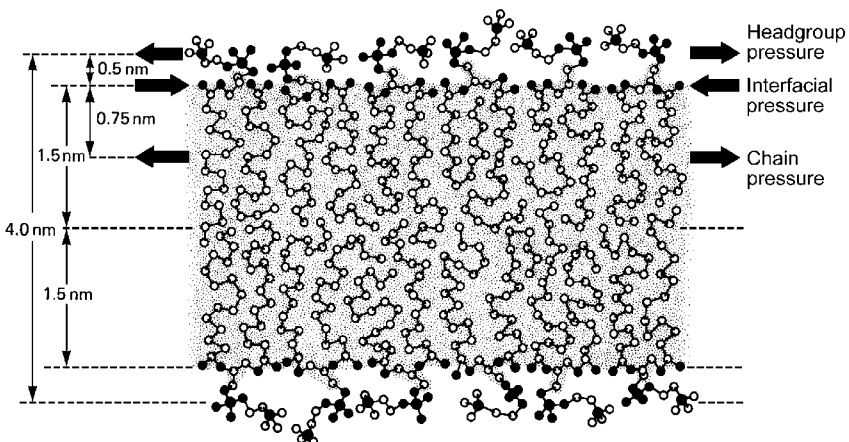


FIGURE 20.6 Lecithin (phosphatidyl choline, PC) bilayer in the fluid state drawn to scale. The lipid bilayer is the basic structure of biological membranes, and most membrane lipids contain two hydrocarbon chains. The lipids diffuse rapidly in the plane of the bilayer, covering a distance of about 1 μm in 1 s. They also cross the bilayer from one side to the other (“flip-flop”), as well as exchange with lipids in the solution, but the rates for these two processes are low, of the order of hours for double-chained lipids compared to 10^{-5} to 10^{-3} s for micelle forming single-chained lyso-lipids. [Modified from Israelachvili et al., 1980a.]

“residence times” τ_R (decreasing the exchange rates) of the molecules within aggregates. Self-assembled structures are usually highly dynamic, with the molecules in constant thermal motion within the aggregates as well as exchanging with monomers in the bulk solution (Pfeiffer et al., 1989). This diffusive exchange may be understood as an activation process, whereby a certain activation energy ΔE has to be surmounted before a molecule can escape from the micelle or bilayer into the bulk solution. Consider the molecules within a bilayer to be jumping about with some characteristic “collision time,” τ_0 . Since the probability of a molecule leaving the bilayer each time it hits the interface is $e^{-\Delta E/kT}$, the mean lifetime of a molecule is therefore $\tau_R = \tau_0 e^{\Delta E/kT}$. After a little thought it becomes clear that ΔE is essentially the same as the energy ($\mu_1^0 - \mu_N^0$) that determines the CMC in Eq. (19.13), which allows us to express the residence time in the simple form:

Residence time⁶

$$\tau_R = \tau_0 / e^{-\Delta E/kT} \approx 55\tau_0 / \text{CMC}, \quad (20.13)$$

where the CMC is in units of M. Typical motional correlation times for amphiphiles in micelles and bilayers are in the range $\tau_0 = 10^{-9}$ – 10^{-7} sec. Thus, for micelles and bilayers we find

$$\tau_R(\text{micelles}) \sim 55 \times 10^{-9} / 10^{-3} \sim 10^{-4} \text{ s},$$

and

$$\tau_R(\text{bilayers}) \sim 55 \times 10^{-7} / 10^{-10} \sim 10^{+4} \text{ s}.$$

⁶This is essentially the same as the inverse of the exchange or transfer rate (in units of s^{-1}).

These values are typical of those measured (Wimley and Thompson, 1990; Kleinfield and Storch, 1993). Furthermore, from the measured CMCs of lipids (Table 19.2) Eq. (20.13) suggests that exchange rates should fall by a factor of about 4–10 per two CH₂ groups added to the chains, in good agreement with measured values of about 8 for phospholipids (Homan and Pownall, 1988). Note, however, that residence times depend on the individual molecules and not on the structures. Thus, when a double-chained lipid bilayer hosts a single-chained surfactant molecule, the residence time of the guest molecule will be much shorter than that of the host lipids.

Another dynamic effect in bilayers is transbilayer lipid exchange, or the “flip-flop” of molecules from one side to the other. This may also be viewed as a diffusive exchange process, except that the energy ΔE in Eq. (20.13) now refers to the energy needed to put the hydrophilic headgroup into the hydrophobic region of the bilayer, which, unlike interbilayer exchange, depends more on the headgroup than on the chains. Flip-flop energies are therefore more difficult to calculate but appear to be of similar magnitude to those involved in the exchange of double-chained lipids, given the similarity in the rates that range from 10² to 10⁵ s—that is, from minutes to days (Wimley and Thompson, 1990).

Another mechanism for the flip-flop of lipids as well as other molecules is diffusion around the inner walls of transient pores (Figures 20.15 and 20.16c). In this case, the process is expected to depend critically both on the lipids in the membrane capable of forming pores (see Problems 20.7 and 20.9) and on the molecules diffusing through them (Herce and Garcia, 2007).

When a bilayer is stretched from its equilibrium state, it expands elastically. For fluid bilayers the 2D area expansion or compressibility modulus k_a may be readily estimated from Eq. (20.3), since by definition

$$\text{Elastic energy} = \frac{1}{2}k_a(a - a_0)^2/a \approx \frac{1}{2}k_a\Delta a^2/a_0 \text{ J} \quad (20.14)$$

which gives

$$k_a \approx 2\gamma \quad \text{per monolayer}, \quad (20.15a)$$

and

$$\approx 4\gamma \quad \text{per bilayer (in units of N m}^{-1} \text{ or J m}^{-2}\text{)}. \quad (20.15b)$$

Given that $\gamma = 20\text{--}50 \text{ mJ m}^{-2}$, we therefore expect $k_a \approx 4\gamma \approx 80\text{--}200 \text{ mJ m}^{-2}$ for bilayers. This estimate compares well with measured values on fluid lipid bilayers and free biological cell membranes which range from 100–250 mJ m⁻² (Kwok and Evans, 1981; Evans and Rawicz, 1990; Marsh, 1990; Rawicz et al., 2000; Ly et al., 2002).

The stress on a bilayer, given by the derivative of the energy with respect to a , is (cf. Eq. (19.19))⁷

$$\tau = k_a\Delta a/a \approx k_a\Delta a/a_0 \text{ N m}^{-1} \text{ or J m}^{-2} \quad (20.16)$$

⁷Note the units for bilayer stress, N m⁻¹, the same as for surface tension. In contrast, the 3D stress on a volume of space is in units of N m⁻² (Pa), the same as for pressure.

which may be positive or negative. However, a stressed bilayer is unlike a conventional elastic or ductile material such as an aluminum sheet: (1) on stretching the area beyond a few percent a bilayer develops pores that rapidly grow leading to rupture, and (2) on compressing, it bends into folds so that the area per molecule does not change.⁸ (3) With time, tensile stresses can be relaxed by having lipids diffuse into the bilayer. (4) Monolayers and bilayers also have a particular kind of elastic bending or curvature modulus, k_b , which is discussed in Section 20.8. When a bilayer is stressed by stretching, the strain $\Delta a/a$ has contributions both from the area elastic modulus determined by Eq. (20.16): $\Delta a/a = \tau/k_a$, but also from the suppression of the thermal undulations, determined by the bending modulus k_b (Helfrich and Servuss, 1984). For most fluid state bilayers, the latter contribution is small except at low strains, typically $\Delta a/a < 0.01$ (1%).

When a bilayer is stretched laterally or compressed normally, it initially deforms elastically, and this deformation can be expressed in terms of an effective 3D Young's modulus (Chapter 17). Thus, for a square bilayer of thickness t with sides of length x under tension τ , where each side expands by Δx , the Young's modulus is $Y = \text{stress}/\text{strain} = (\text{total tensile force along an edge/area of edge})/(\Delta x/x) = (\tau x/t)/(x/\Delta x) = \tau t/\Delta x$. Using Eqs. (20.15b) and (20.16) where $\Delta a = x\Delta x$ and $a_0 = x^2$ gives

$$Y = \tau t/\Delta x \approx k_a/t \approx 4\gamma/t \quad (20.17)$$

for a bilayer (in units of Pa). For a fluid bilayer of thickness $t = 4$ nm, we therefore expect $Y \approx 4(50 \times 10^{-3})/(4 \times 10^{-9}) = 50$ MPa which is a typical value measured for fluid membranes (Table 17.2).

So far, it has been implicitly assumed that the hydrocarbon chains in micelles and bilayers are in the fluid state. At room or body temperature this is the case for most micelle-forming single-chained surfactants, as well as for bilayer-forming double-chained lipids having less than 14–16 carbons per chain. Unsaturated and branched chained lipids remain in the fluid state down to much lower temperatures. Some typical lipid chain melting temperatures, T_c , are given in Table 20.1. We see that these are well above the melting points of the corresponding *n*-alkane—that is, without the headgroup. At temperatures below T_c , bilayers cease to be fluid-like: the elastic moduli increase,⁹ lateral diffusion and flip-flop rates fall, and so on. However, bilayers below T_c do not always freeze into crystalline solids but often retain some of their fluid-like properties; for example, the headgroups may still be highly mobile even though the chains are not. Such bilayers are usually referred to as being in the *gel* state (see Table 17.2), and these can have another transition to a more solid-like or crystalline state at some lower temperature. For excellent compendiums covering all aspects of the physical properties of lipid bilayers, see *Phospholipid Bilayers* by Cevc and Marsh (1987) and the *CRC Handbook of Lipid Bilayers* (Marsh, 1990).

⁸This is only true for isolated or “free” bilayers. Confined bilayers—for example, on a surface or in a lamellar structure (cf. Figure 20.8)—may remain intact and planar when subjected to normal or lateral stresses.

⁹At the transition temperatures the moduli are lower than on either side of T_c , giving rise to increased fluctuations in thickness, solute permeability and ease of rupture.

Table 20.1 Chain Melting (Phase Transition) Temperatures, T_c , of Some Common Double-Chained Lipid Bilayers in Water (at pH 7) in Order of Increasing T_c

Lipid (giving number of carbons per chain)	Headgroup type ^a				Melting point of <i>n</i> -alkane with same number of carbon atoms
	PC	PG ⁻	PS ⁻	PE	
<i>Saturated</i>					
Dilauroyl (12)	−2	0	13	30	−9.6
Dimyristoyl (14)	23	24	36	49	5.9
Dipalmitoyl (16)	41	41	52	64	18.2
Distearoyl (18)	55	55	68	74	28.2
<i>Unsaturated (cis)^c</i>					
Dioleoyl (18)	−22	−18	−7	−16	−30

^aPC: phosphatidylcholine (zwitterionic); PG⁻: phosphatidylglycerol (negatively charged); PS⁻: phosphatidylserine (negatively charged); PE: phosphatidylethanolamine (zwitterionic).

^bCompiled from Cevc and Marsh (1987) and Marsh (1990). Also T_m

^cDepends on the location of the double bond. Most biological lipids have two chains, with a double bond near the middle of one of the chains.

20.7 Vesicles

Under certain conditions it becomes more favorable for closed spherical bilayers (vesicles) to form rather than infinite planar bilayers. This arises because in a closed bilayer the energetically unfavorable edges are eliminated at a finite, rather than infinite, aggregation number, which is also entropically favored. Thus, as long as the lipids in a curved bilayer can maintain their areas at their optimal value, vesicles should be the preferred structures. What then determines the radii of vesicles? First, let us note that if $v/a_0\ell_c = 1$, only planar bilayers will form. For a bilayer to curve, the lipids in the outer monolayer must be able to pack, on average, into truncated cones. This requires that $v/a_0\ell_c < 1$. Simple geometric considerations show (Israelachvili et al., 1976) that for $1/2 < v/a_0\ell_c < 1$, the radius of the smallest vesicle that may be formed without forcing the headgroup area a in the *outer* monolayer to exceed a_0 is

$$R_c \approx \ell_c \left[\frac{3 + \sqrt{3(4v/a_0\ell_c - 1)}}{6(1 - v/a_0\ell_c)} \right] \approx \frac{\ell_c}{(1 - v/a_0\ell_c)} \quad (20.18)$$

which is the critical radius below which a bilayer cannot curve without introducing unfavorable packing stresses on the lipids. Note that no such unfavorable stresses arise for the inner layer molecules, since they can maintain their optimum area without requiring their chains to extend beyond ℓ_c . Thus, as long as a vesicle's radius does not fall below R_c the lipids in both the inner and outer monolayers can pack with their surface areas at the optimal value a_0 and with the two hydrocarbon chain regions not exceeding ℓ_c . For $R < R_c$, a must exceed a_0 in the outer monolayer, and such vesicles are energetically unfavored, while for $R > R_c$ the vesicles are entropically unfavored. For a vesicle of radius R_c and bilayer hydrocarbon thickness $t \approx 2v/a_0$, the aggregation number is

$$N \approx 4\pi[R_c^2 + (R_c - t)^2]/a_0 \approx 8\pi R_c^2/a_0. \quad (20.19)$$

As an example, we may apply the above equations to the much-studied egg lecithin vesicles for which $a_0 \approx 0.717 \text{ nm}^2$ and $v \approx 1.063 \text{ nm}^3$. Taking $\ell_c \approx 1.75 \text{ nm}$ (i.e., $v/a_0\ell_c \approx 0.85$), Eqs. (20.18) and (20.19) then yield $R_c \approx 11 \text{ nm}$, $N \approx 3000$, $t \approx 3.0 \text{ nm}$, and an outside-to-inside lipid ratio of $R_c^2/(R_c - t)^2 \approx 1.9$, all in good agreement with measured values.



Worked Example 20.2

Question: A 12-carbon chain ionic surfactant in aqueous solution has an optimum area of $a_0 \approx 62 \text{ \AA}^2$ in low salt and $a_0 \approx 45 \text{ \AA}^2$ in high salt or near the isoelectric point (pH = iep). What types of structures are likely to be formed by single-chained surfactants in each case, and by double-chained surfactants in high salt?

Answer: For a 12-carbon fluid chain Eqs. (20.4) and (20.5) give $\ell_c \approx 17 \text{ \AA}$ and $v \approx 350 \text{ \AA}^3$ for the critical chain length and single-chain volume. For the single-chained surfactants in low salt to form spherical micelles with $a_0 \approx 62 \text{ \AA}^2$, the micellar radius would have to be $R = 3v/a_0 = 17 \text{ \AA}$, which just happens to be what the surfactant's chain can extend to. Thus, spherical micelles will be the preferred aggregate structure. Smaller spheres will require an expansion of the headgroup area a above a_0 , making them energetically unfavorable, while larger structures with $a = a_0$ will be entropically unfavored. Table 20.2 shows the radii R or chain lengths ℓ

Table 20.2 (for Worked Example 20.2)

12 carbon chain (saturated) $v \approx 350 \text{ \AA}^3$ $\ell_c \approx 17 \text{ \AA}$	Sphere $R = 3v/a_0 (\text{\AA})$	Cylinder $R = 2v/a_0 (\text{\AA})$	Planar bilayer $\ell = v/a_0 (\text{\AA})$	Vesicle $\ell = l_c > v/a_0 (\text{\AA})$
single chain $a_0 = 62 \text{ \AA}^2$	17	11	∅	
single chain $a_0 = 45 \text{ \AA}^2$	28	16	∅	
double chain $a_0 = 45 \text{ \AA}^2$ $v = 700 \text{ \AA}^3$	47	31	16	17

required for the surfactants to pack into the four structures shown, with the crossed out numbers representing those structures that are eliminated for energetic reasons ($\ell > \ell_c$) or entropic reasons (larger N with no energetic advantage). Based on Eq. (20.18) the double chained surfactants in high salt should form vesicles of mean radii $R_c \approx 200 \text{ \AA}$.



For lipids with very small optimal headgroup areas (e.g., $a_0 < 0.42 \text{ nm}^2$ for double-chained lipids) or with bulky polyunsaturated chains (large v , small ℓ_c), their value of $v/a_0\ell_c$ will exceed unity. According to Eq. (20.18), when $v/a_0\ell_c > 1$, R_c becomes negative. What this means is that such lipids form inverted micellar structures (see Figures 20.3 and 20.4) or precipitate out of solution (e.g., unsaturated phosphatidylethanolamines, negatively charged lipids in the presence of Ca^{2+} ions, MGDG, cholesterol).

Certain biological lipids as well as synthetic surfactants and mixtures can spontaneously self-assemble into stable vesicles, and many people believe that vesicles represent the prototypes of early living cells.

20.8 Curvature/Bending Energies and Elasticities of Monolayers and Bilayers

The above treatment offers a rough and ready recipe for analyzing the packing properties of lipid structures, but it is nevertheless incomplete due to the neglect of curvature effects—that is, the effect of a curved (convex or concave) headgroup-water interface on the interaction energy μ_N^0 in Eq. (20.3), which determines which aggregate forms, its mean size, and the distribution about the mean. Curvature effects naturally arise when we consider at which planes the different lateral interactions between adjacent amphiphilic molecules occur. There are three interactions to consider: those between the headgroups, those between the chains, and those occurring at the hydrocarbon-water interface.

Up to now, the lateral attractive and repulsive forces between adjacent amphiphiles, which determine a_0 and μ_N^0 in Eq. (20.3), were all assumed to act in the same plane, at the hydrocarbon-water interface, at which the surface area per molecule has been defined. This is only true for the attractive interfacial tension force, determined by γ but, as illustrated in Figures 20.1 and 20.3, this is not the case for the headgroup repulsive forces, which are centered at some finite distance D above the interface (D positive), or for the chain-chain repulsion, which is centered below that interface (D negative). Thus, the assumption that the chains are entirely fluid and to not oppose any distortion until they become forced to extend beyond ℓ_c is an oversimplification. The assumption of fluidity in bilayers is much less valid than it is in micelles where only one chain needs to reach the center. In a theoretical analysis Gruen and de Lacey (1984) concluded that $\ell_c \approx \ell_{\max}$ in spherical and cylindrical micelles, but $\ell_c \approx 0.7\ell_{\max}$ in bilayers (cf. the assumed value of $\ell_c \approx 1.75 \text{ nm} \approx 0.75\ell_{\max}$ for egg PC vesicles in Section 20.7). The restriction of chain freedom in bilayers gives rise to a lateral chain pressure acting inside the hydrocarbon region—that is, at some negative distance, $-D$, from the hydrocarbon-water interface (Fig. 20.6).

Thus, taking the effects of finite headgroup size and chain repulsion into account, the net repulsive pressure, expressed by K/a in Eq. (20.1), may act at a positive or negative distance D away from the hydrocarbon water interface. This results in an additional curvature- or R -dependent contribution to μ_N^0 . For monolayers this contribution is

$$\mu_N^0 \approx 2\gamma a_0(1 - D/R) \quad \text{per molecule}^{10} \quad (20.20)$$

where for “normal structures” D is positive if the headgroup repulsion dominates over the chain repulsion but negative for “inverted structures.” For example, micelles having a positive D will be more highly curved and therefore smaller than the size predicted by the packing parameter alone. A positive D commonly occurs for micelle-forming, single-chained surfactants. For double-chained surfactants the reverse is often true, and D can be negative—that is, the plane of D lies inside the chain region. Positive and negative D values can lead to qualitatively very different effects, as the next two Worked Examples will show. For planar monolayers, $R = \infty$, and there are no curvature corrections to the energy.

For amphiphiles in bilayers rather than in single monolayers, the situation is more complex because the outer and inner monolayers have opposite curvature, so that the bending energy contributions have opposite signs. But since the outer and inner radii R_o and R_i are different on each side (by the thickness of the bilayer, t), and also because the number of molecules in the outer and inner monolayers is different if each maintains its optimum area a_0 , the *mean* energy for a molecule in a spherical vesicle turns out to be (see Problem 20.6)

$$\mu_N^0 = 2\gamma a_0 \left[1 - \frac{2\pi Dt}{Na_0} \right] = 2\gamma a_0 \left[1 - \frac{Dt}{4R^2} \right] = \mu_\infty^0 - \frac{\gamma a_0 Dt}{2R^2} \quad \text{per molecule} \quad (20.21)$$

which corresponds to a bending energy contribution of

$$\Delta E \approx -\gamma Dt/2R^2 \quad \text{per unit area of the bilayer,} \quad (20.22)$$

where R is the radius of the bilayer, and where D is again positive if the headgroup repulsion dominates (for both monolayers). Note that since the energy goes as $1/R^2$ for bilayers, it is the same for bending in either direction, as indeed it should be by symmetry.

It is conventional to define the curvature energy in terms of a curvature or bending modulus, k_b , where for a spherical elastic sheet the bending energy per unit area is defined by

$$\Delta E = \frac{1}{2}k_b/R^2 \text{ J m}^{-2} \quad (20.23)$$

giving (cf. Eq. 20.22)

$$k_b = -\gamma Dt \text{ J.} \quad (20.24)$$

¹⁰For cylindrically curved structures $\mu_N^0 \approx 2\gamma a_0(1 - D/R)^{1/2}$. These expressions assume that there is no additional interaction at the other (hydrocarbon) end of the molecules—for example, that $\gamma_i = 0$ at the chain-oil interface of the swollen micelles in Figure 20.9.

Using typical bilayer parameters such as $\gamma = 50 \text{ mJ m}^{-2}$, $t = 4.0 \text{ nm}$, and $D = \pm(0\text{--}0.2) \text{ nm}$, we obtain $k_b = \mp\gamma Dt \approx \mp(0\text{--}4) \times 10^{-20} \text{ J} = \mp(0\text{--}10) \text{ kT}$.

A number of papers have addressed the question of how and under what conditions bilayer fragments will close up to form vesicles or liposomes. A circular bilayer disk of radius R will curl up into a closed vesicle if the line tension energy, which favors curling, exceeds the bending energy, which for positive k_b opposes bending. It can be shown (Fromherz, 1983; Lasic, 1988) that the bilayer will close up into a vesicle if $R > 4k_b/\lambda$. For typical values of $k_b = +2.5 \times 10^{-20} \text{ J}$ ($\sim 6 \text{ kT}$) and $\lambda = 10^{-12}\text{--}10^{-11} \text{ N}$, we obtain $R > (10\text{--}100) \text{ nm}$. Thus, only small fragments of (unclosed) bilayers should be found in solution. However, due to the enhanced hydrophobic attraction of their exposed edges (see Section 21.5), these fragments will usually quickly fuse to form larger bilayers. In other words, R will increase until it exceeds the critical size for spontaneous vesicle formation (see Problem 20.16).

It is important to bear in mind that curvature effects start as soon as a monolayer or bilayer starts to curve or bend. That is, as soon as R is no longer infinite. But the energy involved in the initial bending is usually much less than that encountered once the molecules reach their “hard” packing limit, determined by $v/a_0\ell_c$, which usually sets the final limit on the minimum size or radius of an aggregate. We may refer to these two regimes as the “soft” and “hard” packing regimes (Figure 20.7): the first, for $R > R_c$, is determined by the balance of lateral headgroup and chain interactions at roughly constant molecular area ($a \approx a_0$); and the second, for $R < R_c$, when $a > a_0$, by the optimum area and fully extended length of the chains. In the hard packing regime, the opposition to bending comes both from a finite D as well as from the increasing area $a > a_0$ as soon as the bilayer begins to curve. The mean energy associated with changes in radius below R_c due to the increasing a is (Israelachvili et al., 1976):

$$\bar{\mu}_N^0 = 2\gamma a_0 + \frac{\pi\gamma t^2}{N} \left(1 - \frac{R}{R_c}\right)^2 \quad \text{per molecule} \quad (20.25)$$

which leads to a “hard” bending modulus k_b in the hard packing regime of (van Zanten and Zasadzinski, 2005)

$$k_b \approx +\gamma t^2/8 \quad (20.26)$$

which may be compared to the value of $k_b = -\gamma Dt$ in the soft packing regime given by Eq. (20.24). Using the same values as above: $\gamma = 50 \text{ mJ m}^{-2}$ and $t = 4.0 \text{ nm}$, we may therefore expect k_b in the hard packing regime to be of order $k_b \approx +10 \times 10^{-20} \text{ J} \approx +25 \text{ kT}$, which is always positive.

The above calculated values are within the range of measured values for the bending moduli of fluid lipid and surfactant bilayers which range from $+(0.06 \text{ to } 20) \times 10^{-20} \text{ J}$ (Evans and Rawicz, 1990; Marsh, 1990; Abillon and Perez, 1990; Rawicz et al., 2000; Ly et al., 2002; van Zanten and Zasadzinski, 2005; Marsh, 2006), where the positive values indicate opposition to bending.

In the hard packing regime the radius distribution profile is expected to be Gaussian, given by $\exp-(R - R_c)^2 / 2\sigma^2$, with a standard deviation of (Israelachvili et al., 1976; van Zanten and Zasadzinski, 2005)

$$\sigma_R = \frac{2R_c}{t} \sqrt{\frac{kT}{8\pi\gamma}} = R_c \sqrt{\frac{kT}{16\pi k_b}} \propto R_c \propto M^{1/2}, \quad (20.27)$$

which is typically a few percent of R_c .

Equation (20.27) is often used to determine the bending moduli of bilayers from the measured distribution of vesicle sizes. Unfortunately, it is usually impossible to distinguish between the hard and soft bending moduli, which determine the distribution at small and large radii (Figure 20.7). It is also important to distinguish between different types or modes of bending. Unlike areal (pure stretching) expansions or contractions determined by k_a where both monolayers undergo the same deformation, bending can result in different stresses on the outer and inner monolayers in more than one way. The bending moduli derived above assume that both monolayers can relax their headgroup areas to the optimum value, which may require flip-flop when a bilayer curves. However, if an initially planar bilayer, having the same number of molecules on either side, bends

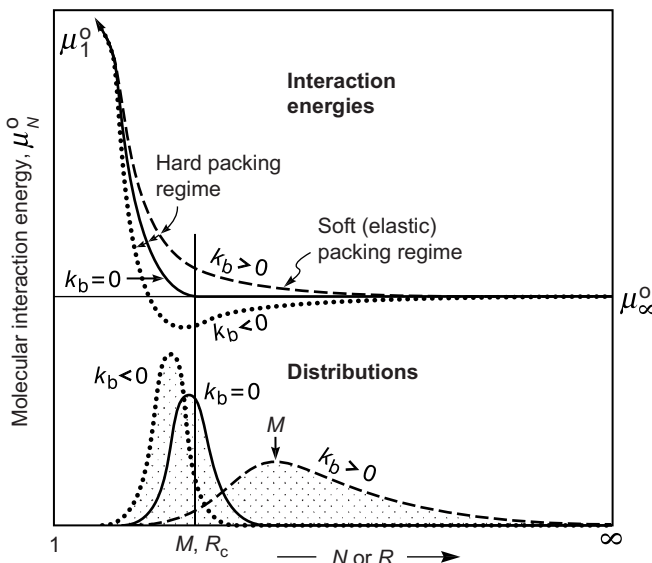


FIGURE 20.7 Schematic variation of interaction energy per molecule in a vesicle with aggregation number N or radius R showing the very different equilibrium size distributions of vesicles depending on the sign of the soft bending modulus k_b , and vesicle radii in the soft ($R > R_c$) and hard ($R < R_c$) packing regimes. In the case of $k_b = 0$, unfavorable hard packing energies prevent the formation of vesicles below a certain size (radius $\sim R_c$ or aggregation number $\sim M$), while entropy disfavors larger vesicles (because of the improbability of so many molecules coming together for no energetic advantage). Solid lines: no soft curvature elasticity ($k_b = 0, D = 0$). Dashed lines: positive soft curvature elasticity ($k_b > 0, D < 0$). Dotted lines: negative soft curvature elasticity ($k_b < 0, D > 0$). The corresponding overall distributions of vesicle sizes (X_N/N) is also shown. The inverse of R_c is also referred to as the *spontaneous curvature* of a membrane (Deuling and Helfrich, 1976 a,b).

into a vesicle without flip-flop occurring, then the outer and inner monolayers will have the same number of molecules and, therefore, different areas from a_0 , giving rise to a much higher bending energy than predicted by Eqs. (20.24) and (20.26). Equilibrium vesicles always have more molecules in their outer monolayer than the inner so that all have (roughly) the same area, close to a_0 (see Worked Example 20.2). It is important in any system involving membrane deformations to establish how the molecules of the two monolayers are coupled.

For large vesicles, those in the soft packing regime, the cases of positive and negative D can give rise to *qualitatively* very different distributions since the first enhances the entropic force toward small aggregates, while the second opposes it. It is worth considering these two cases in more detail.

Negative curvature modulus ($D > 0, k_b < 0$). A negative elasticity favors bending of a monolayer or bilayer right from the start and leads to smaller micelles and vesicles than expected from simple packing considerations (Fig. 20.7). As illustrated in Figures 20.1 and 20.3, the effect is enhanced for large repulsive head groups, as well as for single and/or shorter hydrocarbon chains. Thus, below a certain chain length, no stable vesicles should form; instead, cylindrical or spherical micelles become the preferred structures as occurs for double-chained lecithins with 12 or fewer carbons per chain.



Worked Example 20.3

Question: Figures 20.15 and 20.16 show membranes containing holes or pores. Such holes can be short-lived transient pores involving only lipid molecules, or longer-lived channels usually associated with a protein molecule. Transient lipid pores can provide a low-energy path for ions as well as lipids to traverse (“flip” or “flop”) across membranes. The energetics of a lipid pore requires a careful analysis of how the molecules pack to form the pore walls. Consider a pore in a bilayer whose geometry is like that of the inner surface of a doughnut or torus. There is a strong repulsion between the headgroups that prevents the aqueous hole from having a diameter smaller than 3 nm. The hydrocarbon chain thickness of the bilayer is $t \approx 2\ell_c = 3$ nm and its double-chained lipids have an optimum area of $a_0 = 0.6 \text{ nm}^2$. A small fraction of cone-shaped lysolipids having the same optimum area and chain length but smaller volume v are progressively added to the bilayer. Below what critical packing parameter $v/a_0\ell_c$ will the lysolipids be able to form a pore without any packing constraints, and how many such molecules N will be required to form the pore? If the curvature energy is given by Eq. 20.20, where $\gamma = 50 \text{ mJ m}^{-2}$ and $D = 0.4 \text{ nm}$, show that pores will form fairly abruptly when the mole fraction of the lysolipids reaches a certain critical value, C_{crit} —the CMC for pore formation.

Answer: Consider a torus of inner and outer radii h and $h + 2r$, respectively—that is, whose pore radius is h and whose circular cross section has radius r . The volume and inner area of the part of the torus of radius $h + r$ can be shown to be $V = \pi^2 r^2 (h + r) - \frac{4}{3}\pi r^3$ and $A = 2\pi^2 r(h + r) - 4\pi r^2$. If this volume were to be occupied by lysolipids of chain length $r = \ell_c = 1.5 \text{ nm}$, putting $h = 1.5 \text{ nm}$, we obtain a packing parameter of $v/a_0\ell_c = V/Ar = 0.58$ (typical for lysolipids that form cylindrical micelles), and $N = A/a_0 = 101$. In the absence of curvature contributions to the energy, there is no energetic reason for the lysolipids to form

a pore; and entropy strongly disfavors any aggregation. However, a favorable curvature energy can lead to pores forming above a certain concentration, just as in the case of micelles. Inserting Eq. (20.20): $\mu_N^0 \approx 2\gamma a_0(1 - D/R) = \mu_1^0 - 2\gamma a_0 D/R$ into Eq. (19.3b) gives the distribution of molecules in pores as $X_N = N[X_1 \exp(2\gamma a_0 D/RkT)]^N$. The CMC or C_{crit} is therefore given by $C_{\text{crit}} = \exp(-2\gamma a_0 D/RkT)$, where all the parameters are well defined except for the inner radius of the pore R , which has different principal radii, both convex and concave, at different locations. Still, taking R to be between $r = 1.5$ nm and $2r = 3.0$ nm gives a C_{crit} between 2.0 and 14%. Normal biological membranes usually have no more than a few percent of lysolipids in them, above which they become leaky or break up (undergo “lysis”).

Positive curvature modulus ($D < 0$, $k_b > 0$). A positive bending modulus favors inverted structures, or larger vesicles with very different properties from the small, monodisperse vesicles that have a negative bending modulus. To see why, consider that for $D < 0$ the mean interaction energy per molecule in a vesicle, given by Eq. (20.21), is

$$\bar{\mu}_N^0 = 2\gamma a_0 - \gamma a_0 D t / 2R^2 = \mu_\infty^0 + k_b a_0 / 4R^2 = \mu_\infty^0 + 2\pi k_b / N, \quad (20.28)$$

where $N \approx 8\pi R^2/a_0$ is the number of molecules per vesicle. Equation (20.28) is the same as Eq. (19.6) with $\alpha = 2\pi k_b/kT$. Inserting this expression for α into Eq. (19.32) gives for the mean vesicle aggregation number:

$$M = \sqrt{Ce^\alpha} = e^{2\pi k_b/kT} \sqrt{C}, \quad (20.29)$$

where C is the total lipid concentration in dimensionless mole fraction units ($M/55.5$). The number density of vesicles will decay exponentially with the aggregation number N according to Eq. (19.34), giving for the asymptotic vesicle distribution for $N > M$ (see $k_b > 0$ curves in Figure 20.7):

$$X_N/N = \text{Const.} e^{-N/M}. \quad (20.30)$$

Worked Example 20.4

Question: Based on the packing parameter, the critical vesicle radius of a lipid system is $R_c \approx 20$ nm. Above what positive bending modulus will the size distribution of the vesicles be determined by the “soft” bending modulus rather than the “hard” bending modulus? Assume that the double-chained lipids have a headgroup area of $a_0 = 0.6$ nm² and hydrocarbon length $\ell_c = 1.65$ nm, and that the CMC is 5×10^{-11} M.

Answer: Taking the hydrocarbon thickness of the bilayer to be $t = 2\ell_c = 3.3$ nm, the number of molecules per vesicle with outer and inner radii $R_o = R_c = 20$ nm and $R_i = (R_o - t) = 16.7$ nm is $4\pi(20^2 + 16.7^2)/0.6 \approx 14,200$. R_c is usually not very sensitive to the lipid concentration C . However, the aggregation number given by Eq. (20.29) is. Since C can be as low as the CMC ($C = 5 \times 10^{-11}/55.5 \approx 10^{-12}$), and as high as ~ 10 mM ($C \approx 2 \times 10^{-4}$), the vesicle size will peak at $M > 14,200$ for bending moduli k_b above 1.5×10^{-20} J at the CMC, and 0.9×10^{-20} J at 10 mM. These vesicles will be large and polydisperse, and their mean radius will increase with the total lipid concentration ($R \propto M^{1/2} \propto C^{1/4}$).

The discussion in Worked Example 20.4 strictly applies to *dilute, noninteracting vesicles at equilibrium*. In practice, three effects can limit the sizes of vesicles:

- 1. Time.** The time to equilibrate thousands of low CMC amphiphiles into their equilibrium structure can take months, so that in practice vesicle dispersions often tend to remain in the state they were prepared (by sonication, extrusion, gentle solubilization, etc.). More generally, as discussed in Sections 11.4, aggregates of large macromolecules, nanoparticles, and colloidal particles are often nonequilibrium structures, determined by the method of preparation. These issues are taken up again in Chapter 22, which further explores the differences between *self-assembled* structures and those produced by *directed- or engineered-assembly*.
- 2. Excluded volume.** Single-walled vesicles cannot continue to grow and remain spherical once they exceed a vesicle volume fraction of ~ 0.5 . For example, using the values of the above example, for $k_b = 1.5 \times 10^{-20} \text{ J}$ at a concentration of $\sim 1 \text{ mM}$ ($C = 2 \times 10^{-5}$), Eq. (20.29) gives $M = 4 \times 10^7$, which corresponds to a vesicle radius of $R = \sqrt{Ma_0/8\pi} = 1.0 \times 10^{-6} \text{ m}$ ($1 \mu\text{m}$). Now for a large vesicle of radius R ($R \gg t$) the mole fraction occupied by lipid *in the vesicle* is approximately $4\pi R^2 t \rho_L / \frac{4}{3}\pi R^3 \rho_W = 3t v_w / R v_L$, where v_w and v_L are the molecular volumes of water ($\sim 0.03 \text{ nm}^3$) and lipid ($\sim 1.0 \text{ nm}^3$). In the present example this volume fraction turns out to be $3 \times (4 \times 10^{-9}) \times (0.03) / 10^{-6} = 3.6 \times 10^{-4}$. This is 18 times greater than $C (= 2 \times 10^{-5})$, so that there will be no overlap or crowding—that is, only about 5% of the solution will be occupied by vesicles. However, a repeat calculation at a concentration of $\sim 10 \text{ mM}$ ($C = 2 \times 10^{-4}$), gives $M = 1.4 \times 10^8$, $R = 1.8 \times 10^{-6} \text{ m}$ ($1.8 \mu\text{m}$), and a volume fraction of lipid in the vesicles of 2.0×10^{-4} , which is now the same as C . These vesicles cannot therefore remain spherical, since all the water that is supposed to be their bathing solution is actually inside them. Once the lipid concentration reaches the “crowding limit”—less than 10 mM in this example—the vesicles will be forced to deform and/or adopt different structures. If the bilayers repel, they will order into liposomes or lamellar structures, or into one of the mesophase structures shown in Figure 20.8.
- 3. Interaggregate interactions.** If the bilayers attract, they will order into a lamellar phase already before the vesicles have reached the crowding limit, forming a separate phase in equilibrium with the more dilute vesicle phase (i.e., a two-phase system), as discussed in Section 19.14. If they repel, they may order into a one-phase lamellar system, as also discussed in Section 19.14.

The above approach also applies to other amphiphilic systems (see Figure 20.8), such as coacervates and microemulsions, polymer amphiphiles, and diblock polymers, where one block mimics the hydrocarbon chains of surfactants or lipids and the other mimics the headgroups (Israelachvili, 1985, 1994a; Bates and Fredrickson, 1990; Zheng et al., 1999; Ly et al., 2002). Blocks with more than 40 segments can be analyzed using theories for polymers (Chapter 16).

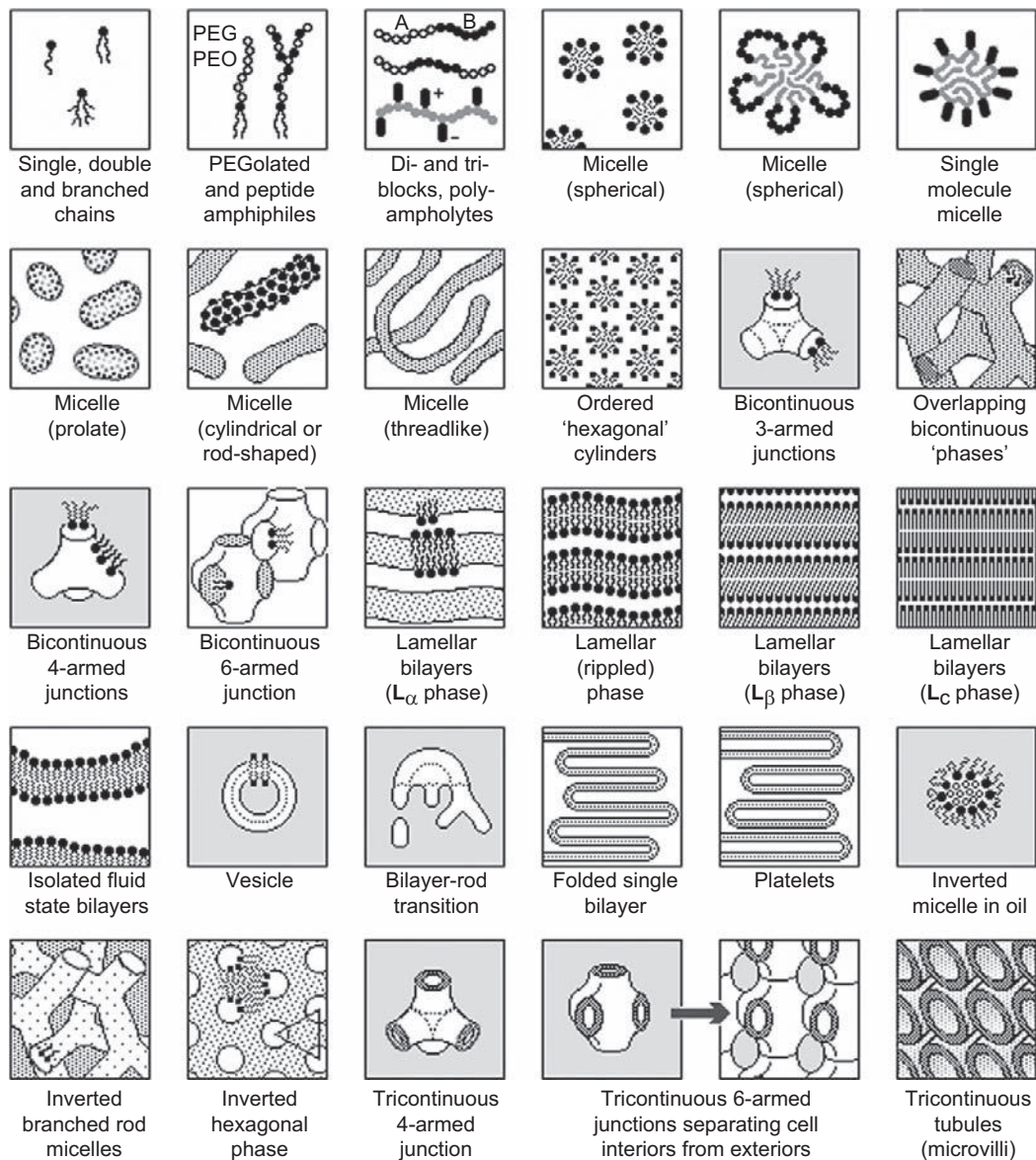


FIGURE 20.8 Some of the more complex structures and mesophases formed by amphiphiles, especially in the cubic and lamellar regimes where $v/a_0 l_c$ is close to 1.0 as well as when aggregates attract or repel each other, and/or at high amphiphile concentrations. Some of these structures are found naturally in both plant and animal cells. Note the 3D bicontinuous and tricontinuous structures where the membrane and aqueous phases are continuous throughout space. In the case of tricontinuous structures the two aqueous regions never overlap; these can be the internal (cytoplasmic) and external (extracellular) regions of a biological cell (see also Figure 20.10). Lamellar structures can also have alternating cytoplasmic and extracellular aqueous regions, as occurs in myelin. The molecular structures of amphiphiles are also becoming increasingly complex, and include *bola* amphiphiles, with a headgroup at either end of the chain (Nagarajan, 1987), polysoaps, with many headgroups along a chain (Borisov and Halperin, 1995), and so on. Some of the structures shown are equilibrium structures, while others may be nonequilibrium but steady-state structures, requiring a continuous input of energy to maintain them (see *self-assembly* and *directed-assembly* in Chapter 22).

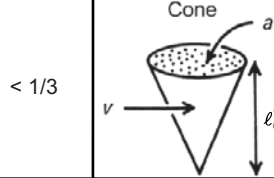
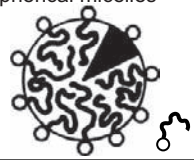
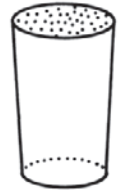
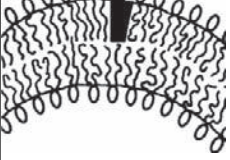
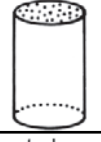
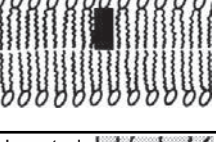
The simple hard and soft packing models developed so far takes us about as far as one can go without resorting to much more sophisticated theoretical methods in which the various intermolecular and interaggregate interactions are treated to a full statistical thermodynamic analysis or a computer simulation. These have been done for micelles (Jönsson and Wennerström, 1981; Gruen, 1985; Szleifer et al., 1985, 1986; Jokela et al., 1987; Blanckstein et al., 1986) and bilayers (Leermakers and Scheutjens, 1988; Egberts and Berendsen, 1988; Cevc and Marsh, 1987; De Loof et al., 1991; Stevens, 2003). Even more complex structures are considered in the next Section.

20.9 Other Amphiphilic Structures and the Transitions between Them

We have seen that the geometric packing properties of different lipids may be conveniently expressed in terms of the packing parameter $v/a_0\ell_c$ characteristic for each lipid in a given solution environment, the value of which determines the type of aggregate formed. Table 20.3 illustrates the structures formed by some common surfactants and lipids, and how these can be modified by their ionic environment, temperature, chain unsaturation, and so on, as will now be summarized (see also Figure 20.3).

- 1. Factors affecting headgroup area.** Lipids with smaller headgroup areas (high $v/a_0\ell_c$) form larger vesicles, less-curved bilayers, or inverted micellar phases. For anionic headgroups, this can be brought about by increasing the salt concentration, particularly Ca^{2+} or lowering the pH. This also has the effect of straightening (condensing) the chains.
- 2. Factors affecting chain packing.** Introducing chain branching and unsaturation, particularly of cis double bonds, reduces ℓ_c and thus increases $v/a_0\ell_c$. Similar effects occur when the effective volume, v , of the chains is increased due to the penetration of organic molecules such as low MW alkanes into the chain regions. Both of the above effects lead to larger vesicles and ultimately to inverted structures. In the case of microemulsions (surfactant/water/oil mixtures), they lead to larger oil-in-water droplets and ultimately to inverted water-in-oil droplets (Figure 20.9).
- 3. Effects of temperature T .** The effects of temperature are more subtle and generally less well understood. The areas of more hydrophilic headgroups usually increase with T due to the increased steric repulsion between them, and this acts to decrease $v/a_0\ell_c$. Thus, with increasing temperature charged micelles usually shrink (Misset et al., 1980). But spherical micelles of nonionic surfactants grow and become more cylindrical, probably due to the reduced repulsion between the headgroups with increasing T (see Figure 21.10). Zwitterionic micelles appear to behave somewhere in between, and their aggregation numbers hardly change with temperature (Malliaris et al., 1985).
- 4. Lipid mixtures.** When an aggregate is composed of a lipid mixture, as long as the different molecules mix ideally and do not phase-separate, the aggregate properties may be treated, in a first approximation, in terms of some mean packing parameter

Table 20.3 Mean (Dynamic) Packing Shapes of Lipids and the Structures They Form[†]

Lipid	Critical packing parameter $v/a_0 \ell_c$	Critical packing shape	Structures formed
Single-chained lipids (surfactants) with large head-group areas: <i>SDS in low salt</i>	< 1/3	Cone 	Spherical micelles 
Single-chained lipids with small head-group areas: <i>SDS and CTAB in high salt, nonionics</i>	1/3–1/2	Truncated cone 	Cylindrical micelles 
Double-chained lipids with large head-group areas, fluid chains: <i>Phosphatidyl choline (lecithin), Phosphatidyl serine, Phosphatidyl glycerol, Phosphatidyl inositol, Phosphatidic acid, sphingomyelin, DGDG^a, dihexadecyl phosphate, dialkyl dimethyl ammonium salts</i>	1/2–1	Truncated cone 	Flexible bilayers, vesicles 
Double-chained lipids with small head-group areas, anionic lipids in high salt, saturated frozen chains: <i>phosphatidyl ethanolamine, phosphatidyl serine + Ca²⁺</i>	~1	Cylinder 	Planar bilayers 
Double-chained lipids with small head-group areas, nonionic lipids, poly (<i>cis</i>) unsaturated chains, high T: <i>unsat. phosphatidyl ethanolamine, cardiolipin + Ca²⁺, phosphatidic acid + Ca²⁺, cholesterol, MGDG^b</i>	>1	Inverted truncated cone or wedge 	Inverted micelles 

^aDGDG, digalactosyl diglyceride, diglucosyl diglyceride.^bMGDG, monogalactosyl diglyceride, monoglucosyl diglyceride.

[†]Fluorocarbon chains are more rigid than hydrocarbon chains. Consequently, fluorocarbon surfactants form less curved structures, and often assemble only into planar bilayers.

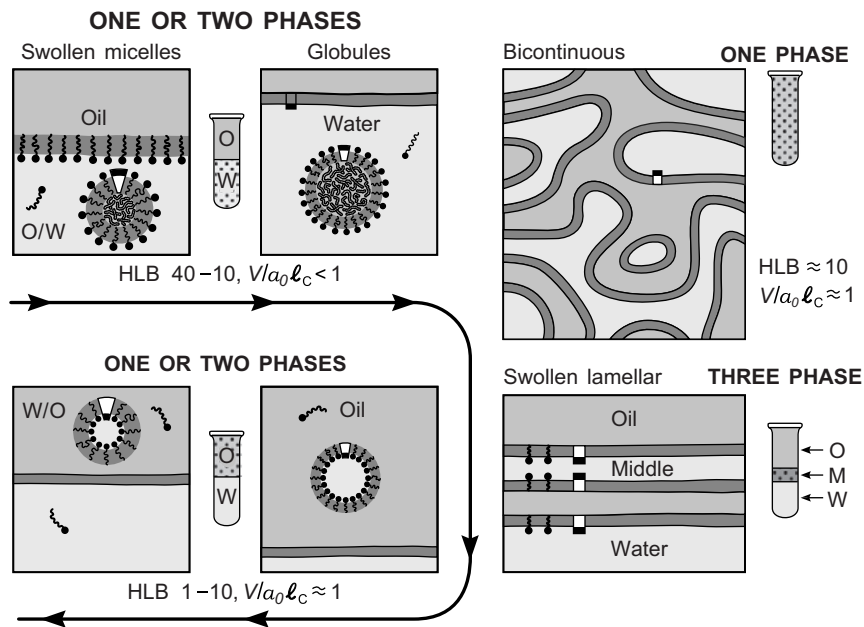


FIGURE 20.9 Various microemulsion structures and phases arising in three-component surfactant-water-oil systems. Notice how, as the packing parameter $v/a_0\ell_c$ increases above 0.33, the structures can now grow as spheres ("swollen micelles," "oil-in-water," or O/W microemulsion droplets) by imbibing oil, something they cannot do in pure aqueous solution—that is, in the absence of oil (Figure 20.4). When $v/a_0\ell_c \approx 1.0$, a "middle phase" of ordered or disordered "sponge phase" lamellae can form if the bilayers attract each other. [From Israelachvili, 1994a.]

intermediate between those of the individual components (Carnie et al., 1979). The sizes of vesicles may thus be conveniently increased or decreased by adding an appropriate amount of another component whose packing parameter is larger or smaller than that of the host lipid. In the case of microemulsion droplets, their sizes are often modulated in this way by adding a "cosurfactant." In other cases, totally new structures may be obtained by a suitable choice of lipid additive. For example, micelle-forming lysolecithin ($v/a_0\ell_c < 0.5$) and non-aggregate forming cholesterol ($v/a_0\ell_c > 1.0$) mix in certain proportions to form bilayer vesicles ($0.5 < v/a_0\ell_c < 1.0$). These and other physical properties of *mixed* lipid bilayers, vesicles, and biological membranes have been discussed by Carnie et al., (1979), Murphy (1982), Kaler et al., (1989), and Yuet and Blankschtein (1996).

Amphiphilic surfactants and polymers can assemble into many other types of structures than the simple ones considered so far, some of which are shown in Figure 20.8. This variety is due to the great variability in molecular design that occurs, either naturally or through advances in synthesizing new types of molecules. These molecules now include surfactants with multiple headgroups or tails, poly-soaps or poly-ions, polymer diblocks and triblocks, random copolymers, branched and dendritic (star-shaped)

polymers, polyelectrolytes, and peptide amphiphiles whose headgroups can be longer than their tails (Discher, 1999; Bates and Fredrickson, 1990; Tirrell et al., 2002). Proteins, with their unique *linear* sequence of amino acid (AA) groups usually fold into unique structures, and are best considered separately (Section 20.13).

Aggregates can also form in other hydrogen-bonding liquids than water, such as ethylene glycol, formamide, and hydrazine (N_2H_4), but their properties have not been as extensively studied. The main requirement for the solvent appears to be that it must have a high interfacial energy with hydrocarbons (see Table 17.1). In addition, there may be more than one solvent—for example, water and oil—where the surfactants may segregate into one or the other phase (as normal O/W or inverted W/O microemulsion droplets) or collect at the interface (see “Middle Phase” in Figure 20.9). The solvent or solvents need not be water or oil, but two immiscible polymer liquids. In such cases terms such as hydrophobic and hydrophilic are replaced by solvophobic and solvophilic.

As shown in Figures 20.4 and 20.8, amphiphiles can order into 3D interconnected structures, often referred to as being biocontinuous or tricontinuous, depending on how many separate percolation channels exist within the structure. Some of these structures occur naturally, for example, the two type of tricontinuous membranous structures shown in Figure 20.10, which are found in plants. Others are synthetic, as in bar soaps where their 3D structure gives the soap its strength.

Many of these structures can be readily transformed from one to the other by changing the temperature or solution conditions. The ease with which this often happens is because the energies are not very different in the different structures, even though they may “look” very different. For example, the two structures shown in Figure 20.10 can have zero net curvature, defined by $1/R_1 + 1/R_2$, because each part of the surface has the same

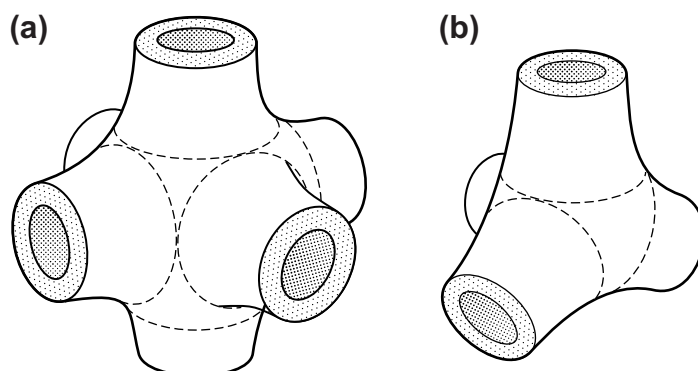


FIGURE 20.10 Two examples of periodic tricontinuous 6-arm and 4-arm membrane structures in water, where a single lipid bilayer or biomembrane folds its way through the whole of space, at the same time separating two aqueous compartments from each other. Such membranous structures occur naturally in leaves (prolamellar bodies). Their mean curvature is close to zero and they can easily transform from one to the other, including lamellae (by the action of light on the proteins within the membranes), since there is little difference in the energies among the different structures despite the large difference in shape (morphology). There are many different types of surfaces whose curvature is everywhere the same (not necessarily zero), known as *minimal surfaces*.

two principal radii but of opposite sign (one convex, the other concave). Thus, both the hard (packing) and soft (bending) energies in these two structures are not very different, and are also the same as in planar bilayers.

20.10 Self-Assembly on Surfaces and Interfaces: 2D Micelles, Domains, and Rafts

For aggregates that self-assemble on a surface or interface the interaction energy μ_N^0 now has an additional energy contribution from the molecule-surface interaction. Interfaces can be vapor-liquid (e.g., “air-water” as in Langmuir monolayers), liquid-liquid (e.g., oil-water), or liquid-solid, and the analysis is more complex because there are now at least three components in the system: the solute molecules, the solvent, and the surface (rather than just the solute and solvent). The structures formed at interfaces usually have different shapes from those in the bulk, as well as a different (usually lower) CMC. For example, surfactant monolayers form at the air-water interface or on hydrophobic surfaces at about 1/10th of the CMC (see Problem 20.10). At solid surfaces the surface aggregates can be planar monolayers or bilayers, although they can also be rippled monolayers, hemicylinders, hemimicelles, or patchy domains (Subramanian and Ducker, 2001).

Domains or “rafts” in monolayers can be considered as 2D micelles (Ruckenstein and Li, 1995, 1996; Israelachvili, 1994b), which, like 3D micelles, may be equilibrium or nonequilibrium but long-lived structures undergoing slow Ostwald ripening or coalescence toward a separate phase (Figure 19.6). Bilayer pores (Figures 20.15 and 20.16) can also be considered as equilibrium 2D (inverted) micelles.¹¹ However, unlike simple 2D aggregates on a surface, those in bilayers and biological membranes usually involve the correlated interactions of the molecules from both monolayers, as occurs, for example, when a pore forms. Another example is “coupled domains,” where the domains in each monolayer are attracted laterally, causing them to overlap—that is, to form a coupled domain as in Figure 20.11(b) and (c).



Worked Example 20.5

Question: A planar bilayer of fluid lipids B contains some lipids of type A in the bottom monolayer that aggregate into isolated circular domains as shown in Figure 20.11(b, left side). The same amount of lipid A is now introduced into the top monolayer. Will the top and bottom domains remain separated (effectively repel each other laterally) or join up to form “coupled domains” as in Figure 20.11(b, right side)? If the latter, will the equilibrium domain radius of the coupled domain be different from that of the isolated domains, R ? Assume that the domains are equilibrium 2D micelles, as in Figure 19.6(a), rather than a separate phase, as in Figure 19.6(c).

¹¹Note that, due to thermal fluctuations, the lifetimes of these “equilibrium” structures, or of any one particular structure, is finite, and can be as short as 0.1 ms (sect. 20.6).

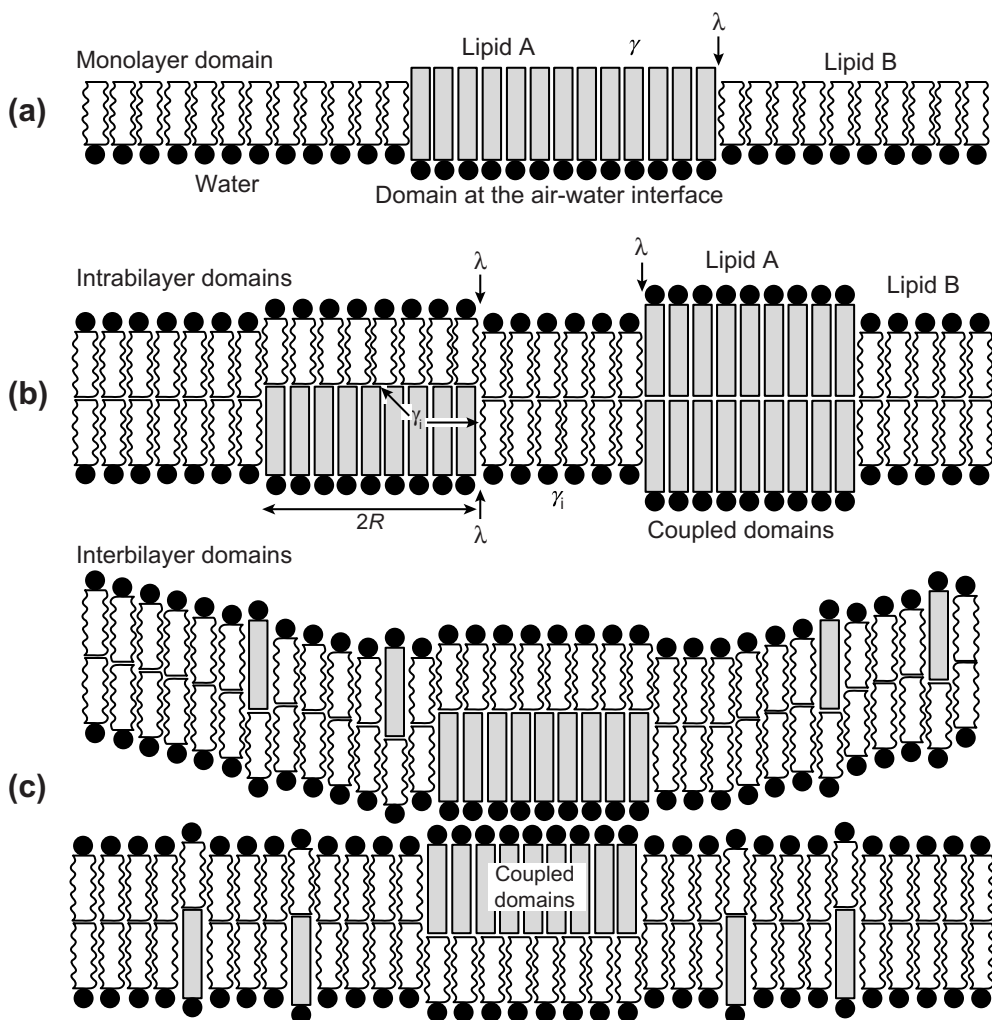


FIGURE 20.11 Examples of isolated and coupled intramonomolayer (top), intrabilayer (middle) and interbilayer (bottom) domains of lipid A in a fluid lipid B. Domains are 2D micelles that arise when the headgroups, chain lengths or phase states of lipids A and B are significantly different. These differences give rise to line tensions λ and interfacial energies γ_i as shown. Figure 21.15 shows how coupled intermembrane domains can occur at the adhesion junctions of biological membranes composed of both lipids and proteins. For images of both isolated and coupled lipid domains see Baumgart et al., (2003), Veatch and Keller (2003), and Gordon et al., (2006).

Partial answer: The difference in the total interfacial energies between two isolated domains and two coupled domains ΔE contains contributions from the line tensions and interfacial energies of the isolated and coupled domains, as defined in Figure 20.11, and that can be expressed as $\Delta E(b, \text{left} \rightarrow \text{right}) = 2\pi R \Delta \lambda - 2\pi R^2 \gamma_i$. Where $\gamma_i = \gamma_{AB}$ is the interfacial energy of the A-B interface. Thus, for large R coupled domains become increasingly favored. For typical values: $\gamma_{AB} = 1-5 \text{ mN m}^{-1}$; $\Delta \lambda = 10^{-13}-10^{-11} \text{ N}$ (Veatch and Keller, 2003), we would

expect the critical domain radius R_c to be $R_c \approx \frac{\Delta\lambda}{\gamma_{AB}} = \frac{10^{-13} - 10^{-11}}{10^{-3} - 5 \times 10^{-3}} = 2 \times 10^{-11} - 10^{-8}$ m = 0.2 – 100 Å, above which coupled domains become the favored structures.

20.11 Biological Membranes

Membranes are the most common cellular structures in both animals and plants (Figure 20.12), where they are involved in almost all aspects of cellular activity, ranging from simple mechanical functions such as motility, food entrapment, and transport to highly specific biochemical processes such as energy transduction, immunological recognition, nerve conduction, and biosynthesis. Biological membranes are very complex and varied. They commonly contain 50 or more different proteins and a host of phospholipids and glycolipids with various headgroups, numbers of chains, chain lengths, and degrees of unsaturation, as well as steroids (e.g., cholesterol) and pure hydrocarbon molecules (e.g., squalane). Yet, in spite of their complexity, there are many aspects of membrane structure that may be qualitatively understood in terms of the concepts we have already outlined, and it is best to start with a consideration of membrane lipids.

20.12 Membrane Lipids

Most biological membrane lipids are double-chained phospholipids or glycolipids, with 16 to 18 carbons per chain, one of which is unsaturated or branched (see Tables 20.1 and 20.3). These properties are not accidental but carefully designed by nature to ensure (1) that biological lipids will self-assemble into thin bilayer membranes that can compartmentalize different regions within a cell as well as protect the inside of the cell from the outside; (2) that because of their extremely low CMC the membranes remain intact even when the bathing medium is grossly depleted of lipids; and (3) that because of the unsaturation or branching the membranes are in the fluid state at physiological temperatures.

For example, as shown in Table 20.1, the chain melting temperatures T_c of saturated di-C₁₈ phospholipids are well above typical physiological temperatures, whereas the unsaturated lipids have their T_c below 0°C. As a consequence of this fluidity, most biological membranes can easily deform and bend until limited by geometric packing constraints. Fluid membranes also allow various solute molecules to pass through them and protein molecules to diffuse along them. Physical and chemical reactions also occur much more rapidly in 2D than in 3D, where the reactant molecules take much longer to find each other by natural diffusion.

A further important aspect of lipid chain fluidity is that different lipid types can pack together—that is, mutually accommodate one another—as well as pack with other molecules while remaining within a planar or curved bilayer configuration (Figure 20.13). In addition, the curvature can be regulated by altering the ratio of its constituent lipids. For example, addition of cone-shaped lipids such as lysolecithin to lecithin vesicles results in smaller vesicles, since a mixture of such lipids can pack into more highly curved

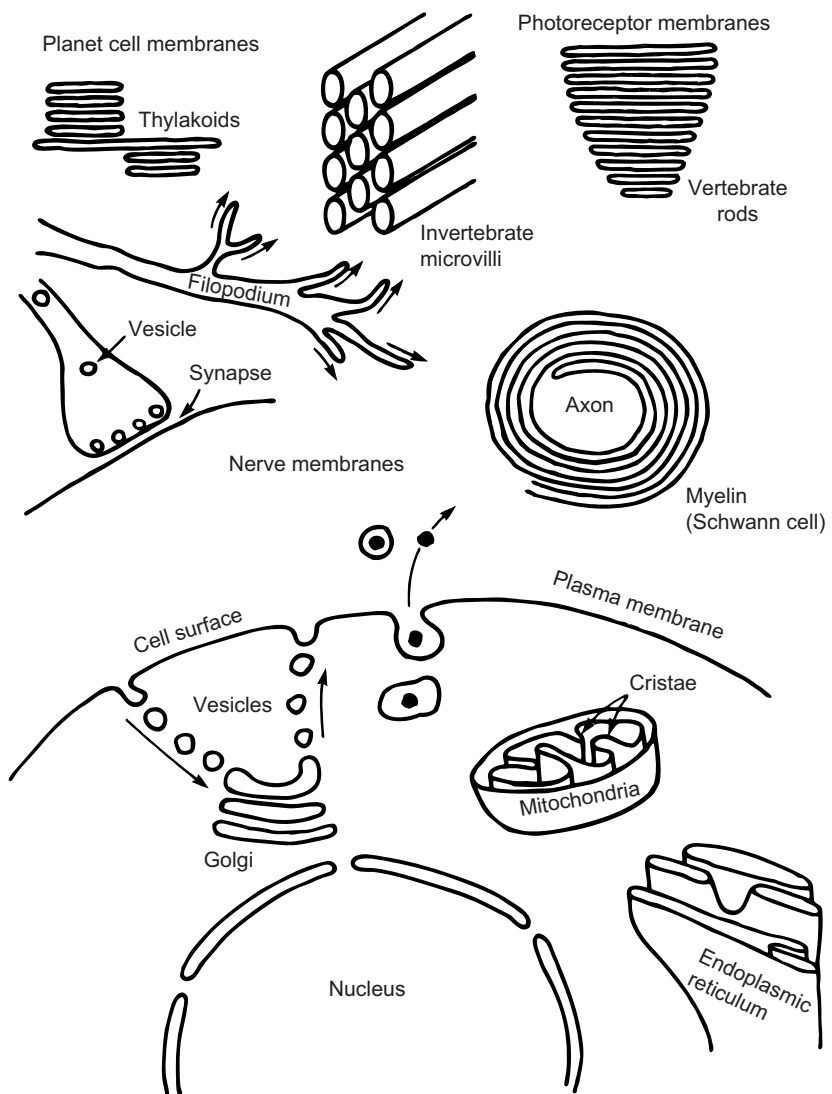


FIGURE 20.12 Cellular membranes are thin sheets of lipids and proteins. Both the surface and internal “intracellular organelles” of cells are bounded by membranes, and it has been estimated that no part within a cell is farther from a membrane than 10 nm. Most biological membranes offer little resistance to bending down to their critical packing radius, R_c , or (inverse) spontaneous curvature.

bilayers. Lysolipids can also form pores, and eventually destabilize a membrane (see Worked Example 20.3).

On the other hand, addition of inverted-cone lipids ($v/a_0\ell_c > 1$) such as phosphatidylethanolamine and cholesterol increases the radius of bilayers, straightens the hydrocarbon chains and reduces their fluidity, causing the “condensation” of the lipids and “stiffening” of membranes.

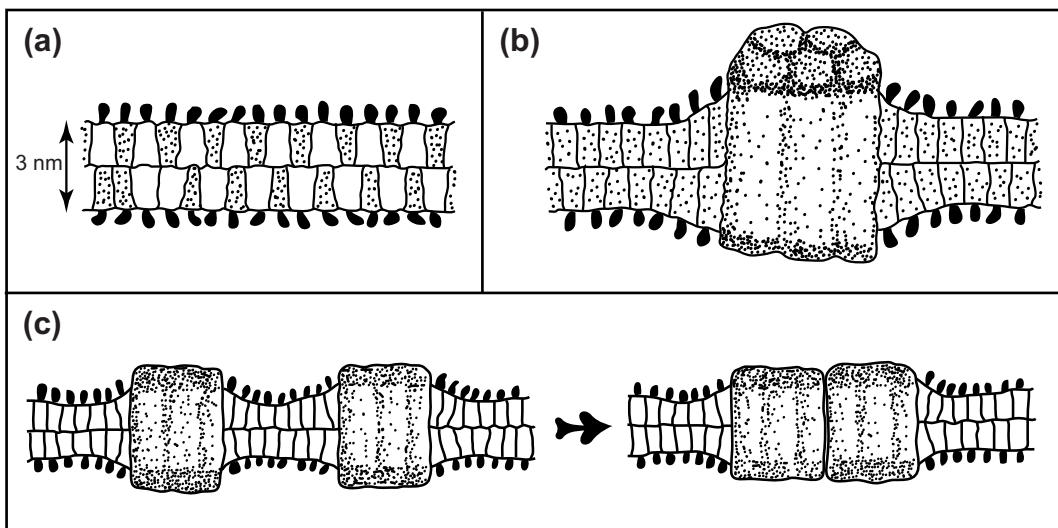


FIGURE 20.13 Packing stresses and their relaxation in multicomponent membranes. (a) Mixture of two different lipids packing together within a planar membrane. The shaded lipid are cone-shaped ($v/a_0\ell_c < 1$); the white lipids are inverted cone-shaped ($v/a_0\ell_c > 1$). (b) Packing constraints induced in the hydrocarbon chain regions of lipids around a protein molecule, which may be relaxed when proteins aggregate, as shown in (c).

It is instructive to note that the most common lipids in animal cells are the two phospholipids phosphatidylcholine (PC) and phosphatidylethanolamine (PE), while in plant cells they are the glycolipids digalactosyl diglyceride (DGDG) and monogalactosyl diglyceride (MGDG). In each case the first lipid packs as a cone ($v/a_0\ell_c < 1$), while the second packs as an inverted cone ($v/a_0\ell_c > 1$) (see Table 20.3). Thus, depending on the ratio of these lipid types in a bilayer, they can pack together into planar bilayers (Figure 20.13a) or into bilayers of varying curvature and flexibility, a facility that is made use of by the lipid synthesis machinery of cells. It is also worth noting that each of these four lipids has an uncharged headgroup. Their headgroup interactions are therefore due entirely to steric-hydration forces that are fairly insensitive to changes in the ionic environment of the cytoplasm. The invariant packing properties of PC, PE, DGDG, and MGDG make these lipids the ideal structural building blocks for stable membrane organization.

The interactions of such lipids may be considered as being nonspecific. Lipids can also interact specifically, usually through complementary ionic (Coulombic) interactions (cf Figure 21.11). For example, when a positively charged lipid or surfactant is next to a negatively charged one, their headgroup areas contract as they bind to each other electrostatically, which in turn changes their packing geometry and the structures they form. Thus, when the two micelle-forming surfactants CTAB (cationic) and SDS (anionic) are mixed 50/50, the resulting structure in water is a bilayer due to the reduced mean headgroup area per surfactant (Kaler et al., 1992).

20.13 Membrane Proteins and Membrane Structure

Membrane proteins are long-chained polypeptide polymers consisting of a long linear string of amino acid (AA) groups or residues. The particular sequence of residues determines the “primary” structure of a protein, and the total molecular weight can exceed 1 million. Compared to membrane lipids, most membrane proteins fold into rigid structures. The chains fold into cylindrical α -helical segments or β -pleated sheets (the secondary structure of proteins), which then self-organize into a globule (the tertiary structure).

While proteins belong to the class of “linear random heteropolymers,” they are really quite special in that unlike synthetic polymers and polyelectrolytes, their segments include positively and negatively charged, zwitterionic, hydrogen bonding, and hydrophobic AA groups. This diversity, together with the different shapes of the 20 “standard” AA groups,¹² means that they fold in a very specific way to produce a unique structure.¹³ In this sense, they are quite different from, say, homopolymers that usually collapse into a structureless “blob.” The 3D conformations (secondary and tertiary structure) of folded proteins are thought to be uniquely determined by the primary sequence of AA groups. This is known as the “central dogma” of molecular biology: that the biologically “active” structure—the natural or “native” structure—is also the structure of lowest energy—that is, the most stable. There is also the hidden supposition that all natural folding pathways lead to the native structure (see Levinthal paradox). Unfortunately, there are no universal theories or models that can be applied to specific interactions and structures, since each is unique. There are only guidelines for understanding protein structure and folding/unfolding dynamics (Dill, 1990).

Soluble proteins have a totally hydrophilic surface, whereas membrane-associated proteins are usually amphiphilic with their surface exposing both hydrophobic and hydrophilic AA groups. If the geometry is right, such proteins can be incorporated into a lipid bilayer where the hydrophobic region penetrates into or totally spans the bilayer and where the hydrophilic residues are exposed to the aqueous phase on one or both sides of the membrane.

When proteins are incorporated into a lipid bilayer in the fluid state, they usually induce stresses on the lipids in their vicinity. Such perturbed lipids are known as boundary lipids. Stresses arise if the hydrophobic regions of the protein and bilayer have different lengths, for then the lipids become stretched or compressed in order to accommodate the protein. This results in a shift of the lipid headgroup area from the optimal value. Such packing stresses around a protein usually involve more than one lipid layer as illustrated in Figure 20.13b.

¹²Some amino acid groups undergo chemical modification after their synthesis and assembly to form the parent protein. This is known as *posttranslational modification*, which greatly increases the number of active amino acid groups.

¹³Given the almost infinite ways that AA groups can be strung together, it is believed by some that only those few that can rapidly fold into ordered structures have evolved into the proteins that exist today. If so, the sequence of AA groups is anything but “random.”

Additional lipid-protein interactions include any specific electrostatic or hydrogen-bonding interactions between the hydrophilic headgroups and the exposed amino acid residues of the proteins. Such lipid-protein interactions often result in a preferential clustering of specific lipids around a protein—the favored lipids being those that can be packed most easily around the protein or specifically interact with it. Since most lipids are negatively charged, the two amino acid groups on protein surfaces that interact electrostatically with bilayer lipids are the positively charged lysine and arginine.

We now turn to consider the forces between proteins *within* a fluid membrane (those *between* membranes are considered in Chapter 21). In Chapters 2, 6, and 19, we saw how 2D structures can be analyzed—for example, in terms of the 2D van der Waals equation of state—to understand phase transitions and domains in surfactant or lipid monolayers and bilayers. In biomembranes, however, the forces between the proteins are more complex and we must really think of it as a three-dimensional system, where both attractive and repulsive forces can now occur between various membrane components at different depths and lateral locations. Repulsive forces can arise between two proteins if they have a strong affinity for the lipids—for example, via ionic bonds. Attractive forces can arise if the proteins can bind to each other directly—for example, via molecular tethers or Ca^{2+} bridges. Attraction can also arise if the protein-lipid packing mismatch is so great that it results in a strong depletion attraction between them where the stresses on the lipids are relieved when the proteins aggregate, as illustrated in Figure 20.13c (for a nice example of this effect, see Sternberg et al., (1993)). In this case the interaction is indirect—mediated by the lipids.

A biological membrane is a dynamic structure. Both the lipids and the proteins move about rapidly in the plane of the membrane (Singer and Nicholson, 1972). However, heterogeneous domains and local clustering of lipids and proteins also occur (Figures 20.15 and 20.16), and these are important for the normal functioning of the membrane and its components. How does a cell maintain and regulate the structural integrity of its membranes? The main criterion for membrane stability appears to be that the heterogeneous lipid mixture should be able to self-assemble into bilayers, even though individual species, such as cholesterol, may not. Thus, many organisms change their lipid composition in response to a change in ambient temperature, for example, synthesizing more unsaturated lipids at lower temperatures. This ensures the stability of the bilayer structure, since the higher packing parameter (higher $v/a_0\ell_c$) of unsaturated lipids offsets the lowering of $v/a_0\ell_c$ at lower temperatures (cf. Figure 20.3 and Table 20.3). Likewise, Wieslander and colleagues (1980) showed that the *in vivo* response of the bacterium *Acholeplasma laidlawii* to external stimuli, such as temperature changes and incorporation of fatty acids and cholesterol, is such that the cell synthesizes just those lipids that will compensate for these stimuli so as to maintain packing compatibility within the membrane—for example, synthesizing more DGDG ($v/a_0\ell_c < 1$) and less MGDG ($v/a_0\ell_c > 1$) after cholesterol (for which $v/a_0\ell_c > 1$) is introduced.

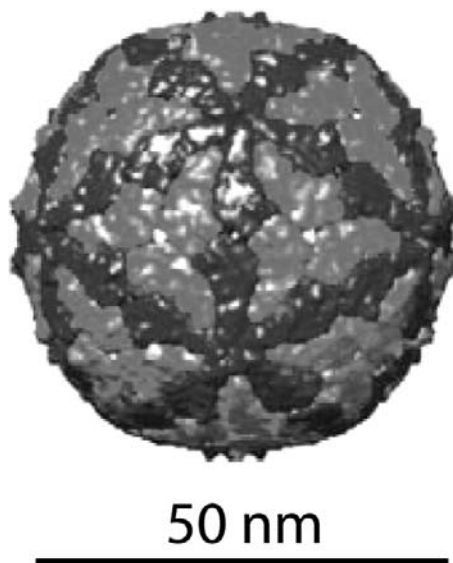


FIGURE 20.14 Association of 72 identical proteins that form the spherical shell (capsid) of the bluetongue virus. The proteins are held together at the common edges by hydrophobic interactions while exposing hydrophilic amino acid groups on their outer and inner surfaces. [Reproduced from Goddard et al., 2005, with permission.]

These examples illustrate the manner in which cells control their membrane structure. They do not do this by a crude mechanical pushing and pulling of components. The cell synthesizes the appropriate lipids and proteins and then leaves them to do their job. The final Chapter (Chapter 22) we shall be looking more into the *dynamics* of cellular and biological structures and processes.

PROBLEMS AND DISCUSSION TOPICS

- 20.1** With the help of Table 19.2 and other literature sources, give possible explanations for the following: (i) The CMCs of surfactants are higher than the solubilities of the corresponding alkanes with the same number of carbon atoms. (ii) The CMC increment per CH_2 is greater for single-chained than for double-chained surfactants. (iii) The smaller the bare ion size of the counterion the larger is its effect on increasing the CMC. (iv) Coions have almost no effect on the CMC. (v) The CMC increment per CH_2 group is greater for nonionic than for ionic and zwitterionic surfactants. (vi) Addition of salt to an ionic micelle decreases the CMC and increases the CMC increment per CH_2 group to the value for nonionic micelles. (vii) The CMC often decreases then increases with temperature. (viii) All other things being equal, reducing the headgroup size decreases the CMC. (ix) Chain branching and unsaturation do not have as strong an effect on the CMC, but usually cause a small increase (so long as the number

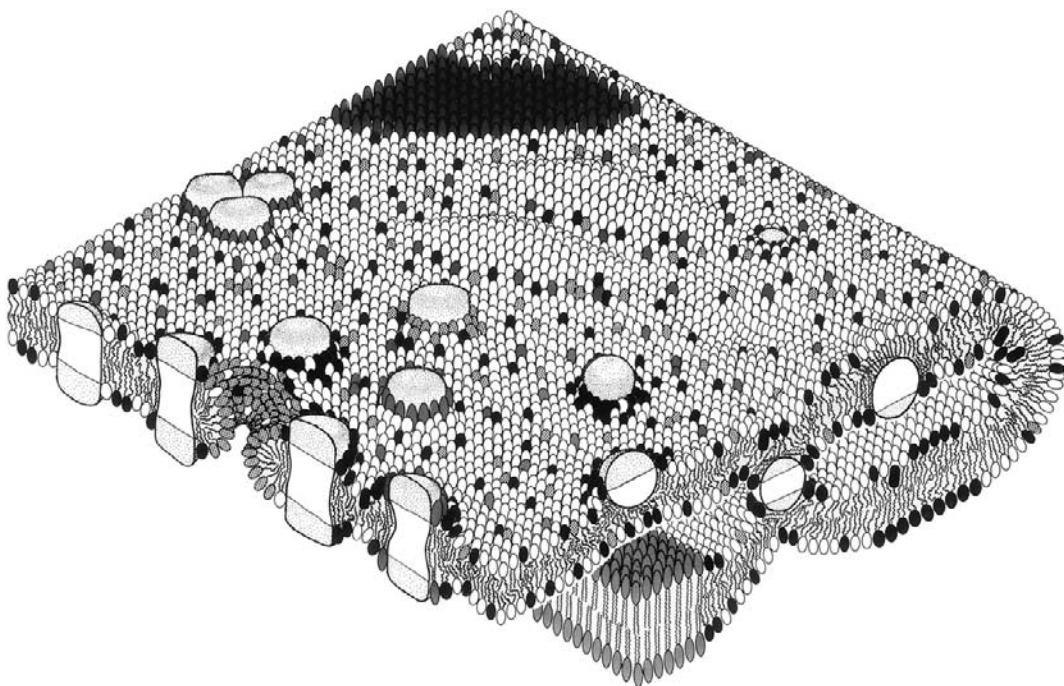


FIGURE 20.15 Schematic figure of a biological membrane. The lipid contents of different membranes vary from as little as 25% up to 80% by weight. At highly curved regions the outer convex face contains mainly cone-shaped lipids, while the inner concave face has more wedge-shaped lipids. Note how stressed regions may expose more of their hydrophobic chain interiors and/or adopt a locally nonbilayer structure, some of which are shown in more detail in Figure 20.16. Lipids have lateral diffusion coefficients of $D \sim 10^{-8} \text{ cm}^2/\text{s}$ in fluid membranes and $D < 10^{-10} \text{ cm}^2/\text{s}$ in gel and frozen state membranes, and therefore diffuse $2\sqrt{Dt} \approx 2$ to $<0.1 \mu\text{m}$ in one second, while free proteins have diffusion coefficients of $D < 10^{-7} \text{ cm}^2/\text{s}$ in fluid membranes. Since two molecules can find each other much faster when confined to diffuse in a membrane (in 2D) than in the bulk solution (in 3D), most biochemical reactions occur between membrane-associated proteins. Even faster reactions occur when the reactant proteins are already associated in clusters, known as reaction centers.

of carbon atoms remains unchanged). [Hint: Think of how electrostatic, steric-hydration and interchain interactions affect the headgroup area and packing parameter, $\nu/a_0\ell_c$, and how this in turn affects micelle size, μ_N^0 and the CMC.]

- 20.2** You are God, and you are unhappy with the planet Earth. You have decided to raise its average temperature by 20°C . How would you modify the membrane lipids to make them more suitable as membrane structure regulators in their new environment? Consider such properties as chain length, degree of branching and unsaturation, type of head-group, and so on.
- 20.3** Two small spherical oil droplets of radius R in water coalesce into one larger droplet. If γ is the interfacial free energy of the interface, obtain an expression for the net change in surface energy during this process. If, due to the presence of charged lipids, each of the original droplets also carries a net charge Q evenly

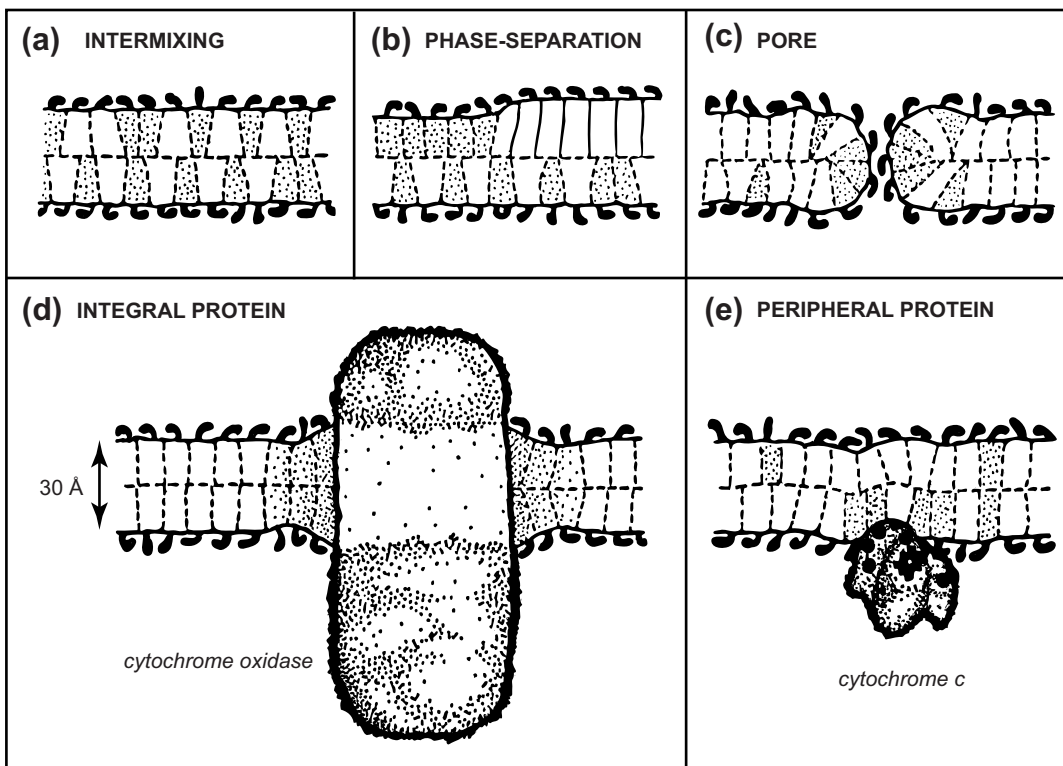


FIGURE 20.16 Mean packing conformations of mixed lipid and lipid-protein membranes, showing how local packing stresses may cause clustering of specific lipids and/or nonbilayer shapes (shaded lipid regions). All figures have been drawn to scale. Note the relatively large size of the cytochrome oxidase protein molecule which protrudes greatly from the bilayer. Both lipid domains (c) and lipid pores (d) may be considered as 2D micelles or inverted micelles, and treated in the same way as 3D micelles (Section 20.10). Pores are usually highly transient structures, although their opening, however brief, can have important effects such as allowing molecules to diffuse or be driven from one monolayer to the other, and/or for polyions to traverse the bilayer (Herce and Garcia, 2007). [Figure adapted from Israelachvili *et al.*, 1980a.]

spread on its surface, what is the additional electrostatic contribution to the total energy change? If $\gamma = 50 \text{ mJ m}^{-2}$ and $Q = 100e$, calculate the critical radius below which the total energy change is positive (i.e., when the coalescence becomes energetically unfavorable). Assume that the dispersion is dilute and that the solvent is pure water with no added electrolyte.

20.4 Derive Eq. (20.18).

20.5 Derive Eq. (20.21) by applying Eq. (20.20) to the outer and inner layer molecules of a vesicle of outer and inner radii R_o and R_i , and thickness $t = R_o - R_i$, where the interfacial areas of the molecules are the same and equal to the optimum area a_0 in each monolayer. Your value of R should be the root mean square average of R_o and R_i —namely, $\sqrt{(R_o^2 + R_i^2)/2}$.

- 20.6** Derive Eq. (20.25).
- 20.7** Amphiphilic surfaces do not always have simple spherical, cylindrical or planar geometries. They can be highly convoluted, where at any point the curvature is theoretically defined by $(1/R_1 + 1/R_2)$. This can lead to interesting situations where what appears as a highly curved surface may actually have no curvature at all. Read up on “minimal surfaces,” and discuss which of the structures in Figure 20.8 need not necessarily have a net curvature at any point on their surfaces—that is, that they are everywhere mathematically *flat*.
- 20.8** Show that for packing parameters $v/a_0\ell_c$ between about 0.75 and 0.85 three-armed junctions of rod-like micelles (Figure 20.17) are energetically favorable. This is the regime where amphiphilic structures form cubic and bicontinuous phases (Figure 20.8).
- 20.9*** (i) A potential difference of 50 mV is applied across an uncharged fluid bilayer (e.g., of DMPC) of nonpolar hydrocarbon-chain thickness 4.0 nm and dielectric constant $\epsilon = 2.5$, in aqueous 150 mM NaCl solution at 300 K. What is the potential drop across the two aqueous regions on either side of the bilayer, and across the nonconducting nonpolar region? You may assume that the external circuit is conducting—that is, that electrons are free to move between the two electrodes immersed in the bulk aqueous phase on either side of the bilayer. (ii) Repeat your calculation when the bilayer is composed of a mixture of 10% charged and 90% uncharged lipids where the headgroup area is 60 \AA^2 for both lipids. If the bilayer is initially symmetrical in its composition, will the application of a field induce asymmetry through flip-flop? (iii) Explain why bilayers and membranes become permeable when subjected to high electric fields. If the above potential difference is applied only across a section of the uncharged bilayer, of area elastic modulus $k_a = 150 \text{ mJ m}^{-2}$, by how much will the section of

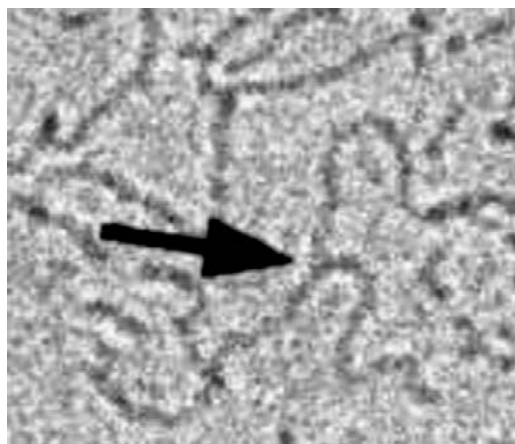


FIGURE 20.17 Three-armed junctions of cylindrical micelles. [Courtesy of Y. Talmon.]

the bilayer thin? Will the thinning be different if the same potential is applied across the whole bilayer rather than just a part of it? [Hint for (i) and (ii): Apply Gauss's Law (Section 3.3) when calculating the surface charge densities and potentials of the two double-layers and bilayer interior. Suggestion for (iii): See Electrocompression and Electroporation.]

- 20.10** The cmc of a single-chained micelle-forming surfactant is 1 mM. Estimate the concentration at which a monolayer forms on a hydrophobic surface immersed in the same surfactant solution. Assume a headgroup area of $a_0 = 25 \text{ \AA}^2$ and $T = 25^\circ\text{C}$. [Answer: About 0.05 mM or 1/20th the cmc.]
- 20.11*** Figure 20.18 shows six different configurations of two immiscible fluids **1** and **2** in fluid medium **3**. (i) If liquids **1** and **2** have the same volume, what are the relationships between γ_{12} , γ_{23} , and γ_{31} that determine which of configurations (a) to (d) has the lowest energy? (ii) If the volumes of **1** and **2** are different, could configurations (e) or (f) be stable thermodynamically? ... against coalescence? ... against Ostwald ripening? For a biological example of this phenomenon as it arises in cell sorting, see Forty et al., 1996. [Advice: Refer to Chapter 17.]
- 20.12** Two water-soluble globular proteins have molecular weights of 50 and 100 kDa, respectively. Which one has a higher fraction of hydrophilic AA residues and why? Assuming that the molecules are spherical, estimate the number of hydrophilic and hydrophobic residues associated with each protein. Describe and analyze how the shape and above numbers change if both proteins span

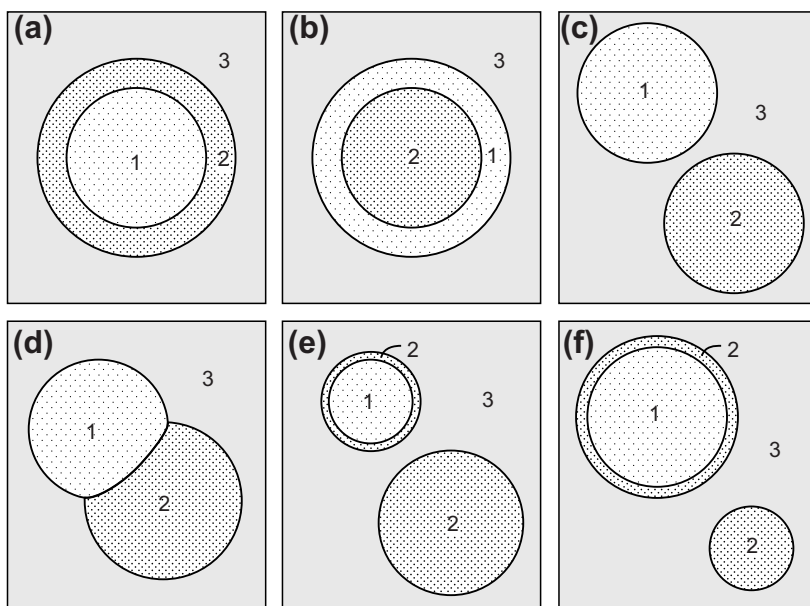


FIGURE 20.18

a lipid bilayer without stressing it when the hydrophobic region is 50 Å thick. Assume that each residue has a molecular weight of 125 Da and occupies a volume of $v \approx 200 \text{ \AA}^3$.

- 20.13*** For a particular anionic surfactant in water the optimum headgroup area is 65 Å², the liquid-like hydrocarbon volume is 400 Å³ and the fully extended chain length is 20 Å. What is the likely structure of the aggregate formed at the CMC and what is the likely aggregation number? As the surfactant concentration increases well above the CMC, it is found that at a surfactant volume fraction of 50% a phase transition occurs to an ordered array of cylindrical micelles. At what volume fraction would another phase transition be expected and what is the likely structure of that phase? Would further mesophases be expected at even higher concentrations? If the water contained a small amount of salt (say, 0.1 M NaCl), would the phase boundaries shift to higher or lower volume fractions? Would these mesophases be separated by two-phase regions and if so would these be wider or narrower than the single-phase regions?
- 20.14*** In Problem 19.3 the surfactants are non-ionic with short-chained PEO headgroups whose optimum area a_0 is sensitive to the temperature, decreasing with increasing temperature. Thus, with increasing temperature the micelles grow and start to imbibe oil from the oil phase, becoming swollen micelles or *oil-in-water* (O/W) microemulsion droplets as the packing parameter $v/a_0\ell_c$ approaches 1.0 (see Figure 20.9). As the temperature continues to increase, $v/a_0\ell_c$ becomes greater than 1.0 and the surfactants now assemble in the oil phase as *water-in-oil* (W/O) droplets that shrink in size. Thus the radius of the droplets, R , first increases in the water phase (R positive), then decreases in the oil phase (R negative). (i) For a system where the surfactant concentration is $C = 0.06$ mole/mole and $a_0 = 0.4 \text{ nm}^2$ (40 Å²) at room temperature, estimate (i) the interfacial tensions of the oil-water interface when $R = 10 \text{ nm}$ assuming no attractive interactions between the micelles. (ii) If there is an attractive interaction between the nonionic headgroups in water, giving rise to an energy minimum of $g_0 = -0.002 kT$ per molecule at $D_w \sim 2 \text{ nm}$ (cf. Figure 21.3), at what droplet radius R will the O/W micelles stop growing but form a lamellar phase at the oil-water interface (essentially a third or “middle” phase as shown in Figure 20.9), and (iii) estimate the interfacial tension of that interface? [Answer: (i) $\gamma_i \approx 0.035 \text{ mJ m}^{-2}$. (ii) $R \approx 13 \text{ nm}$. (iii) $\gamma_i \approx 0.021 \text{ mJ m}^{-2}$.]
- 20.15*** (i) Derive an expression for the line tension λ (energy per unit length, in units of J m⁻¹ or N) of the hemi-cylindrical edge or rim of a fluid bilayer (cf. top rim of Fig. 20.19a) in terms of γ_i , $v/a_0\ell_c$ and ℓ_c . (ii) Estimate the maximum value of λ for a fluid bilayer for which $\gamma_i = 40 \text{ mJ m}^{-2}$ and $\ell_c = 1.5 \text{ nm}$. [Hint: See May, 2000; Umeda et al., 2005. Answer to (ii): $4.7 \times 10^{-11} \text{ N}$.]
- 20.16*** Figure 20.19(b) shows a vesicle of radius R_0 being incompletely engulfed by a fluid bilayer of radius R and area $A < 4\pi R_0^2$ so that a circular hole of radius r

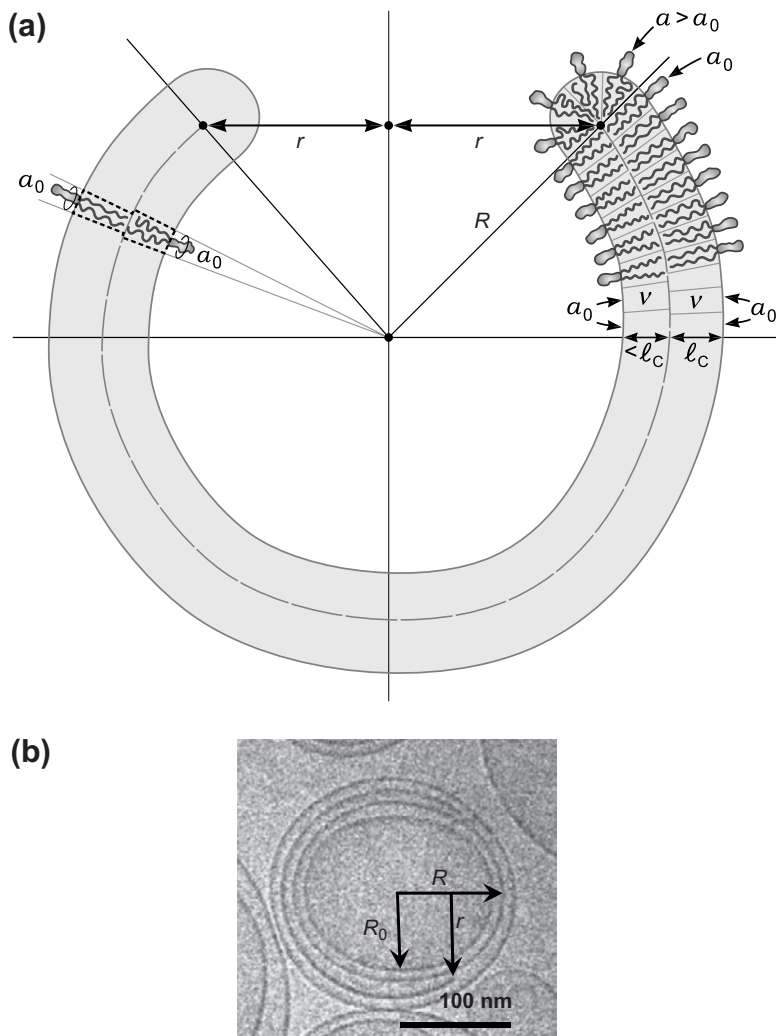


FIGURE 20.19 (a) Schematic of an initially circular planar bilayer disk closing up into a spherical vesicle. The line tension λ at the circular edge of radius r promotes closure which is opposed by the (positive) bending energy (see Lasic, 1988). Assumptions: (i) Fixed number of lipids; (ii) lipids from the inner layer go to the outer layer as R decreases to minimize the energy of the structure at any value of R . (b) Cryo-TEM image of engulfing vesicle. [Courtesy of Bob Reeder and Janet Burns, Procter & Gamble Co.]

remains open. The line tension of the rim of the hole is $\lambda = 10^{-11}$ N. The bilayers repel each other with a short-range repulsion that can be modeled as a hard wall at a bilayer-bilayer separation of D ($D \ll R_0$) such that the radius of the engulfing bilayer is $R = (R_0 + D)$. Derive an approximate expression for the pressure P pressing the bilayer onto the (rigid spherical) vesicle, and calculate P for

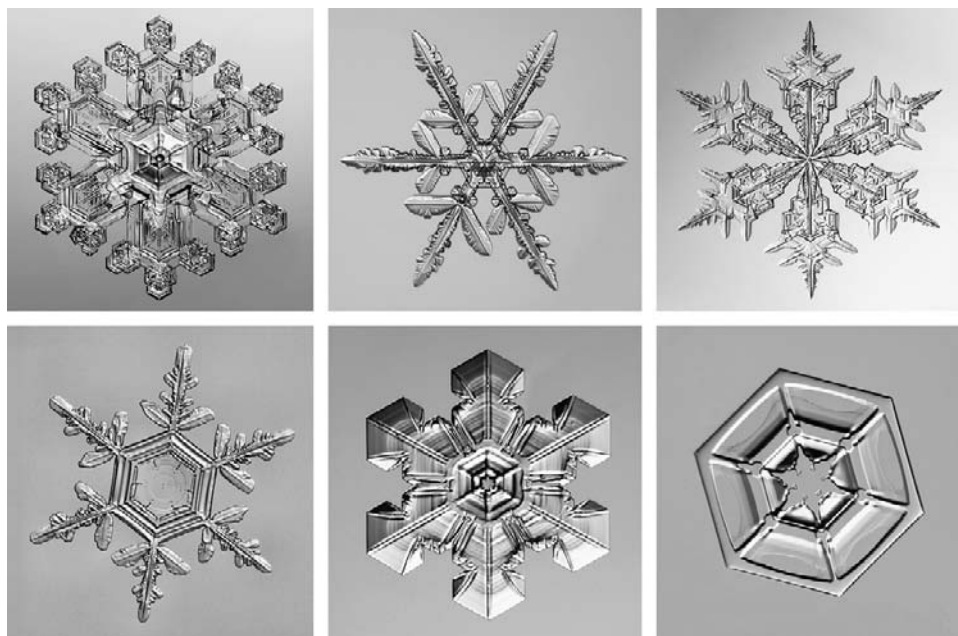


FIGURE 20.20 Snowflakes. [Reproduced from Kenneth Libbrecht www.snowcrystals.com, with permission.]

$R_0 = 45 \text{ nm}$, $D = 5 \text{ nm}$, $A = 0.9 \times 4\pi R_0^2$, and $\lambda = 10^{-11} \text{ N}$. Assume no stretching of the bilayer (infinite stretch modulus) so that $A = \text{constant}$, and no bending energy (zero bending modulus). Ignore the finite thickness of the bilayers. Is the pressure uniform all round?

- 20.17** Discuss the conditions that determine whether circular monolayer domains in a single mixed lipid bilayer as in Figure 20.11 attract or repel each other when present in the *same* monolayer (leading to coalescence in the case of attraction).
- 20.18** (a) Describe and contrast the different mechanisms of the adsorption from solution of surfactants and polymers. (b) Why do you think that nature has evolved proteins to be linear polymers rather than branched which could offer a greater variety of interactions and structures?
- 20.19** Equation 20.17 was derived by considering the lateral stress on a stretched bilayer—that is, when the area is expanded. Derive Eq. 20.17 from a consideration of the normal stress on a compressed bilayer—that is, when the thickness is increased.
- 20.20** Ice crystals are very beautiful, highly elaborate structures that usually exhibit almost perfect six-fold symmetry (Figure 20.20). No two ice crystals are exactly the same in shape or size. As an ice crystal grows, how do the water molecules correlate their growth (self-assembly) on the six arms when these can be very far apart from each other? Could similar arguments apply to some symmetrical biological structures?

Interactions of Biological Membranes and Structures

The interactions of biomolecular assemblies are generally far more complex than can be described by just one or two of the potentials or force functions shown in Figure 21.1. In this chapter we shall first review some of the forces already considered in Part II, but now focusing on how they arise in complex fluid and biological systems. We shall also see how these nonspecific interactions combine to give rise to highly specific ones, and how they act together in regulating the organization and morphologies of biological structures. Given that biological systems are living systems, their interactions are never at equilibrium, even in the steady state where a constant supply of energy is required. Thus, we must also consider the nonequilibrium or dynamic aspects of these interactions, which are further explored in the last chapter.

21.1 Van der Waals Forces

Approximate expressions for the van der Waals interactions between bodies of various shapes are given in Table 13.1. Both experimental and theoretical values for the Hamaker constants of fluid lipid bilayers suggest values of $A = (7.5 \pm 1.5) \times 10^{-21}$ J in pure water and $A \approx 5 \times 10^{-21}$ J in salt solutions at distances beyond the Debye length. These values are higher than for pure hydrocarbon liquids (refractive index $n = 1.42$) due to their higher refractive index (of $n \approx 1.42\text{--}1.48$), which has a significant contribution from the polar headgroups. The Hamaker constants for proteins in aqueous solutions are more difficult to calculate and measure, but based on their refractive index of $n \approx 1.55$ we expect values in the range $A = (10\text{--}16) \times 10^{-21}$ J (Roth et al., 1996).

In the absence of any other forces, unstressed bilayers attract each other via the van der Waals force (see Chapter 13, and Parsegian (2006)). However, fluid bilayers have an additional short-range repulsion arising from their thermal undulation and protrusion forces (described in Section 16.9 and again in Section 21.3) which prevents their surfaces from coming together closer than 1–2 nm for free bilayers, about 1.0 nm for supported (surface-adsorbed or self-assembled) fluid-state bilayers where the undulation forces (but not the protrusion forces) are suppressed, and ~0.5 nm for frozen or gel-state bilayers with one to two layers of strongly bound water molecules on each surface.

Using the equations derived in Chapter 13, one can estimate the binding energy and adhesion or “detachment” force for a spherical particle such as a vesicle or AFM tip of

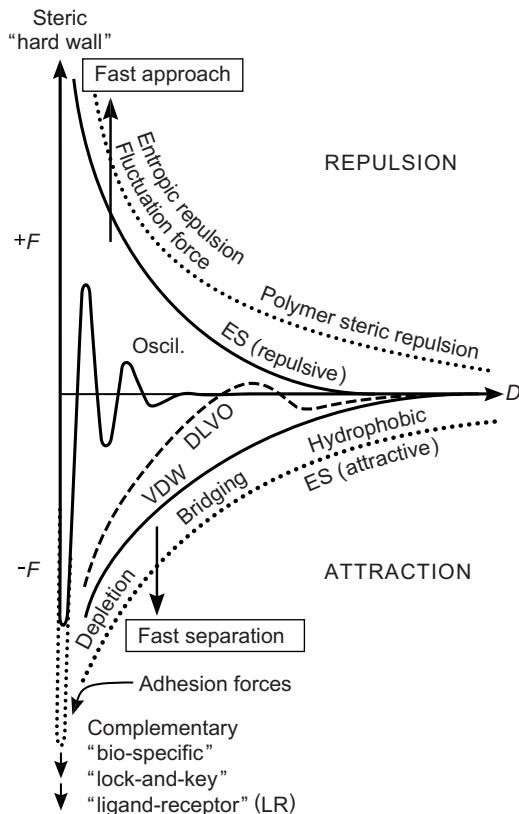


FIGURE 21.1 Generic interaction potentials between two complex macromolecules or biomembrane surfaces. Many colloidal systems display just one or two of these interactions at the same time. However, biological molecules and surfaces often interact via four or more of these forces either simultaneously or following on one another in some systematic order in space and/or time (Chapter 22), although oscillatory forces due to solvent structure that occur between hard, molecularly smooth crystalline surfaces (Ch. 15) are rarely encountered in biological systems. In addition, unlike colloidal interactions which occur mainly between similar or “symmetric” particles, biological interactions often occur between dissimilar molecules or “asymmetric” particles, which add new levels of complexity to the simpler interactions considered in Part II.

radius $R = 10$ nm (diameter = 20 nm) and a flat surface in water. This knowledge may be required to establish whether a measured adhesion force is due only to van der Waals forces. Thus, using the appropriate equations from Table 13.1 for the sphere-on-flat geometry, with a Hamaker constant of $A = 10 \times 10^{-21}$ J and a cut-off distance of $D_0 = 1.0$ nm (more appropriate for supported and/or free gel-state hydrated bilayers at $T < T_m$), we estimate for the vesicle-substrate binding energy:

$$E_{\text{ad}} = -AR/6D_0 \approx -1.7 \times 10^{-20} \text{ J} \approx 4kT, \quad (21.1)$$

and for the adhesion (detachment) force:

$$F_{\text{ad}} = -AR/6D_0^2 \approx -1.7 \times 10^{-11} \text{ N} \approx 20 \text{ pN}. \quad (21.2)$$

whereas for two planar membranes in adhesive contact, we estimate for the thermodynamic adhesion energy per unit area:

$$W_0 = A/12\pi D_0^2 = -F_{ad}/2\pi R \approx 0.3 \text{ mJ/m}^2, \quad (21.3)$$

and for the adhesive pressure:

$$P_{ad} = -A/6\pi D_0^3 \approx -5 \times 10^5 \text{ N/m}^2 \approx 5 \text{ atm}. \quad (21.4)$$

Table 21.1 shows various values measured for the detachment forces F_{ad} and adhesion energies W_0 of various lipid bilayers, both free and supported. We see that for the uncharged bilayers (PCs, PEs) agreement with the above theoretical predictions are reasonable, although accurate comparisons are not possible due to the uncertainties in how to define or measure distances such as D_0 for dynamically rough surfaces.¹ Most values for W_0 are obtained from measurements of pull-off or detachment forces F_{ad} of curved surfaces, Eq. (21.3), and it is important to appreciate that the above equations apply only to rigid, undeformable particles or surfaces. In Section 21.9 we shall see that for soft, deformable particles, such as giant vesicles, cells and soft supporting substrates, while the detachment force F_{ad} is little affected, the adhesion energy of the vesicle-substrate or vesicle-vesicle “bond” is very much larger than given by Eq. 21.1 and depends on the elastic properties of the deformable particle(s). In Chapter 22 we shall further consider how this energy determines the lifetime of the “bond” or associated state.

The van der Waals force between bilayers and membranes—especially in physiological solutions where the zero-frequency contribution is *screened*, or at separations $D > 10 \text{ nm}$ where the dispersion contribution is *retarded*—is fairly weak and has an effective range of at most 15 nm, beyond which it is too weak to be of any major significance.

21.2 Electrostatic (Double-Layer) and DLVO Forces

The double-layer repulsion, unlike the van der Waals attraction, is much more sensitive to the type and concentration of electrolyte present, the pH, and the surface charge density or potential. Approximate expressions for the double-layer interactions between bodies of various shapes are given in Figure 14.10; exact solutions for similar surfaces are plotted in Figures 14.11 and 14.12, and approximate equations for dissimilar surfaces are given in Section 14.18.

As described in Chapter 14, the interplay between attractive van der Waals forces and repulsive double-layer forces forms the basis of the so-called DLVO theory of colloid science. Both of these forces have been directly measured between various

¹If $D = 0$ is defined as the location of the plane that divides equal volumes of the two media on either side of it, it is a simple matter to show that the van der Waals interaction will be stronger than for two flat surfaces at the same separation—that is, it will be underestimated.

Table 21.1 Adhesion Energies per Unit Area W_0 Measured between Various Uncharged (Zwitterionic or Non-ionic) and Anionic Lipid Bilayer Surfaces, Divided into Van der Waals-Dominated and Other, Stronger, Adhesion Forces^a

System and Solution Conditions		Adhesion (in the primary or innermost energy minimum at D_0)		
Monovalent (e.g., NaCl): 1–150 mM	Method of Measurement ^b	Distance of energy minimum D_0 (nm) relative to 'dehydrated' contact at $D = 0$.	Measured adhesion energy W_0 (mJ/m ²) ^c or, when stated, adhesion force F_{ad} (pN), at D_0 .	Is the measured adhesion energy accountable by the VDW force at D_0 ?
Adhesion Determined by Balance of Attractive VDW Force and Repulsive Steric-Hydration Force				
Uncharged (zwitterionic) solid-supported bilayers in monovalent solutions above or below the chain melting temperature, T_c .	SFA DMPC, DLPC ($T > T_c$) DMPC, DPPC ($T < T_c$) DPPE ($T < T_c$)	2.4 2.1 1.2	0.10 0.15 0.80	Yes, after allowing for the repulsive short-range stabilizing steric-hydration force.
Free bilayers or vesicles in solution. ^d	Vesicle adhesion MPA, BFP Bilayer adhesion	Not measured Not measured Not measured	0.002–0.3 0.015 <0.001	Probably yes, after allowing for the undulation repulsion. ^d
MGDG and DGDG bilayers	SFA	0.6–1.2 nm	0.03–0.05	Somewhat weaker
Glycine bilayers, first contact	JKR Apparatus	Not measured	0.14	Yes
DGDG bilayers	MPA	Not measured	0.4	Yes
$C_{12}E_5$ monolayers in water at different temperatures	SFA SFA	~3 nm ~1 nm	0.03 at 20°C 0.13 at 37°C	Yes Yes
Frozen DSPG [−] and fluid DMPG [−] bilayers in NaCl solutions	SFA	No adhesion measured, and none expected: the double-layer repulsion between these charged bilayers dominates at small separations. ^e		

Adhesion in Water or Salt Solutions Determined by Stronger, Non-Van der Waals Forces

DSPG ⁻ and DMPG ⁻ bilayers in CaCl ₂ above and below T_c .	SFA	0.2 ± 0.2 nm (0–2 water layers)	0.5–1.0	Stronger due to ion-correlation forces
Glycine headgroup bilayers	JKR Apparatus	Not measured	16	Stronger due to H-bonds
Increasingly stressed bilayers, partially to fully hydrophobic	SFA	2 nm → 0 nm	0.1 → 100	Stronger due to hydrophobic interaction ^d
Complementary (biospecific) ligand-receptor bonds	SFA/JKR apparatus AFM OT SFD MPA	<1 nm Not measured Not measured Not measured Not measured	>6–16 mJ/m ² 90–400 pN 0.7–55 pN 0.1–120 pN 0.01–1,000 pN	Generally much stronger than ~40 pN (typical van der Waals bonding energy), due to complementary interaction. ^f

^a Adapted from Table 6 in Leckband and Israelachvili (2001).

^b The various techniques used as described in Chapter 12. AFM & MC (Atomic Force Microscopy and Micro Cantilever); SFA (Surface Forces Apparatus, including JKR adhesion apparatus); OT (Optical Tweezers or Optical Trapping); MPA and BFP (Micro Pipette Aspiration and Bio Force Probe), SFD (Shear Flow Detachment); TIRM and RICM (Total Internal Reflection Microscopy and Reflectance Interference Contrast Microscopy); Vesicle adhesion (imaging of adhering structures in solution using freeze-fracture or cryo-electron microscopy).

^c Adhesion energies in a secondary minimum can be very weak, well below 10^{-3} mJ m⁻² corresponding to only 10^{-3} kT per molecule ($<10^{-3}$ kJ mol⁻¹) as illustrated in Fig. 21.3; but between large vesicles or extended surfaces of contact area exceeding $0.1 \mu\text{m} \times 0.1 \mu\text{m} = 0.01 \mu\text{m}^2$, the total adhesion energy can exceed many kT (Section 21.9).

^d Increasing the tensile stress decreases the undulation repulsion and increases the hydrophobic attraction.

^e Note that the plane of origin of the electrostatic interaction, also known as the Outer Helmholtz Plane (OHP), is not generally located at the same place as the van der Waals plane both for lipid bilayers (Marra and Israelachvili, 1985; Marra 1986b) and colloidal surfaces (Frens and Overbeek, 1972; Shubin and Kekicheff, 1993; Vigil et al., 1994).

^f Pull-off forces depend on the pulling rate or waiting time (Chapter 22).

inorganic, organic and, more recently, biological surfaces in aqueous solutions of both monovalent 1:1 and divalent 2:1 electrolytes, although biological surfaces and macromolecules usually interact through various other forces as well (Leckband and Israelachvili, 2001).

Figure 21.2 shows the measured forces between negatively charged bilayers of DPPG⁻ in dilute electrolyte solutions of NaCl and CaCl₂. The effectiveness of divalent cations in reducing the double-layer repulsion and increasing the adhesion force, even at sub-mM concentrations, is quite remarkable, and appears to parallel their effectiveness as adhesogens and fusogens of biological membranes. Indeed, in the presence of divalent counterions, measured short-range forces are often significantly more attractive than can be accounted for by van der Waals forces (see jumps J in Figure 21.2), an effect that has been attributed to the *ion-correlation* force between the divalent ions in the diffuse double-layers (see Section 14.19).

The charged groups at the interfaces of lipid bilayers and proteins are often far from being fully dissociated even though the isolated (acidic or basic) groups in solution are. This phenomenon is partially due to the low dielectric constant environment of the

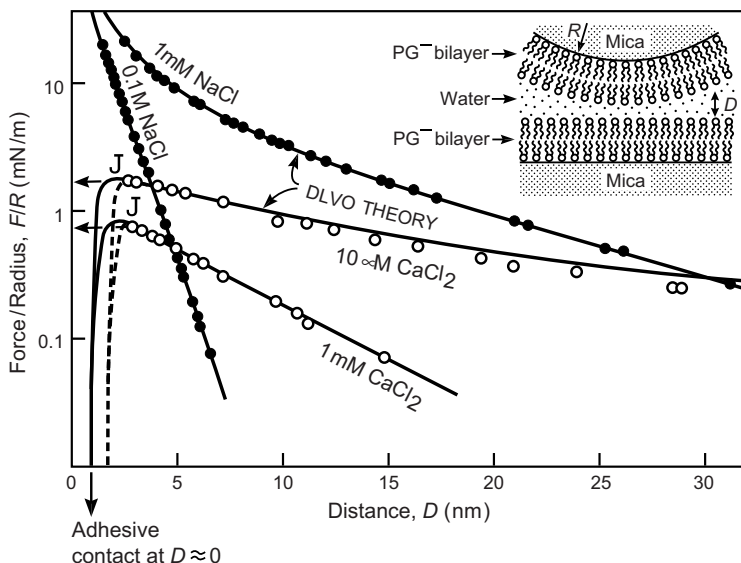


FIGURE 21.2 Measured DLVO forces between solid-supported bilayers of the negatively charged lipid dipalmitoyl-phosphatidyl glycerol (DPPG⁻) supported on crossed cylindrical mica surfaces of radius R in different electrolyte solutions at 22°C. The solid lines are the theoretically predicted DLVO force profiles assuming a Hamaker constant of $A = 6 \times 10^{-21}$ J. In NaCl solutions the double-layer repulsion corresponds to two fully charged surfaces. In CaCl₂ solutions the surface charge has been reduced due to ion binding. From the force maxima at J the two surfaces jump into strong adhesive bilayer-bilayer contact at $D \approx 0.4$ nm. Note that in CaCl₂ solutions at small separations the measured forces (dashed lines) are more attractive than expected from the DLVO theory (solid lines), an effect that is believed to be due to attractive ion correlation forces. [Data from SFA experiments with surfaces in the crossed-cylinder geometry, equivalent to a sphere of radius R near a flat surface or two spheres of radius $2R$, adapted from Marra, 1986b.]

bilayer and protein interiors just below the dissociable groups, composed mainly of hydrophobic groups with a dielectric constant of $\epsilon \approx 2-3$, which makes it energetically very unfavorable for the headgroups to dissociate. In contrast, surfactant and lipid headgroups in small micelles and isolated molecules are much more exposed to the aqueous solution ($\epsilon \approx 80$), and are much more dissociated, typically 25% in small micelles, and close to 100% for isolated molecules in solution. Geometric factors also play a role. The electric field outside a curved charged surface decays faster than from a planar charged surface, so that the counterions around a cylinder (e.g., DNA) or a small sphere (e.g., a micelle or small hydrophilic protein) have a weaker electrostatic force pulling the counterions back onto the surfaces. This effect is known as the *Manning condensation* of ions (see Section 14.19). All things being equal, the surface charge density or degree of ionization usually follows the following order: spheres > cylinders > planar surfaces (Manning, 1969; Shklovskii, 1999).

At higher ionic strength in monovalent electrolytes such as NaCl, the double-layer repulsion usually remains strong enough to keep biological surfaces apart; this is because the van der Waals attraction is weak. Figure 21.3 illustrates this effect for two bilayers in physiological saline solution (~0.15 M NaCl), where the secondary minima occur at 4–7 nm for typical values of the Hamaker constant A and surface potentials ψ_0 . The energy maximum occurs at very small separations, $D < 2$ nm, where the continuum mean-field equations and other approximations inherent in the DLVO theory break down and where other forces (discussed below) now usually dominate the interaction.

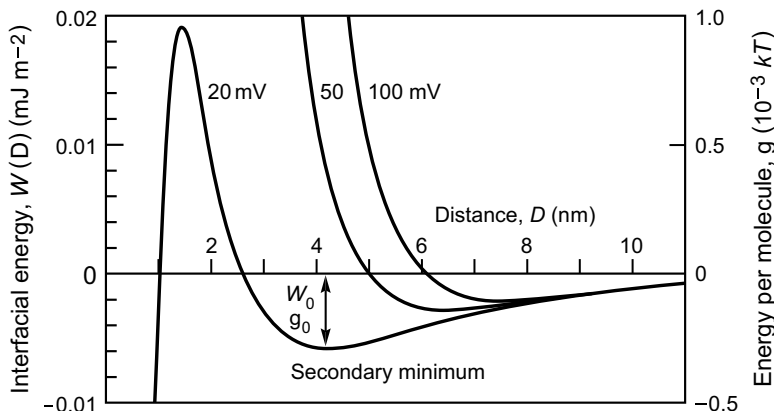


FIGURE 21.3 Theoretical DLVO interaction energy per unit area $W(D)$ between two bilayers in 0.15 M NaCl. The nonretarded Hamaker constant is assumed to be $A = 6 \times 10^{-21}$ J and the surfaces are assumed to interact at constant surface potential ψ_0 (at constant charge density σ the short-range repulsion would be greater). The three curves at $\psi_0 = 100, 50$, and 20 mV correspond to surface charge densities of $1e$ per $1, 3$, and 8.5 nm^2 , respectively. The adhesion energy per molecule (right axis) $g_0 = \frac{1}{2}W_0$ is calculated for a headgroup area of $a_0 = 0.4\text{ nm}^2$. Note that for the deepest and innermost secondary minimum the adhesion energy of $W(D_0) = W_0 \approx 0.006 \times 10^{-3}\text{ mJ m}^{-2}$ corresponds to an energy of about $g_0 = 3 \times 10^{-4}\text{ kT}$ per molecule. At separations below 2 nm other, non-DLVO, forces usually dominate the interactions between biological surfaces or macromolecules.

Worked Example 21.1

Question: Two similar membranes cannot approach closer than 0.4 nm due to a layer of strongly bound water molecules on each surface, but beyond this “hard-wall” barrier the interaction is pure DLVO. The membranes have a surface potential of $\psi_0 = -75$ mV, a Hamaker Constant of $A = 1 \times 10^{-20}$ J, and they exist as rigid vesicles of radius $R = 20$ nm in 0.15 M NaCl solution at $T = 37^\circ\text{C}$. Is the net interaction of any two vesicles at their contact separation of $D = 0.4$ nm attractive or repulsive?

Answer: Equation (14.54) gives $Z = 3.44 \times 10^{-11} \text{ J m}^{-1}$, and Figure 14.10 gives for the electric double-layer interaction between two vesicles of radius $R = 20$ nm at $D = 0.4$ nm:

$$E_{\text{DL}} = +2.1 \times 10^{-19} \text{ J} \approx +50 kT \quad \text{for the energy,}$$

and

$$F_{\text{DL}} = +2.6 \times 10^{-10} \text{ N} \approx 260 \text{ pN} \quad \text{for the (repulsive) force.}$$

These values may be compared with the values for the attractive van der Waals interaction (using Figure 13.1) at the same separation:

$$E_{\text{VDW}} = -4 \times 10^{-20} \text{ J} \approx 10 kT \quad \text{for the binding energy,}$$

and

$$F_{\text{VDW}} = -1 \times 10^{-10} \text{ N} \approx -100 \text{ pN} \quad \text{for the adhesion (detachment) force.}$$

Thus, at a separation of 0.4 nm the double-layer repulsion still wins out over the van der Waals attraction, which, theoretically, eventually wins out only below 0.2 nm.

In Worked Example 21.1, one may readily verify that the force becomes again attractive at $D = 5.1$ nm, where the energy is a minimum, the “secondary minimum,” at $E_{\text{min}} = -2.8 \times 10^{-21} \text{ J} \approx 0.7 kT$. The maximum (adhesion) force occurs at $D = 6.6$ nm where $F_{\text{ad}} = -3 \times 10^{-13} \text{ N}$ (~ 0.3 pN). This energy is not large enough to bind two 20 nm radius vesicles for any appreciable time before the thermal energy drives them apart. Since the interaction energy and force scale in direct proportion to the radius R , the binding energy for vesicles 10 times larger ($R = 200$ nm) will be $7 kT$, which will significantly increase the lifetime of adhering vesicles and, most probably, lead to fusion and coalescence, resulting in phase separation into a dilute vesicle phase in equilibrium with a lamellar or liposome phase, as discussed in Chapters 19 and 20.

But even more important than the effect of size is the effect of finite bilayer elasticity—that is, the fact that vesicles and cells are not rigid but deformable. In Section 21.9 we shall see that membranes with finite stretch and/or bending moduli flatten when they come into adhesion contact in a similar way to the adhesive flattening of elastic spheres considered in Section 17.7. And just as in the case of elastic spheres, their adhesion energy (but not the detachment force) increases well above the value for rigid spheres.

In the limit of small D (typically D below 1.5 nm in physiological saline solutions), the double-layer interaction energy depends on whether the surfaces remain at constant potential ψ_0 , as assumed in the above equations, or at constant charge σ . In most cases, the interaction lies somewhere in between these two limits. In the constant charge case,

as D falls below 1.5 nm (or below the Debye length), the double-layer force per unit area between two surfaces approaches the osmotic limit of the trapped counterions; that is, the limiting double-layer pressure between two approaching surfaces is simply the osmotic pressure P of the excess ions (counterions) that are electrostatically trapped in the aqueous gap between them, which asymptotes to infinity as $D \rightarrow 0$ according to Eq. (14.59): $P(D \rightarrow 0) = +\rho kT = +2\sigma kT/zeD$ for $D < \kappa^{-1}$, where z is the valency of the counterions.

Worked Example 21.2

Question: Referring to the membranes of Worked example 21.1, what is the double-layer pressure between two such planar membranes at $D = 0.4$ nm when the interaction is (1) at constant potential, and (2) at constant charge?

Answer: The potential of the isolated membranes is -75 mV which, according to the Grahame equation, Eq. (14.30), implies a surface charge density of $\sigma = 0.086 \text{ C/m}^2$ in 0.15 M NaCl solution at 37°C. For interactions at constant potential the parameter Z was previously calculated to be $Z = 3.44 \times 10^{-11} \text{ J m}^{-1}$, and the Debye length is $\kappa^{-1} = 0.78 \text{ nm}$. The repulsive double-layer pressure P at $D = 0.4$ nm is therefore $P = (\kappa^2/2\pi)Ze^{-\kappa D} = 5.4 \text{ MPa}$ (~54 atm). The pressure at constant charge is determined by the osmotic limit at small D , Eq. (14.59), giving $P = 46.0 \text{ MPa}$ (~460 atm)—almost an order of magnitude higher.

As already mentioned, the DLVO theory is a simple continuum and mean-field theory: it assumes that the surface charges are smeared out uniformly over the surfaces rather than existing at discrete sites, and that the solvent has no structure. Both assumptions break down at separations below 1–2 nm. The interactions at separations below 3 nm are further complicated by the appearance of other forces, including repulsive thermal fluctuation and steric-hydration forces, and attractive ion-correlation and hydrophobic forces, not to mention specialized biological interactions such as ligand-receptor and polymer bridging forces. Figure 21.4 shows an example of how additional ion-specific repulsive steric-hydration forces affect the short-range forces between supported surfactant bilayers of di-hexadecyl phosphate (see Problem 21.3 for a detailed analysis of the data shown in the figure). These and other non-DLVO forces are discussed further in the following sections.

21.3 Repulsive Entropic (Thermal Fluctuation, Steric-Hydration) Forces: Protrusion, Headgroup Overlap, and Undulation Forces

As we saw in Chapter 15, hydrophilic groups or surfaces that strongly bind water molecules to them experience a short-range repulsive steric-hydration force because of the energy needed to dehydrate these groups as the surfaces approach each other. Between

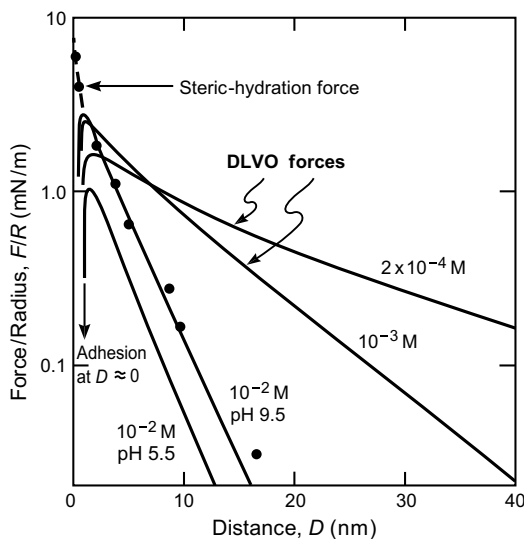


FIGURE 21.4 Forces between layers of di-hexadecyl phosphate (DHP) supported on crossed cylindrical surfaces of radius R , in aqueous NaCl solutions. The solid lines are the theoretical DLVO forces which agree with the measured forces except in 10^{-2} M NaCl at pH 9.5, where the extra repulsion at $D < 2$ nm (black data points and dashed line) cannot be explained by the DLVO theory. This figure also shows that at separations above about 1.5 nm, or 6 molecular diameters of water, the continuum Lifshitz theory of van der Waals forces and the continuum (Poisson-Boltzmann) equations of double-layer forces are valid, at least for monovalent ions such as NaCl. This also suggests that water films as thin as 1.5 nm may be expected to exhibit their bulk continuum properties, at least as far as their interaction forces are concerned. Whenever deviations do occur at small, or even large, separations it is more likely that some other force is also operating than that the DLVO theory has broken down. [Data from SFA experiments with surfaces in the crossed-cylinder geometry, equivalent to a sphere of radius R near a flat surface or two spheres of radius $2R$, adapted Claesson et al., 1989.]

solid crystalline surfaces the hydration force is usually oscillatory. The oscillations have a periodicity of the diameter of the water molecule, about 0.25 nm, and reflect the ordering of water molecules into semi-discrete layers between the smooth, rigid surfaces. Between bilayer and other biological surfaces no such ordering into well-defined layers is possible (or has so far been reported) because (1) the headgroups are rough on the scale of a water molecule, and (2) the surfaces are usually thermally mobile giving rise to a repulsive thermal fluctuation force (Chapter 16). Consequently, any oscillatory force becomes smeared out and one is left with only a monotonic force.

Monotonically repulsive hydration forces were first proposed to arise between amphiphilic surfaces by Langmuir (1937). They were first measured between surfactant monolayers across soap films by Clunie et al., (1967), and later across surfactant and lipid bilayers using a variety of techniques, including the Osmotic Stress and SFA techniques (LeNeveu et al., 1976; Homola and Robertson, 1976; Parsegian et al., 1979; McIntosh and Simon, 1986; Marra and Israelachvili, 1985; Marra, 1985, 1986a; Claesson et al., 1989). Because of their short-range repulsion and exponential decay with a decay length close to the size of a water molecule, these forces were originally believed to arise from water

ordering or structuring effects, and that they reflected some unique or characteristic property of water. However, it is now known that these repulsive forces also exist in other liquids (Figure 21.5). Moreover, they appear to become stronger with *increasing* temperature, which is unlikely for a force that originates from solvent ordering effects. Computer simulations (Granfeldt, 1991) and further investigations into the origin of these forces (see Figure 21.5, and Israelachvili and Wennerström, 1992, 1996) showed them to have an entropic origin—arising from the osmotic repulsion between thermally mobile surface groups once these overlap in a liquid. These repulsive forces therefore have the same origin as the “steric” forces between polymer-coated surfaces in liquids, described in Chapter 16. When they arise in water, they will be referred to as “steric-hydration” forces.

There are three main types of monotonically repulsive thermal fluctuation forces that arise between fluid-like structures such as surfactant micelles, microemulsion droplets, lipid bilayers and membranes: the exponential protrusion and headgroup overlaps forces, and the power-law undulation force (see Figs 16.14 and 16.15). Steric-hydration forces can be considered as special cases of these forces when the solvent is water and when the headgroups are hydrated; this gives the headgroups a finite excluded volume which enhances the range of these repulsive forces (see Eq. 21.8 below).

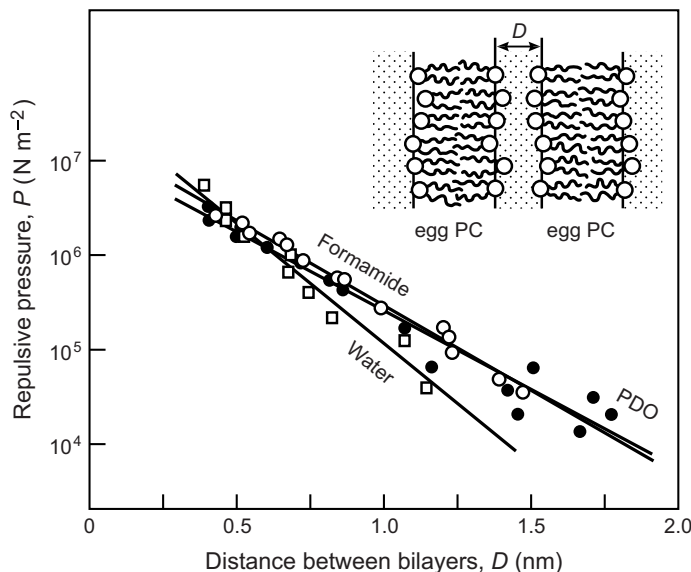


FIGURE 21.5 Pressure between egg lecithin (phosphatidylcholine) bilayers in water, formamide and the alcohol 1,3-propanediol (PDO: HO-CH₂-CH₂-CH₂-OH). The forces may be approximated by exponential functions such as $P = P_0 e^{-D/\lambda}$. The trends are for the decay length λ or range of the forces to increase with decreasing interfacial tension γ_i of the hydrocarbon-solvent interface: viz. $\gamma_i = 53 \text{ mJ m}^{-2}$ with water, $\gamma_i = 32 \text{ mJ m}^{-2}$ with formamide, and $\gamma_i = 21 \text{ mJ m}^{-2}$ with PDO. In addition, the preexponential factor P_0 decreases as λ increases. These trends are as expected if the forces are due to steric-protrusion effects, described by Eq. (21.5). For solvents having much lower interfacial tensions with hydrocarbons—for example, 1,2-propanediol, the aggregates become progressively more diffuse and the pressure approaches the (ideal) osmotic limit, Eq. (16.23). [Reproduced from McIntosh et al., 1989a, with permission.]

The protrusion pressure between two flat surfaces is given by the approximate equation, Eq. (16.22), for the protrusion force:

$$P(D) \approx +2.7\Gamma\alpha e^{-D/\lambda} = +2.7(\Gamma kT/\lambda)e^{-D/\lambda} \text{ N m}^{-2}, \quad (21.5)$$

where Γ is the surface density of protruding molecules in units of m^{-2} , where $\lambda = kT/\alpha$ is the decay length, and where α is the (hydrophobic or solvophobic) protrusion energy per unit length to pull the molecule out of the bilayer or membrane. Theoretical and experimental considerations (see Section 19.7 and Table 19.2) show that the protrusion energy is 1–4 kJ mol^{-1} or $(1.7\text{--}6.6) \times 10^{-21} \text{ J}$ per CH_2 group in water. Since the $\text{CH}_2\text{-CH}_2$ length is 0.126 nm, this energy corresponds to $\alpha = (1.3\text{--}5.3) \times 10^{-11} \text{ J/m}$, giving decay lengths between 0.08 and 3.2 nm at around 25°C, as typically observed (Marsh, 1989; Rand and Parsegian, 1989). Figure 21.6 shows examples of the short-range monotonically

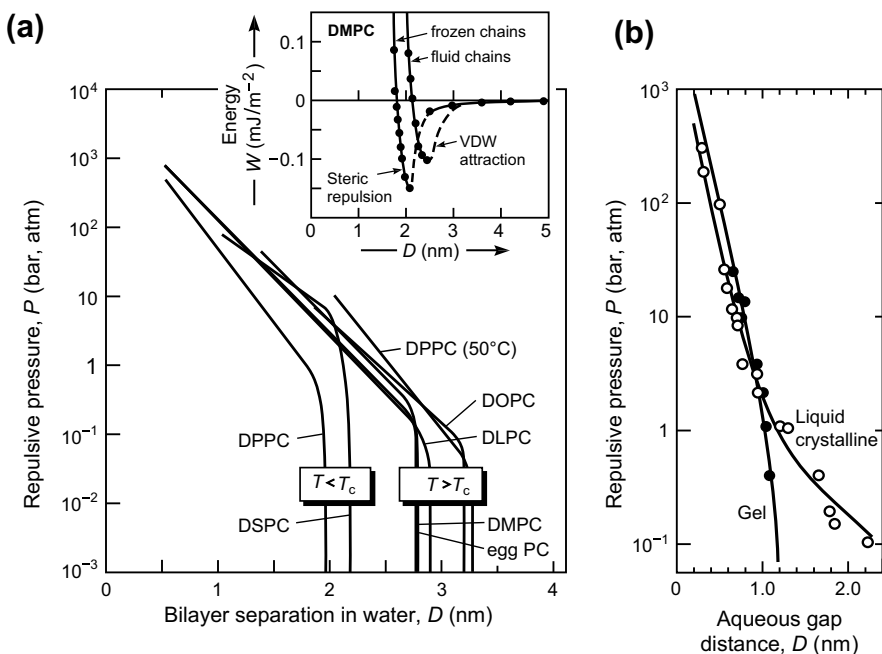


FIGURE 21.6 Repulsive forces between various lipid and surfactant interfaces in the frozen, gel, liquid crystalline and fully liquid-like (fluid) states in water (see also Figure 21.5). **(a)** Forces between various phosphatidylcholines in lamellae as measured by the Osmotic Pressure technique. Most of the exponential decay lengths λ fall between 0.2 and 0.3 nm. **Inset:** Forces between supported DMPC bilayers below and above the main (chain melting) transition temperature ($T_c \sim 24^\circ\text{C}$) as measured by the Surface Forces Apparatus technique. [Adapted from Israelachvili, 1985; Marra and Israelachvili, 1985.] **(b)** Repulsive forces in water between uncharged monoelaidin bilayers in the gel state and monocaprylin bilayers in the liquid-crystalline state (both bilayers have the same $\text{CH}_2\text{OH-CHOH-CH}_2\text{-O-CO-}$ headgroup), as measured by the Osmotic Pressure technique (McIntosh et al., 1989b). At short distances, below about 1 nm, the forces between both bilayers are roughly exponential with a decay length of $\lambda \approx 0.13 \text{ nm}$. However, between the liquid-crystalline bilayers the tail end of the interaction decays as $1/D^3$, and appears to be well described by Eq. (21.7) for the undulation force between bilayers having a bending modulus of $k_b = 3.2 \times 10^{-20} \text{ J}$. [Reproduced from McIntosh et al., 1989b, with permission.]

repulsive forces measured between various bilayers in aqueous solutions, most showing steric-hydration forces.

Another, even shorter-range repulsion is the steric-headgroup overlap force that arises when the hydrated flexible headgroups overlap (even in the absence of molecular, i.e., chain, protrusions). Some lipids have fairly long, and flexible, headgroups. For example, the headgroup of PC of chemical formula, $-\text{PO}_4^- - \text{CH}_2 - \text{CH}_2 - \text{N}^+(\text{CH}_3)_3$, is about 1 nm long when fully extended. If such headgroups are treated as brush layers of thickness L , then the pressure between two such layers has been found to be well-described by Eqs. (16.5)–(16.6) even for very short headgroups (Figure 16.4, see also Problem 16.6). We may therefore write for the Headgroup overlap force:

$$P(D) \approx 100\Gamma^{3/2}kTe^{-\pi D/L} = 100\Gamma^{3/2}kTe^{-D/\lambda} \text{ N m}^{-2}, \quad (21.6)$$

where the decay length is $\lambda \approx L/\pi$. Equation (21.6) gives an interaction of range $2L$, as expected for a steric force.

The third major thermal fluctuation force is the long-range undulation force, arising from long wavelength thermal ripples of membranes that become confined as two membranes approach each other (Fig. 16.15). This confinement reduces the entropy of the system which results in a repulsive force that follows a power-law distance dependence given by Eq. (16.28) for the Undulation force:

$$P(D) \approx +\frac{(kT)^2}{2k_b D^3} \text{ N m}^{-2} \quad (21.7)$$

where k_b is the curvature or bending modulus of the membrane which, typically, lies in the range $k_b \approx 10^{-21} \text{ J} = 0.1\text{--}10 \text{ kT}$ (Section 20.8). Undulation forces have similar magnitudes and the same distance dependence as van der Waals forces but are of opposite sign.

Each of the above three equations assume point molecules or headgroups. The effect of finite headgroup size especially for highly hydrated headgroups acts to enhance entropic forces as previously discussed with regard to the van der Waals equation of state (see Section 2.5 and Worked Example 14.7). Thus, if v is the (hydrated) volume of the headgroups, the force curves of Eqs. (21.5)–(21.7) will be shifted out by the *hard wall thickness* (cf. Figures 15.14 and 15.15).²

$$\delta \approx 4v\Gamma \text{ per surface.} \quad (21.8)$$

For example, if $v = 0.12 \text{ nm}^3$ (4 water molecules) and $\Gamma = 2.0 \text{ nm}^{-2}$ (50 \AA^2 per molecule), $\delta \approx 1 \text{ nm}$, which gives the hard wall separation and defines the effective $D = 0$.

At smaller separations, below about 2 nm, the protrusion and headgroup overlap forces are expected to dominate the undulation repulsion. Figure 21.7 shows theoretical plots of the above four steric interactions, computed using values appropriate for double-chained lipid bilayers in the fluid state. The attractive van der Waals interaction

²A similar layer thickness or length occurs in fluid flow that defines the location of the nonslip shear plane relative to a solid surface, is known as the *hydrodynamic layer thickness* or *slip length*.

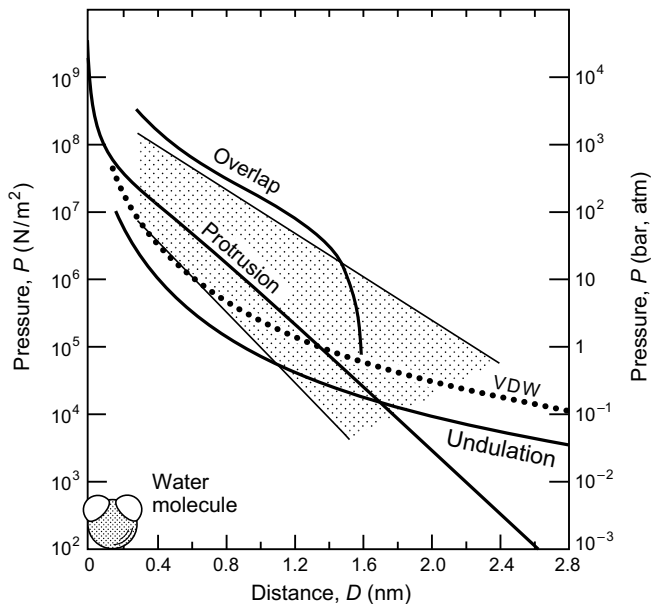


FIGURE 21.7 Theoretical undulation, protrusion (steric-hydration), headgroup overlap, and van der Waals forces between two bilayers in the fluid state in water at $T = 25^\circ\text{C}$. The following values were used in the computations, these being typical for phospholipid bilayers in the fluid state. For the van der Waals force or pressure, $F = -A/6\pi D^2$: Hamaker constant, $A = 5 \times 10^{-21} \text{ J}$. For the undulation force (Eq. (21.7)): bending modulus, $k_b = 10^{-19} \text{ J}$. For the protrusion force (Eq. 21.5): surface density of protruding groups or chains, $\Gamma = 2 \times 10^{18} \text{ m}^{-2}$ (50 \AA^2 per headgroup); protrusion energy, $\alpha = 2.5 \times 10^{-11} \text{ J m}^{-1}$ (corresponding to $\lambda = 0.17 \text{ nm}$). For the headgroup overlap force (Eq. (21.6)): mean separation between headgroups, $s = 0.8 \text{ nm}$; layer thickness of hydrated headgroup region, $L = 0.8 \text{ nm}$ (corresponding to $\lambda = 0.25 \text{ nm}$). Note that all the forces plotted are repulsive except for the van der Waals force, which is attractive, but which has been plotted together with the other forces for convenience of comparison. The shaded region gives the limits of the repulsive forces measured between egg lecithin bilayers whose lipids are mainly unsaturated (McIntosh and Simon, 1986; Rand and Parsegian, 1989; McIntosh et al., 1989a). Pure saturated-chain bilayers generally exhibit shorter-range repulsions.

force is also shown for comparison. The computed curves of Figure 21.7, taken together, appear to satisfactorily account for the magnitude and range of the force-profiles measured between the much studied egg lecithin bilayers (Israelachvili and Wennerström, 1992). However, given the many contributions to the total interaction and the experimental uncertainties of defining the zero of separation, a detailed comparison between theory and experiment is not possible.

The forces shown in Figure 21.7 may be significantly stronger or weaker, depending on the type of lipid and solution conditions—for example, the type and hydration of the headgroup, the electrolyte and its ionic strength, the pH, and the temperature. Some of these force-regulating mechanisms are explored below. Meanwhile, we may summarize two important conclusions for fluid bilayers:³ (1) Under natural conditions, fluid bilayers are unlikely to approach closer than 2 nm, and any adhesion between them is likely to be

³The biological membranes in healthy tissues of animals are mostly in the fluid state.

very weak even between uncharged bilayers (the situation is very different between rigid, globular proteins that have no repulsive entropic forces). (2) With the recent interpretation of the short-range repulsive forces in terms of thermal fluctuations rather than structured water layers, there is no longer any need to explain how membranes, proteins, ligands, receptors, and other hydrophilic surfaces or groups “overcome” the “hydration force barrier” to come into contact and interact (fuse or react chemically). Indeed, it is this very contact or molecular collisions that gives rise to the short-range repulsion. The only real force barrier, which may or may not be present, is the first layer of water molecules directly in contact with the surfaces—that is, the primary hydration shell of strongly bound water.

Given that there are at least four fairly different repulsive entropic forces between fluid interfaces in aqueous electrolyte solutions, it is worth considering how each of these is determined and how it can be controlled.

The **double-layer** interaction depends on the surface charge or potential and the Debye length (ionic strength) and has been discussed at length in Chapter 14 and Section 21.2. Further aspects of this interaction, especially situations where the force is attractive, are described later in this chapter.

The **steric-hydration** forces are determined by how easy it is for lipid molecules to protrude from bilayer surfaces (for the **protrusion** force) and the hydrated size of the headgroups (for the **headgroup overlap** force). These forces therefore depend on the hydrophilicity of the interface and on the hydration of the headgroup. Some lipid headgroups are intrinsically hydrophilic—for example, those with zwitterionic, ethylene oxide, or sugar groups—while others become hydrophilic on binding hydrated ions, especially Na^+ , Li^+ , or Mg^{2+} . The first class of lipids has *intrinsic* hydration forces, and the second has hydration forces that can be “charge regulated” by ion binding or “ion exchange” (Chapter 14). We now consider some examples and consequences of regulated hydration forces.

Figure 21.4 shows the measured forces between bilayers of a double-chained anionic surfactant as a function of salt concentration. For NaCl concentrations below 10^{-2} M, the forces are well described by the DLVO theory: the double-layer repulsion dominates at separations greater than 2 nm, and the van der Waals attraction dominates at smaller separations. But at concentrations above 10^{-2} M NaCl and high pH, a strongly repulsive hydration force comes in at separations below 2 nm that dominates over the van der Waals attraction and prevents the surfaces from coming into adhesive contact as before. This behavior is believed to arise from the binding of hydrated Na^+ ions to the surfaces under conditions of high salt and high pH, effectively increasing the hydrated volume v in Eq. (21.8), and is qualitatively very similar to that occurring between colloidal particle surfaces, described in Section 15.8.⁴

⁴As discussed in Chapter 14, with increasing electrolyte concentration (increasing κ) the double-layer interaction at constant surface potential can also lead to an enhanced repulsion at small separations (as $D \rightarrow 0$), and therefore to a reduced adhesion energy.

There are many other examples where repulsive hydration forces appear to be induced by the binding or exchange of hydrated ions, generally following one of the Hofmeister Lyotropic Series. Thus, negatively charged phospholipid vesicles aggregate or fuse in dilute CaCl_2 solutions, as expected from the DLVO theory, but not in concentrated NaCl solutions, where the DLVO theory predicts strong irreversible adhesion in molecular contact. This is an example of the commonly observed “antagonistic effect” of Na and Ca, where high concentrations of Na enhance stability, while Ca promotes instability. Also, phosphatidylserine vesicles fuse in dilute (approximately millimolar) CaCl_2 solutions but not in MgCl_2 solutions, most likely because the more hydrated Mg^{2+} ions prevent the surfaces from coming into sufficiently close contact to fuse.

As a further example of cation-regulated hydration forces, Princen and colleagues (1980) studied the interactions between oil-in-water emulsion droplets whose surfaces were covered by an alkyl sulfate monolayer. They found that the adhesion between the droplets in concentrated salt solutions decreases with the increasing hydration of the cation bound to the surfaces—namely, KCl (maximum adhesion) $>$ $\text{NaCl} >$ LiCl (almost no adhesion).

Finally, Petsev and Vekilov (2000) found that certain proteins in aqueous solution experiences an additional “hydration” repulsion in high salt, similar to that observed between charge-exchangeable bilayers, colloids and surfaces (in surface force experiments).

Of the four steric-fluctuation forces being discussed here, the **undulation force** has by far the longest range. The full force, described by Eq. (21.7), arises between free, unstressed bilayers in solution. Mechanically or osmotically stretched bilayers and those supported on rigid surfaces have their thermal undulations suppressed, which reduces the magnitude and range of their undulation repulsion and increases their adhesion, as previously discussed (see also Fig. 21.8).

The undulation force depends mainly on the bending modulus of a membrane that can vary over a very large range from $k_b < 10^{-21}$ to $> 10^{-19}$ J. Safinya and colleagues (1986) carried out an x-ray study of the repulsive forces between two oil-water interfaces each bounded by a sodium dodecyl sulfate (SDS) monolayer for which the bending modulus is small ($k_b = 5 \times 10^{-21}$ J). The undulation force was therefore large and accurately measurable, and the results confirmed the inverse third distance dependence of the Helfrich equation, Eq. (21.7). McIntosh et al., (1989b), and Abillon and Perez (1990), also measured a $1/D^3$ tail in the interaction between bilayers whose bending moduli were about ten times higher. The main determinant of the bending modulus of a bilayer is the phase state—whether liquid, gel, frozen amorphous, or frozen crystalline—which is in turn determined by the headgroup type, the number of length of hydrocarbon chains, the degree of unsaturation, and the temperature.

PEGolated lipids and polyelectrolyte amphiphiles are a class of lipids where the headgroups are longer than the hydrocarbon chains. The repulsive entropic forces between membranes containing these molecules were described and illustrated in Chapter 16. PEG or PEO are particularly useful as implant materials because they are biologically inert (biocompatible), and so do not trigger an immune response when, for

example, artificially produced particles or drug-delivery vesicles coated with PEG are administered into the body. The repulsive forces between certain classes of proteins that expose polyelectrolyte chains or domains, such as the polysaccharide domains of mucins and lubricins (Zappone et al., 2007) and the neuro-filaments of actin (Brown and Hoh, 1997), also appear to be well-described by current theories of the steric interactions between polyelectrolyte brushes (Section 16.7).



Worked Example 21.3

Question: In an SFA or AFM experiment (see Sections 12.7 and 12.8) two rigid substrate surfaces of finite area, each supporting a lipid bilayer membrane, are brought together in an “infinite” reservoir of water. There is a monotonically repulsive electrostatic and/or steric-hydration pressure between the charged membrane surfaces across the water film. In a separate experiment, stacks of the same bilayers are studied using the OP technique (Section 12.7), where the membranes are brought together by osmotically removing the water from the dialysis bag encapsulating the membrane stacks in a hypertonic solution. As the membrane surfaces come together in each type of experiment, will they become thinner or thicker? The membranes may be treated as elastic sheets of unstressed thickness D_b .

Answer: In the SFA experiment, as the water gap distance D_w falls, the bilayers are increasingly compressed due to the repulsive pressure between them. This causes them to become thinner—that is, D_b also falls, forcing the excess lipid out of the contact zone into the noninteracting bilayer region that acts as a “lipid reservoir.” In the OP experiment, the situation is different. The whole bilayer stack is confined within the dialysis bag and there is no separate noninteracting lipid reservoir. Imagine the situation after some water has been osmotically sucked out from the bag and the bilayers have come closer together—that is, where D_w has decreased but not D_b . Remove the system from the dialysis bag and observe it in a sealed chamber of fixed total volume. Can the unfavorable repulsive energy across the now thinner water gap be reduced by some rearrangement of the lipid and water molecules at constant lipid-water volume fraction? Yes, by an *increase* in the bilayer separation D_w . But at fixed lipid-water volume fraction this can only be achieved if the bilayers thicken in the same proportion. Thus, both D_w and D_b increase in the sealed chamber—that is, the bilayers become *thicker* until a new equilibrium is reached, where the unfavorable electrostatic and elastic energies are a minimum (see Problem 21.4 (iii)). If the total energy becomes too unfavorable, a phase transition to a different, nonlamellar structure may occur.



21.4 Attractive Depletion Forces

Here we will consider the very different *attractive* depletion force between biological surfaces mediated by *nonadsorbing* polymers or particles, which was previously introduced in Section 16.6. The depletion energy per unit area of two planar surfaces, Eq. (16.10), is given by

$$W(D) = -\rho R_g kT(1 - D/R_g) \quad (21.9)$$

where ρ is the polymer concentration (number density) or, more correctly, the *activity* ρ' . For dilute polymer solutions in a theta solvent R_g is the radius of gyration, while in a “good” solvent it becomes replaced by the larger Flory radius, R_F . In concentrated solutions, above the overlap concentration, the depletion interaction diminishes in magnitude and becomes shorter ranged.

Depletion forces between biological surfaces were first measured between giant vesicles using the Micropipette Aspiration Technique (Evans, 1988), where good agreement was obtained between theory and experiment. Figure 16.11 showed measured depletion forces between supported lecithin bilayers in 10k PEO, where again the agreement between experiment and theory was very good. Depletion forces have also been measured between surfaces in micellar solutions where the charged, repelling micelles replace the polymers as the noninteracting particles (Richetti and Kekicheff, 1992).

Worked Example 21.4

Question: Estimate the expected depletion force contribution to the adhesion force needed to detach a spherical particle of radius R from a flat surface in a 5% by weight 10k PEO solution. Compare your result with the measured adhesion force of $F_{\text{ad}}/R \approx -1.2 \text{ mN/m}$ in Figure 16.11, which translates to a surface energy of $W_0 = 2F_{\text{ad}}/3\pi R = -0.25 \text{ mJ m}^{-2}$. The effective radius of gyration of 10k PEO may be taken to be $R_g = 4.2 \text{ nm}$.

Answer: The concentration corresponds to a number density of $\rho = 0.05 \times 6.02 \times 10^{23}/10,000 = 3.0 \times 10^{24} \text{ m}^{-3}$, which according to Eq. (21.9) leads to an adhesion energy $W(D)$ at $D = 0$ of $W_0 = -\rho R_g kT = -(3.0 \times 10^{24}) \times (4.2 \times 10^{-9}) \times (4.2 \times 10^{-21}) = -0.053 \text{ mJ m}^{-2}$. This is about 20% of the measured value. However, as previously mentioned, it is strictly the *activity* ρ' that should be used for the concentration in Eq. (21.9), rather than the number density ρ . For PEO solutions at 5 wt%, $\rho' \approx 4\rho$, which increases the theoretical prediction to $W_0 \approx -0.21 \text{ mJ m}^{-2}$, or $F_{\text{ad}}/R = -1.0 \text{ mN/m}$, which is now much closer to the measured value. But this is still only part of the analysis. The experimental force curve of Figure 16.11 includes other forces as well, so that to obtain the depletion contribution we must subtract out the other, nondepletion, contributions to the net (measured) adhesion force. In this system, at the point of detachment the attractive van der Waals force contribution is -0.5 mN/m (dotted curve in Figure 16.11), and there is a *possible* additional double-layer force contribution of approximately $+0.5 \text{ mN/m}$. The estimated experimental value for the depletion force contribution to the net adhesion force is therefore $-(0.7-1.2) \text{ mN/m}$, which corresponds to a depletion energy of $W_0 = -(0.15-0.25) \text{ mJ m}^{-2}$, in good agreement with the theoretical estimate of -0.21 mJ m^{-2} .

Depletion forces mediated by PEO or PEG are often used in biomedical experiments to induce cells to adhere or fuse to form “hybrid” cells or “hybridomas,” and they are most effective at molecular weights in the region of 10 kDa and at concentrations above 5 wt % (see Problem 21.10 and Boni et al., 1984; Sowers, 1987; Hui et al., 1999; Safran et al., 2001). Just as in the case of calcium-induced fusion of mixed lipid bilayers (see Figure 21.9), PEO-induced fusion is probably associated with the opening of hydrophobic patches on opposing membranes that have been brought together by the attractive depletion force.

21.5 Attractive Hydrophobic Forces

Since the pioneering work of Kauzman (Kauzmann, 1959) the hydrophobic interaction and force⁵ have been known to be stronger than the van der Waals force and to be of entropic origin—that is, strongly temperature-dependent. It is only more recently that direct measurements of this force have shown it to be of long-range, at least between macroscopic surfaces (Christenson and Claesson, 2001; Meyer et al., 2006). The broader implications of these measurements for biomolecular interactions such as membrane fusion and protein folding are still largely unexplored. Indeed, the physical origin of this important interaction is still not understood, and there is still no agreed-upon potential function or force law for this interaction.

As we saw in Section 15.9, the attractive hydrophobic interaction between hydrocarbon surfaces is of surprisingly long range—much stronger than the van der Waals attraction. In the case of free (unstressed) bilayers, the hydrophilic headgroups “shield” the underlying hydrocarbon groups from the aqueous phase, which effectively masks the hydrophobic interaction between them. However, when bilayers are subjected to a stretching force or tensile stress, they expand laterally, and the increased hydrophobic area exposed to the aqueous phase now allows the hydrophobic interaction to emerge. Stresses can be induced globally (osmotically or mechanically)—that is, uniformly throughout a membrane, as in Figure 21.8, or locally, for example, via local packing mismatches (Figure 20.15) or changes in a protein’s conformation due to Ca^{2+} ion binding, or a combination of local and global stresses (Figure 21.9).

Figure 21.8 shows this effect on the measured forces between two globally stressed lecithin bilayers supported on mica surfaces. A long-range, strongly attractive hydrophobic force emerges as more hydrocarbon groups become exposed to the aqueous phase. It is remarkable that the attraction could be enhanced so significantly by simply increasing the mean headgroup area by a few percent above the optimal value.

A number of different experiments (see inset in Figure 21.8) have shown that to a good approximation, the hydrophobic adhesion energy contribution to a partially hydrophobic interface is simply proportional to the applied stress on the bilayer or membrane τ according to

$$W_0 \approx \tau \quad \text{N/m or J/m}^2. \quad (21.10)$$

In other words, an applied *lateral* stress or tension translates into an enhanced *normal* adhesion energy of about the same magnitude. Further, according to the Derjaguin approximation, this increase would be directly proportional to the increased adhesion force between two vesicles or a cell and a surface.

We may further note that from the definition of a membrane’s elastic stretch modulus (Eq. (20.16)): $k_a = \text{stress}/\text{strain} = \frac{\tau}{\Delta a/a}$, where $\Delta a = (a - a_0)$, the increased adhesion

⁵The term “interaction” is used to cover all aspects and manifestations of a force, including how it determines solute solubility, membrane shape changes, and so on, in contrast to the force-law, $F(D)$.

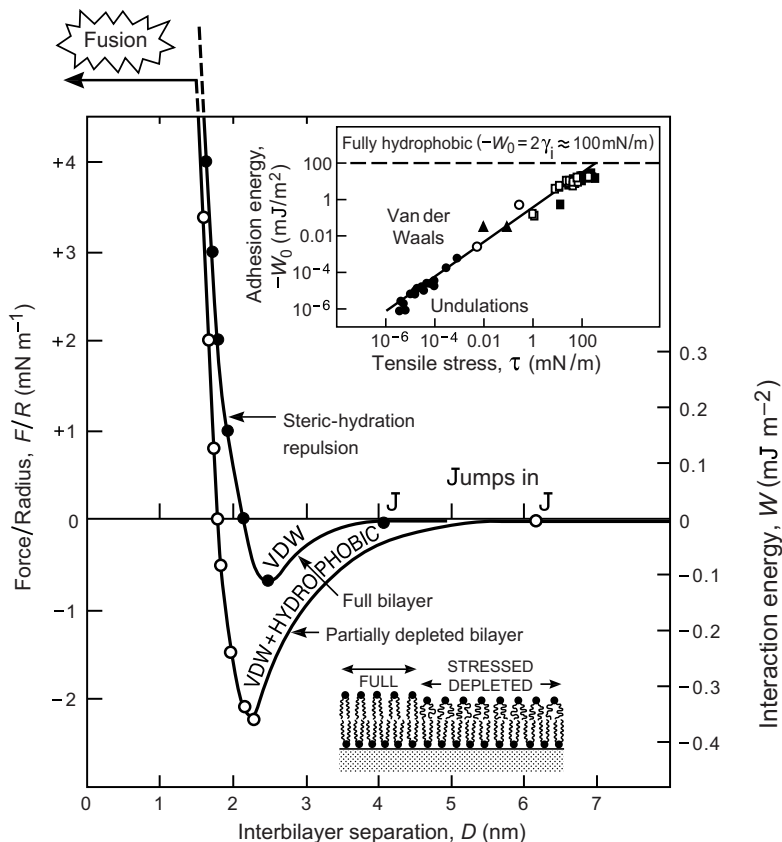


FIGURE 21.8 Van der Waals, steric-hydration and hydrophobic forces measured between (i) unstressed, fully hydrophilic, and (ii) stressed, partially hydrophobic bilayers using the SFA technique (with surfaces in the crossed-cylinder geometry, equivalent to a sphere of radius R near a flat surface or two spheres of radius $2R$). In the unstressed state the bilayers have their hydrocarbon chains effectively shielded from the aqueous phase by the hydrophilic headgroups. Partially hydrophobic bilayers are under a lateral tension or stress τ . Such stressed or "depleted" bilayers are thinner than full bilayers, and expose additional, unshielded hydrophobic groups to the aqueous phase that results in an additional hydrophobic contribution to the adhesion force and energy W_0 as determined from the pull-off force. The inset shows values obtained for W_0 by different authors using different experimental techniques for stressing the bilayers. [Figure and inset adapted from Evans and Metcalfe (1984), Servuss and Helfrich (1989), Bailey et al., (1990), Helm et al., (1992), and Leckband and Israelachvili (2001).]

energy is also proportional to the increased (hydrophobic) area per molecule exposed to the aqueous phase—that is,

$$W_0 \approx \tau \approx k_a \Delta a / a, \quad (21.11)$$

where a is the expanded or stressed area per molecule and a_0 is the equilibrium, unstressed area (the optimum area). Further, for a fluid monolayer, Eq. (20.15a) gives: $k_a \approx 2\gamma_i$. Thus, for an unstressed membrane the hydrophobic contribution is zero, while for a highly stressed membrane where $a \gg a_0$, we have $\Delta a/a \rightarrow 1$, and the adhesion energy

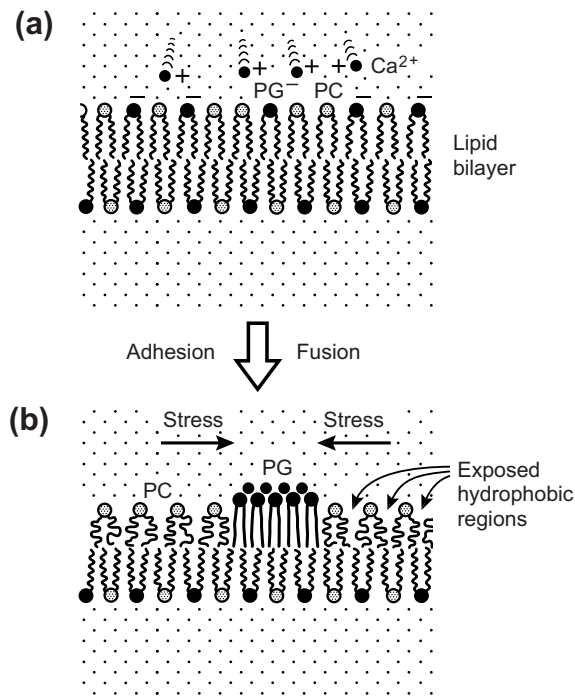


FIGURE 21.9 Example of synergistic rearrangements of lipids resulting from a combination of electrostatic and hydrophobic interactions acting on (and between) two mixed lipid bilayers composed of charged PG⁻ and uncharged PC lipids. Adsorbing calcium ions (a) cause condensation of the negatively charged PG⁻ into domains (b). These domains will preferentially adhere to similar domains on an apposing bilayer through calcium-mediated ionic bonds, or cross-bridges, as illustrated in the coupled interbilayer domains in Figure 20.11(c). Alternatively, or in addition, condensation of PG forces the surrounding sea of uncharged PC lipids to expand and become more hydrophobic, creating hydrophobic regions (or domains) that will adhere and fuse to similar (hydrophobic) regions on an opposing bilayer. Note that because the PC lipids in the top monolayer become uniformly stressed over the whole area (globally stressed), hydrophobic adhesion and fusion may occur anywhere, including far from the calcium binding sites. Note, too, that before Ca^{2+} ions were introduced to the solution, the charged and uncharged lipids form well-mixed bilayers (for example, DMPG and DMPC are completely miscible), with no domains and no attractive or fusion-inducing forces between them. [Adapted from Leckband et al., 1993. See also Eastman et al., 1992.]

(at $D = 0$) tends to $W_0 \rightarrow k_a \rightarrow 2\gamma_i$, which is the same as for two fully hydrophobic surfaces adhering in water. Most interesting, for an area expansion of only 1% above the unstressed area ($\Delta a/a = 0.01$), the hydrophobic contribution to the adhesion energy is $2\gamma_i/100 = 1 \text{ mJ/m}^2$. This is already significantly higher than the van der Waals contribution. Indeed, it is worth recalling that the hydrophobic force is probably the strongest of all the physical nonspecific interaction forces operating between biological surfaces and molecules (Table 21.1). Clearly, even small lateral stresses and local stress-gradients can produce large changes in the normal attractive force between surfaces composed of conformationally adaptable amphiphilic molecules such as fluid lipids or flexible proteins. Hydrophobic adhesion can also lead to fusion, which is discussed in Section 21.10.

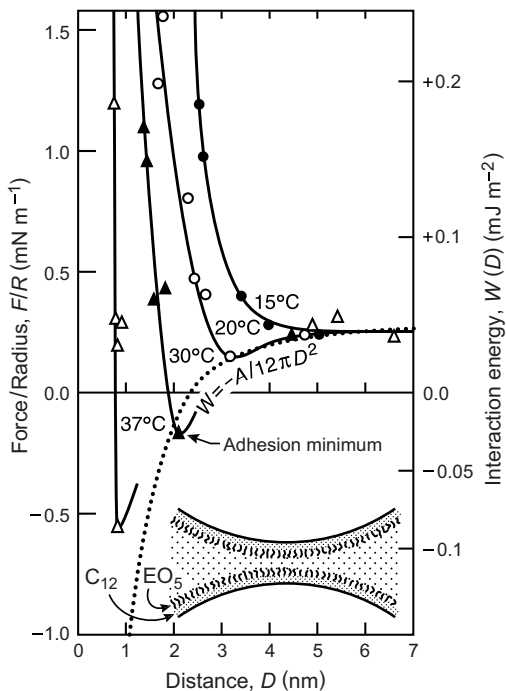


FIGURE 21.10 Measured forces between adsorbed monolayers of the nonionic ethylene-oxide headgroup surfactant $C_{12}EO_5$ (also $C_{12}E_5$) in water at different temperatures. The dotted line shows the expected van der Waals force contribution, $F/R = -A/6D^2$ or $W = F/2\pi R = -A/12\pi D^2$, based on a Hamaker Constant of $A = 10^{-20}$ J. The increased attraction and adhesion in this case may be due to a reduced repulsion, due to dehydration of the ethylene oxide segments, rather than to an enhanced temperature-dependent hydrophobic attraction. [Data from SFA experiments with surfaces in the crossed-cylinder geometry, equivalent to a sphere of radius R near a flat surface or two spheres of radius $2R$, adapted from Claesson et al., 1986.]

Since the hydrophobic interaction increases with temperature,⁶ it is tempting to attribute any observed attraction that increases with the temperature to the hydrophobic interaction. But the strength of an adhesive junction is often not due to the strength of the *attractive* force but to that of the *repulsive* force. Figure 21.10 illustrates a still controversial example of this effect. Here we see an increasing adhesion between two PEO surfactant monolayers with increasing temperature, which we may interpret as being due to an apparently increasing attraction. This effect is responsible for the Lower Consolute Temperature (LCT)⁷ of many surfactant and lipid micelles containing headgroups of PEO

⁶Not all hydrophobic interactions increase with T . The free energies of transferring hydrocarbon solutes into water do increase with T (Tanford, 1980), but the interfacial tensions of most hydrocarbon-water interfaces decrease with T . See also Temperature Effects on CMCs in Table 19.2.

⁷On increasing the temperature of a micellar solution, at the LCT the one-phase system becomes a two-phase system due to the onset of aggregation or a structural change, usually from small micelles to larger structures. This is in contrast to “normal” solutions that usually go from a two-phase to a one-phase system with increasing T at the “Upper Consolute Temperature.” (See Problem 8.5.)

or its analogs and has long been attributed to the entropic nature of the hydrophobic interaction. Figure 21.10, however, shows that the adhesion and attraction can be quantitatively accounted for by the *unchanging* van der Waals force (dotted line in Figure 21.10), where the main effect of increasing the temperature is the reduction in the range of the repulsive steric-hydration force. This could be due to the dehydration of the PEO groups at higher temperature, which is a well-known effect (Bekiranov, 1997; Kjellander and Florin, 1981) that would reduce the excluded volume of each PEO group and, thus, the steric-repulsion between them (see Problem 8.5).

21.6 Biospecificity: Complementary, Site-Specific and Ligand-Receptor (LR) Interactions

Many biological interactions such as those involved in immunological recognition and cell-cell contacts are totally specific for one, and only one, molecule. Early last century, biologists such as Paul Erlich proposed that certain biomolecules may have a perfect geometrical fit which allows them to bind together extremely strongly via a purely mechanical mechanism that is essentially a molecular lock-and-key. Specific interactions arise when a unique combination of physical (noncovalent) bonds between two macromolecules act together cooperatively to give rise to a strong bond. But a specific bond does not have to be strong; it only has to be selective. For example, an ionic bond is usually very strong, but not selective: any anion will bind strongly to any cation in any direction according to the isotropic Coulomb potential, Eq. (3.3). In contrast, some of the H-bonding pairs shown in Figure 8.2, in DNA, and in Figure 10.3 may bond only when mutually aligned in a specific way (see also Fig. 8.3), but not necessarily strongly. Indeed, one of the strongest specific bonds is between biotin and avidin, whose binding energy is “only” $35\text{ }kT$ —significantly stronger than an H-bond ($\sim 10\text{ }kT$) but falling well below the strength of covalent bonds (100–200 kT). Table 21.2

Table 21.2 Bond Energies and Lifetimes of LR Bonds¹

Binding Protein (Receptor, R)	Target (Ligand, L)	Affinity [K_D (M)]	Energy ² (kT)	Lifetimes of Bonds ³
Avidin	Biotin	10^{-15}	35	months
Antibody	Antigen	$10^{-7}\text{--}10^{-11}$	16–25	seconds–hours
Receptor	Hormone	10^{-9}	21	seconds
Enzyme	Substrate	$10^{-3}\text{--}10^{-9}$	7–21	μs –seconds
Transport protein	Hormone	$10^{-6}\text{--}10^{-8}$	14–18	<seconds
Lectins ⁴	Glycoconjugates	$10^{-3}\text{--}10^{-5}$	$7\text{--}12^5$	μs – ms^5

¹Ligand-receptor, but commonly also referred to as complementary, lock-and-key, specific, or biospecific.

²The bond energy is fixed, the pull-off or adhesion force depends on the temperature and pulling rate (see Sections 9.2 and 22.3).

³Calculated using Eq. (9.2) assuming a characteristic vibration time of 10^{-8} s .

⁴Lectins are specific to sugars: saccharides and glyco groups.

⁵Note that specific bonds do not have to be strong or long-lived.

[Courtesy of D. Leckband.]

shows the strengths of some specific bonding pairs, which are now commonly referred to as ligand-receptor or LR bonds, but also site-specific, complementary, lock-and-key, and recognition bonds or interactions.

Table 21.2 reveals the somewhat surprising feature of the *weakness* of LR bonds, rather than their strength, and their short natural lifetimes. Originally it was thought that all LR bonds are of the lock-and-key type, with a deep receptor pocket (the lock) and a precise and tight-fitting ligand (the key). But as illustrated in Figure 21.11, both shape and chemical complementarity can be achieved between two fully exposed regions of

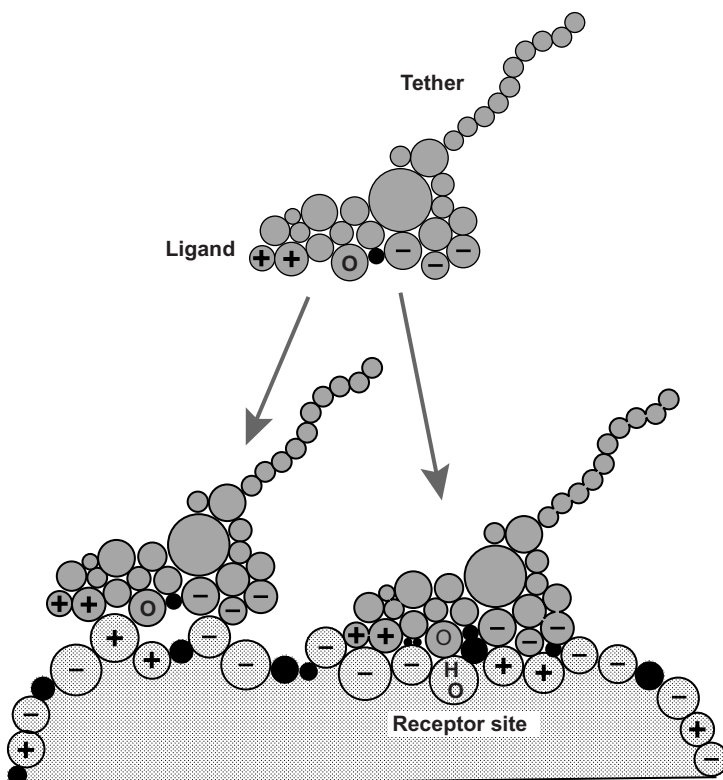


FIGURE 21.11 Example of a bio-specific or complementary interaction between two surfaces, a ligand (top) and a receptor (bottom), where the various ionic (\oplus , \ominus), H-bonding ($H \cdots OH$) and hydrophobic (●) groups shown represent amino acid (AA) groups or subgroups on protein and ligand surfaces. Note that the two surfaces that eventually come into adhesive contact (right side) have more negative charges than positive charges: 3 negatives and 2 positives on the ligand, and 4 negatives and 2 positives on the receptor binding site. Each surface is therefore overall negatively charged, which is the way they appear from afar. These surfaces will therefore repel each other at large separations due to the double-layer interaction, but they attract each other when in contact due to the preponderance of favorable discrete ion-pair interactions: 7 favourable ionic $\oplus \ominus$ bonds, and only one unfavorable $\ominus \ominus$ configuration (on the far right of the adhesion site). Note, too, the favorable juxtaposition of the H-bonding pair and two hydrophobic groups. This electrostatic and hydrophobic complementarity, together with the perfect geometric fit (shape or van der Waals complementarity), together give rise to a strong conformationally specific ligand-receptor (LR) bond. Lock-and-key type bonds involving receptor "pockets" are shown schematically in Figures 10.3 and 21.12.

a protein and ligand. The figure shows seven ionic bonds, one nonbonding ionic configuration, one H-bond, and one hydrophobic “bond.” If we assume the mean energy per favorable bond to be $5 kT$ and that the interactions are additive, this site has an energy of $40 kT$ and, therefore, a lifetime of many months (cf. Table 21.2). It is easy to see how the addition or removal of just one or two ionic or H-bonds can make a very large difference to the lifetime of an LR bond. Thus, a site with only four bonds might have a lifetime of less than 1 s, which increases to hours on adding just two more bonds.

The reason for the weakness and short lifetimes of LR bonds is that nature does not actually want all of its bonds to be long-lived, just long enough for them to perform some function that requires a certain time—not less, but not more either. For example, a specific bond may be required to open a pore or channel in a membrane to allow a certain number of ions through, or to lower the energy barrier to the adhesion or fusion of a vesicle with a membrane (cf. Figure 21.12). In such cases, it may well be desirable to

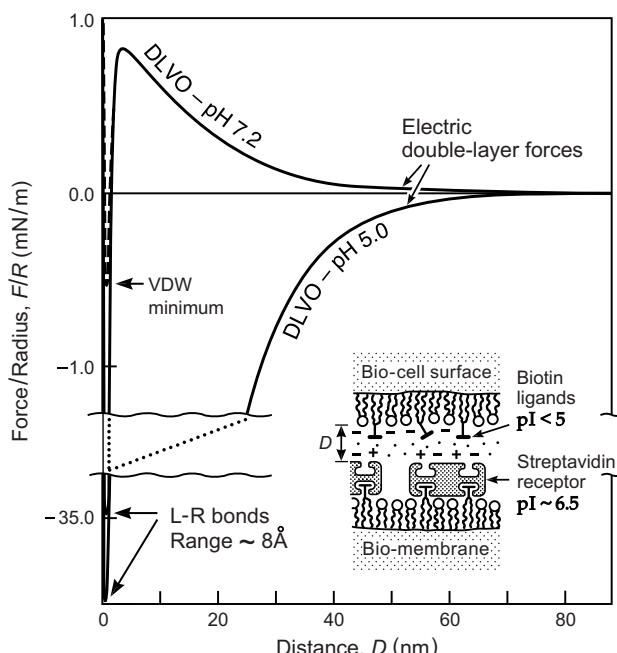


FIGURE 21.12 Example of long-range (>1 nm) DLVO and short-range (<1 nm) ligand-receptor interactions working together in an “asymmetric” biomimetic system. The avidin-biotin LR bond is highly specific, of short-range (<1 nm), and strong (Table 21.2). In this system, at pH 7.2 both surfaces are negatively charged and the electrostatic double-layer force is repulsive; but at pH 5.0 the Streptavidin surface ($pI = 6.5$) is positively charged so that the double-layer force is attractive. Thus, lowering the pH below 6.5, or introducing Ca^{2+} ions around the binding site (not shown), lowers or removes the energy barrier and pulls the surfaces together allowing them to bind via the LR bond that is almost two orders of magnitude stronger than the van der Waals bond. Energy barriers that need to be removed before biological surfaces or sites can bind can be due to other forces, such as discrete electrostatic (Figure 21.11) or hydrophobic interactions. [Data from SFA experiments with surfaces in the crossed-cylinder geometry, equivalent to a sphere of radius R near a flat surface or two spheres of radius $2R$, adapted from Leckband et al., 1994.]

have the pore open or the energy barrier lowered for only a specific time. While this lifetime will be statistical, it is nevertheless a natural mechanism that would not require any complex capping or terminating reaction. Further aspects of dynamic (i.e., nonequilibrium) biological interactions are discussed in the last chapter.

Biospecific interactions can be more varied than so far presented. First, the range of specific bonds, which is typically less than 1 nm (see Izrailev (1997) for details of the avidin-biotin bond), can be effectively extended by having the ligand attached to the end of a flexible polyelectrolyte—for example, polysaccharide, tether, or protein domain (see Sections 22.4 and 22.5). Second, vesicles aggregating via nonspecific adhesion forces, which are determined by the adhesion energy per unit area or interfacial energy, show deformational stresses as illustrated in Figure 21.13 (left) and described in Section 21.7. Such stresses pervade the whole structure and can even lead to rupture. In contrast, vesicle-vesicle attachments via site-specific or tethered LR bonds produce more controlled assemblies without stressing the membranes (Figure 21.13, right).

The geometry of a binding pocket or surface can change to enable the ligand and receptor to lock together. This is known as an *induced-fit interaction*. Also, a physical or

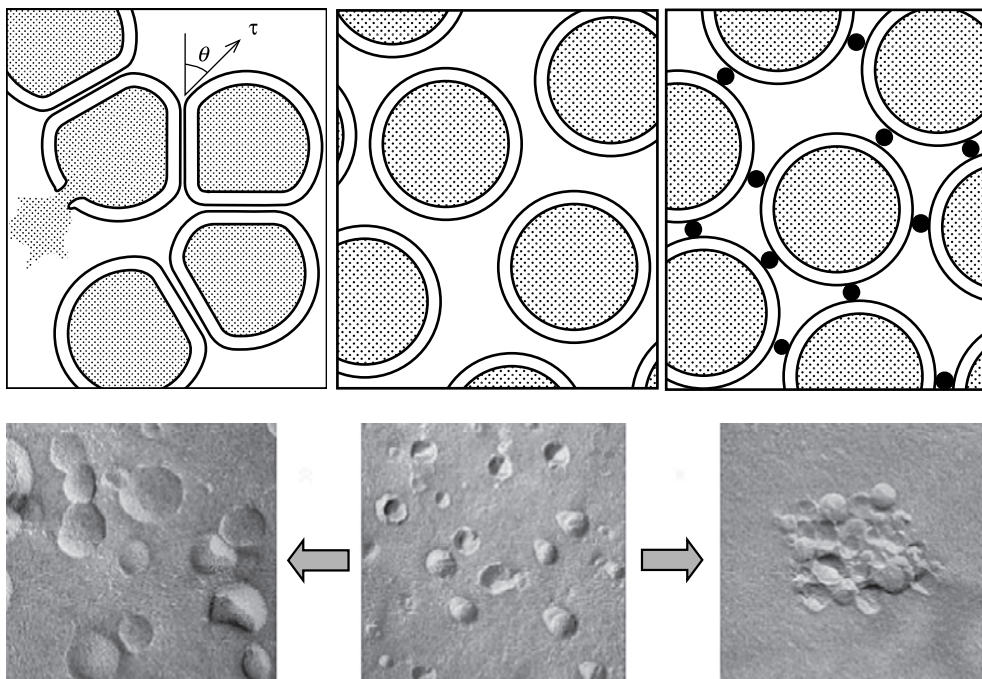


FIGURE 21.13 Left: Vesicles aggregating via nonspecific forces, showing deformation stresses as in Figure 21.16. Right: Stress-free aggregation via site-specific binding, showing no deformations. Controlled self-assembly of such stable multivesicular aggregates or “vesosomes” can now be bioengineered in the laboratory (Zasadzinski, 1997) and offers a path toward the processing of biomaterials and biomimetic cells, such as the one shown in Figure 22.6.

chemical reaction at some point of a macromolecule can cause a change at another point, transforming it from an inert to an active ligand or receptor site. This is known as an *allosteric interaction*.

21.7 Bridging (Tethering) Forces

A surface-bound polymer may contain functional groups along its chain or a specific ligand group at its free end. When the guest molecule or membrane approaches a host that exposes binding sites for these functional groups, a specific bridging attraction can result between the two structures once they are close enough for some initial binding to occur (see Figures 16.8 and 22.3). Following this initial binding, the two structures will be pulled further together thereby allowing for even more bonds to form. The resulting bridging force can be of long range—almost the fully extended “contour” length of the polymer chains $L_c = n\ell$, which is much longer than the Radius of Gyration R_g , or the Flory Radius R_F (Section 16.2) because a significant fraction of chains actually extend well beyond R_g at any moment, and these instantly bind to the opposite surfaces (if the LR binding energy is high). A full analysis of specific bridging interactions shows that they are very much dynamic processes: as two surfaces approach each other to a certain distance D (where $R_g < D < L_c$), there is only a certain *probability* that an LR bond will form *at this separation* during any particular *time* interval (Fig. 22.3). Specific “capture” processes are therefore just as rate-, time-, and temperature-dependent as is the “rupture” or detachment processes on separation, discussed in Section 9.2. We shall defer discussion of the dynamic (nonequilibrium and rate-dependent) aspects of specific interactions to the last chapter, and here concentrate on the equilibrium interaction potentials and forces.

A simple approximate expression for the bridging energy between two site-specific binding sites that are linked together by a single flexible tether (Figure 16.8) is

$$W(D) \approx -1.5nkT(D - R_g)^2/(L_c^2 - D^2) \text{ per tether} \quad (21.12)$$

where $L_c = n\ell$ is the fully extended length of the tether. We may note that this function diverges as D approaches the fully extended tether length, $D \rightarrow L_c$, and has a minimum at $D \approx R_g$, as expected. Also, for small displacements about the equilibrium separation at $D \approx R_g$, assuming that $D \ll L_c$, the force $F = -dW/dD$ is given by

$$F(D) \approx 3nkT(D - R_g)/L_c^2 \approx 3kT(D - R_g)/R_g^2 \text{ per tether} \quad (21.13)$$

which is linear in D and, therefore, “elastic-like” (cf. de Gennes, 1976; Pincus, 1976)—the energy being parabolic around $D \approx R_g$. Thus, as could have been expected, a stretched coil tries to pull its two ends together but resists further compression once it has reached its equilibrium configuration. In the large distance regime ($D \rightarrow L_c$) the force diverges as either

$$F(D) \approx -nkT/(L_c - D) \text{ per tether} \quad (21.14a)$$

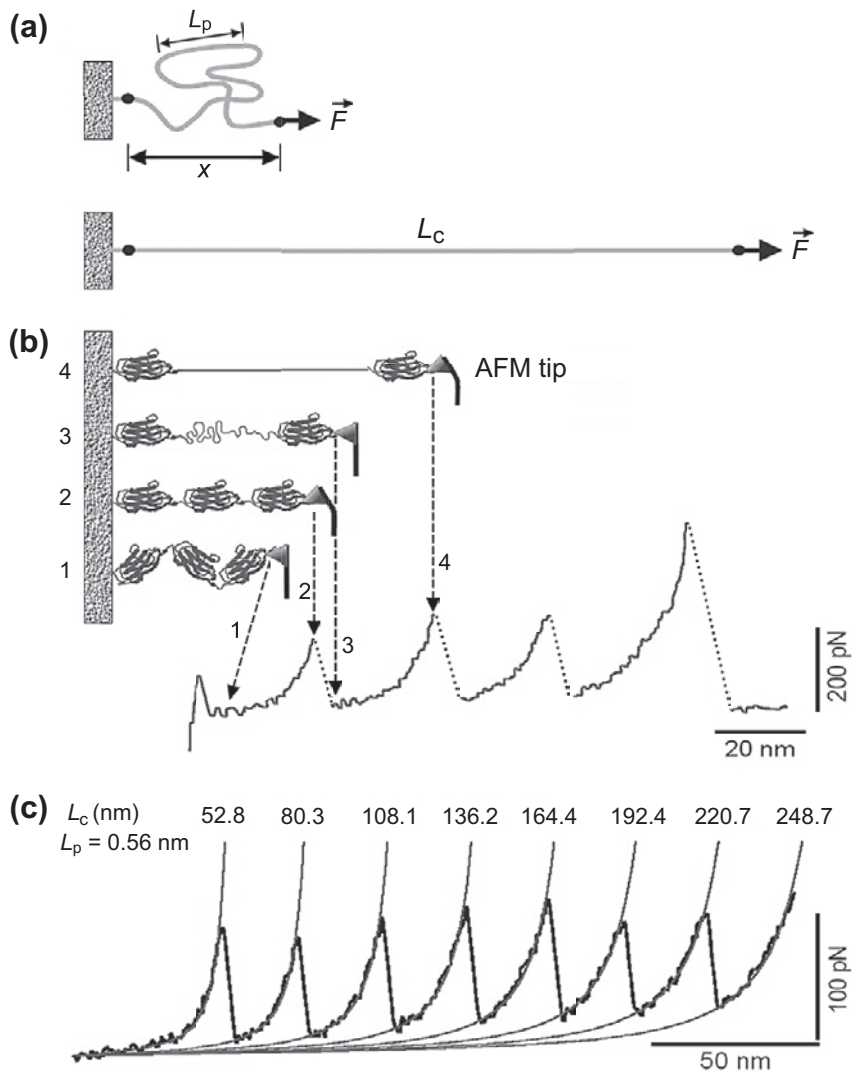


FIGURE 21.14 Force-induced protein unfolding. Panel (a) shows the forced extension of a structureless polymer coil modeled as a worm-like chain (WLC), described by Eq. (21.15). Panel (b) shows the measured force extension profile and the hypothesized changes in the protein structure that generate the different features in the curves. Panel (c) shows the fits of the WLC model to the regions of the force-extension curves between the force maxima. In these regimes, the extension of the unfolded protein initially follows that of a stretched elastic chain. The sudden drops suggest that each domain suddenly snaps opens or unfolds. The worm-like chain model does not apply to freely jointed chains (Eqs. (21.12)–(21.14)), but the two equations are similar except at small extensions, near R_g . Note that such force measurements do not necessarily take the system through its natural unfolding path. [Figure from Fisher et al., 1999.]

or

$$F(D) \approx kT \log_e [2.15(1 - D/L_c)] \text{ per tether} \quad (21.14b)$$

depending on the method of derivation (Jeppeson et al., 2001).

The above is the *freely jointed chain* model. In the alternative *worm-like chain* (WLC) model (Bustamante, 1994), where the tether is viewed as an elastic element, the force is given by

$$F(x) = \frac{L_c^2 kT}{L_p} \left[\frac{1}{4(L_c - D)^2} - \frac{(L_c - D)}{L_c^3} + \frac{3}{4L_c^2} \right] \text{ per coil} \quad (21.15)$$

where L_p is the persistence length. In the limit of $D \rightarrow L_c$ the force asymptotes as $F(D) = -L_c^2 kT / 4L_p (L_c - D)^2$, which differs from Eq. (21.14a), mainly in the squared term in the denominator.

Figure 21.14 shows the results of AFM pulling experiments on a protein, showing the progressive unwinding and intermittent snapping of its domains. Note that the measured force-distance curve, which can be converted into an energy-distance curve, does not necessarily give the *natural* “energy landscape” of the protein: the measured forces are along an unfolding direction dictated by where the protein is attached to the AFM tip and surface (Figure 21.14b). The unfolding path may therefore be quite different from that taken by the protein when it unfolds naturally—that is, due to heating or some change in the solution conditions. Likewise, any folding forces measured using a linear force-measuring device will not necessarily give the natural force or energy path.

Strongly adhesive bridging forces of a different kind also arise between charged surfaces that are bridged or cross-linked by divalent counterions such as Ca^{2+} whose two positive charges can bring together two negative charges. Such ionic bridges can occur both *out-of-plane*, between two surfaces, and *in-plane*, on a single surface. An example of the latter is the bringing together of the anionic headgroups of phosphatidylserine or phosphatidylglycerol lipids in a monolayer or bilayer composed of a mixture of charged and uncharged lipids (Fig. 21.9). Divalent and multivalent ion bridges can have a dramatic effect both on the internal structure of a membrane, causing phase separation, clustering, and local changes in membrane curvature, and on the gross membrane structure, causing adhesion and multilamellar stacking (see Section 21.8). They also cause a dramatic rise in the liquid-to-gel and/or liquid-to-solid phase transition temperatures of bilayers.

21.8 Interdependence of Intermembrane and Intramembrane Forces

Since the electrostatic, solvation, and steric interactions between different bilayers are essentially the same as those acting between adjacent headgroups within one bilayer, we should expect to find many correlations between *interbilayer* forces and *intrabilayer*

forces. Thus, we might expect larger headgroup areas a_0 to be accompanied by larger repulsive forces between bilayers. This is borne out by experiments. For example, the large hydration of the lecithin headgroup results in a large surface area of $a_0 \approx 0.7 \text{ nm}^2$ as well as a large swelling in fully hydrated lecithin multilayers. By contrast the headgroup repulsion in phosphatidylethanolamines is much less, which leads to a smaller headgroup area of $a_0 \approx 0.5 \text{ nm}^2$ and a much reduced swelling.

Analogous correlations occur for charged lipid bilayers where, in general, a decrease in pH or addition of divalent cations reduces the electrostatic headgroup repulsion and thus the surface area per lipid and also leads to reduced bilayer swelling in multilayer phases and to increased adhesion of vesicles.

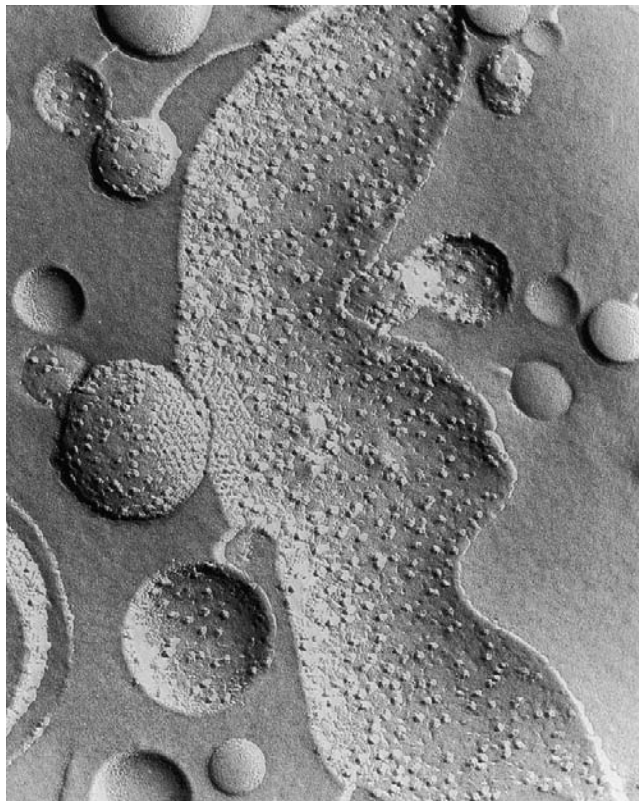


FIGURE 21.15 Example of synergy between intramembrane interactions leading to clustering or domains and intermembrane coupling interactions leading to enhanced adhesion and “tight junctions.” The image shows a freeze-fracture electron micrograph of reconstituted plant thylakoid membranes containing lipids and the two major thylakoid proteins known as photosystem I (mean diameter 9 nm) and the light-harvesting complex (LHC) of photosystem II (LHC-II of mean diameter 7 nm). In the presence of 5 mM Mg²⁺ the LHC-II aggregate into two-dimensional crystalline domains. These also act as adhesion sites between membranes, as seen here and also in intact thylakoids. The adhering vesicle in the figure has a diameter of 220 nm. [Micrograph: I. J. Ryrie]. Similar effects are seen in giant mixed lipid vesicles (Lee et al., 2003; Gordon et al., 2006. See also Figure 20.11c).

As a further example, the aggregation number of alkyl sulfate micelles increases as the electrolyte is changed from LiCl → NaCl → KCl → CsCl (Misset et al., 1982). This implies a reduced headgroup area a_0 , which arises from the reduced hydration repulsion of the bound counterions as we go from Li^+ to Cs^+ . The reduced headgroup area correlates with the increasing adhesion between oil-in-water emulsion droplets, stabilized by alkyl sulfate monolayers, as monitored by the contact angles between them (Princen et al., 1980).

In the area of biological membrane interactions, we may consider the structure of plant thylakoid membranes (Figure 21.15), where isolated (unstacked) membranes have a random distribution of proteins, whereas adhesion junctions or stacked regions (grana) show a denser and nonrandom distribution, as well as different proteins from those in the unstacked (stroma) regions. Figure 21.15 illustrates this phenomenon, showing how two reconstituted membranes have adhered at the sites where specific proteins have aggregated.

21.9 Biomembrane Adhesion, Bioadhesion

When a liquid droplet settles on a surface, or when two soap bubbles adhere, they distort into truncated spheres. For a drop on a surface (Figure 17.6), the contact angle θ is given by the Young-Dupré equation, Eq. (17.23), in terms of the liquid surface tension, γ , and the adhesion energy (work of adhesion) per unit area of the solid-liquid interface, W . In such cases the adhesion-induced flattening or spreading of the liquid on the solid surface is energetically resisted by the increased area of the liquid, as quantified by the surface tension γ . Similar effects occur when two elastic spheres adhere, as described by the JKR theory (Section 17.7), where now the energy resisting the adhesion-induced flattening comes, not from the increased area, but from the elastic energy of the deforming bodies, as quantified by their elastic moduli K .

The adhesive flattening associated with adhering vesicles (Figures 21.13 and 21.16) is yet another feature of interparticle adhesion, this time of elastic sheets, where the opposition to flattening now comes from the elastic area and bending moduli, k_a and k_b . Thus, while for a liquid surface, a change in its surface area by ΔA is accompanied by a surface free energy change of $\gamma\Delta A$, for small areal expansions of an elastic membrane this becomes replaced by $\frac{1}{2}k_a\Delta A^2/A_0 = \frac{1}{2}k_a(A - A_0)^2/A_0$, where A_0 is the unstressed area. On first contact two adhering vesicles of initial radius R_0 , volume $V_0 = \frac{4}{3}\pi R_0^3$ and unstressed area $A_0 = 4\pi R_0^2$, will deform rapidly and elastically at constant water volume V_0 until the adhesion and elastic stresses balance. The equilibrium condition is given by the Young-Dupré equation, $W = 2\tau(1 - \cos \theta)$,⁸ where W is the adhesion energy (or work of adhesion) per unit area of the two membrane surfaces, $\tau \approx k_a\Delta A/A_0 = k_a(A - A_0)/A_0$ is the membrane tension, and where θ is the contact angle measured outside the vesicles as defined in Figures 21.13 and 21.16. (see also Figure on p. xxvii). The above two equations

⁸Note that there are two deformed membranes at the junction, each developing a stress τ .

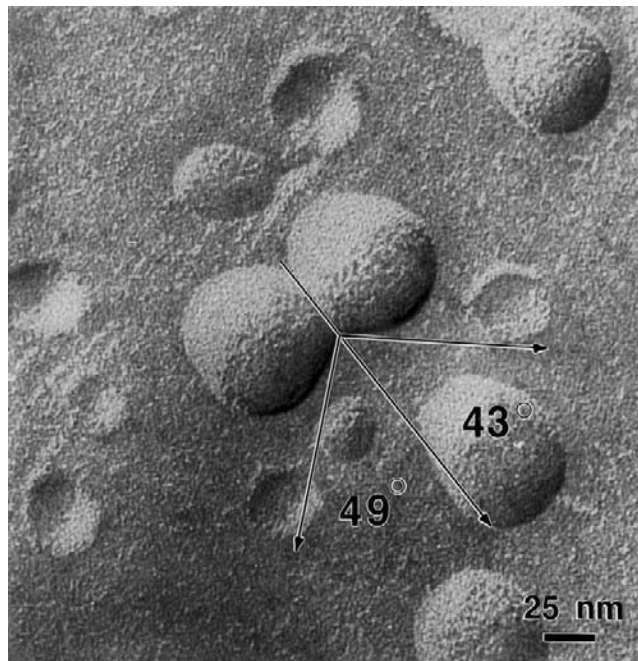


FIGURE 21.16 Deformation associated with the adhesion of two initially spherical lecithin vesicles imaged by cryo-transmission electron microscopy (cryo-TEM). By measuring the deformations, such as the contact angles θ , of the adhering vesicles one can estimate the elastic moduli and stresses on the bilayers or membranes (see Figure 21.13), and the adhesion force and energy, using Eqs. 21.16–21.18 (Bailey, 1990; Chiruvolu, 1995; Ramachandran et al., 2010). [Micrograph courtesy of J. Zasadzinski.]

can be combined to give the contact angle θ in terms of W and the area elastic modulus k_a for deformations at constant vesicle volume:

$$W = 2k_a(1 - \cos \theta) \left\{ \frac{(3 - \cos \theta)}{\left[2(1 + \cos \theta)^{1/2} (2 - \cos \theta) \right]^{2/3}} - 1 \right\}, \quad (21.16a)$$

which for small angles θ is well approximated by

$$\theta \approx (16|W|/k_a)^{1/6}. \quad (21.16b)$$

It may be further established that for two identical vesicles of initial radius R_0 : (1) the adhesion or pull-off force is $F_{ad} = \pi R_0 W$, which is independent of the elastic modulus, just as for rigid (undeformable) spheres, and proportional to R_0 ; and (2) the *total* adhesion energy at contact equilibrium is

$$W_{ad} \approx -W^{4/3} \pi R^2 k_a^{-1/3}, \quad (21.17)$$

or for two vesicles: $W_{ad} \approx -\frac{1}{4}W \times \text{flattened contact area, and}$ (21.18a)

$$\text{for a vesicle on a flat surface: } W_{\text{ad}} \approx -\frac{3}{4}W \times \text{flattened contact area.} \quad (21.18b)$$

which increases (becomes more negative) as k_a decreased. The adhesion energy of deformable vesicles is therefore seen to be much higher than for rigid (undeformable) spheres for which $k_a = \infty$. For typical values of $k_a \approx 100 \text{ mJ m}^{-2}$, the contact angle θ will exceed 45° once the work of adhesion W exceeds 1 mJ m^{-2} . When this occurs the total surface area of each vesicle will be stretched by more than 2% of its initial (presumed unstressed) value. Since most lipid bilayers and biological membranes cannot be stretched beyond 2–4% without rupturing, this could lead to rupture followed by reassociation of the burst vesicles, which is one of a number of different pathways by which vesicles can fuse (see Section 21.10).

The situation is more complex when adhering membranes are water-permeable. Following the initial rapid flattening, water will start to permeate out of the vesicles, pushed out by the pressure $P = 2\tau/R$ exerted on it by the stressed bilayers. If there is only pure water both inside and outside the vesicles, then the expulsion of water will continue indefinitely until the bilayers collapse and fold into tightly packed lamellae or so-called cochleate cylinders. But if the internal solution contains nonpermeable electrolyte ions or some other nonpermeating solute of initial concentration ρ_0 , the water will stop its outward diffusion once the osmotic pressure $\Delta\rho = kT = \rho_0kT(V_0 - V)/V$ equals $P = 2\tau/R$. Thus, a new equilibrium is established where the vesicle volume V is now less than the original volume V_0 and where the adhesion energy is even higher than that given by Eq. (21.17), which is already significantly larger than for rigid (undeformable) spheres. Interestingly, at physiological electrolyte concentrations ρ_0 only a small decrease in water volume results in a large change in the osmotic pressure, so that the deformation and adhesion energy are effectively at constant internal volume.

While the above equations may be formally correct, the situation is far more complex in practice. First, a complete treatment must also include the bending energy changes during vesicle deformations. And—as we have already seen—there are both soft and hard bending regimes. Second, we have also seen that by stretching bilayers their adhesion energy, W , increases due to an increased hydrophobic attraction. Thus, in general, we cannot assume that W is independent of τ . Third, the initial vesicles may already be stressed. Fourth, a number of additional molecular and structural rearrangements, each having its own fast or slow relaxation time, may also be involved during vesicle and biomembrane adhesion in multicomponent (lipid-protein) systems. These include flip-flop; a lateral redistribution and/or phases separation of lipids and proteins giving rise to, for example, *tight junctions*; lipid exchange with other membranes (leading to *Ostwald ripening*), and slow diffusion of ions and other solute molecules across the vesicle walls which again modify the above equations and the final structure; for example, the limiting thermodynamic structure may be a lamellar or liposome phase where the energy *per molecule* is $-Wa_0$, which far exceeds that of the (mean) energy per molecule when two vesicles simply adhere, $-W_{\text{ad}}a_0/8\pi R^2$, where W_{ad} is given by Eq. (21.17).

The term *bioadhesion* covers much more than the adhesion of biological membranes; it also covers the adhesion (and often cohesion) of tissues, cartilage to bone, surgical adhesives, dental glues, geckos to walls and ceilings, mussel feet or plaques to rock surfaces, and so on—a field that is beyond the scope of this book. Figure 21.17 shows some of the rearrangements that occur when biological surfaces or tissues adhere to substrates or to each other. The adhesion forces generated may be very high, even when only noncovalent van der Waals or H-bonds are involved. It is important to note that a high effective adhesion (pull-off) force does not necessarily imply a high thermodynamic surface or interfacial energy: a molecular contact area that is higher than the projected area, as in Figures 17.11(d) and 17.17(b), can give rise to a high adhesion force, as can a rigid substrate or tissue supporting the adhesive layer, as in Figure 17.2. Also, a high friction force when resolved along the pulling direction can also give rise to a high adhesion/pull-off force, a phenomenon that is known as *frictional adhesion* (see Problem 21.7).

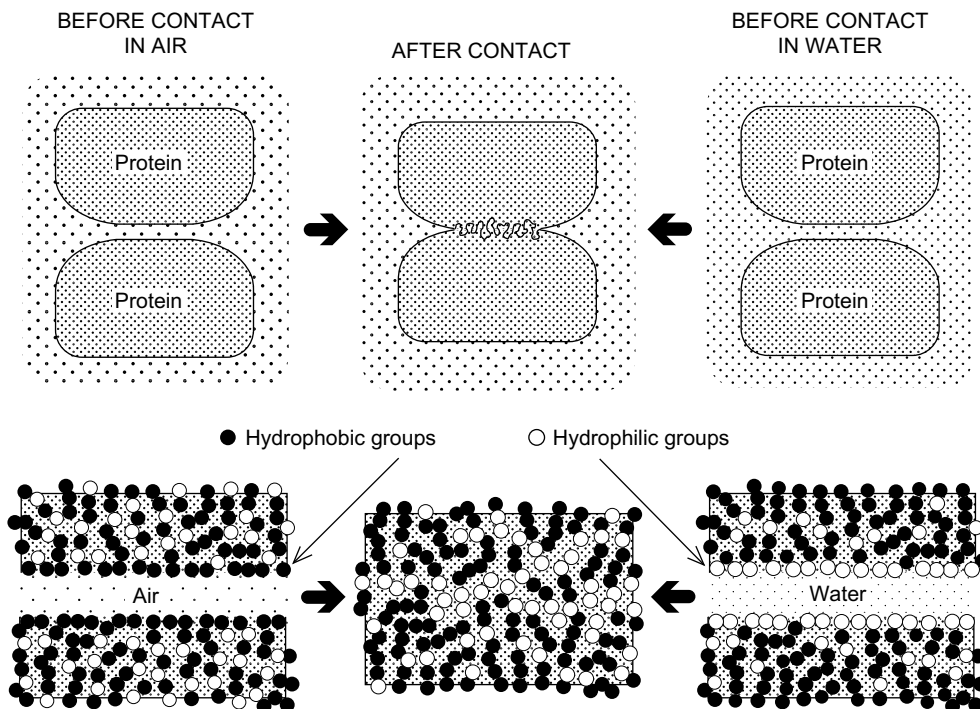


FIGURE 21.17 Surface rearrangements associated with the adhesion of biological (e.g., protein) surfaces in air (left) and water (right). The strong reversible adhesion of geckos to surfaces is an example of the former; the adhesion of mussels to rock surfaces in sea water is an example of the latter. The amino acid groups exposed to air or water before the proteins come into contact will be either hydrophobic (left) or hydrophilic (right). After coming into contact, the various groups will attempt to rearrange so that H-bonding donors link up with acceptors, cations (basic groups) with anions (acidic groups), and hydrophobic groups with each other. These rearrangements can be instantaneous or take a long time (minutes to hours), during which the protein structure changes and the adhesion increases. Similar effects occur when individual proteins bind or adsorb to surfaces.

21.10 Membrane Fusion

Fusion is not a common event for most living membranes, while for some—especially the membranes of small transport vesicles—it may be their main function. Membrane fusion can be divided into hemi-fusion and full fusion (Figure 21.18e and f), as well as into nonspecific and specific fusion.

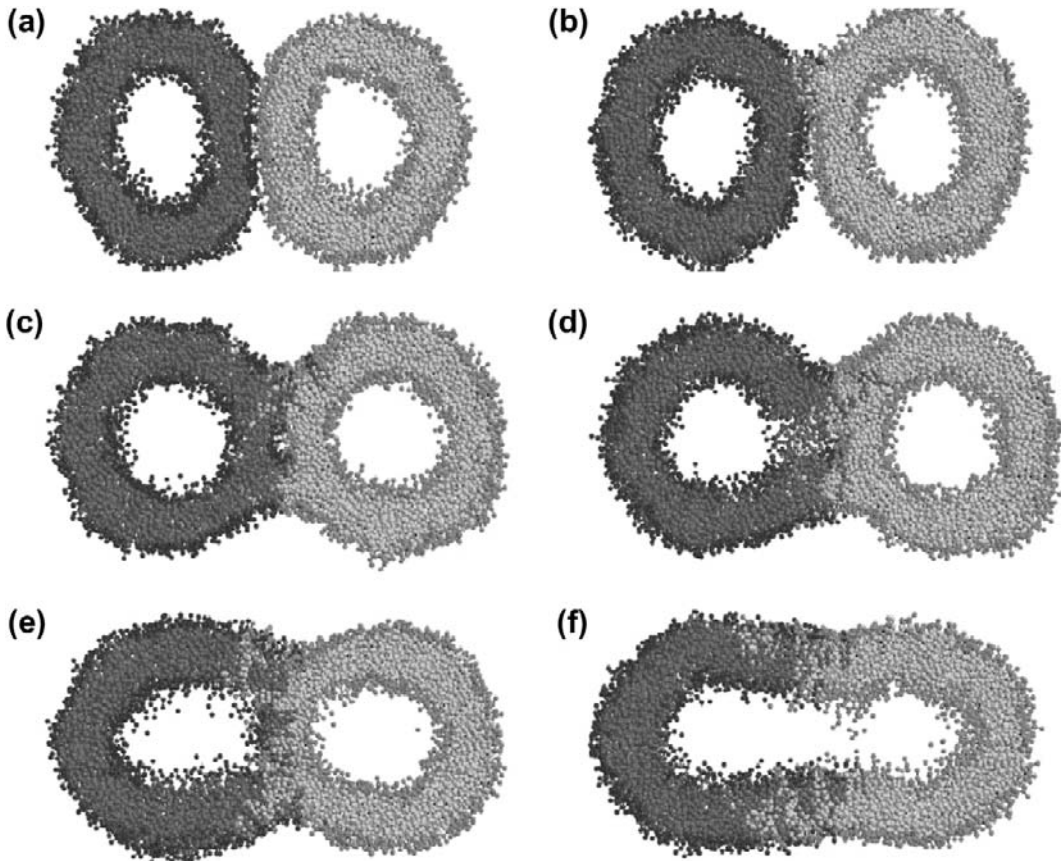


FIGURE 21.18 Probable molecular events taking place during the critical step leading to the hemi-fusion and full-fusion of bilayers. For fusion to occur, adhesion between the exterior surface groups of membranes may not be enough; hydrophobic patches or “pockets” need to be “opened” so that the *interiors* of the bilayers can attract each other across the water gap. Various stresses can lead to the exposure of hydrophobic surface regions: strong local adhesion leading to an increase in the lateral (tensile) tension elsewhere (Figures 21.8 and 21.9); a change in osmotic pressure resulting in tensile stresses; asymmetric or curvature-inducing stresses (Figures 20.15 and 20.16), electric field effects that cause membranes to thin, thereby exposing hydrophobic groups (Problem 20.9), and so on. The images shown are from a computer simulation of two osmotically swollen vesicles that fuse via a “breakthrough” stage (b) at $t \approx 100 \mu\text{s}$ at the edges (note that this is also where the tensile bending stresses on the two outer monolayers facing each other are highest), followed by hemi-fusion (e) at $t \approx 200 \mu\text{s}$, leading to final full fusion (f) at $t \approx 230 \mu\text{s}$. [Reproduced from Stevens et al., (2003) with permission.]

Nonspecific fusion. A stressed or stretched bilayer or membranes exposes hydrophobic regions that will readily fuse with the exposed hydrophobic regions of another membrane or protein due to the enhanced long ranged hydrophobic attraction between stretched bilayers. Such “nonspecific” stresses can be induced osmotically, mechanically, or by applying electric field gradients.

It is worth considering why hydrophobic adhesion often leads to fusion, while other, stronger adhesion forces (e.g., calcium bridging forces between anionic bilayers) do not. Fusion (including hemi-fusion) should be distinguished from adhesion, however strong. In the case of adhesion, two molecules or surfaces are “happy” once they are in contact; in the case of fusion, the membrane or protein *interiors* must be pulled together—the adhesion stage being merely one of the steps on the way to fusion. The critical step, shown in Figure 21.18b, involves the local separation of hydrophilic groups on the surfaces and exposure or opening of hydrophobic pockets on opposite sites; this generates a strong medium-to-long range hydrophobic force that rapidly pulls the hydrophobic (hydrocarbon) *interiors* of the two surfaces together—the “breakthrough” step (Papahadjopoulos et al., 1977; Chernomordik et al., 1987; Helm and Israelachvili, 1991). The various stages shown in Figure 21.18 leading to complete fusion appear to be generic, with minor variations, for all bilayer fusion events (Chernomordik et al., 1987). As discussed below, the same scenario may well apply, albeit in a much more complex way, to the fusion of proteins, given that most proteins are now believed to fuse via the exposure of hydrophobic pockets (Rosenthal, 1998; Skehel, 1998; Sutton, 1998).

What are the factors that cause the sort of stresses on membranes or proteins that can lead to fusion? These can be divided into intra-membrane stresses and inter-membrane stresses: (1) Pure lipid vesicles (e.g., phosphatidylcholines) in water are often stable for months but fuse into larger vesicles when the temperature is lowered much below the chain melting temperature, T_c . This is because the curved bilayers of small vesicles become highly stressed below T_c as the chains now attempt to line up and pack into less or differently curved bilayers. The stressed vesicles easily rupture during collisions, and then fuse with each other to form larger, less curved vesicles. This type of fusion is driven by a change in the internal or intra-membrane forces that have induced packing stresses in the membranes. (2) As we established quantitatively in the previous section, and illustrated in Figures 21.13 and 21.18, one can induce vesicles to fuse by increasing their interfacial adhesion energy ($W_0 = 2\gamma_i$), whether due to a hydrophobic or other interaction, beyond a certain critical value. The resulting deformations stretch the membranes, exposing new hydrophobic areas, which then fuse due to the enhanced long ranged hydrophobic interaction. Unlike (1), this type of nonspecific fusion is due to changes in the inter-membrane forces.

Specific fusion. Specific fusion is more localized or “site-specific” and “selective”—usually caused by specific ligand-receptor type interactions. Specific fusion involves specialized *fusogenic* proteins in specialized membranes or vesicles whose structure and function are geared toward hemi-fusion, full fusion, or some variant of these—for

example, having a vesicle transported through a membrane while selectively exchanging some of the lipids and proteins with that membrane, or having the light and dark lipids of the original vesicles in Figure 21.18 ending up exclusively in the inner and outer monolayers, respectively, of the final vesicle. Such fusion events are usually triggered by conformational changes in proteins rather than lipids; for example, the fusion of the common protein fusogens Hemagglutinin A (Rosenthal, 1998) and SNAREs (Sutton, 1998) are attributed to triggered conformational changes in the local pH and calcium ion concentrations, respectively.

Hydrophobic and electrostatic interactions often work together to induce fusion. For example, the top half of Figure 21.9 shows the structure and intermembrane forces between two mixed lipid bilayers of neutral PC and charged PG⁻ in monovalent electrolyte; the forces are the expected monotonic DLVO forces with no major structural effects on the bilayers. In the presence of even small amounts of calcium, lateral phase separation or clustering occurs (bottom of Figure 21.9) where the PG⁻ lipids are pulled close together (condensed) by Ca²⁺ binding. The condensed PG-calcium domains result in a tensile stress on the remaining PC-rich regions, which become more hydrophobic and thereby act as adhesion and/or fusion sites (Leckband et al., 1992). In this system, fusion would not occur unless a number of favorable factors are present simultaneously: mixed rather than single-component bilayers, divalent counterions on one side of the bathing solution, and fluid membranes that allow molecular rearrangements to occur. Note, too, that with this type of “hydrophobic” fusion mechanism, the fusion will occur at a different location from the calcium binding sites.

As in the case of bilayers, changes in protein structure that cause them to expose hydrophobic domains leading to fusion do not have to occur at the ultimate adhesion nor fusion site; for example, an osmotic or mechanical pressure change triggered in one region of a cell may alter the tension of the entire cell membrane, causing it to fuse with vesicles in a completely different place.

Specific fusion is selective, not only in space, but also in time. For example, synaptic nerve transmission, exocytosis (vesicle incorporation) and pinocytosis (vesicle shedding) require fusion to occur at a particular location, at a particular time, and also for a particular *duration* – the changes in the local electrochemical conditions (e.g., local pH or concentration of Ca²⁺) need to be maintained only for the time required to effect the required fusion event, but no longer.

PROBLEMS AND DISCUSSION TOPICS

- 21.1** (i) List four types of repulsive forces and four types of attractive forces between biological molecules (e.g., lipids, peptides, nucleotides), macromolecular structures (e.g., capsids, vesicles) and extended surfaces (e.g., plasma membranes, gecko toe pads), and briefly describe realistic situations where each would dominate the interaction over a certain distance regime. (ii) Describe three realistic ways in which the adhesion of biomembranes can be enhanced by increasing the strength of an

attractive force between them, and three by decreasing the strength of a repulsive force. (iii) Will increasing the magnitude and range of the repulsive interaction between *self-assembled* structures increase or decrease their size? (iv) Are the following statements true when applied to the interaction in a liquid or vapor of any two unconstrained but similar electroneutral particles or surfaces? (a) The total purely electrostatic contribution to the interaction is always attractive. (b) Apart from the hard-core repulsion at molecular contact, all the repulsive contributions have an entropic origin.

- 21.2** In Figure 21.3, if the solution concentration were increased to 1M NaCl show that the secondary minimum at $\psi_0 = 50$ mV moves in from $D = 6$ nm to about $D = 2$ nm and its depth increases about tenfold.
- 21.3** Consider the forces measured between the two DHP bilayers in 10^{-3} M NaCl (Figure 21.4). (i) How does the Debye length compare with theory? (ii) What is the surface potential and surface charge density? (iii) What fraction of molecules is charged (dissociated)? (iv) Is the interaction “charge regulated”? (v) Estimate the Hamaker constant. (vi) Down to what separation and fraction of the Debye length does the DLVO theory appear to work? Assume that the DHP headgroup area is 0.60 nm^2 . [Answers: (i) Measured decay length: 8.5 nm; theoretical Debye length: 9.5 nm. (ii) $\psi_0 = -49$ mV, $\sigma = -3.8 \times 10^{-3}\text{ C/m}^2$. (iii) 1.4% of the phosphate headgroups are dissociated. (iv) Yes. (v) $A \gtrsim 1 \times 10^{-21}\text{ J}$. (vi) About 1.25 nm, which is ~15% of the Debye length.]
- 21.4*** **(i)** Consider a lipid bilayer in the fluid state in water where the hydrophilic headgroups interact with each other laterally (i.e., in the plane of the bilayer) via a repulsive steric-hydration force whose interaction pair potential is given by $w(r) = +(C/r)e^{-r/\lambda}$, where r is the distance between headgroups each of hard-core diameter σ , and where C and λ are constants. In addition, there is a laterally attractive force between the lipids described by the normal expression for the interfacial energy of a hydrocarbon-water interface—that is, γa , where γ is the interfacial energy per unit area, and a is the mean area-occupied per molecule. Using an analysis similar to that used to derive the two-dimensional (2D) van der Waals equation of state (Problem 2.2 and Eqs. (6.15) and (6.16)), derive the 2D equation of state for bilayers giving the lateral pressure Π (in units of N m^{-1} or J m^{-2}) as a function of the area a , in terms of γ , σ , C , λ and kT . What is the optimum area a_0 occupied by each lipid in the bilayer in the unstressed bilayer ($\Pi = 0$)? Estimate its value at 25°C for the following parameters: $\gamma = 50\text{ mJ/m}^2$, $\sigma = 0.5\text{ nm}$, $C = 0$ —that is, when the only repulsion between the headgroups is due to the hard-core thermal energy. How realistic is your answer, and what does it imply regarding the neglect of any contribution from repulsive headgroup-headgroup interactions? [Note: The area occupied per hydrocarbon chain in the fully-extended frozen state is $\sim 19\text{ \AA}^2$.]

- (ii) Derive an approximate expression for the area elastic modulus of the bilayers, k_a (in units of N m^{-1} or J m^{-2}), for small deviations of the area a about the optimal area a_0 , in terms of γ , a_0 , and kT , and estimate its value for a bilayer having the above values. Compare your result with typically measured values of $k_a \approx 200 \text{ N m}^{-1}$ for lipid bilayers and biological membranes, and comment on the significance of the difference.
- (iii) Next, consider two opposing bilayers at a distance D_w apart in water whose headgroups occupy the same optimum area a_0 . If each headgroup is also assumed to interact with each headgroup in the opposite bilayer via the same repulsive potential function as given by the above equation, show that the repulsive “hydration” pressure $P(D_w)$ between two such bilayers is a pure exponentially decaying function of their separation D_w , and obtain $P(D_w)$ in terms of D_w , C , λ , and a_0 . Discuss qualitatively the different situations (a) where the two bilayers are pressed together from their opposite sides—for example, mechanically—and (b) where they are brought together by sucking out the water between them—for example, osmotically. [Answer to (iii): In (a) as D_w decreases the bilayers thin; in (b) they become thicker (see Worked Example 21.3).]
- 21.5** The phase diagrams of many amphiphile-water systems, which includes both surfactant and amphiphilic polymers, display a common feature where on increasing the surfactant concentration above 20–50 % there are a series of structural transitions having the following characteristic sequence: spherical micelles → aligned cylindrical micelles → oriented planar bilayers (lamellar phase) → “inverted” cylindrical structures. The transitions between these one-phase systems are usually separated by narrow two-phase regions.
- Explain this phenomenon. If the various surfactant aggregates repel each other with a strongly repulsive steric-hydration force coming in sharply at a surface separation of 1.5 nm, and if the fully extended length of the hydrocarbon chain in each type of aggregate is also 1.5 nm, estimate the volume fractions of surfactant at which the transitions from spheres to cylinders, and cylinders to lamellae are expected to occur.
- 21.6** (i) Calculate the lateral tension τ , in units of mN m^{-1} , that must be applied to a bilayer for its mean thickness to decrease by 2%. (ii) Calculate the electric potential difference (in volts) that must be applied across a bilayer in water for its thickness to change by 2%. Will the thickness increase or decrease? What possible effects could these stresses have on the forces and interactions between two adjacent bilayers? [Assume an initial bilayer thickness of 3.0 nm, an elastic modulus of $k_a = 150 \text{ mJ m}^{-2}$, and a dielectric constant of the hydrocarbon core of $\epsilon = 2.2$.]
- 21.7** The legs of a 4-legged insect have the shape of ball-ended pillars. The tissue is made of a stiff (assume totally rigid) biopolymer that adheres via van der Waals forces to a smooth surface. When pulled along its length, the adhesion force of each

leg is $F_{\perp} = 1 \text{ mg}$. When sheared laterally, the friction force is $F_{\parallel} = 1 \text{ gm}$ (cf. the low adhesion but high friction of rubber and many polymer surfaces: Chapters 17 and 18). The four legs come away from the body like the four edges of pyramid, each subtending an angle θ to the horizontal plane. (i) What is the normal adhesion (pull-off) force $F_{\text{ad}}(\theta)$ in terms of F_{\perp} , F_{\parallel} , and θ ? (ii) At what angle will the pull-off force of the four legs be 10 times that of four vertical legs ($\theta = 90^\circ$)? This is an example of *frictional adhesion*, showing how insects and small animals such as *geckos* make use of the articulation of their limbs to enhance both their adhesion and friction forces so that they can attach to ceilings and walls.

[Hint: First show that the force F_{θ} along the axis of a tilted pillar is related to F_{\perp} and F_{\parallel} by $F_{\perp} = F_{\theta} \sin \theta$ and $F_{\parallel} = F_{\theta} \cos \theta$, which leads to a simple expression for $F_{\text{ad}}(\theta)$ using $\sin^2 \theta + \cos^2 \theta = 1$.]

- 21.8** A three-phase oil-water-surfactant system has a water-rich and an oil-rich phase separated by a thin film “middle phase” consisting of alternate oil-swollen bilayers separated by a thin water gap, as illustrated in Figure 20.9. The bilayers in the middle phase are sitting in a secondary potential energy well of energy $0.001 kT$ per surfactant pair where $a_0 = 50 \text{ \AA}^2$ (cf. Figure 21.3). What is the interfacial tension of the film?
- 21.9** The planar membrane of a cell contains receptor proteins R that irreversibly bind ligand groups L. The (different) membrane of a spherical cytoplasmic vesicle contains a small fraction of lipids, each of chain length ℓ with a hydrophilic headgroup tether of length d terminated by a ligand group L. The “protrusion” energy to pull a lipid out from the vesicle membrane is α_p per unit length (see *protrusion forces*, Sections 16.10 and 21.3). Show that the force-distance curve describing the interaction between the vesicle and the planar membrane has the shape of a square well—that is, where the maximum (adhesion) force is constant over a finite distance rather than at a particular separation.
- 21.10*** To answer the following questions, you will need to refer to some papers, review articles, or books that discuss the solution properties and biological use and activity of polyethylene-glycol (PEG) and/or polyethylene-oxide (PEO). (i) What is the difference between PEG and PEO? (ii) Why is PEO considered to be a good candidate for producing biocompatible surfaces? (iii) What are its benefits and disadvantages? (iv) What molecular interactions are responsible for this? (v) Why does *free* PEG or PEO in solution of intermediate molecular weight (~2,000 Da) cause cells to aggregate and even fuse, but low MW (<400 Da) and high MW (>10,000 Da) PEO have no effect or keep cells apart? Discuss whether this effect could be related to the observation that blood platelets are observed to adhere to surfaces *grafted* with PEO 200 and 4,000, but are much less adherent to surfaces grafted with PEG 1,000. (vi) Explain why PEO-mediated depletion attraction between vesicles or cells can cause the membranes to fuse, while other types of attractive forces between membranes only cause them to adhere.

Dynamic Biointeractions

22.1 Subtleties of Biological Forces and Interactions

While the intermolecular forces between biological molecules are no different from those that arise between any other types of molecules, a “biological interaction” is usually very different from a simple chemical reaction or physical change of a system. This is due in part to the higher complexity of biological macromolecules and systems that typically exhibit a hierarchy of non-equilibrium structures ranging in size from proteins to membranes and cells, to tissues and organs, and finally to whole organisms. Moreover, biological interactions do not occur in a linear, stepwise fashion, but involve competing interactions, branching pathways, feedback loops, and regulatory mechanisms.

In addition, biological interactions are essentially “dynamic” rather than “static”: biological systems are never at thermodynamic equilibrium, and they are not, rigorously speaking, closed systems. While it may be common to investigate processes in isolation, *in vivo* they are coupled to other reactions or interactions that control the many biological processes, which together maintain the organism. A “complete” biological interaction, even if such a concept could be clearly defined, would involve a sequence of tightly-orchestrated events, whose effects propagate out in both space and time in a regulated manner (Figure 22.1).

22.2 Interactions that Evolve in Space and Time: Some General Considerations

Dynamic, nonequilibrium, interactions can be classified as (1) those that are undergoing change toward the equilibrium state or some “local” metastable low energy state,

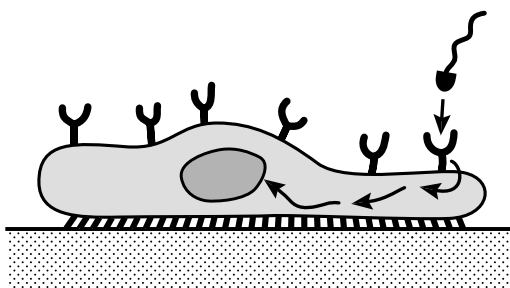


FIGURE 22.1 Biological interactions have no beginning and no end, and should be thought of more as ongoing energy-consuming “processes” evolving in space and time.

(2) those that are driven in response to an external stimulus (force or energy input), or (3) those that remain unchanged in a “steady state” configuration by a continuous input of energy. Yet a fourth type of dynamic interaction is one that is only apparently not at equilibrium, this being a random thermally driven “fluctuation” about the equilibrium configuration. Each of these processes occur in both biological and nonbiological systems, and we shall consider their fundamental origin first before proceeding to consider their occurrence in biological systems which are also usually much more complex.

In the first and second kinds of nonequilibrium interactions, the system is slowly changing *in a certain direction*, and the slowness of the process usually implies that the activation barriers are high or that the multiple potential energy minima are deep. There is no easy way of knowing whether the direction of change is toward the global free energy minimum or some local metastable state.¹ In the third case, the system is not changing, but neither is it in the thermodynamically equilibrium state. In the fourth case, the fluctuation, which may be slow, is eventually reversed; the system is at equilibrium but only when averaged over time. It is ironic that an interaction that is not changing in time may be far from equilibrium, but one that is (or appears to be) continually changing may be in the equilibrium state.

When it comes to the interaction forces and pair potentials, we have seen (see Bell Theory in Section 9.1) that in general the adhesion or binding *forces* depend on the pulling rates and waiting times even when the interaction *energy* or *potential* is a fixed function of the separation. In other words, the measured adhesion force can be very different from the value of $F_{ad} = -(dw/dr)_{max}$ expected from the pair potential. We have also seen (see WLF Theory and Deborah Number in Chapters 9 and 18) that the work done, or energy expended, in any process or cycle depends on the “measurement time” or “observation time.” We shall further see how in biological systems such nonequilibrium effects lead to hysteresis, irreversibility, transient phenomena, discontinuous or sudden changes, diffusion-limited interactions, important rare interactions, and differences between local versus global effects.

Single-bond energies and interparticle adhesion energies encountered in nature fall within the range <0.001 to >200 kT , the higher values being for covalent bonds. In contrast, most noncovalent biological interactions in solution have energies that fall in the range of <1 to 35 kT as we go from weak van der Waals or bio-colloidal interactions to strong ligand-receptor (LR) binding (see also Tables 21.1 and 21.2). Now, adhesion or binding energies (the wells as well as the energy barriers) E_{ad} invariably appear as $e^{-E_{ad}/kT}$ in equations to do with bond lifetimes, aggregation or dissociation dynamics, structural relaxations, and equilibration times. The lifetimes of covalent bonds can exceed the age of the universe, but those of biological “bonds” or “assemblies”

¹Such a system may be moving toward “mechanical equilibrium” but not “thermodynamic equilibrium,” which requires uniformity of the pressure, temperature and chemical potentials of all species throughout the system (Chapter 2).

usually range from microseconds to many days, which is precisely the desired lifetimes of biological associations and processes. Thus, when viewed over “everyday lifetimes” most biological structures are neither at thermodynamic equilibrium nor in some kinetically trapped metastable state, but somewhere in between.

22.3 Biological Rupture and Capture: the Bell and Jarzynski Equations

The Bell equation. In Chapter 9 we saw how even at the single molecule level the pull-off or adhesion force needed to break or separate two molecules depends not only on the equilibrium interaction energy-distance curve, $w(r)$, but also on the temperature and the time scale of the measurement—the pulling time or pulling rate (as previously illustrated in Figure 9.2). The Bell theory (Bell, 1978) shows us that the effective adhesion force is not simple given by when dw/dr is a maximum, but by the far more subtle equation (Eq. 9.3b): $F(t) = kT \ln(\tau/t)/r_0$, where $\tau = \tau_0 e^{-w_0/kT}$, which gives the effective adhesion or pull-off force needed to separate two molecules or particles after a time t in terms of the bond (or rupture) energy w_0 , the bond length r_0 , and the natural molecular vibration or collision time τ_0 .² This equation can be rearranged and also expressed more generally in terms of the work $W = Fr_0$ needed to be done *on* the system to affect the separation, giving an alternative form for

$$\text{the Bell equation: } te^{Fr_0/kT} = te^{W/kT} = \tau_0 e^{-w_0/kT} = \text{constant} = t_0 \quad (22.1)$$

where t_0 (which has replaced τ in Eq. (9.3)) is the natural lifetime of the bond under zero external force, $F = 0$. In what follows, when multiple bonds are considered, N refers to the bond number and n to the number of experiments or rupture-capture measurements performed on that bond.



Worked Example 22.1

Question: A ligand of MW 2 kDa is bound noncovalently to a receptor via a lock-and-key type bond of length $r_0 = 1$ nm and energy $w_0 = -35$ kT at 37°C (body temperature). What pulling force will be needed to detach the ligand within ~ 1 s?

Answer: The mean velocity of the ligand is given by relating the ligand’s kinetic energy to the thermal energy: $\frac{1}{2}mv^2 = \frac{1}{2}kT$. For a ligand of MW = 2,000 Da, its mass is $m = 3.3 \times 10^{-24}$ kg. At 37°C ($T = 310$ K) its mean velocity is therefore $v = 36$ m/s, giving a mean collision time of $\tau_0 = r_0/v = 2.8 \times 10^{-11}$ s, and a mean natural bond lifetime of $t_0 = \tau_0 e^{-w_0/kT} = \tau_0 e^{35} = 4.4 \times 10^4$ s

²Strictly, τ_0 is not a constant but fluctuates due to thermal (Brownian) motion—that is, it is the velocity or kinetic energy of the ligand that is continually changing, according to the Boltzmann distribution, until it is high enough to overcome the activation barrier $w_0 - Fr_0$ (see Worked Example 9.1).

(about 12 hours³). To reduce the bond lifetime to $t = 1.0\text{ s}$ will require a force of $F = (kT/r_0)\ln(t_0/t) = (kT/r_0)\ln(4.4 \times 10^4/1.0) = 4.6 \times 10^{-11}\text{ N} = 46\text{ pN}$.

³Finite viscosity effects will slow down the collision rate and extend the natural lifetime from this value.



While the Bell equation nicely captures the underlying physics of forced bond rupture, it assumes an unrealistically simple energy-distance profile with only one energy minimum rather than the complex 3D energy landscape with multiple energy minima and maxima that is more characteristic of L-R bonds. Evans and Ritchie (1997) and Isailev et al., (1998) extended the Bell approach to include more complex energy landscapes; they also considered viscous dissipation which further affects the lifetimes of bonds.

The Bell model, and its later refinements, shows that the bond rupture force is not an equilibrium or time-independent value but depends on the intrinsic lifetime of the bond and the temperature.⁴ The faster we want to separate two molecules or particles, the larger the force we need to apply and the more work we need to do on (or energy we need to supply to) the system. Another way of looking at this is that the faster or more rapidly we move two particles apart, the *more attractive* the interaction appears, or the greater is the apparent energy barrier needed for the separation.

Equation (22.1) is quite general and applies to the rupture of covalent and noncovalent bonds, to L-R bonds, molecules, particles, and so on. It also applies to the binding or “capture” of molecules, to be discussed further below, where in this case the more rapidly the two molecules or particles approach or collide with each other the *less attractive* (or *more repulsive*) does the interaction appear. Figure 21.1 illustrates the generality of this effect, showing the effective (measured) forces at increasing rates of approach or separation.⁵ Indeed, the overall trend applies not only to molecular forces but to all types of interactions, including frictional, viscous, and hydrodynamic forces. Thus, whenever there is continuous motion in a system, as in a living biological system, the steady-state forces are different from the equilibrium (static or quasi-static forces), and maintaining steady-state conditions requires a constant supply of energy to overcome these forces.⁶

The Jarzynski equation. One may still ask how or whether a dynamic interaction or process can be unambiguously related to the equilibrium interaction potential w_0 . Now, Eq. (22.1) applies to a *single* detachment (or binding) event, giving the *most probable* adhesion force F or energy W needed for a given detachment time t or, conversely, the most probable detachment time for a given pulling force or input energy. Equation (22.1) shows that the work done W can take on any value, both larger and smaller than w_0 , accompanied by pull-out times t that are, respectively, smaller and larger than τ_0 .

⁴Note that the length of the bond also enters into the picture, which gives an additional length-dependent scaling to bond dynamics.

⁵Note that a larger repulsion on approach and a larger attraction on separation both involve an increase in the force in the direction opposing the motion (an example of Le Chatelier's Principle and of the requirement that the friction force and viscosity are always positive).

⁶Commonly referred to as nonconservation forces.

More interesting things happen when multiple detachments and attachments occur over a given time or repeatedly (cyclically as in a Carnot cycle), as well as when many bonds are broken simultaneously. In a ground-breaking paper, Jarzynski (1997a, 1997b) showed that when any one of these processes is repeated many times, n , the average of the *exponential* of the work done W is a constant and equal to the exponential of the thermodynamic work w_0 according to (cf. Eq. (22.1))

the Jarzynski equation:

$$\langle e^{W/kT} \rangle_{n \rightarrow \infty} \rightarrow e^{-w_0/kT} \quad (22.2)$$

which applies to both detachment (pull-off) and attachment (binding) processes, as well as full cycles.

The Jarzynski equation takes into account that fact that while for a single event—say, a pull-off—the work done will most likely be less than w_0 , when multiple pull-offs are performed on the same bond, there will always be some requiring greater work than w_0 (cf. Eq. (22.1)). For example, consider a multiple bond-rupture experiment involving three ruptures ($n = 3$), where the following values are obtained for W_n : 1.0, 3.0, 5.0. The average value is $\langle W \rangle = (1 + 3 + 5)/3 = 3.0$, but the average of $\langle e^{W/kT} \rangle$ is 57.1, which corresponds to $W = 4.0$. With such meager statistics we cannot say what the true value of w_0 is, except that it is more likely to be closer to 4.0 than the average value of 3.0.

The Jarzynski equation has been tested experimentally (Liphardt et al., 2002), but is not as useful experimentally as might be hoped: as pointed out by Lua and Grosberg (2005), the faster the measurements the larger will be the discrepancy between W_n and w_0 and, therefore, the greater the number of measurements n that need to be made to satisfy Eq. (22.2). If one has only a certain time to make measurements, it turns out that one is more likely to obtain the real value for w_0 by making one slow measurement than many fast measurements.

The Jarzynski and Bell equations have further implications for measurements of pull-off times or rates. Thus, on combining Eqs. (22.1) and (22.2), we immediately find that

$$\tau_0 = 1/\langle 1/t \rangle \quad (22.3)$$

which gives the natural vibration or collision time of the interacting groups τ_0 from measurements of the pull-off times t , which are on average much longer than τ_0 . As in the case of the work done, the correct value is again obtained because of the way the averaging skews the results toward shorter times, as illustrated in Worked Example 22.2.



Worked Example 22.2

Question: A single pull-off measurement of a macromolecule from a membrane, when subjected to a given pulling force, is found to be $t = 10 \mu\text{s}$. Three more repeat measurements give the following distribution times:⁷ 1, 10, and $100 \mu\text{s}$. What is the likely molecular vibration or oscillation time of the molecule, τ_0 ?

Answer: The average or mean pull-off time for the four measurements is $\langle t \rangle = (1 + 10 + 10 + 100)/4 = 30$ ms. However, to get t_0 , we need to perform the averaging according to Eq. (22.3),—that is, $\tau_0 = 1/\langle 1/t \rangle = 1/[(1 + 1/10 + 1/10 + 1/100)/4] = 3.3$ s, which is the most likely value for τ_0 given the limited data available. Note how this value is much smaller than both the first and average values measured.

⁷Times, frequencies, and velocities usually have logarithmic (i.e., more spread out) distributions (e.g., 1, 10, 100 Hz) compared with energies that tend to have arithmetic (i.e., more closely spaced) linear distributions (e.g., 1ϵ , 2ϵ , 3ϵ , 4ϵ , ...).

22.4 Multiple Bonds in Series and in Parallel

When a junction that consists of many L-R bonds breaks—for example, when a leukocyte cell detaches from the wall of a blood vessel (Figure 22.2)—many bonds are involved in both the attachment and detachment processes. These bonds can be “in parallel” (next to each other, like a zipper) or “in series” (on top of each other, like the links of a chain). As might be expected intuitively, the lifetime of a junction with bonds in parallel will be longer than given by the Bell equation, Eq. (22.1), which applies to the breaking of a single bond. This is because for the junction to rupture all the bonds must break at about the same time. Conversely, the lifetime of a junction consisting of bonds in series will be shorter than given by Eq. (22.1), since now the whole junction will open as soon as any one (normally the weakest) of the bonds breaks. We will now consider the two types of multiple bonds in turn.

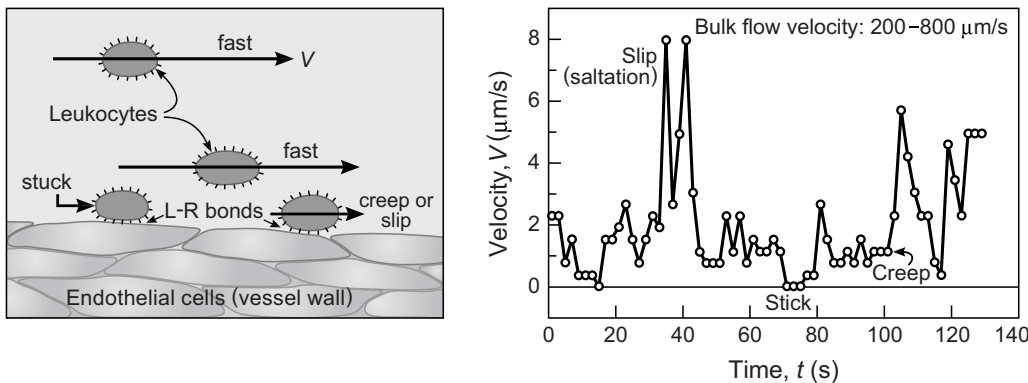


FIGURE 22.2 An example of an ongoing biological process that is increasingly being understood in terms of models that have been successfully applied to stick-slip friction phenomena (Chapter 18). “Leukocyte rolling” along the endothelium *in vitro* (left) involves sticking ($V = 0$), “rolling” or “creep” ($V \approx 1 \mu\text{m/s}$), stick-slip or saltation ($V \approx 5 \mu\text{m/s}$), and free or bulk flow ($V = 200 – 800 \mu\text{m/s}$). Each rolling process involves many mobile molecules, known as selectins, on both surfaces that interact via ligand-receptor bonds that in turn form and break in a complex yet well-orchestrated way. [Adapted from Goetz *et al.*, 1994.]

Bonds in Series

Consider two bonds ($N = 2$) subjected a pulling force F , where the mean lifetime t_N of each bond is $t_{N=1} = 2.0$ and $t_{N=2} = 4.0$ sec, as given by Eq. (22.1). The probability that each will break during a given (short) time interval of, say, 1 sec is therefore $p_1 \approx 1/t_1 = 1/2.0 = 0.5$ and $p_2 \approx 1/t_2 = 1/4.0 \approx 0.25$, respectively, so that the probability that each bond is still intact—that is, not broken—is $(1 - p_1) = (1 - 0.5) = 0.5$ and $(1 - p_2) = (1 - 0.25) = 0.75$, respectively. If these two bonds are now linked together in series and subjected to the same force F , the probability that both are still intact after $t = 1$ sec is $(1 - p_1)(1 - p_2) = 0.5 \times 0.75 = 0.375$, so that the probability of rupture of the 2-link chain or junction is $t[1 - (1 - p_1)(1 - p_2)] = (1 - 0.375) = 0.625$, which, as expected, is higher than that of the weakest link. The mean lifetime of the junction is $1/0.625 = 1.6$ sec, which is shorter than either of the individual bonds. This analysis can be readily extended to N links or bonds in series (Saterbak, 1996). As $N \rightarrow \infty$ the probability of rupture goes to 1.0 and the lifetime of the junction therefore goes to zero (the natural collision time τ_0 or inverse vibration time $1/\nu_0$).

The preceding scenario was confirmed by shear flow detachment measurements of the strength of linkages between beads linked by L-R (antibody-antigen) bonds in series (Saterbak, 1996), where the average rupture force was found to be 2–10 times smaller than the strength of the weakest bond in the chain in agreement with the predicted behavior.

The Bell equation has interesting and unintuitive consequences for the way we should think about the meaning of “the weakest link” in a chain or, more generally, in the way different bonds compete for rupture (or binding). Equation (22.1) shows that the force to rupture a bond depends on the time to rupture. Thus, high pulling forces generally (but not always) lead to short rupture times according to

$$t \rightarrow \tau_0 \text{ as } F \rightarrow w_0/r_0; \quad (22.4)$$

that is, the detachment or adhesion force is given by the slope of the energy-distance curve, which is the classical or mechanistic force first discussed in Section 1.7. At the other extreme of weak forces, the rupture time approaches the natural lifetime of the bond—that is,

$$t \rightarrow \tau_0 e^{-w_0/kT} = t_0 \text{ as } F \rightarrow 0 \quad (22.5)$$

where quite different parameters now determine the relationship between F and t —for example, the energy rather than the slope of the energy.

Thus, when a junction held by a number of different bonds in series is subjected to a pulling force F , the bond that actually breaks (or breaks first) may be different depending on the magnitude of F . For example, if there are two bonds in series, the one with the lowest energy w_0 will break first when the pulling force is low or zero, whereas the bond with the lowest slope w_0/r_0 will break when the pulling force exceeds a certain value (cf. Evans and Ritchie, 1999, and Problem 22.1 (iii)).

A more complex situation involves the adhesion of two dissimilar membrane-coated particles that are connected by tethers, as shown in Figure 22.3. There are now four possibilities for how and where rupture could occur when the particles are pulled apart: at the ligand-protein L-R bonds, at the lipid-protein L-R bonds, at the lipid-membrane

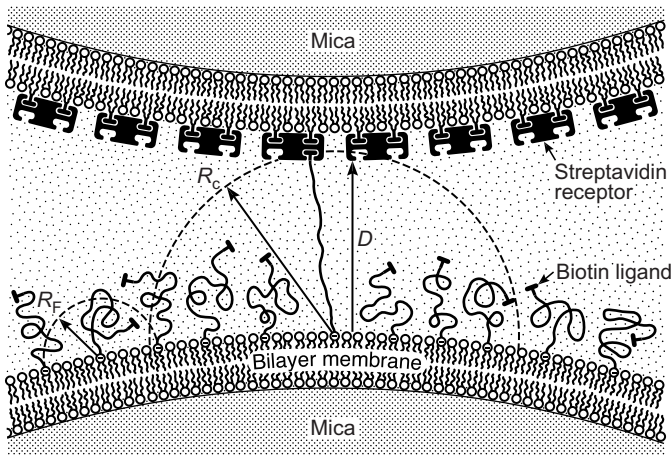


FIGURE 22.3 The probability of a successful binding of a tethered ligand to a receptor at a large distance away (the capture distance, R_c) increases with the waiting time and depends more on the dynamics of the tether (polymer dynamics) than the L-R bond energy. As in the reverse case of separation or pull-out (Figure 9.2), capture depends on a statistically rare event. The statistics of the whole process involves not only the L-R binding energies, but also the dynamic spatial distribution and 3D diffusion of both the ligand and receptor molecules, and also the shapes and relative motion of the two surfaces. [Adapted from Wong et al., 1997, and Jeppesen et al., 2001.]

bonds of the top surface (involving lipid pullout), and at the lipid-membrane bonds of the bottom surface. Such a system was studied experimentally by Leckband et al., (1995), who used an SFA to measure the strength of the adhesion forces and identify the failure mechanism when two supported lipid bilayers linked by biotin-streptavidin L-R bonds were separated. In this system, when the membranes are separated, adhesive failure can occur either at the L-R bonds on either side of the protein or via lipid pull-out from the membranes. Experiments with a series of biotin analogs having different streptavidin affinities showed that the bonds with the lowest rupture *force*, estimated using Eq. (22.1), rather than the lowest *energy*, failed first.

Figure 22.3 further illustrates the equally subtle dynamic effects that determine the attachment or capture mechanisms of two bonds, as well as of whole adhesion junctions consisting of multiple bonds. For the single bond case shown, the probability of binding is again statistical and depends on the likelihood that, over a given time period, the ligand gets sufficiently close to the receptor pocket to bind to it (here defined by the capture distance R_c), which depends on how close the two surfaces approach each other during that time, D , and the spatial sampling rate or diffusion rates of the tethered ligands and protein receptors.

Bonds in Parallel

Multiple bonds in parallel occur at cell-substrate and cell-cell adhesion junctions such as those shown in Figures 22.2 and 22.3 when multiple tethers bridge the two surfaces. The rapture of a chain consisting of N bonds in series occurs when the first link is broken; the

rapture of an adhesive junction consisting of N bonds in parallel (N independent links) occurs when the last link is broken.

Returning to the numerical example of two bonds where the probability that each will break during a given time interval of 1 sec is $p_1 = 0.5$ and $p_2 = 0.25$, the probability that a junction consisting of these two bonds in parallel will open in 1 sec is simply $p_1 p_2 = 0.125$ —that is, it is *less* likely than the rupture of the *strongest* bond. This may be compared with the probability of rupture when the bonds are in series of 0.625, which, as previously discussed, is *more* likely than that of the *weakest* bond.

When more realistic values are used, the quantitative differences between bonds in series and in parallel, and the importance of the number of bonds N or surface coverage Γ become more starkly apparent. Since bond lifetimes are proportional to $e^{-w_0/kT}$, where w_0 can be many kT , the probabilities p_N are usually very much smaller than 1—for example, 10^{-8} or less—so that two or three bonds acting together can change a short-lived association to a long-lived complex. For example, if the vibration time of a typical H-bond of strength $w_0 = -10 kT$ is $\tau_0 = 10^{-12}$ s, the natural lifetime of the bond will be $t_1 = \tau_0 e^{-w_0/kT} = 2.2 \times 10^{-8}$ s. The lifetime of two bonds (in parallel) will be $10^{-12} \times e^{20} \approx 5 \times 10^{-4}$ s, while three H-bonds will have a lifetime of $10^{-12} \times e^{30} \approx 11$ s. These values are, respectively, 22,000 and 500 million times longer due to a mere twofold and threefold increase of the number of H-bonds.⁸ Such H-bonds typically appear as DOPA groups and sugar rings and explain the high affinities (often coupled to a high geometric specificity) of polysaccharide groups.

In general, for N independent bonds or links, the probability of rupture is $p_1 p_2 p_3 \dots p_N$, which tends to zero for large N . Such junctions will be long-lived, and the total rupture force NF will be (relatively) low when F is determined by the energy w_0 of the bonds according to Eqs. (22.1) and (22.5). In contrast, if a high force is applied rapidly, the force F will be determined by the slope according to Eq. (22.4), which is generally significantly higher than that given by Eq. (22.1). Thus, unless we take note of the role of time to rupture we can encounter unexpected or unintuitive situations where a weak force opens a junction (eventually), but a much larger force does not (at least not immediately). Such effects have been observed in experiments on cell-substrate adhesion where the adhesion force appears to increase the greater the pulling force (Marshall et al., 2003).

The above analysis gives the correct trends but is quantitatively oversimplistic, giving an upper bound to the probability of rupture. This is because during the time interval specified, individual bonds in parallel can reform after they break before the other bonds break, —that is, before the whole junction breaks (Vijayendran, 1998; Seifert, 2000). In addition, in practice, soft biological or membranous junctions detach by deforming and *peeling* away from the edges, as described by the JKR theory in Chapter 17. In such

⁸Although, as mentioned two paragraphs later, if the two bonds are spaced well apart on fluid surfaces, or the detachment involves a peeling motion, or the separation involves two plane parallel rigid surfaces, the lifetimes could be much shorter or longer. The way surfaces deform always plays a critical role in adhesion phenomena (see Figure 17.2).

situations the junction adhesion force is given by Eq. (17.37): $F_{\text{ad}} = 3\pi RW$, where $W = \Gamma w_0$ where $\Gamma = (N/\text{area})$ is the number of bonds per unit area (the surface coverage of bonds). However, for high pulling forces that are applied rapidly F_{ad} will now be determined by the slope, w_0/r_0 , as described above (see also Figure 17.2 and Worked Example 17.8 in Section 17.8 on adhesion hysteresis).

22.5 Detachment versus Capture Processes: Biological Importance of “Rare Events”

Quite often the forces and dynamics involved in biological capture are very different from those involved in detachment. Some of these are illustrated in Figure 22.3, which shows the binding of tethered ligands to receptor molecules on an opposing membrane. As already discussed, both the attachment (capture) and detachment (rupture) rates depend not only on the binding energy w_0 but also on the translational (transporting) and diffusive motions of the various particles, molecules and molecular subgroups involved in the interaction. Figure 22.3 highlights another important feature of biological interactions: the crucial role of “rare events.” The capture of the “target” molecule or particle to which the biotin ligand is attached is a rare event in the random Brownian path of the ligand, but it is the event of importance—the one that decides when and where the two membranes will bind to each other rather than pass by each other. The same concept applies to rare unbinding events that, like β -decay where an electron is ejected once every $\sim 10^{17}$ oscillations, they are the events of importance—the ones that matter, the ones that will go on to immobilize a large particle or switch on or turn off the immune response. Analyzing such events requires statistical methods because mean-field theories do not easily capture rare, out of the ordinary, occurrences that are statistically highly improbable.

22.6 Dynamic Interactions between Biological Membranes and Biosurfaces

Role of membrane fluidity. The fluidity of biological membranes allows for lateral rearrangements of proteins and lipids on and within the membranes that can alter the local composition and geometry and in turn affect the intersurface forces. For example, strong specific adhesion will drive ligands and receptors to accumulate at domains and membrane adhesion junctions (see Figure 21.15), leaving a low density of nonadhering species—for example, lipids, outside the contact region (Noppl-Simson and Needham, 1996). Such lateral desegregation or demixing effects can significantly enhance the surface adhesion energy W over the mean value (in the absence of demixing) and, in turn, the overall adhesion energy of, say, a vesicle and a plasma membrane. This effect is in addition to the enhanced adhesion due to the finite elastic modulus and deformed flattened area of adhering vesicles, discussed in Section 21.9.

However, for desegregation to occur requires time, which is determined by the lateral diffusion coefficients of the interacting species in the planes of the membranes and the

out-of-plane diffusion coefficients of the ligands away from the surfaces (cf. Figure 22.3). The former depends on the phase state of the lipids in the bilayer—that is, whether in the fluid, gel or frozen states. Leckband et al., (1994) used an SFA to measure the binding of lipidated biotin bilayers with lipidated streptavidin bilayers whose fluidities were controlled by raising or lowering the temperature above or below the chain melting temperature T_m of the lipids. At 25°C ($T < T_m$) the molecules could not diffuse to their binding partners on the opposite surface; the number of bonds formed was low, and the measured adhesion energy was only $W = 0.6 \text{ mJ/m}^2$. When the temperature was increased above T_m , the molecules could diffuse laterally on the fluid membranes and bind to their cognate receptors on the opposite surface, leading to a 10-fold higher adhesion energy of $\sim 6 \text{ mJ/m}^2$ for the same contact time. This trend of a sharply increasing adhesion with temperature is particularly interesting because increasing the temperature usually decreases adhesion.

Time-dependent demixing effects on adhesion have also been studied using RICM: Albersdörfor and colleagues (1997) followed the time-dependent changes in the adhesion of giant vesicles containing biotinilated lipids and supported bilayers consisting of a mixture of lipids with headgroups of streptavidin and bulky PEO (known as PEGolated lipids). The former headgroups are attracted to biotin, and the latter are repelled. The contact areas were observed to gradually grow in size as streptavidin and biotin accumulated there while squeezing out the lipids from the “tight” adhesive junctions. Such experiments further demonstrate how attractive and repulsive forces between different membrane components can produce laterally segregated domains, either on single membranes or at membrane-membrane junctions (cf. Section 20.10 and Figure 20.11) that presumably have different biological functions.



Worked Example 22.3

Question: A vesicle of radius $R = 0.1 \mu\text{m}$ is made up of a fluid lipid bilayer containing DMPC lipids doped with a fraction $X = 0.005$ (0.5%) of biotinilated lipid, both lipids occupying the same surface area of $a_0 = 0.60 \text{ nm}^2$. The vesicle approaches a planar cell membrane containing a low density of streptavidin molecules, each occupying an area of 20 nm^2 , and exposing two binding sites for biotin each of binding energy $35 kT$. If the lipids and proteins can diffuse freely in their bilayers, and if the vesicle can deform (flatten) elastically as it adheres to and spreads on the planar membrane up to a certain stress before it ruptures (cf. Section 21.9 and Figure 21.13), describe how this specific interaction differs from that of the nonspecific vesicle-vesicle and vesicle-substrate interactions discussed in Sections 21.9 and 21.10.

Answer: Once the first few L-R bonds have formed, biotinilated lipids and streptavidin will slowly diffuse into the contact junction, increasing the surface energy as each new L-R bond is formed. This “site-specific” surface energy, W_0 , corresponds to the situation where the streptavidin receptors at the junction are close packed and where each binds to two biotin ligands on the vesicle surface. Thus, $W_0 = 2 \times 35 \times (4.2 \times 10^{-21})/20 \times 10^{-18} = 15 \text{ mJ/m}^2$. It is worth noting that this energy is much greater than the van der Waals energy of $W_0 = 2 \gamma_i \approx 0.1\text{--}1.0 \text{ mJ/m}^2$ (Figure 21.8) but much less than that of a hydrocarbon-water interface ($W_0 = 2 \gamma_i \approx 100 \text{ mJ/m}^2$). However, the constraints of site-specific binding—where the binding energy

depends on the number of ligands and receptors available rather than the area—means that one cannot simply plug this surface energy into equations derived for nonspecific interactions. Thus, once all the biotin ligands of the vesicle have accumulated at the flattened contact junction, the density of L-R bonds in the junction will have “saturated” and the surface energy will stop increasing. At saturation, the area occupied by each biotin in the junction—the site binding area—is $a_{\text{site}} = 10 \text{ nm}^2$, and since there are $(4\pi R^2/a_0)X$ biotins per vesicle, the maximum flattened area will therefore be $(4\pi R^2/a_0)Xa_{\text{site}}$. Now, the maximum area increase that a vesicle can take before it ruptures is typically a few percent of the unstressed area (Section 21.9) which corresponds to a flattened area (not the *increased* area) that is typically a fraction $f \sim 0.2$ (~20%) of the original vesicle area of $4\pi R^2$. Thus, the maximum fraction of biotin lipids that the vesicle can have to avoid rupture when it adheres to the planar membrane is given by $(4\pi R^2)Xa_{\text{site}}/a_0 < (4\pi R^2)f$, or

$$X_{\max} = fa_0/a_{\text{site}} \approx 0.2 \times 0.6/10 = 0.012 \text{ or } 1.2\%. \quad (22.6)$$

Thus, for $R = 0.1 \mu\text{m}$ and $X = 0.005$, we may expect the total adhesion energy of the junction to be (cf. Eq. 21.18b): $W_{\text{ad}} \approx 35(4\pi R^2/a_0)X kT = 3.7 \times 10^4 kT = 1.5 \times 10^{-16} \text{ J}$, while the adhesion force should still be given by $F_{\text{ad}} \approx 2\pi RW_0 = 10 \text{ nN}$.⁹

⁹As long as the deformed vesicle retains the shape of a truncated sphere. Otherwise the pull-off force is lower, the lower bound being $2\pi rW_0$, where r is the radius of the contact junction.



The interactions in Worked Example 22.3 all depend on the ability of the interacting molecules and groups to diffuse both normally and laterally, and both within and outside, adhesion junctions, and on the rates of the different diffusion processes. Figure 22.4 illustrates some of the very different scenarios that can arise on approach (binding, capture) and separation (unbinding, detachment) of membrane-bound molecules depending on the rates of approach and separation.

Biological cells have clearly developed means for controlling different interaction forces over different distance- and time-regimes. For example, a transient change in the local pH or calcium ion concentration at a membrane surface could modify the *long-ranged* electrostatic interaction but not the *short-range* ligand-receptor interaction, or a change in the receptor binding site could alter the short-range force but not the long-range double-layer force. A change in the local fluidity could alter the diffusion rates of a tethered ligand and thereby prevent or enhance its probability of capture over a given time window. Changes in membrane fluidity also regulate the opening and relaxation kinetics of ion channels in neurons. Living systems clearly make full use of all of these subtle effects in their control and modulation of complex processes.

22.7 Self-Assembly versus Directed Assembly: Dynamic Phases and Tunable Materials

There are two basic kinds of molecular assembly processes. First, there is the assembly of molecules into clusters or nanoparticles, or even large colloidal aggregates, that occurs

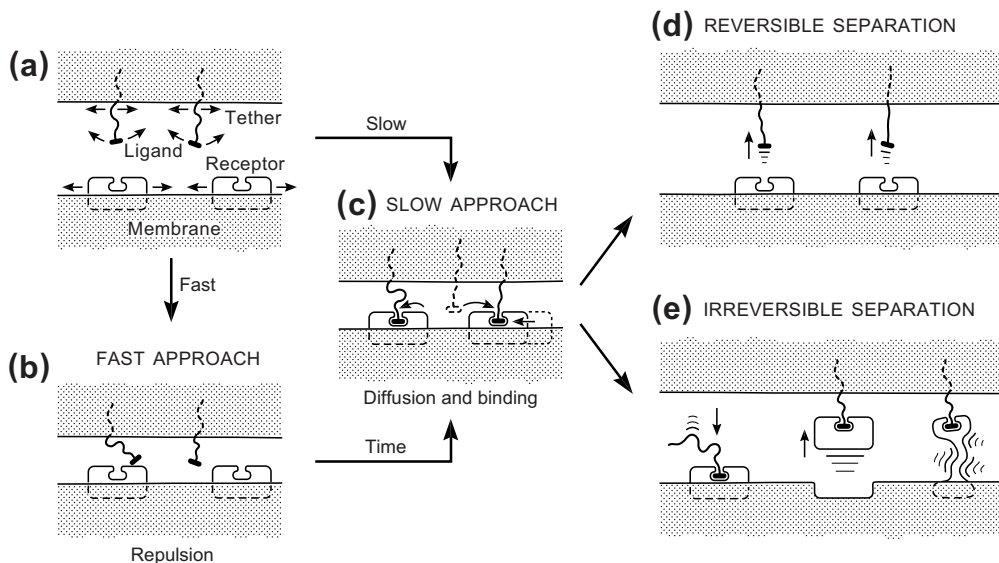


FIGURE 22.4 Examples of molecular binding, transfer and unfolding interactions between membranes. On fast approach (a → b) there is an additional kinetic force barrier because the ligand does not have time to find the binding site until some finite time after the surfaces have been close together (b → c). On separation (c → d, e), depending on the relative bond energies, bond lengths, and rate of separation, the original ligand-receptor bonds may break (d), or lipid molecules may be pulled out of the membrane, or the receptor molecules may be pulled out (cf. Harpooning Effect), or the protein may unfold (e), as in Figure 21.14. Other scenarios are also possible, including statistical combinations of the above.

spontaneously, which is referred to as *self-assembly*. Then there are energy-requiring (external field-driven) processes¹⁰ that lead to long-lived metastable or steady-state structures that are not necessarily the thermodynamically most favored structures or true equilibrium state, which is referred to as *directed-* or *engineered-assembly*. Some of the critical issues that distinguish these two basic processes, including slowly changing and fluctuating structures, have already been discussed in this chapter and in earlier chapters and sections on nonequilibrium interactions.

Biological structures are, in general, not in the equilibrium state. Unfortunately, unlike thermodynamics, nonequilibrium structures and processes have no fundamental equations, similar to the Laws of Thermodynamics, that can predict which structure will be formed even when the type and rate of the energy input is well-specified, although certain “master equations” have been proposed (Schnakenberg, 1976; Bier and van Roij, 2007). Various types of “dynamic phase diagrams” have been presented where the different types of steady-state structures or “dynamic phases” and dynamic phase transitions of a system are displayed on a phase diagram where, for example, the temperature or pressure is plotted against the flow rate or rate of energy supplied to the system.

¹⁰For example, in the form of mechanical work (pressure or flow), heat, light, electric, magnetic or chemical energy.

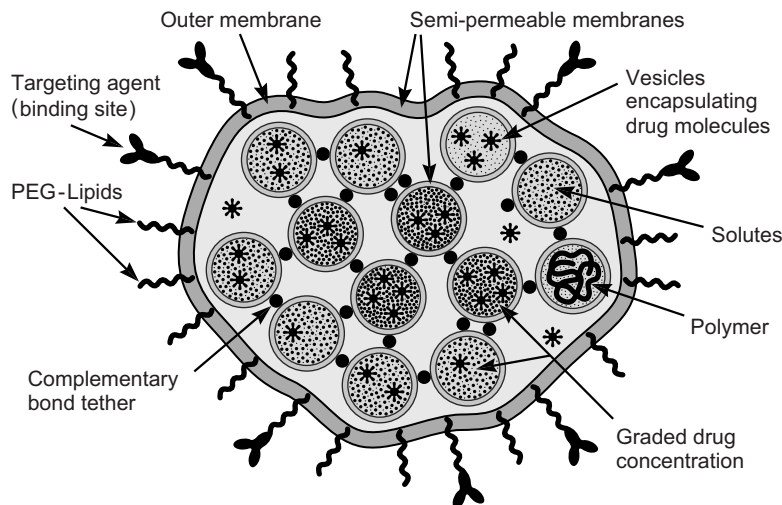


FIGURE 22.5 Schematic of a biomimetic cell-like structure that can be produced by *directed-assembly*, rather than *self-assembly*, for biomedical applications such as drug-delivery (Kisak et al., 2004). See also Figure 21.13 (right side) where a soft nano-structured material has been produced by directed assembly using biospecific bonds. Such structures/materials can be made to have tunable properties.

Steady-state structures can be the same as the equilibrium structures but obtained under different experimental conditions. Or they can be totally different, with no equilibrium equivalent—for example, an equilibrium lamellar phase changing to an ordered micellar or hexagonal phase (Figure 20.8) when sheared.

Highly complex structures and assemblies, such as the one shown in Figure 22.5, can be produced only by a combination of self- and directed- assembly processes, often requiring a number of stages. Such structures, like the biological structures they mimic, can be reversibly “tuned” by modulating the forces within and/or between the structures during use—for example, by applying light of different wavelengths to reversibly photoisomerize the constituent molecules. Such complex fluid materials are currently referred to as “smart,” “tunable,” “switchable,” “responsive,” and/or “adaptable.”

22.8 Motor Proteins, Transport Proteins, and Protein Engines

It is curious that nature did not invent, or at least has made little use of, the wheel.¹¹ Linear motion, however, is common and occurs when “cargos” or molecules such as kinesins are transported along microtubules and when actin filaments grow and push against surfaces (Figure 22.6).

¹¹To the author’s knowledge, there are only three cases of pure rotation in the animal kingdom.

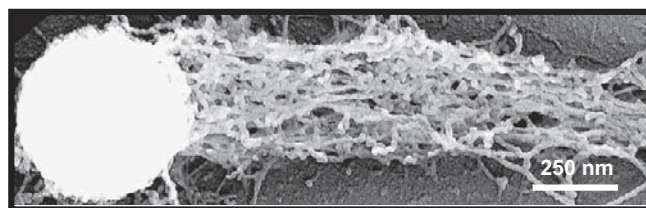


FIGURE 22.6 Actin, an example of a motor protein. A bead containing actin-polymerizing agents on its surface is driven by the actin filaments it polymerizes, leaving behind an actin network. This is the way many cells change their shape, by having the actin filaments push against the membrane, allowing the cell to move along certain directions or engulf nutrients or foreign bodies (phagocytosis). Microtubules, composed of the protein tubulin, function in a similar way, and both actin filaments (bundles) and microtubules can push, pull, or shuttle particles or “cargos” along them, giving rise to “cellular streaming.” [*Image from Plastino et al., 2004.*]

The mechanism by which chemical energy is converted to mechanical work and motion (based on the reaction: $\text{ATP} \rightarrow \text{ADP} + \text{energy}$) is currently not fully understood. Are transport mechanisms essentially the same as pushing mechanisms? Is there a single underlying physico-chemical mechanism for all, or are there many different specialized ones? In the case of growth and pushing, the “Brownian ratchet” or “Brownian motor” model has been proposed that appears to satisfactorily explain the generation of a steady repulsive force. In this model (Peskin et al., 1993) monomers of a janus protein AB (e.g., actin, tubulin) in solution bind to each other vectorially in the presence of ATP to form an actin or microtubule filament, AB–AB–AB–AB–AB– If the filament is already pressed against the surface of a membrane or particle, as in Figure 22.6, the rate of insertion of AB monomers between the particle and the filament is determined by the rate at which the gap between them opens and closes—that is, on the rate of Brownian motion.

Models for transport are usually somewhat different, depending on whether a molecule or cargo is being moved through a medium—for example, the cytoplasm (Howard, 2001)—or through/across a membrane. These models include transport in vesicles, kinesin-type motors, osmotic pressure-driven transport, and electrochemically driven reactions across membranes (see Problems 22.3–22.5).

PROBLEMS AND DISCUSSION TOPICS

- 22.1** A small fibrous α -helical protein has a total hydrophobic length of $r_0 = 15 \text{ \AA}$ that penetrates into a fluid bilayer membrane. The molecule is composed of 20 identical hydrophobic units or segments along its backbone where each unit has a free energy of transfer into water of $\epsilon = -0.5 \times 10^{-20} \text{ J}$. Sketch the interaction potential (energy *versus* distance) for this system as the hydrophilic end of the molecule is pulled out normally from the membrane. The molecule has a natural vibrational frequency in the membrane of $\nu_0 = 1/\tau_0 = 10^8 \text{ s}^{-1}$. Plot the mean time

for detachment t as a function of the applied force f on the molecule. Plot t in units of seconds versus f in units of pN and think carefully about how best to present the different axes (on linear or log scales). Using your plot, estimate the following at $T = 25^\circ\text{C}$:

- (i) The mean lifetime τ_0 of the molecule inside the membrane before it spontaneously hops out into the aqueous phase.
- (ii) The force f_0 needed to rapidly detach the molecule from the membrane. What additional information is needed to calculate the force needed to detach the molecule faster than 10^{-8} s?
- (iii) The hydrophilic end of the protein is replaced by a ligand that is attached to a receptor where the ligand-receptor (L-R) bond length and energy are 5 \AA and $15 kT$, respectively. At what pulling force on the receptor will the probably of breakage at the L-R and protein-membrane sites be equal and what will this time be? [Answer: (i) ~360 s. (ii) ~67 pN. (iii) ~38 pN at $t \sim 0.4 \text{ ms}$.]

22.2 A globular, water-soluble protein has surface residues consisting mainly of Asp, Glu, His, and Ser. (i) Would you expect the folding rate of the protein to increase or decrease at higher pH? (ii) If the protein is also involved in a specific (receptor-ligand type) binding interaction involving a hydrophobic pocket on the protein, how would you expect the on-rate k_{on} , off-rate k_{off} , and overall reaction constant K to be affected (increased or decreased) at the higher pH? [Hint: Check the charges on these AA residues. Draw figures of the net interaction potential to see how the increased double-layer repulsion modifies the net interaction at long and short range.] [Answer: (i) Decreased folding rate. (ii) Decrease, increase, decrease.]

22.3* A hydrophilic polypeptide with 100 quasi-spherical AA groups fits snuggly through hydrophilic pores spanning a cell membrane of thickness 5 nm. Initially, all the polypeptide molecules are outside the cell. The cytoplasm inside the cell contains molecules that are too bulky to pass through the pores, and which readily combine with the AA residues to form long-lived complexes. The diameter of each AA group is 2.5 nm. (i) Estimate the rate (speed) at which the polypeptide moves through the membrane into the cytoplasm, and the time for the transfer. (ii) If the complexes have a short lifetime, comparable to or less than the transfer time, how will this affect the transfer time? (iii) Since no energy—for example, ATP—is used to continually transport molecules into the cell, this system appears to be a thermodynamically impermissible perpetual motion machine. Explain why this is not the case. [Hint: Use the 1D diffusion equation and estimate the 1D diffusion coefficient assuming that the local viscosity around the polypeptide, including the pore, is the same as that of water.]

22.4* In Problem 22.3 the hydrophilic polypeptide consists of negatively charged amino acid groups. There are no specific binding groups in the cytoplasm—that is, the solution is “symmetric” on either side of the membrane, but now the membrane is asymmetric: the outer surface having a higher negative surface charge density σ

than the inner. Sketch the shape of the electrostatic double-layer interaction energy as the polypeptide traverses the membrane. Will this force drive the polypeptide molecules into or out of the cell? If so, by how much, or will it stabilize them partially through the membrane, or will it have no driving effect? Assume that the polypeptide carries its counterions as it traverses the membrane, but consider two possible scenarios for the counterions of the membrane's double-layers: (i) No double-layer counterions ever cross the membrane, so that there is a finite potential difference between the inner and outer bulk solutions (which may be assumed to behave as infinite reservoirs), and (ii) the counterions of the inner and outer double-layers have equilibrated across the membrane so that there is no net potential difference between the inner and outer bulk solutions.

- 22.5** What's wrong with the following explanations: (1) A *Brownian ratchet* along an actin filament, a microtubule, or a plane surface is generated by a skewed sawtooth potential energy profile, with a vertical 90° wall followed by a 45° slope down to the next energy minimum. When thermally activated molecules are kicked up from any one of the minima, they fall back equally on either side of the wall. Thus, about half of the molecules end up falling down the slope to the next well, while the other half end up in the same well. This process repeats itself each time a molecule experiences a Brownian kick. In this way the molecules are moved continuously in one direction driven solely by Brownian motion—that is, without any input of energy. (2) A *protein pump* in a lipid bilayer membrane has a hydrophilic channel through its center that allows ions to diffuse freely between the two aqueous spaces. One of the channel openings is negatively charged. Thus, anions from the solution on that side will be repelled from this opening while cations will be attracted to it. The rate of cation diffusion through the channel from this opening will therefore exceed that of the anions, while the rates in the opposite direction will be the same, since the other opening is not charged. Thus, cations will be pumped through the membrane in one direction, again without the need for any input of energy.

This page intentionally left blank



References

- Abillon, O., & Perez, E. (1990). Swollen lamellar phases between 2 solid walls: undulation forces and generation of defects. *Journal of Physics*, 51(22), 2543–2556.
- Adam, N. K., & Stevenson, D. G. (1953). Detergent Action. *Endeavour*, 12(45), 25–32.
- Adamson, A. W. (1976). *Physical chemistry of surfaces* (3rd ed.). New York: Wiley.
- Adamson, A. W. (1990). *Physical chemistry of surfaces*. New York: Wiley.
- Akulbulut, M., Godfrey Alig, A. R., & Israelachvili, J. (2007). Triboelectrification between smooth metal surfaces coated with self-assembled monolayers (SAMs). *Journal of Physical Chemistry B*, 110(44), 22271–22278.
- Akhmatov, A. S. (1966). *Molecular physics of boundary friction*. Jerusalem, Israel: Wiener Bindery Ltd. Israel Program for Scientific Translations, S. Monson.
- Albersdörfer, A., Feder, T., & Sackmann, E. (1997). Adhesion-induced domain formation by interplay of long-range repulsion and short-range attraction force: a model membrane study. *Biophysical Journal*, 73(1), 245–257.
- Alder, B. J., Hoover, H. G., & Young, D. A. (1968). Studies in molecular dynamics. V. High-density equation of state and entropy for hard disks and spheres. *Journal of Chemical Physics*, 49(8), 3688–3696.
- Allen, M. P., & Tildesley, D. J. (1987). *Computer simulations of liquids*. New York: Clarendon Press.
- Amis, E. S. (1975). Solutions and solubilities. *Solutions and solubilities*. New York: Wiley.
- Anderson, T. H., Donaldson, S. H., Zeng, H., & Israelachvili, J. N. (2010). Direct measurement of double-layer, van der Waals and polymer depletion attraction forces between supported cationic bilayers. *Langmuir*, 26(18), 14458–14465.
- Aniansson, E. A. G. (1978). Dynamics and structure of micelles and other amphiphile structures. *Journal of Physical Chemistry*, 82(26), 2805–2808.
- Aniansson, E. A. G., Wall, S. N., Almgren, M., Hoffmann, H., Kielmann, I., Ulbricht, W., et al. (1976). Theory of kinetics of micellar equilibria and quantitative interpretation of chemical relaxation studies of micellar solutions of ionic surfactants. *Journal of Physical Chemistry*, 80(9), 905–922.
- Argento, C., & French, R. H. (1996). Parametric tip model and force–distance relation for Hamaker constant determination from atomic force microscopy. *Journal of Applied Physics*, 80(11), 6081–6090.
- Ashkin, A. (1992). Forces of a single-beam gradient laser trap on a dielectric sphere in the ray optics regime. *Biophysical Journal*, 61(2), 569–582.
- Ashkin, A., Dziedzic, J. M., Bjorkholm, J. E., & Chu, S. (1986). Observation of a single-beam gradient force optical trap for dielectric particles. *Optics Letters*, 11(5), 288–290.
- Ashkin, A., Dziedzic, J. M., & Yamane, T. (1987). Optical trapping and manipulation of single cells using infrared laser beams. *Nature*, 330, 769–771.
- Aveyard, R., & Saleem, S. M. (1976). Interfacial-tensions at alkane-aqueous electrolyte interfaces. *Journal of the Chemical Society, Faraday Transactions I*, 73, 1609–1617.
- Bailey, S. M., Chiruvolu, S., Israelachvili, J. N., & Zasadzinski, J. A. N. (1990). Measurements of forces involved in vesicle adhesion using freeze-fracture electron microscopy. *Langmuir*, 6(7), 1326–1329.
- Ball, P. (1999). *H₂O – A biography of water*. Phoenix, London: Weidenfeld & Nicolson.
- Banerjee, A., Ferrante, J., & Smith, J. R. (1991). Adhesion at Metal Interfaces. In L. H. Lee (Ed.), *Fundamentals of adhesion* (pp. 325–348). New York: Plenum.

- Barnes, H. A., Hutton, J. F., & Walters, K. (1989). *An introduction to rheology*. Amsterdam: Elsevier.
- Bates, F. S., & Fredrickson, G. H. (1990). Block copolymer thermodynamics—theory and experiment. *Annual Review of Physical Chemistry*, 41, 525–557.
- Baumgart, T., Hess, S. T., & Webb, W. W. (2003). Imaging coexisting fluid domains in biomembrane models coupling curvature and line tension. *Nature*, 425(6960), 821–824.
- Beattie, J. K. (2007). The intrinsic charge at the hydrophobe/water interface. In T. F. Tadros (Ed.), *Colloid stability*, 2 (pp. 153–164). Weinheim, Germany: Wiley.
- Becher, P. (1984). Hydrophile-lipophile balance: history and recent developments Langmuir lecture—1983. *Journal of Dispersion Science and Technology*, 5(1), 81–96.
- Bekiranov, S., Bruinsma, R., & Pincus, P. (1997). Solution behavior of polyethylene oxide in water as a function of temperature and pressure. *Physical Review E*, 55(1), 577–585.
- Bell, G. I. (1978). Models for the specific adhesion of cells to cells. *Science*, 200, 618–627.
- Ben Naim, A., Wilf, J., & Yaacobi, M. (1973). Hydrophobic interaction in light and heavy water. *Journal of Physical Chemistry*, 77(1), 95–102.
- Bergeron, V., & Radke, C. J. (1992). Equilibrium measurements of oscillatory disjoining pressures in aqueous foam films. *Langmuir*, 8(12), 3020–3026.
- Bergeron, V., & Radke, C. J. (1995). Disjoining pressure and stratification in asymmetric thin-liquid films. *Colloid and Polymer Science*, 273(2), 165–174.
- Bergström, L. (1997). Hamaker constants of inorganic materials. *Advances in Colloid and Interface Science*, 70, 125–169.
- Bergström, L., Meurk, A., Arwin, H., & Rowcliffe, D. J. (1996). Estimation of Hamaker constants of ceramic materials from optical data using Lifshitz theory. *Journal of the American Ceramic Society*, 79(2), 339–348.
- Bergström, P. A., Lindgren, J., & Kristiansson, O. (1991). An IR study of the hydration of perchlorate, nitrate, iodide, bromide, chloride and sulfate anions in aqueous solution. *The Journal of Physical Chemistry*, 95(22), 8575–8580.
- Berman, A., Drummond, C., & Israelechvili, J. (1998). Amontons' law at the molecular level. *Tribology Letters*, 4(2), 95–101.
- Bier, M., & van Roij, R. (2007). Relaxation dynamics in fluids of plate-like colloidal particles. *Physical Review E*, 76(2), 10.
- Biggs, S., & Mulvaney, P. (1994). Measurement of the forces between gold surfaces in water by atomic-force microscopy. *Journal of Chemical Physics*, 100(11), 8501–8505.
- Biggs, S., Prieve, D. C., & Dagastine, R. R. (2005). Direct comparison of atomic force microscopic and total internal reflection microscopic measurements in the presence of nonadsorbing polyelectrolytes. *Langmuir*, 21, 5421–5428.
- Binnig, G., & Rohrer, H. (1982). Scanning tunneling microscopy. *Helvetica Physica Acta*, 55(6), 726–735.
- Binnig, G., Quate, C. F., & Gerber, C. (1986). Atomic force microscopy. *Physical Review Letters*, 56, 930–933.
- Binnig, G., Rohrer, H., Gerber, C., & Weibel, E. (1982). Surface studies by scanning tunneling microscopy. *Physical Review Letters*, 49(1), 57.
- Blake, T. D. (1975). Investigation of equilibrium wetting films of n-alkanes on alpha-alumina. *Journal of the Chemical Society, Faraday Transactions I*, 71, 192–208.
- Blanckschtein, D., Thurston, G. M., & Benedek, G. B. (1986). Phenomenological theory of equilibrium thermodynamic properties and phase-separation of micellar solutions. *Journal of Chemical Physics*, 85(12), 7268–7288.
- Block, S. M. (1992). Making light work with optical tweezers. *Nature*, 360, 493–495.
- Bloomfield, V. A. (1991). Condensation of DNA by multivalent cations—considerations on mechanism. *Biopolymers*, 31(13), 1471–1481.
- Bockris, J. O. M., & Reddy, A. K. N. (1970). *Modern electrochemistry*. New York: Plenum.

- Bondi, A. (1968). *Physical properties of molecular crystals, liquids, and glasses*. New York: Wiley.
- Boni, L. T., Hah, J. S., Hui, S. W., Mukherjee, P., Ho, J. T., & Jung, C. Y. (1984). Aggregation and fusion of unilamellar vesicles by poly(ethylene glycol). *Biochimica et Biophysica Acta*, 775(3), 409–418.
- Borisov, O. V., & Halperin, A. (1995). Micelles of polysoaps. *Langmuir*, 11(8), 2911–2919.
- Bowden, F. P., & Tabor, D. (1939). Area of contact between stationary and between moving surfaces. *Proceedings of the Royal Society of London*, 169A, 391–413.
- Bradley, R. S. (1932). The cohesive force between solid surfaces and the surface energy of solids. *Philosophical Magazine Series*, 13(86), 853–862.
- Briscoe, B. J., & Evans, D. C. (1982). The shear properties of Langmuir Blodgett layers. *Proceedings of the Royal Society of London*, A380, 389–407.
- Brown, H. G., & Hoh, J. H. (1997). Entropic exclusion by neurofilament sidearms: a mechanism for maintaining interfilament spacing. *Biochemistry*, 36(49), 15035–15040.
- Buffat, P., & Borel, J. P. (1976). Size effect on melting temperature of gold particles. *Physical Review A*, 13(6), 2287–2298.
- Bustamante, C., Marko, J., & Siggia, E. (1994). Entropic elasticity of λ -phage DNA. *Science*, 265, 1599–1600.
- Cabane, B., Duplessix, R., & Zemb, T. (1985). High resolution neutron scattering on ionic surfactant micelles: SDS in water. *Journal de Physique*, 46, 2161–2178.
- Caffrey, M., & Bilderback, D. H. (1983). Real-time x-ray-diffraction using synchrotron radiation – system characterization and applications. *Nuclear Instruments and Methods in Physics Research*, 208(1–3), 495–501.
- Campbell, D., Pethrick, R. A., & White, J. R. (2000). *Polymer characterization: Physical techniques* (2nd ed.). Cheltenham, UK: Stanley Thornes Ltd.
- Carnie, S. L., & Chan, D. Y. C. (1993). Interaction free energy between plates with charge regulation: a linearized model. *Journal of Colloid and Interface Science*, 161, 260–264.
- Carnie, S., Israelachvili, J. N., & Pailthorpe, B. A. (1979). Lipid packing and transbilayer asymmetries of mixed lipid vesicles. *Biochimica et Biophysica Acta*, 554(2), 340–357.
- Carpick, R. W., Agrait, N., Ogletree, D. F., & Salmeron, M. (1996a). Variation of the interfacial shear strength and adhesion of a nanometer-sized contact. *Langmuir*, 12(13), 3334–3340.
- Carpick, R. W., Agrait, N., Ogletree, D. F., & Salmeron, M. (1996b). Measurement of interfacial shear (friction) with an ultrahigh vacuum atomic force microscope. *Journal of Vacuum Science & Technology B*, 14(2), 1289–1295.
- Casimir, H. B. G. (1948). On the attraction between two perfectly conducting plates. *Proceedings Koninklijke Nederlandse Akademie van Wetenschappen*, 51(7), 793–796.
- Cevc, G., & Marsh, D. (1987). *Phospholipid bilayers*. New York: Wiley.
- Chaikin, P. M., & Lubensky, T. C. (1995). *Principles of condensed matter physics*. Cambridge, New York: Cambridge University Press.
- Chan, D. Y. C. (2002). A simple algorithm for calculating electrical double layer interactions in asymmetric electrolytes. *Journal of Colloid and Interface Science*, 245, 307–310.
- Chan, D. Y. C., & Horn, R. G. (1985). The drainage of thin liquid-films between solid-surfaces. *Journal of Chemical Physics*, 83(10), 5311–5324.
- Chan, D. Y. C., Healy, T. W., & White, L. R. (1976). Electrical double layer interactions under regulation by surface ionization equilibria–dissimilar amphoteric surfaces. *Journal of the Chemical Society, Faraday Transactions I*, 72, 2844–2865.
- Chan, D. Y. C., Mitchell, D. J., Ninham, B. W., & Pailthrope, B. A. (1980a). Solvent structure in particle interactions: low pressure effects and analytic limits. *Journal of the Chemical Society, Faraday Transactions II*, 76, 776–784.

- Chan, D. Y. C., Pashley, R. M., & White, L. R. (1980b). A simple algorithm for the calculation of the electrostatic repulsion between identical charged surfaces in electrolyte. *Journal of Colloid and Interface Science*, 77(1), 283–285.
- Chandler, D. (1987). *Introduction to the modern statistical mechanics*. Oxford: Oxford University Press.
- Chen, Y. L., Chen, S., Frank, C., & Israelachvili, J. (1992). Molecular mechanisms and kinetics during the self-assembly of surfactant layers. *Journal of Colloid and Interface Science*, 153(1), 244–265.
- Cheng, S. F., Luan, B. Q., & Robbins, M. O. (2010). Contact and friction of nanoasperities: effects of adsorbed monolayers. *Physical Review E*, 81(1).
- Chernomordik, L. V., Kozlov, M. M., Leikin, S. L., Markin, V. S., Chizmadzhev, I. A., et al. (1986). Membrane-fusion – local interactions and bilayer structure rearrangements. *Doklady Akademii Nauk SSSR*, 288(4), 1009–1013.
- Chernomordik, L. V., Melikyan, G. B., & Chizmadzhev, Y. A. (1987). Biomembrane fusion: a new concept derived from model studies using 2 interacting planar lipid bilayers. *Biochimica et Biophysica Acta*, 906(3), 309–352.
- Christenson, H. (1983). Experimental measurements of solvation forces in non-polar liquids. *Journal of Chemical Physics*, 78(11), 6906–6913.
- Christenson, H. K. (1988). Non-DVLO forces between surfaces – solvation, hydration and capillary effects. *Journal of Dispersion Science Technology*, 9(2), 171–206.
- Christenson, H. K., & Claesson, P. M. (2001). Direct measurements of the force between hydrophobic surfaces in water. *Advances in Colloid and Interface Science*, 91(3), 391–436.
- Christenson, H. K., & Horn, R. G. (1983). Direct measurement of the force between solid-surfaces in a polar liquid. *Chemical Physics Letters*, 98(1), 45–48.
- Christenson, H. K., & Horn, R. G. (1985). Solvation forces measured in non-aqueous liquids. *Chemica Scripta*, 25(1), 37–41.
- Chu, S., Bjorkholm, J. E., & Ashkin, A. (1986). Experimental observation of optically trapped atoms. *Physical Review Letters*, 57, 314–317.
- Ciccotti, G., Frenkel, D., & McDonald, I. R. (1987). *Simulation of liquids and solids*. Amsterdam: North Holland Publishing Company.
- Claesson, P., Horn, R. G., & Pashley, R. M. (1984). Measurement of surface forces between mica sheets immersed in aqueous quaternary ammonium ion solutions. *Journal of Colloid and Interface Science*, 100(1), 250–263.
- Claesson, P. M., Ederth, T., Bergeron, V., & Rutland, M. W. (1996). Techniques for measuring surface forces. *Advances in Colloid and Interface Science*, 67, 119–183.
- Claesson, P. M., Kjellander, R., Stenius, P., & Christenson, H. K. (1986). Direct measurements of temperature-dependent interactions between nonionic surfactant layers. *Journal of the Chemical Society, Faraday Transactions I*, 82, 2735–2746.
- Claesson, P., Carmona-Ribeiro, A. M., & Kurihara, K. (1989). Dihexadecyl phosphate monolayers: intralayer and interlayer interactions. *Journal of Physical Chemistry*, 93(2), 917–922.
- Cleveland, J. P., Manne, S., Bocek, D., & Hansma, P. K. (1993). A non-destructive method for determining the spring constant of cantilevers for scanning force microscopy. *Review of Scientific Instruments*, 64, 403–405.
- Cleveland, J. P., Schaffer, T. E., & Hansma, P. K. (1995). Probing oscillatory hydration potentials using thermal-mechanical noise in an atomic-force microscope. *Physical Review B*, 52(12), R8692–R8695.
- Clunie, J. S., Goodman, J. F., & Symons, P. C. (1967). Solvation forces in soap films. *Nature*, 216(5121), 1203–1204.
- Coakley, C. J., & Tabor, D. (1978). Direct measurement of van der Waals forces between solids in air. *Journal of Physics D: Applied Physics*, 11(5), L77–L82.
- Cohen, I., Mason, T. G., & Weitz, D. A. (2004). Shear-induced configurations of confined colloidal suspensions. *Physical Review Letters*, 93(4), 046001.

- Cottin-Bizonne, C., Cross, B., Steinberger, A., & Charlaix, E. (2005). Boundary slip on smooth hydrophobic surfaces: intrinsic effects and possible artifacts. *Physical Review Letters*, 94, 056102–056104.
- Cotton, F. A., & Wilkinson, G. (1980). *Advanced inorganic chemistry* (4th ed.). New York: Wiley.
- Coulson, C. A. (1961). *Valence* (2nd ed.). New York: Oxford University Press.
- Cowley, A. C., Fuller, N. L., Rand, R. P., & Parsegian, V. A. (1978). Measurement of repulsive forces between charged phospholipid bilayers. *Biochemistry*, 17(15), 3163–3168.
- Craig, V. S. J. (1997). An historical review of surface force measurement techniques. *Colloids and Surfaces A-Physicochemical and Engineering Aspects*, 130, 75–93.
- Crassous, J., Charlaix, E., & Loubet, J.-L. (1994). Capillary condensation between high-energy surfaces. An experimental study with a surface force apparatus. *Europhysics Letters*, 28, 37.
- Cross, B., Steinberger, A., Cottin-Bizonne, C., Rieu, J.-P., & Charlaix, E. (2006). Boundary flow of water on supported phospholipid films. *Europhysics Letters*, 73(3), 390–395.
- Croxton, C. A. (1975). *Introduction to liquid state physics*. New York: Wiley.
- Dai, J. W., & Sheetz, M. P. (1999). Membrane tether formation from blebbing cells. *Biophysical Journal*, 77, 3363–3370.
- Dang, L. X., Rice, J. E., & Kollman, P. A. (1990). The effect of water models on the interaction of the sodium-chloride ion pair in water: molecular dynamics simulations. *Journal of Chemical Physics*, 93(10), 7528–7529.
- Dasent, W. E. (1970). *Inorganic energetics*. Middlesex, England: Penguin Books.
- Dashevsky, V. G., & Sarkisov, G. N. (1974). Solvation and hydrophobic interaction of non-polar molecules in water in approximation of interatomic potentials: The Monte-Carlo method. *Molecular Physics*, 27(5), 1271–1290.
- Davis, H. T. (1996). *Statistical mechanics of phases, interfaces and thin film*. New York: Wiley-VCH.
- Davies, M. (1965). *Some electrical and optical aspects of molecular behaviour*. Oxford: Pergamon.
- de Boer, J. H. (1936). The influence of van der Waals' forces and primary bonds on binding energy, strength and orientation, with special reference to some artificial resins. *Transactions of the Faraday Society*, 32, 10–38.
- de Gennes, P. G., & Prost, J. (2003). *The physics of liquid crystals*. New York: Oxford University Press.
- De Loof, H., Harvey, S. C., Segrest, J. P., & Pastor, R. W. (1991). Mean field stochastic boundary molecular-dynamics simulation of phospholipid in a membrane. *Biochemistry*, 30(8), 2099–2113.
- De Gennes, P. G. (1976). Dynamics of entangled polymer solutions. 1. The Rouse model. *Macromolecules*, 9(4), 587–593.
- Delville, A. (1993). Structure and properties of confined liquids: a molecular model of the clay–water interface. *Journal of Physical Chemistry*, 97(38), 9703–9712.
- Denbigh, K. G. (1940). The polarisabilities of bonds—I. *Transactions of the Faraday Society*, 36, 936–948.
- Derjaguin, B. V. (1934). Friction and adhesion. IV. The theory of adhesion of small particles. *Kolloid-Zeitschrift*, 69(2), 155–164.
- Derjaguin, B. V., & Churaev, N. V. (1974). Structural component of disjoining pressure. *Journal of Colloid and Interface Science*, 49(2), 249–255.
- Derjaguin, B. V., & Kusakov, M. M. (1939). Anomalous properties of thin polymolecular films. *Acta Physicochimica URSS*, 10(25–44), 153–174.
- Derjaguin, B. V., & Landau, L. (1941). Theory of the stability of strongly charged lyophobic sols and of the adhesion of strongly charged particles in solution of electrolytes. *Acta Physicochimica URSS*, 14, 633–662.
- Derjaguin, B. V., Titijevskaia, A. S., Abricossova, I. I., & Malkina, A. D. (1954). Investigations of the forces of interaction of surfaces in different media and their application to the problem of colloid stability. *Discussions of the Faraday Society*, 18, 24–41.

- Derjaguin, B. V., Abrikossova, I. I., & Lifshitz, E. M. (1956). Direct measurement of molecular attraction between solids separated by a narrow gap. *Quarterly Reviews of the Chemical Society*, 10(3), 295–329.
- Derjaguin, B. V., Rabinovich, Y. I., & Churaev, N. V. (1978). Direct measurement of molecular forces. *Nature*, 272(5651), 313–318.
- Devereux, O. F. (1963). *Interaction of plane-parallel double layers*. Cambridge, MA: MIT Press.
- Diederichs, K., Welte, W., & Kreutz, W. (1985). Determination of interaction forces between higher plant thylakoids and electron-density-profile evaluation using small-angle x-ray-scattering. *Biochimica et Biophysica Acta*, 809(1), 107–116.
- Dill, K. A. (1990). Dominant forces in protein folding. *Biochemistry*, 29(31), 7133–7155.
- Discher, B. M., Won, Y.-Y., Ege, D. S., Lee, J. C. M., Bates, F. S., Discher, D. E., et al. (1999). Polymersomes: tough vesicles made from diblock copolymers. *Science*, 284(5417), 1143–1146.
- Donners, W. A. B., Rijnbout, J. B., & Vrij, J. (1977). Light scattering from soap films. I. Determination of double-layer repulsion forces. *Journal of Colloid and Interface Science*, 61(2), 249–260.
- Drifford, M., Dalbiez, J.-P., Delsanti, M., & Belloni, L. (1996). Structure and dynamics of polyelectrolyte solutions with multivalent salts. *Berichte Der Bunsen-Gesellschaft-Physical Chemistry Chemical Physics*, 100(6), 829–835.
- Drummond, C. J., & Chan, D. Y. C. (1997). van der Waals interaction, surface free energies, and contact angles: dispersive polymers and liquids. *Langmuir*, 13, 3890–3895.
- Drummond, C. J., Georgakis, G., & Chan, D. Y. C. (1996). Fluorocarbons: surface free energies and van der Waals interaction. *Langmuir*, 12(11), 2617–2621.
- Drummond, C., Alcantar, N., & Israelachvili, J. (2002). Shear alignment of confined hydrocarbon liquid films. *Physical Review E*, 66(1). art. no. 011705.
- Drummond, C., Israelachvili, J., & Richetti, P. (2003). Friction between two weakly adhering boundary lubricated surfaces in water. *Physical Review E*, 67(6), 16.
- Dubois, M., Zemb, T., Belloni, L., Delville, A., Levitz, P., & Setton, R. (1992). Osmotic pressure and salt exclusion in electrostatically swollen lamellar phases. *Journal of Chemical Physics*, 96(3), 2278–2286.
- Ducker, W. A., & Clarke, D. R. (1994). Controlled modification of silicon nitride interactions in water via zwitterionic surfactant adsorption. *Colloids and Surfaces*, 94, 275–292.
- Ducker, W. A., Senden, T. J., & Pashley, R. M. (1991). Direct measurement of colloidal forces using an atomic force microscope. *Nature*, 353(6341), 239–241.
- Ducker, W. A., Senden, T. J., & Pashley, R. M. (1992). Measurement of forces in liquids using a force microscope. *Langmuir*, 8(7), 1831–1836.
- Dymond, J. H. (1981). Limiting diffusion in binary nonelectrolyte mixtures. *Journal of Physical Chemistry*, 85(22), 3291–3294.
- Dzyaloshinskii, I. E., Lifshitz, E. M., & Pitaevskii, L. P. (1961). The general theory of van der Waals forces. *Advances in Physics*, 10(38), 165–209.
- Eastman, S. J., Hope, M. J., Wong, K. F., & Cullis, P. R. (1992). Influence of phospholipid asymmetry on fusion between large unilamellar vesicles. *Biochemistry*, 31(17), 4262–4268.
- Egberts, E., & Berendsen, H. J. C. (1988). Molecular dynamics simulation of smetic liquid crystal with atomic detail. *Journal of Chemical Physics*, 89(6), 3718–3726.
- Ekwall, P. (1975). Composition, properties, and structures of liquid crystalline phases in systems of amphiphilic compounds. *Advances in Liquid Crystals*, 1, 1–142.
- Epstein, B. R., Foster, K. R., & Mackay, R. A. (1983). Microwave dielectric-properties of ionic and non-ionic microemulsions. *Journal of Colloid and Interface Science*, 95(1), 218–227.
- Ertl, H., & Dullien, F. A. L. (1973). Self-diffusion and viscosity of some liquids as a function of temperature. *AIChE Journal*, 19(6), 1215–1223.

- Essavaz-Roulet, B., Bockelmann, U., & Heslot, F. (1997). Mechanical separation of the complementary strands of DNA. *Proceedings of the National Academy of Sciences of the United States of America*, 94, 11935–11940.
- Ettelaie, R., & Buscall, R. (1995). Electrical double layer interactions for spherical charge regulating colloidal particles. *Advances in Colloid and Interface Science*, 61, 131–160.
- Evans, E. (1988). Mechanics of cell deformation and cell-surface adhesion. In P. Bongrand (Ed.), *Physical basis of cell adhesion*. Boca Raton: CRC Press.
- Evans, D. F., Wennerström H. (1999). The colloidal domain: where physics, chemistry, biology, and technology meet. New York: Wiley-VCH.
- Evans, E., & Metcalfe, M. (1984). Free energy potential for aggregation of giant, neutral lipid bilayer vesicles by van der Waals attraction. *Biophysical Journal*, 46(3), 423–426.
- Evans, E., & Needham, D. (1988). Attraction between lipid bilayer membranes in concentrated solutions of nonadsorbing polymers: comparison of mean-field theory with measurements of adhesion energy. *Macromolecules*, 21(6), 1822–1831.
- Evans, R., & Parry, A. O. (1990). Liquids at interfaces: what can a theorist contribute? *Journal of Physics: Condensed Matter*, 2, SA15–SA32.
- Evans, E., & Rawicz, W. (1990). Entropy-driven tension and bending elasticity in condensed-fluid membranes. *Physical Review Letters*, 64(17), 2094–2097.
- Evans, E., & Ritchie, K. (1997). Dynamic strength of molecular adhesion bonds. *Biophysical Journal*, 72(4), 1541–1555.
- Evans, E., & Ritchie, K. (1999). Strength of a weak bond connecting flexible polymer chains. *Biophysical Journal*, 76(5), 2439–2447.
- Evans, D. F., Tominaga, T., & Davis, H. T. (1981). Tracer diffusion in polyatomic liquids. *Journal of Chemical Physics*, 74(2), 1298–1305.
- Evans, D. F., Mukherjee, S., Mitchell, D. J., & Ninham, B. W. (1983). Surfactant diffusion: new results and interpretations. *Journal of Colloid and Interface Science*, 93(1), 184–204.
- Farinato, R. S., & Dubin, P. L. (1999). *Colloid-polymer interactions*. New York: Wiley.
- Farrell, J. R., & McTigue, P. (1982). Precise compensating potential difference measurements with a voltaic cell: the surface potential of water. *Journal of Electroanalytical Chemistry*, 139(1), 37–56.
- Ferrante, J., & Smith, J. R. (1985). Theory of the bimetallic interface. *Physical Review B*, 31(6), 3427–3434.
- Ferry, J. D. (1980). *Viscoelastic properties of polymers*. New York: John Wiley.
- Fisher, T., Oberhauser, A. F., Carrion-Vasquez, M., Marszalek, P. E., & Fernandez, J. M. (1999). The study of protein mechanics with the atomic force microscope. *Trends in Biochemical Sciences*, 24, 379–384.
- Florin, E.-L., Moy, V. T., & Gaub, H. E. (1994). Adhesion forces between individual ligand-receptor pairs. *Science*, 264, 415–417.
- Forsyth, P. A., Marcelja, S., Mitchell, D. J., & Ninham, B. W. (1977). Phase-transition in charged lipid-membranes. *Biochimica et Biophysica Acta*, 469(3), 335–344.
- Fowler, P. W., Lazzaretti, P., & Zanas, W. (1989). Anisotropic dispersion forces in methane mixtures. *Molecular Physics*, 68(4), 853–865.
- Franks, F. (1972–1982). *Water: a comprehensive treatise*. New York: Plenum.
- Frantz, P., Agrait, N., & Salmeron, M. (1996). Use of capacitance to measure surface forces. 1. Measuring distance of separation with enhanced spatial and time resolution. *Langmuir*, 12(13), 3289–3294.
- Frechette, J., & Vanderlick, T. K. (2001). Double layer forces over large potential ranges as measured in an electrochemical surface forces apparatus. *Langmuir*, 17(24), 7620–7627.
- Frenkel, D., & Smit, B. (2002). *Understanding molecular simulation: from algorithms to applications*. San Diego, CA: Academic.
- Frens, G., & Overbeek, J. T. G. (1972). Repeptization and the theory of electrostatic colloid. *Journal of Colloid and Interface Science*, 38(2), 376–387.

- Fromherz, P. (1983). Lipid-vesicle structure: size control by edge-active agents. *Chemical Physics Letters*, 94(3), 259–266.
- Fuller, K. N. G., & Tabor, D. (1975). Effect of surface-roughness on adhesion of elastic solids. *Proceedings of the Royal Society of London Series A-Mathematical Physical and Engineering Sciences*, 345(1642), 327–342.
- Gallot, B., & Skoulios, A. (1966). Interactions électriques dans les phases mésomorphes des systèmes amphiphile-eau: Rôle de la teneur en eau, de la longueur de la chaîne paraffinique, de la nature du cation, et de la température. *Kolloid-Zeitschrift and Zeitschrift Fur Polymere*, 208(1), 37–43.
- Gast, A. P., Hall, C. K., & Russel, W. B. (1983a). Polymer-induced phase separations in nonaqueous colloidal suspensions. *Journal of Colloid and Interface Science*, 96(1), 251–267.
- Gast, A. P., Hall, C. K., & Russel, W. B. (1983b). Phase separation induced in aqueous colloidal suspensions by dissolved polymer. *Faraday Discussions of the Chemical Society*, 76, 189–201.
- Gee, M. L., Healy, T. W., & White, L. R. (1989). Ellipsometric studies of alkane adsorption on quartz. *Journal of Colloid and Interface Science*, 131(1), 18–23.
- Gee, M. L., Tong, P., Israelachvili, J. N., & Witten, T. A. (1990a). Comparison of light-scattering of colloidal dispersion with direct force measurements between analogous macroscopic surfaces. *Journal of Chemical Physics*, 93(8), 6057–6064.
- Gee, M. L., Healy, T. W., & White, L. R. (1990b). Hydrophobicity effects in the condensation of water films on quartz. *Journal of Colloid and Interface Science*, 140(2), 450–465.
- Gijs, J., Wuite, R., Davenport, J., Rappaport, A., & Bustamante, C. (2000). An integrated laser trap/flow control video microscope for the study of single biomolecules. *Biophysical Journal*, 79, 1155–1167.
- Gingell, D., & Parsegian, V. A. (1972). Computation of van der Waals interactions in aqueous systems using reflectivity data. *Journal of Theoretical Biology*, 36(1), 41–52.
- Glaser, M. A., & Clarke, N. A. (1990). Statistical geometry of simple liquids in 2 dimensions. *Physical Review A*, 41(8), 4585–4588.
- Goddard, T. D., Huang, C. C., & Ferrin, T. E. (2005). Software extensions to UCSF chimera for interactive visualization of large molecular assemblies. *Structure*, 13(3), 473–482.
- Goetz, D. J., Elsabban, M. E., Pauli, B. U., & Hammer, D. A. (1994). Dynamics of neutrophil rolling over stimulated endothelium in-vitro. *Biophysical Journal*, 66(6), 2202–2209.
- Golan, Y., Martin-Herranz, A., Li, Y., Safinya, C. R., & Israelachvili, J. (2001). Direct observation of shear-induced orientational phase coexistence in a lyotropic system using a modified X-ray surface forces apparatus. *Physical Review Letters*, 86(7), 1263.
- Gordon, V. D., Beales, P. A., Zhao, Z., Blake, C., MacKintosh, F. C., Olmsted, P. D., et al. (2006). Lipid organization and the morphology of solid-like domains in phase-separating binary lipid membranes. *Journal of Physics*, 18, L415–L420.
- Grahame, D. C. (1953). Diffuse double layer theory for electrolytes of unsymmetrical valence types. *Journal of Chemical Physics*, 21(6), 1054–1060.
- Granfeldt, M. K., & Miklavic, S. J. (1991). A simulation study of flexible zwitterionic monolayers: interlayer interaction and headgroup conformation. *Journal of Physical Chemistry*, 95(16), 6351–6360.
- Gregory, J. (1970). The calculation of Hamaker constants. *Advances in Colloid and Interface Science*, 2(4), 396–417.
- Gregory, J. (1975). Interaction of unequal double layers at constant charge. *Journal of Colloid and Interface Science*, 51(1), 44–51.
- Gronbech-Jensen, N., Mashl, R. J., Bruinsma, R. F., & Gelbart, W. M. (1997). Counterion-induced attraction between rigid polyelectrolytes. *Physical Review Letters*, 78(12), 2477–2480.
- Grosberg, A. Y., Nguyen, T. T., & Shklovskii, B. I. (2002). Colloquium: the physics of charge inversion in chemical and biological systems. *Reviews of Modern Physics*, 74, 329–345.

- Gruen, D. W. R. (1985). A model for the chains in amphiphilic aggregates. 1. Comparison with a molecular dynamics simulation of a bilayer. *Journal of Physical Chemistry*, 89(1), 146–152, 153–163.
- Gruen, D. W. R., & de Lacey, E. H. B. (Eds.). (1984). *Surfactant in solution*. New York: Plenum.
- Gruen, D. W. R., & Wolfe, J. (1982). Lateral tensions and pressures in membranes and lipid monolayers. *Biochimica et Biophysica Acta*, 688(2), 572–580.
- Grunewald, T., & Helm, C. A. (1998). Computer-controlled experiments in the surface forces apparatus with a CCD-spectrograph. *Langmuir*, 12(16), 3885–3890.
- Guggenheim, E. A. (1949). *Thermodynamics*. Amsterdam: North Holland Publishing.
- Guillot, B. (2002). A reappraisal of what we have learnt during three decades of computer simulations on water. *Journal of Molecular Liquids*, 101(1–3), 219–260.
- Guldbrand, L., Jönsson, B., Wennerström, H., & Linse, P. (1984). Electrical double layer forces. A Monte Carlo study. *Journal of Chemical Physics*, 80(5), 2221–2228.
- Gunstone, F. D., & Seth, S. (1994). A study of the distribution of eicosapentaenoic acid and docosahexaenoic acid between the alpha and beta glycerol chains in fish oils by C-13-NMR spectroscopy. *Chemistry and Physics of Lipids*, 72(2), 119–126.
- Haberland, M. E., & Reynolds, J. A. (1973). Self-association of cholesterol in aqueous solution. *Proceedings of the National Academy of Sciences of the United States of America*, 70(8), 2313–2316.
- Hagen, M. H. J., Meijer, E. J., Mooij, G. C. A. M., Frenkel, D., & Lekkerkerker, H. N. W. (1993). Does C-60 have a liquid-phase? *Nature*, 365(6445), 425–426.
- Hall, D. G., & Pethica, B. A. (1967). *Nonionic surfactants*. New York: Marcel Dekker.
- Hamaker, H. C. (1937). The London-van der Waals attraction between spherical particles. *Physica*, 4(10), 1058–1072.
- Hammer, M. U. A., Travers, H., Chaimovich, A., Shell, M. S., & Israelachvili, J. (2010). The search for the hydrophobic force law. *Journal of Faraday Transactions*, 146, 299–308.
- Hamnerius, Y., Lundstrom, I., Paulsson, L. E., Fontell, K., & Wennerström, H. (1978). Dielectric properties of lamellar lipid water phases. *Chemistry and Physics of Lipids*, 22(2), 135–140.
- Hänggi, P., Mroczkowski, T. J., Moss, F., & McClintock, P. V. E. (1985). Bistability driven by colored noise: theory and experiment. *Physical Review A*, 32(1), 695.
- Hansma, P. K., Elings, V. B., Marti, O., & Bracker, C. E. (1988). Scanning tunneling microscopy and atomic force microscopy: application to biology and technology. *Science*, 242(4876), 209–216.
- Hardy, W. B. (1899). A preliminary investigation of the conditions which determine the stability of irreversible hydrosols. *Proceedings of the Royal Society of London*, 66, 110–125.
- Hart, J. R., & Rappe, A. K. (1992). Van der Waals functional forms for molecular simulations. *Journal of Chemical Physics*, 97(2), 1109–1115.
- Hasted, J. B. (1973). *Aqueous dielectrics*. London: Chapman & Hall.
- Healy, T. W., & White, L. R. (1978). Ionizable surface group models of aqueous interfaces. *Advances in Colloid and Interface Science*, 9(4), 303–345.
- Healy, T. W., Chan, D., & White, L. R. (1980). Colloidal behavior of materials with ionizable group surfaces. *Pure and Applied Chemistry*, 52(5), 1207–1219.
- Heindl, A., & Kohler, H.-H. (1996). Rod formation of ionic surfactants: a thermodynamic model. *Langmuir*, 12(10), 2464–2477.
- Helfrich, W. (1978). Passages in lecithin-water systems. *Zeitschrift für Naturforschung*, A33(9), 1013–1017.
- Helfrich, W., & Servuss, R. M. (1984). Undulations, steric interaction and cohesion of fluid membranes. *Nuovo Cimento Della Societa Italiana Di Fisica D-Condensed Matter Atomic Molecular and Chemical Physics Fluids Plasmas Biophysics*, 3(1), 137–151.
- Helm, C. A., & Israelachvili, J. N. (1991). The role of the hydrophobic force in bilayer adhesion and fusion. *Makromolekulare Chemie-Macromolecular Symposia*, 46, 433–437.

- Helm, C. A., Israelachvili, J. N., & McGuiggan, P. M. (1992). Role of hydrophobic forces in bilayer adhesion and fusion. *Biochemistry*, 31(6), 1794–1805.
- Herce, H. D., & Garcia, A. E. (2007). Molecular dynamics simulations suggest a mechanism for translocation of the HIV-1 TAT peptide across lipid membranes. *Proceedings of the National Academy of Sciences of the United States of America*, 104(52), 20805–20810.
- Hertz, H. G. (1973). *Water: a comprehensive treatise*. New York: Plenum.
- Hesse, M. B. (1961). *Forces and fields*. New York: Thomas Nelson.
- Heuberger, M. (2001). The extended surface forces apparatus. Part I. Fast spectral correlation interferometry. *Review of Scientific Instruments*, 72, 1700–1707.
- Heuberger, M., Luengo, G., & Israelachvili, J. (1997). Topographic information from multiple beam interferometry in the surface forces apparatus. *Langmuir*, 13(14), 3839–3848.
- Hiemenz, P. C. (1977). *Principles of colloid and surface chemistry*. New York: Dekker.
- Hiemenz, P., & Rajagopalan, R. (1997). *Principles of colloid and surface chemistry*. New York: Marcel Dekker, Inc.
- Hill, T. L. (1960). *An introduction to statistical thermodynamics*. Reading, Massachusetts: Addison-Wesley Pub. Co.
- Hill, T. L. (1963). *Thermodynamics of small systems*. Benjamin, New York: Dover Pubns.
- Hill, T. L. (1963, 1964, 2002). *Thermodynamics of small systems*. Benjamin, New York: Dover Pubns.
- Hirschfelder, J. O., Curtiss, C. F., & Bird, R. B. (1954). *Molecular theory of gases and liquids*. New York: Chapman and Hall.
- Hobbs, P. V. (1974). *Ice physics*. Oxford: Clarendon Press.
- Hogg, R., Healy, T. W., & Fuerstenau, D. W. (1966). Mutual coagulation of colloidal dispersions. *Transactions of the Faraday Society*, 62(522P), 1638–1651.
- Holder, G. D., Mokka, L. P., & Warzinski, R. P. (2001). Formation of gas hydrates from single-phase aqueous solutions. *Chemical Engineering Science*, 56(24), 6897–6903.
- Hollins, G. T. (1964). Configurational statistics + dielectric constant of ice. *Proceedings of the Physical Society*, 84(6), 1001–1016.
- Holz, M., Grunder, R., Sacco, A., & Meleleo, A. (1993). Nuclear magnetic resonance study of self-association of small hydrophobic solutes in water: salt effects and the lyotropic series. *Journal of the Chemical Society, Faraday Transactions*, 89, 1215–1222.
- Homan, R., & Pownall, H. J. (1988). Transbilayer diffusion of phospholipids: dependence on headgroup structure and acyl chain length. *Biochimica et Biophysica Acta*, 938(2), 155–166.
- Homola, A., & Robertson, A. A. (1976). A compression method for measuring forces between colloidal particles. *Journal of Colloid and Interface Science*, 54(2), 286–297.
- Homola, A. M., Israelachvili, J. N., Gee, M. L., & McGuiggan, P. M. (1989). Measurements of and relation between the adhesion and friction of two surfaces separated by molecularly thin liquid films. *Journal of Tribology*, 111, 675–682.
- Homola, A. M., Israelachvili, J. N., McGuiggan, P. M., & Gee, M. L. (1990). Fundamental experimental studies in tribology: the transition from ‘interfacial’ friction of undamaged molecularly smooth surfaces to ‘normal’ friction with wear. *Wear*, 136, 65–83.
- Horn, R. G. (1990). Surface forces and their actions in ceramic materials. *Journal of the American Ceramic Society*, 73(5), 1117–1135.
- Horn, R. G., & Smith, D. T. (1992). Contact electrification and adhesion between dissimilar materials. *Science*, 256(5055), 362–364.
- Horn, R. G., Clarke, D. R., & Clarkson, M. T. (1988). Direct measurement of surface forces between sapphire crystals in aqueous solutions. *Journal of Materials Research*, 3(3), 413–416.
- Horn, R. G., Smith, D. T., & Haller, W. (1989). Surface forces and viscosity of water measured between silica sheets. *Chemical Physics Letters*, 162(4–5), 404–408.

- Hough, D. B., & White, L. R. (1980). The calculation of Hamaker constants from Lifshitz theory with applications to wetting phenomena. *Advances in Colloid and Interface Science*, 14(1), 3–41.
- Howard, J. (2001). *Mechanics of Motor Proteins and the Cytoskeleton*. Sunderland, MA: Sinauer Associates.
- Hui, S. W., Kuhl, T. L., Guo, Y. Q., & Israelachvili, J. (1999). Use of poly(ethylene glycol) to control cell aggregation and fusion. *Colloids and Surfaces B: Biointerfaces*, 14(1–4), 213–222.
- Huibers, P. D. T., Lobanov, V. S., Katritzky, A. R., Shah, D. O., & Karelson, M. (1996). Prediction of critical micelle concentration using a quantitative structure–property relationship approach. 1. Nonionic surfactants. *Langmuir*, 12(6), 1462–1470.
- Hunter, R. J. (1981). *Foundations of colloid science*. Oxford: Clarendon Press.
- Hunter, R. J. (2001). *Foundations of colloid science*. New York: Oxford University Press.
- in't Veld, P. J., Ismail, A. E., & Grest, G. S. (2007). Application of Ewald summations to long-range dispersion forces. *Journal of Chemical Physics*, 127(14), 144711.
- Ise, N., & Yoshida, H. (1996). Paradoxes of the repulsion-only assumption. *Accounts of Chemical Research*, 29(1), 3–5.
- Israelachvili, J. (1994a). The science and applications of emulsions: an overview. *Colloids and Surfaces A: Physicochemical and Engineering Aspects*, 91, 1–8.
- Israelachvili, J. (1994b). Self-assembly in 2 dimensions: surface micelles and domain formation in monolayers. *Langmuir*, 10(10), 3774–3781.
- Israelachvili, J. N. (1972). The calculation of van der Waals dispersion forces between macroscopic bodies. *Proceedings of the Royal Society of London. Series A*, 331(1584), 39–55.
- Israelachvili, J. N. (1973a). Thin-film studies using multiple-beam interferometry. *Journal of Colloid and Interface Science*, 44(2), 259–272.
- Israelachvili, J. N. (1973b). Van der Waals dispersion force contributions to works of adhesion and contact angles on the basis of macroscopic theory. *Journal of the Chemical Society, Faraday Transactions*, 2(69), 1729–1738.
- Israelachvili, J. N. (1974). Van der Waals forces in biological systems. *Quarterly Reviews of Biophysics*, 6(4), 341–387.
- Israelachvili, J. N. (1985). Measurements of hydration forces between macroscopic surfaces. *Chemica Scripta*, 25(1), 7–14.
- Israelachvili, J. N. (1986). Measurement of the viscosity of liquids in very thin films. *Journal of Colloid and Interface Science*, 110(1), 263–271.
- Israelachvili, J. N. (1987a). Physical principles of surfactant self-association into micelles, bilayers, vesicles and microemulsion droplets. In K. L. Mittal, & P. Bothorel (Eds.), *Surfactants in solution: recent developments*, 4 (pp. 3–34). NY: Plenum.
- Israelachvili, J. N. (1987b). Solvation forces and liquid structure, as probed by the direct force measurements. *Accounts in Chemical Research*, 20(11), 415–421.
- Israelachvili, J. N. (1989). Techniques for direct measurements of forces between surfaces in liquids at the atomic scale. *Chemtracts – Analytical and Physical Chemistry*, 1(1), 1–12.
- Israelachvili, J. N., & Adams, G. E. (1978). Measurement of forces between 2 mica surfaces in aqueous electrolyte solutions in range 0–100 nm. *Journal of the Chemical Society, Faraday Transactions*, 74(1), 975–1001.
- Israelachvili, J. N., & McGuiggan, P. M. (1990). Adhesion and short-range forces between surfaces. Part II: effects of lattice mismatch angle on the oscillatory force-law. *Journal of Materials Research*, 5(10), 2223–2231.
- Israelachvili, J. N., & Ninham, B. W. (1977). Intermolecular forces – the long and short of it. *Journal of Colloid and Interface Science*, 58, 14–25.
- Israelachvili, J. N., & Pashley, R. M. (1982b). The hydrophobic interaction is long range, decaying, exponentially with distance. *Nature*, 300, 341–342.

- Israelachvili, J. N., & Tabor, D. (1972). The measurement of van der Waals dispersion forces in the range 1.5 to 130 nm. *Proceedings of the Royal Society of London. Series A*, 331(1584), 19–38.
- Israelachvili, J. N., & Tabor, D. (1973). van der Waals forces: theory and experiment. *Progress in Surface and Membrane Science*, 7(1), 1–55.
- Israelachvili, J. N., & Wennerström, H. (1992). Entropic forces between amphiphilic surfaces in liquids. *Journal of Physical Chemistry*, 96(2), 520–531.
- Israelachvili, J., & Wennerström, H. (1996). Role of hydration and water structure in biological and colloidal interactions. *Nature*, 379(6562), 219–225.
- Israelachvili, J. N., Mitchell, D. J., & Ninham, B. W. (1976). Theory of self-assembly of hydrocarbon amphiphiles into micelles and bilayers. *Journal of the Chemical Society, Faraday Transactions*, 2(72), 1525–1568.
- Israelachvili, J. N., Mitchell, D. J., & Ninham, B. W. (1977). Theory of self-assembly of lipid bilayers and vesicles. *Biochimica et Biophysica Acta*, 470, 185–201.
- Israelachvili, J. N., Marcelja, S., & Horn, R. G. (1980a). Physical principles of membrane organization. *Quarterly Reviews Biophysics*, 13, 121–200.
- Israelachvili, J. N., Tirrell, M., Klein, J., & Almog, Y. (1984). Forces between two layers of adsorbed polystyrene immersed in cyclohexane below and above the theta temperature. *Macromolecules*, 17, 204–209.
- Israelachvili, J., Min, Y., Akbulut, M., Alig, A., Carver, G., Greene, W., et al. (2010). Recent advances in the surface forces apparatus (SFA) technique. *Reports on Progress in Physics*, 73, 1–16.
- Israilev, S., Stepaniants, S., Isralewitz, B., Kosztin, D., Lu, H., Molnar, F., et al. (1998). Steered molecular dynamics. In P. Deufhard, J. Hermans, B. Leimkuhler, A. Mark, S. Reich, & R. D. Skeel (Eds.), *Computational molecular dynamics: challenges, methods, ideas* (pp. 39–65). New York: Springer.
- Jaeger, H. M., & Nagel, S. R. (1992). Physics of the granular state. *Science*, 255(5051), 1523–1531.
- Jain, M. (1988). *Introduction to biological membranes*. New York: Wiley.
- Jammer, M. (1957). *Concepts of force*. Cambridge, Massachusetts: Copyright by General Publishing Company Toronto, Canada.
- Janczuk, B., Bruque, J. M., Gonzalez-Martin, M. L., & Moreno Del Pozo, J. (1993). Determination of components of cassiterite surface free energy from contact angle measurements. *Journal of Colloid and Interface Science*, 161(1), 209–222.
- Jarzynski, C. (1997a). Nonequilibrium equality for free energy differences. *Physical Review Letters*, 78(14), 2690–2693.
- Jarzynski, C. (1997b). Equilibrium free-energy differences from nonequilibrium measurements: a master-equation approach. *Physical Review E*, 56(5), 5018–5035.
- Jasien, P. G., & Fitzgerald, G. (1990). Molecular dipole moments and polarizabilities from local density functional calculations: application to DNA-base pairs. *Journal of Chemical Physics*, 93(4), 2554–2560.
- Jeffrey, G. A. (1997). *An introduction to hydrogen bonding (topics in physical chemistry)*. USA: Oxford University Press.
- Jeppesen, C., Wong, J. Y., Kuhl, T. L., Israelachvili, J. N., Mullah, N., Zalipsky, S., et al. (2001). Impact of polymer tether length on multiple ligand-receptor bond formation. *Science*, 293(5529), 465–468.
- Joesten, M. D., & Schaad, L. J. (1974). *Hydrogen bonding*. New York: Dekker.
- Johnson, K. L. (1985). *Adhesion between elastic bodies. Contact Mechanics*. New York: Cambridge University Press.
- Johnson, K. L., Kendall, K., & Roberts, A. D. (1971). Surface energy and the contact of elastic solids. *Proceedings of the Royal Society of London Series A*, 324(1558), 301–313.
- Jokela, P., Jönsson, B., & Khan, A. (1987). Phase equilibria of catanionic surfactant-water systems. *Journal of Physical Chemistry*, 91(12), 3291–3298.
- Jönsson, B., & Wennerström, H. (1981). Thermodynamics of ionic amphiphile-water systems. *Journal of Colloid and Interface Science*, 80(2), 482–496.

- Jönsson, B., & Wennerström, H. (1983). Image-charge forces in phospholipid-bilayer systems. *Journal of the Chemical Society, Faraday Transactions II*, 79, 19–35.
- Jönsson, B., Wennerström, H., & Halle, B. (1980). Ion distributions in lamellar liquid crystals. A comparison between results from Monte Carlo simulations and solutions of the Poisson-Boltzmann equation. *Journal of Physical Chemistry*, 84(17), 2179–2185.
- Jund, P., Kim, S. G., & Tsallis, C. (1995). Crossover from extensive to nonextensive behavior driven by long-range interactions. *Physical Review B*, 52(1), 50.
- Kaler, E. W., Herrington, K. L., Murthy, A. K., & Zasadzinski, J. A. N. (1992). Phase behavior and structures of mixtures of anionic and cationic surfactants. *Journal of Physical Chemistry*, 96(16), 6698–6707.
- Kallay, N., Biskup, B., Tomic, M., & Matijevic, E. (1986). Particle adhesion and removal in model systems. *Journal of Colloid and Interface Science*, 114(2), 357–362.
- Katsaras, J. (1998). Formation of highly aligned, fully hydrated multibilayers. *Biophysical Journal*, 74(2), A12.
- Kauzmann, W. (1959). Some factors in the interpretation of protein denaturation. *Advances in Protein Chemistry*, 14, 1–63.
- Khan, A., Jönsson, B., & Wennerström, H. (1985). Phase equilibria in the mixed sodium and calcium di-2-ethylhexylsulfosuccinate aqueous system. An illustration of repulsive and attractive double-layer forces. *Journal of Physical Chemistry*, 89(24), 5180–5184.
- Kjellander, R., & Florin, E. (1981). Water structure and changes in thermal stability of the system poly(ethylene oxide)-water. *Journal of the Chemical Society, Faraday Transactions I: Physical Chemistry in Condensed Phases*, 77(9), 2053–2077.
- Kjellander, R., & Marcelja, S. (1984). Correlation and image charge effects in electric double-layers. *Chemical Physics Letters*, 112(1), 49–53.
- Kjellander, R., & Marcelja, S. (1985). Interactions between ionic surface layers. *Chemica Scripta*, 25(1), 112–116.
- Kjellander, R., & Marcelja, S. (1986a). Double-layer interaction in the primitive model and the corresponding Poisson-Boltzmann description. *Journal of Physical Chemistry*, 90(7), 1230–1232.
- Kjellander, R., & Marcelja, S. (1986b). Interaction of charged surfaces in electrolyte solutions. *Chemical Physics Letters*, 127(4), 402–407.
- Kjellander, R., Marcelja, S., Pashley, R. M., & Quirk, J. P. (1988a). Double-layer ion correlation forces restrict calcium-clay swelling. *Journal of Physical Chemistry*, 92(23), 6489–6492.
- Kjellander, R., Marcelja, S., & Quirk, J. P. (1988b). Attractive double-layer interactions between calcium clay particles. *Journal of Colloid and Interface Science*, 126(1), 194–211.
- Kjellander, R., Marcelja, S., Pashley, R. M., & Quirk, J. P. (1990). A theoretical and experimental study of forces between charged mica surfaces in aqueous CaCl_2 solutions. *Journal of Chemical Physics*, 92(7), 4399–4407.
- Klein, J. (1980). Forces between mica surfaces bearing layers of adsorbed polystyrene in cyclohexane. *Nature*, 288(5788), 248–250.
- Klein, J. (1982). Forces between two polymer layers adsorbed at a solid-liquid interface in a poor solvent. *Advances in Colloid and Interface Science*, 16, 101–115.
- Klein, J. (1983). Forces between mica surfaces bearing adsorbed macromolecules in liquid-media. *Journal of the Chemical Society, Faraday Transactions I*, 79, 99–118.
- Klein, J., & Luckham, P. (1982). Forces between two adsorbed polyethylene oxide layers immersed in a good aqueous solvent. *Nature*, 300(5891), 429–431.
- Klein, J., & Luckham, P. (1984a). Long-range attractive forces between two mica surfaces in an aqueous polymer solution. *Nature*, 308(5962), 836–837.
- Klein, J., & Luckham, P. F. (1984b). Forces between two adsorbed poly(ethylene oxide) layers in a good aqueous solvent in the range 0–150 nm. *Macromolecules*, 17(5), 1041–1048.
- Klein, J. (1988). Surface forces with adsorbed and grafted polymers. *Studies in polymer science* (Vol. 2) (pp. 333–352). M. Nagasawa, Amsterdam: Elsevier.

- Kleinfeld, A. M., & Storch, J. (1993). Transfer of long-chain fluorescent fatty acids between small and large unilamellar vesicles. *Biochemistry*, 32(8), 2053–2061.
- Kohler, F. (1972). *The liquid state*. Weinheim: Verlag Chemie.
- Kruus, P. (1977). *Liquids and solutions: structure and dynamics*. New York: Dekker.
- Kumacheva, E. (1998). Interfacial friction measurement in surface force apparatus. *Progress in Surface Science*, 58(2), 75–120.
- Kumar, R., & Prausnitz, J. M. (1975). Solvents in chemical technology. In M. R. J. Dack (Ed.), *Solutions and solubilities* (pp. 259–326). New York: Wiley.
- Kunst, M., & Warman, J. M. (1980). Proton mobility in ice. *Nature*, 288(5790), 465–467.
- Kwok, R., & Evans, E. (1981). Thermoelasticity of large lecithin bilayer vesicles. *Biophysical Journal*, 35(3), 637–652.
- Landau, L. D., & Lifshitz, E. M. (1980). *Statistical physics*. Oxford: Pergamon.
- Landau, L. D., & Lifshitz, E. M. (1984). *Electrodynamics of continuous media*. Oxford: Pergamon.
- Landman, U., Luedtke, W. D., & Ribarsky, M. W. (1989). Structural and dynamical consequences of interactions in interfacial systems. *Journal of Vacuum Science & Technology a-Vacuum Surfaces and Films*, 7(4), 2829–2839.
- Landolt-Börnstein. (1982). *Numerical data and functional relationships in science and technology*. Heidelberg: Springer.
- Langmuir, I. (1938). The role of attractive and repulsive forces in the formation of tactoids, thixotropic gels, protein crystals and coacervates. *Journal of Chemical Physics*, 6(12), 873–896.
- Larson, R. G. (1999). *The structure and rheology of complex fluids*. New York: Oxford University Press.
- Larson, I., Drummond, C. J., Chan, D. Y. C., & Grieser, F. (1993). Direct force measurements between titanium dioxide surfaces. *Journal of the American Chemical Society*, 115(25), 11885–11890.
- Lasic, D. D. (1988). The mechanism of vesicle formation. *Biochemical Journal*, 256(1), 1–11.
- Lau, A. W. C., Levine, D., & Pincus, P. (2000). Novel electrostatic attraction from plasmon fluctuations. *Physical Review Letters*, 84, 4116–4119.
- Laughlin, R. G. (1978). Solvation and structural requirements of surfactant hydrophilic groups. In G. H. Brown (Ed.), *Advances in liquid crystals*, 3 (pp. 41–148). New York: Academic Press.
- Laughlin, R. G. (1981). HLB, from a thermodynamic perspective. *Journal of the Society of Cosmetic Chemists*, 32(6), 371–392.
- Le, T. D., & Weers, J. G. (1995). QSPR and GCA models for predicting the normal boiling points of fluorocarbons. *Journal of Physical Chemistry*, 99(17), 6739–6747.
- Leach, A. R. (2001). *Molecular modeling: principles and applications*. Harlow, England: New York Prentice Hall.
- Leckband, D. (1994). Forces and molecular mechanisms of receptor-mediated interactions between model membranes. *Journal of Cellular Biochemistry*, 240.
- Leckband, D., & Israelachvili, J. (2001). Intermolecular forces in biology. *Quarterly Reviews of Biophysics*, 34(2), 105–267.
- Leckband, D. E., Helm, C. A., & Israelachvili, J. (1993). Role of calcium in the adhesion and fusion of bilayers. *Biochemistry*, 32(4), 1127–1140.
- Leckband, D. E., Schmitt, F. J., Israelachvili, J. N., & Knoll, W. (1994). Direct force measurements of specific and nonspecific protein interactions. *Biochemistry*, 33(15), 4611–4624.
- Leckband, D. E., Kuhl, T., Wang, H. K., Herron, J., Muller, W., & Ringsdorf, H. (1995). 4-4-20 Anti-fluoresceyl IgG Fab' recognition of membrane bound haptens: direct evidence for the role of protein and interfacial structure. *Biochemistry*, 34, 11467–11478.
- Leckband, D., Muller, W., Schmitt, F.-J., & Ringsdorf, H. (1995). Molecular mechanisms determining the strength of receptor-mediated intermembrane adhesion. *Biophysical Journal*, 69(3), 1162–1169.

- Lee, Y.-C., Taraschi, T. F., & Janes, N. W. (1993). Support for the shape concept of lipid structure based on a headgroup volume approach. *Biophysical Journal*, 65(4), 1429–1432.
- Lee, G., Kidwell, D. A., & Colton, R. J. (1994). Sensing discrete streptavidin-biotin interactions with atomic force microscopy. *Langmuir*, 10, 354–357.
- Leermakers, F. A. M., & Scheutjens, J. M. H. M. (1988). Statistical thermodynamics of association colloids. I. Lipid bilayer membranes. *Journal of Chemical Physics*, 89(5), 3264–3274.
- Leikin, S., Parsegian, V. A., Rau, D. C., & Rand, R. P. (2003). Hydration forces. *Annual Review of Physical Chemistry*, 44(1), 369–395.
- Lekkerkerker, H. N. W., Poon, W. C. K., Pusey, P. N., Stroobants, A., & Warren, P. B. (1992). Phase behaviour of colloid + polymer mixtures. *Europhysics Letters*, 20(6), 559–564.
- LeNeveu, D. M., Rand, R. P., & Parsegian, V. A. (1976). Measurement of forces between lecithin bilayers. *Nature*, 259(5544), 601–603.
- Lennard-Jones, J. E., & Dent, B. M. (1928). Cohesion at a crystal surface. *Transactions of the Faraday Society*, 24, 92–108.
- Lewis, B. A., & Engelman, D. M. (1983b). Lipid bilayer thickness varies linearly with acyl chain length in fluid phosphatidylcholine vesicles. *Journal of Molecular Biology*, 166(2), 211–217.
- Li, F., & Pincet, F. (2007). Confinement free energy of surfaces bearing end-grafted, polymers in the mushroom regime and local measurement of the polymer density. *Langmuir*, 23(25), 12541–12548.
- Lifshitz, E. M. (1956). The theory of molecular attractive forces between solids. *Soviet Physics JETP*, 2(1), 73–83.
- Lighthill, M. J. (1970). *Introduction to Fourier analysis and generalized functions*. London and New York: Cambridge University Press.
- Lin, T.-S., Tsen, M.-Y., Chen, S.-H., & Roberts, M. F. (1990). Temperature dependence of the growth of diheptanoylphosphatidylcholine micelles studied by small-angle neutron scattering. *Journal of Physical Chemistry*, 94(18), 7239–7243.
- Liphardt, J., Dumont, S., Smith, S. B., Tinoco, I., Jr., & Bustamante, C. (2002). Equilibrium information from nonequilibrium measurements in an experimental test of Jarzynski's equality. *Science*, 296(5574), 1832–1835.
- Lipkin, D. M., Israelachvili, J. N., & Clarke, D. (1997). Estimating the metal-ceramic van der Waals adhesion energy. *Philosophical Magazine A*, 76(4), 715–728.
- Lis, L. J., McAlister, M., Fuller, N. L., Rand, R. P., & Parsegian, V. A. (1982). Interactions between neutral phospholipid bilayer membranes. *Biophysical Journal*, 37(3), 657–665.
- London, F. (1937). The general theory of molecular forces. *Transactions of the Faraday Society*, 33, 8–26.
- Lua, R. C., & Grosberg, A. Y. (2005). Practical applicability of the Jarzynski relation in statistical mechanics: a pedagogical example. *Journal of Physical Chemistry B*, 109(14), 6805–6811.
- Luckham, P., & Klein, J. (1990). Forces between mica surfaces bearing adsorbed homopolymers in good solvents—the effect of bridging and dangling tails. *Journal of the Chemical Society, Faraday Transactions*, 86(9), 1363–1368.
- Luzar, A., Bratko, D., & Blum, L. J. (1987). Monte-Carlo simulation of hydrophobic interaction. *Chemical Physics*, 86(5), 2955–2959.
- Ly, H. V., Block, D. E., & Longo, M. L. (2002). Interfacial tension effect of ethanol on lipid bilayer rigidity, stability, and area/molecule: a micropipet aspiration approach. *Langmuir*, 18(23), 8988–8995.
- Lyklema, J., & Mysels, K. J. (1965). A study of double layer repulsion and van der Waals attraction in soap films. *Journal of American Chemical Society*, 87(12), 2539–2546.
- Lyle, I. G., & Tiddy, G. J. T. (1986). Hydration forces between surfactant bilayers – an equilibrium binding description. *Chemical Physics Letters*, 124(5), 432–436.
- Lyons, J. S., Furlong, D. N., & Healy, T. W. (1981). The electrical double-layer properties of the mica (muscovite)-aqueous electrolyte interface. *Australian Journal of Chemistry*, 34(6), 1177–1187.

- Mahanty, J., & Ninham, B. W. (1976). *Dispersion forces*. New York: Academic Press.
- Mahoney, M. W., & Jorgensen, W. L. (2000). A five-site model for liquid water and the reproduction of the density anomaly by rigid, nonpolarizable potential functions. *Journal of Chemical Physics*, 112(20), 8910–8922.
- Maitland, G., Rigby, M., Smith, E., & Wakeham, W. (1981). *Intermolecular forces: their origin and determination*. New York: Oxford Univ. Press.
- Malliaris, A., Le Moigne, J., Sturm, J., & Zana, R. (1985). Temperature-dependence of the micelle aggregation number and rate of intramicellar excimer formation in aqueous surfactant solutions. *Journal of Physical Chemistry*, 89(12), 2709–2713.
- Mamedov, S. S., Alexander, D., & Dhinojwala, A. (2002). A device for surface study of confined micron thin films in a total internal reflection geometry. *Review of Scientific Instruments*, 73, 2321.
- Mangipudi, V., Tirrell, M., & Pocius, A. V. (1994). Direct measurement of molecular level adhesion between poly(ethylene terephthalate) and polyethylene films: determination of surface and interfacial energies. *J. Adhesion Sci. Technol*, 8(11), 1251–1270.
- Mangipudi, V., Pocius, A. V., & Tirrell, M. (1995). Direct measurement of the surface energy of corona-treated polyethylene using the surface forces apparatus. *Langmuir*, 11(1), 19–23.
- Manning, G. S. (1969). Limiting laws and counterion condensation in polyelectrolyte solutions. I. Colligative properties. *Journal of Chemical Physics*, 51, 924–933.
- Marcelja, S. (1973). Molecular model for phase transition in biological membranes. *Nature*, 241(5390), 451–453.
- Marcelja, S. (1997). Effects of ion hydration in double layer interaction. *Colloids and Surfaces A*, 130, 321–326.
- Marcelja, S. (2000). Exact description of aqueous electrical double layers. *Langmuir*, 16(15), 6081–6083.
- Marcelja, S., Mitchell, D. J., Ninham, B. W., & Sculley, M. J. (1977). Role of solvent structure in solution theory. *Journal of the Chemical Society, Faraday Transactions*, 2(73), 630–648.
- Margenau, H., & Kestner, N. R. (1971). *Theory of intermolecular forces*. Oxford: Pergamon.
- Marinova, K. G., Alargova, R. G., Denkov, N. D., Velev, O. D., Petsev, D. N., Ivanov, I. B., et al. (1996). Charging of oil-water interfaces due to spontaneous adsorption of hydroxyl ions. *Langmuir*, 12(8), 2045–2051.
- Marra, J. (1986a). Direct measurements of attractive Van der Waals and adhesion forces between uncharged lipid bilayers in aqueous solutions. *Journal of Colloid and Interface Science*, 109(1), 11–20.
- Marra, J. (1986b). Effects of counterion specificity on the interactions between quaternary ammonium surfactants in monolayers and bilayers. *Journal of Physical Chemistry*, 90(10), 2145–2150.
- Marra, J. (1986c). Direct measurement of the interaction between phosphatidylglycerol bilayers in aqueous electrolyte solutions. *Biophysical Journal*, 50(5), 815–825.
- Marra, J., & Israelachvili, J. N. (1985). Direct measurements of forces between phosphatidylcholine and phosphatidylethanolamine bilayers in aqueous-electrolyte solutions. *Biochemistry*, 24(17), 4608–4618.
- Marsh, D. (1989). Water adsorption isotherms and hydration forces for lysolipids and diacyl phospholipids. *Biophysical Journal*, 55(6), 1093–1100.
- Marsh, D. (1990). *Handbook of lipid bilayers*. Boca Raton: CRC Press.
- Marsh, D. (2006). Elastic curvature constants of lipid monolayers and bilayers. *Chemistry and Physics of Lipids*, 144(2), 146–159.
- Marshall, B. T., Long, M., Piper, J. W., Yago, T., McEver, R. P., & Zhu, C. (2003). Direct observation of catch bonds involving cell-adhesion molecules. *Nature*, 423(6936), 190–193.
- May, S. (2000). A molecular model for the line tension of lipid membranes. *The European Physical Journal E: Soft Matter and Biological Physics*, 3(1), 37–44.
- Mazer, N. A., Benedek, G. B., & Carey, M. C. (1976). An investigation of the micellar phase of sodium dodecyl sulfate in aqueous sodium chloride solutions using quasielastic light scattering spectroscopy. *Journal of Physical Chemistry*, 80(10), 1075–1085.

- McConnell, H. M. (1991). Structures and transitions in lipid monolayers at the air–water interface. *Annual Review of Physical Chemistry*, 42, 171–195.
- McGuigan, P., & Israelachvili, J. N. (1990). Adhesion and short-range forces between surfaces. II. Effects of surface lattice mismatch. *Journal of Materials Research*, 5(10), 2232–2243.
- McGuigan, P. M., Wallace, J. S., Smith, D. T., Sridhar, I., Zheng, Z. W., & Johnson, K. L. (2007). Contact mechanics of layered elastic materials: experiment and theory. *Journal of Physics D-Applied Physics*, 40(19), 5984–5994.
- McIntosh, T. J., & Simon, S. A. (1986). Hydration force and bilayer deformation: a reevaluation. *Biochemistry*, 25(14), 4058–4066.
- McIntosh, T. J., Magid, A. D., & Simon, S. A. (1989a). Range of the solvation pressure between lipid membranes: dependence on the packing density of solvent molecules. *Biochemistry*, 28(19), 7904–7912.
- McIntosh, T. J., Magid, A. D., & Simon, S. A. (1989b). Repulsive interactions between uncharged bilayers: Hydration and fluctuation pressures for monoglycerides. *Biophysical Journal*, 55(5), 897–904.
- McLachlan, A. D. (1963a). Retarded dispersion forces between molecules. *Proceedings of the Royal Society of London. Series A. Mathematical and Physical Sciences*, 271(1346), 387–401.
- McLachlan, A. D. (1963b). Retarded dispersion forces in dielectrics at finite temperatures. *Proceedings of the Royal Society of London. Series A. Mathematical and Physical Sciences*, 274(1356), 80–90.
- McLachlan, A. D. (1963c). 3-body dispersion forces. *Molecular Physics*, 6(4), 423–427.
- McLachlan, A. D. (1964). Van der waals forces between an atom and a surface. *Molecular Physics*, 7(4), 381–388.
- McLachlan, A. D. (1965). Effect of the medium on dispersion forces in liquids. *Discussions of the Faraday Society*, 40, 239–245.
- McLaughlin, S. (1989). The electrostatic properties of membranes. *Annual Review of Biophysics and Biophysical Chemistry*, 18, 113–136.
- McLaughlin, S., Mulrine, N., Gresalfi, T., Vaio, G., & McLaughlin, A. (1981). Adsorption of divalent cations to bilayer membranes containing phosphatidylserine. *Journal of General Physiology*, 77(4), 445–473.
- McQuarrie, D. A. (2000). *Statistical mechanics*. New York: Harper & Row.
- Meagher, J. (1992). Direct measurement of forces between silica surfaces in aqueous CaCl₂ solutions using an atomic force microscope. *Journal of Colloid and Interface Science*, 152, 293–295.
- Mehta, A. (1994). *Granular matter: an interdisciplinary approach*. New York: Springer-Verlag.
- Meijer, E. J., & Frenkel, D. (1991). Computer-simulation of polymer-induced clustering of colloids. *Physical Review Letters*, 67(9), 1110–1113.
- Merrill, W. W., Pocius, A. V., Thakker, B. V., & Tirrell, M. (1991). Direct Measurement of Molecular-Level Adhesion Forces between Biaxially Oriented Solid Polymer-Films. *Langmuir*, 7(9), 1975–1980.
- Meurk, A., Luckham, P. F., & Bergström, L. (1997). Direct measurement of repulsive and attractive van der Waals forces between inorganic materials. *Langmuir*, 13(14), 3896–3899.
- Meyer, E., Rosenberg, K., & Israelachvili, J. (2006). Recent progress in understanding hydrophobic interactions. *Proceedings of the National Academy of Sciences of the United States of America*, 103, 15739–15746.
- Milling, A., Mulvaney, P., & Larson, I. (1996). Direct measurement of repulsive van der Waals interactions using an atomic force microscope. *Journal of Colloid and Interface Science*, 180(2), 460–465.
- Min, Y., Akbulut, M., Kristiansen, K., Golan, Y., & Israelachvili, J. (2008). Role of interparticle and external forces in nanoparticle assembly. *Nature Materials*, 7, 527–538.
- Missel, P. J., Mazer, N. A., Benedek, G. B., Young, C. Y., & Carey, M. C. (1980). Thermodynamic analysis of the growth of sodium dodecyl sulfate micelles. *Journal of Physical Chemistry*, 84(9), 1044–1057.
- Missel, P. J., Mazer, N. A., Carey, M. C., & Benedek, G. B. (1982). Thermodynamics of the sphere-to-rod transition in alkyl sulfate micelles. In K. L. Mittal, & E. J. Fendler (Eds.), *Solution behaviour of surfactants*, 1 (pp. 373–388). New York: Plenum.

- Missel, P. J., Mazer, N. A., Benedek, G. B., & Carey, M. C. (1983). Influences of chain-length on the sphere-to-rod transition in alkyl sulfate micelles. *Journal of Physical Chemistry*, 87(7), 1264–1277.
- Missel, P. J., Mazer, N. A., Carey, M. C., & Benedek, G. B. (1989). Influence of alkali-metal counterion identity on the sphere-to-rod transition in alkyl sulfate micelles. *Journal of Physical Chemistry*, 93(26), 8354–8366.
- Mitchell, D. J., & Ninham, B. W. (1981). Micelles, vesicles and microemulsions. *Journal of the Chemical Society, Faraday Transactions II*, 77(4), 601–629.
- Mo, Y. F., Turner, K. T., & Szlufarska, I. (2009). Friction laws at the nanoscale. *Nature*, 457(7233), 1116–1119.
- Moelwyn-Hughes, E. A. (1961). *Physical chemistry*. Oxford: Pergamon.
- Mohideen, U., & Roy, A. (1998). Precision measurement of the Casimir force from 0.1 to 0.9 μm. *Physical Review Letters*, 81(21), 4549–4552.
- Moy, V. T., Florin, E.-L., & Gaub, H. E. (1994). Intermolecular forces and energies between ligands and receptors. *Science*, 266, 257–259.
- Mugele, F., & Baret, J. C. (2005). Electrowetting: from basics to applications. *Journal of Physics – Condensed Matter*, 17(28), R705–R774.
- Mukerjee, P., & Mysels, K. J. (1970). *Critical micelle concentrations of aqueous systems*. Washington D.C.: National Bureau of Standards.
- Mukhopadhyay, A., Zhao, J., Bae, S. C., & Granick, S. (2002). Contrasting friction and diffusion in molecularly thin confined films. *Physical Review Letters*, 89(13), 136103.
- Munday, J. N., Capasso, F., & Parsegian, V. A. (2009). Measured long-range repulsive Casimir-Lifshitz forces. *Nature*, 457(7226), 170–173.
- Murphy, D. J. (1982). The importance of non-planar bilayer regions in photosynthetic membranes and their stabilisation by galactolipids. *FEBS Letters*, 150(1), 19–26.
- Murray, C. A., & Grier, D. G. (1996). Video microscopy of monodisperse colloidal systems. *Annual Review of Physical Chemistry*, 47, 421.
- Nagarajan, R. (1987). Self-assembly of bola amphiphiles. *Chemical Engineering Communications*, 55(1–6), 251–273.
- Nagarajan, R., & Ruckenstein, E. (1977). Critical micelle concentration: a transition point for micellar size distribution: a statistical thermodynamical approach. *Journal of Colloid Interface Science*, 60(2), 221–231.
- Nagarajan, R., & Ruckenstein, E. (1979). Aggregation of amphiphiles as micelles or vesicles in aqueous media. *Journal of Colloid and Interface Science*, 71(3), 580–604.
- Nicholson, D., & Parsonage, N. G. (1982). *Computer simulation and the statistical mechanics of adsorption*. New York: Academic Press.
- Niebel, K. F., & Venables, J. A. (1974). Explanation of crystal-structure of rare-gas solids. *Proceedings of the Royal Society of London Series a-Mathematical Physical and Engineering Sciences*, 336(1606), 365–377.
- Nightingale, E. R. (1959). Phenomenological theory of ion solvation: effective radii of hydrated ions. *Journal of Physical Chemistry*, 63(9), 1381–1387.
- Ninham, B. W., & Parsegian, V. A. (1970). van der Waals forces: special characteristics in lipid-water systems and a general method of calculation based on the Lifshitz theory. *Biophysical Journal*, 10(7), 646–663.
- Ninham, B. W., & Parsegian, V. A. (1971). Electrostatic potential between surfaces bearing ionizable groups in ionic equilibrium with physiologic saline solution. *Journal of Theoretical Biology*, 31(3), 405–428.
- Noppl-Simson, D. A., & Needham, D. (1996). Avidin-biotin interactions at vesicle surfaces: adsorption and binding, cross-bridge formation, and lateral interactions. *Biophysical Journal*, 70(3), 1391–1401.
- Norrish, K. (1954). The swelling of montmorillonite. *Discussions of the Faraday Society*, 18, 120–134.
- Ohshima, H. (1995a). Electrostatic interaction between 2 dissimilar spheres with constant surface-charge density. *Journal of Colloid and Interface Science*, 170, 432–439.

- Ohshima, H. (1995b). Electrostatic interaction between 2 dissimilar spheres: image-interaction correction to the linear superposition approximation. *Journal of Colloid and Interface Science*, 176, 7–16.
- Ohshima, H., Healy, T. W., & White, L. R. (1982a). Improvement on the Hogg—Healy—Fuerstenau formulas for the interaction of dissimilar double layers: I. Second and third approximations for moderate potentials. *Journal of Colloid and Interface Science*, 89(2), 484–493.
- Ohshima, H., Inoko, Y., & Mitsui, T. (1982b). Hamaker constant and binding constants of Ca⁺ and Mg²⁺ in dipalmitoyl phosphatidylcholine water system. *Journal of Colloid and Interface Science*, 86(1), 57–72.
- Okamoto, S., & Hachisu, S. (1977). Ordered structure in monodisperse gold sol. *Journal of Colloid and Interface Science*, 62(1), 172–181.
- Onoda, G. Y., & Liniger, E. G. (1990). Random loose packings of uniform spheres and the dilatancy onset. *Physical Review Letters*, 64(22), 2727–2730.
- Onsager, L. (1949). The effects of shape of the interaction of colloidal particles. *Annals of the New York Academy of Sciences*, 51, 627–659.
- Oosawa, F. (1971). *Polyelectrolytes*. New York: Marcel Dekker.
- Owens, D. K. (1970). Some thermodynamic aspects of polymer adhesion. *Journal of Applied Polymer Science*, 14, 1725–1730.
- Pacheco, J. M., & Ekardt, W. (1992). Microscopic calculation of the vanderwaals interaction between small metal-clusters. *Physical Review Letters*, 68(25), 3694–3697.
- Pallas, N. R., & Pethica, B. A. (1985). Liquid-expanded to liquid-condensed transition in lipid monolayers at the air/water interface. *Langmuir*, 1(4), 509–513.
- Pallas, N. R., & Pethica, B. A. (1987). The liquid-vapour transition in monolayers of n-pentadecanoic acid at the air/water interface. *Journal of the Chemical Society, Faraday Transactions I*, 83(3), 585–590.
- Panella, V., Chiarello, R., & Krim, J. (1996). Adequacy of the Lifshitz theory for certain thin adsorbed films. *Physical Review Letters*, 76(19), 3606–3609.
- Pangali, C., Rao, M., & Berne, B. J. (1979). A Monte Carlo simulation of the hydrophobic interaction. *Journal of Chemical Physics*, 71(7), 2975–2981.
- Papahadjopoulos, D., Vail, W. J., Newton, C., Nir, S., Jacobson, K., Poste, G., et al. (1977). Studies on membrane fusion. III. The role of calcium-induced phase changes. *Biochimica et Biophysica Acta*, 465(3), 579–598.
- Parker, J. L., Christenson, H. K., & Ninham, B. W. (1989a). Device for measuring the force and separation between two surfaces down to molecular separations. *Review of Scientific Instruments*, 60(10), 3135–3138.
- Parsegian, V. A. (1966). Theory of liquid-crystal phase transitions in lipid + water systems. *Transactions of the Faraday Society*, 62(520P), 848–860.
- Parsegian, V. A. (2006). *Van der Waals forces: a handbook for biologists, chemists, engineers, and physicists*. New York: Cambridge University Press.
- Parsegian, V. A., & Gingell, D. (1972). Electrostatic interaction across a salt solution between 2 bodies bearing unequal charges. *Biophysical Journal*, 12(9), 1192–1204.
- Parsegian, V. A., & Weiss, G. H. (1981). Spectroscopic parameters for computation of van der Waals forces. *Journal of Colloid and Interface Science*, 81(1), 285–289.
- Parsegian, V. A., Fuller, N., & Rand, R. P. (1979). Measured work of deformation and repulsion of lecithin bilayers. *Proceedings of the National Academy of Sciences of the United States of America*, 76(6), 2750–2754.
- Parsons, J. M., Siska, P. E., & Lee, Y. T. (1972). Intermolecular potentials from crossed-beam differential elastic scattering measurements. IV. Ar+Ar. *Journal of Chemical Physics*, 56(4), 1511–1516.
- Pashley, R. M. (1977). The van der Waals interaction for liquid water: a comparison of the oscillator model approximation and use of the Kramers—Kronig equation with full spectral data. *Journal of Colloid and Interface Science*, 62(2), 344–347.

- Pashley, R. M. (1980). Multilayer adsorption of water on silica – an analysis of experiment results. *Journal of Colloid and Interface Science*, 78(1), 246–248.
- Pashley, R. M. (1981a). Hydration forces between mica surfaces in aqueous-electrolyte solutions. *Journal of Colloid and Interface Science*, 80(1), 153–162.
- Pashley, R. M. (1981b). DLVO and hydration forces between mica surfaces in Li⁺, Na⁺, K⁺, and Cs⁺ electrolyte solutions: a correlation of double-layer and hydration forces with surface cation exchange properties. *Journal of Colloid and Interface Science*, 83(2), 531–545.
- Pashley, R. M., & Israelachvili, J. N. (1981). A comparison of surface forces and interfacial properties of mica in purified surfactant solutions. *Colloids and Surfaces*, 2(2), 169–187.
- Pashley, R. M., & Kitchener, J. A. (1979). Surface forces in adsorbed multilayers of water on quartz. *Journal of Colloid and Interface Science*, 71(3), 491–500.
- Pashley, R. M., & Ninham, B. W. (1987). Double-layer forces in ionic micellar solutions. *Journal of Physical Chemistry*, 91(11), 2902–2904.
- Pashley, R. M., & Quirk, J. P. (1984). The effect of cation valency on DLVO and hydration forces between macroscopic sheets of muscovite mica in relation to clay swelling. *Colloids and Surfaces*, 9(1), 1–17.
- Pashley, R. M., McGuiggan, P. M., Ninham, B. W., Brady, J., & Evans, D. F. (1986). Direct measurements of surface forces between bilayers of double-chained quaternary ammonium acetate and bromide surfactants. *Journal of Physical Chemistry*, 90(8), 1637–1642.
- Pass, G. (1973). *Ions in solution 3: inorganic properties*. London: Clarendon Press.
- Patel, S. S., & Tirrell, M. (1989). Measurement of forces between surfaces in polymer fluids. *Annual Review of Physical Chemistry*, 40, 597–635.
- Pauling, L. (1935). The structure and entropy of ice and of other crystals with some randomness of atomic arrangement. *Journal of the American Chemical Society*, 57(12), 2680–2684.
- Pauling, L. (1960). *The nature of the chemical bond*. Ithaca: Cornell University Press.
- Payens, T. A. J. (1955). Ionized monolayers. *Philips Research Reports*, 10, 425–481.
- Perkin, S., Chai, L., Kampf, N., Raviv, U., Briscoe, W., Dunlop, I., et al. (2006). Forces between mica surfaces, prepared in different ways, across aqueous and nonaqueous liquids confined to molecularly thin films. *Langmuir*, 22, 6142–6152.
- Perkin, S., Goldberg, R., Chai, L., Kampf, N., & Klein, J. (2009). Dynamic properties of confined hydration layers. *Faraday Discussions*, 141, 399–413.
- Peskin, C. S., Odell, G. M., & Oster, G. F. (1993). Cellular motions and thermal fluctuations: the Brownian ratchet. *Biophysical Journal*, 65(1), 316–324.
- Petsev, D. N., & Vekilov, P. G. (2000). Evidence for non-DLVO hydration interactions in solutions of the protein apoferritin. *Physical Review Letters*, 84(6), 1339–1342.
- Pettitt, B. M., & Rossky, P. J. (1986). Alkali halides in water: ion–solvent correlations and ion–ion potentials of mean force at infinite dilution. *Journal of Chemical Physics*, 84(10), 5836–5844.
- Pfeiffer, W., Henkel, Th., Sackmann, E., Knoll, W., & Richter, D. (1989). Local dynamics of lipid bilayers studied by incoherent quasi-elastic neutron scattering. *Europhysics Letters*, 8(2), 201–206.
- Pincus, P. (1976). Excluded volume effects and stretched polymer chains. *Macromolecules*, 9(3), 386–388.
- Podgornik, R., Rau, D. C., & Parsegian, V. A. (1994). Parametrization of direct and soft steric-undulatory forces between DNA double helical polyelectrolytes in solutions of several different anions and cations. *Biophysical Journal*, 66(4), 962–971.
- Pratt, L. R., & Chandler, D. (1977). Theory of the hydrophobic effect. *Journal of Chemical Physics*, 67(8), 3683–3704.
- Prieve, D. C. (1999). Measurement of colloidal forces with TIRM. *Advances in Colloid and Interface Science*, 82(1–3), 93–125.
- Prieve, D. C., & Frej, N. A. (1990). Total internal reflection microscopy: a quantitative tool for the measurement of colloidal forces. *Langmuir*, 6(2), 396–403.

- Prieve, D. C., & Ruckenstein, E. (1976). The surface potential of and double-layer interaction force between surface characterized by multiple ionizable groups. *Journal of Theoretical Biology*, 56, 205–228.
- Prieve, D. C., & Russel, W. B. (1988). Simplified predictions of Hamaker constants from Lifshitz theory. *Journal of Colloid and Interface Science*, 125(1), 1–13.
- Prieve, D. C., Bike, S. G., & Frej, N. A. (1990). Brownian motion of a single microscopic sphere in a colloidal force field. *Faraday Discussions of the Chemical Society*, 90, 209–222.
- Princen, H. M., Aronson, M. P., & Moser, J. C. (1980). Highly concentrated emulsions. II. Real systems. The effect of film thickness and contact angle on the volume fraction in creamed emulsions. *Journal of Colloid and Interface Science*, 75(1), 246–270.
- Pryde, J. A. (1966). *The liquid state*. London: Hutchinson University Library.
- Pugh, R. J., & Yoon, R. H. (1994). Hydrophobicity and rupture of thin aqueous films. *Journal of Colloid and Interface Science*, 163(1), 169–176.
- Pusey, P. N., Poon, W. C. K., Ilett, S. M., & Bartlett, P. (1994). Phase behavior and structure of colloidal suspensions. *Journal of Physics: Condensed Matter*, 6, A29–A39.
- Puvvada, S., & Blanckstein, D. (1990). Molecular-thermodynamic approach to predict micellization, phase behavior and phase separation of micellar solutions. I. Application to nonionic surfactants. *Journal of Chemical Physics*, 92(6), 3710–3724.
- Quirk, J. P. (1994). Interparticle forces: a basis for the interpretation of soil physical behavior. *Advances in Agronomy*, 53, 121–183.
- Ramachandran, A., Anderson, T. H., Leal, L. G., & Israelachvili, J. N. (2011). Adhesive interactions between vesicles in the strong adhesion limit. *Langmuir*, 27, 59–73.
- Rand, R. P., & Parsegian, V. A. (1989). Hydration forces between phospholipid bilayers. *Biochimica et Biophysica Acta*, 988(3), 351–376.
- Rau, D. C., Lee, B., & Parsegian, V. A. (1984). Measurement of the repulsive force between polyelectrolyte molecules in ionic solution: hydration forces between parallel DNA double helices. *Proceedings of the National Academy of Sciences*, 81(9), 2621–2625.
- Raviv, U., Pierre, L., & Klein, J. (2002a). Fluidity of bound hydration layers. *Science*, 297, 1540–1543.
- Raviv, U., Giasson, S., Frey, J., & Klein, J. (2002b). Viscosity of ultra-thin water films confined between hydrophobic or hydrophilic surfaces. *Journal of Physics: Condensed Matter*, 14(40), 9275–9283.
- Rawicz, W., Olbrich, K., McIntosh, T., Needham, D., & Evans, E. (2000). Effect of chain length and unsaturation on elasticity of lipid bilayers. *Biophysical Journal*, 79(1), 328–339.
- Ray, J., & Manning, G. S. (1994). An attractive force between two rodlike polyions mediated by the sharing of condensed counterions. *Langmuir*, 10(7), 2450–2461.
- Read, A. D., & Kitchener, J. A. (1969). Wetting films on silica. *Journal of Colloid and Interface Science*, 30(3), 391–398.
- Reiss-Husson, F. (1967). Structure des phases liquide-cristallines de différents phospholipides, mono-glycérides, sphingolipides, anhydres ou en présence d'eau. *Journal of Molecular Biology*, 25(3), 363–382.
- Requena, J., Billett, D. F., & Haydon, D. A. (1975). Van der Waals forces in oil-water systems from the study of thin lipid films. I. Measurement of the contact angle and the estimation of the van der Waals free energy of thinning of a film. *Proceedings of the Royal Society of London. Series A*, 347(1649), 141–159.
- Restagno, F., Crassous, J., Charlaix, E., Cottin-Bizonne, C., & Monchanin, M. (2002). A new surface forces apparatus for nanorheology. *Review of Scientific Instruments*, 73(6), 2292–2297.
- Richetti, P., & Kekicheff, P. (1992). Direct measurement of depletion and structural forces in a micellar system. *Physical Review Letters*, 68(12), 1951–1954.
- Rosenthal, P. B., Zhang, X., Formanowski, F., Fitz, W., Wong, C.-W., Meier-Ewert, H., et al. (1998). Structure of the haemagglutinin-esterase-fusion glycoprotein of influenza C virus. *Nature*, 396(6706), 92–96.

- Roth, C. M., Neal, B. L., & Lenhoff, A. M. (1996). Van der Waals interactions involving proteins. *Biophysical Journal*, 70(2), 977–987.
- Rouzina, I., & Bloomfield, V. A. (1996). Macroion attraction due to electrostatic correlation between screening counterions. 1. mobile surface-adsorbed ions and diffuse ion cloud. *Journal of Physical Chemistry*, 100(23), 9977–9989.
- Rowlinson, J. S. (2002). *Cohesion: a scientific history of intermolecular forces*. Cambridge, UK: Cambridge University Press.
- Ruckenstein, E., & Bhakta, A. (1994). Clustering and its effects on adsorption. *Langmuir*, 10(8), 2694–2698.
- Ruckenstein, E., & Li, B. Q. (1995). A surface equation of state-based on clustering of surfactant molecules of insoluble monolayers. *Langmuir*, 11(9), 3510–3515.
- Ruckenstein, E., & Li, B. Q. (1996). A simple surface equation of state for the phase transition in phospholipid monolayers. *Langmuir*, 12(9), 2308–2315.
- Rugar, D., & Hansma, P. (1990). Atomic force microscopy. *Physics Today*, 43(10), 23–30.
- Rushbrooke, G. S. (1940). On the statistical mechanics of assemblies whose energy levels depend on the temperature. *Transactions of the Faraday Society*, 36, 1055–1062.
- Russel, W. S., Saville, D. A., & Schowalter, W. R. (1999). *Colloidal dispersions*. Cambridge, UK: Cambridge University Press.
- Ruths, M., Alcantar, N. A., & Israelachvili, J. N. (2003). Boundary friction of aromatic silane self-assembled monolayers measured with the surface forces apparatus and friction force microscopy. *Journal of Physical Chemistry B*, 107(40), 11149–11157.
- Ruths, M., & Israelachvili, J. N. (2010). Surface forces and nanorheology of molecularly thin films. In B. Bhushan (Ed.), *Springer handbook of nanotechnology* (3rd ed.), (pp. 857–922) Springer-Verlag.
- Ruths, M., Heuberger, M., Scheumann, V., Hu, J., & Knoll, W. (2001). Confinement-induced film thickness transitions in liquid crystals between two alkanethiol monolayers on gold. *Langmuir*, 17(20), 6213–6219.
- Sabisky, E. S., & Anderson, C. H. (1973). Verification of the Lifshitz theory of the van der Waals potential using liquid-helium films. *Physical Review A*, 7(2), 790–806.
- Safinya, C. R., Roux, D., Smith, G. S., Sinha, S. K., Dimon, P., Clark, N. A., et al. (1986). Steric interactions in a model multimembrane system: a synchrotron X-ray study. *Physical Review Letters*, 57(21), 2718–2721.
- Safran, S. A., Kuhl, T. L., & Israelachvili, J. N. (2001). Polymer-induced membrane contraction, phase separation, and fusion via Marangoni flow. *Biophysical Journal*, 81(2), 659–666.
- Saluja, P. P. S. (1976). Environment of ions in aqueous solutions. *Int. Rev. Sci. Electrochemistry. Physical Chemistry Series 2*. London, Butterworth: A.D. Buckingham. 6, 1–52.
- Saterbak, A., & Lauffenburger, D. A. (1996). Adhesion mediated by bonds in series. *Biotechnology Progress*, 12(5), 682–699.
- Schmitz, K., Holcomb-Wygle, D. L., Oberski, D. J., & Lindermann, C. B. (2000). Measurement of the force produced by an intact bull sperm flagellum in isometric arrest and estimation of the dynein stall force. *Biophysical Journal*, 79, 468–478.
- Schnakenberg, J. (1976). Network theory of microscopic and macroscopic behavior of master equation systems. *Reviews of Modern Physics*, 48(4), 571–585.
- Schneider, J., & Tirrell, M. (1999). Direct measurement of molecular level forces and adhesion in biological systems. In E. Mathiowicz, D. E. Chickering & C.-M. Lehr (Eds.), *Bioadhesive drug delivery systems: fundamentals, novel approaches, and development*, Vol. 98 (pp. 223–256). NY: Marcel Dekker.
- Schuster, P., Zundel, G., & Sandorfy, C. (1976). *The hydrogen bond*. Amsterdam: North-Holland Publ.
- Seifert, U. (2000). Rupture of multiple parallel molecular bonds under dynamic loading. *Physical Review Letters*, 84(12), 2750.
- SenGupta, A. K., & Papadopoulos, K. D. (1997). Electrokinetic transport of a slender particle through a pore. *Journal of the Chemical Society, Faraday Transactions*, 93(20), 3695–3701.

- Servuss, R. M., & Helfrich, W. (1989). Mutual adhesion of lecithin membranes at ultralow tensions. *Journal of Physics (France)*, 50(7), 809–827.
- Shinoda, K., Nakagawa, T., Tamamushi, B., & Isemura, T. (1963). *Colloidal surfactants*. New York: Academic Press.
- Shklovskii, B. I. (1999). Wigner crystal model of counterion induced bundle formation of rodlike polyelectrolytes. *Physical Review Letters*, 82, 3268–3271.
- Shubin, V. E., & Kékicheff, P. (1993). Electrical double layer structure revisited via a surface force apparatus: mica interfaces in lithium nitrate solutions. *Journal of Colloid and Interface Science*, 155, 108–123.
- Singer, S. J., & Nicholson, G. L. (1972). The fluid mosaic model of the structure of cell membranes. *Science*, 175(4023), 720–731.
- Skehel, J. J., & Wiley, D. C. (1998). Coiled coils in both intracellular vesicle and viral membrane fusion. *Cell*, 95(7), 871–874.
- Small, P. A. (1953). Some factors affecting the solubility of polymers. *Journal of Applied Chemistry*, 3(2), 71–80.
- Smith, C. P., Maeda, M., Atanasoska, L., White, H. S., & McClure, D. J. (1988). Ultrathin platinum films on mica and the measurement of forces at the platinum/water interface. *Journal of Physical Chemistry*, 92(1), 199–205.
- Smith, D. E., Zhang, L., & Haymet, A. D. J. (1992). Entropy of association of methane in water: a new molecular dynamics computer simulation. *Journal of the American Chemical Society*, 114(14), 5875–5876.
- Smyth, C. P. (1955). *Dielectric behaviour and structure*. New York: McGraw-Hill.
- Sogami, I., & Ise, N. (1984). On the electrostatic interaction in macroionic solutions. *Journal of Chemical Physics*, 81(12), 6320–6332.
- Sowers, A. E. (Ed.). (1987). *Cell fusion*. New York: Plenum.
- Stafford, R. E., Fanni, T., & Dennis, E. A. (1989). Interfacial properties and critical micelle concentration of lysophospholipids. *Biochemistry*, 28(12), 5113–5120.
- Standard, J. M., & Certain, P. R. (1985). Bounds to 2-body and 3-body long-range interaction coefficients for S-state atoms. *Journal of Chemical Physics*, 83(6), 3002–3008.
- Stecki, J. (1961). Molecular theory of electrostatic interactions between ions in a solvent. *Bulletin De L Academie Polonaise Des Sciences-Serie Des Sciences Chimiques*, 9, 429–434.
- Sterba, M., & Sheetz, M. P. (1998). Basic laser tweezers. *Methods in Cell Biology*, 55, 29–41.
- Stern, O. (1924). The theory of the electrolytic Double-layer. *Z. Elektrochemie und Angewandte Physikalische Chemie*, 30, 508.
- Sternberg, B., Watts, A., & Cejka, Z. (1993). Lipid-induced modulation of the protein packing in two-dimensional crystals of bacteriorhodopsin. *Journal of Structural Biology*, 110(3), 196–204.
- Stevens, M. J., Hoh, J. H., & Woolf, T. B. (2003). Insights into the molecular mechanism of membrane fusion from simulation: evidence for the association of splayed tails. *Physical Review Letters*, 91(18), 188102/1–188102/4.
- Stone, A. J. (1996). *The theory of intermolecular forces*. New York: Oxford University Press.
- Stroud, W., Curry, J., & Cushman, J. (2001). Capillary condensation in nanoscale contacts. *Langmuir*, 17(3), 688–698.
- Subramanian, V., & Ducker, W. (2001). Proximal adsorption of cationic surfactant on silica at equilibrium. *Journal of Physical Chemistry B*, 105, 1389–1409.
- Sutton, R. B., Fasshauer, D., Jahn, R., & Brunger, A. T. (1998). Crystal structure of a SNARE complex involved in synaptic exocytosis at 2.4 Å resolution. *Nature*, 395(6700), 347–353.
- Svoboda, K., & Block, S. M. (1994). Biological applications of optical forces. *Annual Review of Biophysics and Biomolecular Structure*, 23(1), 247–285.

- Szczesniak, M. M., Chalasinski, G., Cybulski, S. M., & Scheiner, S. (1990). Intermolecular potential of the methane dimer and trimer. *Journal of Chemical Physics*, 93(6), 4243–4253.
- Szleifer, I., Ben-Shaul, A., & Gelbart, W. M. (1985). Chain organization and thermodynamics in micelles and bilayers. II. Model calculations. *Journal of Chemical Physics*, 83(7), 3612–3620.
- Szleifer, I., Ben-Shaul, A., & Gelbart, W. M. (1986). Chain statistics in micelles and bilayers: effects of surface roughness. *Journal of Chemical Physics*, 85(9), 5345–5358.
- Tabor, D. (1982). Attractive surface forces. In J. W. Goodwin (Ed.), *Colloid dispersions* (pp. 23–46). London: Royal Society of Chemistry.
- Tabor, D., & Winterton, R. H. S. (1969). The direct measurement of normal and retarded van der Waals forces. *Proceedings of the Royal Society of London. Series A*, 312(1511), 435–450.
- Tadmor, R., Hernández-Zapata, E., Chen, N., Pincus, P., & Israelachvili, J. N. (2002). Debye length and double-layer forces in polyelectrolyte solutions. *Macromolecules*, 35(6), 2380–2388.
- Takano, K., & Hachisu, S. (1978). Spectroscopic study of monodisperse latex: I. Short-range order in monodisperse latex. *Journal of Colloid and Interface Science*, 66(1), 124–129.
- Tanford, C. (1980). *The hydrophobic effect*. New York: John Wiley & Sons.
- Tang, J. X., Wong, S., Tran, P. T., & Janmey, P. A. (1996). Counterion induced bundle formation of rodlike polyelectrolytes. *Berichte Der Bunsen-Gesellschaft-Physical Chemistry Chemical Physics*, 100(6), 796–806.
- Taylor, A. J., & Wood, F. W. (1957). The electrophoresis of hydrocarbon droplets in dilute solutions of electrolytes. *Transactions of the Faraday Society*, 53(4), 523–529.
- Thomas, G. F., & Meath, W. J. (1977). Dipole spectrum, sums and properties of ground-state methane and their relation to molar refractivity and dispersion energy constant. *Molecular Physics*, 34(1), 113–125.
- Thompson, D. W. (1968). *On growth and form*. New York: Cambridge University Press.
- Thompson, P. A., & Robbins, M. O. (1990). Origin of stick-slip motion in boundary lubrication. *Science*, 250(4982), 792–794.
- Tiddy, G. J. T. (1980). Surfactant-water liquid crystal phases. *Physics Reports*, 57(1), 1–46.
- Tirrell, M. (1996). Measurement of interfacial energy at solid polymer surfaces. *Langmuir*, 12(19), 4548–4551.
- Tirrell, M., Kokkoli, E., & Biesalski, M. (2002). The role of surface science in bioengineered materials. *Surface Science*, 500(1–3), 61–83.
- Tolansky, S. (1948). *Multiple beam interferometry of surfaces and films*. London: Oxford University Press.
- Tolansky, S. (1955). *An introduction to interferometry*. London: Longmans, Green & Co.
- Tonck, A., Georges, J. M., & Loubet, J. L. (1988). Measurements of intermolecular forces and the rheology of dodecane between alumina surfaces. *Journal of Colloid and Interface Science*, 126(1), 150–163.
- Torrie, G. M., & Valleau, J. P. (1979). A Monte Carlo study of an electrical double layer. *Chemical Physics Letters*, 65(2), 343–346.
- Torrie, G. M., & Valleau, J. P. (1980). Electrical double layers. I. Monte Carlo study of a uniformly charged surface. *Journal of Chemical Physics*, 73(11), 5807–5816.
- Tsao, Y. H., Yang, S. X., Evans, D. F., & Wennerstroem, H. (1991). Interactions between hydrophobic surfaces – dependence on temperature and alkyl chain length. *Langmuir*, 7(12), 3154–3159.
- Tsao, Y. H., Evans, D. F., & Wennerstroem, H. (1993). Long-range attraction between a hydrophobic surface and a polar surface is stronger than that between 2 hydrophobic surfaces. *Langmuir*, 9(3), 779–785.
- Tucker, E. E., Lane, E. H., & Christian, S. D. (1981). Vapor pressure studies of hydrophobic interactions. Formation of benzene-benzene and cyclohexane-cyclohexanol dimers in dilute aqueous solution. *Journal of Solution Chemistry*, 10(1), 1–20.
- Umeda, T., Suezaki, Y., Takiguchi, K., & Hotani, H. (2005). Theoretical analysis of opening-up vesicles with single and two holes. *Physical Review E*, 71(1), 011913.

- Umeyama, H., & Morokuma, K. (1977). The origin of hydrogen bonding. An energy decomposition study. *Journal of the American Chemical Society*, 99(5), 1316–1332.
- Usui, S., Sasaki, H., & Matsukawa, H. (1981). The dependence of zeta potential on bubble size as determined by the dorn effect. *Journal of Colloid and Interface Science*, 81(1), 80–84.
- van Blokland, P. H. G. M., & Overbeek, J. T. G. (1978). van der Waals forces between objects covered with a chromium layer. *Journal of the Chemical Society, Faraday Transactions I*, 74, 2637–2651.
- van Blokland, P. H. G. M., & Overbeek, J. T. G. (1979). Dispersion forces between objects of fused silica. *Journal of Colloid and Interface Science*, 68(1), 96–100.
- van Olphen, H. (1977). *An introduction to clay colloid chemistry*. Wiley, Krieger.
- Van Oss, C. J., Absalom, D. R., & Neumann, A. W. (1980). Applications of net repulsive van der Waals forces between different particles, macromolecules, or biological cells in liquids. *Colloids and Surfaces*, 1(1), 45–46.
- van Zanten, R., & Zasadzinski, J. A. (2005). Using cryo-electron microscopy to determine thermodynamic and elastic properties of membranes. *Current Opinion in Colloid & Interface Science*, 10(5–6), 261–268.
- Veatch, S. L., & Keller, S. L. (2003). Separation of liquid phases in giant vesicles of ternary mixtures of phospholipids and cholesterol. *Biophysical Journal*, 85(5), 3074–3083.
- Velamakanni, B. V., Chang, J. C., Lange, F. F., & Pearson, D. S. (1990). New method for efficient colloidal particle packing via modulation of repulsive lubricating hydration forces. *Langmuir*, 6(7), 1323–1325.
- Velamakanni, B. V., et al. (1990). *PhD Thesis*. Santa Barbara: University of California.
- Verschuur, G. L. (1993). *Hidden attraction: the history and mystery of magnetism*. New York and Oxford: Oxford University Press.
- Verwey, E. J. W., & Overbeek, J. T. G. (1948). *Theory of the stability of lyophobic colloids*. Amsterdam: Elsevier.
- Vigil, G., Xu, Z., Steinberg, S., & Israelachvili, J. (1994). Interactions of silica surfaces. *Journal of Colloid and Interface Science*, 165(2), 367–385.
- Vijayendran, R., Hammer, D., & Leckband, D. (1998). Simulations of the adhesion between molecularly bonded surfaces in direct force measurements. *Journal of Chemical Physics*, 108(18), 7783–7794.
- Visscher, K., Gross, S. P., & Block, S. M. (1996). Construction of multiple-beam optical traps wih nanometer-resolution position sensing. *IEEE Journal of Selected Topics in Quantum Electronics*, 2, 1066–1076.
- Watkins, M., & Tweed, M. (2000, 2005). *Useful mathematical and physical formulae*. Glastonbury, Somerset, UK: Wooden Books.
- Wawra, H. (1975). Surface-energy of solid materials as measured by ultrasonic and conventional test methods. 1. *Zeitschrift Fur Metallkunde*, 66(7–8), 395–401, 492–498.
- Wennerström, H., & Lindman, B. (1979). Micelles. Physical chemistry of surfactant association. *Physics Reports*, 52(1), 1–86.
- Wennerström, H., Jönsson, B., & Linse, P. (1982). The cell model for poly-electrolyte systems-exact statistical mechanical relations, Monte-Carlo simulations, and the Poisson-Boltzmann approximation. *Journal of Chemical Physics*, 76, 4665–4670.
- Wesson, L. G. (1948). *Tables of electric dipole moments*. Cambridge: The Technology Press MIT.
- Widom, B. (1963). Some topics in the theory of fluids. *Journal of Chemical Physics*, 39(11), 2808–2812.
- Wiener, M. C., & White, S. H. (1992). Structure of a fluid dioleoylphosphatidylcholine bilayer determined by joint refinement of x-ray and neutron diffraction data. III. Complete structure. *Biophysical Journal*, 61(2), 434–447.
- Wieslander, A., Christiansson, A., Rilfors, L., & Lindblom, G. (1980). Lipid bilayer stability in membranes. Regulation of lipid composition in *Acholeplasma laidlawii* as governed by molecular shape. *Biochemistry*, 19(16), 3650–3655.
- Williams, D. E. G. (1998). Packing fraction of a disk assembly randomly close packed on a plane. *Physical Review E*, 57(6), 7344.

- Wimley, W. C., & Thompson, T. E. (1990). Exchange and flip-flop of dimyristoyl phosphatidylcholine in liquid-crystalline, gel and two-component, two-phase large unilamellar vesicles. *Biochemistry*, 29(5), 1296–1303.
- Wong, J. Y., Kuhl, T. L., Israelachvili, J. N., Mullah, N., & Zalipsky, S. (1997). Direct measurement of a tethered ligand-receptor interaction potential. *Science*, 275(5301), 820–822.
- Woodcock, L. V. (1997). Entropy difference between the face-centred cubic and hexagonal close-packed crystal structures. *Nature*, 385(6612), 141–143.
- Xie, H. W., Song, K. Y., Mann, D. J., & Hase, W. L. (2002). Temperature gradients and frictional energy dissipation in the sliding of hydroxylated alpha-alumina surfaces. *Physical Chemistry Chemical Physics*, 4(21), 5377–5385.
- Yamada, S. (2003). Layering transitions and tribology of molecularly thin films of poly(dimethylsiloxane). *Langmuir*, 19(18), 7399–7405.
- Yamada, S. (2009). Structural aging and stiction dynamics in confined liquid films. *Journal of Chemical Physics*, 131(18), 9.
- Yoshizawa, H., Chen, Y.-L., & Israelachvili, J. (1993). Fundamental mechanisms of interfacial friction I: relation between adhesion and friction. *Journal of Physical Chemistry*, 97, 4128–4140.
- Yuet, P. K., & Blankschtein, D. (1996). Effect of surfactant tail-length asymmetry on the formation of mixed surfactant vesicles. *Langmuir*, 12(16), 3819–3827.
- Zäck, M., Vanicek, J., & Heuberger, M. (2003). The extended surface forces apparatus: III. High-speed interferometric distance measurement. *Review of Scientific Instruments*, 74, 260–266.
- Zappone, B., Ruths, M., Greene, G. W., Jay, G. D., & Israelachvili, J. (2007). Adsorption, lubrication, and wear of lubricin on model surfaces: polymer brush-like behavior of a glycoprotein. *Biophysical Journal*, 92, 1693–1707.
- Zasadzinski, J. A. (1997). Novel approaches to lipid based drug delivery. *Current Opinion in Solid State & Materials Science*, 2(3), 345–349.
- Zheng, Y., Won, Y. Y., Bates, F. S., Davis, H. T., Scriven, L. E., & Talmon, Y. (1999). Directly resolved core-corona structure of block copolymer micelles by cryo-transmission electron microscopy. *Journal of Physical Chemistry B*, 103(47), 10331–10334.
- Zhulina, E. B., Borisov, O. V., & Priamitsyn, V. A. (1990). Theory of steric stabilization of colloid dispersions by grafted polymers. *Journal of Colloid and Interface Science*, 137(2), 495–511.
- Zhulina, E. B., Borisov, O. V., Pryamitsyn, V. A., & Birshtein, T. M. (1991). Coil globule type transitions in polymers .1. Collapse of layers of grafted polymer-chains. *Macromolecules*, 24(1), 140–149.
- Zwanzig, R. (1963). Two assumptions in the theory of attractive forces between long saturated chains. *Journal of Chemical Physics*, 39(9), 2251–2258.



Index

A

Additive interactions, 29
Additivity, 209, 213
Adhesion
 biomembrane, 607
 capillary forces, 455
 contact angle hysteresis, 439
 contact angles and wetting films, 429
 energies versus forces, 419
 force, 237, 444
 friction controlled by, 477, 499
 and friction forces, 475
 highly curved surfaces and interfaces, 422
 hysteresis, 173, 448, 476, 477, 499
 JKR and Hertz theories, 442
 mechanics of, 453
 plastic deformations, 453
 of rough and textured surfaces, 452
 of solid particles, 442
 strength of, 455
 surface and interfacial energies, 415
 wetting of rough, textured, and chemically heterogeneous surfaces, 434
Adhesion energy, 196, 255, 275, 419
Adsorbed layers, 281
Adsorbed polymers, 385
Adsorbed surface films, 201
Adsorption, 198
AFM (Atomic Force Microscope), 14, 21, 147, 174, 245
Aggregates
 dimensionality and geometry, effects of, 510
 formation of, conditions necessary for, 509
 infinite versus finite sized, 513
 mesophases and multilayers, 528
 nucleation and growth of, 515
Aggregation number, 526, 528
Alder transitions, 116
Allosteric interaction, 601
Amontons' laws of friction, 479
Amorphous solid, 142
Amphiphiles, 506
Amphiphilic structures. *See also* Biological structures; Biological systems
 fluid, 535
 large and complex, 527, 557
 transitions between, 558

Amphiphilic surfaces, 363
Amphoteric surfaces, 311
Analytical methods, 37
Angle-averaged potential, 84
Anions, 55
Anisotropy, 127
Aqueous systems, solvation forces in, 361, 370
Archimedes, principle, 197
Area
 of contact, 493
 interaction, 211
 optimal headgroup, 536
Argon-Argon potential, 137
Associated colloids, 503
Associated liquids, 83, 153, 155
Associated molecules, 191
Asymmetric molecules, 359
Asymmetric surfaces, 321
Asymmetrical electrolytes, 313
Atomic Force Microscope (AFM), 14, 21, 147, 174, 245
Atomistic theories, 37
Atoms
 polarizability of, 91
 size of, 133
Attractive forces
 depletion, 398, 593
 hydrophobic, 370, 594
 intersegment and bridging, 394
Available energy. *See* Free energy
Azimuthal angles, 84

B

Bacon, Francis, 19
Bare ion radius, 133
Bell equation, 170, 619
Bending energy, 550
Bernal-Fowler rule, 378
Bilayers, 544, 550, 614
Bioadhesion, 606, 609
Biointeractions. *See* Dynamic biointeractions
Biological structures. *See also* Biological systems;
 Dynamic biointeractions
amphiphilic structures, transitions
 between, 558
bilayers, 544

- Biological structures (*Continued*)
 biological membranes, 564
 curvature effects, 550
 fluid amphiphilic structures, equilibrium considerations of, 535
 geometric packing, 538
 membrane lipids, 564
 membrane proteins and structure, 567
 nonspherical and cylindrical micelles, 543
 optimal headgroup area, 536
 self-assembly on surfaces and interfaces, 562
 spherical micelles, 540
 vesicles, 547
- Biological systems. *See also* Biological structures;
 Dynamic biointeractions
 attractive depletion forces, 593
 attractive hydrophobic forces, 594
 bioadhesion, 606
 biomembrane adhesion, 606
 bridging (tethering) forces, 601
 complementary and ligand-receptor interactions, 599
 DLVO forces, 579
 electrostatic forces, 579
 intermembrane and intramembrane forces, 604
 membrane fusion, 610
 repulsive entropic forces, 585
 van der Waals forces, 577
- Biomembrane adhesion, 606
- Biospecificity, 599
- Biosurfaces, 626
- Bjerrum length, 322
- Body forces, 218
- Boiling point, 33
- Boltzmann distribution, 26, 43, 229
- Bond
 chemical, 35, 53, 54
 covalent, 35, 53, 54, 133
 electronic polarizability of, 93
 hydrogen, 83, 151, 152
 ionic, 55
 moment, 71, 72
 in parallel, 622, 624
 physical non-covalent, 54
 polarizabilities of, 92
 in series, 622
- Bonding-unbonding processes, 178
- Born energy, 61, 65, 98
- Born repulsion, 133
- Boundary conditions, 294
- Branched chain molecules, 357
- Bridging force, 394, 601
- Brownian ratchet, 633
- Brownian velocity, 207
- C**
- CAC (critical aggregation concentration), 509, 512
- Capacitor, 57, 298
- Capillary condensation, 455
- Capillary forces, 456
- Capture, biological, 619, 626
- Casimir force, 272
- Casimir-Polder equation, 131
- Cassie equation, 373
- Cavities, 422
- Cell Sorting, 573
- Cellular membranes, 565
- Cellular streaming, 631
- Chain melting temperature, 548
- Chain packing, 558
- Chaotropes, 165
- Chaotropic agents, 165
- Charge regulation, 305, 318
- Charge-charge interactions, 54
- Charged surfaces
 in electrolyte solutions, 306
 pressure between, in water, 299
- Charge-dipole interaction, 76, 84
- Charging mechanism, 292
- Chemical bond, 35, 53, 54
- Chemical potential, 26, 27
- Chemically heterogeneous surfaces, 434
- Chord Theorem, 194, 215, 218
- Classical limit, 35
- Clathrate cage, 159
- Clays, swelling, 363
- Close-packing, 25
- Clusters, 422
- CMC (critical micelle concentration), 325, 509, 512
- Coagulation, 327
- Cohesion energy, 196
- Cohesive energy, 59
- Collisions
 energy transfer during molecular, 175
 multiple, 43
 time of, 173, 176
 two-body, 39
- Colloid science, 17
- Colloidal dispersion, 227
- Colloidal particle, 83
- Combining laws, 197
- Combining relations, 191, 197, 274
- Competitive adsorption, 311
- Complementary interactions, 195, 599
- Complex fluids, 503

- Compressibility Cell technique, 225
 Computer simulations, 37, 67, 495
 Conducting media, van der Waals forces between, 261
 Contact angle hysteresis, 439
 Contact angles, 203, 429, 441
 Contact electrification, 59
 Contact mechanics, 453
 Contact value theorem, 299, 349
 Continuum theories, 8, 35, 66
 Contour lengths, 382
 Core-shell nanoparticles, 288
 Couette flow, 485
 Coulomb forces, 54
 Coulomb friction, 472
 Coulomb interactions, 60, 62
 Counterions, 292, 293, 296. *See also* Electrostatic forces
 “Counterions only” systems, 293
 Covalent bond, 35, 53, 54, 133
 Covalent forces, 53
 Critical aggregation concentration (CAC), 509, 512
 Critical coagulation concentration, 327
 Critical micelle concentration (CMC), 325, 509, 512
 Curvature effects, 550
 Curved surfaces, 422
 Cyclic bonding-unbonding processes, 178
 Cylinders, 510
 Cylindrical micelles, 543
- D**
- De Broglie wavelength, 30
 Debonding (detachment) forces, 171, 626
 Deborah Number, 175, 182, 187, 492
 Debye interaction, 99
 Debye length, 274, 312
 Debye unit, 71
 Debye-Hückel equation, 313
 Deformations, 443, 453, 607
 Density distribution function, 26
 Depletion forces, attractive, 398, 593
 Derjaguin approximation, 215, 231, 442
 Desorption, 194, 202
 Detachment (debonding) forces, 171, 626
 Detailed Balance, 321
 Dewetting, 202
 Dielectric constants, 65, 55
 Dielectric permittivity, 55, 260, 265
 Diffuse double-layer, 295, 312
 Diffuse interfaces, 381
 Di-hexadecyl phosphate (DHP), 586
 Dipalmitolphosphatidyl glycerol (DPPG), 582
- Dipolar molecules, 71
 Dipolar polarizability, 93
 Dipole moment, 71, 72, 75
 Dipole-dipole interaction, 81, 85
 Dipoles
 dipole-induced interactions of, 99
 discrete surface charges and, 335
 magnetic, 83
 polarizability of, 91
 rotating, 84
 self-energy, 73
 Direct experiments, 5
 Direct force-measuring, 223, 227
 Directed-assembly, 503, 630
 interactions of, 214
 versus self-assembly, 628
 structures of, 555
 Directional bonding, 527
 Discrete atoms, 54
 Discrete surface charge, 335
 Discs, 510
 Disjoining pressure, 267, 303
 Dispersed molecules, 191
 Dispersion forces
 anisotropy of, 127
 London equation, 107
 strength of, 109
 Dissipation. *See* Energy transfer
 Distribution function, 510
 Divalent cations, 134
 Divalent ions, 311
 DLVO theory, 326, 331, 579
 Docking, 18
 Domains, 562
 Double-layer forces, 325, 331, 579
 Double-layer interaction, 313, 591
 Doubly charged ions, 311
 DPPG (dipalmitolphosphatidyl glycerol), 582
 Droplets, 511, 512
 Dry friction, 479
 Dupré equation, 417
 Dynamic biointeractions
 biological forces and interactions, subtleties of, 617
 biological membranes and biosurfaces, 626
 biological rupture and capture, 619
 bonds in parallel, 622, 624
 bonds in series, 622
 detachment versus capture processes, 626
 interactions evolving in space and time, 617
 motor proteins, 630
 protein engines, 630
 self-assembly versus directed-assembly, 628
 transport proteins, 630

Dynamic effects, 213
 Dynamic phases, 628

E

Ejection, 200
 Elastic coefficient, 169
 Elastic surfaces, 453
 Elasticity of monolayers and bilayers, 546, 550
 Elastohydrodynamic (EHD) friction, 474
 Electric dipole, 71
 Electric double-layer, 292
 Electric fields, 293, 298
 Electric susceptibility, 98
 Electro-capillarity effect, 433
 Electrokinetic forces, 334
 Electrolyte solutions
 charged surfaces in, 306
 electrostatic screening effects in, 273
 Electronegative atoms, 83
 Electroneutrality, 294
 Electronic polarizability, 92, 93, 102
 Electrostatic forces, 60
 asymmetric surfaces, 321
 biological systems, 579
 charge regulation, 318
 charged surfaces in electrolyte solutions, 306
 charged surfaces in water, 292
 charging of surfaces in liquids, 291
 contact value theorem, 299
 counterion concentration profile away from surface, 296
 Debye length, 312
 discrete surface charges and dipoles, 335
 divalent ions, effect of, 311
 DLVO theory, 325, 331
 double-layer interaction, 313
 electric field, origin of, 298
 electrokinetic, 334
 finite ion-size effects, 324
 finite reservoir systems, 324
 Grahame equation, 308
 ion-condensation, 322
 ion-correlation, 322
 ionic distribution, origin of, 298
 osmotic limit and charge regulation, 305
 Poisson-Boltzmann equation, 293
 pressure, origin of, 298
 pressure between two charged surfaces in water, 299
 surface charge and potential of isolated surfaces, 309
 surface charge, electric field, and counterion concentration at surface, 293
 surface potential, origin of, 298

thick wetting films, 303
 variation of potential gradient and ionic concentrations, 313
 Electrostatic interaction, 94, 613
 Electrostatic screening effects, 273
 Electro-wetting effect, 433
 Energetic instabilities, 237
 Energetics, 9
 Energy transfer (dissipation)
 during cyclic bonding-unbonding processes, 178
 during molecular collisions, 175, 469
 Energy-distance potential functions, 496
 Engineered-assembled structures, 555
 Engineered-assembly interactions, 214
 Engulfing, 198, 200
 Entropic effects, 86
 Entropy, 43
 Equation of state (EOS), van der Waals, 29, 113
 Equilibrium, 27, 43
 Ergodicity, 50
 Excess polarizability, 100, 101, 122
 Exchange repulsion, 133
 Exchangeable ions, 309
 Exchangeable surfaces, 309
 Exponential potential, 133, 136

F

Film
 adsorbed surface, 201
 liquid- and solid-like, transitions between, 489
 liquid-like, 489
 solid-like, 489
 thin, molecular ordering in, 342
 wetting, 201, 267, 303, 429
 Finite ion-size effects, 324
 Finite reservoir systems, 324
 Finite sized aggregates (micellization), 513
 First Bohr radius, 108
 First hydration shell, 80
 First ionization potential, 108
 First Law of Thermodynamics, 42
 Flat punch geometry, 454
 Flocculation, 327
 Flory radius, 382, 593
 Flow stress, 453
 Fluid amphiphilic structures, 535
 Fluidity, 360
 Fluid-like interfaces, 405
 Force law, 9
 Forced simple harmonic motion, 492
 Force-distance functions, 179, 234, 496
 Force-measuring techniques

adhesion, 237
 Atomic Force Microscopy, 245
 direct methods, 223, 227, 229
 energetic instabilities, 237
 force-distance functions, 234
 indirect methods, 223
 mechanical instabilities, 236
 Microfiber Cantilever, 250
 optical tweezers or optical trapping, 248
 Osmotic Pressure or Osmotic Stress, 244
 problems of interpretation, 229
 surface forces apparatus, 240
 thermodynamic instabilities, 237
 total internal reflection microscopy, 247
 Forces. *See also* Force-measuring techniques
 interaction, 215
 of nature, 3
 Franklin, Benjamin, 15
 Free energy, 23, 86, 86, 86
 Free space, interaction of molecules in, 23
 Freely jointed chain, 382
 Friction forces
 Amontons' laws of friction, 479
 chaotic, 496
 coefficients, 473
 liquid- and solid-like films, transitions
 between, 489
 lubricated sliding, 485
 origin of, 469
 real area of contact of rough surfaces, 493
 relationship between adhesion and, 475
 rolling friction, 494
 smooth and stick-slip sliding, 482, 496
 theoretical modeling of friction mechanisms,
 495
 Friction trace, 482
 Frictional adhesion, 615
 Full pair potentials, 137
 Fusion of membranes, 611
 Fusogenic proteins, 612

G
 Galileo, 5, 19
 Gas-liquid phase transitions, 114
 Gauss's Law, 54
 Geometric packing, 538
 Gibbs adsorption isotherm, 523
 Gibbs equation, 524
 Glass transition temperature, 493
 Glycine, 64, 88
 Gouy-Chapman theory, 313
 Grahame equation, 308
 Greek science, 3
 Group polarizabilities, 92

H

Hamaker constant, 257
 for interactions in vacuums or air, 262
 Lifshitz theory, applications to interactions in
 media, 266
 negative, 267
 nonretarded, 260, 263
 van der Waals forces, 253
 Hard core repulsion, 133
 Hard spheres, 25, 113, 133, 136
 Hard wall thickness, 589
 Harpooning effect, 59, 415
 Hauksbee, Francis, 8
 Headgroup area, 536, 558
 Headgroup overlap forces, 585
 Hellman-Feynman theorem, 16
 Helmholtz layers, 292, 298
 Hertz theory, 442
 Hertzian limit, 448
 Heuristic models, 495
 Hexagonal close packed (HCP), 424
 History of intermolecular forces
 eighteenth century, 7
 first estimates of molecular sizes, 14
 forces of nature, 3
 Greek notions, 3
 interaction potentials, 9
 intermolecular force-laws, 9
 Medieval notions, 3
 nineteenth century, 8
 phenomenological theories, 12
 recent trends, 17
 seventeenth century, 5
 twentieth century, 16
 Hogg-Healy-Fuerstenau equation, 321
 Homologous molecules, 358
 Hydrated ions, 78
 Hydrated radius, 79
 Hydration forces, 80, 302, 329, 361, 585
 Hydration number, 78
 Hydration regulation, 365
 Hydration shells, 63
 Hydrocarbon chains, 540
 Hydrocarbon interiors, 536
 Hydrodynamic layer thickness, 589
 Hydrogel, 163
 Hydrogen bond, 83, 151, 152
 Hydrogen-bond polymerization, 155
 Hydronium ion, 80
 Hydrophile-Liphophile Balance (HLB)
 number, 540
 Hydrophilic headgroups, 540
 Hydrophilic interaction, 163
 Hydrophilic polypeptide, 632

- Hydrophobic attraction, 163
 Hydrophobic compounds, 117
 Hydrophobic effect, 117, 151, 158
 Hydrophobic energy of transfer, 514
 Hydrophobic force, 370, 595
 Hydrophobic hydration, 158
 Hydrophobic interaction, 161, 371, 613
 Hydrophobic solvation, 158
 Hydrophobic surface, 461
 Hydrophobicity, 370, 371
 Hygroscopic, 163
 Hysteresis
 adhesion energy, 448
 contact angle, 439
- I**
- Ideal Gas Law, 12
 Ideal solvent, 384
 Iep (isoelectric point), 311
 Image charges, 257
 Imaginary frequencies, 119
 Incommensurate lattices, 281
 Incomplete wetting, 203
 Indirect force-measuring, 223
 Induced dipole moment, 91, 97
 Induced-fit interaction, 601
 Induction interaction, 99
 Inert ions, 309
 Infinite aggregates (phase separation), 513
 In-plane bridges, 604
 In-plane ordering, 342
 Insoluble monolayers, 520
 Integral equations, 67
 Interaction. *See also* Dynamic biointeractions; *specific types of interaction by name*
 common types (classification) of, 36, 219
 of dissimilar molecules, 117
 energies and forces, 215
 gravitational, 10, 267
 in free space and in mediums, 23
 gauging strength of, with thermal energy, 31
 length of, 182
 particle and small molecule, qualitative differences in, 205
 of particles, 212
 relative strengths of, 157
 time of, 176, 180, 181
 volume of, 31
 Interaction parameter, 406
 Interaction potential, 9, 208, 212. *See also* Pair potential
- Interfaces
 molecular ordering at, 342
 self-assembly on, 562
 Interfacial energy, 29, 196, 415
 Interfacial width, 344, 406
 Intermembrane forces, 604
 Intermolecular forces
 adsorbed surface films, 201
 body forces and surface forces, 218
 direct and indirect measurements, 223
 effective interaction area of two spheres, 211
 engulfing and ejection, 200
 interaction energies and interaction forces, 215
 interaction potentials between macroscopic bodies, 208
 interactions of particles versus those between atoms or small molecules, 212
 interdependence of, 606
 laws of, 9
 like molecules or particles in medium, association of, 191
 particle-surface and particle-interface interactions, 198
 short-range and long-range effects of, 11, 205
 surface and interfacial energy, 196
 unlike molecules, particles, or surfaces, association of, 197
 Intermolecular pair potential, 136
 Intermolecular potential functions, 180
 Interparticle forces
 adsorbed surface films, 201
 body forces and surface forces, 218
 direct and indirect measurements, 223
 effective interaction area of two spheres, 211
 engulfing and ejection, 200
 interaction energies and interaction forces, 215
 interaction potentials between macroscopic bodies, 208
 interactions of particles versus those between atoms or small molecules, 212
 like molecules or particles in medium, association of, 191
 particle-surface and particle-interface interactions, 198
 in pure polymer liquids, 392
 short-range and long-range effects of, 11, 205
 surface and interfacial energy, 196
 unlike molecules, particles, or surfaces, association of, 197
 Interparticle interaction potential, 212
 Intersegment forces, 394
 Intersurface forces
 body forces and surface forces, 218
 direct and indirect measurements, 223

- effective interaction area of two spheres, 211
- interaction energies and interaction forces, 215
- interaction potentials between macroscopic bodies, 208
- interactions of particles versus those between atoms or small molecules, 212
- short-range and long-range effects of, 205
- Intramembrane forces, 604
- Intramolecular expansion factor, 382
- Inverse power-law potential, 133
- Inverted-cone lipids, 565
- Ion exchangeable surfaces, 291
- Ion-condensation forces, 322
- Ion-correlation forces, 322
- Ion-dipole interactions, 73, 78
- Ionic concentrations, 295, 313
- Ionic crystals, 58
- Ionic distribution, 298
- Ionic liquids, 55
- Ionic surface lattice, 335
- Ions
- Born energy of, 61
 - divalent, 311
 - hydrated, 78
 - interactions with uncharged molecules, 96
 - in polar solvents, 77
 - size of, 133
 - solubility of, in different solvents, 62
 - specific ion-solvent effects, 66
- Ion-solvent molecule interaction, 98
- Irreversible path, 234
- Isoelectric point (iep), 311
- Isolated polymer chains, 384
- J**
- Jamming molecules, 354
- Jarzynski equation, 619
- JKR apparatus, 233
- JKR theory, 442
- K**
- Keesom interaction, 85
- Kelvin equation, 456, 532, 533
- Kelvin radius, 456, 532, 533
- Kepler Conjecture, 142
- Kinetic energy, 40, 43, 469
- Kinetic state, 206
- Kirkwood-Alder transition, 116
- Kitchen sink experiment, 21
- Kuhn length, 384
- L**
- Langbein approximation, 211
- Langmuir adsorption isotherm, 166
- Langmuir equation, 303
- Laplace equation, 269
- Laplace pressure, 269, 427, 428, 429, 455
- Lateral stress, 595
- Lecithin bilayer, 545
- Lennard-Jones potential, 15, 14, 68, 136, 139, 140, 475
- Lifshitz theory, 372
- as continuum theory, 264
 - interactions in mediums, applications to, 264
 - nonretarded Hamaker constants calculated on basis of, 260
 - of van der Waals forces, 256
- Ligand-receptor (LR) interactions, 599
- Line tension, 521, 563
- Linear chain molecules, 357
- Linear superposition approximation (SLA), 314
- Lipids
- bilayers of, 614
 - mean packing shapes of, 559
 - membrane, 564
 - mixtures of, 558
 - reservoirs of, 593
- Liquid crystals, 279
- Liquid helium, 268
- Liquid-like film, 489
- Liquids. *See also* Electrostatic forces
- associated, 83, 155, 153
 - charging of surfaces in, 291
 - diffuse interfaces in, 381
 - effect of liquid structure on molecular forces, 147
 - models of, 155
 - repulsive force in, 145
 - van der Waals forces, 109
- Liquid-solid phase transitions, 114
- Lock and key mechanisms, 18, 195
- London equation, 107
- Long-range undulation forces, 408
- Long-ranged interactions, 628
- Lorenz-Lorentz equation, 102
- Loss of entropy, 87
- Lower consolute temperature, 166
- LR (ligand-receptor) interactions, 599
- Lubrication forces
- Amontons' laws of friction, 479
 - liquid- and solid-like films, transitions between, 489
 - lubricated sliding, 485
 - origin of, 469

Lubrication forces (*Continued*)

- real area of contact of rough surfaces, 493
- relationship between adhesion and friction forces, 475
- rolling friction, 494
- smooth and stick-slip sliding, 482
- theoretical modeling of friction mechanisms, 495

M**Macroscopic bodies**

- molecule-surface interaction, 208
- sphere-surface and sphere-sphere interaction, 210
- surface-surface interaction, 211

Madelung constant, 59

Magnetic colloidal particles, 83

Magnetic dipoles, 83

Manning condensation, 323, 582

Many-body effects, 128

Many-body interaction, 23

Many-body systems, 67

Mass action equation, 309

Mass action, law of, 505

Mathematical methods, 5

MBI (Multiple Beam Interferometry), 241

MC (Microfiber Cantilever), 250

MC (Monte Carlo) computer simulation, 37, 297

McLachlan's expression, 120

MD (Molecular Dynamics) computer simulation, 37

Measuring techniques. *See Force-measuring techniques*

Mechanical instabilities, 236

Medieval science, 3

Melts, polymer, 392

Membranes. *See also Biological systems*

biological, 564, 626

fluidity of, 626

fusion of, 610

lipids, 564

proteins of, 567

structure of, 567

Mesophases, 528, 539

Metals, surface energies of, 280

Metastable state, 206

Micelles

2D, 521, 562

nonspherical and cylindrical, 543

spherical, 540

Micellization (finite sized aggregates), 513

Microfiber Cantilever (MC), 250

Micropipette Aspiration Technique, 594

Minimal surfaces, 458

Miscible components, 358

Mismatched lattices, 281

Molar cohesive energy, 109

Molar lattice energy, 59, 109

Molecular Dynamics (MD) computer simulation, 37

Molecular ordering, 145

Molecular packing, 18

Molecular polarizability, 120

Molecular theories, 8, 35, 66, 67

Molecular volume, 31

Molecules. *See also* Polar molecules; Polarization of molecules

branched chain, 357

dispersion self-energy of, 126

distribution of, in systems at equilibrium, 27

electronic polarizability of, 93

energy transfer during collisions of, 175

first estimates of sizes, 14

flexible (soft), 357

homologous, 358

interaction of, 23, 205

jamming, 354

like, association of, 191

linear chain, 357

liquid structure, effect on molecular forces, 147

nonspherical, ordering of between structured surfaces, 347

ordering at surfaces, interfaces, and in thin films, 342

polarizability of, 91

size of, 133

in solids, packing of, 142

spherical, ordering of between smooth structures, 345

uncharged, 96

unlike, association of, 197

Van der Waals forces between, 119

Molecule-surface interaction, 208

Molten salts, 55

Momentum, 40

Monodisperse micelles, 530

Monolayers

curvature effects, 550

soluble, and Gibbs adsorption

isotherm, 523

soluble and insoluble, 520

Monomers, 505

Monotonically repulsive hydration forces, 361

Monovalent anions, 134

Monovalent cations, 134

Monte Carlo (MC) computer simulation, 37, 297
 Motor proteins, 630
 Multilayers, 528
 Multimolecular systems, 35
 Multiple Beam Interferometry (MBI), 241
 Multivalent polyelectrolytes, 402

N

Nanoparticles, 212, 422
 Natural frequency, 471
 Natural philosophers, 9
 Negative adsorption, 198
 Negative Hamaker constant, 267
 Negative hydration, 79
 Nernst equation, 27
 Newton, Isaac, 5, 6, 7, 39
 Newton's Cradle, 470
 Nonadditivity, 128, 213
 Nonadsorbing polymers, 593
 Noncovalent interactions, 230
 Nondirectional bonding, 527
 Non-DLVO forces, 341
 Nonequilibrium effects, 213
 Nonequilibrium interactions
 biological, 617
 Deborah Number, 175
 energy transfer during cyclic bonding-unbonding processes, 178
 energy transfer during molecular collisions, 175
 polymers, 404
 rate- and time-dependent detachment forces, 171
 time, temperature, and velocity in complex processes, 169
 time- and rate-dependent interactions and processes, 169
 Noninteracting solute molecules, 244
 Nonlinear chain molecules, 357
 Nonretarded Hamaker constants, 260, 263
 Nonspecific fusion, 611
 Nonspherical micelles, 543
 Nonspherical molecules, 347
 Nonwetting, 201
 Nucleation, 515, 532
 Numerical methods, 37

O

OHP (Outer Helmholtz Plane), 298
 Oil-in-water (O/W) droplets, 574
 One-component aggregates, 526
 One-dimensional aggregates, 510

Optical trapping (OT), 248
 Optical tweezers, 248
 Optimal headgroup area, 536
 Orientation interaction, 85
 Orientational distribution, 33
 Orientational polarizability, 93
 Orienting molecules, 78
 Orthogonal cylinders, 218
 Oscillatory force, 68, 146, 349, 355
 Osmotic limit, 305, 320
 Osmotic Pressure (OP) technique, 225, 226, 244
 Osmotic Stress (OS) technique, 225, 226, 244
 Ostwald ripening, 515, 519, 609
 Outer Helmholtz Plane (OHP), 298
 Out-of-plane bridges, 604
 Out-of-plane ordering, 342
 Overlap repulsion, 387
 O/W (oil-in-water) droplets, 574
 Oxonium ion, 80

P

P-A (pressure-area) curve, 115
 Packing densities, 355
 Packing factor, 539
 Packing parameter, 539
 Packing properties, 538
 Packing radii, 134
 Packing stresses, 566
 Pair potential
 classification of, 34, 219
 of common types of interactions, 36, 219
 defined, 23
 interaction potentials, 9
 between macroscopic bodies, 208
 self-energy and, 24
 Pairwise additive, 128
 Parallel bonds, 622, 624
 Partial-wetting, 203
 Particle-interface interactions, 198
 Particles
 distribution of, in systems at equilibrium, 27
 interaction of, versus that of molecules, 205
 interactions of, compared to atoms or small molecules, 212
 like, association of, 191
 in solids, packing of, 142
 unlike, association of, 197
 Particle-surface interactions, 198
 PB (Poisson-Boltzmann) equation, 293, 294
 Periodic boundary conditions, 50
 Permanent dipole, 97
 Persistence lengths, 382
 Phase separation (infinite aggregates), 513

- Phase transitions
 gas-liquid, 114
 liquid-solid, 114
- Phenomenological theories, 12
- Physical (non-covalent) bond, 54
- Pitch Drop Experiment website, 447
- Plastic deformations, 453
- Point of zero charge (pzc), 311
- Poisson equation, 293
- Poisson-Boltzmann (PB) equation, 293, 294
- Polar angles, 84
- Polar molecules
 angle-averaged potentials, 84
 defined, 71
 dipole self-energy, 73
 dipole-dipole interactions, 81
 entropic effects, 86
 hydrated ions, 78
 hydration forces, 80
 hydrogen bonds, 83
 ion-dipole interactions, 73, 78
 ions in polar solvents, 77
 magnetic dipoles, 83
 polarizability of, 93
 rotating dipoles, 84
 solvation forces, 80
 structural forces, 80
 Van der Waals forces between, 117
- Polarizability. *See also* Polarization of molecules
 of atoms and molecules, 91
 determined from molecular and bulk properties, 103
 excess, 100, 101, 122
 of polar molecules, 93
- Polarization interactions, 34
- Polarization of molecules
 dipole-induced dipole interactions, 99
 effects of on electrostatic interactions, 94
 excess polarizability, 100
 interactions between ions and uncharged molecules, 96
 ion-solvent molecule interactions and Born energy, 98
 mechanisms for, 94
 polarizability of atoms and molecules, 91
 polarizability of polar molecules, 93
 solvent effects, 100
 unification of polarization interactions, 99
- Polydisaccharide, 402
- Polydispersity, 358
- Polyelectrolytes, 402
- Polymer-mediated forces. *See* Steric forces
- Positive curvature modulus, 555
- Potential determining ions, 310
- Potential gradient, 313
- Power-law potential, 133, 136
- Pressure
 disjoining, 267, 303
 Laplace, 269, 427, 428, 429, 455
 light, 249
 origin of, 298
 radiation, 51
 spreading, 418, 419
 between two charged surfaces in water, 299
- Pressure-area (Π -A) curve, 115
- Pressure-volume (P-V) curve, 115
- Primary hydration shell, 80
- Principia* (Newton), 5, 7
- Protein
 engines, 630
 membrane, 567
 motor, 630
 pump, 633
 transport, 630
- Protrusion decay length, 344
- Protrusion forces, 344, 406, 585
- Pseudo-phase approximation, 530
- Pzc (point of zero charge), 311
- Q**
- Quantum theory of colloids, 5
- R**
- Radius of gyration, 382
- Rafts, 562
- Raleigh Instability, 460
- Random close-packing (RCP), 142
- Random coil shape, 382
- Random loose packing (RLP), 142, 143
- Rankine, William, 9
- Rate and state models, 495
- Rate-dependent interactions. *See also*
 Nonequilibrium interactions
 detachment forces, 171
 energy transfer during molecular collisions, 175
 general discussion, 169, 617
- Rayleigh instability, 236
- Rayleigh limit, 69
- Reduced mass, 173
- Reference states, 59
- Reflectance Interference Contrast Microscopy (RICM), 248
- Relaxation time, 176, 180, 181, 182
- Repeptization, 330
- Repulsive configurations, 125

- Repulsive double-layer interaction energy, 319
- Repulsive force
effect of liquid structure on molecular forces, 147
entropic, 585
in liquids, 145
in noncovalently bonded solids, 140
packing of molecules and particles in solids, 142
between polymer-covered surfaces, 387
repulsive potentials, 136, 137
sizes of atoms, molecules, and ions, 133
steric-hydration, 302, 329, 361, 585
total intermolecular pair potential, 136
van der Waals, 267
- Repulsive potential, 136, 137
- Resonance energy transfer, 492
- Restricted chains, 384
- Retardation effect, 129, 270
- Reversible path, 234
- RICM (Reflectance Interference Contrast Microscopy), 248
- RLP (random loose packing), 142, 143
- Robert Boyle, 6
- Rods, 510
- Rolling friction, 474, 494
- Rotating dipoles, 84
- Rotational correlation time, 79
- Rough surfaces
adhesion of, 452
real area of contact of, 493
wetting of, 434
- Round punch geometry, 454
- Rupture, biological, 619
- S**
- Scaling arguments, 5
- Scaling effects, 212
- Second Law of Thermodynamics, 47
- Secondary minimum, 326
- Self-assembly. *See also* Biological structures
aggregates, conditions necessary for formation of, 509
of amphiphilic molecules, 503
amphiphilic structures, large and complex, 527
critical micelle concentration, 512
dimensionality and geometry, 510
versus directed-assembly, 628
hydrophobic energy of transfer, 514
infinite aggregates versus finite sized aggregates, 513
interactions of, 214
line tension and 2D micelles, 521
- mesophases and multilayers, 528
nucleation and growth of aggregates, 515
overview, 503
size distributions, 524
soluble and insoluble monolayers, 520
soluble monolayers and Gibbs adsorption isotherm, 523
on surfaces and interfaces, 562
thermodynamic equations of, 504
- Self-energy, 24, 61, 73, 126
- Semiempirical models, 495
- Semiflexible chains, 384
- SFA (surface forces apparatus), 240, 245
- Shear Transformation Zone (STZ) model, 495
- Sheet-like aggregates, 510, 511
- Short-range interaction, 628
- Short-range protrusion forces, 406
- Simple systems, 16
- Skin depth effects, 212, 214
- SLA (linear superposition approximation), 314
- Sliding
lubricated, 485
smooth and stick-slip, 482
- Slip length, 589
- Smectic liquid crystal, 279
- Smooth sliding, 482
- Snowflakes, 576
- Soft structures. *See* Biological structures
- Solid particles, adhesion of, 442
- Solid-like films, 489
- Solids
noncovalently bonded, role of repulsive forces in, 140
packing of molecules and particles in, 142
van der Waals forces, 109
- Solubility, 62, 516, 520
- Soluble monolayers, 520, 523
- Solute molecules, 26
- Solutions, state of polymers in, 381
- Solvated ions, 78
- Solvation forces
attractive hydrophobic forces, 370
monotonically repulsive hydration forces, 361
oscillatory force, 68, 146, 349
structural forces, and hydration forces, 80
- Solvation shells, 63
- Solvation zone, 81
- Solvent effect, 24, 65, 100
- Solvents
polar, ions in, 77
solubility of ions in, 62
specific ion-solvent effects, 66
- Space, biointeractions evolving in, 617

- Specific binding sites, 18
 Specific fusion, 612
 Specific interactions, 195, 599
 Spheres
 effective interaction area of, 211
 hard, 25, 113, 133, 136
 self-assembly, 510
 sphere-sphere interactions, 210
 sphere-surface interactions, 210
 Spherical micelles, 540
 Spherical molecules, 134, 345
 Spreading coefficient, 419
 Spreading pressure, 418, 419
 Spring potential functions, 180
 Static dielectric constants, 65
 Statistical aspects of intermolecular forces, 43
 See also Thermodynamics
 Steric (polymer-mediated) forces
 attractive depletion forces, 398
 attractive intersegment and bridging forces, 394
 biological systems, 585
 diffuse interfaces in liquids, 381
 fluid-like interfaces, 405
 interparticle forces in pure polymer liquids, 392
 long-range undulation forces, 408
 nonequilibrium aspects of polymer interactions, 404
 polyelectrolytes, 402
 polymers, 381
 repulsive forces between polymer-covered surfaces, 387
 short-range protrusion forces, 406
 Steric-hydration repulsion, 302, 329, 361, 585
 Steric repulsion, 387
 Stern layers, 292, 298, 299
 Stick-slip adhesion, 452
 Stick-slip sliding, 482
 Stribeck Curve, 495
 Strong intermolecular forces
 Born energy of ions, 61
 charge-charge interactions, 54
 computer simulations, 67
 continuum theories, 66
 Coulomb forces, 54
 covalent or chemical bonding forces, 53
 electrostatic forces, 60
 Gauss's Law, 54
 integral equations of many-body systems, 67
 ionic crystals, 58
 physical and chemical bonds, 54
 reference states, 59
 solubility of ions in different solvents, 62
 specific ion-solvent effects, 66
 Structural forces, 80
 Structured surfaces, 347
 STZ (Shear Transformation Zone) model, 495
 Superhydrophobicity, 371, 438
 Superposition principle, 60
 Surface. *See also* Electrostatic forces
 with adsorbed layers, van der Waals forces between, 281
 asymmetric, 321
 charge, discrete, 335
 charge, electric field, and counterion concentration at surface, 293
 charged, in electrolyte solutions, 306
 charged, in water, 292
 highly curved, 422
 isolated, surface charge and potential of, 309
 in liquids, charging of, 291
 molecular ordering at, 342
 ordering of spherical molecules between smooth, 345
 polymer-covered, repulsive forces between, 387
 polymers, state of at, 381
 pressure between charged, in water, 299
 rough, real area of contact of, 493
 rough, textured, and chemically heterogeneous, wetting of, 434
 rough and textured, adhesion of, 452
 self-assembly on, 562
 structured, ordering of nonspherical molecules between, 347
 unlike, association of, 197
 Surface energy, 196, 275, 280, 415
 Surface forces, 218
 Surface forces apparatus (SFA), 240, 245
 Surface potential, 298
 Surface-area-to-volume scaling effect, 212
 Surface-surface interactions, 211
 Surface tension (See Surface energy)
 Swelling clays, 363
 Symmetric liquid molecules, 359
 Symmetrical electrolytes, 313
- T**
- Temperature, in complex processes, 182
 Temperature-dependent processes.
 See Nonequilibrium interactions
 Tethering forces, 601
 Textured surfaces
 adhesion of, 452
 wetting of, 434
 Thermal energy, 31

- Thermal fluctuation forces
 attractive depletion forces, 398
 attractive intersegment and bridging forces, 394
 biological systems, 585
 diffuse interfaces in liquids, 381
 fluid-like interfaces, 405
 interparticle forces in pure polymer liquids, 392
 long-range undulation forces, 408
 nonequilibrium aspects of polymer interactions, 404
 polyelectrolytes, 402
 polymers, 381
 repulsive forces between polymer-covered surfaces, 387
 short-range protrusion forces, 406
- Thermal wavelength, 30
- Thermally activated processes, 175
- Thermodynamic instabilities, 237
- Thermodynamic surface energy, 421
- Thermodynamic transitions, 236
- Thermodynamically equilibrium, 229
- Thermodynamically stable colloids, 326
- Thermodynamics. *See also* Self-assembly
 Boltzmann distribution, 26, 43
 chemical potential, 26
 computer simulations, molecular approaches via, 37
 distribution of molecules and particles in systems at equilibrium, 27
 entropy, 43
 equilibrium, 43
 forces, classification of, 34
 interaction of molecules, 23
 Molecular Dynamics computer simulation, 37
 Monte Carlo computer simulation, 37
 multimolecular systems, 35
 multiple collisions, 43
 pair potential, 24, 34
 self-energy, 24
 thermal energy, gauging strength of interactions with, 31
 two-body collisions, Newton's laws applied to, 39
 van der Waals equation of state, 29
- Theta solvent, 384
- Theta temperature, 384
- Thick wetting films, 303
- Thin films, 342
- Thomas-Fermi screening length, 274
- Three-dimensional aggregates, 511
- Tight adhesive junctions, 627
- Tight junctions, 609
- Time
 biointeractions evolving in, 617
 in complex processes, 182
 time-temperature superposition, 184
- Time-dependent interactions
 detachment forces, 171
 energy transfer during cyclic bonding-unbonding processes, 178
 energy transfer during molecular collisions, 175
 general discussion, 169, 617
 time, temperature, and velocity in complex processes, 178
- Tolman Equation, 423
- Total energy curves, 180
- Total internal reflection microscopy (TIRM), 247
- Transbilayer lipid exchange, 546
- Translational kinetic energy, 39
- Transport protein, 630
- Triboelectric effect, 499
- Triboelectricity, 59
- Trivalent cations, 134
- Trotton's rule, 31, 32
- Tunable materials, 628
- Two-body collisions, 39
- Two-dimensional aggregates, 510
- Two-dimensional micelles, 521, 562
- Two-dimensional structures on surfaces, 520
- U**
- Uncharged molecules, 96
- Undulation forces, 408, 585
- Univalent polyelectrolytes, 402
- Unstructured surfaces, 345
- Unwetting, 202
- V**
- Vacuums
 Hamaker constants for interactions in, 253, 262
 van der Waals forces between bodies in, 255
 work of adhesion and cohesion, 415
- Van der Waals equation of state (EOS), 29, 113
- Van der Waals forces, 85
 adhesion energies, 275
 anisotropy of dispersion forces, 127
 biological systems, 577
 between bodies in vacuum or air, 255
 for bodies of different geometries, 255
 combining relations, 274
 between conducting media, 261
 dispersion forces, 107, 109

- Van der Waals forces (*Continued*)**
- dispersion self-energy of molecules in mediums, 126
 - electrostatic screening effects in electrolyte solutions, 273
 - experiments on, 282
 - gas-liquid phase transitions, 114
 - Hamaker constant, defined, 253
 - Hamaker constants for interactions in vacuum or air, 262
 - Lifshitz theory applied to interactions in mediums, 264
 - Lifshitz theory of, 256
 - liquid-solid phase transitions, 114
 - London equation, 107
 - many-body effects, 128
 - in mediums, 121
 - between molecules, 119
 - nonadditivity of, 128
 - nonretarded Hamaker constants, 260
 - particle-surface interactions, 258
 - between polar molecules, 117
 - repulsive, 267
 - retardation effect, 129, 270
 - strength of, 109
 - surface energies, 275, 280
 - between surfaces with adsorbed layers, 281
 - Van der Waals interaction, 254
 - Vapor bridges model, 377
 - Velocity, in complex processes, 182
 - Vesicles, 547
 - Vibration time, 173
 - Viscoelastic materials, 453
- W**
- Water
- charged surfaces in, 292
 - hydrogen bonds, 152
 - hydrophilic interaction, 163
 - hydrophobic effect, 158
 - hydrophobic interaction, 161
 - models of, 155
- pressure between two charged surfaces in, 299
- properties of, 151
- strong ion-dipole interactions in, 78
- structure models of, 377
- Water-in-oil (W/O) droplets, 574
- Wavy surfaces, 462
- Weak overlap approximation (WOA), 314
- Wenzel Equation, 436
- Wetting**
- adhesion energies versus adhesion forces, 419
 - adhesion energy hysteresis, 448
 - adhesion of rough and textured surfaces, 452
 - adsorbed surface films, 201
 - capillary forces, 455
 - contact angle hysteresis, 439
 - contact angles and wetting films, 429
 - films, 201, 267, 303, 429
 - highly curved surfaces and interfaces, 422
 - JKR and Hertz theories, 442
 - plastic deformations, 453
 - of rough, textured, and chemically heterogeneous surfaces, 434
 - surface and interfacial energies, 415
- Williams-Landell-Ferry (WLF) theory, 490
- Work of adhesion, 196, 416
- Work of cohesion, 196, 416
- Wormlike chain, 382
- Worm-like chain (WLC) model, 604
- Y**
- Yield stress, 453
- Young, Thomas, 15
- Young equation, 203, 431
- Young-Dupré equation, 203, 431, 439, 606, 607
- Young's modulus, 447
- Z**
- Zwitterionic molecules, 71